2017 Chesapeake Bay Water Quality and Sediment Transport Model

A Report to the US Environmental Protection Agency Chesapeake Bay Program Office

December 2019 Final Report

Carl F. Cerco

Mark R. Noel

US Army Engineer Research and Development Center, Vicksburg, MS

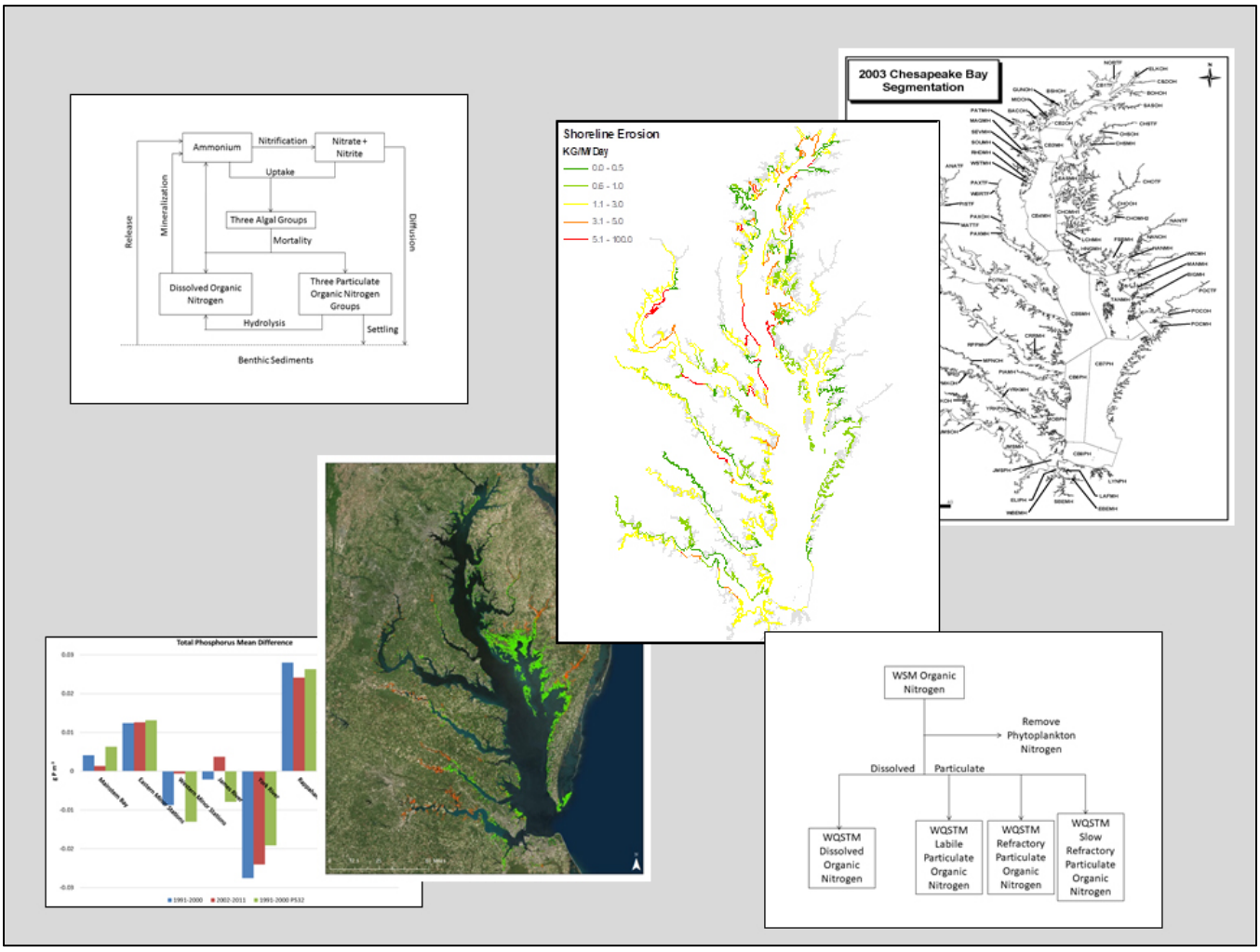

Abstract

This report documents the 2017 version of the Chesapeake Bay Water Quality and Sediment Transport Model (WQSTM). This model version is intended to provide support for the 2017 Midpoint Assessment of the 2010 Chesapeake Bay Total Maximum Daily Load (TMDL). The 2017 WQSTM is calibrated to the years 1991–2000 and is validated with an independent data set from 2002–2011.

The first chapter of this report summarizes revisions since the 2010 version of the WQSTM. Notably, a wetlands module has been added to the 2017 version and three particulate organic matter classes are now specified in the water column, corresponding to the three classes in the sediment diagenesis model. The second chapter of the report details model kinetics, which are largely based on the original kinetics developed in 1992. Silica and zooplankton state variables have been deleted, however, because of data limitations and lack of evidence that they influence the TMDL standards being evaluated. This model version reinstitutes a partial attenuation model for computing light attenuation, as detailed in Chapter 3. The partial attenuation model relaxes data requirements, which limited application of the preceding optical model. The new wetlands module, described in Chapter 4, emphasizes transfer of carbon, nitrogen, phosphorus, and oxygen between wetlands and the adjacent water column. Chapter 5 describes loads to the water column from shoreline erosion. The 2017 WQSTM incorporates shoreline nutrient loads as well as suspended solids loads. Watershed loads for the application period are provided by the Phase 6 Chesapeake Bay Watershed Model (WSM). The processes for linking the WQSTM to loads from the watershed, point sources, and atmosphere are described in Chapter 6, which also details mapping of WSM variables into WQSTM variables. Oysters were active in the 2010 model but received little emphasis. The 2017 model renews the representation of the native oyster population and introduces an aquaculture module, as described in Chapter 7. Chapter 8 presents a statistical summary of 2017 model results in comparison with the 2010 version. The report concludes with recommendations for future model developments in Chapter 9. Primary recommendations include replacing the hydrodynamic model with a model that provides improved detail in near-shore regions and improving transformation of WSM variables to WQSTM variables.

Appendices A-D provide time series and spatial comparisons of the model to observations for calibration and verification. The comparisons emphasize model variables critical to the TMDL, which focuses on dissolved oxygen, chlorophyll, and water clarity. Appendix E compares simulated and observed algal nutrient limitations, and Appendix F compares simulated and observed hypoxic water volumes. Appendix G describes revisions to the relationships between algal growth and temperature employed in the WQSTM calibration. The revisions were implemented to provide more realistic model performance in climate-change scenarios.

Acknowledgements

Funding for this study was provided by the US Environmental Protection Agency's (EPA's) Chesapeake Bay Program Office (CBPO) through an interagency agreement with the US Army Corps of Engineers, Baltimore District. Lewis Linker is the Science and Analysis Team Leader for the Science, Analysis, and Implementation Branch of CBPO and the Chesapeake Bay Program Modeling Coordinator. Appendices E and F were prepared by Dr. Richard Tian, University of Maryland Center for Environmental Science (UMCES); Lewis Linker, EPA; Gary Shenk, US Geological Survey; Dr. Gopal Bhatt, Penn State; Dr. Danny Kaufman, Chesapeake Research Consortium (CRC); Dr. Isabella Bertani, UMCES; and Cuiyin Wu, CRC.

Point of Contact

Carl F. Cerco, PhD, PE
Research Hydrologist (retired)
US Army Engineer Research and Development Center
3909 Halls Ferry Road
Vicksburg, MS 39180
769-230-5543
carlcerco@outlook.com

Contents

Figures

Tables

Abbreviations and Acronyms

3-D	three dimensional
ADH	Adaptive Hydrodynamics (model)
AMD	absolute mean difference
AOM	advanced optical model
BOD5	biological oxygen demand for 5 days
C	carbon
CAST	Chesapeake Assessment and Scenario Tool
CBOPE	Chesapeake Bay Oyster Population Estimate
CBP	Chesapeake Bay Program
CBPO	Chesapeake Bay Program Office
CBPS	Chesapeake Bay Program Segment
CE-QUAL-ICM	Corps of Engineers Integrated Compartment Water Quality Model
CH3D	Computational Hydrodynamics in Three Dimensions (model)
Chl	chlorophyll *a*
CO_2	carbon dioxide
COD	chemical oxygen demand
CRC	Chesapeake Research Consortium
DC	Deep Channel (use)
DIP	dissolved inorganic phosphorus
DO	dissolved oxygen
DOC	dissolved organic carbon
Dsil	dissolved silica

DW	Deep Water (use)
GIS	geographic information system
EPA	US Environmental Protection Agency
FVCOM	Finite Volume Community Ocean Model
HUC	hydrologic unit code
MD	mean difference
MDNR	Maryland Department of Natural Resources
N	number of observations
NH_4^+	ammonium
NO_3^-	nitrate
NWI	National Wetlands Inventory
O	observation
O_2	oxygen
OW	Open Water (use)
P	prediction
PAM	partial attenuation model
PBS	particulate biogenic silica
PIP	particulate inorganic phosphorus
POC	particulate organic carbon
ppt	parts per thousand
RD	relative difference
SALT	salinity
SAV	submerged aquatic vegetation
SCHISM	Semi-implicit Cross-scale Hydroscience Integrated System Model

SI	International System of Units
SLAMM	Sea Level Affecting Marshes Model
SWMP	Shallow Water Monitoring Program
TMDL	Total Maximum Daily Load
TN	total nitrogen
TP	total phosphorus
TSS	total suspended solids
UMCES	University of Maryland Center of Environmental Science
VIMS	Virginia Institute of Marine Science
VMRC	Virginia Marine Resources Commission
VSS	volatile suspended solids
WQSTM	Chesapeake Bay Water Quality and Sediment Transport Model
WSM	Chesapeake Bay Watershed Model

Units of Measure

Abbreviation	Unit
^{o}C	degrees Celsius
^{o}K	degrees Kelvin
cm^{2}	square centimeter(s)
d	day(s)
g	gram(s)
$g\ s^{-1}$	gram(s) per second
kg	kilogram(s)
$kg\ d^{-1}$	kilogram(s) per day (load)
$kg\ m^{-3}$	kilogram(s) per cubic meter (density)
$kg\ m^{-1}\ d^{-1}$	kilogram(s) per meter per day (erosion)
$kg\ yr^{-1}$	kilogram(s) per year (erosion)
km	kilometer(s)
km^{3}	cubic kilometer(s)
lb	pound(s)
µg	microgram(s)
m	meter(s)
m^{2}	square meter(s)
$m^{2}\ kg^{-1}$	square meter(s) per kilogram (attenuation)
m^{3}	cubic meter(s)
$m^{3}\ yr^{-1}$	cubic meter(s) per year (flow rate)
metric ton d^{-1}	metric ton(s) per day (load)
metric ton yr^{-1}	metric ton(s) per year (load)
mg/l	milligram(s) per liter
ppt	part(s) per thousand
s	second(s)

1 Introduction

This study builds on a modeling framework established nearly 30 years ago and subjected to continuous revision since then. Four major study phases preceded this one. The first phase provided modeling technology for the 1991 reevaluation of the 1987 nutrient reduction goals (Cerco and Cole 1994). The second phase refined the computational grid to improve representation in the Virginia tributaries and introduced living resources into the computational framework (Cerco et al. 2002). That phase provided computational tools for the Tributary Strategy management effort. The third phase continued the grid refinements and extended the model into still smaller tributaries (Cerco and Noel 2004a). That version of the model provided verification of a 2003 agreement to cap average annual nitrogen and phosphorus loads to the Bay. The fourth phase provided modeling technology to support development of the 2010 Chesapeake Bay Total Maximum Daily Load (TMDL) (Cerco et al. 2010).

The latest study phase is referred to as the Midpoint Assessment of the 2010 TMDL. This phase employs the 2017 version of the Chesapeake Bay Water Quality and Sediment Transport Model (WQSTM). This study phase had multiple objectives, including the following:

- Extend the model application period to encompass recent observations, including those collected in the Shallow Water Monitoring Program.
- Perform adjustments and recalibration necessary to accommodate loads computed by Phase 6 of the Chesapeake Bay Program Watershed Model (WSM).
- Provide modeling technology to support a 2017 Midpoint Assessment of the 2010 TMDL.

The final objective is considered the most consequential and the schedule of the present study was specified to provide a 2017 product.

1.1 What's New, What's Not?

Each preceding model application employed a different combination of model features and required the addition of capabilities to support project goals. The present study followed that precedent. This study breaks precedent, however, by removing model features that are obsolete or no longer relevant. This section provides brief descriptions of model revisions since the 2010 version. Detailed descriptions of significant revisions are provided in succeeding chapters.

1.1.1 Application Period

The 2017 study introduces a new model application period from 2002 to 2011. The period 1991–2000 is retained as the primary calibration period since the years 1993–1995 form the basis for the TMDL determination. The earlier years also provide a rich data set of living resource and process observations for comparison with relevant model results. The 2002–2011 application provides a classic model verification. All model parameter specification is determined in the 1991–2000 application. Model performance is then tested or verified against an independent data set collected in 2002–2011.

1.1.2 Model Kinetics

1.1.2.1 Particulate Organic Matter

The model of the water column was originally formulated with two classes of particulate organic matter: labile and refractory (Cerco and Cole 1994). Those classes were distinguished by their reaction rates. Labile material decomposed on a time scale of days to weeks while refractory material required more time. Labile and refractory state variables were defined for carbon, nitrogen, and phosphorus.

The sediment diagenesis model (DiToro and Fitzpatrick 1993) was formulated with three classes of organic matter: G1, G2, and G3 (Westrich and Berner 1984). Those classes indicate labile, refractory, and slow refractory material. Upon settling to the sediments, labile state variables in the water column were routed to the G1 sediment state variables. Refractory state variables in the water column were split between G2 and G3 sediment state variables. That arrangement proved unsatisfactory in the 2017 model. Problems developed because the split into G2 and G3 occurred at the sediment-water interface. Distinctions between G2 and G3 content could not be assigned to refractory particles originating from different sources (e.g., phytoplankton vs. shoreline erosion loads). The problem was alleviated by introducing a third reactive class of organic material to the suite of water column state variables. Labile, refractory, and slow refractory particles in the water are now routed directly to G1, G2, and G3 classes in the diagenesis model. Internal and external sources of particulate organic material are provided with individual, potentially distinct particle composition.

1.1.2.2 Silica

Silica was included in the original 1994 model to allow for potential nutrient limitation of diatoms during the spring algal bloom in the Bay and lower tributaries. Two state variables were required: particulate biogenic silica (PBS) and dissolved silica (Dsil). Application of the silica submodel was hindered from the outset by a shortfall of PBS observations. While Dsil was regularly monitored in the water column and at river inputs, only sporadic observations were available for specification of PBS loads and for calibration of PBS in the water

column. Subsequent model applications indicated that phosphorus is the predominant limiting nutrient during the spring algal bloom. Consequently, silica has been eliminated in the 2017 model.

1.1.2.3 Zooplankton

Zooplankton were added to the model circa 2000 during the Virginia Tributary Refinements phase (Cerco et al. 2002). One motivation was an interest in direct computation of living resources (e.g., submerged aquatic vegetation [SAV], zooplankton, and benthos). A second motivation was to improve computation of phytoplankton dynamics by improving predation terms. Two zooplankton classes were added: microzooplankton and mesozooplankton. Both classes prey upon phytoplankton. The model formulation included an additional predation term to represent other planktivores, including menhaden. Despite model limitations, credible representations of zooplankton biomass were obtained (Cerco and Meyers 2000). During an effort to improve computations of primary production, however, we found the formulation of the additional predation term was more important than the zooplankton representation in determining primary production (Cerco and Noel 2004b). Interest in zooplankton has diminished since they were introduced, and their inclusion added little to the model. Consequently, zooplankton have been eliminated in the 2017 model version.

1.1.3 Sediment Diagenesis Model

Testa et al. (2013) revised the denitrification formulation in the original diagenesis model. That revision provided improved computations of sediment-water nitrate flux across a range of environments from freshwater to mesohaline. The revised formulation has been incorporated into the 2017 model.

Deposit-feeding benthos were added to the diagenesis model at the same time other living resources (SAV and zooplankton) were added to the representation of the water column (Cerco and Meyers 2000). The deposit feeders, which fed on and recycled sediment carbon, were living resource indicators but served no purpose in the model. We found they influenced carbon cycling among various reactive classes of organic matter in an unpredictable manner. In view of diminished interest and uncertain influence, deposit feeders have been eliminated in the 2017 model.

1.1.4 Wetlands Module

Tidal wetlands exert a potentially significant influence on the concentrations of dissolved and suspended materials in the adjacent open waters. Wetland processes can play a significant role in estuarine nutrient and solids budgets, largely through removal. In recognition of wetland effects, Dresher and Stack (2015) have developed protocols to provide nutrient and sediment mass

reduction credits for shoreline management projects that include restoration of vegetation.

Wetlands respiration has been represented in the WQSTM since the 2002 version (Cerco and Noel 2004a). Incorporation of wetlands respiration was required to reflect low dissolved oxygen concentrations observed in open waters adjacent to extensive tidal wetlands. Wetlands respiration is now incorporated into a more representative wetlands module, which was developed largely in response to the potential credits allowed in the TMDL for wetlands restoration (Drescher and Stack 2015). The module also improves model performance in regions with extensive wetlands. Development of a mechanistic biogeochemical wetlands model is a formidable task beyond the scope of this study. The new module does, however, provide basic representations of relevant wetlands processes, including deposition of organic and inorganic particles, nitrate uptake, and respiration.

1.1.5 Shoreline Erosion

State-of-the-art quantification of solids loads entering the Bay from shoreline erosion was conducted concurrent with the 2010 model study (Cerco et al. 2010). The loads were derived from long-term shoreline recession rates and accounted for structures and other local features. The quantification added previously unavailable spatial detail to estimated solids loads. The solids loads from the 2010 model have been retained in the 2017 version.

Shoreline erosion adds nutrients as well as solids to the Bay. Phosphorus contributed by erosion is a significant portion of the system total phosphorus load. Nutrients associated with shoreline erosion have been included in various model versions (Cerco and Noel 2004a) but were omitted from the 2010 version because no guidance existed to incorporate them into the TMDL development. A recent panel report recognized the potential for nutrient reduction credits associated with erosion management practices but withheld recommendations pending access to more information on nutrient availability/ reactivity. In view of the recognized contribution of shoreline erosion to the Bay nutrient budget and the pending consideration of those nutrients in TMDL development, nutrient loads from shoreline erosion have been restored in this model version.

1.1.6 Oysters

Bivalve filter feeders were added to the model as part of the Tributary Refinements phase (Cerco et al. 2002). That addition reflected the general interest in living resources as well as a specific mandate to investigate the impact of a tenfold increase in the oyster population on Bay water quality. The filter feeder module incorporated two freshwater bivalve groups as well as oysters. An investigation of the increase in the oyster population led to the following conclusions (Cerco and Noel 2007):

- The contemporary oyster population had little effect on water quality.
- A tenfold increase would improve conditions in the vicinity of oyster reefs but do little to alleviate hypoxia in deep channels of the Bay and tributaries.

Oysters were included in the 2010 model version but received limited attention. Effects of oyster restoration were not considered in the TMDL development. Currently, oysters are receiving increased attention because of the rapid expansion of aquaculture operations and the potential associated beneficial effects (Cornwell et al. 2016). As a result of the increased interest, the oyster module has been updated to reflect contemporary populations on reefs and current aquaculture operations.

1.1.7 Light Attenuation

Bay model versions prior to 2010 calculated light attenuation in the water column through various partial attenuation relationships. Attenuation was the linear sum of contributions from water itself and from suspended particles. The 2010 model version incorporated an advanced optical model that calculated attenuation as a nonlinear function of attenuation from color and attenuation and scattering from solids and chlorophyll. The advanced model added rigor to the calculation of light attenuation but at a cost. The model was demanding in data requirements for parameterization. The complex formulation rendered the model difficult to "tune" to improve agreement between predictions and observations. As a consequence, the 2017 model restores a partial attenuation relationship for calculating light attenuation.

1.1.8 Submerged Aquatic Vegetation

SAV was added to the 2002 model version along with other living resources. The SAV model was basically a representation of SAV production and loss on a unit-area basis. SAV biomass and fluxes between SAV and the surrounding water on the unit-area basis were multiplied by the SAV bed area associated with each cell in the model computational grid to obtain biomass and fluxes associated with the cell.

Specification of bed area has been problematic since the initial model application (Cerco and Moore 2001), especially because the area changes in response to processes that are not entirely understood or predictable. The 2010 model defined SAV cells as distinct from the water quality model computational grid. The potential extent of the SAV cells was determined by the largest historical observed bed area. The actual bed area within each cell was determined by light penetration to the bottom. The algorithm to determine area did not function well, largely because area was determined exclusively by light availability. Processes that allow or prevent SAV propagation in areas with sufficient illumination were absent. The 2017 model specifies bed area based on annual surveys. That

specification enhances the computation of total SAV biomass and ensures the correct representation of mass fluxes between SAV and the Bay water column.

1.1.9 Hydrodynamics

The calculation of hydrodynamics using the Computational Hydrodynamics in Three Dimensions (CH3D) model is unchanged from the 2010 model version. The model application period has been extended to 2011 and hydrodynamic calculations have been updated as revised calculations of hydrology become available from the WSM. Likewise, the calculation of surface waves and bottom shear stress for the WQSTM are unchanged. The sediment transport algorithms are exactly as parameterized and employed in the 2010 model. The reader is referred to the 2010 documentation for details (Cerco et al. 2010).

1.2 References

Cerco, C.F., and T.M. Cole. 1994. *Three-Dimensional Eutrophication Model of Chesapeake Bay*. Technical Report EL-94-4, US Army Corps of Engineers, Waterways Experiment Station, Vicksburg, MS.

Cerco, C., and M. Meyers. 2000. Tributary refinements to the Chesapeake Bay Model. *Journal of Environmental Engineering* 126(2):164-174.

Cerco, C., and K. Moore. 2001. System-wide submerged aquatic vegetation model for Chesapeake Bay. *Estuaries* 24(4):522-534.

Cerco, C., B., Johnson, and H. Wang. 2002. *Tributary Refinements to the Chesapeake Bay Model*. ERDC TR-02-4. US Army Engineer Research and Development Center, Vicksburg, MS.

Cerco, C., and M. Noel. 2004a. *The 2002 Chesapeake Bay Eutrophication Model*. EPA 903-R-04-004. US Environmental Protection Agency, Chesapeake Bay Program Office, Annapolis, MD. https://nepis.epa.gov/Exe/ZyPURL.cgi?Dockey=P1003SK2.txt.

Cerco, C., and M. Noel. 2004b. Process-based primary production modeling in Chesapeake Bay. *Marine Ecology Progress Series* 282:45-58.

Cerco, C., and M. Noel. 2007. Can oyster restoration reverse cultural eutrophication in Chesapeake Bay? *Estuaries and Coasts* 30(2):331-343.

Cerco, C., S.-C. Kim, and M. Noel. 2010. *The 2010 Chesapeake Bay Eutrophication Model*. US Environmental Protection Agency, Chesapeake Bay Program Office, Annapolis, MD. http://www.chesapeakebay.net/publications/title/the_2010_chesapeake_bay_eutrophication_model1.

Cornwell, J., J. Rose, L. Kellogg, M. Luckenbach, S. Bricker, K. Paynter, C. Moore, M. Parker, L. Sanford, B. Wolinski, A. Lacatell, L. Fegley, and K. Hudson. 2016. *Panel Recommendations on the Oyster BMP Nutrient and Suspended Sediment Reduction Effectiveness Determination Decision Framework and Nitrogen and Phosphorus Assimilation in Oyster Tissue Reduction Effectiveness for Oyster Aquaculture Practices*. Draft for CBP Partnership and public review. Oyster Recovery Partnership, Annapolis, MD. https://www.chesapeakebay.net/channel_files/24330/oyster_bmp_report_draft_for_partnership_and_public_review_2016-09-22.pdf.

DiToro, D., and J. Fitzpatrick. 1993. *Chesapeake Bay Sediment Flux Model*. Contract Report El-93-2. US Army Corps of Engineers, Waterways Experiment Station, Vicksburg, MS.

Drescher, S., and B, Stack. 2015. *Recommendations of the Expert Panel to Define Removal Rates for Shoreline Management Projects*. Chesapeake Bay Program Partnership, Annapolis, MD. http://www.chesapeakebay.net/documents/Shoreline_Management_Protocols_Final_Approved_07132015-WQGIT-approved.pdf.

Testa, J., D. Brady, D. DiToro, W. Boynton, J. Cornwell, and W. Kemp. 2013. Sediment flux modeling: Simulating nitrogen, phosphorus, and silica cycles. *Estuarine, Coastal and Shelf Science* 131:245-263.

Westrich, J., and R. Berner. 1984. The role of sedimentary organic matter in bacterial sulfate reduction: The G model tested. *Limnology and Oceanography* 29(2):236-249.

2 Water Quality Model Formulation

The Corps of Engineers Integrated Compartment Water Quality Model (CE-QUAL-ICM) was designed to be a flexible, widely applicable eutrophication model. Initial application was to the Chesapeake Bay (Cerco and Cole 1994). Subsequent applications included the Delaware Inland Bays (Cerco et al. 1994), Newark Bay (Cerco and Bunch 1997), San Juan Estuary in Puerto Rico (Bunch et al. 2000), Virginia Tributary Refinements (Cerco et al. 2002), and 2002 and 2010 versions of the Chesapeake Bay model (Cerco and Noel 2004; Cerco et al. 2010). Each application employed a different combination of model features and required addition of system-specific capabilities.

This chapter describes general features and site-specific developments in the model applied to the water column of the Chesapeake Bay in the 2017 model version.

2.1 Conservation of Mass Equation

The foundation of CE-QUAL-ICM is the solution to the three-dimensional mass conservation equation for a control volume. Control volumes correspond to cells on the model grid. CE-QUAL-ICM solves, for each volume and for each state variable, this equation (equation 1):

$$\frac{\delta V_j \cdot C_j}{\delta t} = \sum_{k=1}^{n} Q_k \cdot C_k + \sum_{k=1}^{n} A_k \cdot D_k \cdot \frac{\delta C}{\delta x_k} + \Sigma S_j \qquad (1)$$

where:

V_j = volume of j^{th} control volume (m^3), where j goes from 1 to the number of cells on the model grid
C_j = concentration in j^{th} control volume (g m^{-3})
t, x = temporal and spatial coordinates
n = number of flow faces attached to j^{th} control volume
Q_k = volumetric flow across flow face k of j^{th} control volume (m^3 s^{-1})
C_k = concentration in flow across face k (g m^{-3})
A_k = area of flow face k (m^2)
D_k = diffusion coefficient at flow face k (m^2 s^{-1})
S_j = external loads and kinetic sources and sinks in j^{th} control volume (g s^{-1})

Solution of equation 1 on a digital computer requires discretizing the continuous derivatives and specifying parameter values. The equation is solved using the

QUICKEST algorithm (Leonard 1979) in the horizontal plane and an implicit central-difference scheme in the vertical direction. Discrete time steps, determined by computational stability requirements, are ≈ 5 minutes.

2.2 State Variables

The 2017 Chesapeake Bay Water Quality and Sediment Transport Model (WQSTM) incorporates 24 state variables in the water column, including physical variables; multiple algal groups; and multiple forms of carbon, nitrogen, and phosphorus (Table 2-1).

Table 2-1. Water Quality Model State Variables

Temperature	Salinity
Fixed Solids	Freshwater Algae
Spring Diatoms	Other Green Algae
Dissolved Organic Carbon	Labile Particulate Organic Carbon
Refractory Particulate Organic Carbon	Slow Refractory Particulate Organic Carbon
Ammonium	Nitrate+Nitrite
Dissolved Organic Nitrogen	Labile Particulate Organic Nitrogen
Refractory Particulate Organic Nitrogen	Slow Refractory Particulate Organic Nitrogen
Phosphate	Dissolved Organic Phosphorus
Labile Particulate Organic Phosphorus	Refractory Particulate Organic Phosphorus
Slow Refractory Particulate Organic Phosphorus	Particulate Inorganic Phosphorus
Chemical Oxygen Demand	Dissolved Oxygen

2.2.1 Algae

Algae are grouped into three model groups: freshwater algae, spring diatoms, and other green algae. The model formulations for the three groups are virtually identical. The definition of three groups provides flexibility in parameter evaluation to fit various regions of the Bay system. In particular, definition of a freshwater group allows maximum flexibility in parameter specification in freshwater portions of the system, which vary greatly in terms of physical characteristics, loading, and surroundings. The spring diatoms are large phytoplankton that produce an annual bloom in the saline portions of the Bay and tributaries. Algae that do not fit in the first two groups are combined under the heading of “other green algae.” The other green algae represent the mixture that characterizes saline waters during summer and autumn, and freshwater regions in which a specific algal group is not defined. Nonbloom-forming diatoms compose a portion of this mixture.

2.2.2 Organic Carbon

The 2017 WQSTM considers four organic carbon state variables: dissolved, labile particulate, refractory particulate, and slow refractory particulate. Labile, refractory, and slow refractory distinctions are based upon the time scale of decomposition. Labile organic carbon decomposes on a time scale of days to weeks while refractory organic carbon requires more time. Slow refractory particulate carbon is virtually inert in the water column. The three particulate organic carbon (POC) groups correspond to the three G groups in the sediment diagenesis model (DiToro and Fitzpatrick 1993), although the decay rates might differ between the water column and sediments.

2.2.3 Nitrogen

Nitrogen is first divided into available and unavailable fractions. “Available” refers to employment in algal nutrition. Two available forms are considered: reduced nitrogen and oxidized nitrogen. Ammonium is the single reduced nitrogen form. Nitrate and nitrite compose the oxidized nitrogen pool. Both reduced and oxidized nitrogen are used to fulfill algal nutrient requirements. The primary reason for distinguishing between the two is that ammonium is oxidized by nitrifying bacteria into nitrite and, subsequently, nitrate. This oxidation can be a significant sink of oxygen in the water column and sediments.

“Unavailable” nitrogen state variables are dissolved organic nitrogen, labile particulate organic nitrogen, refractory particulate organic nitrogen, and slow refractory particulate organic nitrogen.

2.2.4 Phosphorus

As with nitrogen, phosphorus is first divided into available and unavailable fractions. Only a single available form, dissolved phosphate, is considered. Five forms of unavailable phosphorus are considered: dissolved organic phosphorus, labile particulate organic phosphorus, refractory particulate organic phosphorus, slow refractory particulate organic phosphorus, and particulate inorganic phosphorus (PIP).

2.2.5 Chemical Oxygen Demand

Reduced substances produced in anoxic bottom sediments are combined in the chemical oxygen demand pool. The primary component of chemical oxygen demand in saltwater is sulfide. Oxidation of sulfide to sulfate can remove substantial quantities of dissolved oxygen (DO) from the water column. In freshwater, the primary component is methane.

2.2.6 Dissolved Oxygen

DO is required for the existence of higher life forms. Oxygen availability determines the distribution of organisms and the flows of energy and nutrients in an ecosystem. DO is a central component of the WQSTM.

2.2.7 Salinity

Salinity is a conservative tracer that provides verification of the transport component of the model and facilitates examination of conservation of mass. Salinity also influences the DO saturation concentration and can be used in the determination of kinetics constants, which differ in saline and fresh water.

2.2.8 Temperature

Temperature is a primary determinant of biochemical reaction rates. Reaction rates increase as a function of increasing temperature, although extreme temperatures can result in the mortality of organisms and a decrease in kinetics rates.

2.2.9 Fixed Solids

Fixed solids are the mineral fraction of total suspended solids. In previous model versions, fixed solids contributed to light attenuation and formed a site for sorption of dissolved inorganic phosphorus. The former role of fixed solids is now occupied by the four solids classes incorporated into the sediment transport model. The fixed solids variable has been retained but has no present function.

2.3 Algae

Equations governing the three algal groups are largely the same. Differences among the groups are expressed through the specification of parameter values. Generic equations are presented in this section. For notational simplicity, the transport terms are dropped in the reporting of kinetics formulations here and elsewhere.

Algal sources and sinks in the conservation equation include production, metabolism, predation, and settling. These are expressed in equation 2:

$$\frac{\delta}{\delta t}B = \left(G - BM - Wa \times \frac{\delta}{\delta z}\right)B - PR \qquad (2)$$

where:

B = algal biomass, expressed as carbon (g C m^{-3})
G = growth (d^{-1})

BM = basal metabolism (d^{-1})
Wa = algal settling velocity ($m\ d^{-1}$)
PR = predation ($g\ C\ m^{-3}\ d^{-1}$)
z = vertical coordinate

2.3.1 Production

Production by phytoplankton is determined by the intensity of light, by the availability of nutrients, and by the ambient temperature.

2.3.1.1 Light

The influence of light on phytoplankton production is represented by a chlorophyll-specific photosynthesis equation (equation 3) (Jassby and Platt 1976):

$$P^B = P^Bm \frac{I}{\sqrt{I^2 + Ik^2}} \quad (3)$$

where:

P^B = photosynthetic rate ($g\ C\ g^{-1}\ Chl\ d^{-1}$)
P^Bm = maximum photosynthetic rate ($g\ C\ g^{-1}\ Chl\ d^{-1}$)
I = irradiance ($E\ m^{-2}\ d^{-1}$)

Parameter Ik is defined as the irradiance at which the initial slope of the photosynthesis versus irradiance relationship (Figure 2-1) intersects the value of P^Bm (equation 4):

$$Ik = \frac{P^Bm}{\alpha} \quad (4)$$

where:

α = initial slope of photosynthesis versus irradiance relationship ($g\ C\ g^{-1}\ Chl\ (E\ m^{-2})^{-1}$)

The chlorophyll-specific photosynthesis rate is readily converted to a carbon-specific growth rate, for use in equation 2, through division by the carbon-to-chlorophyll ratio (equation 5):

$$G = \frac{P^B}{CChl} \quad (5)$$

where:

CChl = carbon-to-chlorophyll ratio (g C g^{-1} chlorophyll *a*)

Figure 2-1. Photosynthesis versus irradiance curve.

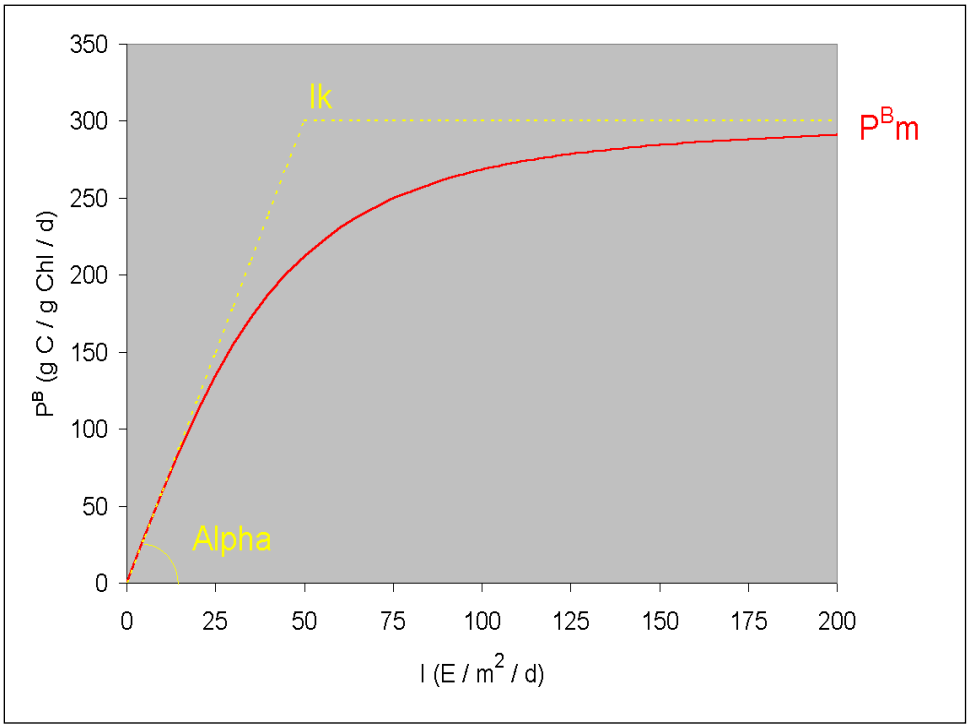

2.3.1.2 *Nutrients*

Carbon, nitrogen, and phosphorus are the primary nutrients required for algal growth. Diatoms require silica as well. Inorganic carbon and silica are usually available in excess and are not considered in the model. The effects of the remaining nutrients on growth are described by the formulation commonly referred to as "Monod kinetics" (Figure 2-2) (Monod 1949), as shown in equation 6:

$$f(N) = \frac{D}{KHd + D} \quad (6)$$

where:

f(N) = nutrient limitation on algal production ($0 \le f(N) \le 1$)
D = concentration of dissolved nutrient (g m^{-3})
KHd = half-saturation constant for nutrient uptake (g m^{-3})

Figure 2-2. Monod formulation for nutrient-limited growth.

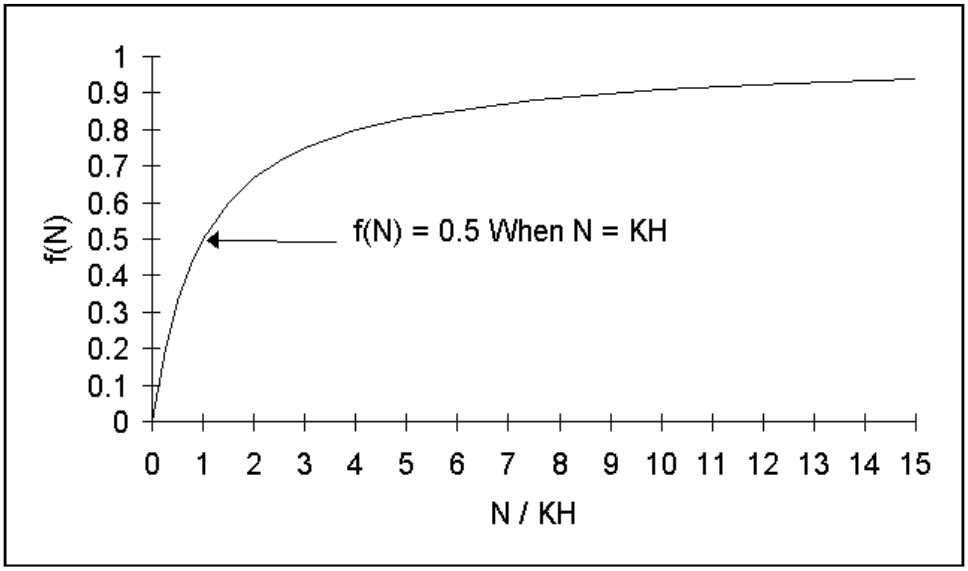

2.3.1.3 Temperature

Algal production increases as a function of increasing temperature until an optimum temperature or temperature range is reached. Above the optimum, production declines until a temperature lethal to the organisms is attained. Numerous functional representations of temperature effects are available. Inspection of growth versus temperature data indicates a function similar to a Gaussian probability curve (Figure 2-3) provides a good fit to observations (equation 7):

$$f(T) = e^{-KTg1 \cdot (T - Topt)^2} \text{ when } T \le Topt$$
$$= e^{-KTg2 \cdot (Topt - T)^2} \text{ when } T > Topt \quad (7)$$

where:

T = temperature (°C)
$Topt$ = optimal temperature for algal growth (°C)
$KTg1$ = effect of temperature below Topt on growth (°C^{-2})
$KTg2$ = effect of temperature above Topt on growth (°C^{-2})

Figure 2-3. Relation of algal production to temperature.

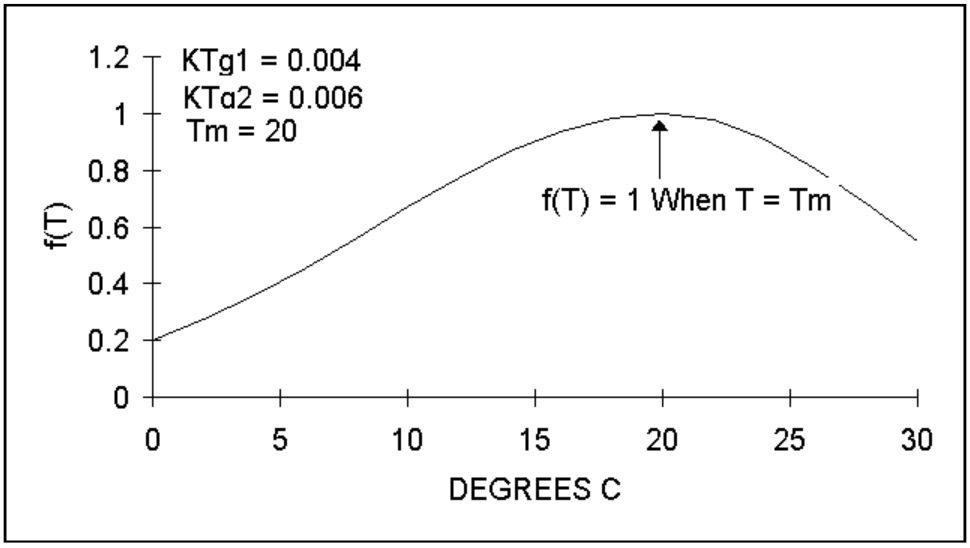

2.3.2 Constructing the Photosynthesis versus Irradiance Curve

A photosynthesis versus irradiance relationship is constructed for each model cell at each time step. First, the maximum photosynthetic rate under ambient temperature and nutrient concentrations is determined (equation 8):

$$P^B m(N,T) = P^B m \times f(T) \times \frac{D}{KHd + D} \tag{8}$$

where:

$P^B m(N,T)$ = maximum photosynthetic rate under ambient nutrient concentrations and temperature (g C g^{-1} Chl d^{-1})

The single most limiting nutrient is employed in determining the nutrient limitation.

Next, parameter Ik is derived from equation 4. Finally, the photosynthesis versus irradiance relationship is constructed using $P^B m(N,T)$ and Ik. The resulting photosynthesis versus irradiance curve exhibits three regions (Figure 2-4). For I >> Ik, the value of the term $I / (I^2 + Ik^2)^{1/2}$ approaches unity, and temperature and nutrients are the primary factors that influence photosynthesis. For I << Ik, photosynthesis is determined solely by α and irradiance I. In the region where the initial slope of the photosynthesis versus irradiance curve intercepts the line, indicating photosynthesis at optimal illumination, I ≈ Ik, photosynthesis is determined by the combined effects of temperature, nutrients, and light.

Figure 2-4. Effects of light and nutrients on photosynthesis versus irradiance curve determined for α = 8 (g C g^{-1} Chl *a* (E m^{-2})$^{-1}$).

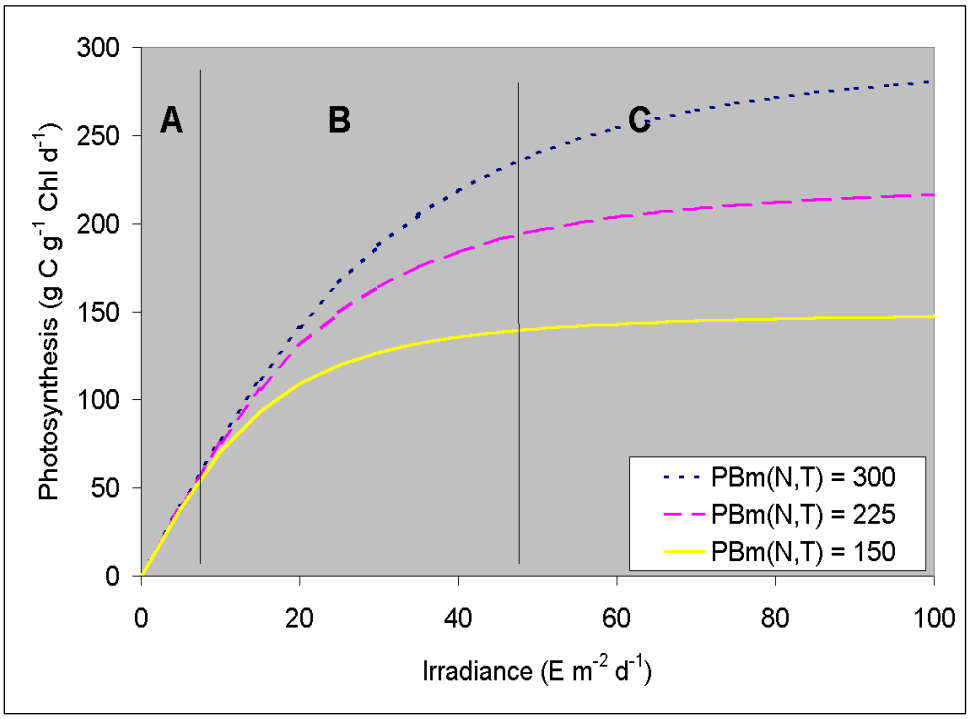

2.3.3 Irradiance

Irradiance at the water surface is evaluated at each model time step. Instantaneous irradiance is computed by fitting a sin function to daily total irradiance (equation 9):

$$Io = \frac{\Pi}{2 \times FD} \times IT \times \sin\left(\frac{\Pi \times DSSR}{FD}\right) \tag{9}$$

where:

Io = irradiance at water surface (E m^{-2} d^{-1})
IT = daily total irradiance (E m^{-2})
FD = fractional daylength (0 < FD < 1)
$DSSR$ = time since sunrise (d)

Io is evaluated only during the interval (equation 10):

$$\frac{1 - FD}{2} \leq DSM \leq \frac{1 + FD}{2} \tag{10}$$

where:

DSM = time since midnight (d)

Outside the specified interval, Io is set to zero.

Irradiance declines exponentially with depth below the surface. The diffuse attenuation coefficient, Ke, is computed as a function of color and concentrations of organic and mineral solids.

2.3.4 Respiration

Two forms of respiration are considered in the model: photorespiration and basal metabolism. Photorespiration represents the energy expended by carbon fixation and is a fixed fraction of production. In the event of no production (e.g., at night), photorespiration is zero. Basal metabolism is continuous energy expenditure to maintain basic life processes. In the model, metabolism is considered to be an exponentially increasing function of rising temperature (Figure 2-5). Total respiration is represented by equation 11:

$$R = Presp \times G + BM \times e^{KTb \times (T - Tr)} \quad (11)$$

where:

Presp = photorespiration ($0 \le Presp \le 1$)
BM = metabolic rate at reference temperature Tr (d^{-1})
KTb = effect of temperature on metabolism ($^oC^{-1}$)
Tr = reference temperature for metabolism (^oC)

Figure 2-5. Exponential temperature relationship employed for metabolism and other processes.

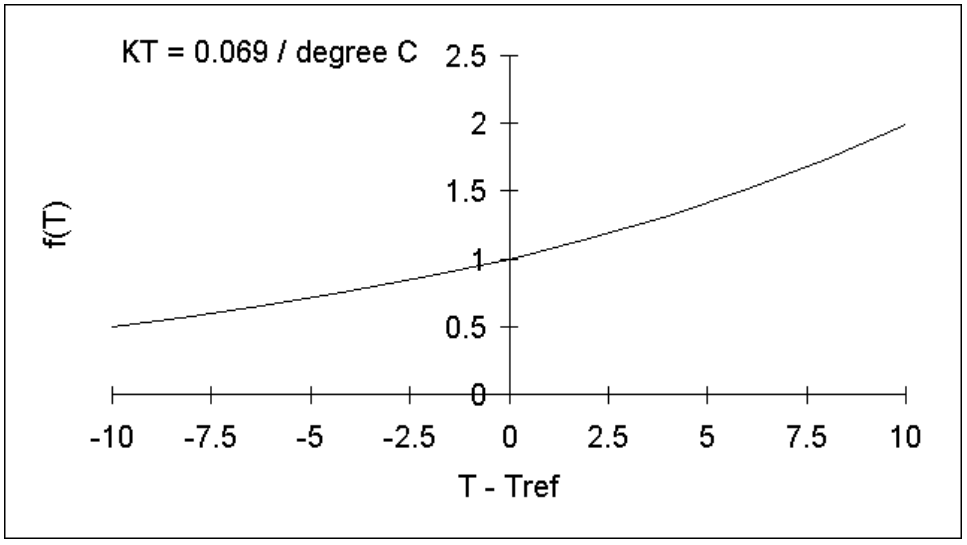

2.3.5 Predation

The predation term in equation 2 includes the activity of zooplankton, planktivorous fish, and other pelagic filter feeders. Predation in the water column is modeled by assuming predators clear a specific volume of water per unit biomass (equation 12):

$$PR = F \times B \times M \tag{12}$$

where:

F = filtration rate ($m^3\ g^{-1}$ predator C d^{-1})
M = planktivore biomass (g C m^{-3})

Detailed specification of the spatial and temporal distribution of the predator population is impossible. One approach is to assume predator biomass is proportional to algal biomass, M = γ B, in which case equation 12 can be rewritten as equation 13:

$$PR = \gamma \times F \times B^2 \tag{13}$$

Since neither γ nor F are known precisely, the logical approach is to combine their product into a single unknown determined during the model calibration procedure. Effect of temperature on predation is represented with the same formulation as the effect of temperature on respiration. The final representation of predation is as follows (equation 14):

$$PR = Phtl \cdot B^2 \tag{14}$$

where:

$Phtl$ = rate of water-column planktivore predation ($m^3\ g^{-1}$ C d^{-1})

Predation by filter-feeding benthos is represented as a loss term only in model cells that intersect the bottom. Details of the benthos computations can be found in Cerco and Noel (2010).

2.3.6 Accounting for Algal Phosphorus

The amount of phosphorus incorporated into algal biomass is quantified through a stoichiometric ratio. Thus, total phosphorus in the model is expressed as in equation 15:

$$TotP = PO_4 + Apc \cdot B + DOP + LPOP + RPOP + G3OP + PIP \tag{15}$$

where:

$TotP$ = total phosphorus (g P m^{-3})
PO_4 = dissolved phosphate (g P m^{-3})
Apc = algal phosphorus-to-carbon ratio (g P g^{-1} C)
DOP = dissolved organic phosphorus (g P m^{-3})
$LPOP$ = labile particulate organic phosphorus (g P m^{-3})
$RPOP$ = refractory particulate organic phosphorus (g P m^{-3})
$G3OP$ = slow refractory particulate organic phosphorus (g P m^{-3})
PIP = particulate inorganic phosphorus (g P m^{-3})

Algae take up dissolved phosphate during production and release dissolved phosphate and organic phosphorus through respiration. The distribution of phosphorus released by respiration is determined by empirical coefficients. The distribution of algal phosphorus recycled by predation is determined by a second set of empirical values.

2.3.7 Accounting for Algal Nitrogen

WQSTM nitrogen state variables include ammonium, nitrate+nitrite, dissolved organic nitrogen, labile particulate organic nitrogen, refractory particulate organic nitrogen, and slow refractory particulate organic nitrogen. The amount of nitrogen incorporated into algal biomass is quantified through a stoichiometric ratio. Thus, total nitrogen in the model is expressed in equation 16:

$$TotN = NH_4 + NO_{23} + Anc \cdot B + DON + LPON + RPON + G3ON \quad (16)$$

where:

$TotN$ = total nitrogen (g N m^{-3})
NH_4 = ammonium (g N m^{-3})
NO_{23} = nitrate+nitrite (g N m^{-3})
Anc = algal nitrogen-to-carbon ratio (g N g^{-1} C)
DON = dissolved organic nitrogen (g N m^{-3})
$LPON$ = labile particulate organic nitrogen (g N m^{-3})
$RPON$ = refractory particulate organic nitrogen (g N m^{-3})
$G3ON$ = slow refractory particulate organic nitrogen (g N m^{-3})

As with phosphorus, the distribution of algal nitrogen released by metabolism and predation is represented by empirical coefficients.

2.3.8 Algal Nitrogen Preference

Algae take up ammonium and nitrate+nitrite during production and release ammonium and organic nitrogen through respiration. Nitrate+nitrite is internally reduced to ammonium before synthesis into biomass occurs (Parsons et al. 1984). Trace concentrations of ammonium inhibit nitrate reduction so that, in the presence of multiple nitrogenous nutrients, ammonium is used first. The "preference" of algae for ammonium is expressed by a modification of an empirical function presented by Thomann and Fitzpatrick (1982) (equation 17):

$$PN = NH_4 \cdot \frac{NO_{23}}{(KHNH_4 + NH_4) \cdot (KHNH_4 + NO_{23})} + NH_4 \cdot \frac{KHNH_4}{(NH_4 + NO_{23}) \cdot (KHNH_4 + NO_{23})} \quad (17)$$

where

PN = algal preference for ammonium uptake ($0 \le PN \le 1$)
$KHNH_4$ = half-saturation concentration for algal ammonium uptake (g N m^{-3})

Our modification substitutes a specific half-saturation concentration for ammonium uptake, $KHNH_4$, for the original use of half-saturation concentration for nitrogen uptake, KHn. We found the modification enforces ammonium use down to lower concentrations than the original formulation.

The preference function has two limiting values (Figure 2-6). When nitrate+nitrite is absent, the preference for ammonium is unity. When ammonium is absent, the preference is zero. In the presence of ammonium and nitrate+nitrite, the preference depends on the abundance of both forms relative to the half-saturation constant for ammonium uptake. When ammonium and nitrate+nitrite are both abundant, the preference for ammonium approaches unity. When ammonium is scarce but nitrate+nitrite is abundant, the preference decreases in magnitude and a significant fraction of algal nitrogen requirement comes from nitrate+nitrite.

Figure 2-6. Algal ammonium preference.

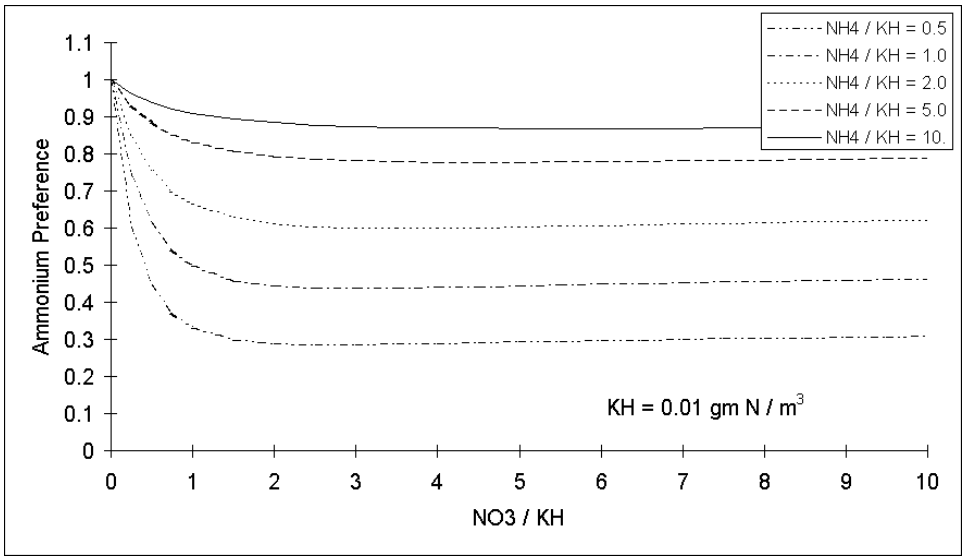

2.3.9 Effect of Algae on Dissolved Oxygen

Algae produce oxygen during photosynthesis and consume oxygen through respiration. The quantity produced depends on the form of nitrogen used for growth. More oxygen is produced per unit of carbon fixed when nitrate is the algal nitrogen source than when ammonium is the source. Equations 18 and 19 describe algal uptake of carbon and nitrogen and production of DO (Morel 1983):

$$106\ CO_2 + 16\ NH_4^+ + H_2PO_4^- + 106\ H_2O \text{ - - >}$$

$$\text{protoplasm} + 106\ O_2 + 15\ H^+ \tag{18}$$

$$106\ CO_2 + 16\ NO_3^- + H_2PO_4^- + 122\ H_2O + 17\ H^+ \text{ - - >}$$

$$\text{protoplasm} + 138\ O_2 \tag{19}$$

When ammonium (NH_4^+) is the nitrogen source, 1 mole of oxygen (O_2) is produced per mole of carbon dioxide (CO_2) fixed. When nitrate (NO_3^-) is the nitrogen source, 1.3 moles of oxygen are produced per mole of carbon dioxide fixed.

Equation 20 describes the effect of algae on DO in the model:

$$\frac{\delta}{\delta t}\mathrm{DO} = \left[(1.3 - 0.3 \times \mathrm{PN}) \times \mathrm{P} - (1 - \mathrm{FCD}) \times \mathrm{BM}\right] \times \mathrm{AOCR} \times \mathrm{B} \tag{20}$$

where:

FCD = fraction of algal metabolism recycled as dissolved organic carbon ($0 \le FCD \le 1$)
AOCR = DO-to-carbon ratio in respiration (2.67 g O_2 g^{-1} C)

The magnitude of AOCR is derived from this basic representation of the respiration process (equation 21):

$$CH_2O + O_2 = CO_2 + H_2O \tag{21}$$

The quantity ($1.3 - 0.3 \cdot PN$) is the photosynthesis ratio and expresses the molar quantity of oxygen produced per mole of carbon fixed. The photosynthesis ratio approaches unity as the algal preference for ammonium approaches unity.

2.3.10 Salinity Toxicity

Some freshwater algae such as the cyanobacteria *microcystis* cease production when salinity exceeds 1–2 parts per thousand (ppt) (Sellner et al. 1988). The potential effect of salinity on freshwater algae is represented by a mortality term in the form of a rectangular hyperbola (equation 22):

$$STOX1 = STF1 \times \frac{S}{KHst1 + S} \tag{22}$$

where

STOX1 = mortality induced by salinity (d^{-1})
STF1 = maximum salinity mortality (d^{-1})
S = salinity (ppt)
KHst1 = salinity at which mortality is half maximum value (ppt)

The spring diatom bloom is limited to saline water. The limiting mechanism is not defined but appears to be related to salinity. The upstream limit of the spring bloom is defined in the model by introducing a mortality term at low salinity (equation 23):

$$STOX2 = STF2 \times \frac{KHst2}{KHst2 + S} \tag{23}$$

where

STOX2 = mortality induced by fresh water on spring diatoms (d^{-1})
STF2 = maximum fresh water mortality on spring diatoms (d^{-1})
KHst2 = salinity at which mortality is half maximum value (ppt)

The salinity-related mortality (Figure 2-7) is added to the basal metabolism.

Figure 2-7. Salinity toxicity relationship.

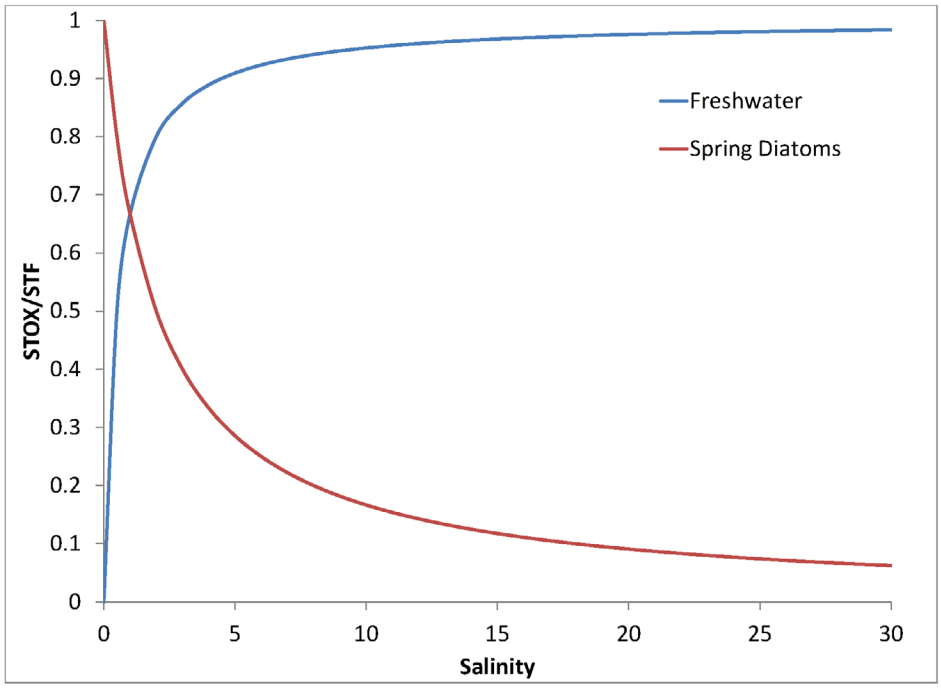

2.4 Organic Carbon

Organic carbon undergoes numerous transformations in the water column. The model carbon cycle consists of the following elements (Figure 2-8):

- Phytoplankton production and excretion
- Predation on phytoplankton
- Dissolution of particulate carbon
- Heterotrophic respiration
- Settling

Algal production is the primary carbon source to the water column, although carbon also enters the system through external loading. Predation on algae by zooplankton and other organisms releases particulate and dissolved organic carbon to the water column. A fraction of the POC undergoes first-order dissolution to dissolved organic carbon. Dissolved organic carbon produced by excretion, by predation, and by dissolution is respired at a first-order rate to inorganic carbon. POC that does not undergo dissolution settles to the bottom sediments.

Organic carbon dissolution and respiration are represented as first-order processes in which the reaction rate is proportional to concentration of the

reactant. An exponential function relates dissolution and respiration to temperature (Figure 2-5).

Figure 2-8. Model carbon cycle.

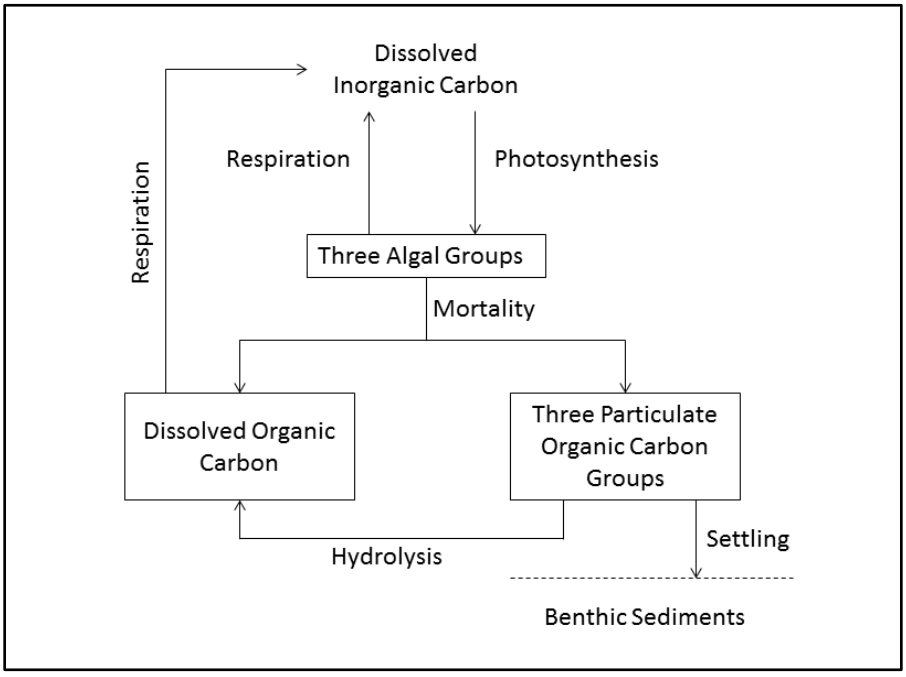

2.4.1 Dissolved Organic Carbon

The complete representation of dissolved organic carbon sources and sinks in the model ecosystem is shown in equation 24:

$$\frac{\delta}{\delta t} DOC = FCD \cdot R \cdot B + FCDP \cdot PR + Klpoc \cdot LPOC + Krpoc \cdot RPOC + Kg3poc \cdot G3OC - \frac{DO}{KHodoc + DO} \cdot Kdoc \cdot DOC \quad (24)$$

where:

DOC = dissolved organic carbon (g m^{-3})
$LPOC$ = labile POC (g m^{-3})
$RPOC$ = refractory POC (g m^{-3})
$G3OC$ = slow refractory POC (g m^{-3})
FCD = fraction of algal respiration released as DOC ($0 \leq FCD \leq 1$)
$FCDP$ = fraction of predation on algae released as DOC ($0 \leq FCDP \leq 1$)
$Klpoc$ = dissolution rate of LPOC (d^{-1})
$Krpoc$ = dissolution rate of RPOC (d^{-1})
$Kg3poc$ = dissolution rate of G3OC (d^{-1})
Kdoc = respiration rate of DOC (d^{-1})

2.4.2 Particulate Organic Carbon

The complete representation of labile POC sources and sinks in the model ecosystem is shown in equation 25:

$$\frac{\delta}{\delta t} LPOC = FCL \times R \times B + FCLP \times PR - Klpoc \times LPOC - Wl \times \frac{\delta}{\delta z} LPOC \quad (25)$$

where:

FCL = fraction of algal respiration released as LPOC ($0 \leq FCL \leq 1$)
$FCLP$ = fraction of predation on algae released as LPOC ($0 \leq FCLP \leq 1$)
Wl = settling velocity of labile particles (m d^{-1})

The equations for refractory and slow refractory POC are analogous.

2.5 Phosphorus

The WQSTM phosphorus cycle includes the following processes (Figure 2-9):

- Algal uptake and excretion
- Predation
- Hydrolysis of particulate organic phosphorus
- Mineralization of dissolved organic phosphorus
- Dissolution of PIP
- Settling and resuspension

External loads provide the ultimate source of phosphorus to the system. Dissolved phosphate is incorporated by algae during growth and released as phosphate and organic phosphorus through respiration and predation. Dissolved organic phosphorus is mineralized to phosphate. A portion of the particulate organic phosphorus hydrolyzes to dissolved organic phosphorus. The balance settles to the sediments. Dissolution of PIP is also possible. Within the sediments, particulate phosphorus is mineralized and recycled to the water column as dissolved phosphate.

Figure 2-9. Model phosphorus cycle.

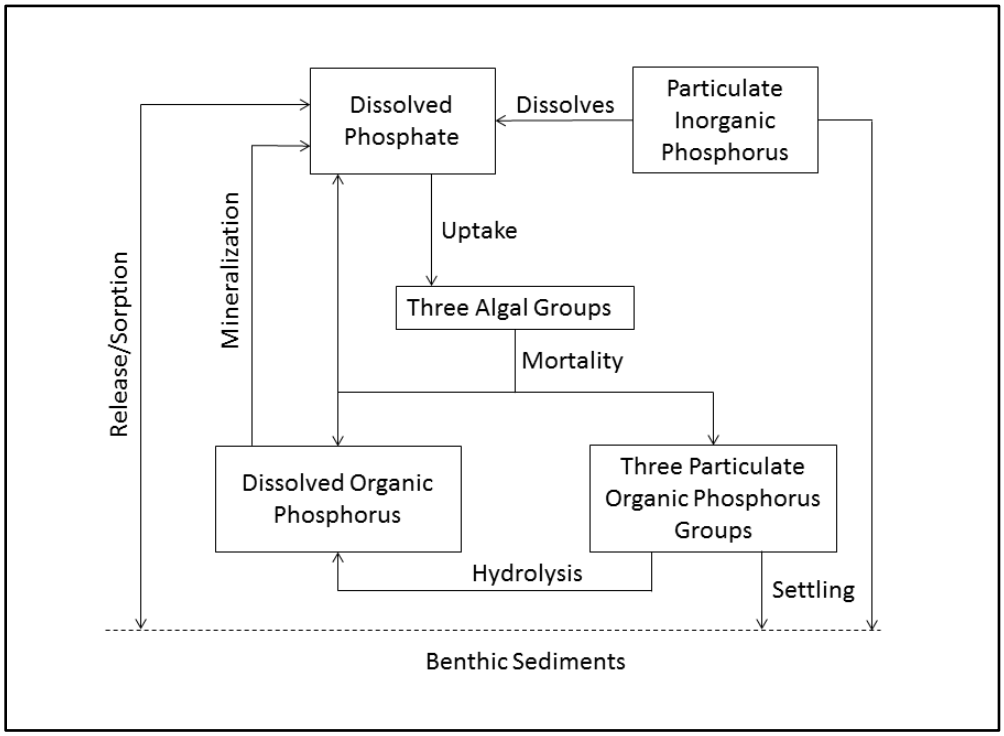

2.5.1 Hydrolysis and Mineralization

Within the WQSTM, "hydrolysis" is defined as the process by which particulate organic substances are converted to dissolved organic form. "Mineralization" is defined as the process by which dissolved organic substances are converted to dissolved inorganic form. Conversion of particulate organic phosphorus to phosphate proceeds through the sequence of hydrolysis and mineralization. Direct mineralization of particulate organic phosphorus does not occur.

Mineralization of organic phosphorus is mediated by the release of nucleotidase and phosphatase enzymes by bacteria (Ammerman and Azam 1985; Chrost and Overbeck 1987) and algae (Matavulj and Flint 1987; Chrost and Overbeck 1987; Boni et al. 1989). Since the algae themselves release the enzyme and bacterial abundance is related to algal biomass, the model relates the rate of organic phosphorus mineralization to algal biomass. A most remarkable property of the enzyme process is that alkaline phosphatase activity is inversely proportional to ambient phosphate concentration (Chrost and Overbeck 1987; Boni et al. 1989). Put in different terms, when phosphate is scarce, algae stimulate production of an enzyme that mineralizes organic phosphorus to phosphate. This phenomenon is simulated by relating mineralization to the algal phosphorus nutrient limitation. The mineralization rate is enhanced when algae are strongly phosphorus limited and is diminished when no limitation occurs.

The expression for mineralization rate is provided in equation 26:

$$Kdop = Kdp + \frac{KHp}{KHp + PO_4} \times Kdpalg \times B \qquad (26)$$

where:

$Kdop$ = mineralization rate of dissolved organic phosphorus (d^{-1})
Kdp = minimum mineralization rate (d^{-1})
KHp = half-saturation concentration for algal phosphorus uptake (g P m^{-3})
PO_4 = dissolved phosphate (g P m^{-3})
$Kdpalg$ = constant that relates mineralization to algal biomass (m^3 g^{-1} C d^{-1})

Potential effects of algal biomass and nutrient concentration on the mineralization rate are shown in Figure 2-10. When nutrient concentration greatly exceeds the half-saturation concentration for algal uptake, the rate roughly equals the minimum. Algal biomass has little influence on the rate. As nutrients become scarce relative to the half-saturation concentration, the rate increases. The magnitude of the increase depends on algal biomass. A factor of two to three increase is feasible. Exponential functions relate mineralization and hydrolysis rates to temperature (Figure 2-5).

Figure 2-10. Effect of algal biomass and nutrient concentration on phosphorus mineralization.

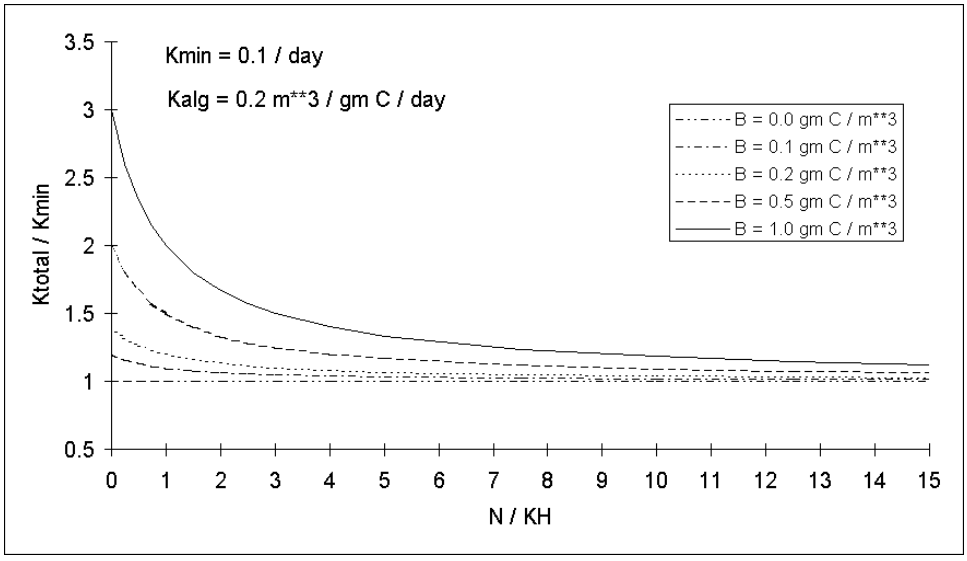

2.5.2 Dissolved Phosphate

The mass balance equation for dissolved phosphate is shown by equation 27:

$$\frac{\delta}{\delta t} PO_4 = Kdop \cdot DOP + Kpip \cdot PIP - APC \cdot G \cdot B + APC \cdot \left[FPI \cdot BM \cdot B + FPIP \cdot PR\right] - Wpo_4 \cdot \frac{\delta}{\delta z} PO_4 \quad (27)$$

where:

PIP = particulate inorganic phosphorus (g P m^{-3})
$Kpip$ = dissolution rate of particulate inorganic phosphorus (d^{-1})
FPI = fraction of algal metabolism released as dissolved phosphate ($0 \le FPI \le 1$)
$FPIP$ = fraction of predation released as dissolved phosphate ($0 \le FPIP \le 1$)
Wpo_4 = settling rate of precipitated phosphate (m d^{-1})

Phosphate settling represents phosphate removal through coprecipitation with iron and manganese during the breakup of seasonal bottom-water anoxia. The settling rate is implemented for a 30-day period in appropriate portions of the system.

2.5.3 Dissolved Organic Phosphorus

The mass balance equation for dissolved organic phosphorus is shown in equation 28:

$$\frac{\delta}{\delta t} DOP = APC \cdot (BM \cdot B \cdot FPD + PR \cdot FPDP) + Klpop \cdot LPOP + Krpop \cdot RPOP + Kg3op \cdot G3OP - Kdop \cdot DOP \quad (28)$$

where:

DOP = dissolved organic phosphorus (g P m^{-3})
$LPOP$ = labile particulate organic phosphorus (g P m^{-3})
$RPOP$ = refractory particulate organic phosphorus (g P m^{-3})
$G3OP$ = slow refractory particulate organic phosphorus (g P m^{-3})
FPD = fraction of algal metabolism released as DOP ($0 \le FPD \le 1$)
$FPDP$ = fraction of predation on algae released as DOP ($0 \le FPDP \le 1$)
$Klpop$ = hydrolysis rate of LPOP (d^{-1})
$Krpop$ = hydrolysis rate of RPOP (d^{-1})
$Kg3op$ = hydrolysis rate of G3OP (d^{-1})
$Kdop$ = mineralization rate of DOP (d^{-1})

2.5.4 Particulate Organic Phosphorus

The mass balance equation for labile particulate organic phosphorus is shown in equation 29:

$$\frac{\delta}{\delta t} LPOP = APC \times (BM \times B \times FPL + PR \times FPLP) - Klpop \times LPOP - Wl \times \frac{\delta}{\delta z} LPOP \quad (29)$$

where:

FPL = fraction of algal metabolism released as LPOP ($0 \leq FPL \leq 1$)
$FPLP$ = fraction of predation on algae released as LPOP ($0 \leq FPLP \leq 1$)

The equations for refractory and slow refractory particulate organic phosphorus are analogous.

2.5.5 Particulate Inorganic Phosphorus

A large fraction of particulate phosphorus in the Chesapeake Bay system is in inorganic form (Keefe 1994). Examination of dissolved phosphate, fixed solids, and PIP observations indicates the PIP cannot be represented through equilibrium partitioning to sediment particles. PIP is represented in the WQSTM as a distinct substance that potentially dissolves into phosphate. Otherwise, the fate of PIP is settling to bottom sediments where it is incorporated into the phosphate pool. The mass balance equation for PIP is shown by equation 30:

$$\frac{\partial}{\partial t} PIP = -Kpip \cdot PIP - Wpip \cdot \frac{\delta}{\delta z} PIP \quad (30)$$

where:

$Wpip$ = settling rate of particulate inorganic phosphorus (m d^{-1})

2.6 Nitrogen

The model nitrogen cycle includes the following processes (Figure 2-11):

- Algal production and metabolism
- Predation
- Hydrolysis of particulate organic nitrogen
- Mineralization of dissolved organic nitrogen
- Settling
- Nitrification

External loads provide the ultimate source of nitrogen to the system. Available nitrogen is incorporated by algae during growth and released as ammonium and organic nitrogen through respiration and predation. A portion of the particulate organic nitrogen hydrolyzes to dissolved organic nitrogen. The balance settles to the sediments. Dissolved organic nitrogen is mineralized to ammonium. In an oxygenated water column, a fraction of the ammonium is subsequently oxidized to nitrate+nitrite through the nitrification process. Particulate nitrogen that settles to the sediments is mineralized and recycled to the water column, primarily as ammonium. Nitrate+nitrite moves in both directions across the sediment-water interface, depending on relative concentrations in the water column and sediment interstices.

Figure 2-11. Model nitrogen cycle.

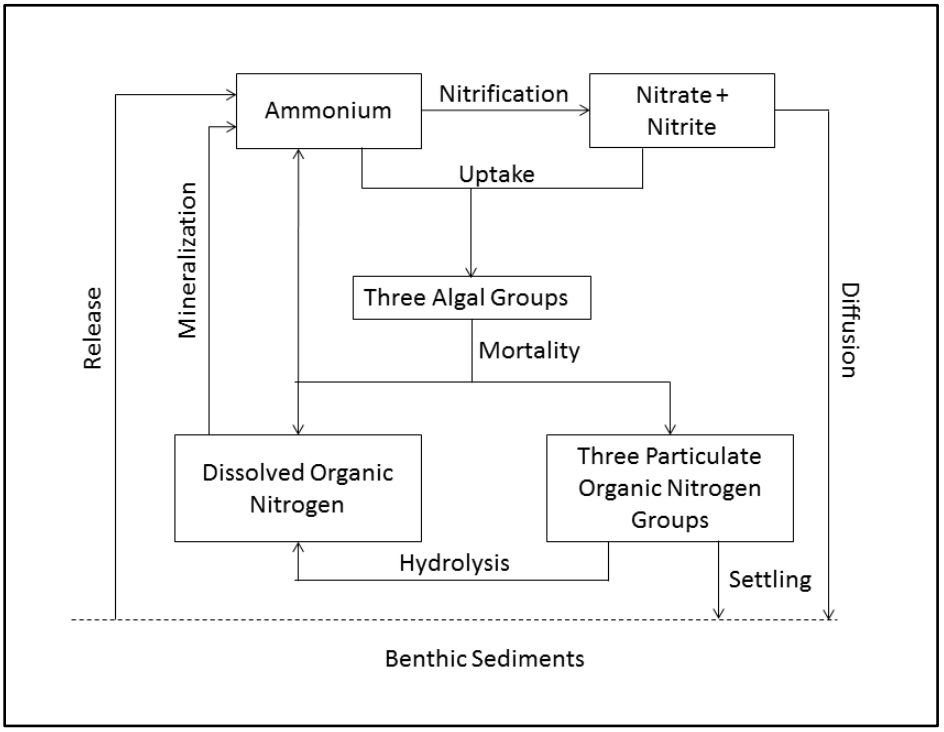

2.6.1 Nitrification

Nitrification is a process mediated by specialized groups of autotrophic bacteria that obtain energy through the oxidation of ammonium to nitrite and oxidation of nitrite to nitrate. A simplified expression for complete nitrification is provided by equation 31 (Tchobanoglous and Schroeder 1987):

$$NH_4^+ + 2\,O_2 \text{ --> } NO_3^- + H_2O + 2\,H^+ \quad (31)$$

The simplified stoichiometry indicates that 2 moles of oxygen are required to nitrify 1 mole of ammonium into nitrate. The simplified equation is not strictly

true, however. Cell synthesis by nitrifying bacteria is accomplished by the fixation of carbon dioxide so that less than 2 moles of oxygen are consumed per mole of ammonium used (Wezernak and Gannon 1968).

The kinetics of complete nitrification are modeled as a function of available ammonium, DO, and temperature (equation 32):

$$NT = \frac{DO}{KHont + DO} \cdot \frac{NH_4}{KHnnt + NH_4} \cdot f(T) \cdot NTm \quad (32)$$

where:

NT = nitrification rate (g N m^{-3} d^{-1})
$KHont$ = half-saturation constant of DO required for nitrification (g O_2 m^{-3})
$KHnnt$ = half-saturation constant of NH_4 required for nitrification (g N m^{-3})
NTm = maximum nitrification rate at optimal temperature (g N m^{-3} d^{-1})

The kinetics formulation incorporates the products of two Monod-like functions (Figure 2-12). The first function diminishes nitrification at low DO concentration. The second function expresses the influence of ammonium concentration on nitrification. When ammonium concentration is low relative to KHnnt, nitrification is proportional to ammonium concentration. For NH4 << KHnnt, the reaction is approximately first order (the first-order decay constant ≈ NTm/KHnnt). When ammonium concentration is high relative to KHnnt, nitrification approaches a maximum rate. This formulation is based on a concept proposed by Tuffey et al. (1974). Nitrifying bacteria adhere to benthic or suspended sediments. When ammonium is scarce, vacant surfaces suitable for nitrifying bacteria exist. As ammonium concentration increases, bacterial biomass increases, vacant surfaces are occupied, and the rate of nitrification increases. The bacterial population attains maximum density when all surfaces suitable for bacteria are occupied. At that point, nitrification proceeds at a maximum rate independent of any additional increase in ammonium concentration.

The optimal temperature for nitrification might be less than peak temperatures that occur in coastal waters. To allow for a decrease in nitrification at superoptimal temperature, the effect of temperature on nitrification is modeled in the Gaussian form of equation 7.

Figure 2-12. Effect of DO and ammonium concentration on nitrification rate.

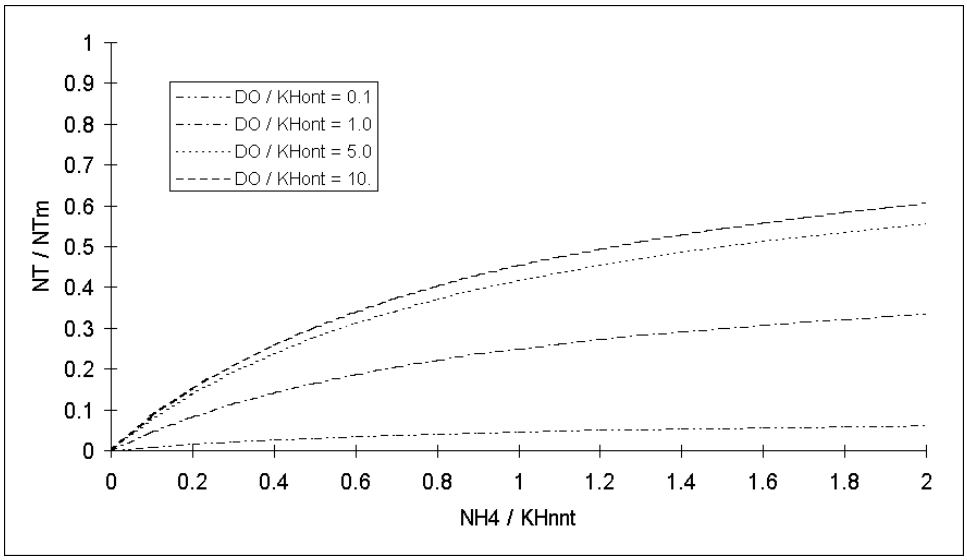

2.6.2 Nitrogen Mass Balance Equations

The mass balance equations for nitrogen state variables are written by summing all previously described sources and sinks, as shown in equation 33, equation 34, and equation 35:

2.6.2.1 Ammonium

$$\frac{\delta}{\delta t} NH_4 = ANC \cdot \left[(BM \cdot FNI - PN \cdot P) \cdot B + PR \cdot FNIP\right] + Kdon \cdot DON - NT \quad (33)$$

where:

FNI = fraction of algal metabolism released as NH4 ($0 \le FNI \le 1$)
PN = algal ammonium preference ($0 \le PN \le 1$)
$FNIP$ = fraction of predation released as NH4 ($0 \le FNIP \le 1$)

2.6.2.2 Nitrate+Nitrite

$$\frac{\delta}{\delta t} NO_{23} = - ANC \cdot (1 - PN) \cdot P \cdot B + NT \quad (34)$$

2.6.2.3 Dissolved Organic Nitrogen

$$\frac{\delta}{\delta t}DON = ANC \cdot (BM \cdot B \cdot FND + PR \cdot FNDP) + Klpon \cdot LPON + Krpon \cdot RPON + Kg3on \cdot G3ON - Kdon \cdot DON \quad (35)$$

where:

DON = dissolved organic nitrogen (g N m^{-3})
$LPON$ = labile particulate organic nitrogen (g N m^{-3})
$RPON$ = refractory particulate organic nitrogen (g N m^{-3})
$G3ON$ = slow refractory particulate organic nitrogen (g N m^{-3})
FND = fraction of algal metabolism released as DON ($0 \leq FND \leq 1$)
$FNDP$ = fraction of predation on algae released as DON ($0 \leq FNDP \leq 1$)
$Klpon$ = hydrolysis rate of LPON (d^{-1})
$Krpon$ = hydrolysis rate of RPON (d^{-1})
$Kg3on$ = hydrolysis rate of G3ON (d^{-1})
$Kdon$ = mineralization rate of DON (d^{-1})

2.6.2.4 Particulate Organic Nitrogen State Variable

The mass balance equation for labile particulate organic nitrogen is provided in equation 36:

$$\frac{\delta}{\delta t}LPON = ANC \times (BM \times B \times FNL + PR \times FNLP) - Klpon \times LPON - WI \times \frac{\delta}{\delta z}LPON \quad (36)$$

where:

FNL = fraction of algal metabolism released as LPON ($0 \leq FNL \leq 1$)
$FNLP$ = fraction of predation on algae released as LPON ($0 \leq FNLP \leq 1$)

The equations for refractory and slow refractory particulate organic nitrogen are analogous.

2.7 Chemical Oxygen Demand

Chemical oxygen demand is the concentration of reduced substances that are produced by reactions in anoxic bottom sediments. The primary component of chemical oxygen demand in saline water is sulfide. A cycle occurs in which sulfate is reduced to sulfide in the sediments and reoxidized to sulfate in the water column. In fresh water, methane might be released to the water column by bottom sediments. Both sulfide and methane are quantified in units of oxygen demand and are treated with the same kinetics formulation (equation 37):

$$\frac{\delta}{\delta t} COD = - \frac{DO}{KHocod + DO} \times Kcod \times COD \quad (37)$$

where:

COD = chemical oxygen demand concentration (g oxygen-equivalents m^{-3})
$KHocod$ = half-saturation concentration of DO required for exertion of chemical oxygen demand (g O_2 m^{-3})
$Kcod$ = oxidation rate of chemical oxygen demand (d^{-1})

An exponential function describes the effect of temperature on exertion of chemical oxygen demand (Figure 2-5).

2.8 Dissolved Oxygen

Sources and sinks of DO in the water column include (Figure 2-13):

- Algal photosynthesis
- Atmospheric reaeration
- Algal respiration
- Heterotrophic respiration
- Nitrification
- Chemical oxygen demand

Figure 2-13. DO sources and sinks.

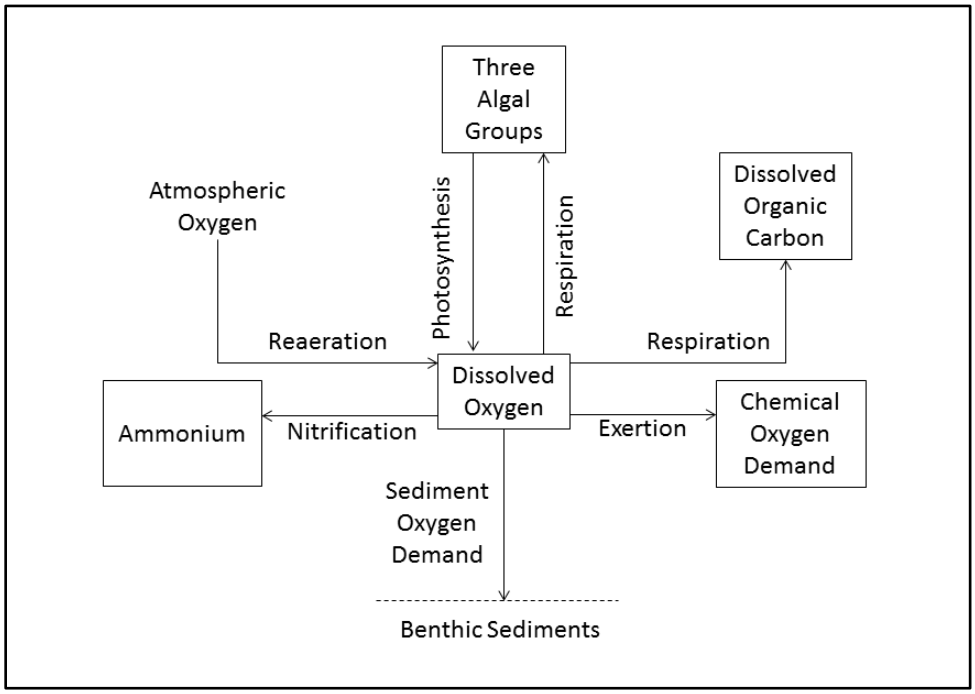

2.8.1 Reaeration

The rate of reaeration is proportional to the DO deficit in model segments that form the air-water interface (equation 38):

$$\frac{\delta}{\delta t} DO = \frac{Kr}{\Delta z} \times (DOs - DO) \tag{38}$$

where:

DO = DO concentration (g O_2 m^{-3})
Kr = reaeration coefficient (m d^{-1})
DOs = DO saturation concentration (g O_2 m^{-3})
Δz = model surface layer thickness (m)

In free-flowing streams, the reaeration coefficient depends largely on turbulence generated by bottom shear stress (O'Connor and Dobbins 1958). In lakes and coastal waters, however, wind effects can dominate the reaeration process (O'Connor 1983). The model code provides three options for the reaeration coefficient:

- Calculate reaeration as a function of stream velocity and depth.
- Calculate reaeration as a function of wind speed.
- Specify a reaeration coefficient.

The relationship of reaeration to velocity and depth is based on O'Connor and Dobbins (1958). In International System of Units (SI) units, the O'Connor-Dobbins relationship is as shown in equation 39:

$$Kr = 3.9\sqrt{u/H} \tag{39}$$

where:

u = stream velocity (m s^{-1})
H = depth (m)

The relationship of reaeration to wind is from Hartman and Hammond (1985) (equation 40):

$$Kr = Arear \bullet Rv \bullet Wms^{1.5} \tag{40}$$

where:

$Arear$ = empirical constant (≈ 0.1)
Rv = ratio of kinematic viscosity of pure water at 20 °C to kinematic viscosity of water at specified temperature and salinity
Wms = wind speed measured at 10 m above water surface (m s^{-1})

Hartman and Hammond (1985) indicate that Arear takes the value 0.157. In the WQSTM Arear is treated as a variable to allow for effects of wind sheltering, for differences in height of local wind observations, and for other factors. An empirical function (Figure 2-14) that fits tabulated values of Rv is shown in equation 41:

$$Rv = 0.54 + 0.0233 \bullet T - 0.0020 \bullet S \quad (41)$$

where:

S = salinity (ppt)
T = temperature (°C)

Figure 2-14. Computed and tabulated values of Rv.

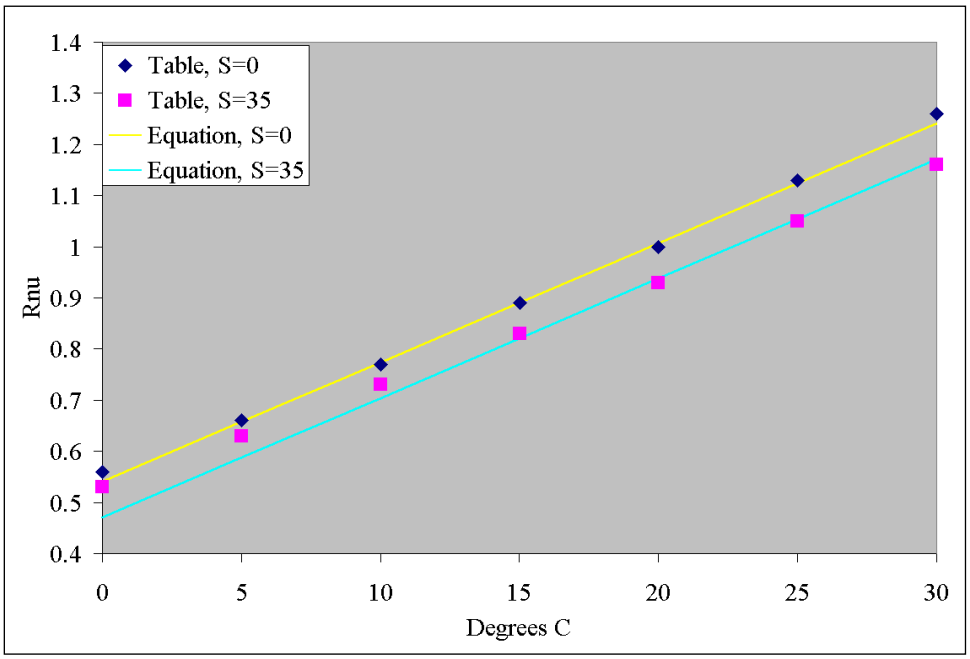

2.8.2 Dissolved Oxygen Saturation

The saturation concentration of DO is influenced by temperature, salinity, and pressure. A general representation of these influences is shown in equation 42:

$$DOs = DOf \cdot Fs \cdot Fp \quad (42)$$

where:

DOf = DO concentration, as a function of temperature, in fresh water (g O_2 m^{-3})
Fs = salinity correction factor
Fp = pressure correction factor

DOf is from Benson and Krause (1980, cited in USGS 2011) (equation 43):

$$DOf = exp\left(-139.34 + \frac{1.58x10^5}{T} - \frac{6.64x10^7}{T^2} + \frac{1.24x10^{10}}{T^3} - \frac{8.62x10^{11}}{T^4}\right) \quad (43)$$

where:

T = temperature ($^oK = {}^oC+273.15$)

Fs is from Benson and Krause (1984, cited in USGS 2011) (equation 44):

$$Fs = exp\left(-S \cdot \left(0.0177 - \frac{10.75}{T} + \frac{2141}{T^2}\right)\right) \quad (44)$$

where:

S = salinity (ppt)

Since reaeration occurs at the air-water interface, where atmospheric pressure prevails, Fp is set to unity.

The mass balance equation for DO accounts for sources and sinks, including algal production and respiration, nitrification, DOC mineralization, chemical oxygen demand, and reaeration, as shown in equation 45:

$$\begin{aligned}\frac{\delta}{\delta t}DO = {} & AOCR \times \left[(1.3 - 0.3 \times PN) \times P - (1 - FCD) \times BM\right] \times B \\ & - AONT \times NT - \frac{DO}{KHodoc + DO} \times AOCR \times Kdoc \times DOC \\ & - \frac{DO}{KHocod + DO} \times Kcod \times COD + \frac{Kr}{H} \times (DOs - DO)\end{aligned} \quad (45)$$

where:

$AOCR$ = oxygen-to-carbon mass ratio in production and respiration (= 2.67 g O_2 g^{-1} C)
$AONT$ = oxygen consumed per mass ammonium nitrified (= 4.33 g O_2 g^{-1} N)

2.9 Temperature

Computation of temperature in the 2017 model employs a conservation of internal energy equation that is analogous to the conservation of mass equation. For practical purposes, the internal energy equation can be written as a conservation of temperature equation. The only source or sink of temperature considered is exchange with the atmosphere. Atmospheric exchange is proportional to the temperature difference between the water surface and a theoretical equilibrium temperature (Edinger et al. 1974), as shown in equation 46:

$$\frac{\delta}{\delta t} T = \frac{KT}{\rho \times Cp \times H} \times (Te - T) \qquad (46)$$

where:

T = water temperature (^{o}C)
Te = equilibrium temperature (^{o}C)
KT = Heat exchange coefficient (watt m^{-2} ^{o}C^{-1})
Cp = specific heat of water (4,200 watt s kg^{-1} ^{o}C^{-1})
ρ = density of water (1,000 kg m^{-3})

2.10 Salinity

Salinity is modeled in the WQSTM by the conservation of mass equation with no internal sources or sinks.

2.11 Parameter Values

Model parameter evaluation is a recursive process. Parameters are selected from a range of feasible values, tested in the model, and adjusted until satisfactory agreement between predicted and observed variables is obtained. Ideally, the range of feasible values is determined by observation or experiment. For some parameters, however, no observations are available. Then, the feasible range is determined by parameter values employed in similar models or by the judgment of the modeler. A review of parameter values was included in documentation of the first CE-QUAL-ICM application to the Chesapeake Bay WQSTM (Cerco and Cole 1994). Parameters from the initial study were refined in successive applications and refined again for the 2017 model. A complete set of parameter values is provided in Table 2-2.

Table 2-2. Parameters in Kinetics Equations for 2017 WQSTM

Symbol	Definition	Value	Units
ANC	Nitrogen-to-carbon ratio of algae	0.175 (fresh) 0.135 (spring) 0.155 (green)	g N g^{-1} C
AOCR	DO-to-carbon ratio in respiration	2.67	g O_2 g^{-1} C
AONT	Mass DO consumed per mass ammonium nitrified	4.33	g O_2 g^{-1} N
APC	Algal phosphorus-to-carbon ratio	0.0125 (fresh) 0.0167 (spring) 0.0167 (green)	g P g^{-1} C
BM	Basal metabolic rate of algae at reference temperature Tr	0.03 (fresh) 0.01 (spring) 0.02 (green)	d^{-1}
CChl	Algal carbon-to-chlorophyll ratio	45 (fresh) 75 (spring) 60 (green)	g C g^{-1} Chl *a*
FCD	Fraction of dissolved organic carbon produced by algal metabolism	0.0	$0 \le FCD \le 1$
FCDP	Fraction of dissolved organic carbon produced by predation	0.5	$0 \le FCDP \le 1$
FCG3	Fraction of slow refractory particulate carbon produced by algal metabolism	0.0	$0 \le FCG3 \le 1$
FCG3P	Fraction of slow refractory particulate carbon produced by predation	0.05	$0 \le FCG3P \le 1$
FCL	Fraction of labile particulate carbon produced by algal metabolism	0.0	$0 \le FCL \le 1$
FCLP	Fraction of labile particulate carbon produced by predation	0.3	$0 \le FCLP \le 1$
FCR	Fraction of refractory particulate carbon produced by algal metabolism	0.0	$0 \le FCR \le 1$
FCRP	Fraction of refractory particulate carbon produced by predation	0.15	$0 \le FCRP \le 1$
FND	Fraction of dissolved organic nitrogen produced by algal metabolism	0.2	$0 \le FND \le 1$
FNDP	Fraction of dissolved organic nitrogen produced by predation	0.15	$0 \le FNDP \le 1$
FNG3	Fraction of slow refractory particulate nitrogen produced by algal metabolism	0.08	$0 \le FNG3 \le 1$
FNG3P	Fraction of slow refractory particulate nitrogen produced by predation	0.12	$0 \le FNG3P \le 1$
FNI	Fraction of inorganic nitrogen produced by algal metabolism	0.45	$0 \le FNI \le 1$
FNIP	Fraction of inorganic nitrogen produced by predation	0.35	$0 \le FNIP \le 1$
FNL	Fraction of labile particulate nitrogen produced by algal metabolism	0.23	$0 \le FNL \le 1$

Symbol	Definition	Value	Units
FNLP	Fraction of labile particulate nitrogen produced by predation	0.28	$0 \leq FNLP \leq 1$
FNR	Fraction of refractory particulate nitrogen produced by algal metabolism	0.04	$0 \leq FNR \leq 1$
FNRP	Fraction of refractory particulate nitrogen produced by predation	0.1	$0 \leq FNRP \leq 1$
FPD	Fraction of dissolved organic phosphorus produced by algal metabolism	0.25	$0 \leq FPD \leq 1$
FPDP	Fraction of dissolved organic phosphorus produced by predation	0.4	$0 \leq FPDP \leq 1$
FPG3	Fraction of slow refractory particulate phosphorus produced by algal metabolism	0.0	$0 \leq FPG3 \leq 1$
FPG3P	Fraction of slow refractory particulate phosphorus produced by predation	0.03	$0 \leq FPG3P \leq 1$
FPI	Fraction of dissolved inorganic phosphorus produced by algal metabolism	0.75	$0 \leq FPI \leq 1$
FPIP	Fraction of dissolved inorganic phosphorus produced by predation	0.5	$0 \leq FPIP \leq 1$
FPL	Fraction of labile particulate phosphorus produced by algal metabolism	0.0	$0 \leq FPL \leq 1$
FPLP	Fraction of labile particulate phosphorus produced by predation	0.06	$0 \leq FPLP \leq 1$
FPR	Fraction of refractory particulate phosphorus produced by algal metabolism	0.0	$0 \leq FPR \leq 1$
FPRP	Fraction of refractory particulate phosphorus produced by predation	0.01	$0 \leq FPRP \leq 1$
Kcod	Oxidation rate of chemical oxygen demand	20 (saltwater) 0.025 (fresh)	d^{-1}
Kdoc	Dissolved organic carbon respiration rate	0.025 – 0.05	d^{-1}
Kdon	Dissolved organic nitrogen mineralization rate	0.035	d^{-1}
Kdp	Minimum mineralization rate of dissolved organic phosphorus	0.025	d^{-1}
Kdpalg	Constant that relates mineralization rate to algal biomass	0.4	$m^3\ g^{-1}\ C\ d^{-1}$
Kg3c	Slow refractory POC hydrolysis rate	0.0	d^{-1}
Kg3n	Slow refractory particulate organic nitrogen hydrolysis rate	0.0	d^{-1}
Kg3p	Slow refractory particulate organic phosphorus hydrolysis rate	0.0	d^{-1}
KHn	Half-saturation concentration for nitrogen uptake by algae	0.01 (fresh) 0.025 (spring) 0.025 (green)	$g\ N\ m^{-3}$
KHNH4	Half-saturation concentration of ammonium in nitrogen preference formula	0.002 (fresh) 0.002 (spring) 0.002 (green)	$g\ N\ m^{-3}$

Symbol	Definition	Value	Units
KHnnt	Half-saturation concentration of NH_4 required for nitrification	1.0	g N m^{-3}
KHocod	Half-saturation concentration of DO required for exertion of COD	0.1	g O_2 m^{-3}
KHodoc	Half-saturation concentration of DO required for oxic respiration	0.1	g O_2 m^{-3}
KHont	Half-saturation concentration of DO required for nitrification	1.0	g O_2 m^{-3}
KHp	Half-saturation concentration for phosphorus uptake by algae	0.0025	g P m^{-3}
KHst	Salinity at which algal mortality is half maximum value	15 (fresh) 2.0 (spring)	ppt
Klpoc	Labile POC dissolution rate	0.15	d^{-1}
Klpon	Labile particulate organic nitrogen hydrolysis rate	0.12	d^{-1}
Klpop	Labile particulate organic phosphorus hydrolysis rate	0.12	d^{-1}
Kpip	Particulate inorganic phosphorus dissolution rate	0.0	d^{-1}
Krdo	Reaeration coefficient	1.5	m d^{-1}
Krpoc	Refractory POC dissolution rate	0.006	d^{-1}
Krpon	Refractory particulate organic nitrogen hydrolysis rate	0.005	d^{-1}
Krpop	Refractory particulate organic phosphorus hydrolysis rate	0.005	d^{-1}
KTb	Effect of temperature on basal metabolism of algae	0.0322	$^oC^{-1}$
KTcod	Effect of temperature on exertion of chemical oxygen demand	0.041	d^{-1}
KTg1	Effect of temperature below Tm on growth of algae	0.005 (fresh) 0.0018 (spring) 0.0035 (green)	$^oC^{-2}$
KTg2	Effect of temperature above Tm on growth of algae	0.004 (fresh) 0.006 (spring) 0.0 (green)	$^oC^{-2}$
KThdr	Effect of temperature on hydrolysis rates	0.069	$^oC^{-1}$
KTmnl	Effect of temperature on mineralization rates	0.069	$^oC^{-1}$
KTnt1	Effect of temperature below Tmnt on nitrification	0.003	$^oC^{-2}$
KTnt2	Effect of temperature above Tmnt on nitrification	0.003	$^oC^{-2}$
KTpr	Effect of temperature on predation	0.032	$^oC^{-1}$
NTm	Maximum nitrification rate at optimal temperature	0.062 to 0.125	g N m^{-3} d^{-1}

Symbol	Definition	Value	Units
Phtl	Predation rate on algae	0.05 (fresh) 0.1 (spring) 0.4 (green)	$m^3\ g^{-1}\ C\ d^{-1}$
Pm^B	Maximum photosynthetic rate	200 (fresh) 300 (spring) 450 (green)	$g\ C\ g^{-1}\ Chl\ d^{-1}$
Presp	Photorespiration fraction	0.25	$0 \leq Presp \leq 1$
STF	Salinity toxicity factor	0.3 (fresh) 0.1 (spring)	d^{-1}
Tmnt	Optimal temperature for nitrification	30	^oC
Topt	Optimal temperature for growth of algae	29 (fresh) 16 (spring) 25 (green)	^oC
Tr	Reference temperature for metabolism	20	^oC
Trcod	Reference temperature for COD oxidation	23	^oC
Trhdr	Reference temperature for hydrolysis	20	^oC
Trmnl	Reference temperature for mineralization	20	^oC
Trpr	Reference temperature for predation	20	^oC
Wa	Algal settling rate	0.0 (fresh) 0.6 (spring) 0.1–0.5 (green)	$m\ d^{-1}$
Wg3	Settling velocity of slow refractory particles	1.0	$m\ d^{-1}$
Wl	Settling velocity of labile particles	1.0	$m\ d^{-1}$
Wpip	Settling velocity of particulate inorganic phosphorus	0.1 to 0.5	$m\ d^{-1}$
Wpo4	Settling velocity for precipitated phosphate	1.0	$m\ d^{-1}$
Wr	Settling velocity of refractory particles	1.0	$m\ d^{-1}$
α	Initial slope of production versus irradiance relationship	3.15 (fresh) 8.0 (spring) 10.0 (green)	$g\ C\ g^{-1}\ Chl\ (E\ m^{-2})^{-1}$

Notes: fresh = freshwater algae; green = other green algae; spring = spring diatoms.

2.12 References

Ammerman, J., and F. Azam. 1985. Bacterial 5'-nucleodase in aquatic ecosystems: A novel mechanism of phosphorus regeneration. *Science* 227:1338-1340.

Boni, L., E. Carpene, D. Wynne, and M. Reti. 1989. Alkaline phosphatase activity in *Protogonyaulax Tamarensis*. *Journal of Plankton Research* 11:879-885.

Bunch, B., C. Cerco, M. Dortch, B. Johnson, and K. Kim. 2000. *Hydrodynamic and Water Quality Model Study of San Juan Bay and Estuary*. ERDC TR-00-1. US Army Engineer Research and Development Center, Vicksburg, MS.

Cerco, C., and T. Cole. 1994. *Three-Dimensional Eutrophication Model of Chesapeake Bay*. Technical Report EL-94-4. US Army Engineer Waterways Experiment Station, Vicksburg, MS.

Cerco, C., B. Bunch, M. Cialone, and H. Wang. 1994. *Hydrodynamic and Eutrophication Model Study of Indian River and Rehoboth Bay, Delaware*. Technical Report EL-94-5. US Army Engineer Waterways Experiment Station, Vicksburg, MS.

Cerco, C., and B. Bunch. 1997. *Passaic River Tunnel Diversion Model Study, Report 5, Water Quality Modeling*. Technical Report HL-96-2. US Army Engineer Waterways Experiment Station, Vicksburg, MS.

Cerco, C., B. Johnson, and H. Wang. 2002. *Tributary Refinements to the Chesapeake Bay Model*. ERDC TR-02-4, US Army Engineer Research and Development Center, Vicksburg, MS.

Cerco, C., and M. Noel. 2004. *The 2002 Chesapeake Bay Eutrophication Model*. EPA 903-R-04-004. US Environmental Protection Agency, Chesapeake Bay Program Office, Annapolis, MD.

Cerco, C., S.-C. Kim, and M. Noel. 2010. *The 2010 Chesapeake Bay Eutrophication Model*. US Environmental Protection Agency, Chesapeake Bay Program Office, Annapolis, MD.

Cerco, C., and M. Noel. 2010. Monitoring, modeling, and management impacts of bivalve filter feeders in the oligohaline and tidal fresh regions of the Chesapeake Bay system. *Ecological Modeling* 221:1054-1064.

Chrost, R., and J. Overbeck. 1987. Kinetics of alkaline phosphatase activity and phosphorus availability for phytoplankton and bacterioplankton in Lake Plubsee (north German eutrophic lake). *Microbial Ecology* 13:229-248.

DiToro, D., and J. Fitzpatrick. 1993. *Chesapeake Bay Sediment Flux Model*. Contract Report EL-93-2. US Army Corps of Engineers Waterways Experiment Station, Vicksburg, MS.

Edinger, J., D. Brady, and J. Geyer. 1974. *Heat Exchange and Transport in the Environment*. Report 14. Johns Hopkins University, Department of Geography and Environmental Engineering, Baltimore, MD.

Hartman, B., and D. Hammond. 1985. Gas exchange in San Francisco Bay. *Hydrobiologia* 129:59-68.

Jassby, A., and T. Platt. 1976. Mathematical formulation of the relationship between photosynthesis and light for phytoplankton. *Limnology and Oceanography* 21:540-547.

Keefe, C. 1994. The contribution of inorganic compounds to the particulate carbon, nitrogen, and phosphorus in suspended matter and surface sediments of Chesapeake Bay. *Estuaries* 17:122-130.

Leonard, B. 1979. A stable and accurate convection modelling procedure based on quadratic upstream interpolation. *Computer Methods in Applied Mechanics and Engineering* 19:59-98.

Matavulj, M., and K. Flint. 1987. A model for acid and alkaline phosphatase activity in a small pond. *Microbial Ecology* 13:141-158.

Monod, J. 1949. The growth of bacterial cultures. *Annual Review of Microbiology* 3:371-394.

Morel, F. 1983. *Principles of Aquatic Chemistry*. John Wiley and Sons, New York, NY.

O'Connor, D. 1983. Wind effects on gas-liquid transfer coefficients. *Journal of the Environmental Engineering Division* 190:731-752.

O'Connor, D., and W. Dobbins. 1958. Mechanisms of reaeration in natural streams. *Transactions of the American Society of Civil Engineers* 123:641-666.

Parsons, T., M. Takahashi, and B. Hargrave. 1984. *Biological Oceanographic Processes*. 3rd ed. Pergamon Press, Oxford.

Sellner, K., R. Lacoutre, and C. Parrish. 1988. Effects of increasing salinity on a cyanobacteria bloom in the Potomac River Estuary. *Journal of Plankton Research* 10:49-61.

Tchobanoglous, G., and E. Schroeder. 1987. *Water Quality*. Addison-Wesley, Reading, MA.

Thomann, R., and J. Fitzpatrick. 1982. *Calibration and Verification of a Mathematical Model of the Eutrophication of the Potomac Estuary*. Prepared for District of Columbia Department of the Environment. HydroQual Inc., Mahwah, NJ.

Tuffey, T., J. Hunter, and V. Matulewich. 1974. Zones of nitrification. *Water Resources Bulletin* 10:555-564.

USGS (US Geological Survey). 2011. *Change to Solubility Equations for Oxygen in Water*. Office of Water Quality Technical Memorandum 2011.03. US Geological Survey. Accessed April 2019. https://water.usgs.gov/admin/memo/QW/qw11.03.pdf.

Wezernak, C., and J. Gannon. 1968. Evaluation of nitrification in streams. *Journal of the Sanitary Engineering Division* 94(SA5):883-895.

3 Light Attenuation

Light attenuation is computed using a "partial attenuation model" (PAM) in which light attenuation is considered as the sum of the contributions from individual components. The components include water itself, colored organic matter, and suspended particles. The selection of components depends on available observations. The contribution from each component depends on local conditions.

3.1 Methods

Observations of light attenuation (Ke) and contributors to attenuation for the years 2000–2010 were obtained from the Chesapeake Bay Program's online database at http://www.chesapeakebay.net/data/downloads/cbp_water_quality_database_1984_present. The observations were generated through the Tidal Water Quality Monitoring Program and Shallow Water Monitoring Program. Contributors included particulate organic carbon (POC), dissolved organic carbon (DOC), volatile suspended solids (VSS), total suspended solids (TSS), salinity (SALT), and chlorophyll *a* (Chl). DOC and SALT were included as potential indicators of color while the other contributors represented various fractions of suspended solids. Negative values and outliers were removed from the 2000–2010 data, leaving nearly 18,000 observations of Ke and contributing factors.

Stepwise regression was used to evaluate additive models, which included various combinations of contributing factors. Superior results ($R^2 = 0.623$) were obtained for a simple model that related Ke to TSS and SALT (equation 1):

$$Ke = a1 + a2 \cdot TSS + a3 \cdot SALT \quad (1)$$

where:

Ke = coefficient of diffuse light attenuation (m^{-1})
$a1$ = background attenuation (m^{-1})
$a2$ = attenuation by TSS ($m^2\ g^{-1}$)
$a3$ = relationship between attenuation and salinity ($m^2\ kg^{-1}$)
TSS = TSS concentration ($g\ m^{-3}$)
$SALT$ = salinity ($kg\ m^{-3}$)

Chl was an additional significant contributor to attenuation ($p < 0.0001$) but the marginal improvement in R^2 was small at 0.012, so Chl was neglected in the model.

After the model was established, residuals were examined by monitoring station. Background attenuation (parameter a1) was adjusted in regions of the Bay judged to have significant, consistent residuals. Additional adjustments to parameter a1 were made in a few regions based on model data comparisons following operation of the Water Quality and Sediment Transport Model (WQSTM).

3.2 Results

The following parameter values were obtained through regression:

- a1 = 1.647 m^{-1}
- a2 = 0.0557 $m^2 g^{-1}$
- a3 = -0.0624 $m^2 kg^{-1}$

The negative value for a3 implies that fresh water is more highly colored than ocean water. Attenuation caused by color diminishes as the fraction of ocean water at the sample location increases. Examination of residuals indicated the following:

- Negative residuals (observed attenuation less than modeled) near the James, Rappahannock, Potomac, and Susquehanna river fall lines.
- Negative residuals in the lower Potomac and St. Marys rivers.
- Positive residuals (observed attenuation greater than modeled) in the York and Mattaponi rivers.
- Positive residuals in the lower James and Elizabeth rivers.

Table 3-1 lists adjustments made to background attenuation for Chesapeake Bay Program Segments (CBPSs), as shown in Figure 3-1.

Table 3-1. Adjustments to Background Attenuation

CBPS	Adjustment	CBPS	Adjustment
ANATF	-0.4	LAFMH	+0.6
BOHOH	+0.7	MATTF	-0.4
BSHOH	+0.5	MPNOH	+0.5
CB1	-0.4	MPNTF	+0.5
CB2	-0.3	PAXMH	-0.5
CB3	-0.3	PISTF	-0.4
CB4	-0.3	POTMH	-0.4
CB5	-0.3	POTOH	-0.4
CHOOH	+0.6	POTTF	-0.4
CHSTF	+0.7	SBEMH	+0.6
EBEMH	+0.6	WBEMH	+0.6
ELIPH	+0.6	YRKMH	+0.5

Figure 3-1. Background attenuation was adjusted on a segmentwide basis for CBPSs in Table 3-1.

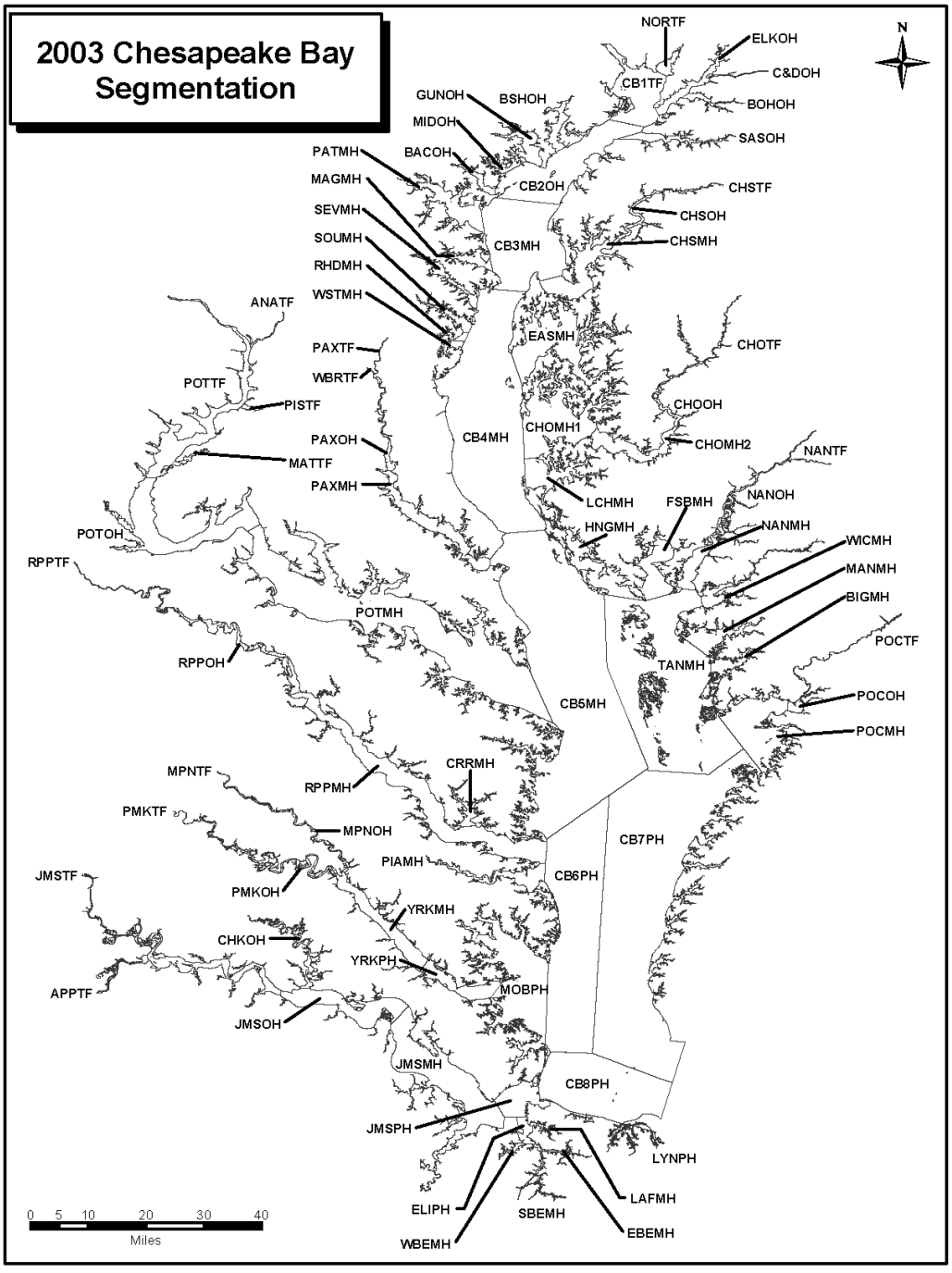

3.3 Additional Model Considerations

Observed TSS in the attenuation relationship is the sum of organic and inorganic particulate matter. Multiple WQSTM state variables must be summed to obtain TSS for use in the relationship. Concentration of inorganic solids is obtained from the WQSTM as the sum of the fine clay, clay, silt, and sand state variables. Observed organic (volatile) solids correspond to model POC state variables. For idealized organic matter, represented as CH_2O, organic solids concentration would be 2.5 times POC concentration. In reality, that ratio can vary. The appropriate ratio for the Chesapeake Bay was obtained using Type II regression of observed VSS on observed POC (Laws and Archie 1981). The result indicated organic solids = 2.9 * POC (R^2 = 0.889). Model POC is the sum of the three algal groups and three POC variables.

The negative relationship between Ke and SALT can result in negative values for Ke under conditions of high salinity coupled with low TSS. To avoid negative values, a minimum Ke value of 0.15 m^{-1} is imposed.

3.4 Comparison of Optical Models

The PAM used in this study replaces an advanced optical model (AOM) used in the 2010 model study (Cerco et al. 2010). Following parameterization of the PAM and implementation in the WQSTM, a model run was made to compare the PAM's results with those of the previous optical model. Computations of Ke were compared using the absolute mean difference (AMD) statistic developed for the initial Chesapeake Bay model (Cerco and Cole 1994) and used thereafter to examine model performance (equation 2):

$$AMD = \frac{\sum|P-O|}{N} \quad (2)$$

where:

AMD = absolute mean difference
O = observation
P = prediction
N = number of observations

The AMD is a measure of the characteristic difference between individual observations and computations. An AMD of zero indicates that the model perfectly reproduces each observation.

Statistics were determined using the model-data pairs employed in the model validation time series plots and grouped into systems. Results indicate the AOM and PAM deliver comparable performance in the mainstem Bay (Figure 3-2). For most other regions in the system, AMD is lower for the PAM than for the AOM.

Only in the Potomac River are results from the AOM superior to the PAM. Those results should not be interpreted to mean that PAMs are superior to AOMs. AOMs such as the one employed in the 2010 study are based on rigorous physics and are preferred in applications that emphasize optical properties of surface waters. The less rigorous PAM used here is suitable, however, to describe light attenuation in a study such as this one and is advantageous in terms of computational and data requirements.

Figure 3-2. Light attenuation AMD statistic for the PAM vs. the AOM.

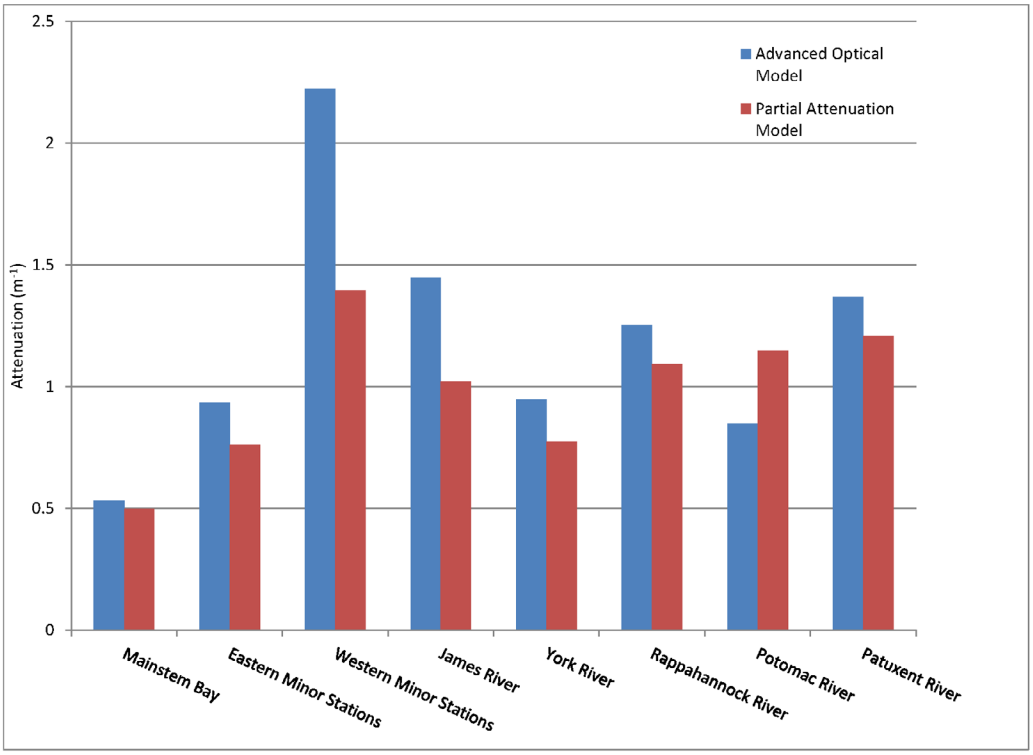

3.5 References

Cerco, C.F., and T.M. Cole. 1994. *Three-Dimensional Eutrophication Model of Chesapeake Bay*. Technical Report EL-94-4. US Army Engineer, Waterways Experiment Station, Vicksburg, MS.

Cerco, C., S.-C., Kim, and M. Noel. 2010. *The 2010 Chesapeake Bay Eutrophication Model*. US Environmental Protection Agency, Chesapeake Bay Program Office, Annapolis, MD. http://www.chesapeakebay.net/publications/title/the_2010_chesapeake_bay_eutrophication_model1.

Laws, E., and J. Archie. 1981. Appropriate use of regression analysis in marine biology. *Marine Biology* 65:13-16.

4 Wetlands Module

A decades-long, abundant literature describes tidal wetlands processes and interactions between tidal wetlands and open waters of the Chesapeake Bay system. Wetlands processes relevant to water quality management include the following:

- Nitrogen removal through denitrification (Merrill and Cornwell 2002; Neubauer et al. 2005; Hopfensperer et al. 2009; Seldomridge and Prestegaard 2014)
- Nitrogen removal through burial (Morse et al. 2004; Neubauer et al. 2005; Boynton et al. 2008; Palinkas and Cornwell 2012)
- Phosphorus removal through burial (Morse et al. 2004; Boynton et al. 2008; Palinkas and Cornwell 2012)
- Production and burial of organic carbon (Flemer et al. 1978; Neubauer et al. 2000, 2002; Morse et al. 2004)
- Burial of organic and inorganic solids (Stevenson et al. 1985; Ward et al. 1998; Morse et al. 2004; Palinkas et al. 2013)
- Dissolved oxygen (DO) consumption through respiration (Neubauer et al. 2000, 2002; Neubauer and Anderson 2003)

In recognition of nutrient and solids removal by wetlands, Drescher and Stack (2015) developed protocols to provide nutrient and sediment mass reduction credits for shoreline management projects that include restoring vegetation. Loss of wetlands in the Bay, associated with sea-level rise and diminishing sediment inputs, has been noted for decades (Stevenson et al. 1985; Ward et al. 1998; Kearney et al. 2002). Concern over potential wetlands loss is increasing in parallel with concern over sea-level rise associated with climate change (Glick et al. 2008).

The 2010 Chesapeake Bay Model included the effect of wetlands respiration on adjacent open water (Cerco et al. 2010). In view of the load reduction credits recommended for restoring wetlands and the potential ecosystem effects of wetlands loss, a more detailed wetlands module has been incorporated into the 2017 Chesapeake Bay Water Quality and Sediment Transport Model (WQSTM). The new module focuses on wetlands processes that have management implications: nutrient removal, solids removal, and respiration.

This chapter describes the wetlands module as implemented in the 2017 Midpoint Assessment of the 2010 Total Maximum Daily Load. The module was still undergoing evaluation and development at the time the 2017 WQSTM was delivered for use in the Midpoint Assessment. A revised module, accompanied by

revised documentation, will be implemented in upcoming climate-change scenarios.

4.1 Module Formulations

Formulating a detailed model of wetlands biogeochemical processes is a formidable task considering the process complexity and the variety of wetlands in the Chesapeake Bay system. Instead we have focused on basic relationships that describe the desired processes. The relationships incorporate rate-limiting functions that provide "feedback" between the rate of material removal by wetlands and the amount of material available in the adjacent open water column. Potential effects of wetlands location and type can be accommodated by local variations in parameter assignment.

4.1.1 Denitrification

The effect of wetland denitrification on adjacent open water is represented through a nitrate-removal algorithm. Nitrate removal is not exactly equivalent to denitrification (Neubauer et al. 2005; Seldomridge and Prestegaard 2014), but the removal process is readily inferred and easily parameterized through nitrate observations in the water column. Equation 1 represents nitrate removal:

$$V \cdot \frac{dC}{dT} = Transport + Kinetics - MTC \cdot f(T) \cdot C \cdot Aw \qquad (1)$$

where:

V = volume of water-quality model cell adjacent to wetlands (m^3)
C = nitrate concentration ($g\ m^{-3}$)
MTC = mass-transfer coefficient ($m\ d^{-1}$)
$f(T)$ = temperature effect
Aw = area of wetland adjacent to water-quality model cell (m^2)

The temperature effect is an exponential relationship in which denitrification doubles for a 10-degree Celsius (^oC) temperature increase.

4.1.2 Particle Settling

Settling of all particles, organic and inorganic, is represented by the same formulation (equation 2):

$$V \cdot \frac{dC}{dT} = Transport + Kinetics - WSw \cdot C \cdot Aw \qquad (2)$$

where:

C = particle concentration (g m^{-3})
WSw = wetland settling velocity (m d^{-1})

Differences in settling rates for different types of particles are accommodated by varying the WSw parameter.

4.1.3 Respiration

Net DO uptake is represented in equation 3:

$$V \cdot \frac{dDO}{dT} = Transport + Kinetics - f(DO) \cdot f(T) \cdot WOC \cdot Aw \qquad (3)$$

where:

DO = DO concentration (g m^{-3})
$f(DO)$ = limiting factor: DO/(Kh + DO)
Kh = DO concentration at which uptake is halved (g m^{-3})
WOC = wetlands oxygen consumption (g m^{-2} d^{-1})

If oxygen consumption is reduced by oxygen availability in the water column, chemical oxygen demand equivalent to the reduction is released from the wetlands so the total respiration, in oxygen equivalents, is constant.

4.2 Process Observations

Reported observations of relevant wetlands processes are concentrated in several "hot spots" around the Bay system (Figure 4-1). Those hot spots include reaches in the York River (MPNOH and PMKOH) and the Patuxent River (PAXOH), and in the vicinity of the Nanticoke River (NANOH, NANMH, FSBMH, and WICMH). Additional observations useful for evaluating parameters and comparing with the WQSTM are found in the Potomac River (POTTF), Bush River (BSHOH), and Chester River (CHSMH). The observations were collected by study authors for varying purposes and represent a wide variety of methods, reporting units, and time frames. Results from multiple sources were assembled (Table 4-1), converted to relevant units, and summarized for use in the wetlands module (Table 4-2).

Figure 4-1. Regions with wetlands observations used to parameterize the 2017 WQSTM wetlands module.

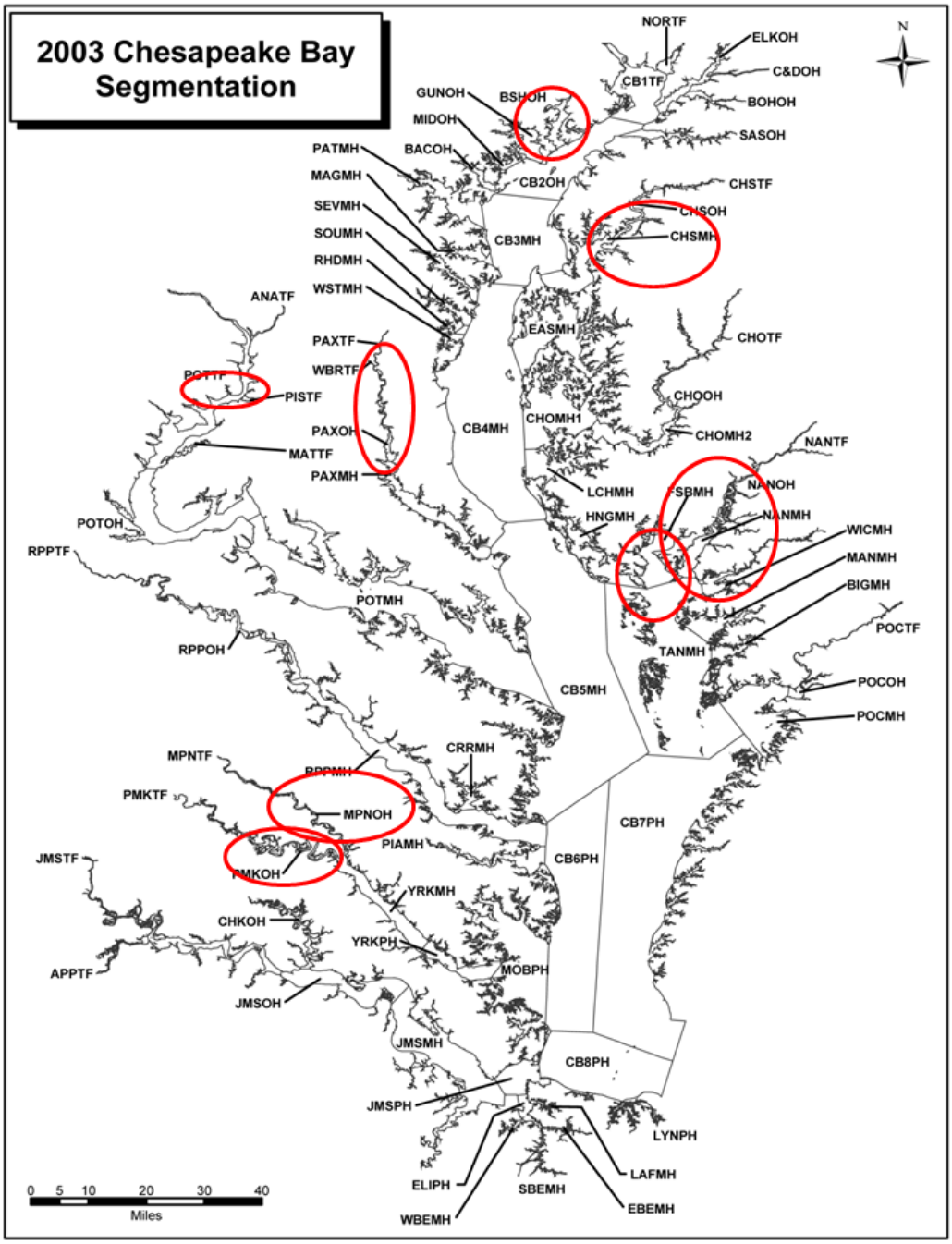

Table 4-1. Process Database Sources

Authors	Year	Published in
Boynton, W., Hagy, J., Cornwell, J., Kemp, W., Greene, S., Owens, M., Baker, J., and Larsen, R.	2008	*Estuaries and Coasts* 31:623-651
Flemer, D., Heinle, D., Keefe, C., and Hamilton, D.	1978	*Estuaries* 1(3):157-163
Hopfensperer, K., Kaushal, S., Findlay, S., and Cornwell, J.	2009	*Journal of Environmental Quality* 38:618-626
Merrill, J., and Cornwell, J.	2002	*Concepts and Controversies in Tidal Marsh Ecology,* pp 425-441
Morse, J., Megonigal, J., and Waldbridge, M.	2004	*Biogeochemistry* 69:175-206
Neubauer, S., Miller, W., and Anderson, I.	2000	*Marine Ecology Progress Series* 199:13-30
Neubauer, S., Anderson, I., Constantine, J., and Kuel, S.	2002	*Estuarine, Coastal and Shelf Science* 54:13-727
Neubauer, S., and Anderson, I.	2003	*Limnology and Oceanography* 48(1):299-307
Neubauer, S., Anderson, I., and Neikirk, B.	2005	*Estuaries* 28(6):909-922
Palinkas, C., and Cornwell, J.	2012	*Estuaries and Coasts* 35:546-558
Palinkas, C., Engelhardt, K., and Cadol, D.	2013	*Estuarine, Coastal and Shelf Science* 129:152-161
Seldomridge, E., and Prestegaard, K.	2014	*Wetlands* 34:641-651
Stevenson, J., Kearney, M., and Pendleton, E.	1985	*Marine Geology* 67:213-235
Ward, L., Kearney, M., and Stevenson, J.	1998	*Marine Geology* 151:111-134

Table 4-2. Summary of Wetlands Process Observations Used in Parameterizing and Validating the Module

CBPS	C Deposition ($g\ m^{-2}\ d^{-1}$)	N Deposition, ($g\ m^{-2}\ d^{-1}$)	P Deposition, ($g\ m^{-2}\ d^{-1}$)	Denitrification ($g\ N\ m^{-2}\ d^{-1}$)	Solids Deposition ($g\ m^{-2}\ d^{-1}$)	Respiration ($g\ DO\ m^{-2}\ d^{-1}$)
BSHOH		0.008 to 0.032	0.001 to 0.006			
CHOMH		0.053 to 0.074	4.9 e-4 to 0.005			
CHSMH		0.02 to 0.064	0.01 to 0.019		3.6	
FSBMH	0.39 to 0.82				0.3	
MPNOH	0.42 to 0.93	0.034 to 0.082	0.006 to 0.026		2.8 to 14.2	
NANMH	0.22 to 0.43				1.61 to 8.12	
NANOH	0.22 to 0.43				1.61 to 8.12	
PAXOH		0.037	0.006		3.8	
PAXTF		0.037 to 0.064	0.006 to 0.01	0.054 to 0.098	3.8	
PMKOH	1.42	0.05		0.023		1.12 to 2.77
POTTF	1.27			0.043 to 0.06	6.35	
WICMH	0.22 to 0.43	0.037	2.74 e-5 to 0.004		1.61 to 8.12	

Notes: C = carbon; CBPS = Chesapeake Bay Program Segment; $g\ m^{-2}\ d^{-1}$ = grams per square meter per day; N = nitrogen; P = phosphorus.

4.3 Wetlands Areas

Tidal wetlands areas were obtained from an application of the Sea Level Affecting Marshes Model (SLAMM) (WPC 2018). The SLAMM application projected how wetlands areas in the Chesapeake Bay and Delaware Bay regions would be affected by sea-level rise associated with climate change (Glick et al. 2008). Geographic information system (GIS) files of wetlands areas adjoining the Chesapeake Bay were provided by Dr. Lora Harris of the University of Maryland Center for Environmental Science. These were previously extracted from the complete SLAMM results as part of a study of nitrogen removal by Chesapeake Bay tidal wetlands (Bryan 2014).

Wetlands areas from SLAMM for the year 1996 were employed in the WQSTM. Chesapeake Bay tidal wetlands totaled 130,000 hectares. More than 90 percent of that area was classified as salt or brackish marsh with the remainder classified as tidal freshwater (Figure 4-2). The SLAMM areas were compared to projections from a 1996 National Wetlands Inventory (NWI) provided by the Chesapeake Bay Program (CBP). The SLAMM wetlands areas were nearly equal to the sum of NWI "emergent" wetlands at 125,000 hectares.

GIS projections of tidal wetlands were combined with projections of local Bay watersheds and of the model grid (Figure 4-3). Next, contiguous wetlands were divided into a "fishnet" of subsegments (Figure 4-4). Those subsegment areas were assigned to the nearest model surface cell (Figure 4-5), with care being taken not to cross local hydrologic unit code- (HUC-) 10 watershed boundaries (Figure 4-6).

The final product was a table of tidal wetlands areas associated with surface cells on the model grid. Roughly 2,300 of the total 11,000 surface cells adjoin tidal wetlands. The tidal wetlands area is roughly 11 percent of the open-water area of the Bay system, as represented on the model grid. For some regions, however, the area of adjacent tidal wetlands equals or exceeds the open-water area (Figure 4-7 and Figure 4-8).

Figure 4-2. Chesapeake Bay tidal wetlands. Salt and brackish wetlands are shown in green; freshwater wetlands are shown in red.

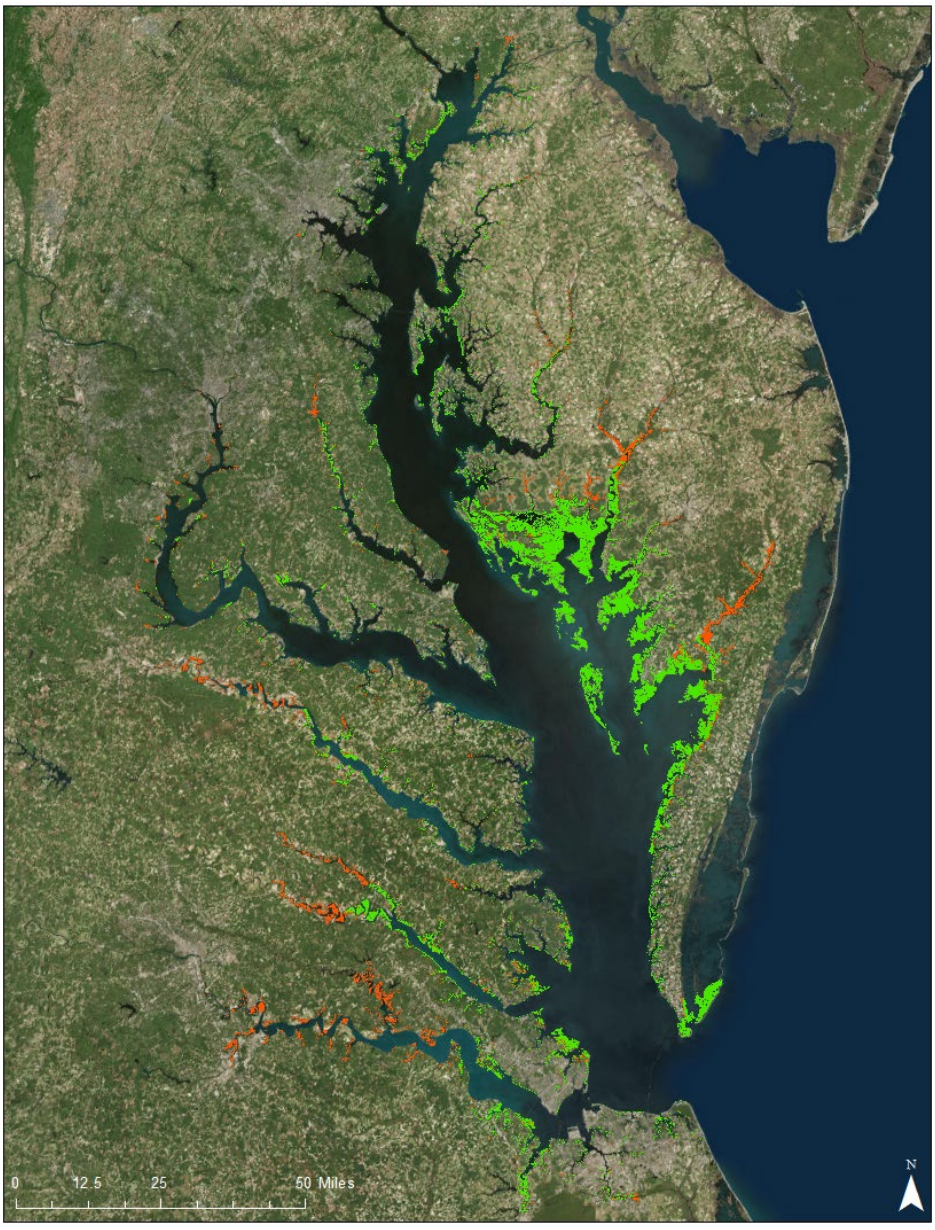

Figure 4-3. Example of wetlands areas combined with the model grid and Bay watersheds.

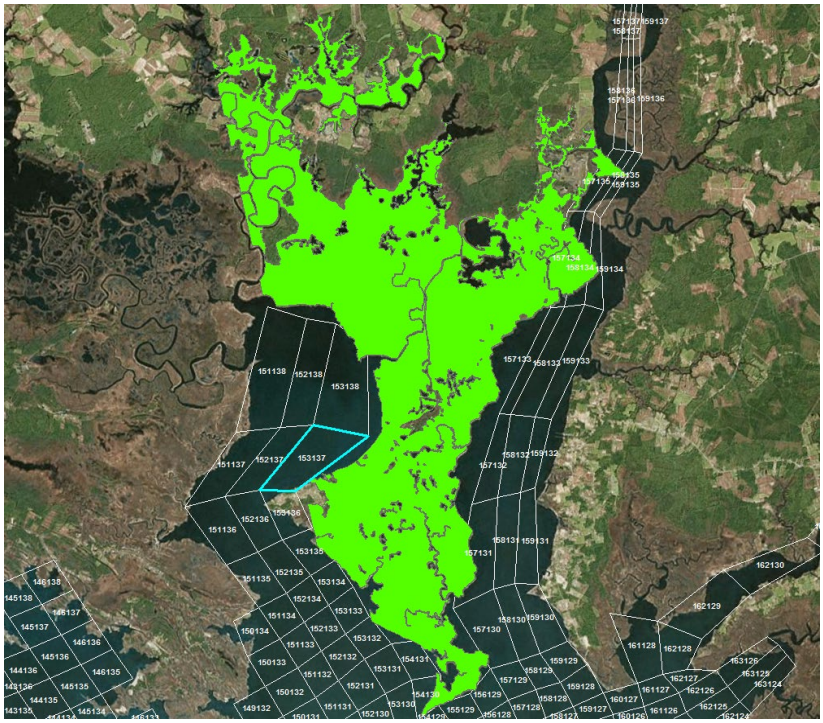

Figure 4-4. Example of subsegment "fishnet" superimposed on wetlands areas.

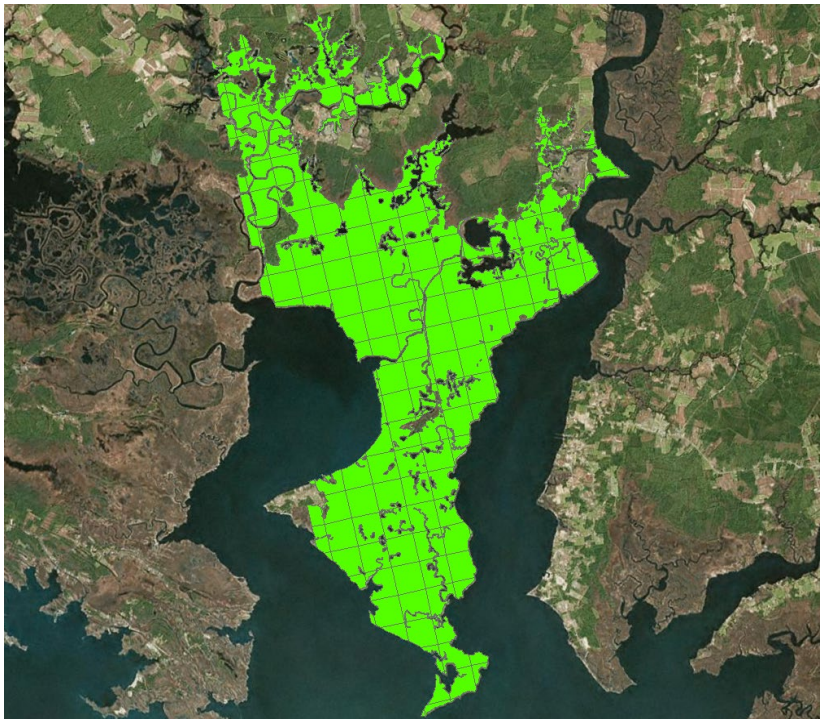

Figure 4-5. Example of wetlands areas mapped to model cells. Wetlands subsegments from the fishnet are shown in the same color as the cells to which they are mapped.

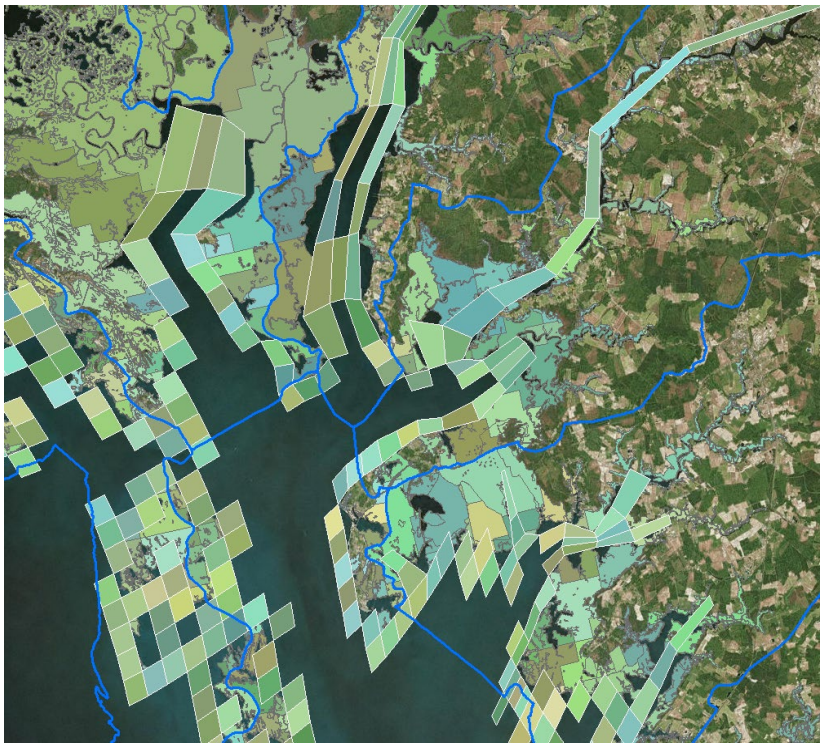

Figure 4-6. Example of HUC-10 local watershed boundaries superimposed on a map of Bay watersheds. Mapping of wetlands to model cells was restricted so as not to cross local watershed boundaries.

Figure 4-7. Ten regions of the Bay with the highest ratio of tidal wetlands area to open-water area. Open-water areas are as represented on the model grid.

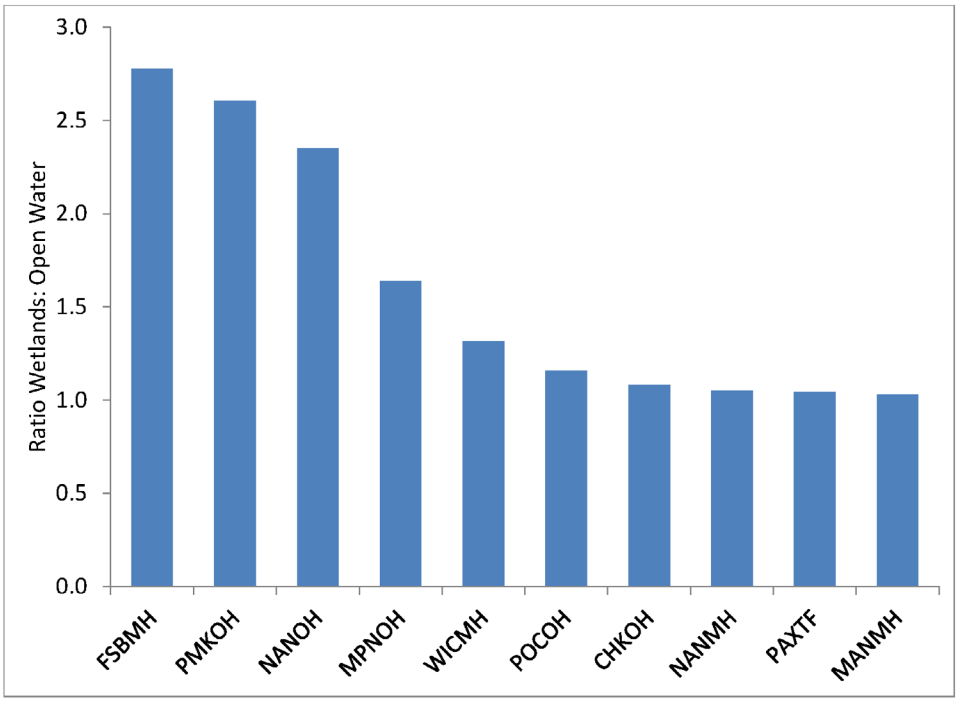

Figure 4-8. Locations of 10 regions with the highest ratio of tidal wetlands area to open-water area.

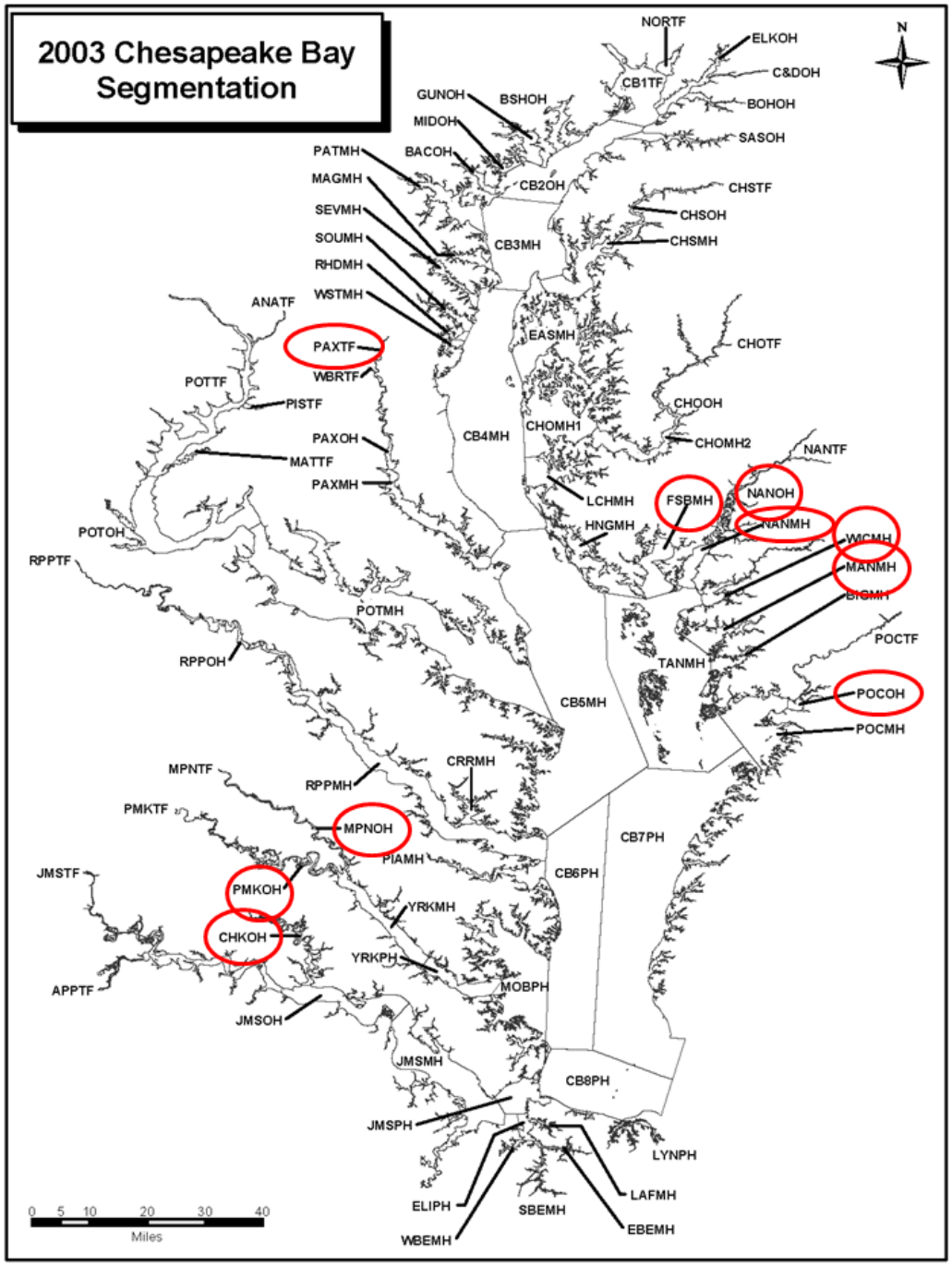

4.4 Initial Model Results

4.4.1 Areal Removal Rates

Observed removal rates are often quantified by methods such as analysis of sediment profiles, which provide rates averaged over years to decades. Some studies also describe rates at small spatial scales not represented in the WQSTM. The various methodologies, time scales, and spatial scales restrict the nature of model-data comparisons. The comparisons provided in this section are of long-term average model rates versus the range of rates observed in each of the regions with observations (Figure 4-1).

Figure 4-9, Figure 4-10, Figure 4-11, and Figure 4-12 show comparisons for deposition of carbon, nitrogen, phosphorus, and fixed solids based on the parameter set presented in Table 4-3.

Figure 4-9. Comparison of computed daily average of wetlands carbon deposition (*blue bars*) with range of reported rates (*red bars*). Observed rates in MPNOH, PMKOH, and POTTF represent accumulation on tiles. Remaining observations are long-term burial rates.

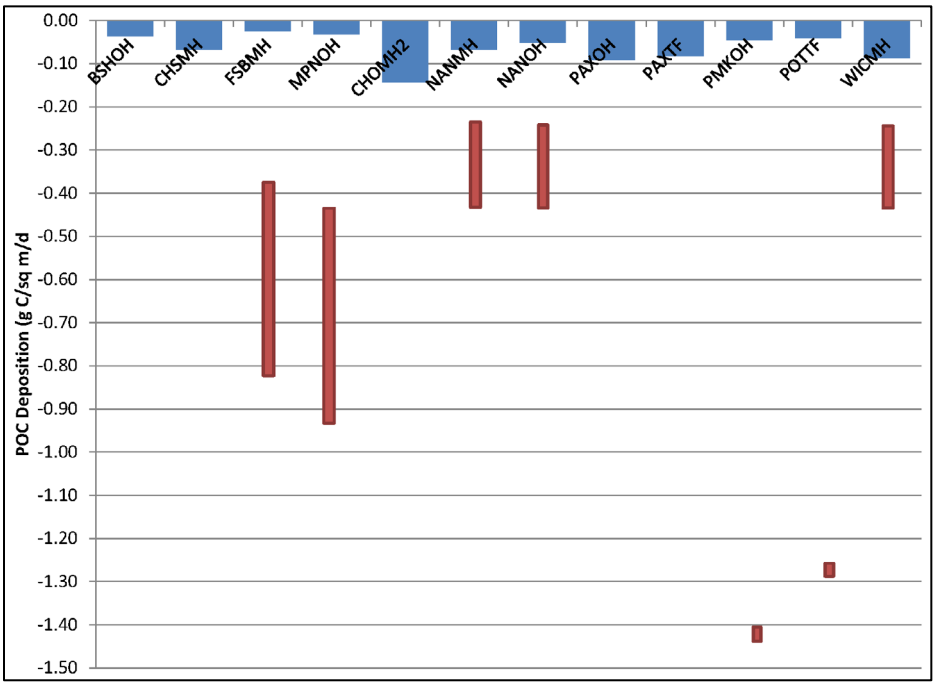

Figure 4-10. Comparison of computed daily average of wetlands particulate nitrogen deposition (*blue bars*) with range of reported rates (*red bars*). Observed rates in MPNOH represent accumulation on tiles. Remaining observations are long-term burial rates.

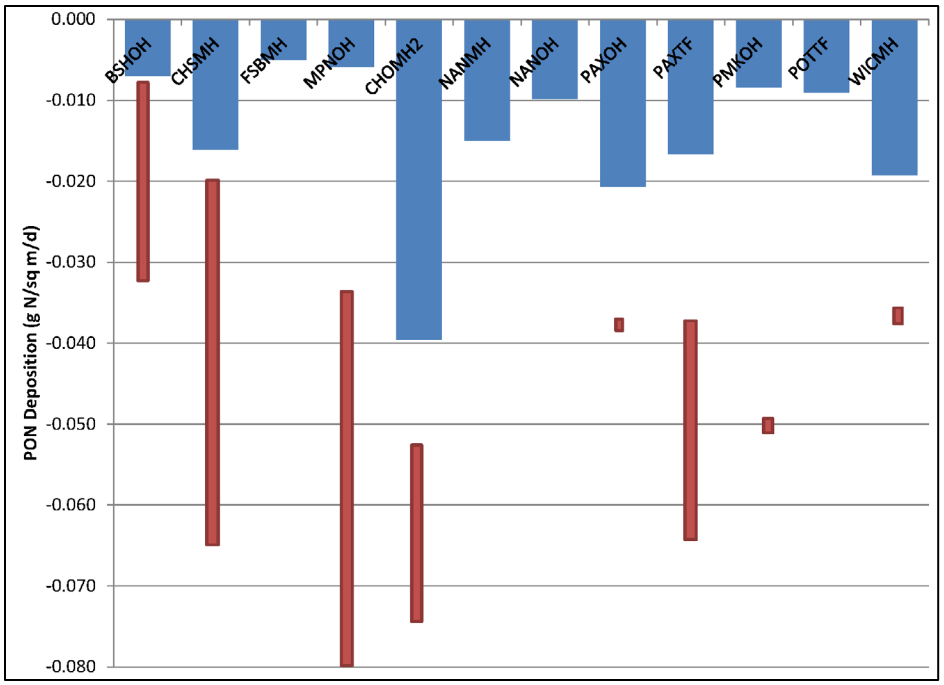

Figure 4-11. Comparison of computed daily average of wetlands particulate phosphorus deposition (*blue bars*) with range of reported rates (*red bars*). Observed rates in MPNOH represent accumulation on tiles. Remaining observations are long-term burial rates. The *red line* shows the allowance for wetlands phosphorus removal recommended by the Water Quality Goal Implementation Team.

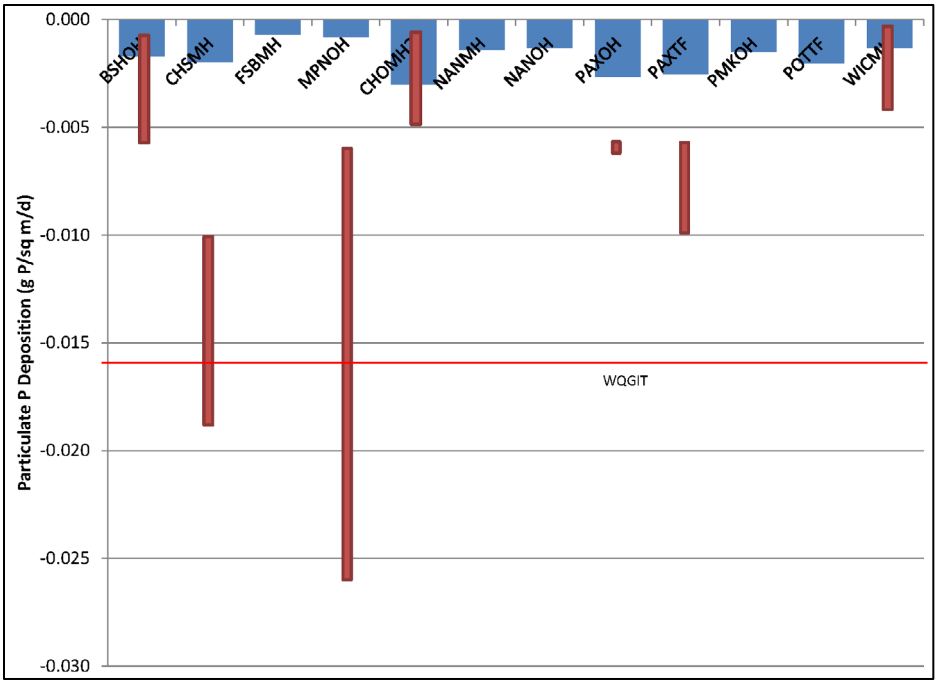

Figure 4-12. Comparison of computed daily average of wetlands fixed solids deposition (*blue bars*) with range of reported rates (*red bars*). Observed rates in MPNOH and POTTF represent accumulation on tiles. Remaining observations are long-term burial rates.

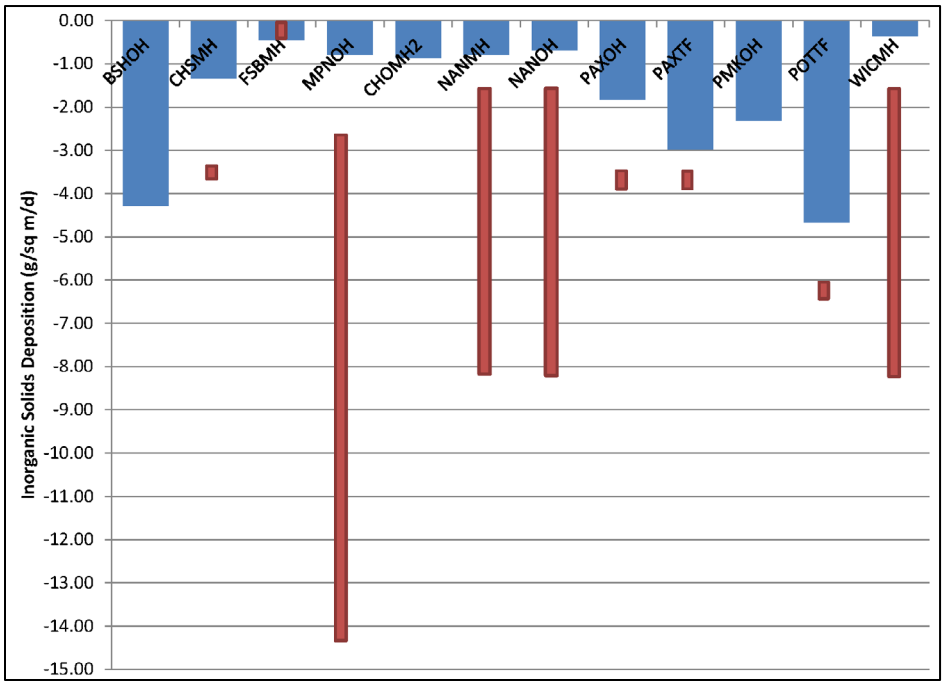

Table 4-3. Wetlands Module Parameters

Parameter	Definition	Value	Units
WSl	Settling velocity of labile organic particles	0.05	m d^{-1}
WSr	Settling velocity of refractory organic particles	0.05	m d^{-1}
WSg3	Settling velocity of slow refractory organic particles	0.05	m d^{-1}
WSb1	Settling velocity of Group 1 phytoplankton	0.005	m d^{-1}
WSb2	Settling velocity of Group 2 phytoplankton	0.005	m d^{-1}
WSb3	Settling velocity of Group 3 phytoplankton	0.005	m d^{-1}
WSpip	Settling velocity of particulate inorganic phosphorus	0.01	m d^{-1}
WSfclay	Settling velocity of fine clay	0.05	m d^{-1}
WSclay	Settling velocity of clay	0.13	m d^{-1}
WSsilt	Settling velocity of silt	0.432	m d^{-1}
WOC	Wetlands oxygen consumption at 20 ^{o}C	1.25	g DO m^{-2} d^{-1}
Kh	DO concentration at which wetlands consumption is halved	1	g m^{-3}
MTC	Nitrate mass-transfer coefficient	0.05	m d^{-1}

Notes: g m^{-2} d^{-1} = grams per meter per day; g m^{-3} = grams per meter; m d = meters per day.

An initial explanation of the results is that less material is deposited in the model wetlands than is depicted in the range of observations. One inference from that explanation is that the initial wetlands settling rates should be increased. An

alternate explanation is that the observations, which are largely burial rates, are not composed exclusively of particulate material removed from the water column, as represented in the module. Burial could include carbon fixed by wetlands vegetation and dissolved nutrients converted by vegetation to particulate organic form. Modeled wetlands nitrate uptake is predominantly less than the range of observations, suggesting the need to revise the initial nitrate mass-transfer coefficient (Figure 4-13).

Figure 4-13. Comparison of computed daily average of wetlands nitrate uptake (*blue bars*) with range of reported rates (*red bars*). Observations in PAXTF are wetlands nitrate retention. Observations in PMKOH are diffusive flux at the sediment-water interface. Observations in POTTF are denitrification as gaseous nitrogen flux.

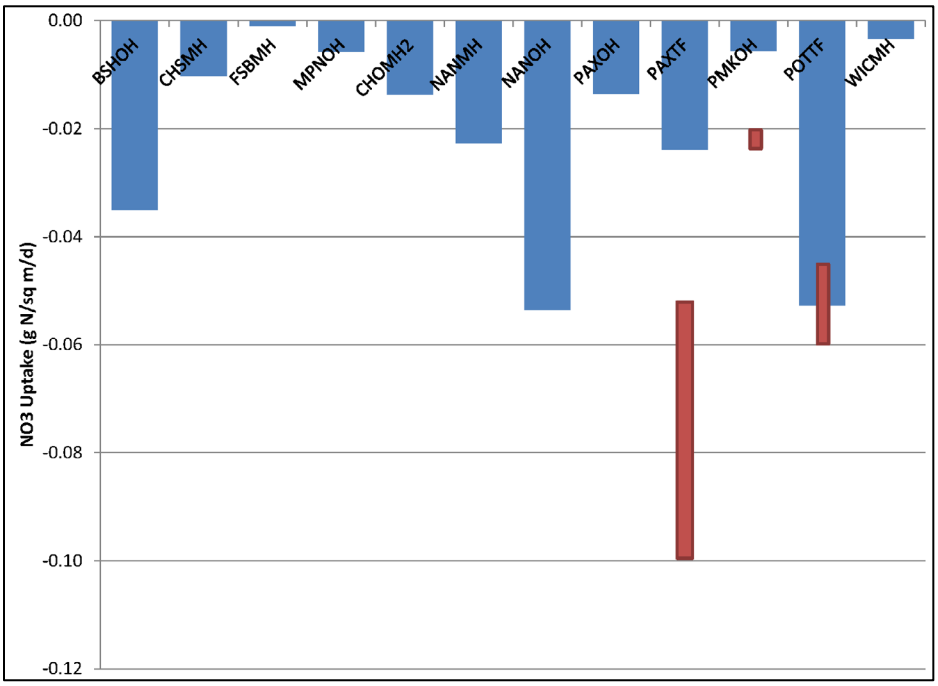

CBP's Water Quality Goal Implementation Team has provided values for nutrient reduction credits associated with vegetation restoration (Drescher and Stack 2015). The values for nitrogen and phosphorus credits, 0.026 g N m^{-2} d^{-1} and 0.016 g P m^{-2} d^{-1}, respectively, are based on an extensive literature survey that included studies outside the limited geographic range of this study. The model nitrogen removal rates, which combine denitrification and burial, are representative of the recommended credits (Figure 4-14). The model phosphorus removal value, equivalent to particle deposition, is much lower than the recommended credit (Figure 4-11). Model phosphorus removal can be increased through an increase in the wetlands settling velocity, but the recommended credit is higher than the majority of observed burial rates considered in this study.

Figure 4-14. Comparison of computed daily average of wetlands nitrogen removal (*blue bars*) with the allowance recommended by the Water Quality Goal Implementation Team (*red line*).

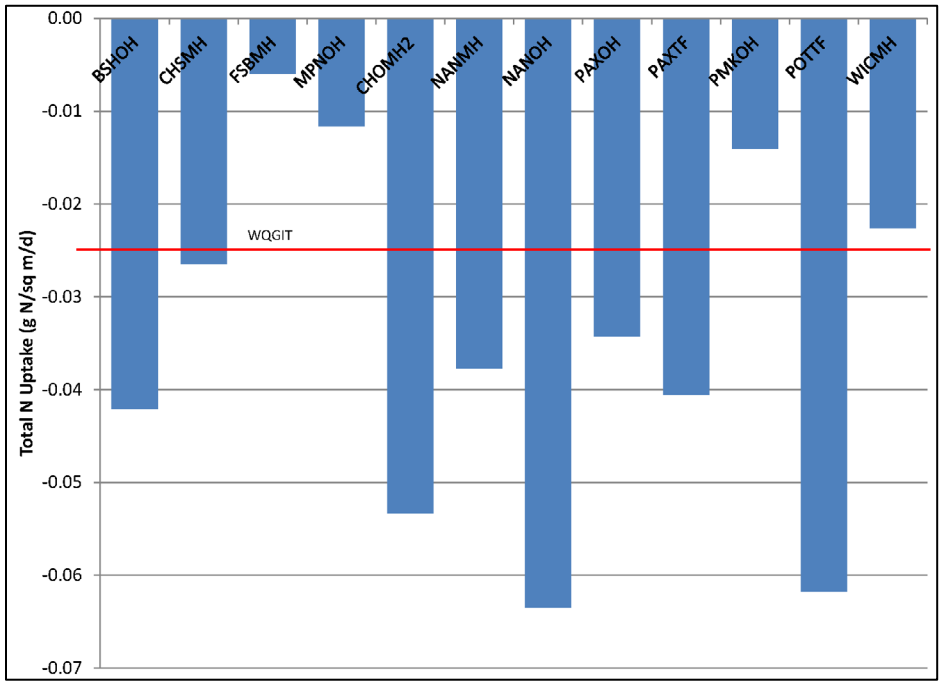

4.4.2 Mass Removed

Local watershed nutrient loads were compared to wetlands nutrient removal for the same segments examined for areal removal rates (Table 4-4). The fraction of loads removed varies widely and often exceeds unity for the segments considered. A fraction greater than unity indicates that the segment imports nutrients from adjacent waters, which are subsequently removed in local wetlands. The segments with the greatest fractional removal have large ratios of wetlands to open-water area (e.g., FSBMH, NANOH, and PMKOH) (Figure 4-7). Anomalies exist, however, notably in the PAXTF segment (tidal fresh Patuxent), which exhibits minimal fractional removal despite a relatively high ratio of wetlands to open-water area. The low removal fractions in that segment reflect the influence of local watershed area and residence time. PAXTF receives loads from the entire upland Patuxent River watershed, which is of tremendous extent relative to the area of the segment. The upland runoff accompanying the loads minimizes the residence time of nutrients in the segment and the opportunity for wetlands removal.

Table 4-4. Watershed Load and Wetlands Removal 1991–2000

CBPS	Total N Load (kg d^{-1})	Total P Load (kg d^{-1})	Total N Removed, (kg d^{-1})	Total P Removed (kg d^{-1})	N Fraction Removed	P Fraction Removed
BSHOH	831	45.0	194	7.9	0.233	0.175
CHOMH2	848	45.6	372	21.0	0.439	0.460
CHSMH	1,157	76.8	311	23.3	0.269	0.303
FSBMH	1,334	88.2	1,220	143.0	0.914	1.622
MPNOH	267	8.3	162	11.1	0.608	1.344
NANMH	613	30.5	1,490	55.5	2.431	1.823
NANOH	754	29.8	1,590	32.5	2.108	1.092
PAXOH	591	54.4	380	29.5	0.643	0.543
PAXTF	2,946	256.9	252	15.8	0.086	0.061
PMKOH	134	7.1	311	33.1	2.322	4.629
POTTF	66,776	5,708.7	565	18.6	0.008	0.003
WICMH	1,777	93.4	1,190	69.0	0.670	0.739
System	335,318	21,607.5	26,000	1,860.0	0.078	0.086

Notes: CBPS = Chesapeake Bay Program Segment; kg d^{-1} = kilogram per day; N = nitrogen; P = phosphorus.

The WQSTM indicates that 7.8 percent of the total nitrogen load and 8.6 percent of the total phosphorus load to the Bay are removed in tidal wetlands (Table 4-4). Boynton et al. (2008) reported that 46 percent and 74 percent of the upland nitrogen and phosphorus loading, respectively, were removed in the oligohaline Patuxent estuary and adjacent tidal marshes. The WQSTM indicates that the wetlands remove 18 percent and 15 percent of the nitrogen and phosphorus loads, respectively, to the PAXTF and PAXOH segments. The Boynton et al. estimates include loss to estuarine sediments. Thus, the estimates are expected to exceed the loss exclusively through wetlands computed in this study. The disparity between the independent estimate and the present computations, however, reinforces the earlier indications that the present wetlands module underestimates wetlands nutrient removal.

4.4.3 Influence on WQSTM Calibration

Preliminary sensitivity runs demonstrate the ability of the wetlands module to improve WQSTM performance. Nitrate computations in a 40-kilometer reach of the York River are improved when wetlands nitrate uptake is represented in the model (Figure 4-15). DO sags in the Patuxent and York rivers are explained by wetlands respiration (Figure 4-16), and total nitrogen computations in the Nanticoke River are improved when wetlands nitrogen removal is considered (Figure 4-17).

The wetlands module is still under development. Revised and improved comparisons to observations are expected following additional assessment of the module formulation and revisions to parameter assignments.

Figure 4-15. Sensitivity of York River model nitrate concentration to wetlands removal. Comparison shown for summer 2004.

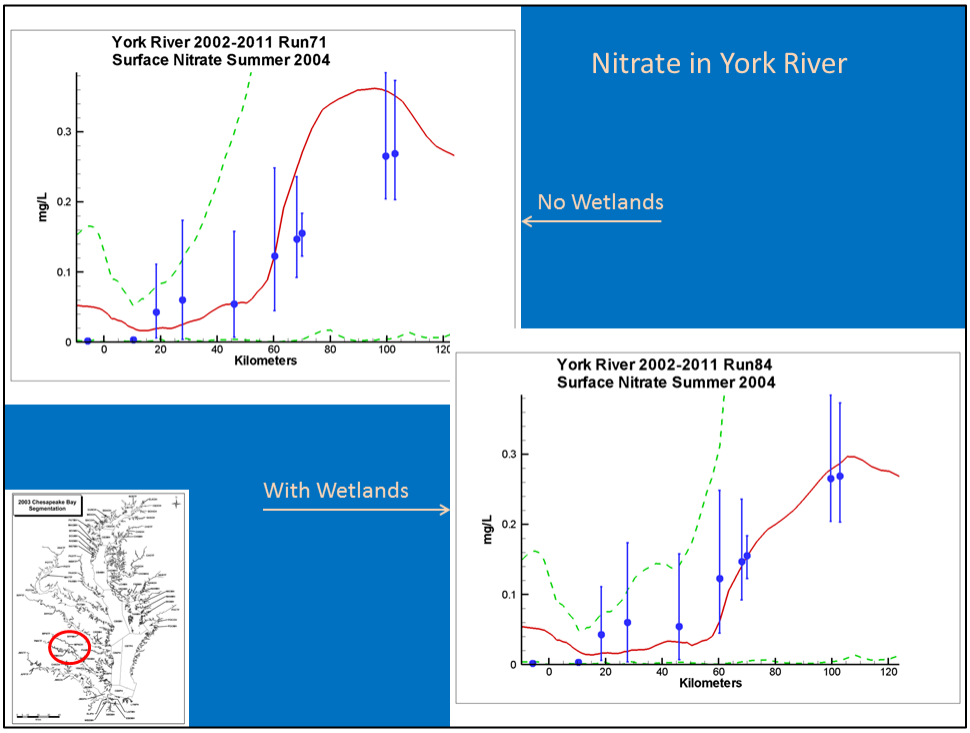

Figure 4-16. Effect of wetlands oxygen uptake on DO computations in the Patuxent and York rivers. Results shown for summer 2004.

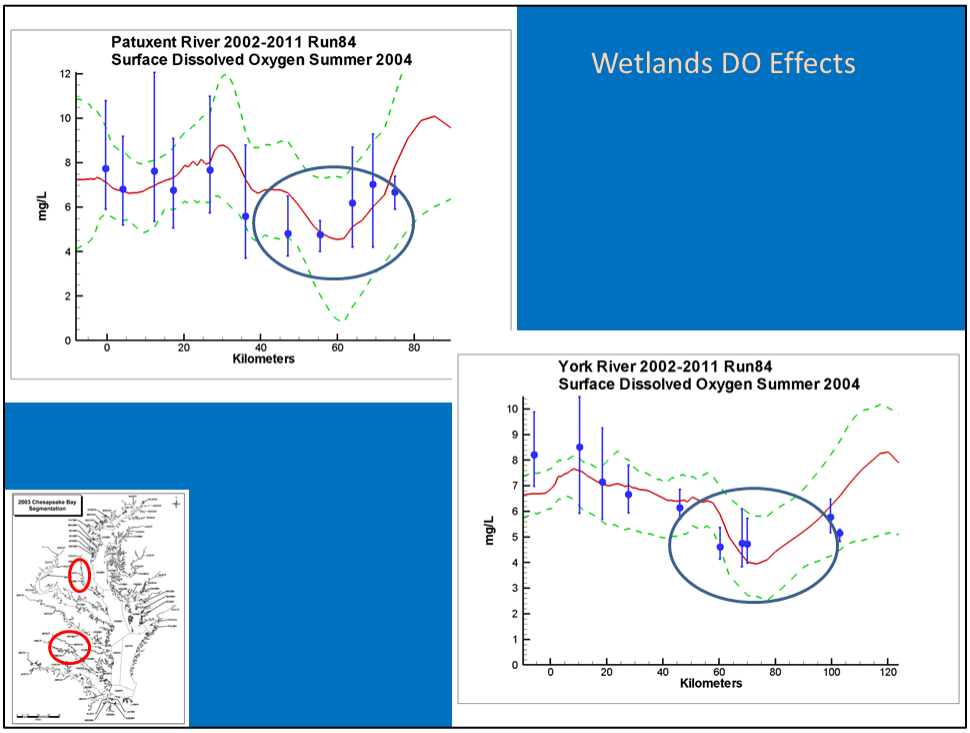

Figure 4-17. Effect of wetlands nitrogen removal on computed total nitrogen concentration in the Nanticoke River. Ten-year time series 2002–2011.

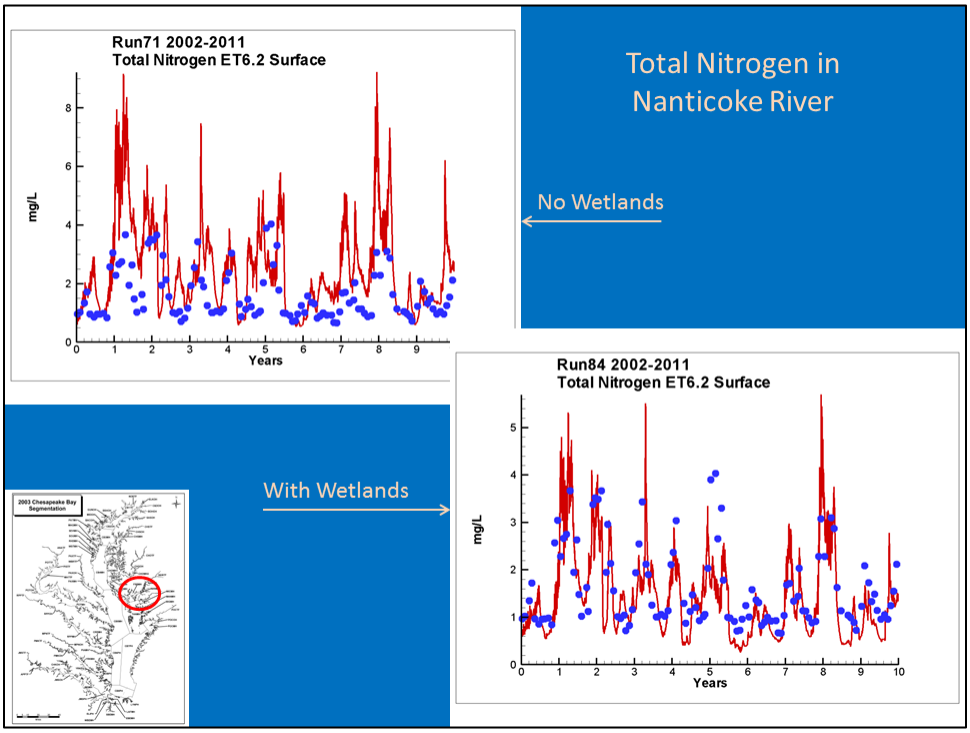

4.5 References

Boynton, W., J. Hagy, J. Cornwell, W. Kemp, S. Greene, M. Owens, J. Baker, and R. Larsen. 2008. Nutrient budgets and management actions in the Patuxent River estuary. *Estuaries and Coasts* 31:623-651.

Bryan, J. 2014. Effects of Sea Level Rise on Tidal Marshes. Master's thesis, University of Maryland, College Park.

Cerco, C., S.-C. Kim, and M. Noel. 2010. *The 2010 Chesapeake Bay Eutrophication Model*. US Environmental Protection Agency, Chesapeake Bay Program Office, Annapolis, MD. http://www.chesapeakebay.net/publications/title/the_2010_chesapeake_bay_eutrophication_model1.

Drescher, S., and B. Stack. 2015. *Recommendations of the Expert Panel to Define Removal Rates for Shoreline Management Projects*. Chesapeake Bay Partnership, Annapolis, MD. http://www.chesapeakebay.net/documents/Shoreline_Management_Protocols_Final_Approved_07132015-WQGIT-approved.pdf.

Flemer, D., D. Heinle, C. Keefe, and D. Hamilton. 1978. Standing crops of marsh vegetation of two tributaries of Chesapeake Bay. *Estuaries* 1(3):157-163.

Glick, P., J. Clough, and B. Nunley. 2008. *Sea-Level Rise and Coastal Habitats in the Chesapeake Bay Region*. National Wildlife Federation. https://www.nwf.org/~/media/PDFs/Global-Warming/Reports/SeaLevelRiseandCoastalHabitats_ChesapeakeRegion.ashx.

Hopfensperer, K., S. Kaushal, S. Findlay, and J. Cornwell. 2009. Influence of plant communities on denitrification in a tidal freshwater marsh of the Potomac River, United States. *Journal of Environmental Quality* 38:618-626.

Kearney, M., J. Rogers, E. Townshend, E. Rizzo, D. Stutzer, J. Stevenson, and K. Sundborg. 2002. Landsat imagery shows decline of coastal marshes in Chesapeake and Delaware bays. *Eos* 83(16):173, 177-178.

Merrill, J., and J. Cornwell. 2002. The Role of Oligohaline Marshes in Estuarine Nutrient Cycling. Chapter in *Concepts and Controversies in Tidal Marsh Ecology*, ed. M. Weinstein and D. Kreeger, pp 425-441. Springer, Dordrecht.

Morse, J., J. Megonigal, and M. Waldbridge. 2004. Sediment nutrient accumulation and nutrient availability in two tidal freshwater marshes along the Mattaponi River, Virginia, US. *Biogeochemistry* 69:175-206.

Neubauer, S., W. Miller, and I. Anderson. 2000. Carbon cycling in a tidal freshwater marsh ecosystem: A carbon gas flux study. *Marine Ecology Progress Series* 199:13-30.

Neubauer, S., I. Anderson, J. Constantine, and S. Kuel. 2002. Sediment deposition and accretion in a Mid-Atlantic (U.S.) tidal freshwater marsh. *Estuarine, Coastal and Shelf Science* 54:713-727.

Neubauer, S., and I. Anderson. 2003. Transport of dissolved inorganic carbon from a tidal freshwater marsh to the York River estuary. *Limnology and Oceanography* 48(1):299-307.

Neubauer, S., I. Anderson, and B. Neikirk. 2005. Nitrogen cycling and ecosystem exchanges in a Virginia tidal freshwater marsh. *Estuaries* 28(6):909-922.

Palinkas, C., and J. Cornwell. 2012. A preliminary sediment budget for the Corsica River (MD): Improved estimates of nitrogen burial and implications for restoration. *Estuaries and Coasts* 35:546-558.

Palinkas, C., K. Engelhardt, and D. Cadol. 2013. Evaluating physical and biological influences on sedimentation in a tidal fresh marsh with 7Be. *Estuarine, Coastal and Shelf Science* 129:152-161.

Seldomridge, E., and K. Prestegaard. 2014. Geochemical, temperature, and hydrologic transport limitations on nitrate retention in tidal freshwater wetlands, Patuxent River, Maryland. *Wetlands* 34:641-651.

Stevenson, J., M. Kearney., and E. Pendleton. 1985. Sedimentation and erosion in a Chesapeake Bay brackish marsh system. *Marine Geology* 67:213-235.

Ward, L., M. Kearney, and J. Stevenson. 1998. Variations in sedimentary environments and accretionary patterns in estuarine marshes undergoing rapid submergence, Chesapeake Bay. *Marine Geology* 151:111-134.

WPC (Warren Pinnacle Consulting). 2018. SLAMM: Sea Level Affecting Marshes Model. Warren Pinnacle Consulting Inc., Waitsfield, VT. http://warrenpinnacle.com/prof/SLAMM/.

5 Shoreline Erosion

The 2002 study identified solids loads from shoreline erosion as a major source of suspended solids to the Bay and tributaries (Cerco and Noel 2004). The database for quantification of loads (USACE 1990) was sparse, however, and the loads were input to the model on a spatially and temporally uniform basis. For the 2010 study, we determined to complete the best possible quantification of bank loads (Cerco et al. 2010). Those revised loads were based on contemporary information and reflected spatial variability caused by local shoreline characteristics and the presence of shoreline structures. The resulting estimates were multi-decadal averages based on shoreline recession determined from aerial surveys and hydrographic maps.

The significant potential contribution of shoreline erosion to Chesapeake Bay total phosphorus was noted in the earliest phase of the Chesapeake Bay model (Cerco and Cole 1993). Carbon, nitrogen, and phosphorus from shoreline erosion were included in the 2002 model version (Cerco and Noel 2004). These loads were omitted, however, from the 2010 model version used to guide the determination of the Total Maximum Daily Load (TMDL) (Cerco et al. 2010). The loads were omitted because no guidance existed for incorporating them into the TMDL development. In addition, there was no authoritative source for specification of shoreline carbon and nutrient loads.

More recently, an expert panel provided protocols to define pollutant load reductions associated with shoreline management practices (Drescher and Stack 2015). One protocol provided an annual mass sediment reduction credit for qualifying shoreline management practices that prevent tidal shoreline erosion that delivers sediment to nearshore/downstream waters. The panel report recognized potential nutrient reduction credits associated with erosion management practices but withheld recommendations pending review of additional information on nutrient availability/reactivity. In view of the recognized contribution of shoreline erosion to the Bay nutrient budget and the pending consideration of those nutrients in TMDL development, we have restored nutrient loads from shoreline erosion to this model version. This chapter describes the loads and their availability.

5.1 Methods for Determining Solids Loads

Primary references for the determination of shoreline erosion loads are a report by Hennessee et al. (2006) and a PowerPoint presentation (Halka and Hopkins 2006). Methods for determining solids loads, gleaned from those reports, are summarized in this section.

Quantifying solids loads from bank erosion requires two fundamental calculations. First, calculating the volume of sediment lost from erosion, and second, converting sediment volume into sediment mass.

The volume is determined using equation 1:

$$V = L \cdot W \cdot H \quad (1)$$

where:

V = volume of annual sediment loss from shore erosion ($m^3\ yr^{-1}$)
L = shoreline length (m)
W = rate of shoreline retreat (m yr^{-1})
H = bank height or marsh elevation (m)

Volume is converted to mass using equation 2:

$$Mtotal = Bd \cdot V \quad (2)$$

where:

$Mtotal$ = total mass of annual sediment (sand, silt, and clay) loss from bank erosion (kg yr^{-1})
Bd = dry bulk density of eroding bank (kg m^{-3})

Approximately 250,000 shoreline-normal transects were available for the Maryland shoreline alone to determine the rate of shoreline retreat. Available Maryland shorelines spanned the period from approximately 1850 to 1990. For model calculations, the two most recent shorelines in each analyzed reach or section were used. For most areas, the two most recent shorelines dated from about 1940 and about 1990, although intervals shorter and longer than 50 years occurred. Shoreline characteristics, notably the presence of protective structures, were reported in surveys conducted by Virginia Institute of Marine Science (Hardaway et al. 1992). Still, complete information for the systemwide characterization of shorelines was missing. When necessary, missing information (e.g., recession rate, presence of structures, and bulk density) was based on adjacent shoreline reaches or on regional average characteristics.

Other key assumptions included the following:

- Erosion of fastland from unprotected shorelines represents 65 percent of the total load; nearshore erosion represents 35 percent (Figure 5-1).
- No sediment is eroded from either fastland or nearshore along accreting shorelines.

- No sediment is delivered to the Bay from fastland protected by structures. The nearshore in regions protected by structures, however, erodes at the same rate as nearby unprotected reaches.
- The average dry bulk density of banks is 1.38 g cm^{-3} and of marshes is 0.62 g cm^{-3}.
- On average, silts and clays constitute 56 percent of sediment eroded from banks and 44 percent of sediment eroded from marshes.
- Organic matter is delivered only from marsh erosion and constitutes 34 percent of that material.
- Bulk density and composition of nearshore sediments are the same as those of adjacent fastland sediments.

Figure 5-1. Fastland versus nearshore erosion (*Source*: Hennessee et al. 2006).

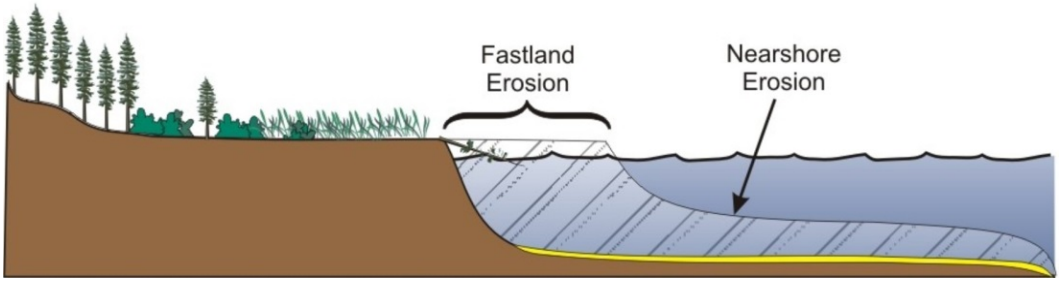

5.1.1 Summary

Results indicate that the Bay shoreline above the Potomac River junction produces the largest sediment mass per unit shoreline length (Figure 5-2). Reaches with high erosion levels are also found in the Potomac River, the Rappahannock River, and the James River. Although the Virginia shoreline is longer and less protected than the Maryland shoreline (Table 5-1), the largest sediment loads originate in the Maryland portion of the Bay system. Both the total loading and the loading per unit shoreline length are higher in Maryland than in Virginia.

Figure 5-2. Long-term average shoreline erosion in the Chesapeake Bay system (*Source*: Halka and Hopkins 2006).

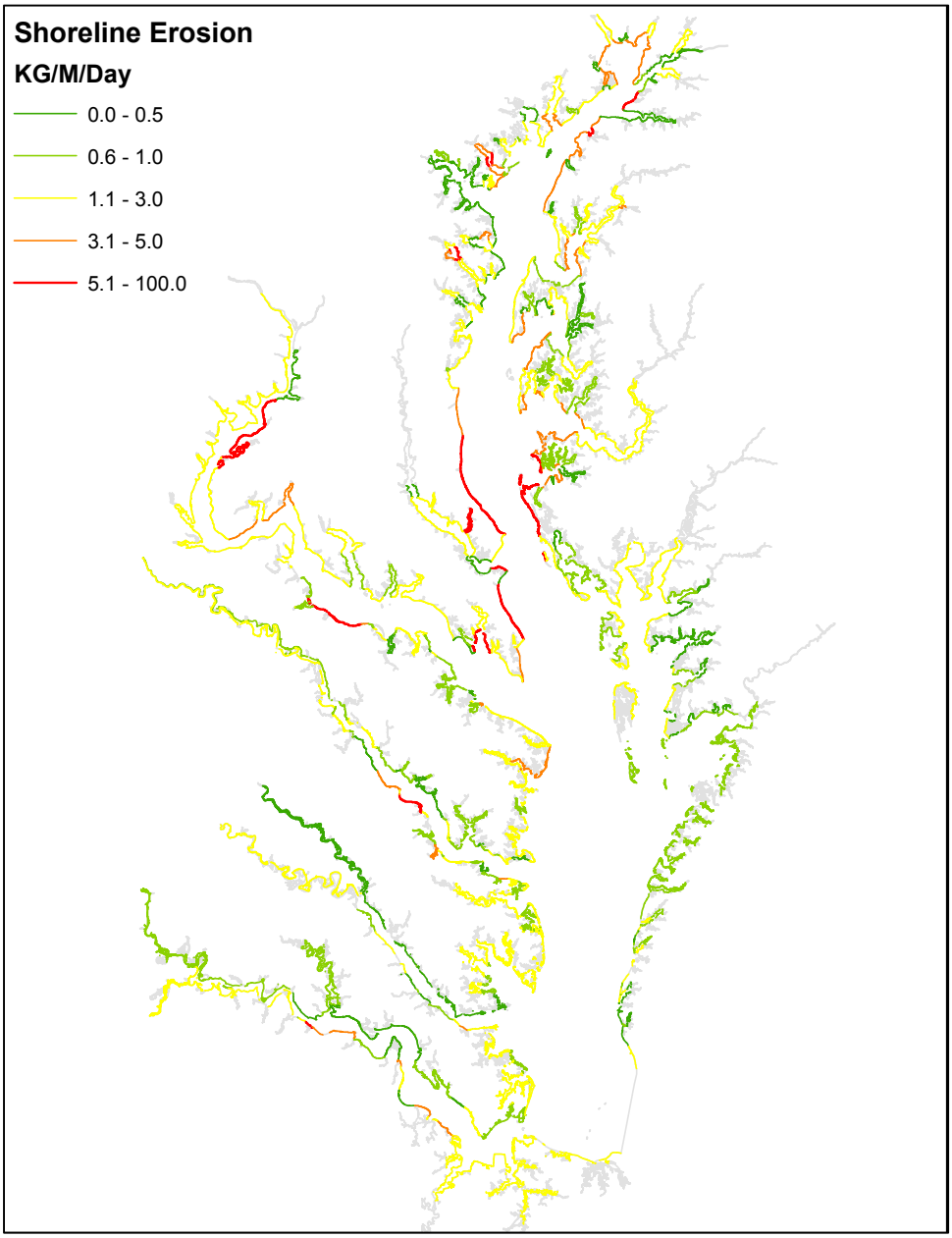

Table 5-1. Summary of Shoreline Erosion Loads to Chesapeake Bay (*Source*: Halka and Hopkins 2006)

Unit	Maryland	Virginia
Total Length, m	2,912,000	4,060,000
Unprotected Length, m	1,993,000	3,276,000
Percent Protected	32	19
Loading, metric ton yr^{-1}	2,425,000	1,500,000
Fines	1,331,000	506,000
Coarse	1,018,000	994,000
Organic	76,000	-
Loading, kg m^{-1} d^{-1}	2.28	1.01
Fines	1.25	0.34
Coarse	0.96	0.67
Organic	0.07	0.00

5.2 Mapping Shoreline Loads to the 2017 Model

The shoreline erosion study resulted in decadal-average mass erosion rates per unit shoreline length throughout the Bay system. For some regions with complete information, rates were available on the spatial scale of shoreline structures. For other regions, necessary information was lacking (Figure 5-3 and Figure 5-4) and uniform erosion rates were employed for kilometers of shoreline length. The Chesapeake Bay Program (CBP) geographic information system (GIS) team merged three key pieces of information: mass erosion rates, shoreline length, and the Water Quality and Sediment Transport Model (WQSTM) computational grid. Shoreline length was assigned to each cell adjoining the shore (2,928 cells), and the mass loading to each cell was computed. That information was supplied to the WQSTM team in the original categories employed by the developers: coarse material, fine material, and organic material. The modelers converted the loads to model units, kg d^{-1}, and mapped the loads into WQSTM state variables: fine clay, clay, silt, and sand.

Figure 5-3. Maryland shoreline data with no small creeks or upper headwaters and only 30% of Maryland shoreline surveyed (*Source*: Halka and Hopkins 2006).

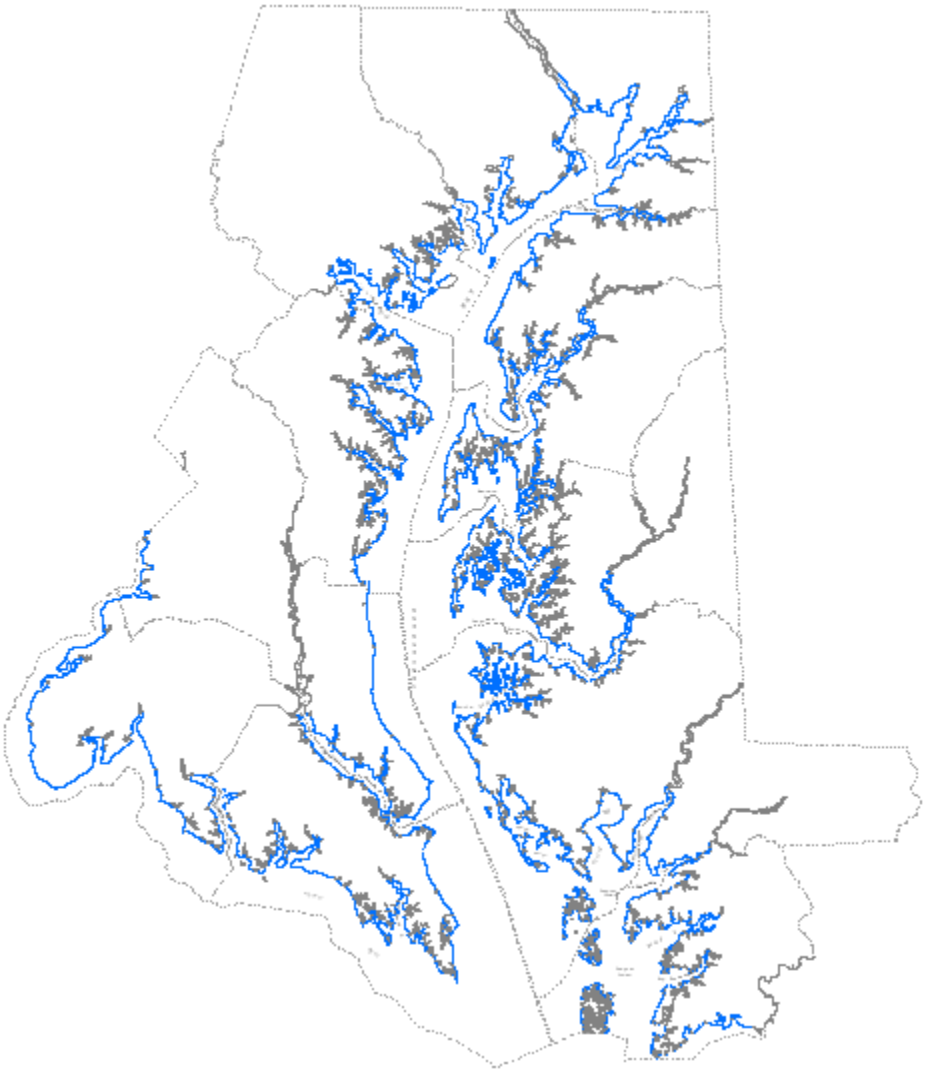

Figure 5-4. Virginia erosion data available from 1992 Bank Erosion Study, which ends at Westmoreland County on the Potomac. Headwaters of Potomac, Rappahannock, York, and James rivers missing (*Sources*: Halka and Hopkins 2006; Hardaway et al. 1992).

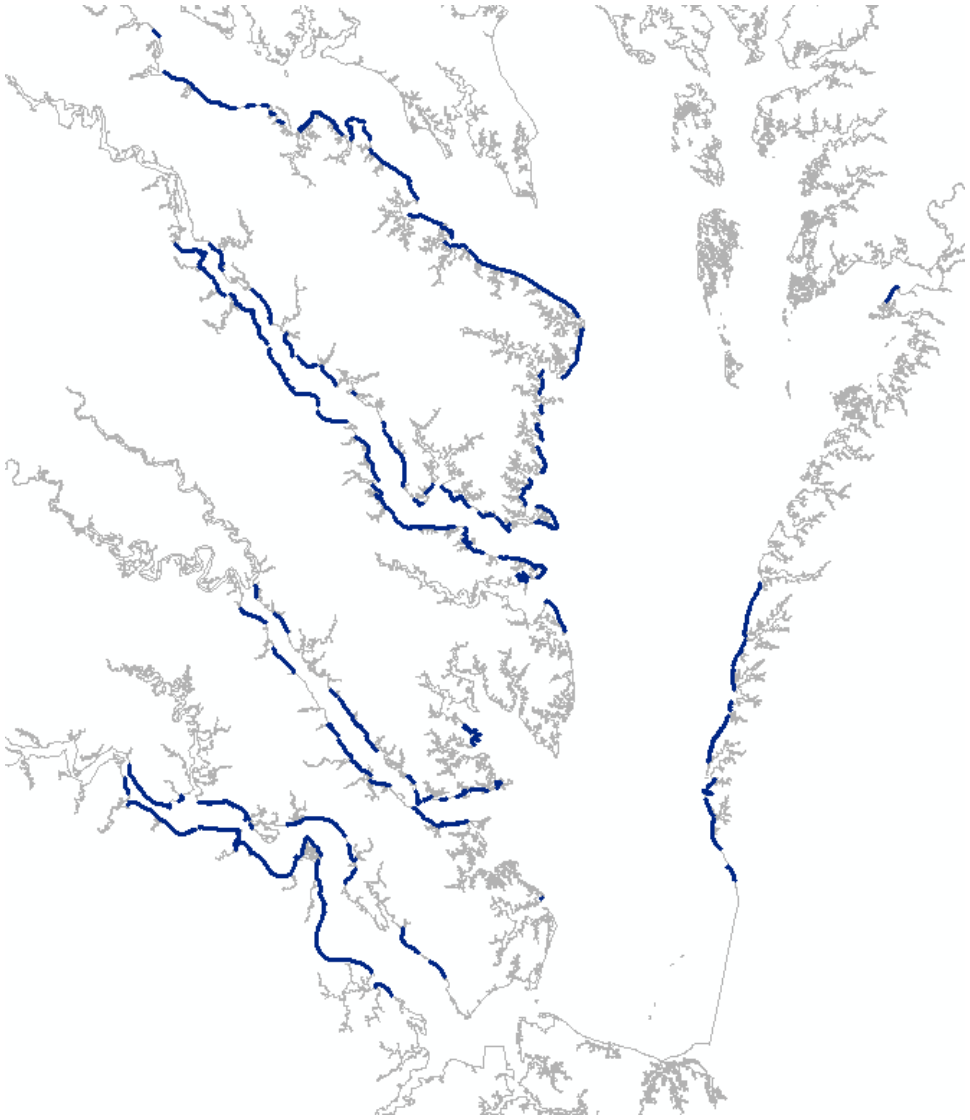

5.3 Shoreline Nutrient Loads

The nutrient content attributed to eroded sediments was specified by the CBP: 0.29 mg N g^{-1} solids and 0.205 mg P g^{-1} solids. Using these values, the total nitrogen and total phosphorus shoreline erosion loads to the Bay are readily computed (Table 5-2). Comparing them to other watershed loads indicates the contribution of shoreline erosion to the Bay nitrogen budget is minor: less than 1 percent of the total watershed load. Total phosphorus loading from shoreline erosion is comparable in magnitude to alternate sources and comprises 11 percent of the decadal average total load.

Table 5-2. Nonpoint Source Load Summary in metric ton d^{-1} 1991–2000[a]

Load Source	Total Nitrogen	Total Phosphorus	Total Suspended Solids
Susquehanna	191.2	7.32	3,761
Potomac	49.2	3.47	2,141
James	12.2	1.47	1,570
Other Tributaries	12.6	1.31	961
Below-Fall-Line	106.2	5.14	1,832
Shoreline Erosion	3.3	2.33	11,375

Note:
[a] Watershed loads are from the Phase 6 Beta 4 (Dec. 2016) version of the Watershed Model.

Little guidance exists for partitioning the total nutrients into model state variables. The nitrogen content of sediments must be mapped into labile, refractory, and slow refractory organic particles. Sediment phosphorus must be mapped into particulate inorganic form as well as into the three organic classes. Initial model sensitivity runs indicated the model could not withstand an 11-percent increase in available phosphorus without deviating significantly from observed conditions. Those model experiments suggested the shoreline nutrient loads must be largely nonreactive. A second interpretation of the model experiments might be that previously the reactivity of loads from alternate sources was overestimated so that additional reactive material from shoreline erosion could not be accommodated. Likely both interpretations contain a grain of truth.

Subsequent model experiments were performed that kept the total reactive nutrient load constant. Reactive loads from alternate sources were reduced to compensate for newly introduced reactive loads from shoreline erosion. The final fractionation of shoreline erosion loads was:

- 14 percent of total phosphorus in particulate inorganic form (Ibison et al. 1990).
- 20 percent of total nitrogen and remaining phosphorus in refractory particulate organic form.
- 80 percent of total nitrogen and remaining phosphorus in slow refractory particulate organic form.

5.4 Acknowledgements

Jeff Halka, of the Maryland Department of Natural Resources–Maryland Geological Survey, led the team that computed loads from bank and marsh erosion. Kate Hopkins, of the University of Maryland and the US Environmental Protection Agency Chesapeake Bay Program, performed the GIS operations. Scott Hardaway, of the Virginia Institute of Marine Science, provided invaluable assistance in computing shoreline erosion loads in the Virginia portion of the Bay.

5.5 References

Cerco, C., and T. Cole. 1993. Three-dimensional eutrophication model of Chesapeake Bay. *Journal of Environmental Engineering* 119(6):1006–1025.

Cerco, C., and M. Noel. 2004. *The 2002 Chesapeake Bay Eutrophication Model*. EPA 903-R-04-004. US Environmental Protection Agency, Chesapeake Bay Program Office, Annapolis, MD. https://nepis.epa.gov/Exe/ZyPURL.cgi?Dockey=P1003SK2.txt.

Cerco, C., S.-C., Kim, and M. Noel. 2010. *The 2010 Chesapeake Bay Eutrophication Model*. US Environmental Protection Agency, Chesapeake Bay Program Office, Annapolis, MD. http://www.chesapeakebay.net/publications/title/the_2010_chesapeake_bay_eutrophication_model1.

Drescher, S., and B. Stack. 2015. *Recommendations of the Expert Panel to Define Removal Rates for Shoreline Management Projects*. Chesapeake Bay Partnership, Annapolis, MD. http://www.chesapeakebay.net/documents/Shoreline_Management_Protocols_Final_Approved_07132015-WQGIT-approved.pdf.

Hennessee, L., K. Offerman, and J. Halka. 2006. *Suspended Sediment Load Contributed by Shore Erosion in Chesapeake Bay, Maryland*. Coastal and Estuarine Geology File Report No. 2006-03. Maryland Geological Survey, Baltimore, MD.

Halka, J., and K. Hopkins. 2006. Final WQM Shoreline Report. PowerPoint presentation to Chesapeake Bay Program Modeling and Research Subcommittee, Annapolis, MD. Available from Jeff Halka, Maryland Geological Survey, JHalka@dnr.state.md.us.

Hardaway, S., G. Thomas, J. Glover, J. Smithson, M. Berman, and A. Kenne. 1992. Bank Erosion Study. SRAMSOE 391. Virginia Institute of Marine Science, Gloucester Point, VA.

Ibison, N., C. Frye, J. Frye, C. Hill, and N. Berger. 1990. *Sediment and Nutrient Contributions of Selected Eroding Banks of the Chesapeake Bay Estuarine System*. Division of Soil and Water Conservation, Shoreline Programs Bureau, Gloucester Point, VA.

USACE (US Army Corps of Engineers). 1990. *Chesapeake Bay Shoreline Erosion Study*. Feasibility Report. US Corps of Engineers, Baltimore District, Baltimore, MD.

6 Linking in the Loads

Loads input to the Water Quality and Sediment Transport Model (WQSTM) come from a variety of sources and are reported in multiple forms. The loads must be linked or mapped to specific WQSTM state variables. The linkage process has evolved as the WQSTM has evolved and as the sources of loads have changed. The current linkage process combines methods developed for this phase of the study along with methods inherited from earlier phases. This chapter describes the methods employed to link to loads from the watershed, from point sources, from shoreline erosion, and from direct atmospheric deposition.

6.1 Watershed Loads

Watershed loads from the Phase 6 version of the Chesapeake Bay Program (CBP) Watershed Model (WSM) were provided in late November 2017. The WSM output is provided in annual files in which daily loads and flows are routed to WQSTM surface cells around the perimeter of the Bay and its tributaries. Several WSM state variables have direct equivalents in the WQSTM while others require conversion to WQSTM state variables (Table 6-1). Two differences in the models require attention. The first is the conversion of the general WSM organic nitrogen and organic phosphorus state variables to the detailed suite of WQSTM variables. The second is the provision of watershed organic carbon loads in the absence of a WSM state variable corresponding to the WQSTM organic carbon variable suite. The linkage process allows for individual specification of the parameters involved in the linkage at seven river inputs: Susquehanna, Patuxent, Potomac, Rappahannock, York, James, and Choptank. The remaining distributed loads are converted with one more available parameter set.

6.1.1 Organic Nitrogen

The steps required to map WSM organic nitrogen into WQSTM variables (Figure 6-1) are as follows:

1. Remove the amount of nitrogen associated with phytoplankton loads.
2. Split organic nitrogen into particulate and dissolved forms.
3. Split particulate organic nitrogen into three reactive classes: labile particulate organic nitrogen, refractory particulate organic nitrogen, and slow refractory particulate organic nitrogen.

Table 6-1. Constituents in Watershed and Water Quality Models

WSM Variable	Maps to	WQSTM Variable
Ammonium	----->	Ammonium
Nitrate	----->	Nitrate
Organic nitrogen	----->	• Dissolved organic nitrogen • Labile particulate organic nitrogen • Refractory particulate organic nitrogen • Slow refractory particulate organic nitrogen
Dissolved phosphate	----->	Phosphate
Organic phosphorus plus particulate inorganic phosphorus	----->	• Dissolved organic phosphorus • Particulate inorganic phosphorus • Labile particulate organic phosphorus • Refractory particulate organic phosphorus • Slow refractory particulate organic phosphorus

Figure 6-1. Routing WSM organic nitrogen into WQSTM state variables.

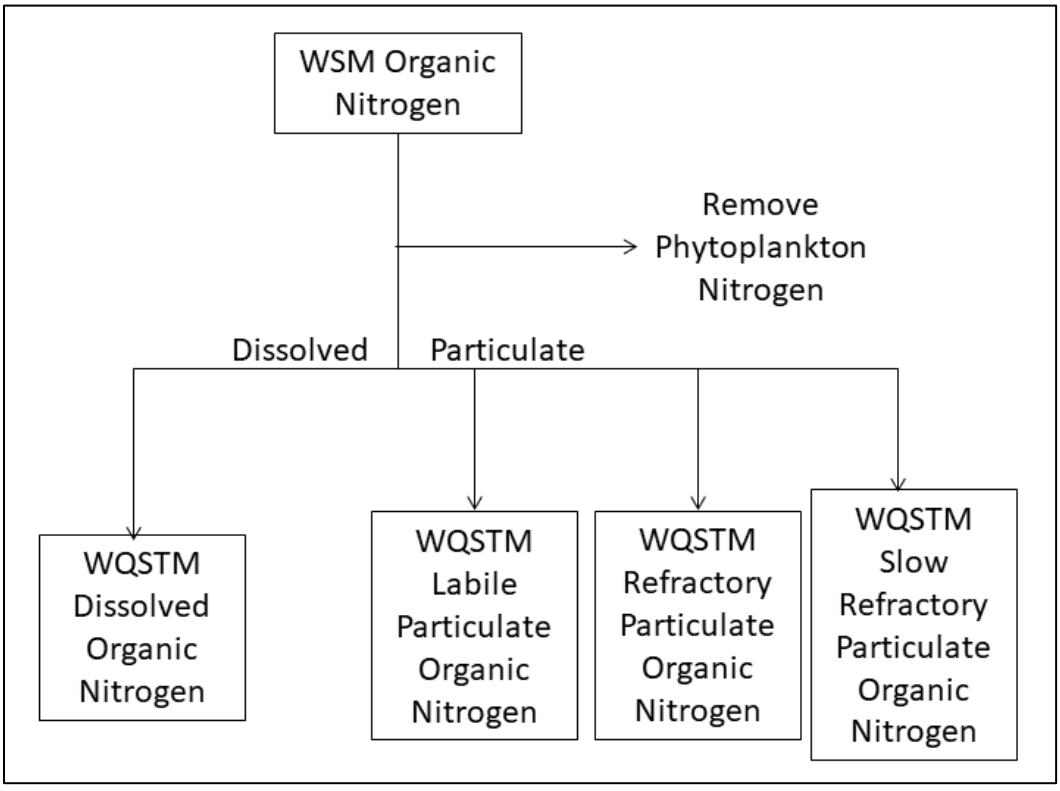

Phytoplankton nitrogen is represented implicitly in the WQSTM. That is, the nitrogen is represented as a fraction of phytoplankton carbon (see Chapter 2, *Water Quality Model Formulation*). The 2017 version of the WQSTM employs WSM chlorophyll to compute phytoplankton entering tributaries from the watershed. To load the WQSTM with precisely the quantity of nitrogen provided by the WSM, the implicit nitrogen load incorporated into phytoplankton is removed from the explicit organic nitrogen load provided by the WSM.

The split of organic nitrogen into particulate and dissolved organic form is difficult to quantify definitively. Some uncertainty results from the multiple databases and analyses available to inform the splits. Earlier analyses detected an influence of river flow (Cerco and Cole 1994; Cerco and Noel 2004). For this phase of the study, we examined particulate and dissolved organic nitrogen at the first tidal monitoring station downstream of each river inflow. Our assumption was that the observations at those stations are representative of the material entering from the watershed. This approach ensured consistency between the methodologies used to determine the splits and the data used to calibrate and validate the WQSTM. Little or no influence of flow was evident in the database (Figure 6-2 and Figure 6-3). Splits were determined from the median fractions of particulate and dissolved organic nitrogen at each location (Table 6-2).

Figure 6-2. Dissolved organic nitrogen concentration at Station CB1.1, below Susquehanna River inflow. Note absence of relationship to flow.

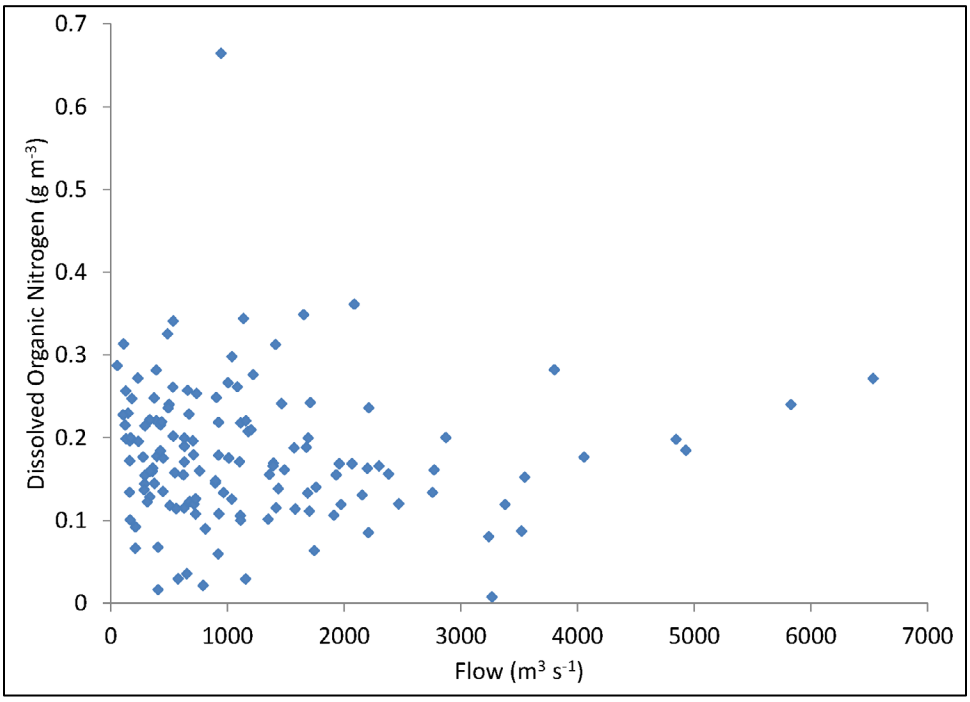

Figure 6-3. Dissolved organic nitrogen concentration at Station TF2.1, below Potomac River inflow. Note absence of relationship to flow.

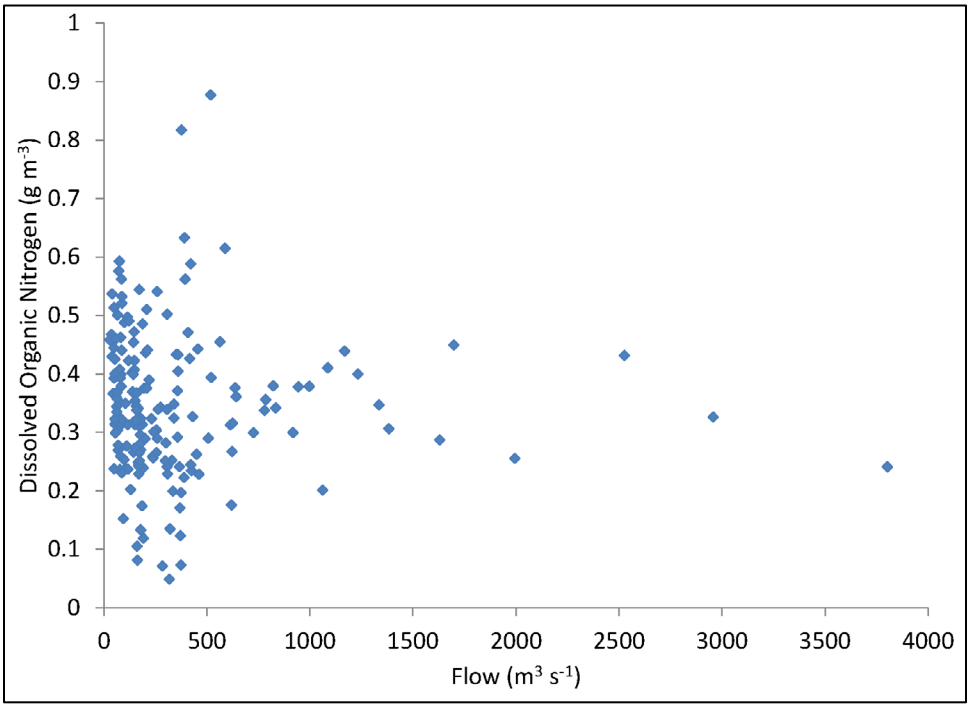

Table 6-2. Routing WSM Organics into WQSTM State Variables

River	Fraction Particulate, Nitrogen and Carbon	Fraction Particulate, Phosphorus	Fraction Particulate Inorganic Phosphorus	Carbon-to-Nitrogen Ratio
Susquehanna	0.4	0.65	0.58	8
Patuxent	0.26	0.692	0.6	6
Potomac	0.26	0.65	0.47	8
Rappahannock	0.36	0.772	0.6	8
York	0.21	0.516	0.6	8
James	0.21	0.61	0.6	8
Choptank	0.33	0.645	0.7	8
Other	0.3	0.65	0.6	8

Splits of particulate organic nitrogen into reactive classes were obtained from an ongoing study of the Conowingo Reservoir, Maryland (Zhang 2017). The study estimated the splits through a mass balance analysis of solids entering and leaving the reservoir and of sediment-water nutrient fluxes within the reservoir. For the Susquehanna River, the reactive splits are influenced by flow above 6,500 $m^3\ s^{-1}$. The relationships used to determine the reactive classes are of the form shown in equation 1, equation 2, and equation 3:

$$Fg1 = FLPON{-}\propto 1 \cdot (Q - 6500) \quad (1)$$

$$Fg2 = FRPON{-}\propto 2 \cdot (Q - 6500) \quad (2)$$

$$Fg3 - 1 - Fg1 - Fg2 \quad (3)$$

where:

$Fg1$ = labile fraction of particulate organic nitrogen (0 < Fg1 < 1)
$Fg2$ = refractory fraction of particulate organic nitrogen (0 < Fg2 < 1)
$Fg3$ = slow refractory fraction of particulate organic nitrogen (0 < Fg3 < 1)
$\alpha 1$ = Effect of flow more than 6,500 $m^3\ s^{-1}$ on Fg1 ($s\ m^{-3}$)
$\alpha 2$ = Effect of flow more than 6,500 $m^3\ s^{-1}$ on Fg2 ($s\ m^{-3}$)
Q = Flow at Conowingo Reservoir outfall ($m^3\ s^{-1}$)

The α1 and α2 parameters have nonzero values only when flow exceeds 6,500 $m^3\ s^{-1}$ (Table 6-3). In the absence of information, the values of FLPON and FRPON determined for the Susquehanna River are transferred to the other river inputs without flow effects.

Table 6-3. Calculation of Reactive Fractions of Watershed Particles

Parameter	Nitrogen	Phosphorus	Carbon
Fraction labile	0.15	0.3	0.15
Fraction refractory	0.45	0.4	0.35
α1	7.49×10^{-6}	1.091×10^{-5}	7.64×10^{-6}
α2	1.638×10^{-5}	9.49×10^{-6}	1.33×10^{-5}

6.1.2 Organic and Particulate Inorganic Phosphorus

Routing WSM organic phosphorus into WQSTM state variables is similar to routing organic nitrogen into the variables. The presence of particulate inorganic phosphorus (PIP), however, requires an additional step. Both the WSM and the WQSTM include PIP state variables but the nature of the variables differs. PIP in the WSM is loosely sorbed to sediment particles. The amount sorbed is determined by a linear partition coefficient. Reversible exchange is possible between dissolved and particulate form. In the WQSTM, PIP is an independent form of phosphorus that potentially decays to dissolved inorganic form at a first-order rate. In view of the differences between the two PIP variables, WSM PIP is first combined with organic phosphorus. The combination is then mapped to WQSTM variables (Figure 6-4).

The steps necessary to route WSM organic phosphorus and PIP into WQSTM state variables are as follows:

1. Combine WSM organic phosphorus and PIP.
2. Remove the amount of phosphorus associated with phytoplankton loads.
3. Split the combination into particulate and dissolved forms.
4. Split particulate phosphorus into organic and inorganic forms.
5. Split particulate organic phosphorus into three reactive classes: labile particulate organic phosphorus, refractory particulate organic phosphorus, and slow refractory particulate organic phosphorus.

Figure 6-4. Routing WSM organic phosphorus and PIP into WQSTM state variables.

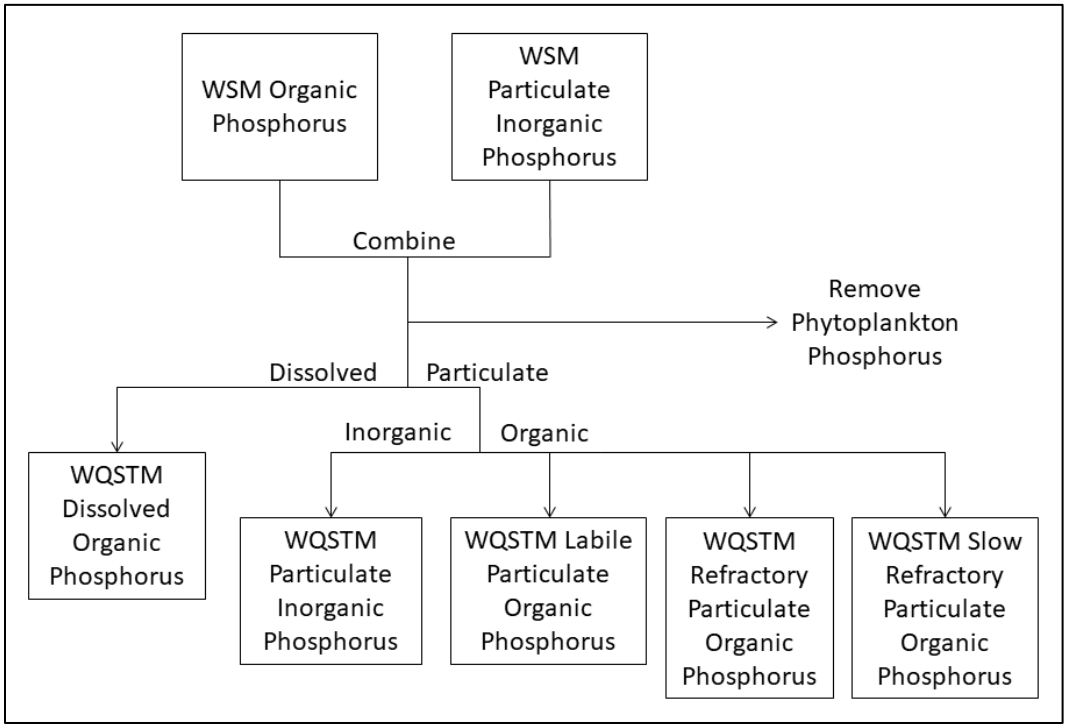

The reasoning behind the removal of algal phosphorus is analogous to the removal of algal nitrogen. The splits between dissolved and particulate phosphorus are determined for individual river inflows based on median fractions observed immediately below the river inputs (Table 6-2). Observations collected at the river inputs indicate PIP represents a consistent fraction of particulate phosphorus (Figure 6-5 and Figure 6-6). Fractions based on observations (Table 6-2) were used to split particulate phosphorus into organic and inorganic forms at each river inflow location. Particulate organic phosphorus was split into reactive classes using relationships analogous to equations 1–3. Parameters appropriate to phosphorus shown in Table 6-3 were obtained from the same study of the Conowingo Reservoir from which the nitrogen parameters were obtained (Zhang 2017).

6.1.3 Organic Carbon

The WSM contains no state variable corresponding to the WQSTM organic carbon suite. Watershed organic carbon loads are derived by ratio to organic nitrogen. The ratios shown in Table 6-2 were derived from observations at the river inputs and are adapted for the current model from the 2010 Total Maximum Daily Load model (Cerco et al. 2010). Distributing watershed organic carbon into WQSTM state variables is similar to the process for distributing organic nitrogen. First, organic carbon is split into dissolved and particulate forms. Then the particulate organic carbon is routed into three reaction classes. The splits between particulate and dissolved forms of carbon are the same as they are for organic nitrogen. Routing particulate organic carbon into reaction classes is achieved using relationships analogous to equations 1–3. Parameters appropriate to carbon (Table 6-3) were obtained from the Conowingo Reservoir study that provided the nitrogen parameters (Zhang 2017).

Figure 6-5. PIP vs. particulate phosphorus at Susquehanna River fall line. PIP is a consistent fraction of particulate phosphorus.

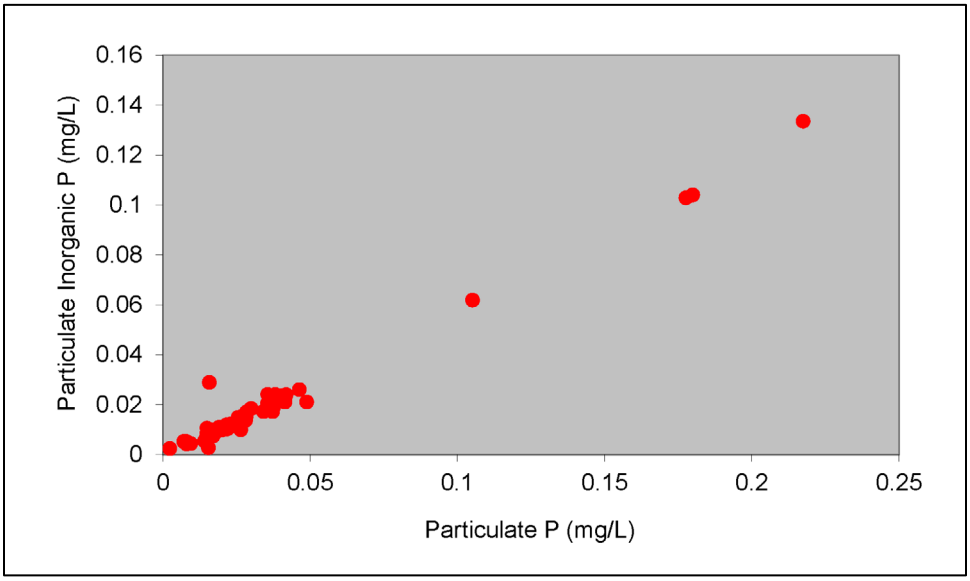

Figure 6-6. PIP vs. particulate phosphorus at Potomac River fall line. PIP is a consistent fraction of particulate phosphorus.

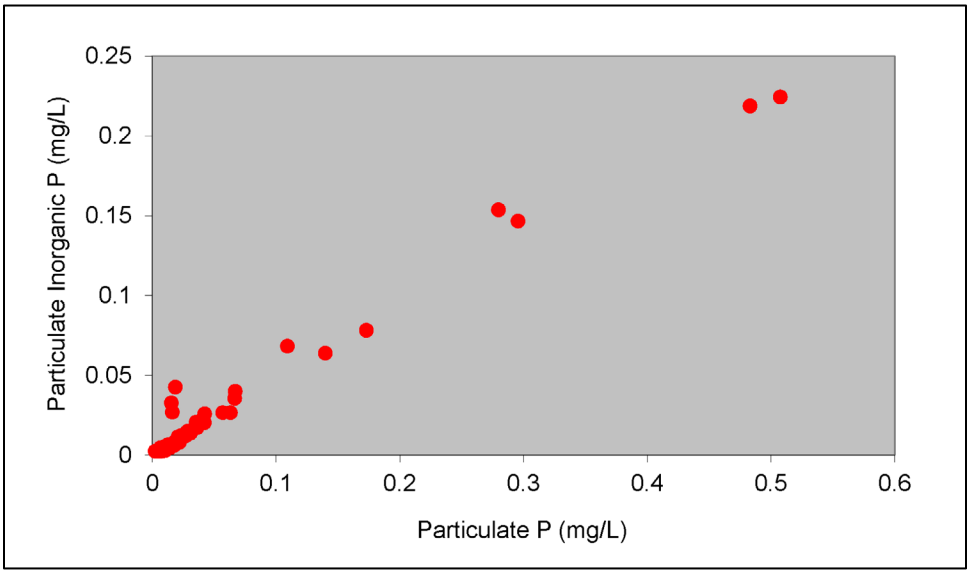

6.2 Point-Source Loads

The WQSTM considers loads from municipal and industrial sources located along the tidal shoreline of the Bay and its tributaries. Loads from point sources above the fall lines of major tributaries are included in the watershed loads. Point-source loads are provided by the CBP in a format similar to watershed loads. They are provided in annual files that contain daily loads routed to WQSTM surface cells. Constituents in the files are similar to outputs from the WSM (Table 6-1). Routing of point-source loads into WQSTM state variables follows a process similar to the routing of WSM loads. Point-source loads of organic nitrogen and phosphorus must be routed to the detailed suite of WQSTM state variables. Since no point-source carbon loads are provided, they must be derived from available information.

The data available to guide mapping of point-source loads into WQSTM state variables is sparse. Most values employed in the 2017 model (Table 6-4) are adopted from the 2002 version (Cerco and Noel 2004). Those values were based on sampling of Virginia point sources and on preliminary experiments to determine reactivity. The determination of point-source carbon load has been revised from the 2002 model, however, and is now based on the ratio to biological oxygen demand over 5 days (BOD5) rather than nitrogen load.

Table 6-4. Routing Point-Source Loads into WQSTM Variables

	Fraction Dissolved	Fraction Labile Particles	Fraction Refractory Particles	Fraction Slow Refractory Particles
Organic N	0.5	0.15	0.28	0.07
Organic P	0.4	0.07	0.42	0.11
Organic C	0.8	0.15	0.04	0.01

Note: C:BOD5 ratio = 1.0.

6.3 Shoreline Erosion

Nutrient loads from shoreline erosion were initially calculated and implemented by the WQSTM team. Subsequently, those loads were incorporated into the WSM. Incorporation into the WSM facilitated implementation of credits for management actions to control shoreline erosion. Shoreline erosion loads of solids and nutrients were provided by the CBP as annual files containing daily loads routed to WQSTM surface cells. Daily loads were assigned in proportion to runoff. Care was taken to ensure annual loads to each WQSTM cell equaled the loads computed using long-term average shoreline recession rates (Chapter 5, *Shoreline Erosion*).

Following precedent for distributed and point-source loads, we computed carbon loads from shoreline erosion from available information since organic carbon is not a WSM variable. The carbon fraction of shoreline solids, 4.35 mg C g^{-1} solids, was taken as the mean of values reported by Ibison et al. (1990). Daily loads were computed as the product of carbon fraction and daily solids loads. Organic carbon was split into 20 percent refractory particulate and 80 percent slow refractory particulate, consistent with values employed for nitrogen and phosphorus (Chapter 5, *Shoreline Erosion*).

6.4 Atmospheric Loads

The WQSTM incorporates atmospheric nitrogen and phosphorus loads into the water surface. Atmospheric loads to the land surface are incorporated into the watershed loads. Atmospheric loads were provided by the CBP in annual files that contained daily loads to WQSTM surface cells. Loads included ammonium, nitrate, organic nitrogen, phosphate, and organic phosphorus. Organic nitrogen and phosphorus loads were split into 20 percent refractory particulate and 80 percent slow refractory particulate, consistent with shoreline erosion loads.

6.5 References

Cerco, C.F., and T.M. Cole. 1994. *Three-Dimensional Eutrophication Model of Chesapeake Bay*. Technical Report EL-94-4. US Army Engineer Waterways Experiment Station, Vicksburg, MS.

Cerco, C., and M. Noel. 2004. *The 2002 Chesapeake Bay Eutrophication Model*. EPA 903-R-04-004. US Environmental Protection Agency, Chesapeake Bay Program Office, Annapolis, MD. https://nepis.epa.gov/Exe/ZyPURL.cgi?Dockey=P1003SK2.txt.

Cerco, C., S.-C. Kim, and M. Noel. 2010. *The 2010 Chesapeake Bay Eutrophication Model*. US Environmental Protection Agency, Chesapeake Bay Program Office, Annapolis, MD. http://www.chesapeakebay.net/publications/title/the_2010_chesapeake_bay_eutrophication_model1.

Ibison, N., C. Frye, J. Frye, C. Hill, and N. Berger. 1990. *Sediment and Nutrient Contributions of Selected Eroding Banks of the Chesapeake Bay Estuarine System*. Virginia Department of Conservation and Recreation, Division of Soil and Water Conservation, Shoreline Programs Bureau, Gloucester Point, VA.

Zhang, Q. 2017. Fractions of G1/G2/G3 Organics Scoured from the Conowingo Reservoir. PowerPoint presentation. Chesapeake Bay Program Modeling Workgroup April 2017 Quarterly Review, Annapolis, MD. https://www.chesapeakebay.net/channel_files/24719/2017-04-04_conowingo_hdr_g1g2g3_2.pdf.

7 Oysters

Bivalve filter feeders were introduced in the Chesapeake Bay Model as part of the Tributary Refinements phase (Cerco et al. 2002). The initial representation included two freshwater species, *Corbicula flumenea* and *Rangia cuneata*, and one saltwater species, *Macoma balthica*. Subsequently, native oysters, *Crassostrea virginica*, were substituted for *Macoma* to investigate the potential impact of a tenfold increase in native oyster population (Cerco and Noel 2007). Oysters were included in the 2010 model version but received limited attention. Their activity was not explicitly incorporated into the 2010 Total Maximum Daily Load. Oysters are the subject of renewed attention because of increases in the natural population in sanctuaries and the tremendous growth of the aquaculture industry. Nutrient removal credits associated with oyster restoration and with aquaculture will be included in future nutrient management plans. Renewed management attention demands a corresponding renewal of the oyster module in the 2017 Chesapeake Bay Water Quality and Sediment Transport Model (WQSTM). Representation of the freshwater bivalves is unchanged from the previous model version (Cerco and Noel 2010).

7.1 Model Basics

The revised oyster module considers three populations:

- Natural populations on reefs and subject to harvest
- Natural populations in sanctuaries and not subject to harvest
- Aquaculture operations

Application of the model to each population requires resolution of the following issues:

- Location
- Biomass
- Model parameterization

7.1.1 Mass-Balance Equation

The fundamental mass-balance equation for the filter feeders is shown in equation 1:

$$\frac{dO}{dt} = \propto \cdot Fr \cdot POC \cdot IF \cdot (1 - RF) \cdot O - BM \cdot O - \beta \cdot O - H \cdot O \qquad (1)$$

where:

O = oyster density (g C m^{-2})
α = assimilation efficiency ($0 < \alpha < 1$)
Fr = filtration rate (m^3 g^{-1} C d^{-1})
POC = particulate organic carbon (g m^{-3})
IF = ingestion fraction ($0 < IF < 1$)
RF = respiration fraction ($0 < RF < 1$)
BM = basal metabolism (d^{-1})
β = mortality (d^{-1})
H = harvest rate (d^{-1})

Parameter values in the governing equation are largely as described by Cerco and Noel (2007).

Oyster reefs occupy small fractions of model computational cells, which average 1 km by 1 km in extent. The "foraging arena" concept was introduced in the model to represent the limited encounters between predators and prey induced by the small fraction of each computational cell occupied by reefs (Cerco and Noel 2010). We found, however, that the computed biomass of oysters, in g C, was excessive when the computed density, in g C m^{-2}, was multiplied by the cell area. We also found that the potential impact of oysters on prey was exaggerated despite the foraging arena. Consequently, the concept of "coverage" is introduced in the WQSTM. Coverage is the fraction of cell area occupied by oyster reefs. Biomass is computed as the product of density, cell area, and fraction of cell covered by reefs. Corrections for coverage are also introduced into the mass-balance equations for mass transfers between oysters and their surroundings.

7.1.2 Modifications for Aquaculture

Oyster density in each cell, as computed by equation 1, varies spatially and temporally depending on local conditions. Aquaculture operations, including year-round planting and harvesting, tend to reduce the intraannual and interannual oscillations that occur in natural oyster beds. The spatial distribution of oyster biomass depends on the location of aquaculture operations. Water quality managers wish to explore the impacts of varying levels of aquaculture activity, which has led to a model representation in which oyster density in each cell is a specified constant value. Setting $dO/dt = 0$ in equation 1 leads to the representation in equation 2:

$$IF = \frac{BM+\beta+H}{\alpha \cdot Fr \cdot POC \cdot (1-RF)} \quad (2)$$

The ingestion fraction becomes a variable rather than a parameter, as in equation 1. Employment of the variable ingestion fraction in the balance of the model formulations results in a constant oyster density, which is specified at model initiation.

In the event the rate of biomass loss (represented in the numerator on the right-hand side of equation 1) exceeds food intake (represented in the denominator), the computed ingestion fraction will exceed unity. That situation is physically impossible, although the model will operate under those conditions. Consistent computation of an ingestion fraction greater than unity indicates that oysters cannot persist at the specified density under modelled conditions. Either sufficient food resources are unavailable or losses from respiration, mortality, and harvest exceed sustainable levels.

7.2 Location

7.2.1 Natural Population

More than 8,000 oyster bars were located as part of a 2008 study of oyster restoration alternatives (MDNR 2008). Bar locations were mapped to the model grid and consolidated by cell (Figure 7-1). The total bar area in each cell was employed to compute coverage (see section 7.1, *Model Basics*). Oyster bars occurred in 2,068 of the 11,064 model surface cells. Coverage for those 2,068 cells ranged from less than 0.01 percent to 100 percent. The median coverage was 5 percent and was less than 10 percent for the vast majority of cells with oyster bars.

Figure 7-1. Location of natural oyster bars mapped to model grid.

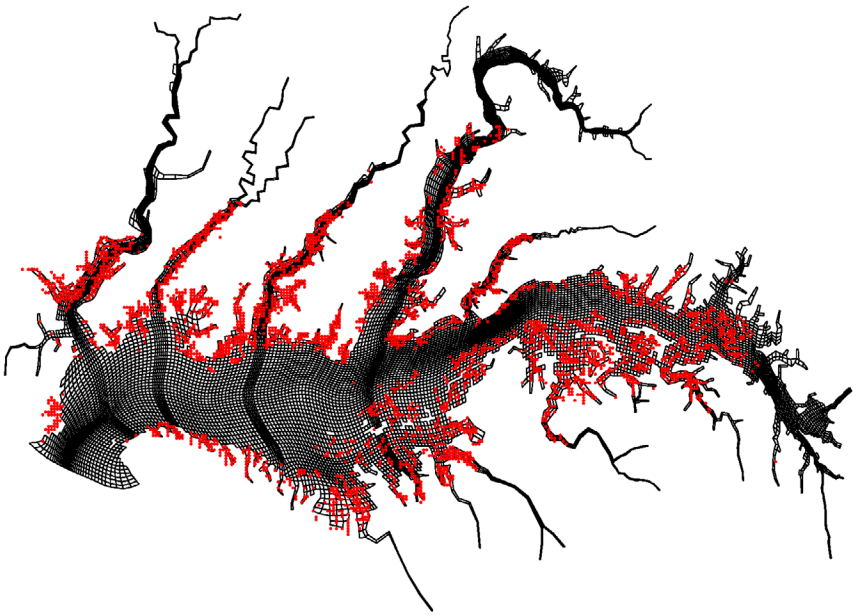

7.2.2 Sanctuaries

Locations of oyster sanctuaries in Maryland were obtained by the project sponsor and mapped to the model grid. Considerable overlap occurred between the location of reefs determined in 2008 and the present location of sanctuaries. In the event a natural bar and a sanctuary were coincident, we assumed the bar is presently a sanctuary.

7.2.3 Aquaculture

Locating aquaculture operations presented a considerable challenge. Although various state agencies have that information, they cannot release anything considered proprietary. For the state of Maryland, we were provided with the aquaculture harvest totals by county for the years 2014–2016 (Julie Reichert-Nguyen, Oyster Recovery Partnership, personal communication, December 21, 2016). We created a map of potential model aquaculture cells within those counties by assuming aquaculture is restricted to water less than 12 feet deep and with salinity greater than 7 parts per thousand (ppt) (Figure 7-2). The depth constraint was based on assumptions regarding accessibility. The salinity constraint was determined by Cerco and Noel (2007) as the minimum required for a healthy natural population.

A geographic information system file was available that mapped private lease areas in Virginia. That map was superimposed on the model grid to indicate cells that contain leases (Figure 7-3). Potential aquaculture cells were then limited to lease areas less than 12 feet deep and with greater than 7 ppt salinity.

Figure 7-2. Potential aquaculture cells in Maryland. Criteria are depth ≤ 12 feet and salinity > 7 ppt.

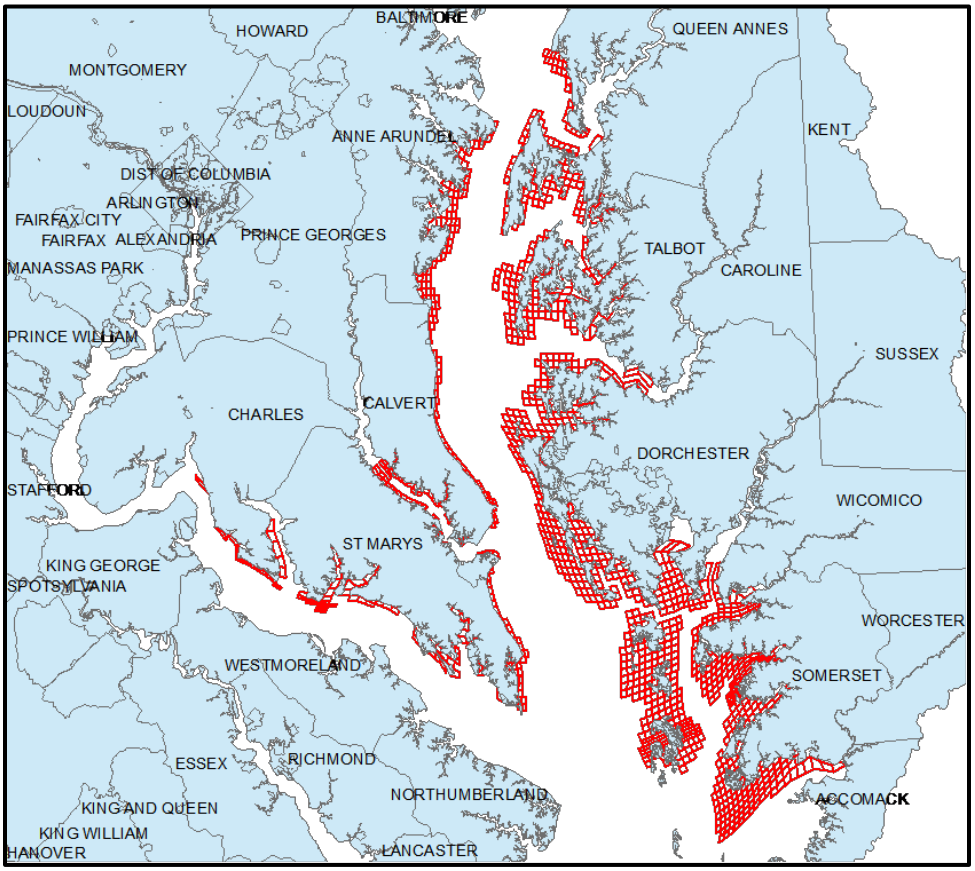

Figure 7-3. Potential aquaculture cells in Virginia. Cells shown include private lease areas and meet the criteria depth ≤ 12 feet and salinity > 7 ppt.

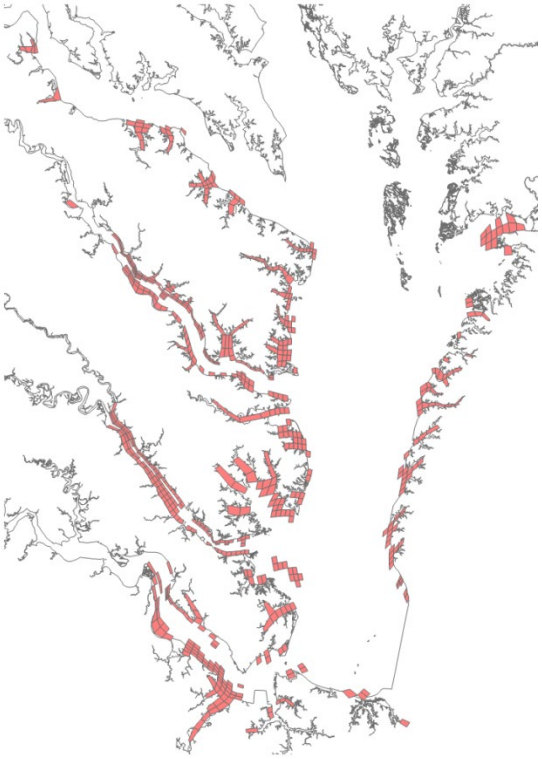

As noted in section 7.1, *Model Basics*, it is possible to assign aquaculture to a cell that cannot support the specified level of activity. We minimized this possibility through a "self-locating" process. An exploratory model run was conducted in which oysters were assigned to all potential aquaculture cells. They were modelled as a natural population that was allowed to thrive or perish according to ambient conditions. We restricted aquaculture cells to those that supported a density of 10 mg C m^{-2} (Figure 7-4).

Figure 7-4. Self-location of aquaculture cells. Aquaculture is restricted to areas capable of supporting a density of 10 mg C m^{-2}.

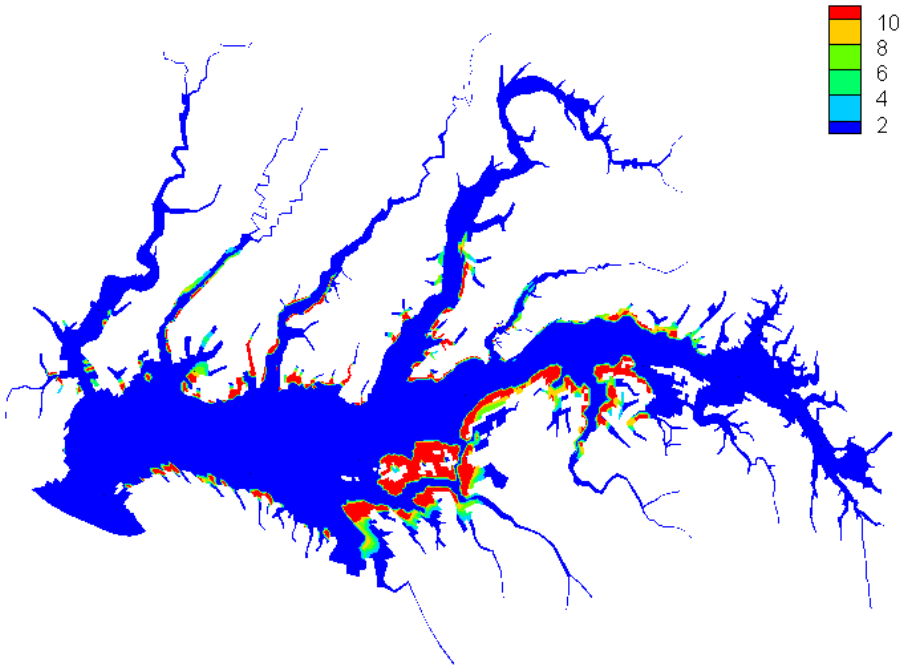

7.3 Biomass

7.3.1 Natural Population and Sanctuaries

The primary data source for the population on oyster bars is the website for the Chesapeake Bay Oyster Population Estimate (CBOPE) project, which is maintained by the Virginia Institute of Marine Science (VIMS) (VIMS 2017). The CBOPE project was conducted to monitor progress towards a tenfold increase in Chesapeake Bay oyster population called for in the Chesapeake 2000 Agreement. The site reports various categories of standing stock and harvest for Virginia (1994–2008) and Maryland (1994–2002). The state totals are reported for various basins within each state in various years. Major population categories include the following:

- Fishery-Independent Data—Collected during annual patent tong surveys in Virginia and annual dredge surveys in Maryland.
- Fishery-Dependent Data–Public/Commercial—Based on annual oyster landings reported to the Virginia Marine Resources Commission (VMRC) and the Maryland Department of Natural Resources (MDNR).
- Fishery-Dependent Data–Private Fishery—Based on reports by private leaseholders to VMRC and MDNR.

The total population in each state was considered to be the sum of the fishery-independent data plus the amount removed in public and private landings (Table 7-1). For Virginia, the private landings were adjusted to remove aquaculture activities from 2005 onward. The landings, adjusted for aquaculture, were tracked separately to assist in parameter assignment of the harvest rate in equation 1.

Table 7-1. Reef Biomass and Harvest

Year	VA Biomass (kg DW)	VA Harvest (kg DW)	VA Harvested Fraction	MD Biomass (kg DW)	MD Harvest (kg DW)	MD Harvested Fraction
1994	512560	23548	0.046	411614	21614	0.053
1995	511522	7519	0.015	512930	51930	0.101
1996	681933	9923	0.015	561680	70680	0.126
1997	471609	8606	0.018	631470	68470	0.108
1998	581486	20475	0.035	721221	122221	0.169
1999	582623	9615	0.017	736000	147000	0.200
2000	657979	9753	0.015	720555	129555	0.180
2001	698260	13246	0.019	698568	138568	0.198
2002	561166	18215	0.032	184000	40000	0.217
2003	575272	9997	0.017			
2004	734962	33864	0.046			
2005	993351	71780	0.072			
2006	819680	37747	0.046			
2007	651726	29950	0.046			
2008	1039207	28039	0.027			

7.3.1.1 Assignment to Basins

CBOPE reporting by basins was sporadic and the state data could not be reliably split by basin over the reporting period. Based on alternative data sources, 13 basins were defined (Table 7-2). The Virginia basins were defined to coincide with harvest data provided by the VMRC (Jim Wesson, department head, Conservation and Replenishment, personal communication, December 30, 2016). The Virginia population was split into basins in proportion to the total public harvest taken in each basin. The Maryland basins were defined to coincide with a 1994–2006 population estimate (Greenhawk and O'Connell 2007). The Maryland population was split into basins according to the proportions in the estimate.

Table 7-2. Basin Fractions of Total Reef Biomass

VA Basin	Fraction	MD Basin	Fraction
Chesapeake	0.294	Chester	0.151
James	0.354	Eastern Bay	0.076
York	0.082	Choptank	0.118
Rappahannock	0.262	Little Choptank	0.026
Potomac	0.007	Tangier Sound	0.136
		Potomac	0.074
		Patuxent	0.037
		Chesapeake	0.371

7.3.2 Aquaculture

The aquaculture biomass was difficult to estimate because of the proprietary nature of the data on operations. In addition, necessary information was obtained through personal communication and sources were not always in agreement. The original source for Virginia aquaculture biomass was a summary of surveys conducted by VIMS (Hudson and Murray 2016). The surveys reflect the number of oysters sold through Virginia aquaculture operations for the years 2005–2015. The surveys risk underreporting the sales because of a lack of response from some operators. Alternatively, the surveys risk overestimating the sales since operations on the Atlantic side of the Delmarva peninsula are included. Nevertheless, the survey report is the primary citable source for Virginia aquaculture data.

The number of oysters sold was converted to dry tissue weight using the factor for market-size oysters of 2.1 g DW per oyster (Cerco and Noel 2007). Converting the harvest to standing stock required consideration of aquaculture practices and grow-out period from seed to harvest. Aquaculture practices can be broadly divided into “cage culture” and “bottom culture.” We were advised that roughly 80 percent of aquaculture in Virginia is conducted in cages and 20 percent is conducted on bottom. We were further advised that the grow-out period for cage culture is 2 years while the grow-out period for bottom culture is 3 years (Mike Parker, University of Maryland Extension, personal communication, February 16, 2017). Assuming linear growth and continuous planting and harvest, the standing stock of oysters in cages is 1.5 times the annual harvest. The standing stock of oysters on bottom is twice the annual harvest. Combining these factors indicates the biomass of aquaculture oysters in Virginia is 1.6 times the annual harvest (Table 7-3).

Table 7-3. Aquaculture Biomass and Harvest

Year	VA Biomass (kg DW)	VA Harvest (kg DW)	MD Biomass (kg DW)	MD Harvest (kg DW)
2005	3398	2124		
2006	11892	7433		
2007	16989	10618		
2008	25483	15927		
2009	32279	20174		
2010	56063	35039		
2011	79847	49904		
2012	93438	58399		
2013	103631	64770		
2014	134211	83882	40905	21529
2015	118921	74326	60612	31901
2016			64550	33974
2025	508032	317520	241315	127008

Note: Data for the year 2025 are projections employed in management scenarios as detailed in section 7.5.1.1, *Estimate of Aquaculture Activity through 2025*.

Data for Maryland aquaculture originated with the MDNR and was provided through the Oyster Recovery Partnership (Julie Reichert-Nguyen, Oyster Recovery Partnership, personal communication, December 21, 2016). The original data consisted of the number of bushels harvested for the years 2014–2016. Statewide totals as well as data for some counties were provided. Bushels were converted to number of oysters using the factor of 300 oysters per bushel provided along with the data. The number of oysters was subsequently converted to dry tissue weight using the factor of 2.1 g DW per oyster for market-size oysters (Cerco and Noel 2007). We were advised that, in Maryland, roughly 80 percent of aquaculture is conducted on the bottom while 20 percent is conducted in cages. Those proportions are the inverse of operations in Virginia. Using the grow-out periods quoted previously, the Maryland aquaculture standing stock is 1.9 times the annual harvest (Table 7-3).

7.3.2.1 Assignment to Basins

Data on private landings for major basins in Virginia were provided by the VMRC (Jim Wesson, department head, Conservation and Replenishment, personal communication, December 30, 2016). The Virginia aquaculture biomass was assigned to basins according to the fraction of the total private landings in each basin (Table 7-4).

Table 7-4. Basin Fractions of Aquaculture Biomass

VA Basin	Fraction	MD Basin	Fraction
Chesapeake	0.293	Anne Arundel	0.022
James	0.360	Calvert	0.030
York	0.128	Dorchester	0.475
Rappahannock	0.050	St. Marys	0.215
Potomac	0.170	Somerset	0.025
		Talbot	0.072
		Wicomico	0.162

Maryland aquaculture biomass was assigned to counties in proportion to the fraction of the total harvest represented by each county (Table 7-4). Data were not available for all individual counties, however, so fractions were assigned to those counties according to surface area.

7.4 Model Parameterization

7.4.1 Model Calibration to Reef Population

The fundamental parameter values for the oyster module are adapted from the 2005 study of the impact of a tenfold increase in natural oyster population (Cerco and Noel 2007). Values of two parameters, mortality and harvest (equation 1), are newly assigned in the 2017 model to match current biomass data. First the harvest is assigned to calculate values representative of data, then the mortality is assigned to obtain representative biomasses. Harvest values range from 1.23×10^{-4} to 6.75×10^{-4} d^{-1} in the months from October through April. Harvest is zero otherwise. The seasonal assignment reflects that harvest from natural reefs is minimal during spawning season. Mortality ranges from 0.025 to 0.05 d^{-1} in the months from June to October. Mortality is zero otherwise. The seasonal assignment reflects the influence of temperature on predators and disease organisms.

The reef biomass data reflect annual surveys (fishery-independent data) combined with annual summaries of oyster landings (fishery-dependent data). They are compared to annual-average biomass computed by the model. Comparison of computations and observations (e.g., Figure 7-5 and Figure 7-6) indicates the model largely reflects the regional biomasses, although intraannual variations in the observations are not reproduced.

Figure 7-5. Computed (annual average) and observed oyster biomass in the Choptank River, MD.

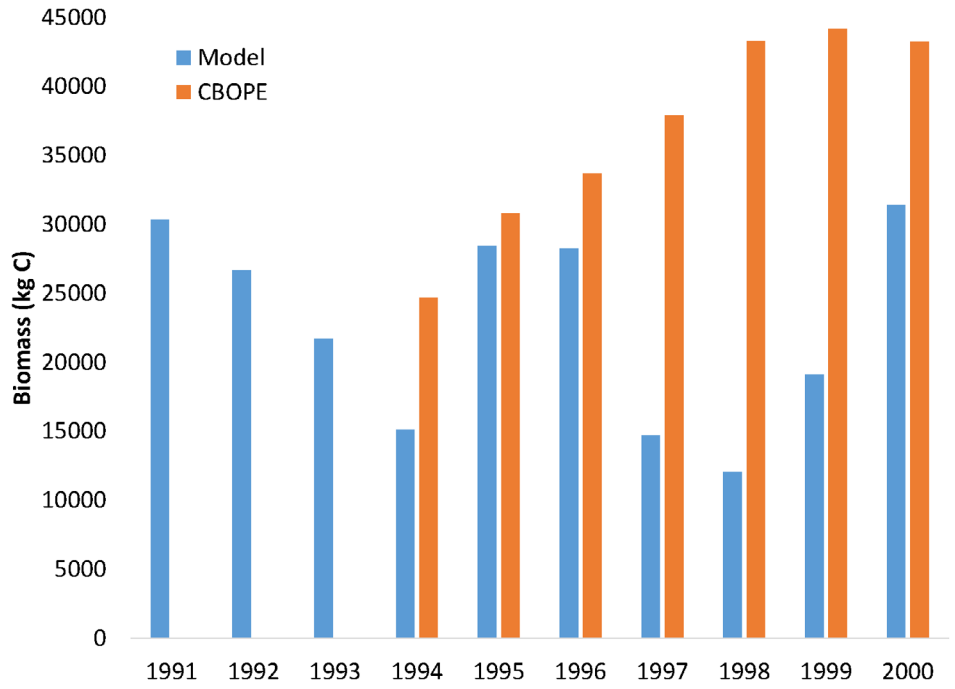

Figure 7-6. Computed (annual average) and observed oyster biomass in the James River, VA.

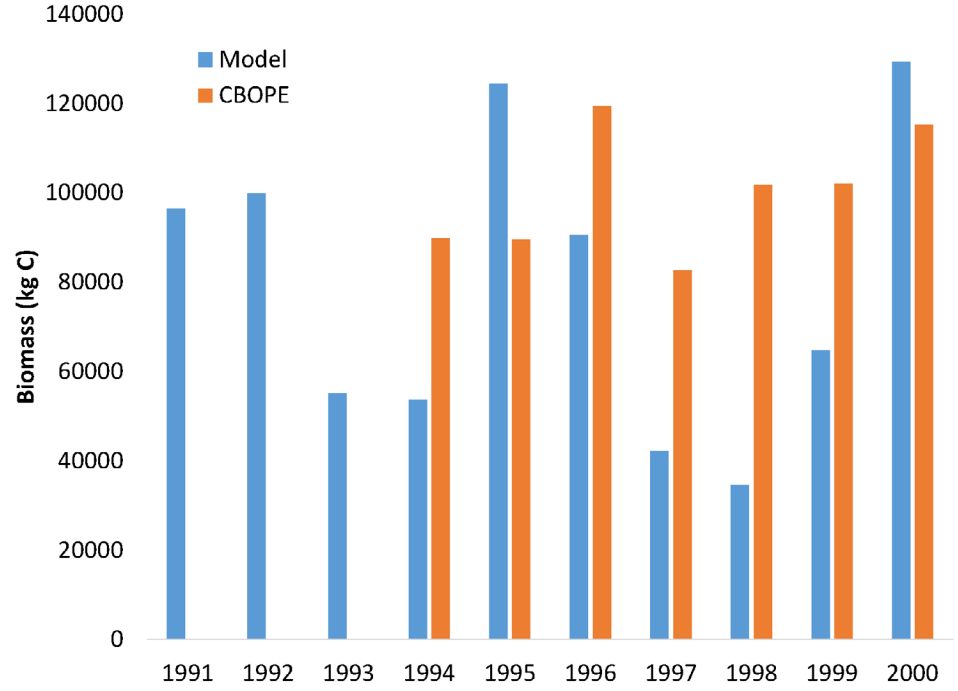

The correlation (R^2) between computed annual-average biomass in Maryland basins and observed biomass is 0.62 and is highly significant ($p < 0.01$) (Figure 7-7). The correlation between computed and observed biomass in Virginia is lower, $R^2 = 0.47$, but remains highly significant nonetheless (Figure 7-8).

Figure 7-7. Computed vs. observed biomass for Maryland basins designated in Table 7-2. Computed values are annual averages for 1994–2000. Observations are derived from CBOPE.

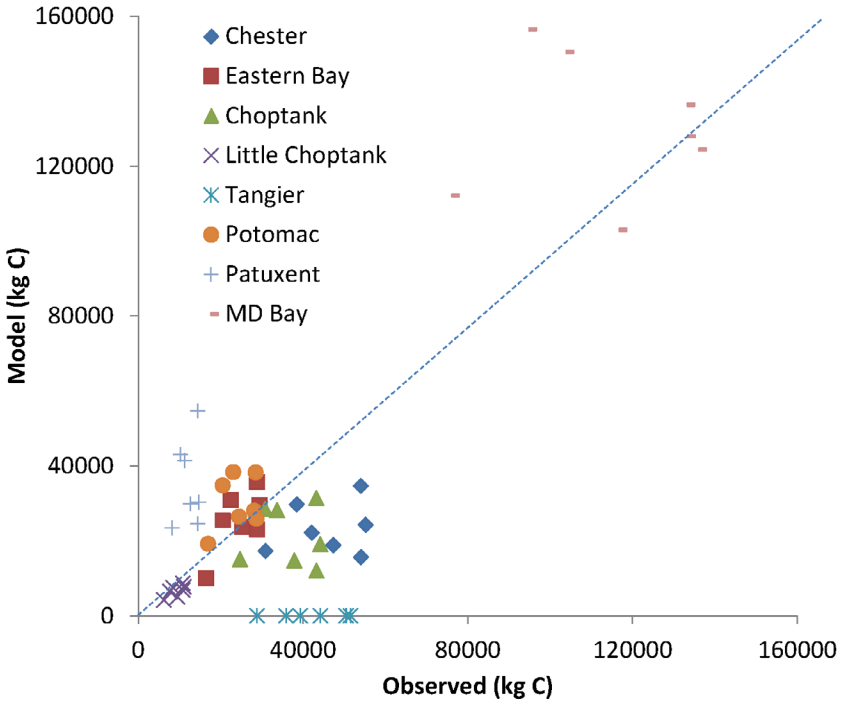

Figure 7-8. Computed vs. observed biomass for Virginia basins designated in Table 7-2. Computed values are annual averages for 1994–2000. Observations are derived from CBOPE.

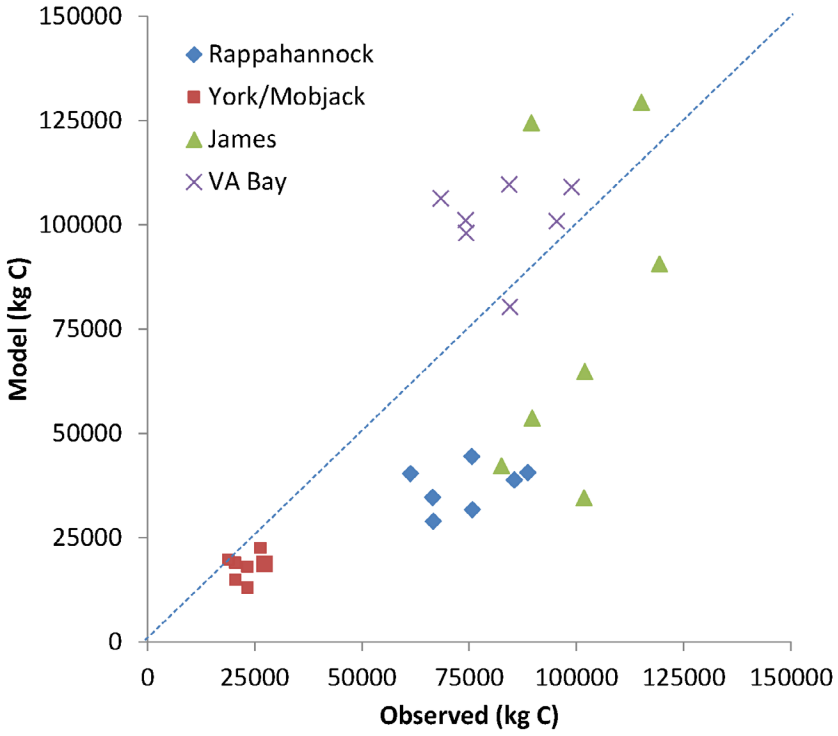

7.5 Management Considerations

7.5.1 Oyster Aquaculture

The Virginia aquaculture biomass was negligible, compared to the reef biomass, through the WQSTM calibration and verification years, 1991–2000 and 2002–2011 (Figure 7-9). Aquaculture in Maryland was nonexistent during those periods. Consequently, the aquaculture feature of the oyster module was not implemented in the calibration or verification periods spanning 1991 to 2011. Aquaculture activities are growing rapidly, however, in both Virginia (Figure 7-9) and Maryland (Figure 7-10) and nutrient removal through aquaculture is now considered a best management practice (Cornwell et al. 2016). Consequently, aquaculture is implemented in various Chesapeake Bay Model scenarios for 2025 conditions.

7.5.1.1 Estimate of Aquaculture Activity through 2025

We were provided with 2025 projections of aquaculture activity by state (Olivia Devereux, Devereux Consulting, personal communication, December 8, 2017). Data included the number of oysters harvested and the nitrogen and phosphorus content of individual oyster soft tissue. Since the WQSTM quantifies oysters as carbon, the total nitrogen removed was multiplied by the WQSTM oyster carbon-to-nitrogen ratio of 6 g C g^{-1} N to convert the projected harvest to model carbon

units. Harvest was converted to standing-stock biomass as described in section 7.3.2, *Aquaculture*.

The aquaculture biomass obtained from the harvest was distributed to model cells capable of supporting aquaculture in each state. The projected harvest and biomass were subsequently converted to dry weight for comparison with previously computed values for the years 2005–2016 (Table 7-3). The 2025 projections are much higher than the most recent data but are consistent with extrapolations from present trends.

The 2025 "full buildout" oyster aquaculture estimates are the approximate maximum biomass of Maryland aquaculture oysters because of constraints in available shallow waters of suitable salinities and water quality. For scenario years of 2025 and beyond, the 2025 full buildout biomass estimates are used. For Progress Scenario years before 2025, Virginia and Maryland provide the annual estimates of aquaculture oyster harvest through the Chesapeake Assessment and Scenario Tool (CAST) (CBPO 2017), which is then used to represent the influence of aquaculture on water quality.

7.5.1.2 Implementing Aquaculture in the WQSTM

CAST operates by reducing the watershed loads to appropriate cells of the WQSTM to account for nutrient removal by harvest and consumption of oyster soft tissue (Cornwell et al. 2016). (Nitrogen and phosphorus content of harvested shells are uncounted and assumed to be net zero because shells from oyster aquaculture are commonly collected and replanted on aquaculture grounds with new oyster spat.) Therefore, in the WQSTM, the harvest of aquaculture oysters is specified as zero (equations 1 and 2) to prevent "double counting" of nutrient removal in both watershed loads and through algorithms in the oyster module. However, oyster functions of particle filtration and nutrient recycling to the water and sediments remain in operation for simulation of oyster aquaculture. Consequently, aquaculture in scenarios provides potential benefits in water clarity and enhanced nutrient burial and denitrification as well as the reductions of nitrogen and phosphorus represented in CAST.

7.5.1.3 Sensitivity Scenario

The overall influence of oyster aquaculture at 2025 full buildout biomass is estimated to increase spring and summer bottom dissolved oxygen (DO) by more than 0.05 mg/l in CB4MH and CB5MH segments (Figure 7-11) (Modeling Workgroup 2018). Improvement in bottom DO from the WQSTM oyster simulated processes of particle filtration and nutrient cycling is more than twice that of nutrient removal by oyster aquaculture harvest alone.

Figure 7-9. Virginia natural reef and aquaculture biomass 1994–2015.

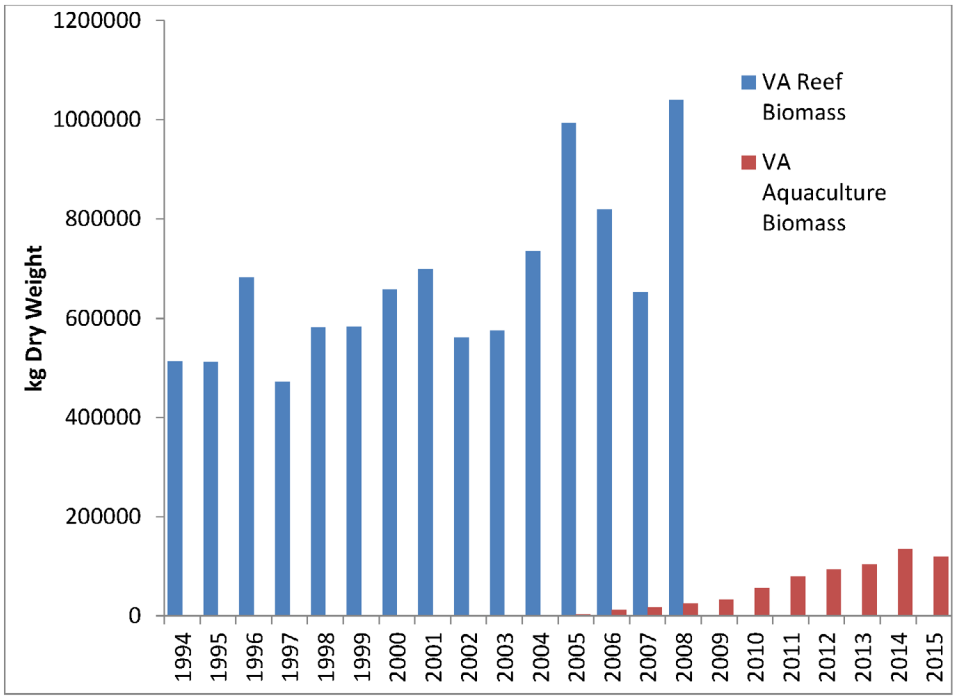

Figure 7-10. Annual harvest of aquaculture (farm-raised) oysters in Maryland 2012–2017. SLL = submerged land lease; WC = water column lease (*Source*: Roscher 2019)

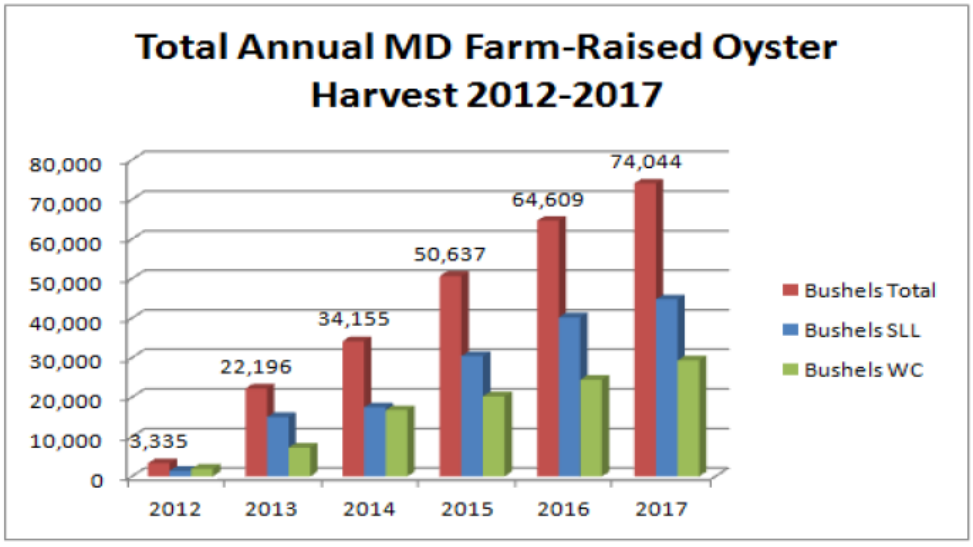

Figure 7-11. Influence of oyster aquaculture at 2025 full buildout biomass on bottom cell DO in CB4MH and CB5MH. Delta DO > 0 indicates an increase in DO (*Source*: Modeling Workgroup 2018).

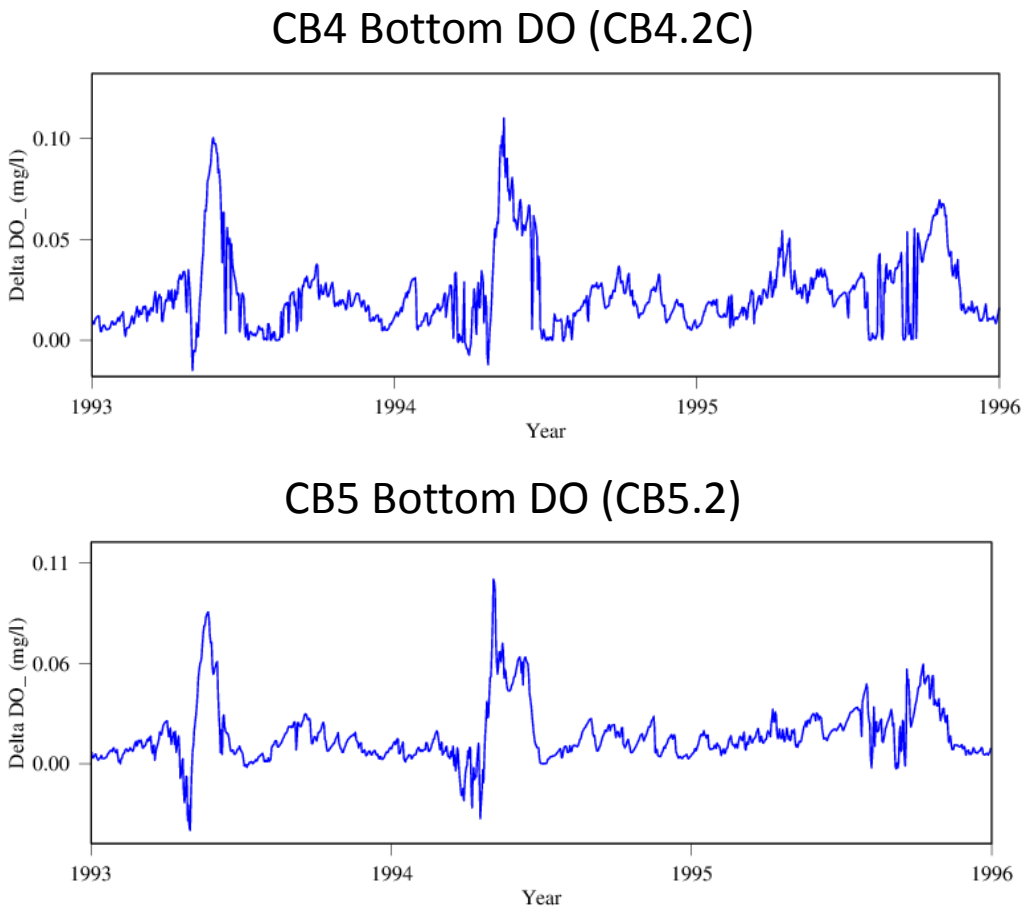

7.5.2 Nutrient Credits for Oyster Habitat Restoration

By 2025, 10 areas of the Chesapeake Bay will have an extensively restored bottom along with oyster spat planting. The 10 areas of existing or planned specific, large, and intensive restoration of oyster habitat are shown in Figure 7-12. Nutrient removal associated with restoration in those areas is equated to load reductions in CAST (CBPO 2019). The credits for restoration are 81 pounds of nitrogen and 4 pounds of phosphorus per acre of restored oyster sanctuary habitat (CBPO 2019). The credits account for nutrient assimilation into oyster tissue and enhanced sediment denitrification. To avoid double counting of nutrient removal in the oyster module and in CAST, the oyster module is disabled in the areas for which specific information on restoration site size and location is available.

Figure 7-12. Location of 10 areas of large-scale oyster habitat restoration to be completed by 2025 (Modified from Bruce and Westby 2018).

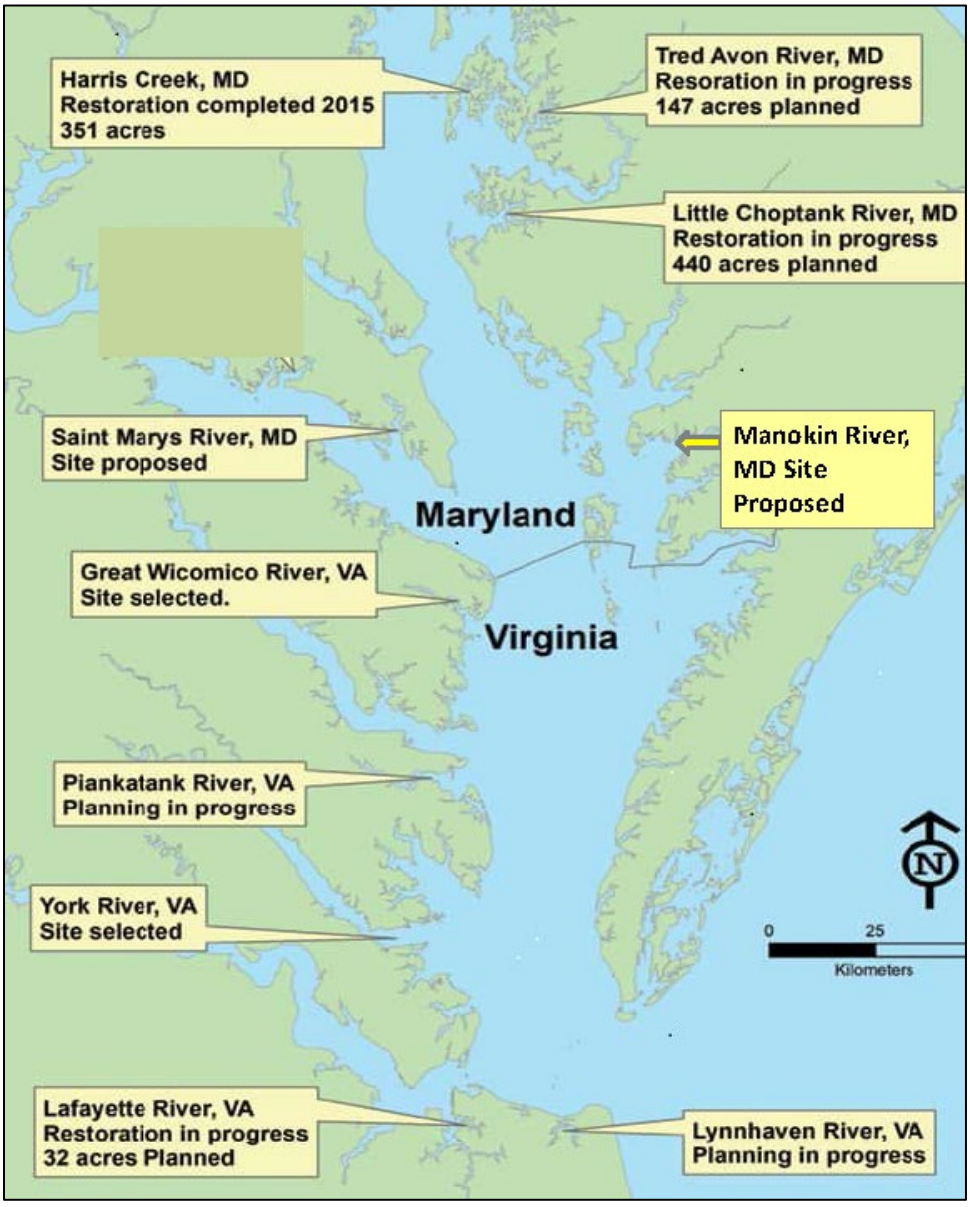

7.6 References

Bruce, D., and Westby, S. 2018. *Restoring Oyster Habitats Requires Geodesign*. ArcNews Fall 2018. Accessed October 10, 2019. https://www.esri.com/content/dam/esrisites/en-us/newsroom/arcnews/G195835_AN_Fal2018_165035_final.pdf.

CBPO (Chesapeake Bay Program Office). 2017. Chesapeake Assessment and Scenario Tool (CAST) Version 2017d. Chesapeake Bay Program Office, Annapolis, MD. Accessed August 6, 2019. https://cast.chesapeakebay.net/Documentation/ModelDocumentation.

CBPO (Chesapeake Bay Program Office). 2019. Chesapeake Assessment and Scenario Tool: Technical Appendix for Oyster Reef Restoration Planning BMPs in the Phase 6 Watershed Model and CAST. Chesapeake Bay Program Office, Annapolis, MD. Accessed August 6, 2019. https://cast.chesapeakebay.net.

Cerco, C., B. Johnson, and H. Wang. 2002. *Tributary Refinements to the Chesapeake Bay Model*. ERDC TR-02-4. US Army Engineer Research and Development Center, Vicksburg, MS.

Cerco, C., and M. Noel. 2007. Can oyster restoration reverse cultural eutrophication in Chesapeake Bay? *Estuaries and Coasts* 30(2):331-343.

Cerco, C., and M. Noel. 2010. Monitoring, modeling, and management impacts of bivalve filter feeders in the oligohaline and tidal fresh regions of the Chesapeake Bay system. *Ecological Modeling* 221:1054-1064.

Cornwell, J., J. Rose, L. Kellogg, M. Luckenbach, S. Bricker, K. Paynter, C. Moore, M. Parker, L. Sanford, B. Wolinski, A. Lacatell, L. Fegley, and K. Hudson. 2016. *Panel Recommendations on the Oyster BMP Nutrient and Suspended Sediment Reduction Effectiveness Determination Decision Framework and Nitrogen and Phosphorus Assimilation in Oyster Tissue Reduction Effectiveness for Oyster Aquaculture Practices*. Oyster BMP Expert Panel First Incremental Report. Oyster Recovery Partnership, Annapolis, MD. https://www.chesapeakebay.net/channel_files/24330/oyster_bmp_report_draft_for_partnership_and_public_review_2016-09-22.pdf.

Greenhawk, K., and T. O'Connell. 2007. *Oyster Population Estimates for the Maryland Portion of Chesapeake Bay 1994–2006*. Maryland Department of Natural Resources, Fisheries Service, Annapolis, MD.

Hudson, K., and T. Murray. 2016. *Virginia Shellfish Aquaculture Situation and Outlook Report*. VIMS Marine Resource Report 2016-4. Virginia Institute of Marine Science, Gloucester Point, VA.

MDNR (Maryland Department of Natural Resources). 2008. *Draft Programmatic Environmental Impact Statement for Oyster Restoration in Chesapeake Bay including the Use of a Native and/or Nonnative Oyster*. Maryland Department of Natural Resources, Annapolis, MD. http://dnr.maryland.gov/fisheries/Pages/EIS.aspx.

Modeling Workgroup. 2018. *Estimated Oyster Aquaculture Influence on Chesapeake Water Quality*. Chesapeake Bay Program, Annapolis, MD. Accessed August 8, 2019. https://www.chesapeakebay.net/channel_files/25850/attachment_e_oyster_aquaculture_influence_on_water_quality_2.pdf.

Roscher, K. 2019. *Maryland Shellfish Aquaculture Conference Policy and Regulatory Developments*. February 2019. Annapolis, MD. Accessed August 6, 2019. https://www.cbf.org/document-library/presentation-webinar-materials/2019-aquaculture-roscher.pdf.

VIMS (Virginia Institute of Marine Science). 2017. *Chesapeake Bay Oyster Population Estimate*. Virginia Institute of Marine Science, Gloucester Point, VA. http://web.vims.edu/mollusc/cbope/overview.htm.

8 Statistical Summary of Model Calibration

Calibrating the Chesapeake Bay Water Quality and Sediment Transport Model (WQSTM) involves the comparison of hundreds of thousands of observations with model results in various formats, including graphical and statistical summaries. Comparisons involve conventional water quality data, process-oriented data, and living resources observations. Graphical comparisons produce thousands of plots, which are challenging to assimilate in their entirety. Evaluating model performance is enhanced by statistical and graphical summaries of results. This chapter summarizes results for major water quality constituents in the mainstem Bay and tributaries in both statistical and graphical formats. Additional graphical comparisons are available in Appendices A through D to this report.

8.1 Methods

We have employed summary statistics developed as part of our initial Chesapeake Bay model study to evaluate the 2017 WQSTM (Cerco and Cole 1994). Using a consistent set of statistics facilitates comparisons with earlier model versions and with model applications to other systems. Statistics computed are mean difference (MD), absolute mean difference (AMD), and relative difference (RD), as shown in equation 1, equation 2, and equation 3, respectively:

$$MD = \frac{\sum(P-O)}{N} \quad (1)$$

$$AMD = \frac{\sum|P-O|}{N} \quad (2)$$

$$RD = \frac{\sum|P-O|}{\sum O} \quad (3)$$

where:

MD = mean difference
AMD = absolute mean difference
RD = relative difference
O = observation
P = prediction
N = number of observations

The MD describes whether the model overestimates (MD > 0) or underestimates (MD < 0) the observations, on average. The MD can attain its ideal value, zero, while discrepancies exist between individual observations and computations. The MD can also be skewed by extreme differences in a few computations and observations. The AMD is a measure of the characteristic difference between individual observations and computations. An AMD of zero indicates the model perfectly reproduces each observation. RD is the AMD normalized by the mean of the observations.

Quantitative statistics are determined using the same model-data pairs as in the time series plots found in Appendices A and B. The statistics are reported for the mainstem Bay and seven subsystems. The stations and number of pairs depend on the system or station grouping (Table 8-1). In most cases, for stations classed as TF, ET, and WT, only surface samples are considered. Surface and bottom samples are considered for most RET and EE stations. Surface, mid-depth, and bottom samples are considered for most CB and LE stations.

Table 8-1. Stations and Observations in 1991–2000 Statistical Summary

Grouping	Stations	Salinity Obs.	Chlorophyll Obs.	Total Nitrogen Obs.	Total Phosphorus Obs.	DO Obs.	TSS Obs.
Chesapeake Bay	CB1.1, CB2.2, CB3.3C, CB4.2, CB5.2, CB6.1, CB7.3, CB7.4, CB7.4N, CB8.1E, EE3.1, EE3.2	5,811	5,695	5,657	5,738	5,803	5,757
James River	TF5.5, RET5.2, LE5.3	823	831	465	812	829	802
York River	TF4.2, RET4.3, LE4.2, WE4.2	1,153	1,134	754	1,114	1,155	1,138
Rappahannock River	TF3.3, RET3.2, LE3.2	844	822	472	820	841	831
Potomac River	TF2.1, RET2.4, LE2.2	1,097	1,068	1,036	1,083	1,097	1,094
Patuxent River	TF1.7, RET1.1, LE1.3	1,190	1,166	1,188	1,188	1,190	1,183
Eastern Shore Tributaries	EE1.1, EE2.1, ET1.1, ET3.2, ET4.2, ET5.2, ET6.2, ET9.1	1,886	1,832	1,762	1,848	1,886	1,866
Western Shore Tributaries	WT1.1, WT2.1, WT5.1, WT8.1	904	870	838	888	904	898

Notes: DO = dissolved oxygen; TSS = total suspended solids.

Statistics are calculated for three distinct applications: the current calibration to the years 1991–2000 (Table 8-2), the current validation to the years 2002–2011 (Table 8-3), and the 1991–2000 model application used to guide development of the 2010 Total Maximum Daily Load (TMDL) (Table 8-4) (Cerco et al. 2010).

Table 8-2. Statistical Summary of Current Model Calibration 1991–2000

Salinity	Bay	Eastern Shore Tribs	Western Shore Tribs	James	York	Rappahannock	Potomac	Patuxent
MD, ppt	0.56	0.30	-1.32	-0.14	0.22	0.44	1.29	0.39
AMD, ppt	2.00	1.35	1.63	1.17	1.74	1.77	1.68	1.63
RD, %	11.2	12.9	24.0	13.0	11.9	15.9	18.7	16.1
Chlorophyll	**Bay**	**Eastern Shore Tribs**	**Western Shore Tribs**	**James**	**York**	**Rappahannock**	**Potomac**	**Patuxent**
MD, µg m^{-3}	0.31	-0.46	-10.14	-1.34	-0.96	-0.17	-0.15	0.48
AMD, µg m^{-3}	3.82	7.26	14.29	7.88	5.42	5.87	8.01	7.29
RD, %	53.0	63.8	65.5	67.2	57.5	60.7	68.3	59.1
Total Nitrogen	**Bay**	**Eastern Shore Tribs**	**Western Shore Tribs**	**James**	**York**	**Rappahannock**	**Potomac**	**Patuxent**
MD, g m^{-3}	0.03	0.24	0.16	0.23	0.10	0.37	0.08	0.33
AMD, g m^{-3}	0.16	0.44	0.36	0.30	0.21	0.39	0.34	0.37
RD, %	23.6	47.1	28.4	41.5	34.1	61.7	26.1	43.9
Total Phosphorus	**Bay**	**Eastern Shore Tribs**	**Western Shore Tribs**	**James**	**York**	**Rappahannock**	**Potomac**	**Patuxent**
MD, g m^{-3}	0.01	0.03	0.01	0.00	-0.02	0.03	0.01	0.01
AMD, g m^{-3}	0.02	0.04	0.04	0.05	0.03	0.05	0.04	0.04
RD, %	46.8	79.5	52.6	45.0	43.5	73.2	56.7	48.1
TSS	**Bay**	**Eastern Shore Tribs**	**Western Shore Tribs**	**James**	**York**	**Rappahannock**	**Potomac**	**Patuxent**
MD, g m^{-3}	2.40	-6.45	2.03	-14.00	-10.37	-0.18	1.71	-0.73
AMD, g m^{-3}	13.00	11.74	16.51	27.05	18.04	13.72	16.50	11.21
RD, %	71.59	63.4	99.7	66.1	60.1	63.3	71.1	63.9
Light Attenuation	**Bay**	**Eastern Shore Tribs**	**Western Shore Tribs**	**James**	**York**	**Rappahannock**	**Potomac**	**Patuxent**
MD, m^{-1}	0.12	-0.08	0.17	-0.33	-0.21	0.21	0.62	-0.88
AMD, m^{-1}	0.41	0.79	1.61	1.00	0.75	0.87	1.13	1.09
RD, %	37.2	41.6	60.9	32.9	33.5	35.9	53.3	44.0
DO	**Bay**	**Eastern Shore Tribs**	**Western Shore Tribs**	**James**	**York**	**Rappahannock**	**Potomac**	**Patuxent**
MD, g m^{-3}	-0.11	-0.40	0.41	1.13	0.91	0.62	0.97	1.05
AMD, g m^{-3}	1.03	1.40	1.25	1.27	1.22	1.05	1.57	1.47
RD, %	13.5	16.2	13.5	14.8	16.0	13.1	21.9	18.9

Notes: DO = dissolved oxygen; TSS = total suspended solids.

Table 8-3. Statistical Summary of Current Model Verification 2002–2011

Salinity	Bay	Eastern Shore Tribs	Western Shore Tribs	James	York	Rappahannock	Potomac	Patuxent
MD, ppt	-0.18	-0.74	-1.94	-1.06	-0.95	-0.41	0.13	-0.30
AMD, ppt	1.68	1.15	2.02	1.44	1.72	1.33	1.09	1.28
RD, %	9.7	11.7	33.4	15.4	11.4	11.9	11.8	13.1
Chlorophyll	**Bay**	**Eastern Shore Tribs**	**Western Shore Tribs**	**James**	**York**	**Rappahannock**	**Potomac**	**Patuxent**
MD, µg m^{-3}	-0.62	-3.16	-12.70	-0.94	-1.60	-1.22	-0.98	-2.98
AMD, µg m^{-3}	3.71	7.55	15.19	6.29	4.88	5.68	7.53	8.59
RD, %	47.1	52.7	63.5	58.7	48.0	50.9	62.6	55.5
Total Nitrogen	**Bay**	**Eastern Shore Tribs**	**Western Shore Tribs**	**James**	**York**	**Rappahannock**	**Potomac**	**Patuxent**
MD, g m^{-3}	0.05	0.17	0.14	0.24	0.10	0.31	0.09	0.31
AMD, g m^{-3}	0.18	0.38	0.35	0.31	0.22	0.36	0.30	0.34
RD, %	26.2	38.1	27.8	41.6	34.4	52.2	27.0	42.0
Total Phosphorus	**Bay**	**Eastern Shore Tribs**	**Western Shore Tribs**	**James**	**York**	**Rappahannock**	**Potomac**	**Patuxent**
MD, g m^{-3}	0.01	0.04	0.03	0.03	-0.01	0.04	0.03	0.02
AMD, g m^{-3}	0.02	0.05	0.04	0.05	0.03	0.05	0.04	0.04
RD, %	55.1	107.3	68.1	66.8	44.8	87.4	78.8	48.2
TSS	**Bay**	**Eastern Shore Tribs**	**Western Shore Tribs**	**James**	**York**	**Rappahannock**	**Potomac**	**Patuxent**
MD, g m^{-3}	10.03	1.11	6.13	-3.77	-11.31	-0.61	13.53	0.81
AMD, g m^{-3}	14.79	10.47	14.04	27.31	17.54	11.19	17.84	11.52
RD, %	110.5	86.3	120.7	77.8	61.3	53.5	129.8	70.4
Light Attenuation	**Bay**	**Eastern Shore Tribs**	**Western Shore Tribs**	**James**	**York**	**Rappahannock**	**Potomac**	**Patuxent**
MD, m^{-1}	0.48	0.27	0.39	0.20	-0.19	0.01	0.46	-0.91
AMD, m^{-1}	0.67	0.48	1.14	1.48	0.74	0.97	0.73	1.19
RD, %	66.9	29.1	51.4	45.3	35.3	35.0	54.4	39.2
DO	**Bay**	**Eastern Shore Tribs**	**Western Shore Tribs**	**James**	**York**	**Rappahannock**	**Potomac**	**Patuxent**
MD, g m^{-3}	-0.01	-0.30	0.77	1.06	0.81	0.59	1.07	1.09
AMD, g m^{-3}	1.00	1.29	1.38	1.31	1.21	1.09	1.62	1.56
RD, %	13.0	14.6	15.3	14.8	15.3	13.4	23.0	20.3

Notes: DO = dissolved oxygen; TSS = total suspended solids.

Table 8-4. Statistical Summary of 2010 TMDL Model 1991–2000

Salinity	Bay	Eastern Shore Tribs	Western Shore Tribs	James	York	Rappahannock	Potomac	Patuxent
MD, ppt	0.04	0.25	-0.73	-1.07	-0.62	-0.24	0.78	0.50
AMD, ppt	1.84	1.15	1.31	1.51	1.40	1.38	1.26	1.20
RD, %	10.3	11.0	19.3	16.8	9.6	12.4	14.1	11.8
Chlorophyll	**Bay**	**Eastern Shore Tribs**	**Western Shore Tribs**	**James**	**York**	**Rappahannock**	**Potomac**	**Patuxent**
MD, $\mu g\ m^{-3}$	-0.15	-0.10	-9.64	-0.72	-1.73	2.34	4.21	2.70
AMD, $\mu g\ m^{-3}$	3.89	7.79	14.39	7.13	5.25	6.94	11.33	9.56
RD, %	54.0	68.4	65.9	60.8	55.7	71.7	96.6	77.5
Total Nitrogen	**Bay**	**Eastern Shore Tribs**	**Western Shore Tribs**	**James**	**York**	**Rappahannock**	**Potomac**	**Patuxent**
MD, $g\ m^{-3}$	-0.07	-0.07	-0.10	0.10	-0.06	0.08	-0.08	-0.03
AMD, $g\ m^{-3}$	0.16	0.37	0.35	0.23	0.17	0.17	0.33	0.19
RD, %	23.4	40.2	27.6	31.2	28.3	27.1	25.7	22.9
Total Phosphorus	**Bay**	**Eastern Shore Tribs**	**Western Shore Tribs**	**James**	**York**	**Rappahannock**	**Potomac**	**Patuxent**
MD, $g\ m^{-3}$	0.006	0.013	-0.013	-0.008	-0.019	0.026	0.006	-0.004
AMD, $g\ m^{-3}$	0.017	0.040	0.036	0.046	0.030	0.045	0.033	0.035
RD, %	41.7	75.8	48.0	44.3	39.1	73.2	45.5	47.0
TSS	**Bay**	**Eastern Shore Tribs**	**Western Shore Tribs**	**James**	**York**	**Rappahannock**	**Potomac**	**Patuxent**
MD, $g\ m^{-3}$	4.13	-4.92	-1.56	-7.92	-11.02	3.72	-0.29	-2.74
AMD, $g\ m^{-3}$	13.55	11.69	14.70	27.42	18.30	16.47	14.95	11.45
RD, %	74.6	63.2	88.8	67.0	61.0	76.0	64.4	65.3
Light Attenuation	**Bay**	**Eastern Shore Tribs**	**Western Shore Tribs**	**James**	**York**	**Rappahannock**	**Potomac**	**Patuxent**
MD, m^{-1}	0.31	0.01	-0.06	0.30	-0.27	0.21	-0.02	-0.82
AMD, m^{-1}	0.53	0.93	2.22	1.45	0.95	1.26	0.85	1.37
RD, %	48.4	49.5	84.0	47.8	42.5	51.8	40.1	55.5
DO	**Bay**	**Eastern Shore Tribs**	**Western Shore Tribs**	**James**	**York**	**Rappahannock**	**Potomac**	**Patuxent**
MD, $g\ m^{-3}$	-0.14	-0.45	-0.80	0.91	0.90	0.52	0.63	0.44
AMD, $g\ m^{-3}$	1.01	1.53	1.72	1.14	1.28	1.09	1.50	1.68
RD, %	13.3	17.8	18.6	13.3	16.7	13.6	20.9	21.7

Notes: DO = dissolved oxygen; TSS = total suspended solids.

8.2 Load Summary

Watershed loads for the 2017 WQSTM are from the Phase 6 version of the Chesapeake Bay Watershed Model (WSM), provided in late November 2017. A summary of the loads for 1991–2000 indicates remarkable consistency with the loads from the Phase 5.3.2 WSM employed in the 2010 WSM (Table 8-5). Although differences exist in individual years and subwatersheds, the daily-average total nitrogen, total phosphorus, and total suspended solids (TSS) loads for the two WSM versions are nearly identical. The small increase in total nitrogen and total phosphorus loads in the 2017 study consists of the new shoreline erosion loads. A significant difference exists, however, in the composition of the nitrogen loads between the two WSM versions. The Phase 6 version provides a 23 percent increase in nitrate loading, accompanied by a corresponding decrease in organic nitrogen and ammonium. Nitrate comprises 68 percent of the total nitrogen load in the current model version versus 54 percent in the 2010 study.

Table 8-5. Daily-Average Loads 1991–2000 from Phase 5 and Phase 6 WSMs

Phase 6	Nitrate (10^3 kg N d^{-1})	Organic N + Ammonium (10^3 kg N d^{-1})	Total Nitrogen (10^3 kg N d^{-1})	Phosphate (10^3 kg P d^{-1})	Organic + Particulate Inorganic P (10^3 kg P d^{-1})	Total Phosphorus (10^3 kg P d^{-1})	TSS (10^3 kg d^{-1})
Susquehanna	137.8	28.8	166.7	1.15	5.80	6.95	4606
Patuxent	1.3	0.8	2.1	0.04	0.12	0.16	76
Potomac	41.2	22.2	63.5	0.80	4.49	5.29	3868
Rappahannock	2.9	3.3	6.2	0.10	0.90	1.00	602
York	1.2	2.0	3.2	0.07	0.24	0.30	121
James	4.5	9.0	13.5	1.16	1.85	3.01	1420
Other	59.1	21.1	80.1	2.05	2.85	4.90	2151
Point Source	28.6	37.0	65.6	2.17	1.09	3.26	
Shoreline		3.3	3.3		2.33	2.33	11371
Total	276.7	127.5	404.2	7.53	19.67	27.20	24217
Phase 5.3.2	**Nitrate (10^3 kg N d^{-1})**	**Organic N + Ammonium (10^3 kg N d^{-1})**	**Total Nitrogen (10^3 kg N d^{-1})**	**Phosphate (10^3 kg P d^{-1})**	**Organic + Particulate Inorganic P (10^3 kg P d^{-1})**	**Total Phosphorus (10^3 kg P d^{-1})**	**TSS (10^3 kg d^{-1})**
Susquehanna	101.7	78.7	180.4	1.15	5.73	6.88	3471
Patuxent	0.9	1.1	2.0	0.04	0.09	0.13	97
Potomac	42.3	14.0	56.3	1.35	4.41	5.77	3010
Rappahannock	3.0	3.1	6.1	0.08	1.15	1.23	1433
York	1.7	2.2	3.9	0.07	0.27	0.34	153
James	3.1	11.6	14.7	0.67	2.16	2.83	1553
Other	34.8	35.1	69.9	2.39	2.48	4.87	1956
Point Source	29.1	37.9	67.0	2.20	1.08	3.28	
Shoreline							11371
Total	216.6	183.7	400.3	7.95	17.37	25.33	23044

8.3 Model Statistics

Performance statistics from a single model run alone provide little insight. Comparing them with statistics from alternate runs provides grounds for interpreting model behavior and the effects of various developments. This section presents three sets of statistics that allow for two significant comparisons. The first significant comparison is between the current calibration to 1991–2000 and the 2010 calibration to the same data. The stated goal of the sponsor is that the current calibration should be "as good or better" than the previous calibration. The second comparison is between the 1991–2000 calibration and the validation to more recent data from 2002–2011. The latter application is a classic validation in that model parameter adjustment was restricted to the 1991–2000 application. The 2002–2011 application provides validation of the parameters since the model was not "tuned" to match observations collected in that period.

8.3.1 Salinity

Model salinity is determined solely by transport processes. The structure of the Computational Hydrodynamics in Three Dimensions (CH3D) model is unchanged from the version that provided hydrodynamics for the 2010 TMDL determination (Kim 2013). New hydrodynamic runs were completed for 1991–2000, however, based on revised freshwater runoff from the updated WSM. Completely new CH3D runs were also conducted to extend the application period through 2011. An additional factor that influences transport is specification in the current WQSTM of a minimum vertical diffusivity: 2.2×10^{-5} m^2 d^{-1}. The minimum was determined empirically to improve computations of bottom-water dissolved oxygen (DO).

The salinity MD statistic indicates salinity in the current model calibration is largely higher than in the 2010 version (Figure 8-1). The increase in salinity is accompanied by a decrease in accuracy as indicated by the AMD statistic (Figure 8-2). The almost universal deterioration in the AMD statistic might represent the impact of the newly imposed minimum vertical diffusivity or it might represent a change in freshwater runoff provided by the WSM. In contrast to the 1991-2000 statistic, the salinity MD for the 2002–2011 validation is primarily negative, indicating salinity is underpredicted despite the minimum vertical diffusivity. Consequently, the impact of the newly imposed minimum vertical diffusivity is unclear. In view of the premier role of DO computations in the model, a slight deterioration in salinity computations, if it exists, is acceptable.

Figure 8-1. Salinity MD statistic.

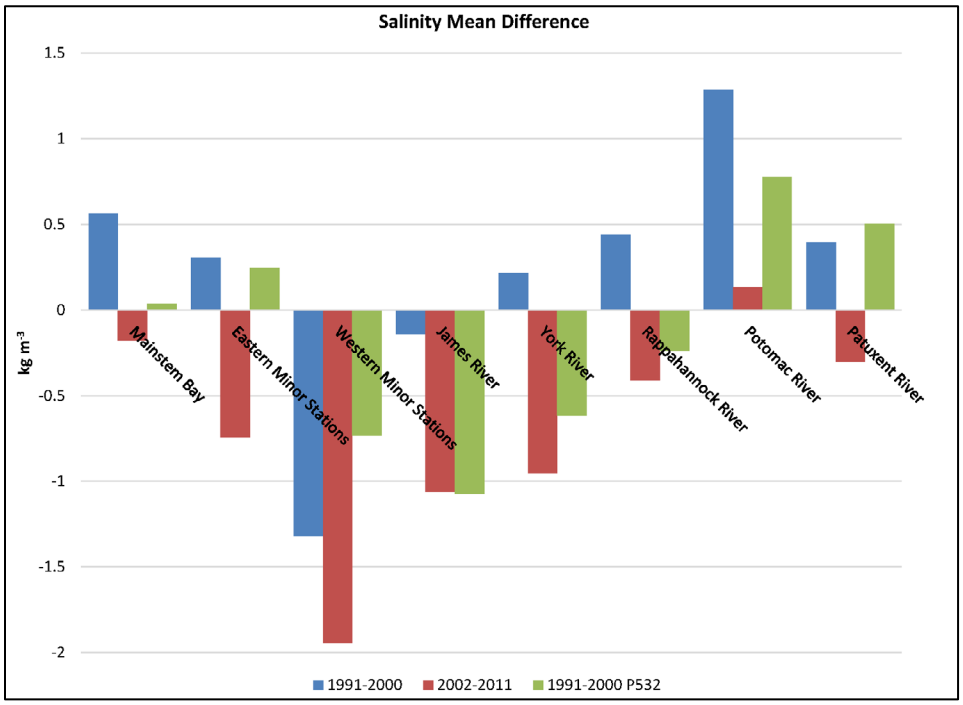

Figure 8-2. Salinity AMD statistic.

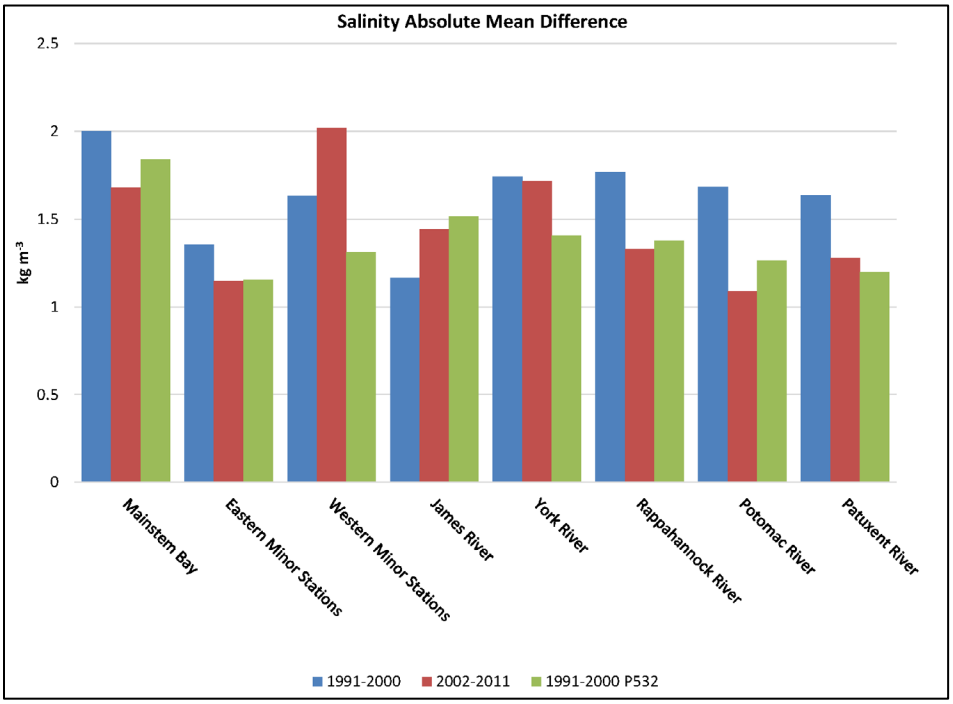

8.3.2 Chlorophyll

The standout in the chlorophyll MD summary is a consistent underprediction of chlorophyll concentration in the western minor tributaries. On average, chlorophyll in those reaches is 10 mg m^{-3} less than observed for any calibration state, application period, or watershed model version (Figure 8-3). The western minor tributaries also exhibit greater AMD in chlorophyll computation than in any other reaches (Figure 8-4). In the 2010 report, we attributed the chlorophyll shortfall in western minor tributaries to a deficiency in phosphorus loading. The computed average total phosphorus in those tributaries for 1991–2000 and 2002–2011 is now in excess, however, while the chlorophyll MD statistic shows no improvement over alternate periods or WSM versions (Figure 8-5). Close examination of model results (e.g., Station WT1.1) indicates a phosphorus deficiency persists, however, during the summer months (Figure 8-6). The impact at specific stations for limited periods might be lost in the summary statistics.

Figure 8-3. Chlorophyll MD statistic.

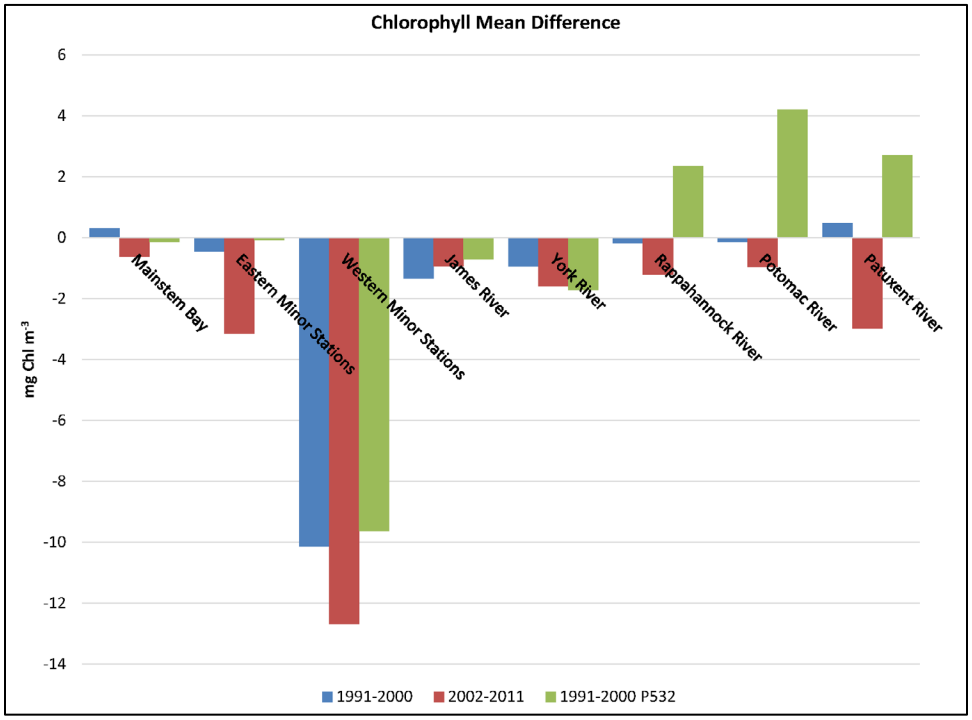

Figure 8-4. Chlorophyll AMD statistic.

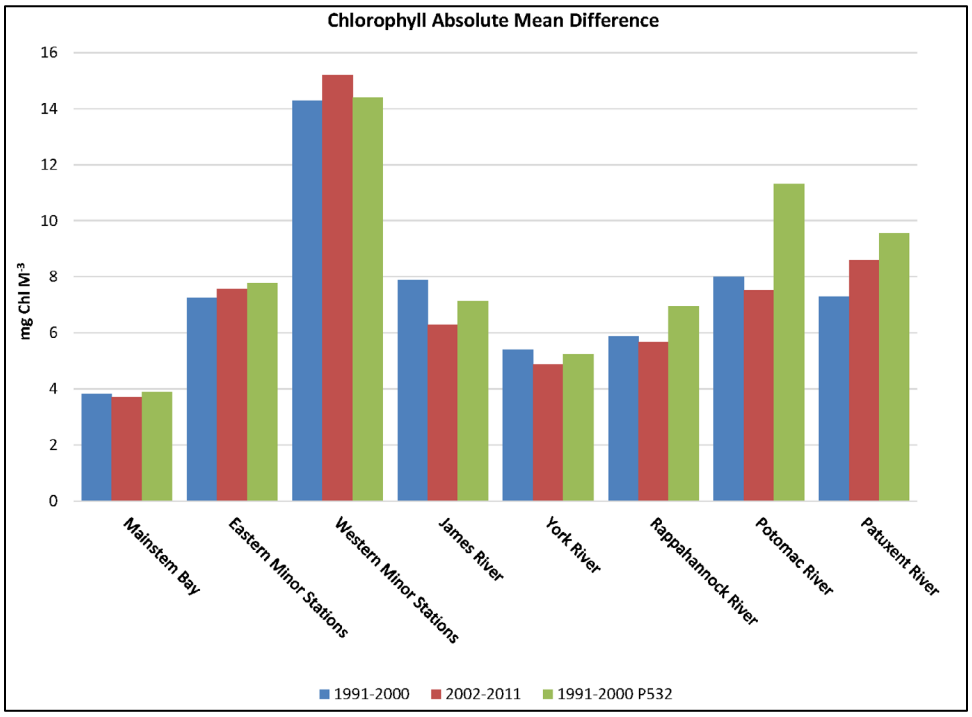

Figure 8-5. Total phosphorus MD statistic.

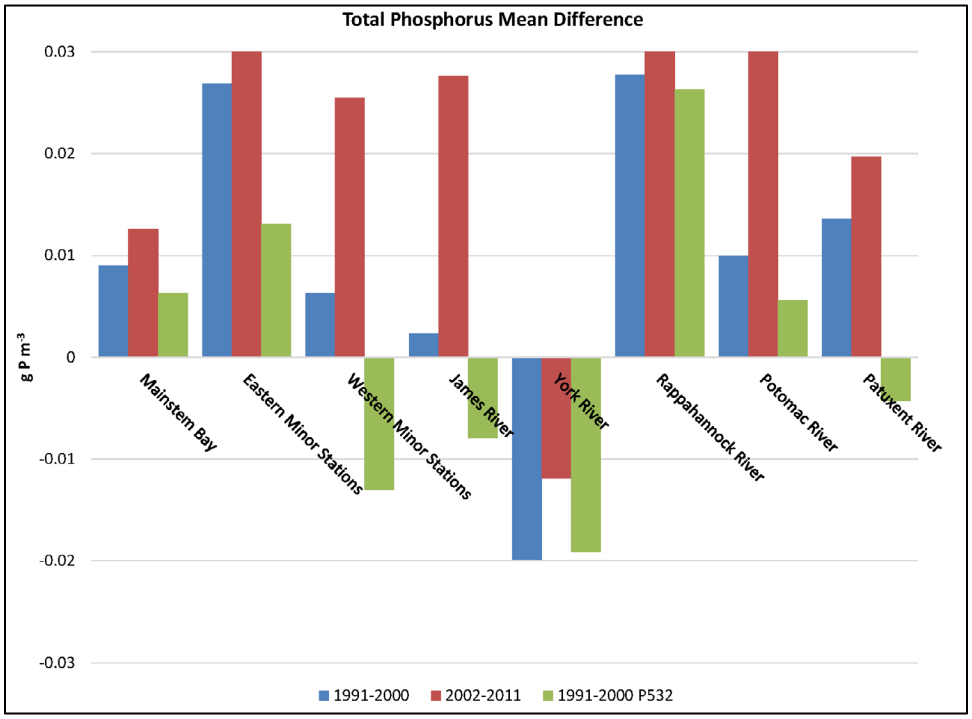

Figure 8-6. Computed chlorophyll and total phosphorus in the Bush River. Note the shortfall in computed total phosphorus during summer months.

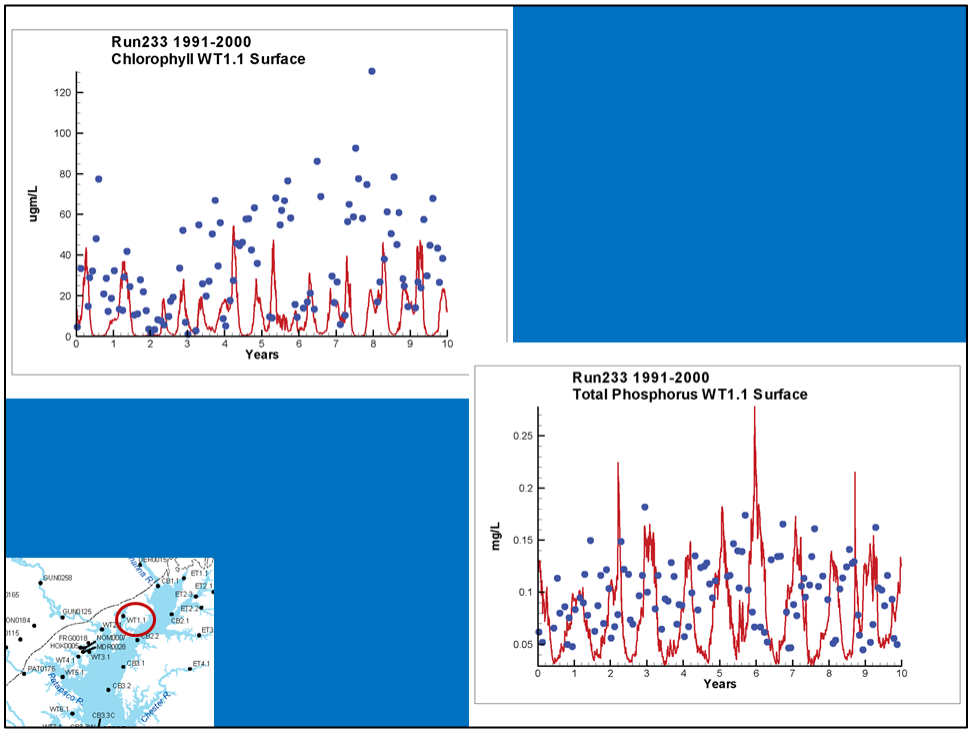

Computed chlorophyll averages 2–4 mg m^{-3} less in the 2017 WQSTM than in the 2010 version in the Rappahannock, Potomac, and Patuxent rivers (Figure 8-3). The lower average chlorophyll concentration is accompanied by improvement in comparison of computations with individual observations (Figure 8-4). Clear, consistent changes in computed chlorophyll between the 2017 model and the 2010 version are difficult to perceive in remaining systems. The MD statistic indicates the average computed chlorophyll in most systems is 1–2 mg m^{-3} lower in the 1992–2011 verification than in the 1991–2000 calibration (Figure 8-3). The reason for the shortfall is not apparent, although it coincides with a shortfall also in computed salinity compared to the 1991–2000 period (Figure 8-1).

8.3.3 Total Phosphorus

The MD statistic indicates that the computed average total phosphorus is almost universally higher in the 2017 model than in the 2010 version (Figure 8-5). With one exception, the present computed average exceeds the observed mean whereas the MD was more evenly distributed around zero in the 2010 model. Differences in the AMD statistic for the two model versions are minor, although, where differences occur, the 2010 version is slightly better at representing individual observations (Figure 8-7). The total phosphorus MD is consistently greater for the 2002–2011 simulation than for 1991–2000 (Figure 8-5). For several systems, the AMD is also greater for 2002–2011 than for 1991–2000 (Figure 8-7). Since the WQSTM parameter set is consistent between the two current simulation

periods, the statistics might indicate that phosphorus loads are more accurate for the earlier interval.

Figure 8-7. Total phosphorus AMD statistic.

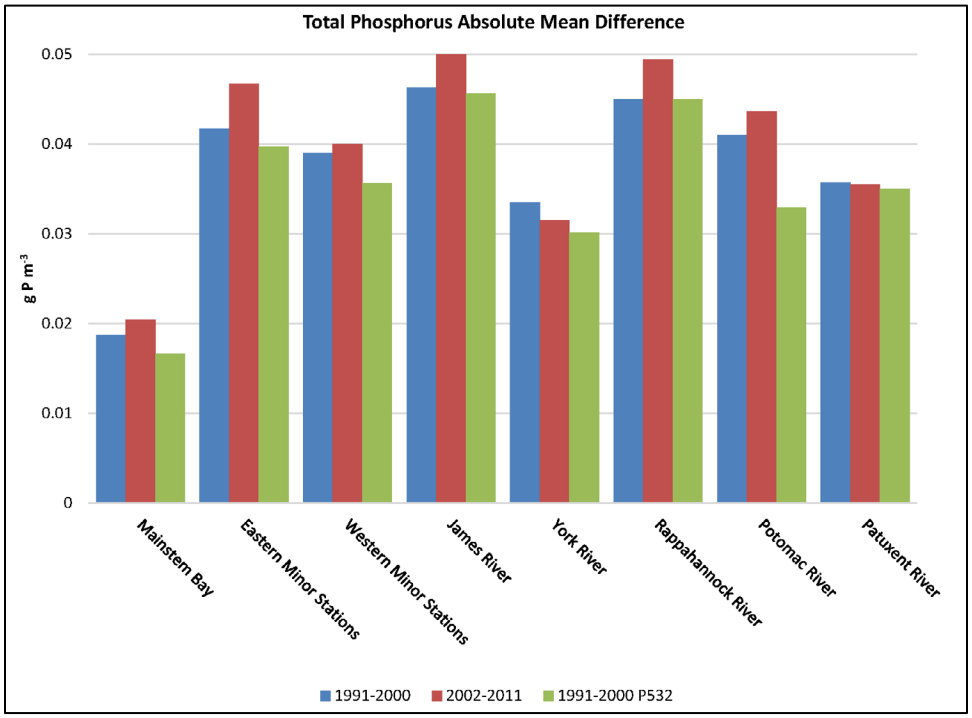

8.3.4 Total Nitrogen

The total nitrogen MD statistic indicates total nitrogen has increased by 0.1–0.3 g m^{-3} or more in the simulations based on Phase 6 loads compared to Phase 5.3.2 loads (Figure 8-8). Systemwide, the total nitrogen loads from the two WSM versions differ by only a small amount. There is a difference in the composition of the loads. The Phase 6 loads contain a larger fraction of nitrate than the Phase 5.3.2 loads (Table 8-5). The MD for nitrate, however, indicates that nitrate in the 2017 model version is not responsible for the increase in total nitrogen (Figure 8-9). The excess in the present model must be organic nitrogen. The AMD statistic shows no consistent difference between the 2010 and 2017 WQSTM versions (Figure 8-10). In the mainstem Bay, for example, the statistic is virtually identical for all WQSTM versions and simulation periods. Where differences exist, however, the 2010 WQSTM calibrated to Phase 5.3.2 WSM loads provides superior representation of total nitrogen observations.

The statistical summaries for total phosphorus and nitrogen present a dilemma when viewed in combination with the load summaries.

Figure 8-8. Total nitrogen MD statistic.

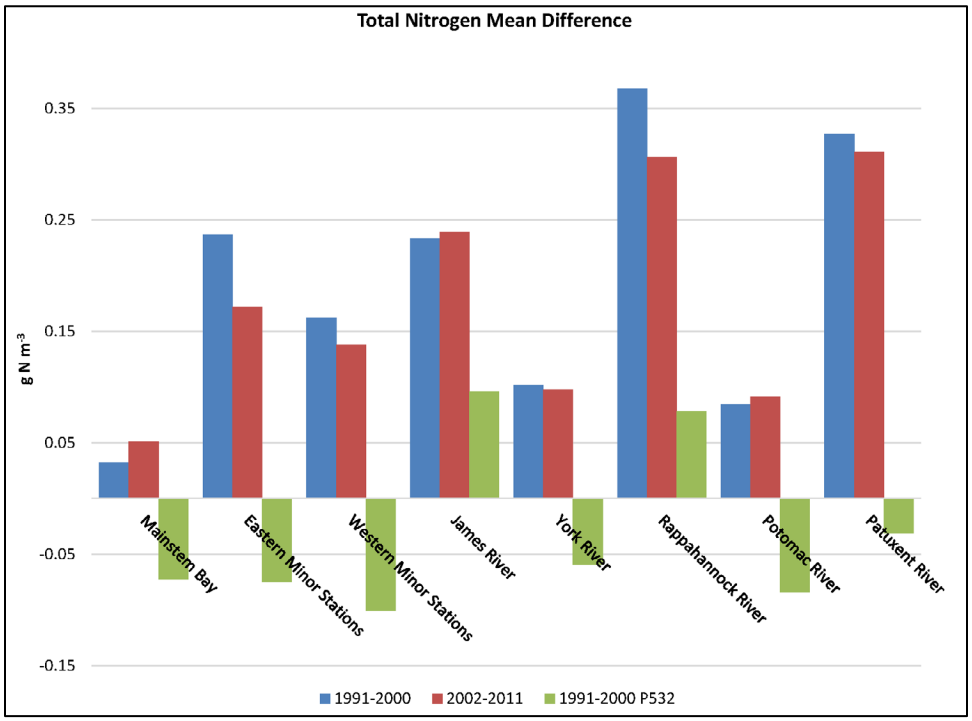

Figure 8-9. Nitrate MD statistic.

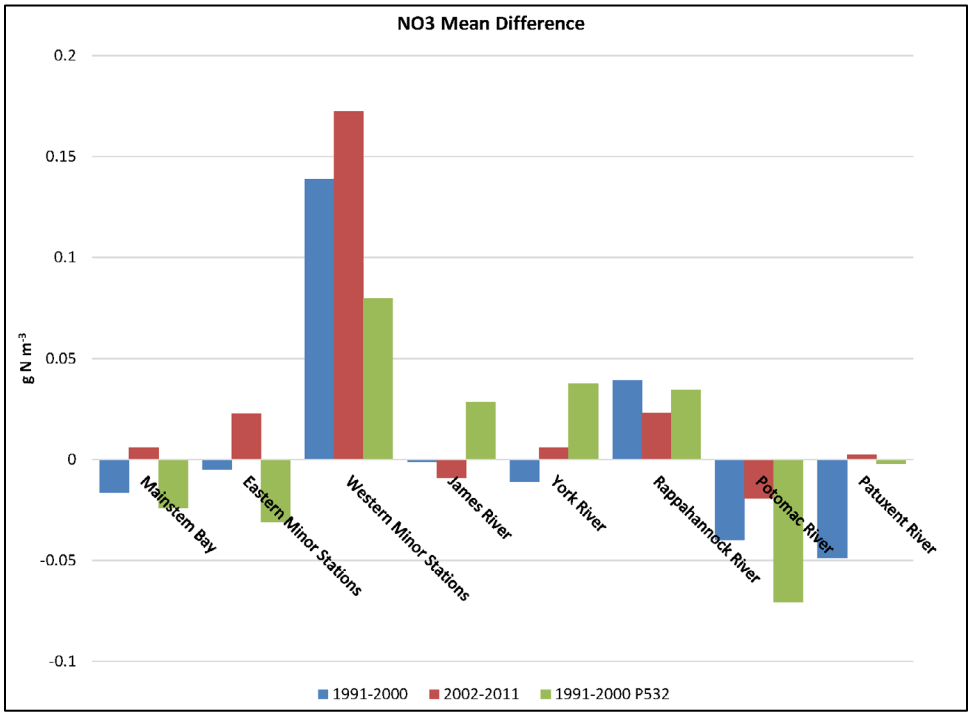

Figure 8-10. Total nitrogen AMD statistic.

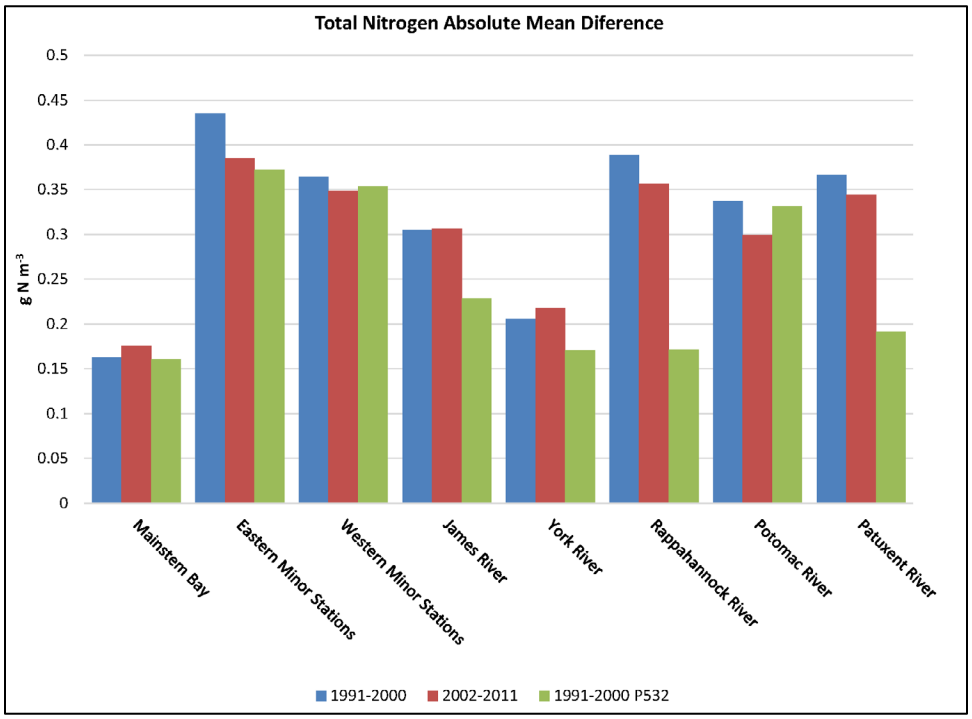

Total phosphorus and nitrogen are higher in the 2017 WQSTM than in the 2010 version despite nearly identical loadings. A review of model parameters leads to the hypothesis that the differences originate in the mapping of WSM organic phosphorus and nitrogen to WQSTM variables. The 2010 WQSTM employed constant concentrations for the dissolved organic components. An increase in total organic loading from a scour event, for example, would lead to an increase in the particulate fraction of the load since the dissolved concentration is constant. The particulate fraction would be subject to settling, removing organic phosphorus and nitrogen from the water column. The 2017 WQSTM employs a constant proportion of dissolved organic material in the load. Consequently, the dissolved organic concentration increases along with loading. The proportion of dissolved organic nitrogen and phosphorus in a large load would be larger than in the 2010 representation, resulting in less settling of the total organic loads.

Definitive mapping of the WSM organic variables into WQSTM variables is difficult to achieve. The mapping is confounded by variations in the analyses conducted in fall-line samples and by the sampling procedures. For example, sampling is often limited in high-flow events. The initial dissolved/particulate splits employed in the present model were determined prior to the extensive analysis of particulate material reactivity in the Conowingo loads (Zhang 2017). That study could provide useful guidance for the future. Review of that study and of observations is recommended when linking the next versions of the Chesapeake Bay WQSTM and WSM.

8.3.5 Dissolved Oxygen

On average, DO calculations for the mainstem Bay in the 2017 model are virtually identical to those in the 2010 model (Figure 8-11). Performance is also nearly identical for the 1991–2000 calibration and 2002–2011 verification periods. Where differences do exist, the 2017 model version computes higher DO concentrations than the 2010 version. That difference is attributed to the introduction of a new minimum vertical diffusivity of 2.2 x 10^{-5} m^2 d^{-1} in the 2017 WQSTM. At several stations (e.g., WT5.1), the new diffusivity eliminates the computation of excess hypoxia (Figure 8-12). The improvement might result in slight deterioration elsewhere (e.g., LE2.2) (Figure 8-13).

Overall model accuracy, as indicated by the AMD statistic, shows little difference between the 2017 and 2010 model versions (Figure 8-14). We view the consistent computations in the mainstem Bay, the elimination of excess hypoxia at several stations, and the negligible changes in overall agreement between computations and observations as evidence that the DO results in the 2017 WQSTM are as good or better than in the 2010 WSM.

Figure 8-11. DO MD statistic.

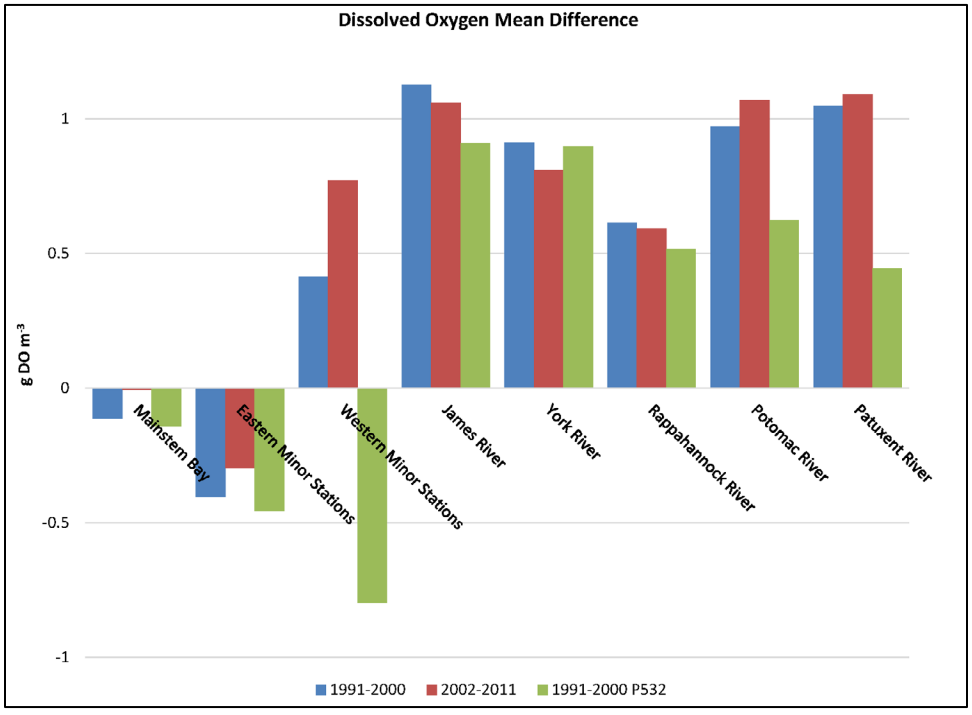

Figure 8-12. The effect on DO at Station WT5.1 of increasing minimum vertical diffusivity from 0.014 cm² s⁻¹ (CH3D) to 0.22 cm² s⁻¹ (WSM).

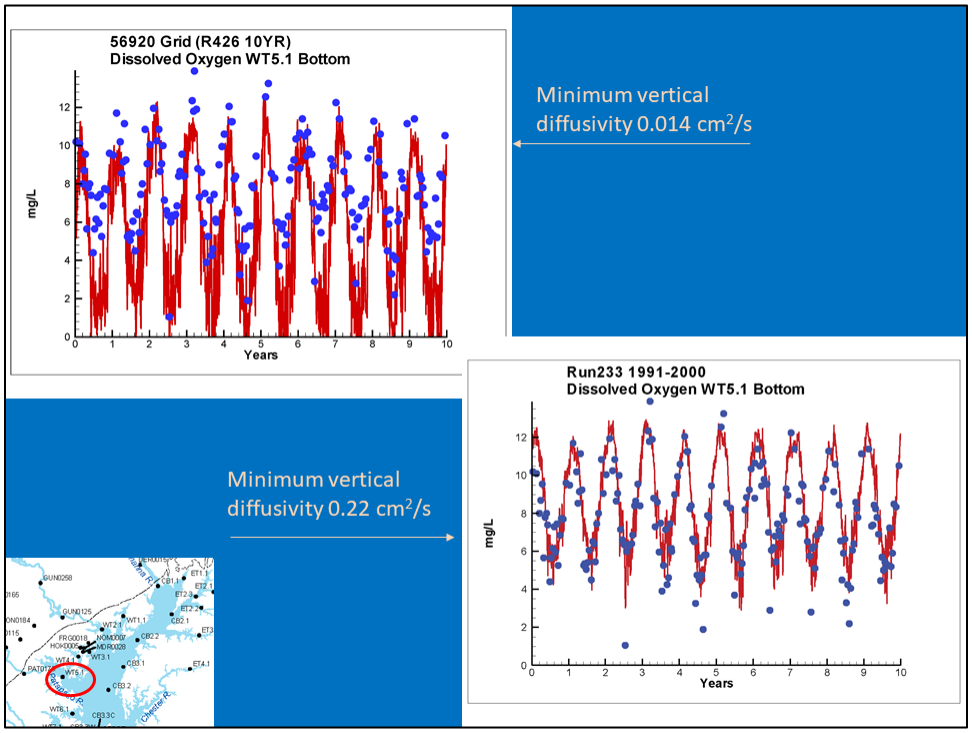

Figure 8-13. The effect on DO at Station LE2.2 of increasing minimum vertical diffusivity from 0.014 cm² s⁻¹ (CH3D) to 0.22 cm² s⁻¹ (WSM).

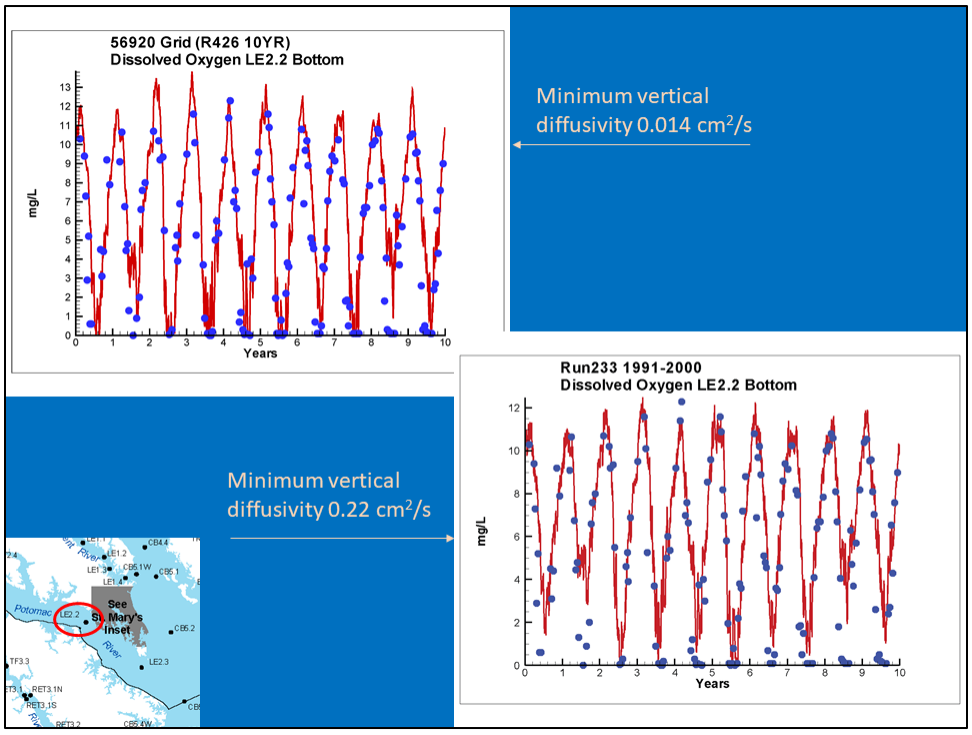

Figure 8-14. DO AMD statistic.

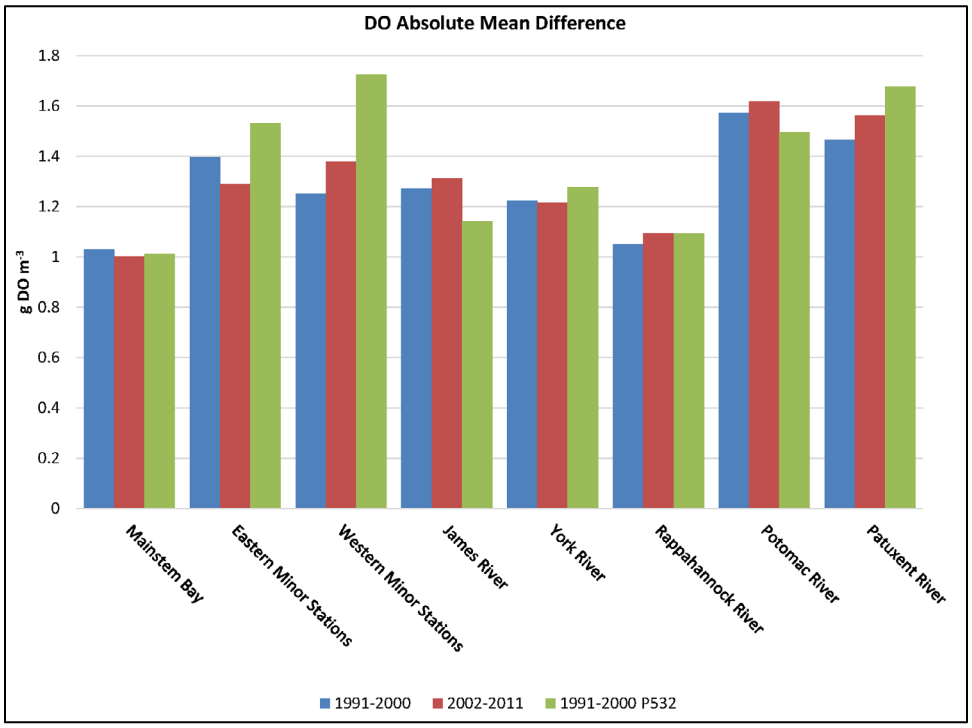

8.3.6 Total Suspended Solids

The sediment transport parameters are unchanged between the 2010 WQSTM and the 2017 WQSTM. Changes in computed solids concentrations are then largely attributable to changes in loading, although the organic fraction of the TSS concentration is potentially influenced by WQSTM parameterization. Examples can be found for each model version and calibration period in which average TSS computations are nearly perfect or erroneous (Figure 8-15). The MD statistic can be highly influenced by extreme differences in a few observations. We suspect the erratic behavior of the TSS MD statistic results from individual loading events represented with varying degrees of accuracy in different systems and model versions. The summary of individual computations and observations shows little difference between model versions and calibration periods (Figure 8-16), consistent with the similarity in loading between WSM versions and identical parameter sets in the WQSTM versions.

Figure 8-15. TSS MD statistic.

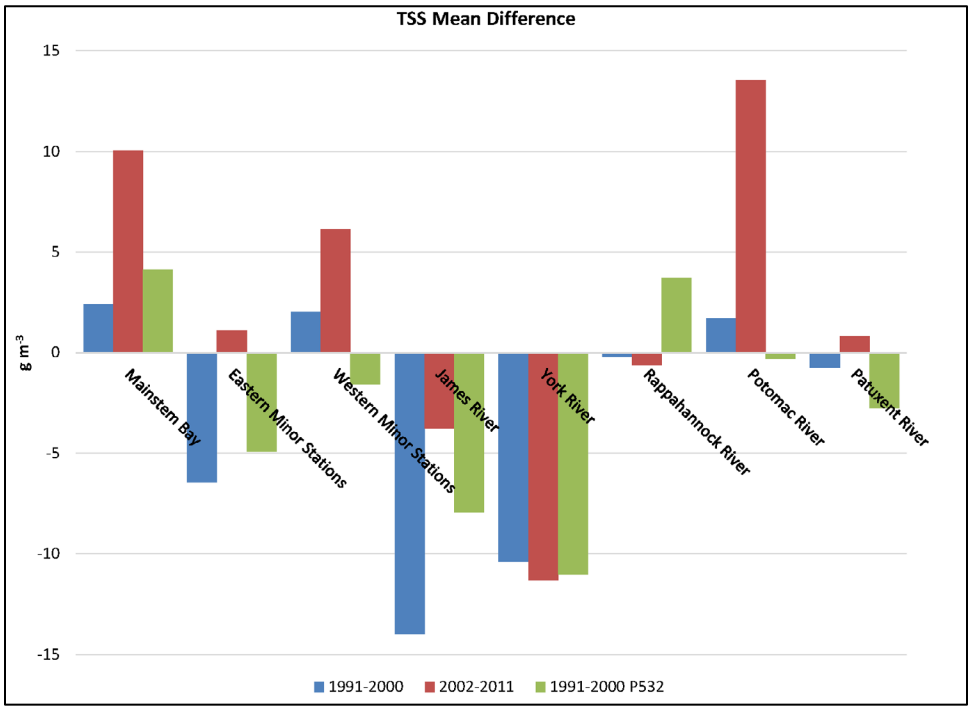

Figure 8-16. TSS AMD statistic.

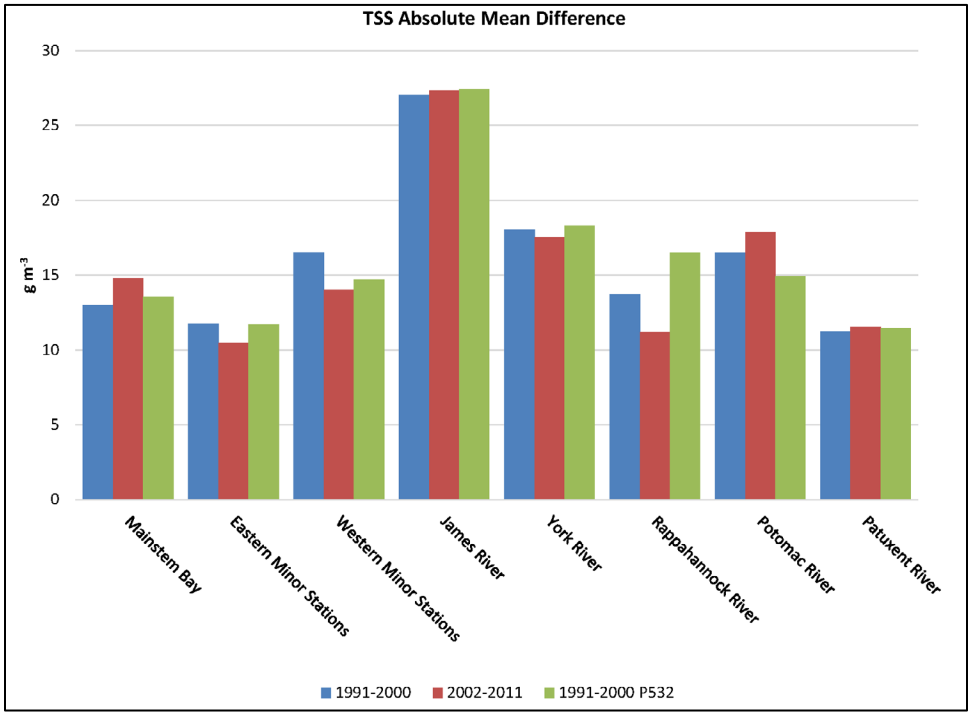

8.3.7 Light Attenuation

As with TSS, consistent differences in computed light attenuation between model versions or application periods are difficult to discern (Figure 8-17). Similarities occur in that all versions and application periods underestimate attenuation in the York and Patuxent rivers. The underestimate in the York River coincides with an underestimate of TSS (Figure 8-15), although correspondence between shortfall of computed attenuation and computed solids in the Patuxent River is not evident. Seven of the eight subsystems considered demonstrate improved agreement between individual computations and observations for the 2017 WQSTM compared to the 2010 WQSTM (Figure 8-18). Those results support the decision to revert to a partial attenuation relationship for light attenuation rather than to continue with the advanced optical model.

Figure 8-17. Light extinction MD statistic.

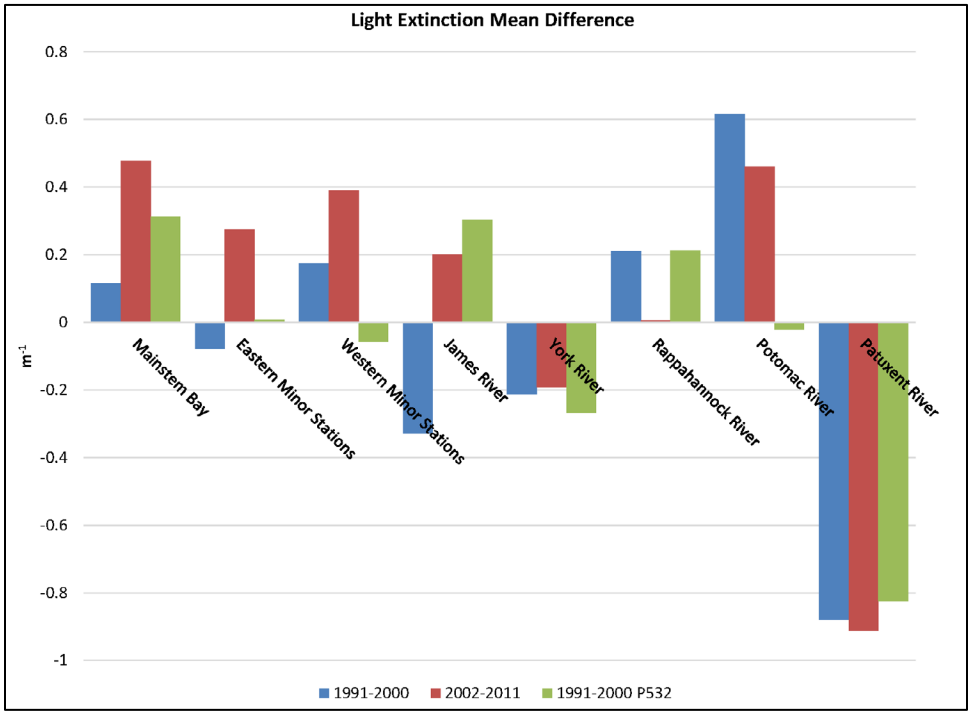

Figure 8-18. Light extinction AMD statistic.

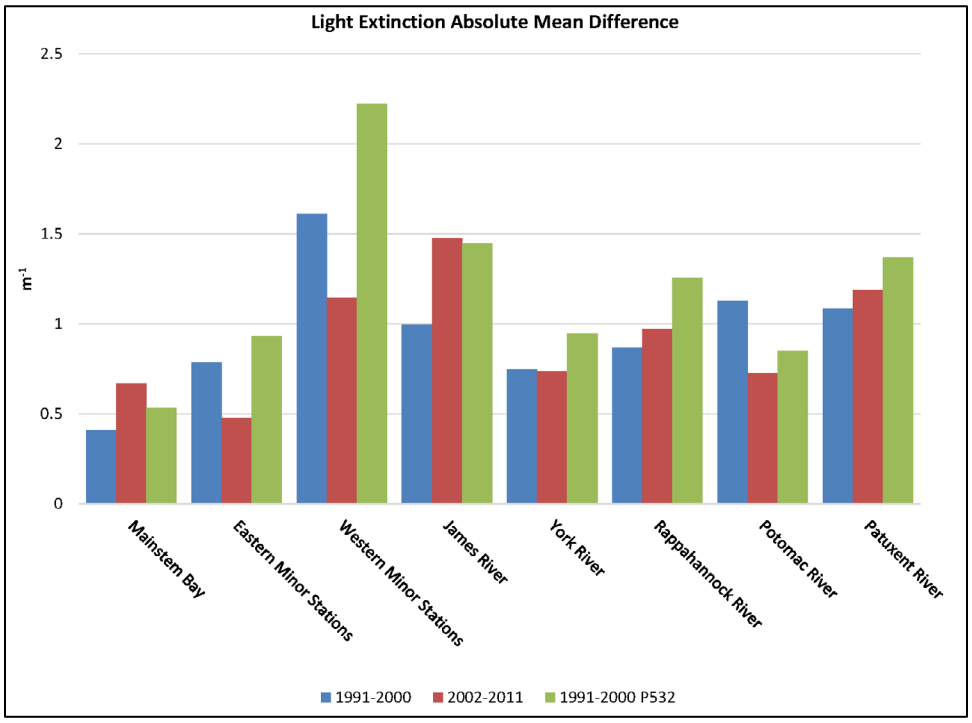

8.4 References

Cerco, C.F., and T.M. Cole. 1994. *Three-Dimensional Eutrophication Model of Chesapeake Bay*. Technical Report EL-94-4. US Army Engineer Waterways Experiment Station, Vicksburg, MS.

Cerco, C.F., S.-C. Kim, and M.R. Noel. 2010. *The 2010 Chesapeake Bay Eutrophication Model: A Report to the US Environmental Protection Agency Chesapeake Bay Program and to the US Army Engineer Baltimore District*. US Environmental Protection Agency, Chesapeake Bay Program Office, Annapolis, MD. https://www.chesapeakebay.net/content/publications/cbp_55318.pdf.

Kim, S-C. 2013. Evaluation of a three-dimensional hydrodynamic model applied to Chesapeake Bay through long-term simulation of transport processes. *Journal of the American Water Resources Association* 49(5):1078–1090.

Zhang, Q. 2017. *Fractions of G1/G2/G3 Organics*. Chesapeake Bay Program Modeling Workgroup April 2017 Quarterly Review, Annapolis, MD. https://www.chesapeakebay.net/channel_files/24719/2017-04-04_conowingo_hdr_g1g2g3_2.pdf.

9 Recommendations for the Future

The model framework for the present study was established 30 years ago to provide verification of the 1987 Chesapeake Bay nutrient reduction goals. The framework included a three-dimensional (3-D), intra-tidal hydrodynamic model (Johnson et al. 1991); an independent, 3-D eutrophication model (Cerco and Cole 1994); and a benthic sediment diagenesis model (DiToro and Fitzpatrick 1993) that interacted with the eutrophication model. That groundbreaking study set the pattern for subsequent studies in the Chesapeake Bay system and elsewhere.

The existing model structure is robust and proven. Technology has advanced, however, making it possible for newer elements more suited to the current needs of the Chesapeake Bay Program (CBP) to replace components of the existing framework. In addition, phenomena are observed in the Bay that defy simulation within the current formulations despite decades of revision and adjustment. This chapter recommends improvements in the model framework and investigations necessary to improve model representation of the Chesapeake Bay system.

9.1 The Hydrodynamic Model

The Computational Hydrodynamics in Three Dimensions (CH3D) model currently in use operates on a structured grid of quadrilateral elements. The CH3D computational grid employs a unique, non-orthogonal, curvilinear coordinate system that provides optimal capability to represent curvilinear shorelines and channels with quadrilateral grid elements. The continual extension of the model into smaller, geometrically complex systems, however, has pushed CH3D capabilities to their limit. A move to a hydrodynamic model that employs triangular grid elements, which allow for more detailed representation of complex geometry, is necessary.

Several alternatives to CH3D are already available. The Semi-implicit Cross-scale Hydroscience Integrated System Model (SCHISM) has been applied to the Chesapeake Bay and used in a detailed study of the Chester River (Ye et al. 2018; Wang et al. 2016). The Finite Volume Community Ocean Model (FVCOM) has been linked to the Corps of Engineers Integrated Compartment Water Quality Model (CE-QUAL-ICM) and also applied to the Chesapeake Bay and the Chester River (Kim et al. 2009; Xia and Jiang 2016; Tian 2016). Additional alternatives may also exist.

In modeling the Bay, the CH3D application employs Z-plane vertical coordinates. The vertical layers are of a constant thickness. Variations in depth are represented by varying the number of layers in a vertical column. That

representation was adapted in the original Chesapeake Bay study, when it was discovered the initial vertical coordinate system, sigma coordinates, confounded representation of vertical density stratification. (In the sigma system, the number of vertical layers does not vary. Variations in depth are represented by varying layer thickness.) Hydrodynamic models using sigma coordinates have since been applied to the Bay (CCMP 2018). Successful use of sigma coordinates could be attributable to advances in numerical algorithms and/or to grid refinements. If the CBP replaces the CH3D model as the hydrodynamic model for the Bay, they should carefully examine the capability in the potential replacement to represent vertical stratification before a selection is made.

In the present model framework, the hydrodynamic and eutrophication models are completely independent. Computed hydrodynamics are exported from the hydrodynamic model and saved for subsequent use in the eutrophication model. That scheme provides tremendous computational efficiency since, once computed, hydrodynamics can be used repeatedly by the eutrophication model. The scheme, however, requires meticulous attention to the software that links the two models. Advanced capabilities such as wetting and drying algorithms in the SCHISM and FVCOM models render the export, storage, and subsequent use of hydrodynamics extremely complex. Attempts to export hydrodynamics for subsequent use in a eutrophication model from the US Army Corps of Engineers' Adaptive Hydrodynamics (ADH) model—which employs triangular elements on an adaptive grid— have proved unsuccessful. Instead, eutrophication algorithms from CE-QUAL-ICM were incorporated into the ADH framework. Eutrophication model runs were conducted by running the hydrodynamic model with calls to eutrophication subroutines. In the event the CBP adapts the SCHISM, FVCOM, or a similar model, the most likely path will be incorporating eutrophication algorithms directly into the hydrodynamic model rather than running two models independently.

9.2 Dissolved Oxygen

9.2.1 Chesapeake Bay Bottom-Water Hypoxia

The present model provides good representation of bottom-water hypoxia at the head of the deep trench, roughly 200 km from the mouth of the Bay (Figure 9-1 and Figure 9-2). During the summer months, however, computed bottom-water dissolved oxygen (DO) can average roughly 1 g m^{-3} above observed in the lower Bay, from km 50 to km 150. The computed excess appears to be inversely related to spring and summer flow in the Susquehanna River; greater excesses occur in years with lower flows (Figure 9-1 and Figure 9-2). That characteristic existed in the earliest version of the model (Cerco and Cole 1994) and has persisted through various model grid refinements and recalibrations.

Figure 9-1. Computed (*red*) and observed (*blue*) bottom DO along Bay axis, summer 1994. Mar–Aug flow in Susquehanna River = 2,034 $m^3 s^{-1}$.

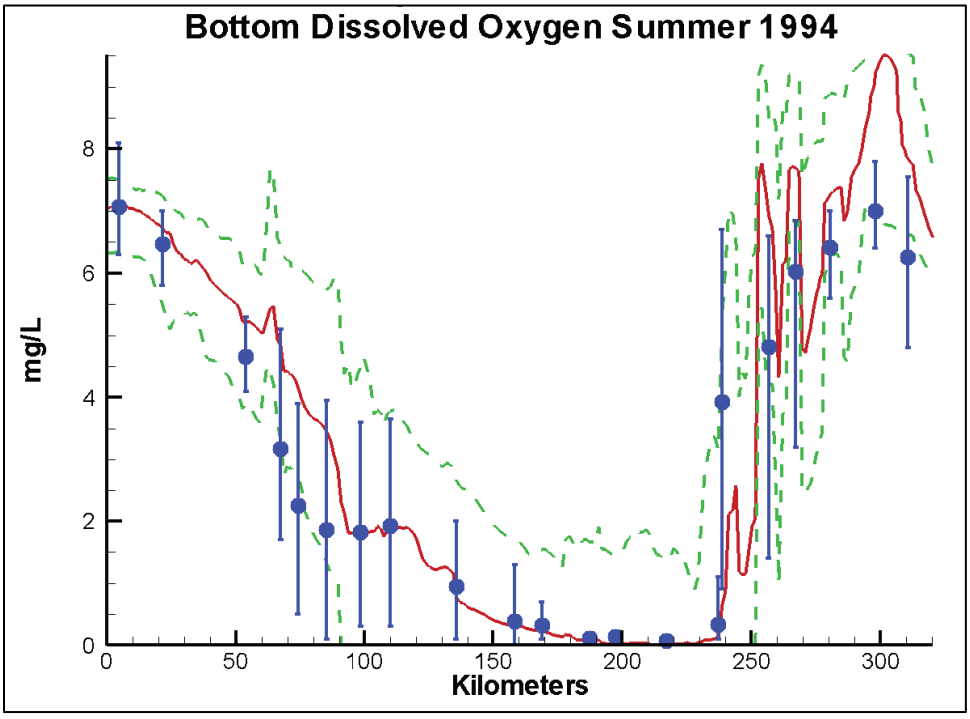

Figure 9-2. Computed (*red*) and observed (*blue*) bottom DO along Bay axis, summer 1999. Mar–Aug flow in Susquehanna River = 690 $m^3 s^{-1}$.

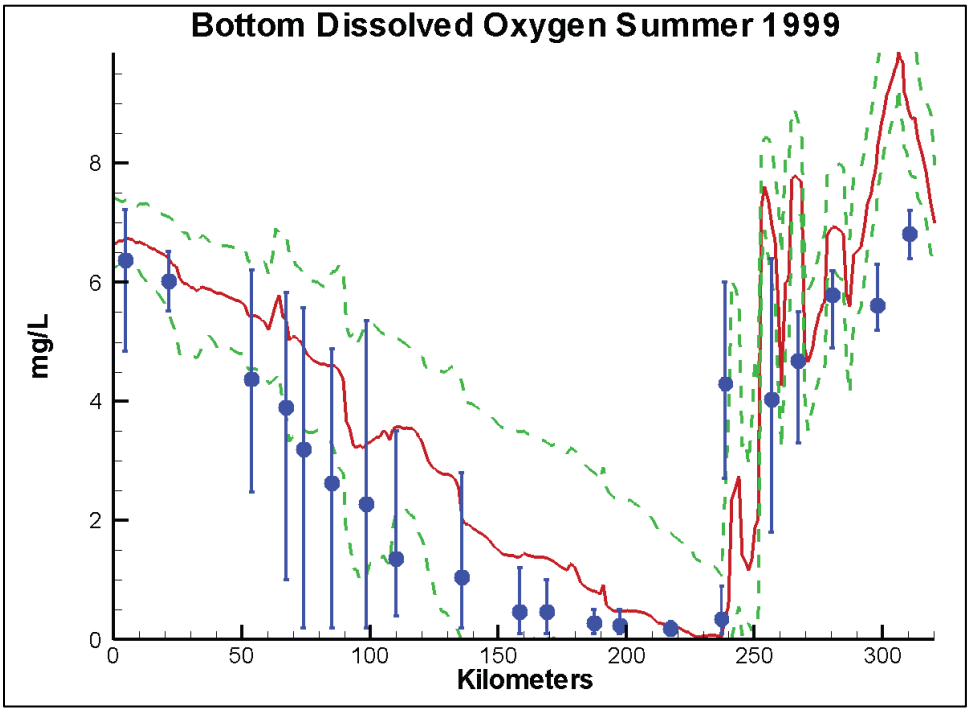

The excess bottom DO coincides with a shortfall in computed respiration in the lower Chesapeake Bay Program Segments (CBPS) (Figure 9-3 and Figure 9-4). Oxygen consumption cannot be increased, however, by simply increasing the model dissolved organic carbon (DOC) respiration rate. Ultimately, more oxidizable carbon is required to consume more oxygen.

Figure 9-3. Computed (*red*) and observed (*blue*) respiration in CBPS CB6, 1991–2000.

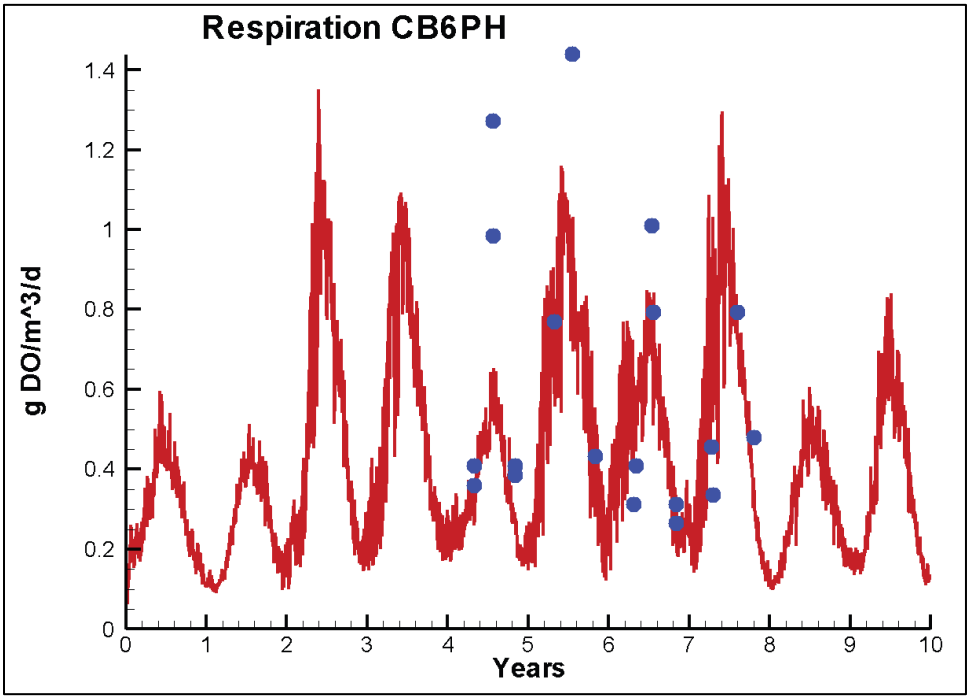

Figure 9-4. Computed (*red*) and observed (*blue*) respiration in CBPS CB7, 1991–2000.

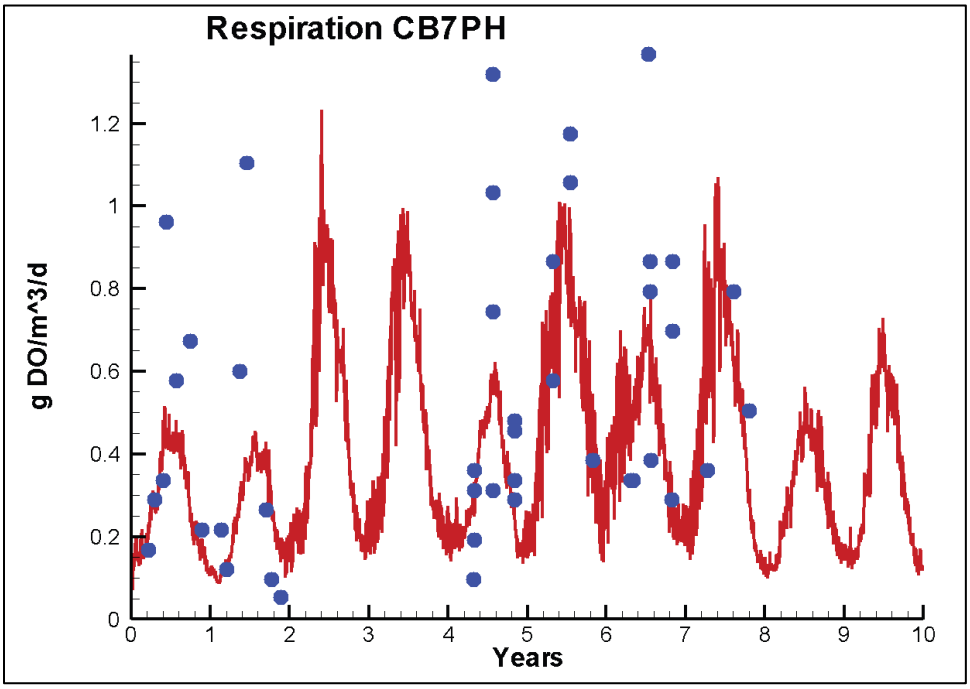

The carbon can be produced by increasing primary production (Figure 9-5 and Figure 9-6). While the steps to produce and respire more carbon, thereby consuming additional bottom-water DO, are readily visualized, implementing them in the model is not as straightforward. Increasing primary production also produces DO, so it is necessary to separate production from respiration in space and/or time. Otherwise, additional carbon respiration will be offset by the additional oxygen production. In addition, attempts to alter model parameters to improve results in the lower Bay have resulted in deteriorated performance elsewhere.

Figure 9-5. Computed (*red*) and observed *(blue*) net primary production in CBPS CB6, 1991–2000.

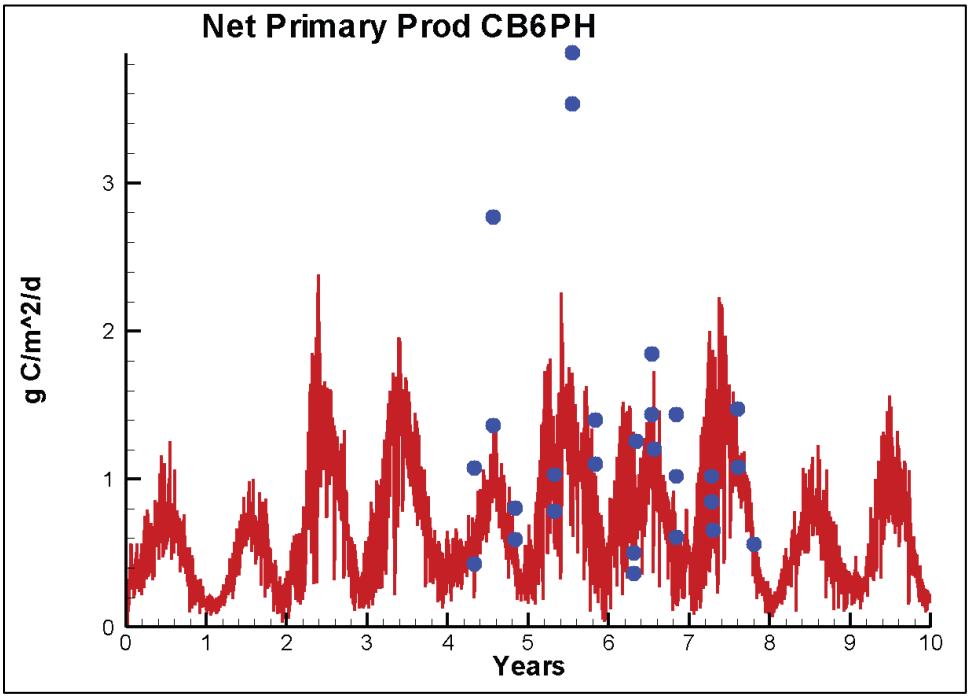

Figure 9-6. Computed (*red*) and observed (*blue*) net primary production in CBPS CB7, 1991–2000.

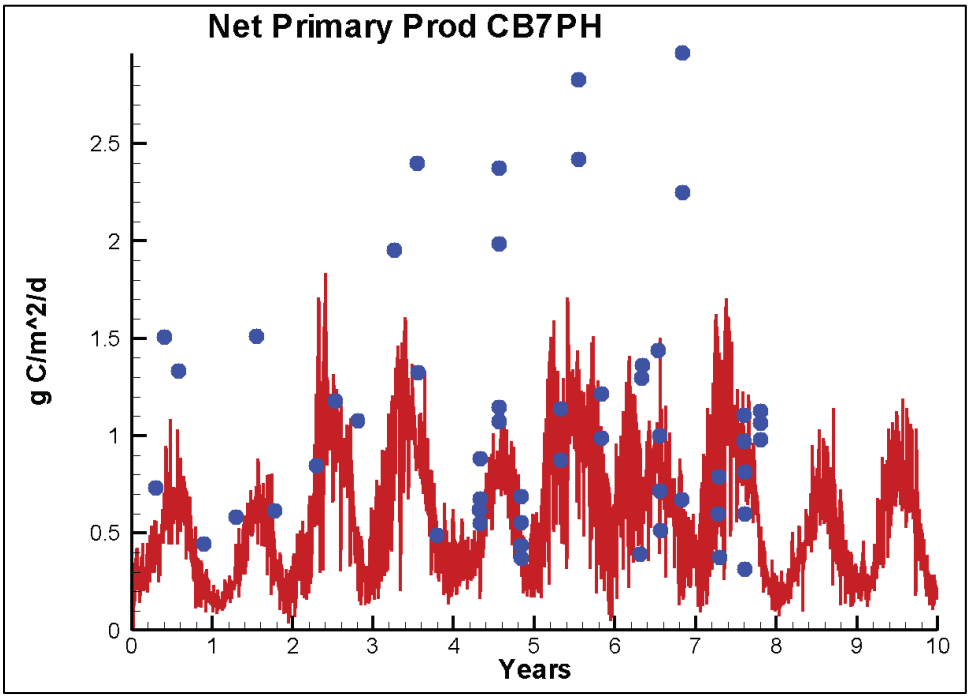

Successful representation of production, respiration, and DO in the lower Bay might require a distinct set of model parameters and/or creation of a new algal group for the lower Bay.

9.2.2 Potomac River Bottom-Water Hypoxia

The 2017 Water Quality and Sediment Transport Model (WQSTM) persistently misses the bottom-water hypoxia in the lower 50 km of the Potomac River (Figure 9-7). Model extremes attain near-zero DO, but the average computed DO is 1–2 g m^{-3} in excess of the observed average. As with the DO simulation in the lower Bay, that behavior has been characteristic of the model through multiple versions. The lower Potomac resembles the lower Bay in that the region is expansive and distant from the primary loading source near the head of tide. Those similarities suggest that the remedy for the lower Bay—increased production and respiration—would be appropriate for the lower Potomac as well. Measures of production and respiration to compare to model values, however, are lacking.

Figure 9-7. Computed (*red*) and observed (*blue*) bottom DO along Potomac River axis, summer 1996.

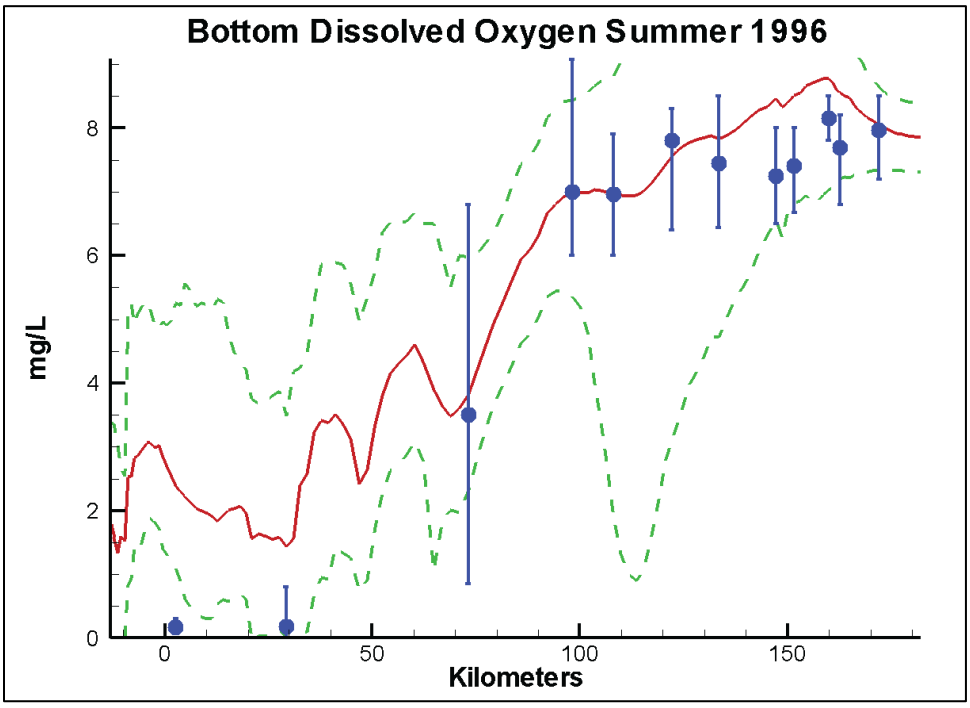

An alternate hypothesis for model behavior in the lower Potomac involves bathymetry as represented in the model. A sill exists across the mouth of the Potomac that is penetrated by a channel connecting to the Chesapeake Bay (Figure 9-8). Computed bottom DO increases as depth diminishes over the sill. Consequently, oxidation of organic matter is required to simply return bottom water to its initial oxygen concentration before passing over the sill. Examination and adjustment of the model geometry to provide a more direct connection to deep water in the Chesapeake Bay might lower the DO concentration of water entering the lower Potomac (Figure 9-9). Respiration would then contribute to further reducing the DO concentration rather than compensating for reaeration over the sill.

Figure 9-8. Profile view of Potomac River model grid. Note the sill at the junction with Chesapeake Bay (km 0).

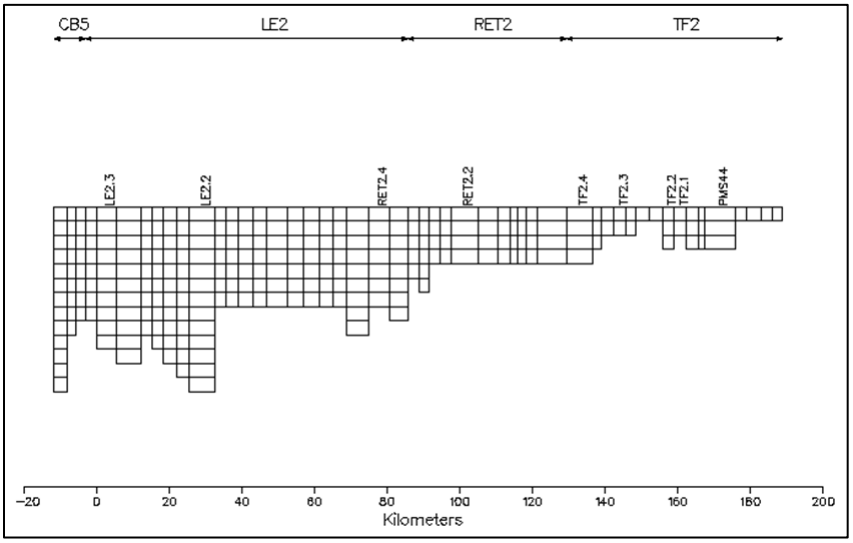

Figure 9-9. Plan view of model grid near the Potomac River mouth. Deep channels are shown in *blue* and shoals in *red*. Note the shallow sill separating the Chesapeake Bay and Potomac River deep water.

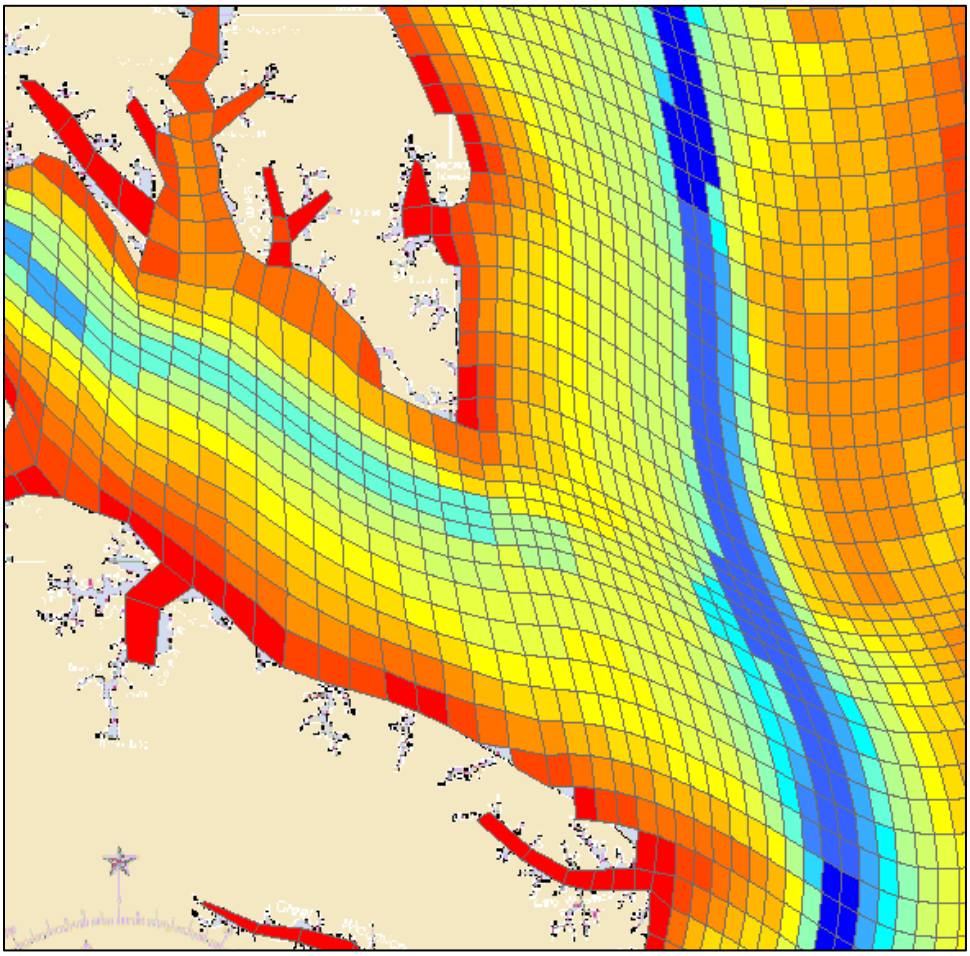

Experiments to validate the hypothesis regarding the Potomac River entrance channel are demanding of resources and, given the recommended replacement of CH3D, unlikely to be conducted. Clearly, however, great care should be taken in representing the connection of the Potomac to the Chesapeake Bay in the next model version. In the event that problems persist in simulating lower Potomac DO, attention would then be devoted to a review of production and respiration.

9.2.3 Tributary Surface Dissolved Oxygen Sag

Several of the western tributaries exhibit a surface DO sag in the lower to mid-estuary (Figure 9-10 through Figure 9-13). The sags are a persistent feature in multiple years of varying hydrology. Minimum DO concentrations in the sags approach 4 g m^{-3}. Model sensitivity analyses indicate the sags cannot be explained by respiration in adjacent wetlands (Figure 9-10). The wetland area in those reaches is small, relative to the extent of the open waters.

Figure 9-10. Computed (*red*) and observed (*blue*) surface DO along York River axis, summer 1996. Note the observed DO sag km 25–45. The sag around km 70 is induced by wetland respiration.

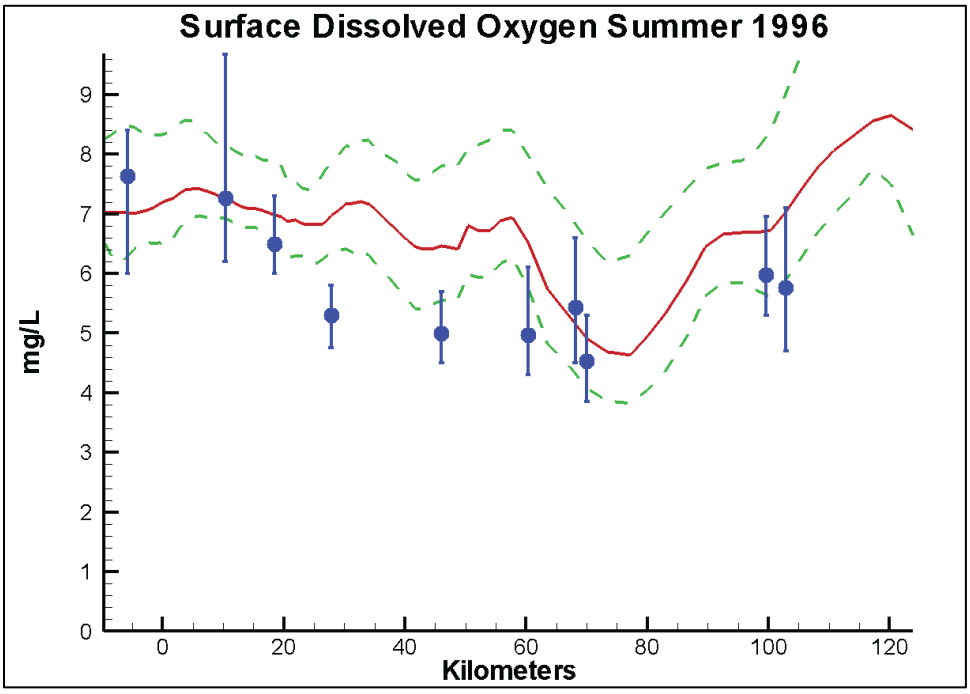

Figure 9-11. Computed (*red*) and observed (*blue*) surface DO along Rappahannock River axis, summer 1999. Note the observed DO sag km 40.

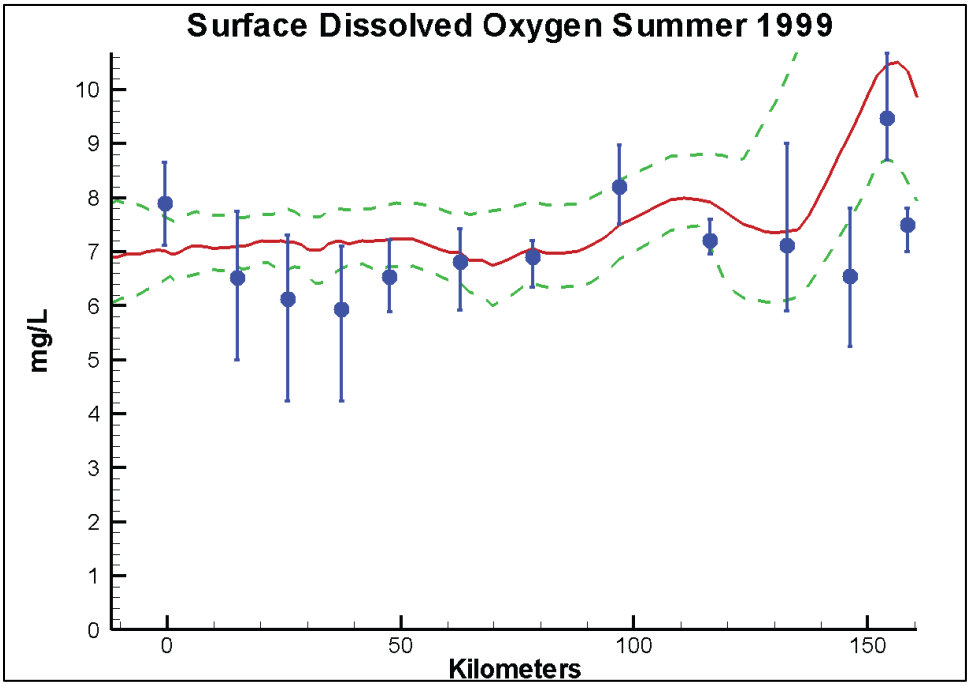

Figure 9-12. Computed (*red*) and observed (*blue*) surface DO along Potomac River axis, summer 1994. Note the observed DO sag km 70.

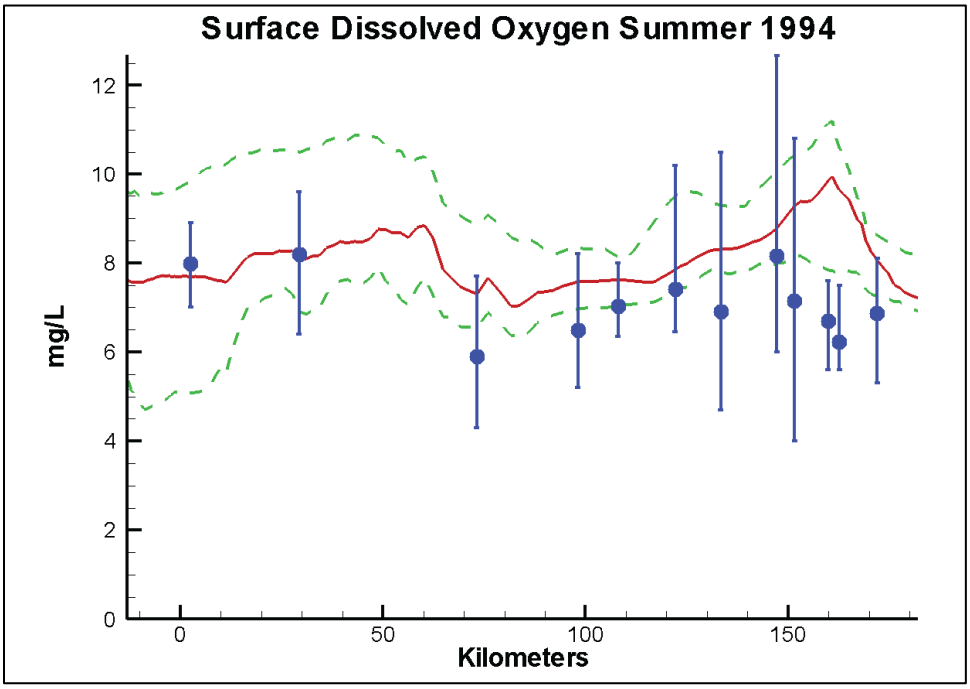

Figure 9-13. Computed (*red*) and observed (*blue*) surface DO along Patuxent River axis, summer 1996. Note the observed DO sag km 35-45.

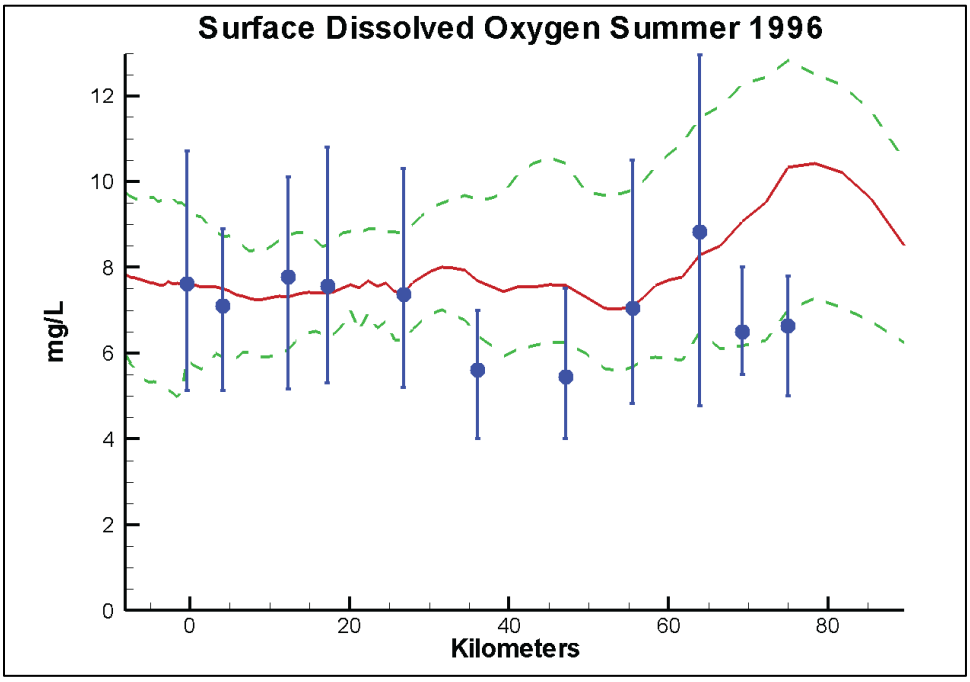

In a study of the Patuxent River, Testa and Kemp (2008) found that observed deep bottom-water respiration in the river was supported by transport of oxidizable material from adjacent shallow flanks. We can speculate that the observed surface oxygen sag is also caused by transport of oxidizable material from the shallow lateral flanks. In the model, we attempt to simulate that process by restricting particle settling in shallow water (i.e., net particle settling from the water column to sediments is a function of depth). That parameterization inhibits settling in flanks although subsequent lateral transport to deeper water overlying the channel is not ensured. The sags are absent in current model computations. Either lateral transport is insufficient or another process is responsible for the sags. If the sags are of concern, research is needed to explain the mechanism before definitive modeling can be conducted.

9.3 Phosphorus

9.3.1 Phosphorus Maximum at the Head of the Salinity Intrusion

The Bay and its western tributaries, including the Patuxent, Potomac, Rappahannock, and York rivers, exhibit a persistent dissolved inorganic phosphorus (DIP) peak coincident with the head of the salinity intrusion (Figure 9-14 through Figure 9-17). Early investigators suggested the DIP maximum results from desorption of phosphate from suspended solids caused by different partition coefficients in freshwater versus saltwater. Detailed experiments, however, indicate desorption linked to salinity is not responsible for the DIP maximum in the Potomac River (UMCES 2007). Investigations in the Patuxent indicate the phenomenon originates with reactions involving iron, phosphorus, and sulfate (Figure 9-18) (Jordan et al. 2008; Hartzell and Jordan 2012). Sulfate in saltwater is reduced to sulfide in anoxic bottom sediments. Iron sulfide is formed, leaving less iron available to form oxy-hydroxides, which sequester phosphorus.

Figure 9-14. Computed (*red*) and observed (*blue*) surface DIP along Bay axis, winter 1994. Note the observed peak km 300.

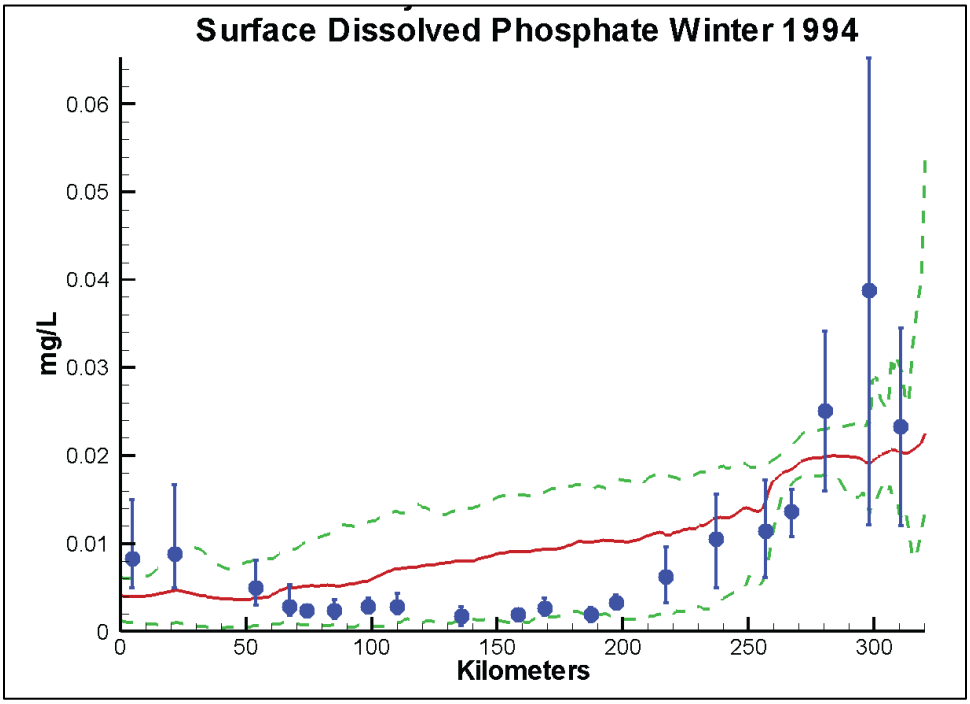

Figure 9-15. Computed (*red*) and observed (*blue*) surface salinity along Bay axis, winter 1994. Note the head of salt intrusion coincides with the DIP peak km 300.

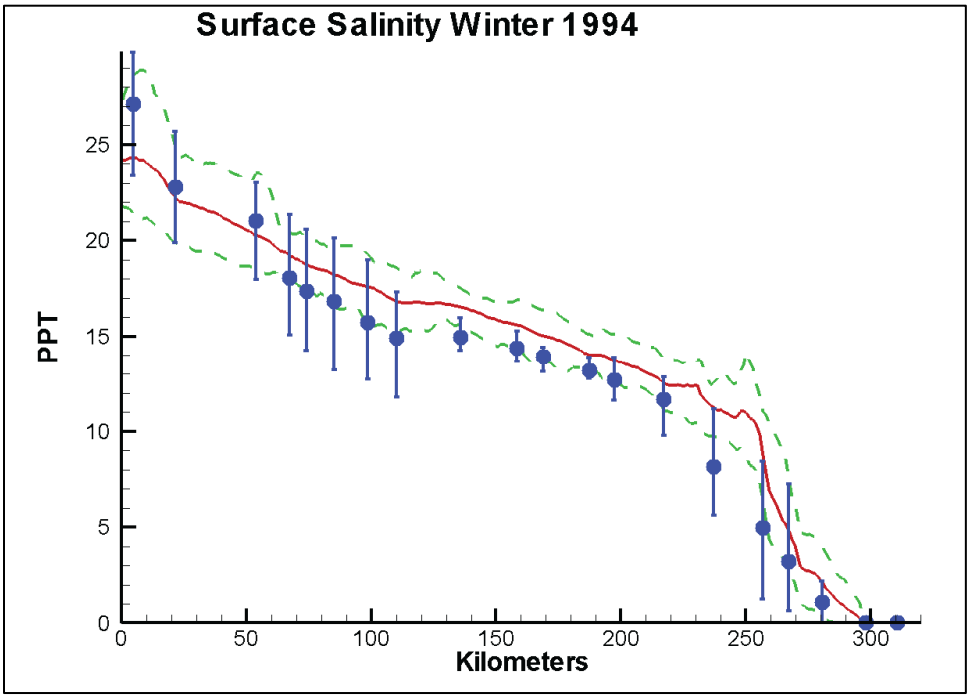

Figure 9-16. Computed (*red*) and observed (*blue*) surface DIP along Potomac River axis, summer 1994. Note the observed peak km 100.

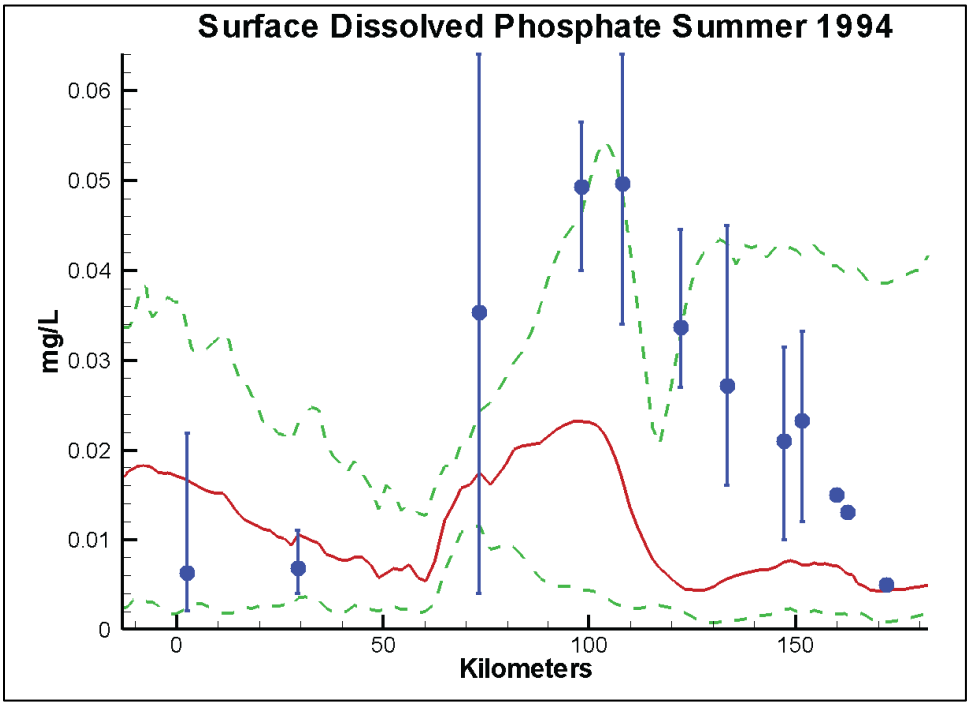

Figure 9-17. Computed (*red*) and observed (*blue*) surface salinity along Potomac River axis, summer 1994. Note the head of salt intrusion coincides with the DIP peak km 100.

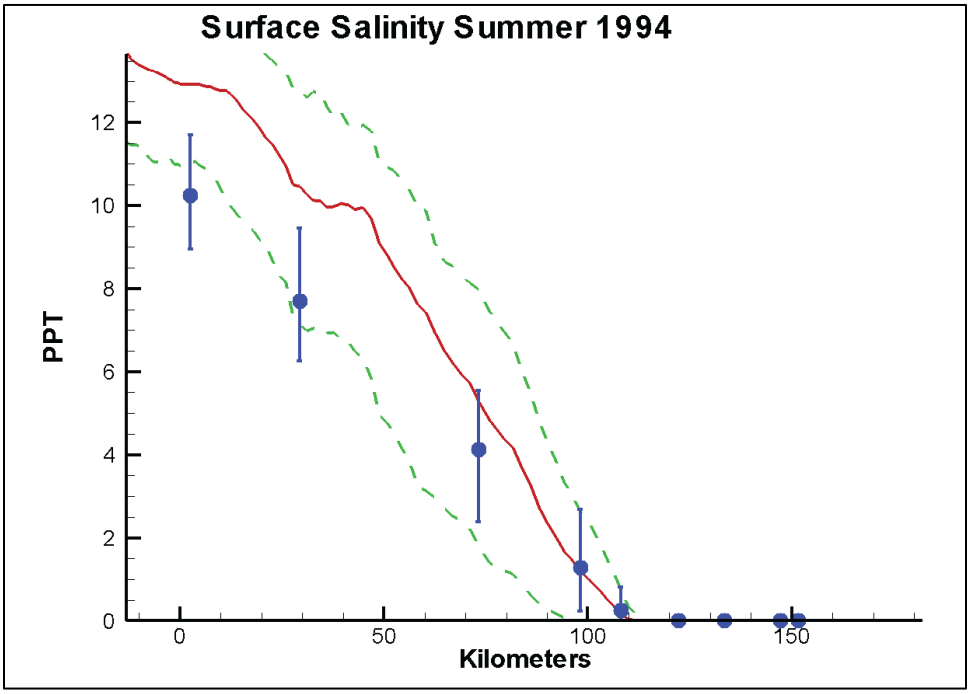

Figure 9-18. Schematic of reactions involving iron, phosphorus, and sulfur in sediments underlying an oxygenated saline system.

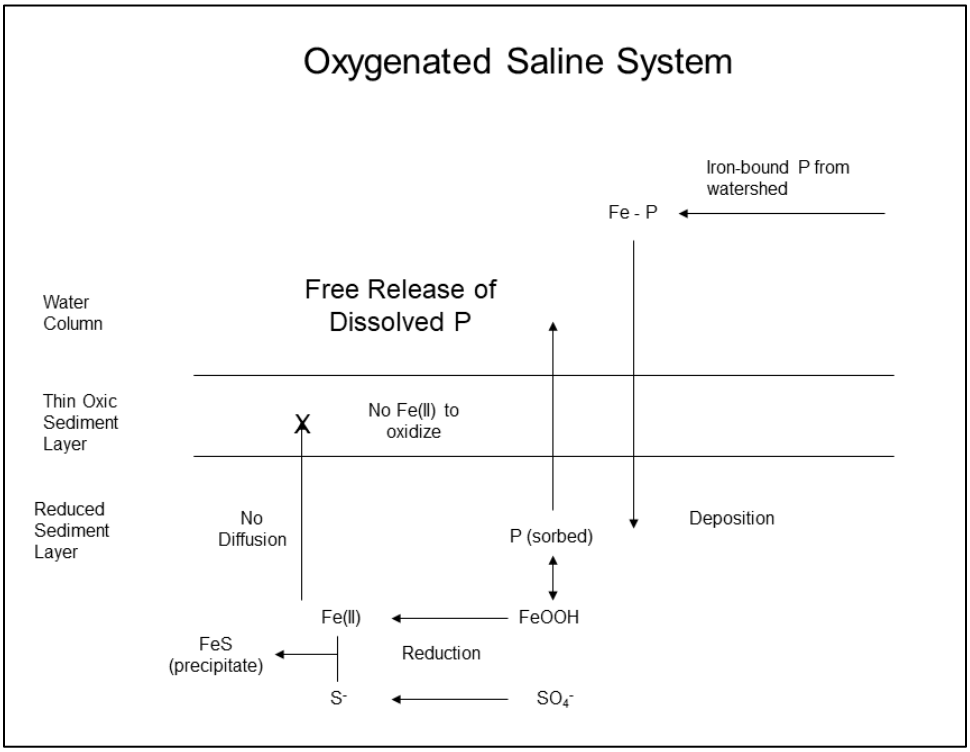

Neither iron nor sulfate is explicitly included in the present sediment diagenesis model. Rather, the role of those substances is represented through parameterization of general model formulations. We have attempted to reproduce the DIP maximum through manipulations of model parameters, in particular DIP sorption parameters, without success. Representation of the DIP maximum requires substantial reformulation of the diagenesis model. Ideally, iron should be added to the model parameter suite. That addition will require revisions to model formulations in the water column and sediments and, potentially, collecting additional observations. Iron observations are available in the Bay and tributary water column, bed sediments, and inflows. Those observations are sporadic, however, and might not support model development and validation without additional field observations.

9.3.2 Phosphorus Coprecipitation with Iron

DIP shows a strong inverse relationship to DO in the deep Bay waters, which experience seasonal hypoxia (Figure 9-19). DIP increases instantaneously at the onset of hypoxia and is depleted rapidly when DO achieves 2 g m^{-3} during fall reaeration of bottom waters. The increase associated with hypoxia onset is readily explained by the release of DIP from bottom sediments (Cowan and Boynton 1996). The origin of the rapid removal is not obvious. We propose that the removal is caused by phosphorus coprecipitation with iron. In the absence of oxygen, iron exists in reduced, dissolved form, Fe(II). When the water column oxygenates, particulate iron oxides, Fe(III), are formed, to which DIP rapidly sorbs. The sorbed phosphorus might persist in the water column or settle to bottom sediments. In either case, the phosphorus is no longer in dissolved form. That mechanism was observed in the Scheldt Estuary when phosphorus was rapidly removed from anoxic headwaters entering the oxygenated lower estuary (Zwolsman 1994).

The rapid depletion of DIP associated with autumn reaeration was noted in the earliest stages of model development (Cerco and Cole 1994). At that time, a “total active metal” state variable, representing iron and manganese, was created to mimic the process. Since then, various approaches to removing DIP from the water column have been employed. The present model invokes a DIP-settling velocity in appropriate segments of the Bay during fall reaeration.

Figure 9-19. Computed (*red*) and observed (*blue*) bottom DO and DIP Station CB4.2C, 1991–2000. Vertical lines indicate phosphorus removal during autumn reaeration events (DO > 2 g m^{-3}).

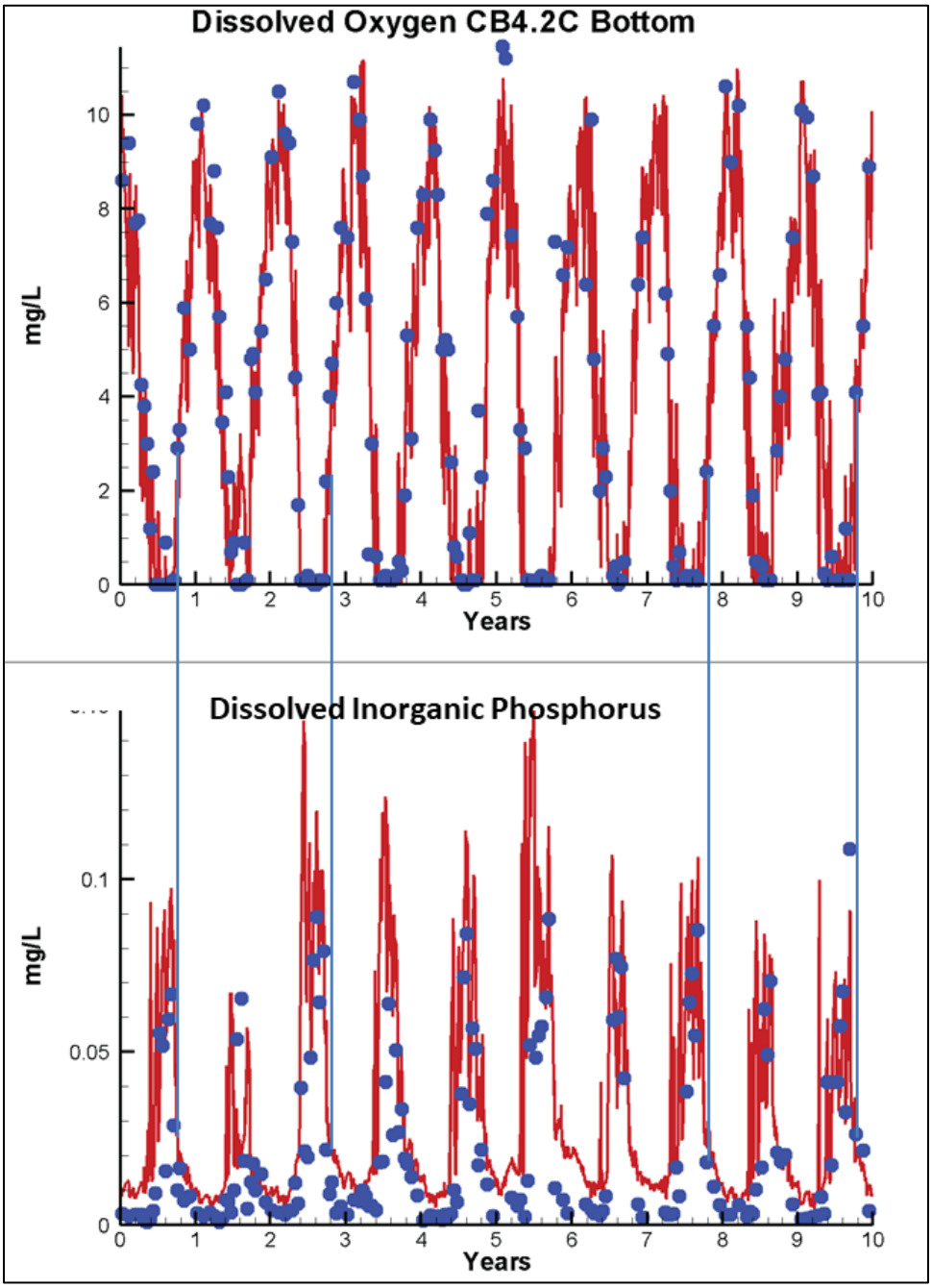

A second phenomenon involving DIP sorption or precipitation with iron oxides might also exist. During summer, the model computes excess DIP in surface waters overlying deep anoxic water (Figure 9-20). The DIP apparently diffuses upward from the anoxic bottom water in which large DIP concentrations are maintained by release from bottom sediments. The diffusion exceeds the rate of algal DIP uptake and the model, consequently, computes excess DIP. We

speculate the excess surface DIP is not observed in the Bay because DIP is removed from the water column at the transition from hypoxic to oxygenated water, either by coprecipitation with iron or by sorption to existing particulate iron. That mechanism is more speculative than the autumn removal described earlier. It is not readily apparent in observations and might be otherwise explained, for example, by luxury phytoplankton phosphorus uptake.

Figure 9-20. Computed (*red*) and observed (*blue*) surface DIP Station CB4.2C, 1991–2000. Note the computed excess during summer, coincident with sediment release into anoxic bottom water.

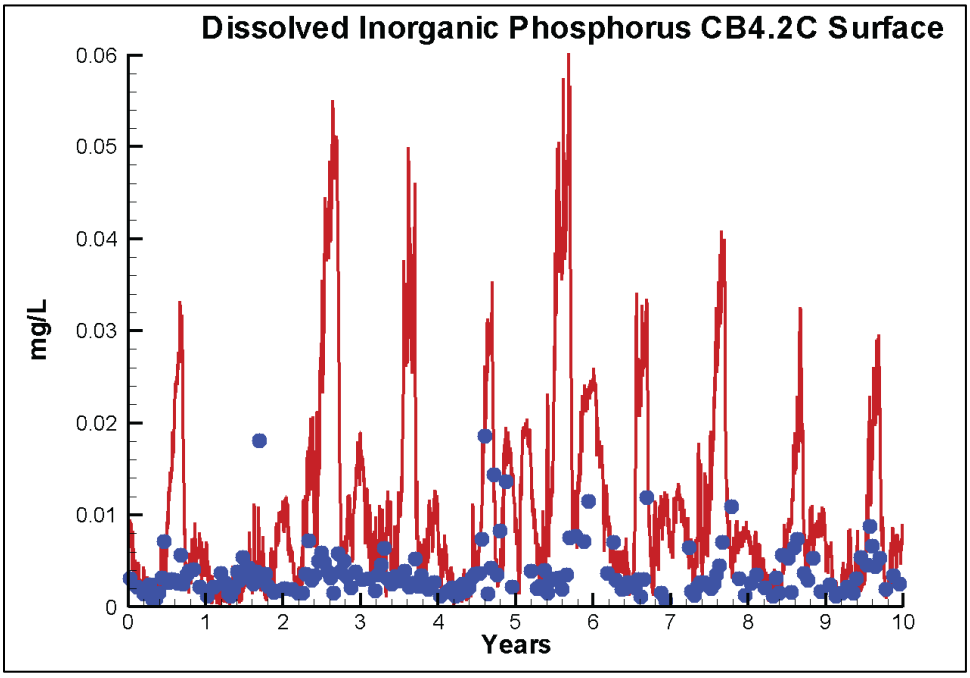

Correct representation of the autumn DIP precipitation event requires addition to the model suite of multiple forms of iron and supports the recommendation to add iron to represent the DIP maximum coincident with the head of salt intrusion. Model investigation of the potential for DIP removal at the vertical transition from anoxic to oxygenated water also requires addition of iron to the model. In that instance, collection of appropriate field observations to validate the proposed mechanism also is recommended.

9.3.3 Particulate Inorganic Phosphorus

Particulate phosphorus is the predominant form of phosphorus in the Chesapeake Bay water column (Keefe 1994; Conley et al. 1995). It can be broadly divided into organic (Org P), iron-bound (Fe-P), and apatite-associated (HCL-P) fractions. Depending on location and season, either Org P or Fe-P is the predominant fraction. The combined Fe-P and HCL-P are represented by the model particulate inorganic phosphorus (PIP) state variable. The reactions affecting PIP are largely unknown. Analyses of monitoring data from 1994

indicate the amount of phosphorus associated with inorganic solids is not affected by DIP (Figure 9-21). That is, the fraction associated with solids cannot be represented by linear partitioning. Although outliers exist, observations suggest the phosphorus fraction of fixed solids is roughly constant at 0.0012 g P g^{-1} solids. In the absence of any obvious reactivity, PIP is treated as inert in the model water column. When deposited in the benthic sediments, PIP is combined with inorganic phosphorus produced by diagenesis of organic matter.

A review of the present model provided suggestions for model PIP kinetics in the water column, based on experiments conducted in the Great Lakes (Brady et al. 2018). The interactions of iron, phosphorus, and DO previously discussed indicate DO should affect particle-bound phosphorus in the Chesapeake Bay. The proposed and expected reactions, however, cannot be validated by examining monitoring data alone. Basic laboratory experiments are necessary to determine the reactivity of PIP and the factors that influence PIP reactions.

9.4 Model Parameter Suite

9.4.1 Mapping Watershed Model to Water Quality Model

Chapter 6 describes the process of mapping Watershed Model (WSM) loads to WQSTM inputs. Basically, four particulate and dissolved WQSTM organic nitrogen variables must be derived from one WSM organic nitrogen load. Five WQSTM dissolved and particulate phosphorus variables must be derived from combined WSM organic and PIP loads. Four particulate and dissolved WQSTM organic carbon variables are based on ratio to WSM organic nitrogen since organic carbon is not computed by the WSM.

Guidance for the mapping is obtained from observations collected near the major river inflows to the Bay system. Those observations allow for derivation of particulate/dissolved splits and for carbon-to-nitrogen ratios. Data collected at or above the major fall-lines are extensive but, at times, frustrating to use. Observations are collected by multiple agencies and subject to varying analytical methods. Analyses necessary for the mapping process are not always available. Multiple relationships for particulate/dissolved splits and for carbon-to-nitrogen ratios can be proposed and are, at times, apparent.

For the present study, required mapping parameters were derived from observations at the first in-stream monitoring station downstream of major inflows. That switch provided required information and ensured consistency in analytical methods. A disadvantage was that data were available only for in-stream surveys and likely omitted high flows when conditions prohibited sampling.

One solution to the problems involved in mapping WSM loads to the WQSTM variables is to revise the WSM to include organic carbon and to separate particulate from dissolved organic matter. Otherwise, a study is recommended to examine available data and to obtain definitive relationships between WSM and WQSTM variables. Collection of additional, specific observations might be required when available data are insufficient.

9.4.2 Net Settling of Particulate Organic Matter

The sediment diagenesis model employs a net settling velocity to transfer particulate organic matter from the water column to benthic sediments. Transfer from water to sediments is a one-way process with no resuspension. The net settling velocity is usually lower than settling through the water column to represent the long-term effects of resuspension. Little guidance exists for specifying the net settling velocity. In the initial model application, net settling was 10 percent of settling velocity in the overlying water (Cerco and Cole 1994). In the present study, net settling is 1–100 percent of settling in the overlying water, depending on depth. This parameterization is based on the assumption that the level of resuspension is high in shallow water because of wave-induced shear stress. It is intended to induce the transfer of particulate material from shoals to deep water required to account for bottom-water respiration (Testa and Kemp 2008). While this parameterization does contribute to model respiration in deep channels, net settling in extensive shallow areas not adjacent to deep channels is likely underestimated.

An improved, definitive method of representing transfer of particulate material from water to benthic sediments is required. One option is to include particulate organic matter in the sediment transport algorithms of the WQSTM. In that case, settling and resuspension would be computed dynamically. That method requires modification of the diagenesis model and renders the model system significantly more complicated. A second option is to retain the concept of net settling but introduce a relation to long-term average bottom shear stress. That approach was investigated in the present study. Resources were not available, however, to complete the proposed approach within project deadlines. A weakness of the approach was that the specific functional relationship of net settling to average shear stress was not available. Time-consuming trial and error was required. Regardless of approach, the next study should provide improved quantification of particulate organic matter transfer between water and sediments, validated by comparing computed and observed particulate organic matter concentrations in both water column and benthic sediments.

9.5 References

Brady, D., J. DePinto, S. Chapra, D. DiToro, M. Friedrichs, M. Gray, T. Jordan, and M. Xia. 2018. *Scientific and Technical Advisory Committee Chesapeake Bay Water Quality and Sediment Transport Model Review*. STAC Publication Number 18-002. Chesapeake Research Consortium, Edgewater, MD.

CCMP (Chesapeake Community Modeling Program). 2018. Chesapeake Bay ROMS Community Model. Chesapeake Community Modeling Program. Accessed August 2019. http://ches.communitymodeling.org/models/ChesROMS/index.php.

Cerco, C.F., and T.M. Cole. 1994. Three-Dimensional Eutrophication Model of Chesapeake Bay. Technical Report EL-94-4. US Army Engineer Waterways Experiment Station, Vicksburg, MS.

Conley, D., W. Smith, J. Cornwell, and T. Fisher. 1995. Transformation of particle-bound phosphorus at the land-sea interface. *Estuarine, Coastal and Shelf Science* 40(2):161–176.

Cowan, J., and W. Boynton. 1996. Sediment-water oxygen and nutrient exchanges along the longitudinal axis of Chesapeake Bay: Seasonal patterns, controlling factors, and ecological significance. *Estuaries* 19(3):562–580.

DiToro, D., and J. Fitzpatrick. 1993. Chesapeake Bay Sediment Flux Model. Contract Report El-93-2. US Army Corps of Engineers, Waterways Experiment Station, Vicksburg, MS.

Hartzell, J., and T. Jordan. 2012. Shifts in the relative availability of phosphorus and nitrogen along estuarine salinity gradients. *Biogeochemistry* 107:489-500.

Johnson, B., R. Heath, B. Hsieh, K. Kim, and L. Butler. 1991. *User's Guide for a Three-Dimensional Numerical Hydrodynamic, Salinity, and Temperature Model of Chesapeake Bay*. Technical Report HL-91-20. US Army Engineer Waterways Experiment Station, Vicksburg, MS.

Jordan, T., J. Cornwell, W. Boynton, and J. Anderson. 2008. Changes in phosphorus biogeochemistry along an estuarine salinity gradient: The iron conveyer belt. *Limnology and Oceanography* 53(1):172–184.

Keefe, C. 1994. The contribution of inorganic compounds to the particulate carbon, nitrogen, and phosphorus in suspended matter and surface sediments of Chesapeake Bay. *Estuaries* 17:122–130.

Kim, T., R. Labiosa, T. Khangaonkar, Z. Yang, C. Chen, J. Qi, and C. Cerco. 2009. Development and Evaluation of a Coupled Hydrodynamic (FVCOM) and Water Quality Model (CE-QUAL-ICM). In proceedings of the 11th International Conference on Estuarine and Coastal Modeling, Seattle, Washington, November 4–6, 2009, pp. 373–388. doi: 10.1061/41121(388)23.

Testa, J., and W. Kemp. 2008. Variability of biogeochemical processes and physical transport in a partially stratified estuary: A box-modeling analysis. *Marine Ecology Progress Series* 356:63–79.

Tian, R. 2016. Progress report on FVCOM-ICM application in the Chester River: Evaluation. http://www.chesapeake.org/stac/presentations/262_Tian_STAC_Apr20_2016FVCOM1.pdf.

UMCES (University of Maryland Center for Environmental Science). 2007. Development of an estuarine phosphorus sub-model for incorporation into the next-generation Potomac River environmental model: Phosphorus data and laboratory experiments. TS-563-07. University of Maryland Center for Environmental Science, Horn Point, MD.

Ye, F., Y. Zhang, H. Wang, M. Friedrichs, I. Irby, E. Alteljevich, A. Valle-Levinson, Z. Wang, H. Huang, J. Shen, and J. Du. 2018. A 3D unstructured-grid model for Chesapeake Bay: Importance of bathymetry. *Ocean Modeling* 127:16–39.

Wang, H., Z. Wang, J. Zhang, and F. Ye. 2016. Chester River Hydrodynamic and Water Quality Modeling Using SCHISM/HEM3D. Accessed August 2019. http://www.chesapeake.org/stac/presentations/262_talk-Wang-CBPO-April2016.pdf.

Xia, M., and L. Jiang. 2016. Application of an unstructured grid-based water quality model to Chesapeake Bay and its adjacent coastal ocean. *Journal of Marine Science and Engineering* 4:52. doi:10.3390/jmse4030052.

Zwolsman, J. 1994. Seasonal variability and biogeochemistry of phosphorus in the Scheldt Estuary, south-west Netherlands. *Estuarine, Coastal and Shelf Science* 39:227–248.

Appendix A: Time Series Comparisons 1991–2000

The eutrophication model was applied and calibrated to the period 1991–2000. Data for model calibration was obtained from the database maintained by the US Environmental Protection Agency's Chesapeake Bay Program at http://www.chesapeakebay.net/data/index.htm. Observations were obtained from 40 stations among the larger number in the monitoring program (Figure A-1). We selected one station in each major Chesapeake Bay Program Segment as well as stations in multiple smaller segments. At each station, time series comparisons were completed for 19 water quality components at one to three depth intervals. Comparisons included physical quantities (salinity, temperature, suspended solids, and light attenuation), chlorophyll, dissolved oxygen (DO), and multiple forms of carbon, nitrogen, and phosphorus. This appendix concentrates on the components that correspond closely to chlorophyll, clarity, and DO. The presentation of each component is described, and four pages of plots for each time series station follow the descriptions.

Chlorophyll Surface. Ten-year time series of computed and observed chlorophyll *a*. The time axis on this and the following plots commences on January 1, 1991, and runs through January 31, 2000. Instantaneous observations from the surface sample (1 meter) are plotted along with daily-average model values in the cell that corresponds to the monitoring station.

Light Attenuation. Ten-year time series of computed and observed diffuse light attenuation. Attenuation at the following stations was calculated from disk visibility (coefficient of diffuse light attenuation (Ke) = 1.4 / DV): EE3.1, EE3.2, EE1.1, EE2.1, ET1.1, ET2.3, ET4.2, ET6.2, ET9.1, WT1.1, WT2.1, WT8.1, RET2.4, TF2.1, LE1.3, and RET1.1. Attenuation at the remaining stations was derived from irradiance observed at multiple depths in the water column.

Dissolved Inorganic Nitrogen Surface. Ten-year time series of computed and observed dissolved inorganic nitrogen, which is computed as the sum of ammonium and nitrate nitrogen.

Dissolved Inorganic Phosphorus Surface. Ten-year time series of computed and observed dissolved inorganic phosphorus.

Figure A-1. Monitoring stations. Forty stations were selected from this group for time series analysis.

Algal Limits. Ten-year time series of computed nutrient limitations on phytoplankton production in the model surface cell. Nutrient limits are daily average values. The limitations are biomass weighted according to the algal groups present. A limitation of zero indicates complete limitation to growth. A limitation of unity indicates no limitation.

Total Nitrogen Surface. Ten-year time series of computed and observed total nitrogen.

Total Phosphorus Surface. Ten-year time series of computed and observed total phosphorus.

Statistics. Mean difference and absolute mean difference statistics are provided for the computations and observations at this station. Those statistics are defined in equation 1 and equation 2:

$$MD = \frac{\sum(P-O)}{N} \quad (1)$$

$$AMD = \frac{\sum|P-O|}{N} \quad (2)$$

where:

MD = mean difference
AMD = absolute mean difference
O = observation
P = prediction
N = number of observations

Dissolved Oxygen. Ten-year time series of computed and observed DO. The presentation varies depending on local depth of the monitoring station. Comparisons are always presented for the surface sample. At deeper stations (typically prefixed EE and RET), comparisons are presented at the surface and bottom. At stations deep enough to warrant sampling near the pycnocline (typically prefixed CB and LE), comparisons are presented at the surface, mid-depth, and bottom. Statistics correspond to the number of depths plotted.

Total Suspended Solids Surface. Ten-year time series of computed and observed total suspended solids (TSS). Model TSS is the sum of the four fixed solids variables (fine clay, clay, silt, and sand) plus particulate organic carbon components (algal carbon and labile, refractory, and slow refractory particulate organic carbon). Organic carbon is converted to solids through multiplication by the ratio 2.5 g solids g^{-1} C.

Solids Surface. This graph separates computed fixed (inorganic) and volatile (organic) solids. Volatile solids are obtained from modeled carbon as noted in *Total Suspended Solids Surface*, above. No observations are shown since these fractions are not regularly observed in the monitoring program.

Station CB1.1

Run233 1991-2000
Chlorophyll CB1.1 Surface

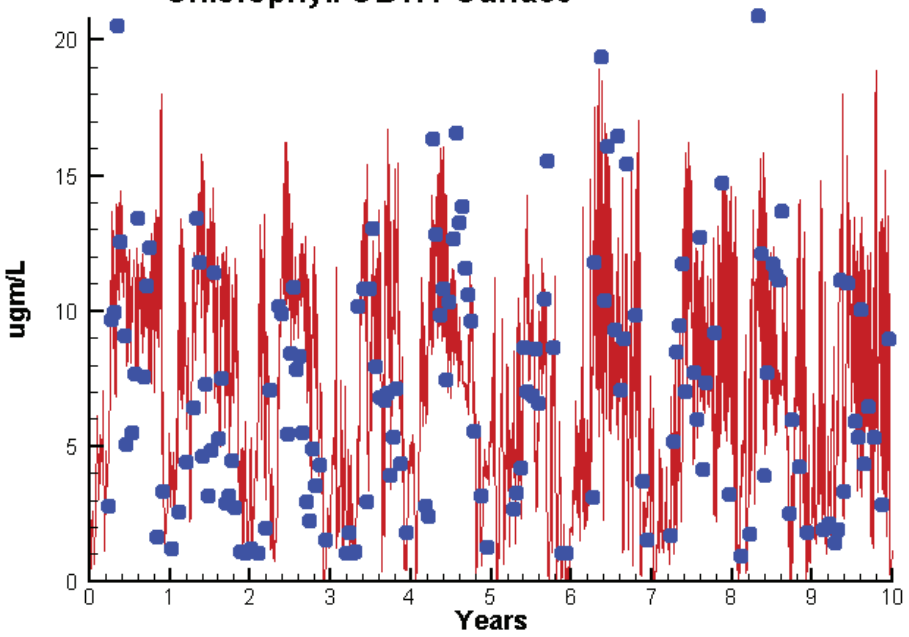

Run233 1991-2000
Light Extinction CB1.1 Surface

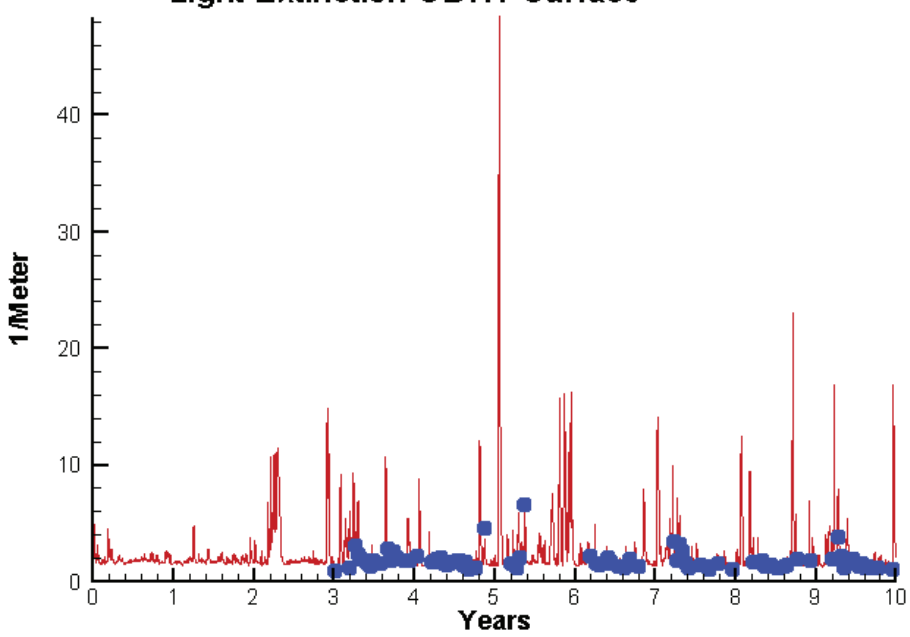

Run233 1991-2000
Dissolved Inorganic Nitrogen CB1.1 Surface

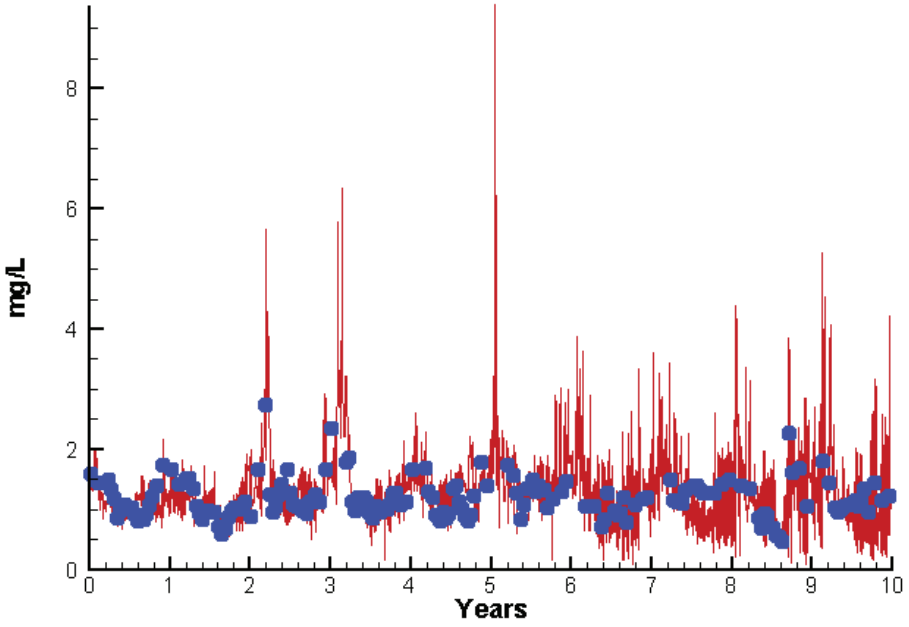

Run233 1991-2000
Dissolved Inorganic Phosphorus CB1.1 Surface

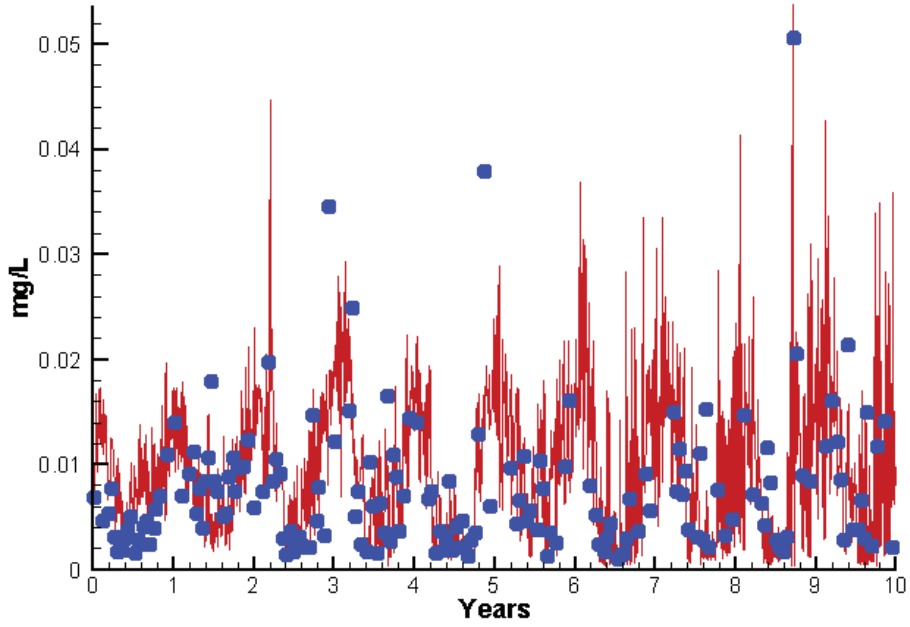

Station CB1.1

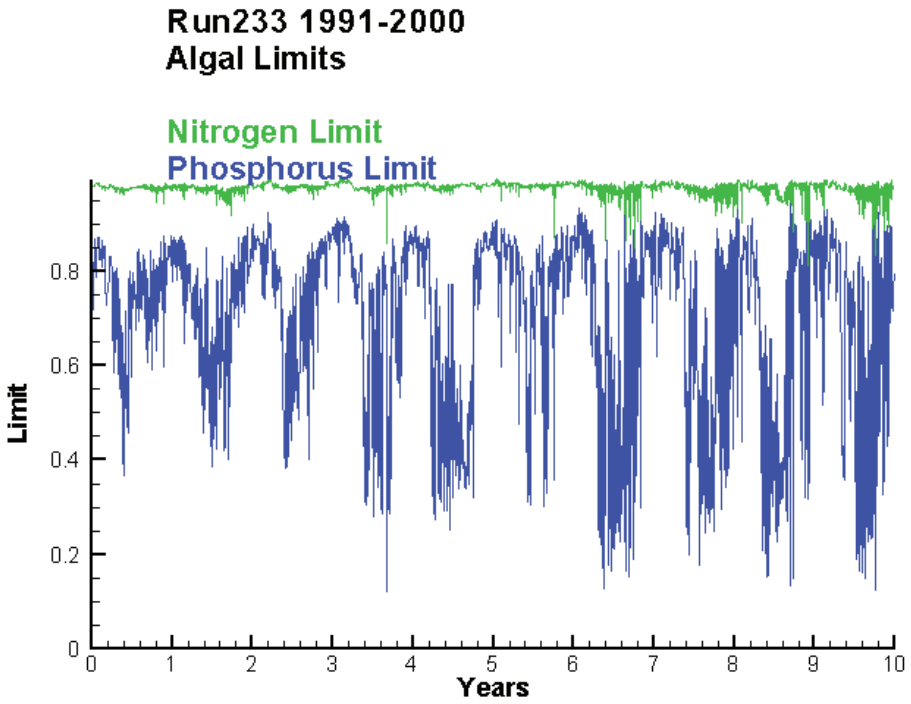

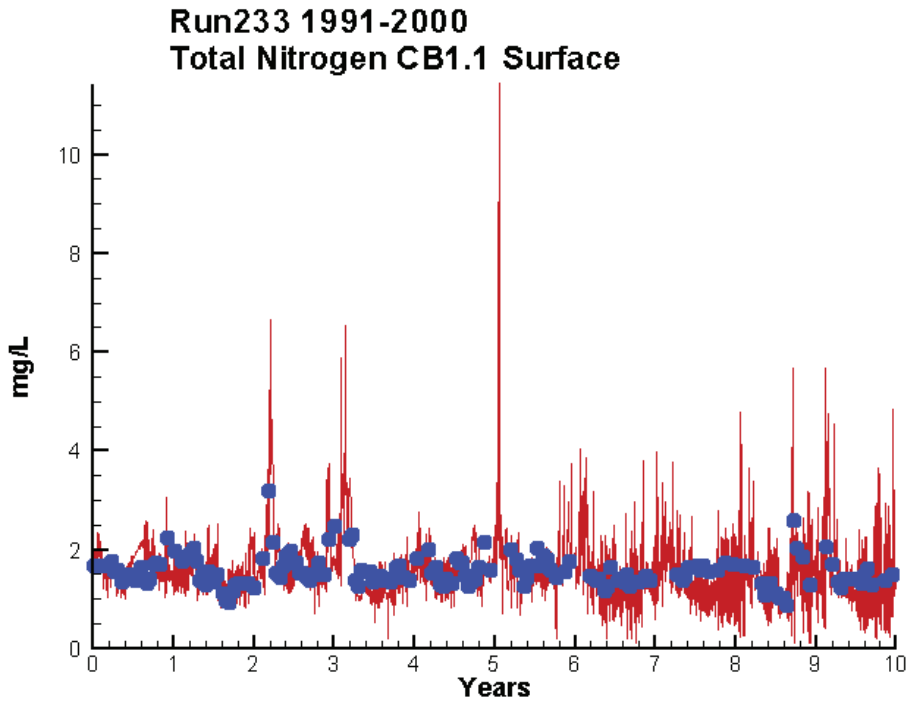

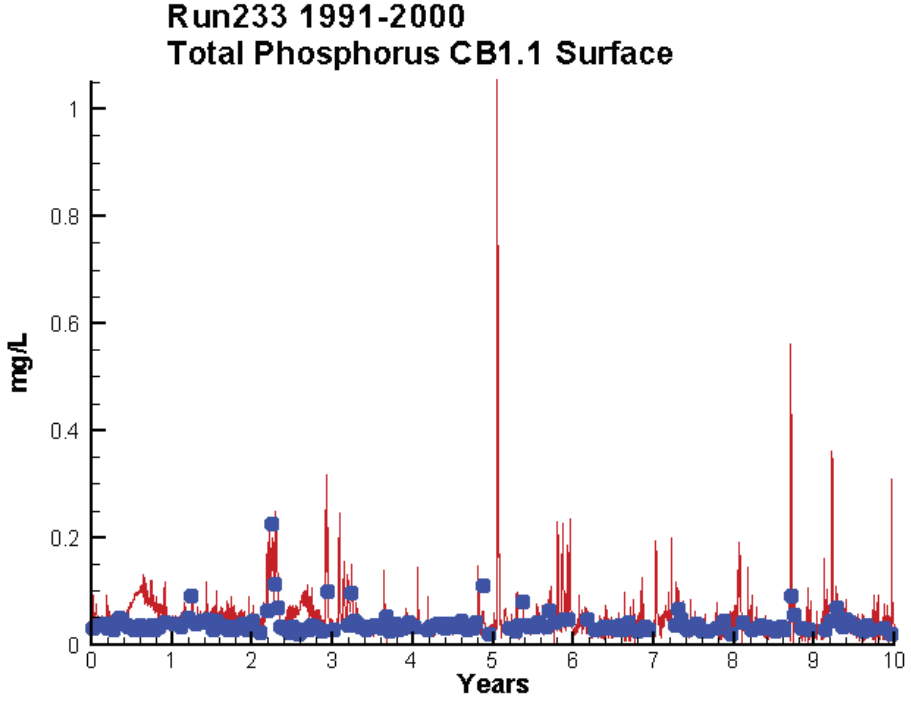

	Mean Difference	Absolute Mean Difference
Chl	1.0995	3.6412
DIN	0.0212	0.2582
KE	0.2237	0.4710
DIP	0.0007	0.0044
TP	0.0098	0.0170
TN	-0.0586	0.3186

Station CB1.1

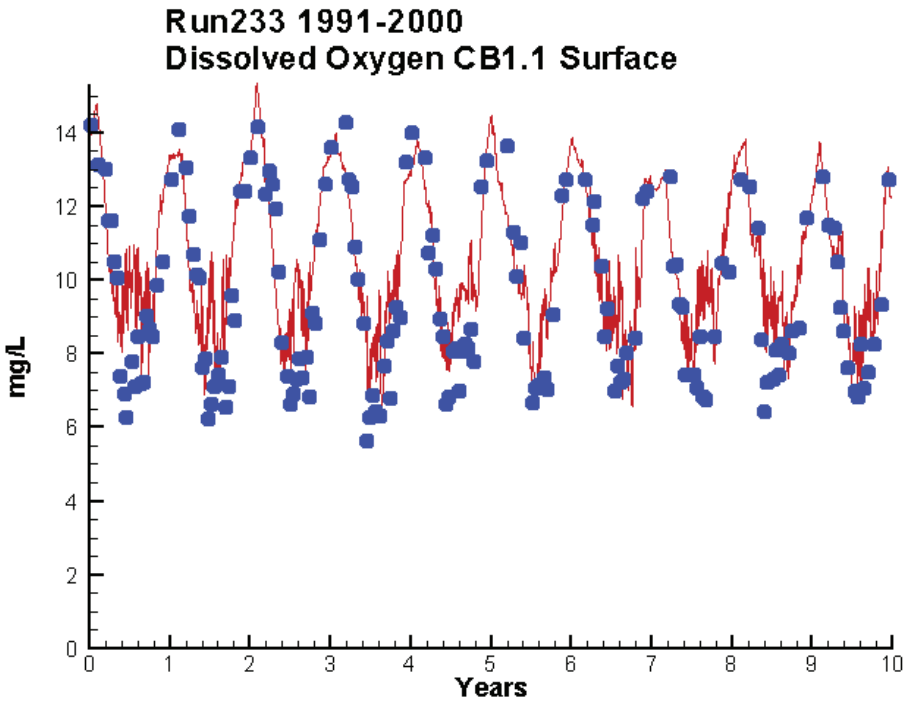

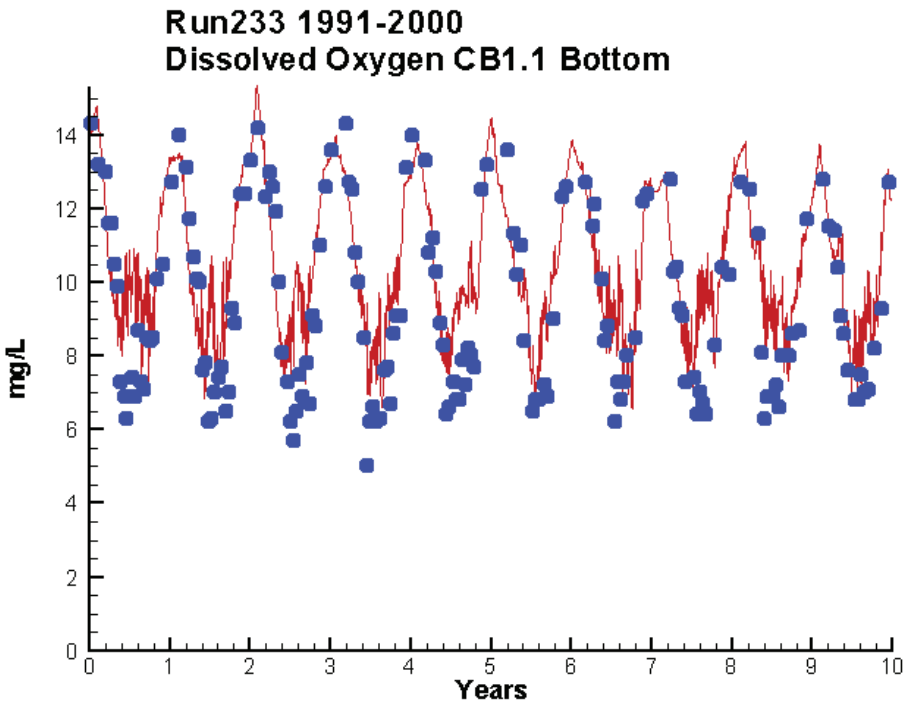

	Mean Difference	Absolute Mean Difference
Top DO	0.5641	1.1447
Bot DO	0.6868	1.2462

Station CB1.1

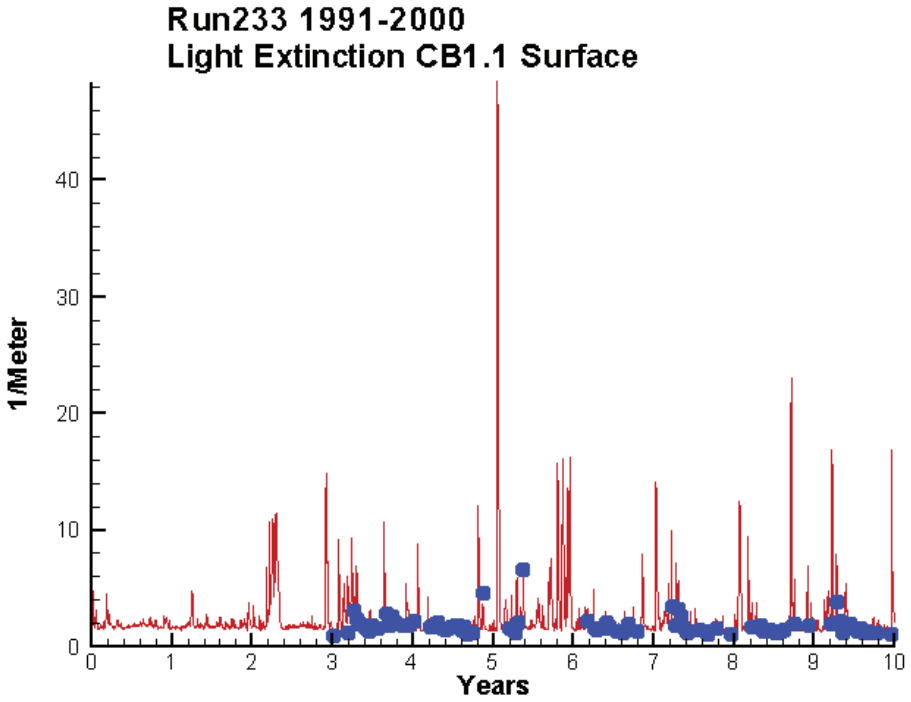

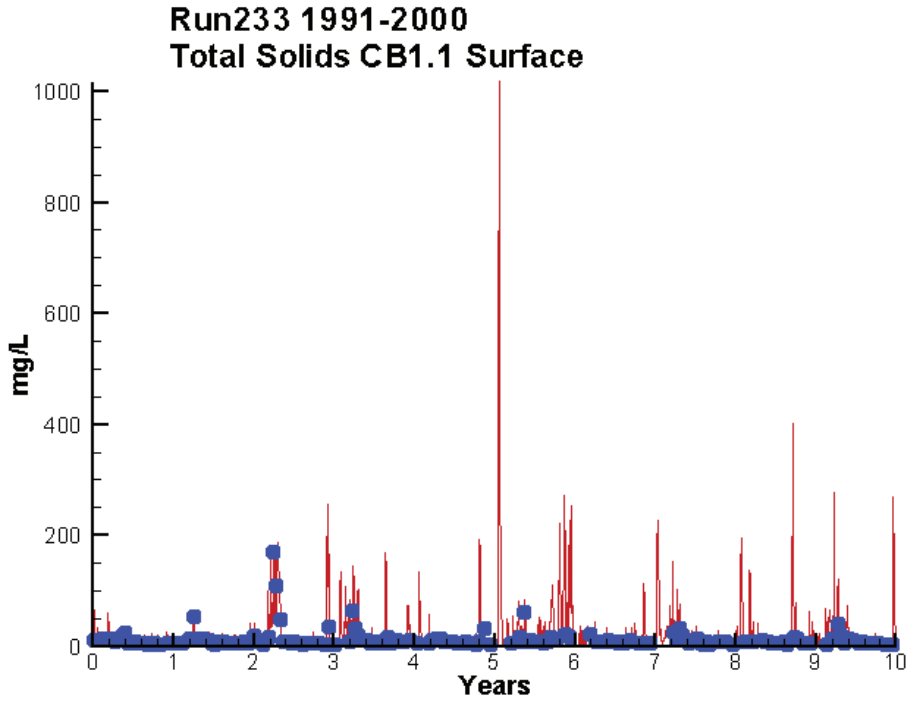

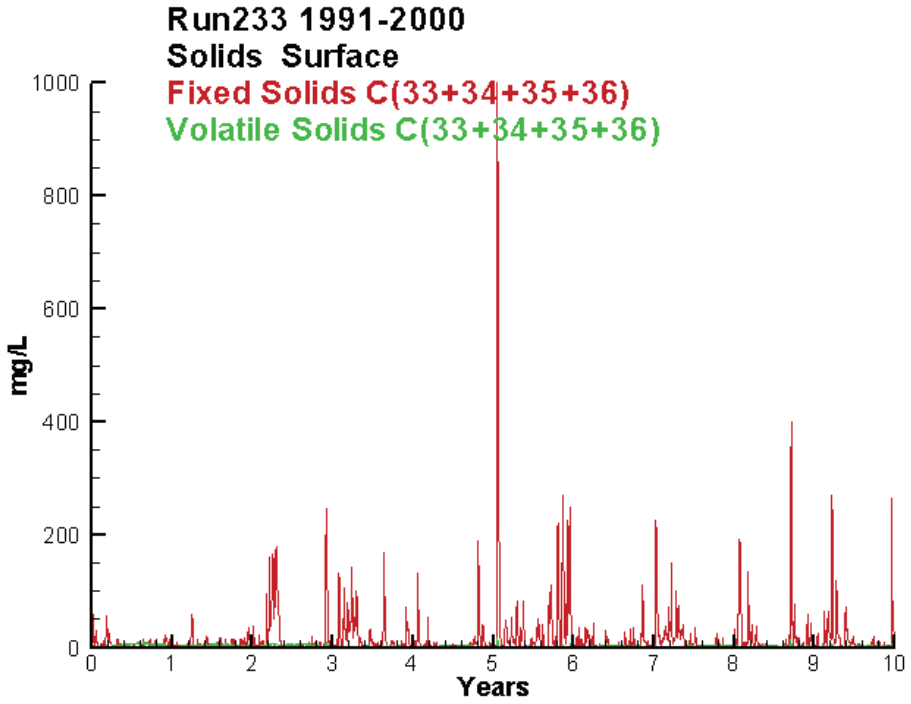

	Mean Difference	Absolute Mean Difference
KE	0.2237	0.4710
TSS	4.5217	7.3689

Station CB2.2

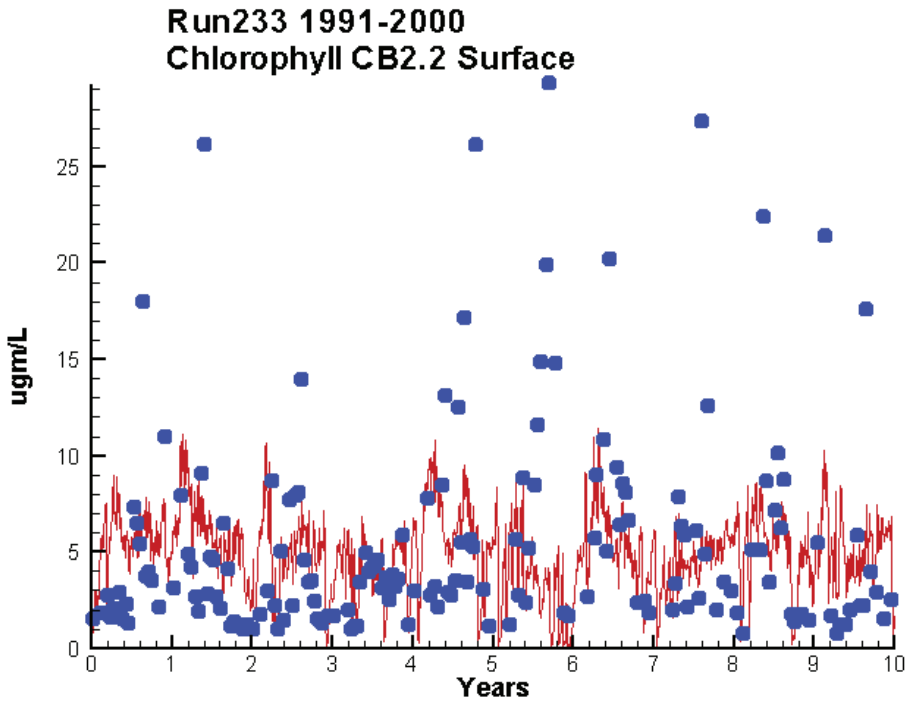

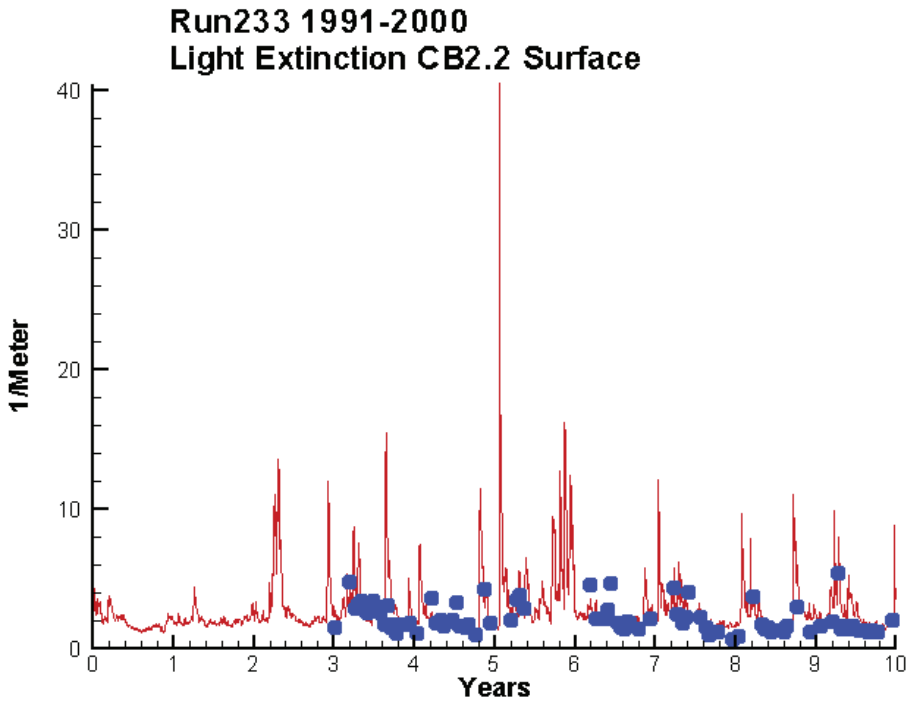

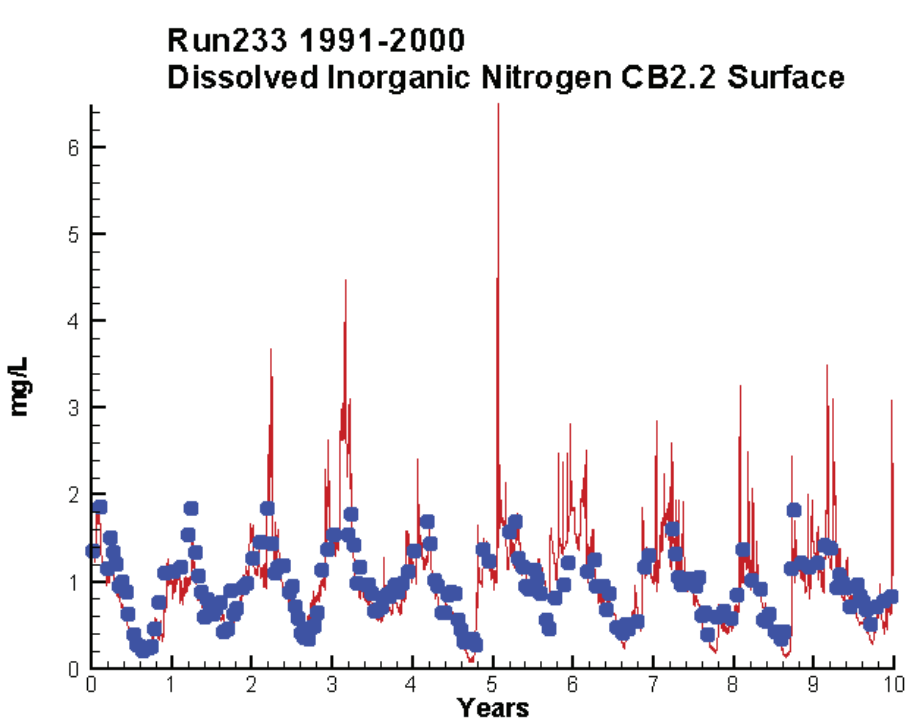

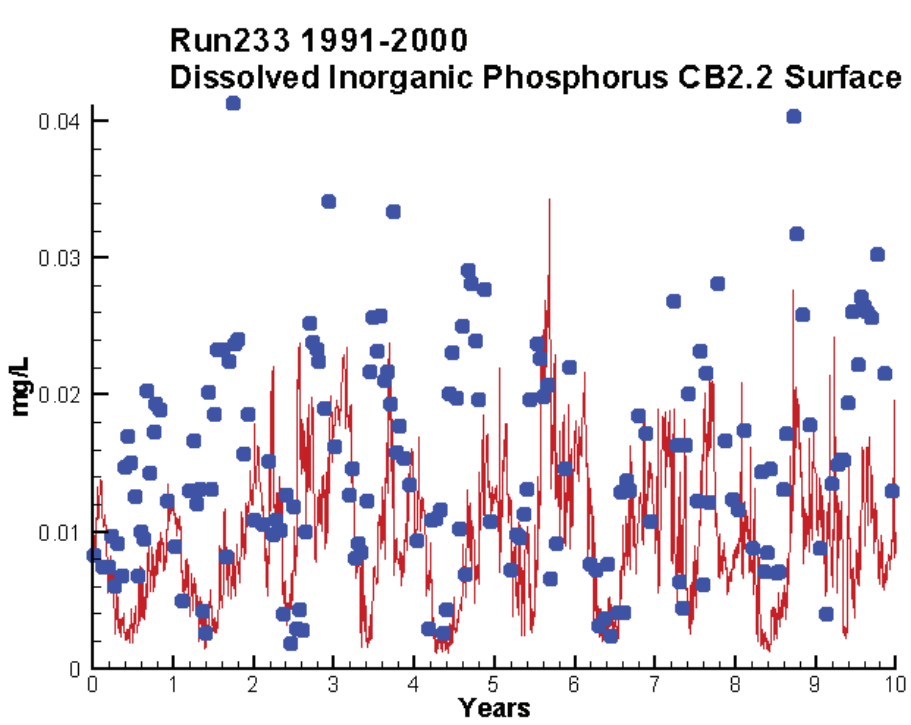

Station CB2.2

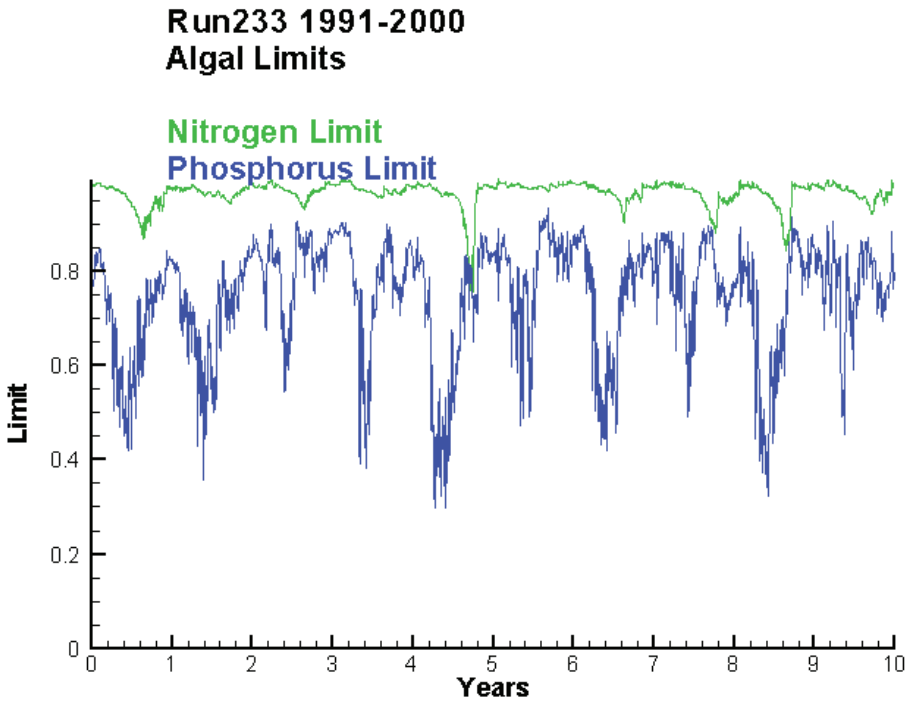

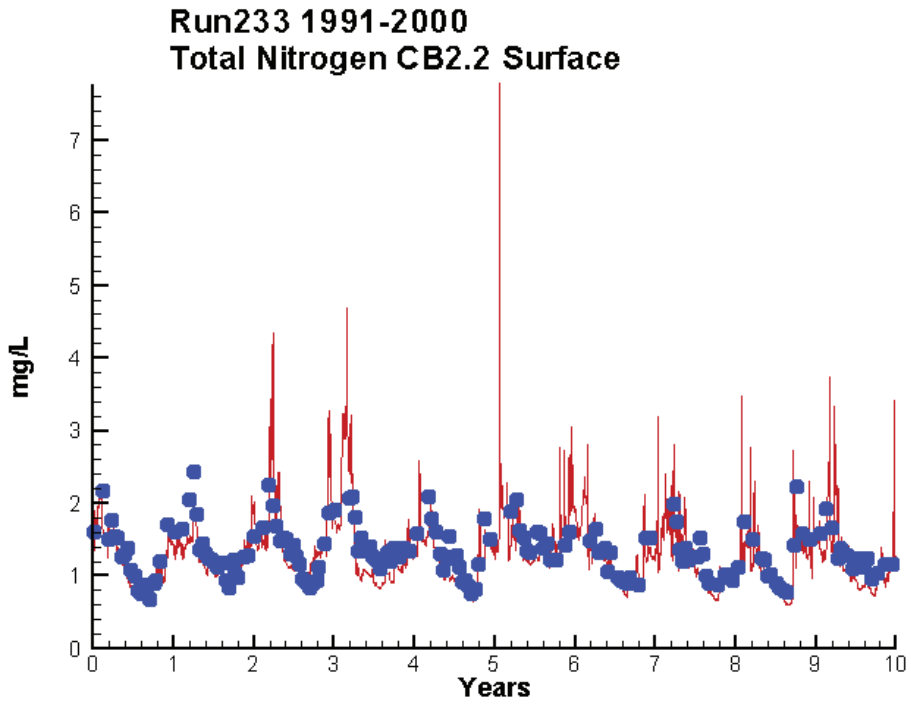

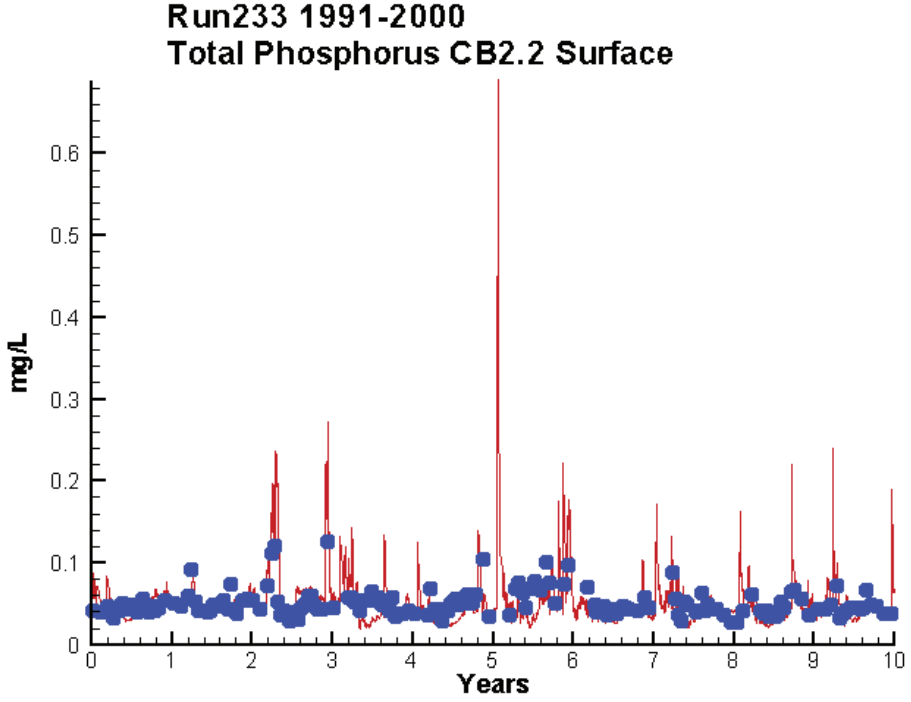

	Mean Difference	Absolute Mean Difference
Chl	-0.3163	3.5172
DIN	-0.0303	0.1860
KE	0.3830	0.8152
DIP	-0.0064	0.0083
TP	-0.0000	0.0154
TN	-0.1015	0.2130

Station CB2.2

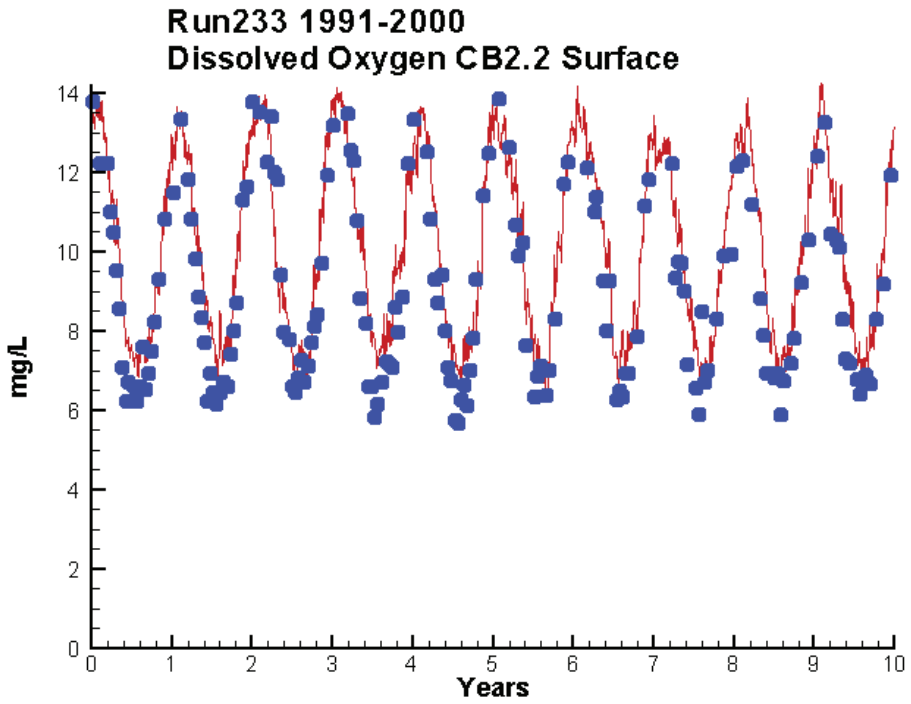

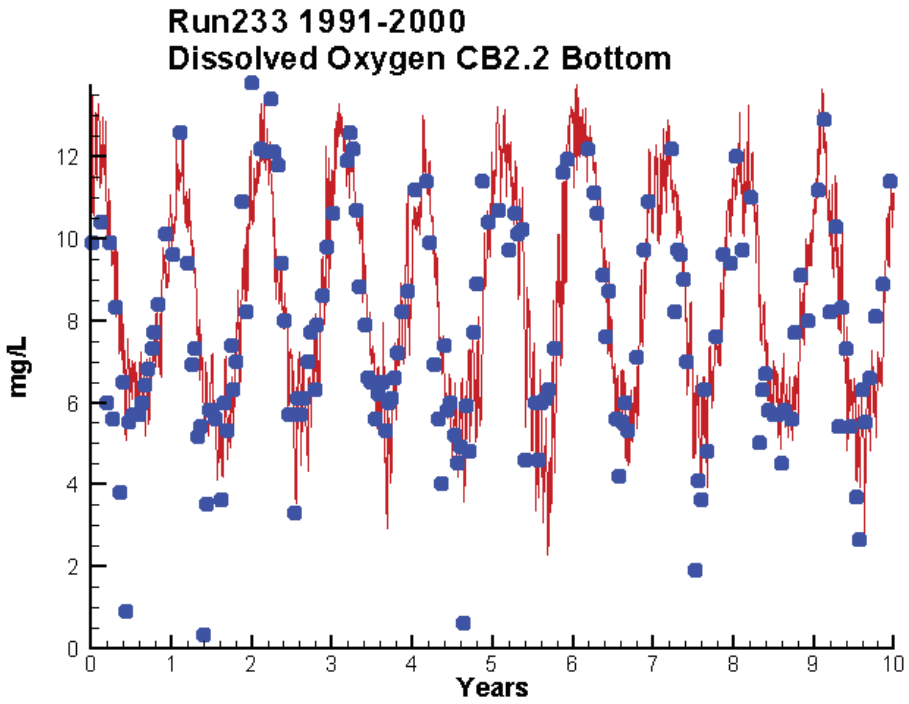

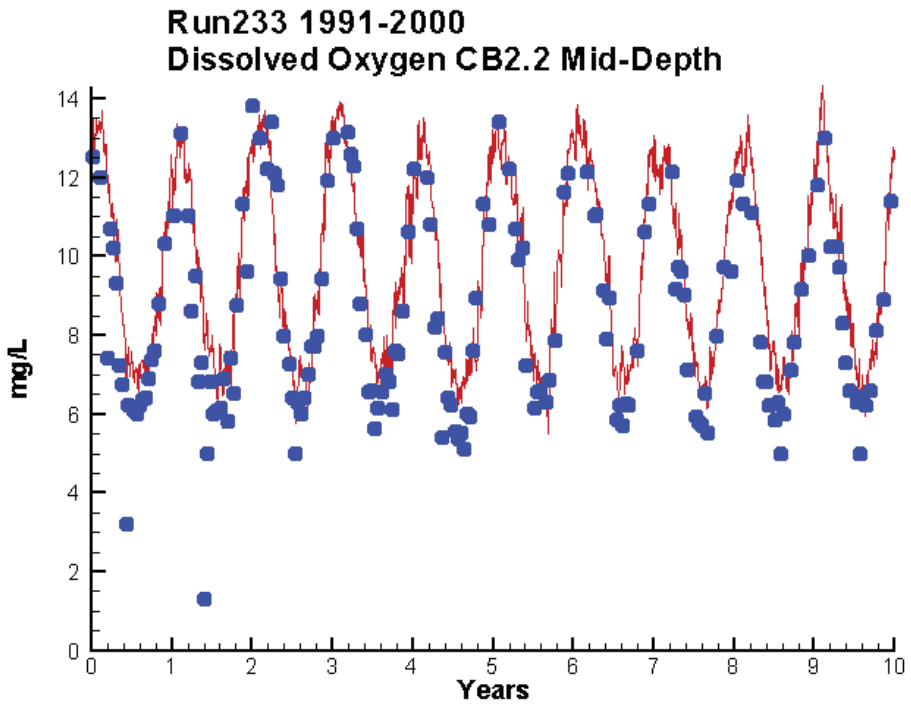

	Mean Difference	Absolute Mean Difference
Top DO	0.6838	0.8848
Mid DO	0.8138	1.0003
Bot DO	0.2920	1.1476

Station CB2.2

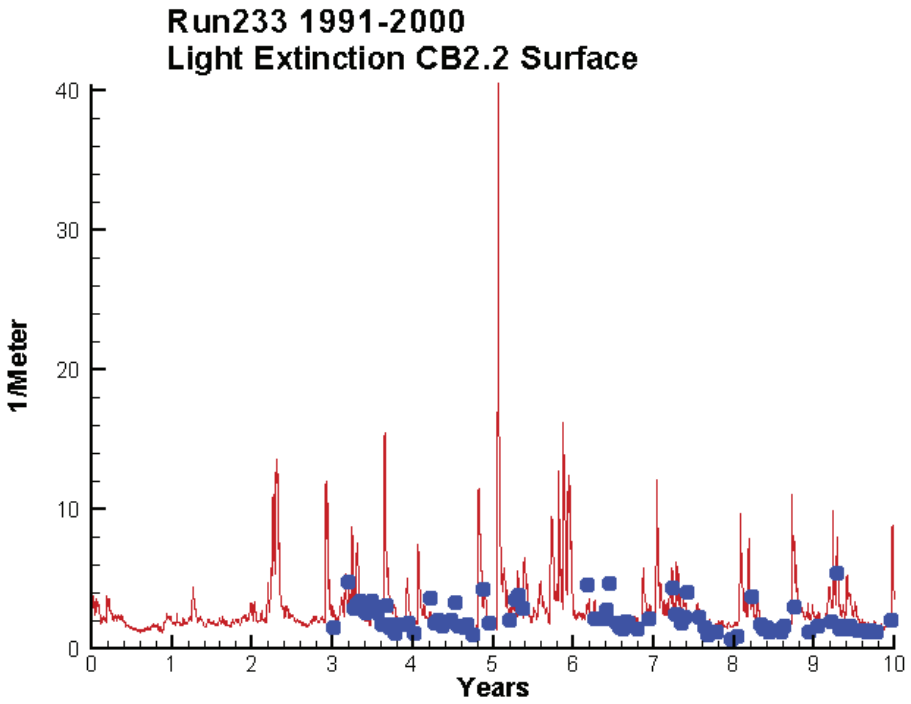

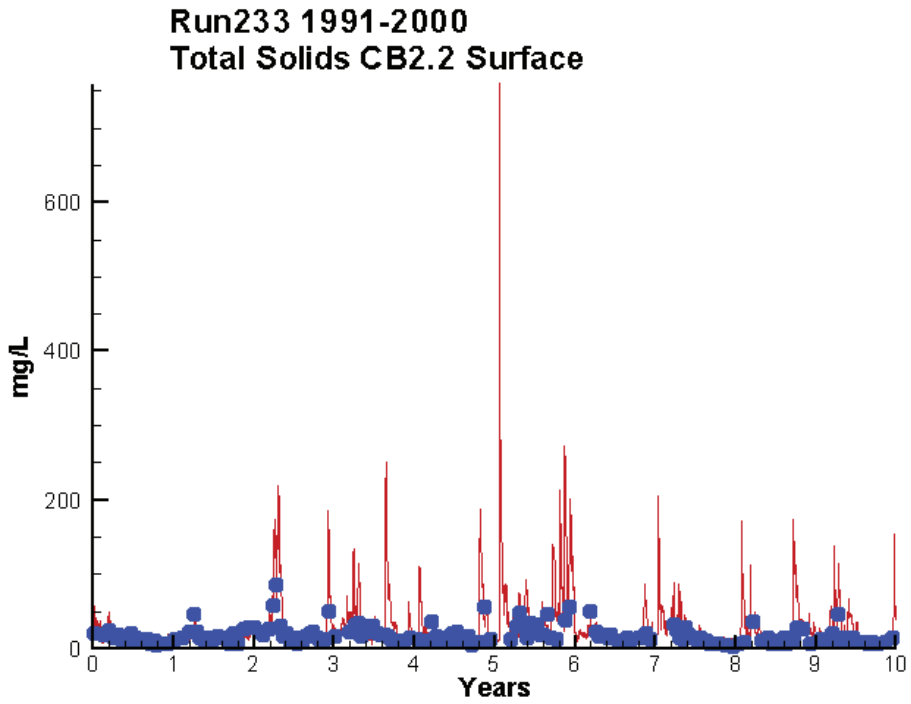

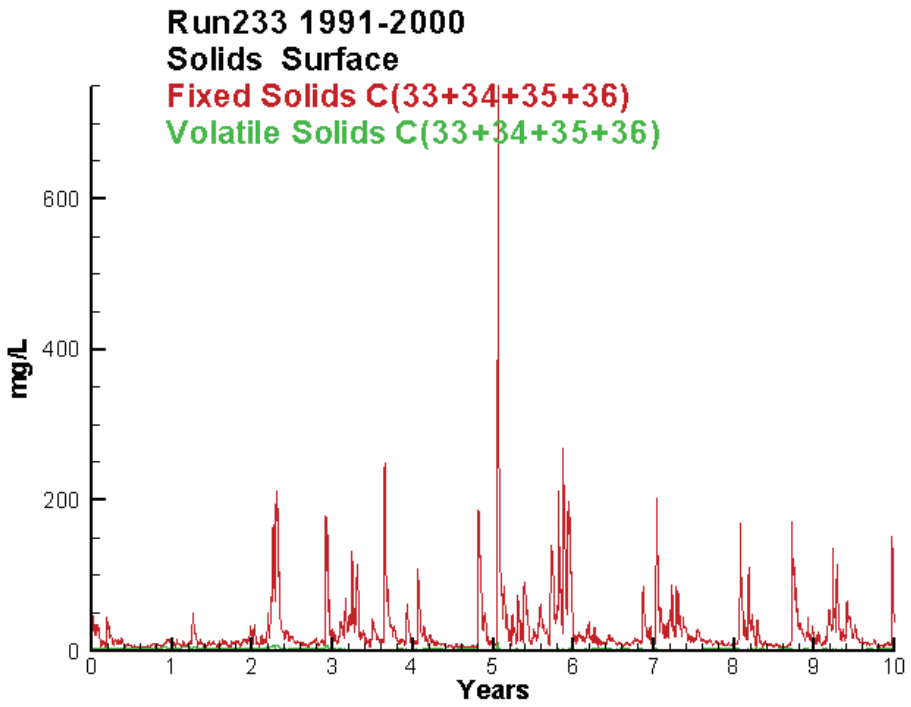

	Mean Difference	Absolute Mean Difference
KE	0.3830	0.8152
TSS	9.2233	13.0661

Station CB3.3C

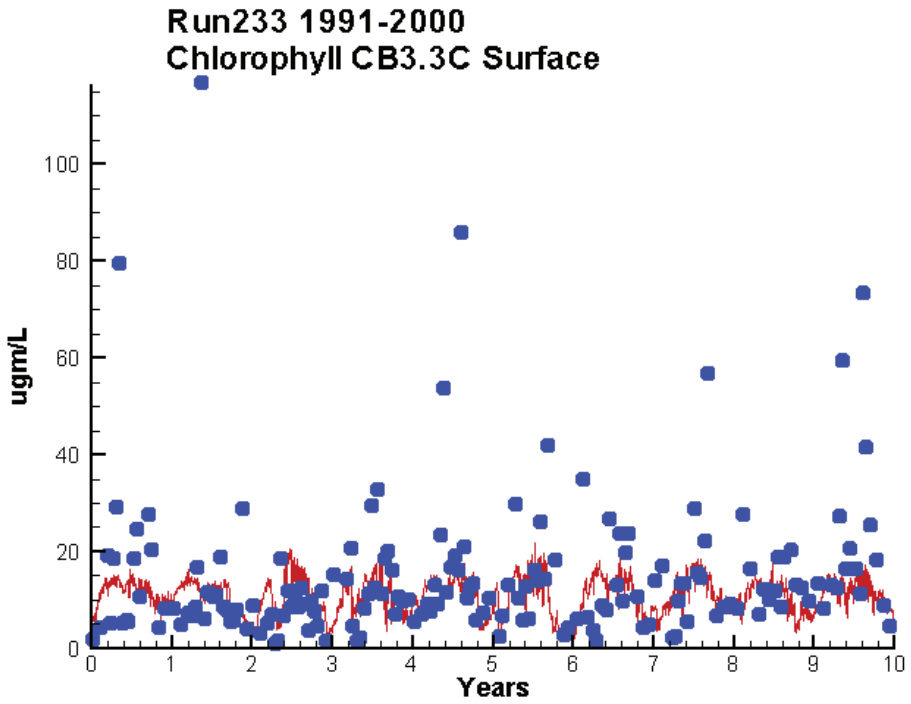

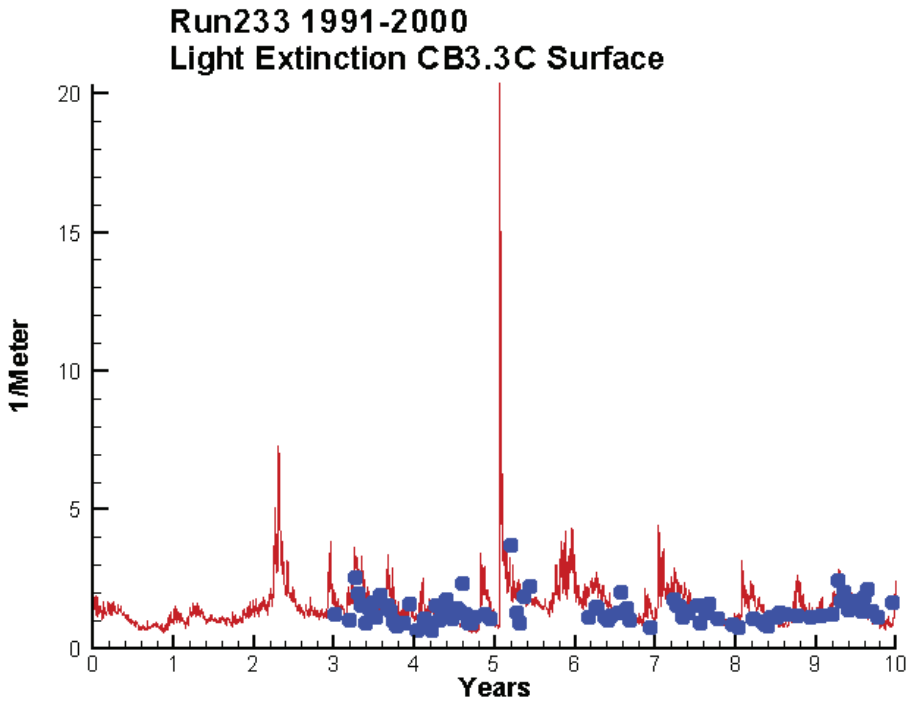

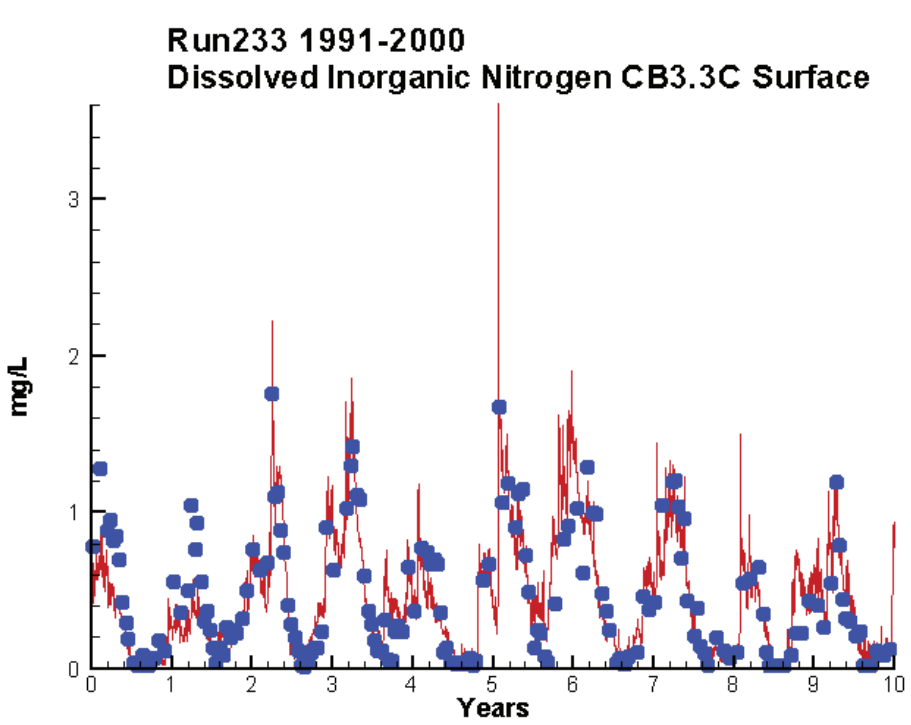

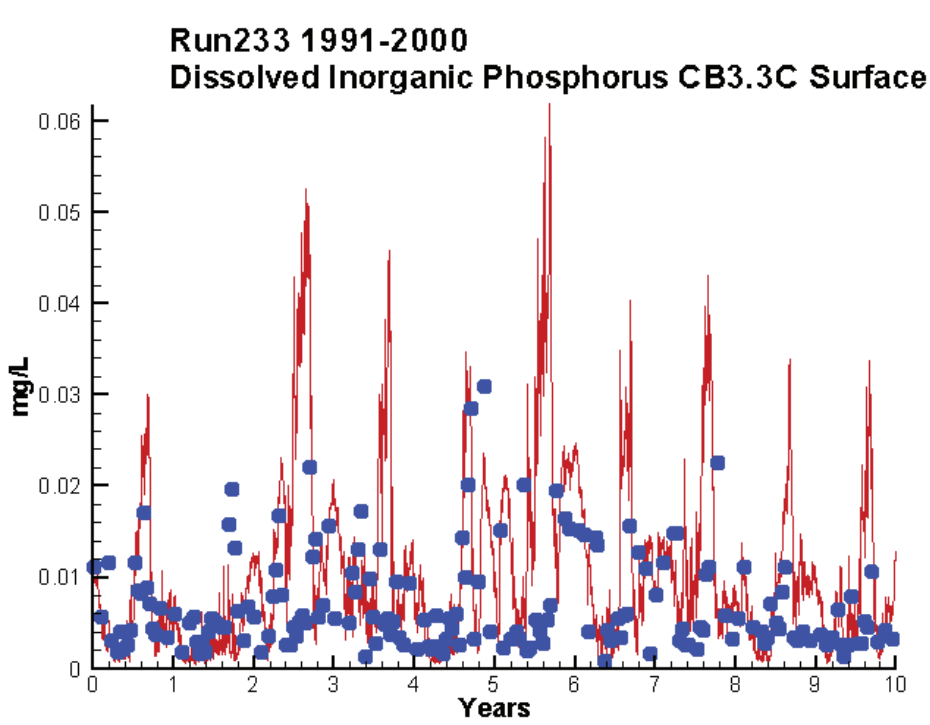

Station CB3.3C

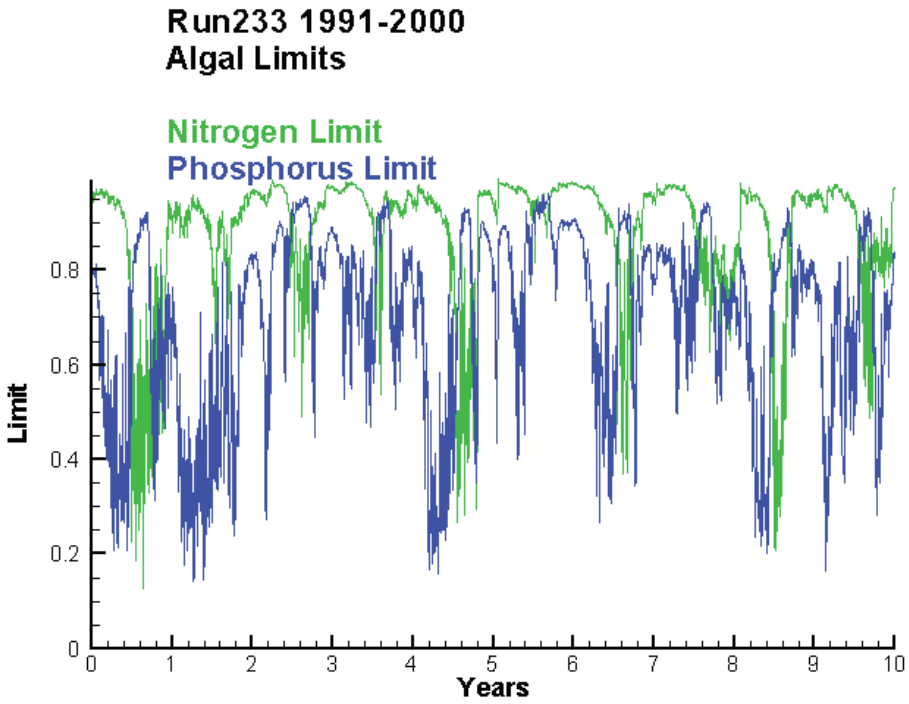

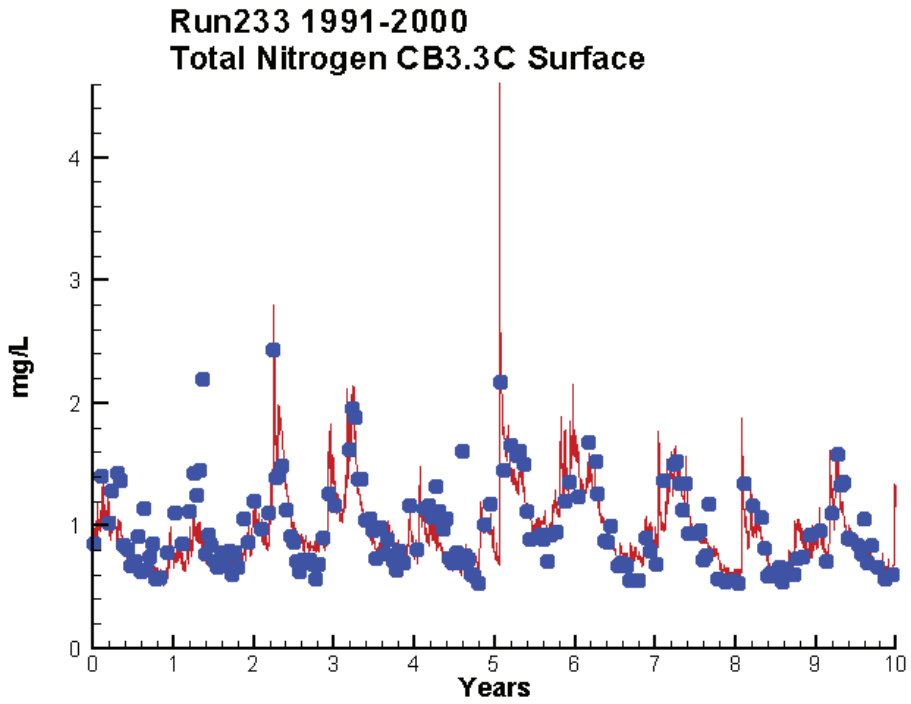

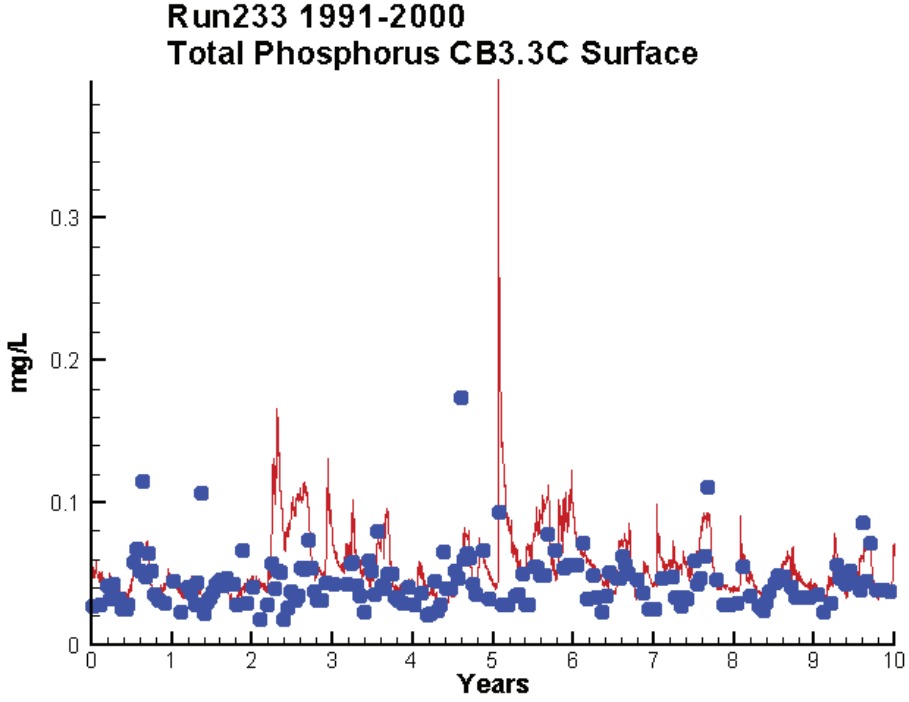

	Mean Difference	Absolute Mean Difference
Chl	-3.4481	8.0504
DIN	-0.0060	0.1301
KE	0.1613	0.4856
DIP	0.0045	0.0076
TP	0.0128	0.0196
TN	-0.0301	0.1528

Station CB3.3C

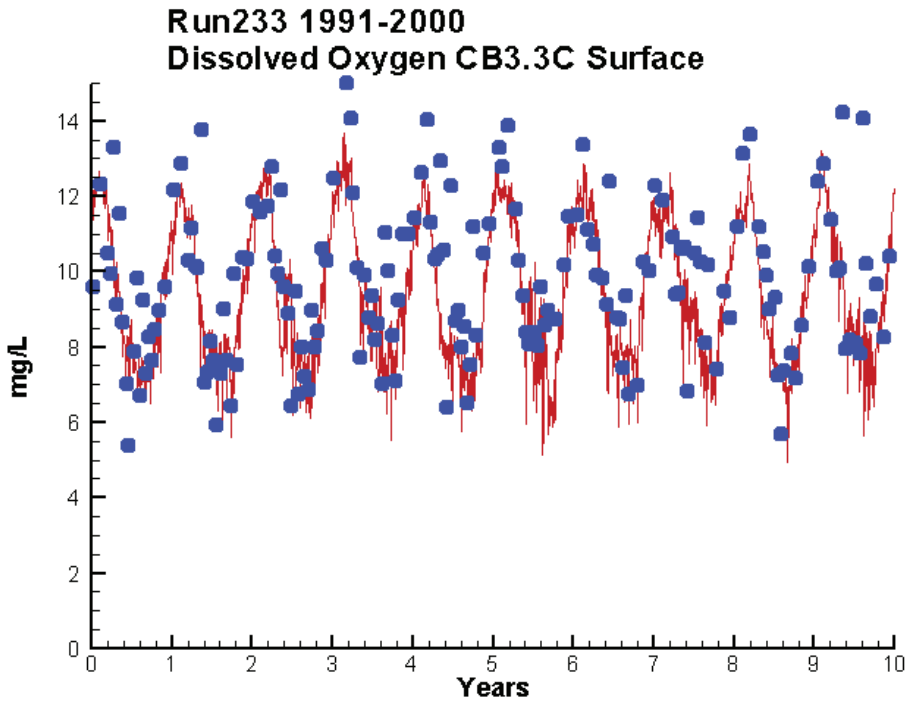

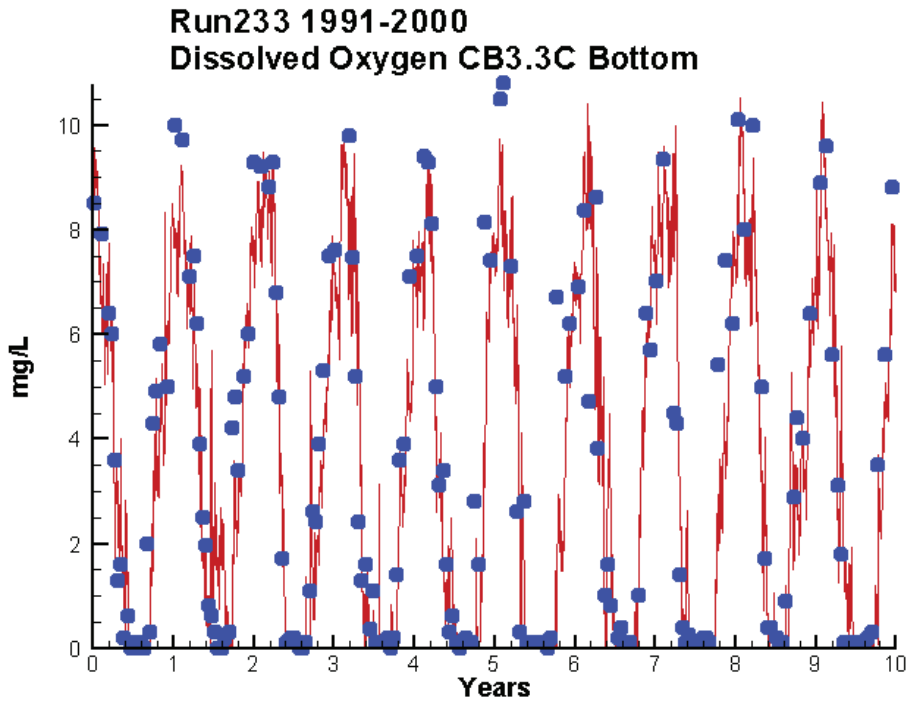

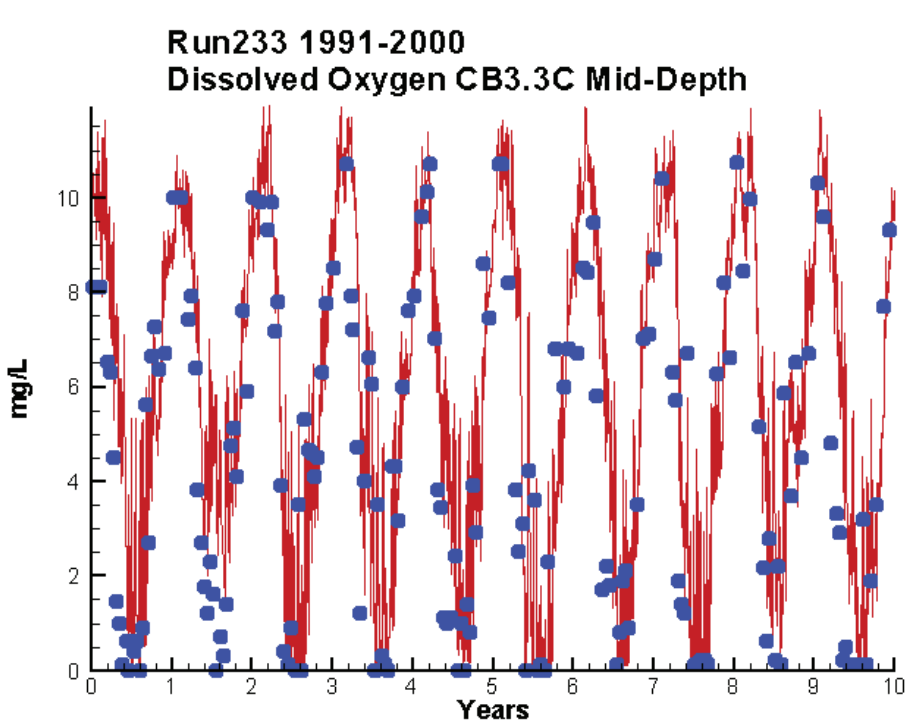

	Mean Difference	Absolute Mean Difference
Top DO	-0.5702	1.0708
Mid DO	1.1151	1.5826
Bot DO	-0.3537	0.9397

Station CB3.3C

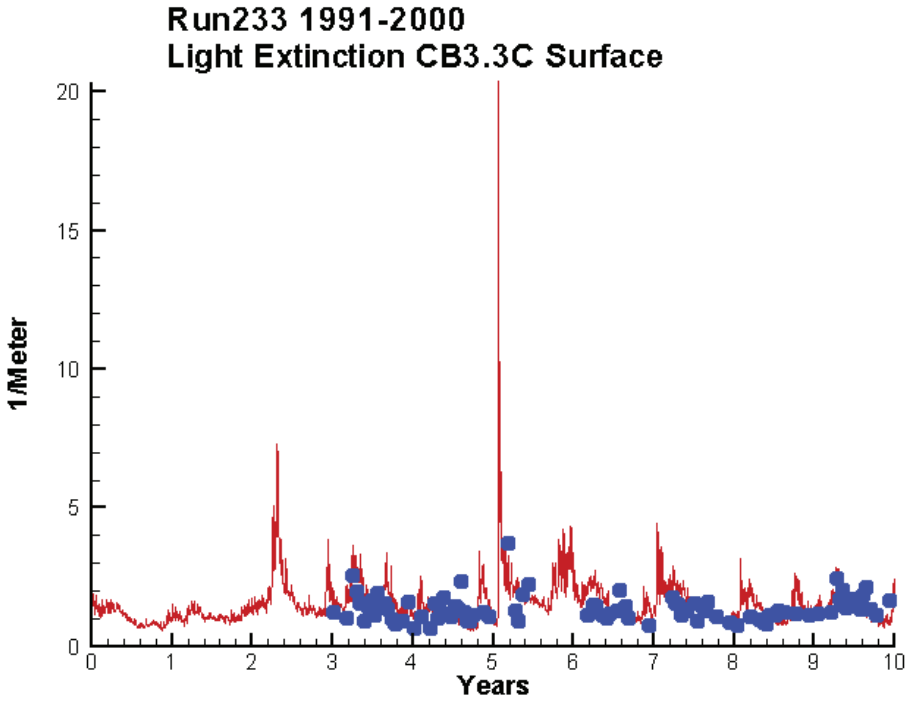

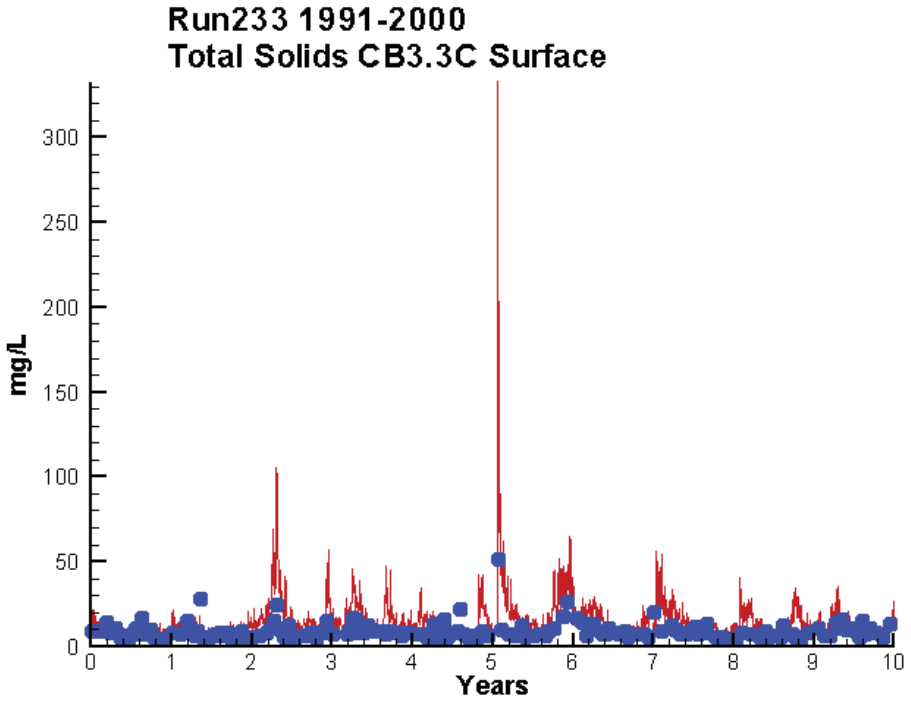

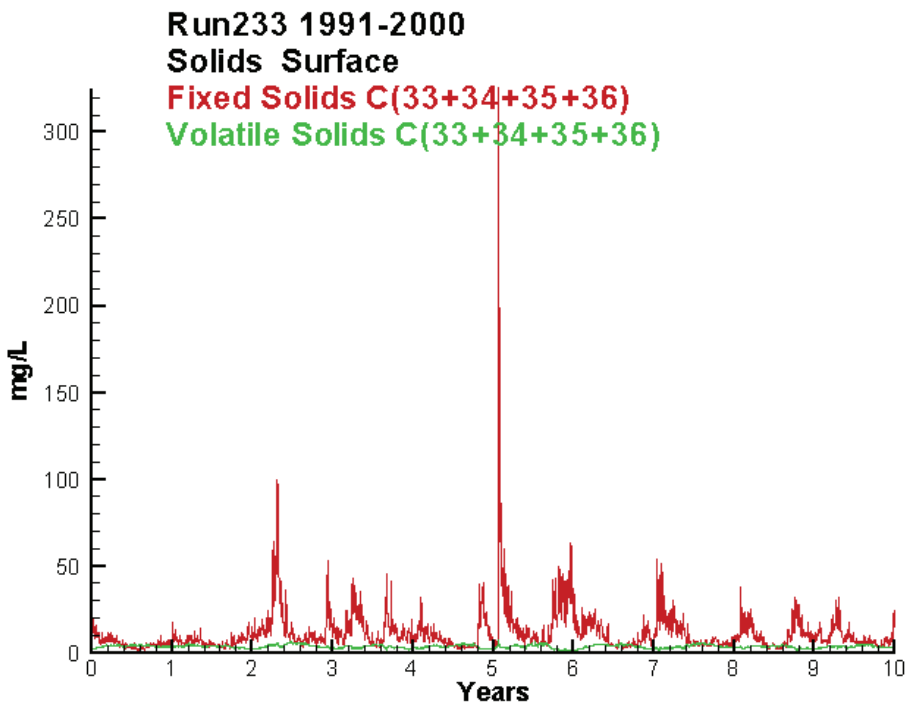

	Mean Difference	Absolute Mean Difference
KE	0.1613	0.4856
TSS	5.9185	6.9430

Station CB4.2C

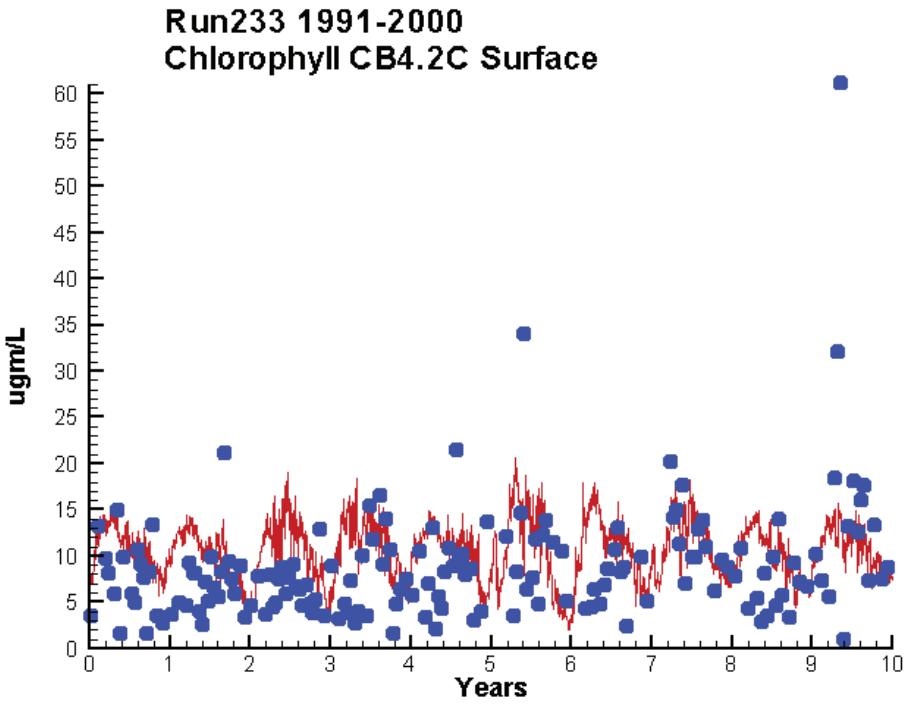

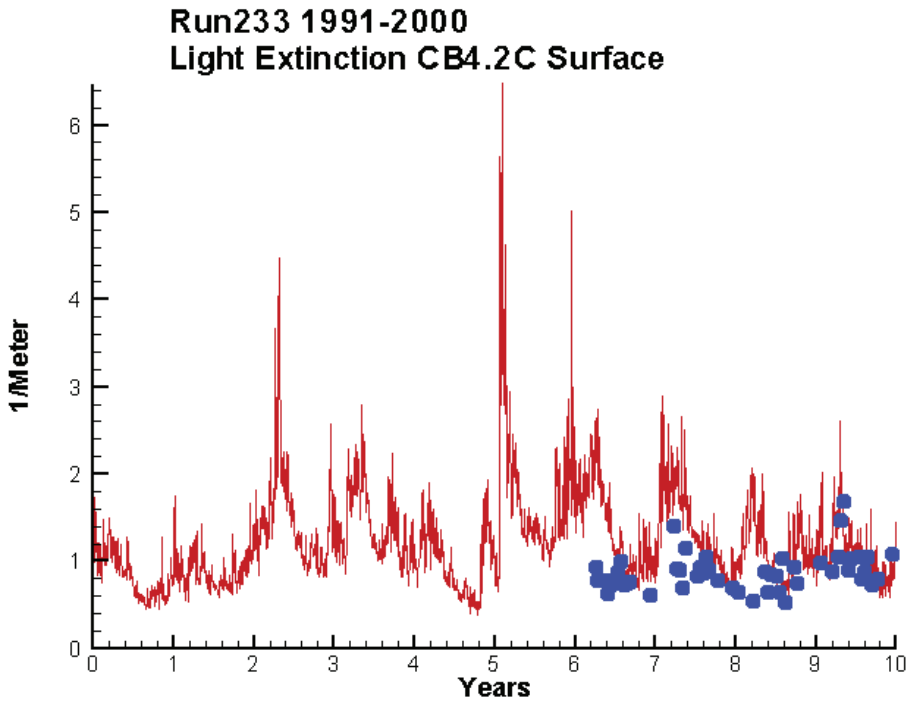

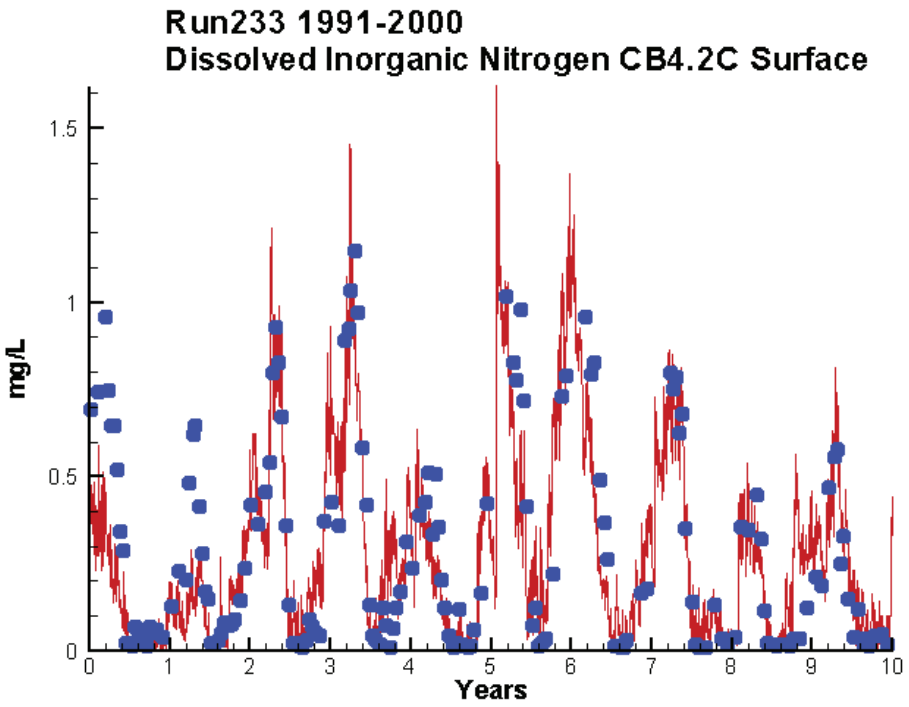

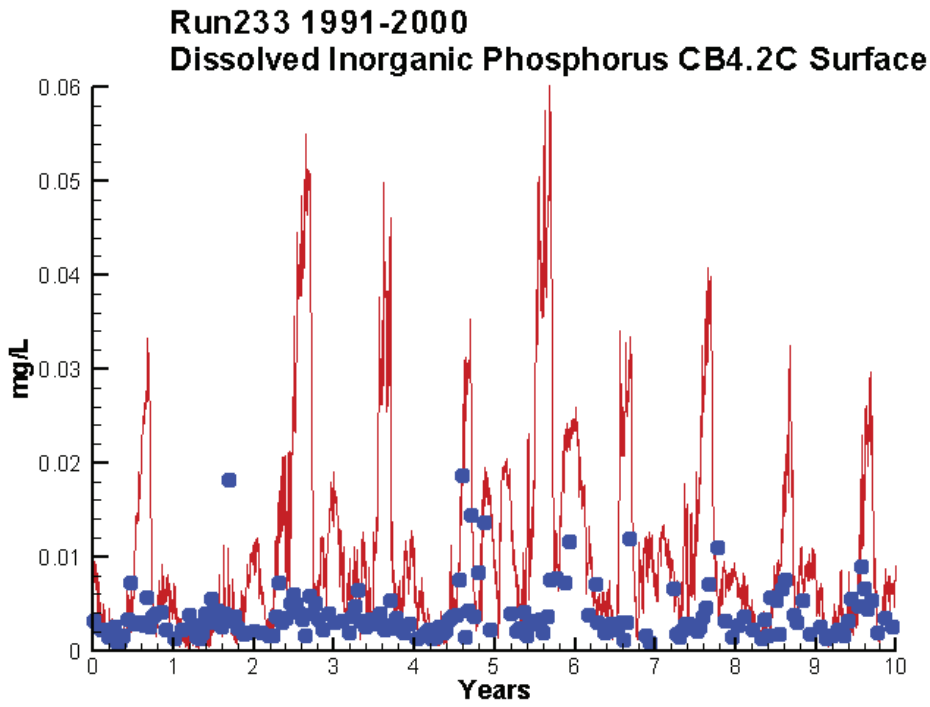

Station CB4.2C

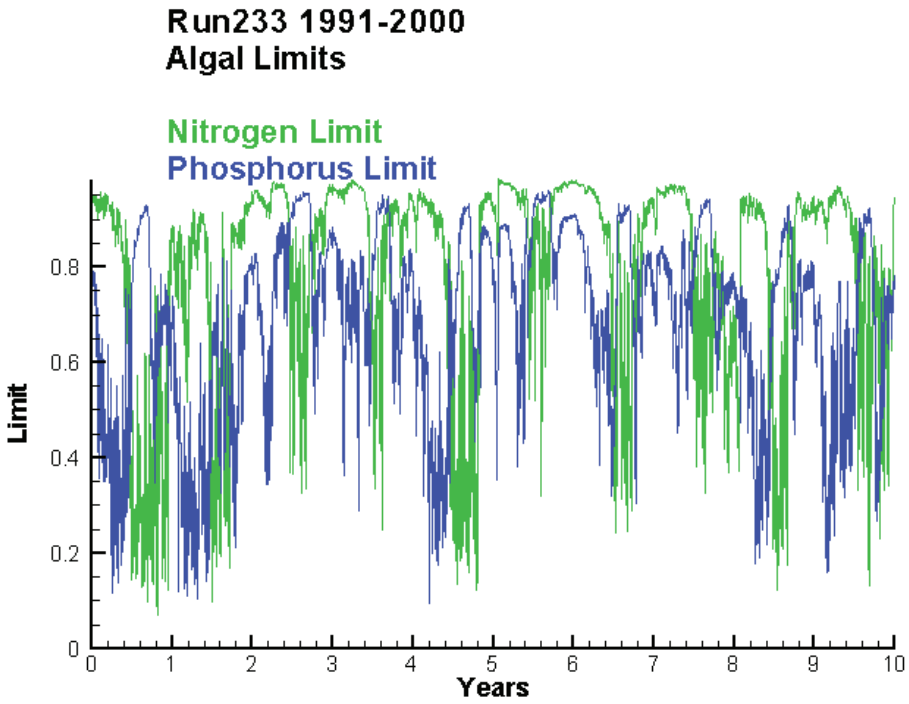

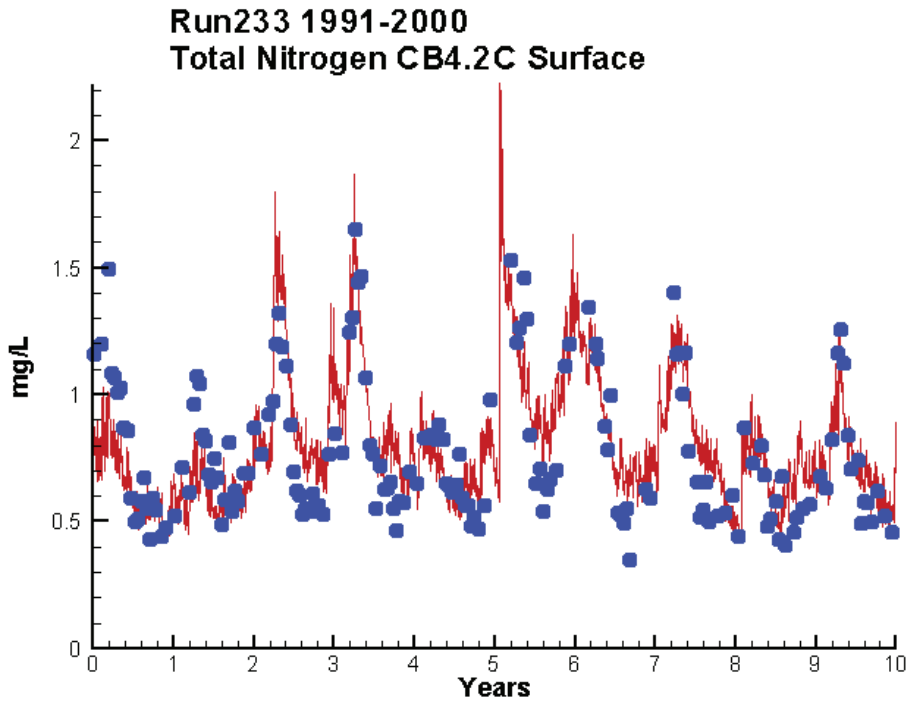

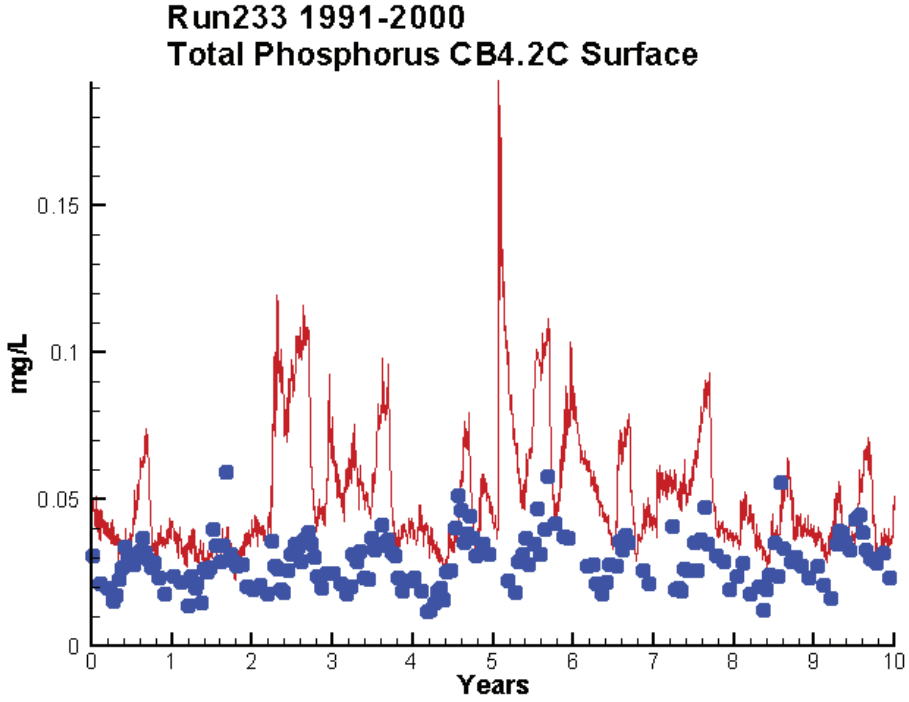

	Mean Difference	Absolute Mean Difference
Chl	2.4634	5.1535
DIN	-0.0288	0.1143
KE	0.3334	0.3857
DIP	0.0077	0.0084
TP	0.0233	0.0239
TN	0.0275	0.1335

Station CB4.2C

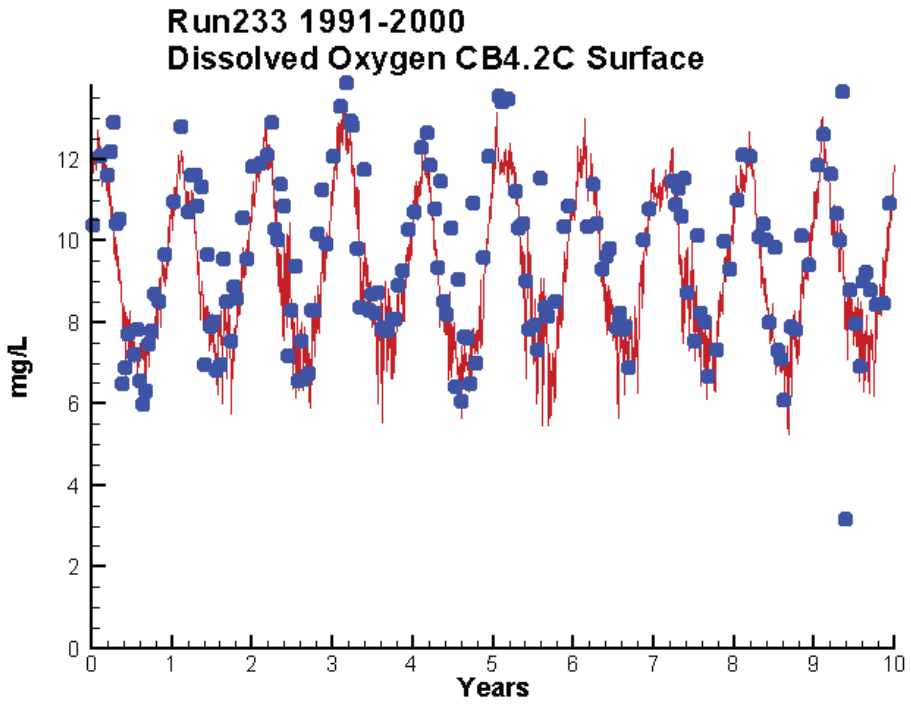

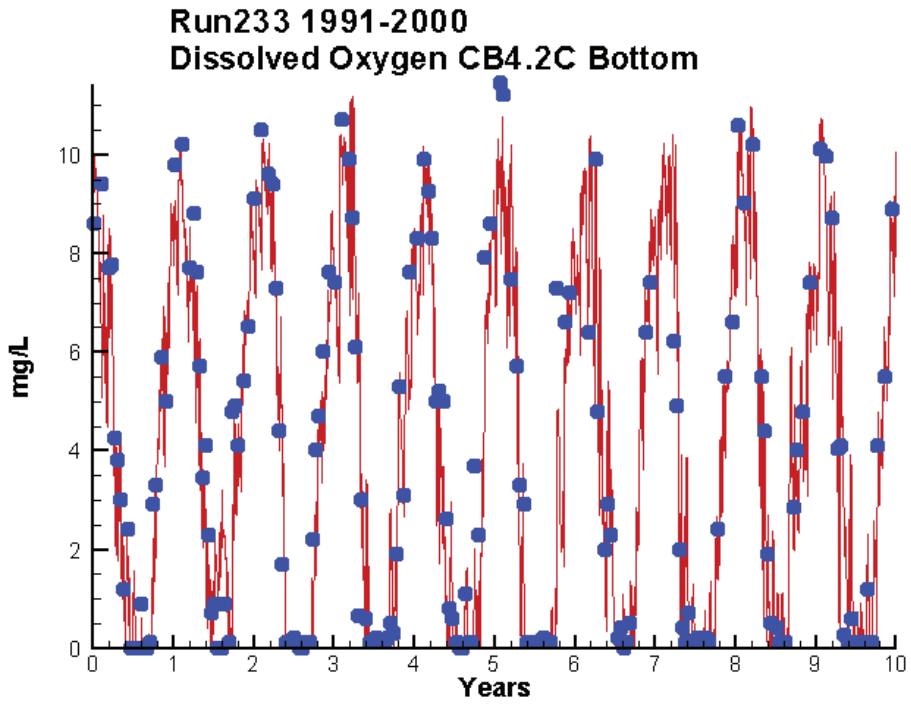

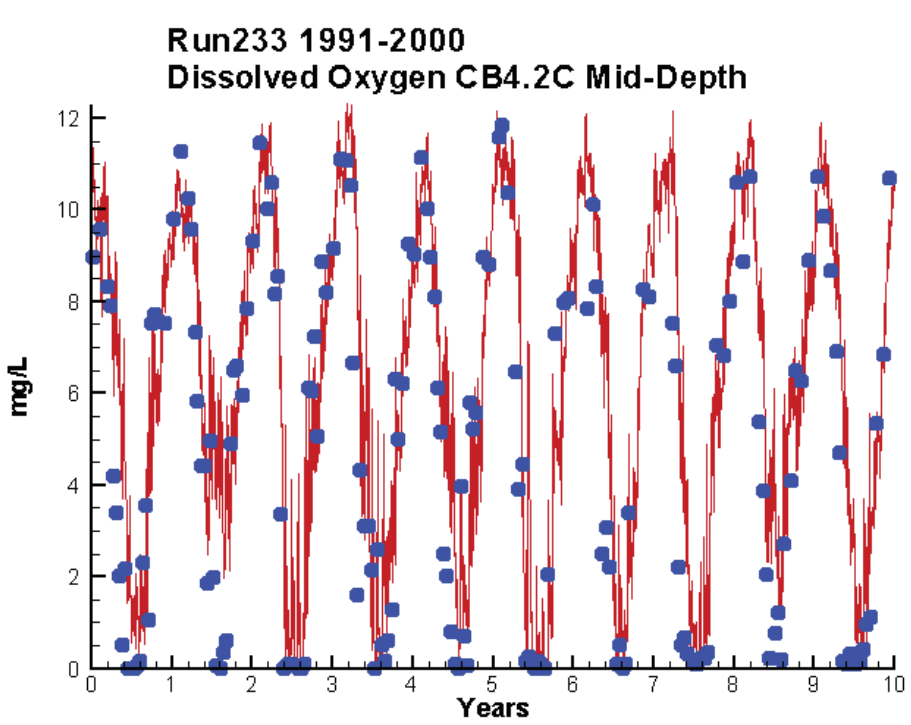

	Mean Difference	Absolute Mean Difference
Top DO	-0.4843	0.8875
Mid DO	1.1015	1.5607
Bot DO	-0.2954	0.9127

Station CB4.2C

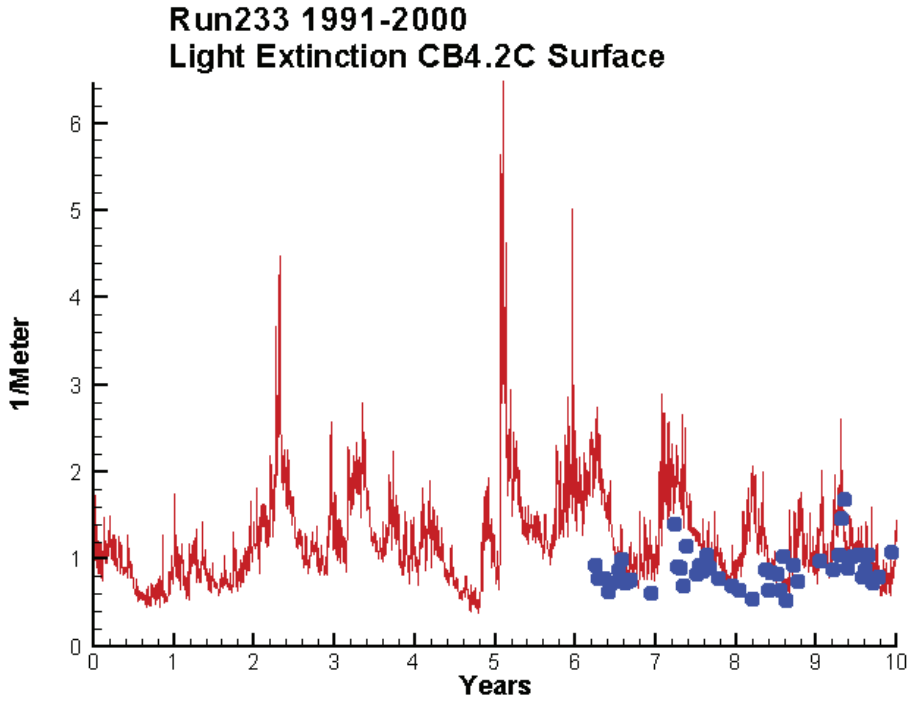

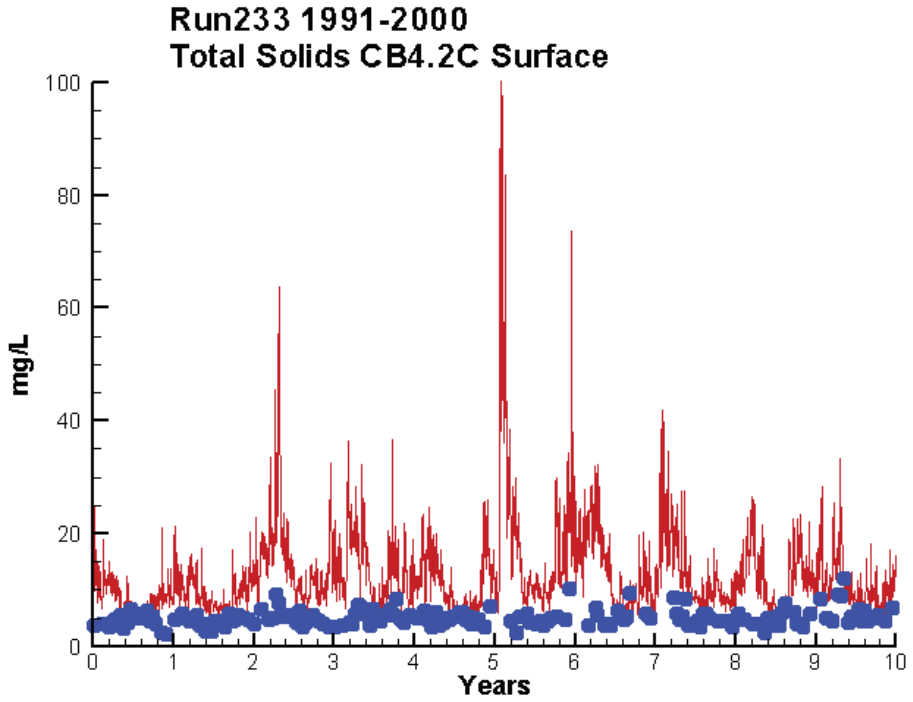

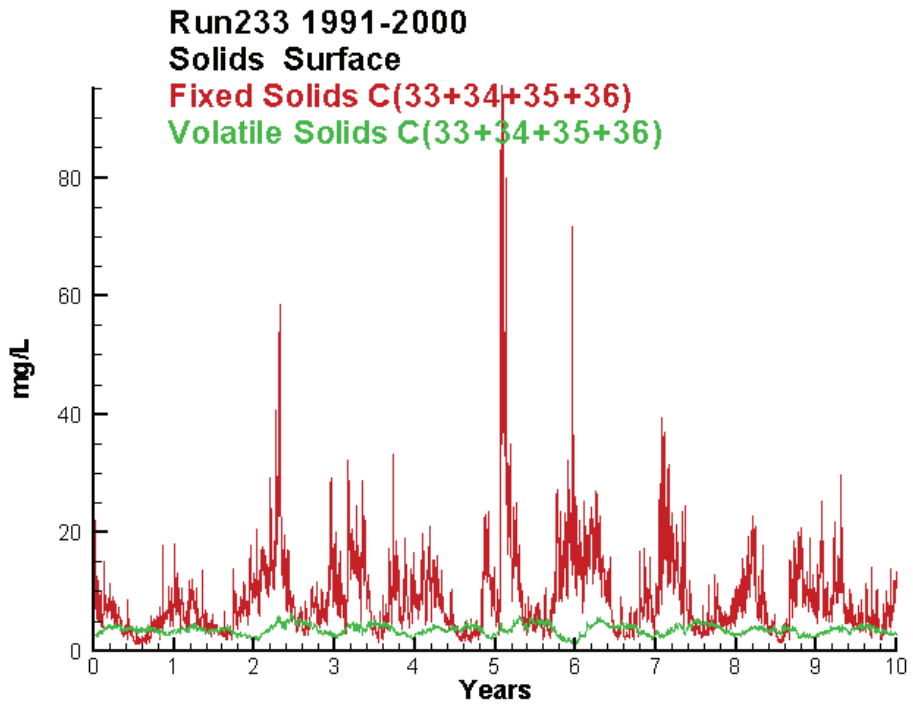

	Mean Difference	Absolute Mean Difference
KE	0.3334	0.3857
TSS	6.6699	6.7705

Station CB5.2

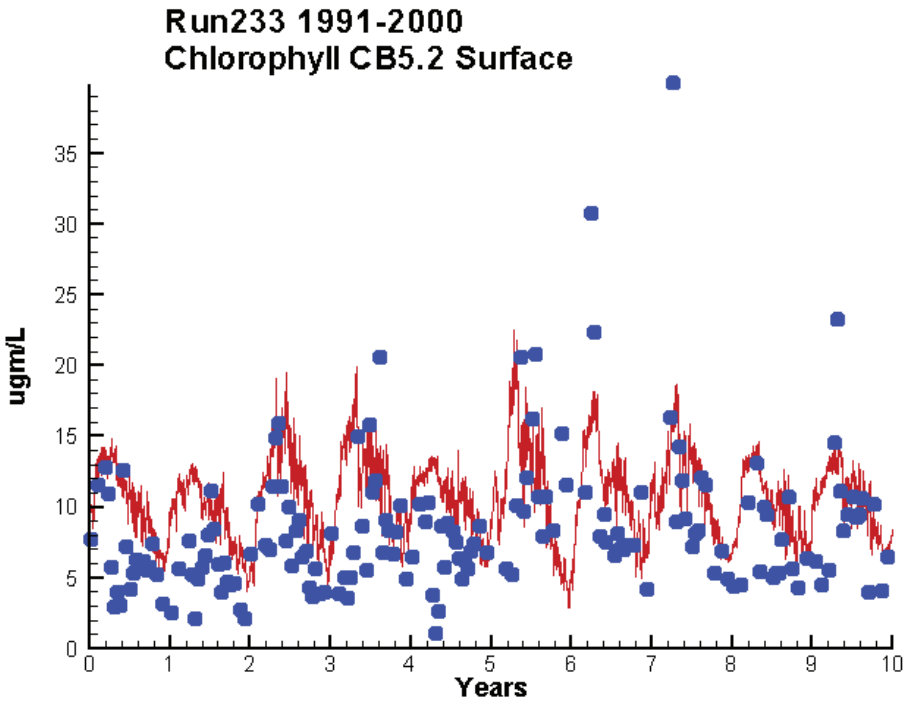

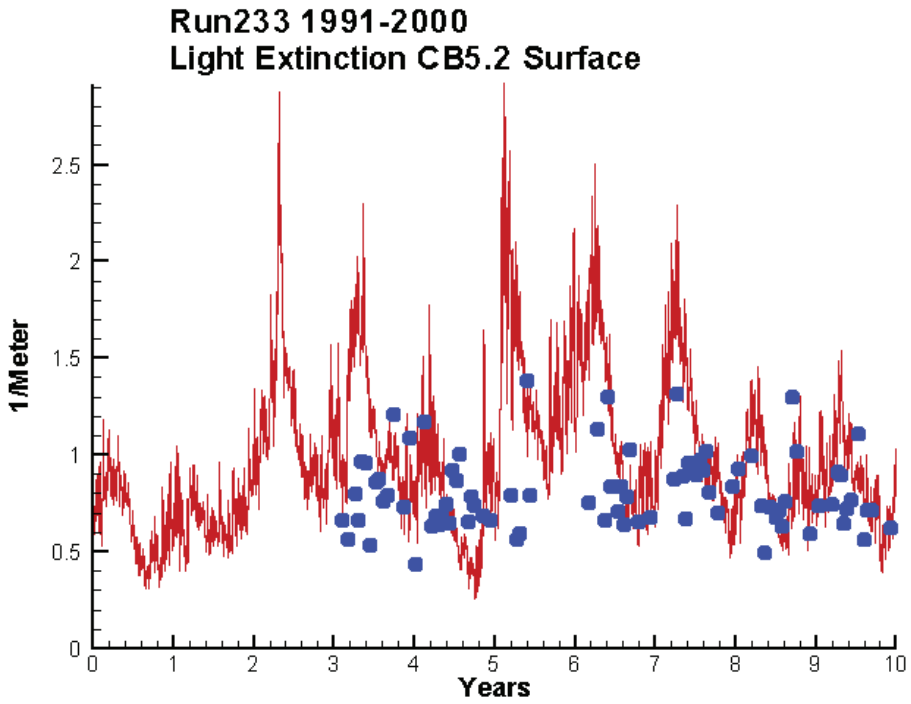

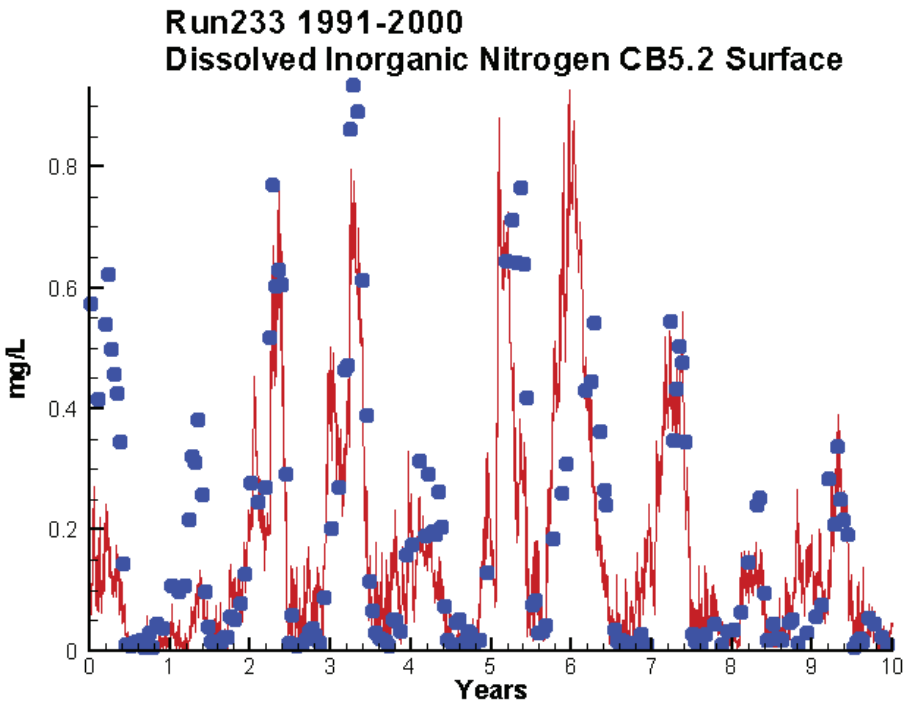

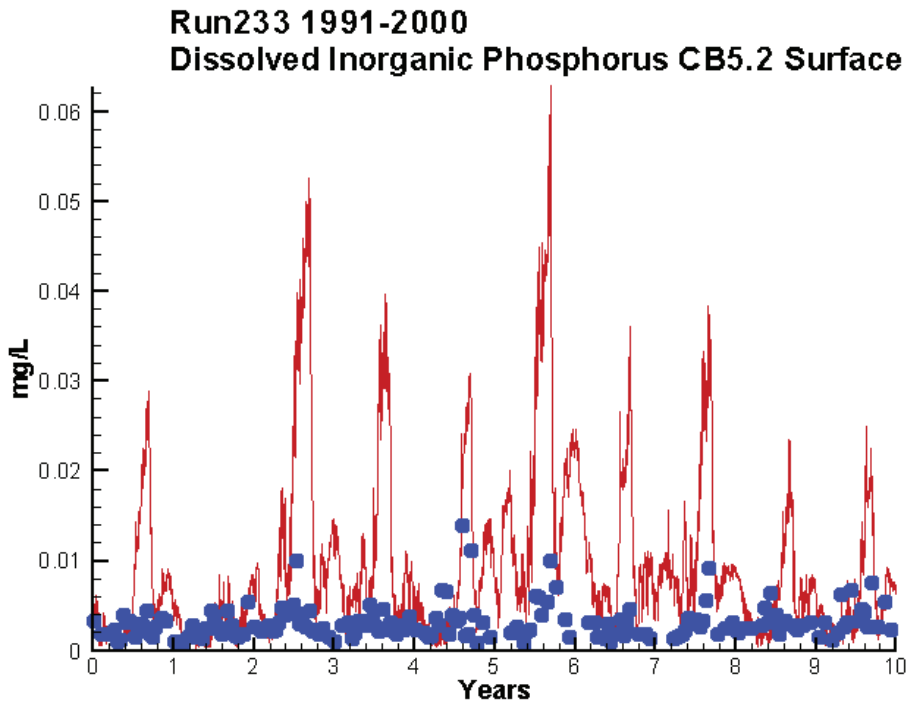

Station CB5.2

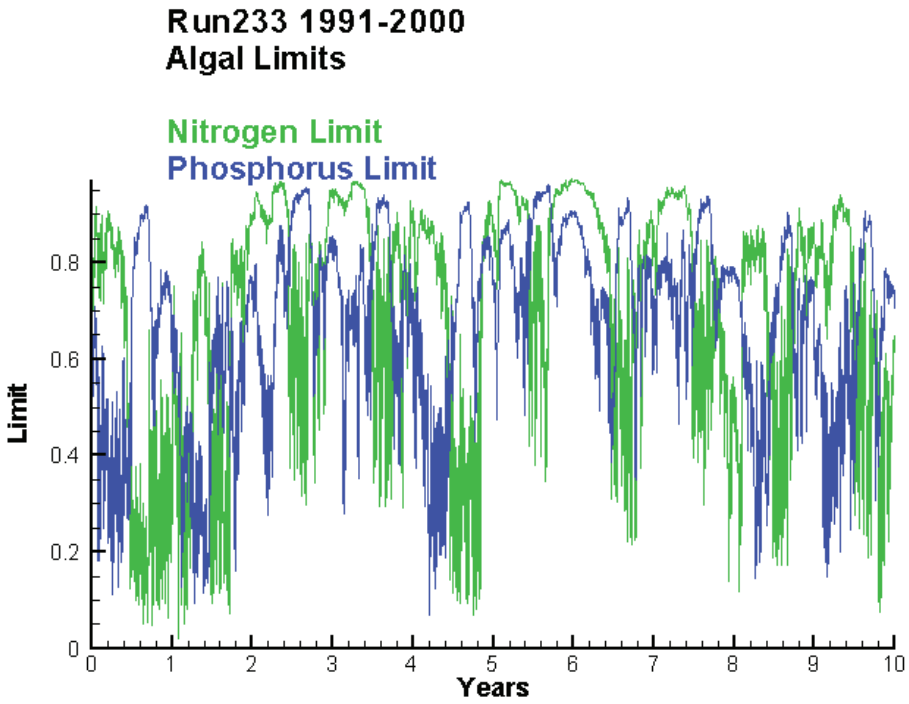

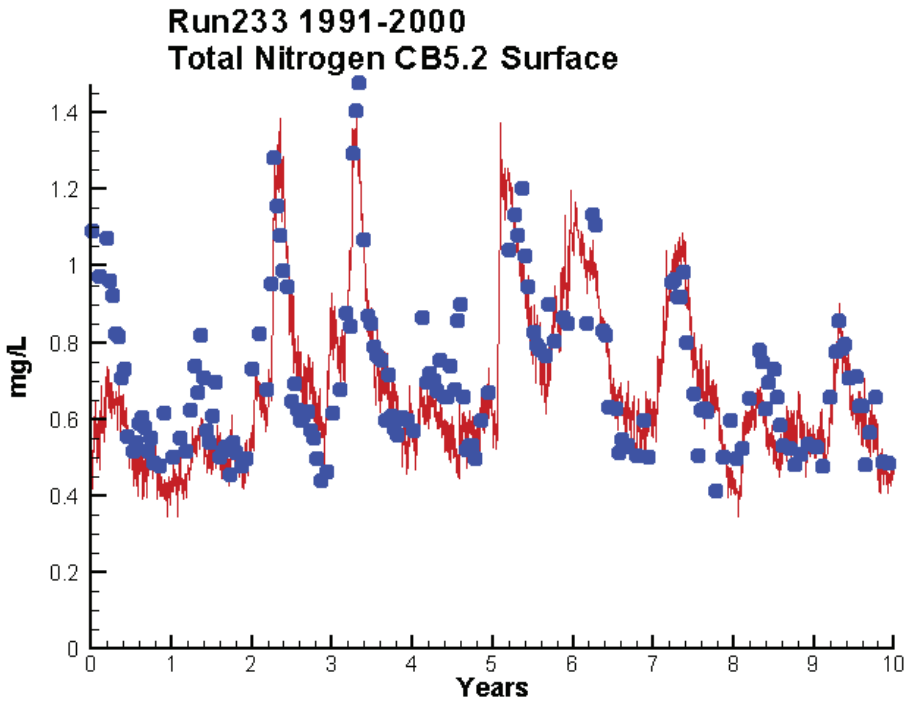

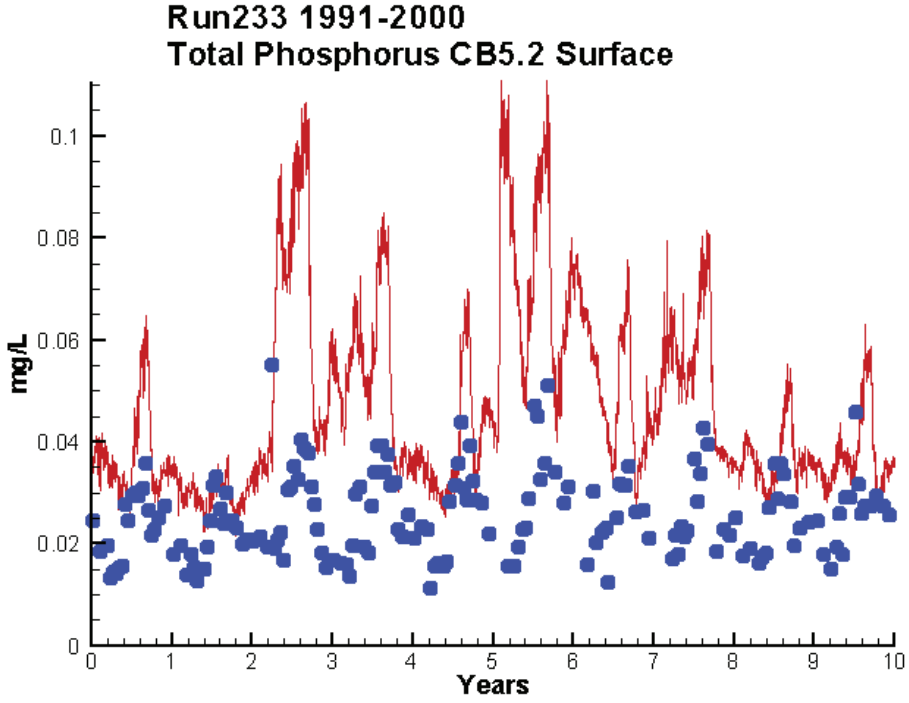

	Mean Difference	Absolute Mean Difference
Chl	2.8207	4.2558
DIN	-0.0410	0.0909
KE	0.2169	0.3438
DIP	0.0072	0.0078
TP	0.0224	0.0228
TN	-0.0297	0.1013

Station CB5.2

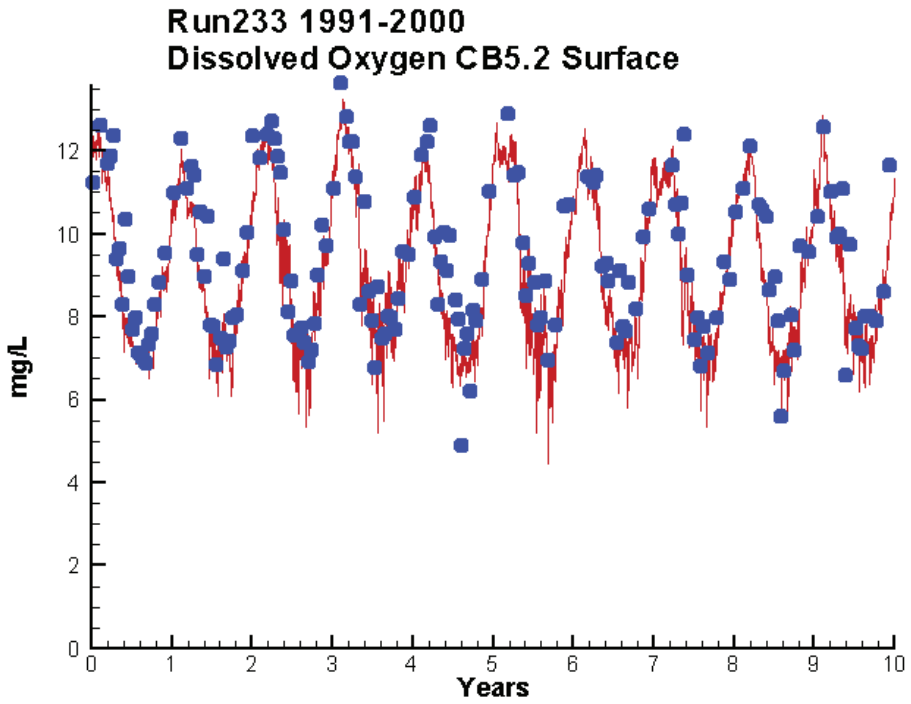

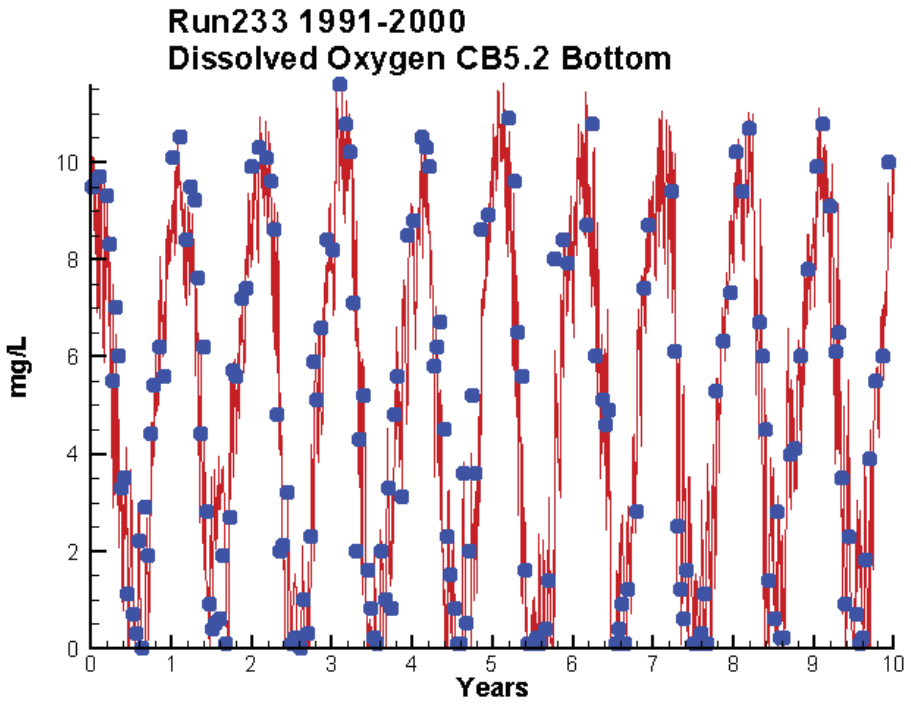

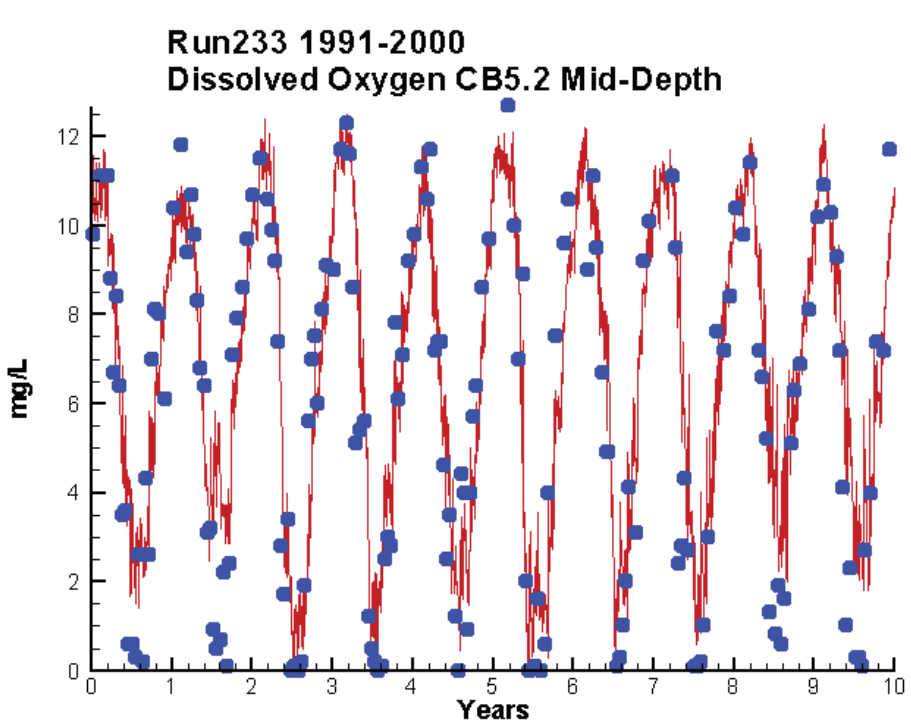

	Mean Difference	Absolute Mean Difference
Top DO	-0.5553	0.7817
Mid DO	0.6179	1.2804
Bot DO	-0.3132	1.1199

Station CB5.2

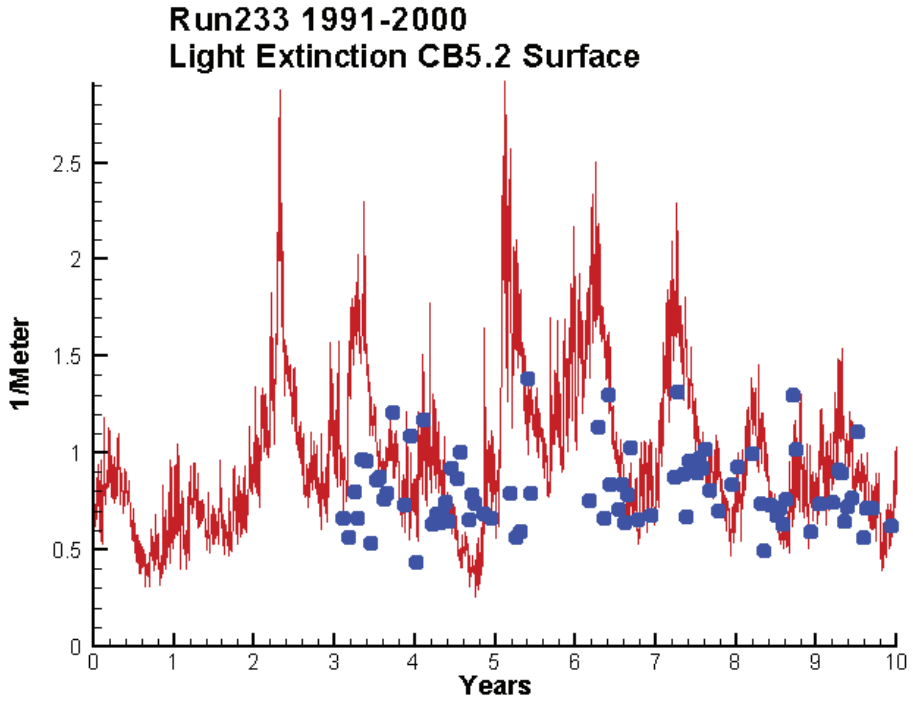

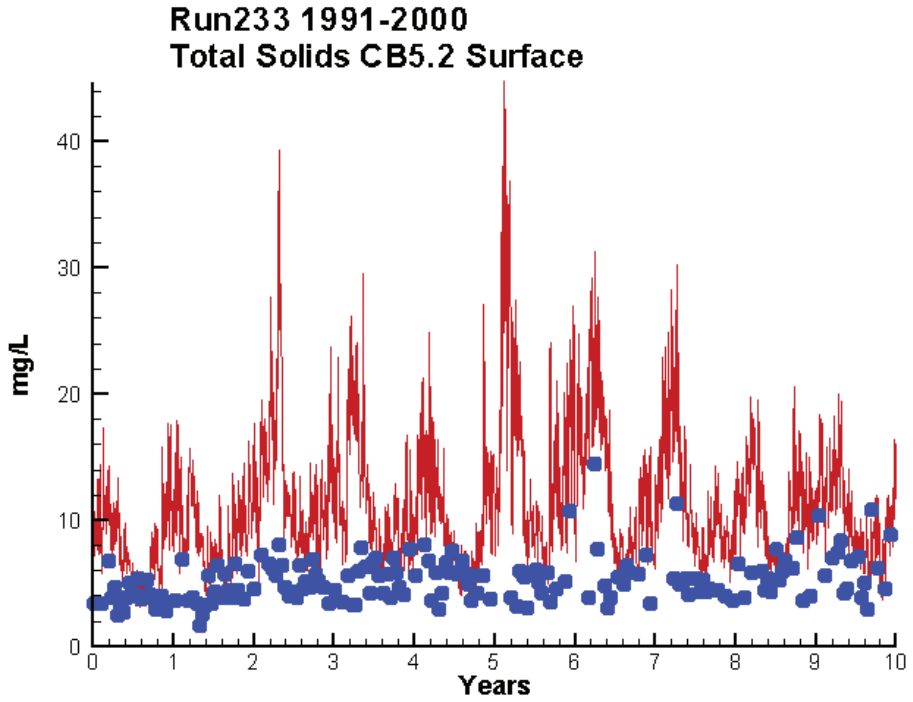

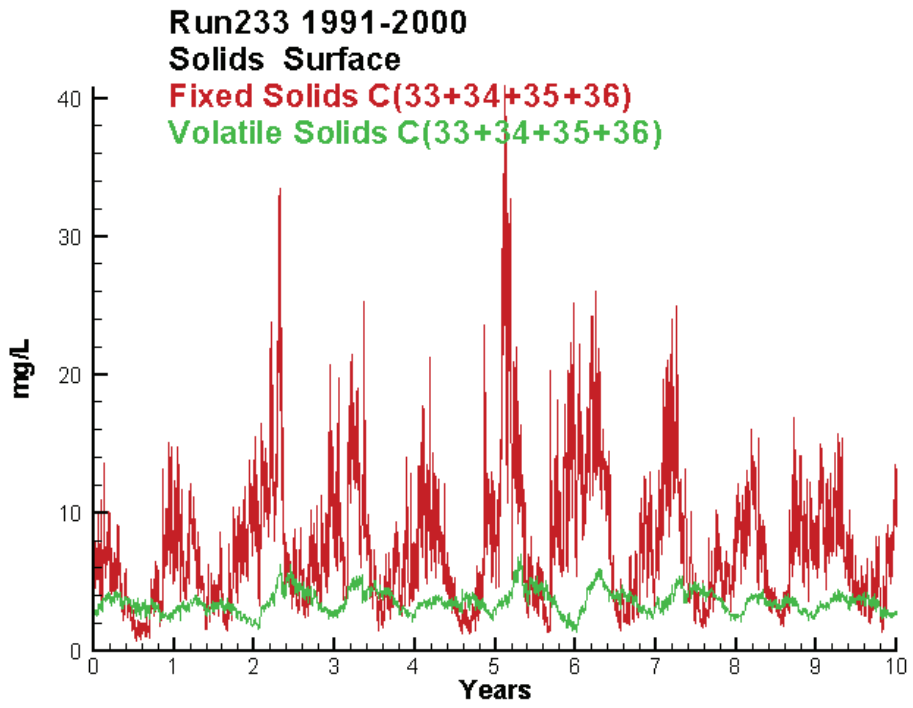

	Mean Difference	Absolute Mean Difference
KE	0.2169	0.3438
TSS	5.4723	5.6606

Station CB6.1

Run233 1991-2000
Chlorophyll CB6.1 Surface

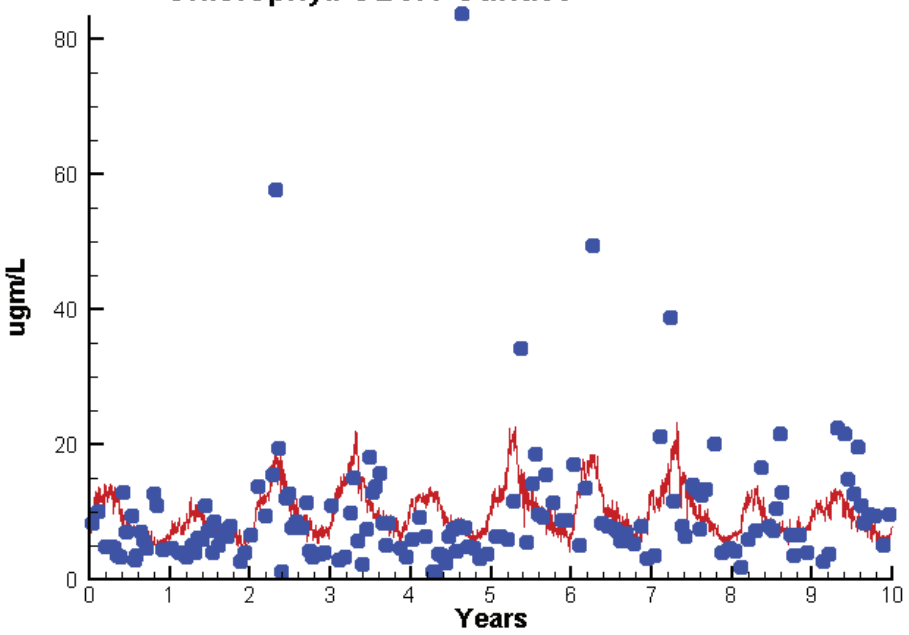

Run233 1991-2000
Light Extinction CB6.1 Surface

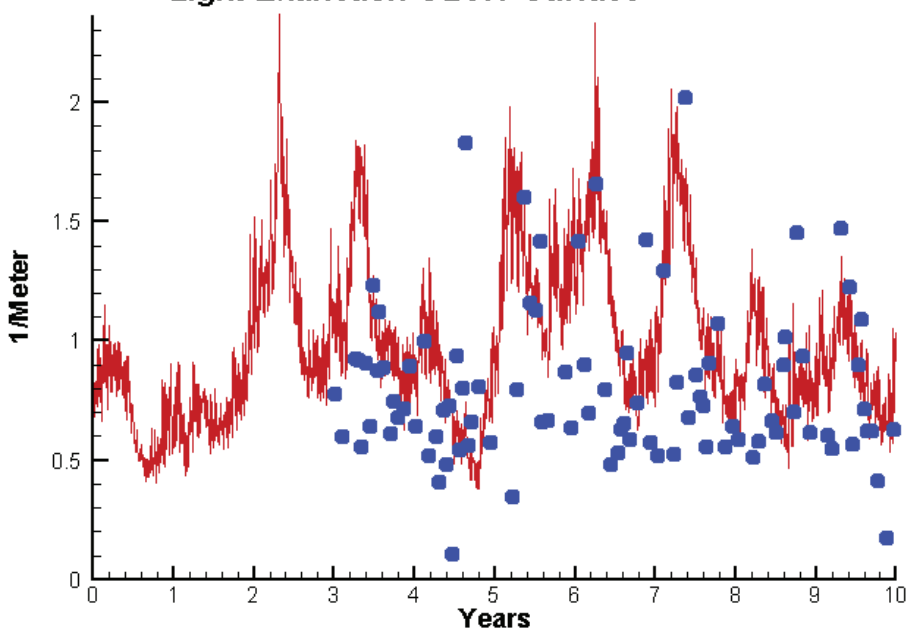

Run233 1991-2000
Dissolved Inorganic Nitrogen CB6.1 Surface

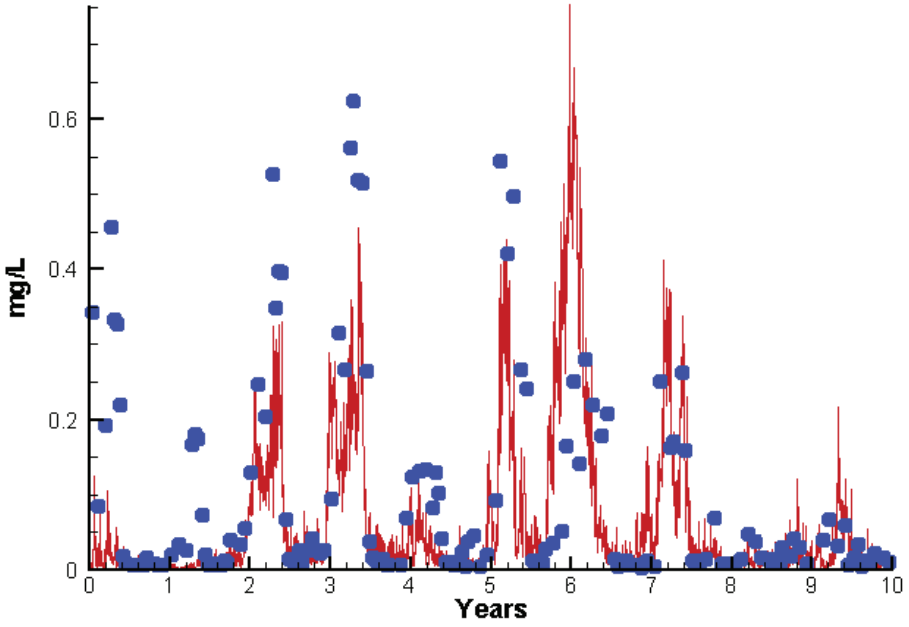

Run233 1991-2000
Dissolved Inorganic Phosphorus CB6.1 Surface

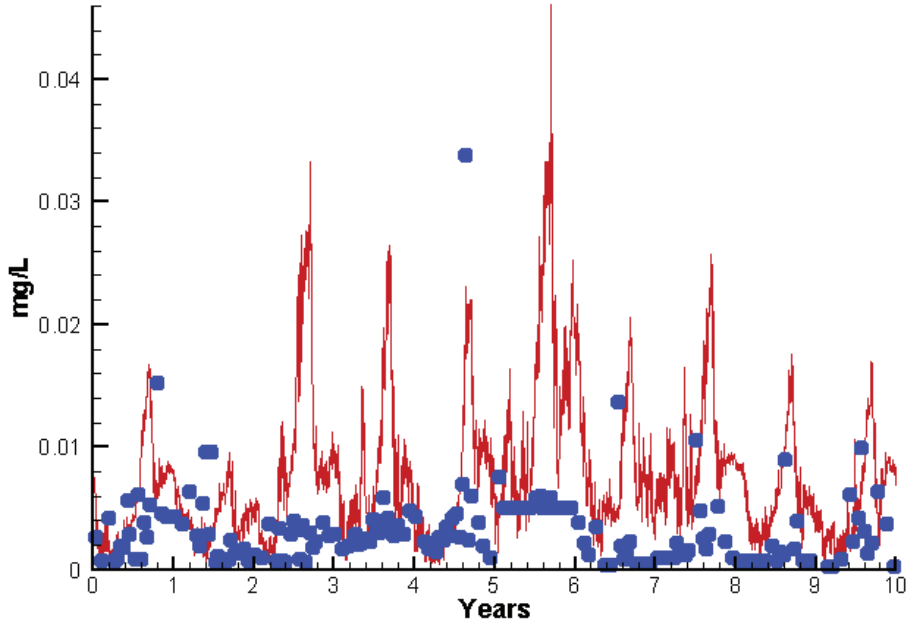

Station CB6.1

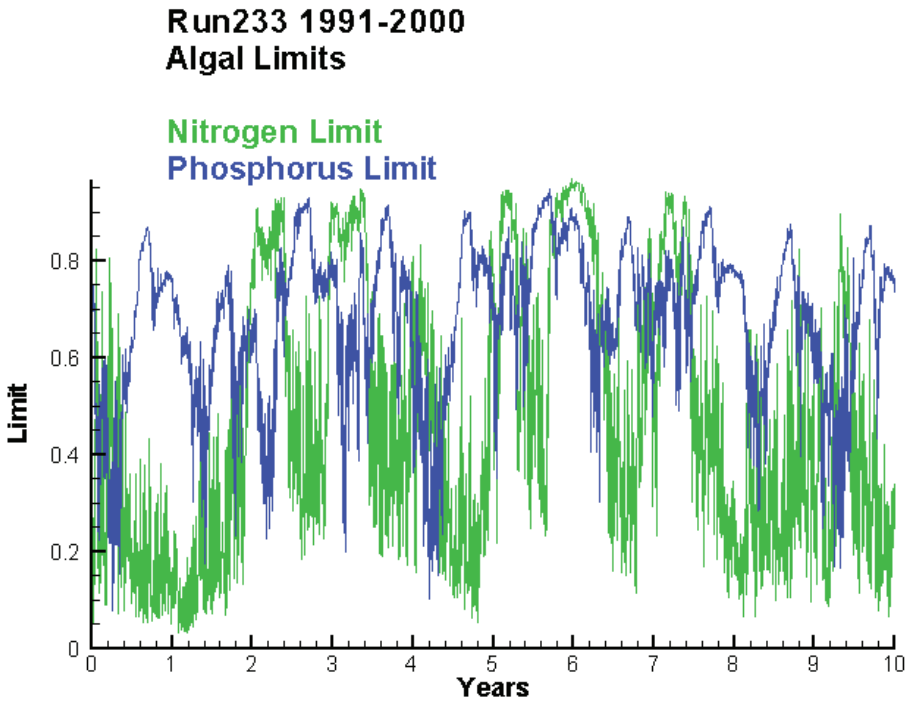

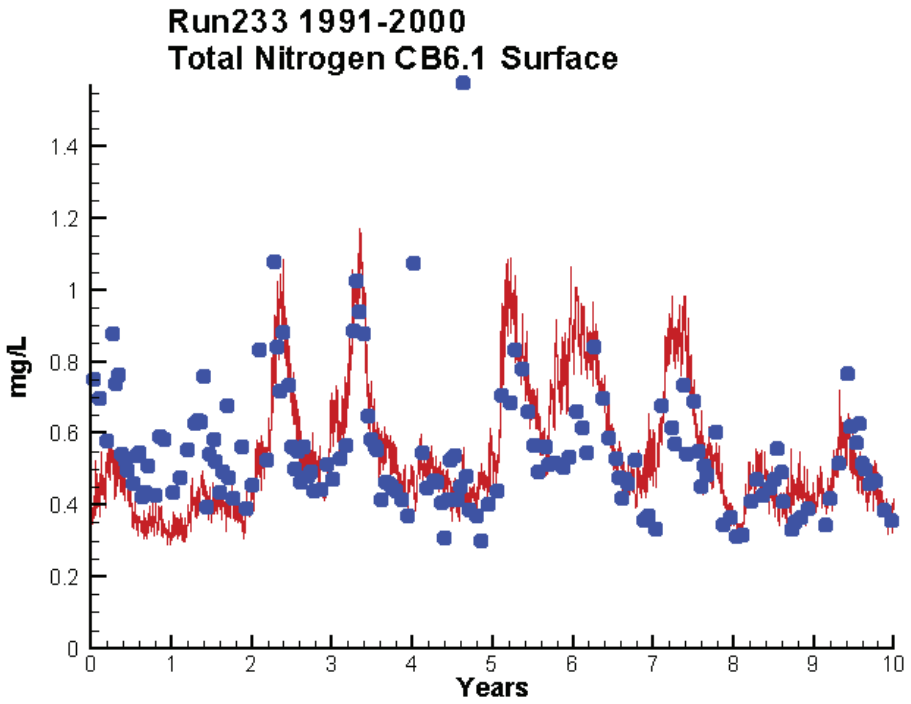

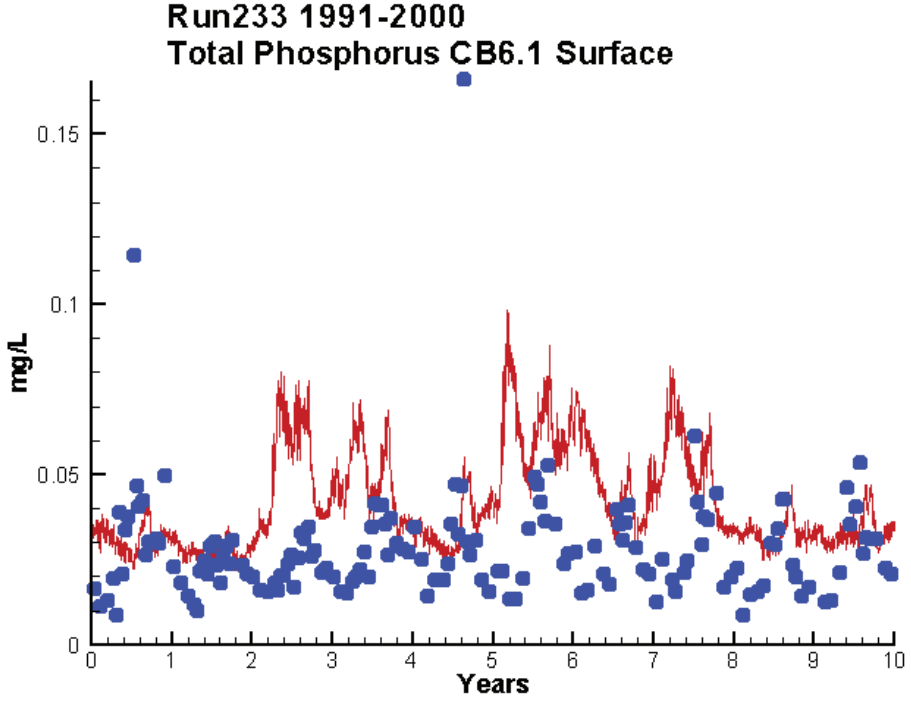

	Mean Difference	Absolute Mean Difference
Chl	0.2994	5.3075
DIN	-0.0356	0.0718
KE	0.2045	0.3367
DIP	0.0052	0.0062
TP	0.0145	0.0199
TN	-0.0002	0.1183

Station CB6.1

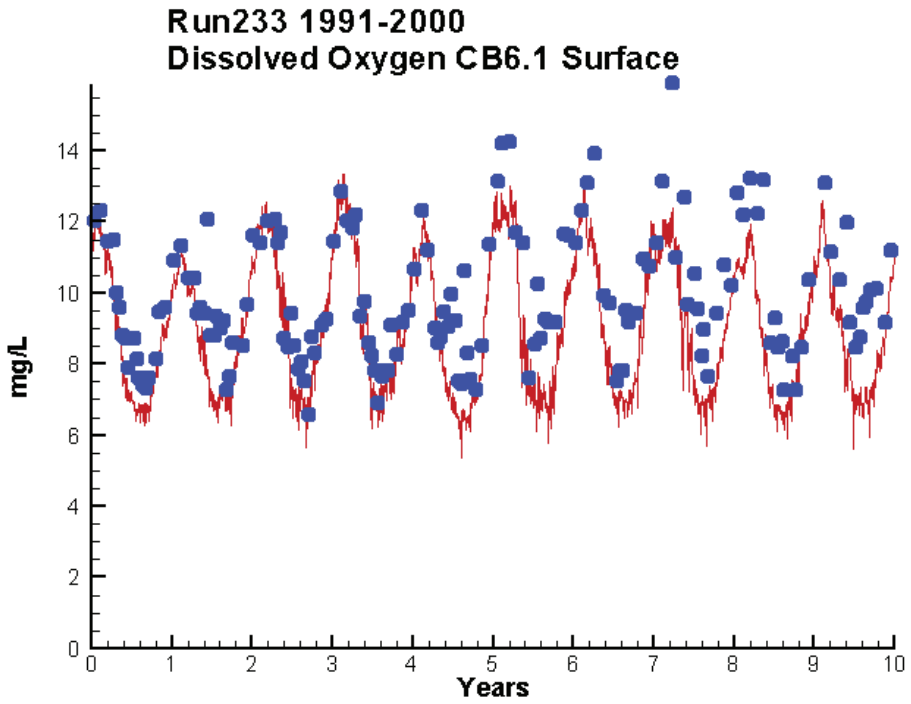

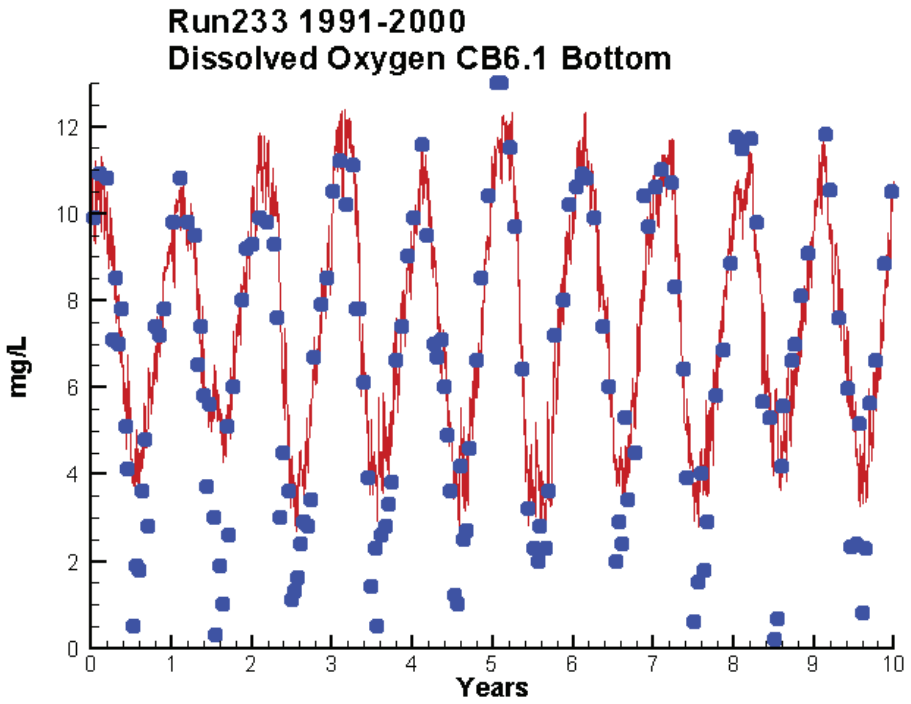

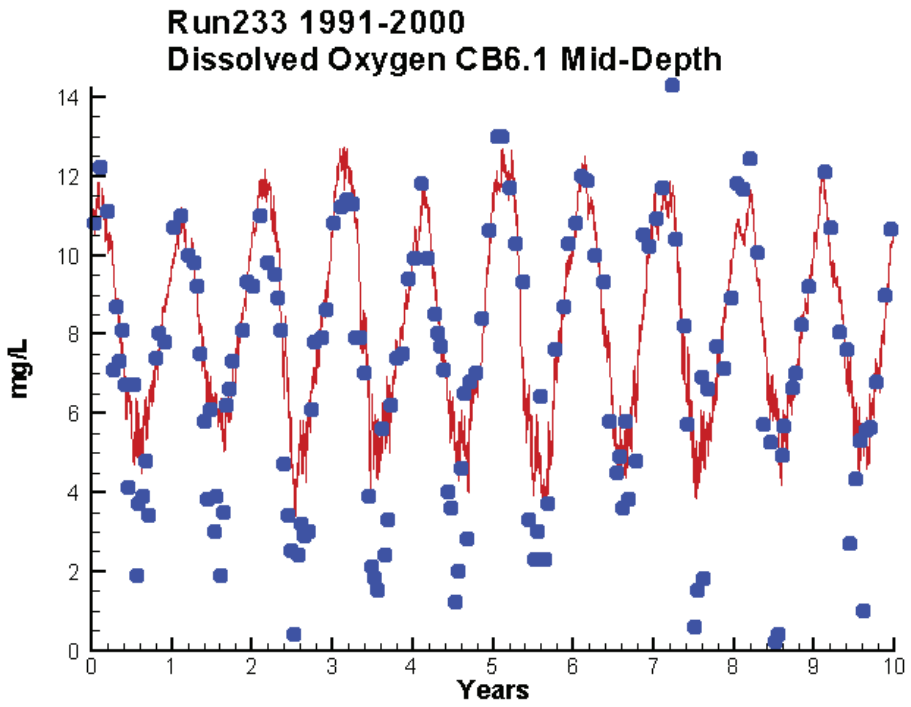

	Mean Difference	Absolute Mean Difference
Top DO	-1.1591	1.2251
Mid DO	0.8089	1.2874
Bot DO	0.7952	1.2241

Station CB6.1

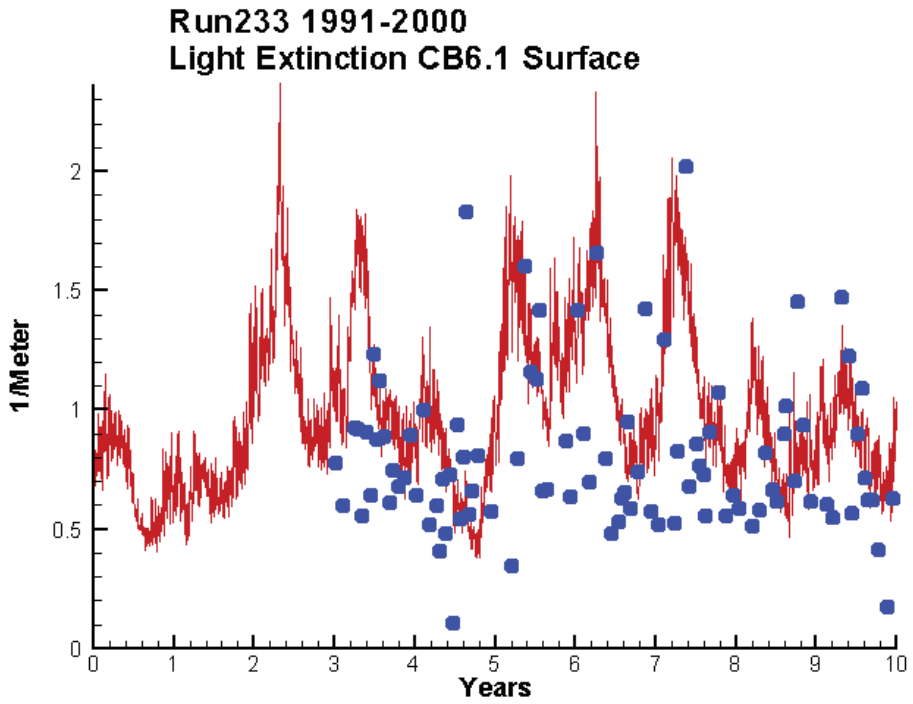

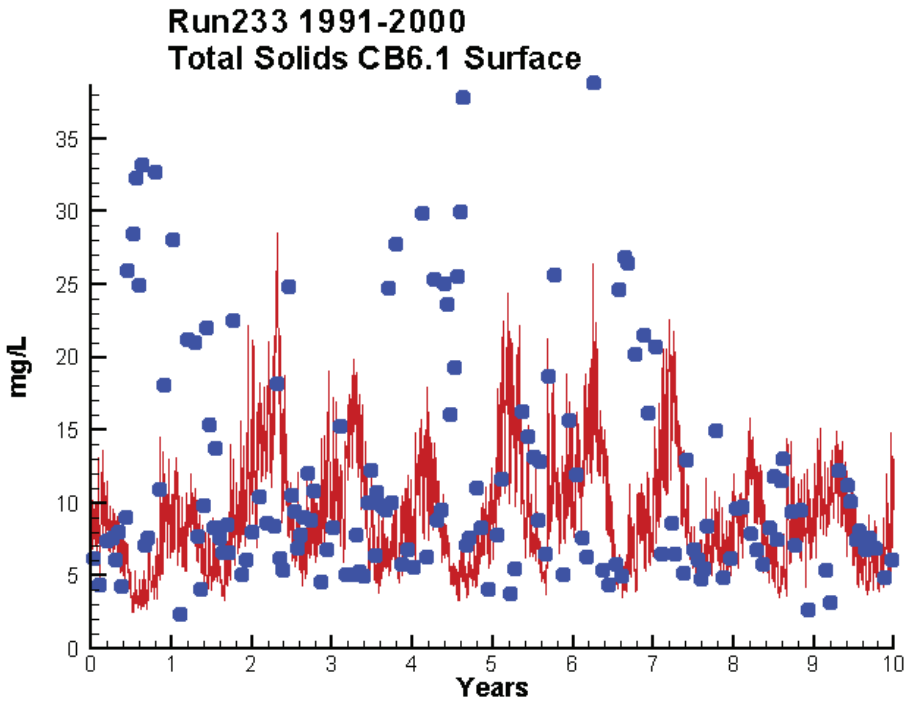

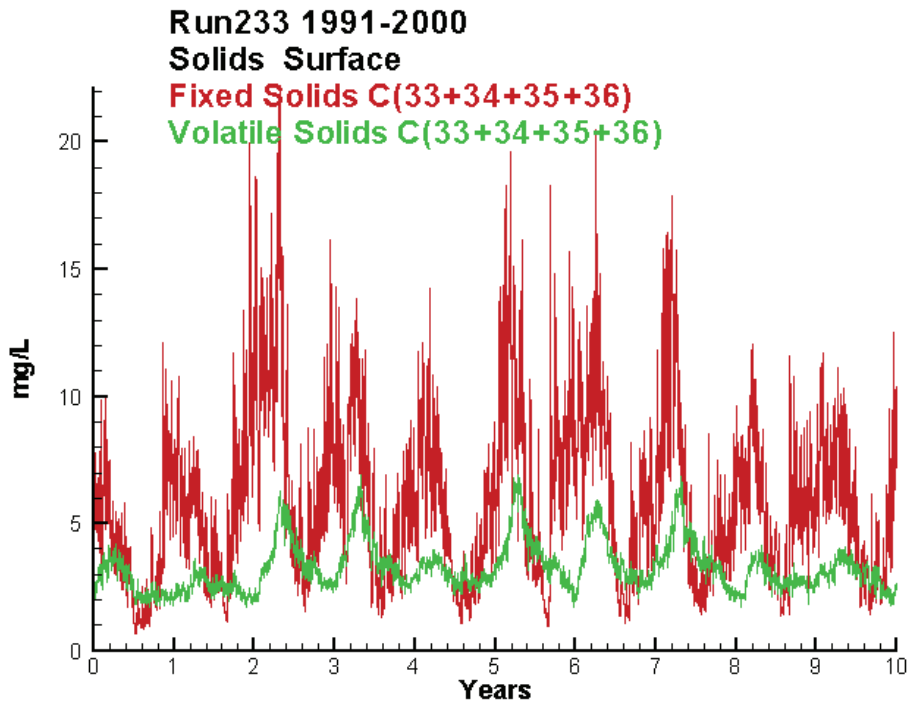

	Mean Difference	Absolute Mean Difference
KE	0.2045	0.3367
TSS	-2.9854	7.0983

Station CB7.3

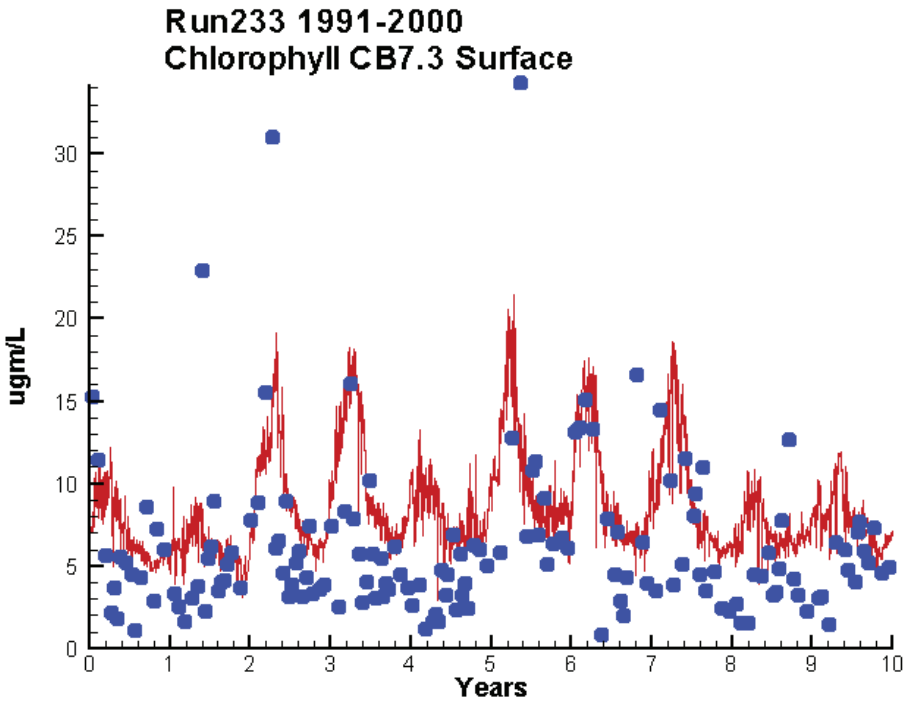

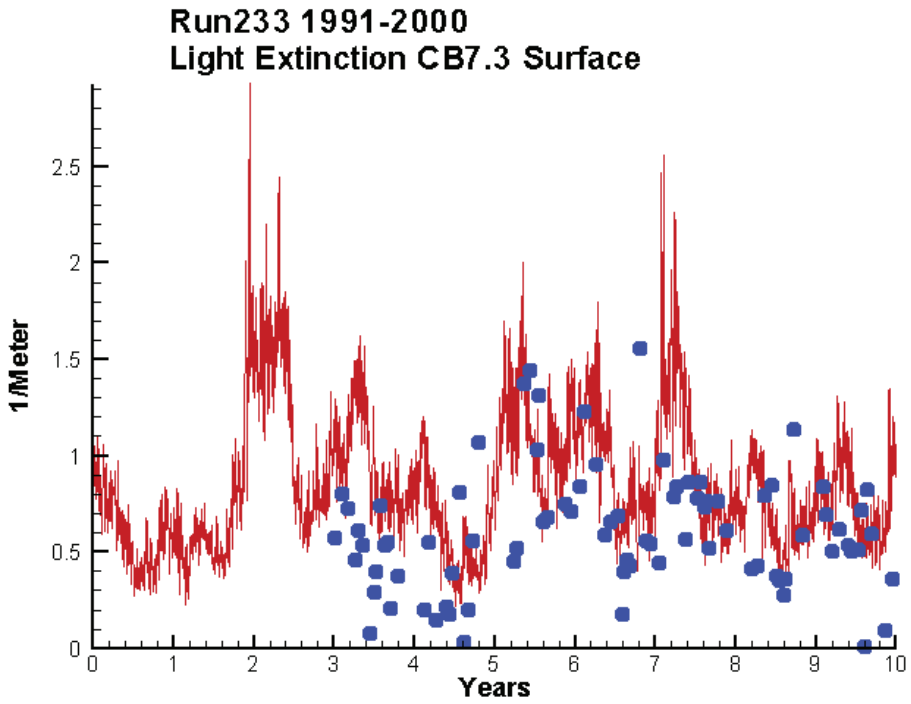

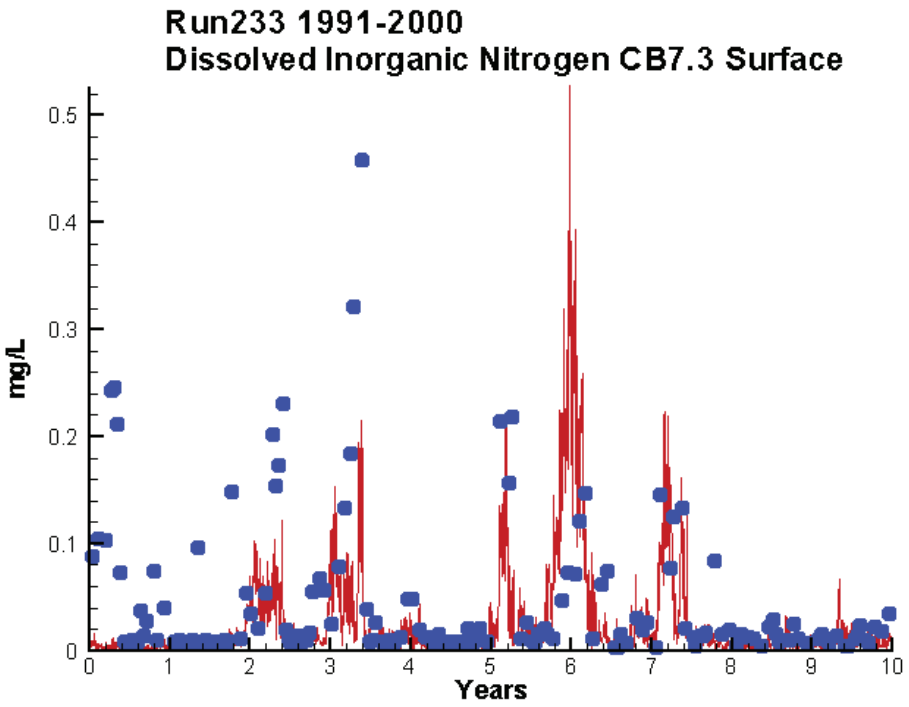

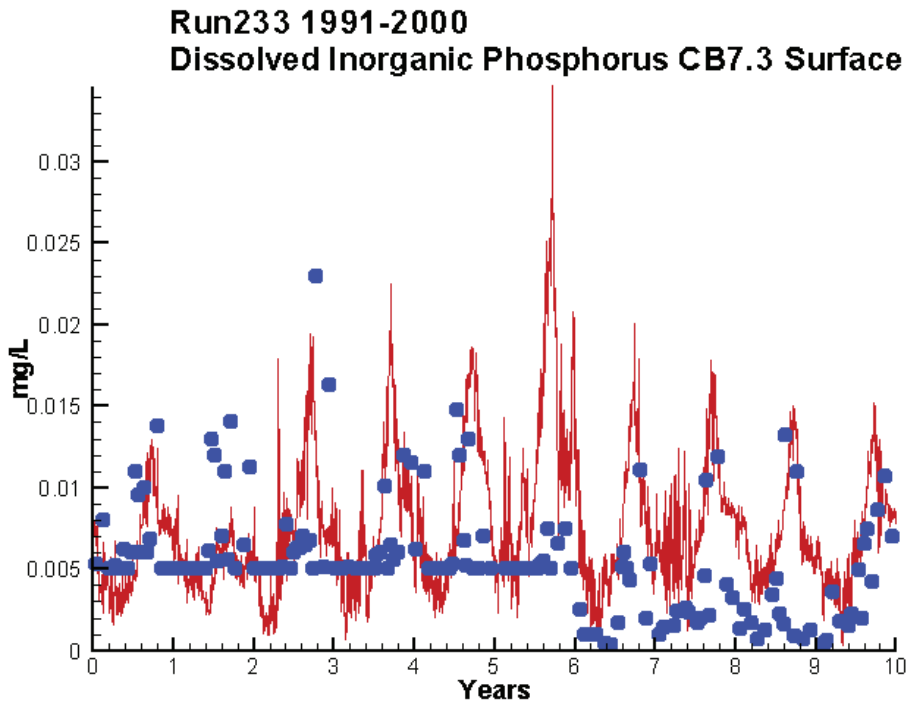

Station CB7.3

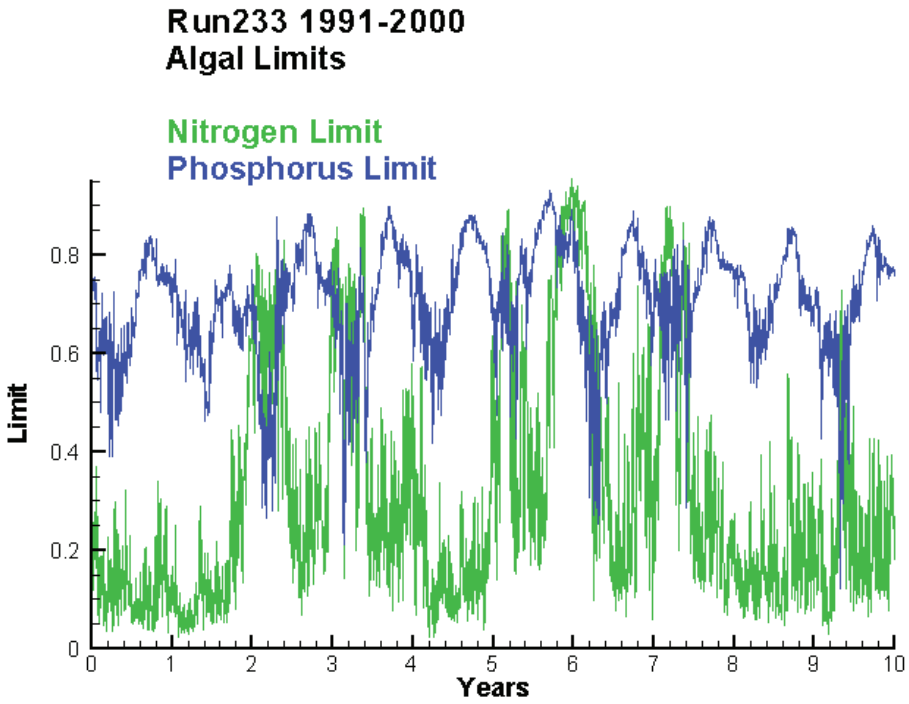

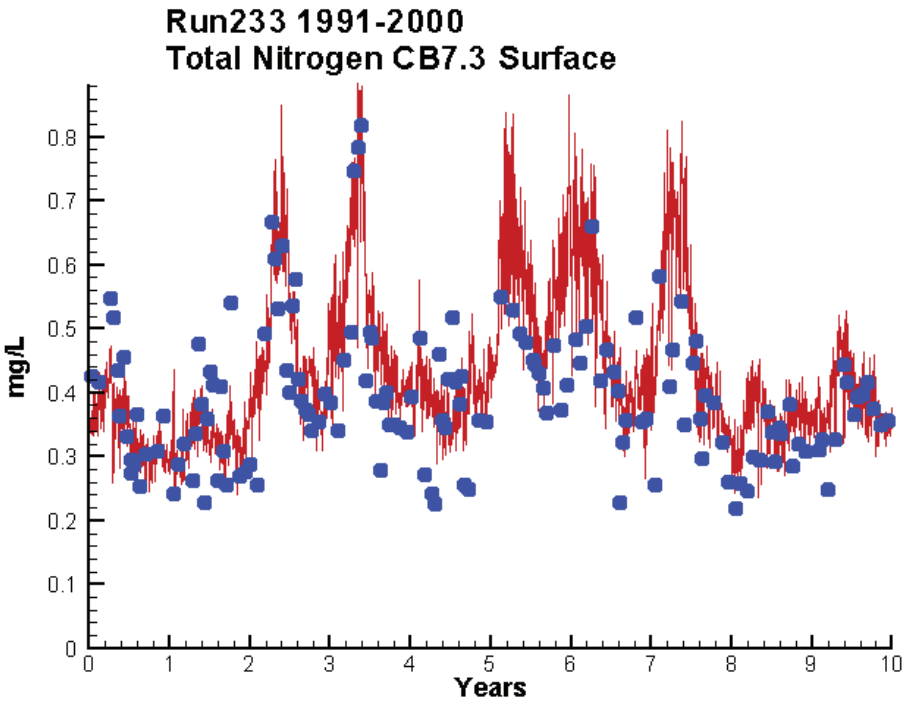

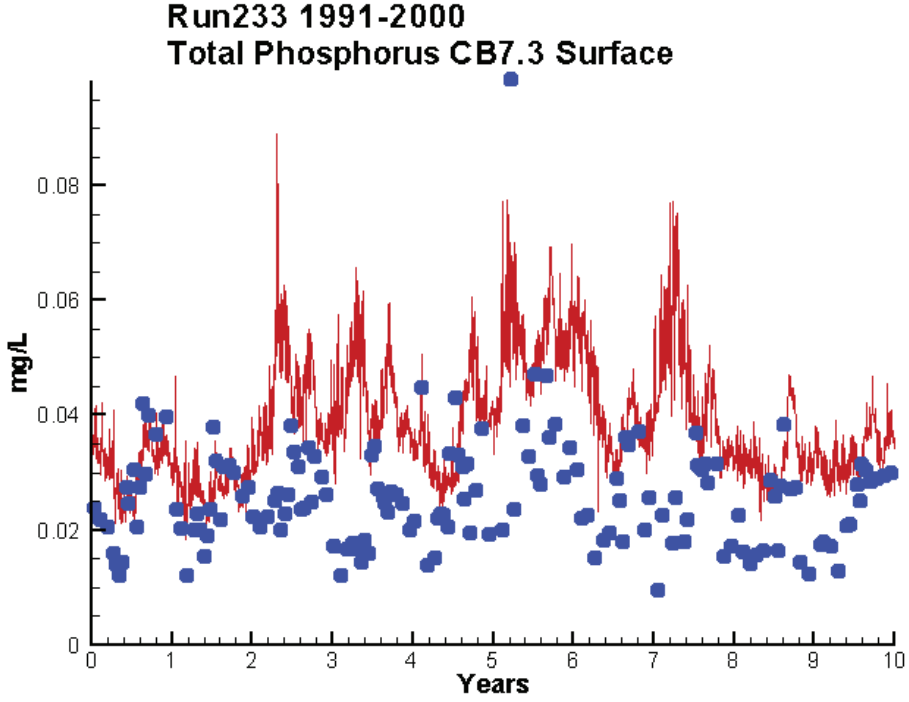

	Mean Difference	Absolute Mean Difference
Chl	2.3340	3.7386
DIN	-0.0245	0.0372
KE	0.2142	0.3315
DIP	0.0020	0.0039
TP	0.0122	0.0140
TN	0.0394	0.0726

Station CB7.3

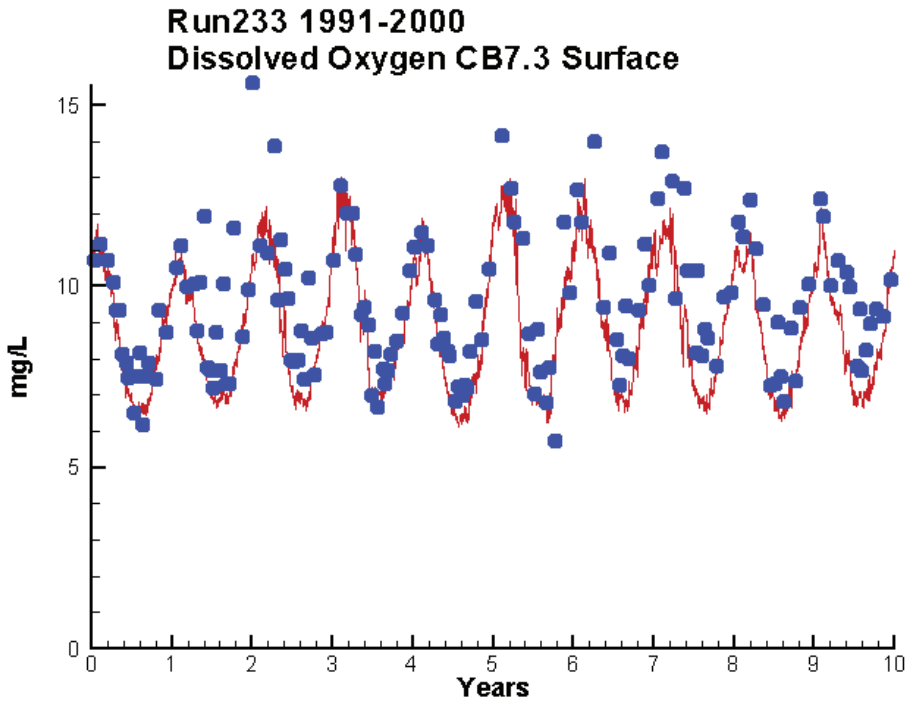

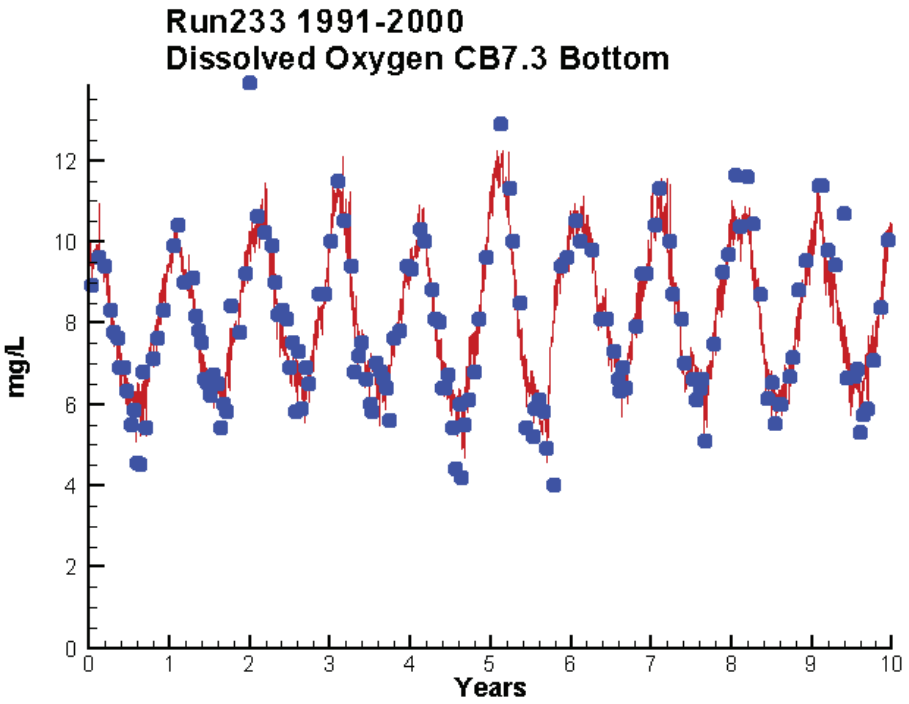

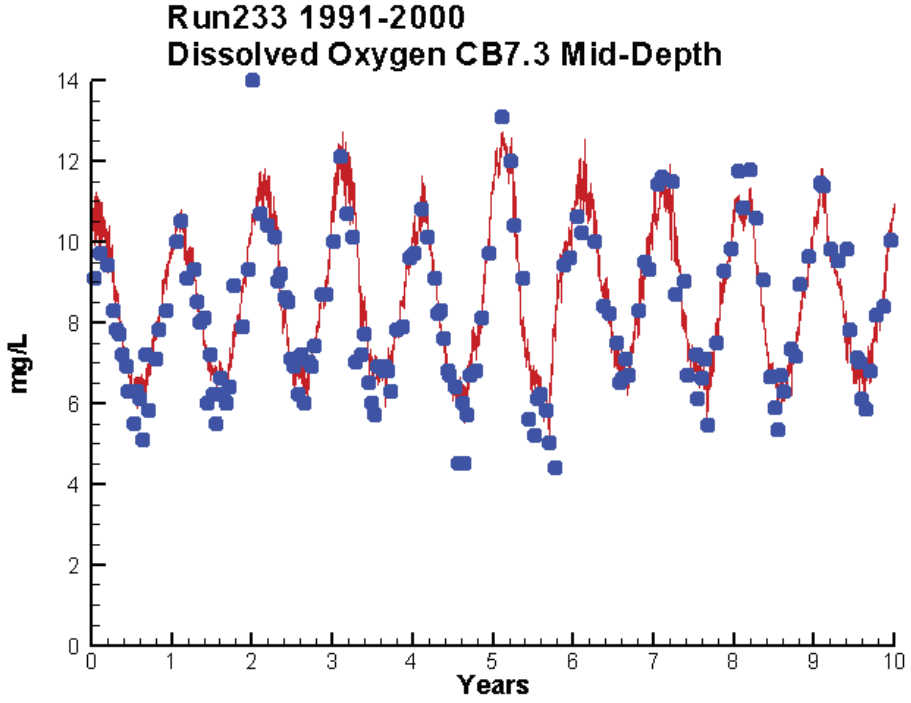

	Mean Difference	Absolute Mean Difference
Top DO	-0.8784	1.0354
Mid DO	0.2194	0.5924
Bot DO	0.0307	0.5584

Station CB7.3

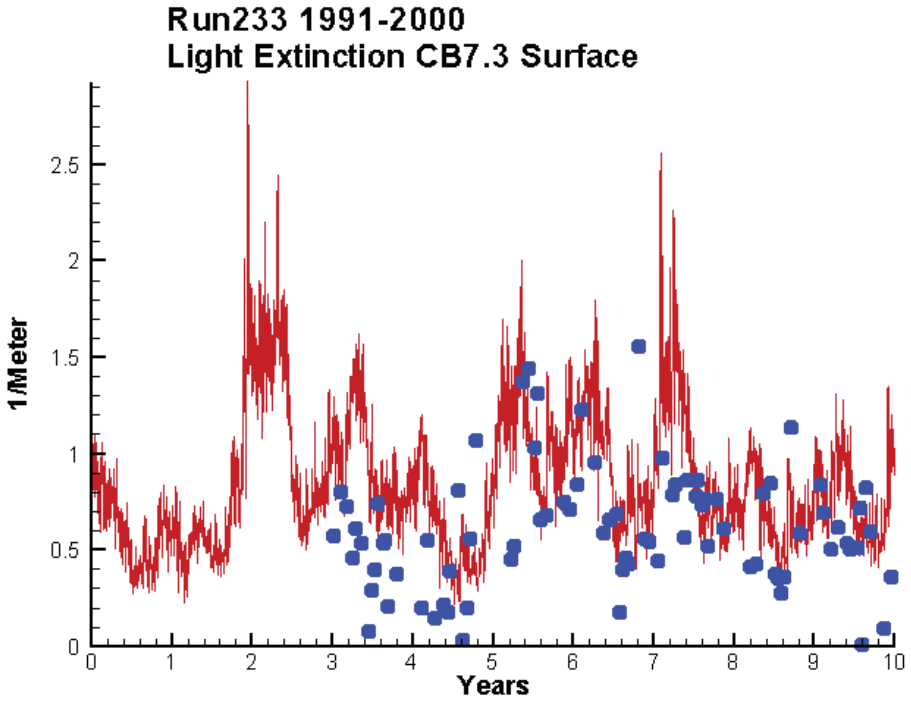

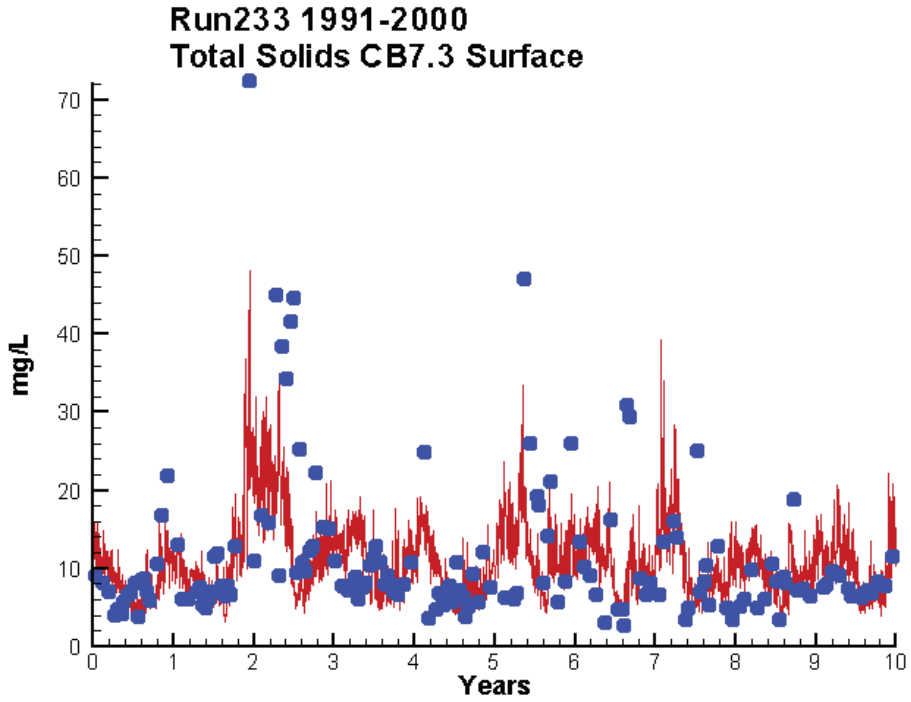

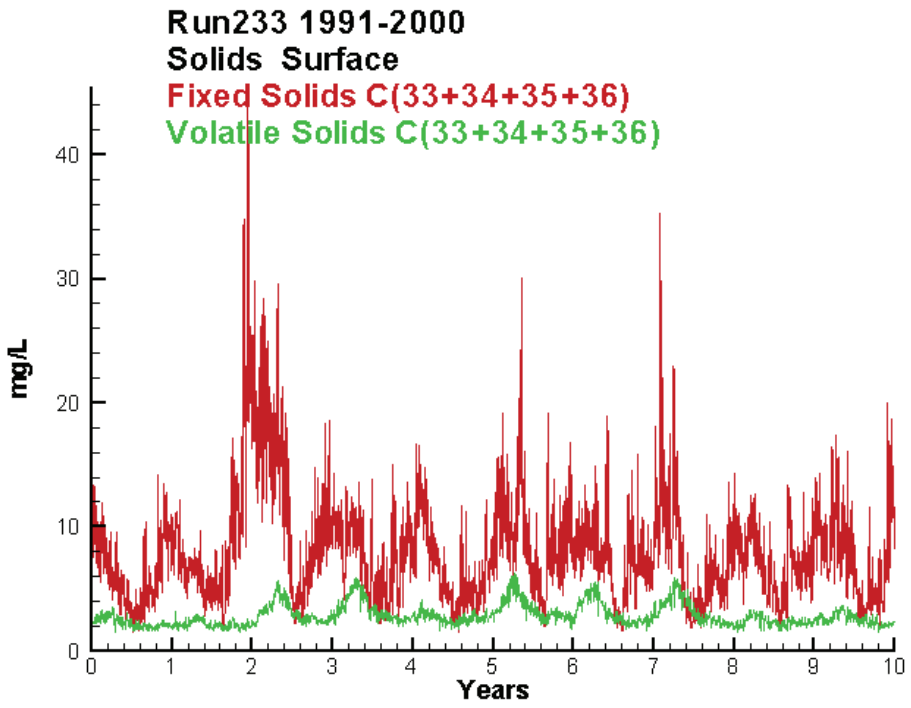

	Mean Difference	Absolute Mean Difference
KE	0.2142	0.3315
TSS	-1.4395	5.4509

Station CB7.4

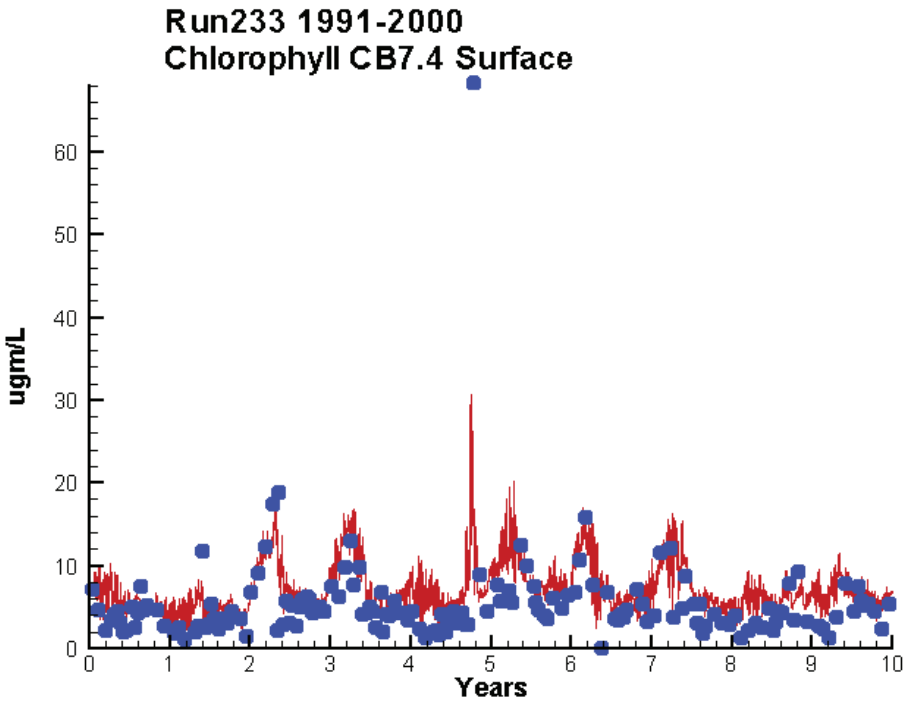

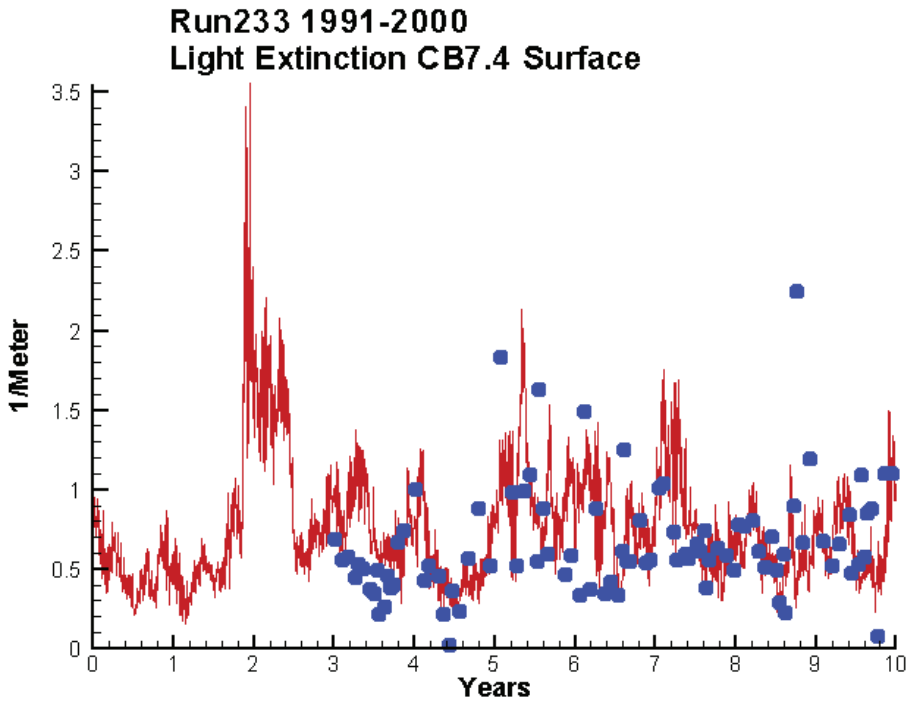

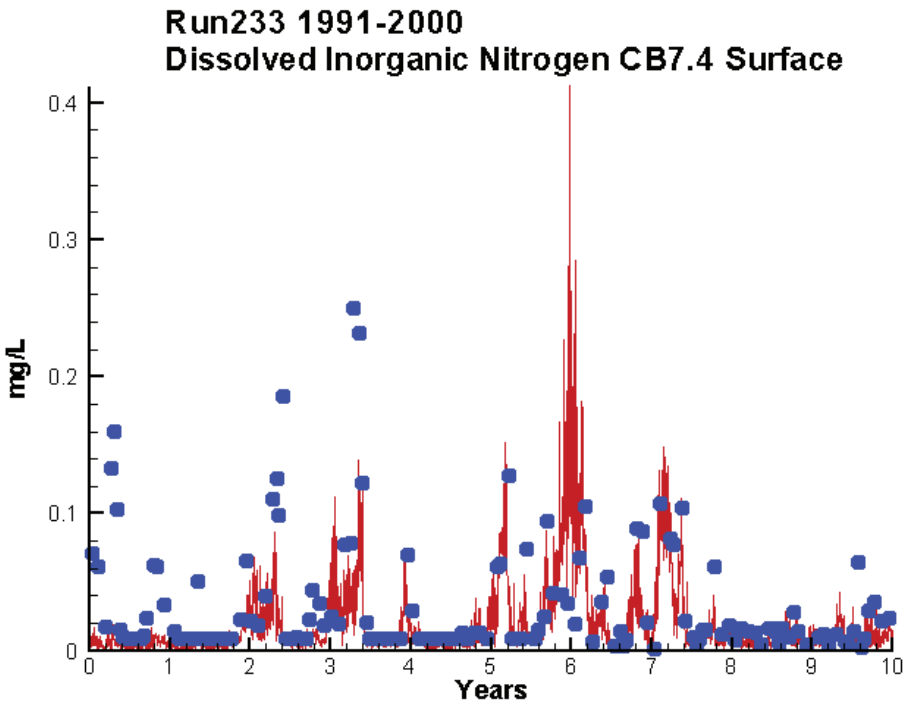

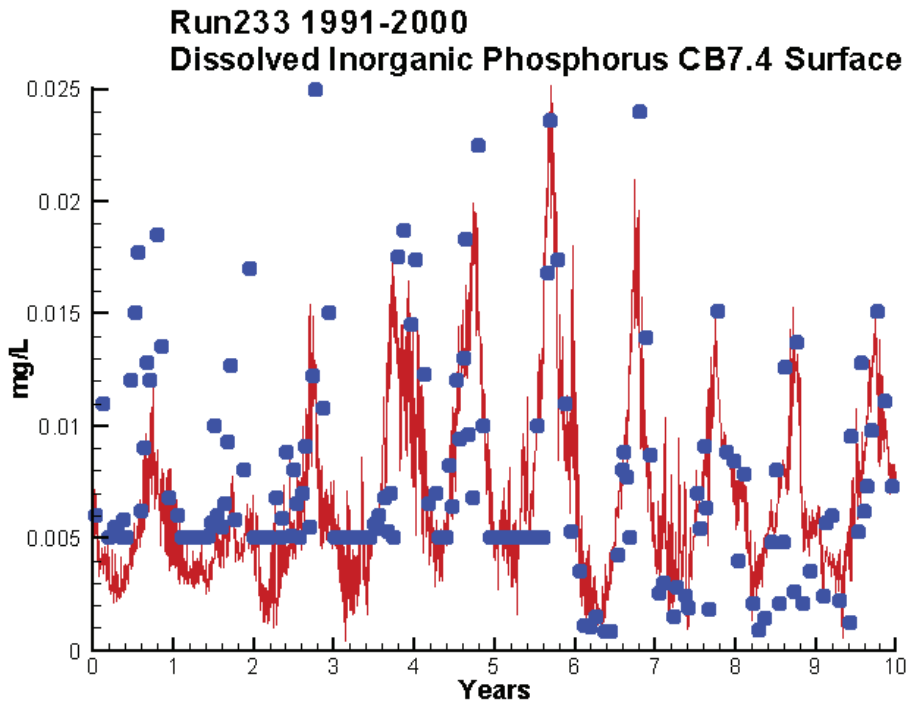

Station CB7.4

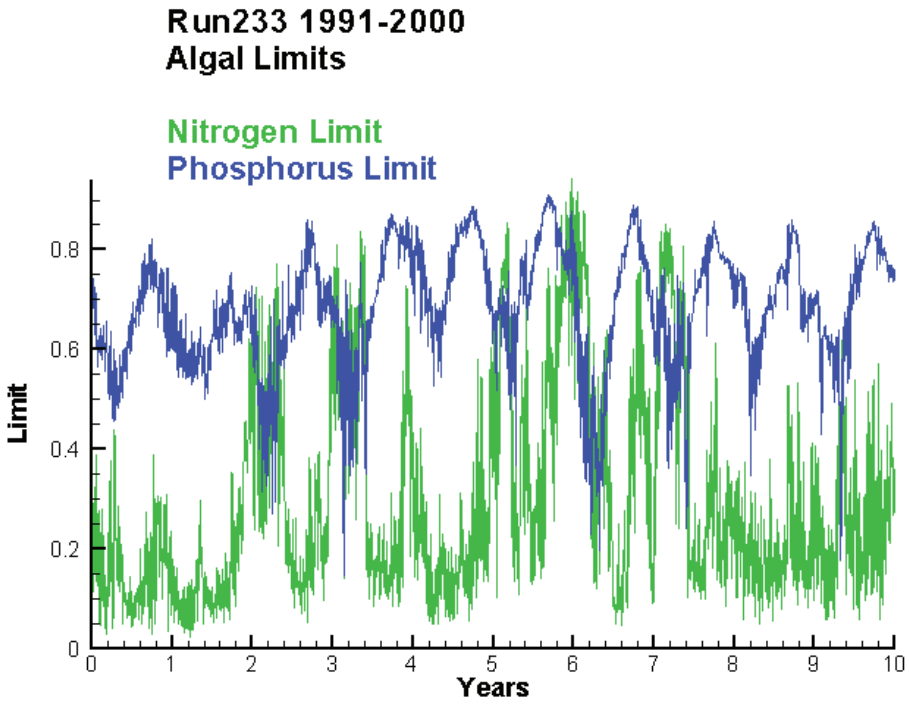

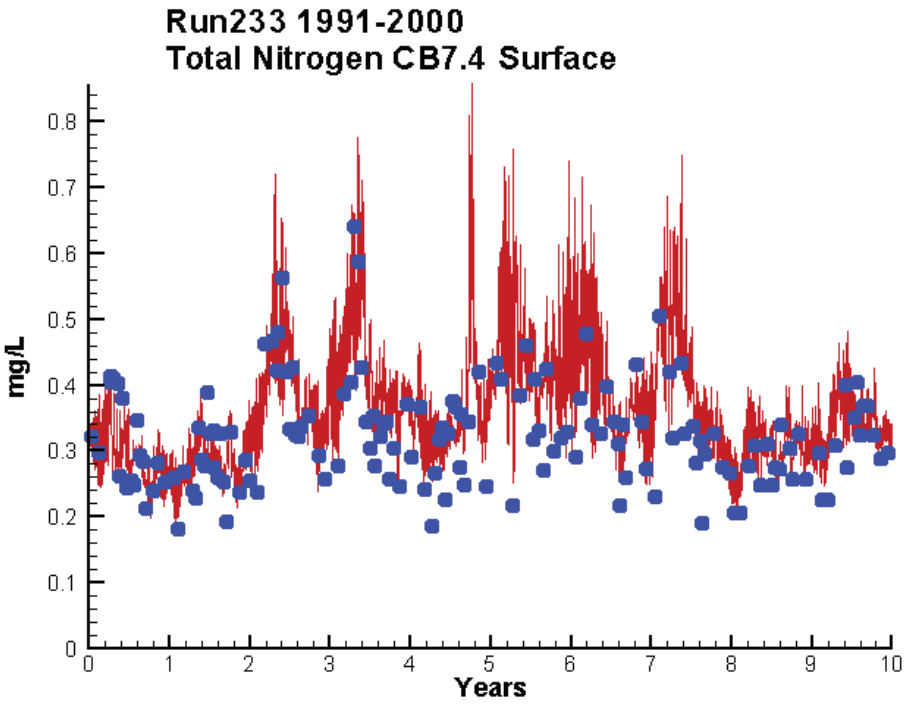

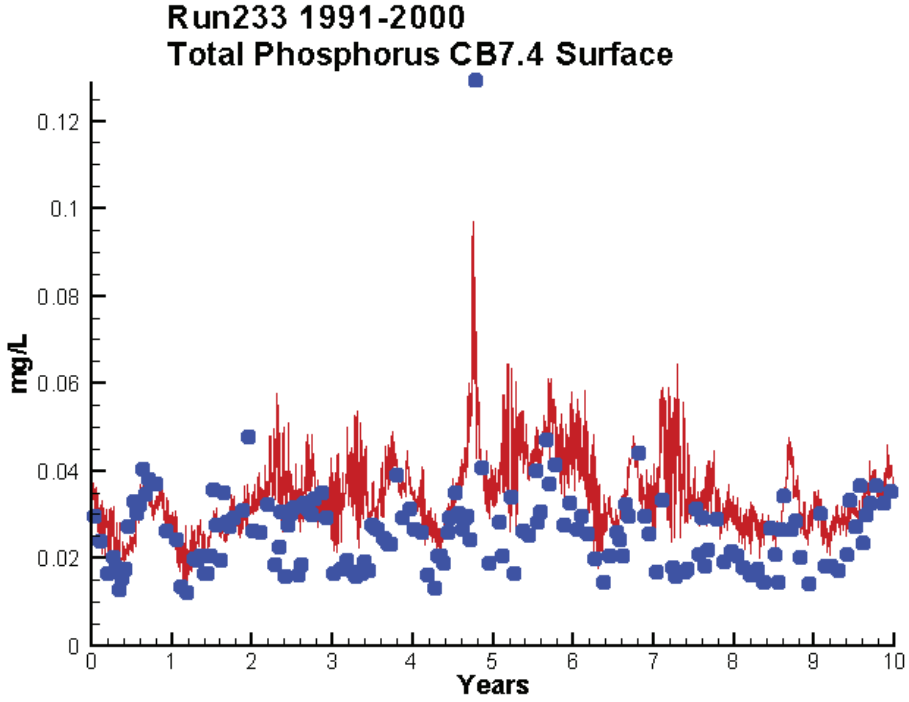

	Mean Difference	Absolute Mean Difference
Chl	1.7352	2.9708
DIN	-0.0162	0.0222
KE	0.0631	0.3128
DIP	-0.0008	0.0031
TP	0.0075	0.0097
TN	0.0354	0.0553

Station CB7.4

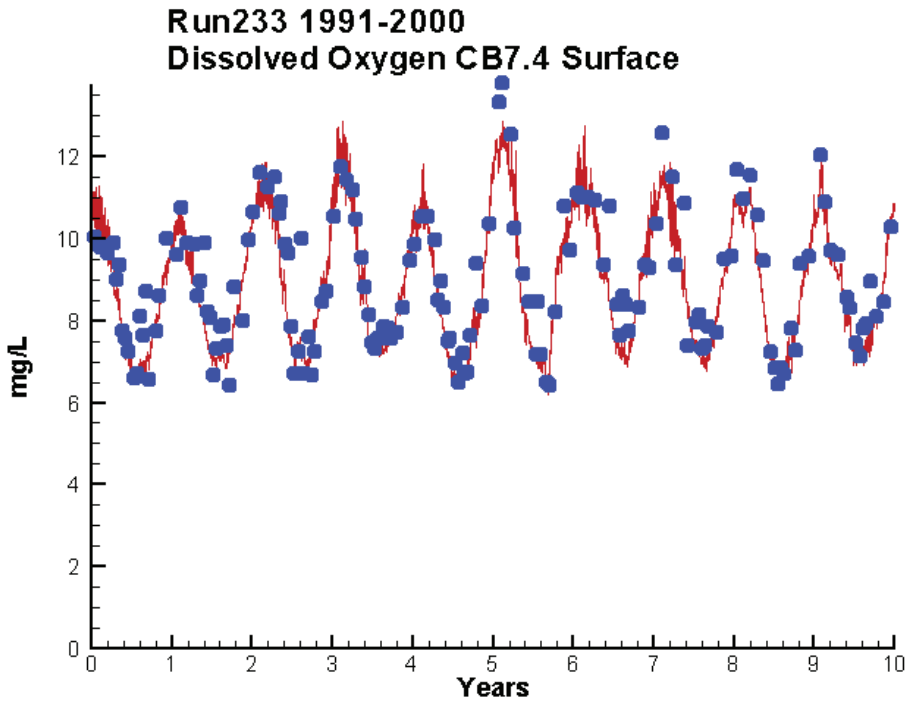

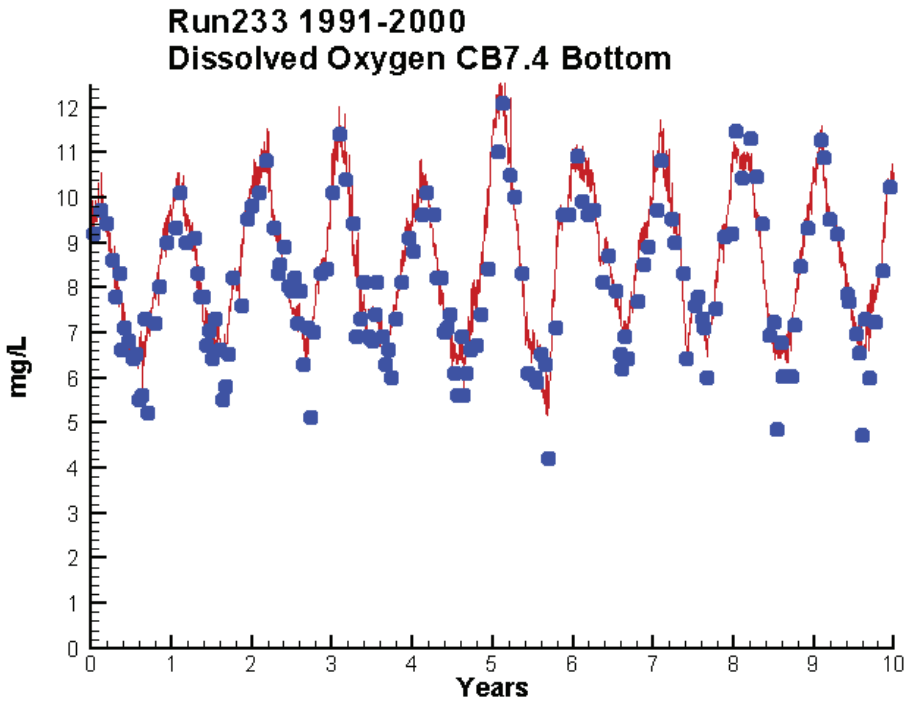

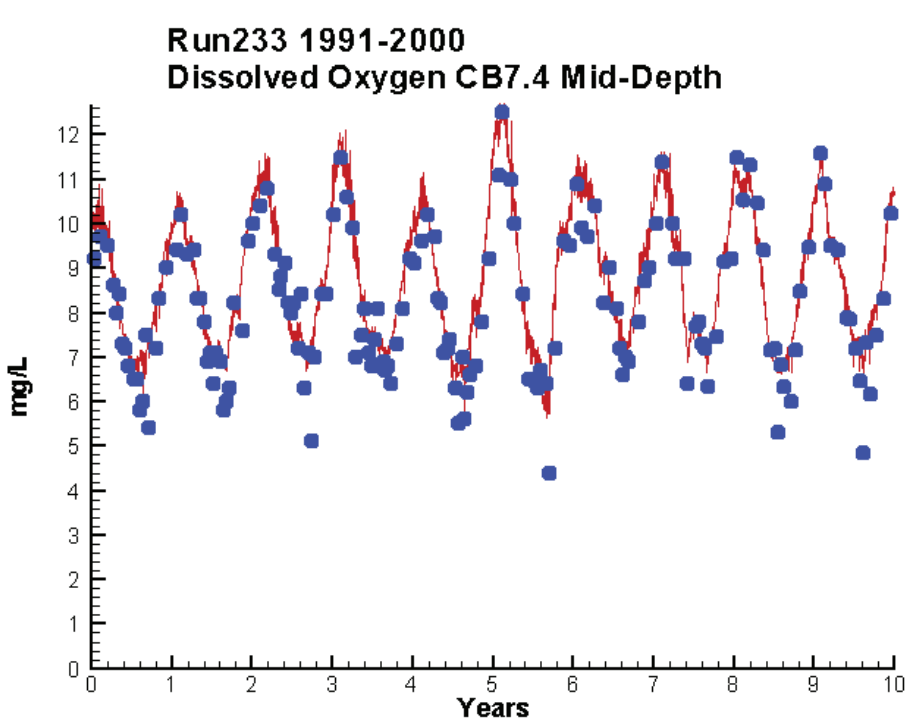

	Mean Difference	Absolute Mean Difference
Top DO	-0.3150	0.6004
Mid DO	0.3690	0.5927
Bot DO	0.3080	0.5574

Station CB7.4

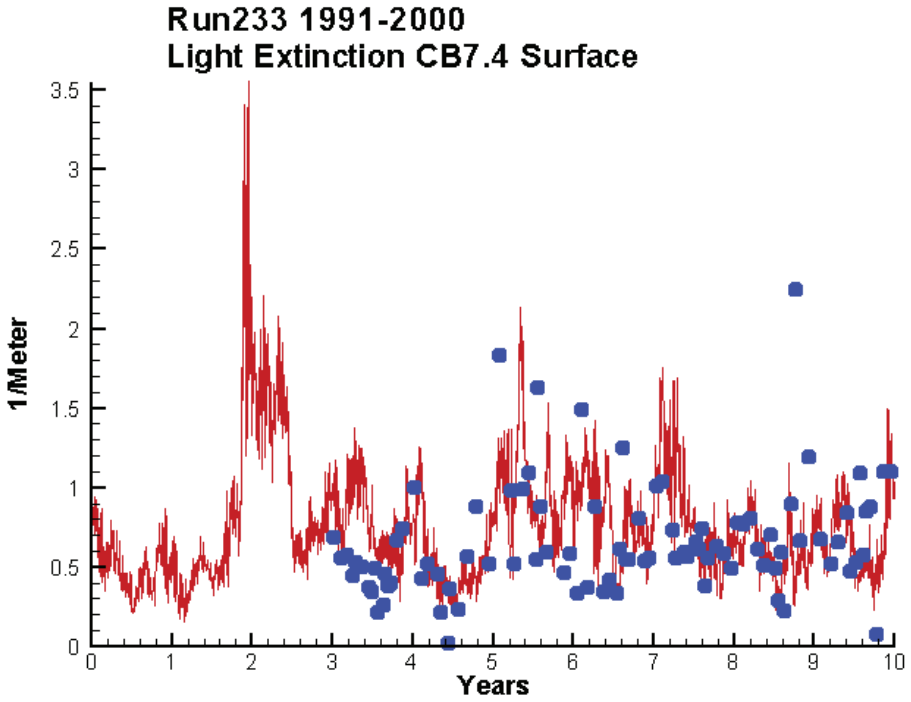

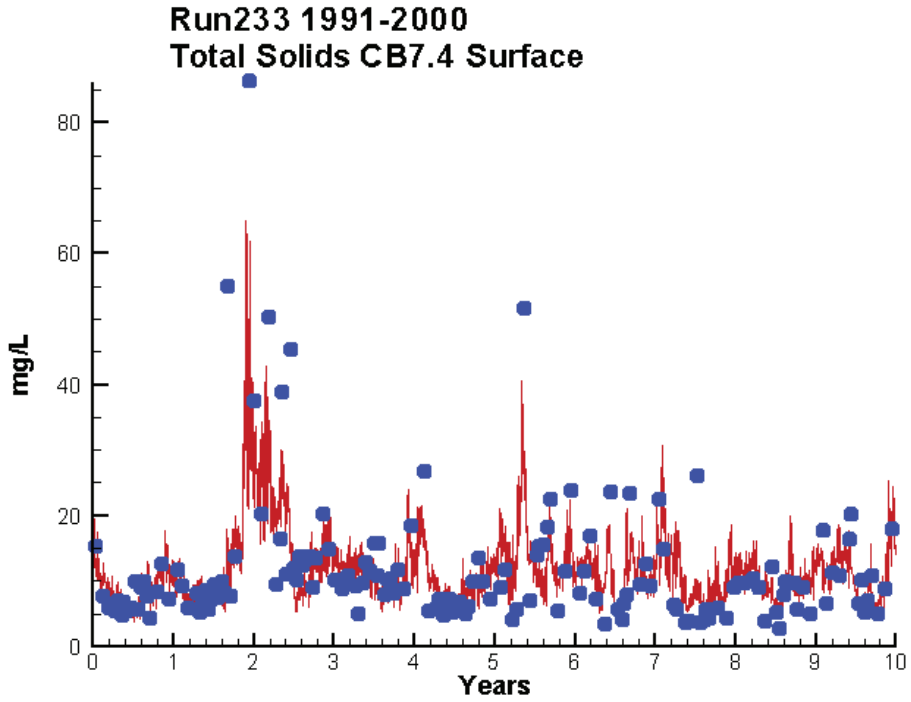

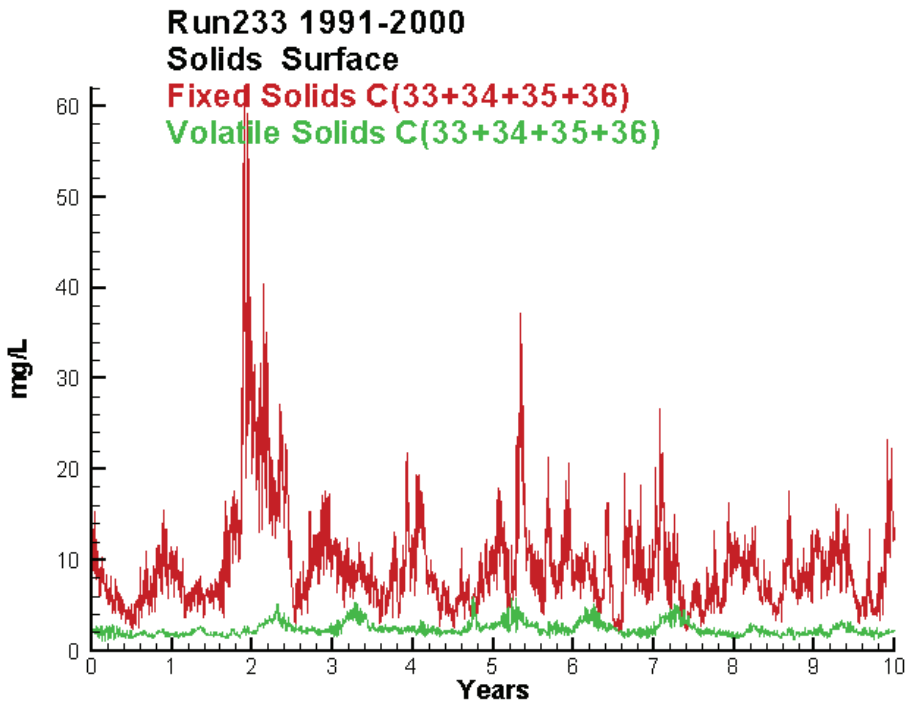

	Mean Difference	Absolute Mean Difference
KE	0.0631	0.3128
TSS	-0.6755	4.6393

Station CB7.4N

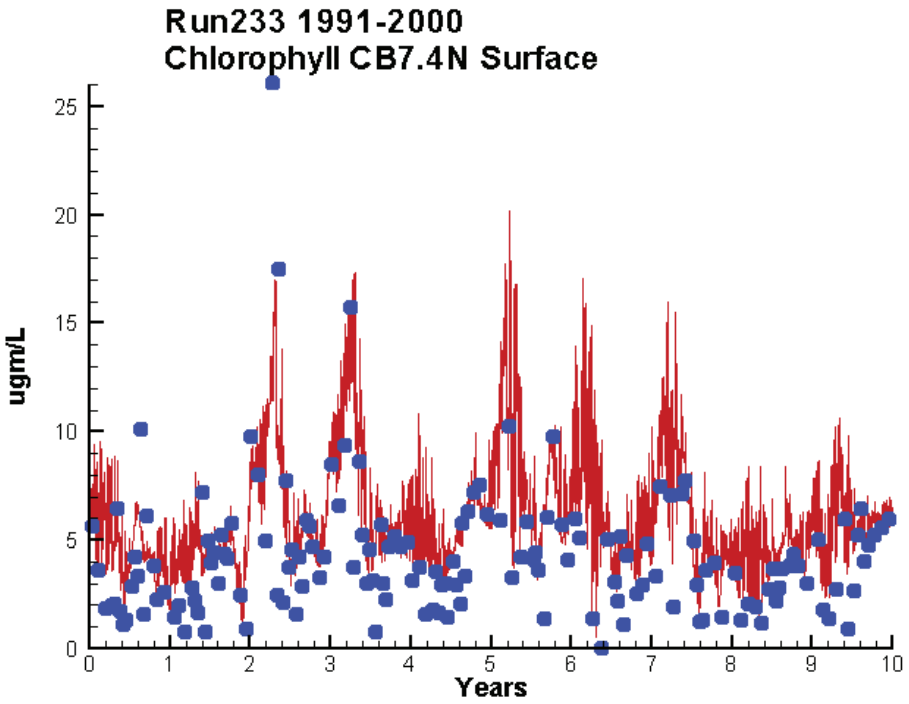

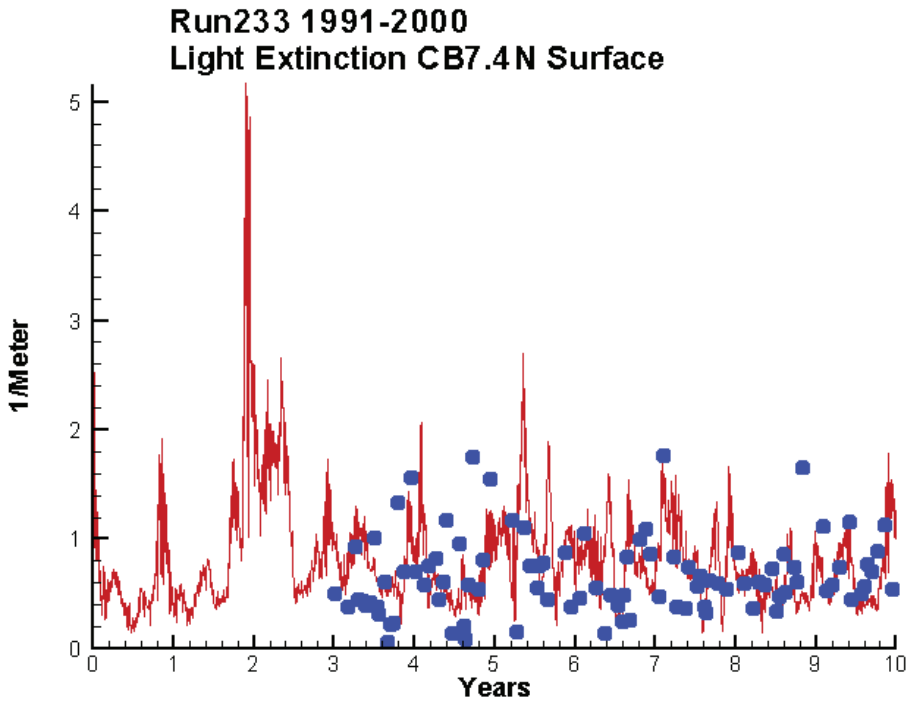

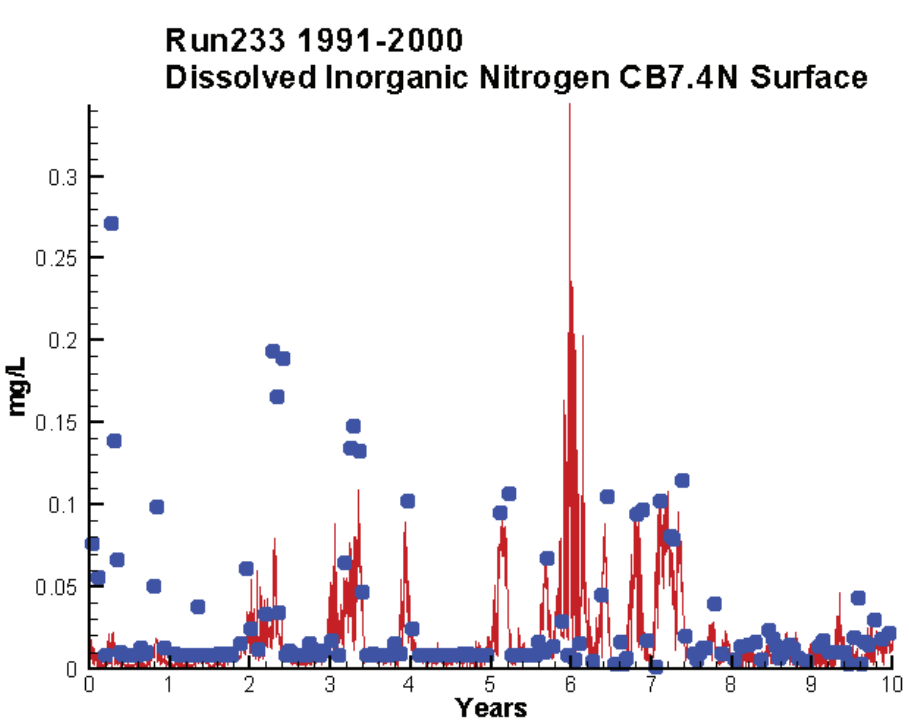

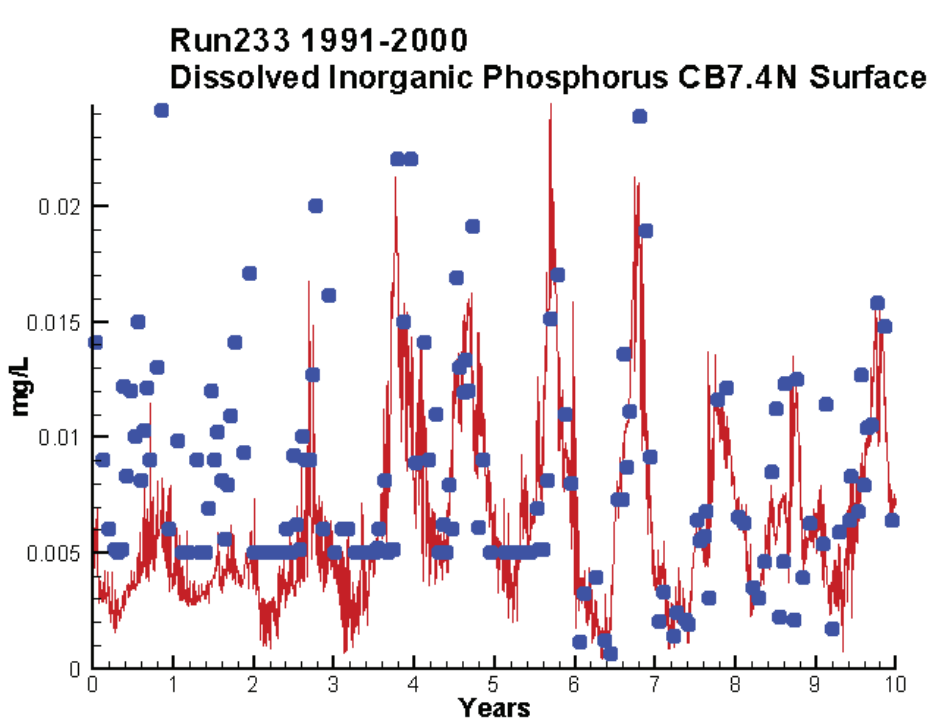

Station CB7.4N

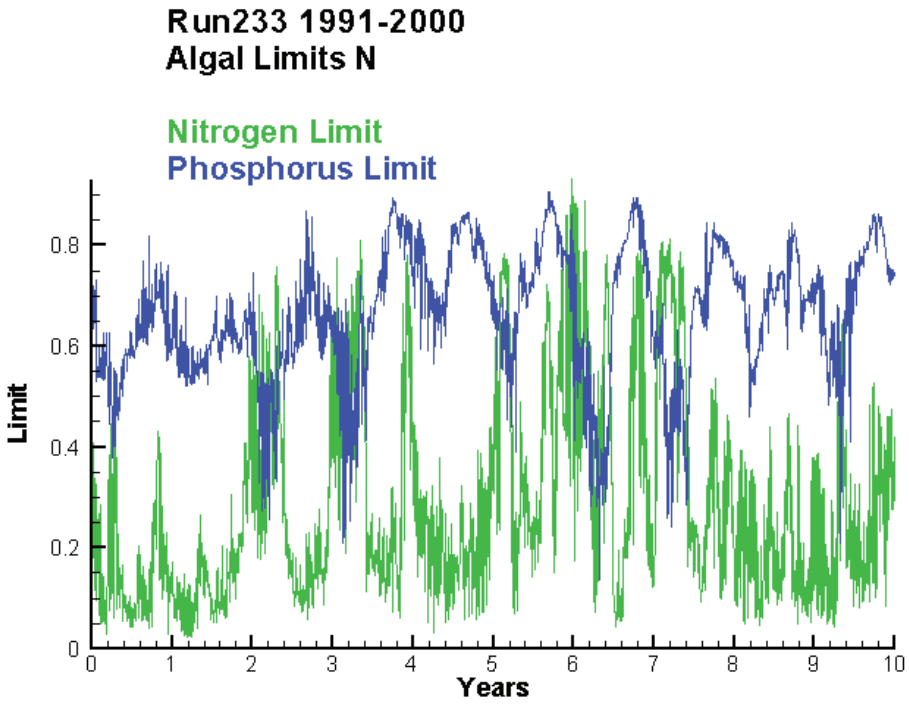

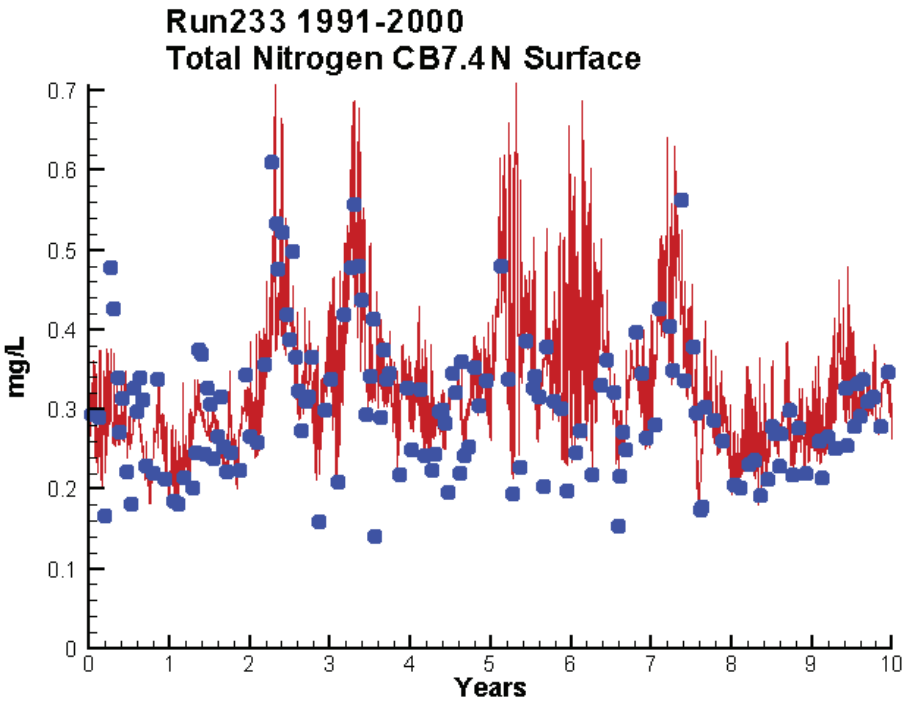

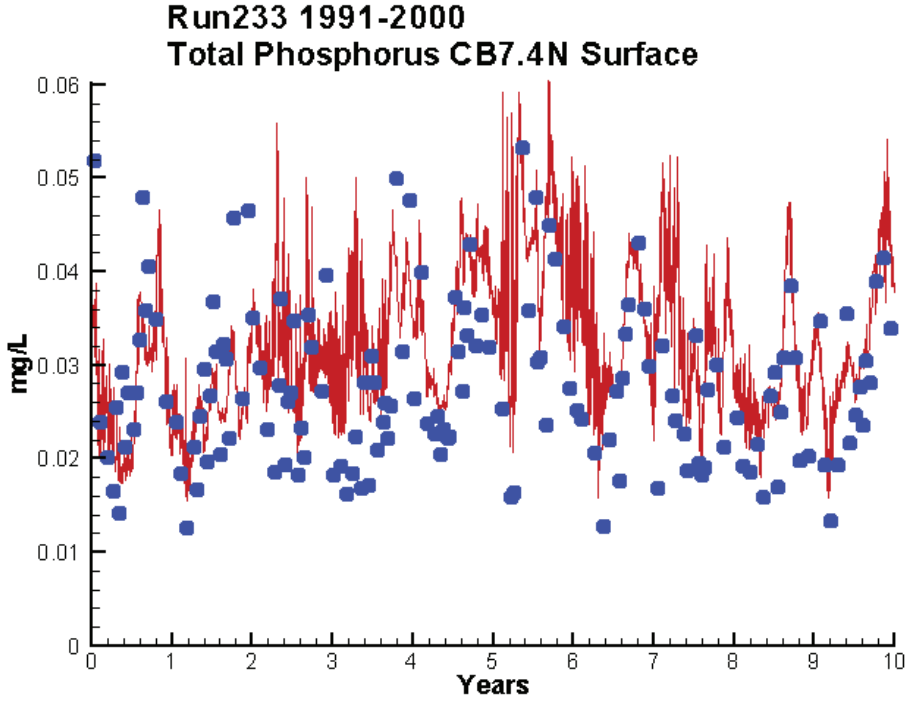

	Mean Difference	Absolute Mean Difference
Chl	1.6509	2.2465
DIN	-0.0152	0.0195
KE	0.0822	0.3447
DIP	-0.0018	0.0033
TP	0.0042	0.0071
TN	0.0223	0.0503

Station CB7.4N

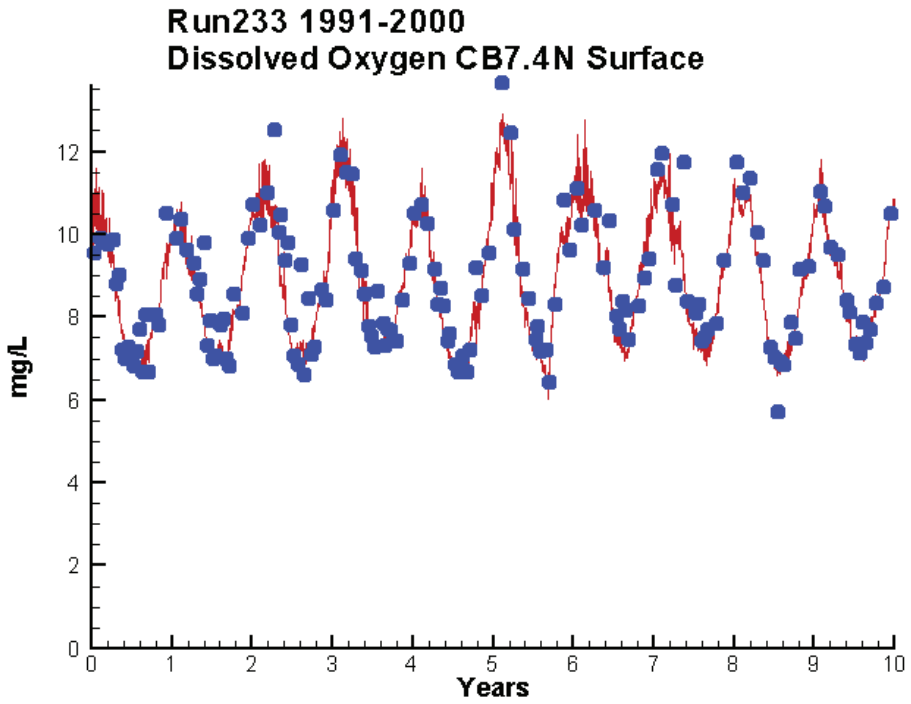

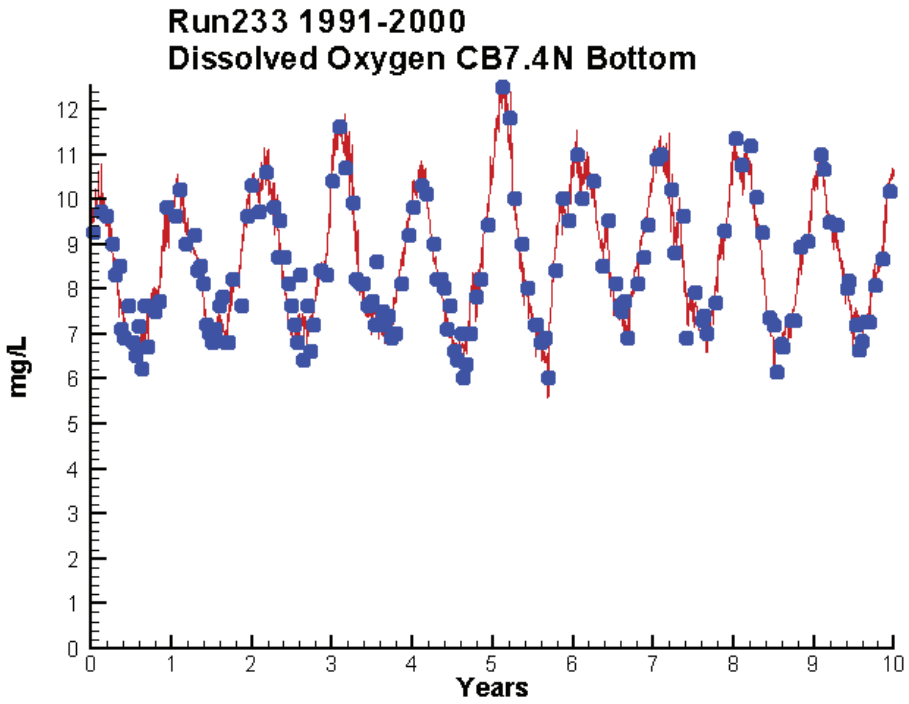

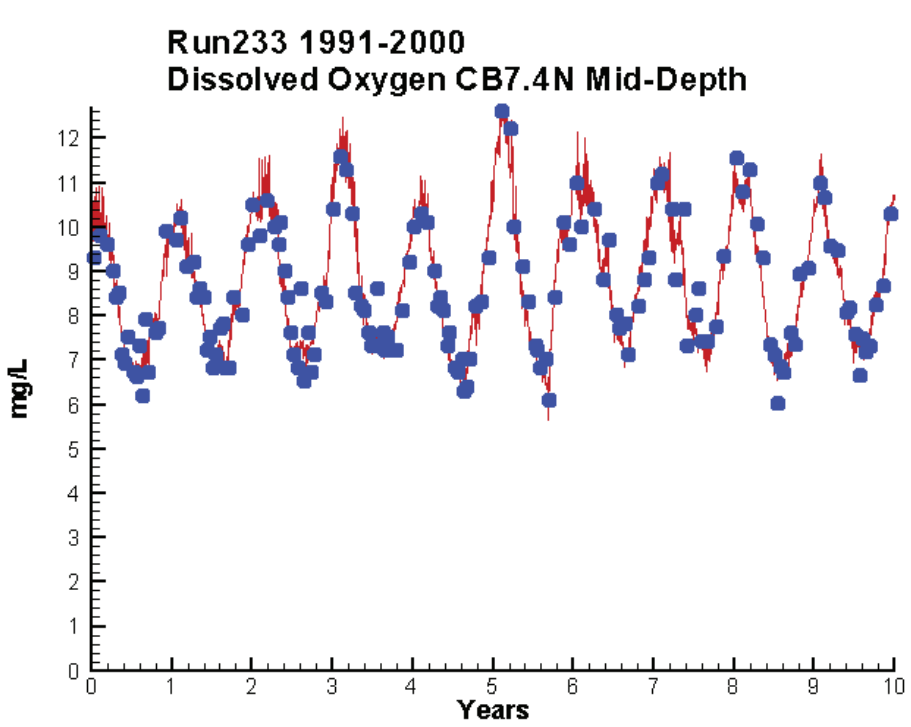

	Mean Difference	Absolute Mean Difference
Top DO	-0.2311	0.5244
Mid DO	0.0022	0.4308
Bot DO	0.0232	0.4028

Station CB7.4N

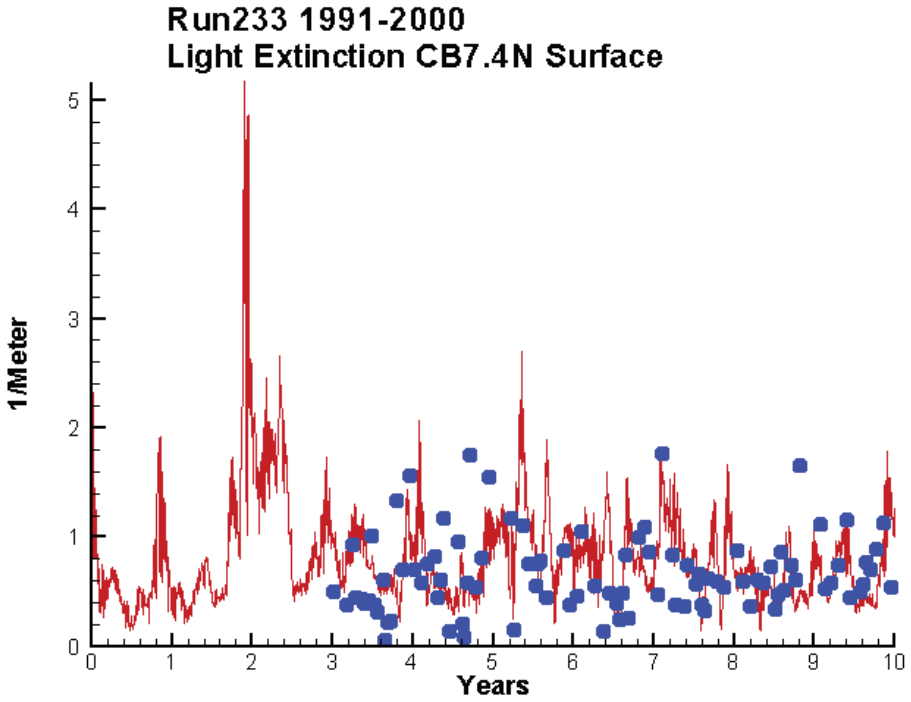

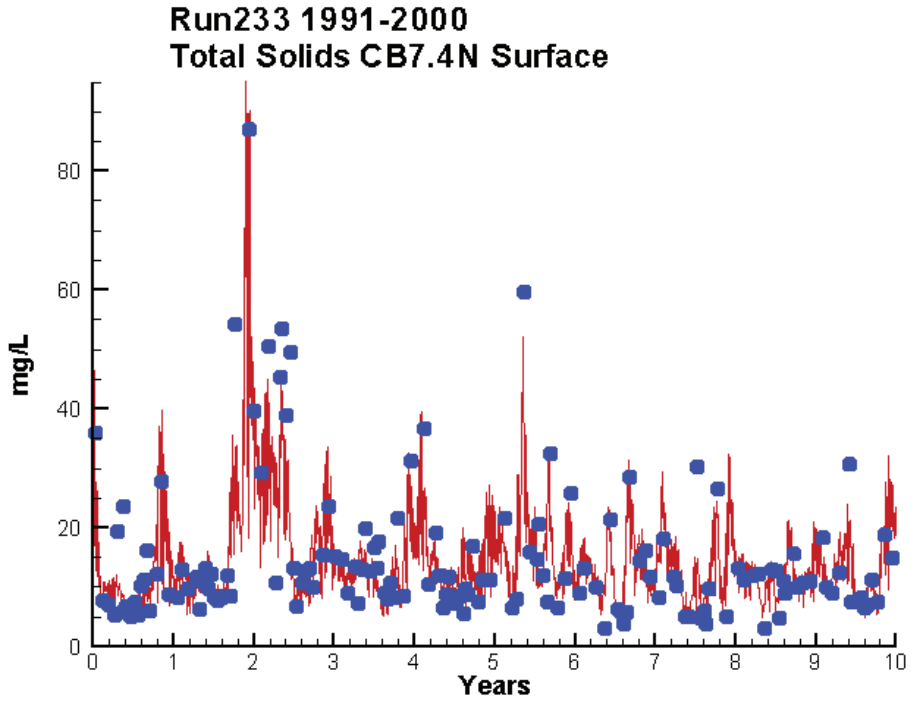

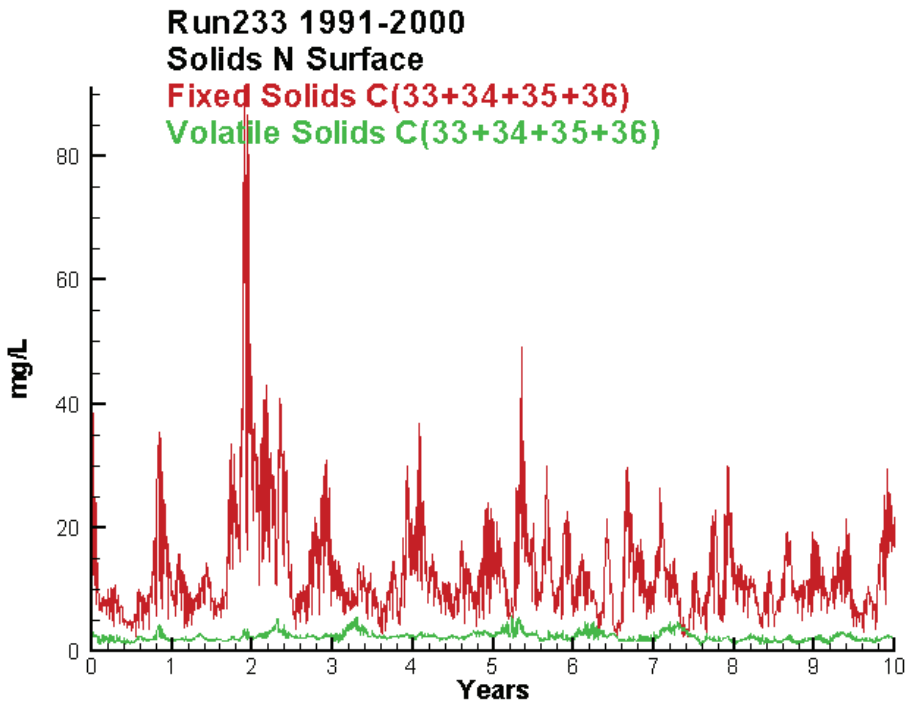

	Mean Difference	Absolute Mean Difference
KE	0.0822	0.3447
TSS	-0.3147	5.6888

Station CB8.1E

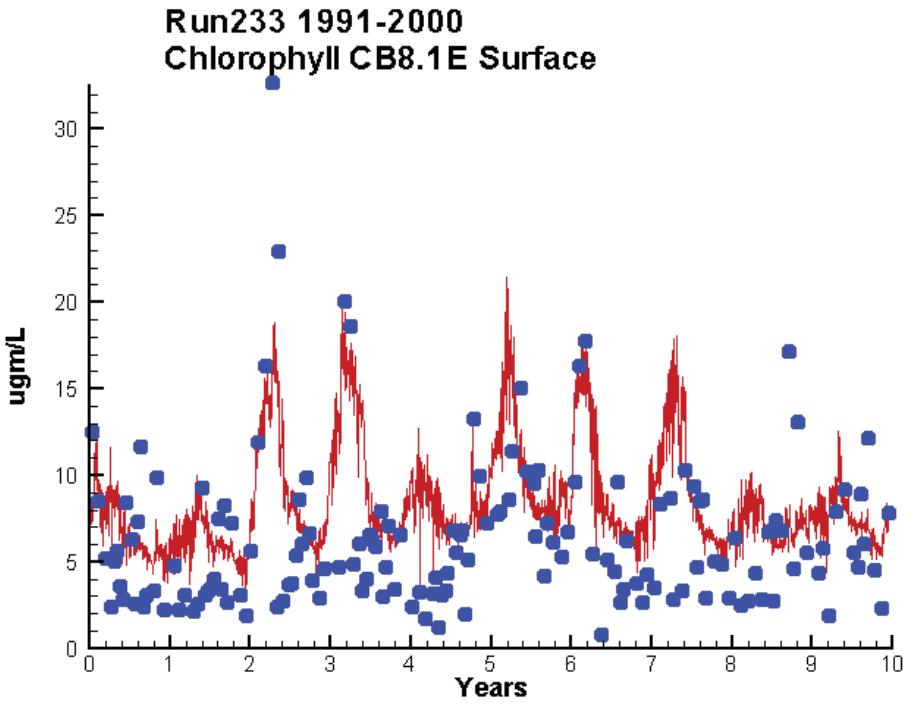

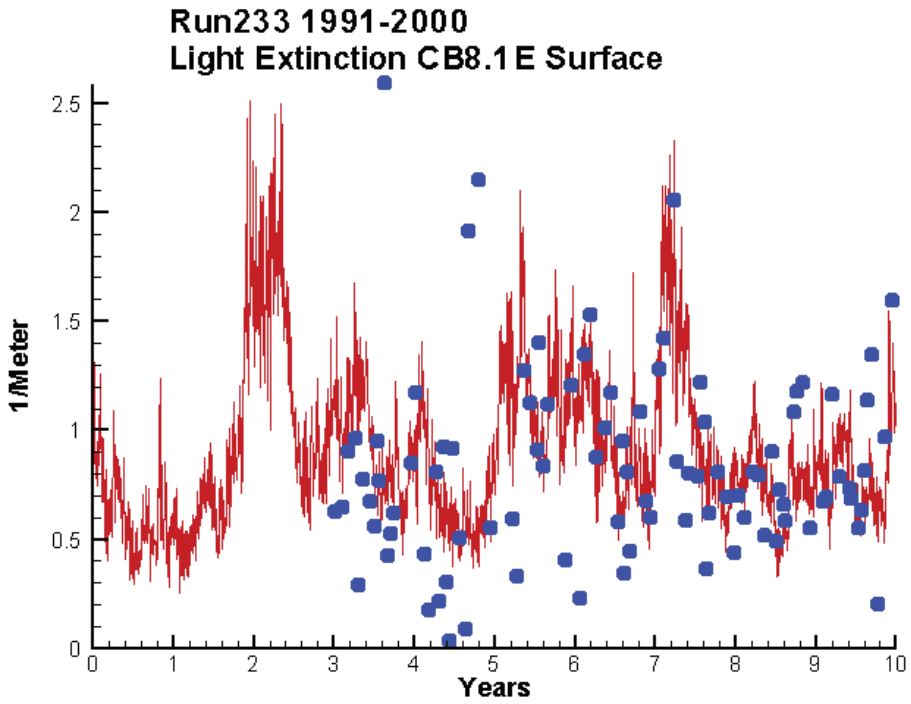

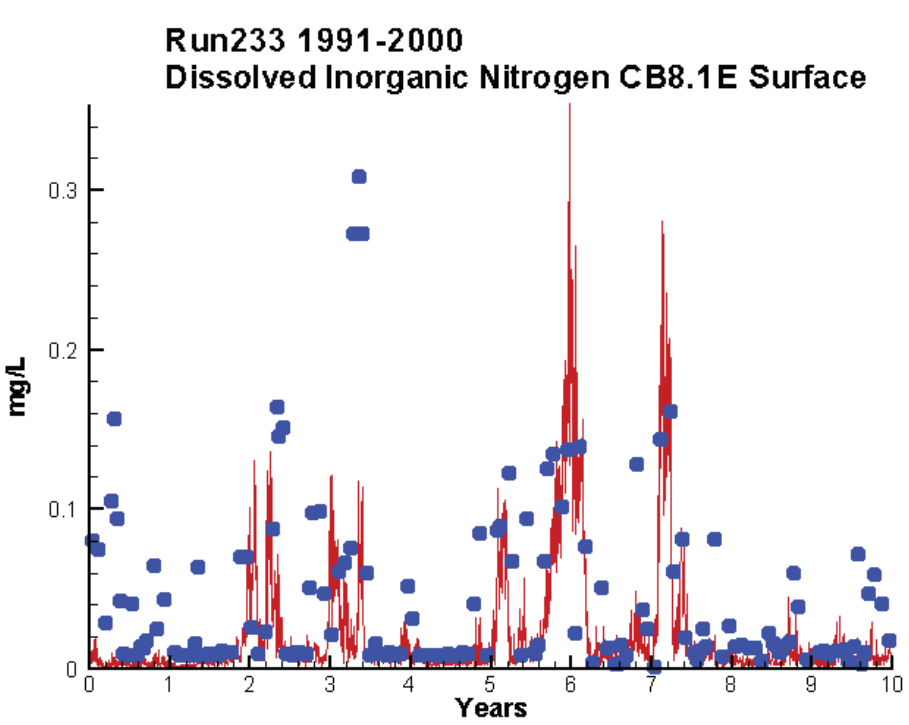

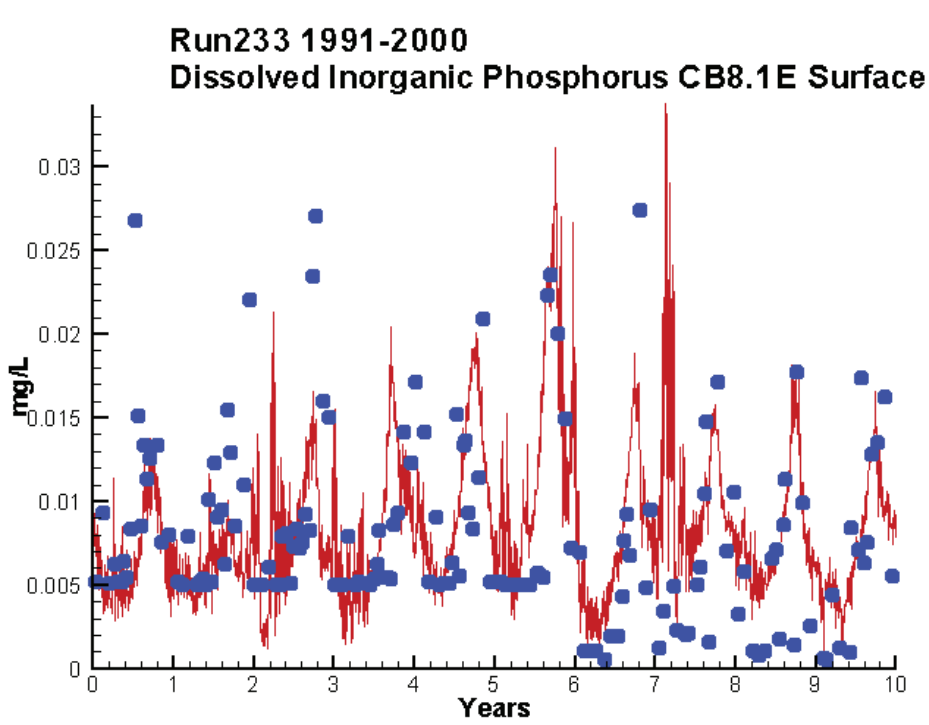

Station CB8.1E

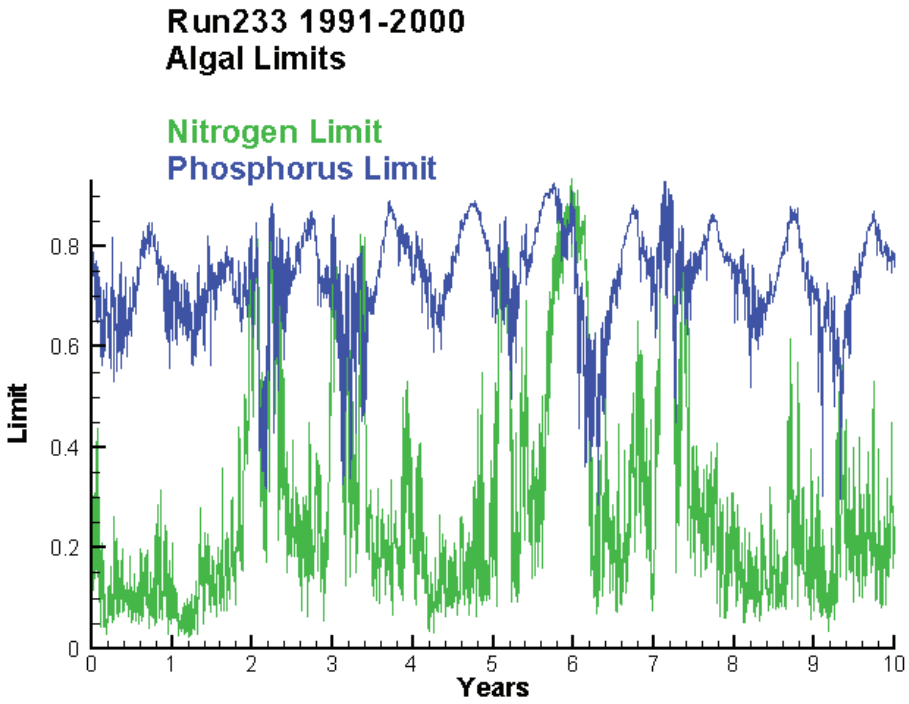

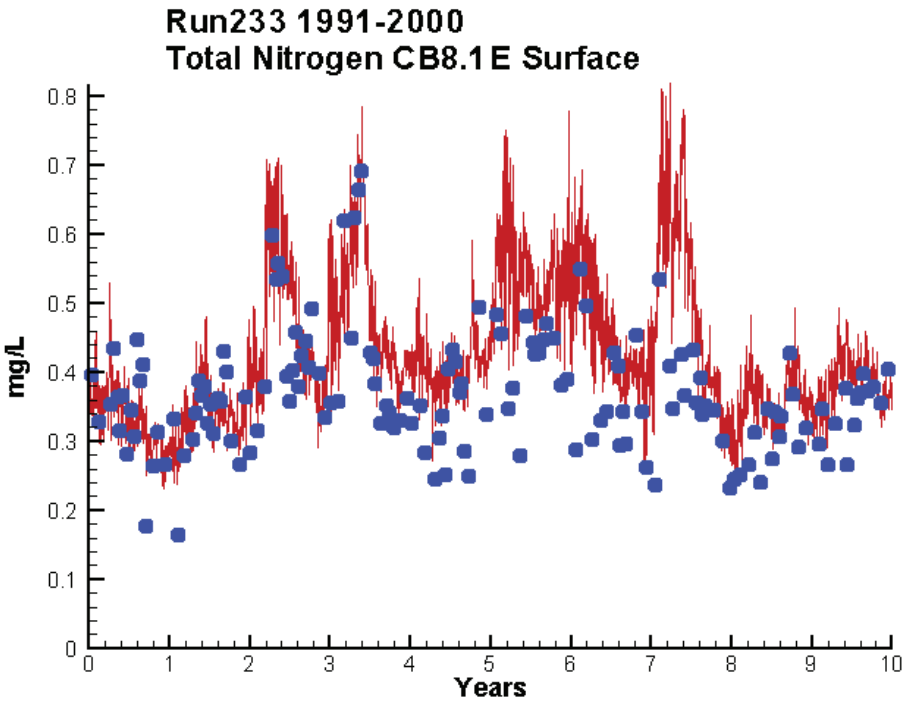

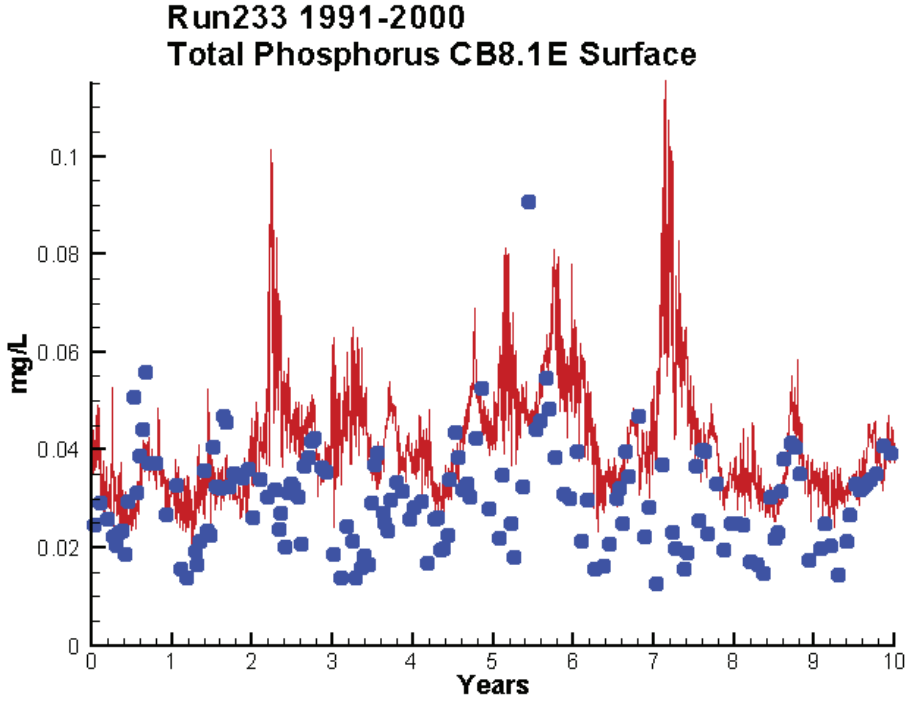

	Mean Difference	Absolute Mean Difference
Chl	1.8603	3.4190
DIN	-0.0228	0.0299
KE	0.0213	0.3158
DIP	0.0004	0.0039
TP	0.0104	0.0130
TN	0.0561	0.0741

Station CB8.1E

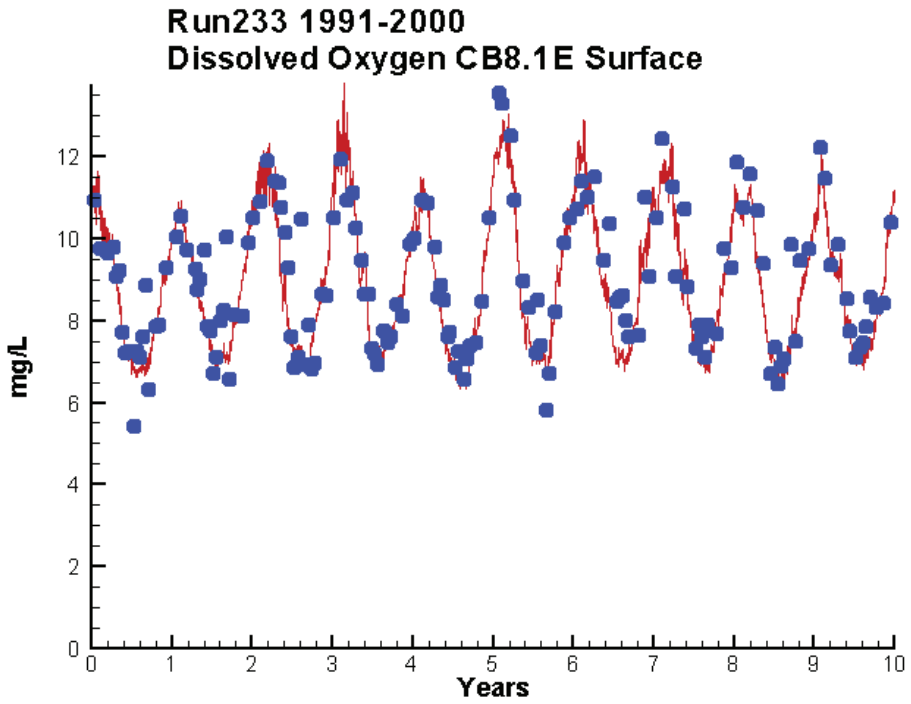

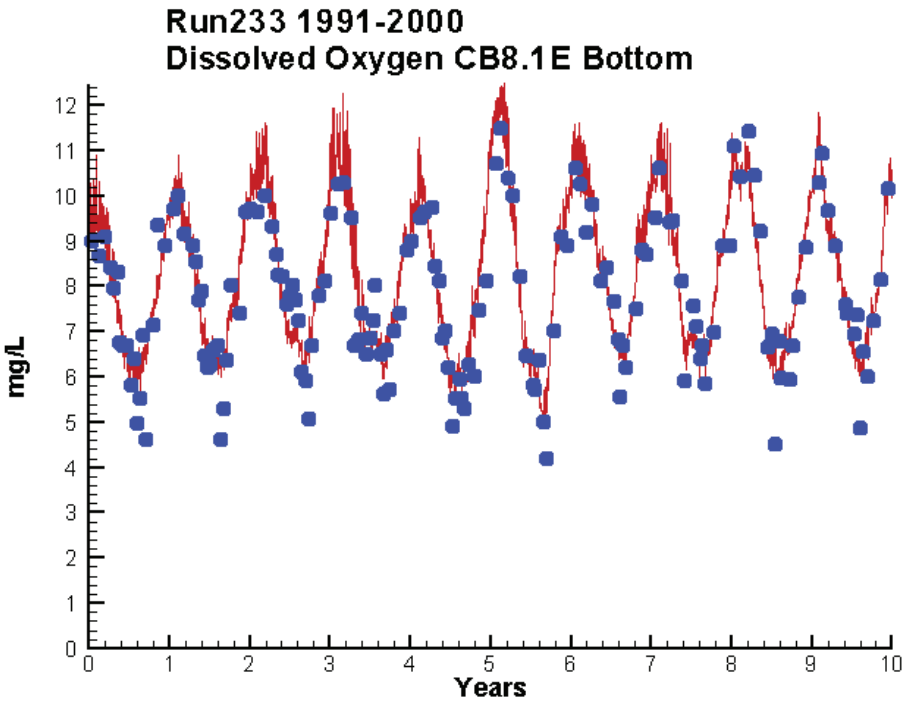

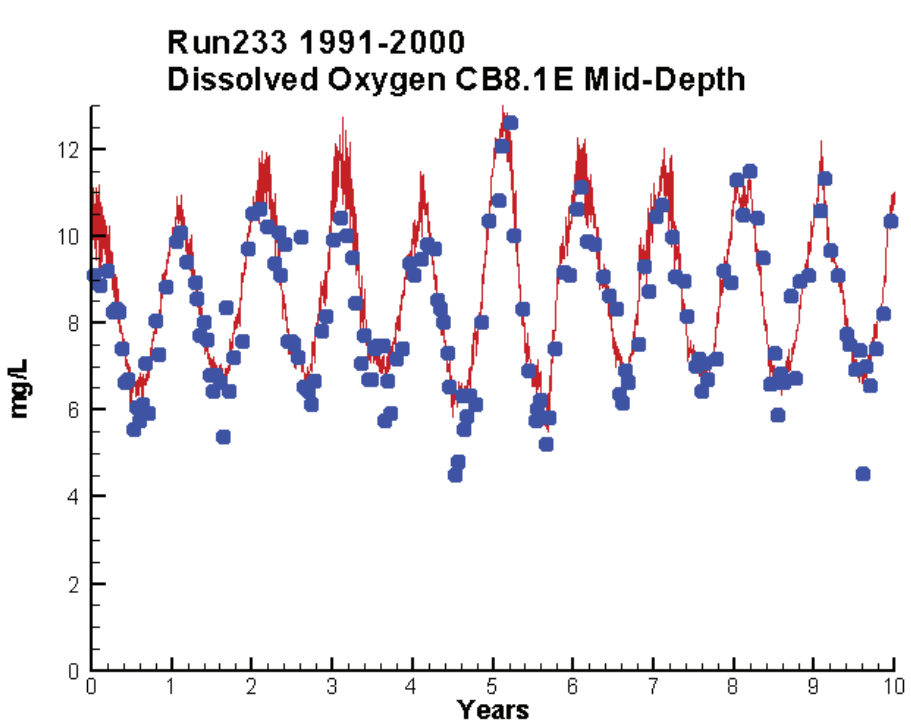

	Mean Difference	Absolute Mean Difference
Top DO	-0.2444	0.6180
Mid DO	0.3602	0.6472
Bot DO	0.2127	0.6105

Station CB8.1E

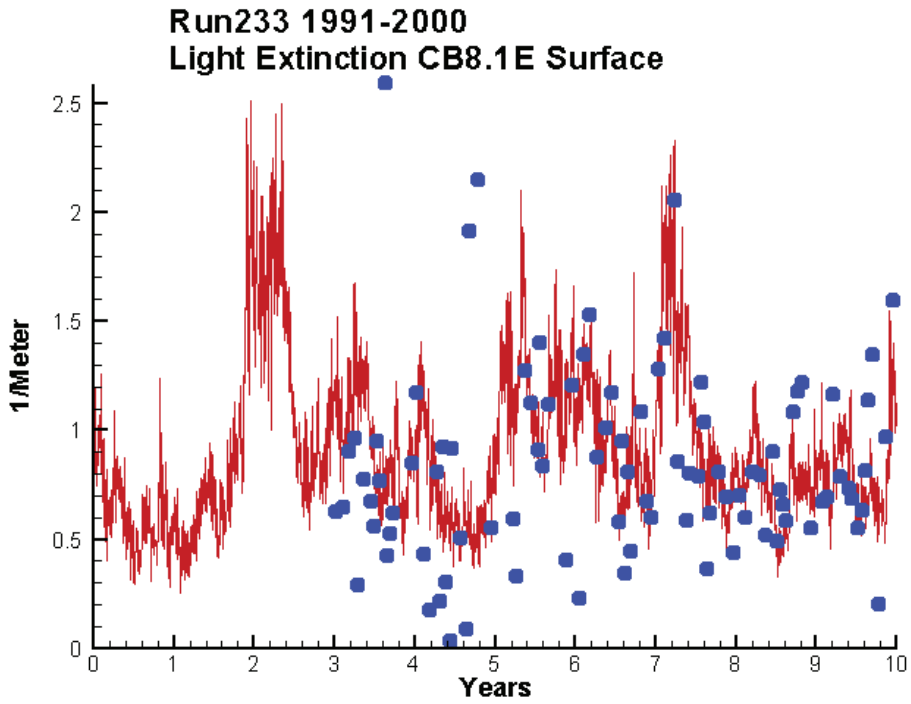

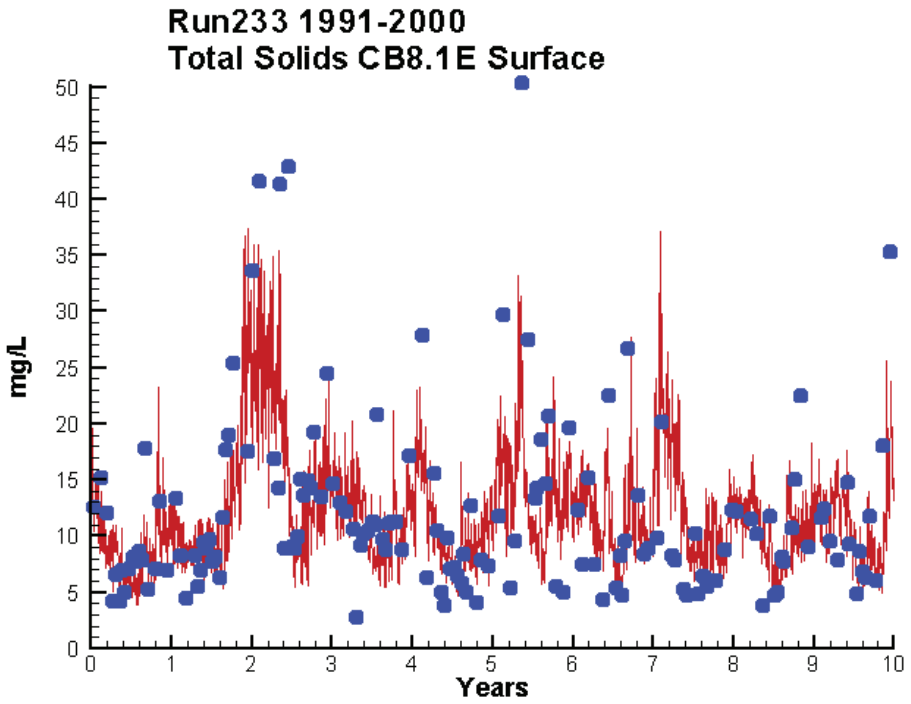

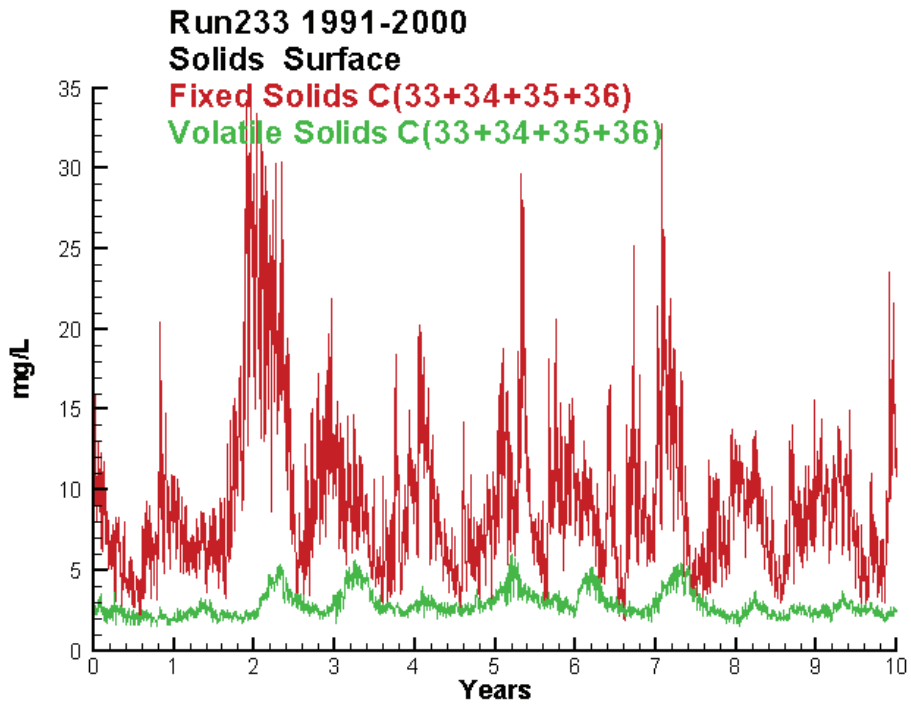

	Mean Difference	Absolute Mean Difference
KE	0.0213	0.3158
TSS	-1.2608	4.2034

Station EE3.2

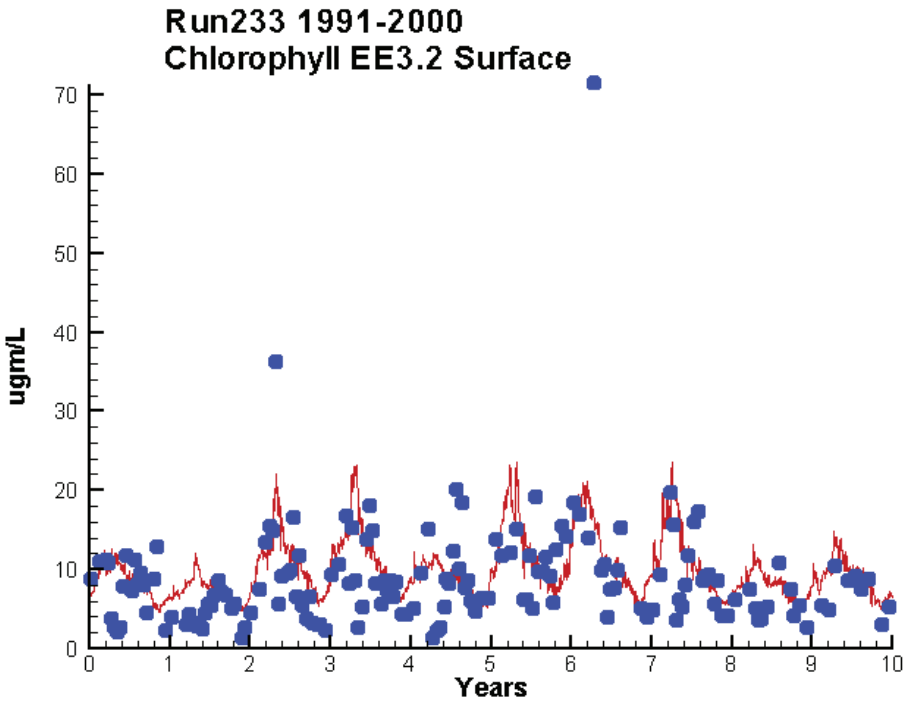

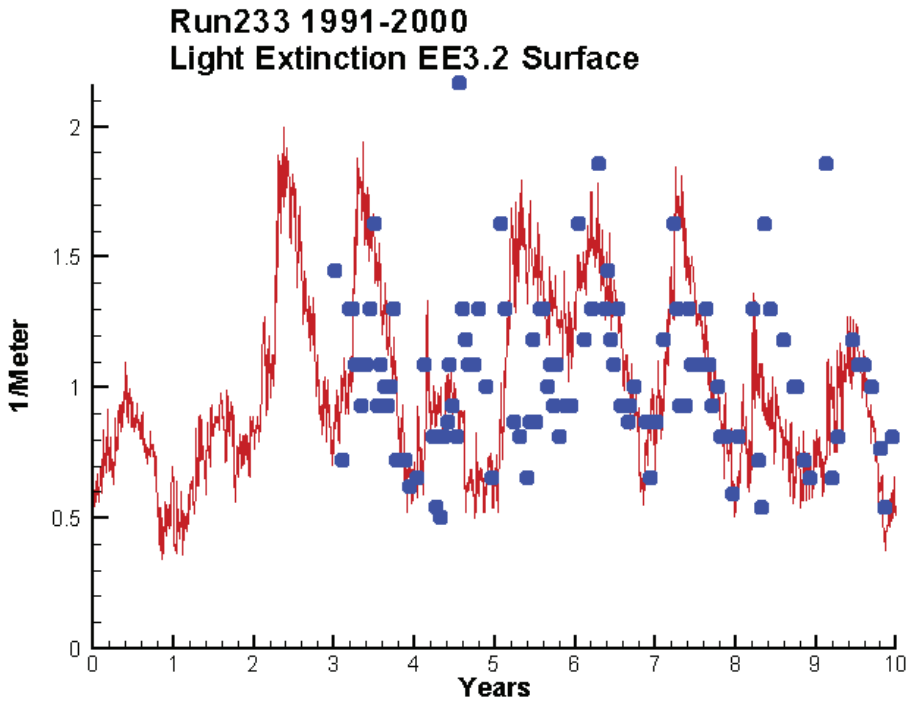

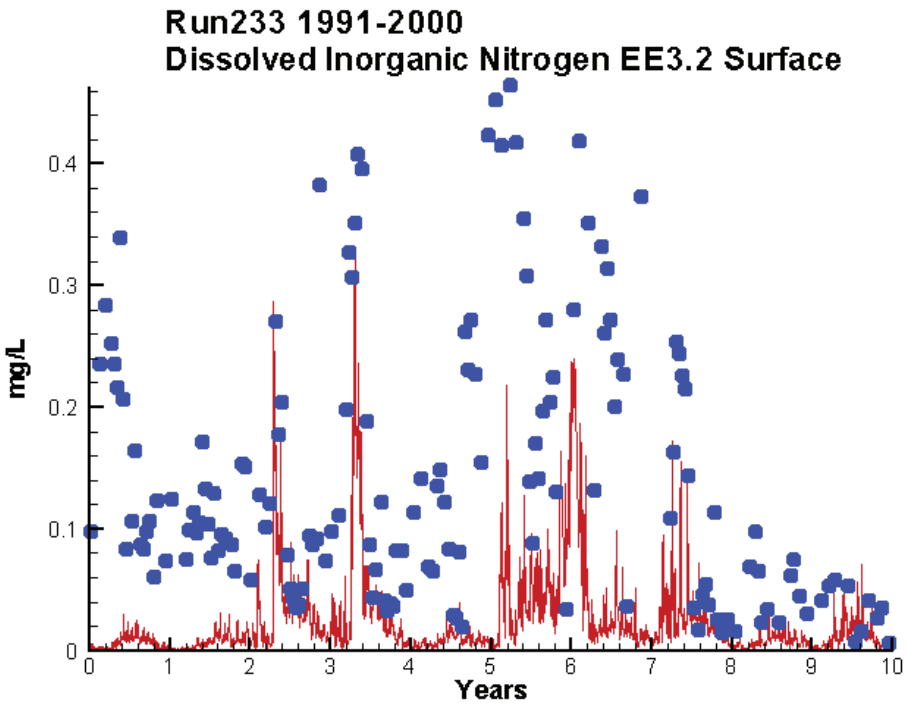

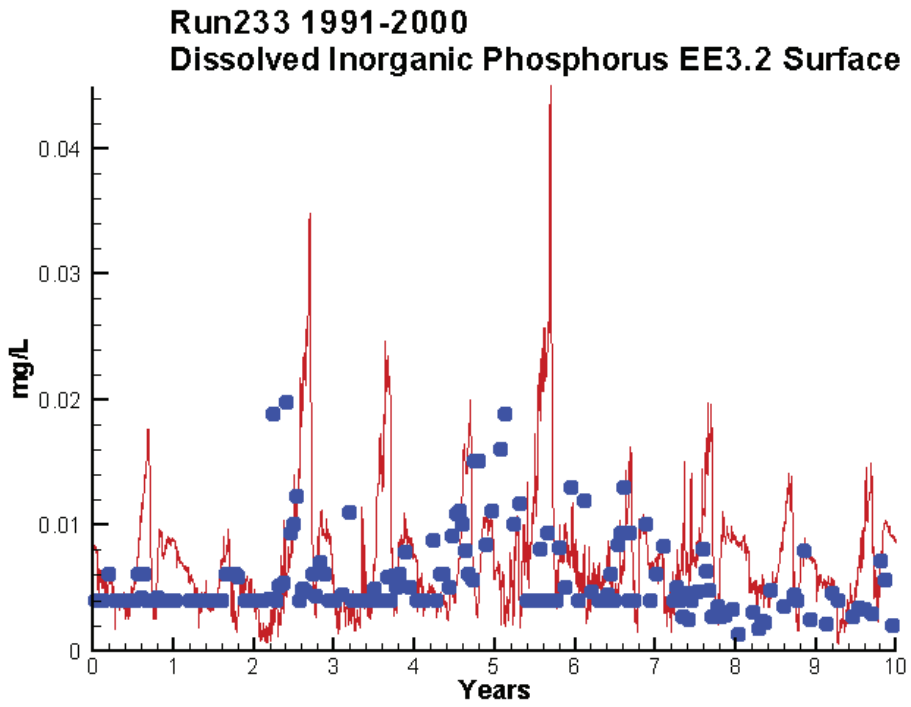

Station EE3.2

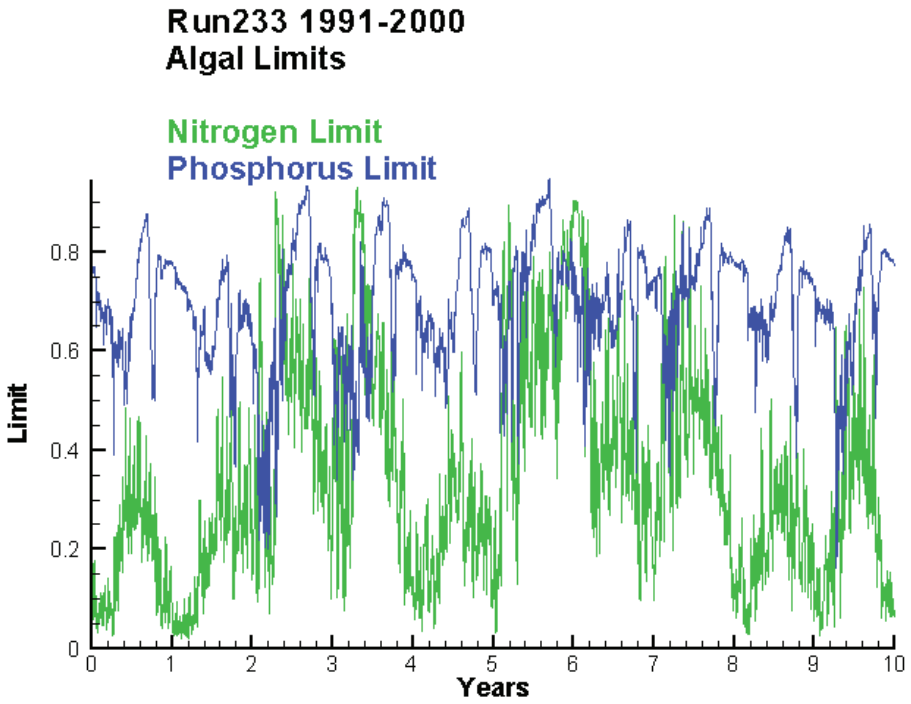

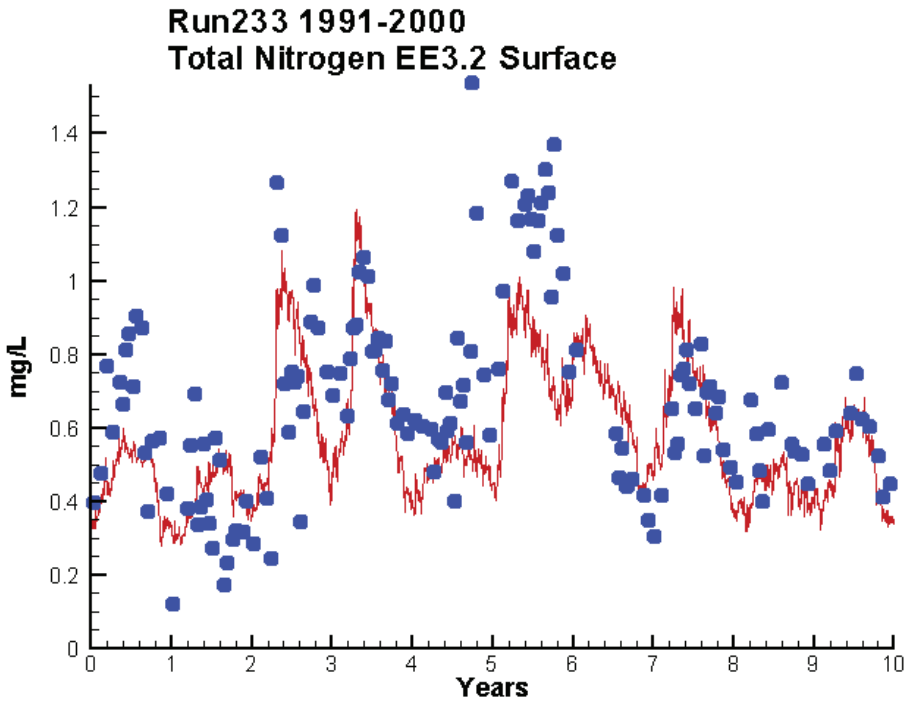

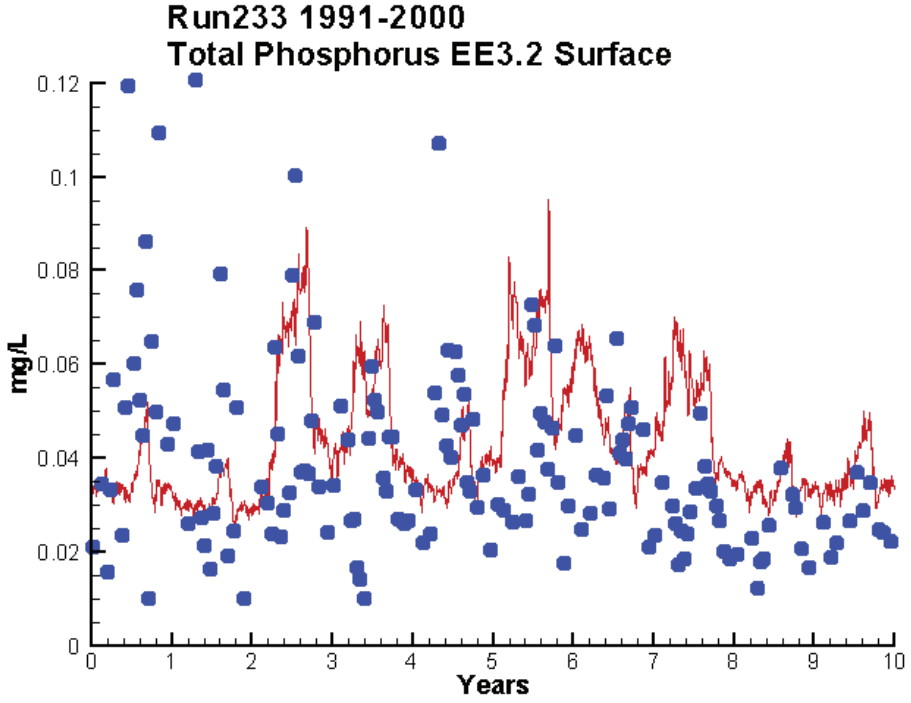

	Mean Difference	Absolute Mean Difference
Chl	1.4134	4.0019
DIN	-0.1174	0.1192
KE	0.0406	0.2860
DIP	0.0022	0.0044
TP	0.0065	0.0193
TN	-0.0764	0.1728

Station EE3.2

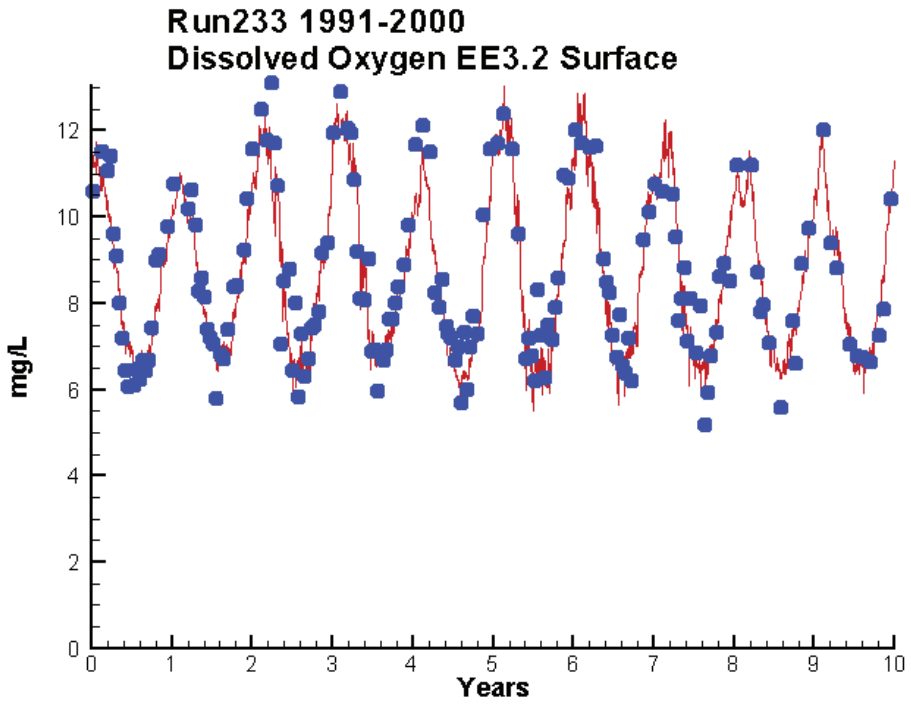

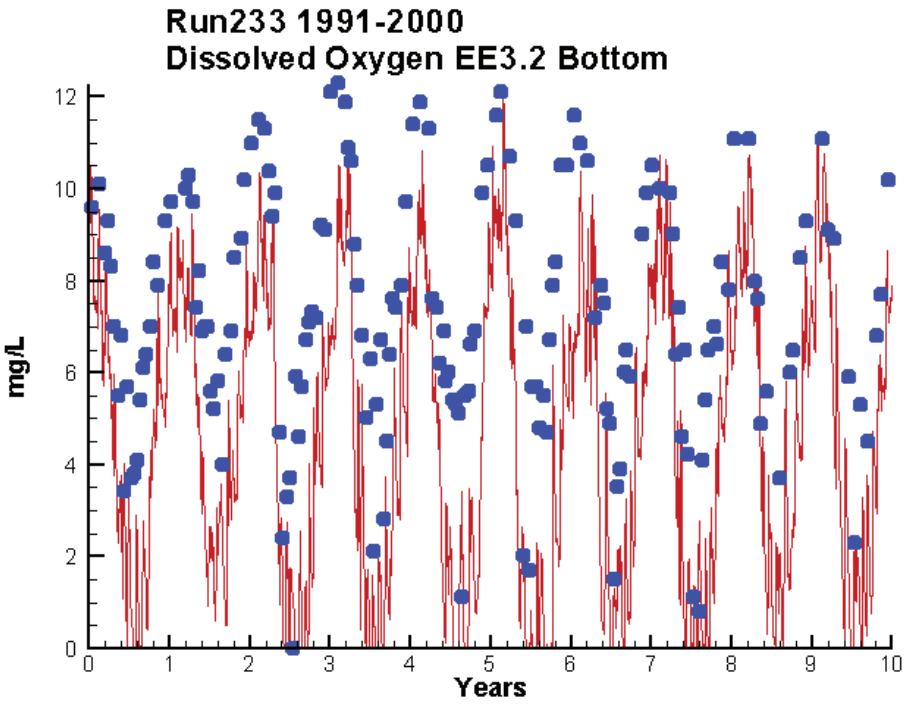

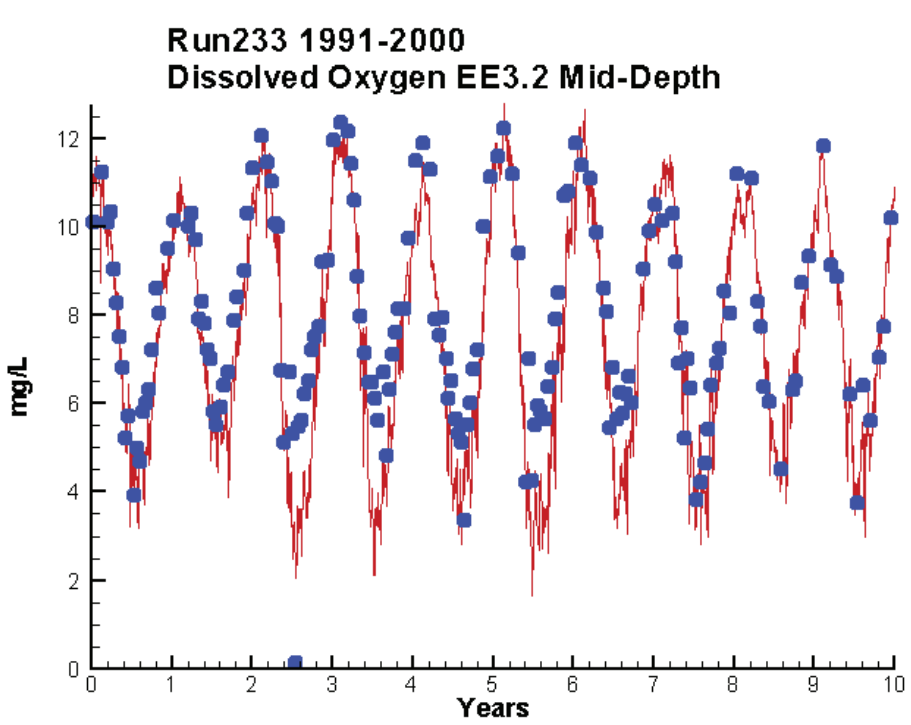

	Mean Difference	Absolute Mean Difference
Top DO	-0.1618	0.5556
Mid DO	-0.8256	1.0530
Bot DO	-3.3713	3.4387

Station EE3.2

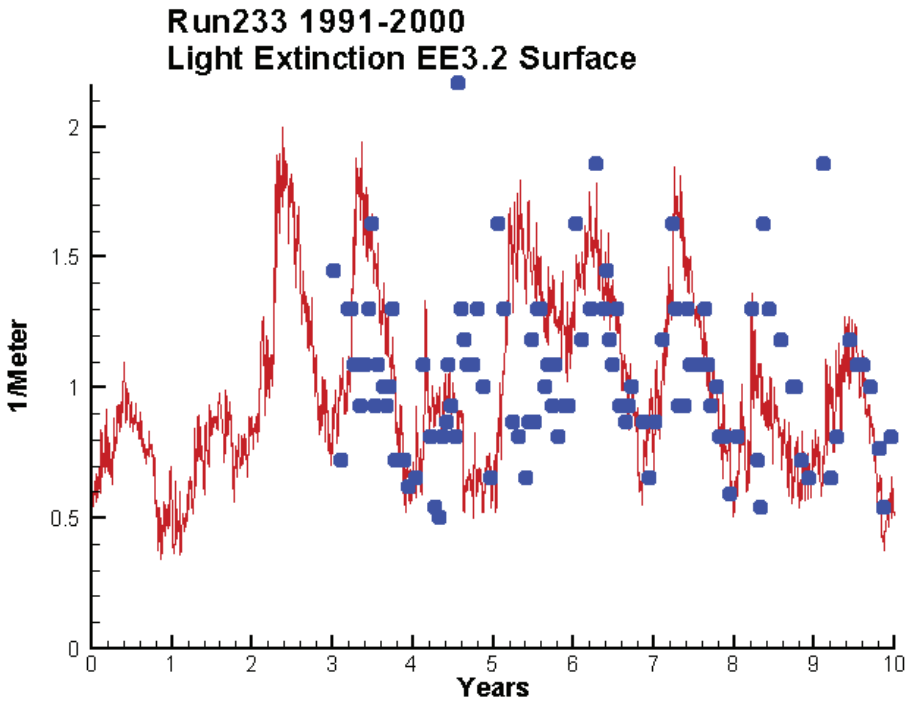

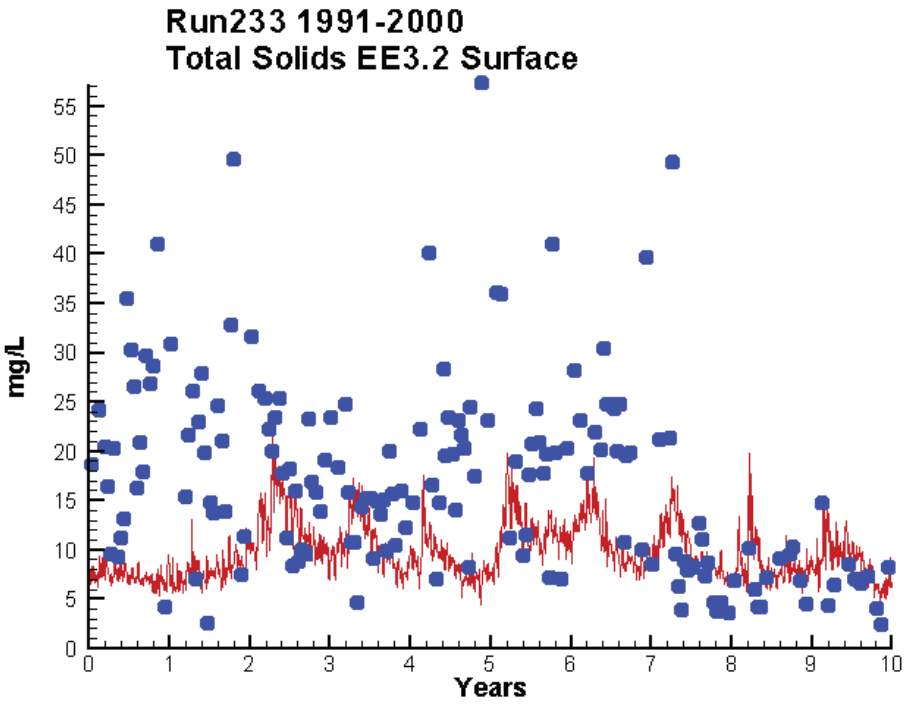

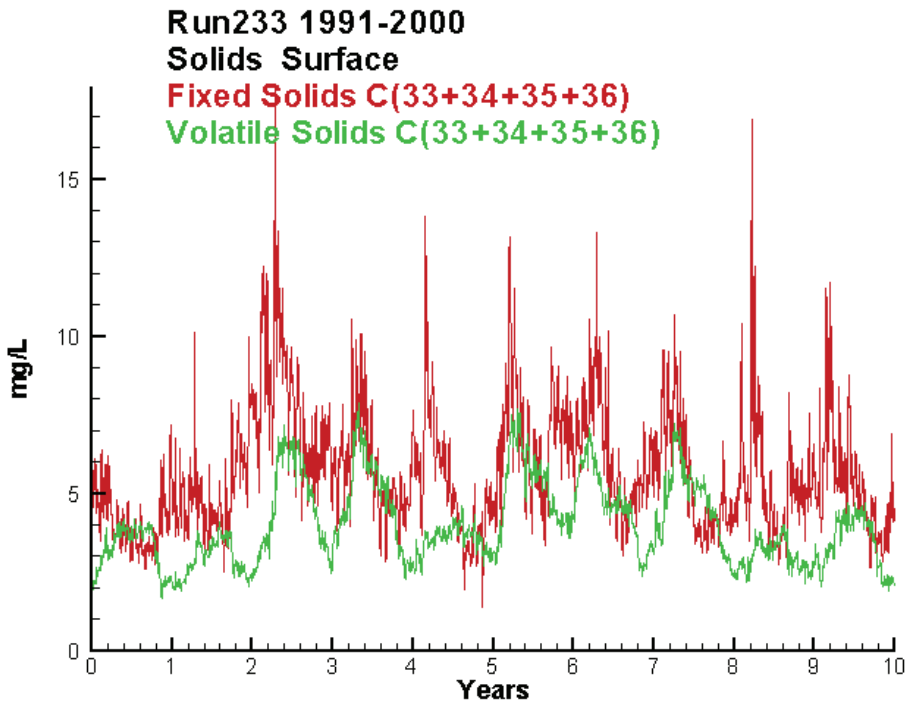

	Mean Difference	Absolute Mean Difference
KE	0.0406	0.2860
TSS	-7.3846	9.0461

Station LE1.3

Run233 1991-2000
Chlorophyll LE1.3 Surface

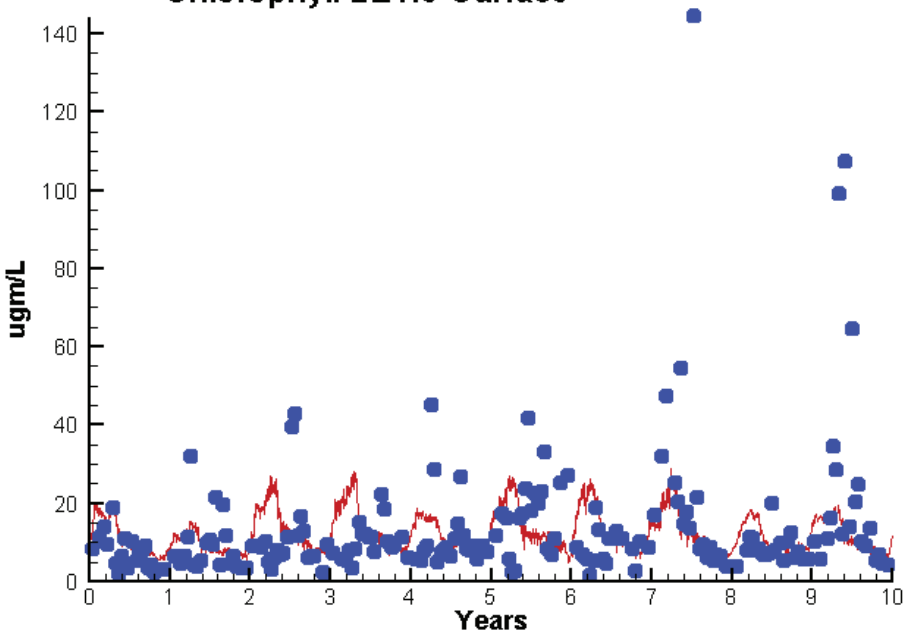

Run233 1991-2000
Light Extinction LE1.3 Surface

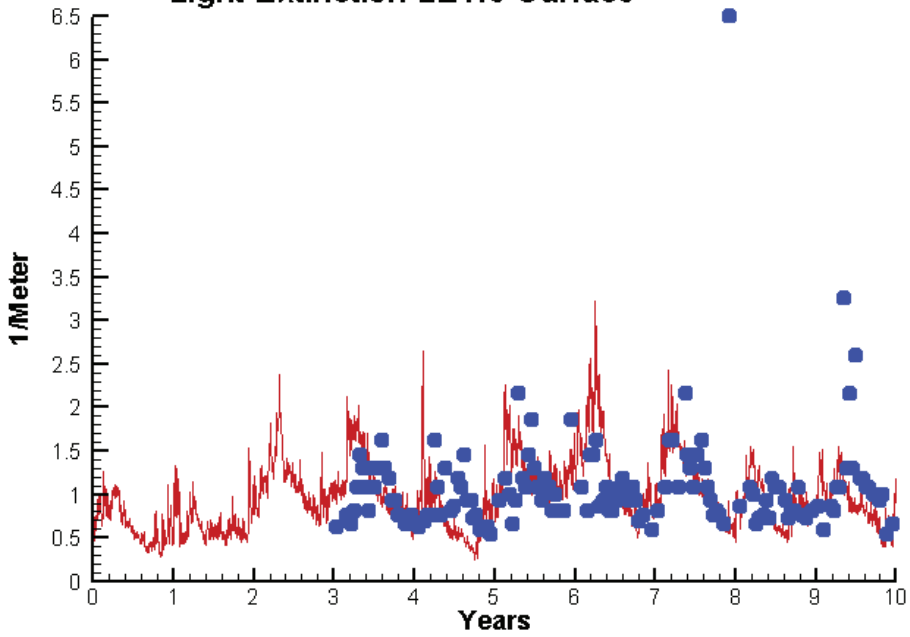

Run233 1991-2000
Dissolved Inorganic Nitrogen LE1.3 Surface

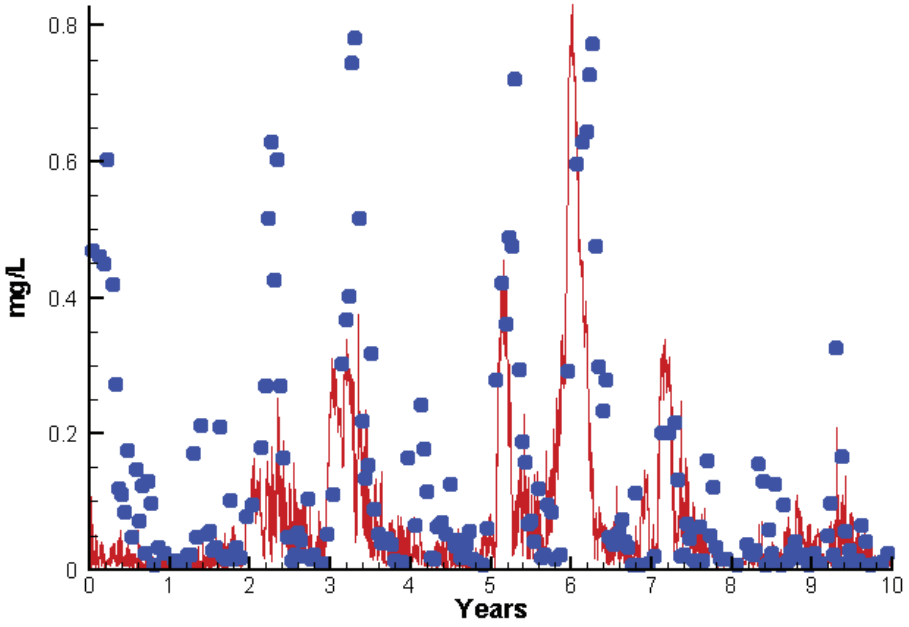

Run233 1991-2000
Dissolved Inorganic Phosphorus LE1.3 Surface

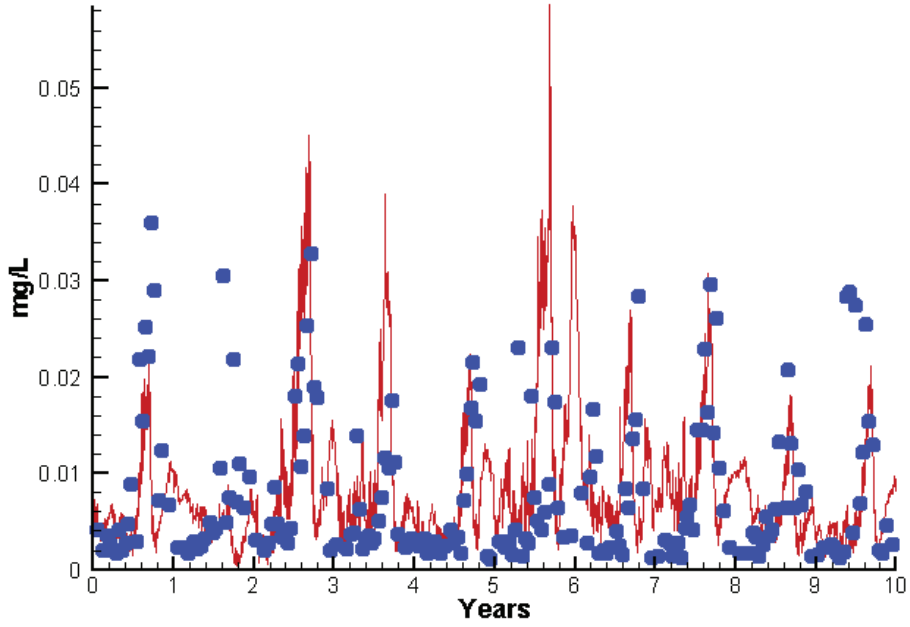

Station LE1.3

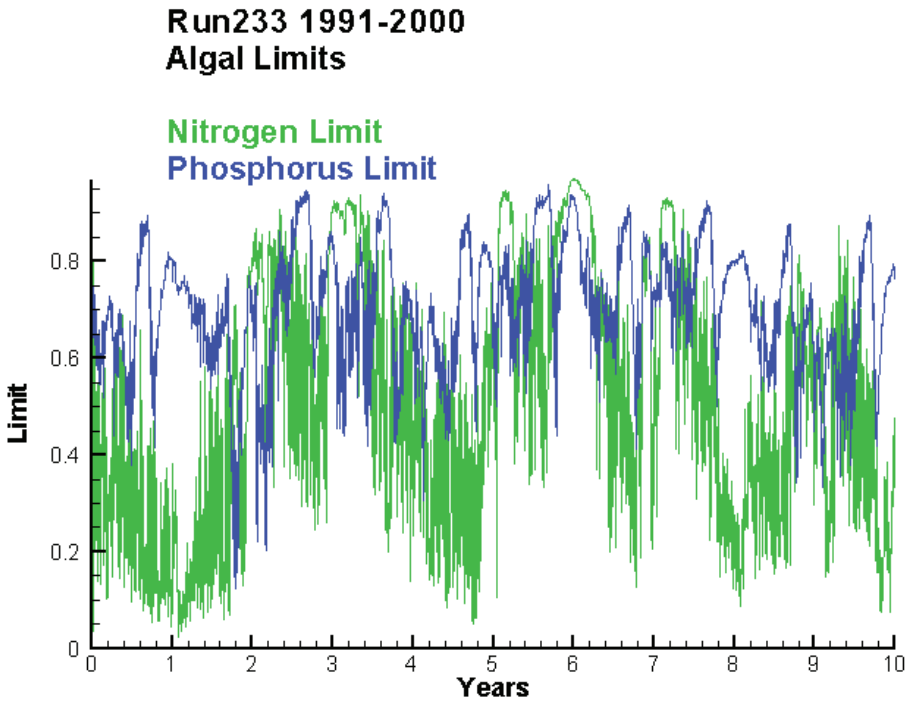

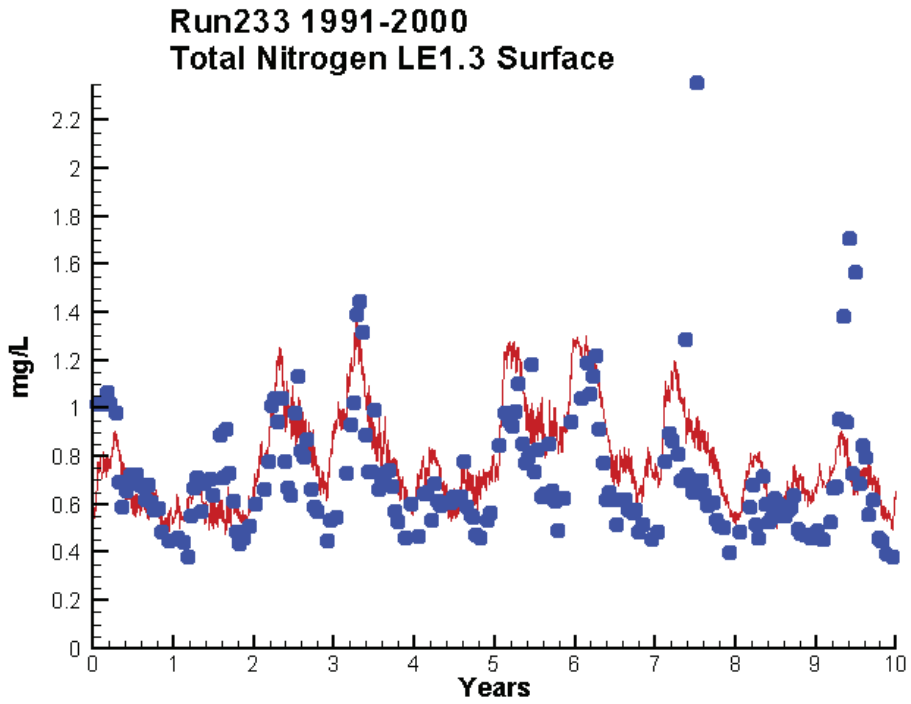

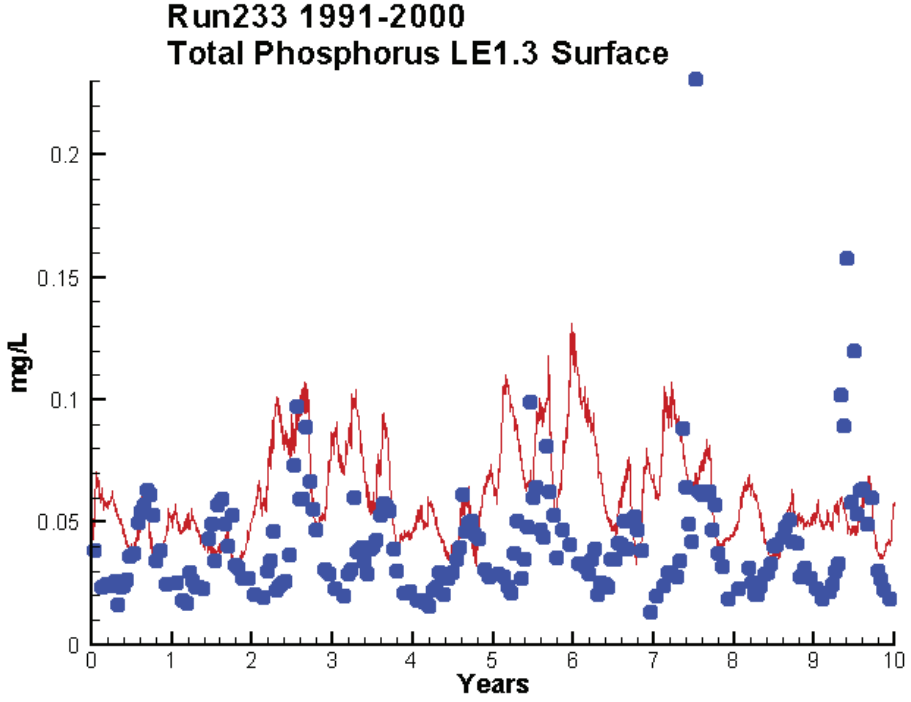

	Mean Difference	Absolute Mean Difference
Chl	-0.9478	8.4340
DIN	-0.0729	0.0986
KE	-0.0512	0.3954
DIP	0.0007	0.0065
TP	0.0202	0.0270
TN	0.0773	0.1688

Station LE1.3

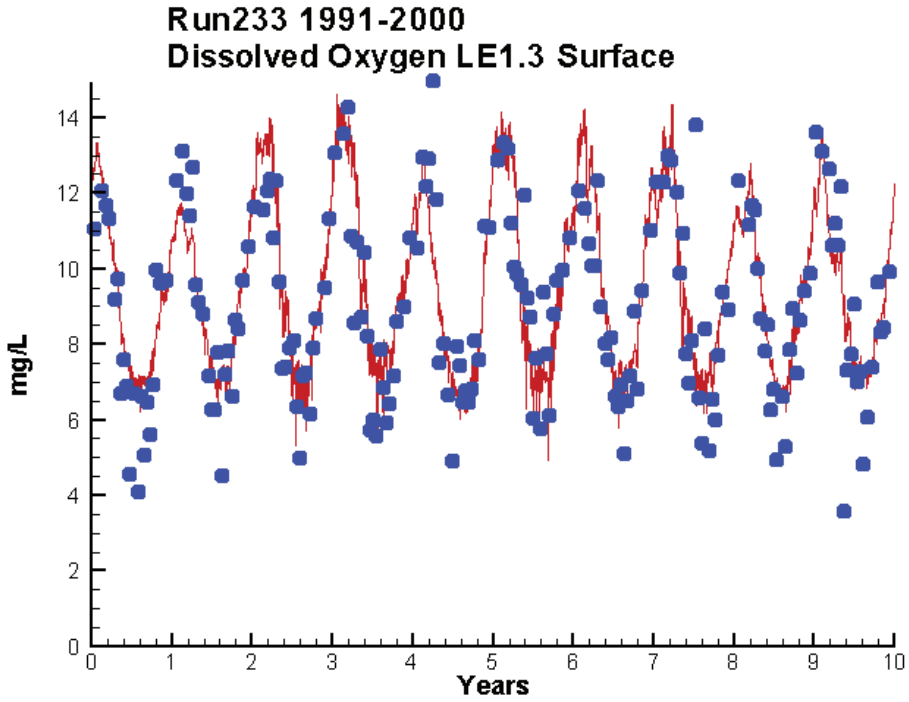

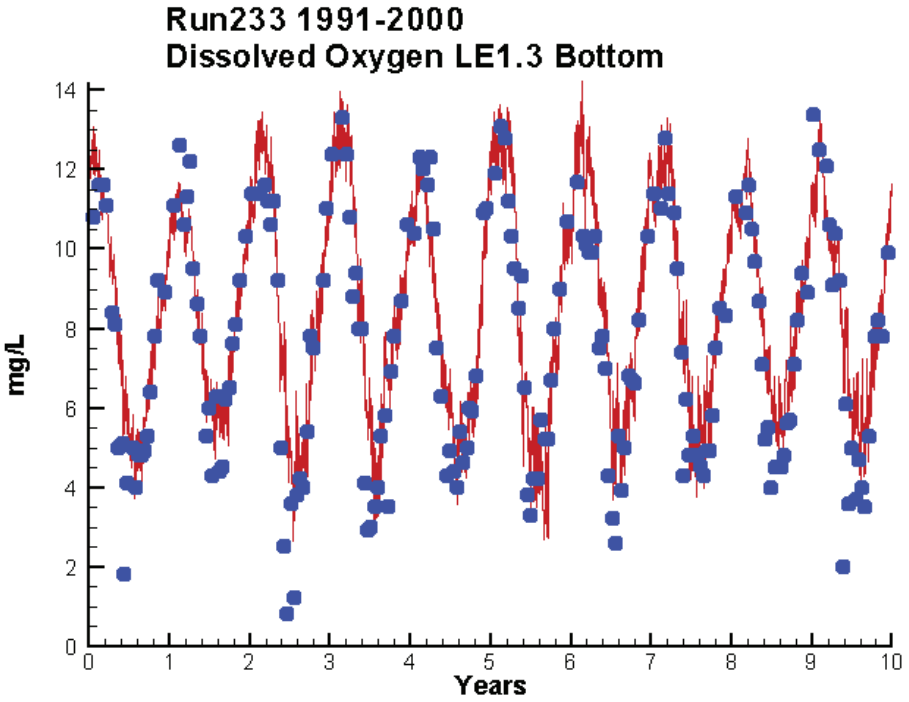

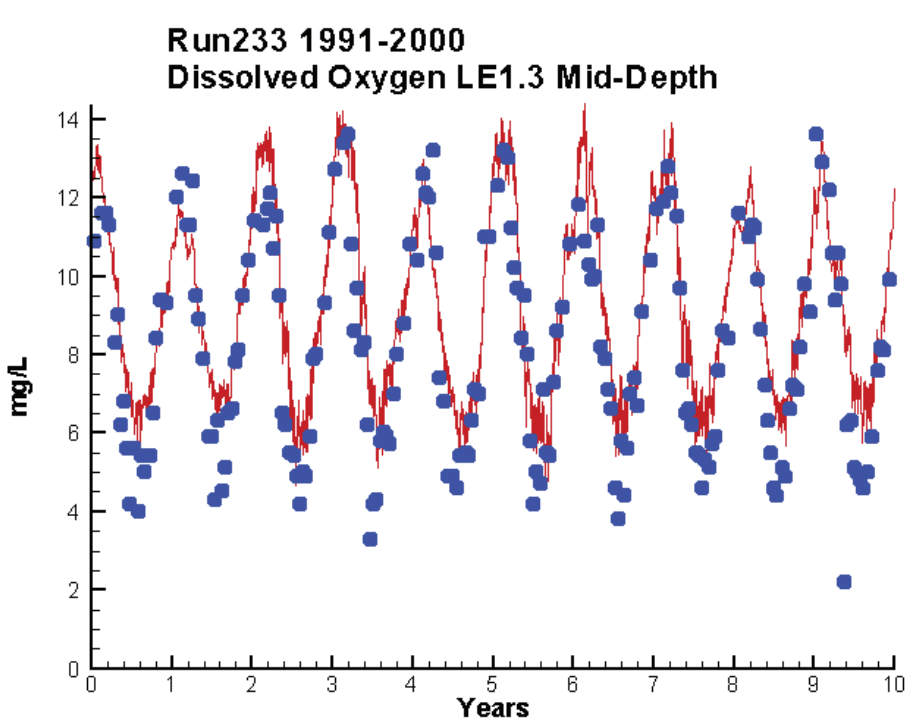

	Mean Difference	Absolute Mean Difference
Top DO	0.2793	1.0107
Mid DO	0.9010	1.1290
Bot DO	0.5826	1.0398

Station LE1.3

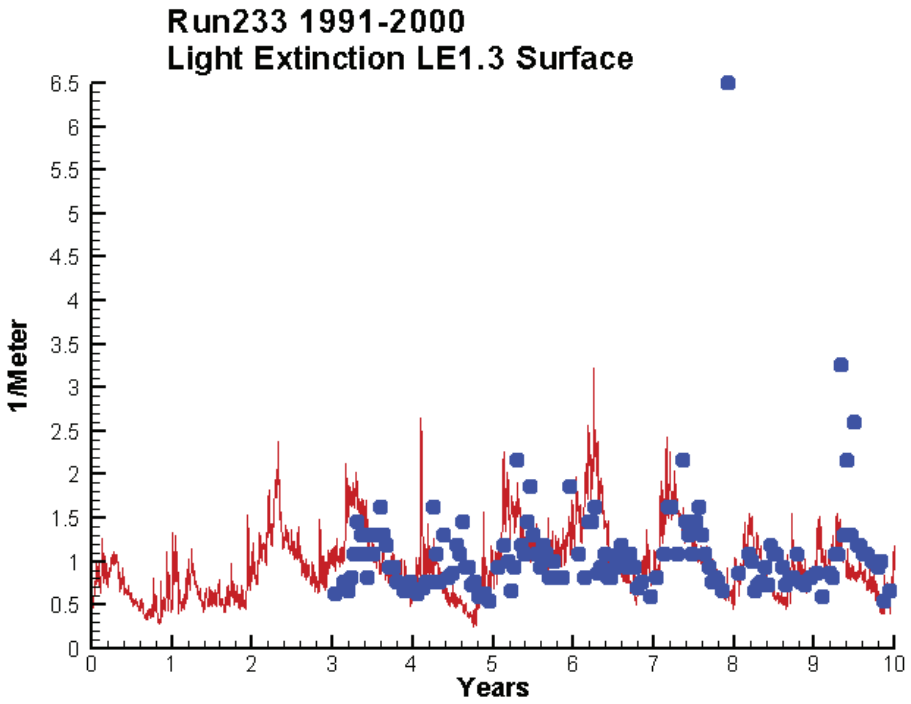

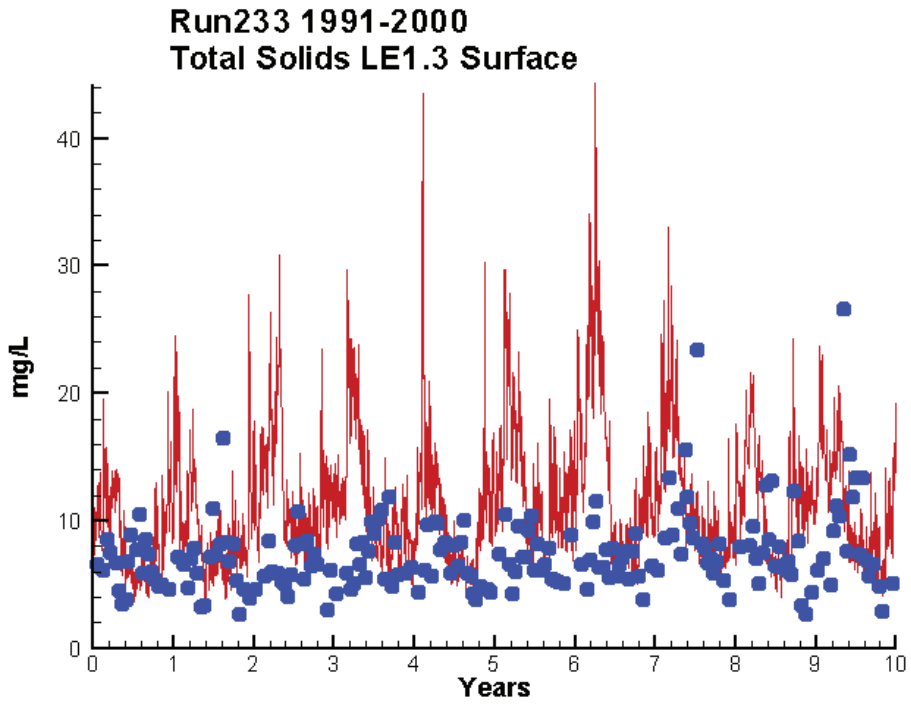

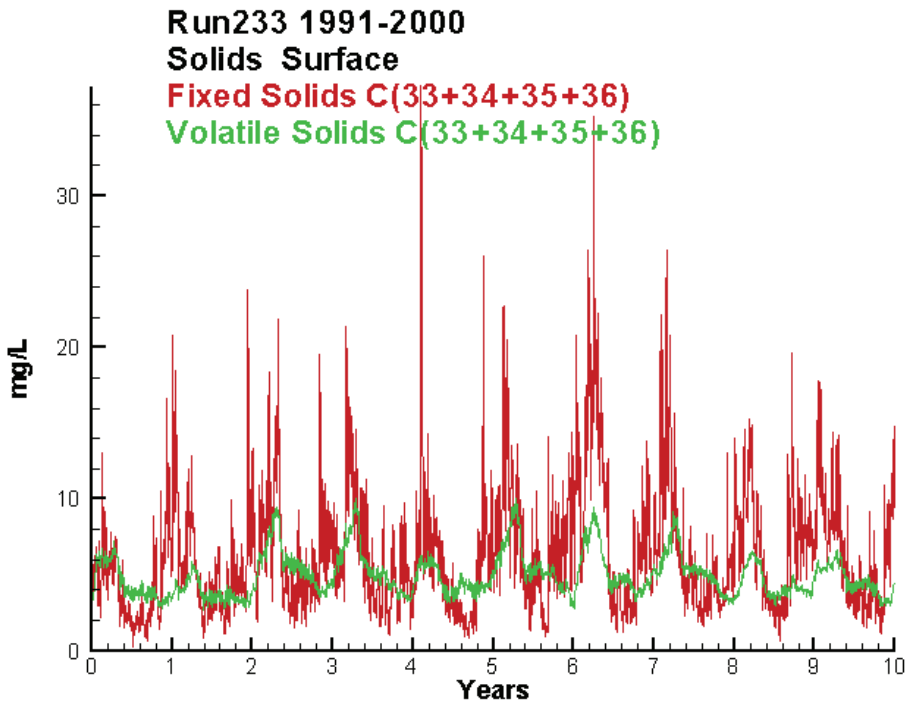

	Mean Difference	Absolute Mean Difference
KE	-0.0512	0.3954
TSS	3.8292	5.2139

Station RET1.1

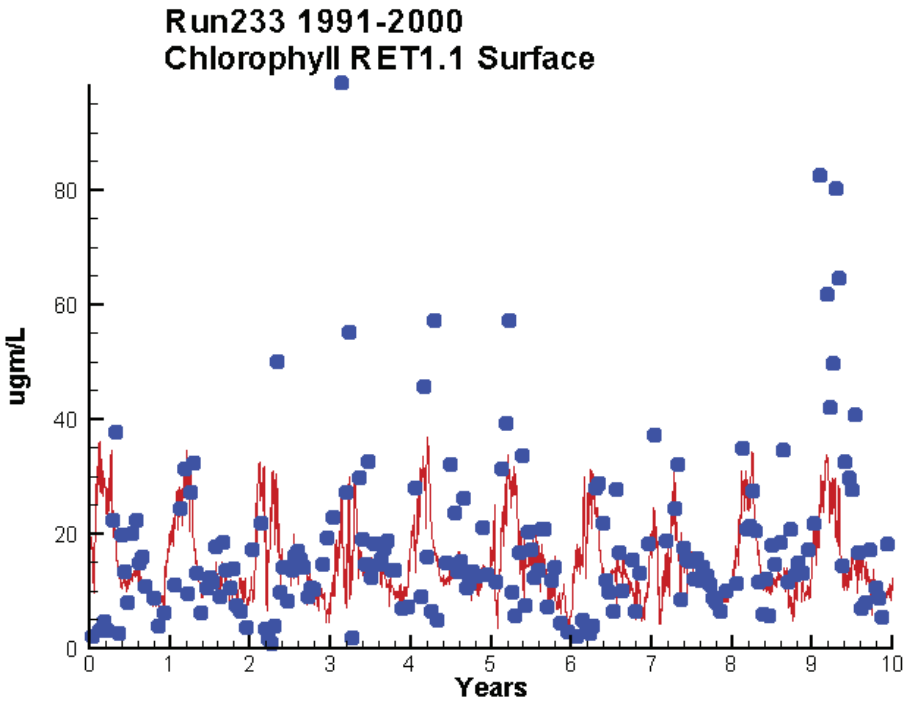

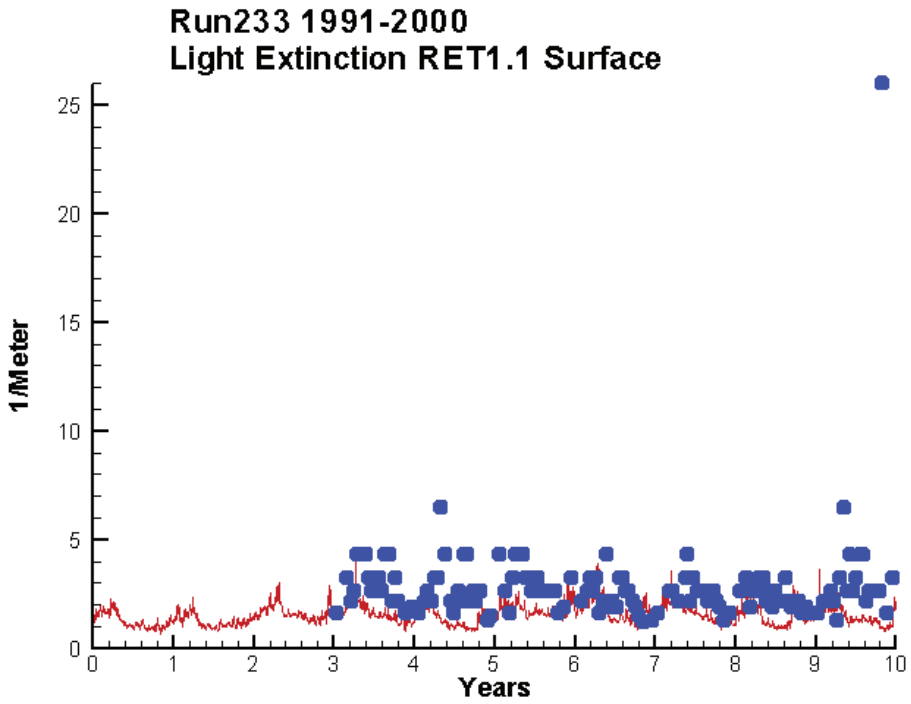

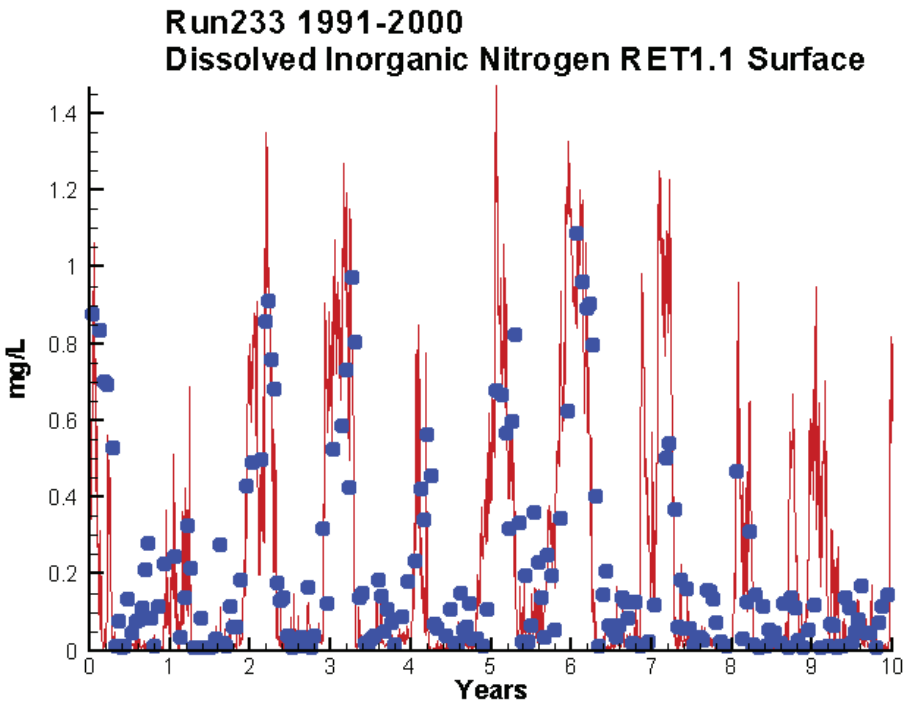

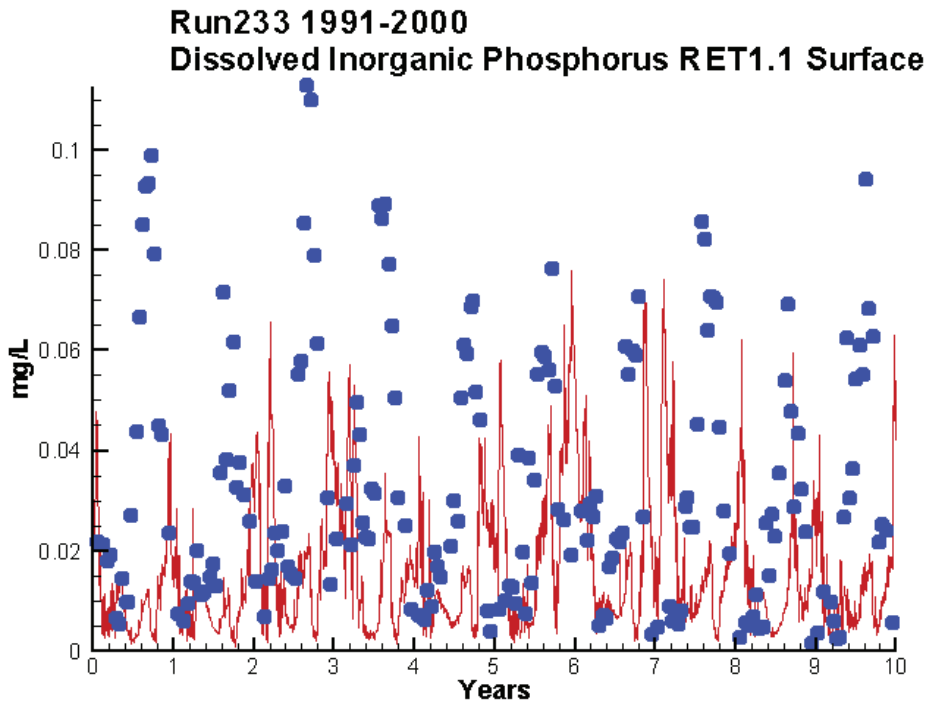

Station RET1.1

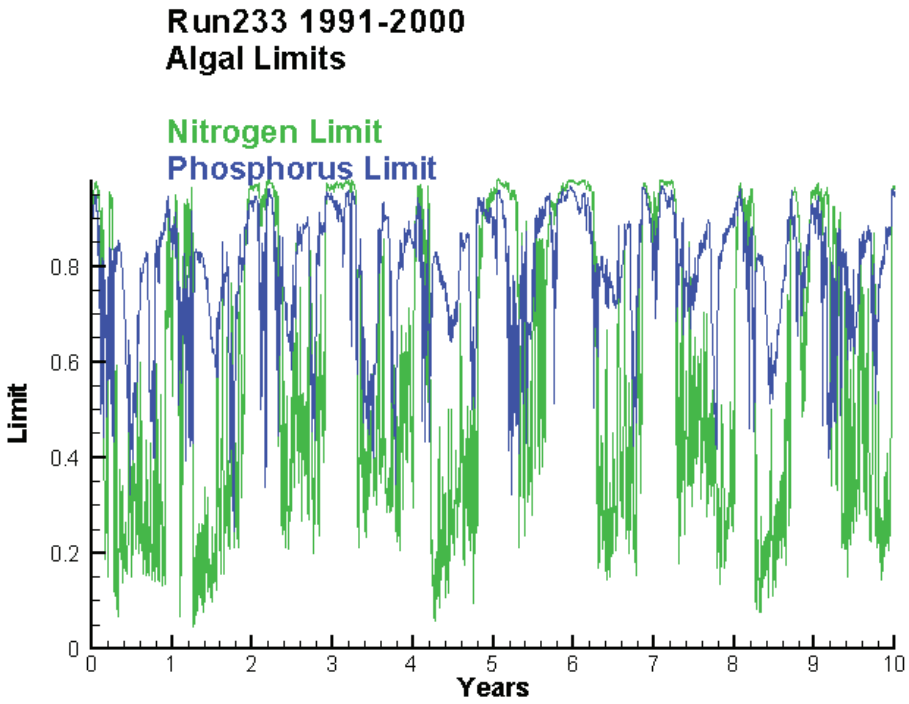

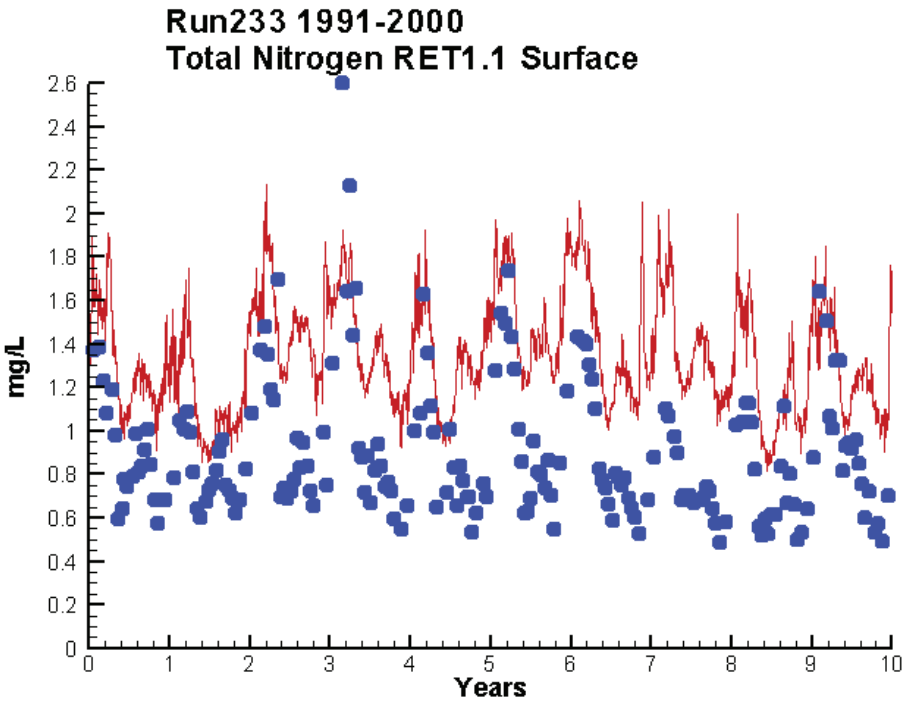

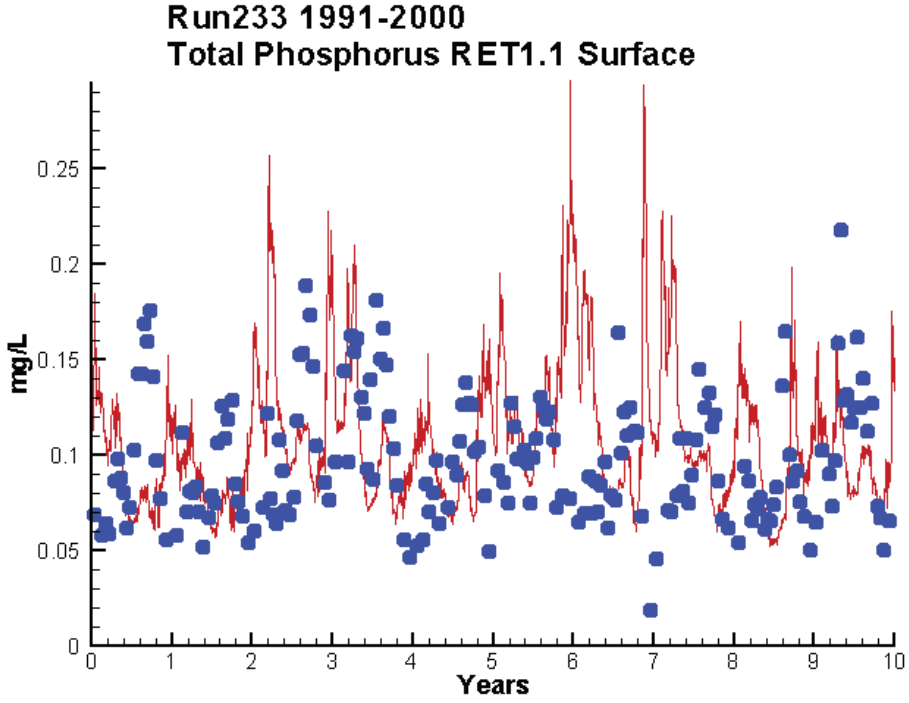

	Mean Difference	Absolute Mean Difference
Chl	-2.4857	8.9143
DIN	-0.0282	0.1356
KE	-1.2715	1.3413
DIP	-0.0197	0.0266
TP	0.0064	0.0382
TN	0.4431	0.4597

Station RET1.1

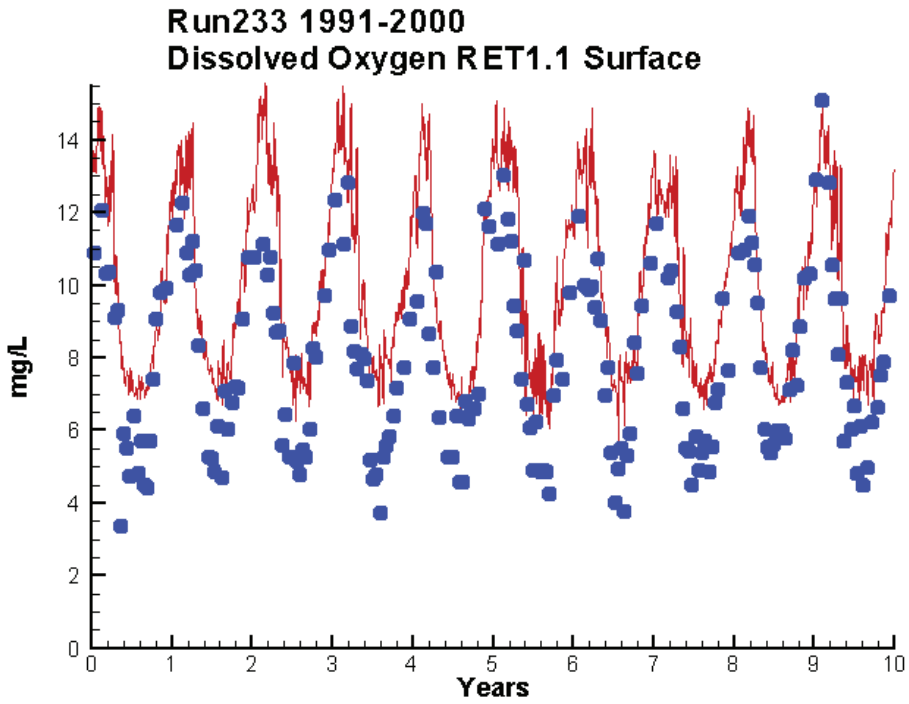

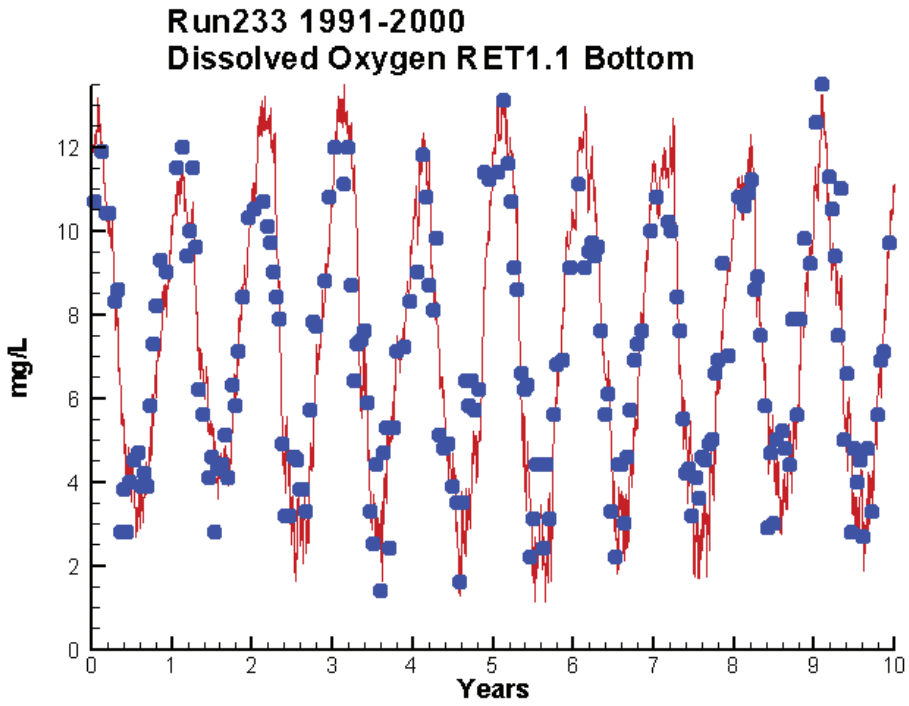

	Mean Difference	Absolute Mean Difference
Top DO	1.7963	1.8650
Bot DO	-0.0097	1.0051

Station RET1.1

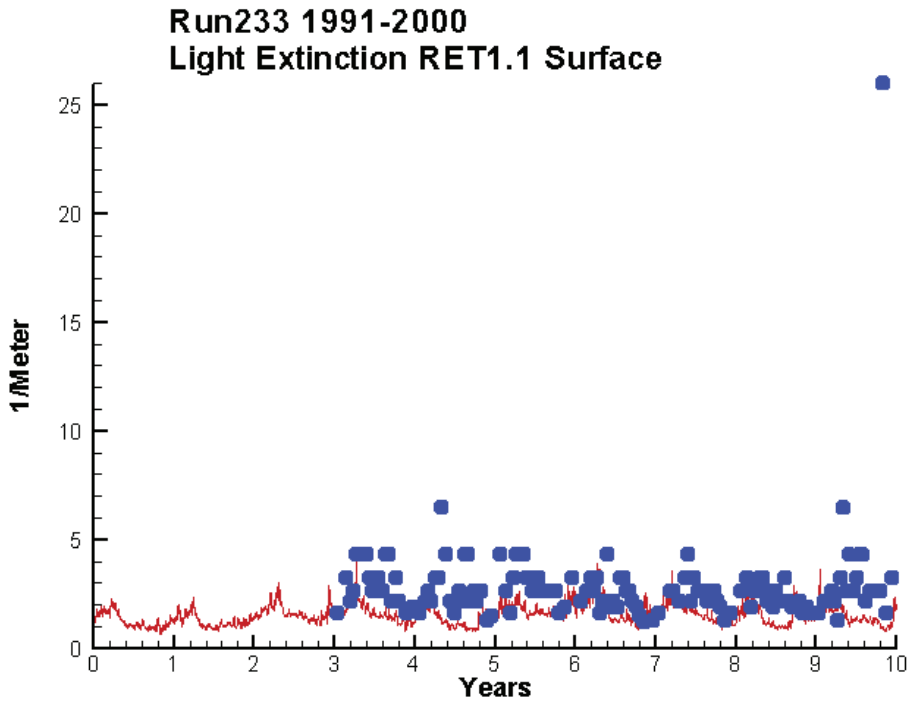

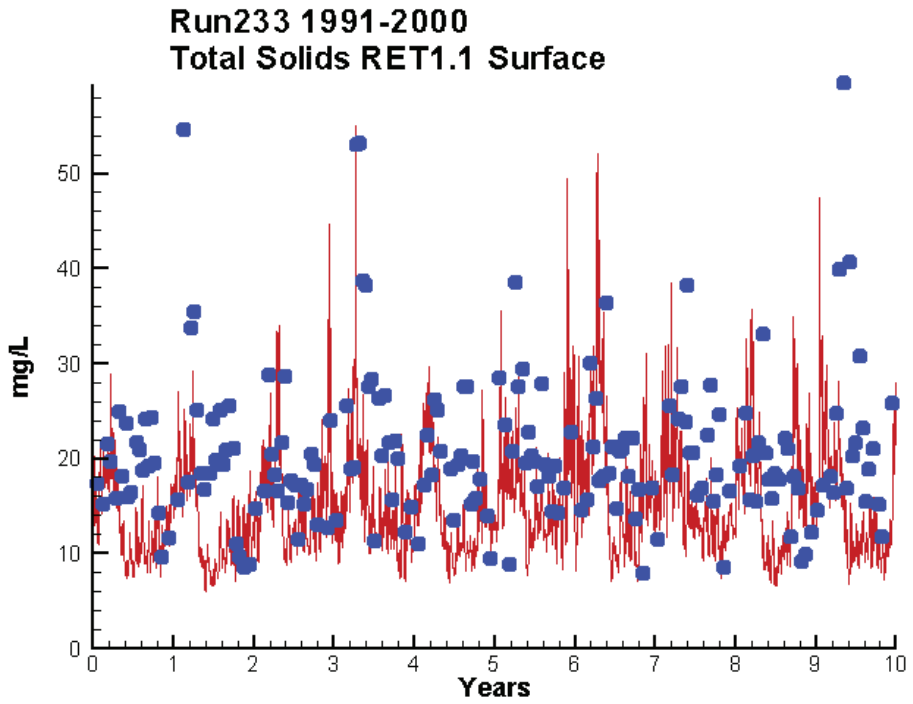

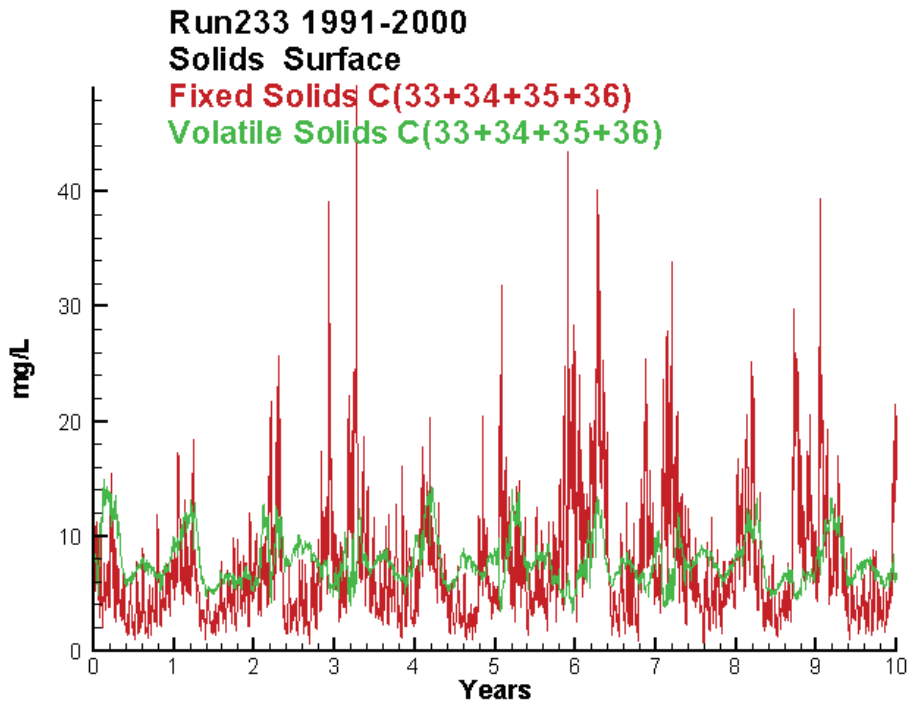

	Mean Difference	Absolute Mean Difference
KE	-1.2715	1.3413
TSS	-4.9168	7.9325

Station TF1.7

Run233 1991-2000
Chlorophyll TF1.7 Surface

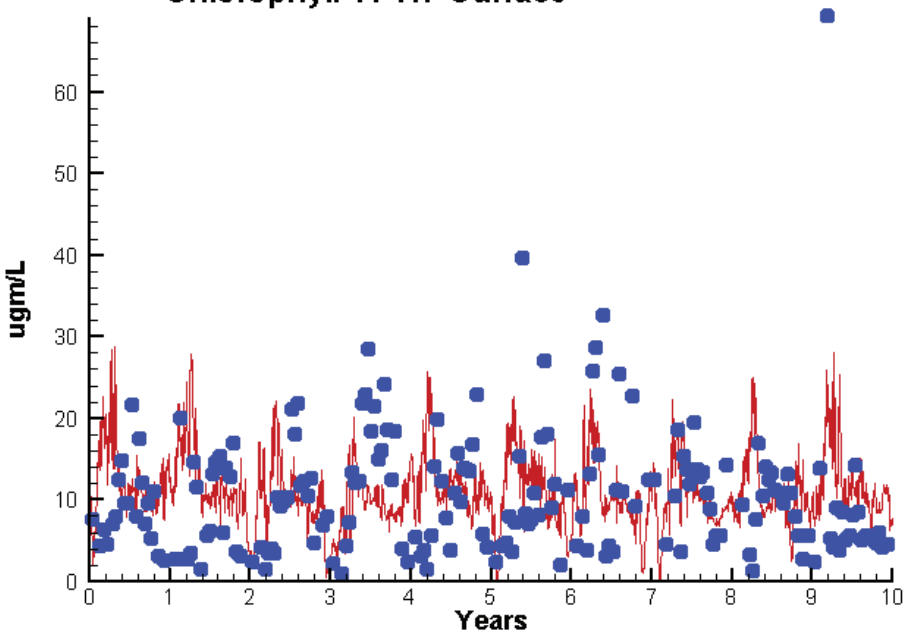

Run233 1991-2000
Light Extinction TF1.7 Surface

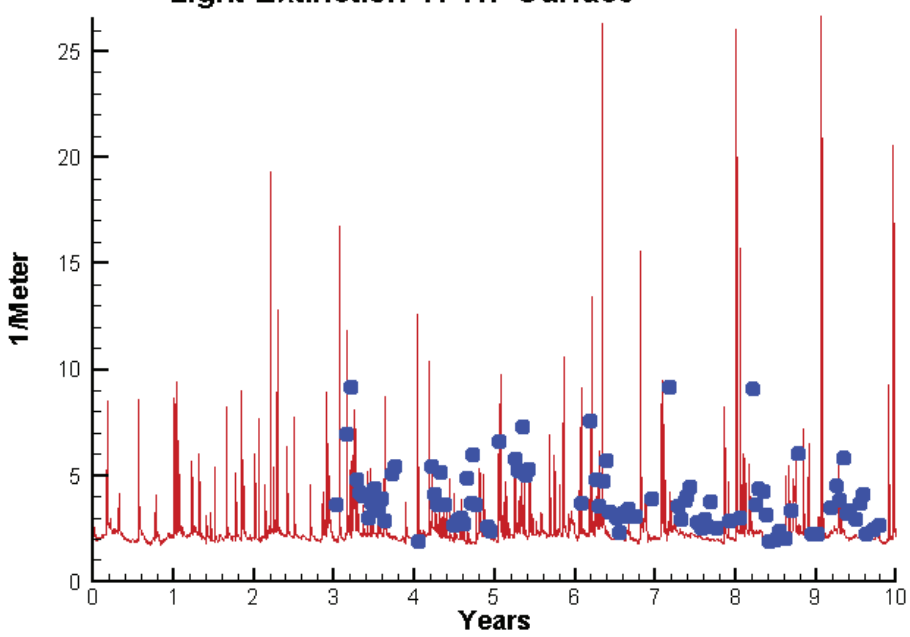

Run233 1991-2000
Dissolved Inorganic Nitrogen TF1.7 Surface

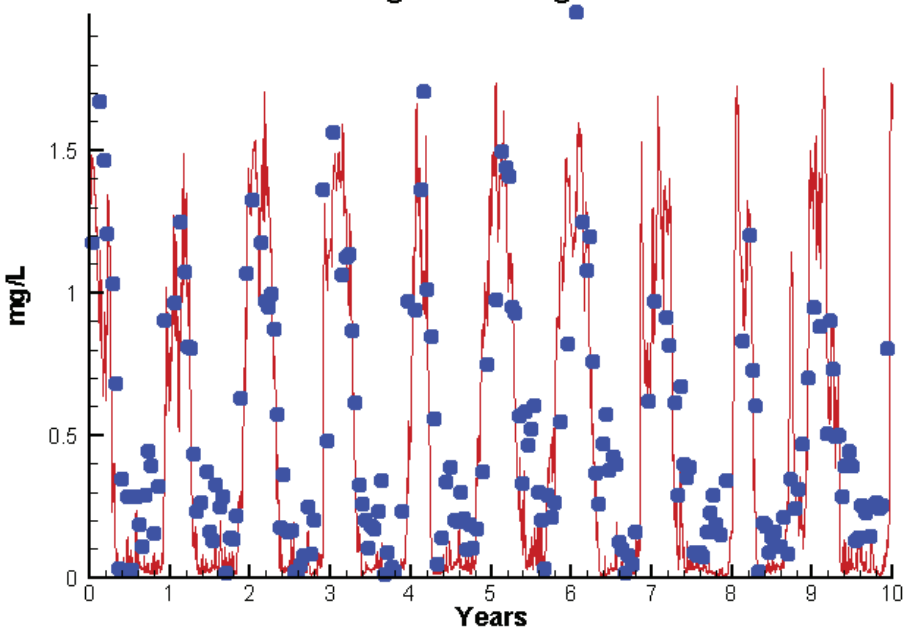

Run233 1991-2000
Dissolved Inorganic Phosphorus TF1.7 Surface

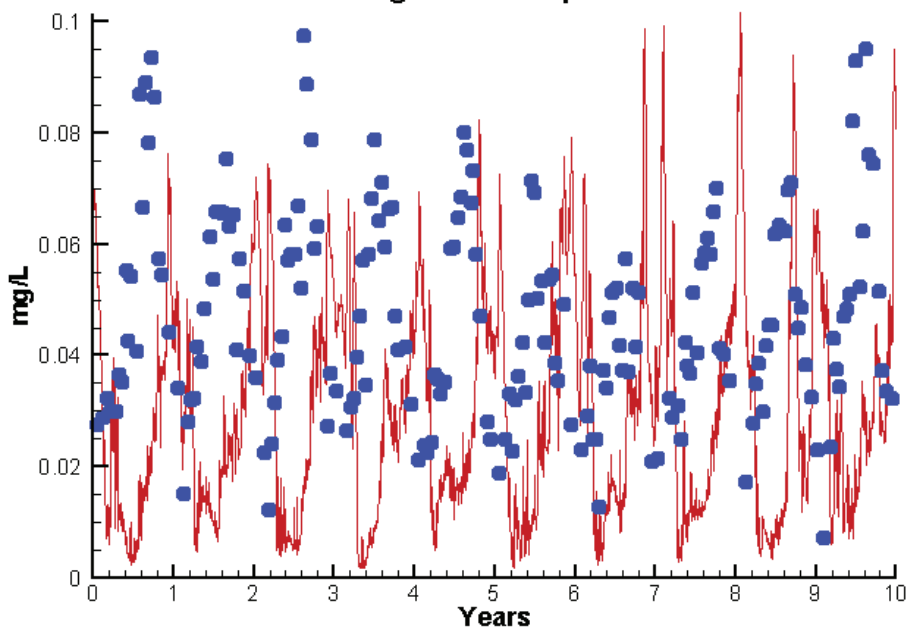

Station TF1.7

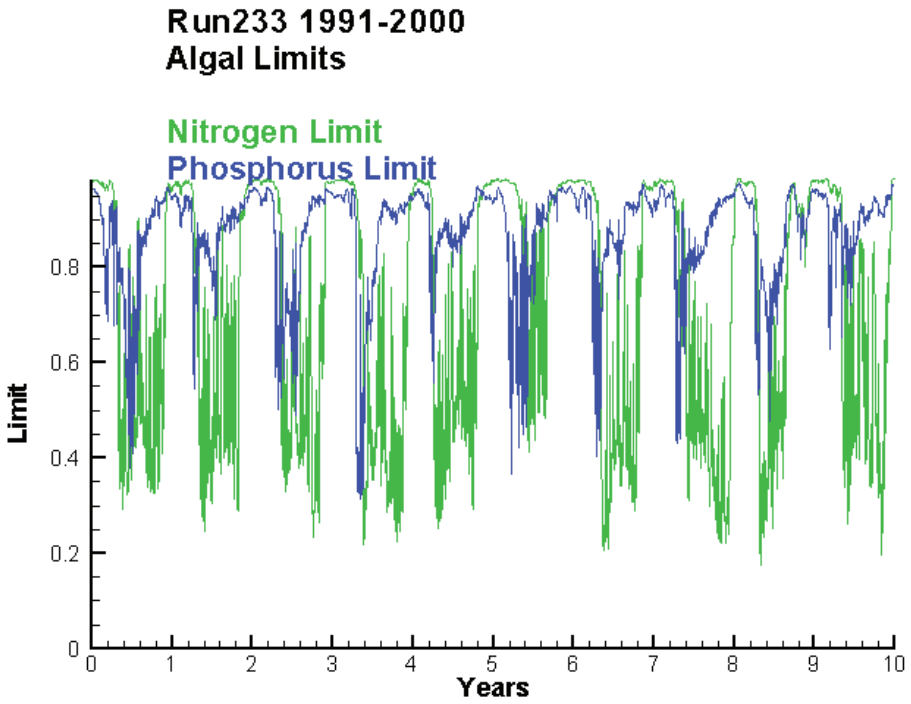

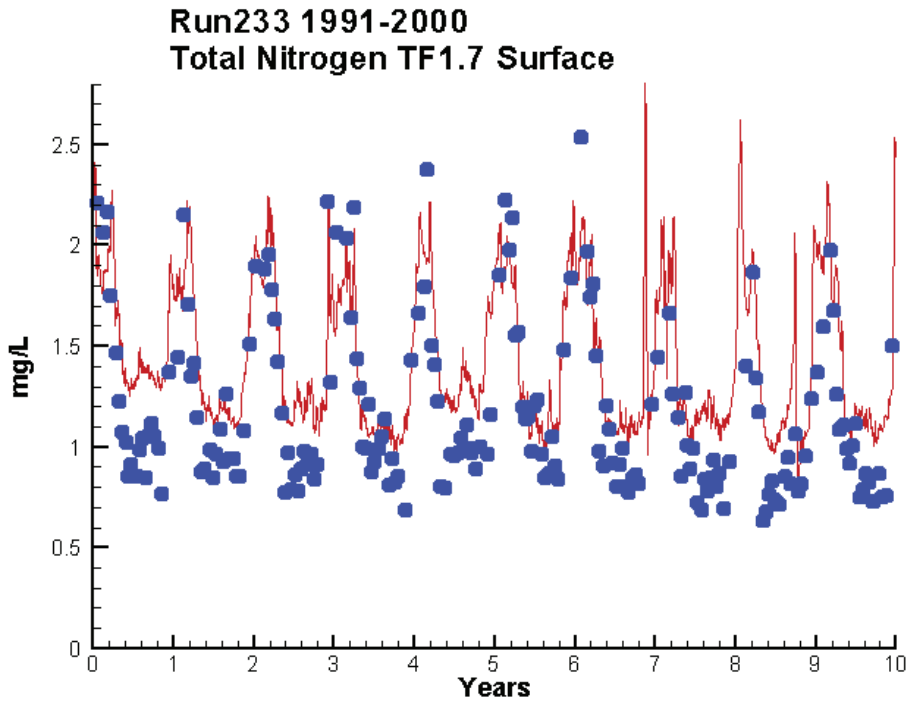

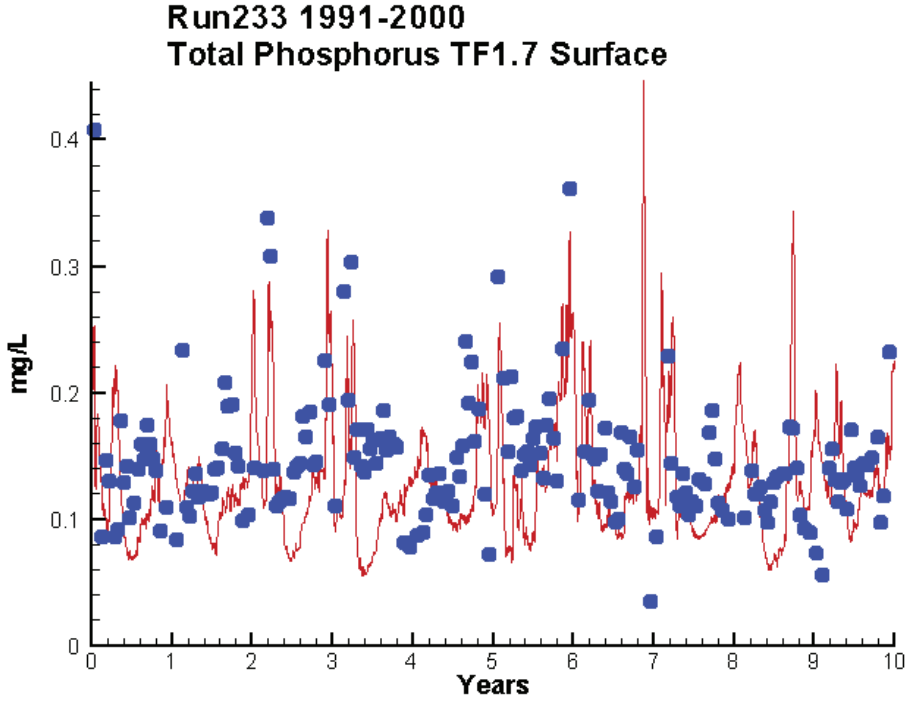

	Mean Difference	Absolute Mean Difference
Chl	1.2926	6.7032
DIN	-0.1238	0.2289
KE	-1.5487	1.7519
DIP	-0.0215	0.0313
TP	-0.0233	0.0477
TN	0.2106	0.2657

Station TF1.7

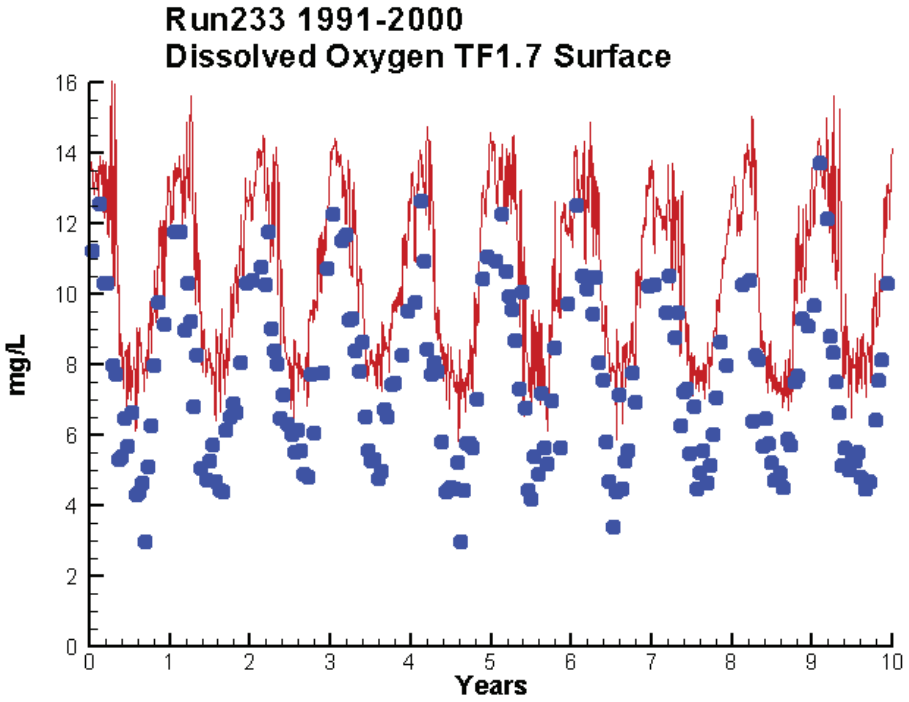

	Mean Difference	Absolute Mean Difference
Top DO	2.7689	2.7689

Station TF1.7

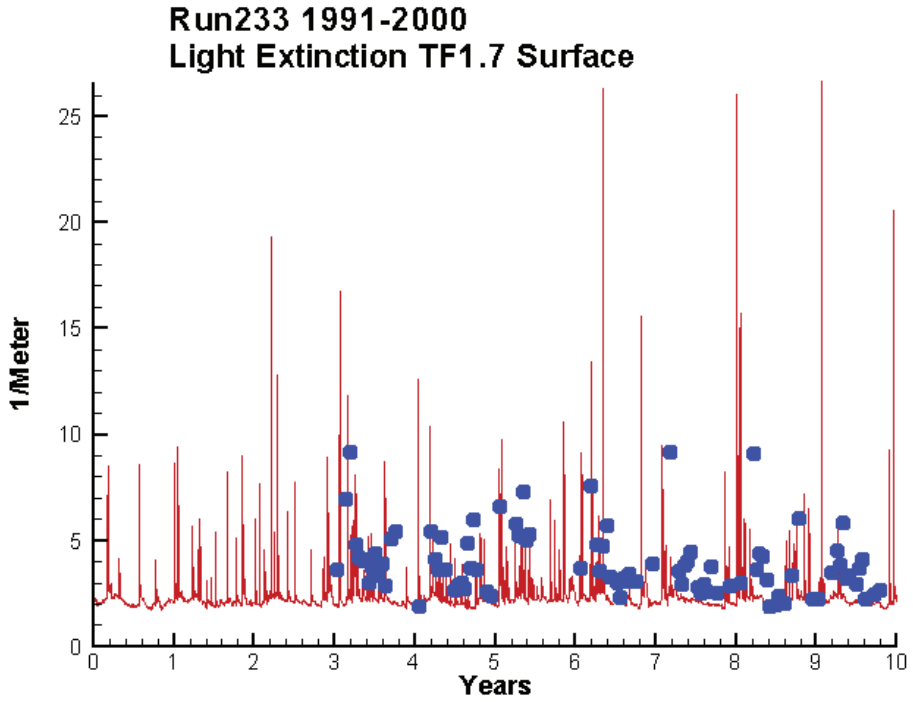

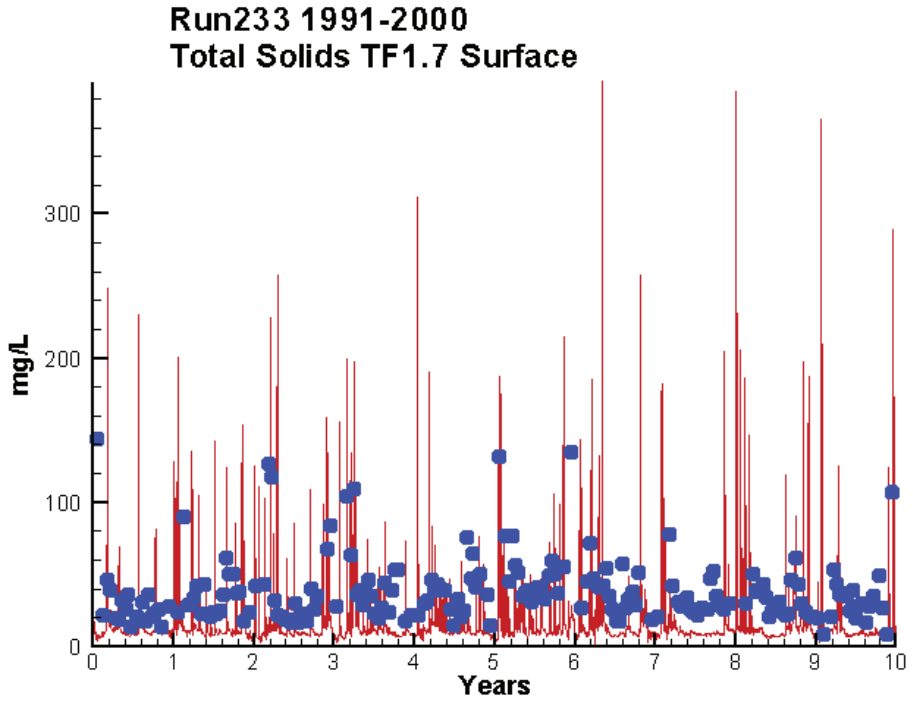

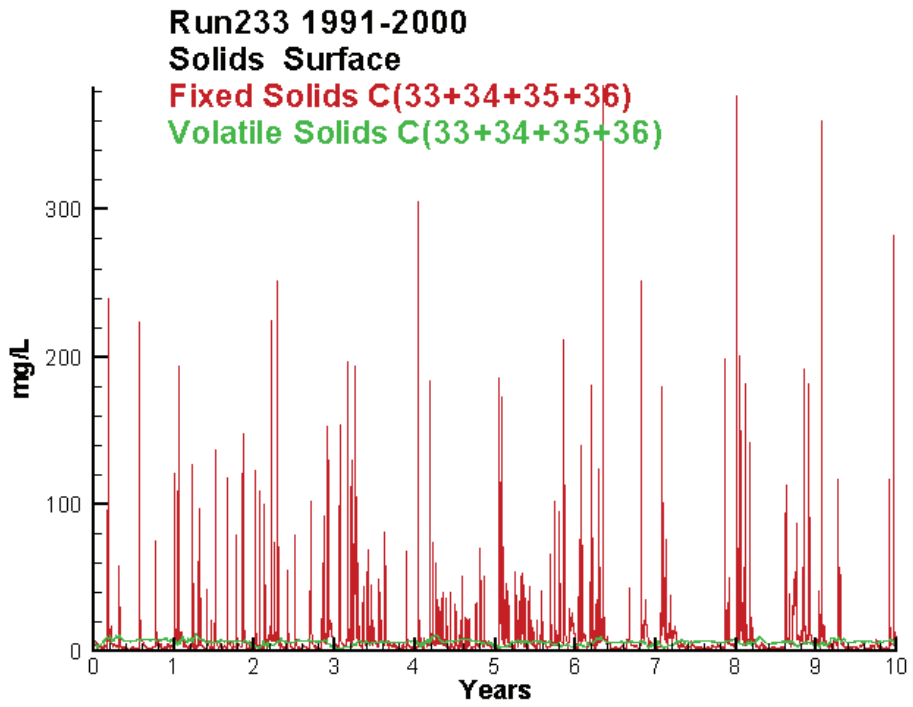

	Mean Difference	Absolute Mean Difference
KE	-1.5487	1.7519
TSS	-22.0227	27.8615

Station LE2.2

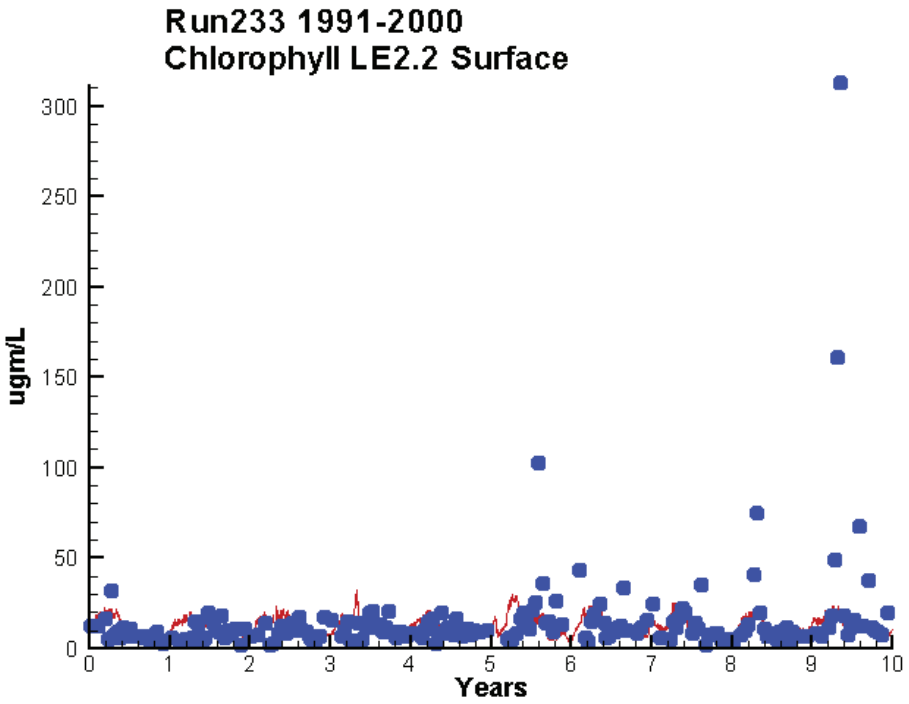

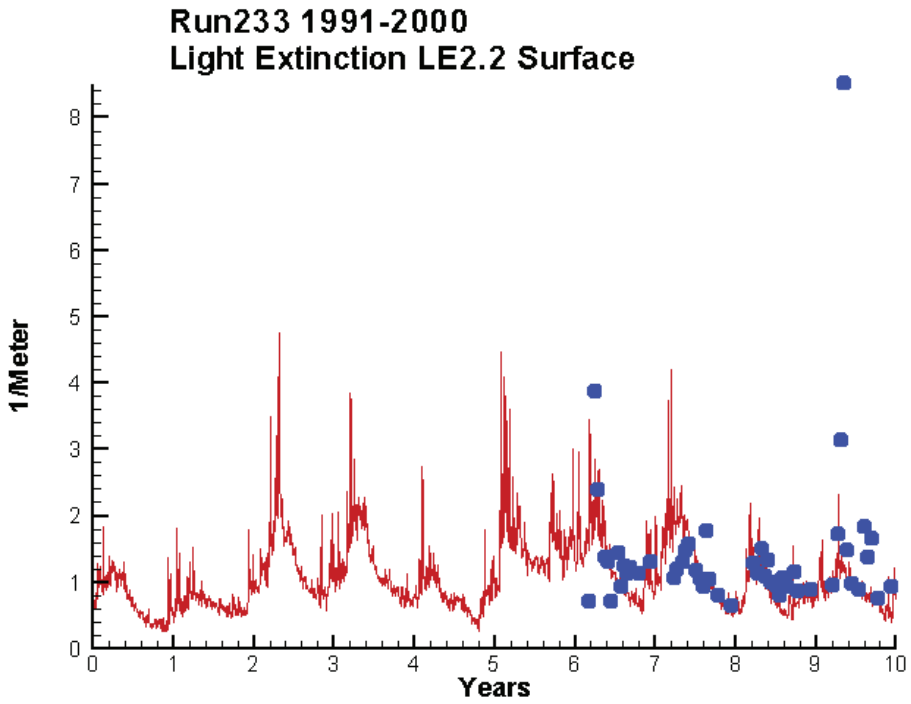

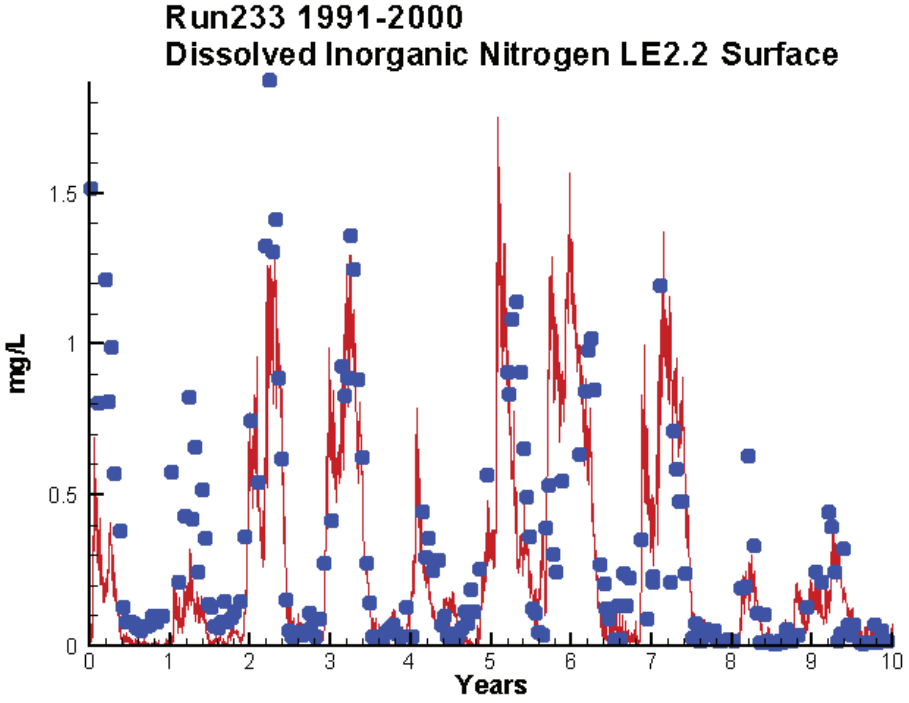

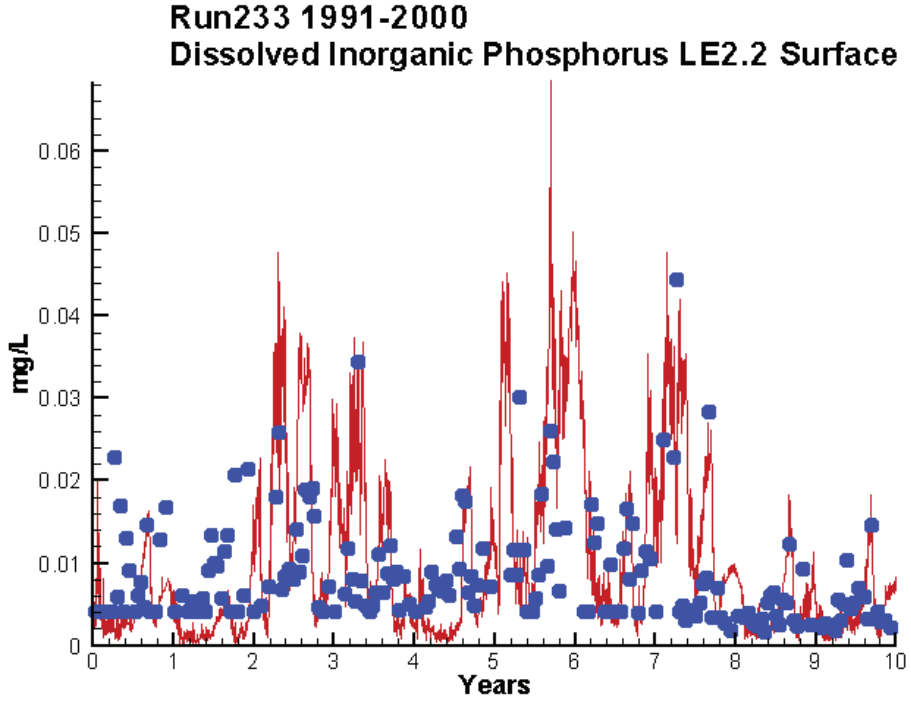

Station LE2.2

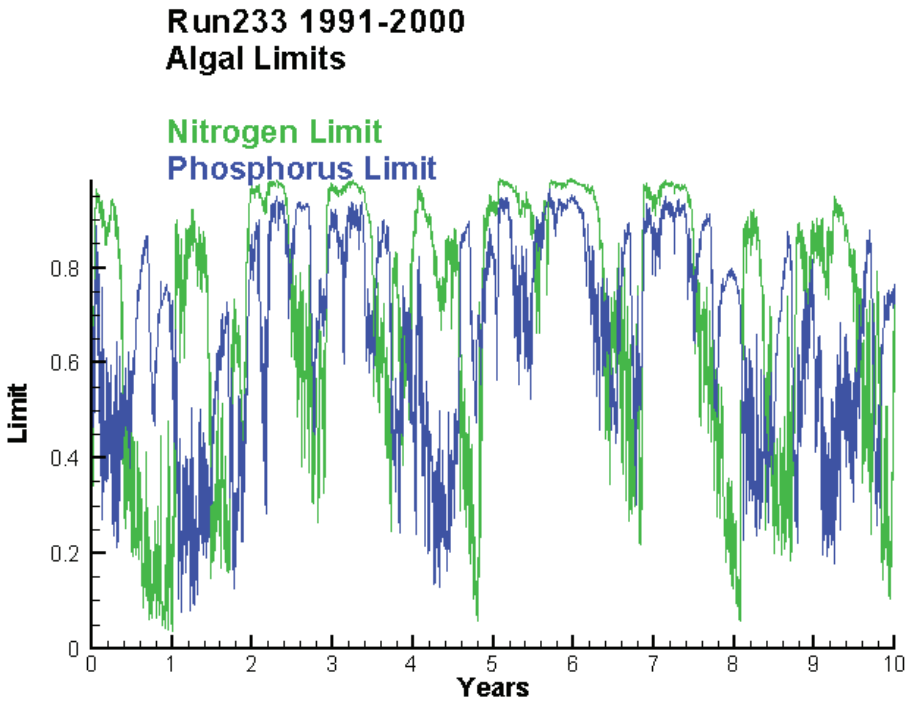

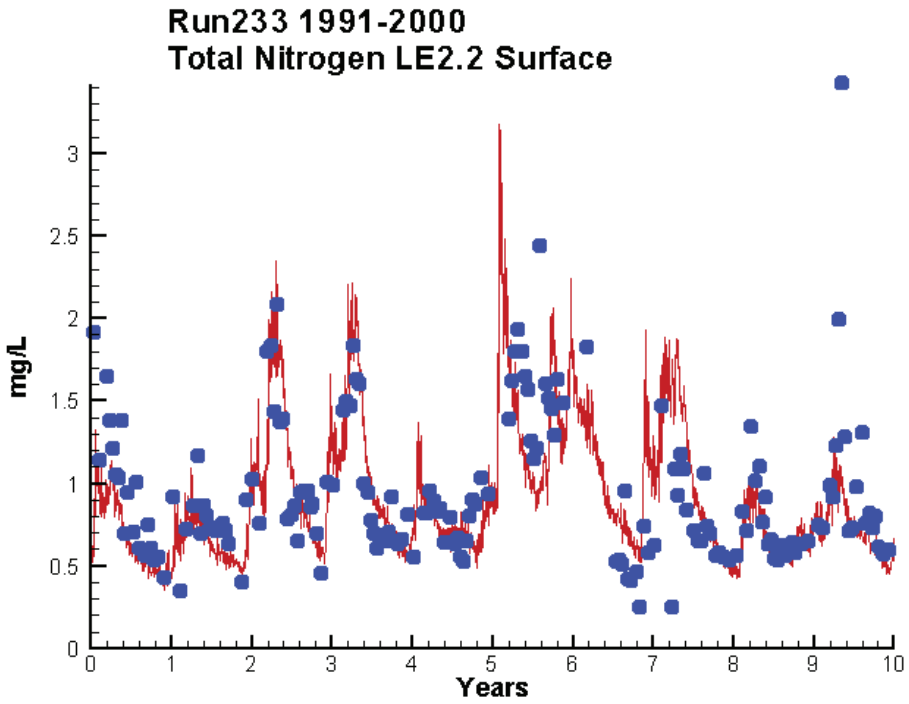

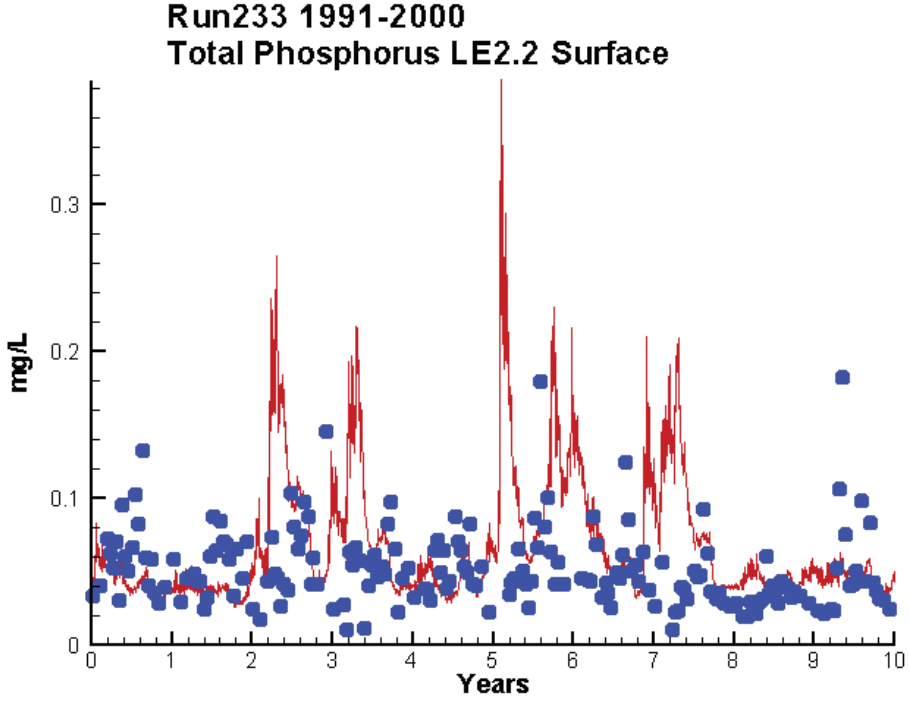

	Mean Difference	Absolute Mean Difference
Chl	-1.5933	9.2717
DIN	-0.0751	0.1719
KE	-0.2916	0.5780
DIP	0.0014	0.0067
TP	0.0145	0.0341
TN	-0.0544	0.2426

Station LE2.2

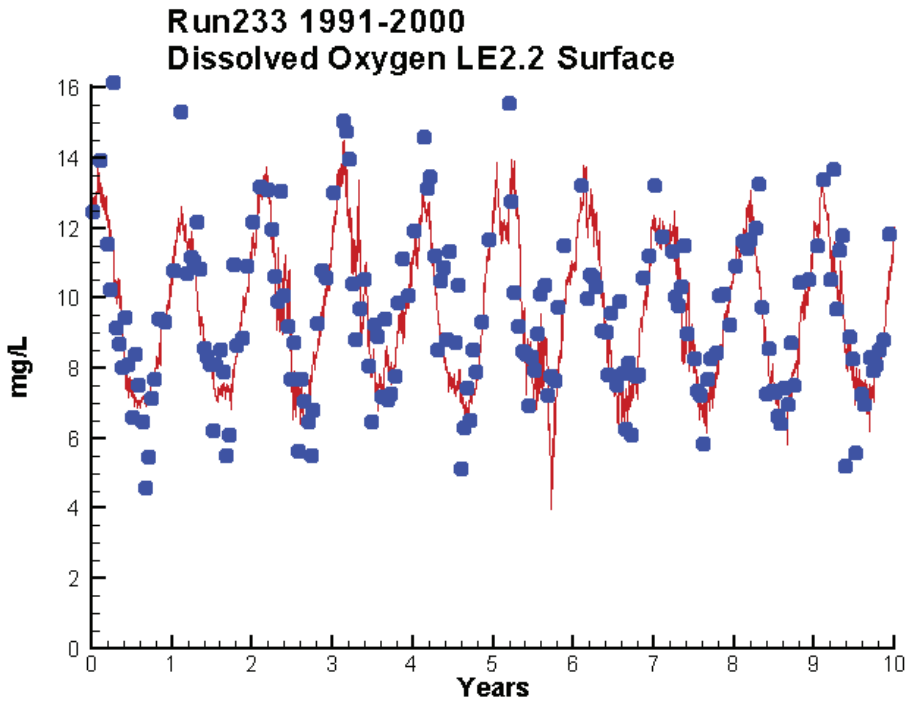

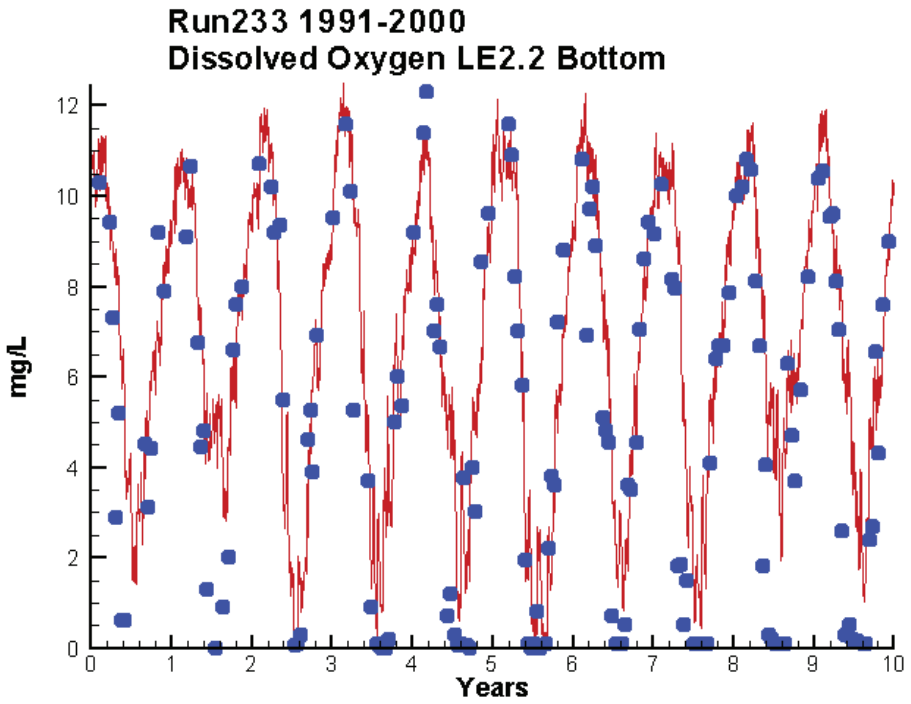

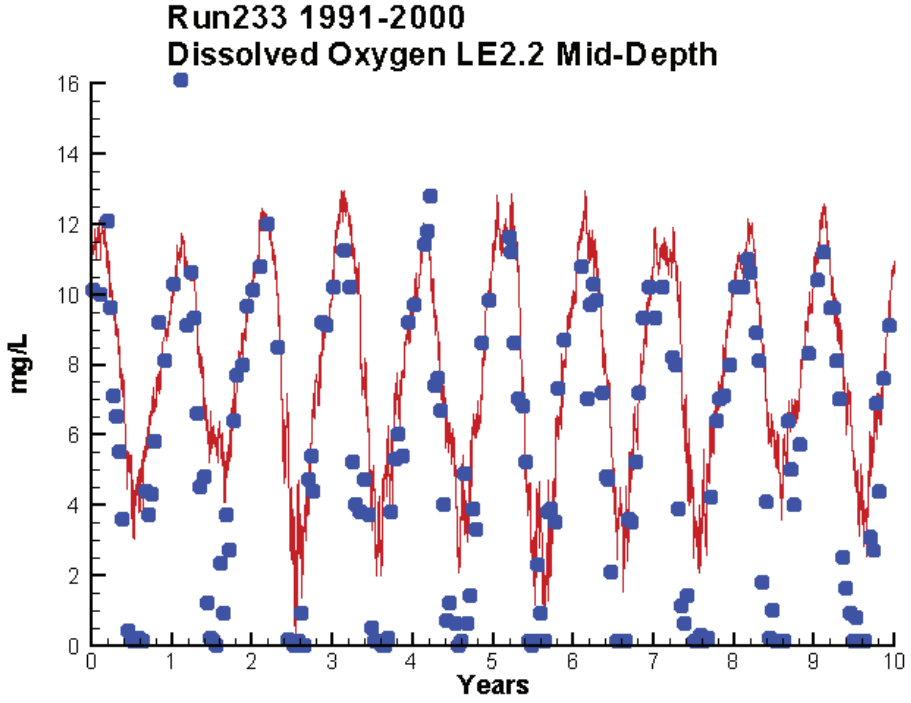

	Mean Difference	Absolute Mean Difference
Top DO	-0.1495	1.0771
Mid DO	2.1977	2.4059
Bot DO	1.2582	1.7246

Station LE2.2

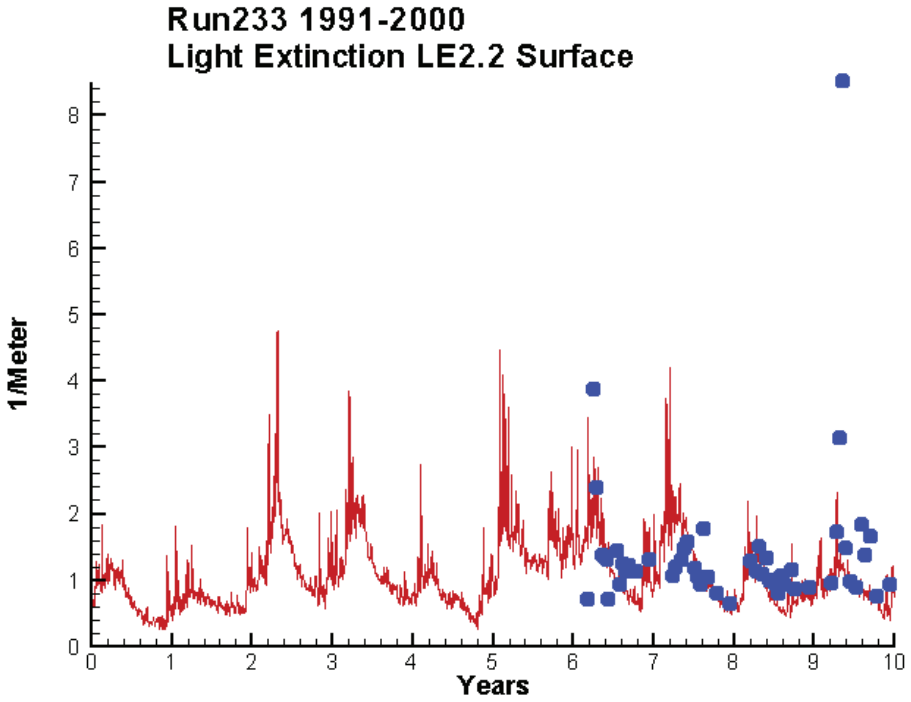

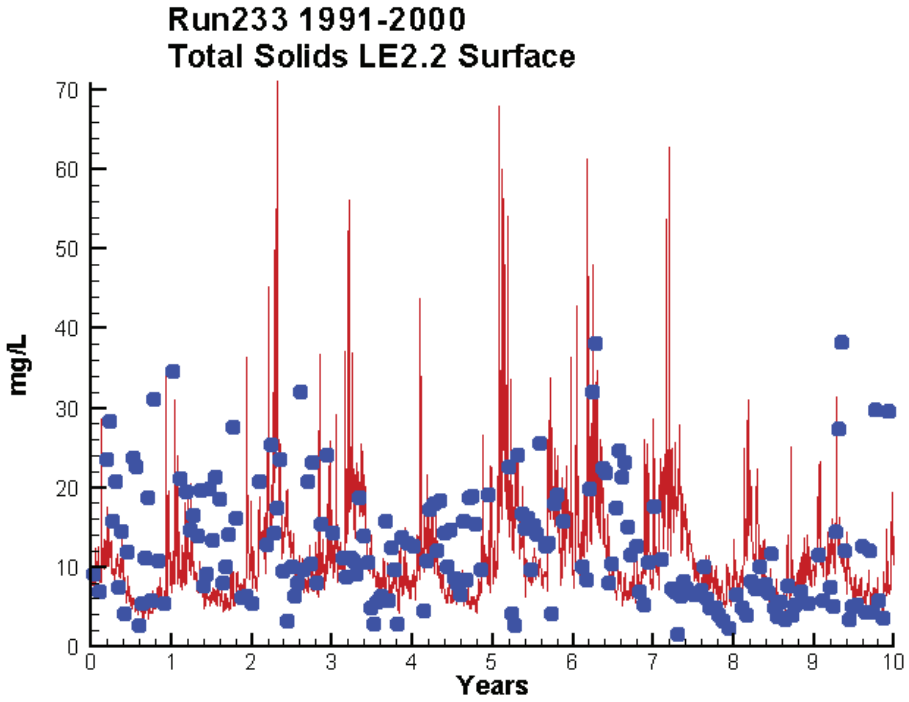

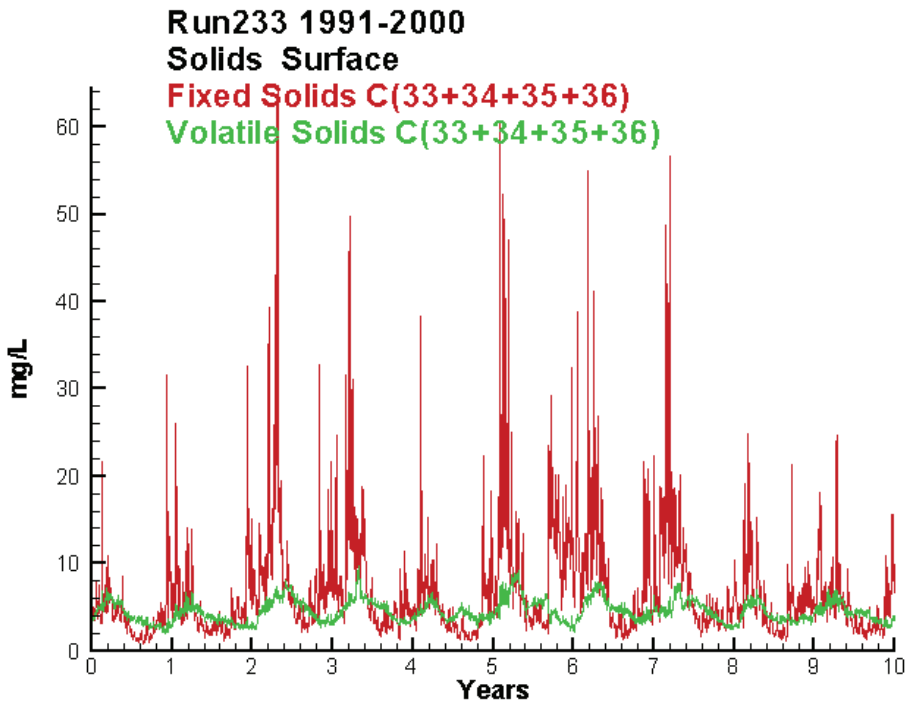

	Mean Difference	Absolute Mean Difference
KE	-0.2916	0.5780
TSS	-1.9217	7.1908

Station RET2.4

Run233 1991-2000
Chlorophyll RET2.4 Surface

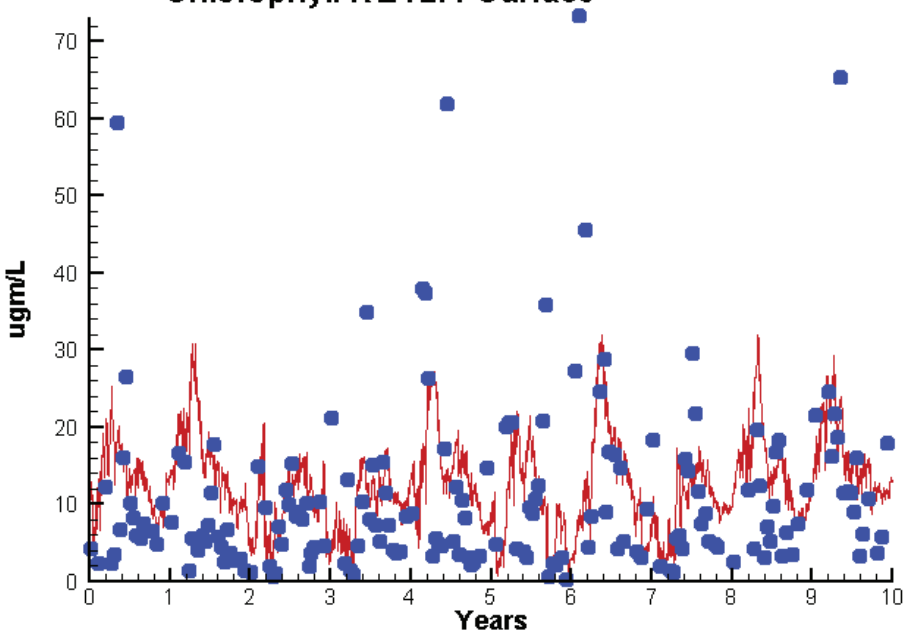

Run233 1991-2000
Light Extinction RET2.4 Surface

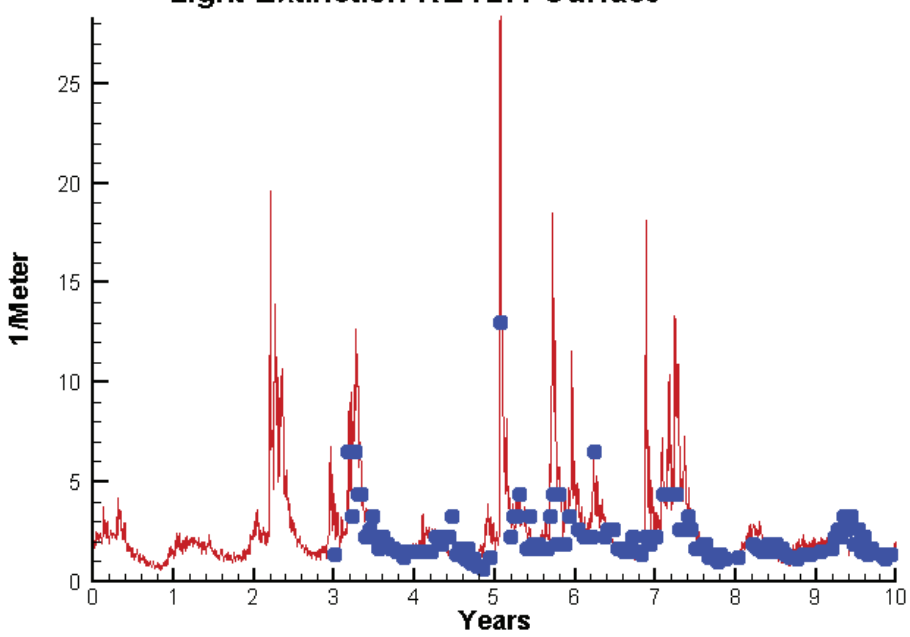

Run233 1991-2000
Dissolved Inorganic Nitrogen RET2.4 Surface

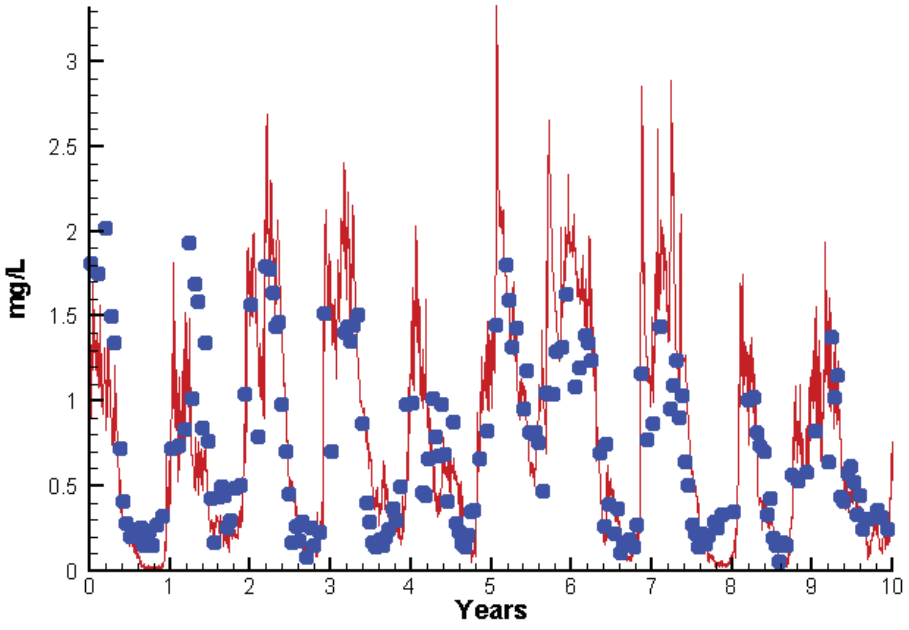

Run233 1991-2000
Dissolved Inorganic Phosphorus RET2.4 Surface

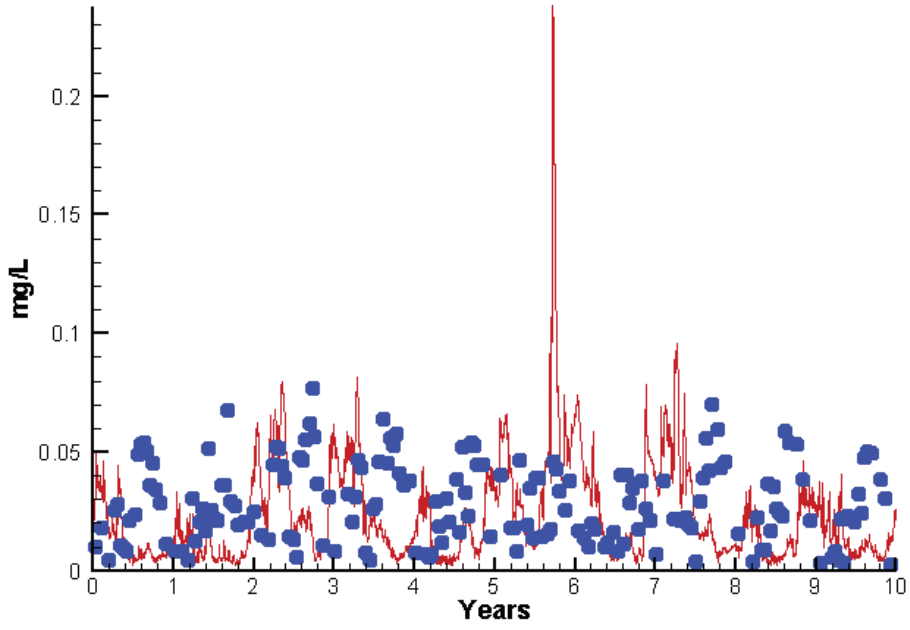

Station RET2.4

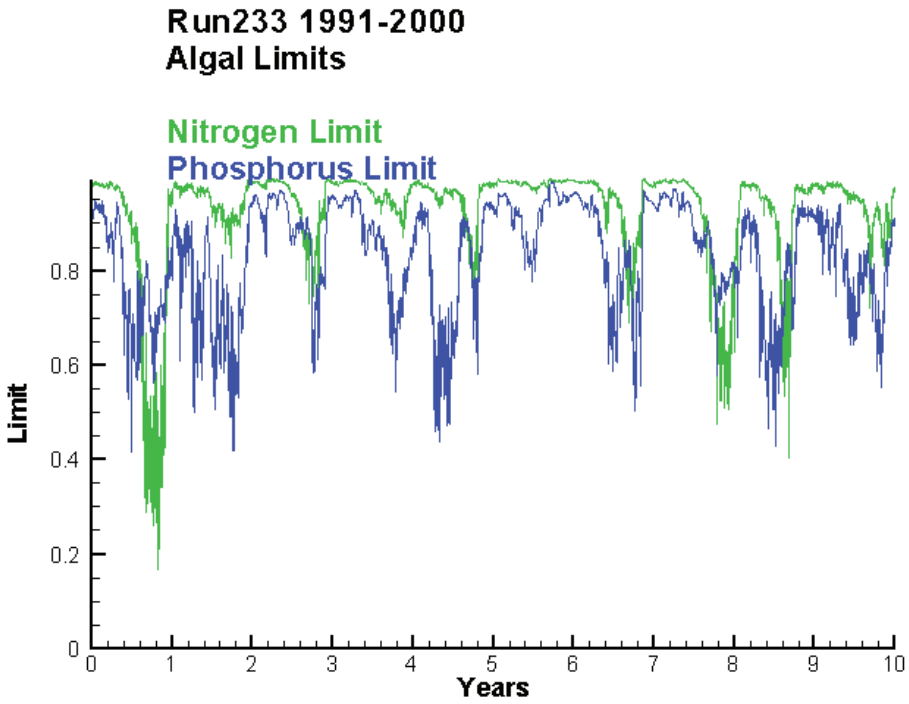

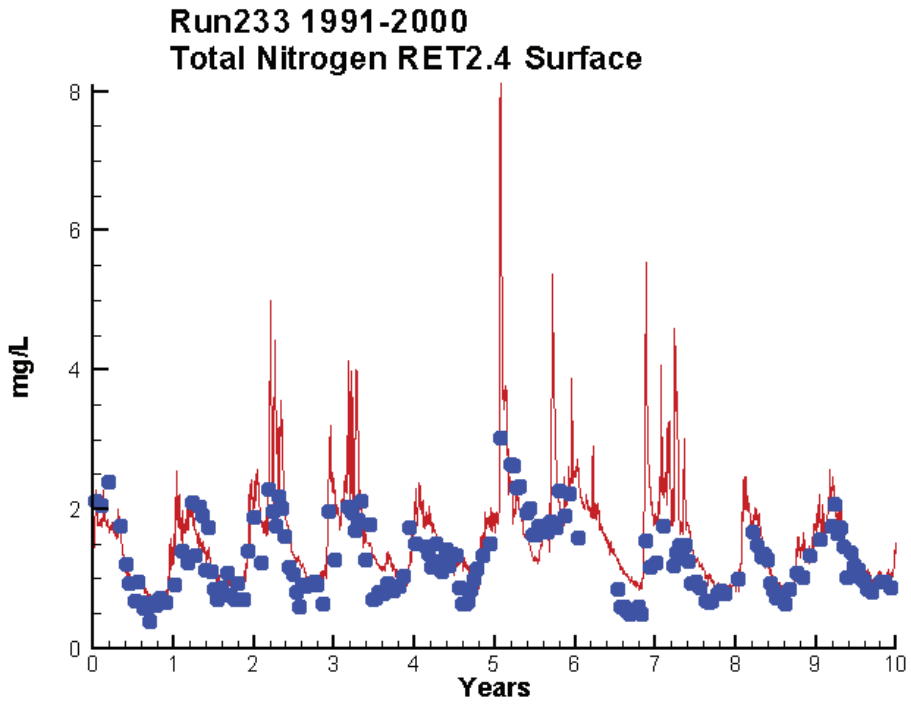

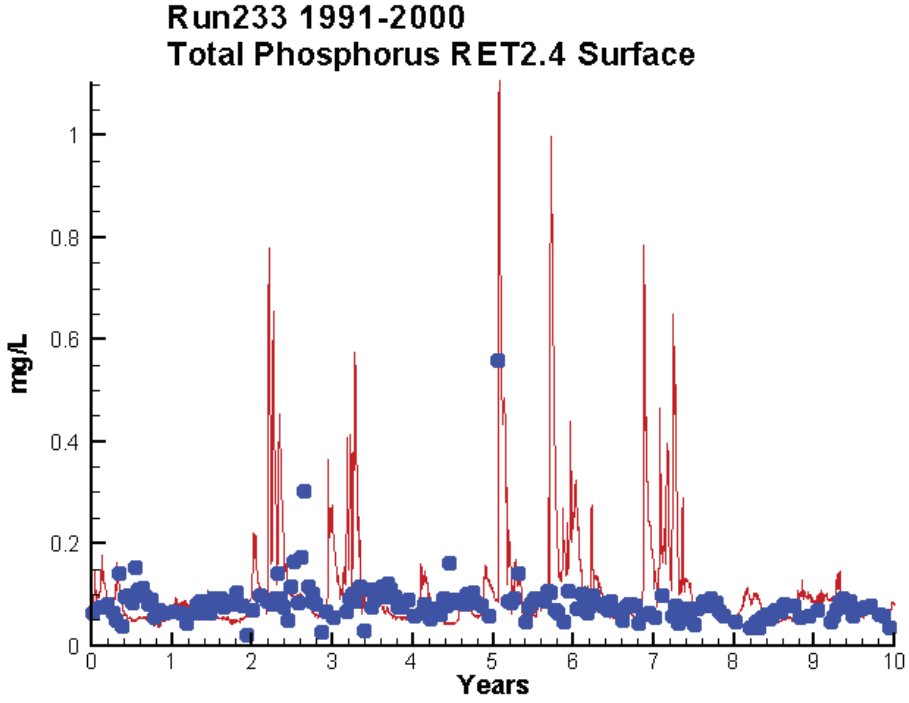

	Mean Difference	Absolute Mean Difference
Chl	2.6386	8.4852
DIN	0.0501	0.2802
KE	0.7330	1.0735
DIP	-0.0066	0.0230
TP	0.0328	0.0612
TN	0.3127	0.4113

Station RET2.4

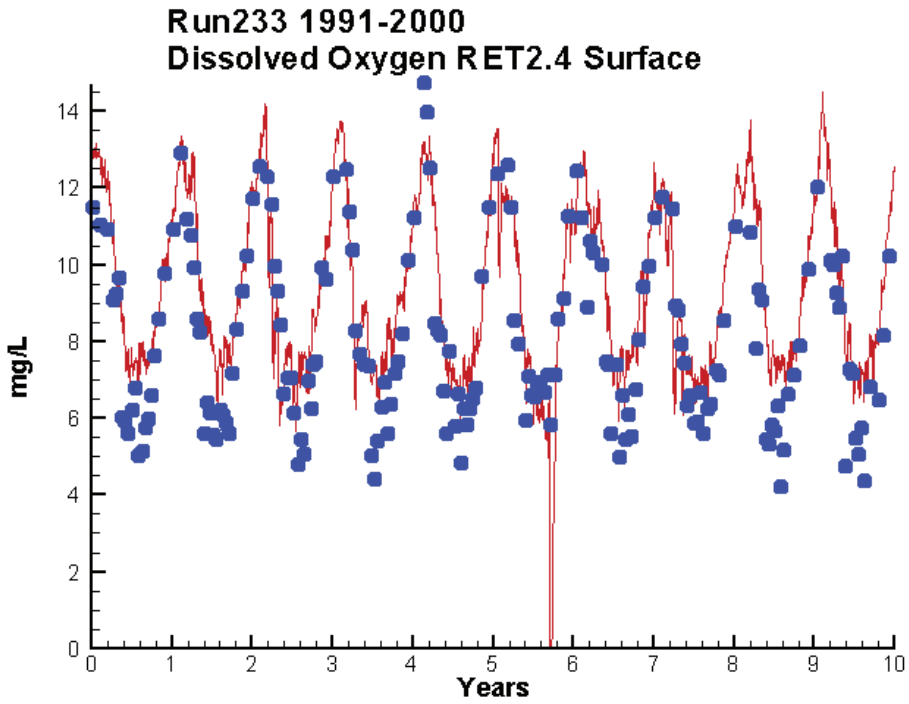

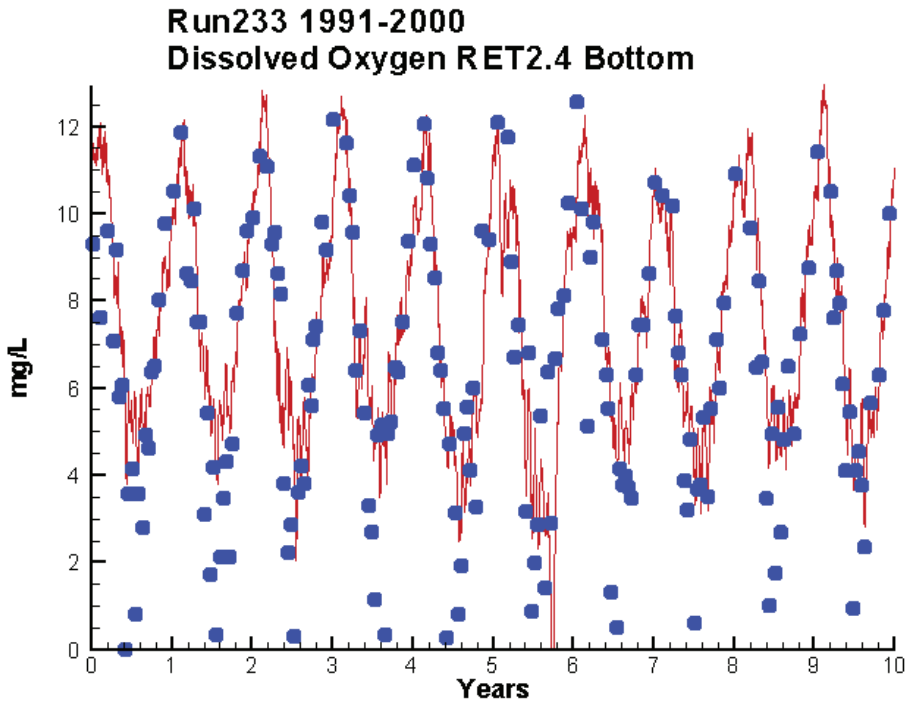

	Mean Difference	Absolute Mean Difference
Top DO	0.8674	1.3007
Bot DO	0.6766	1.3471

Station RET2.4

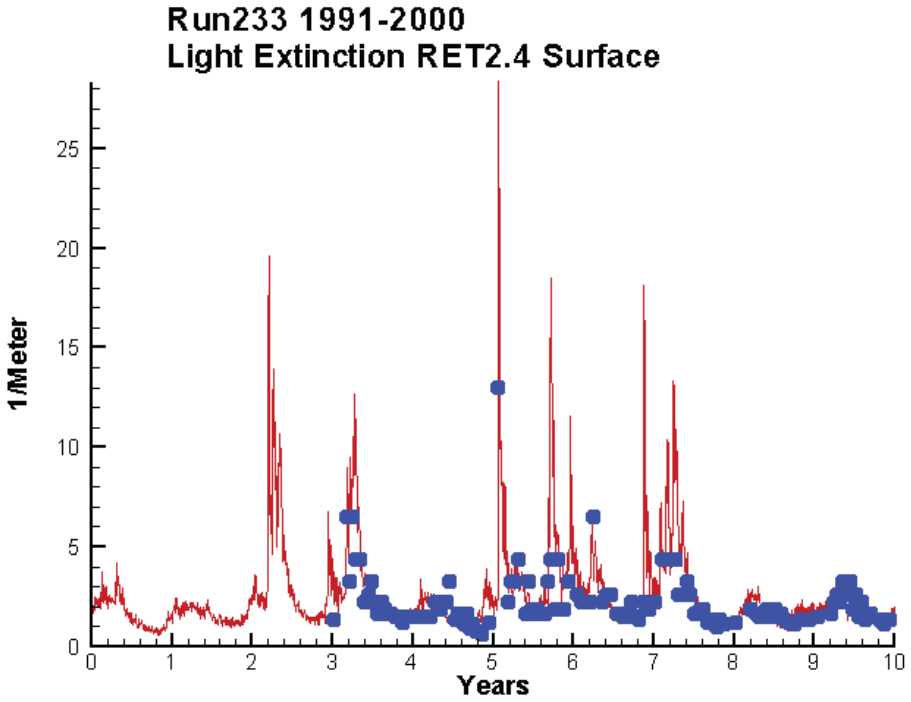

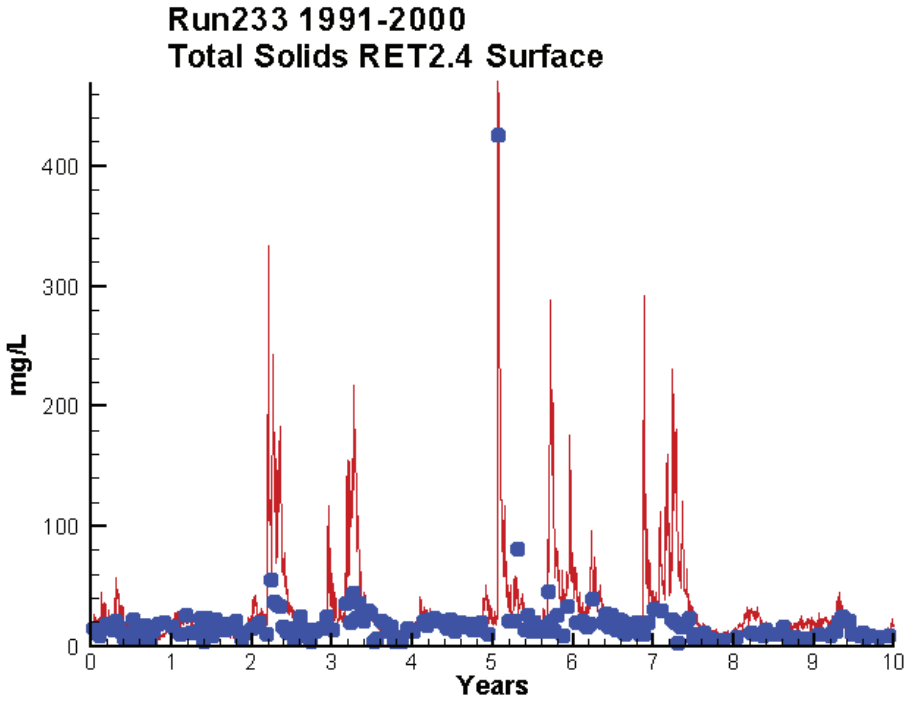

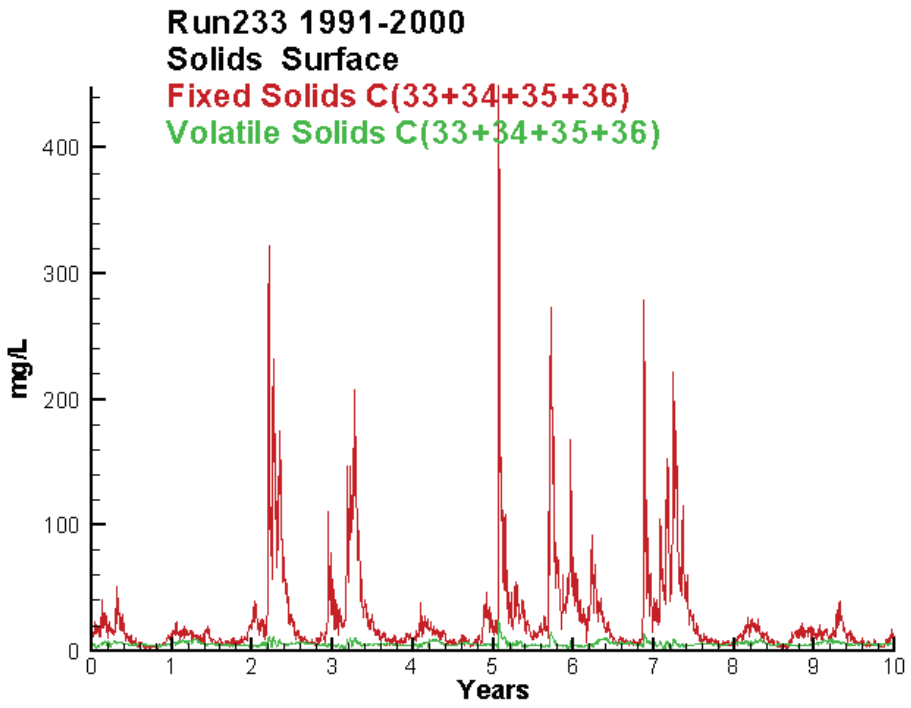

	Mean Difference	Absolute Mean Difference
KE	0.7330	1.0735
TSS	14.2232	17.5176

Station TF2.1

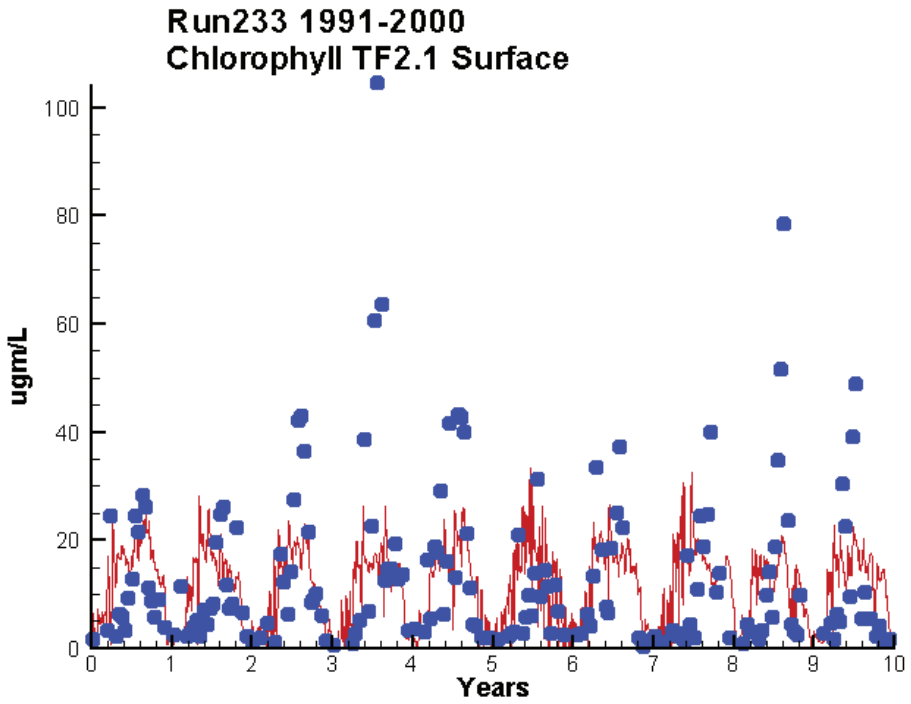

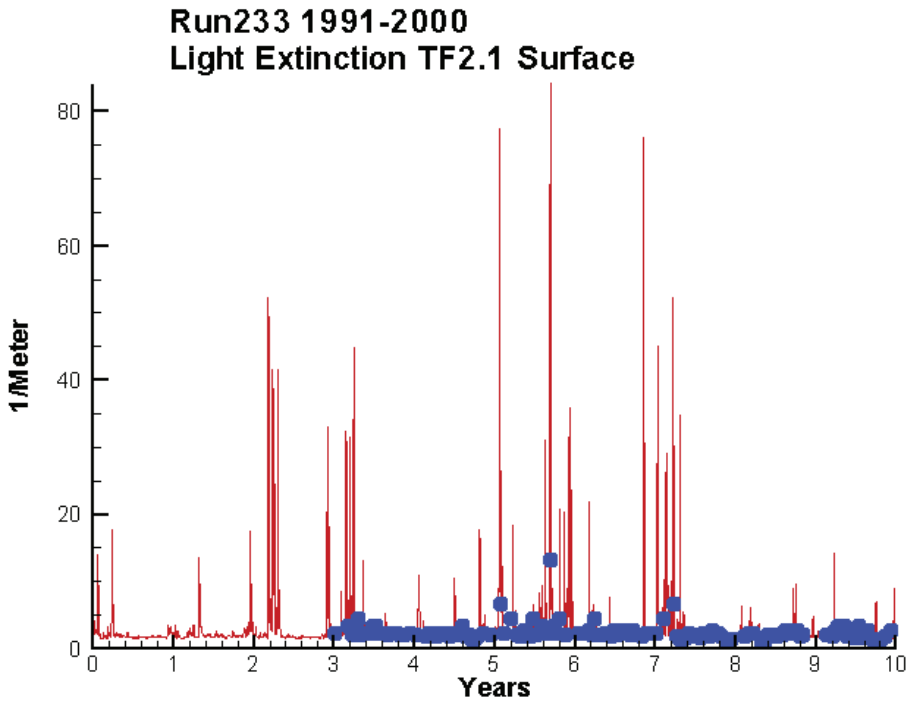

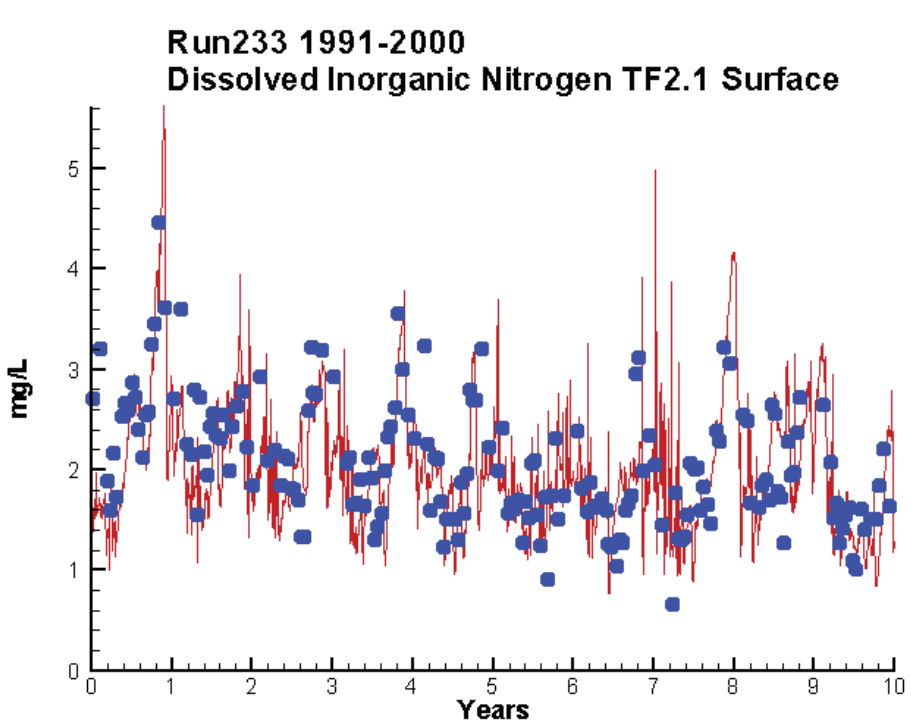

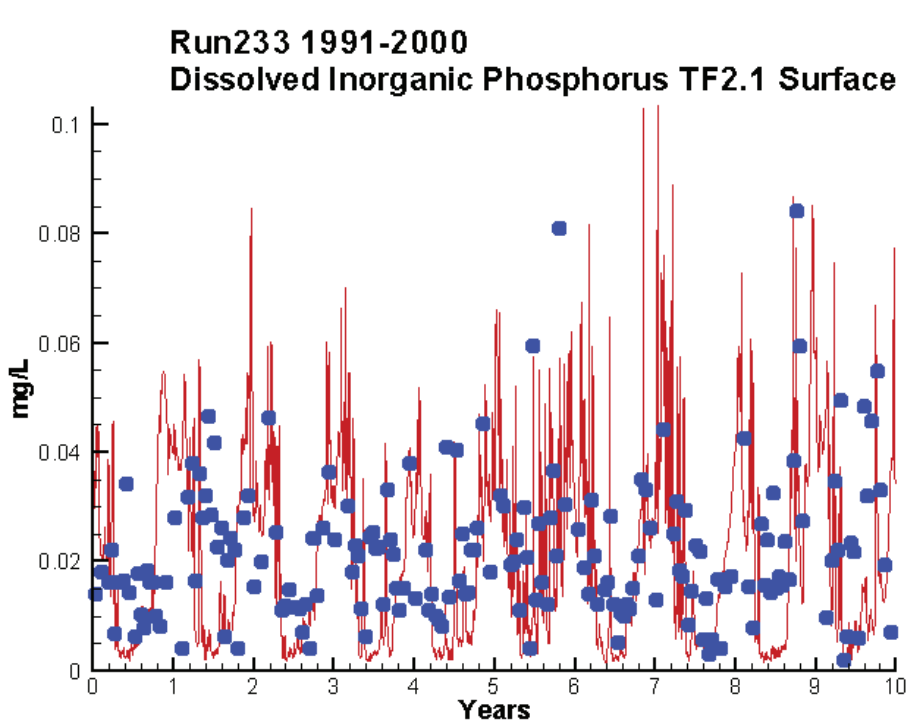

Station TF2.1

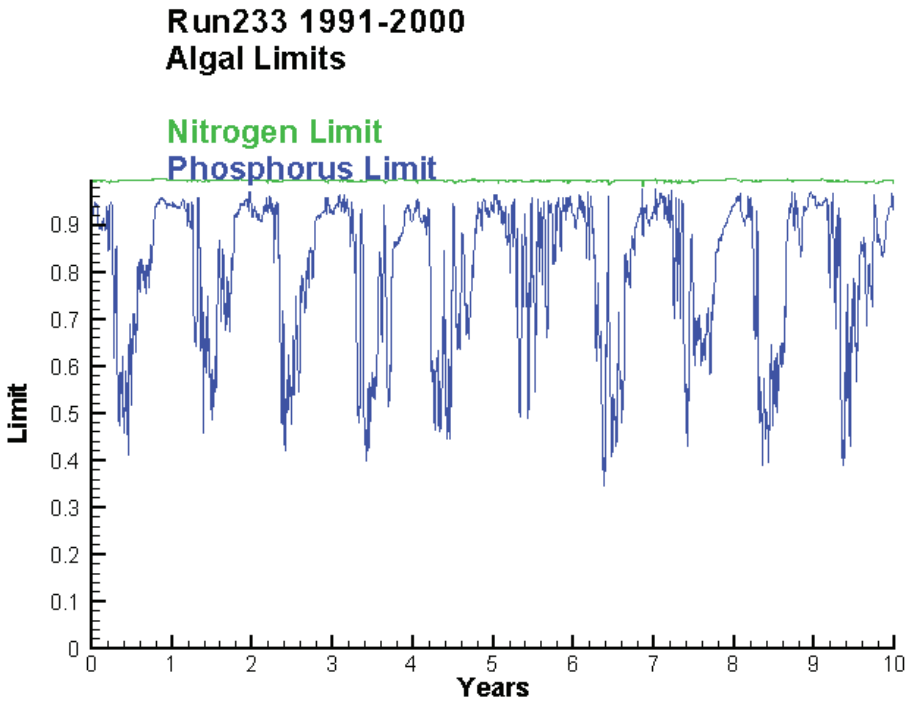

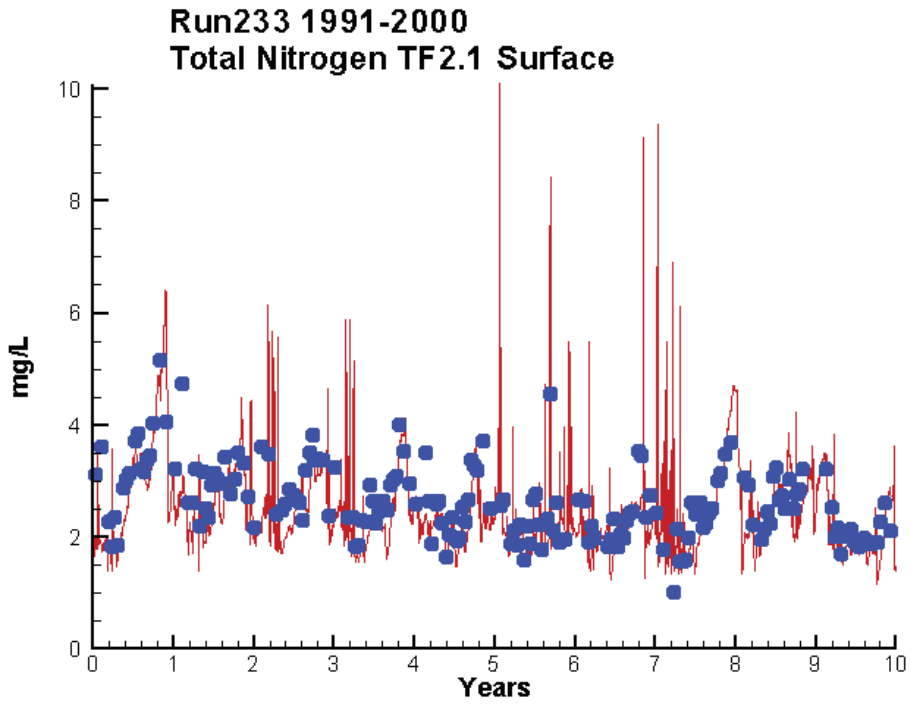

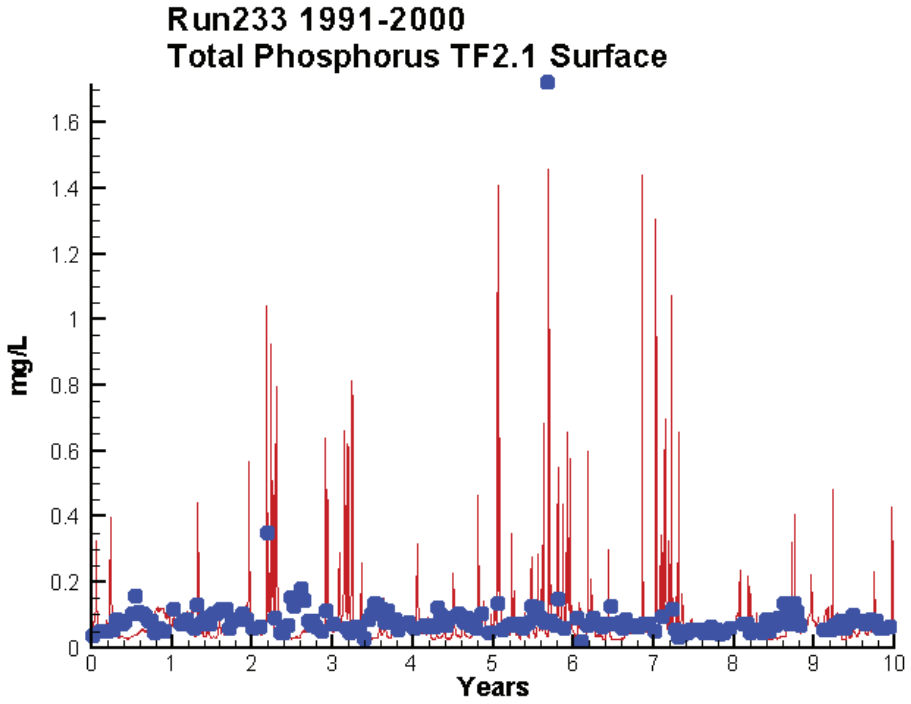

	Mean Difference	Absolute Mean Difference
Chl	-0.0789	9.4997
DIN	-0.1066	0.3837
KE	0.8490	1.3932
DIP	-0.0040	0.0134
TP	-0.0125	0.0479
TN	-0.1901	0.4460

Station TF2.1

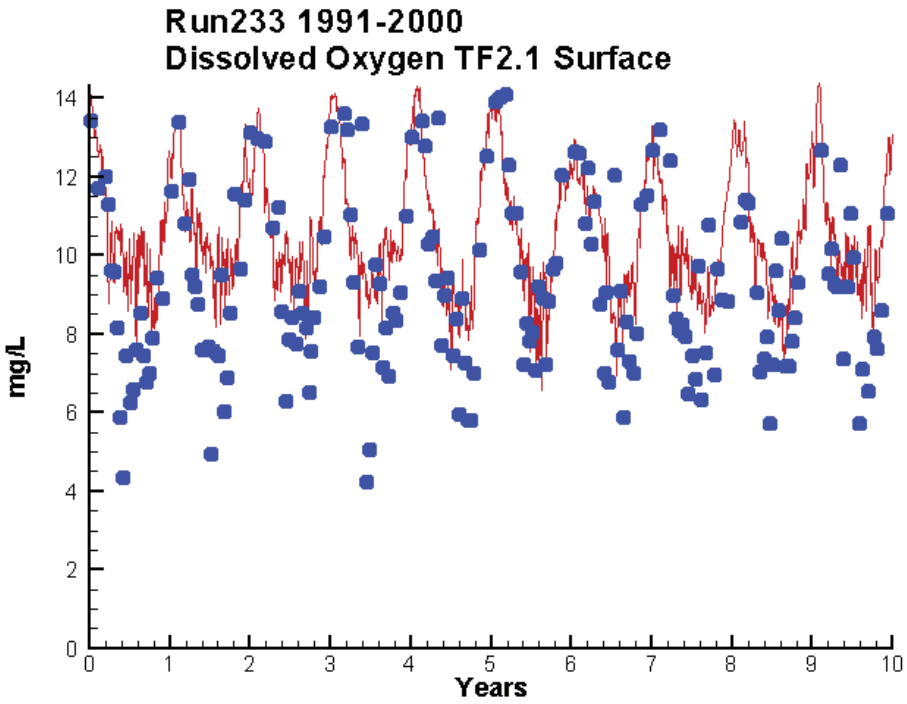

	Mean Difference	Absolute Mean Difference
Top DO	1.0656	1.6279

Station TF2.1

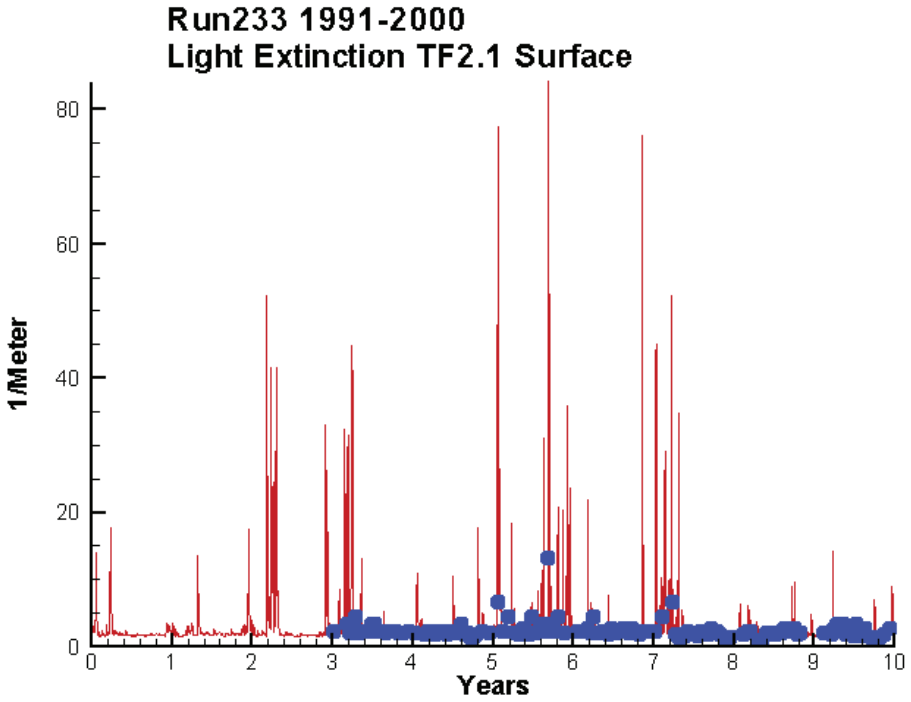

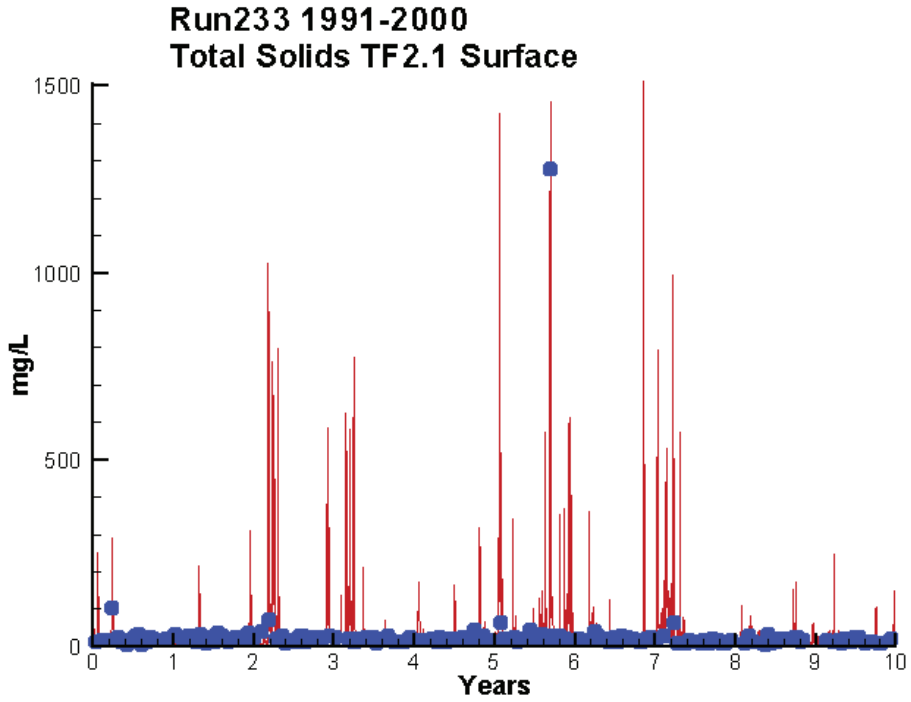

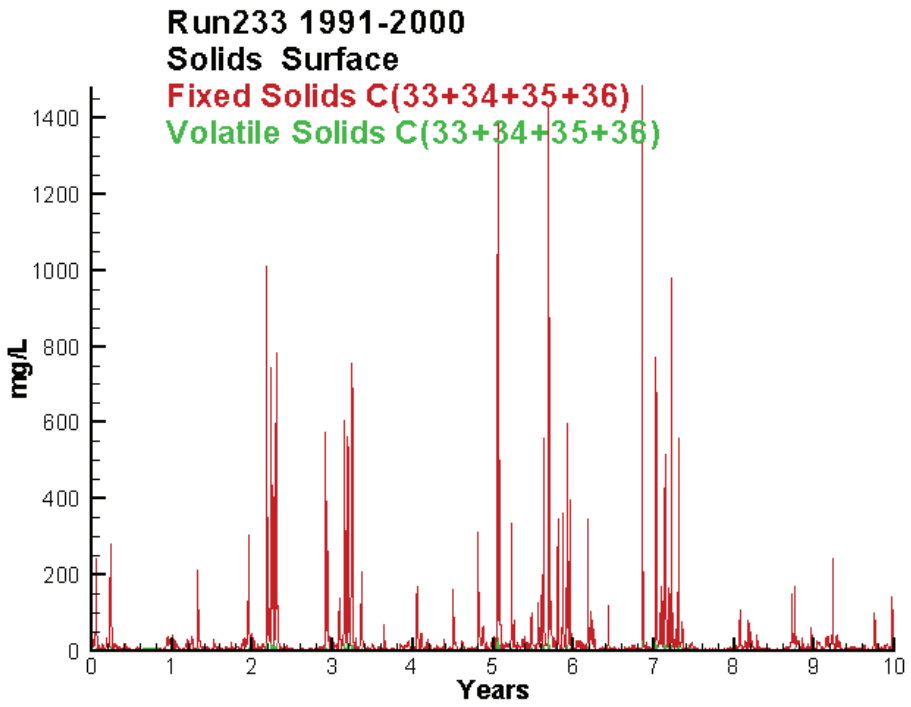

	Mean Difference	Absolute Mean Difference
KE	0.8490	1.3932
TSS	5.4176	20.5400

Station LE3.2

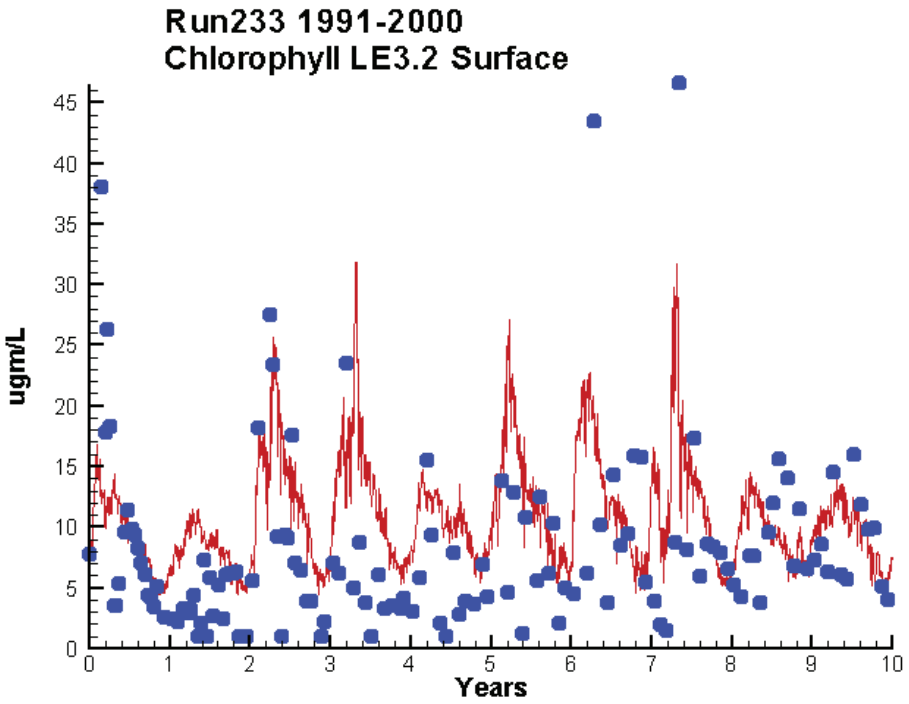

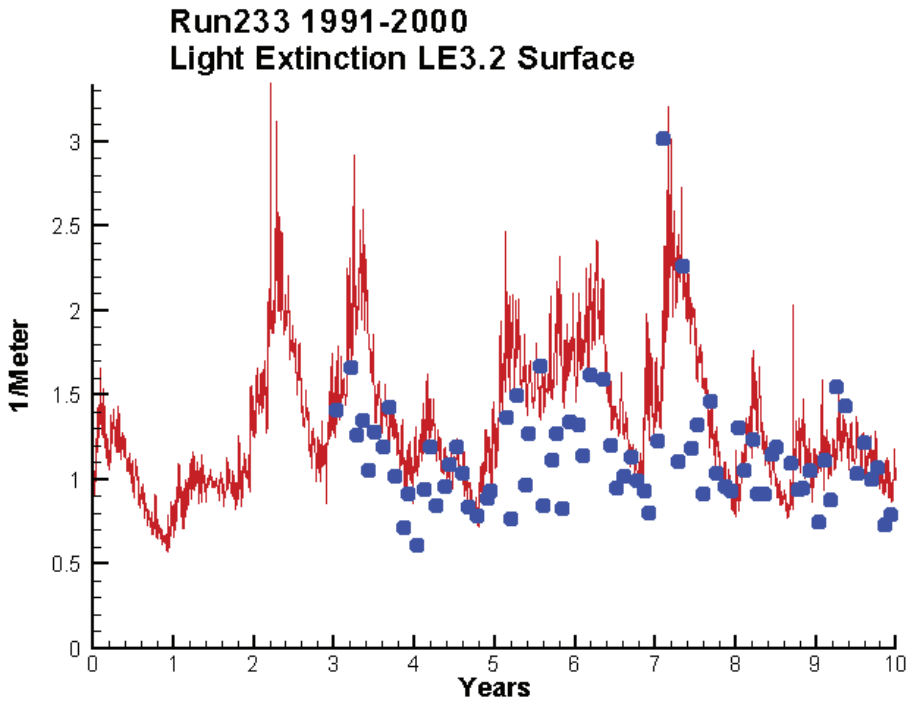

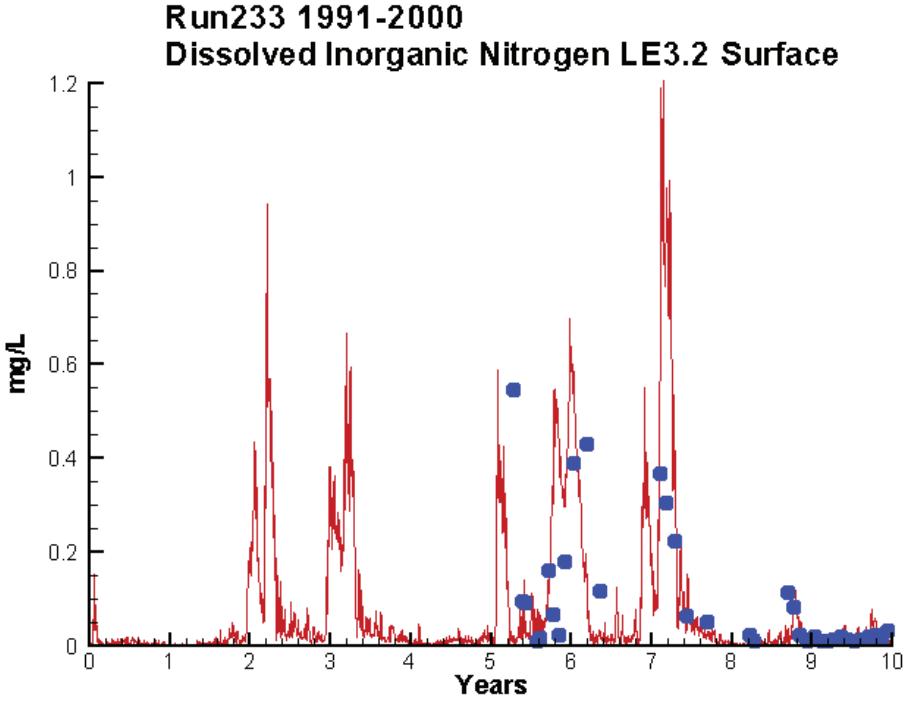

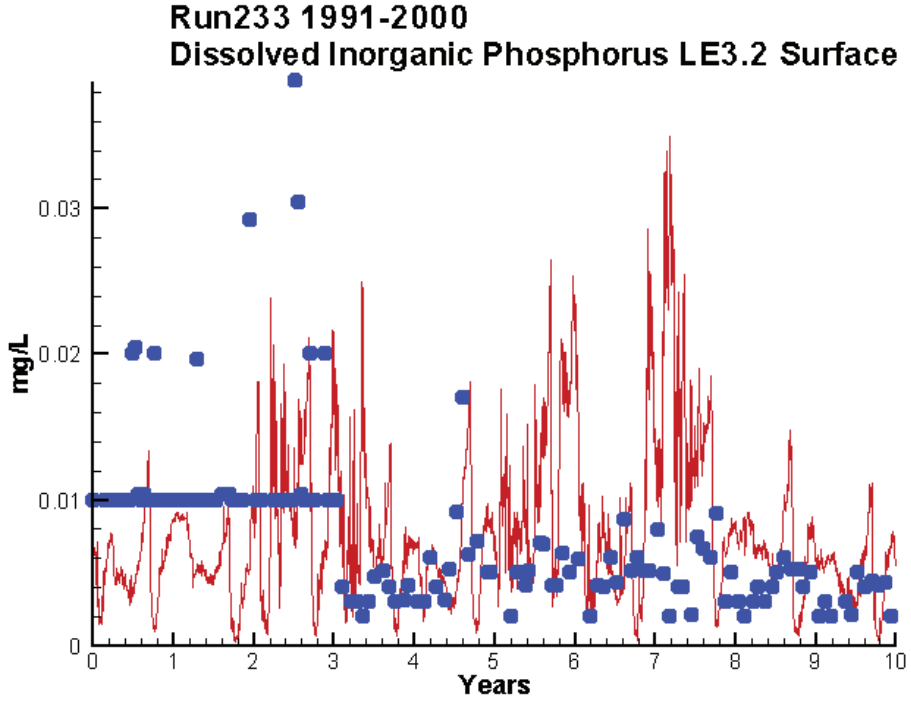

Station LE3.2

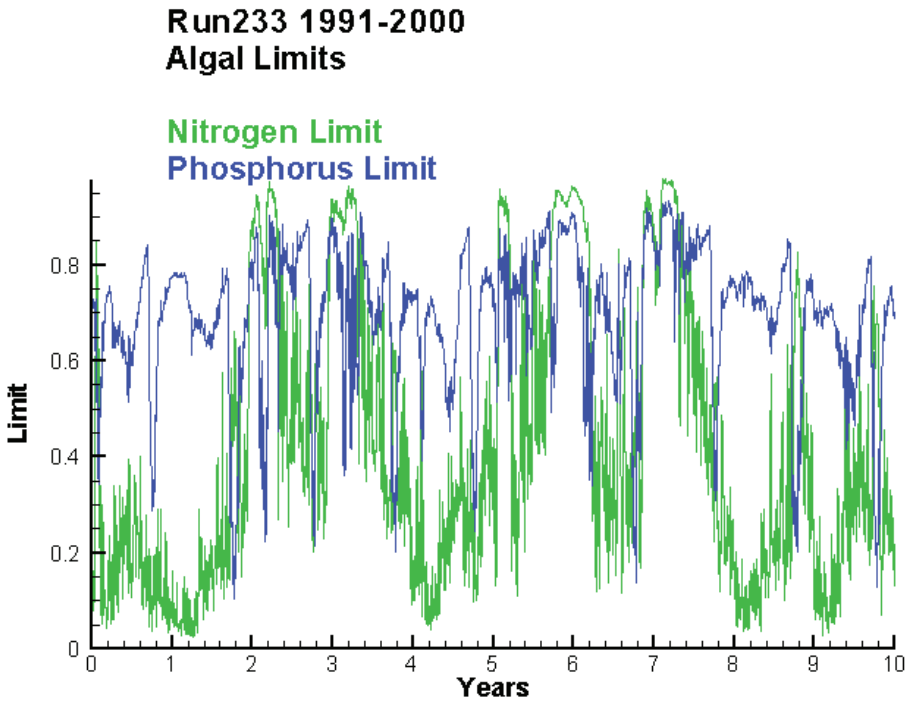

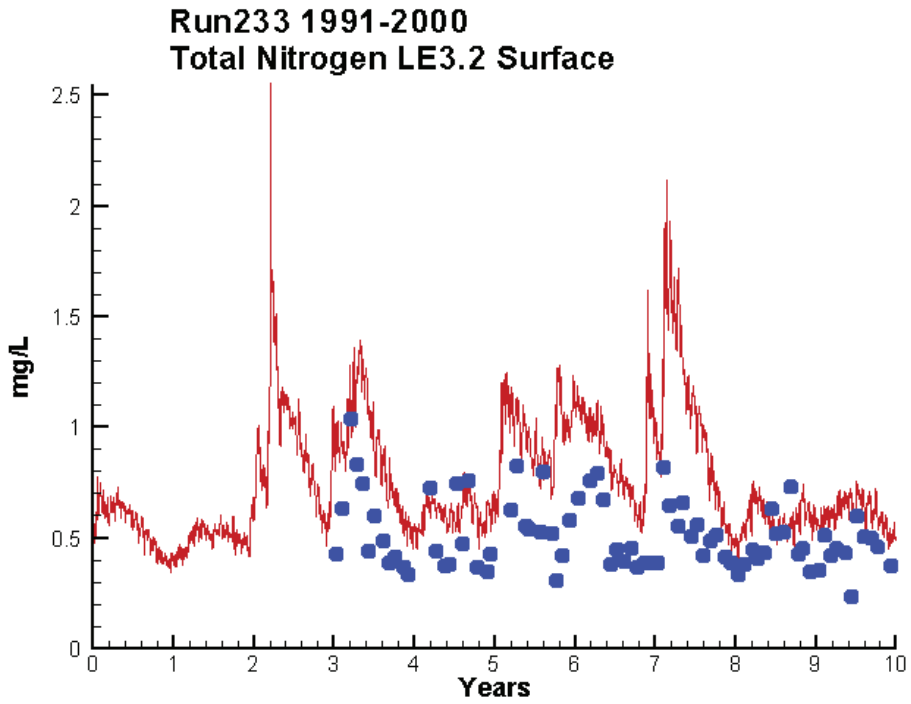

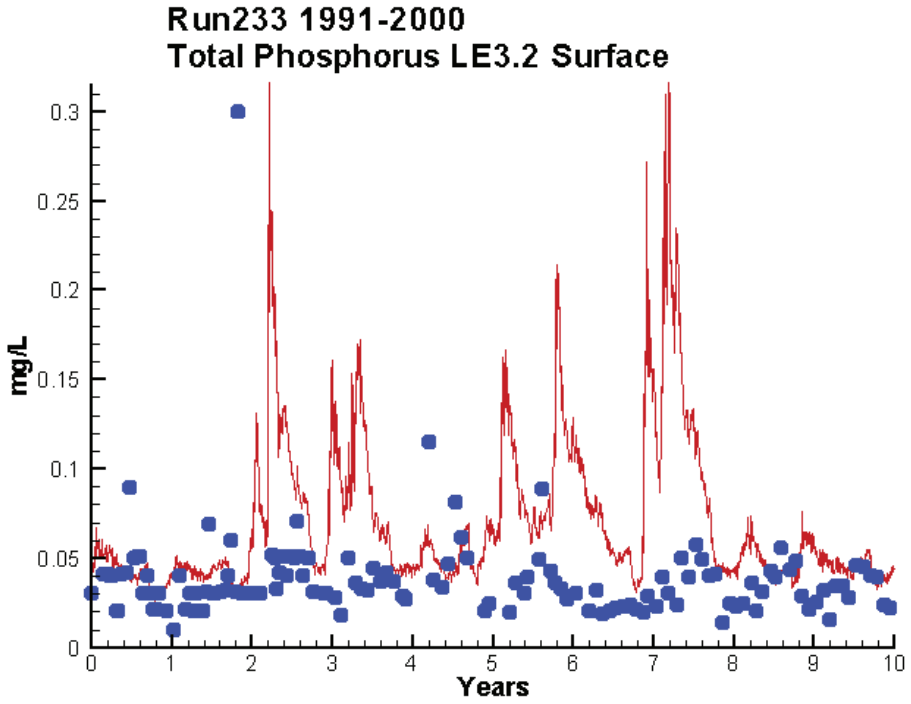

	Mean Difference	Absolute Mean Difference
Chl	2.5154	5.5955
DIN	0.0376	0.1158
KE	0.2626	0.3299
DIP	0.0002	0.0059
TP	0.0322	0.0402
TN	0.2998	0.3098

Station LE3.2

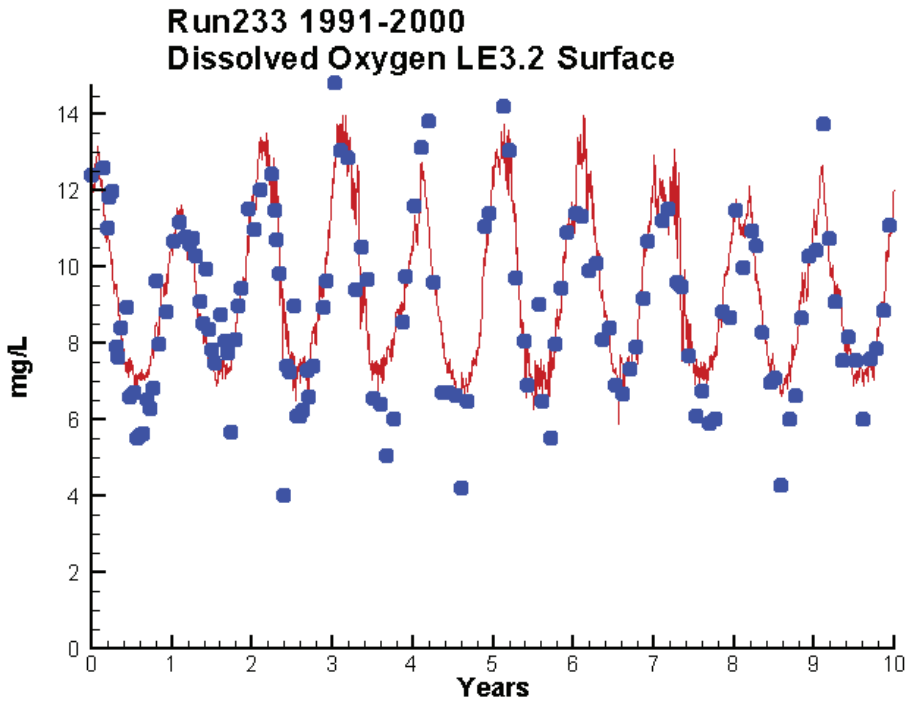

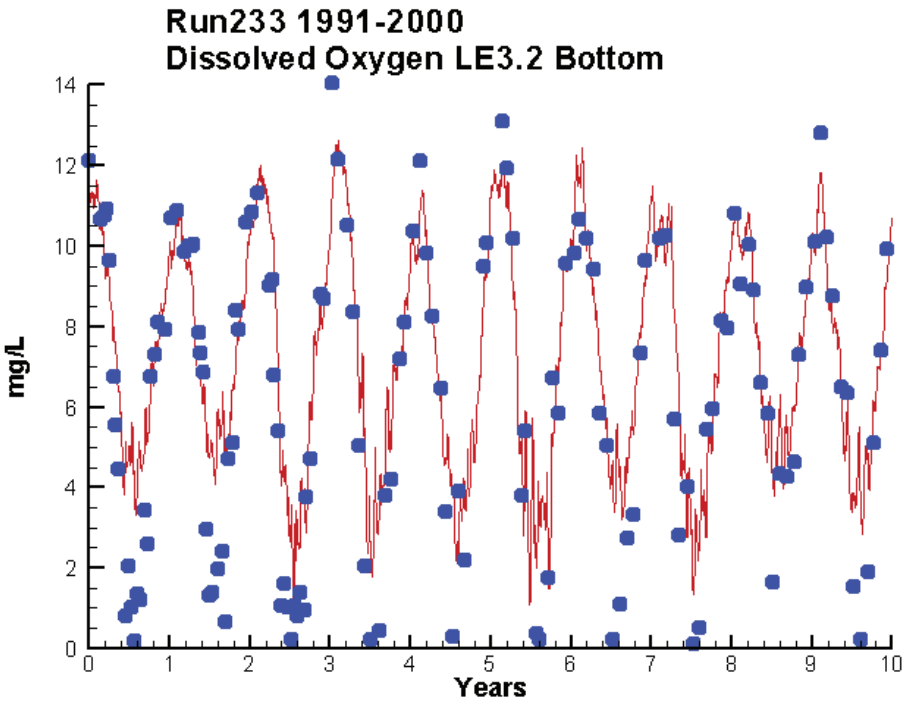

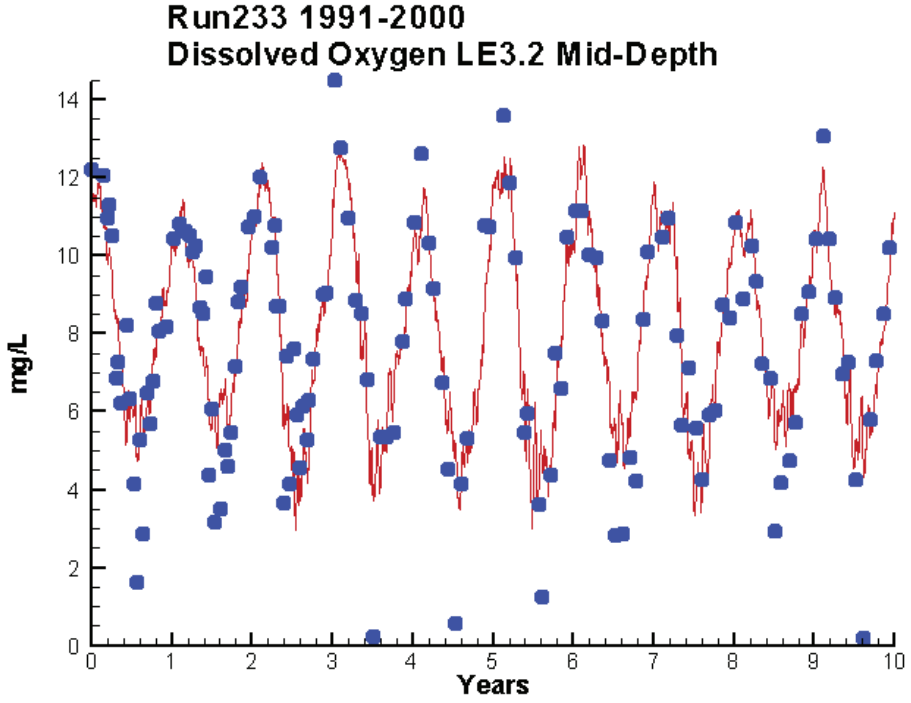

	Mean Difference	Absolute Mean Difference
Top DO	0.2991	0.8889
Mid DO	0.1937	0.9801
Bot DO	0.8060	1.3243

Station LE3.2

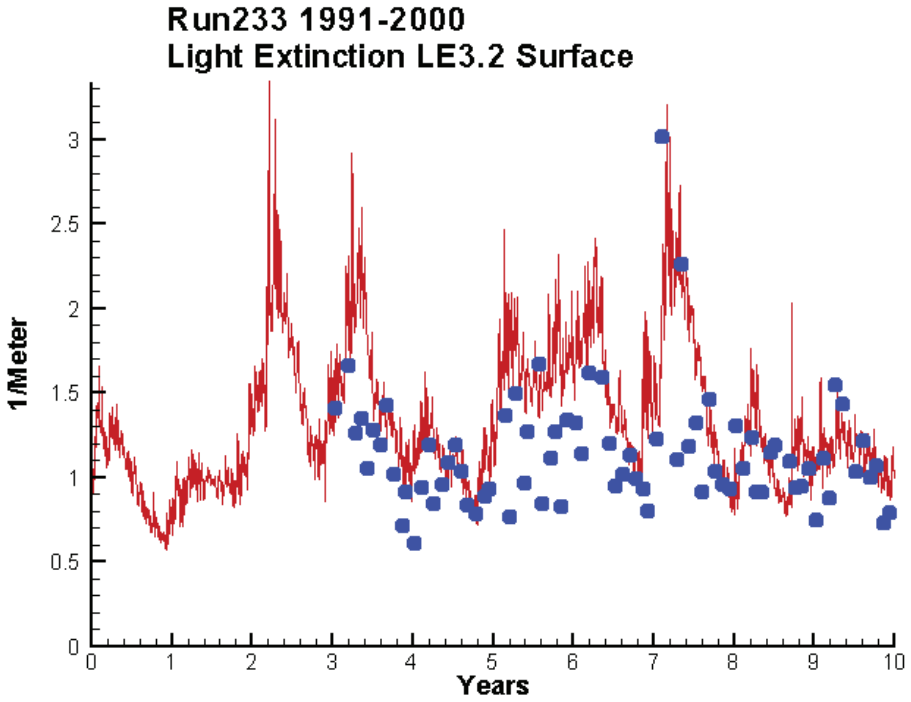

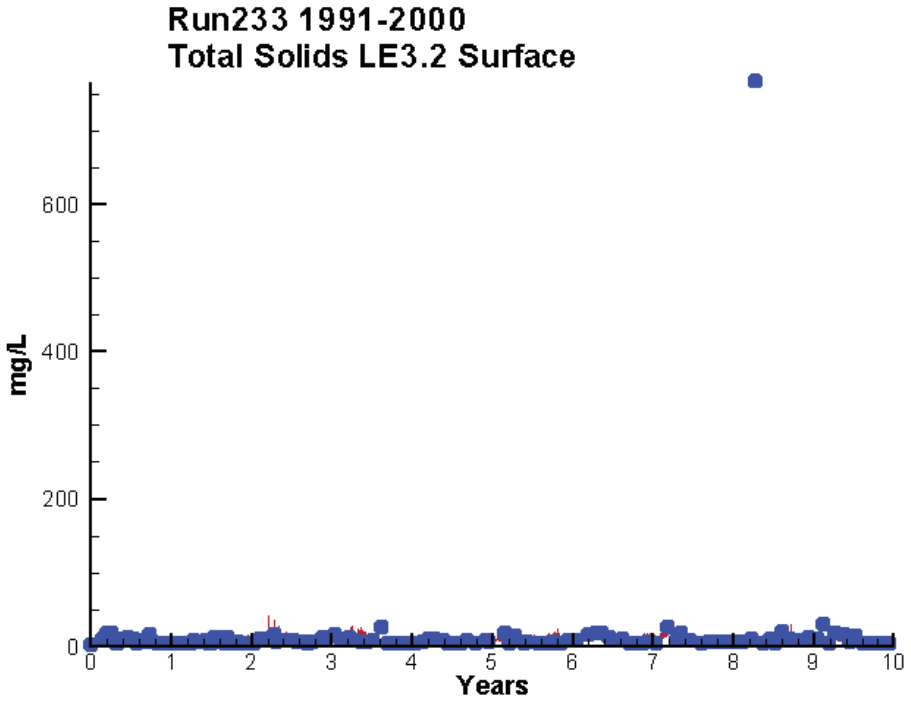

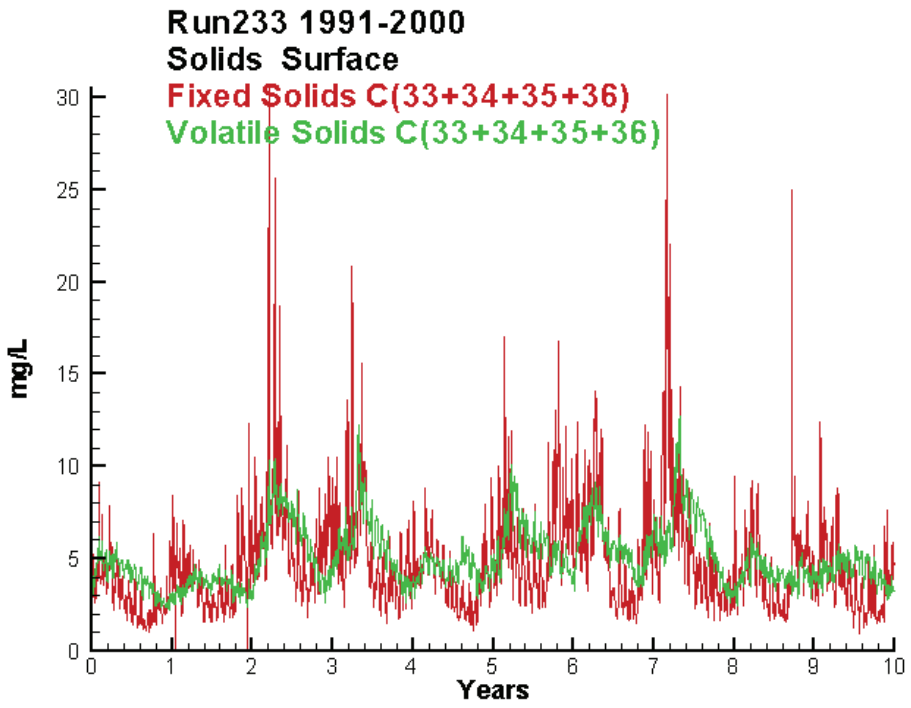

	Mean Difference	Absolute Mean Difference
KE	0.2626	0.3299
TSS	-3.4280	9.8351

Station RET3.2

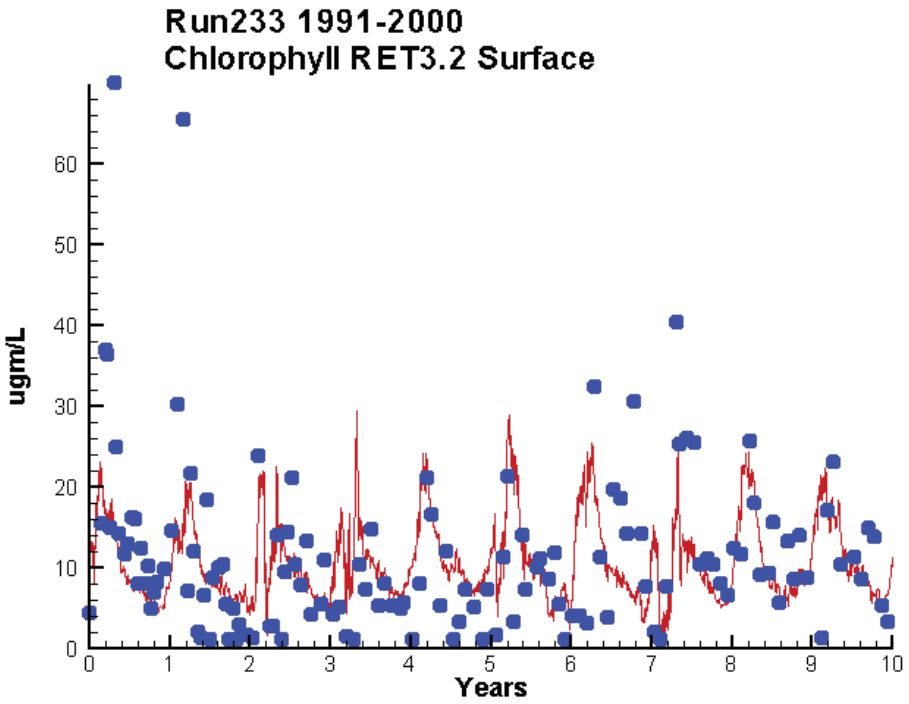

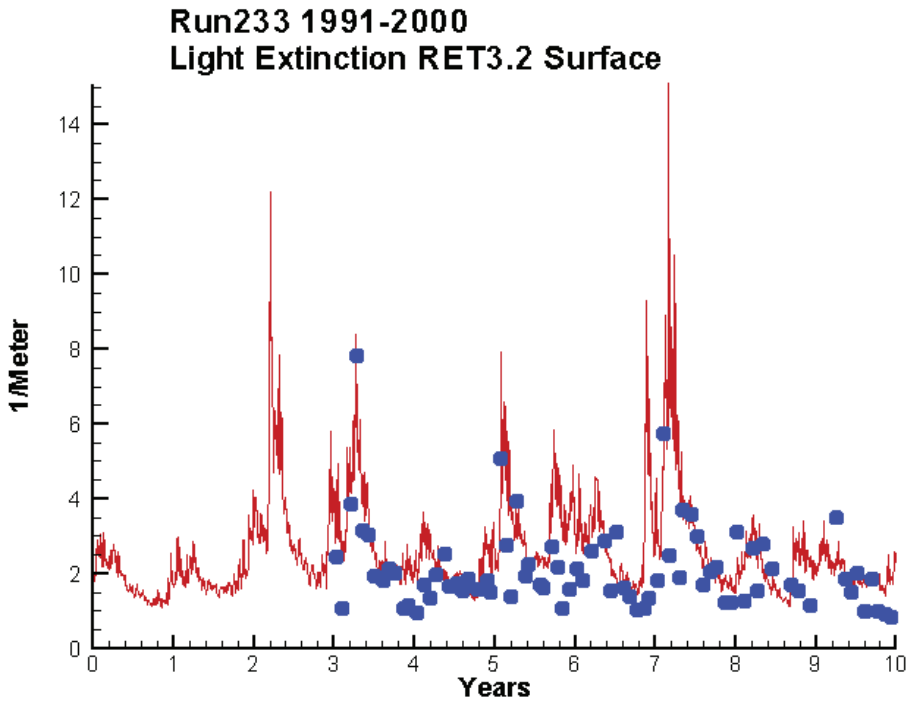

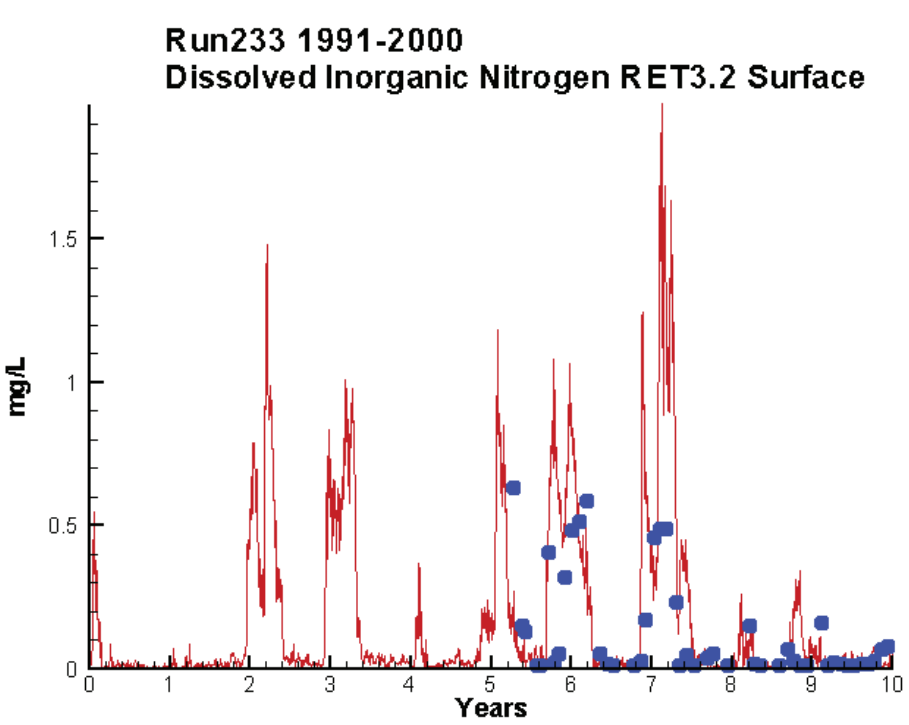

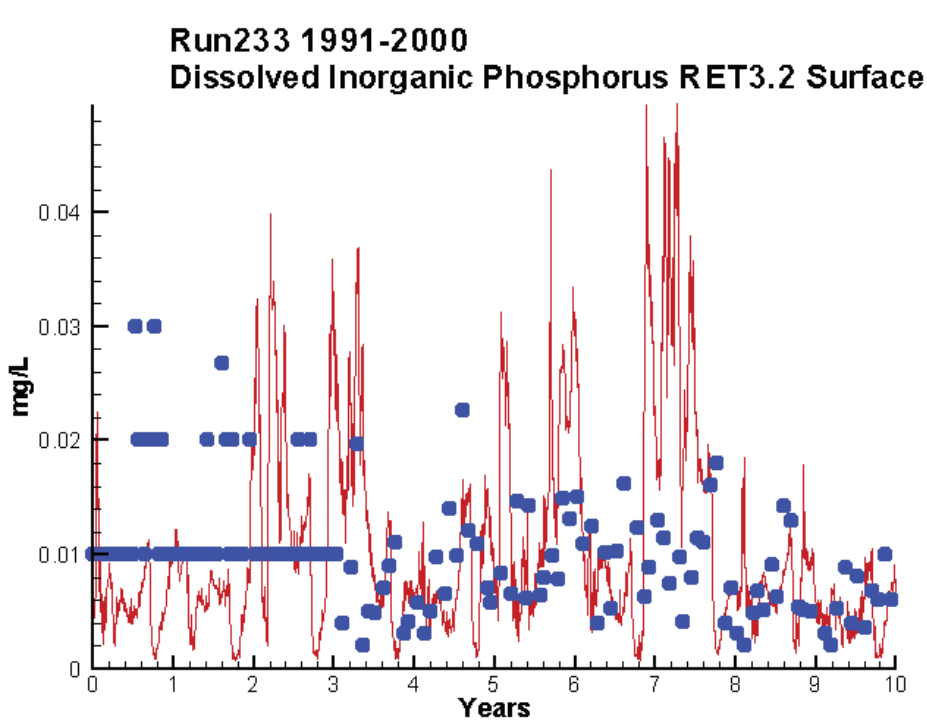

Station RET3.2

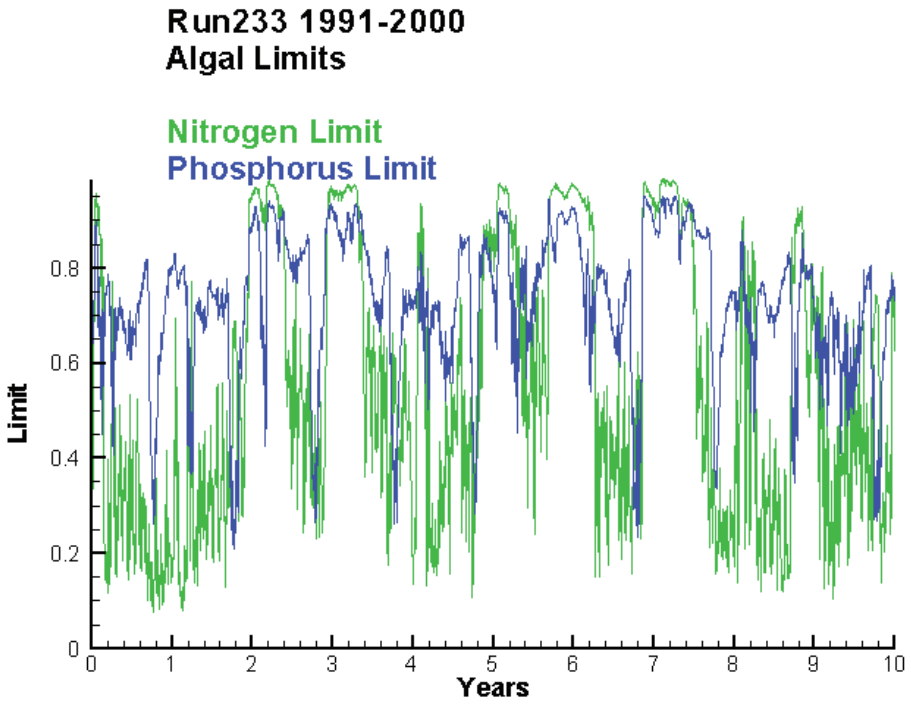

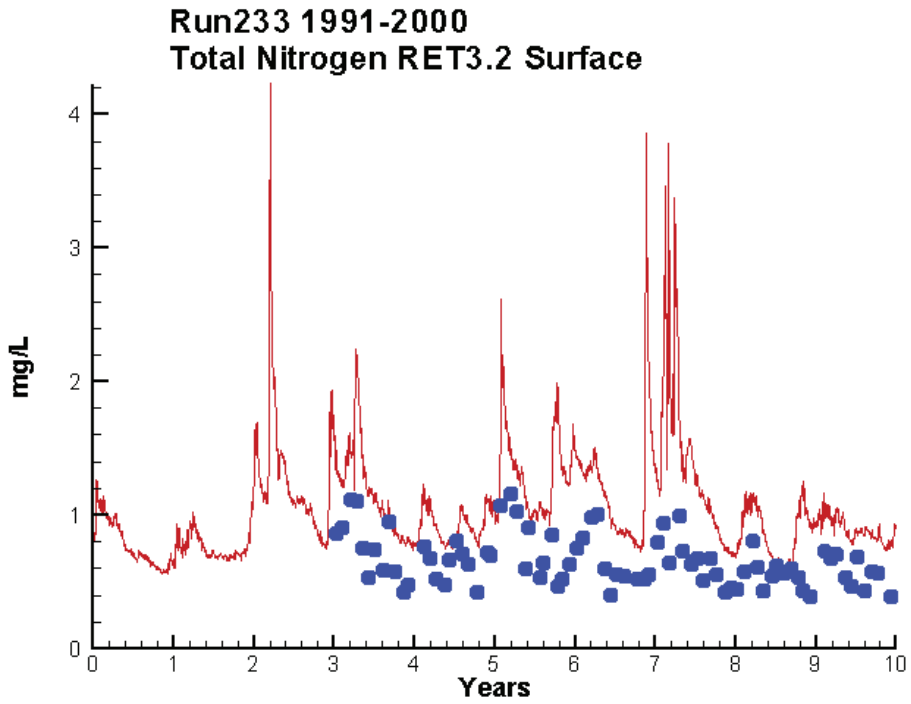

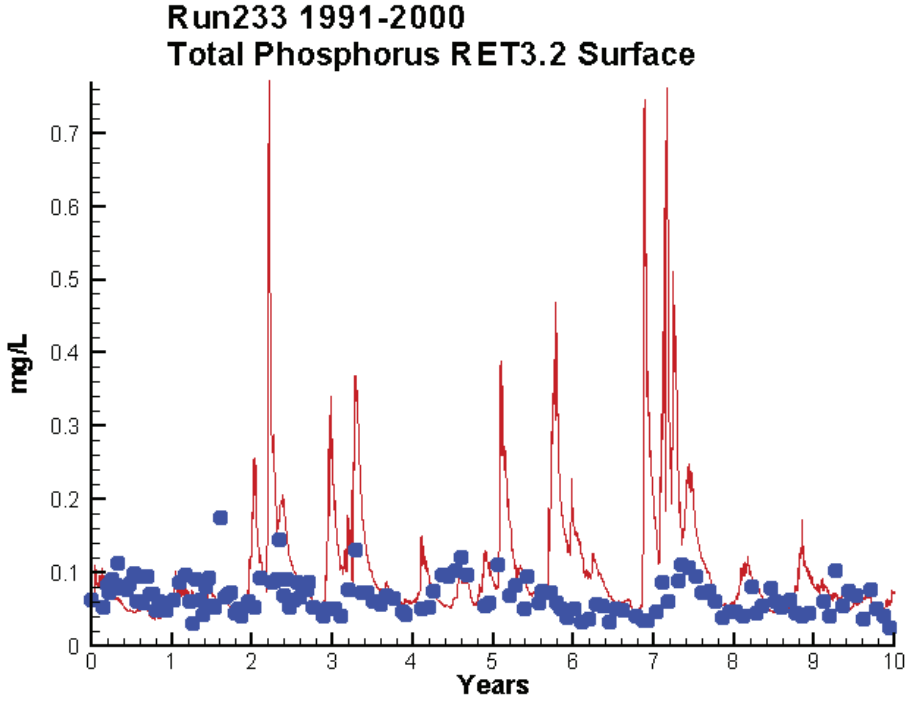

	Mean Difference	Absolute Mean Difference
Chl	-0.9499	6.2753
DIN	0.0938	0.1643
KE	0.7036	0.9236
DIP	0.0002	0.0076
TP	0.0341	0.0489
TN	0.4679	0.4679

Station RET3.2

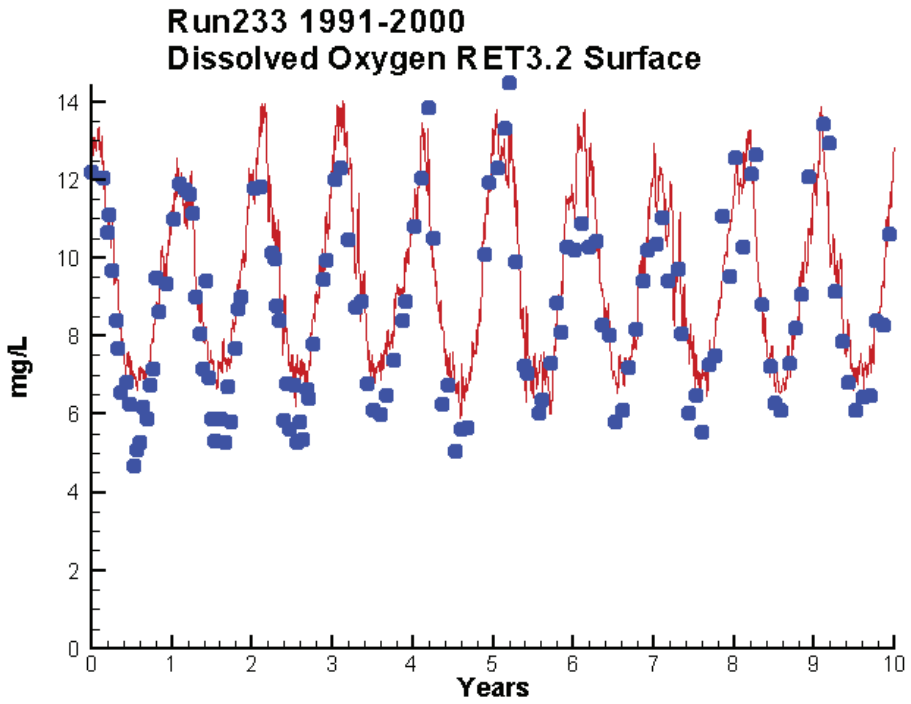

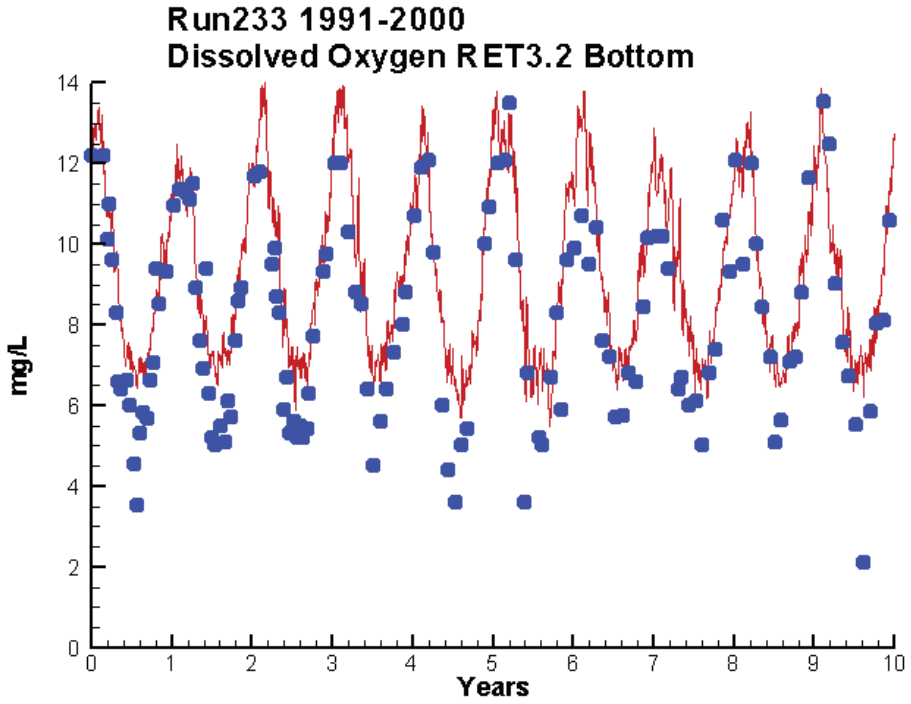

	Mean Difference	Absolute Mean Difference
Top DO	0.6704	0.9732
Bot DO	1.0778	1.2355

Station RET3.2

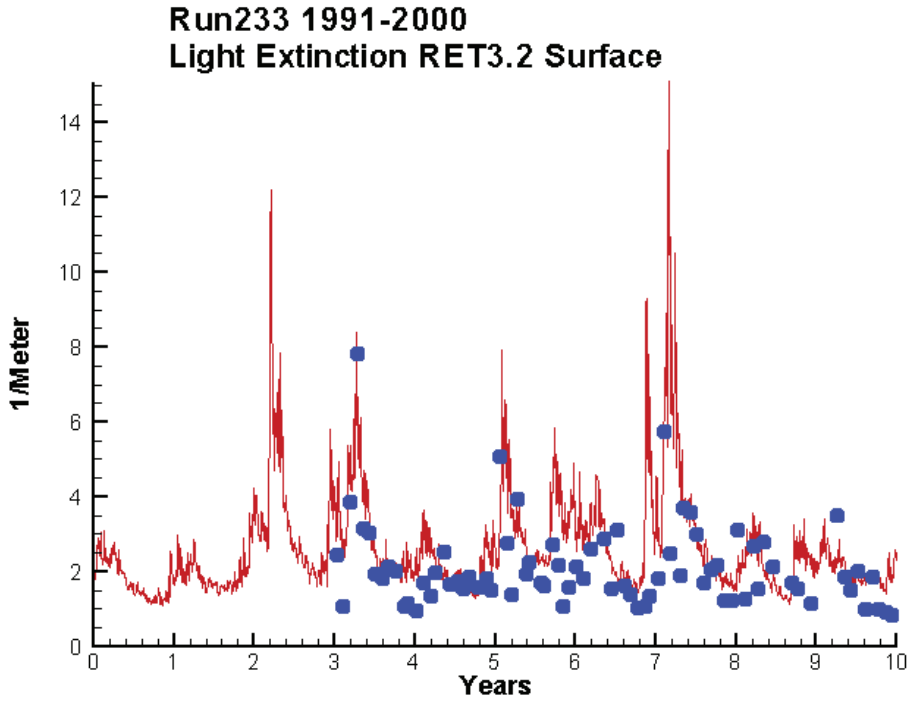

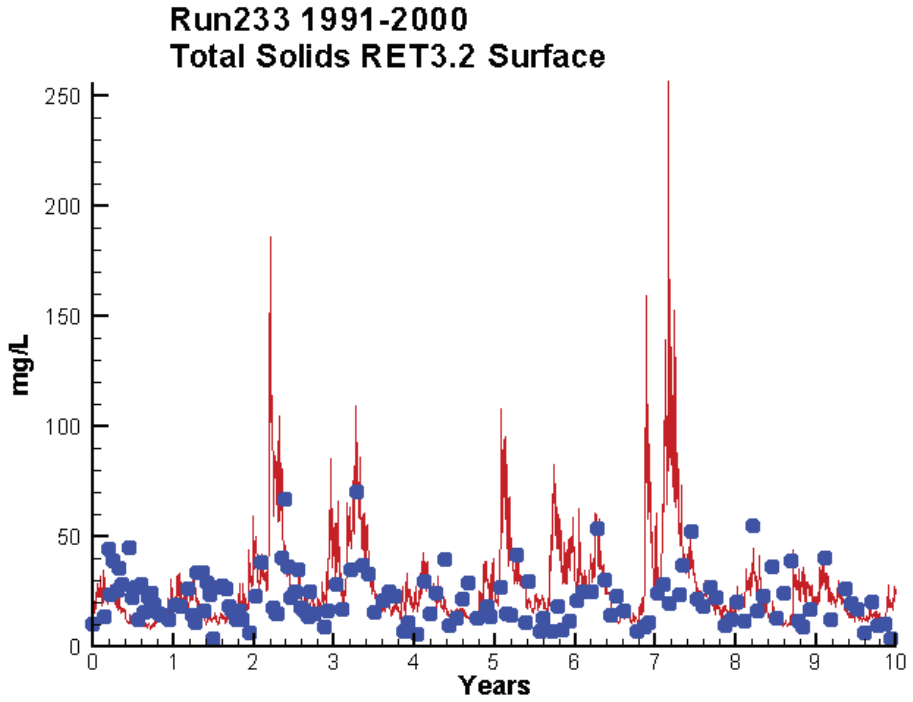

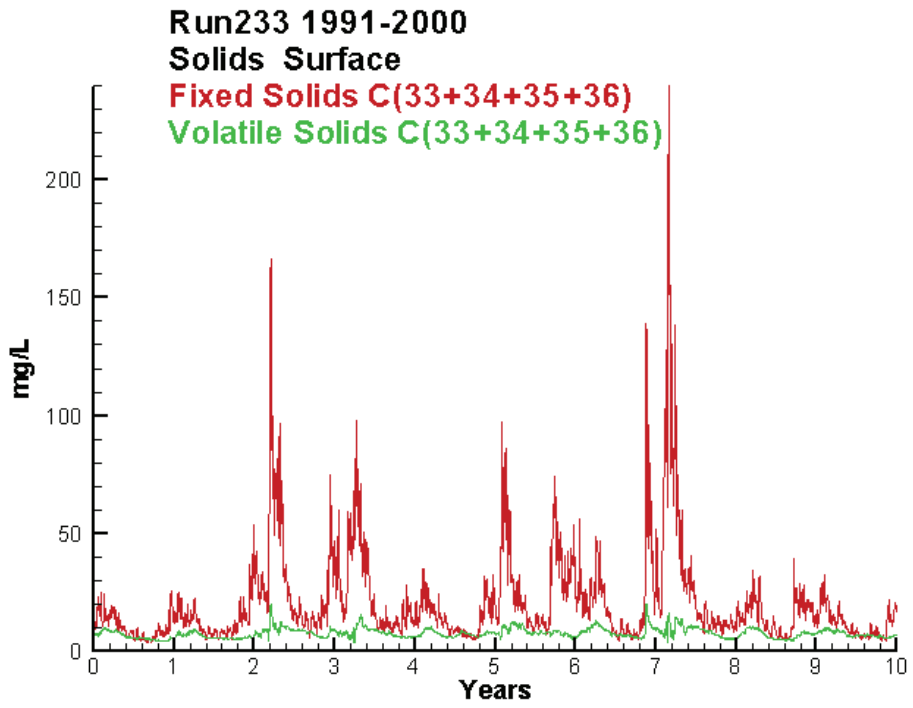

	Mean Difference	Absolute Mean Difference
KE	0.7036	0.9236
TSS	5.1354	13.1470

Station TF3.3

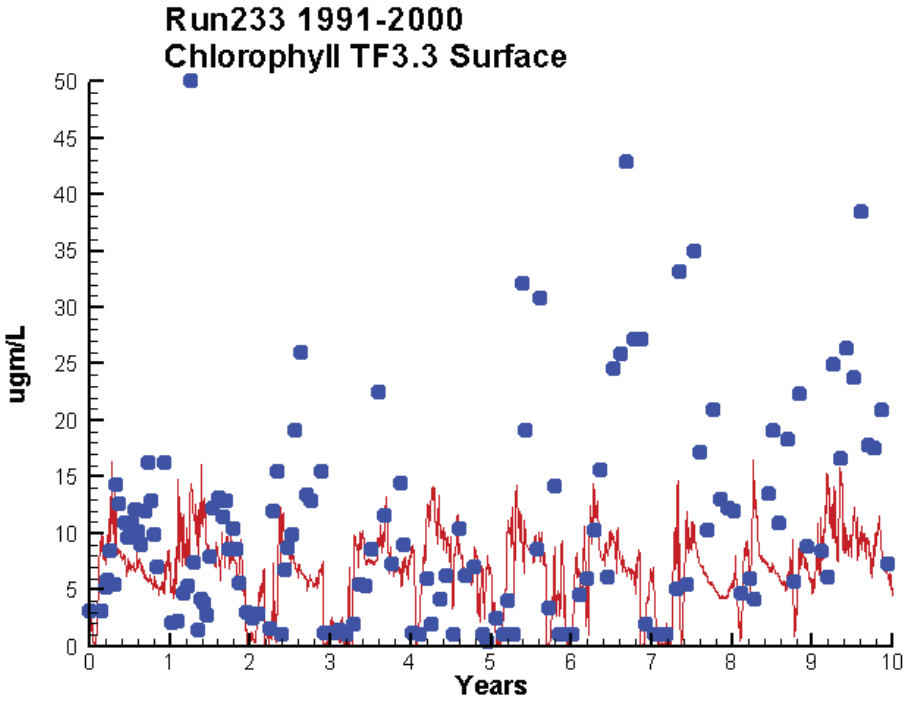

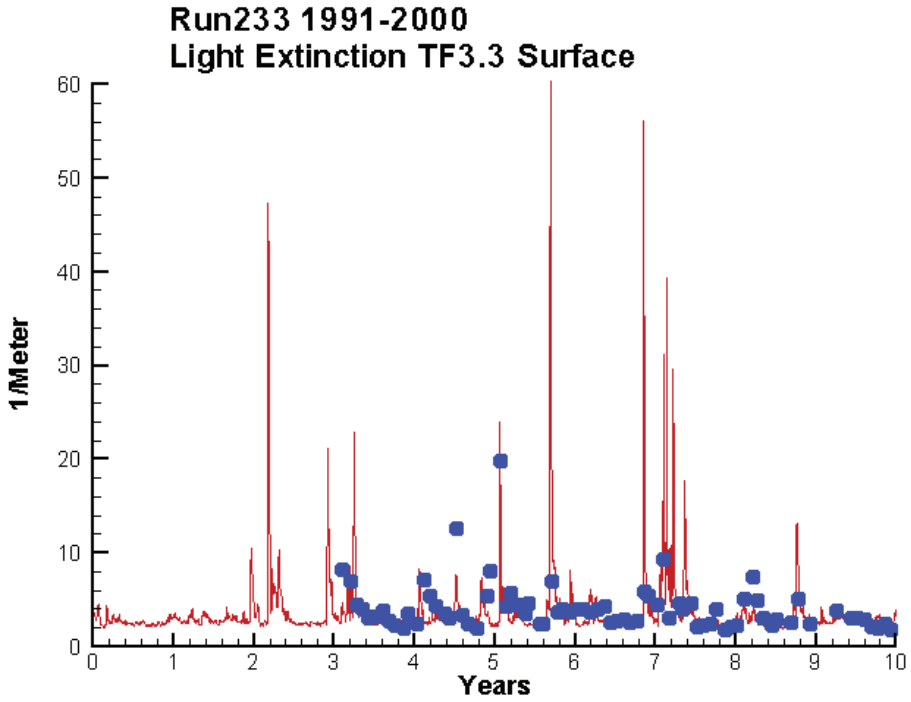

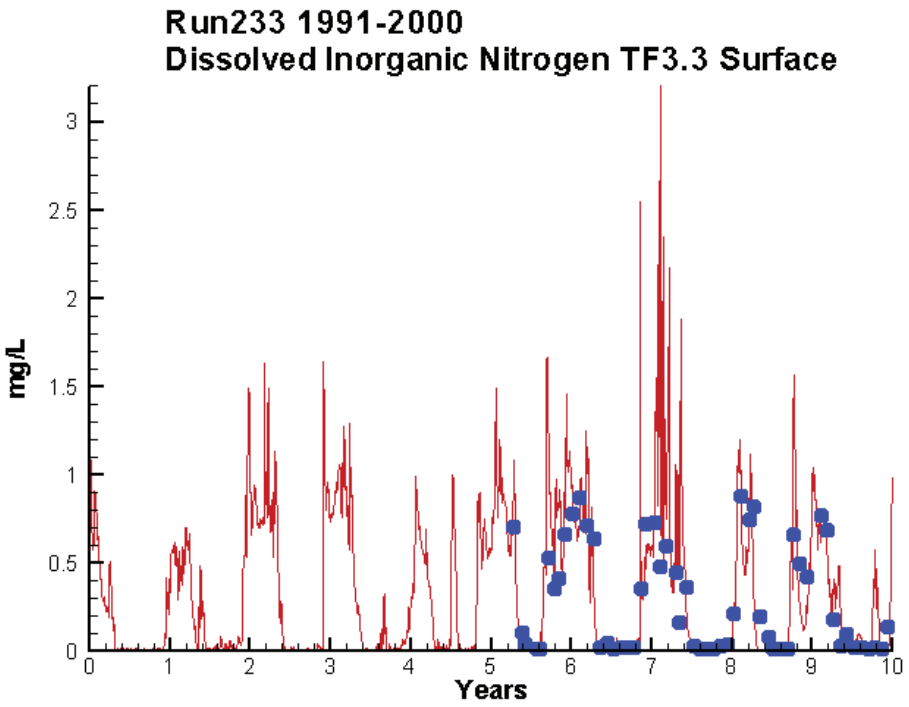

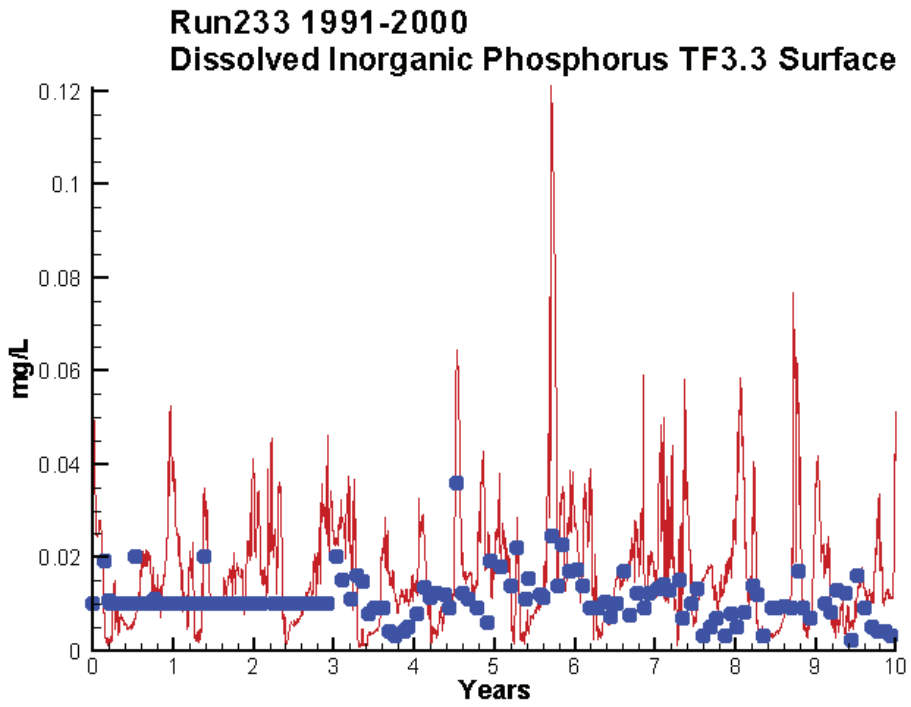

Station TF3.3

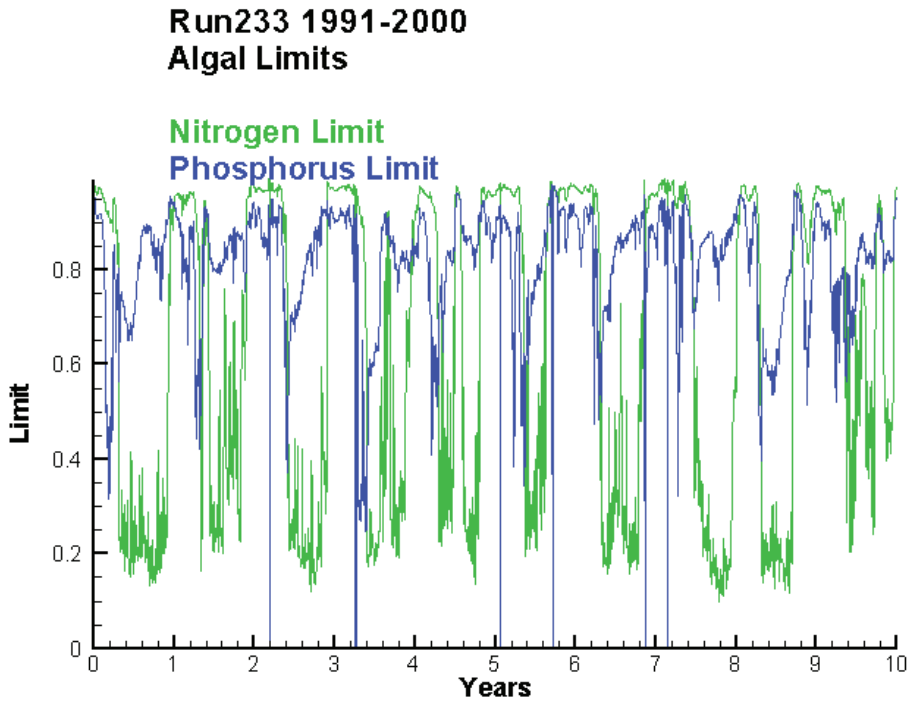

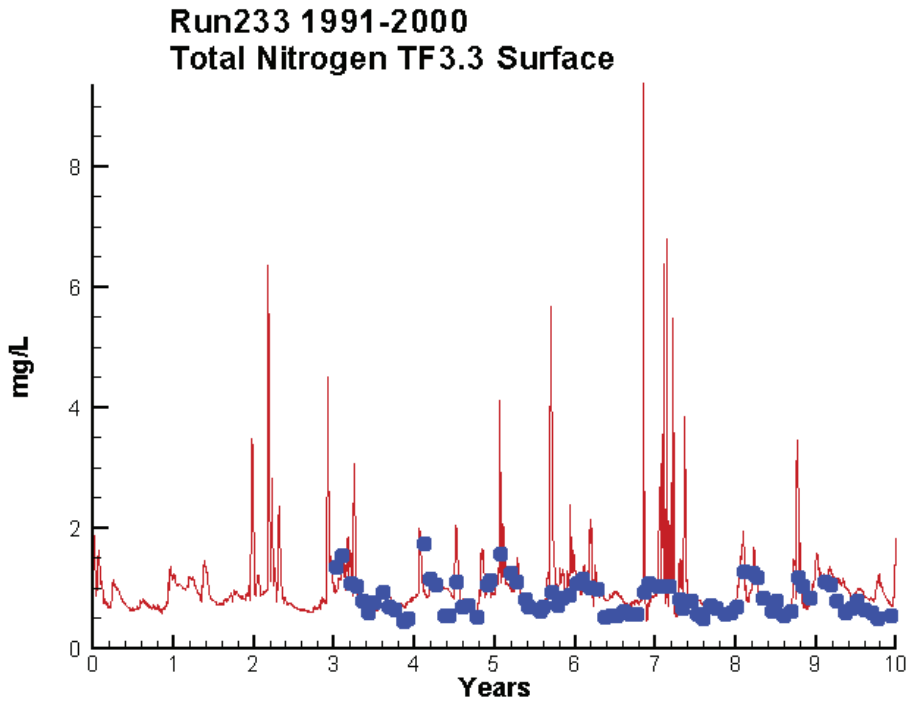

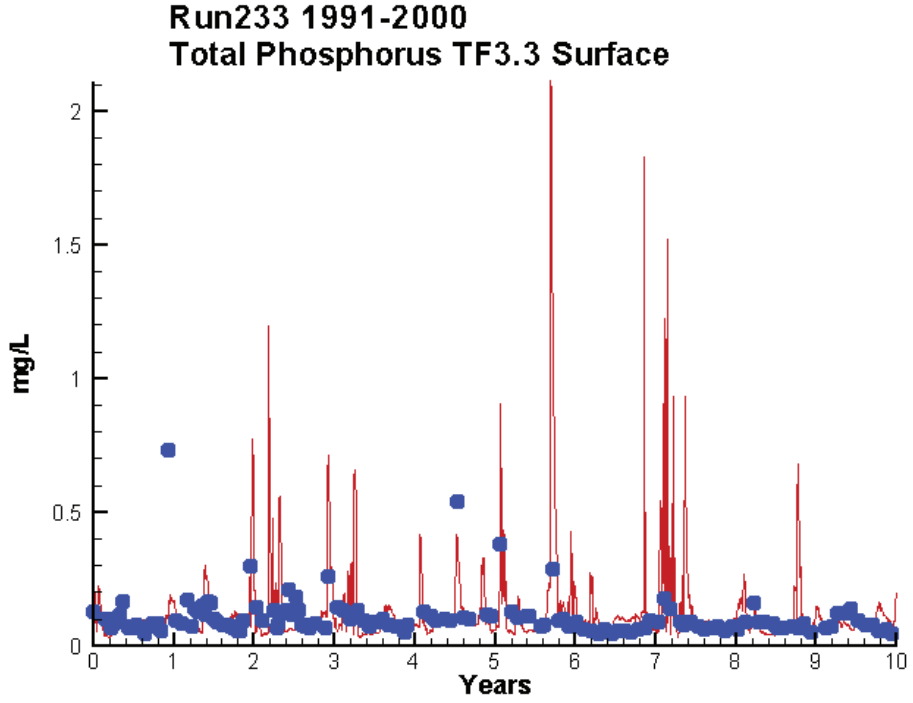

	Mean Difference	Absolute Mean Difference
Chl	-3.4971	6.6671
DIN	0.0550	0.1650
KE	-0.3339	1.3611
DIP	0.0054	0.0087
TP	0.0188	0.0647
TN	0.1737	0.2716

Station TF3.3

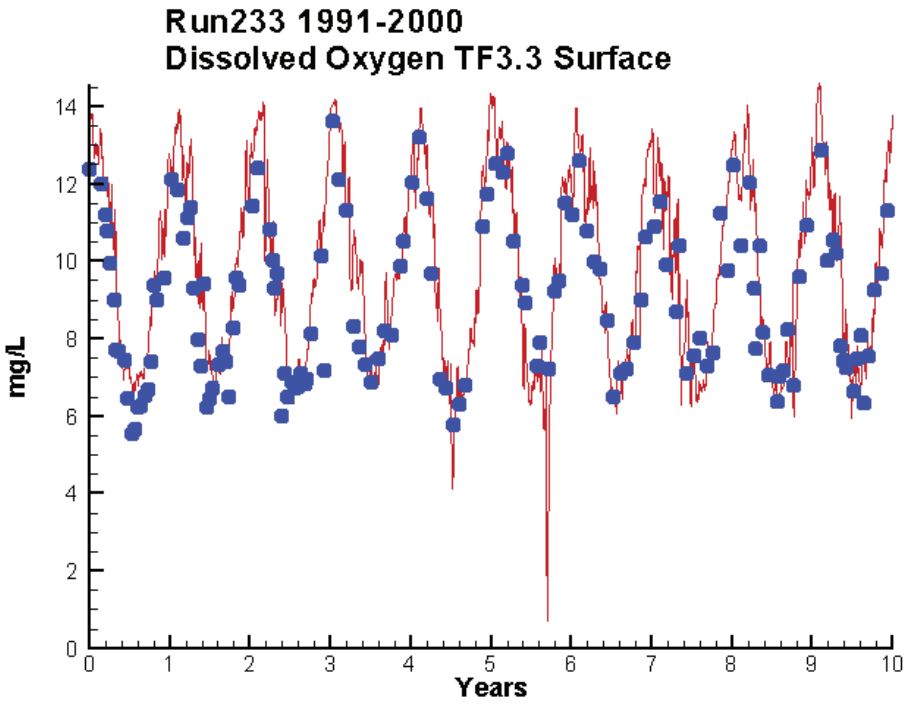

	Mean Difference	Absolute Mean Difference
Top DO	0.6429	0.9029

Station TF3.3

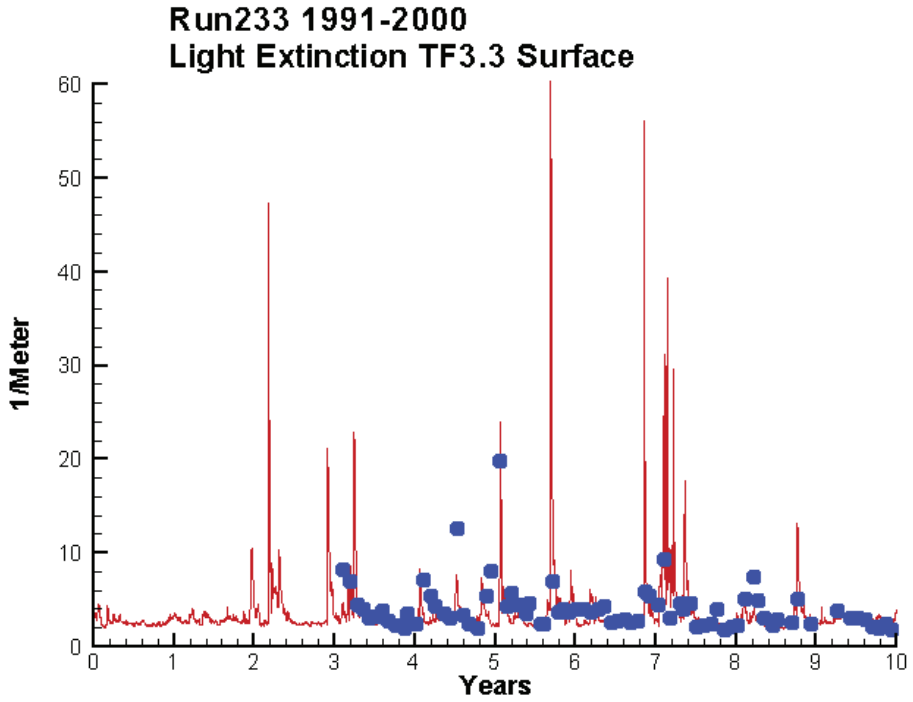

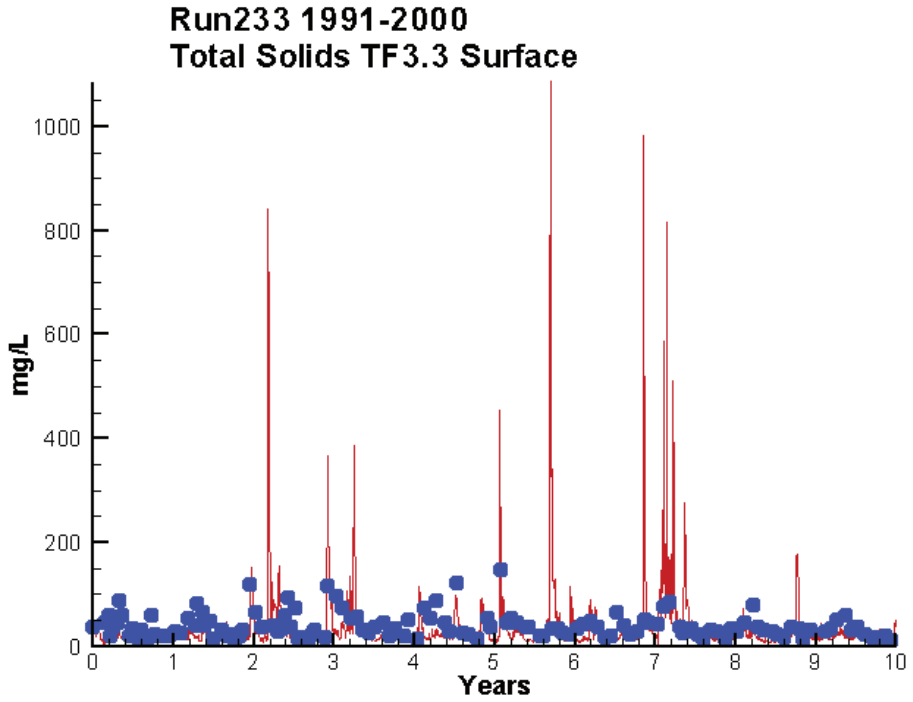

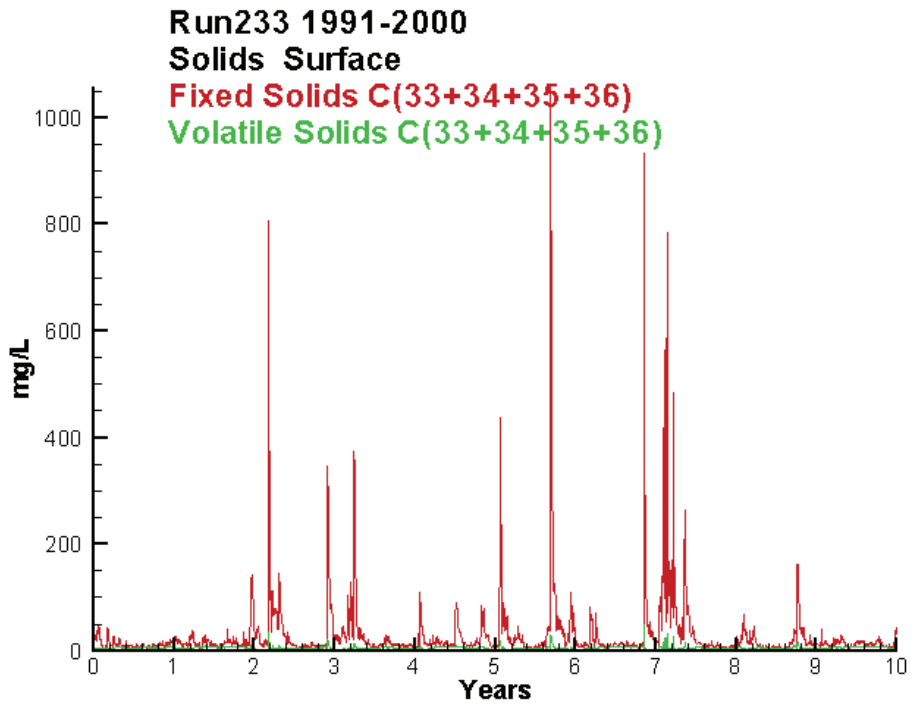

	Mean Difference	Absolute Mean Difference
KE	-0.3339	1.3611
TSS	-5.1986	23.3671

Station LE4.2

Run233 1991-2000
Chlorophyll LE4.2 Surface

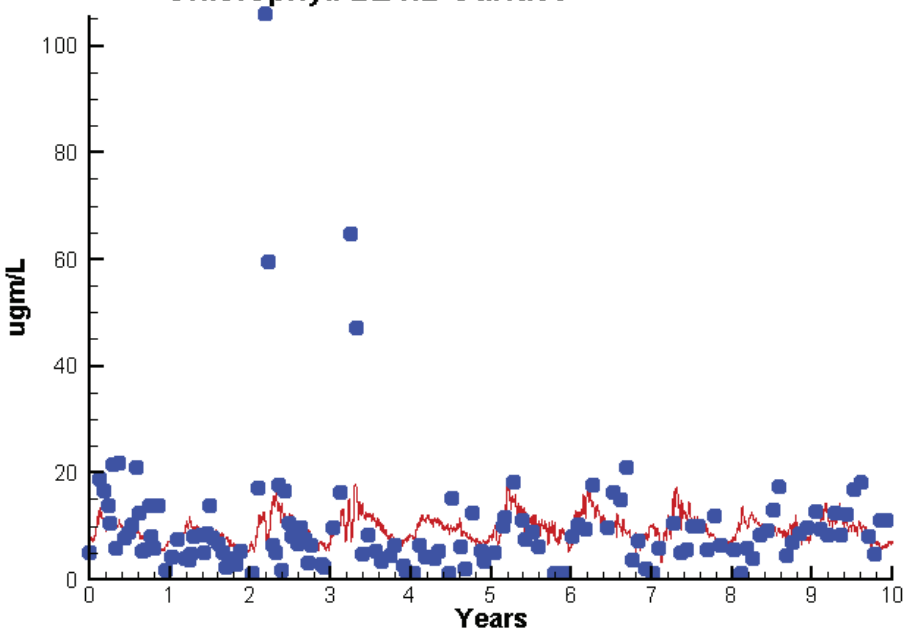

Run233 1991-2000
Light Extinction LE4.2 Surface

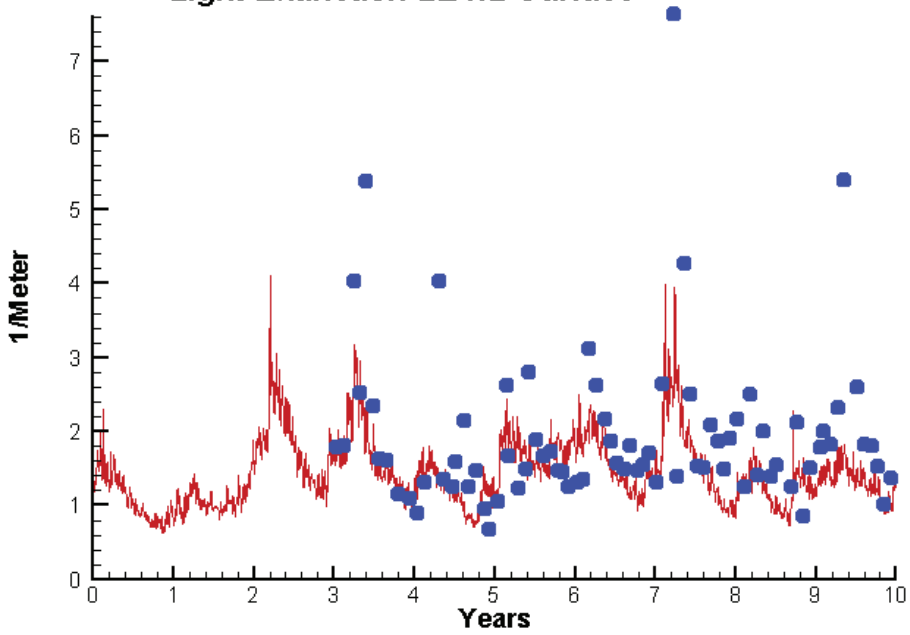

Run233 1991-2000
Dissolved Inorganic Nitrogen LE4.2 Surface

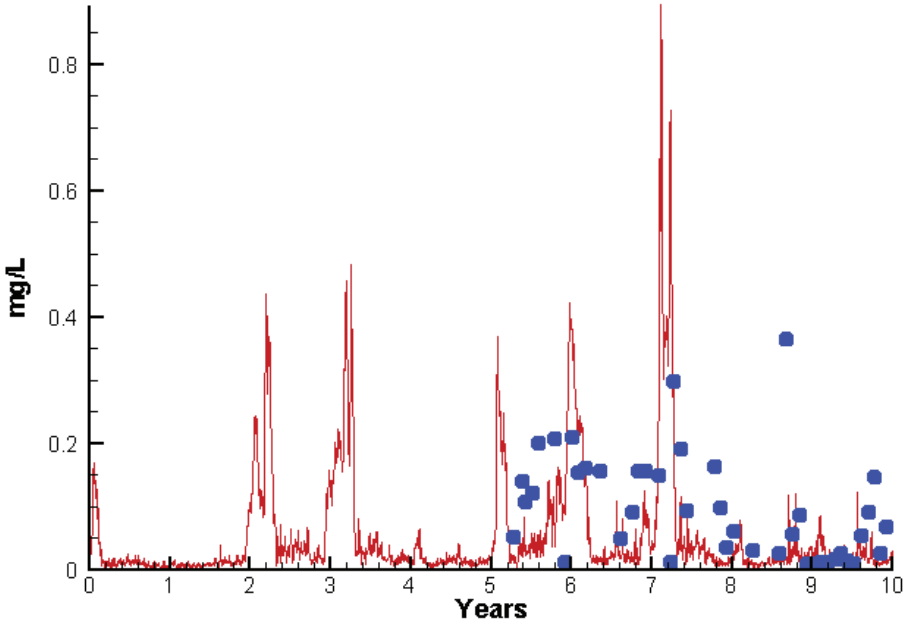

Run233 1991-2000
Dissolved Inorganic Phosphorus LE4.2 Surface

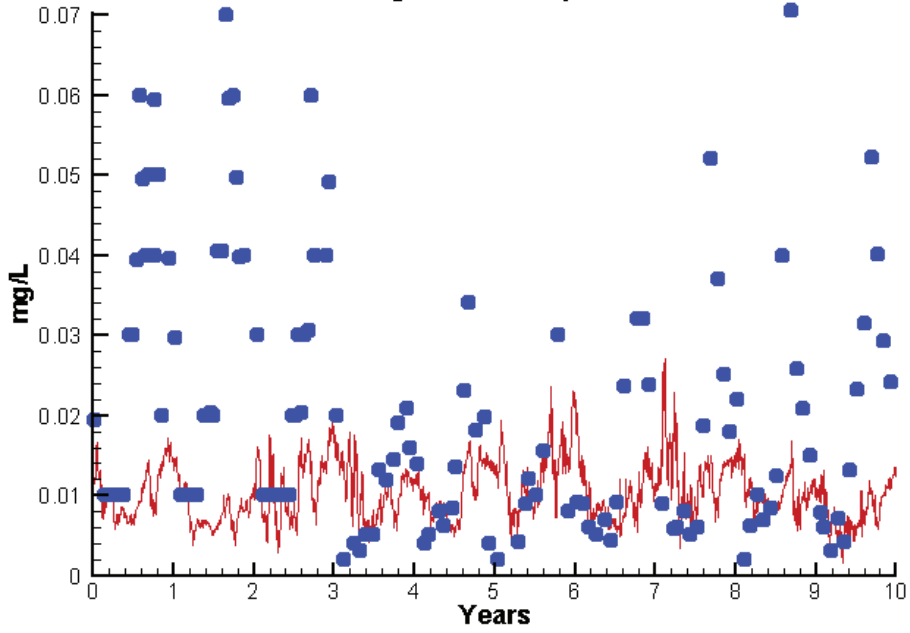

Station LE4.2

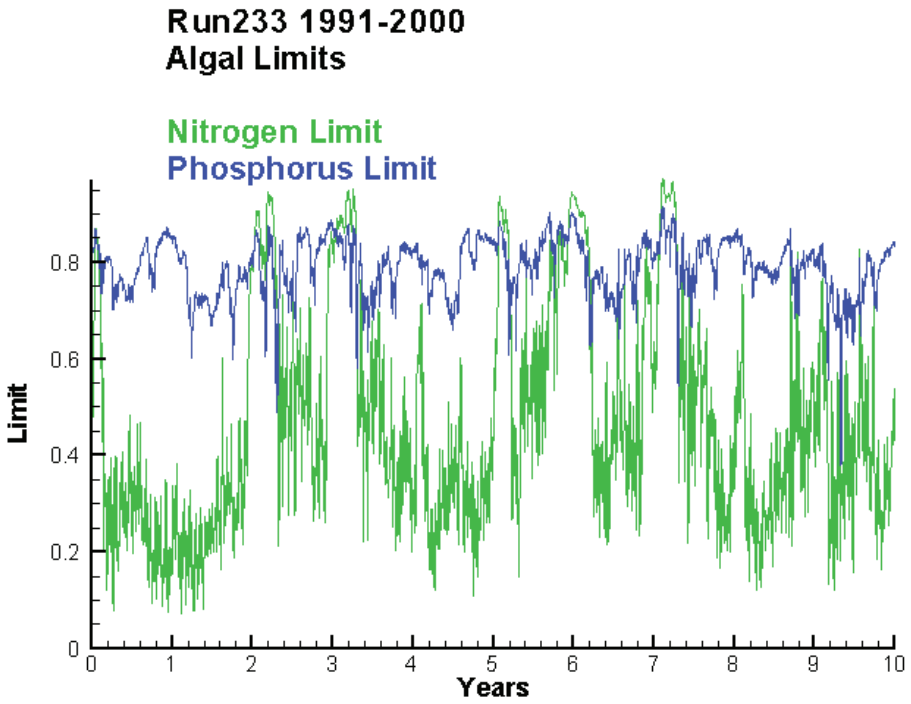

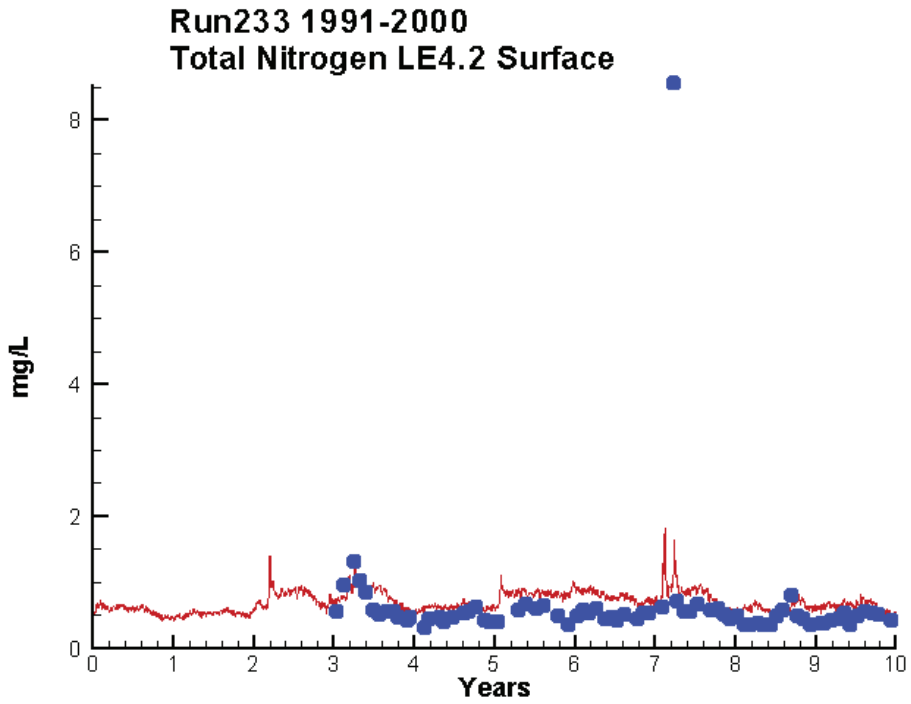

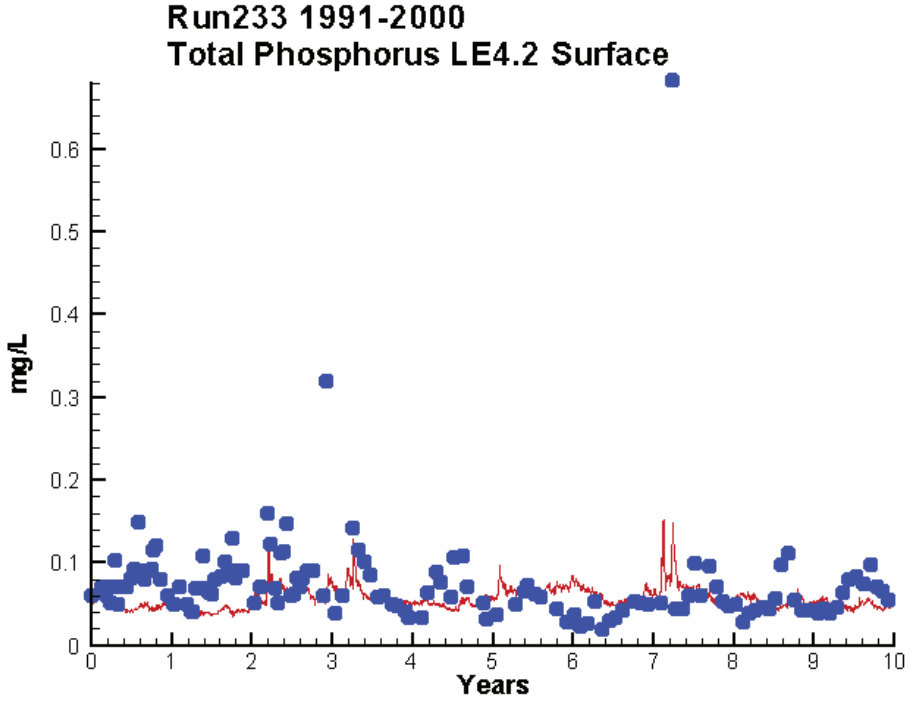

	Mean Difference	Absolute Mean Difference
Chl	-0.4325	5.7484
DIN	-0.0186	0.0950
KE	-0.4321	0.6198
DIP	-0.0108	0.0136
TP	-0.0179	0.0309
TN	0.1069	0.3168

Station LE4.2

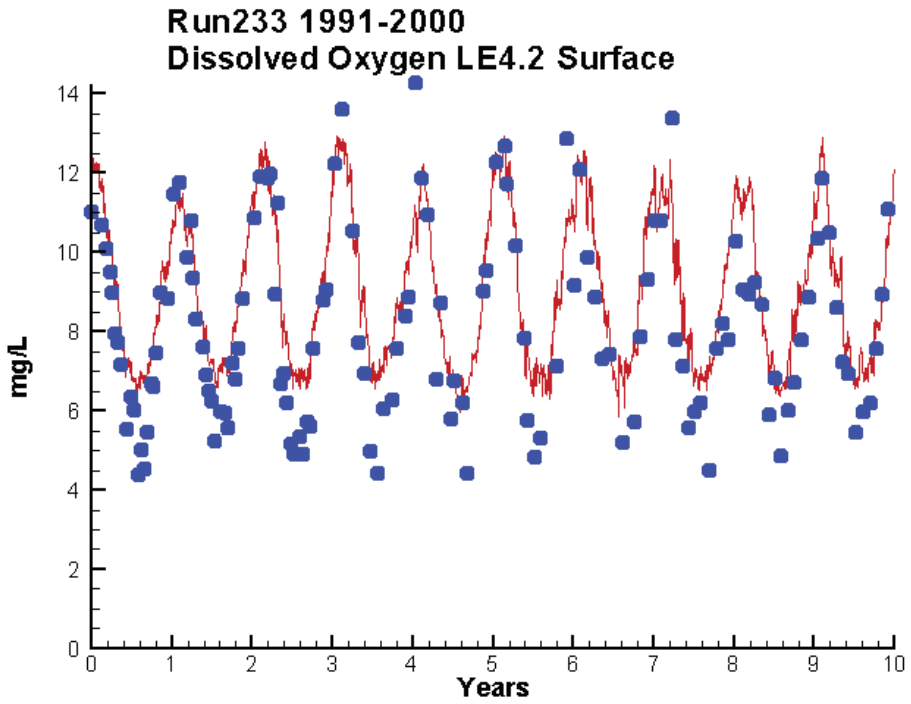

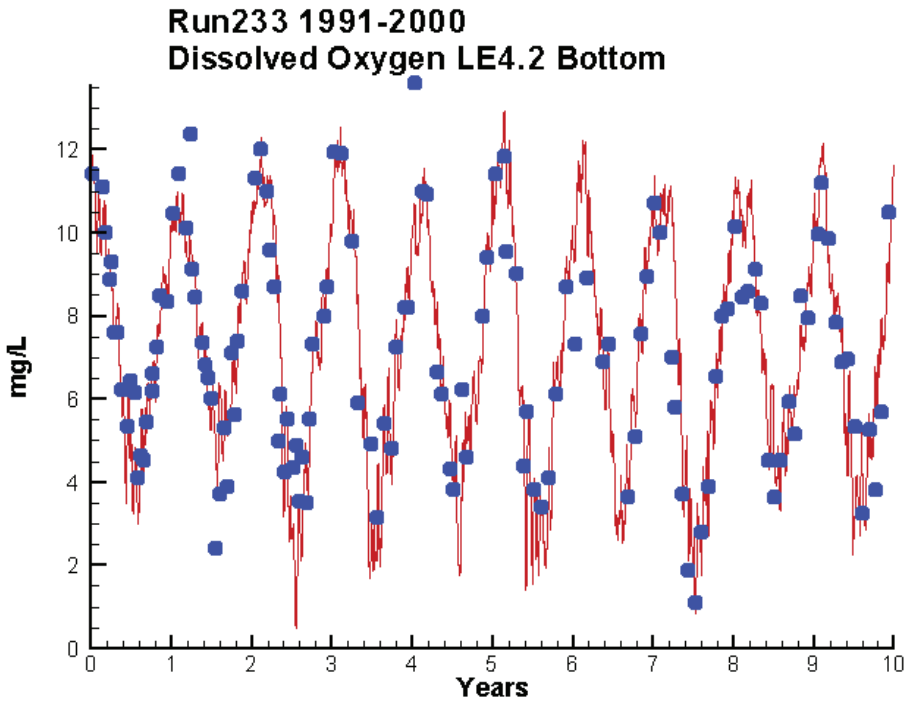

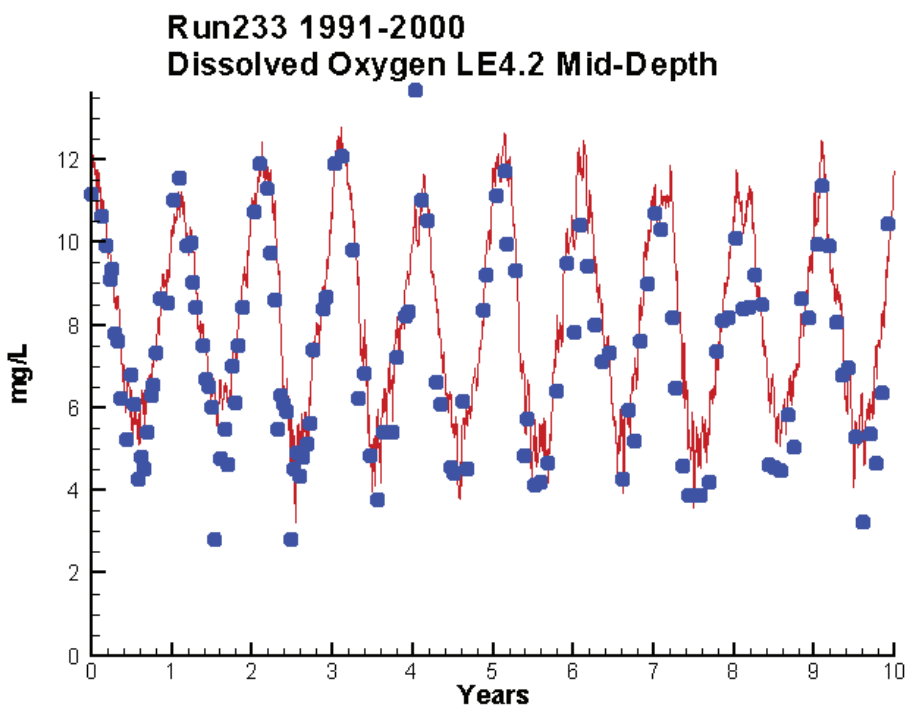

	Mean Difference	Absolute Mean Difference
Top DO	0.9169	1.1479
Mid DO	0.8456	0.9631
Bot DO	0.1300	0.8161

Station LE4.2

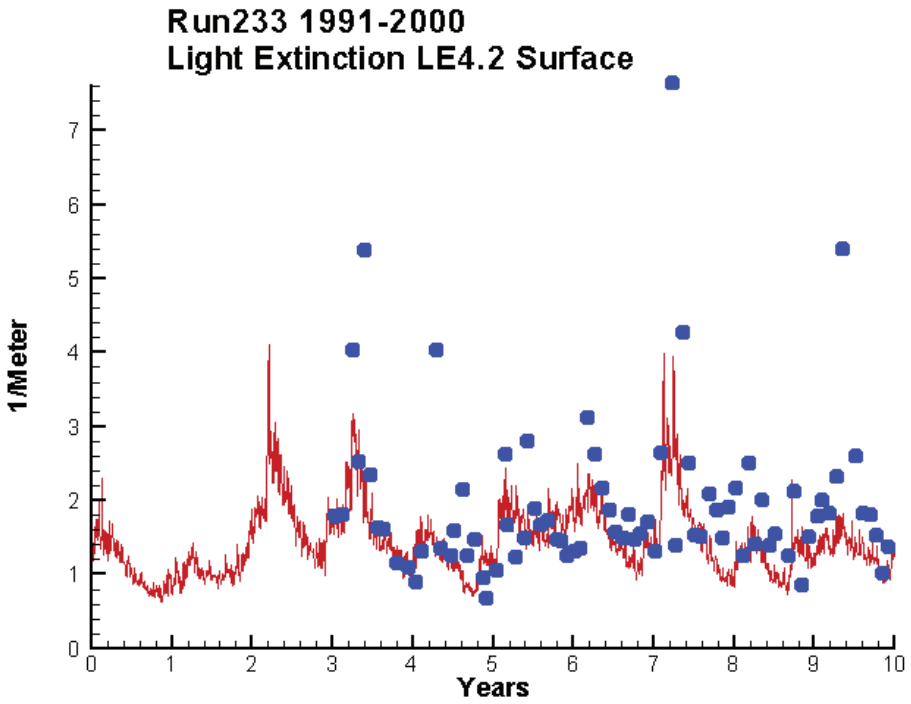

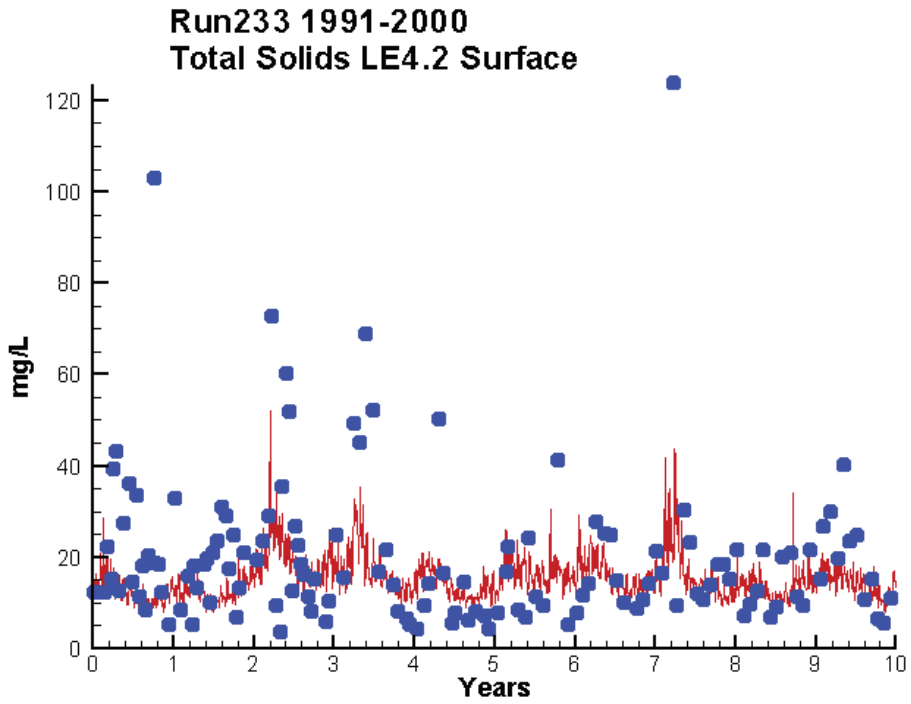

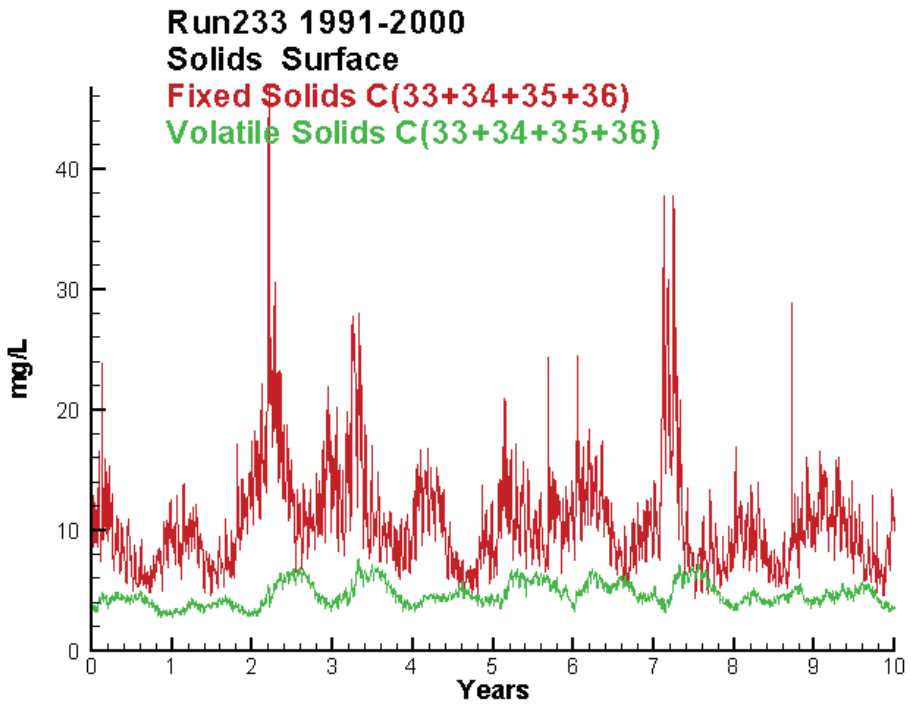

	Mean Difference	Absolute Mean Difference
KE	-0.4321	0.6198
TSS	-4.3303	9.2521

Station RET4.3

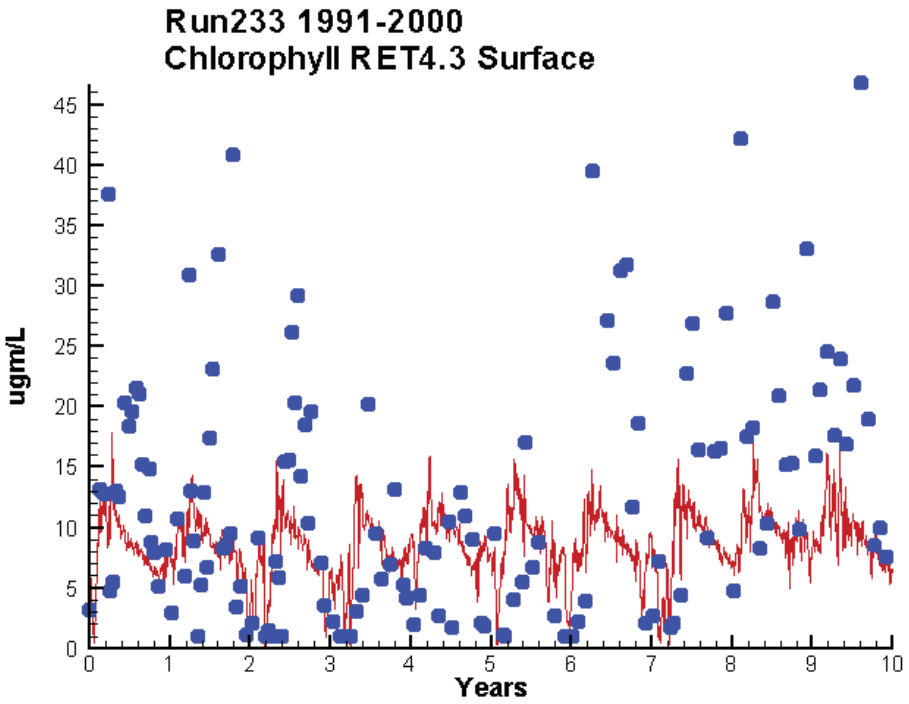

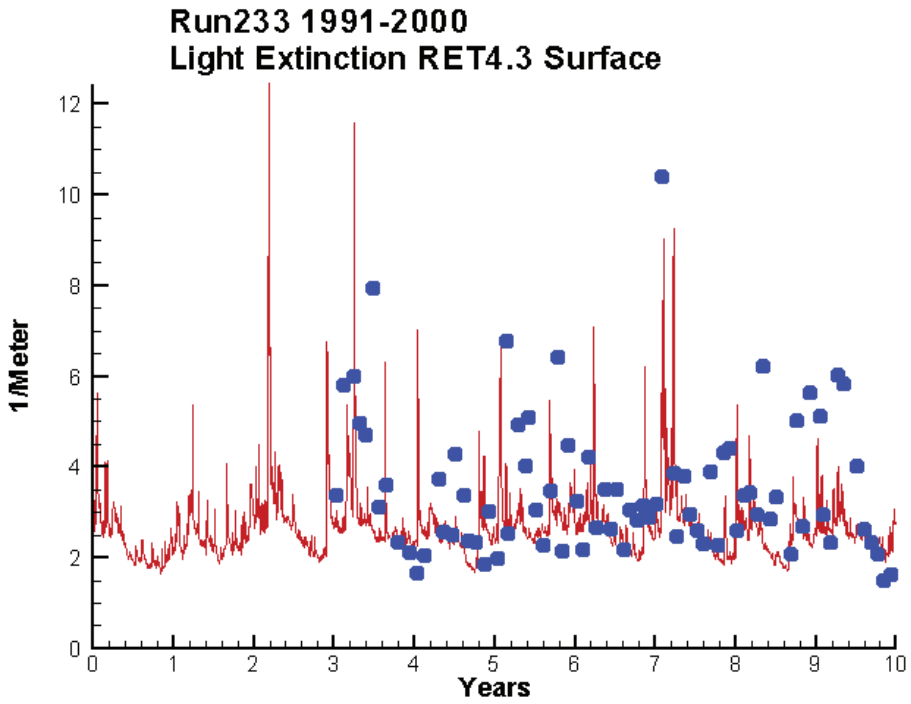

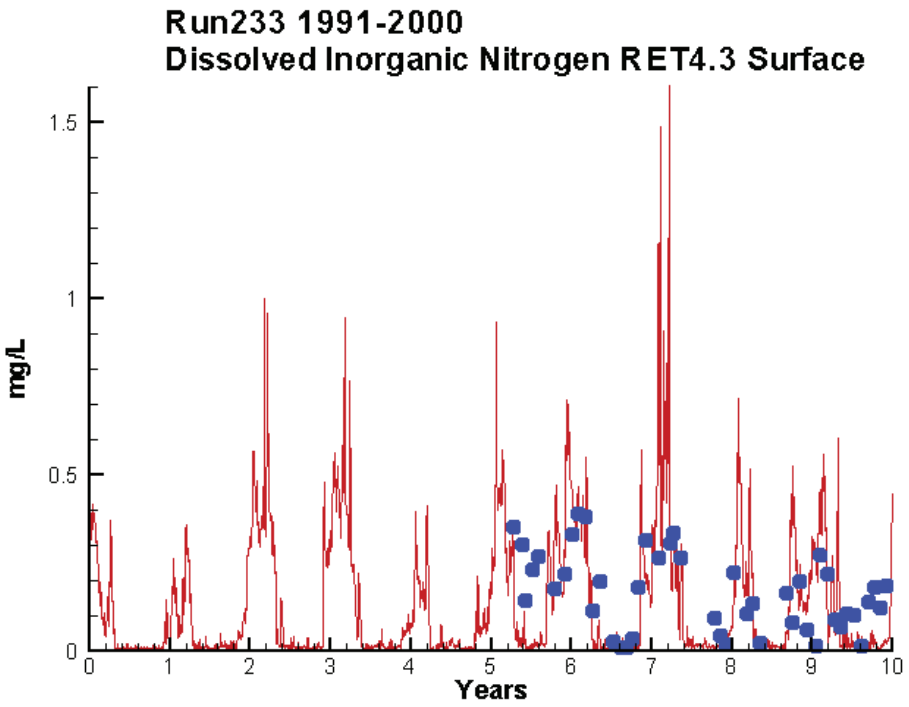

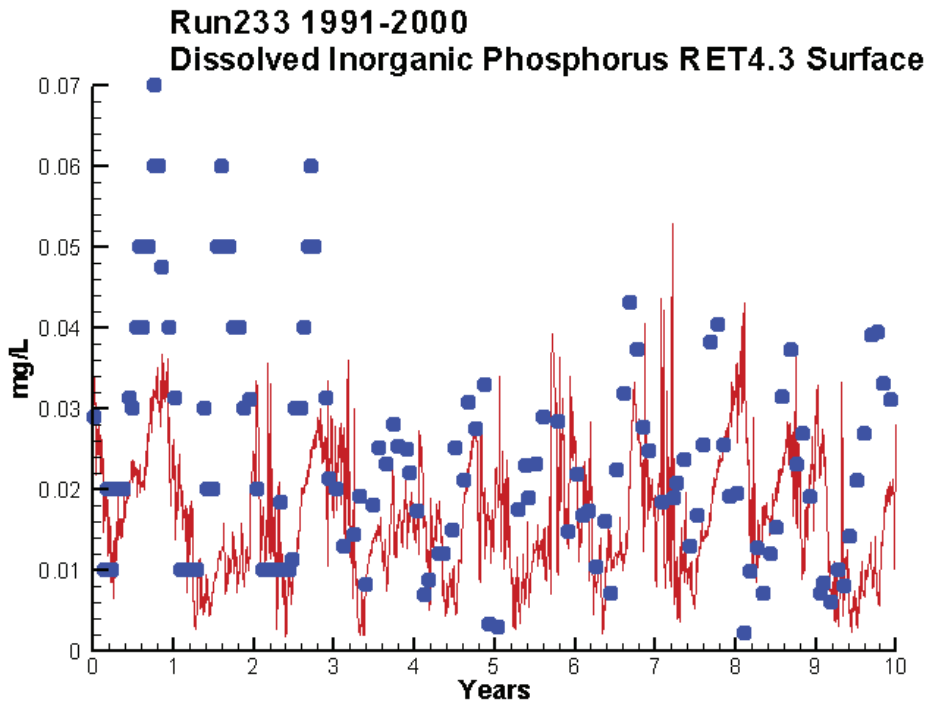

Station RET4.3

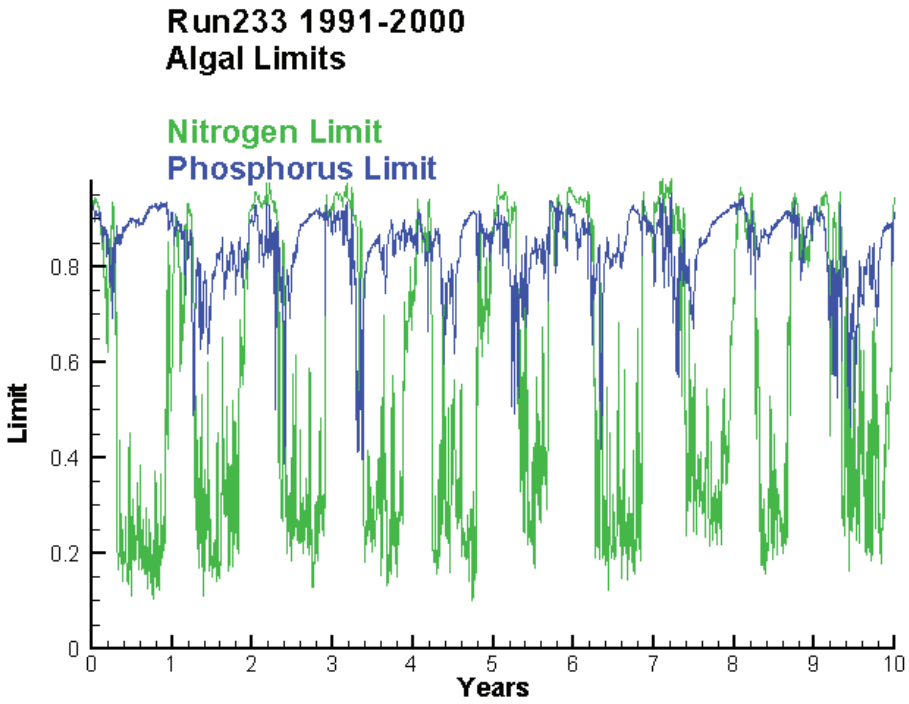

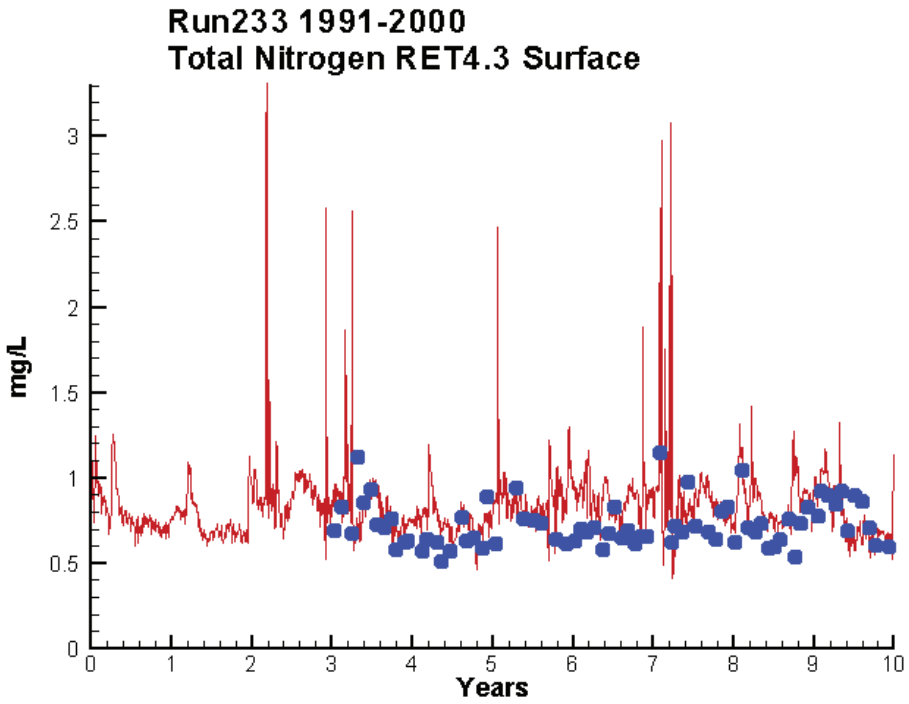

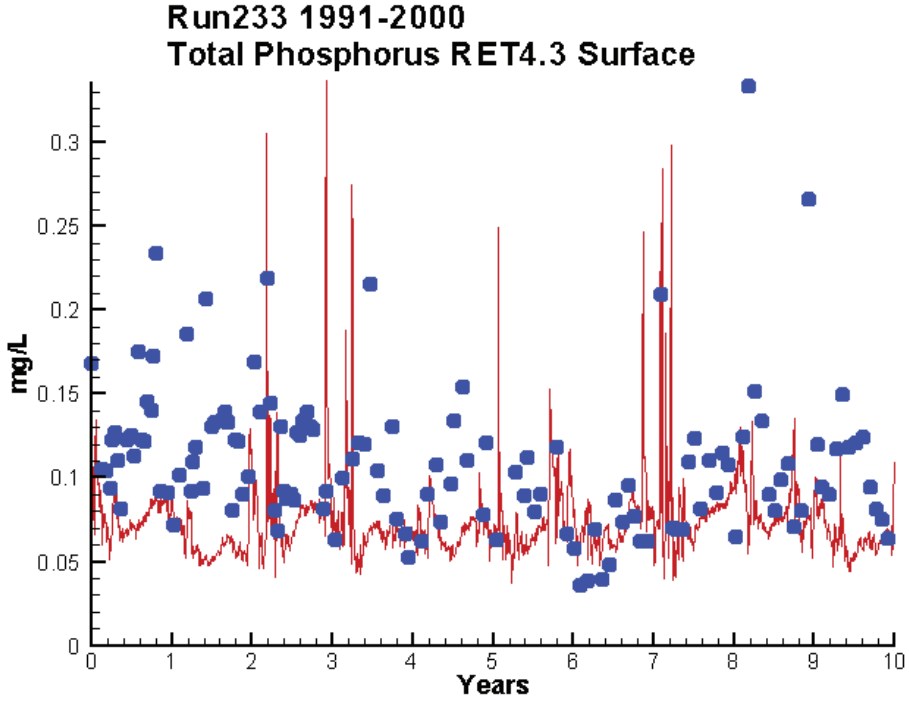

	Mean Difference	Absolute Mean Difference
Chl	-3.5690	7.3037
DIN	-0.0403	0.1094
KE	-0.7642	1.2267
DIP	-0.0087	0.0122
TP	-0.0375	0.0438
TN	0.0930	0.1482

Station RET4.3

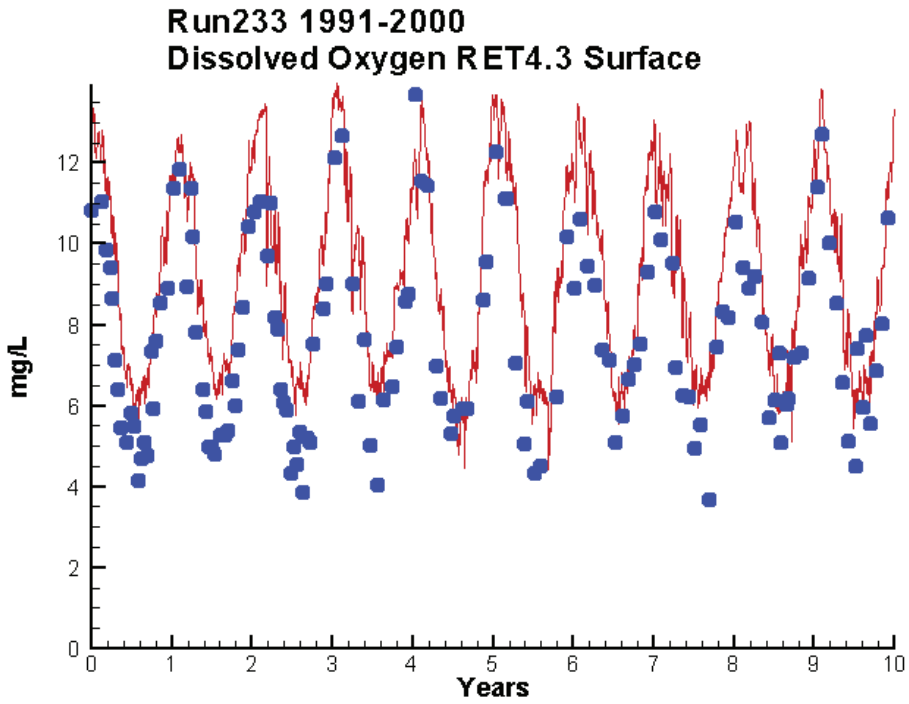

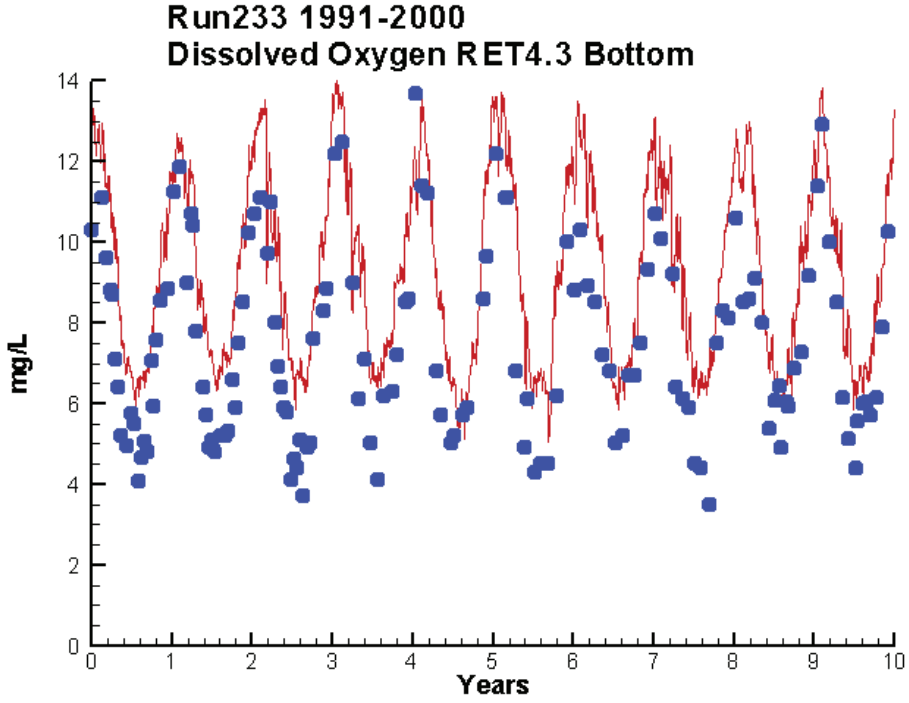

	Mean Difference	Absolute Mean Difference
Top DO	1.5017	1.6014
Bot DO	1.7392	1.7853

Station RET4.3

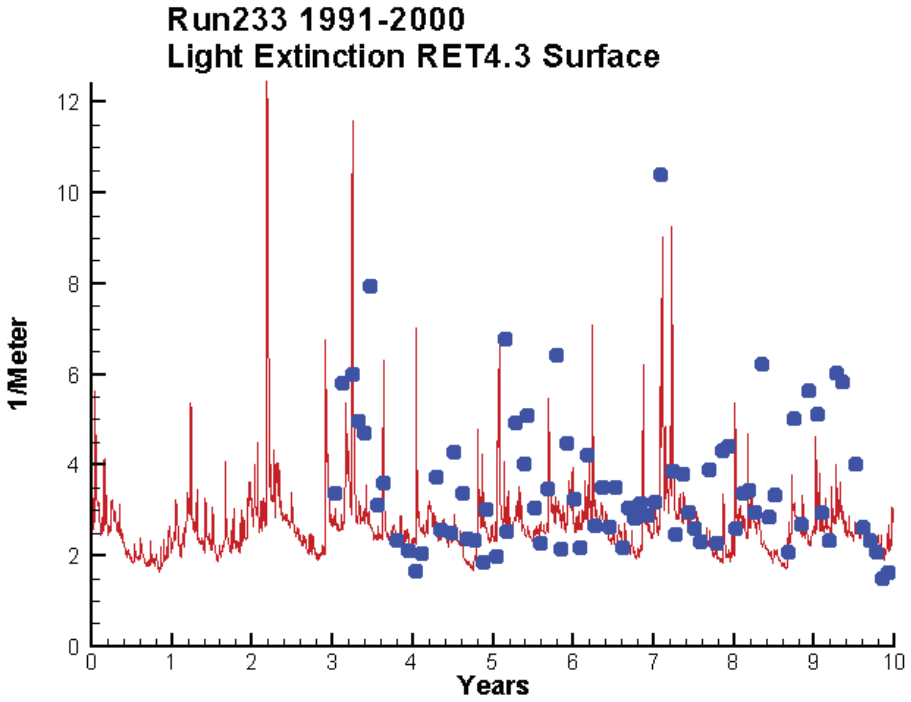

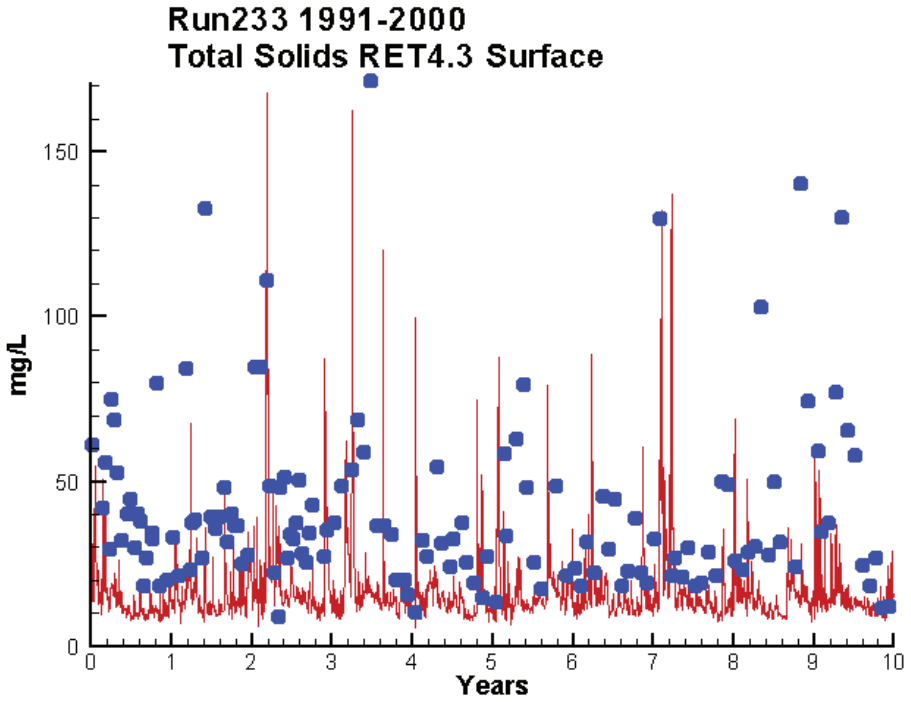

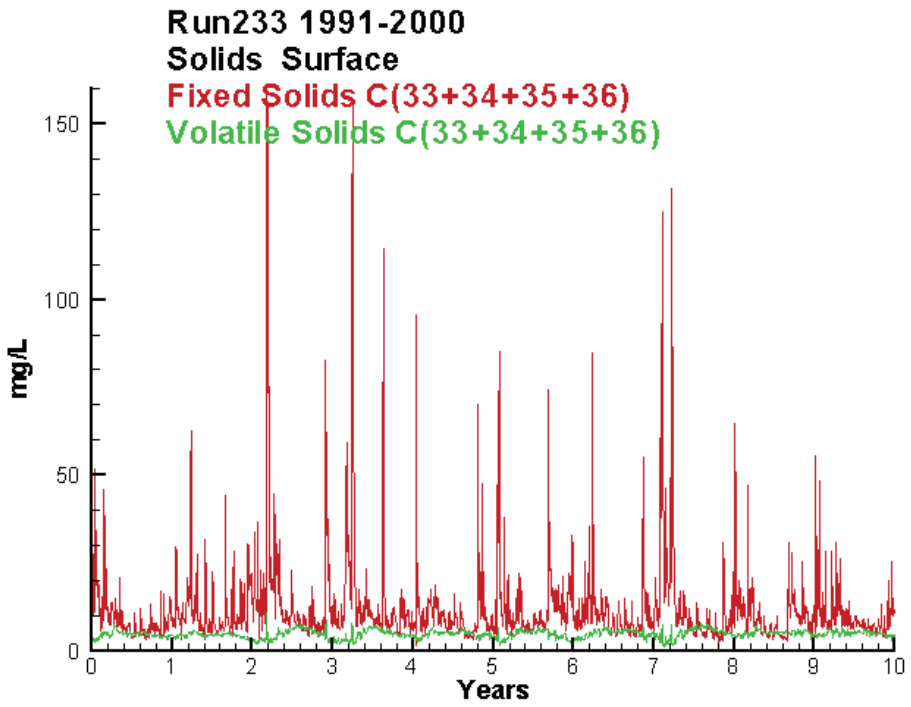

	Mean Difference	Absolute Mean Difference
KE	-0.7642	1.2267
TSS	-24.0439	27.1796

Station TF4.2

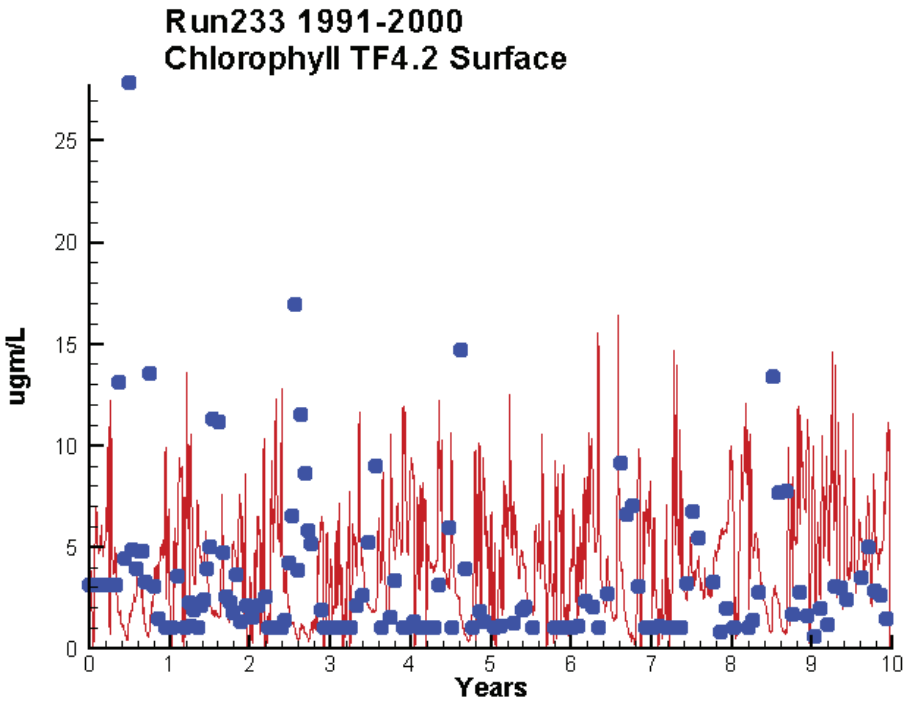

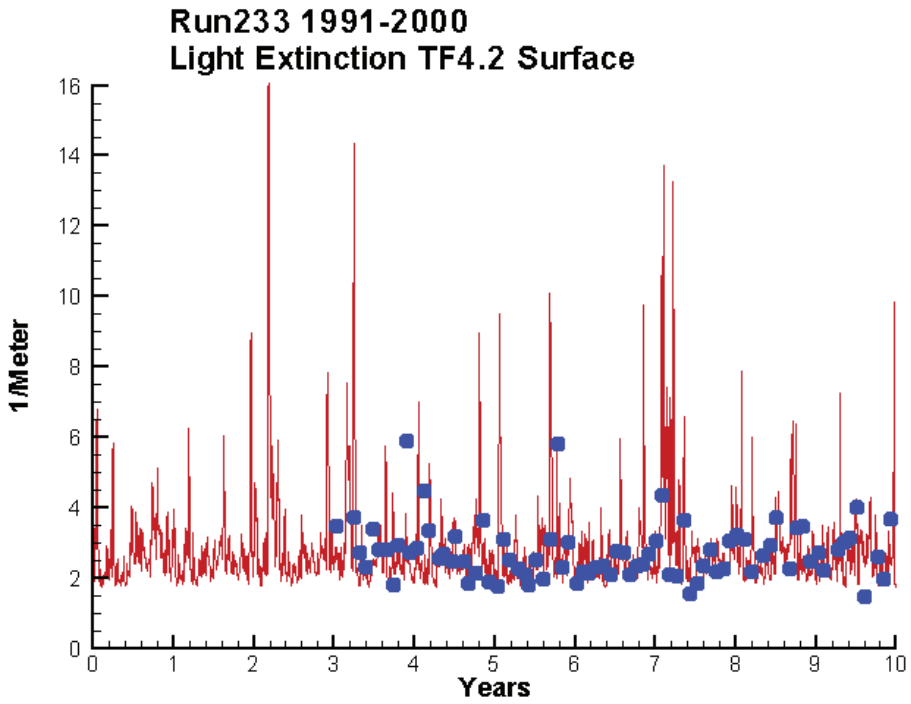

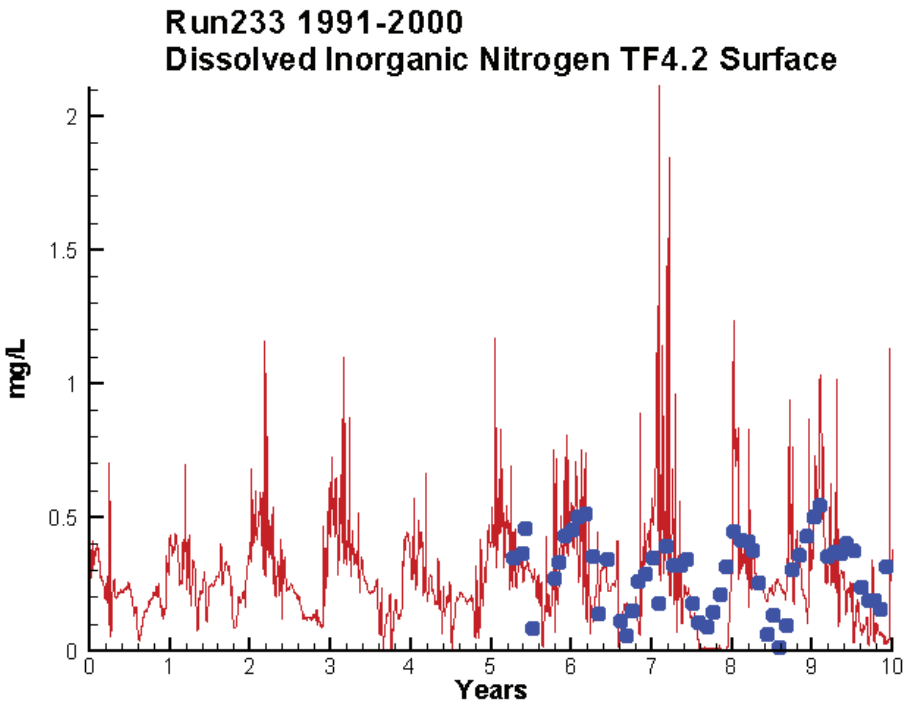

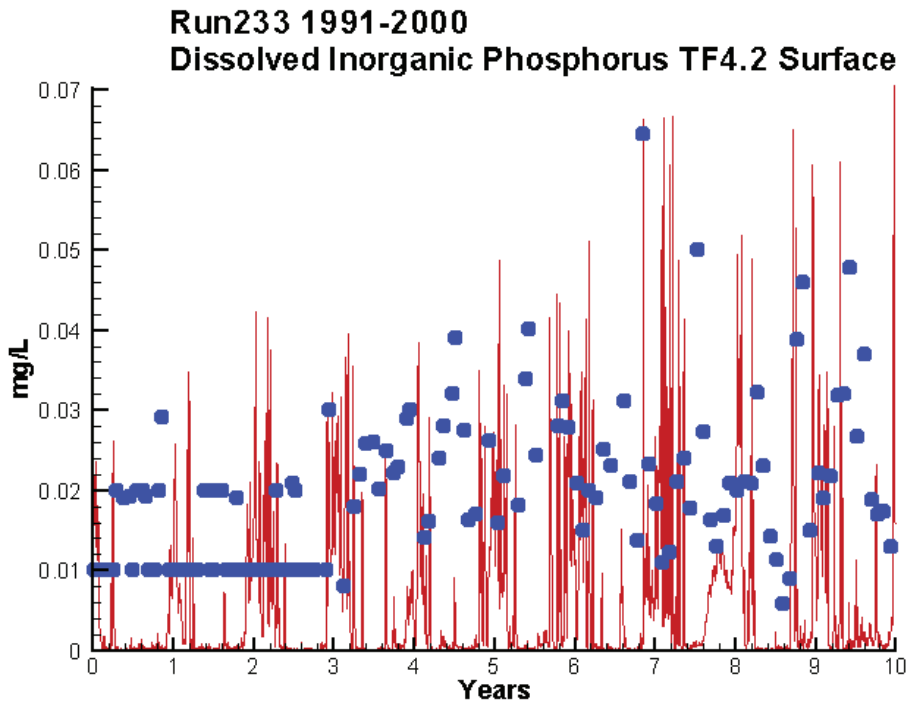

Station TF4.2

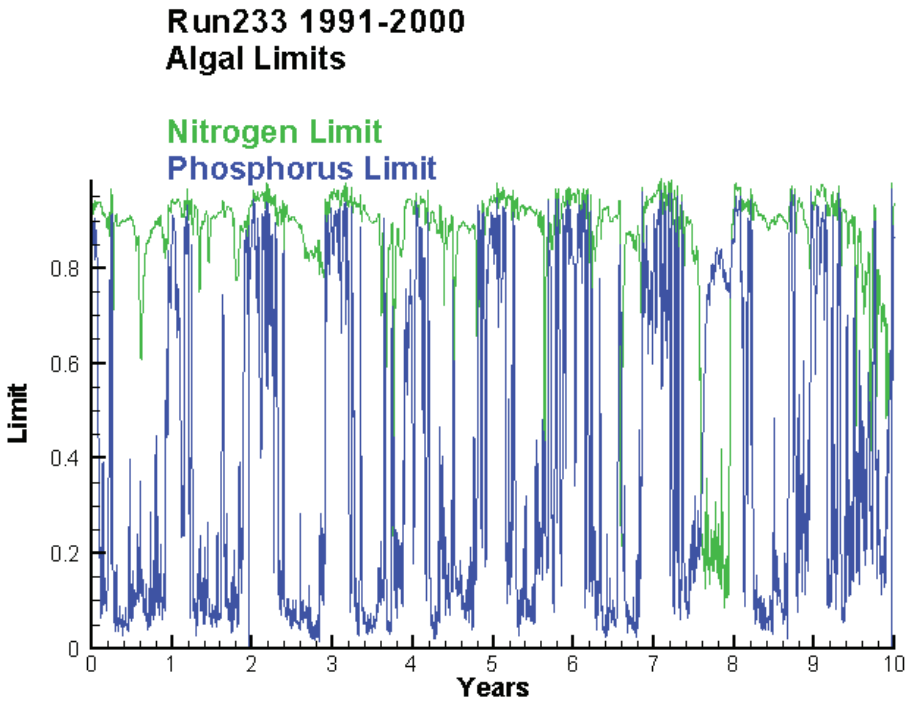

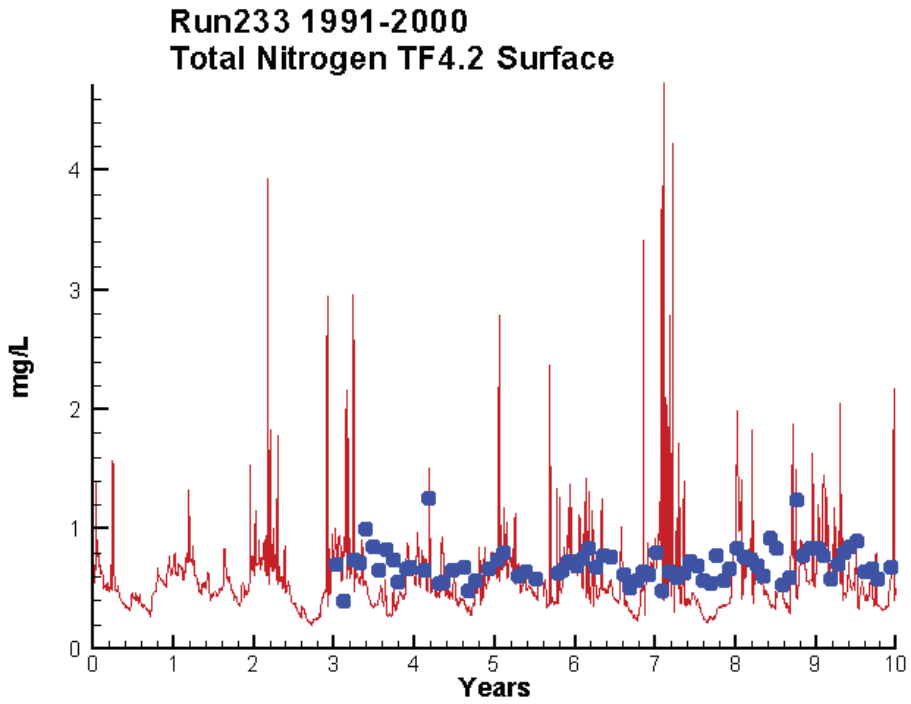

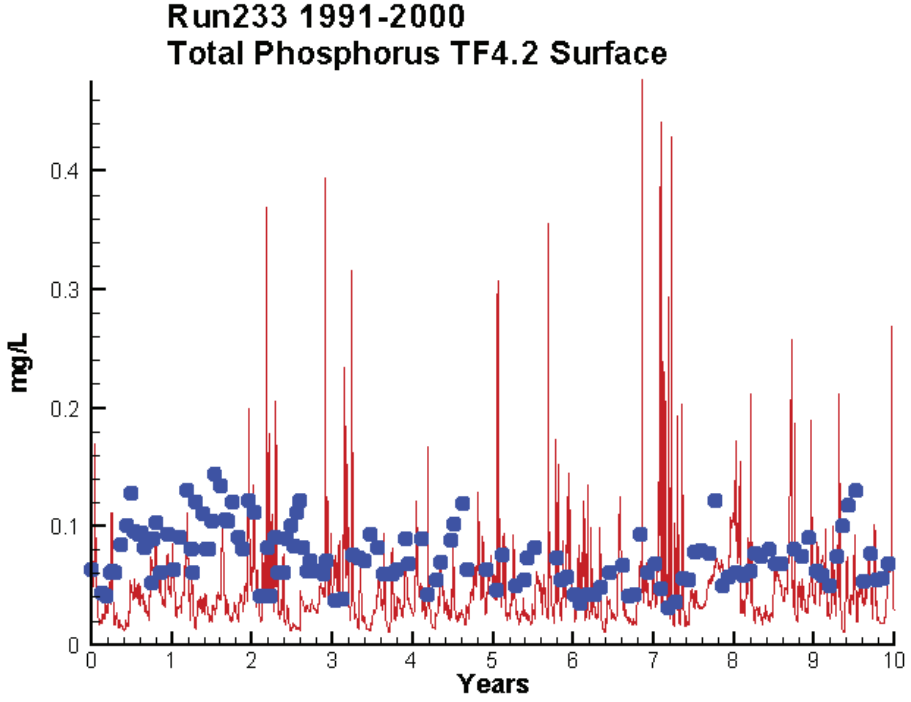

	Mean Difference	Absolute Mean Difference
Chl	0.9257	4.2129
DIN	-0.0083	0.1718
KE	0.0973	0.8570
DIP	-0.0144	0.0166
TP	-0.0305	0.0406
TN	-0.0820	0.2497

Station TF4.2

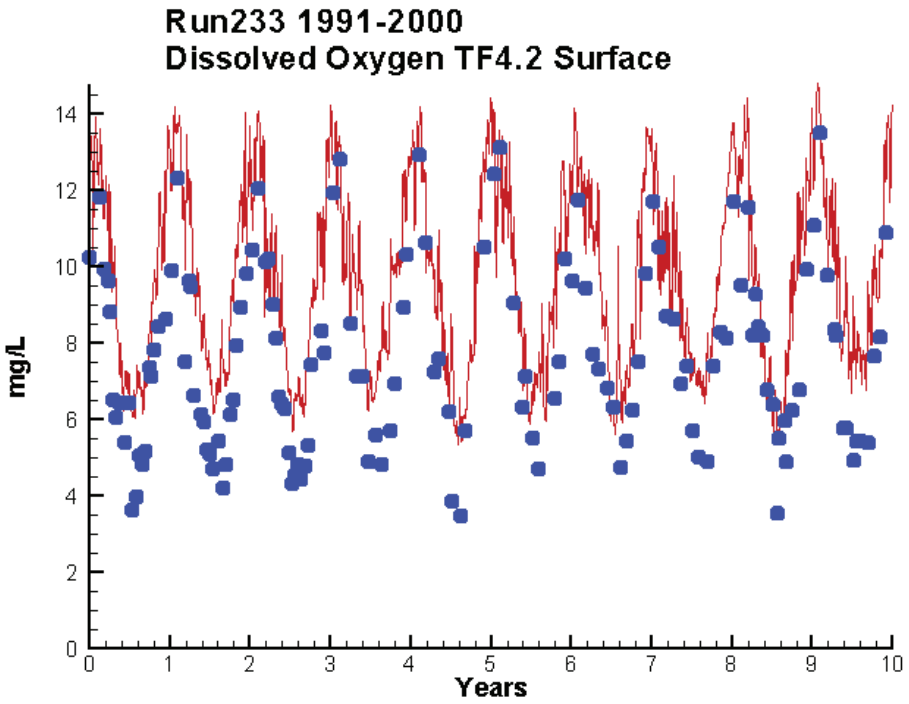

	Mean Difference	Absolute Mean Difference
Top DO	1.9396	1.9905

Station TF4.2

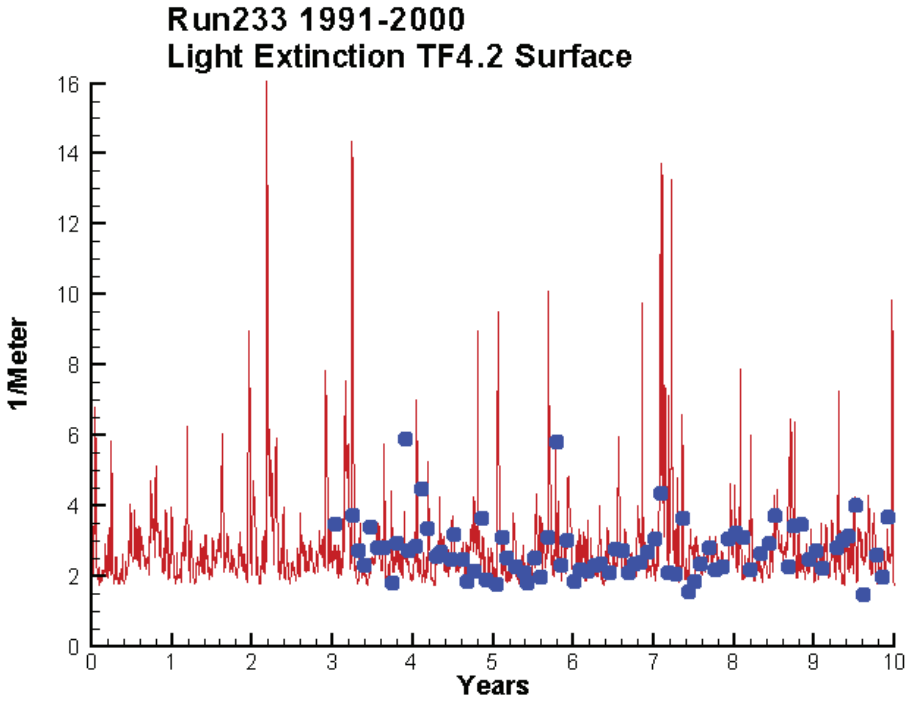

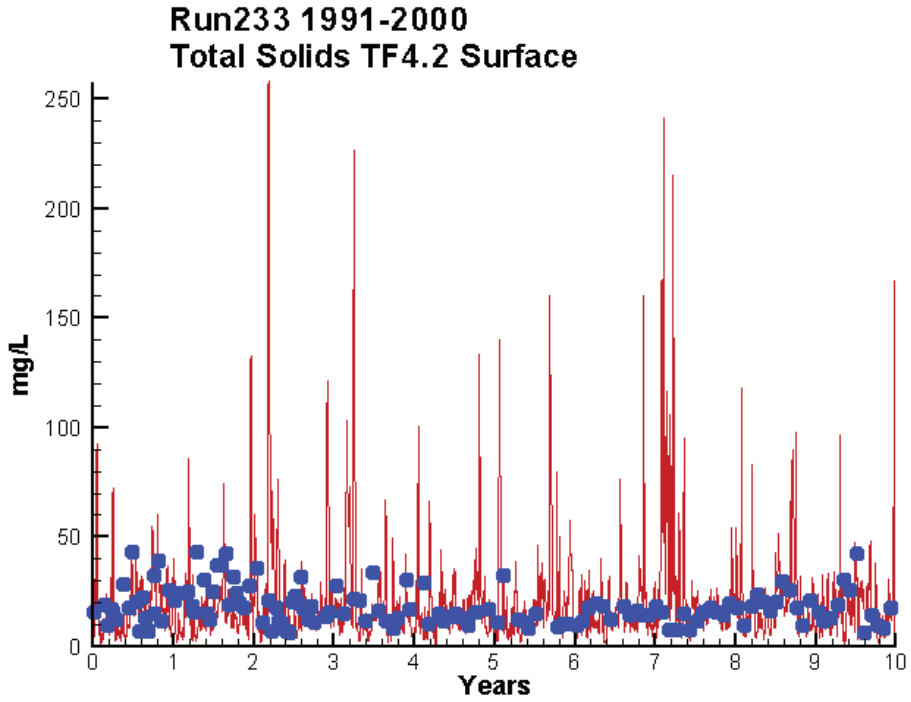

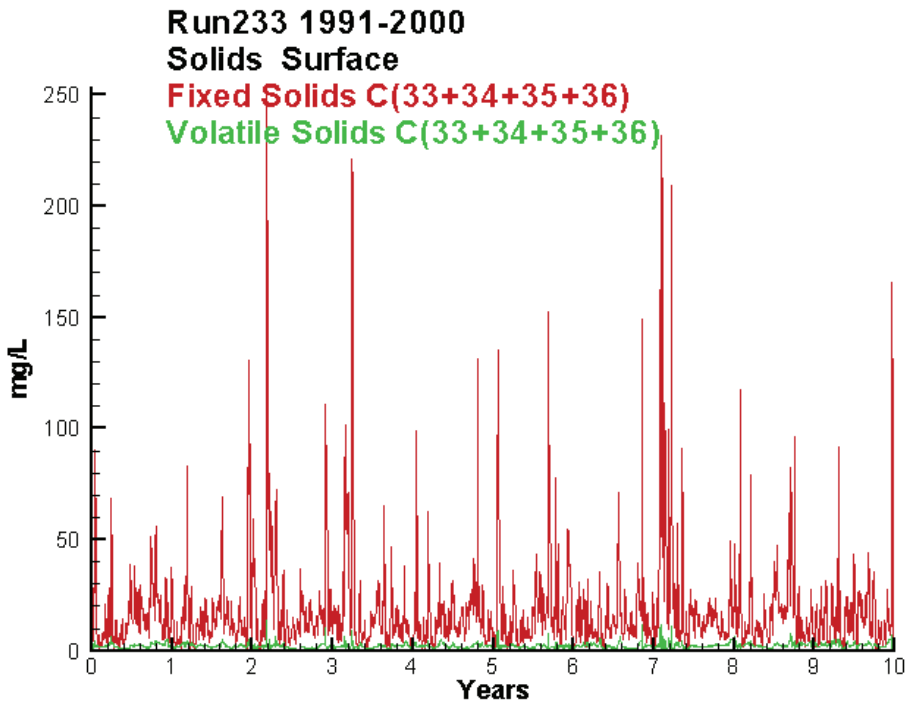

	Mean Difference	Absolute Mean Difference
KE	0.0973	0.8570
TSS	3.4708	13.1598

Station LE5.3

Run233 1991-2000
Chlorophyll LE5.3 Surface

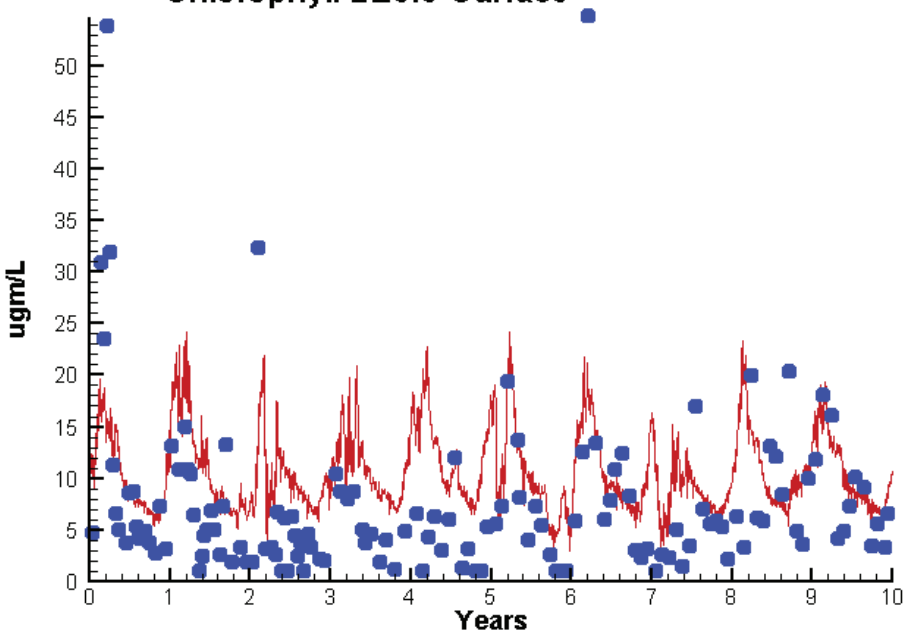

Run233 1991-2000
Light Extinction LE5.3 Surface

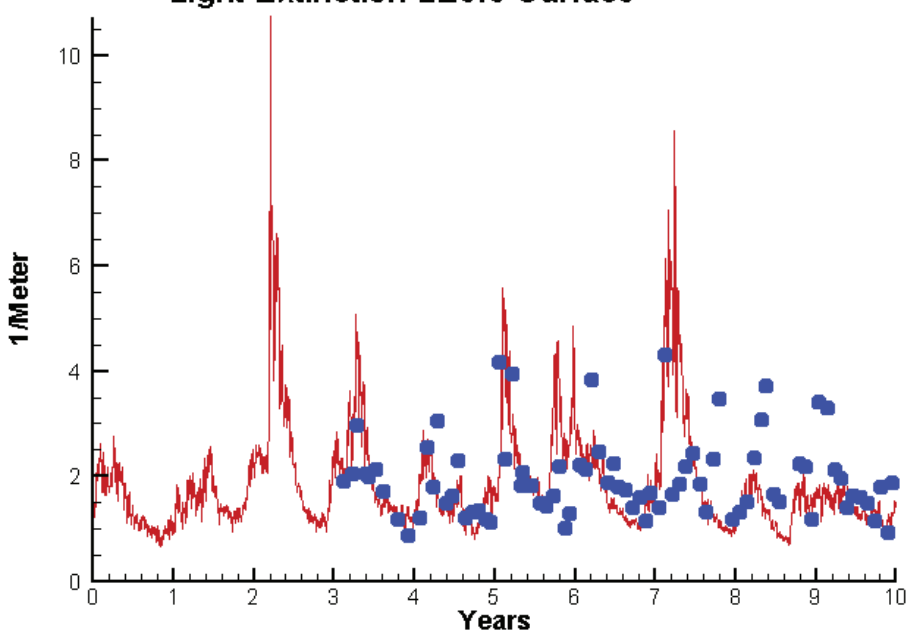

Run233 1991-2000
Dissolved Inorganic Nitrogen LE5.3 Surface

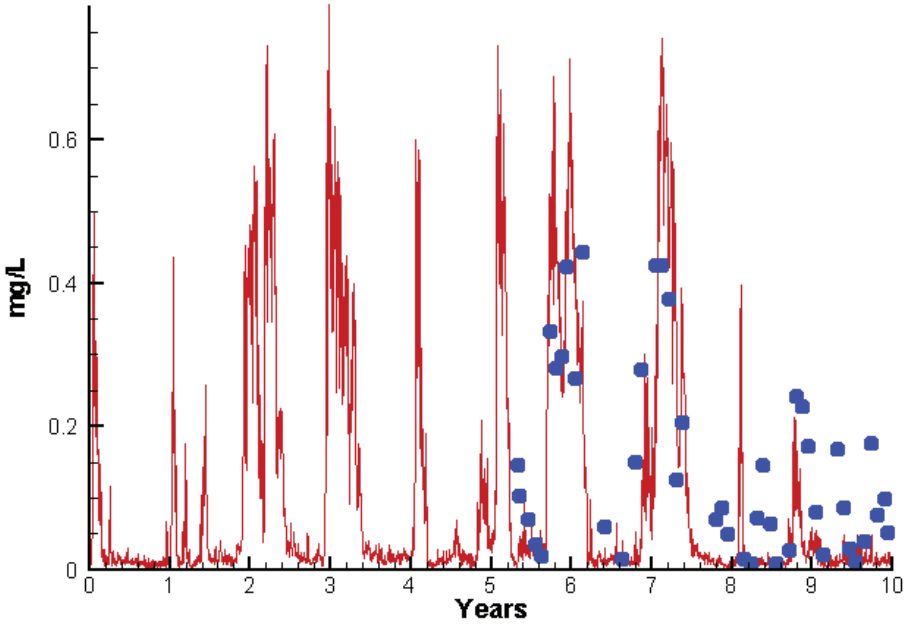

Run233 1991-2000
Dissolved Inorganic Phosphorus LE5.3 Surface

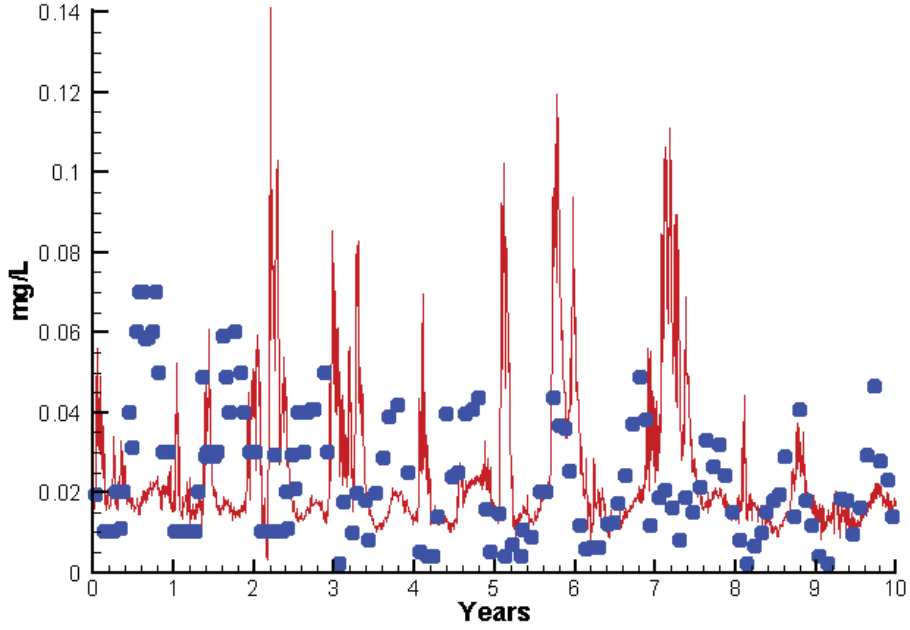

Station LE5.3

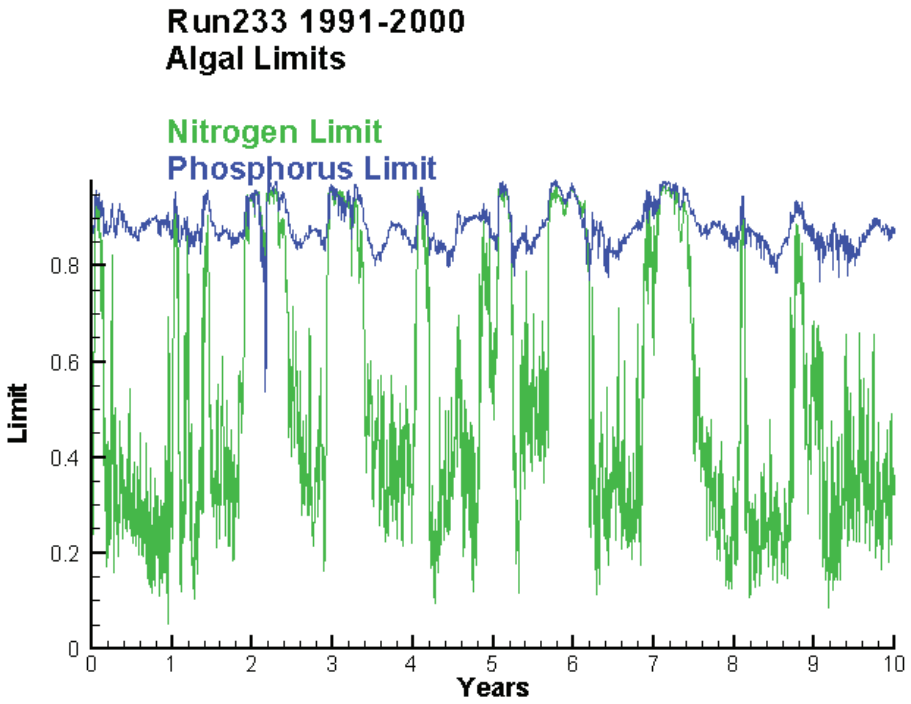

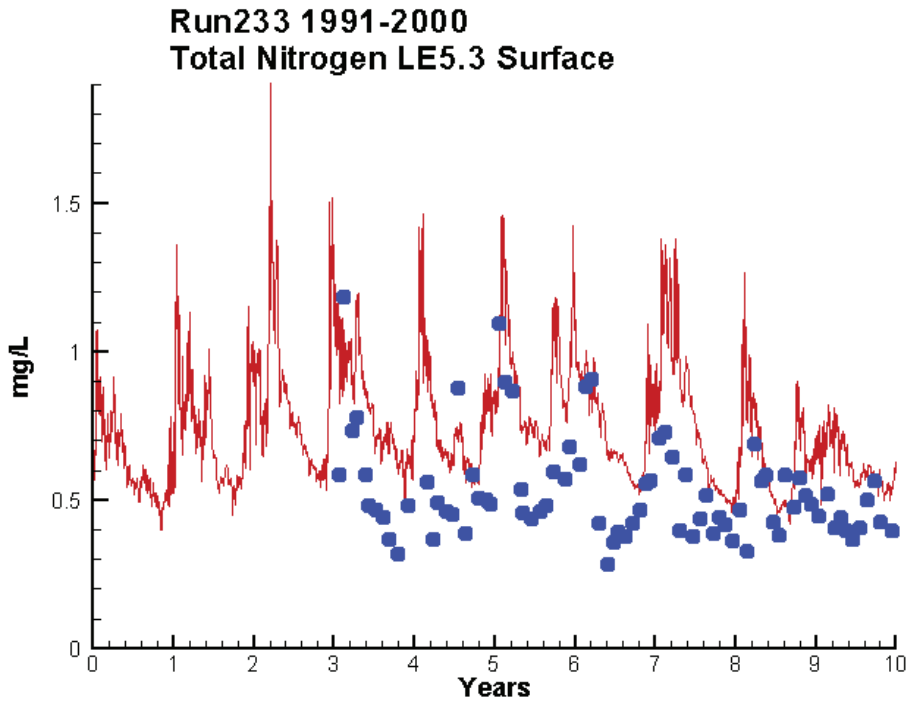

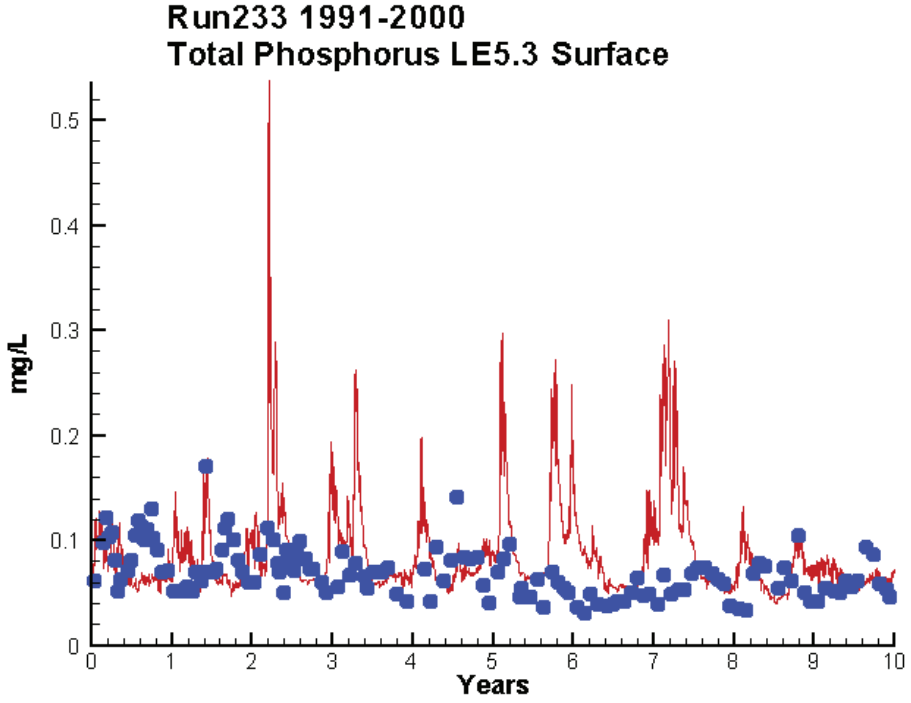

	Mean Difference	Absolute Mean Difference
Chl	3.2559	5.9670
DIN	-0.0295	0.0790
KE	-0.0659	0.6835
DIP	-0.0007	0.0178
TP	0.0156	0.0334
TN	0.2085	0.2220

Station LE5.3

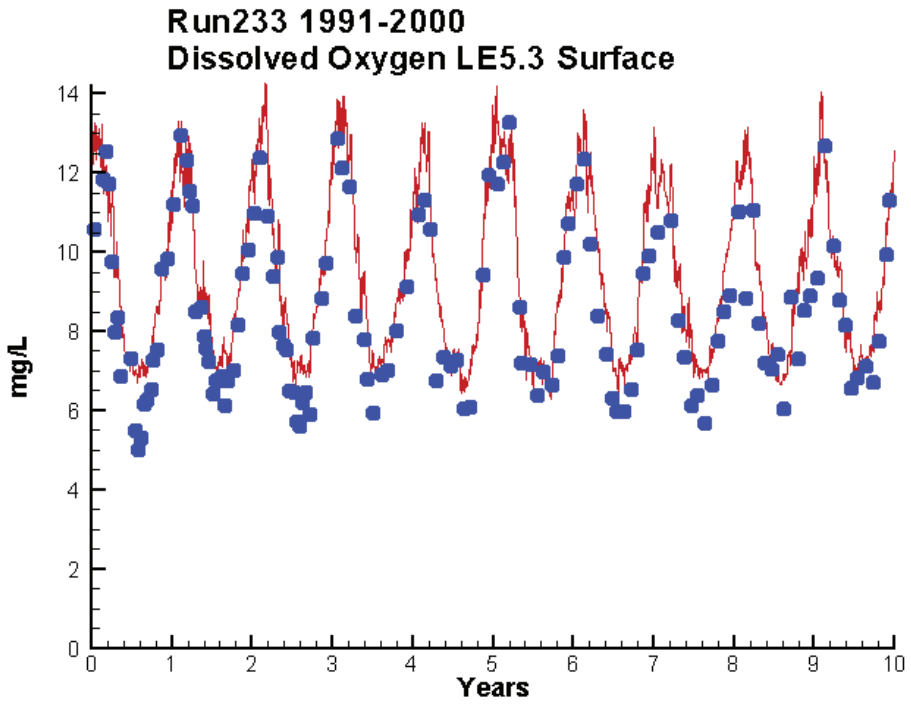

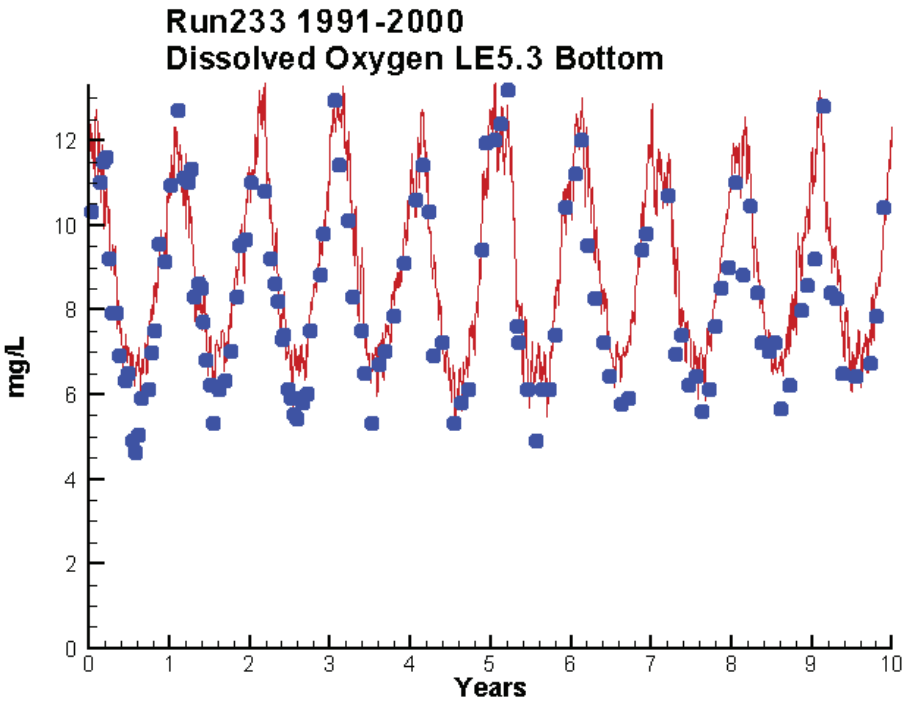

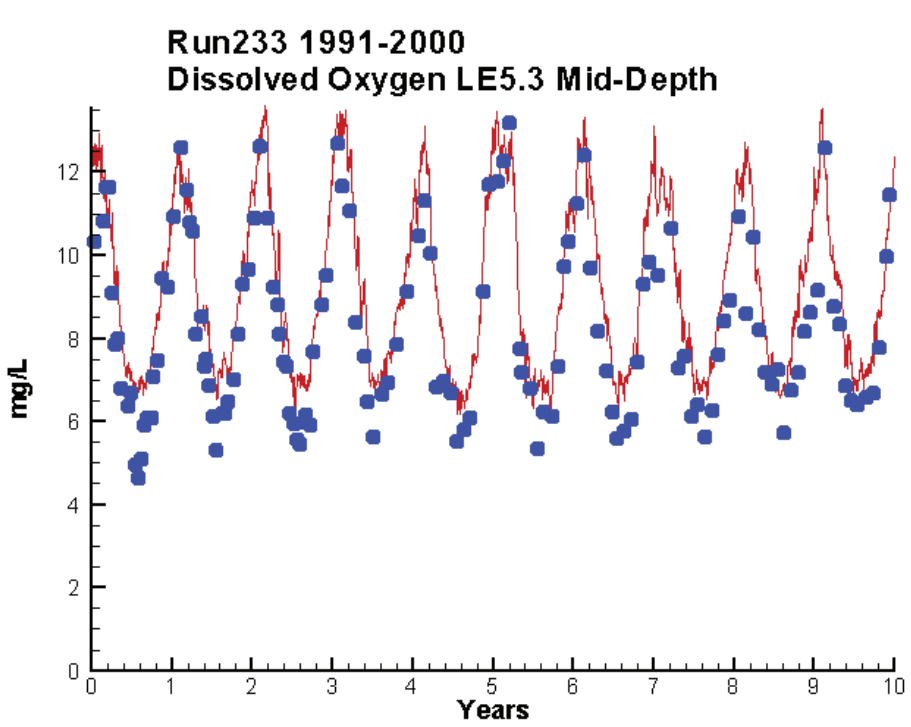

	Mean Difference	Absolute Mean Difference
Top DO	0.8519	0.9281
Mid DO	0.9726	1.0306
Bot DO	0.7325	0.9058

Station LE5.3

Run233 1991-2000
Light Extinction LE5.3 Surface

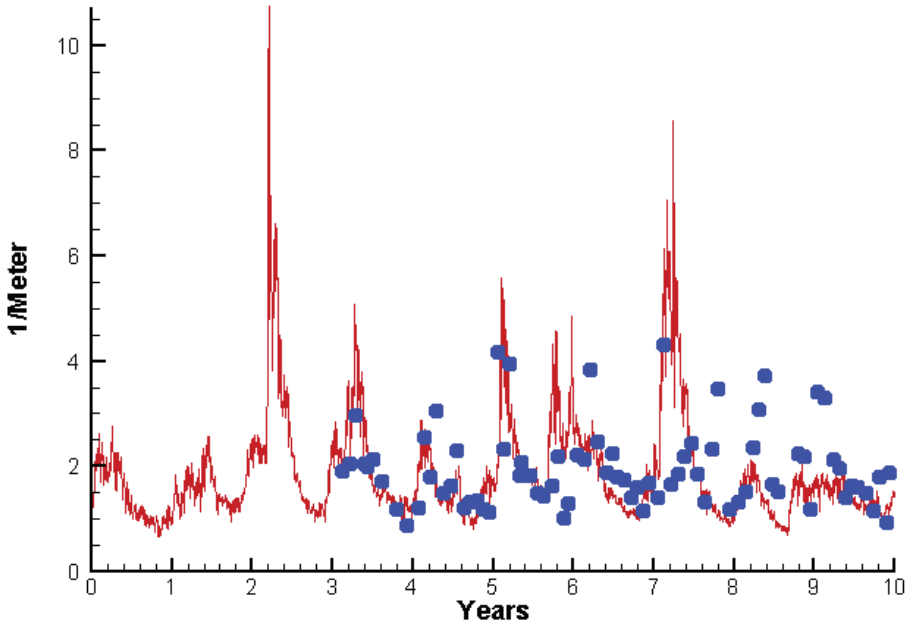

Run233 1991-2000
Total Solids LE5.3 Surface

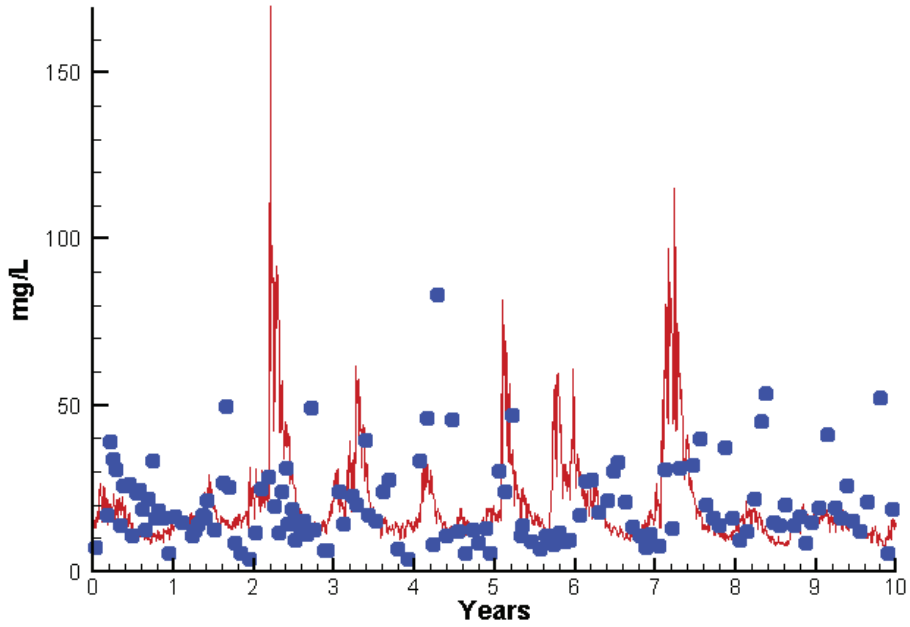

Run233 1991-2000
Solids Surface
Fixed Solids C(33+34+35+36)
Volatile Solids C(33+34+35+36)

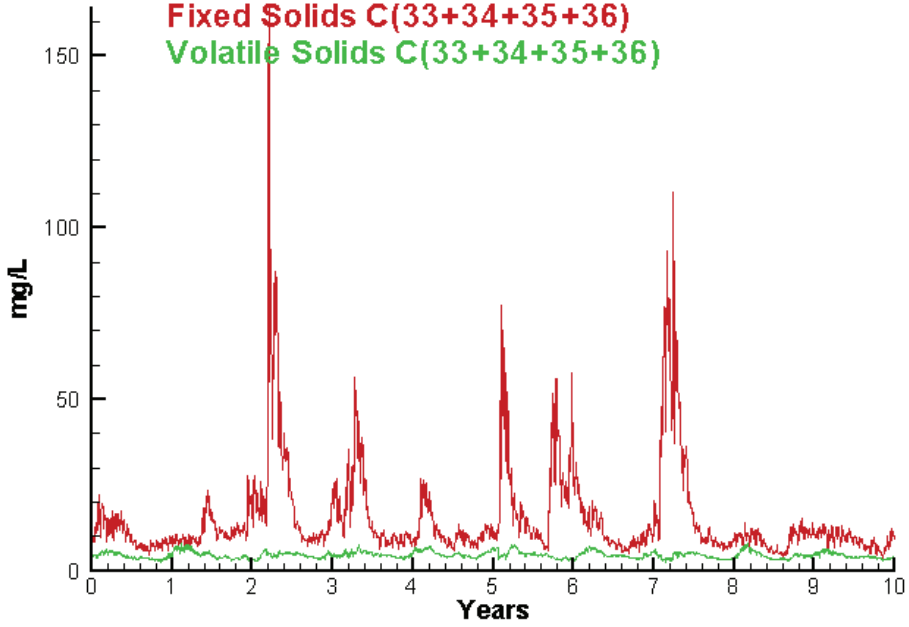

	Mean Difference	Absolute Mean Difference
KE	-0.0659	0.6835
TSS	0.1471	12.1435

Station RET5.2

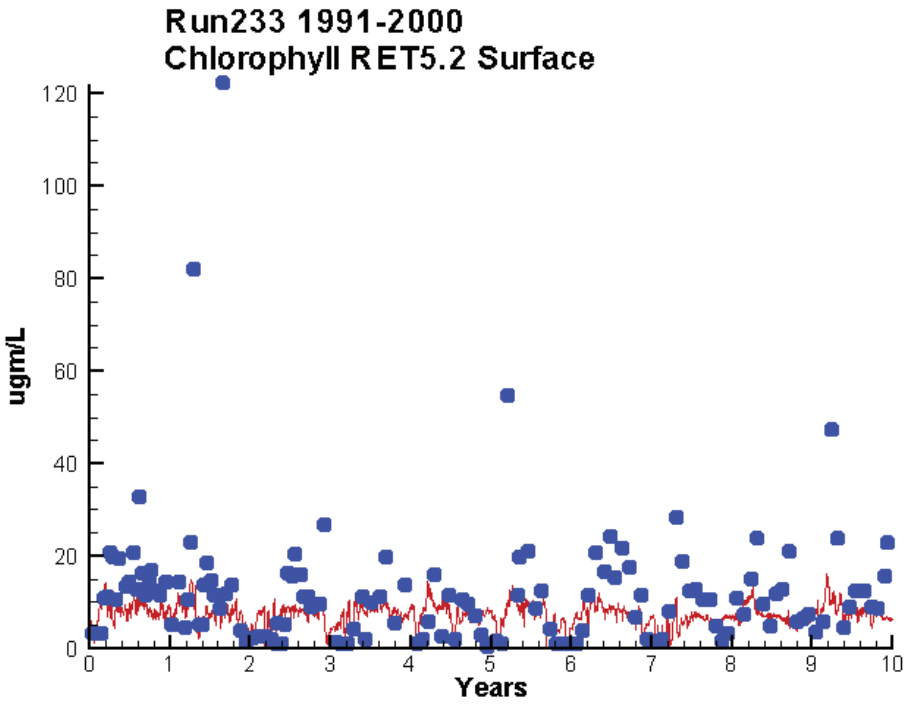

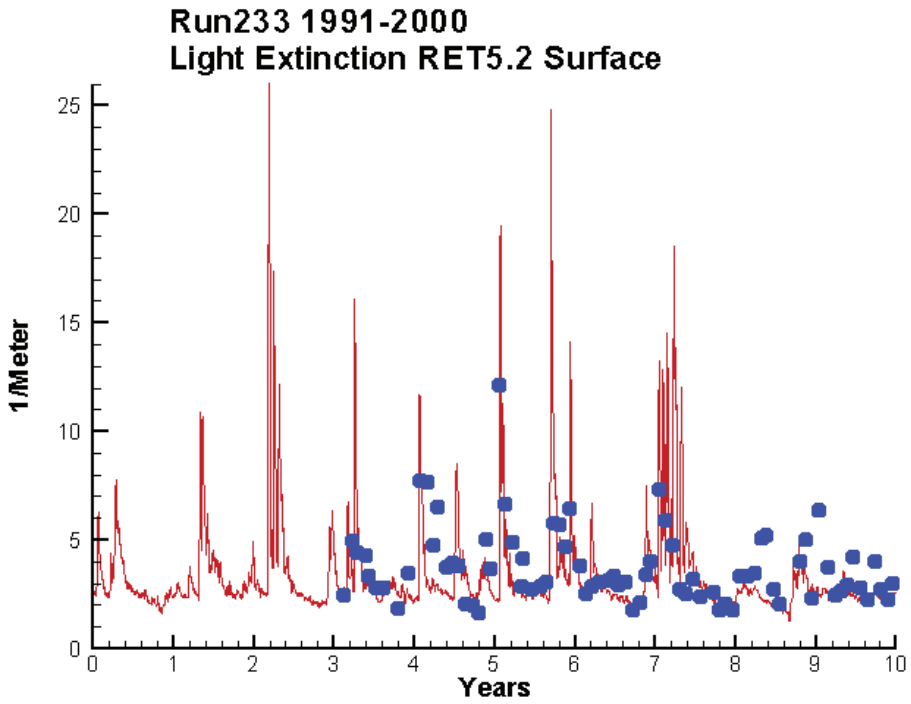

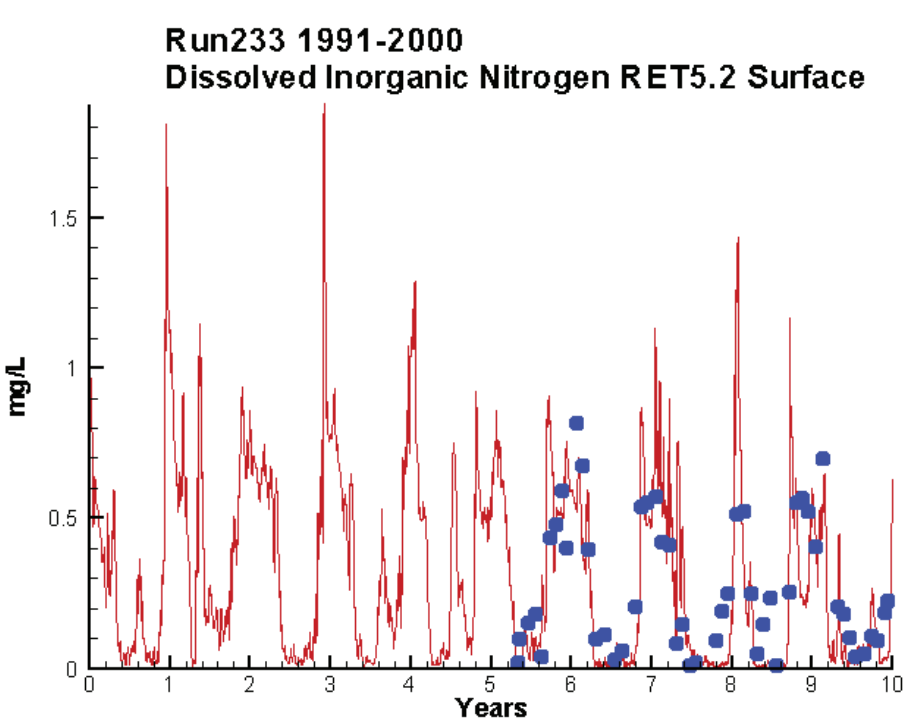

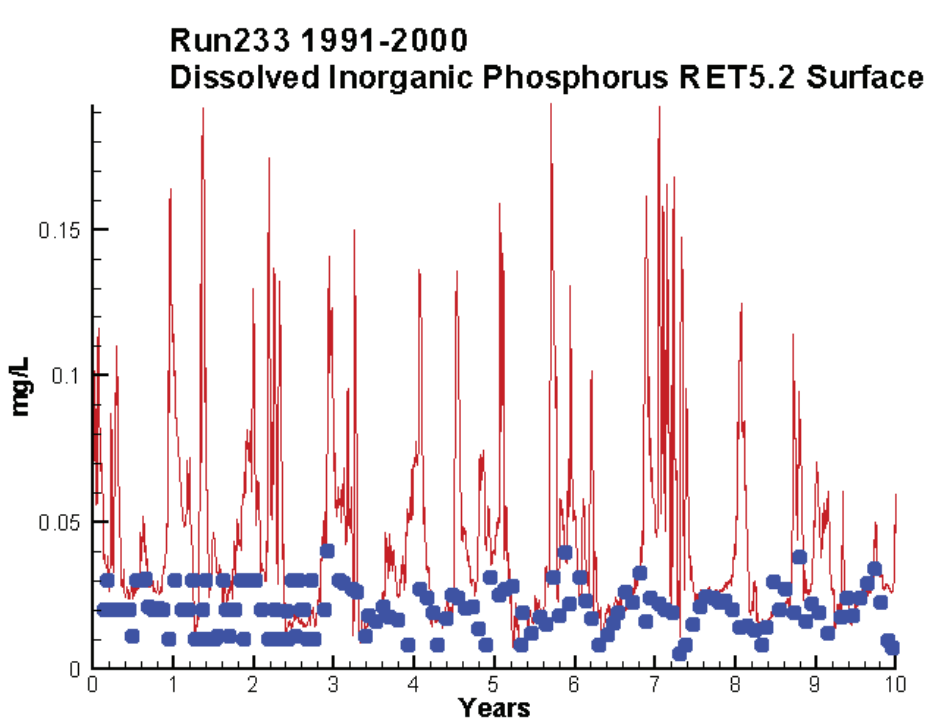

Station RET5.2

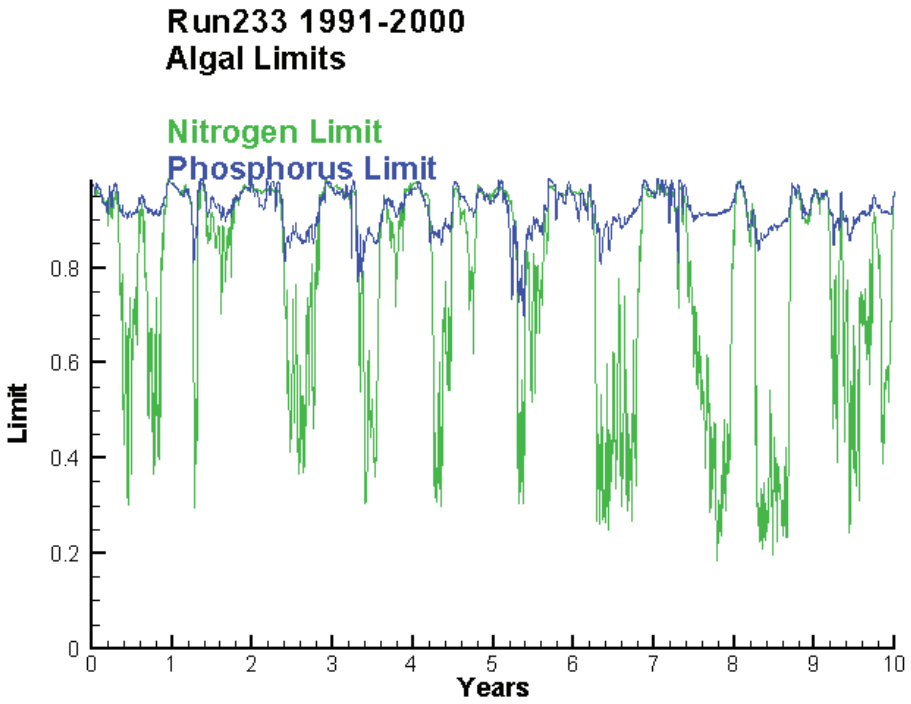

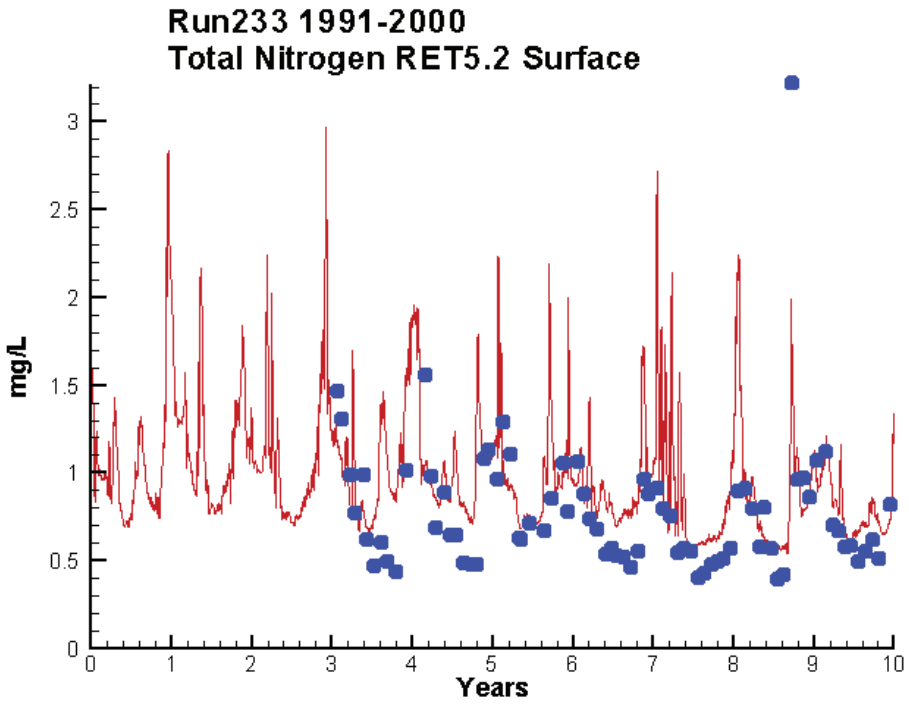

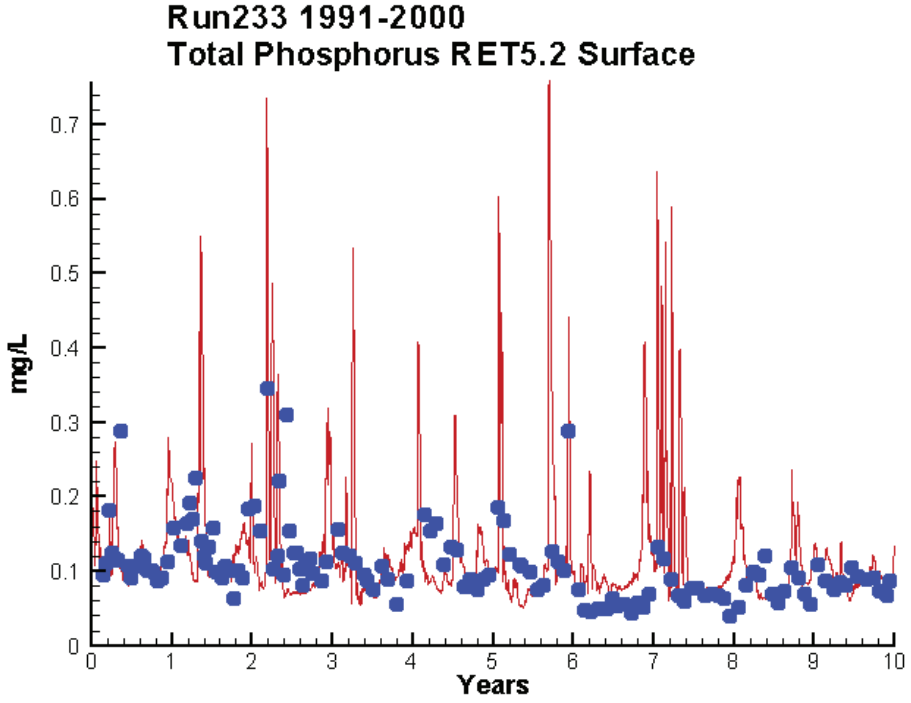

	Mean Difference	Absolute Mean Difference
Chl	-4.7719	7.2410
DIN	0.0113	0.1537
KE	-0.1913	1.1982
DIP	0.0249	0.0267
TP	0.0164	0.0510
TN	0.1678	0.2823

Station RET5.2

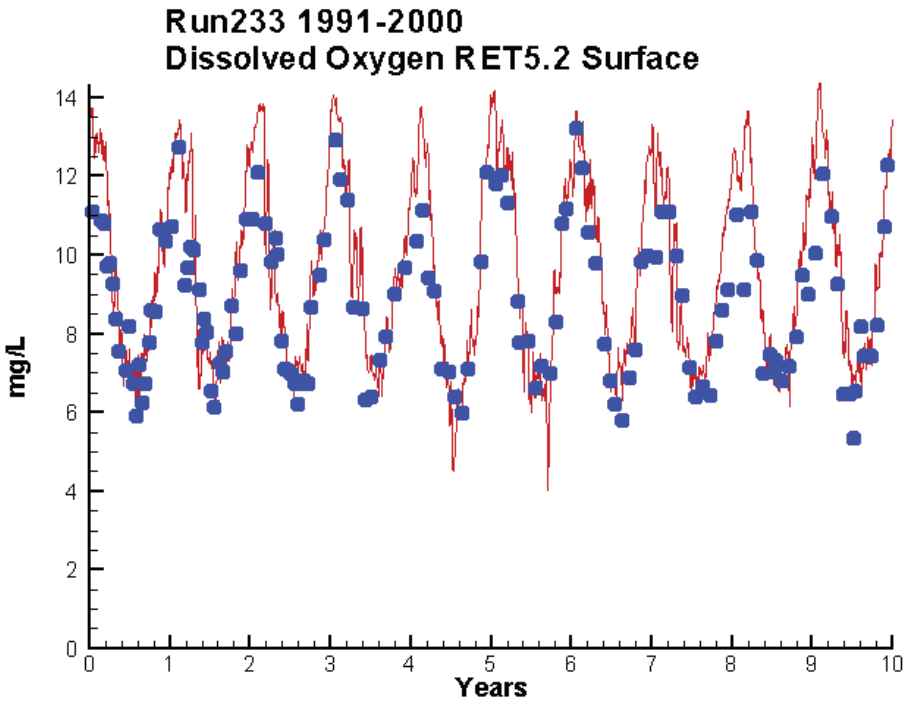

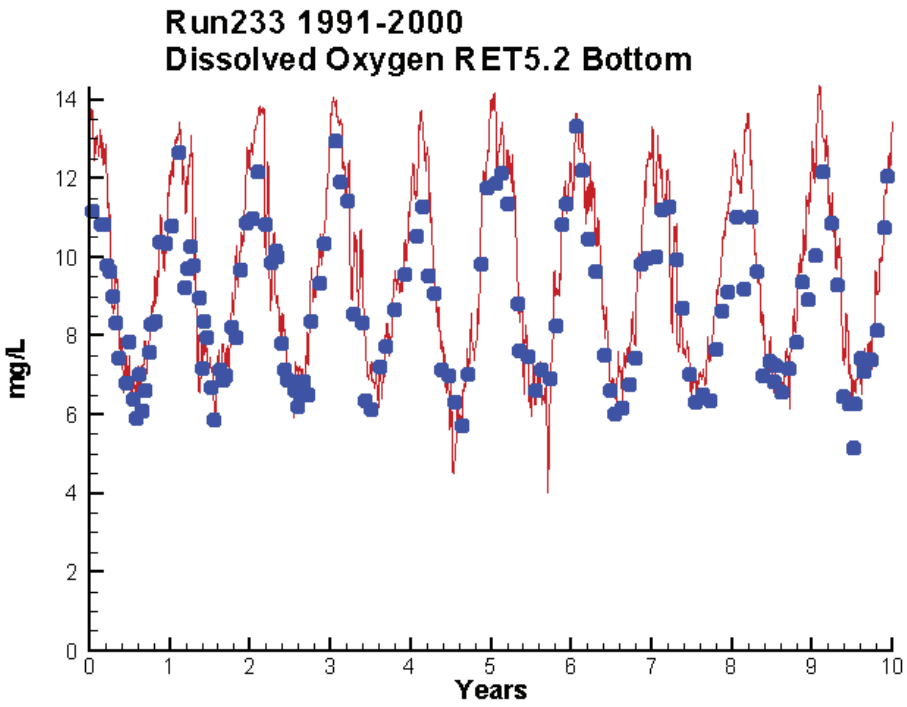

	Mean Difference	Absolute Mean Difference
Top DO	0.6522	0.9214
Bot DO	0.6937	0.9219

Station RET5.2

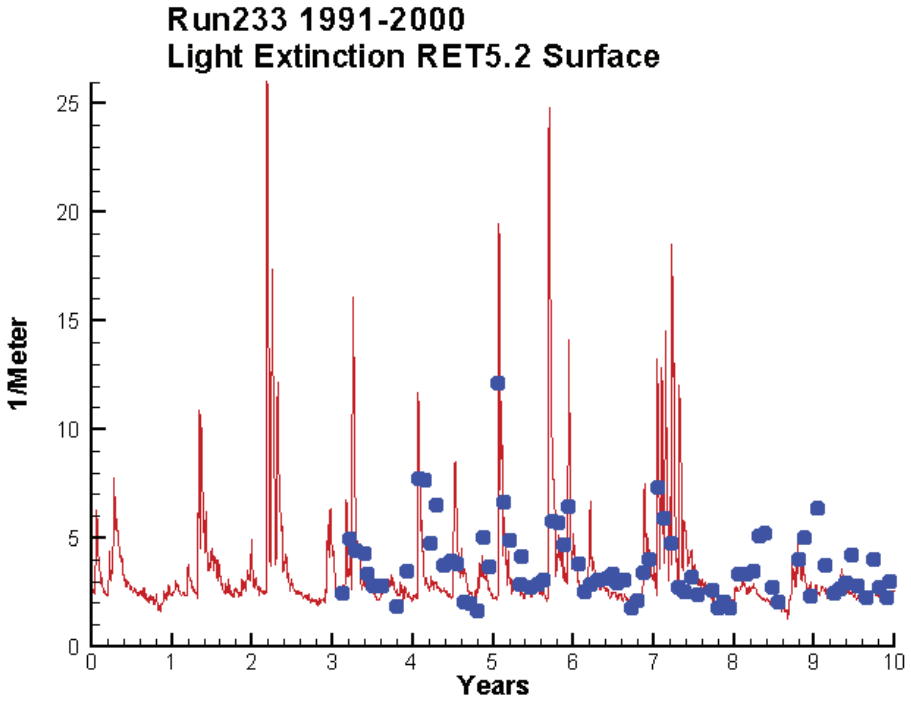

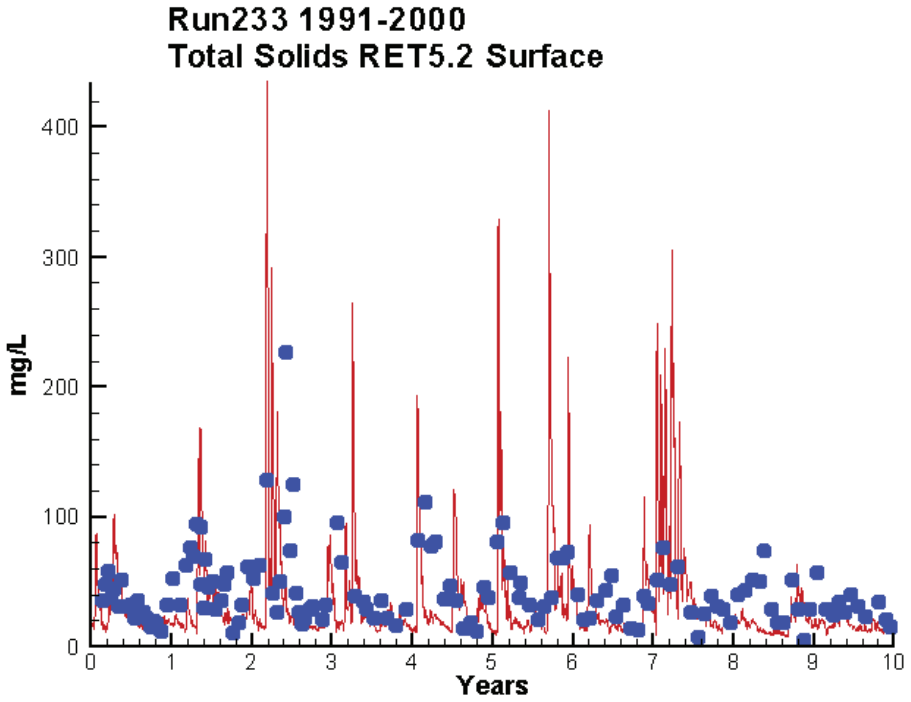

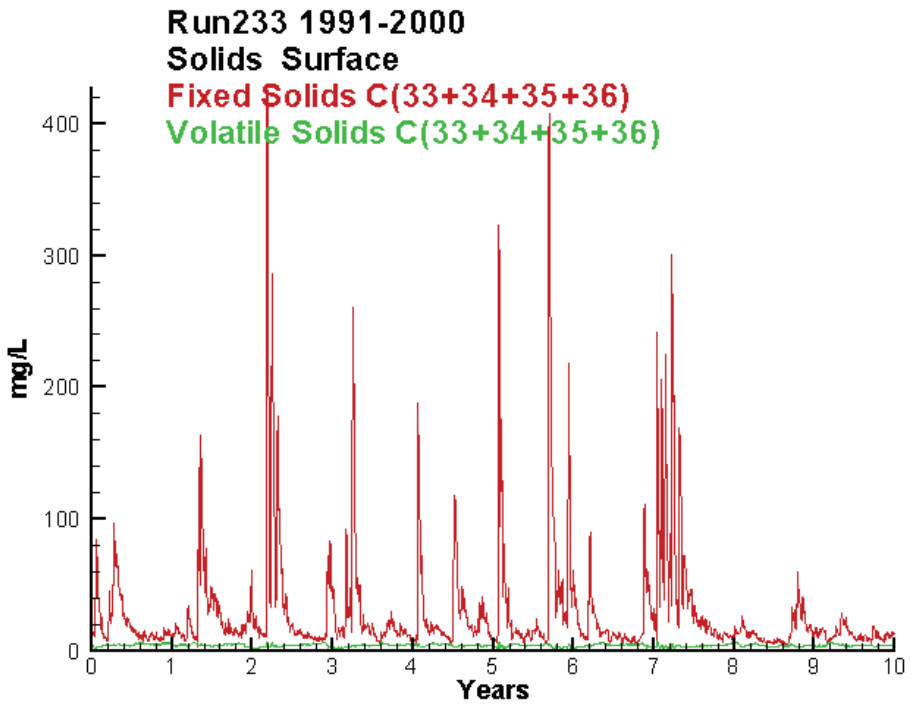

	Mean Difference	Absolute Mean Difference
KE	-0.1913	1.1982
TSS	-5.4701	28.8033

Station TF5.5

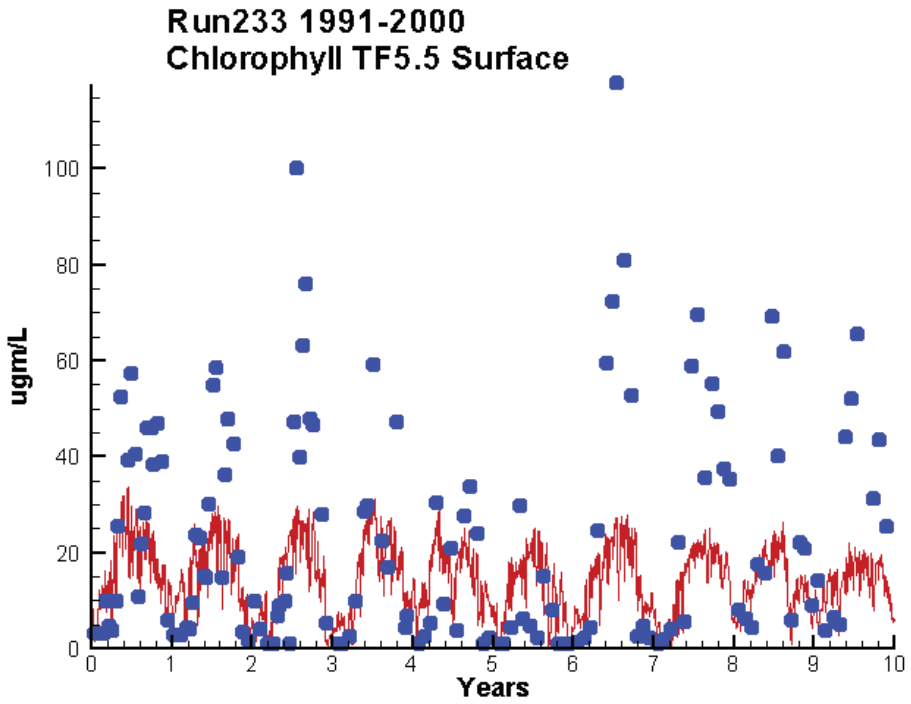

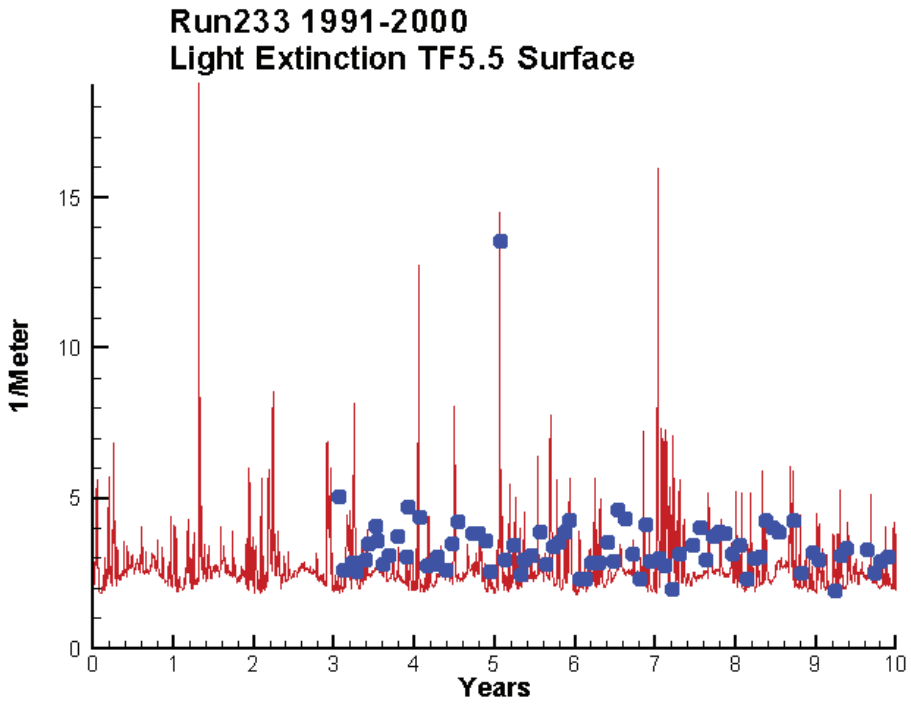

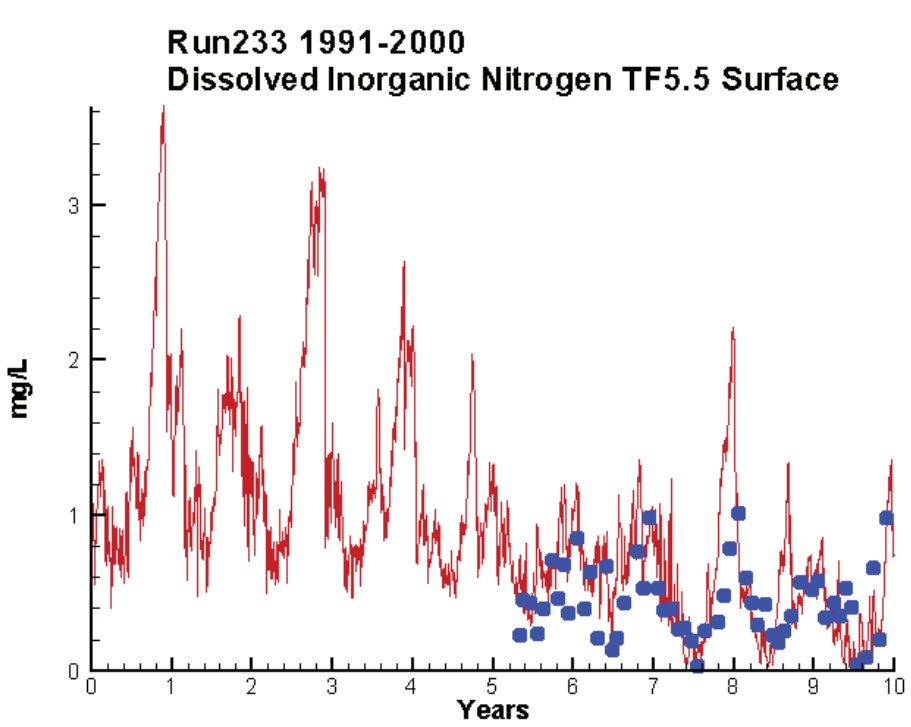

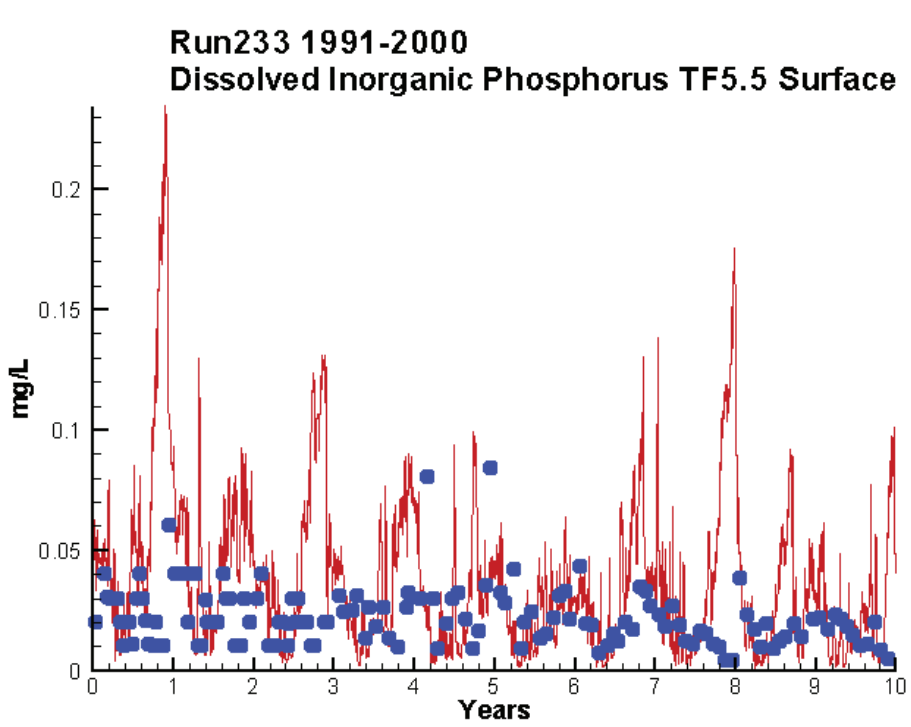

Station TF5.5

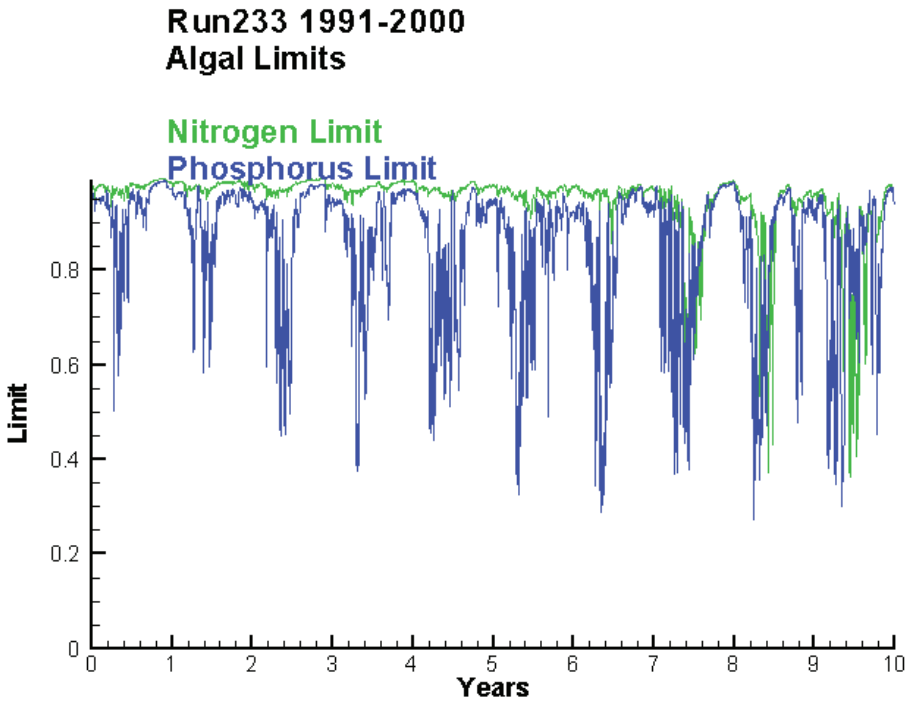

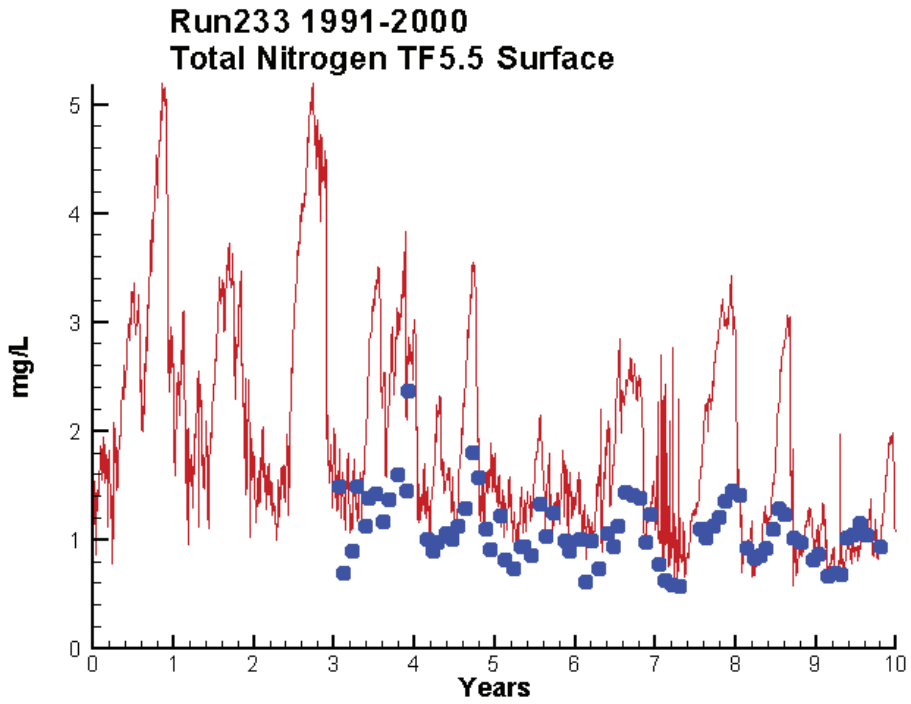

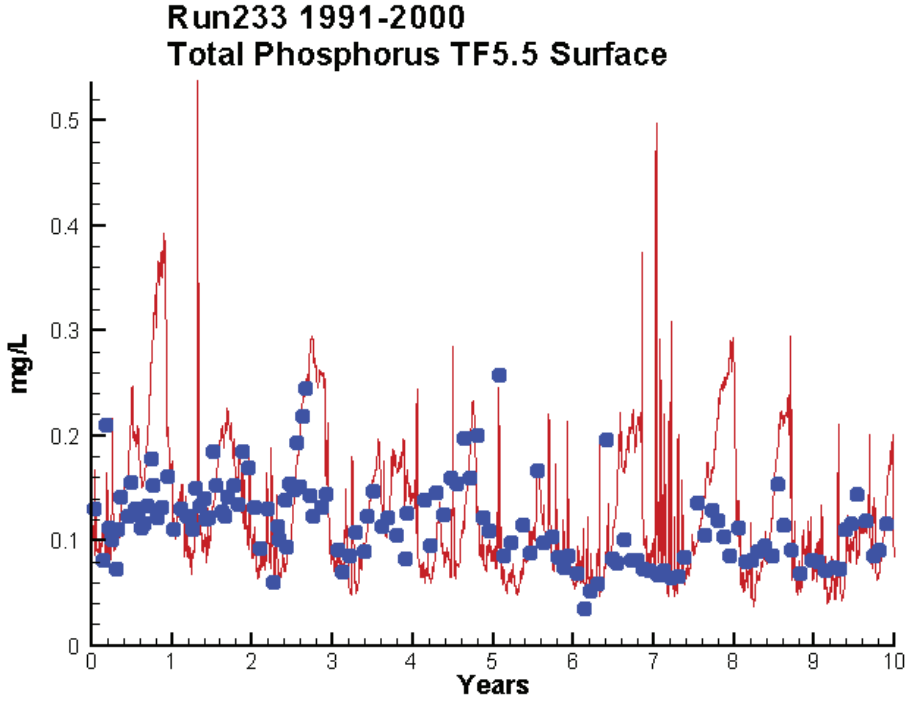

	Mean Difference	Absolute Mean Difference
Chl	-8.1648	14.5077
DIN	0.1337	0.2453
KE	-0.7350	1.1052
DIP	0.0161	0.0253
TP	0.0162	0.0450
TN	0.6113	0.6397

Station TF5.5

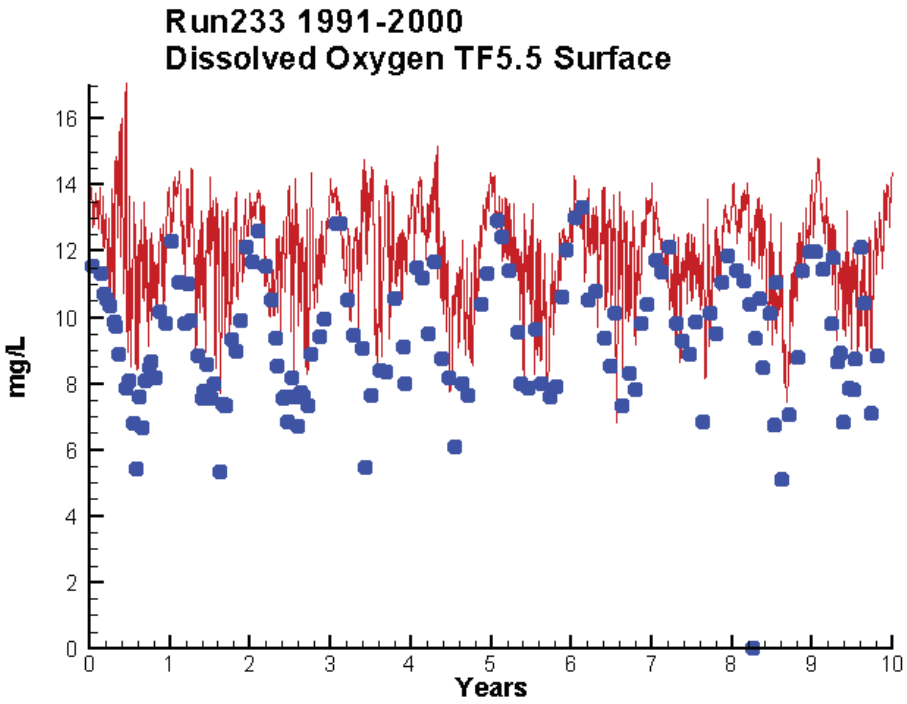

	Mean Difference	Absolute Mean Difference
Top DO	2.7723	2.8329

Station TF5.5

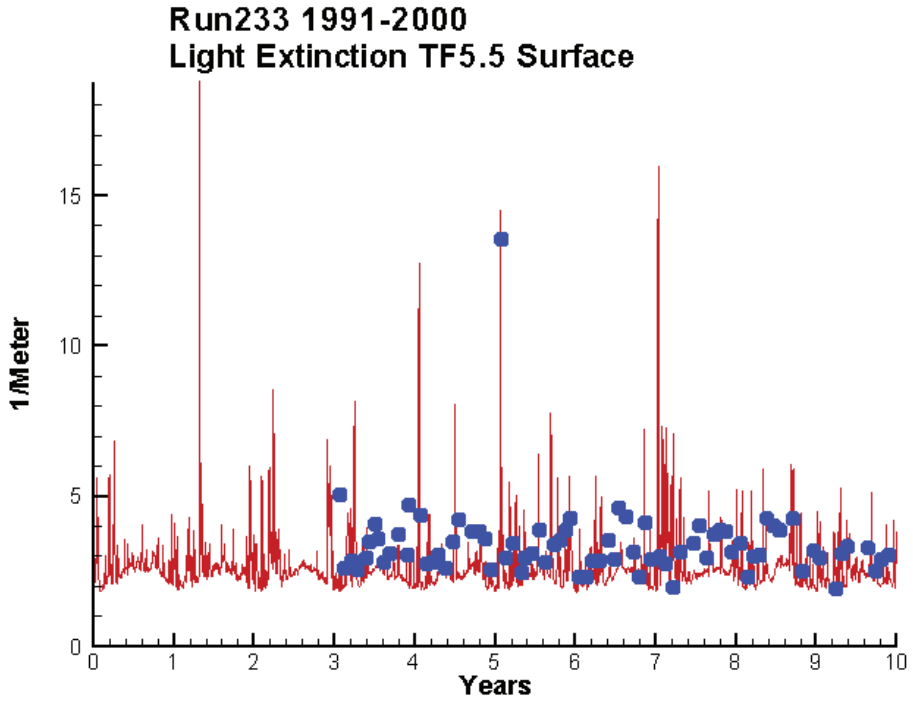

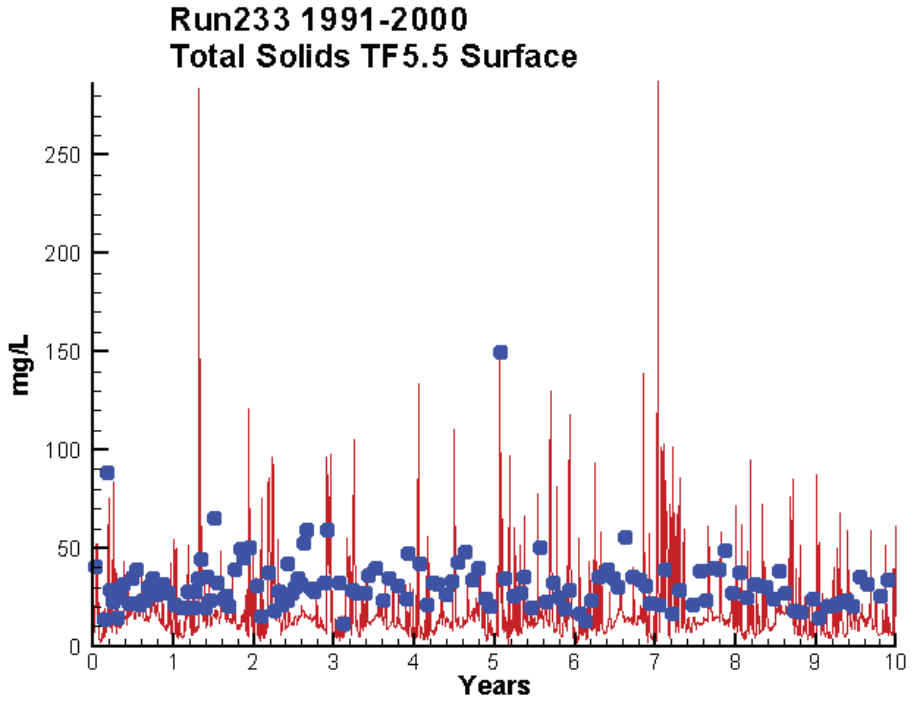

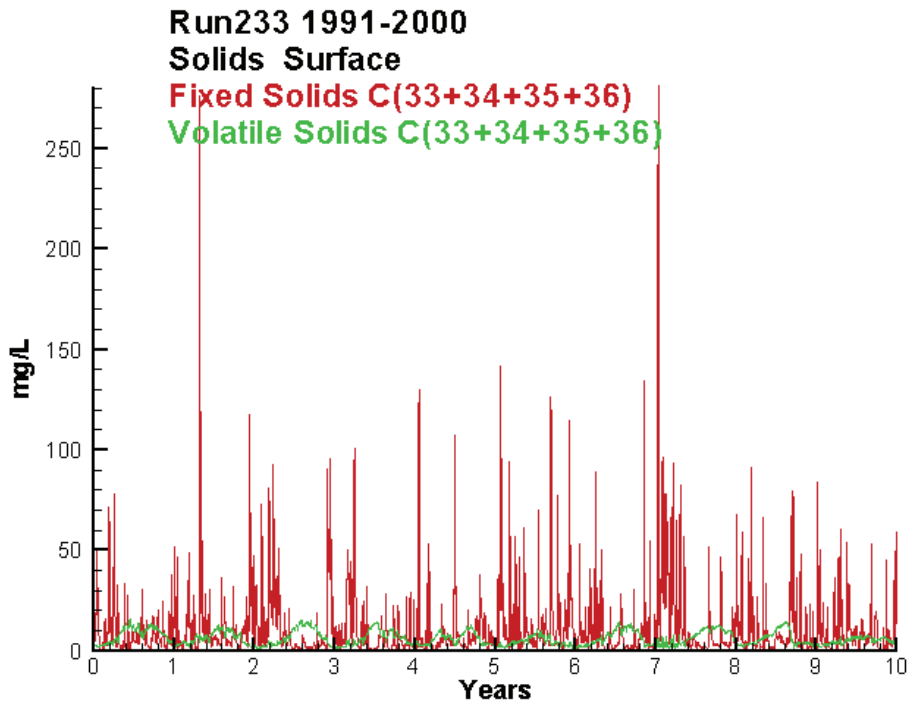

	Mean Difference	Absolute Mean Difference
KE	-0.7350	1.1052
TSS	-13.4461	17.4543

Station EE1.1

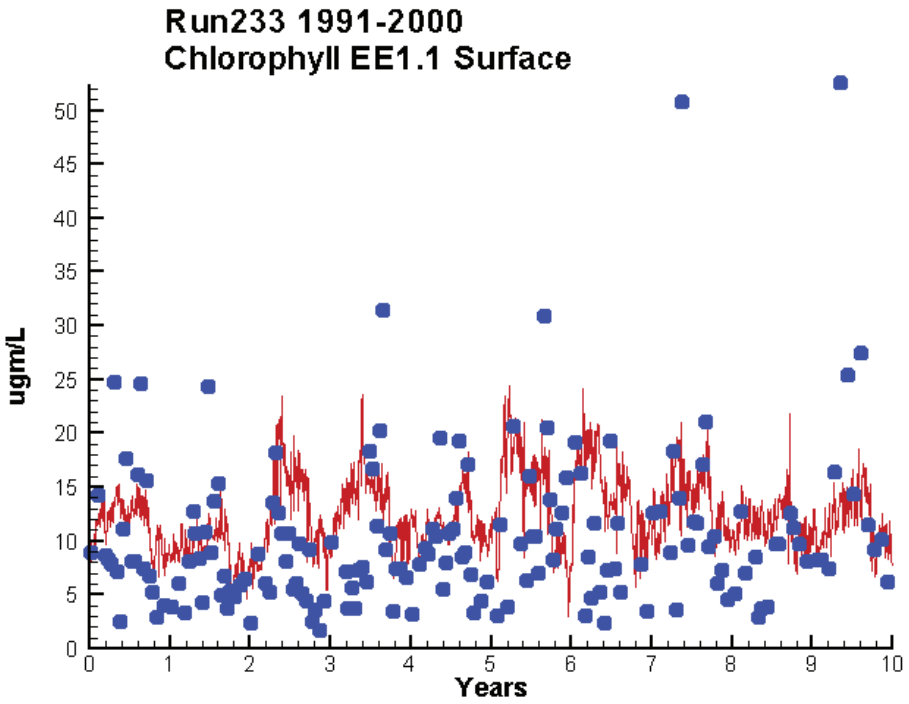

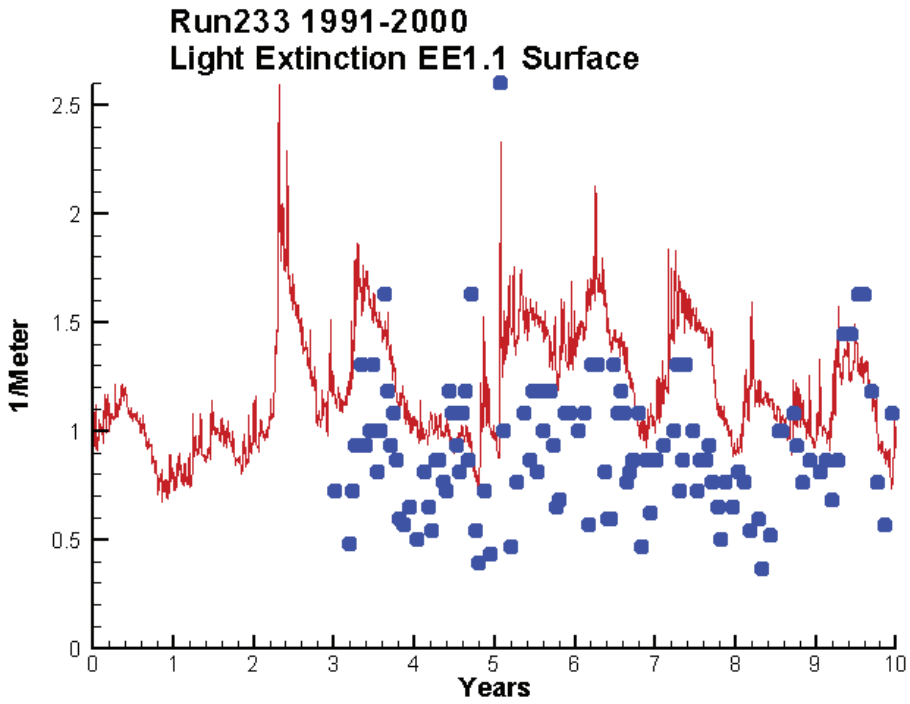

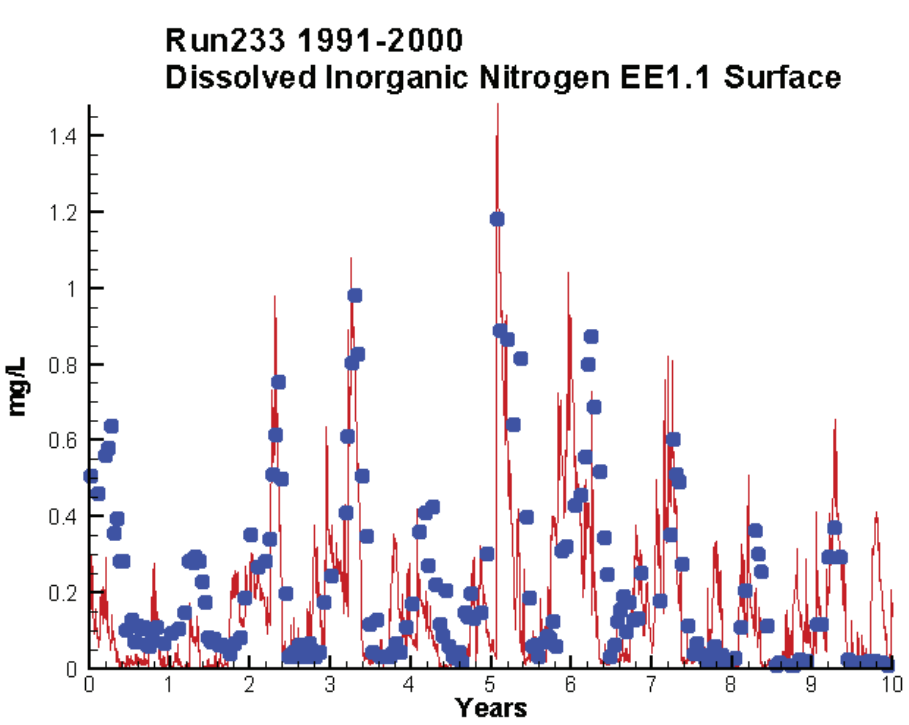

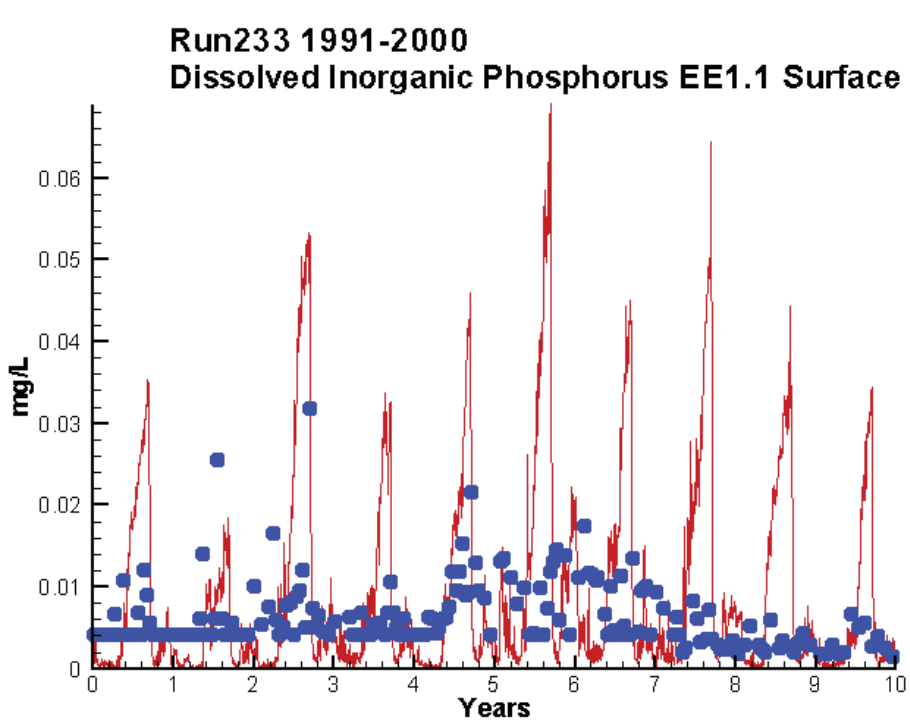

Station EE1.1

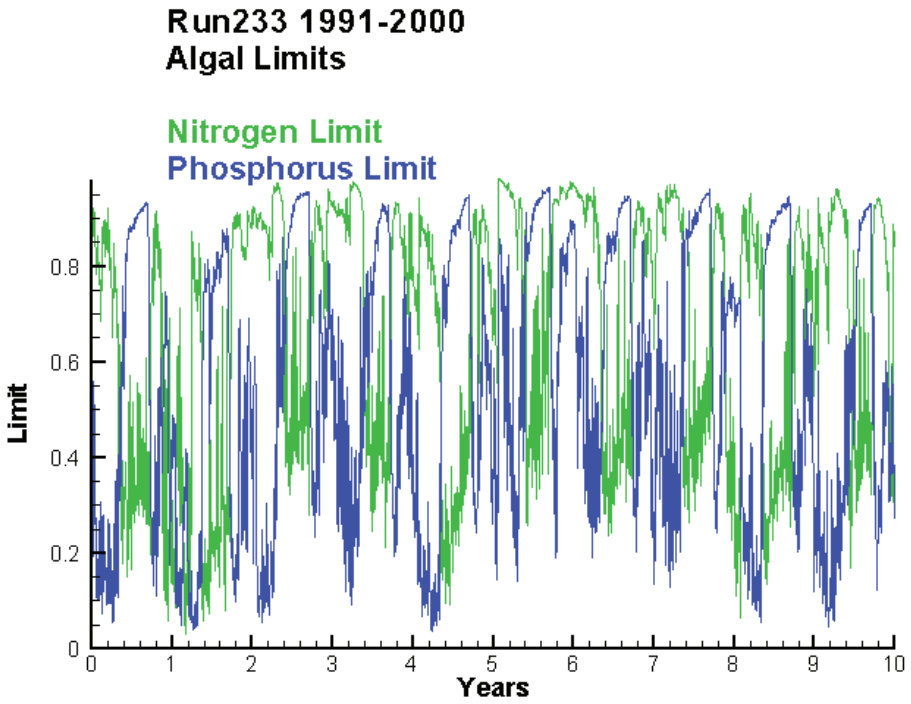

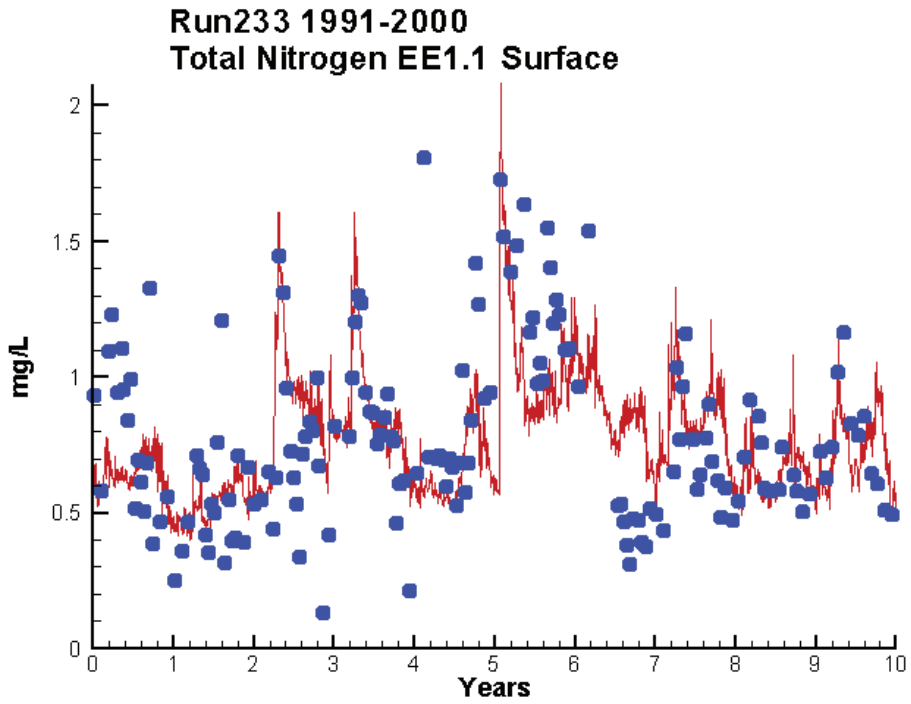

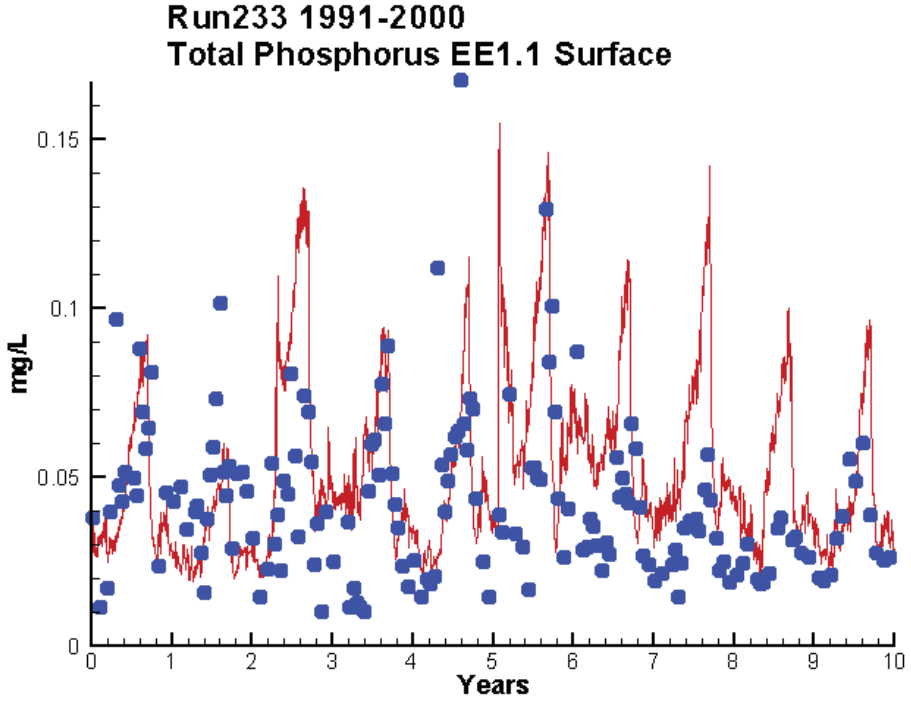

	Mean Difference	Absolute Mean Difference
Chl	2.2476	5.4234
DIN	-0.0661	0.1402
KE	0.3392	0.4082
DIP	0.0042	0.0094
TP	0.0118	0.0231
TN	-0.0051	0.2035

Station EE1.1

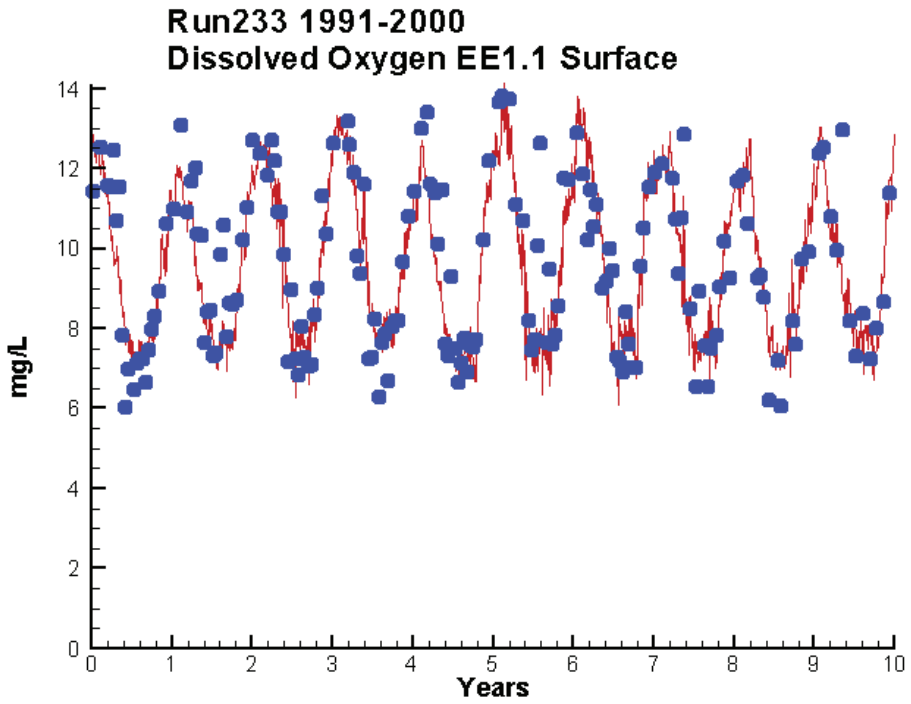

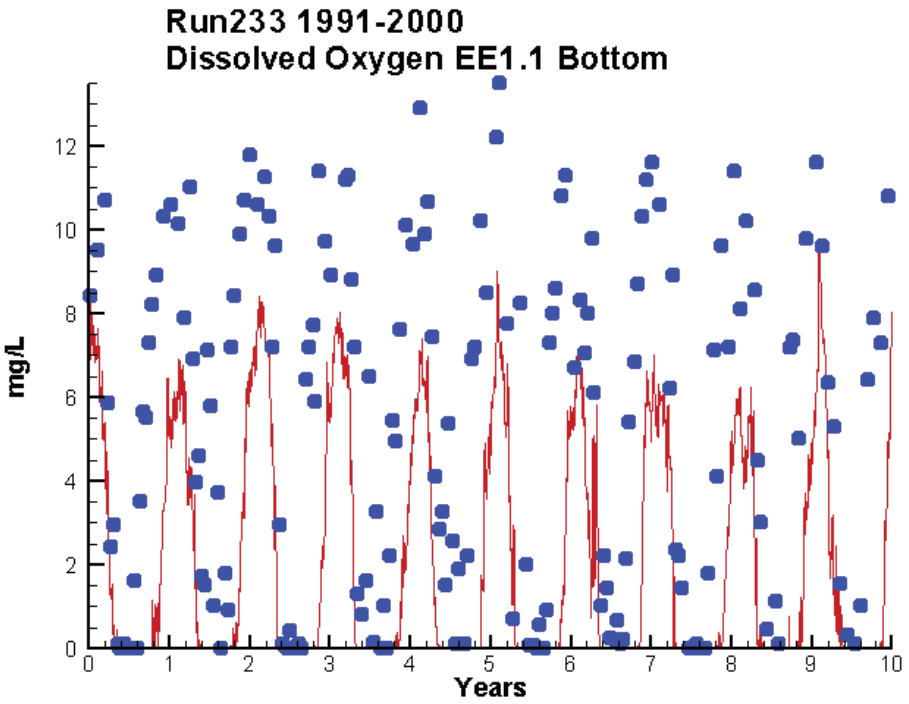

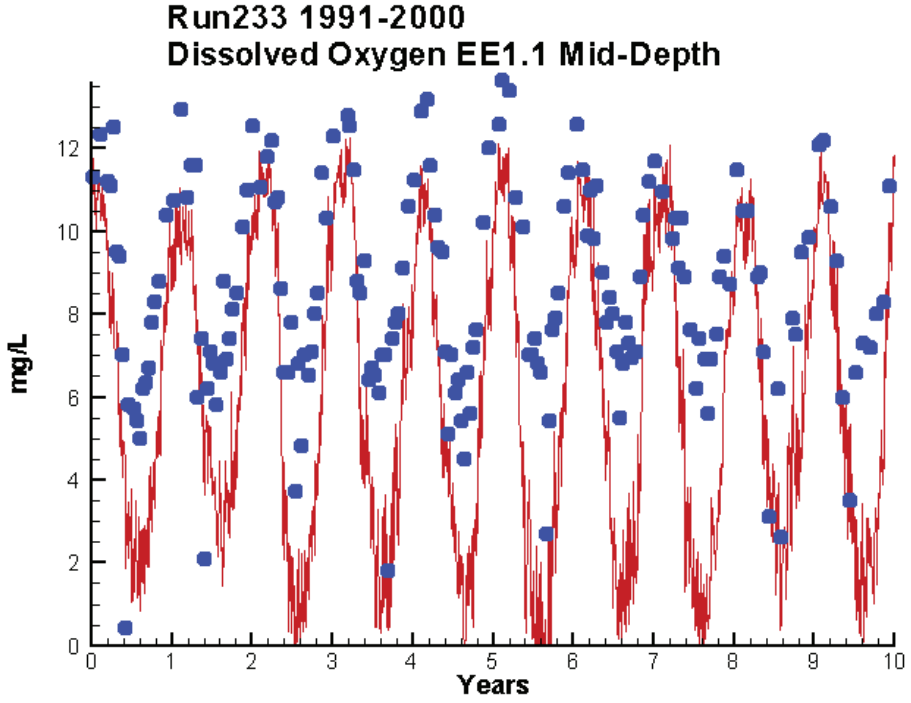

	Mean Difference	Absolute Mean Difference
Top DO	-0.1711	0.7925
Mid DO	-3.1073	3.1919
Bot DO	-3.5841	3.6095

Station EE1.1

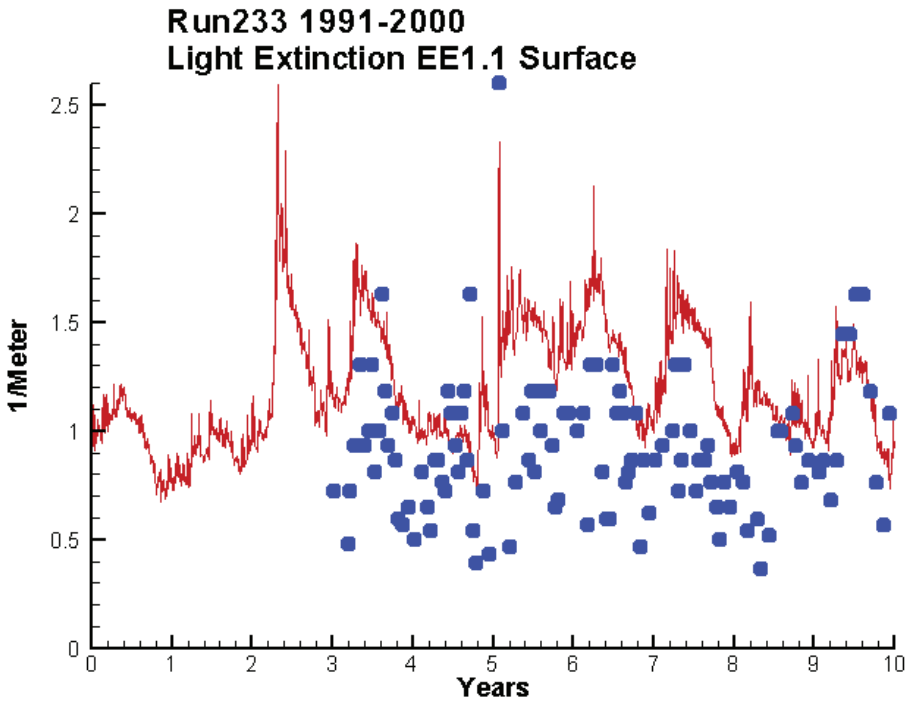

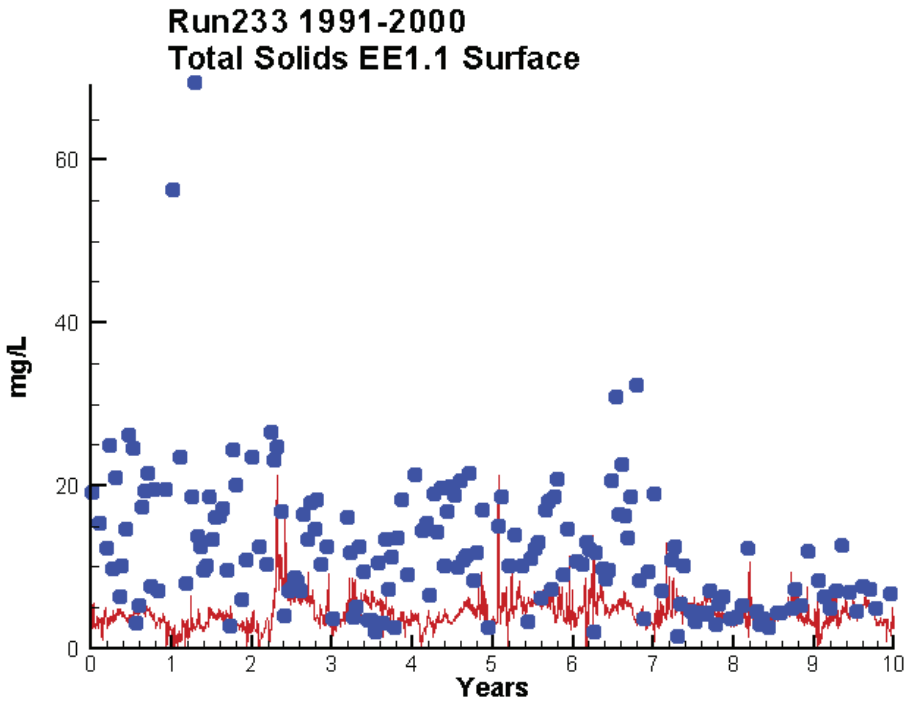

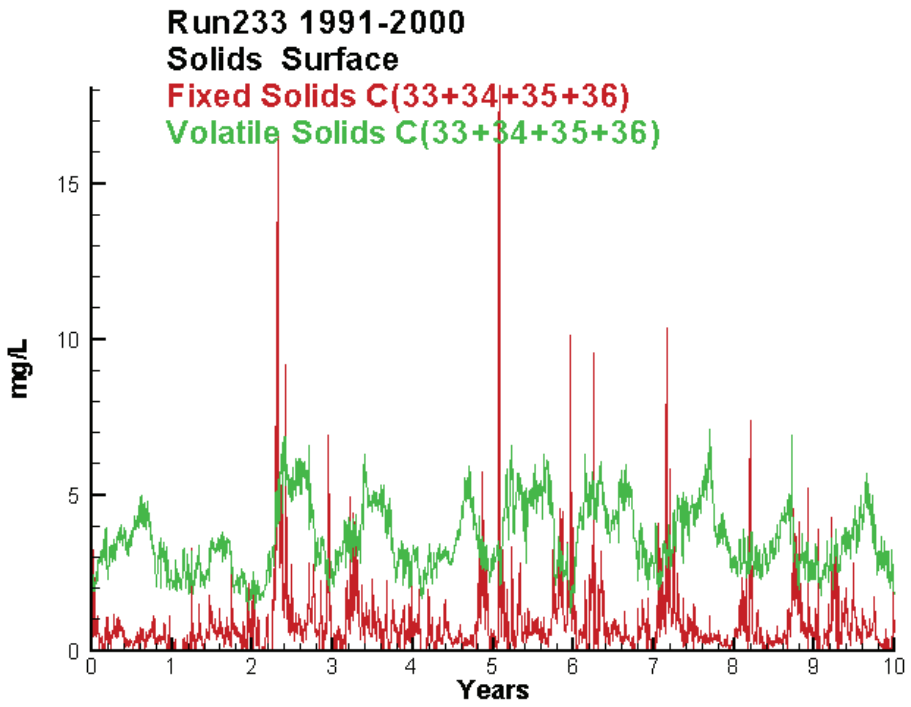

	Mean Difference	Absolute Mean Difference
KE	0.3392	0.4082
TSS	-7.8569	8.3531

Station EE2.1

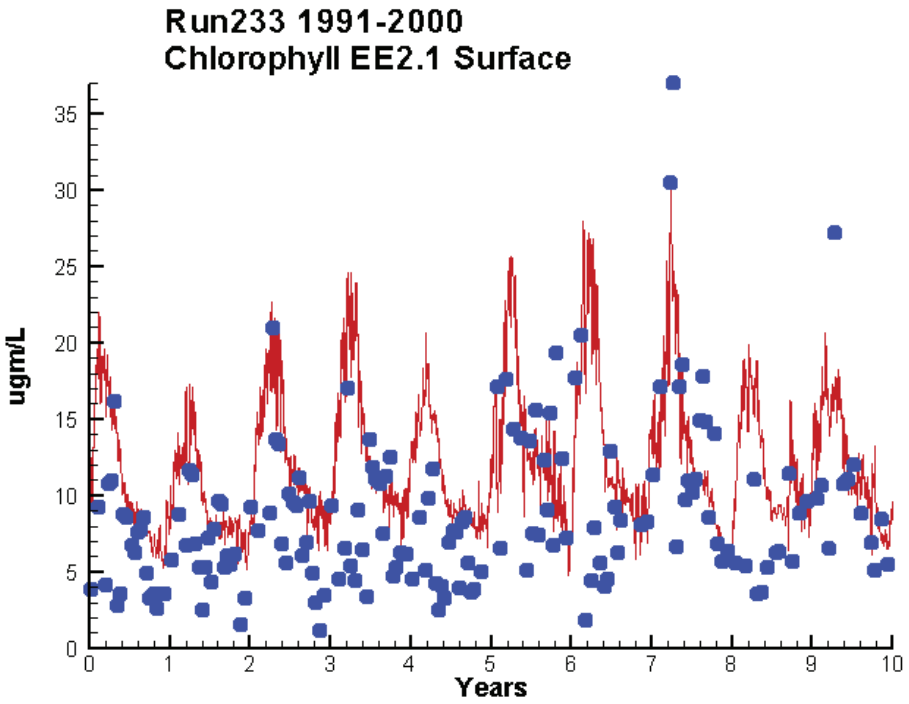

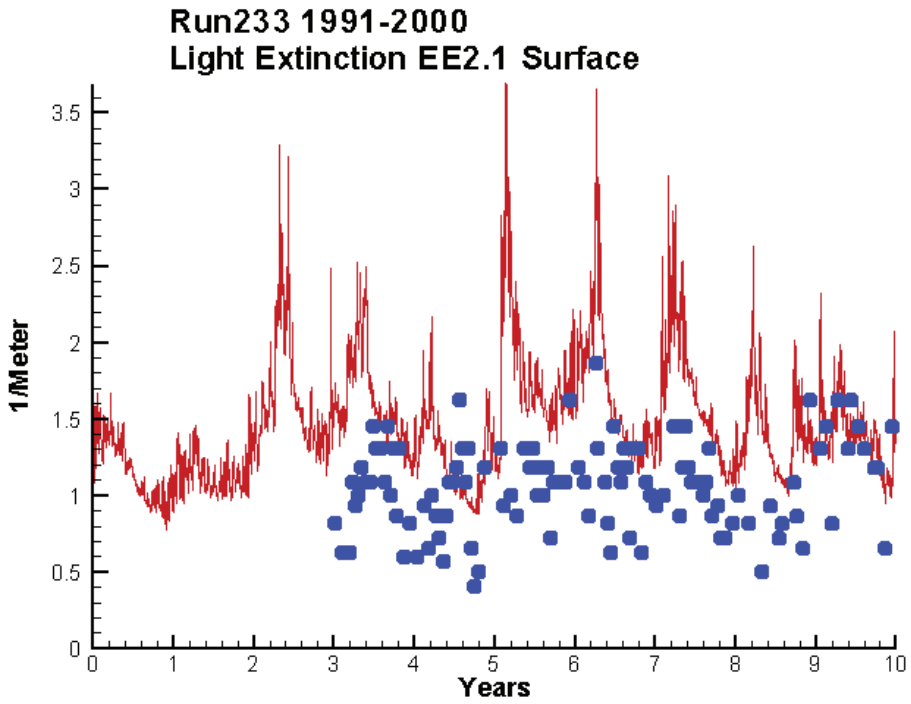

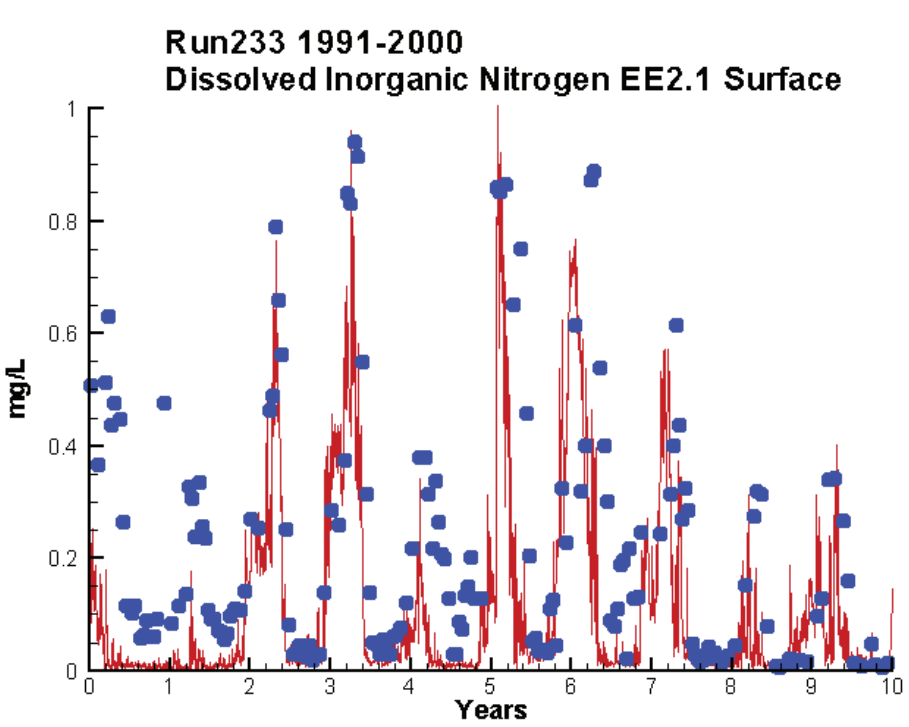

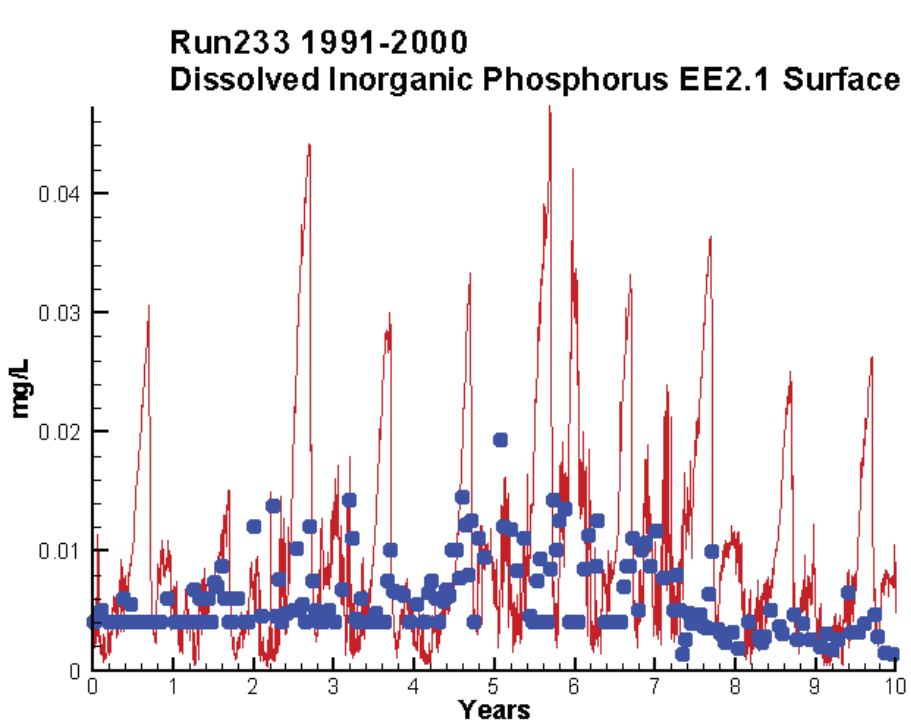

Station EE2.1

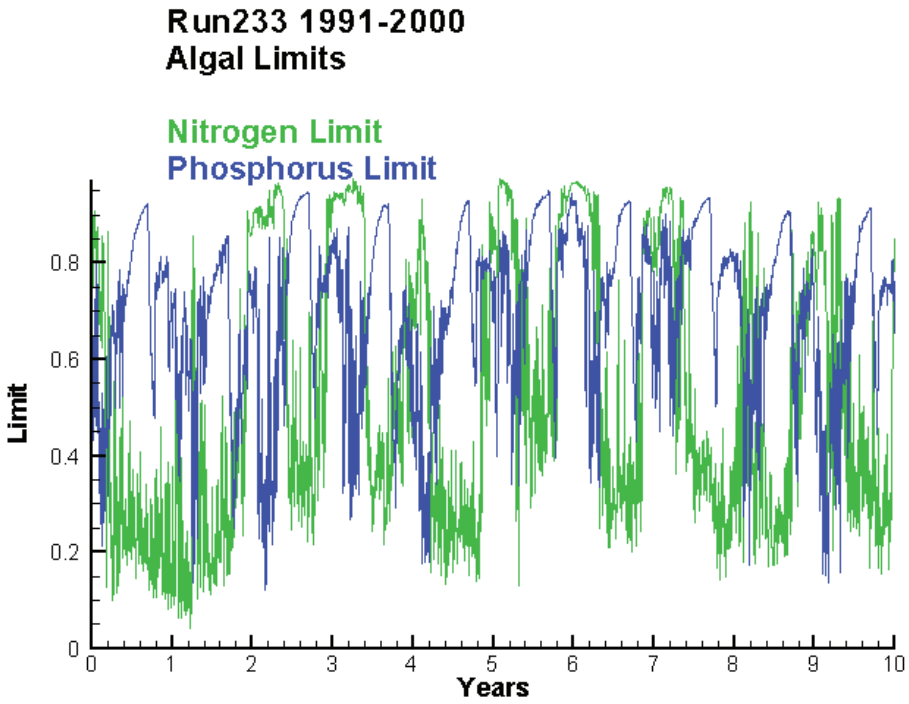

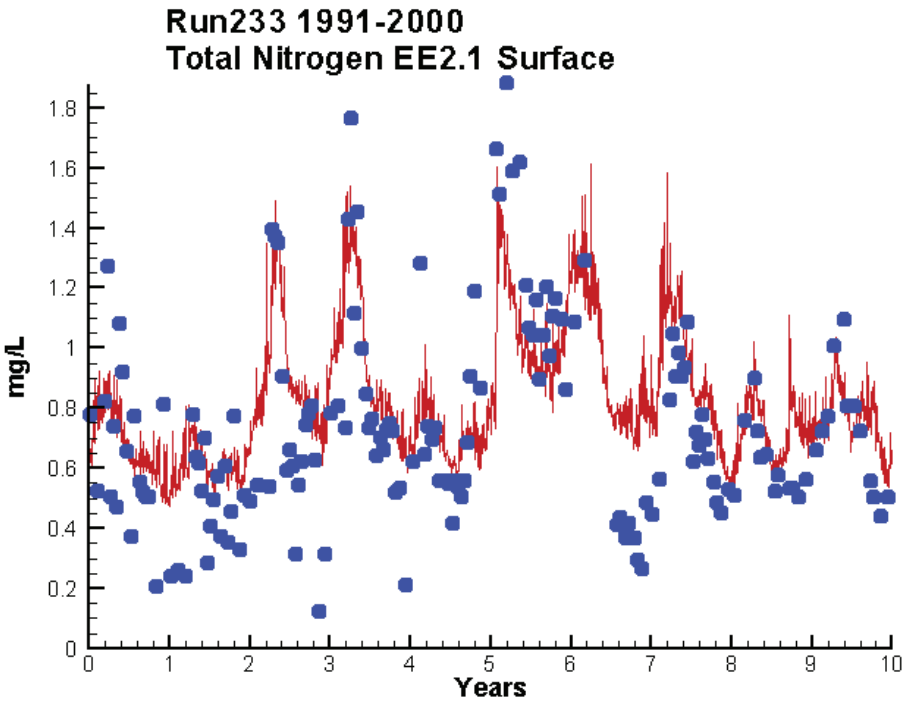

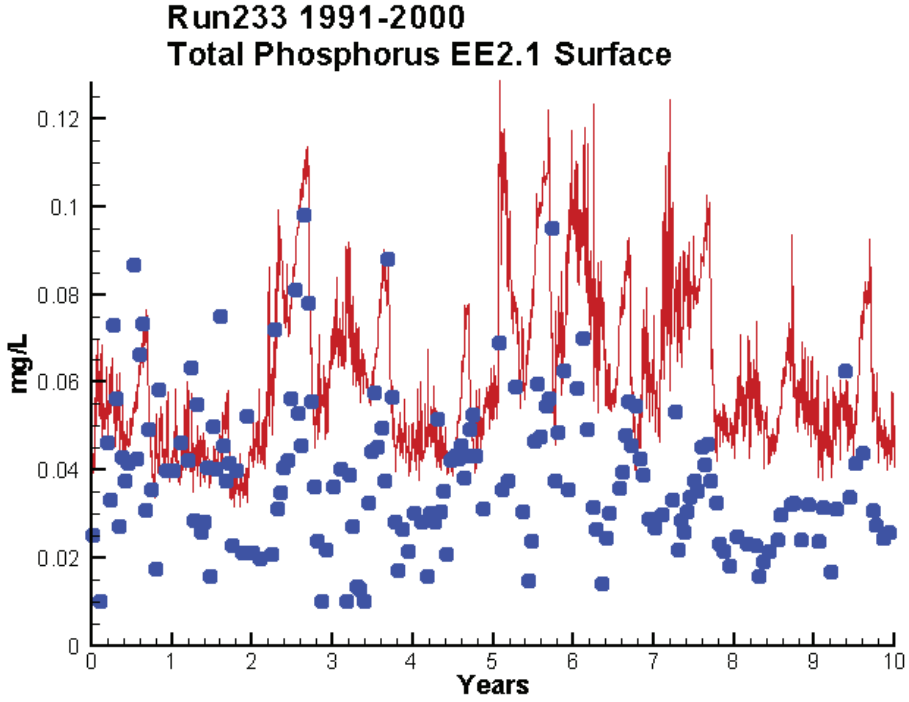

	Mean Difference	Absolute Mean Difference
Chl	3.3357	4.5512
DIN	-0.1187	0.1478
KE	0.4626	0.5068
DIP	0.0052	0.0073
TP	0.0242	0.0268
TN	0.1010	0.1918

Station EE2.1

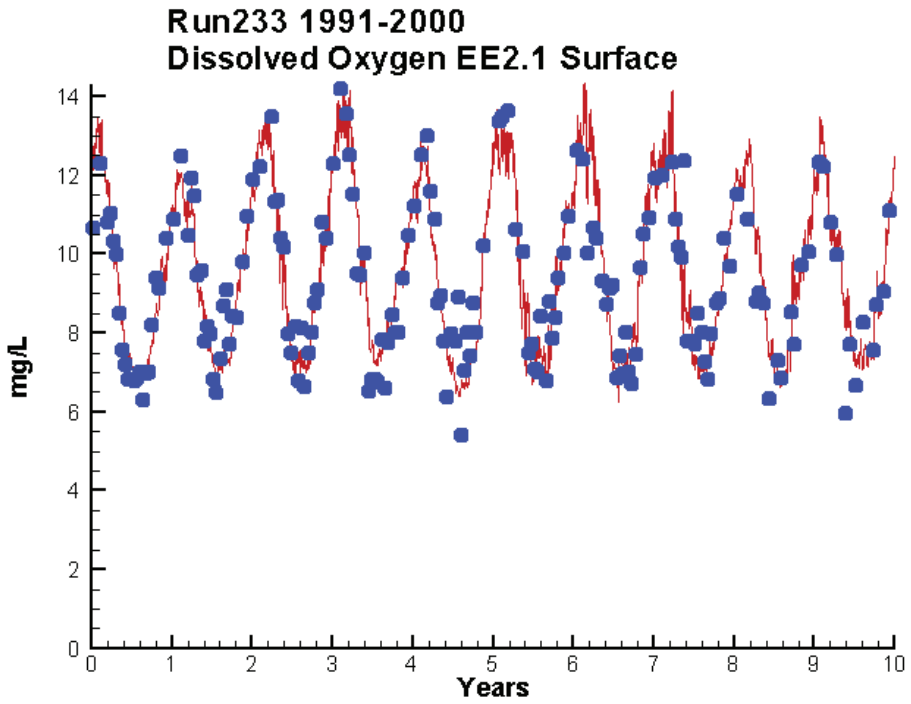

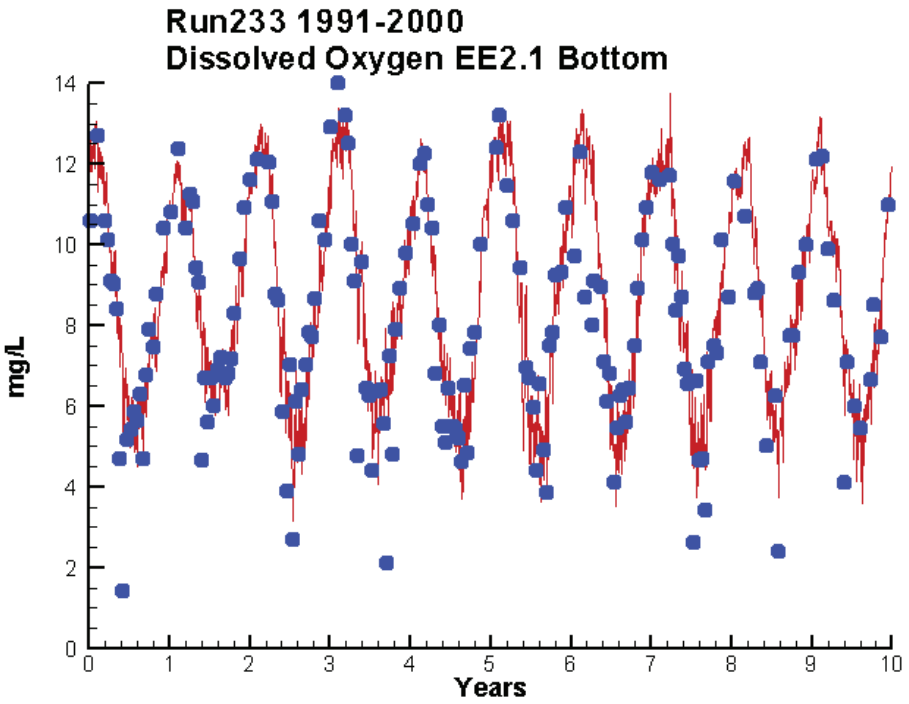

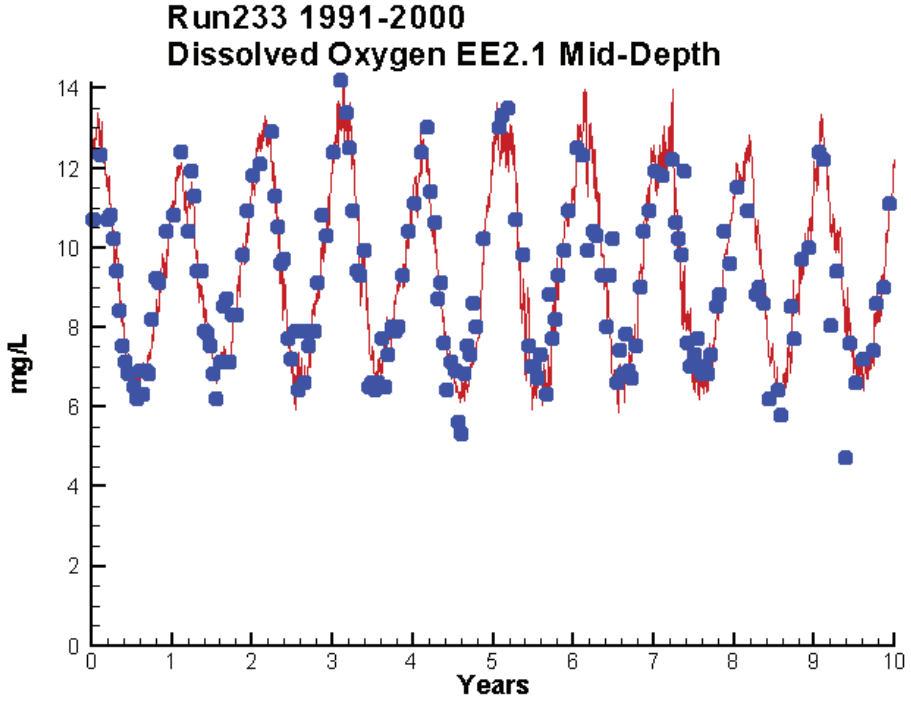

	Mean Difference	Absolute Mean Difference
Top DO	0.0522	0.6692
Mid DO	0.0577	0.6363
Bot DO	0.2528	0.8797

Station EE2.1

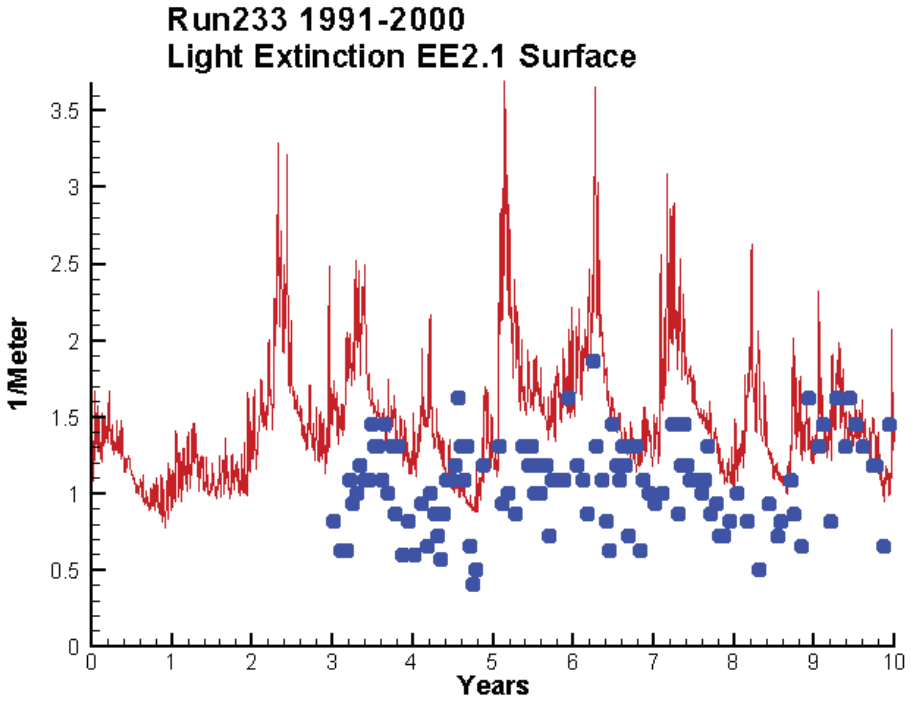

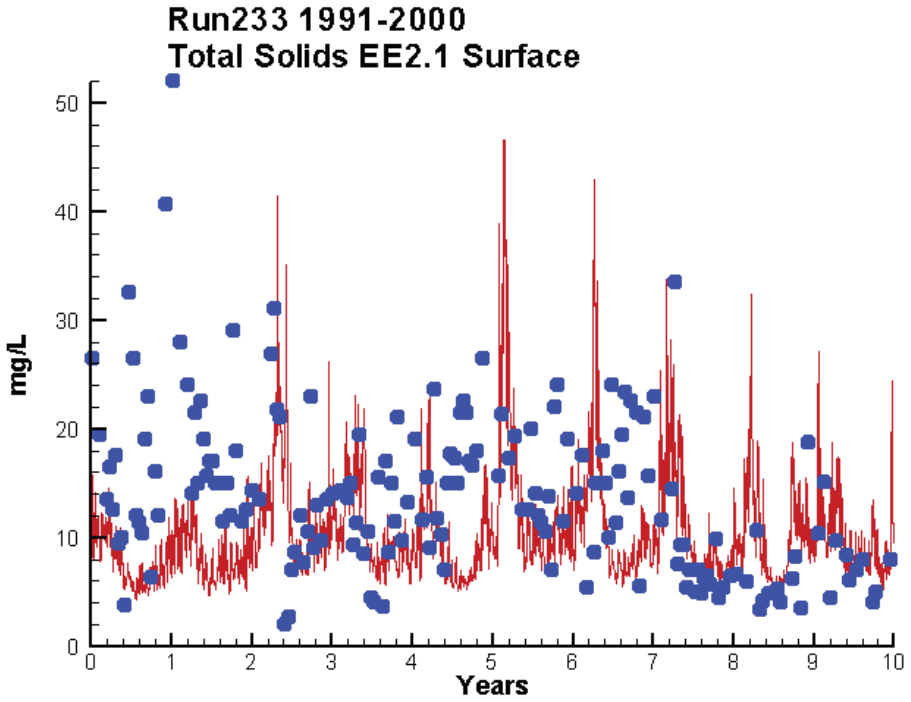

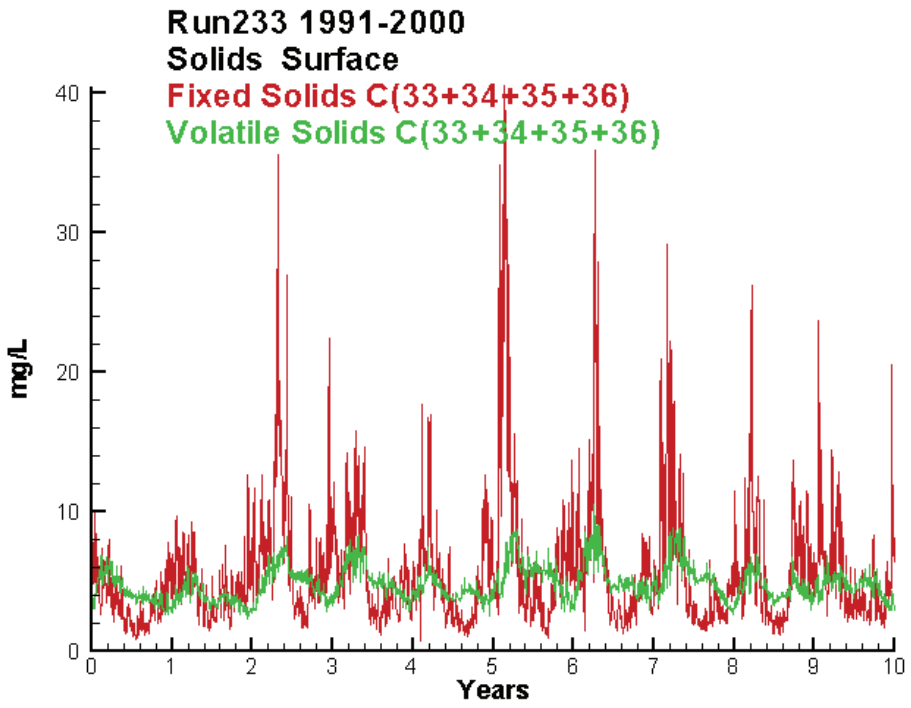

	Mean Difference	Absolute Mean Difference
KE	0.4626	0.5068
TSS	-3.9173	7.0082

Station EE3.1

Run233 1991-2000
Chlorophyll EE3.1 Surface

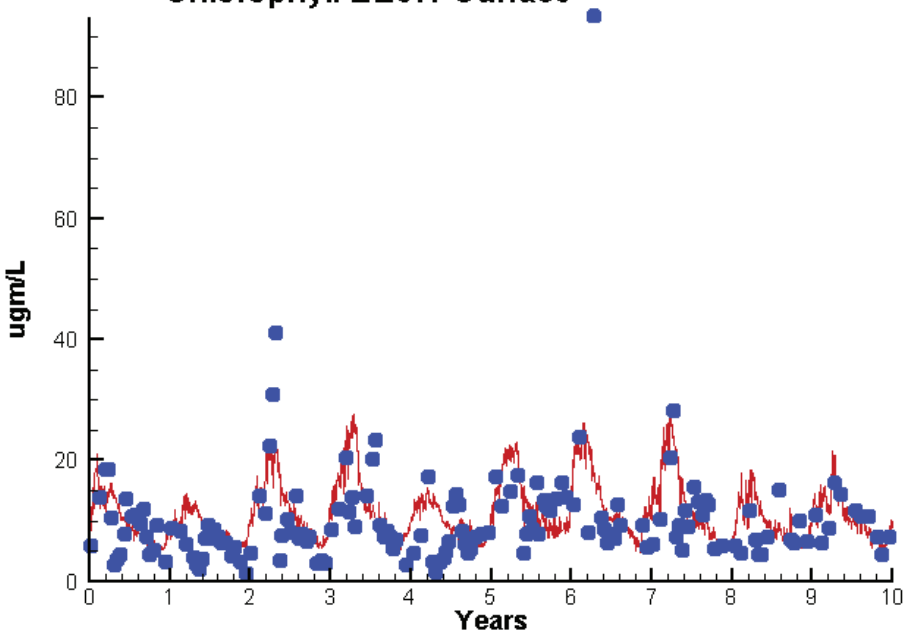

Run233 1991-2000
Light Extinction EE3.1 Surface

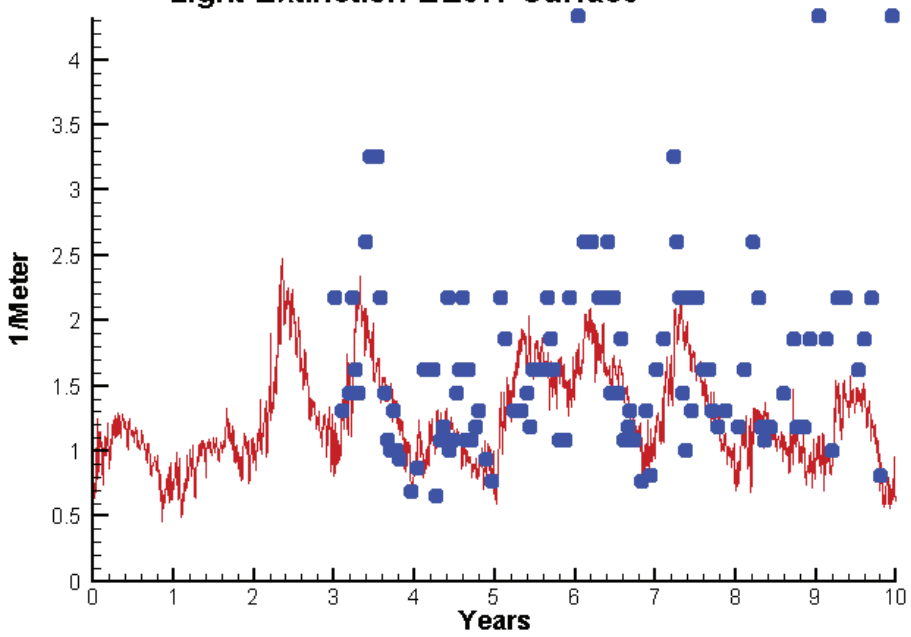

Run233 1991-2000
Dissolved Inorganic Nitrogen EE3.1 Surface

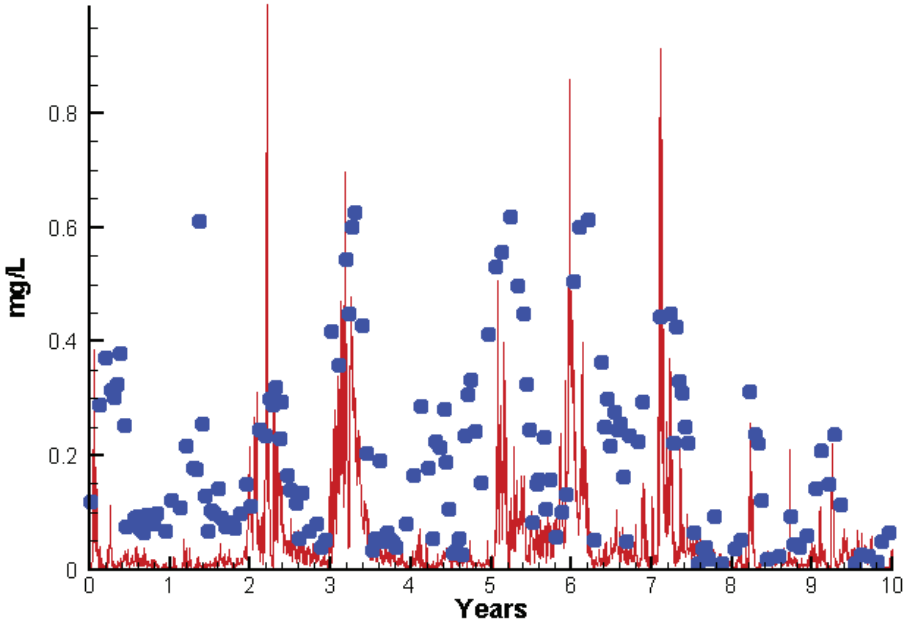

Run233 1991-2000
Dissolved Inorganic Phosphorus EE3.1 Surface

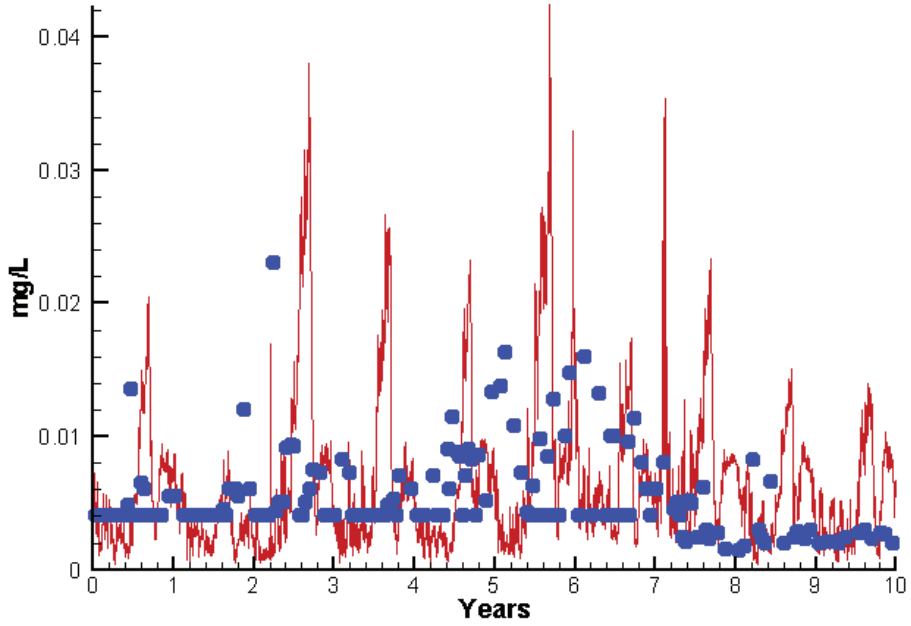

Station EE3.1

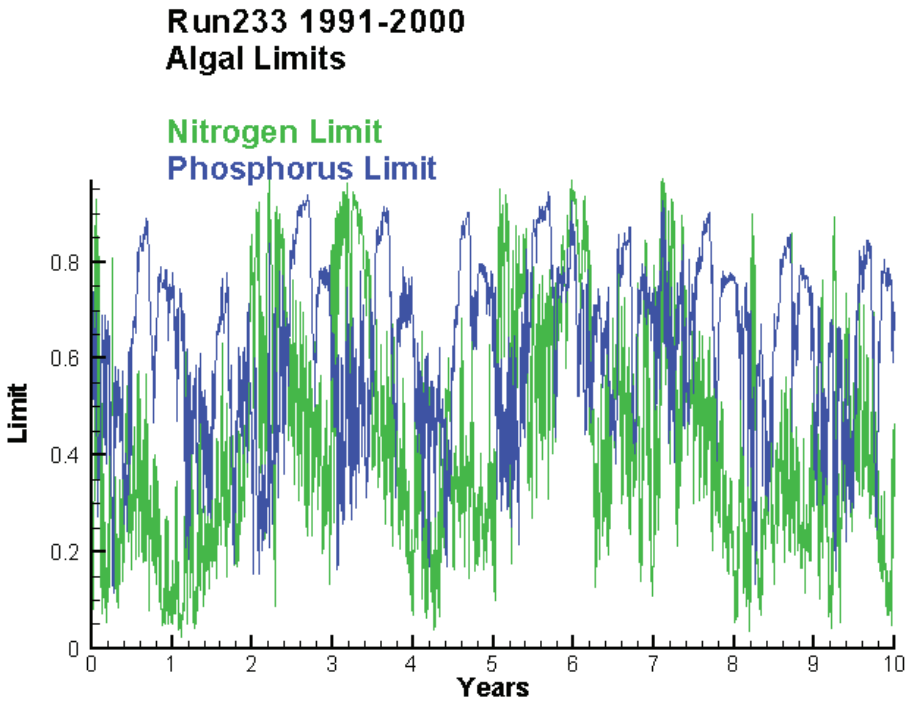

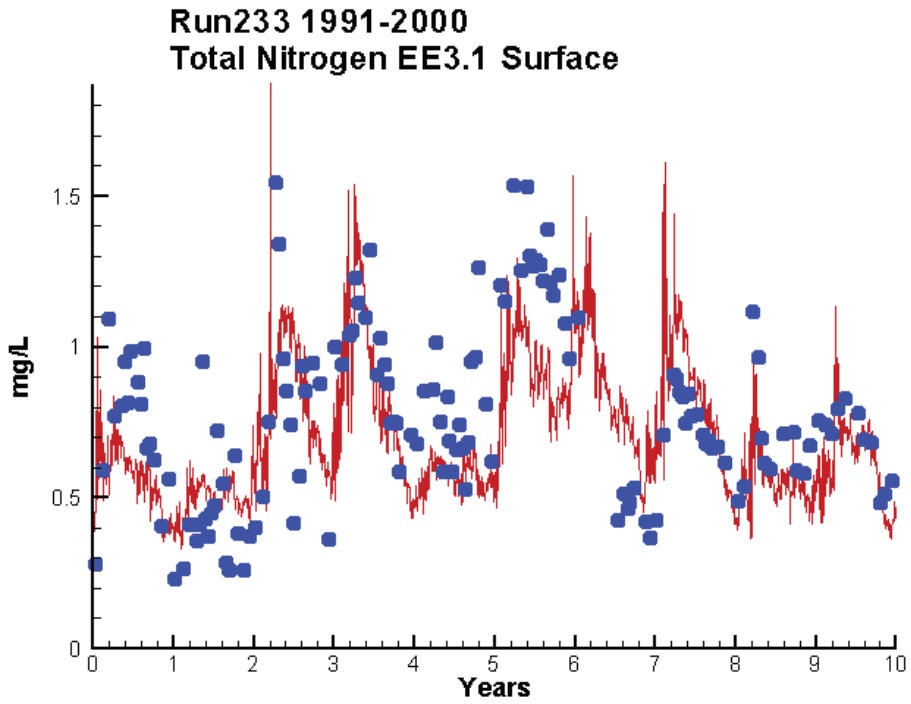

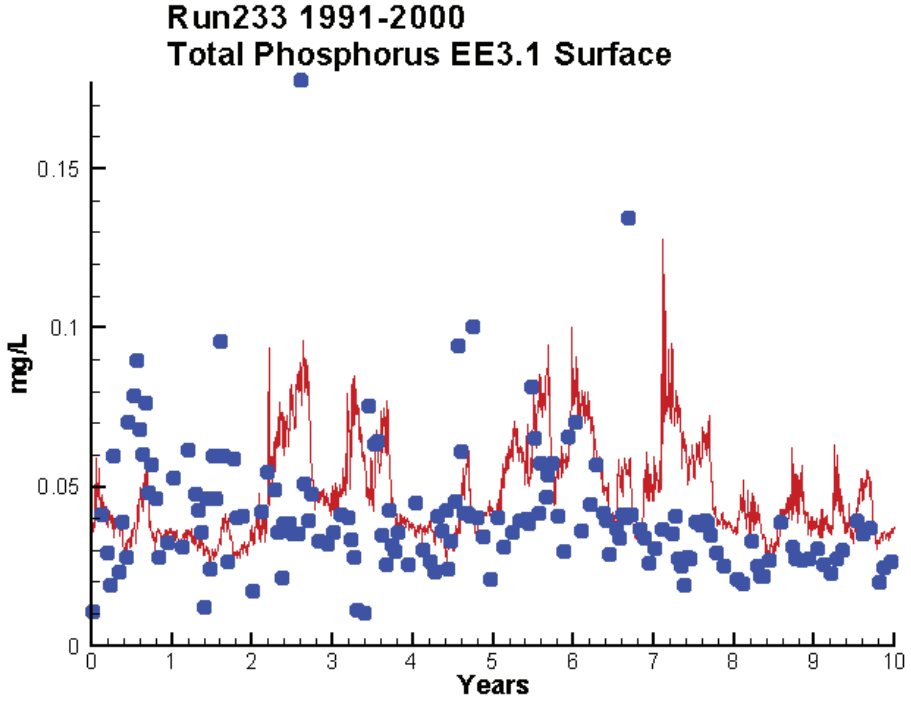

	Mean Difference	Absolute Mean Difference
Chl	1.3142	4.7401
DIN	-0.1451	0.1528
KE	-0.3248	0.5111
DIP	0.0017	0.0051
TP	0.0078	0.0198
TN	-0.0710	0.2057

Station EE3.1

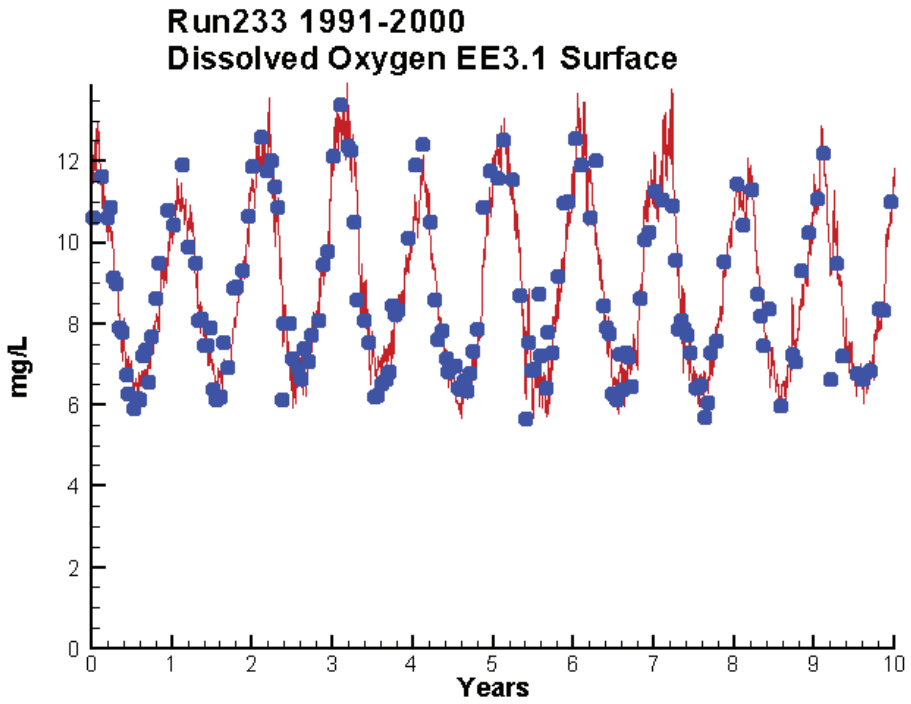

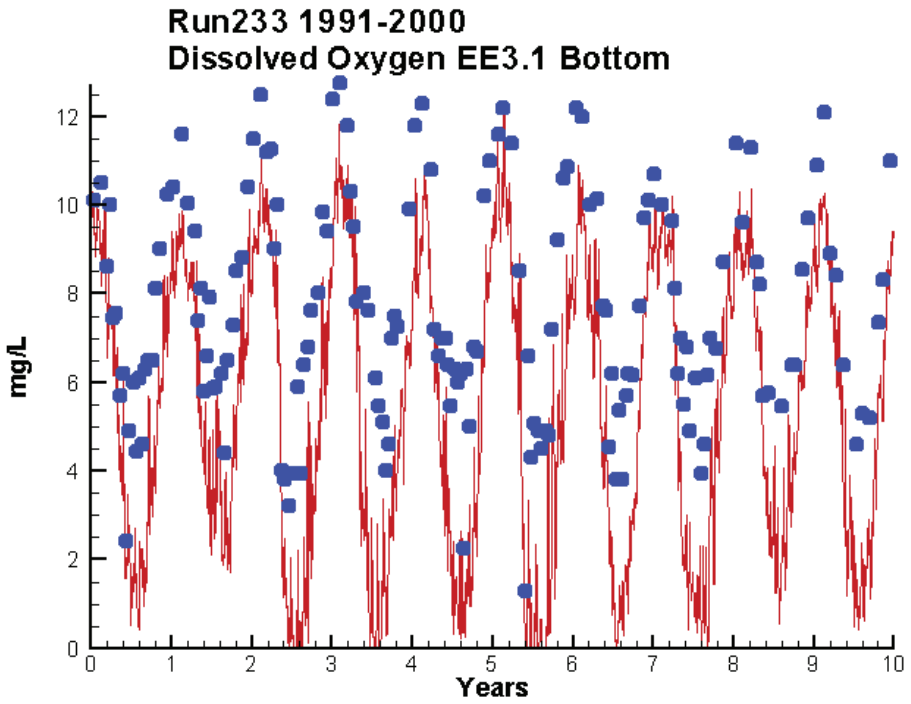

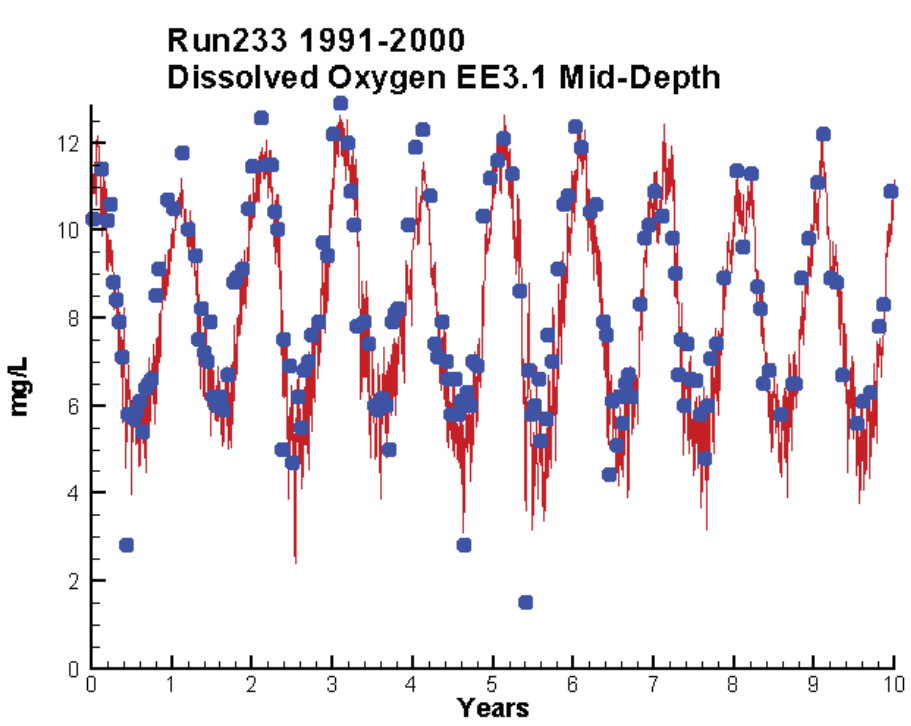

	Mean Difference	Absolute Mean Difference
Top DO	0.0232	0.5461
Mid DO	-0.3924	0.8008
Bot DO	-2.8703	2.8732

Station EE3.1

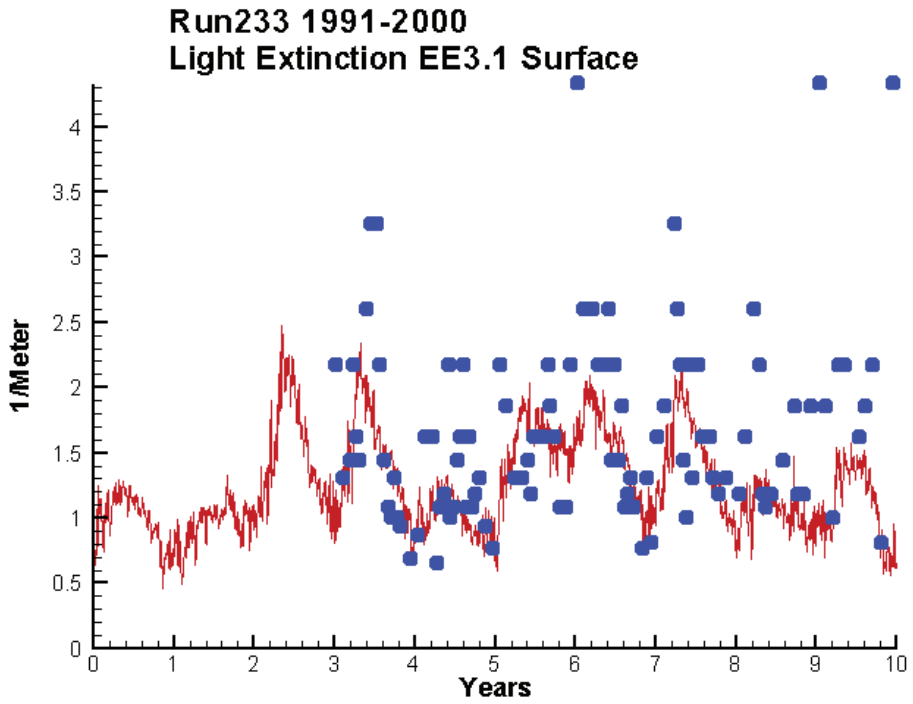

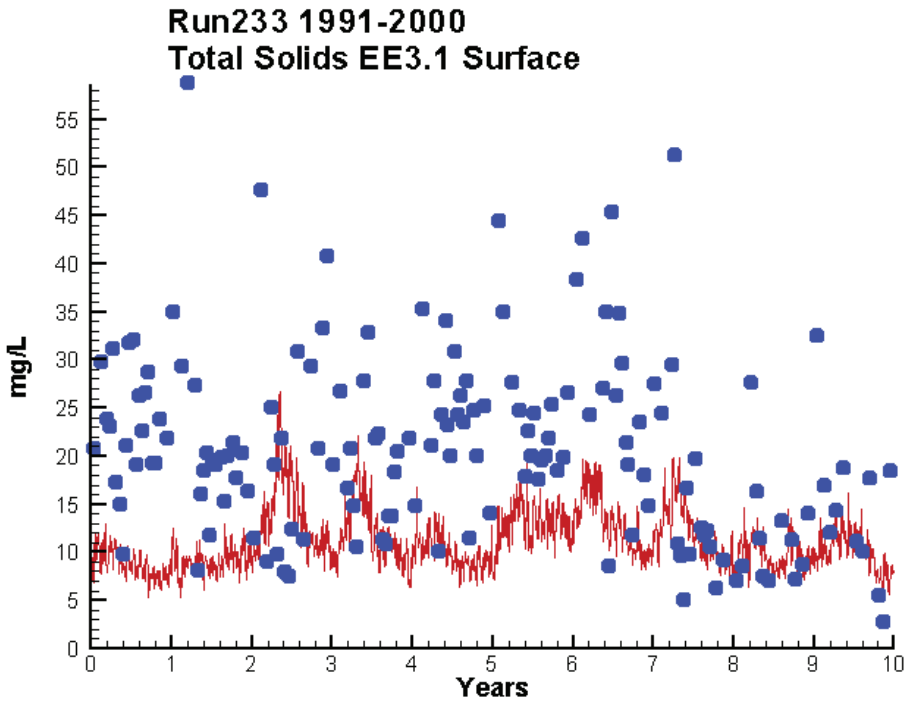

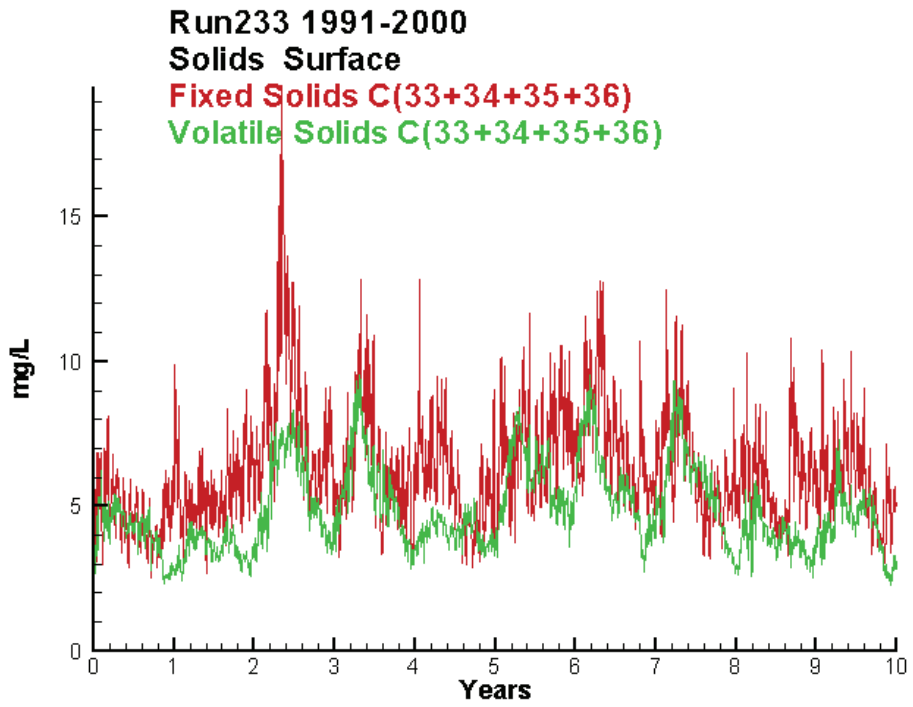

	Mean Difference	Absolute Mean Difference
KE	-0.3248	0.5111
TSS	-9.5482	10.9110

Station ET1.1

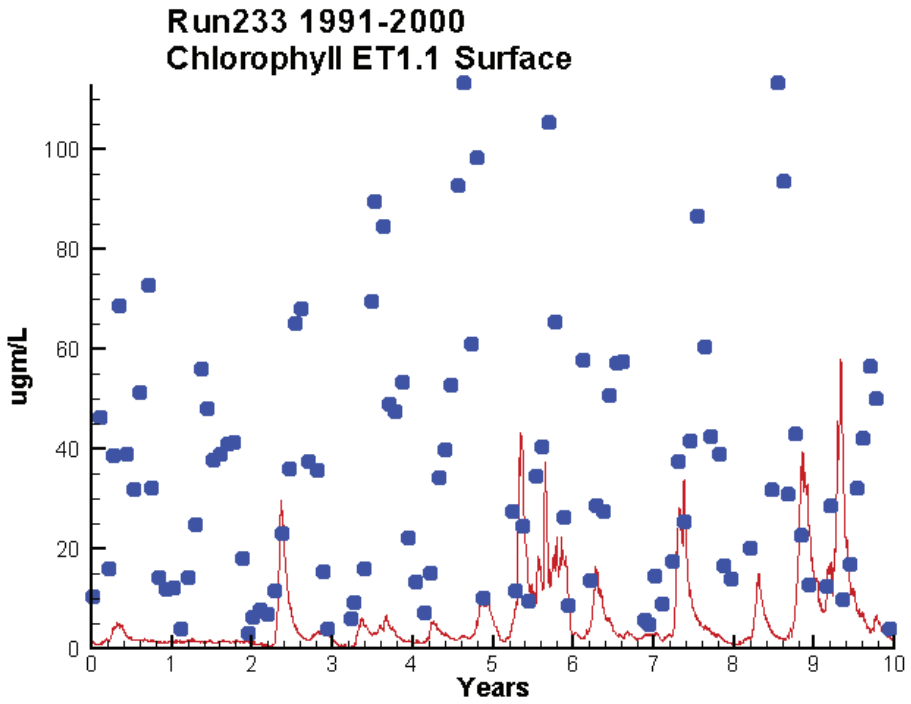

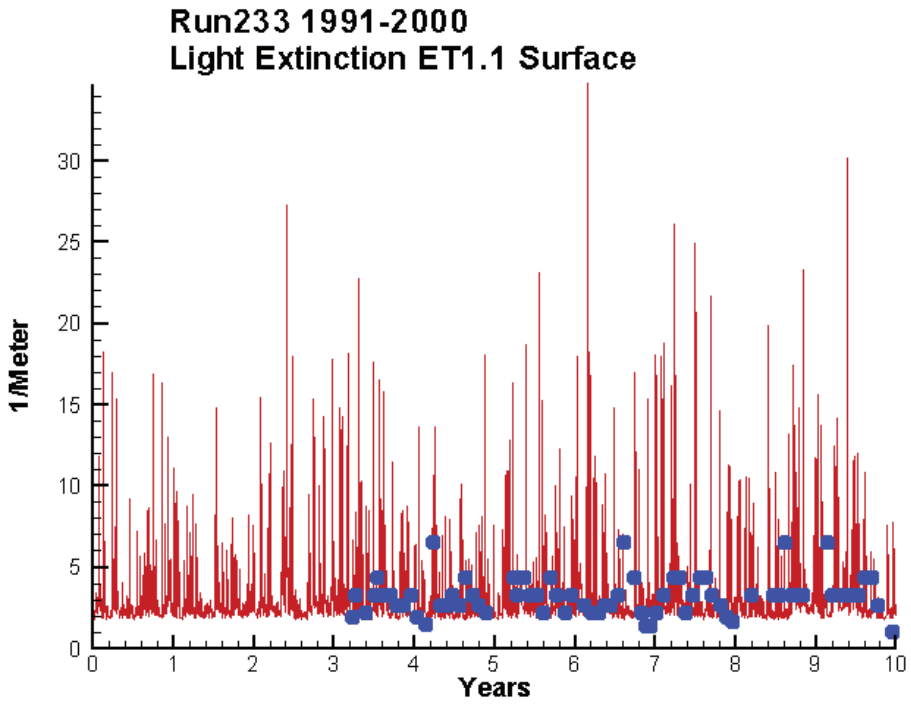

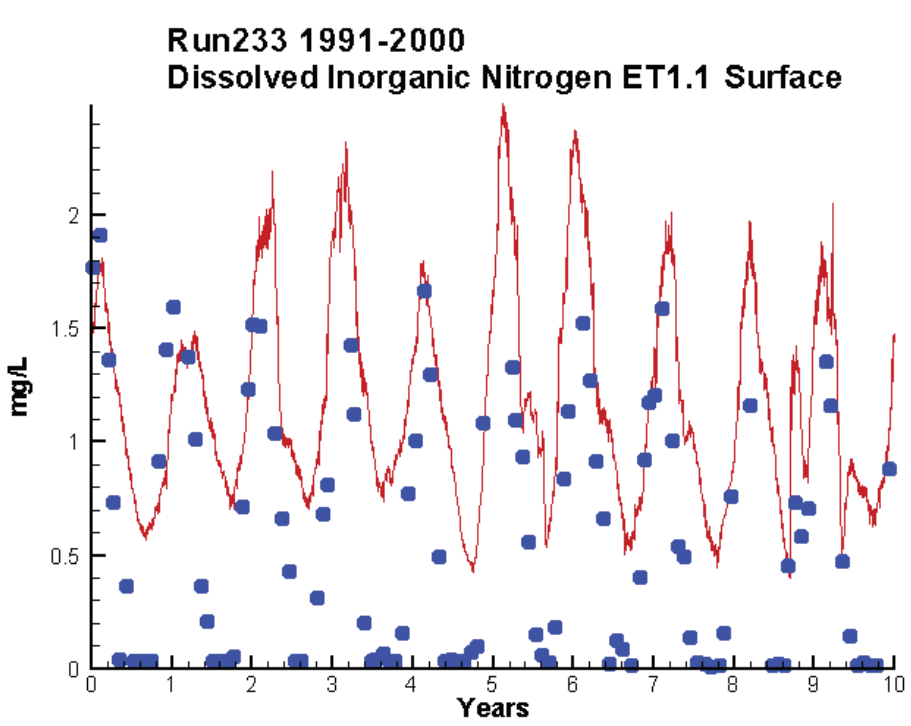

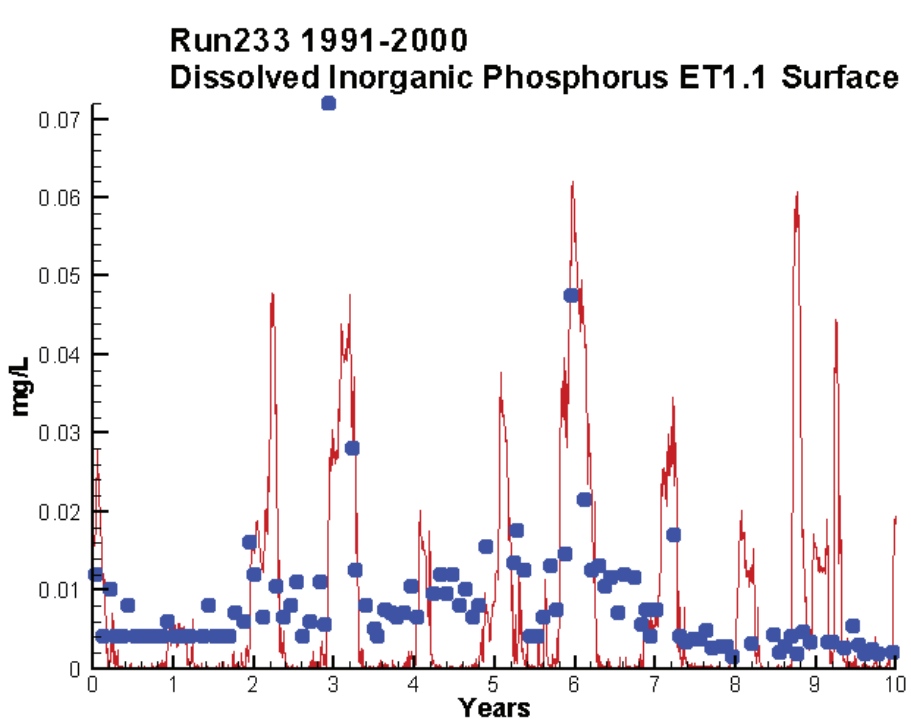

Station ET1.1

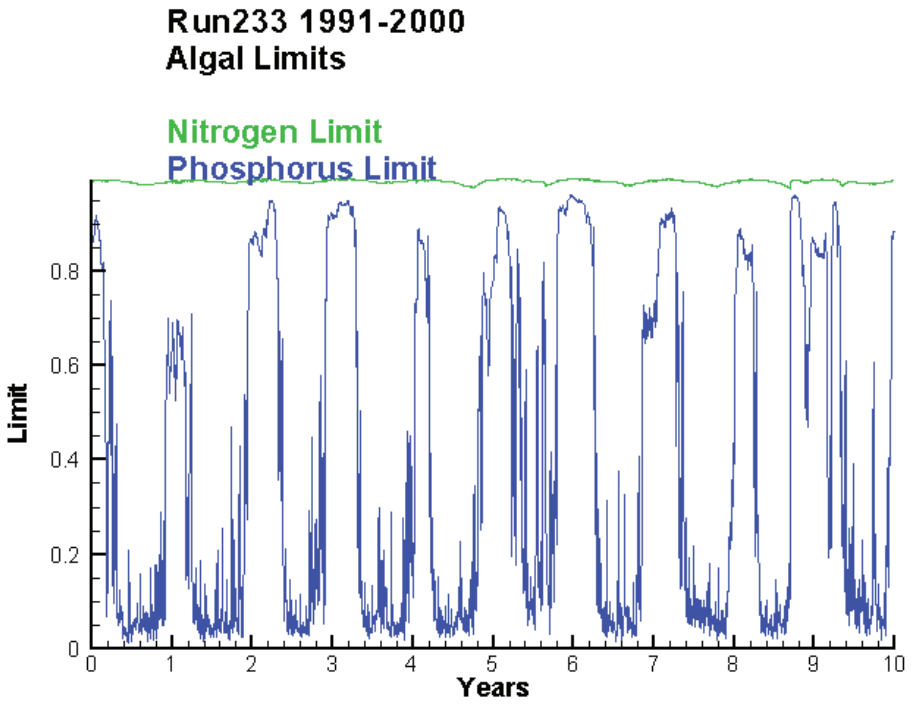

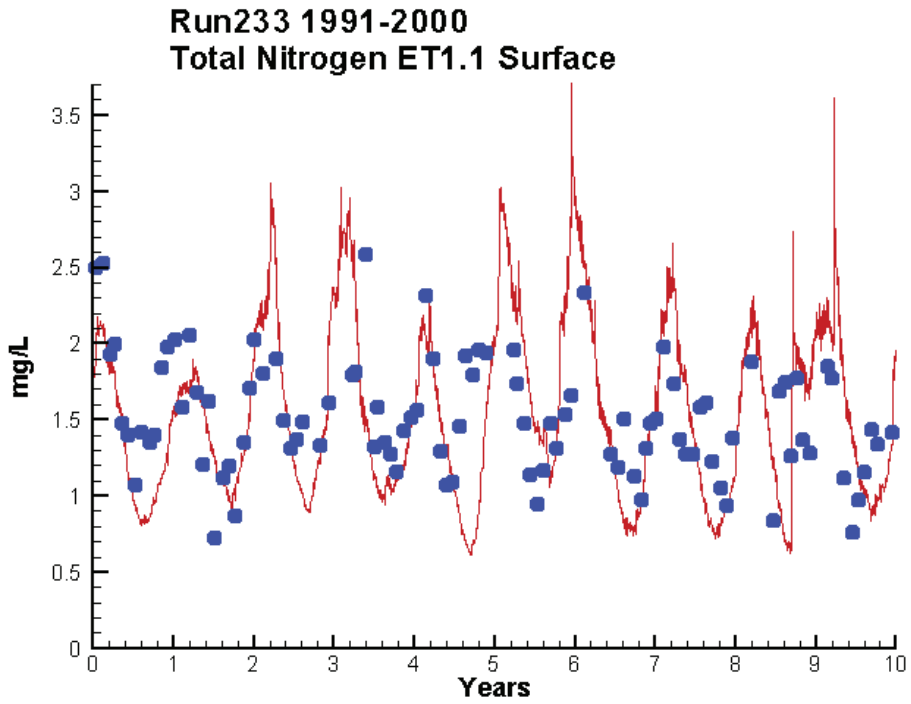

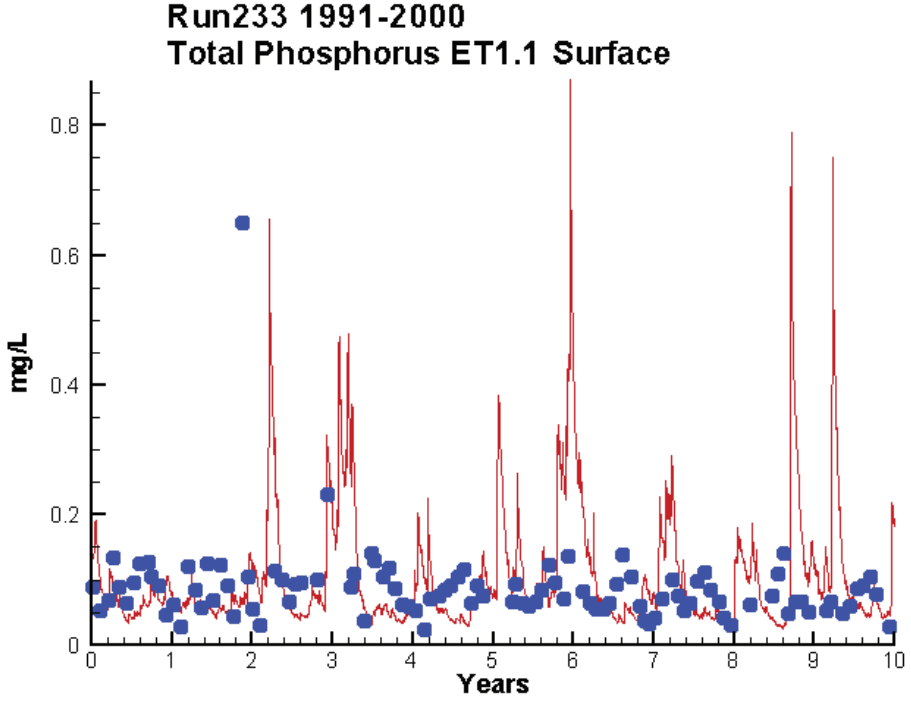

	Mean Difference	Absolute Mean Difference
Chl	-29.7961	30.9980
DIN	0.5370	0.5660
KE	0.3441	1.8023
DIP	-0.0032	0.0067
TP	0.0018	0.0547
TN	-0.0681	0.3582

Station ET1.1

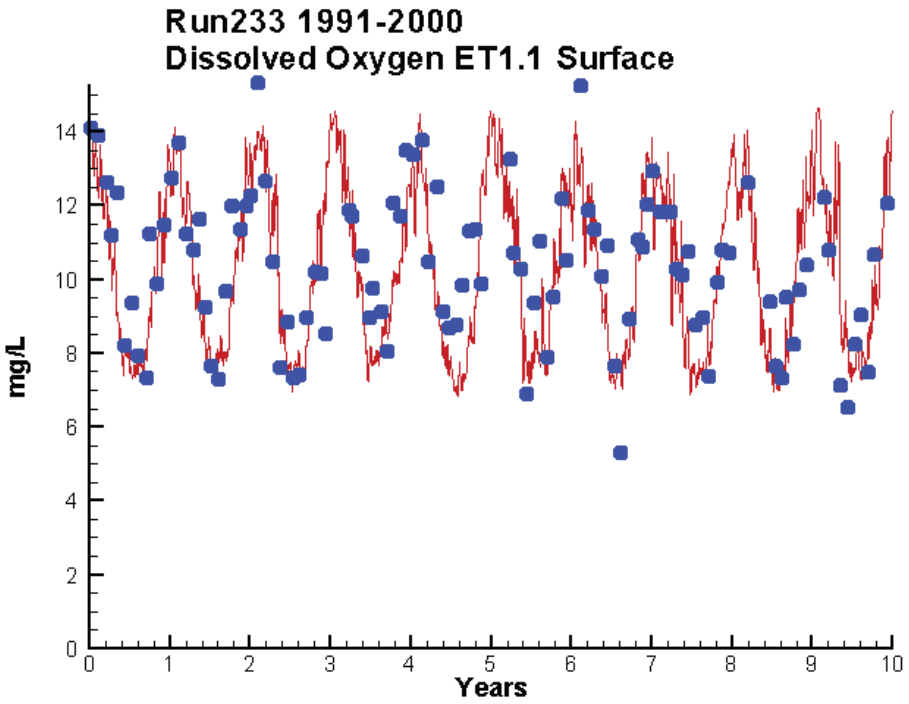

	Mean Difference	Absolute Mean Difference
Top DO	-0.4014	1.1207

Station ET1.1

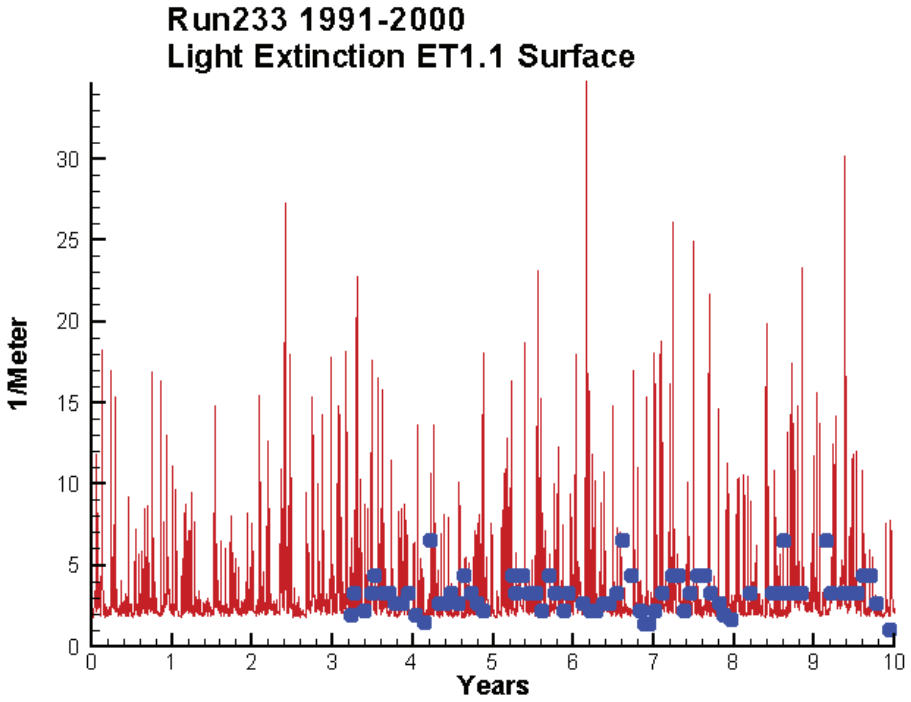

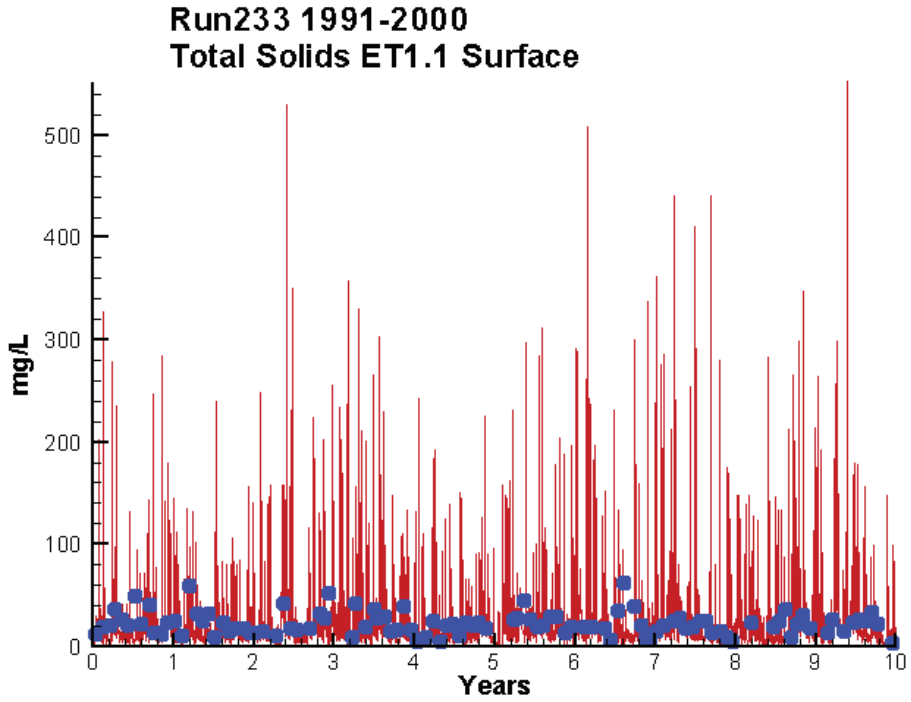

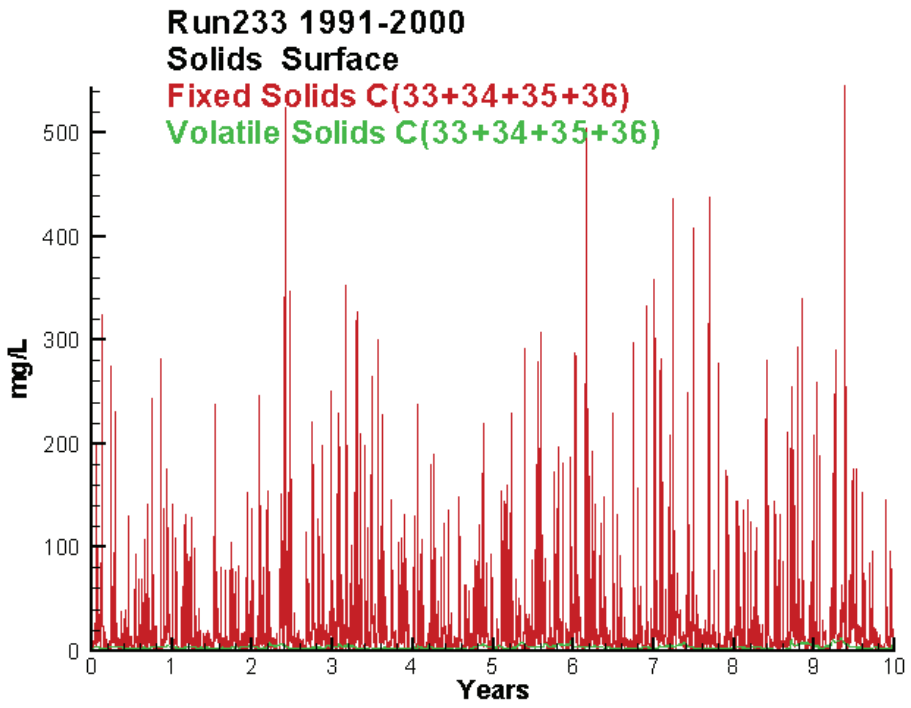

	Mean Difference	Absolute Mean Difference
KE	0.3441	1.8023
TSS	6.9181	22.6333

Station ET2.3

Run233 1991-2000
Chlorophyll ET2.3 Surface

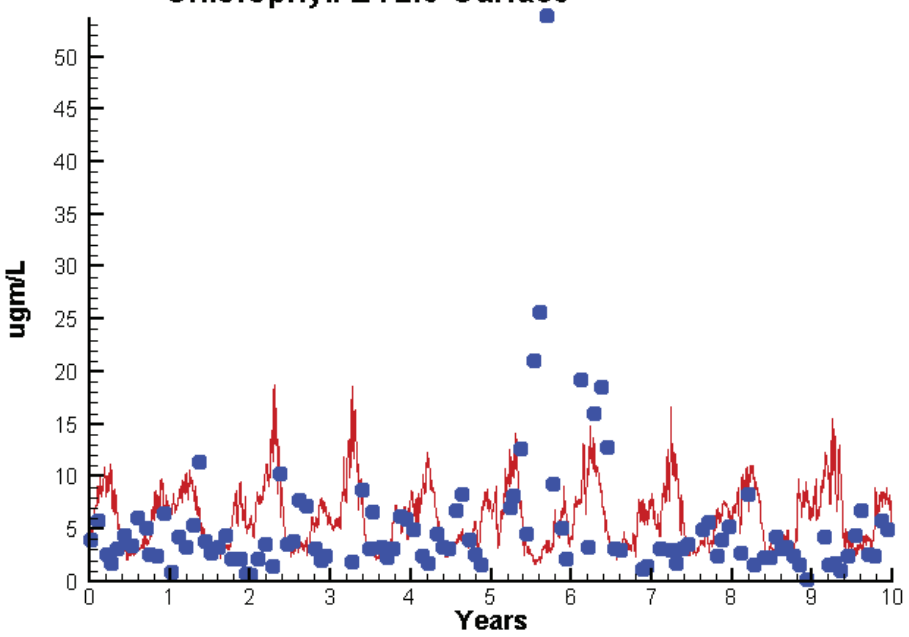

Run233 1991-2000
Light Extinction ET2.3 Surface

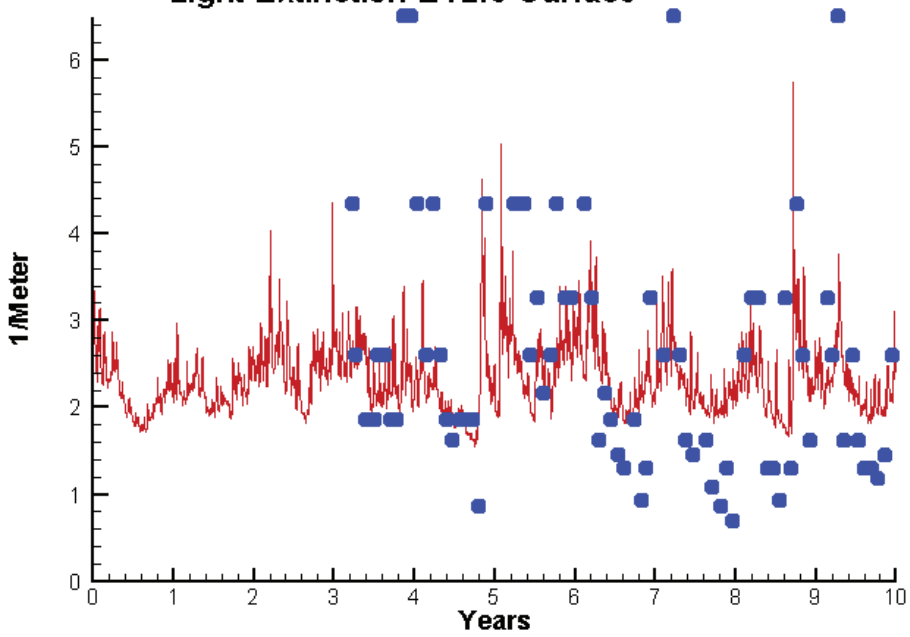

Run233 1991-2000
Dissolved Inorganic Nitrogen ET2.3 Surface

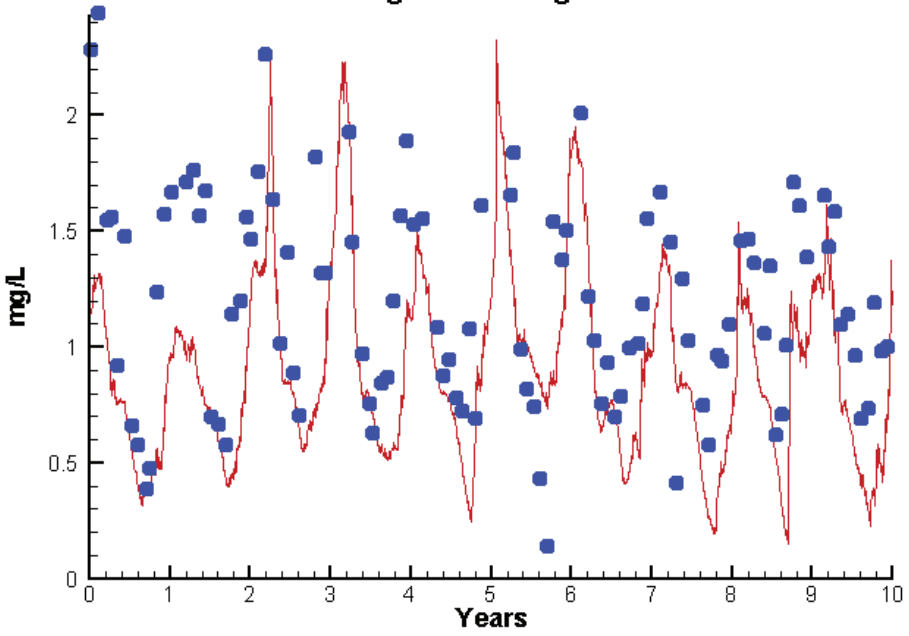

Run233 1991-2000
Dissolved Inorganic Phosphorus ET2.3 Surface

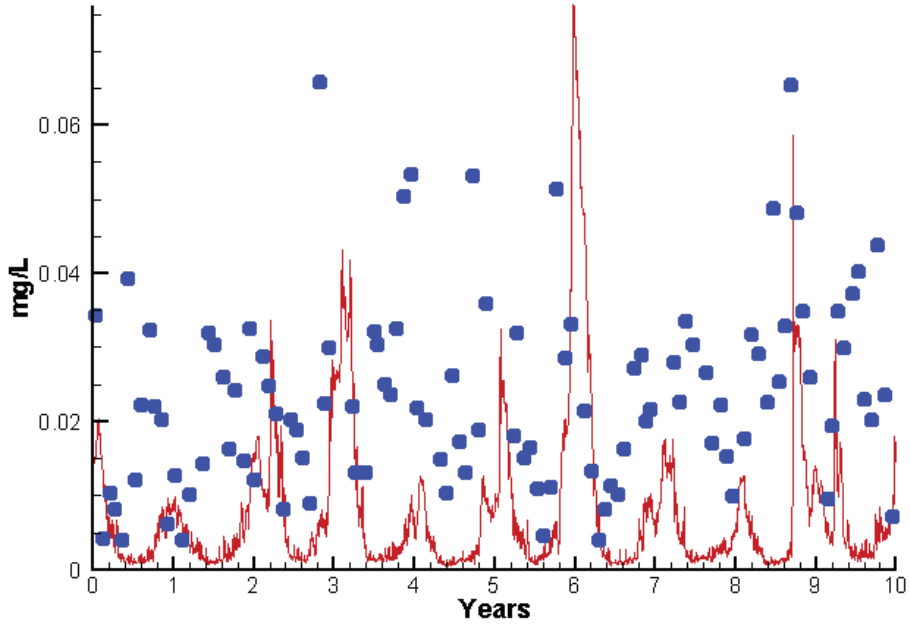

Station ET2.3

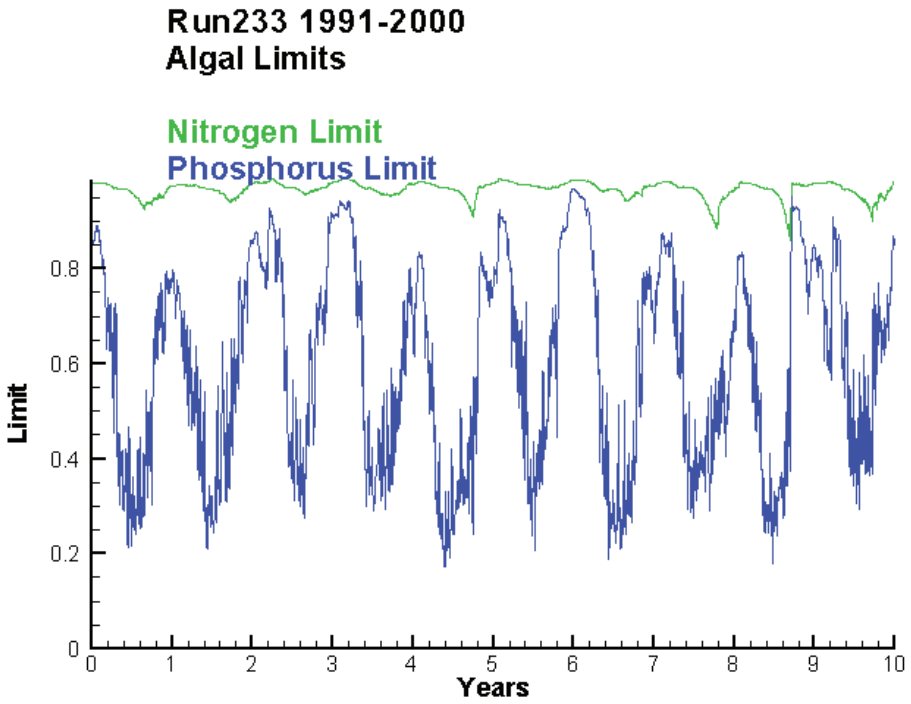

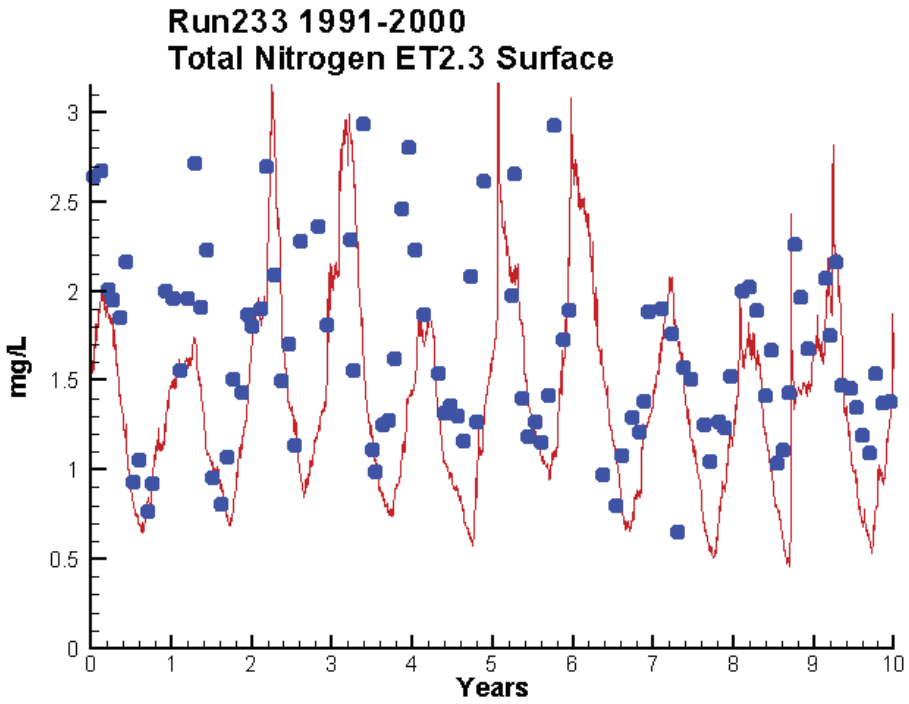

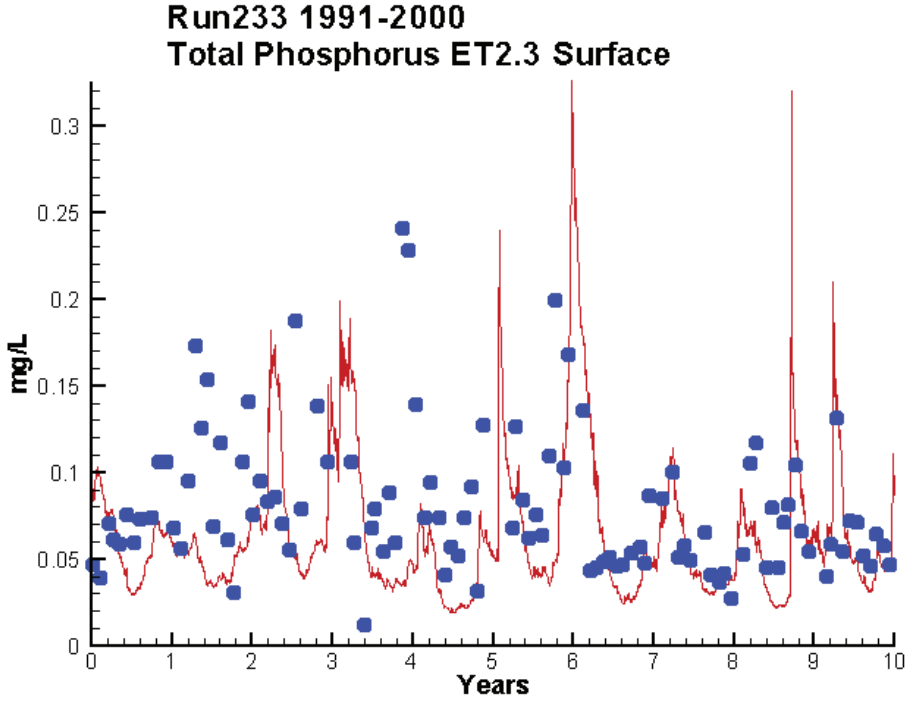

	Mean Difference	Absolute Mean Difference
Chl	0.9991	4.6235
DIN	-0.3532	0.3929
KE	-0.2861	0.9269
DIP	-0.0175	0.0186
TP	-0.0203	0.0365
TN	-0.3457	0.4699

Station ET2.3

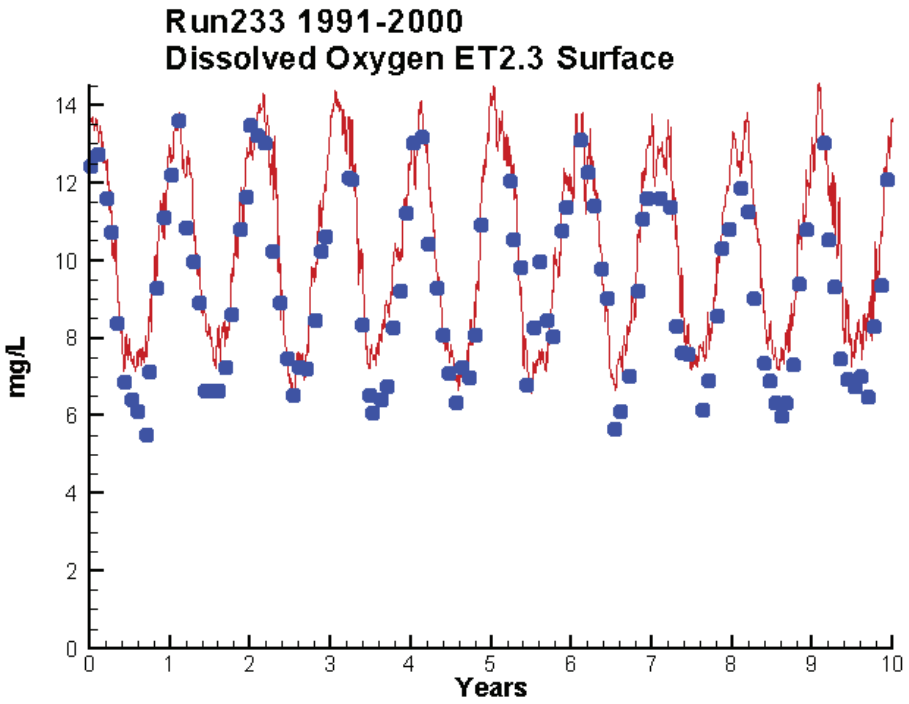

	Mean Difference	Absolute Mean Difference
Top DO	0.9145	1.0461

Station ET2.3

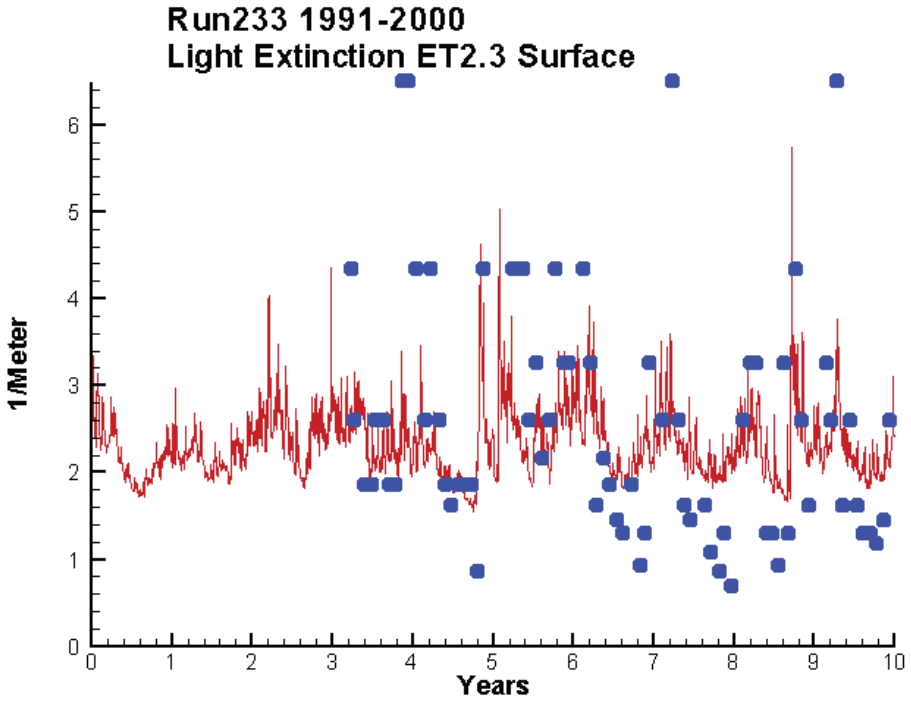

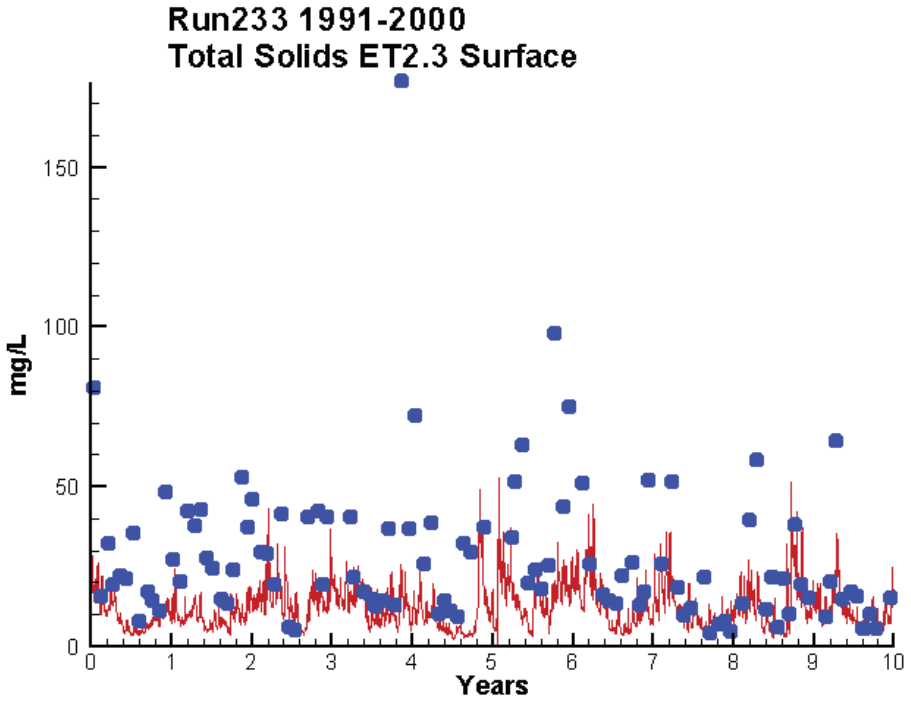

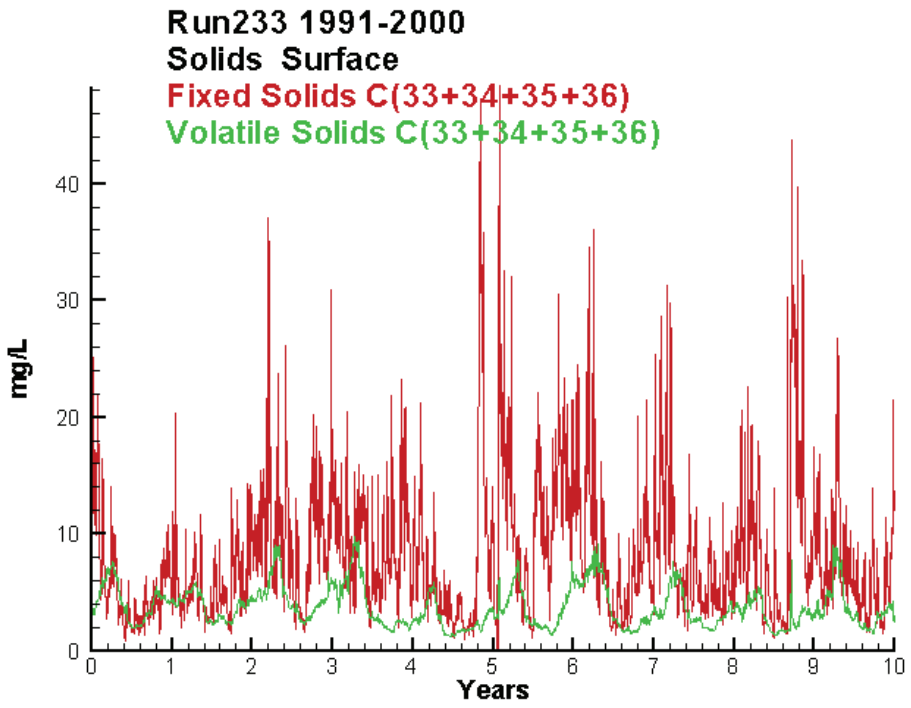

	Mean Difference	Absolute Mean Difference
KE	-0.2861	0.9269
TSS	-16.8182	17.5502

Station ET4.2

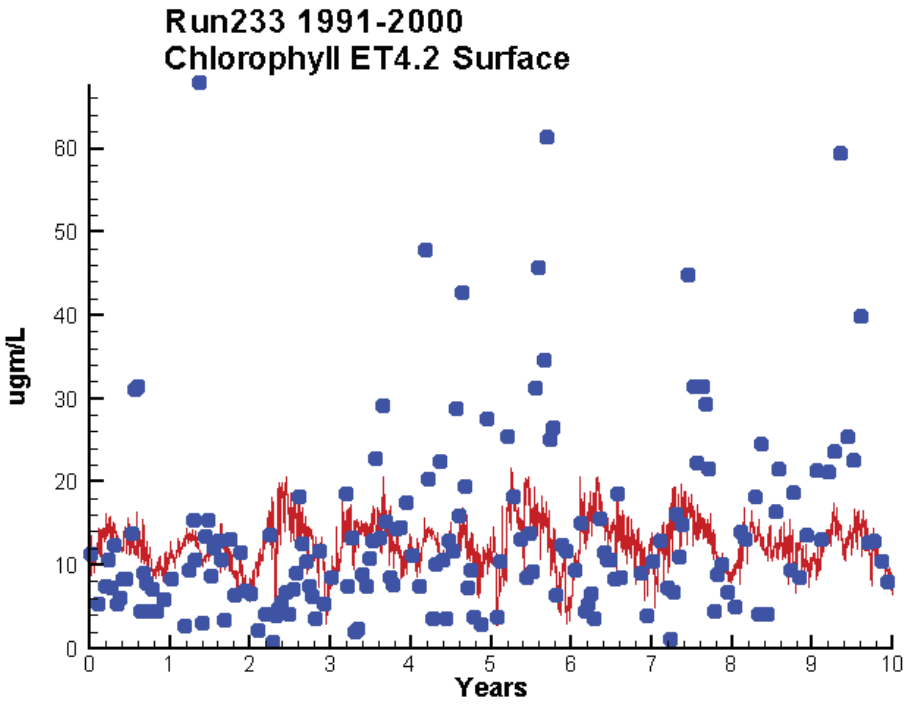

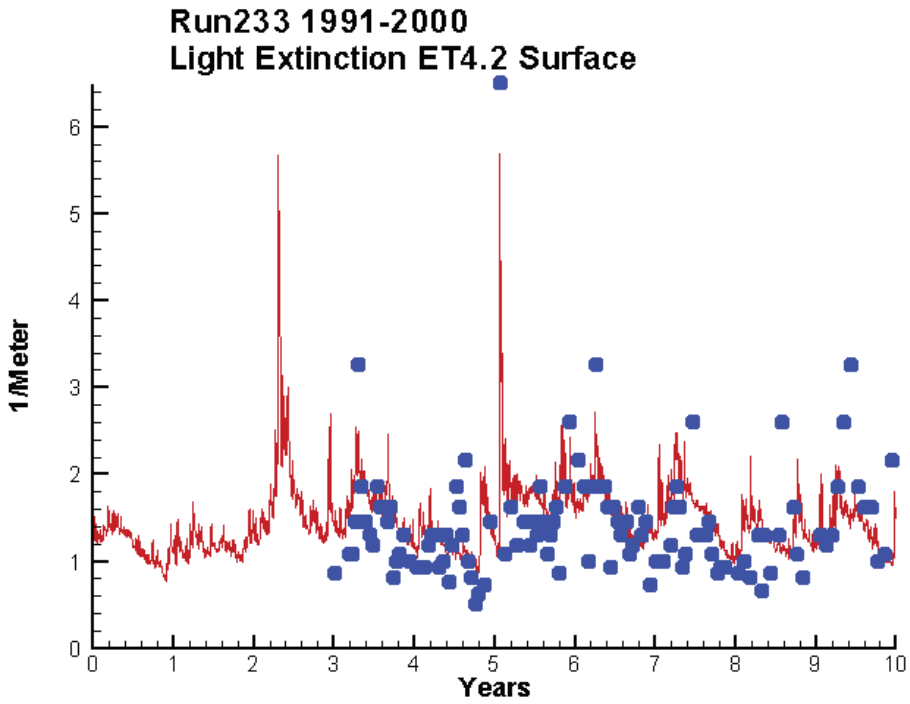

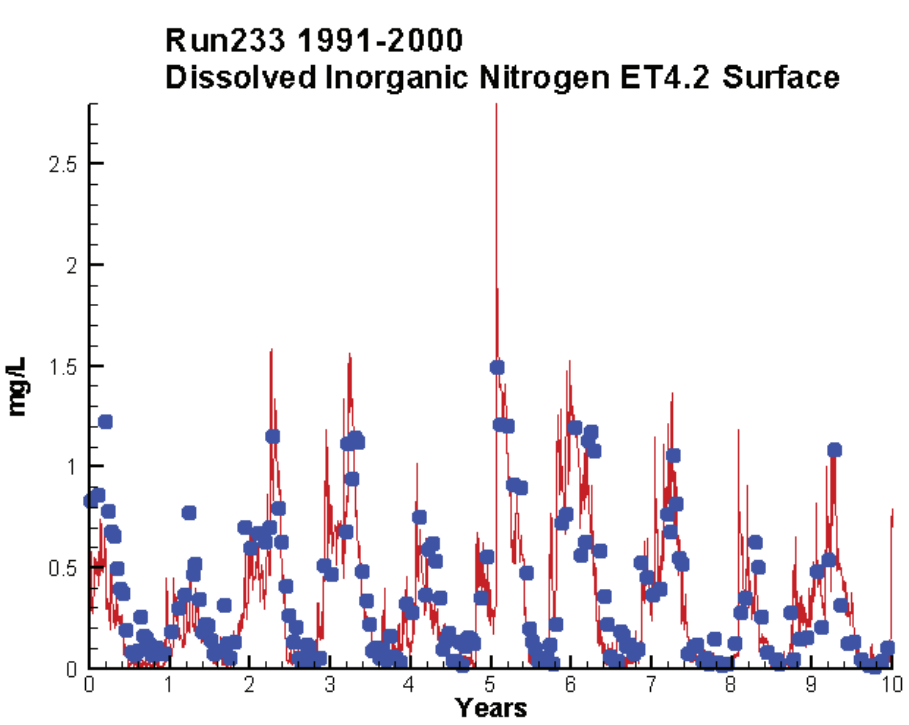

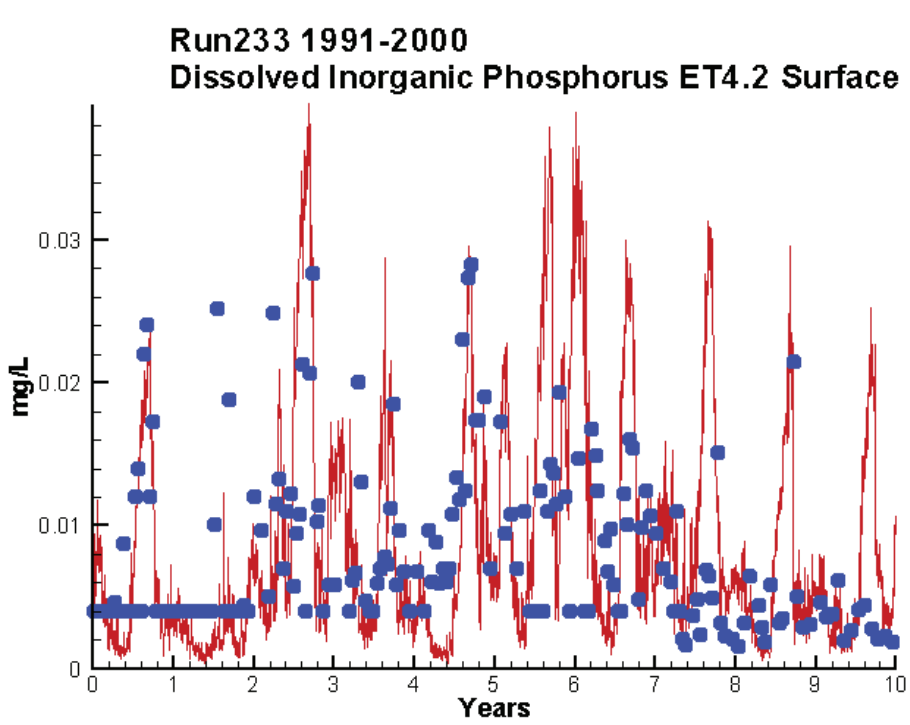

Station ET4.2

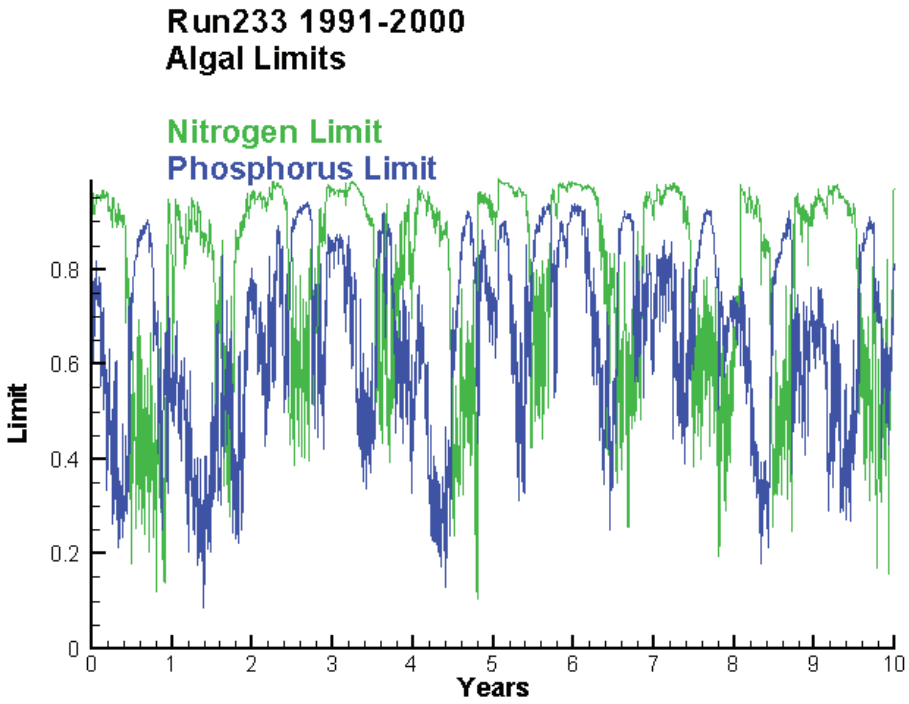

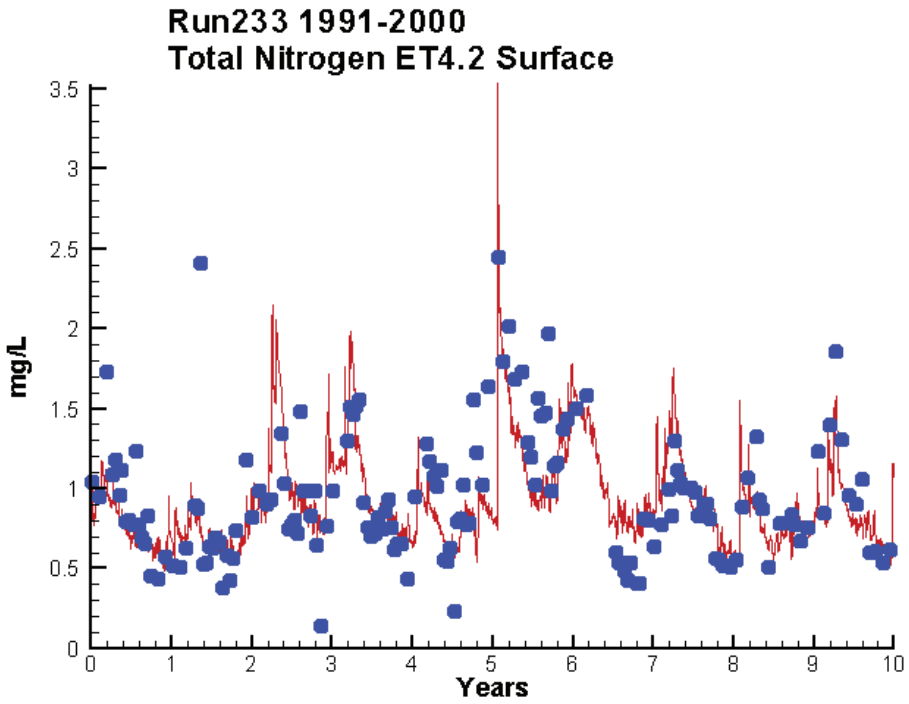

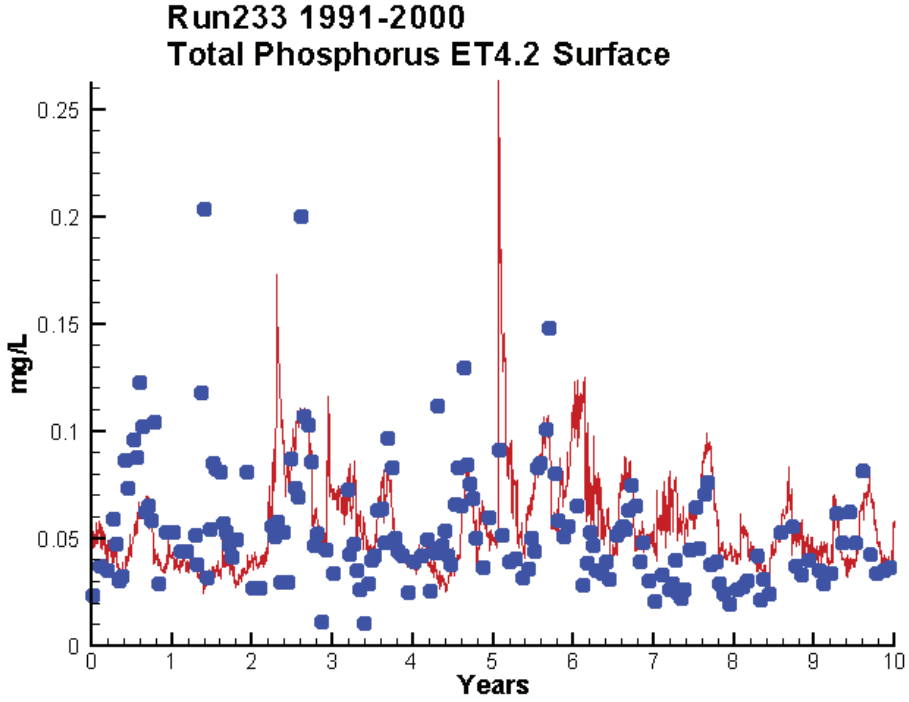

	Mean Difference	Absolute Mean Difference
Chl	-0.9857	7.1855
DIN	-0.0518	0.1470
KE	0.1066	0.4135
DIP	0.0012	0.0064
TP	0.0049	0.0233
TN	-0.0321	0.2089

Station ET4.2

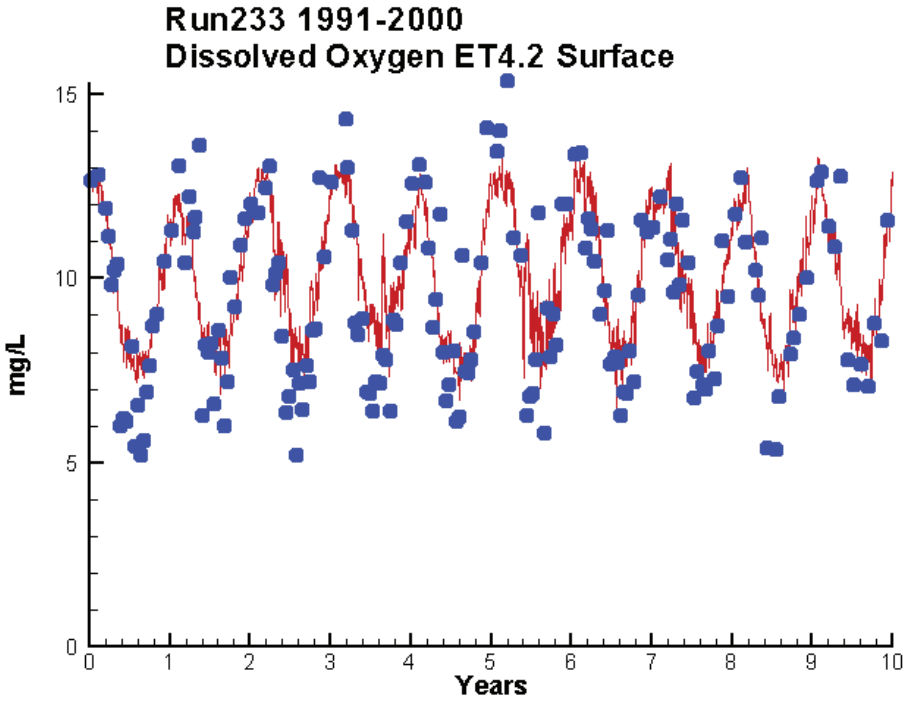

	Mean Difference	Absolute Mean Difference
Top DO	0.4077	1.0637

Station ET4.2

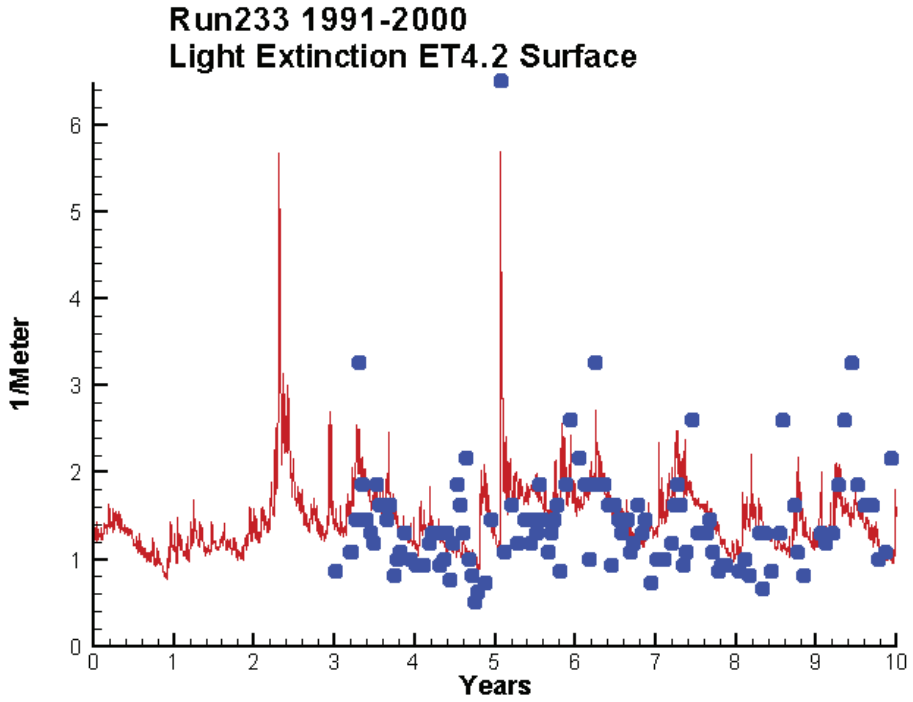

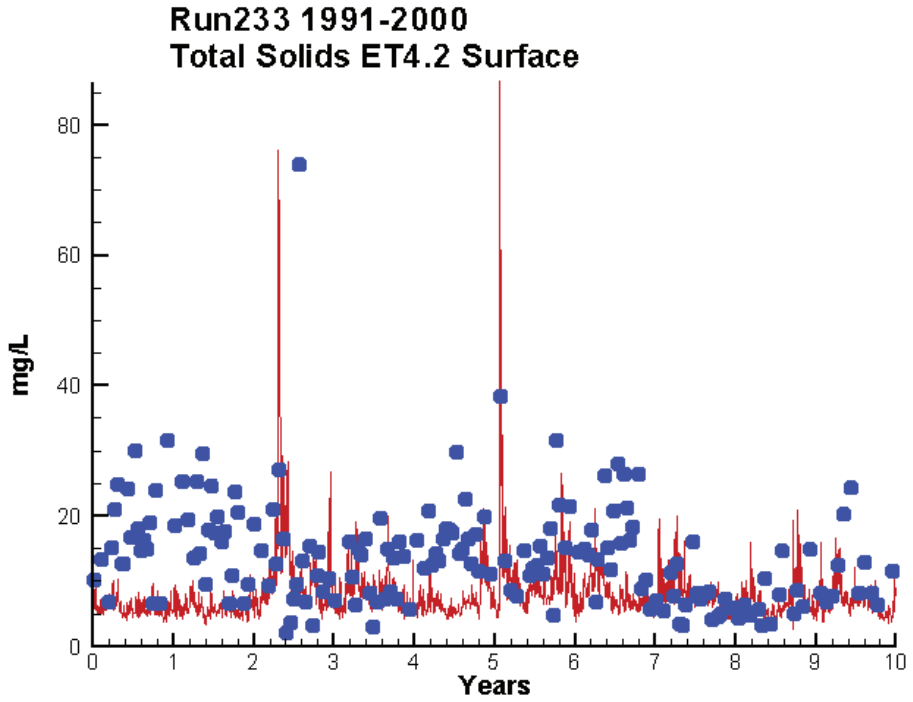

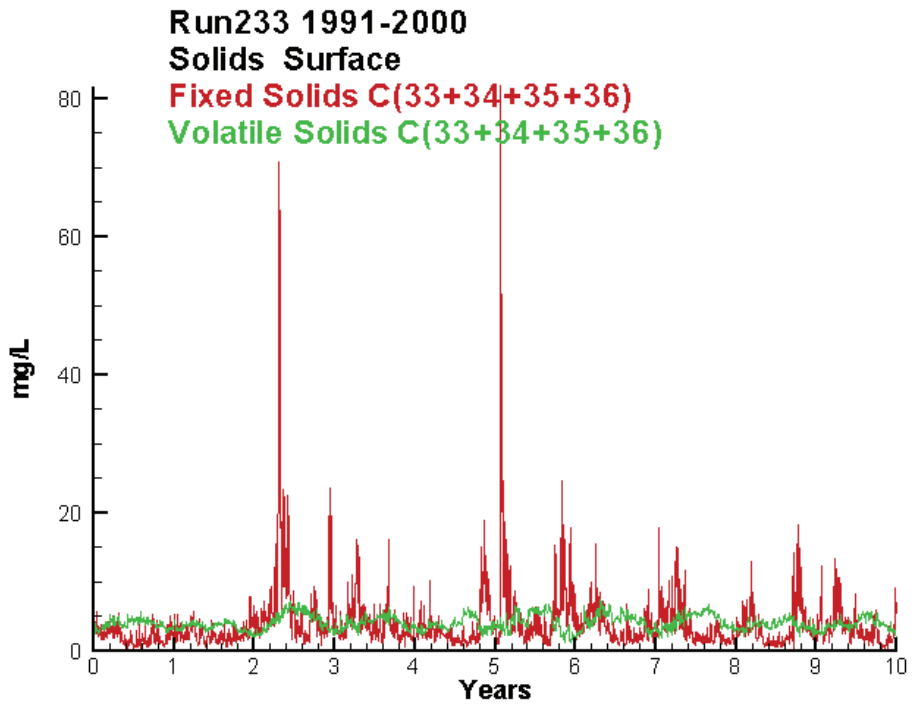

	Mean Difference	Absolute Mean Difference
KE	0.1066	0.4135
TSS	-5.7030	7.8637

Station ET5.2

Run233 1991-2000
Chlorophyll ET5.2 Surface

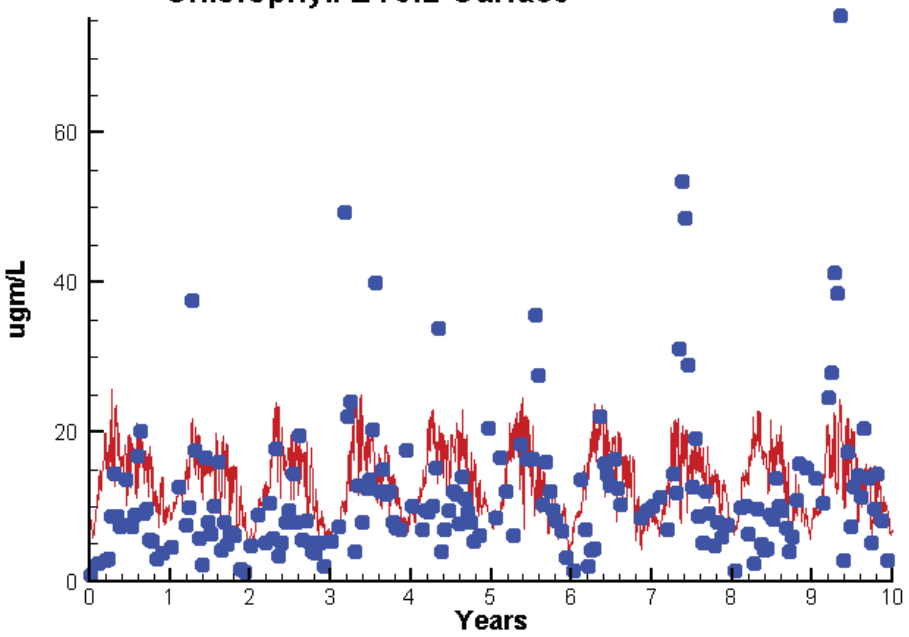

Run233 1991-2000
Light Extinction ET5.2 Surface

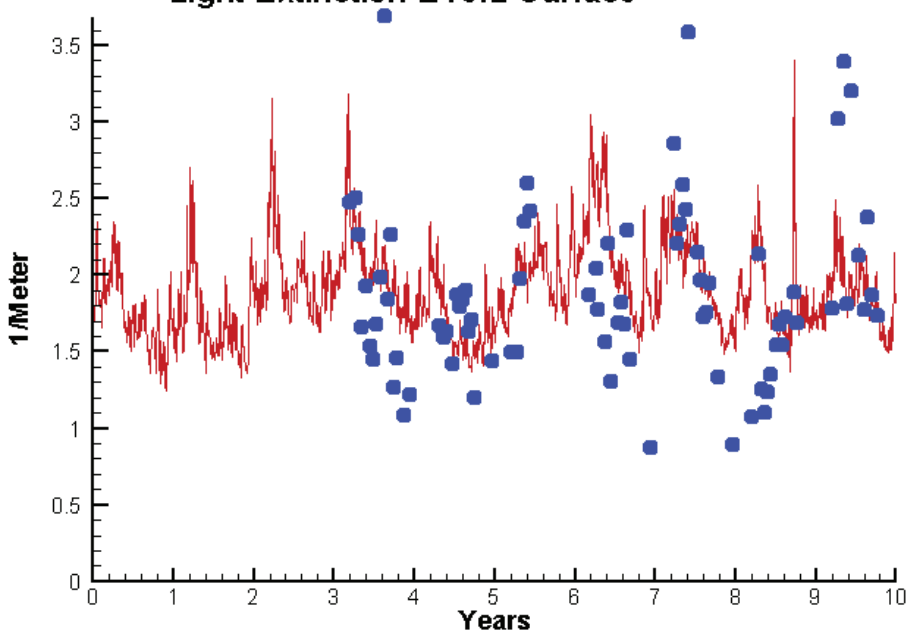

Run233 1991-2000
Dissolved Inorganic Nitrogen ET5.2 Surface

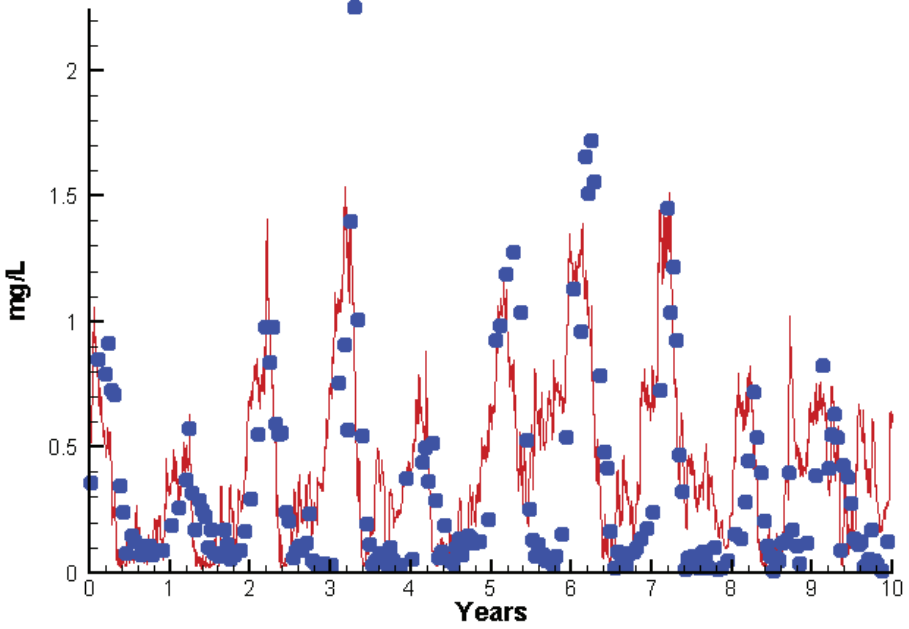

Run233 1991-2000
Dissolved Inorganic Phosphorus ET5.2 Surface

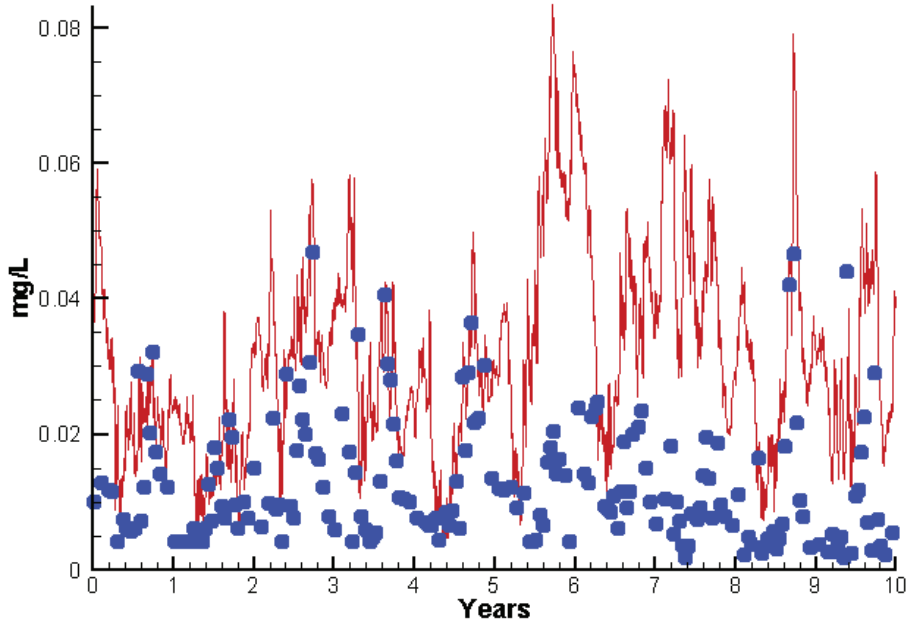

Station ET5.2

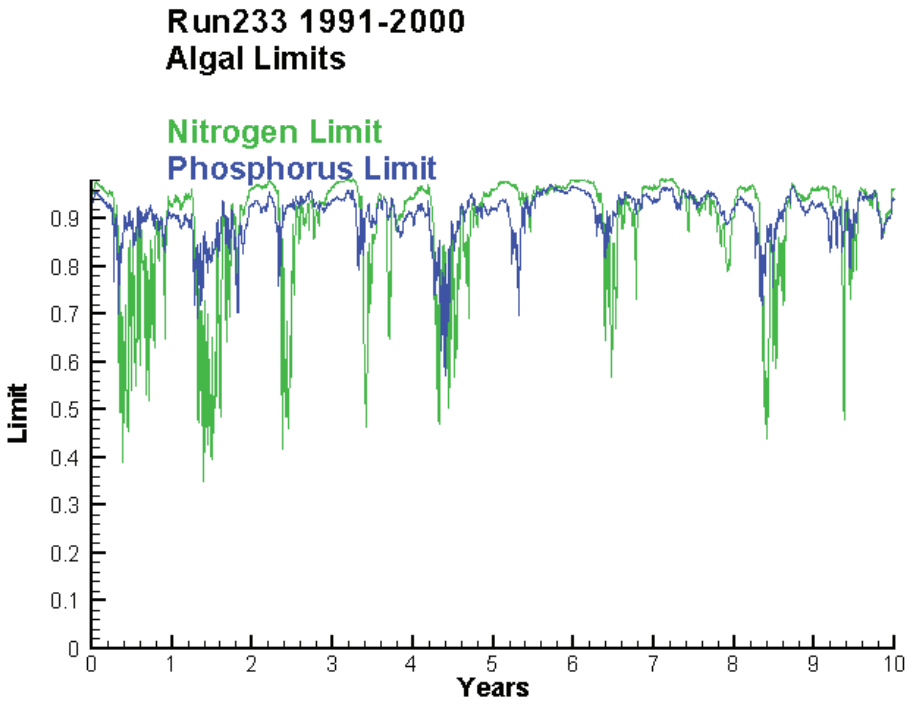

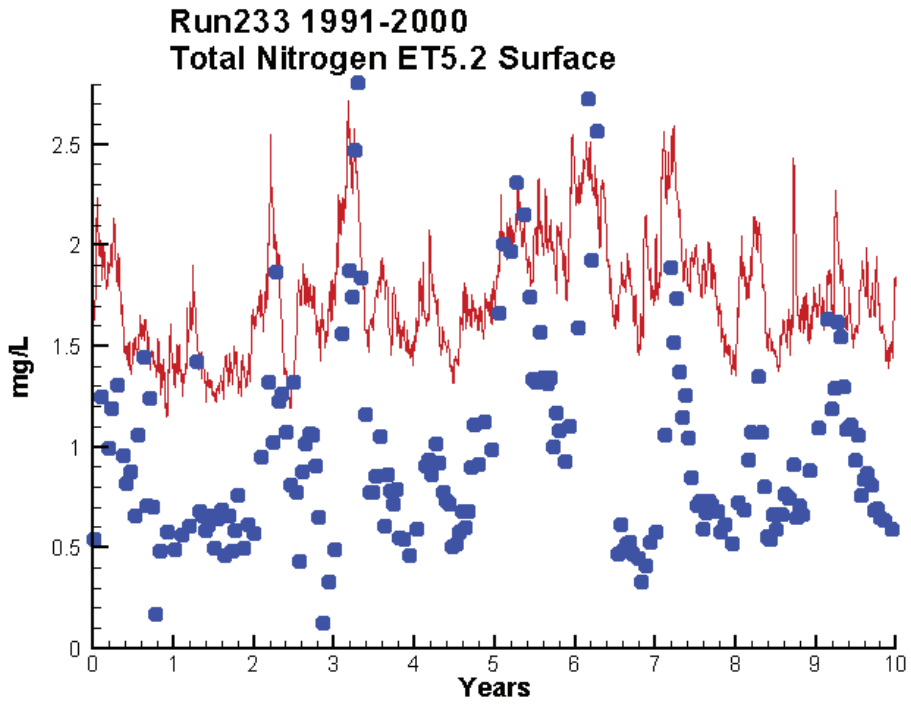

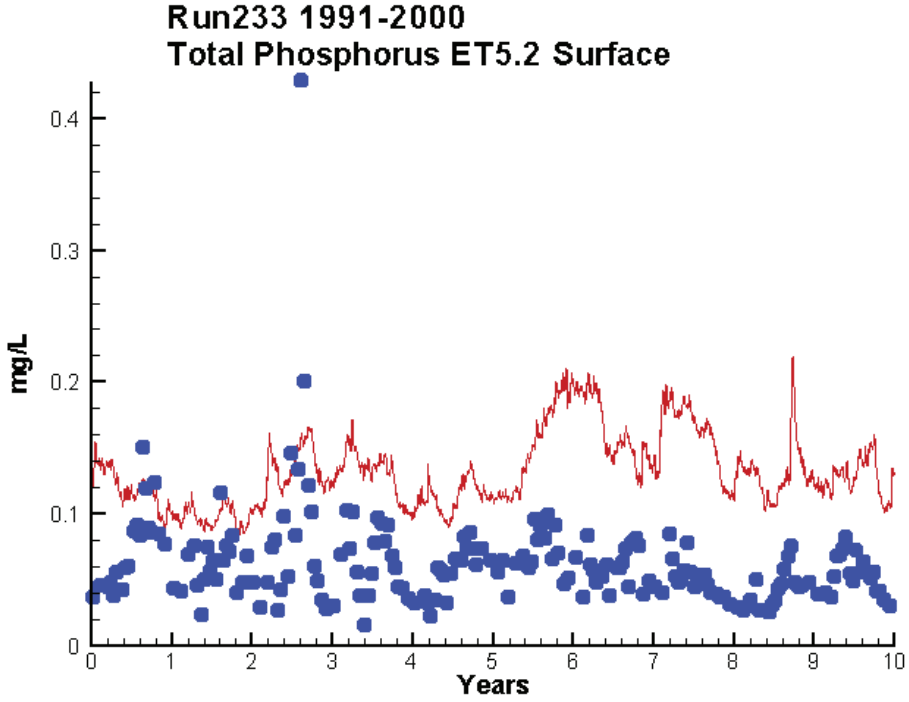

	Mean Difference	Absolute Mean Difference
Chl	2.6585	7.6069
DIN	0.0651	0.2546
KE	0.1105	0.4308
DIP	0.0183	0.0192
TP	0.0719	0.0757
TN	0.7767	0.7926

Station ET5.2

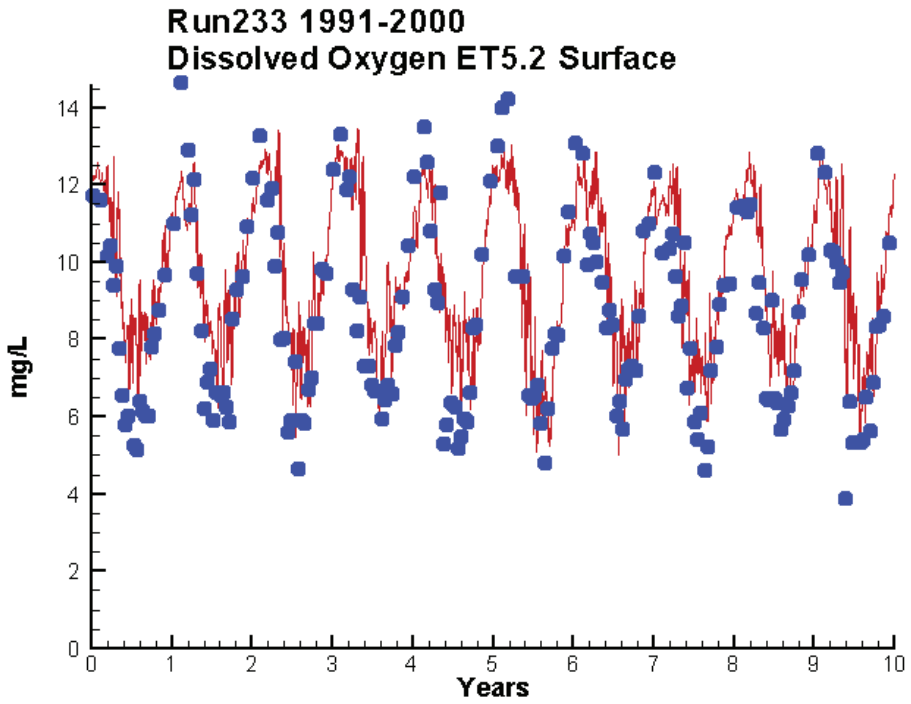

	Mean Difference	Absolute Mean Difference
Top DO	0.9715	1.2724

Station ET5.2

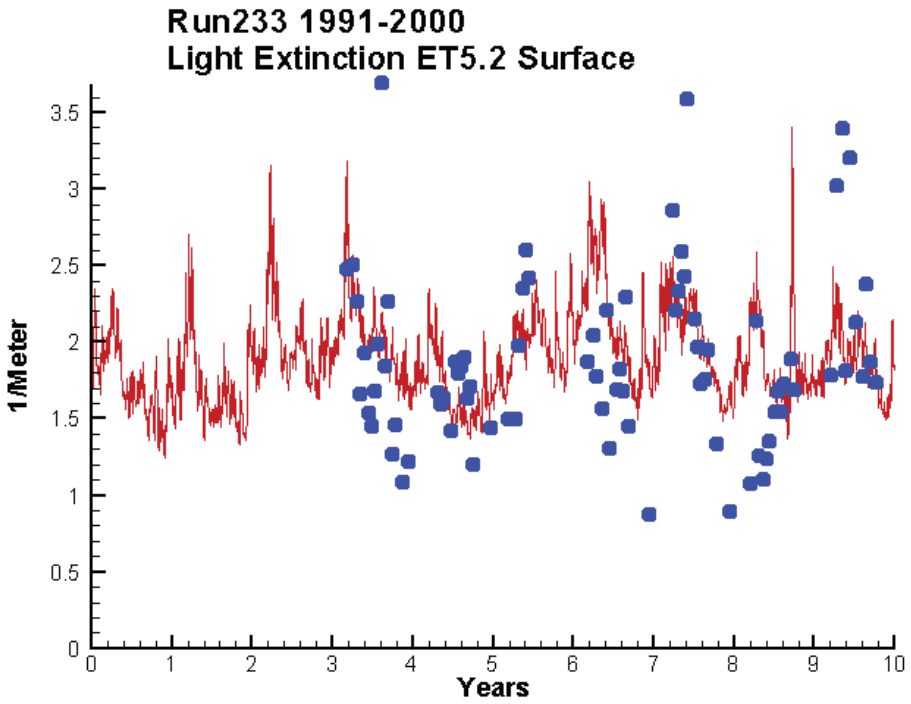

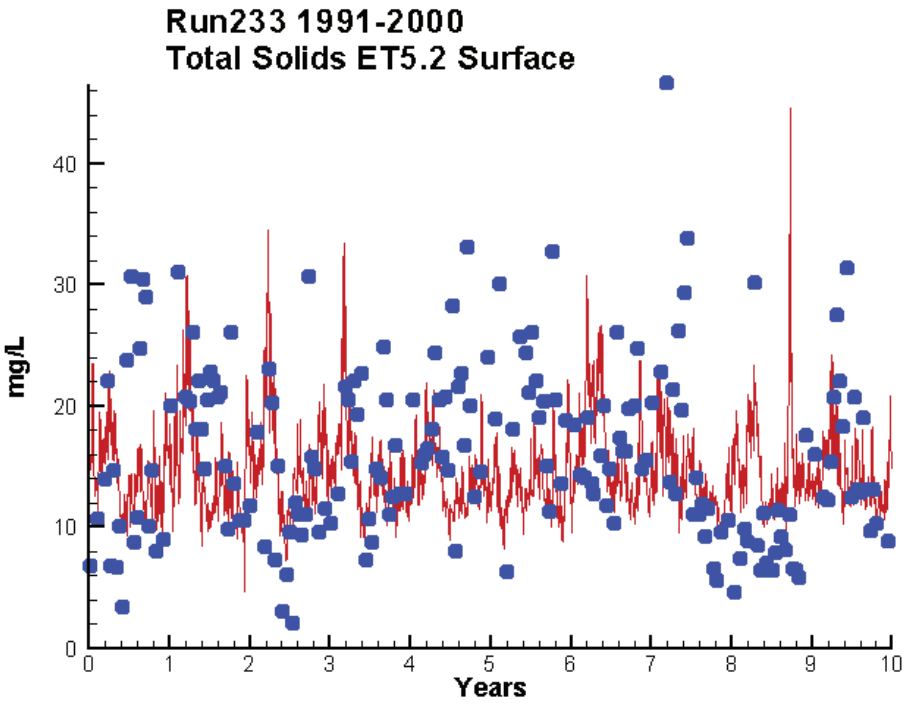

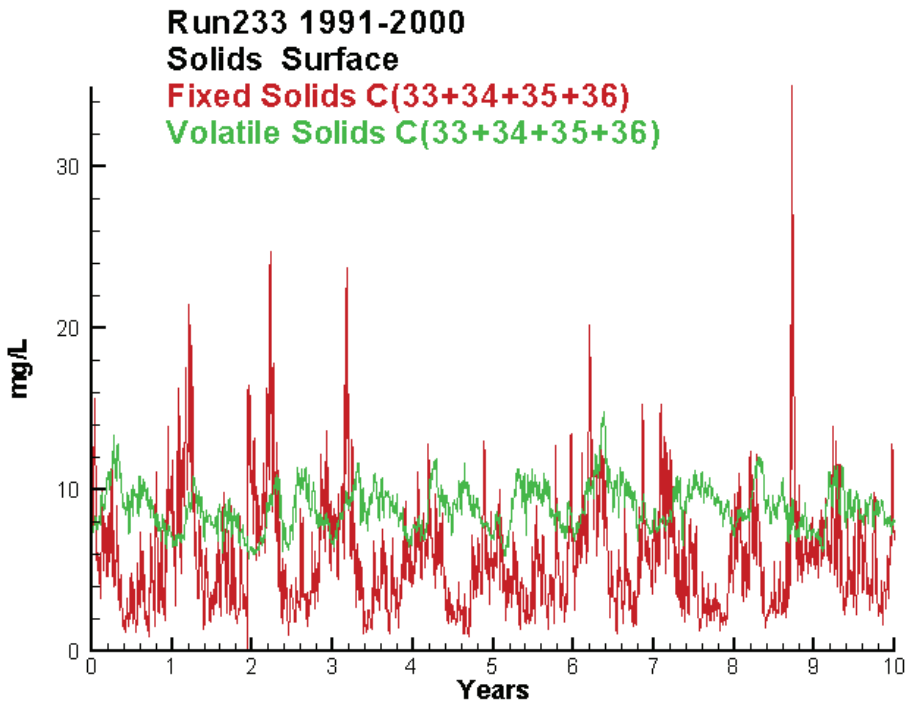

	Mean Difference	Absolute Mean Difference
KE	0.1105	0.4308
TSS	-1.7212	6.1611

Station ET6.2

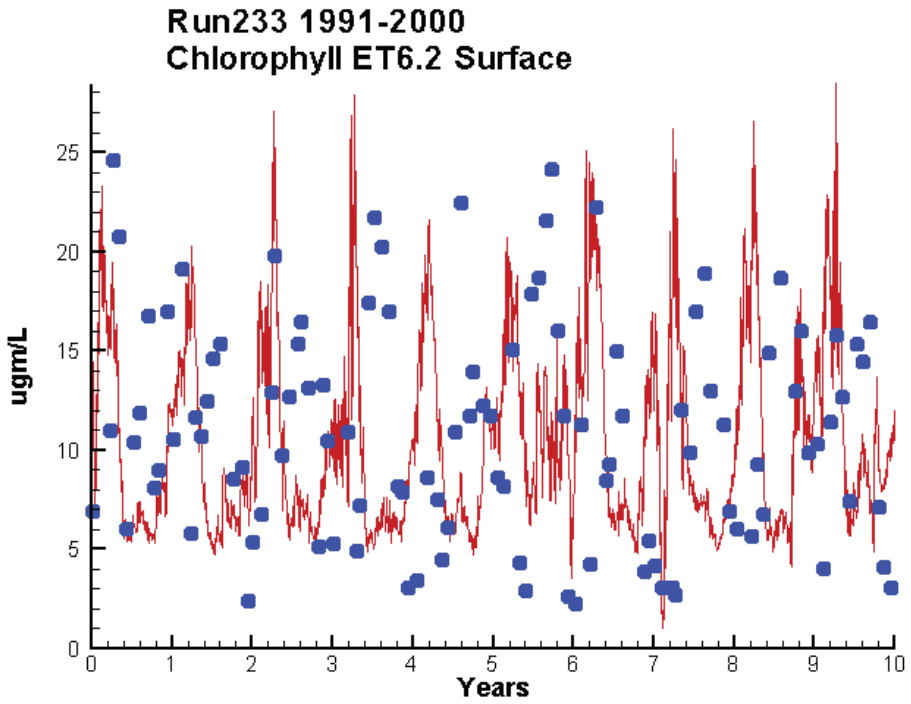

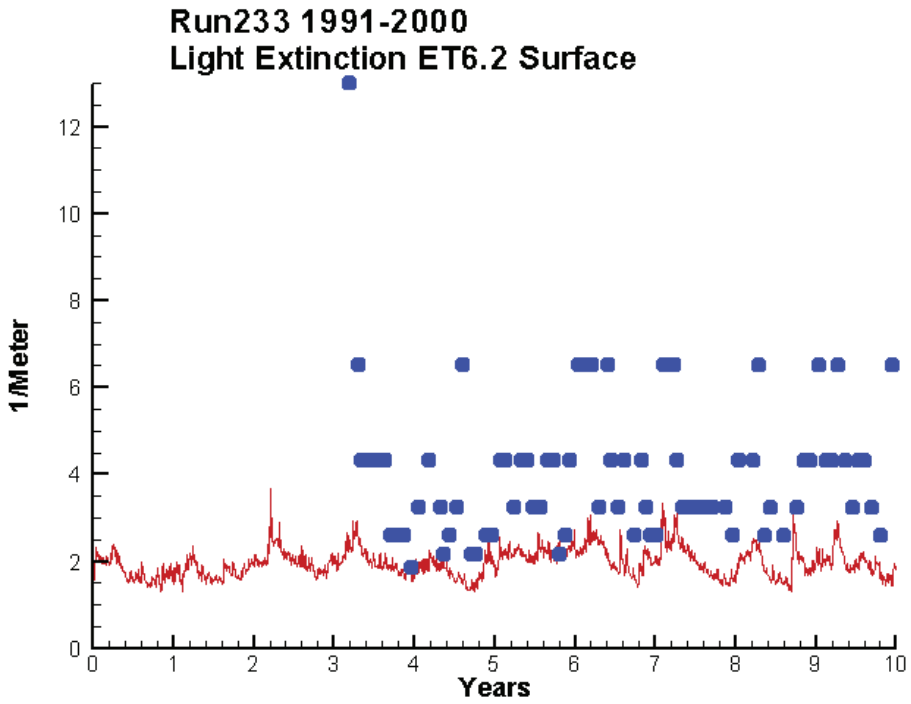

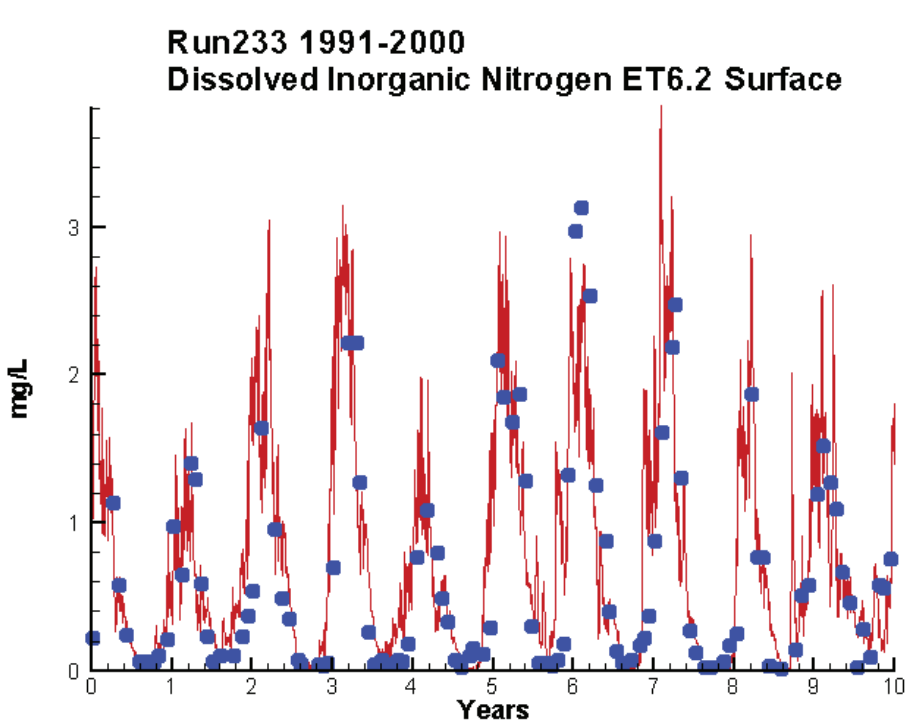

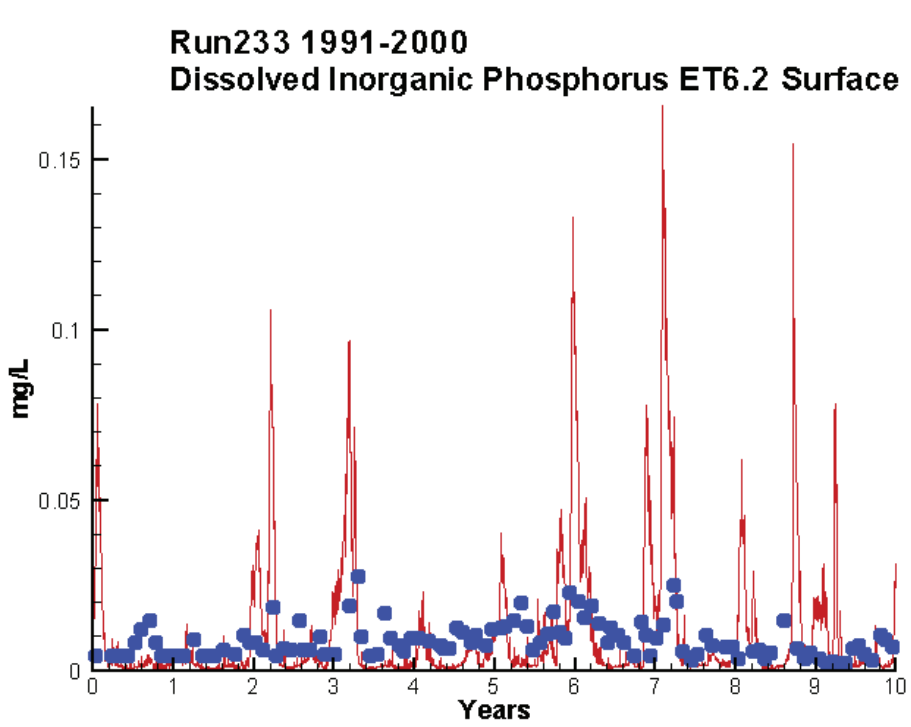

Station ET6.2

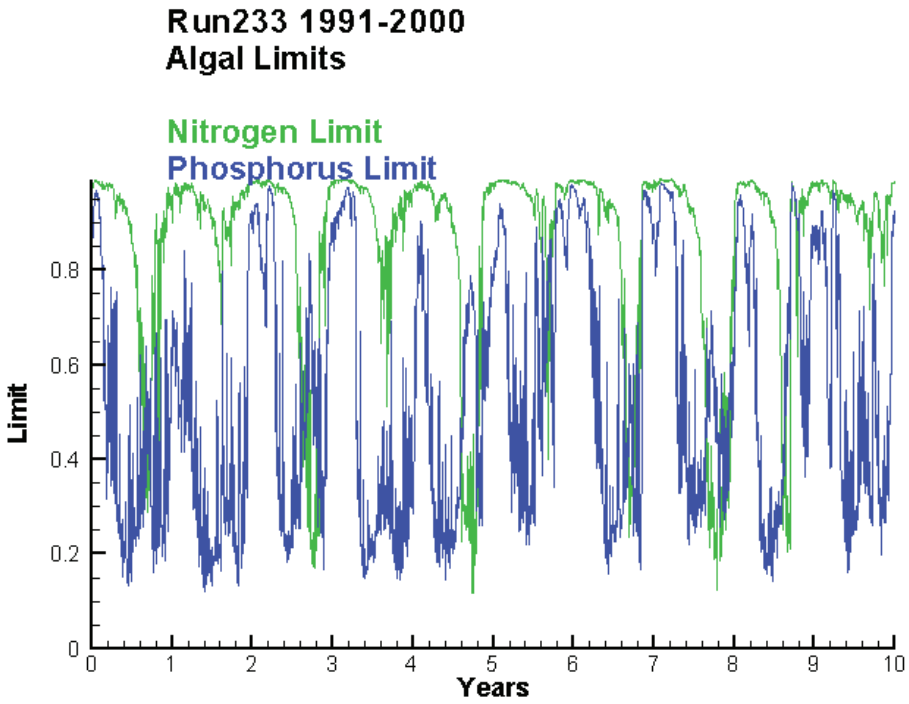

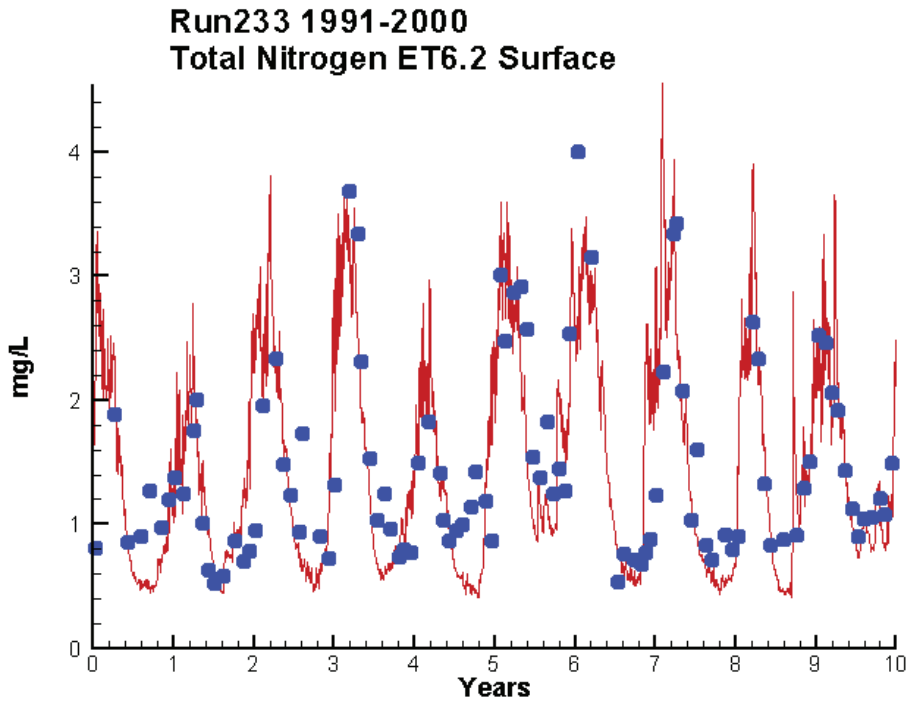

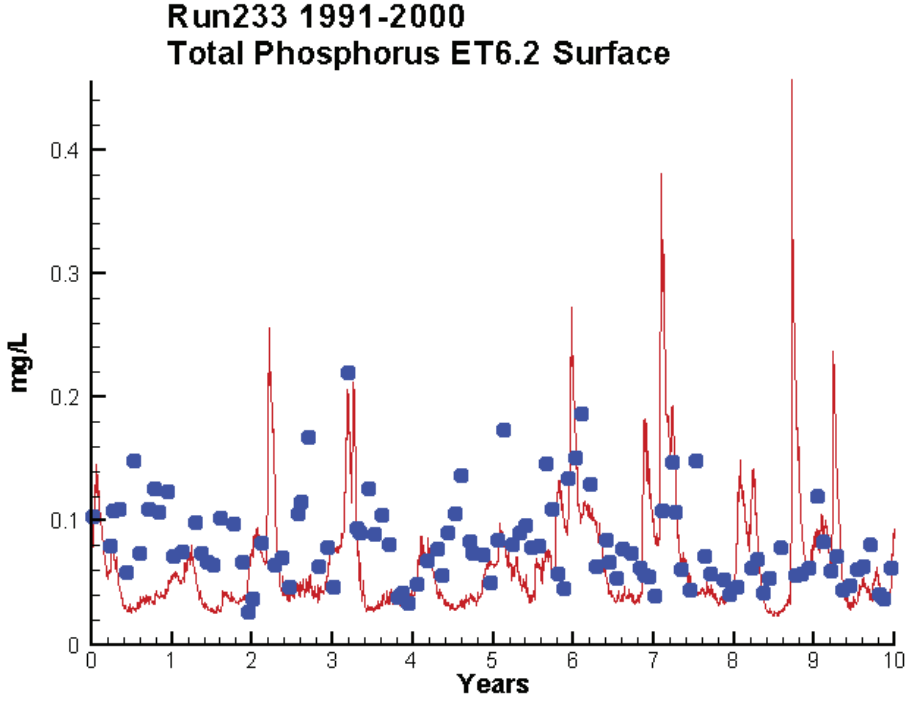

	Mean Difference	Absolute Mean Difference
Chl	-0.3937	6.2418
DIN	0.0776	0.3607
KE	-2.0497	2.0515
DIP	0.0022	0.0104
TP	-0.0163	0.0395
TN	-0.0017	0.4250

Station ET6.2

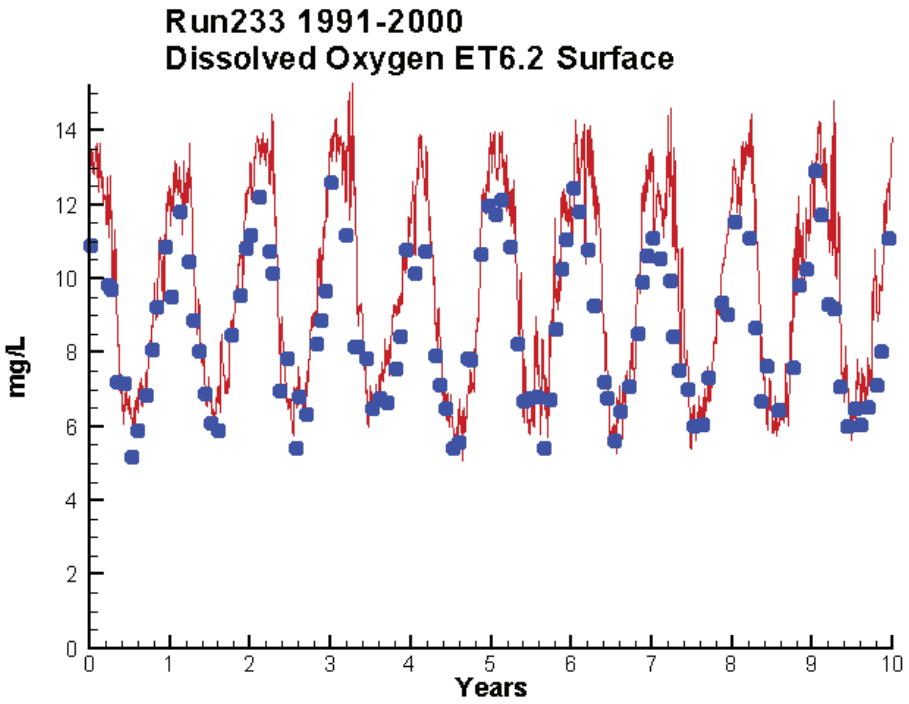

	Mean Difference	Absolute Mean Difference
Top DO	1.0665	1.1980

Station ET6.2

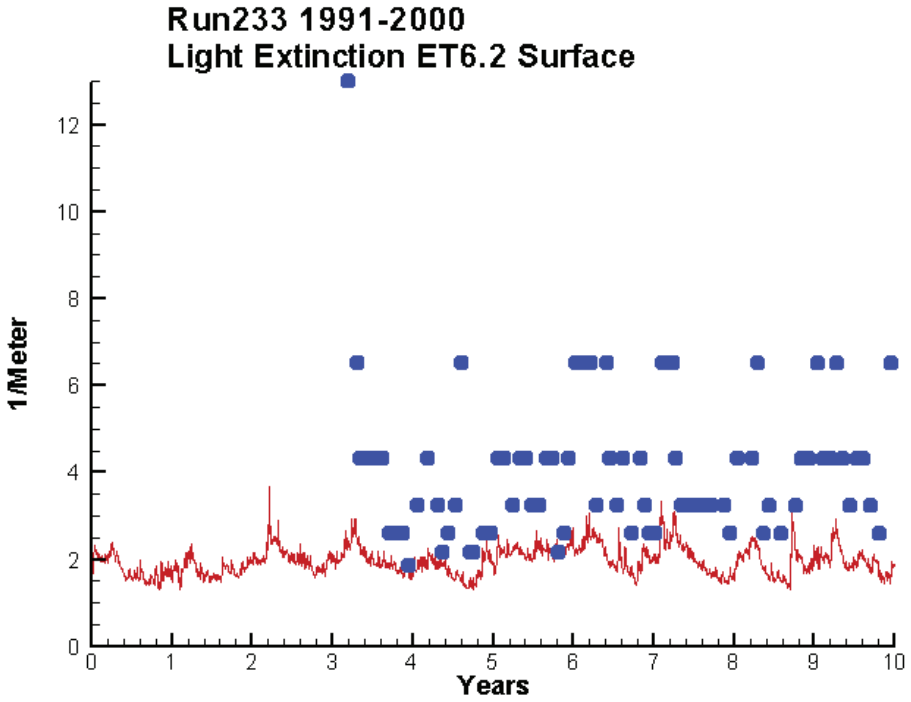

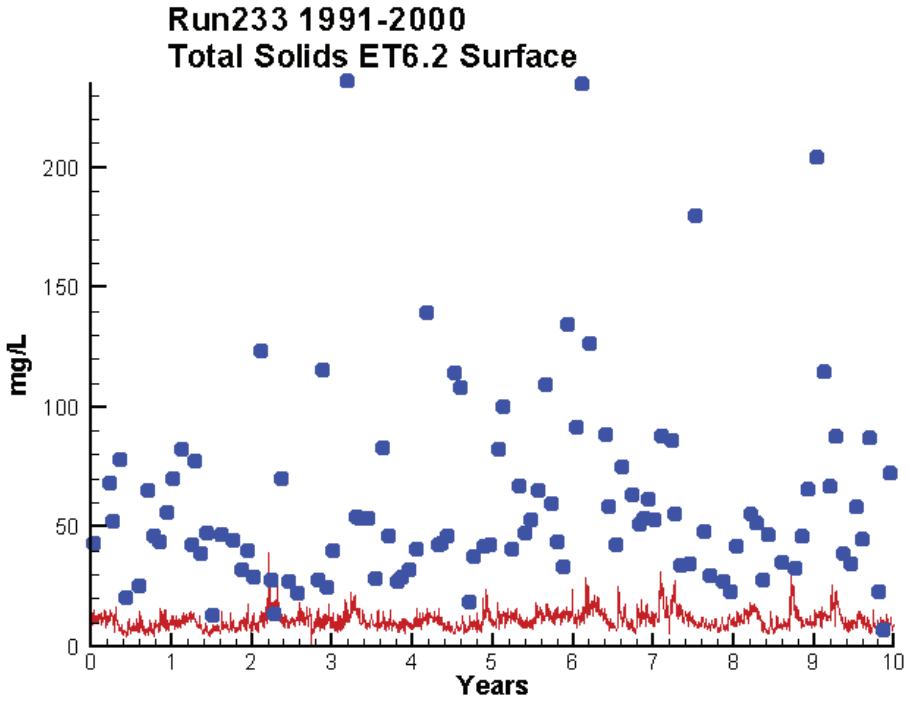

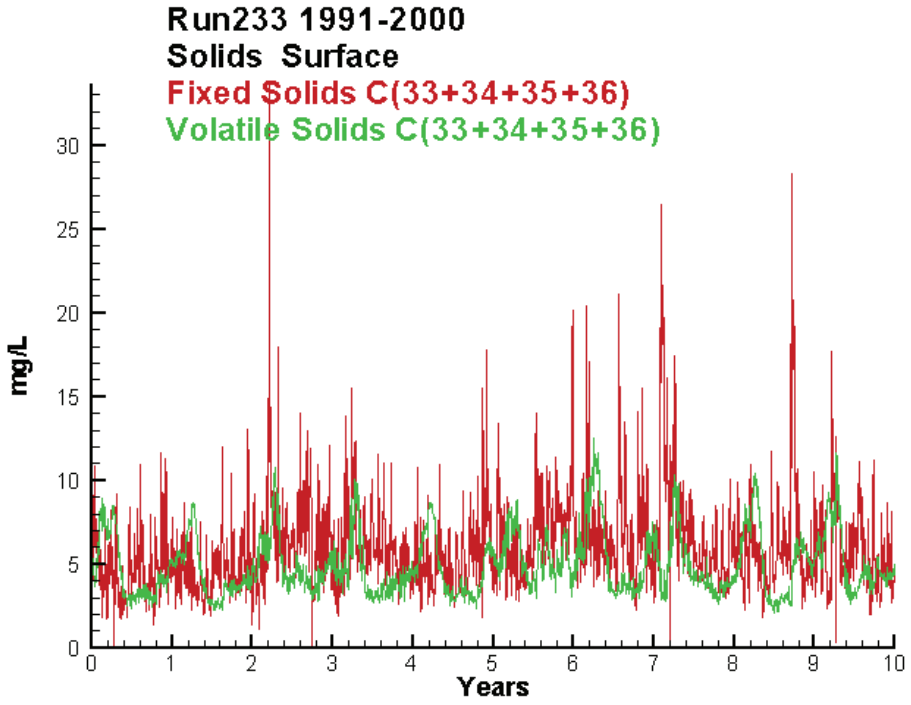

	Mean Difference	Absolute Mean Difference
KE	-2.0497	2.0515
TSS	-49.2552	49.4478

Station ET9.1

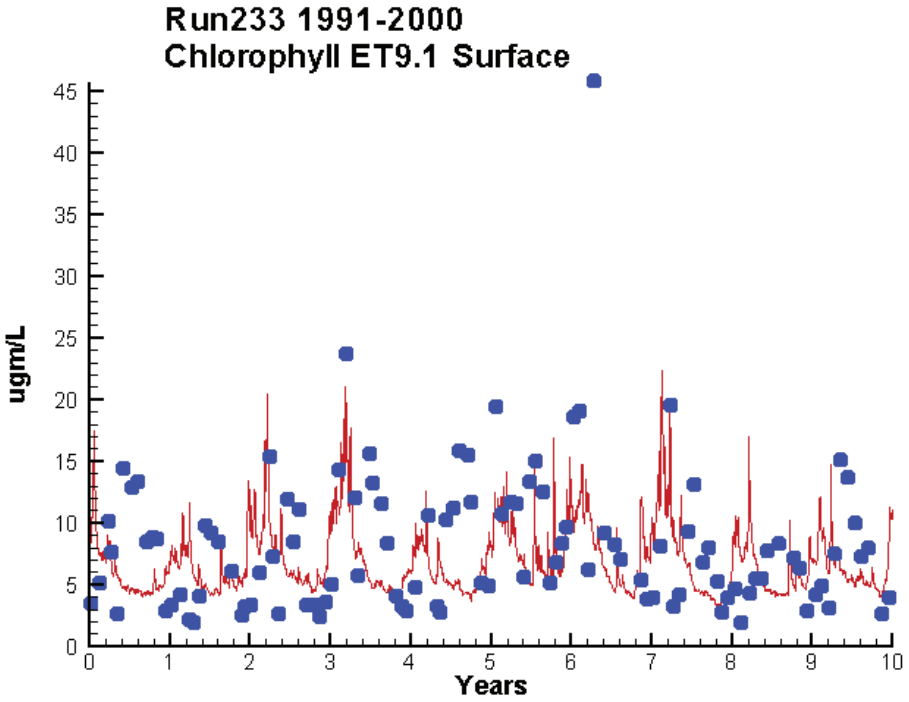

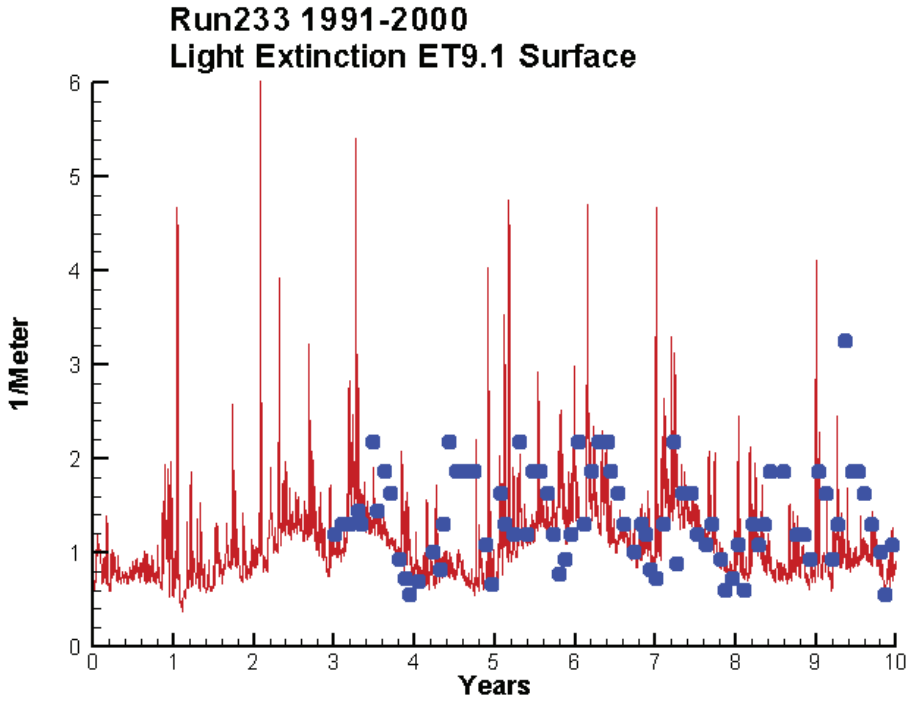

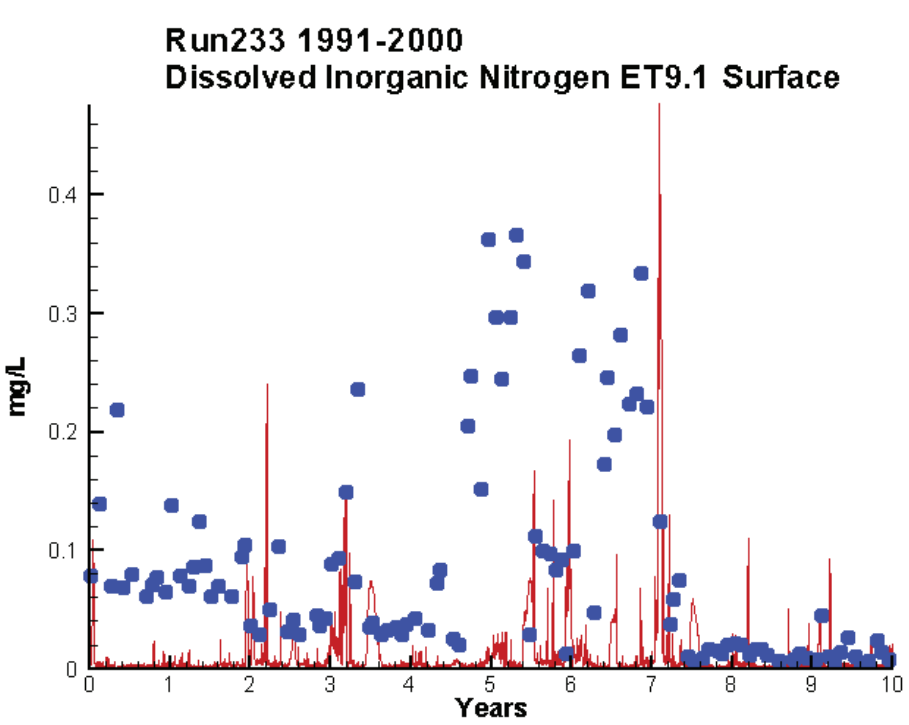

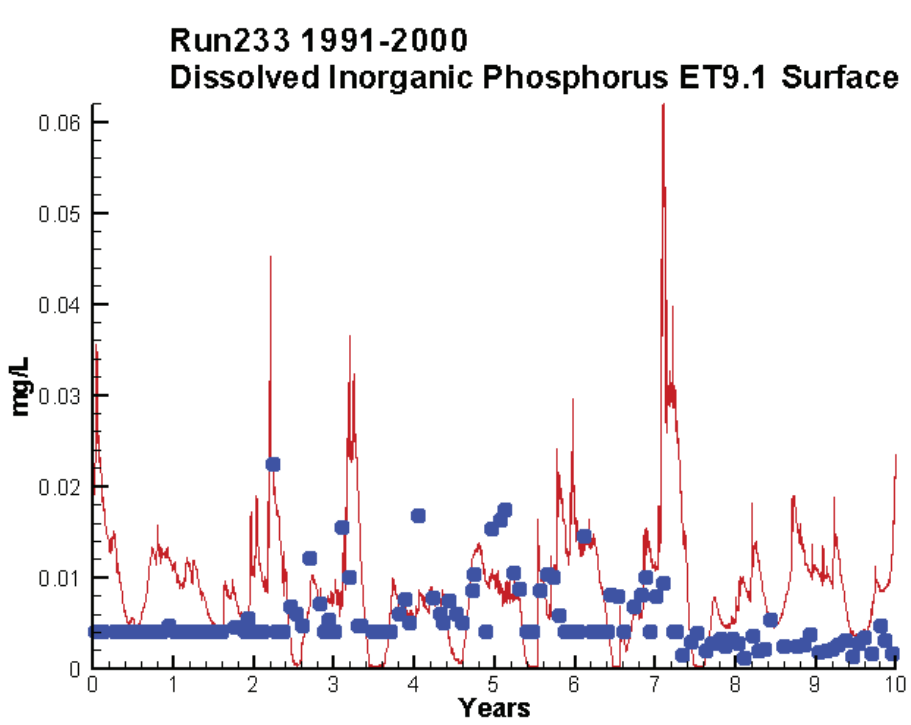

Station ET9.1

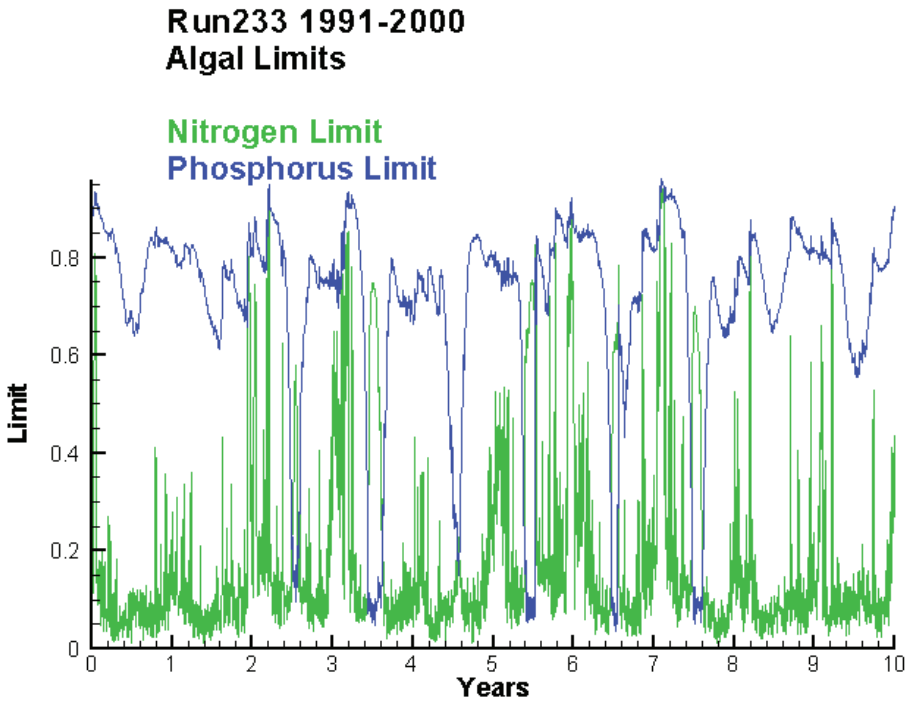

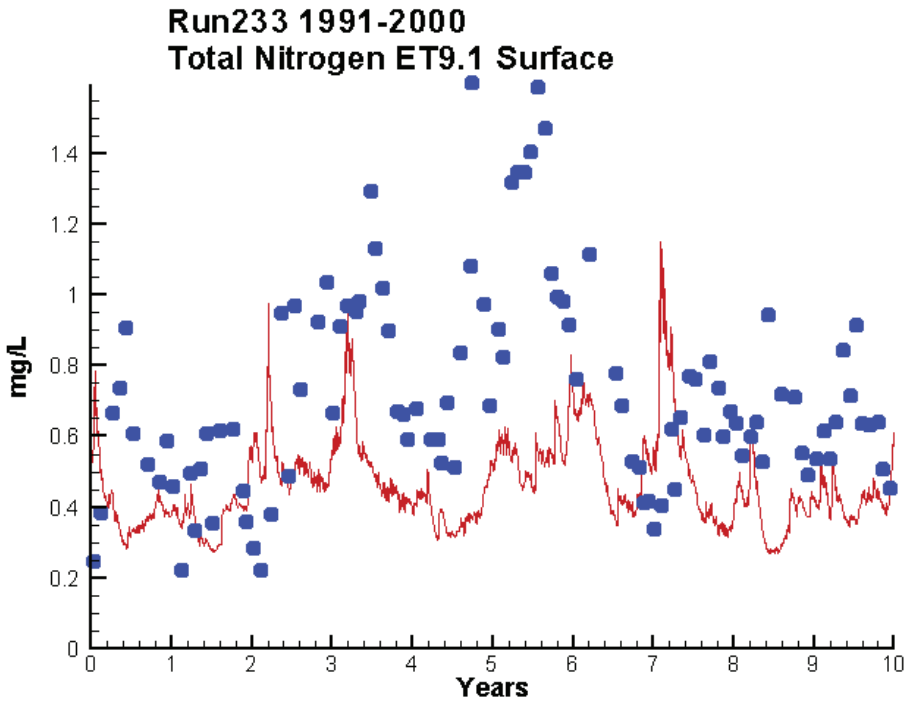

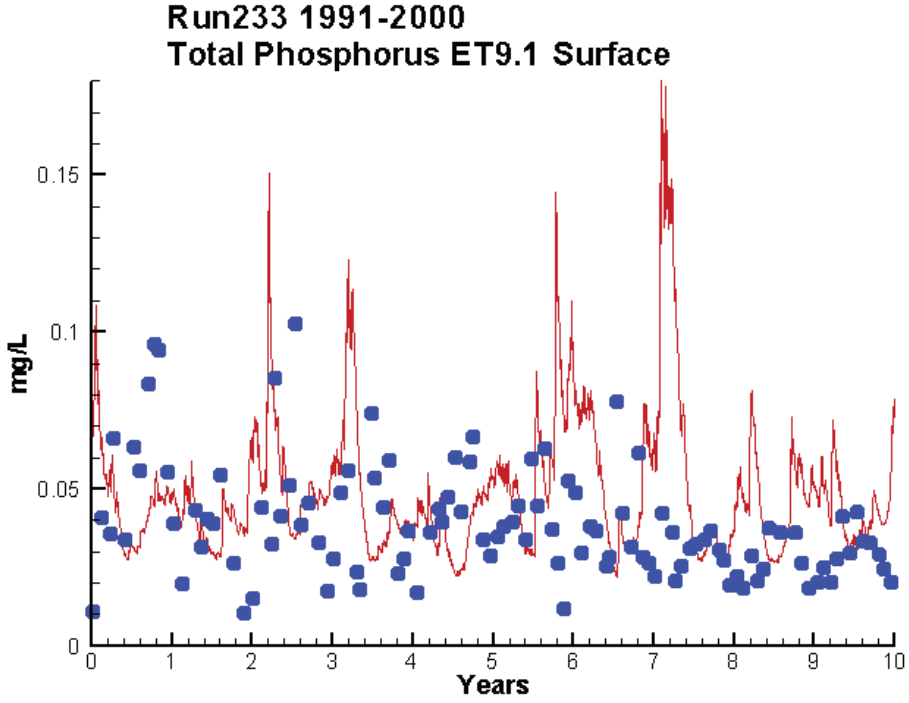

	Mean Difference	Absolute Mean Difference
Chl	-1.3415	4.5276
DIN	-0.0759	0.0838
KE	-0.2233	0.4292
DIP	0.0039	0.0060
TP	0.0111	0.0245
TN	-0.2585	0.3175

Station ET9.1

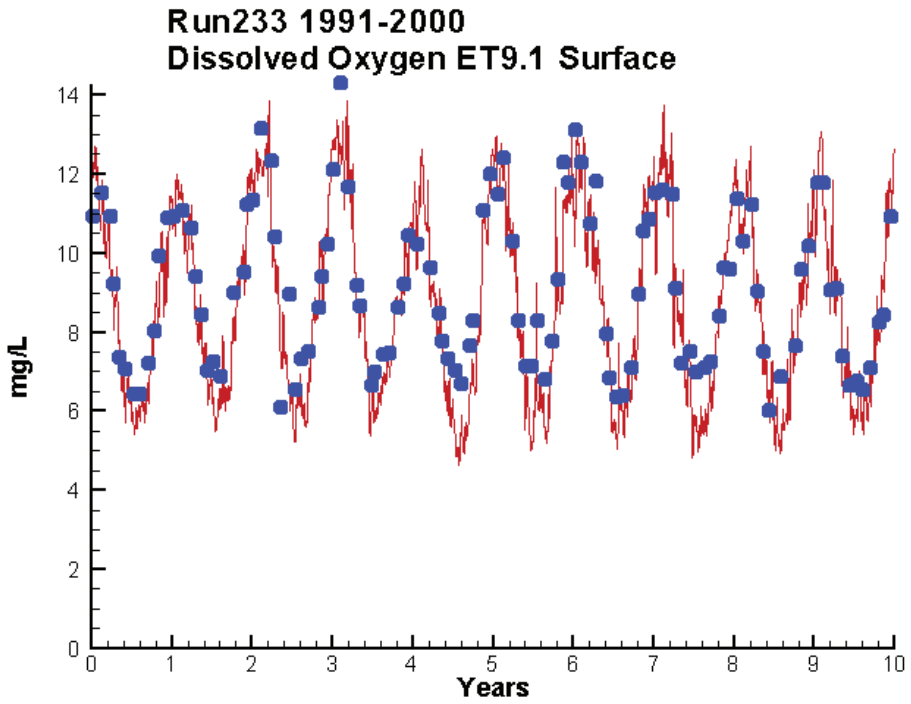

	Mean Difference	Absolute Mean Difference
Top DO	-0.3809	0.7239

Station ET9.1

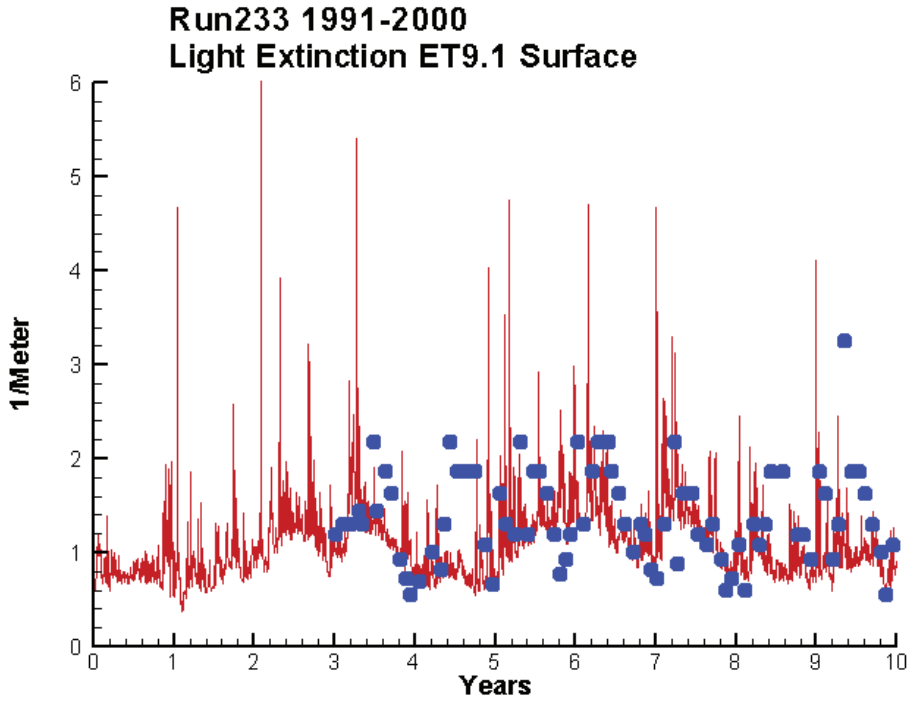

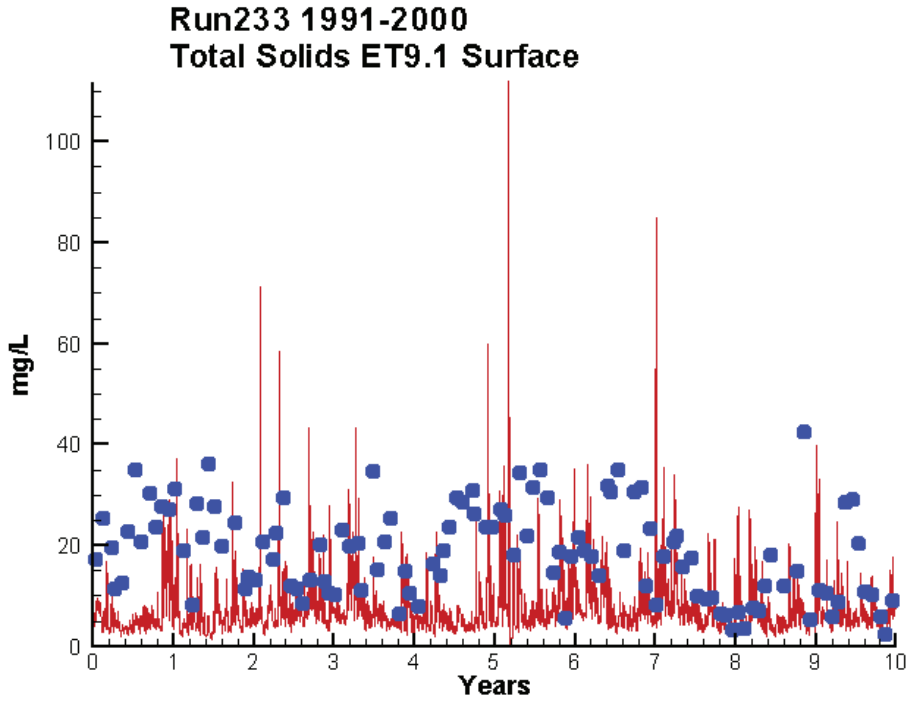

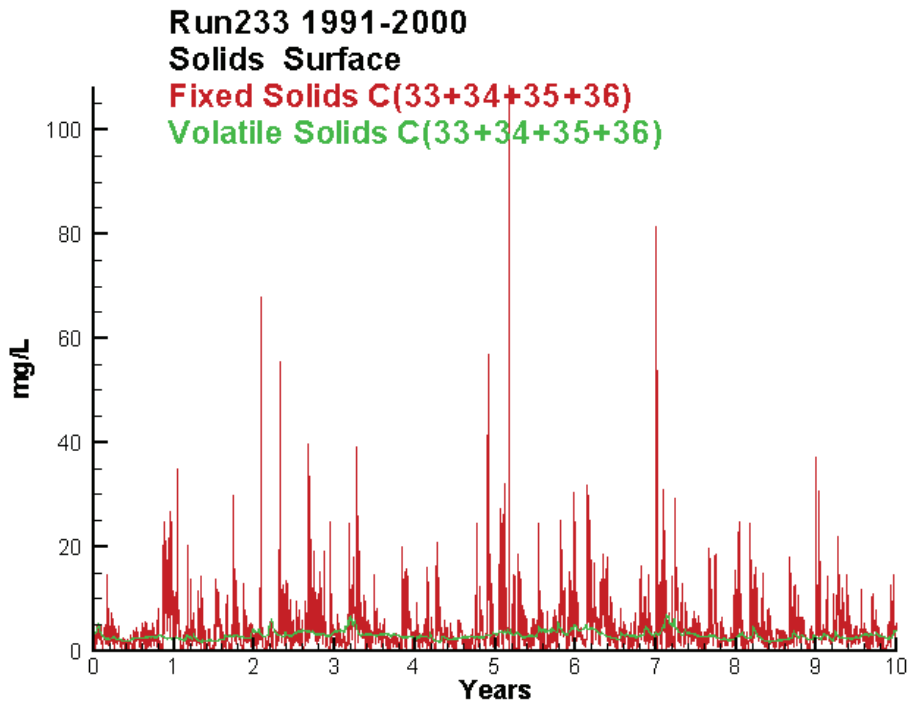

	Mean Difference	Absolute Mean Difference
KE	-0.2233	0.4292
TSS	-11.7015	12.1239

Station WE4.2

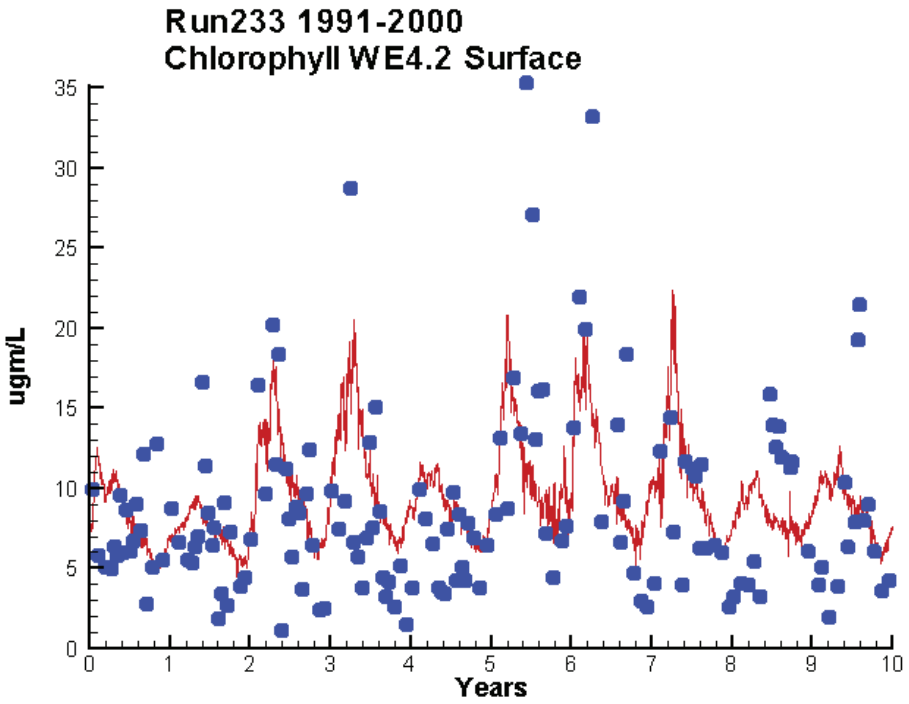

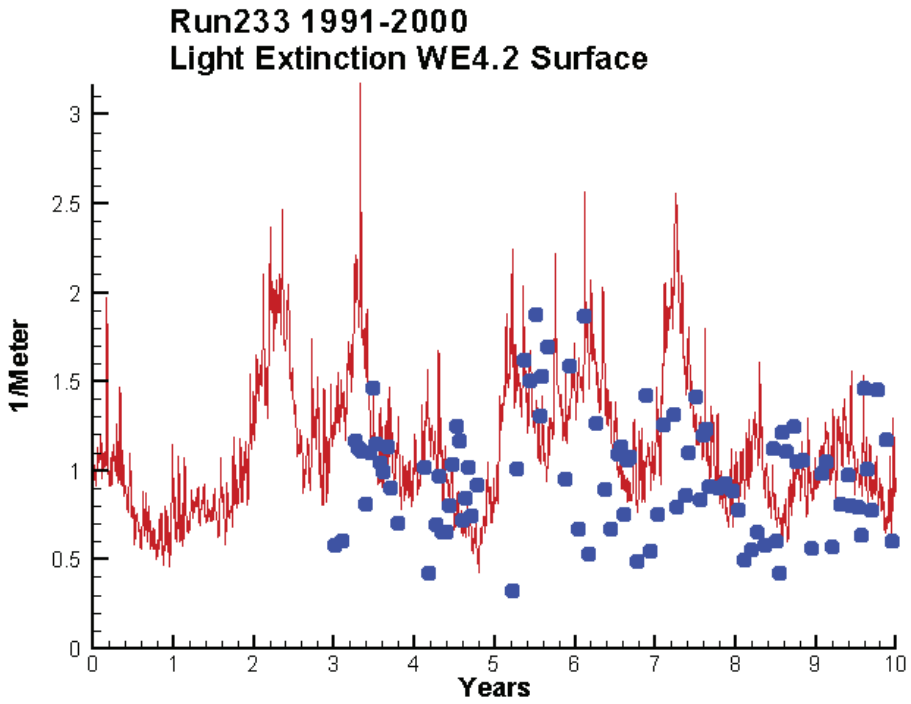

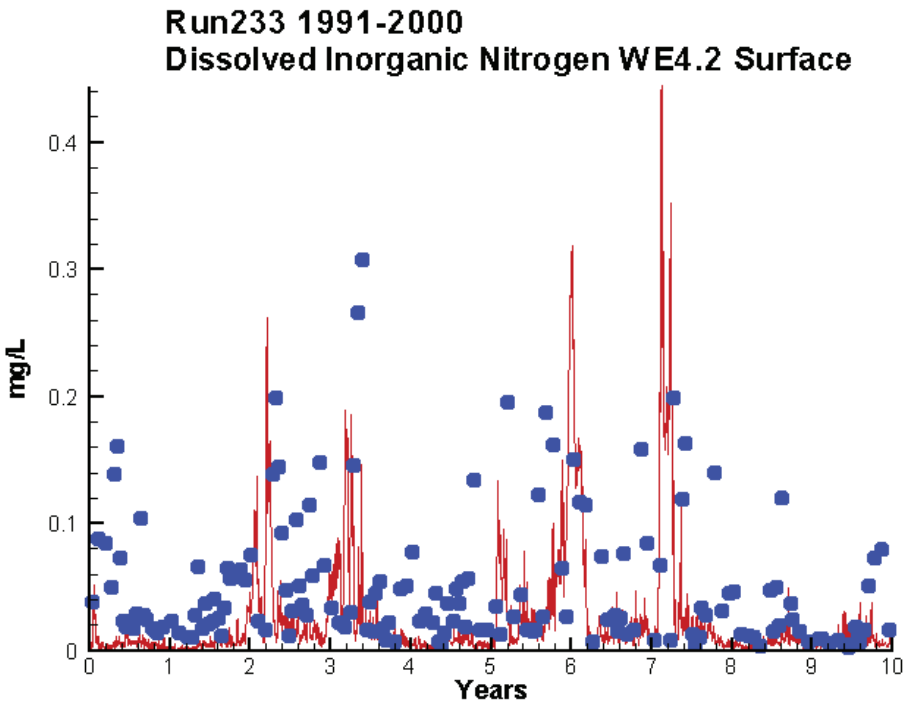

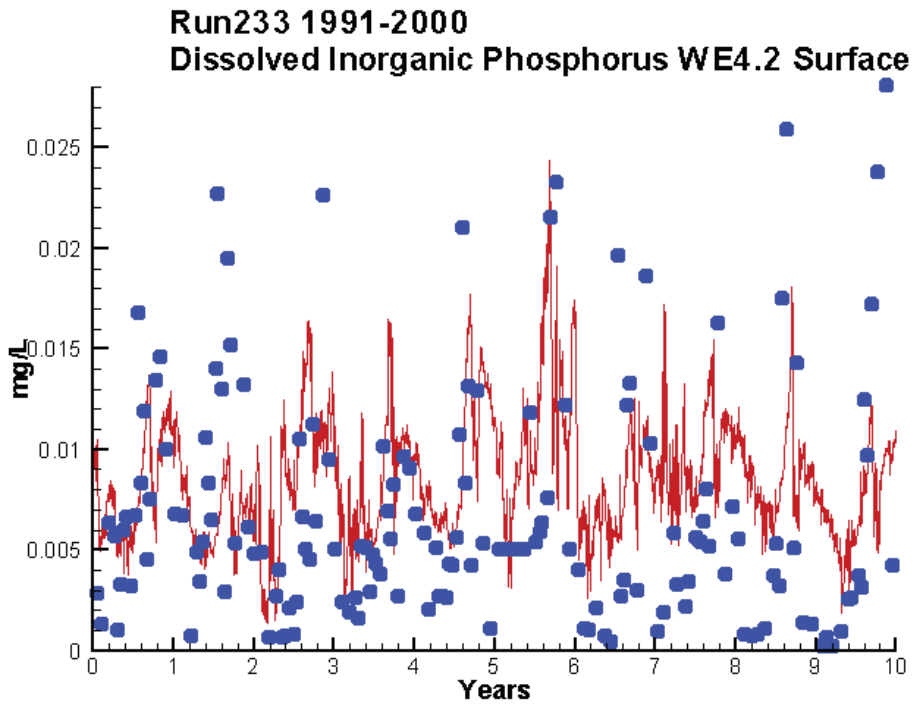

Station WE4.2

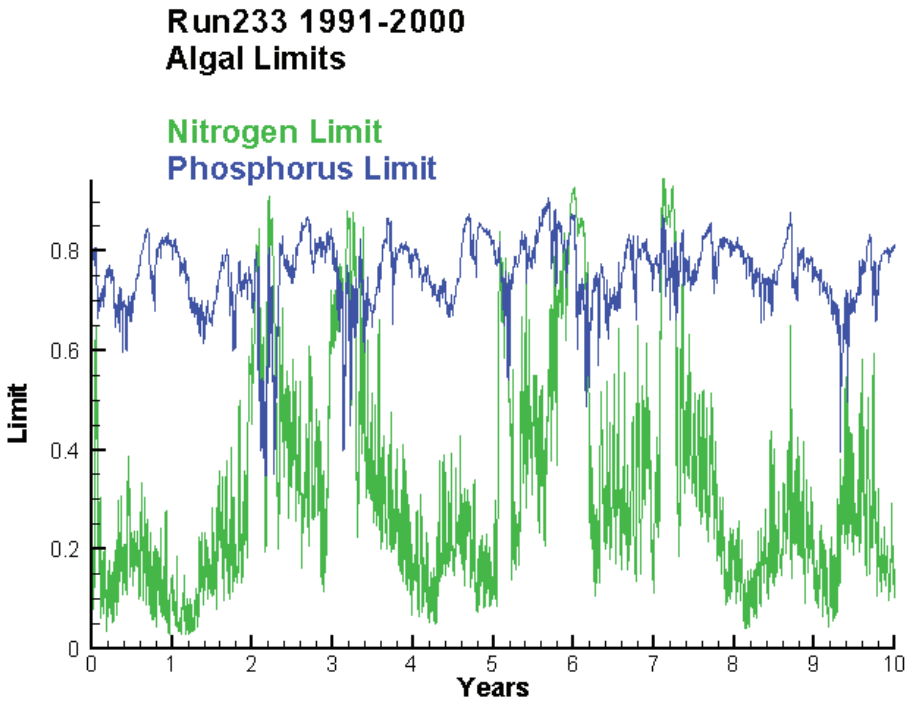

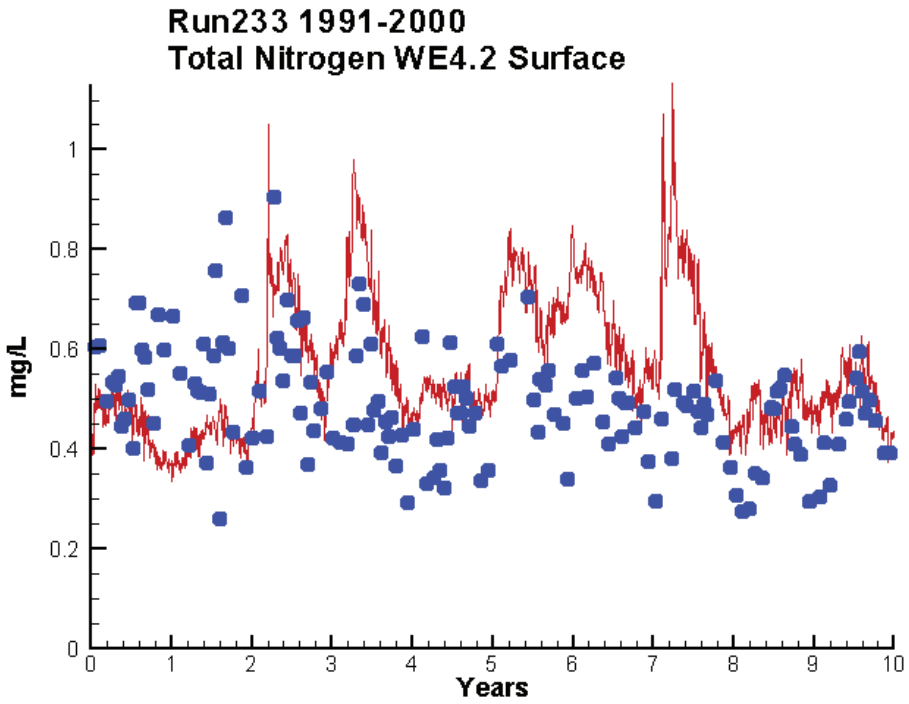

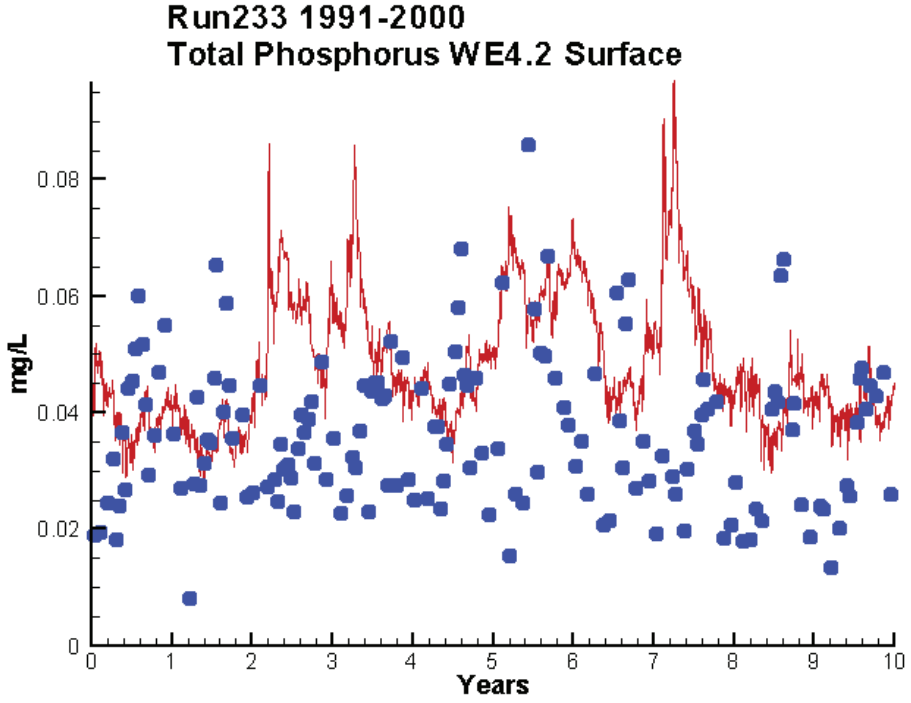

	Mean Difference	Absolute Mean Difference
Chl	0.8793	3.9943
DIN	-0.0283	0.0449
KE	0.1693	0.3633
DIP	0.0017	0.0049
TP	0.0118	0.0172
TN	0.0748	0.1412

Station WE4.2

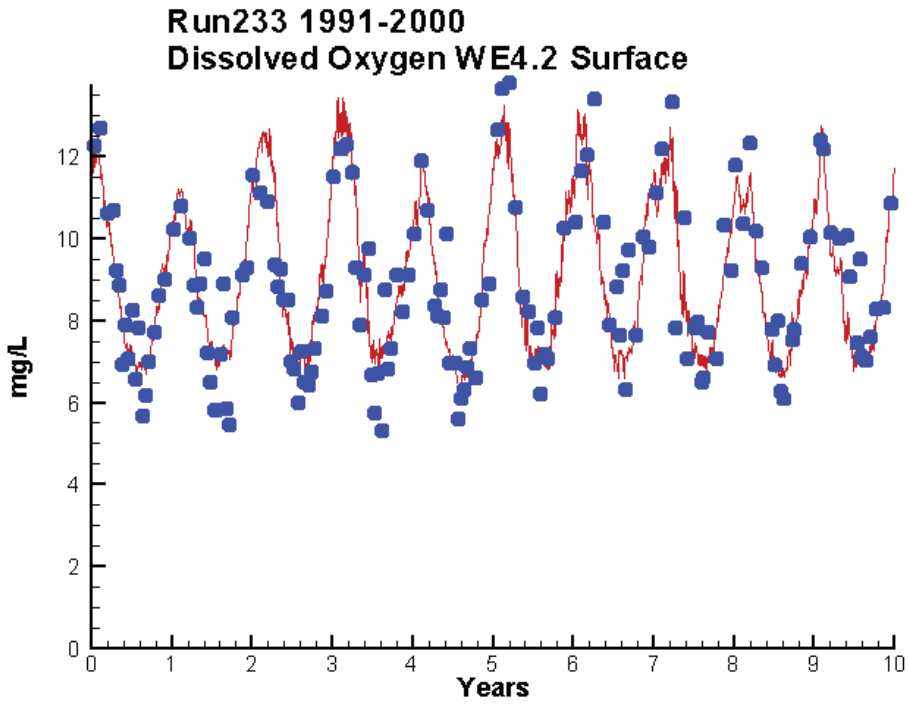

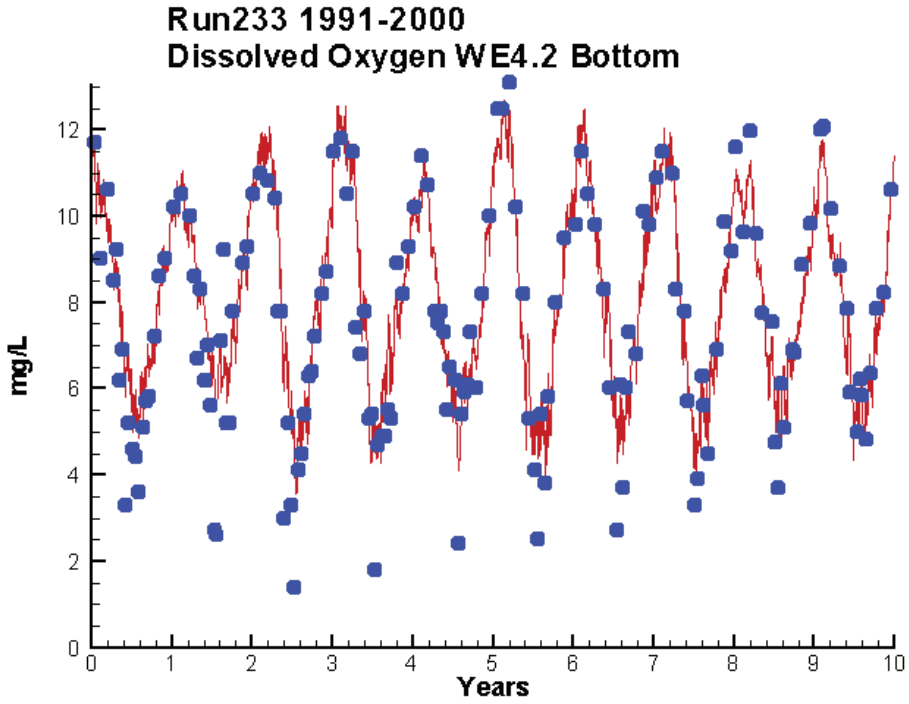

	Mean Difference	Absolute Mean Difference
Top DO	0.0382	0.7650
Bot DO	0.2839	0.7689

Station WE4.2

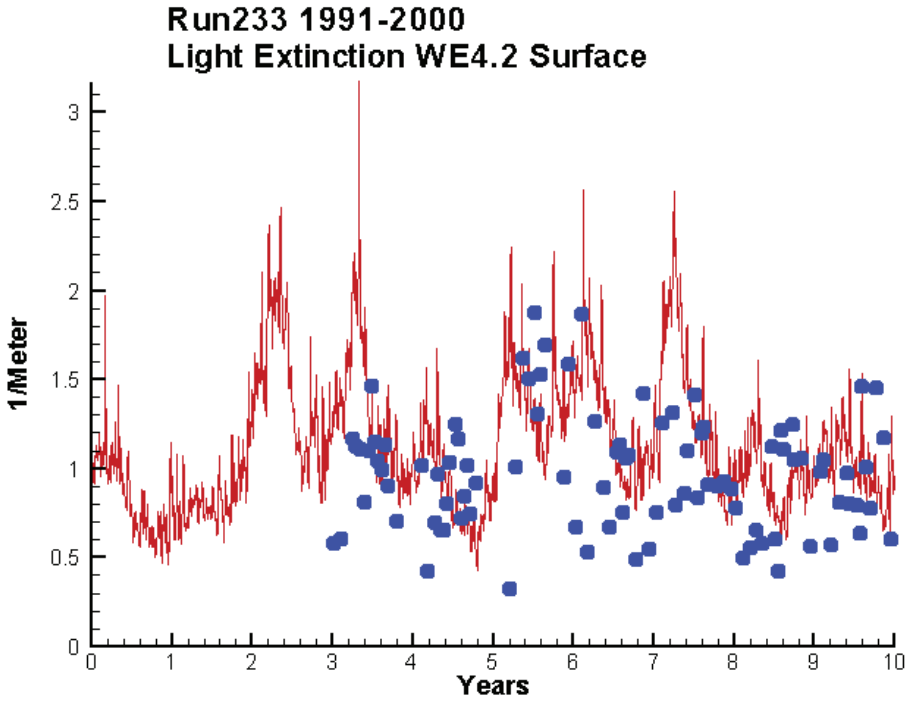

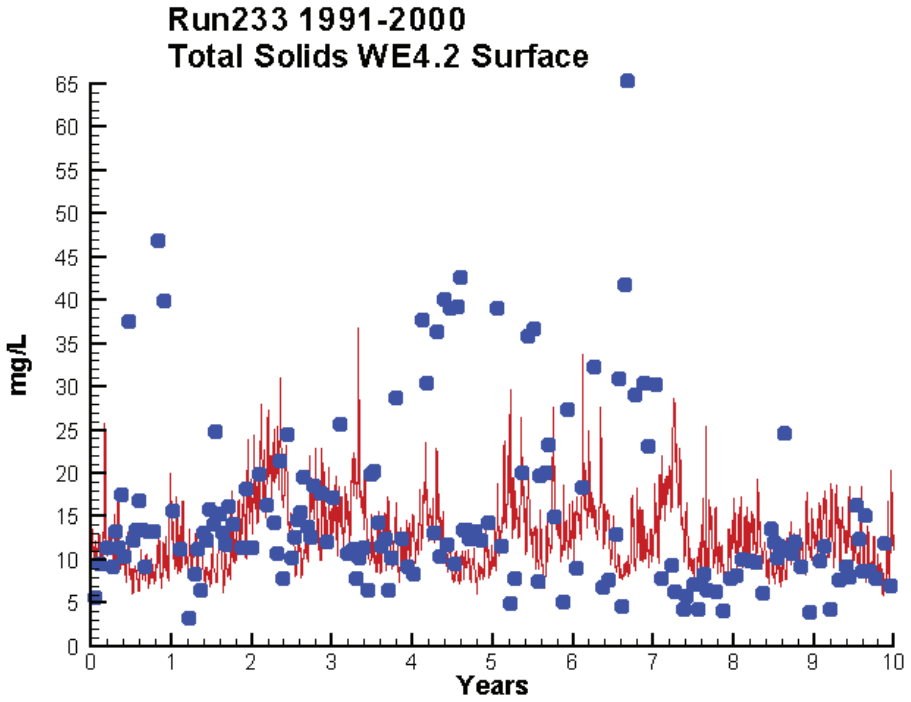

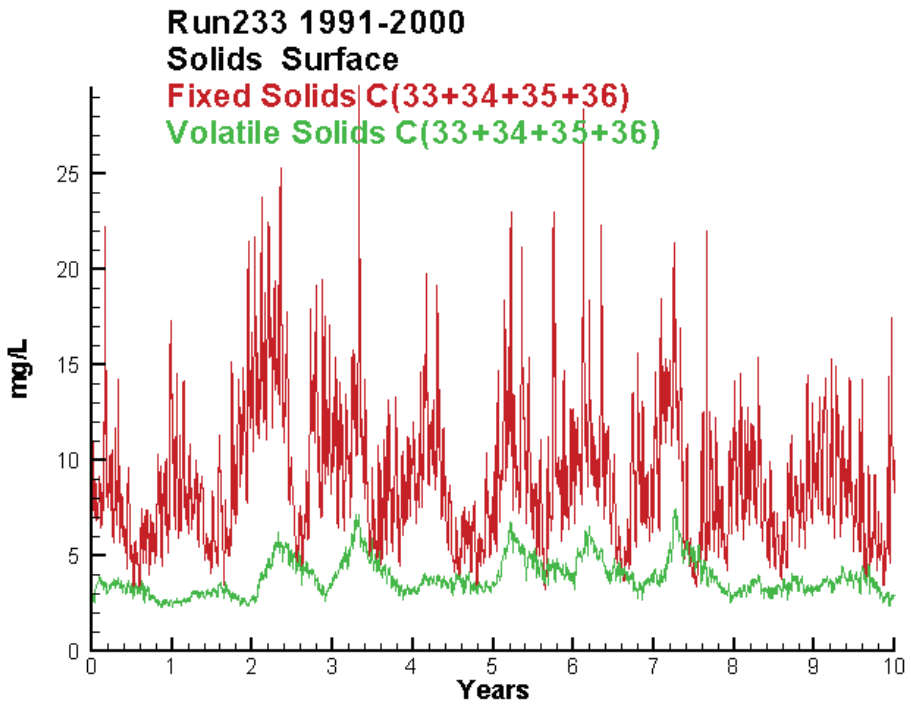

	Mean Difference	Absolute Mean Difference
KE	0.1693	0.3633
TSS	-3.2755	7.7011

Station WT1.1

Run233 1991-2000
Chlorophyll WT1.1 Surface

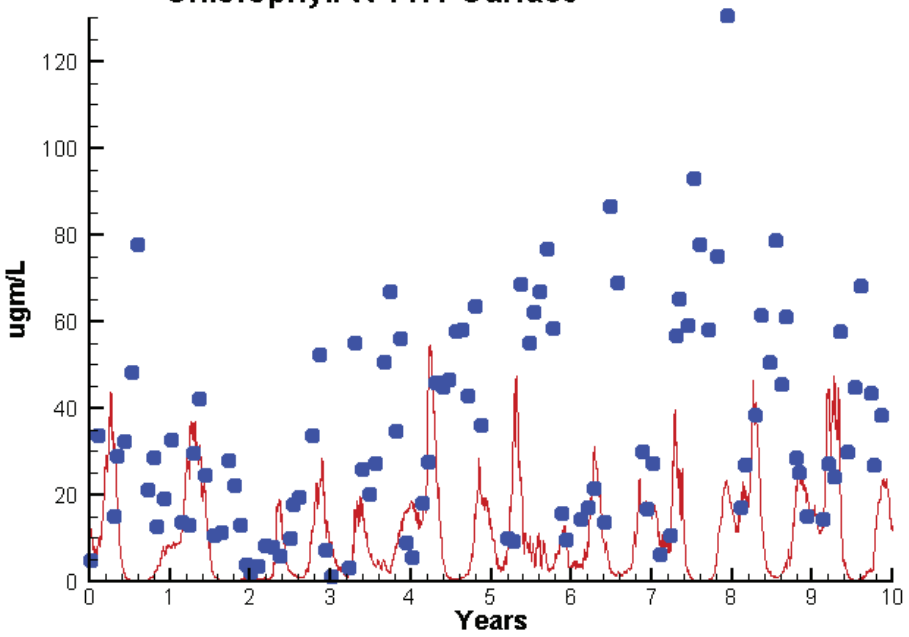

Run233 1991-2000
Light Extinction WT1.1 Surface

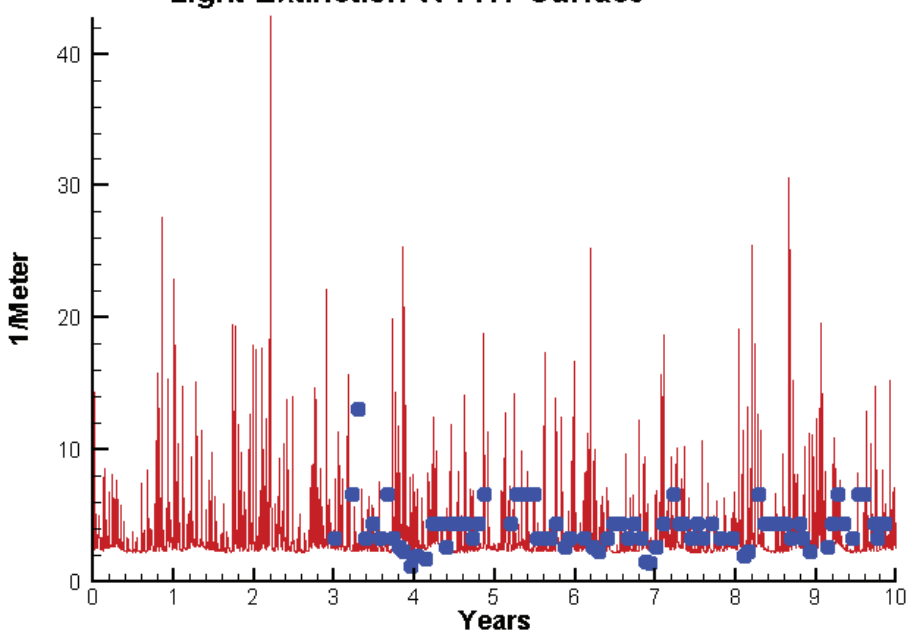

Run233 1991-2000
Dissolved Inorganic Nitrogen WT1.1 Surface

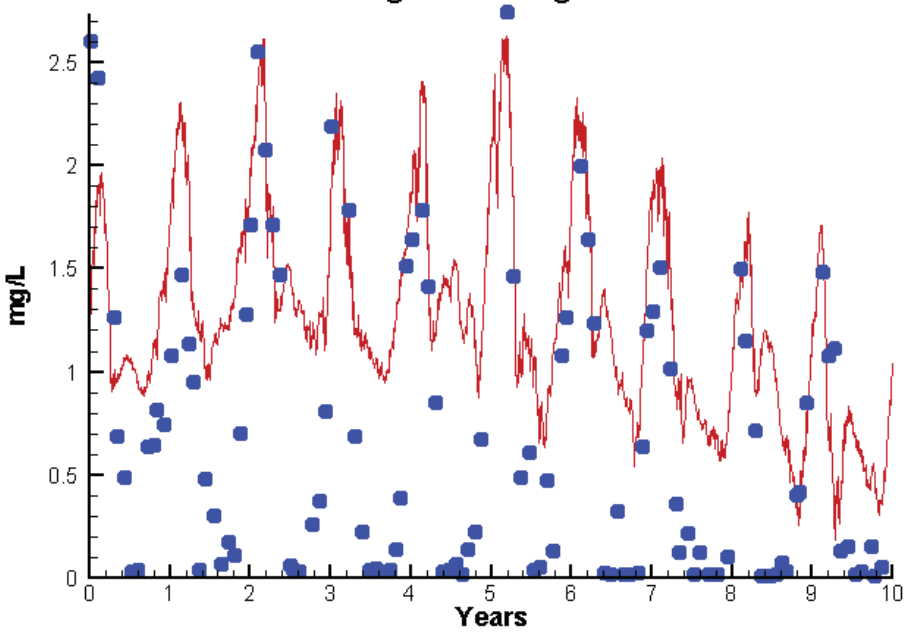

Run233 1991-2000
Dissolved Inorganic Phosphorus WT1.1 Surface

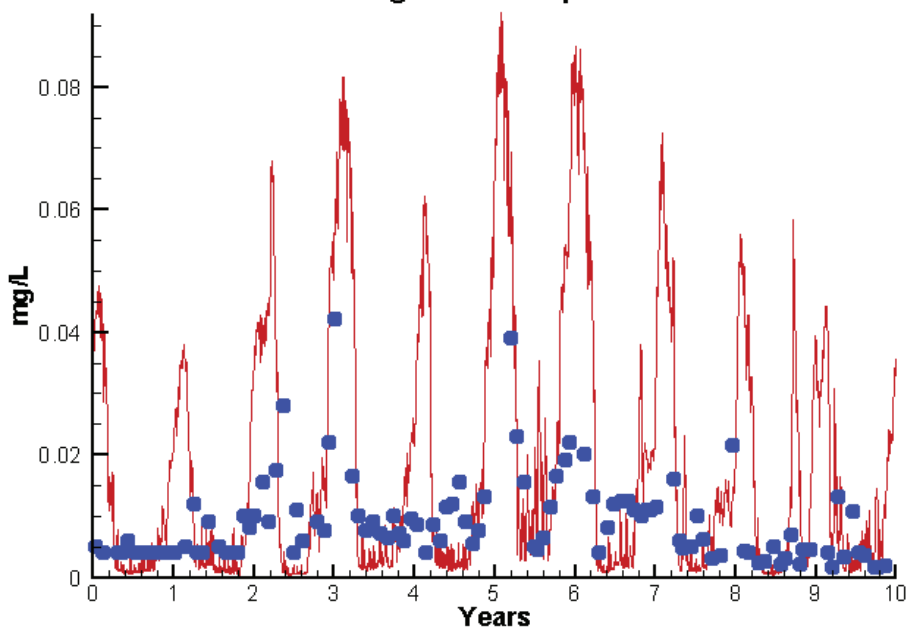

Station WT1.1

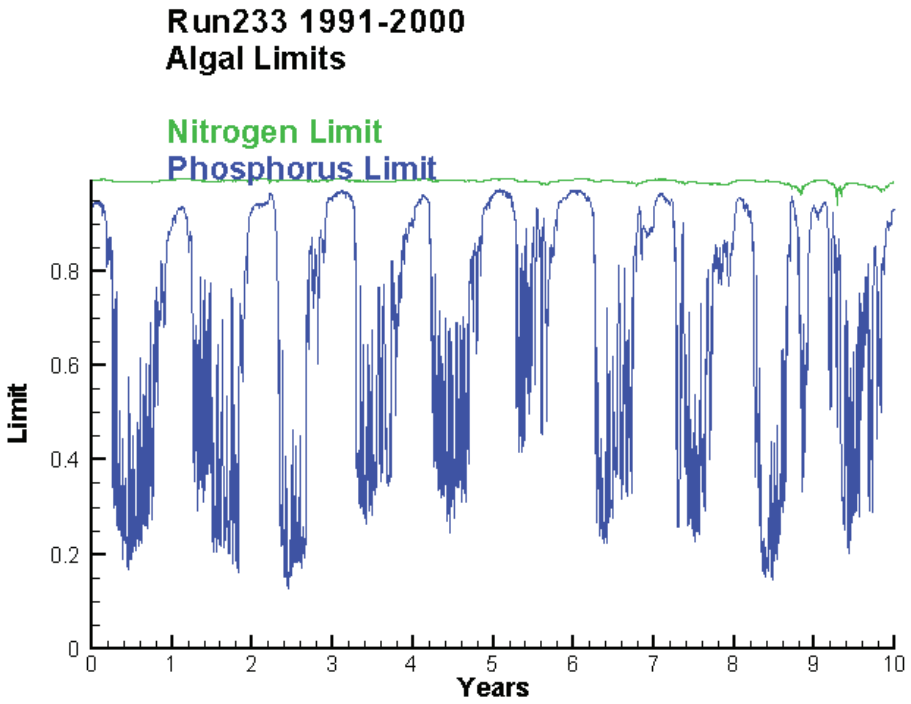

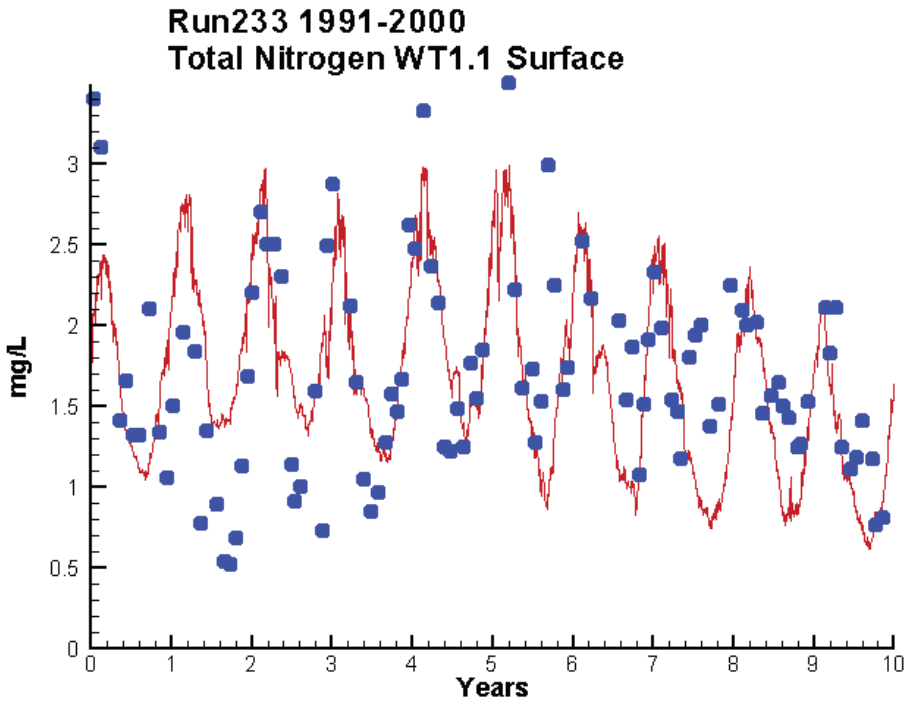

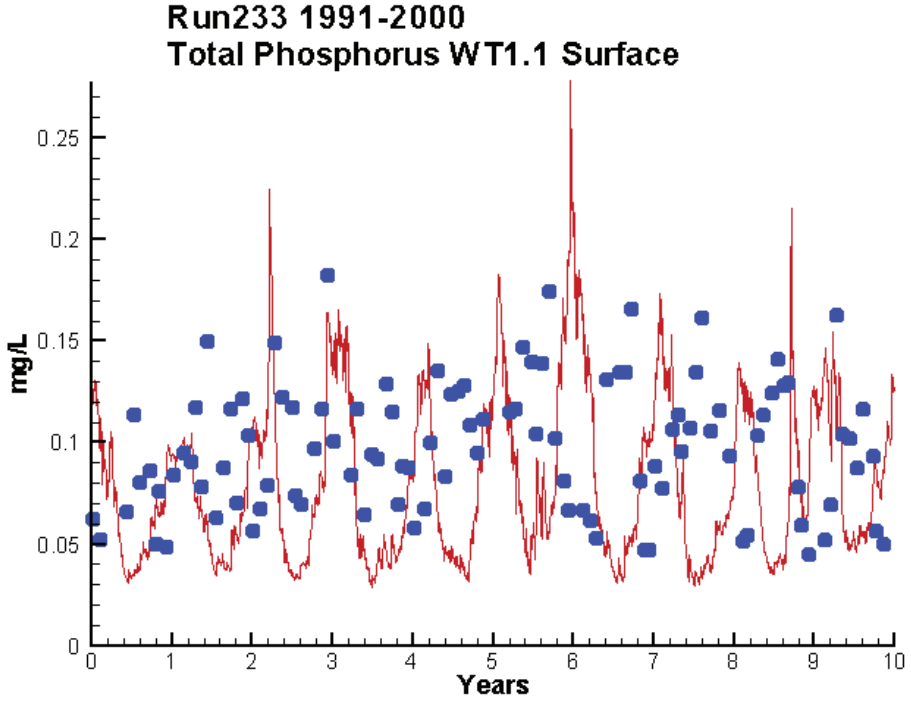

	Mean Difference	Absolute Mean Difference
Chl	-23.6567	27.5333
DIN	0.5604	0.6404
KE	-0.6288	2.1079
DIP	0.0064	0.0116
TP	-0.0208	0.0497
TN	-0.0513	0.4211

Station WT1.1

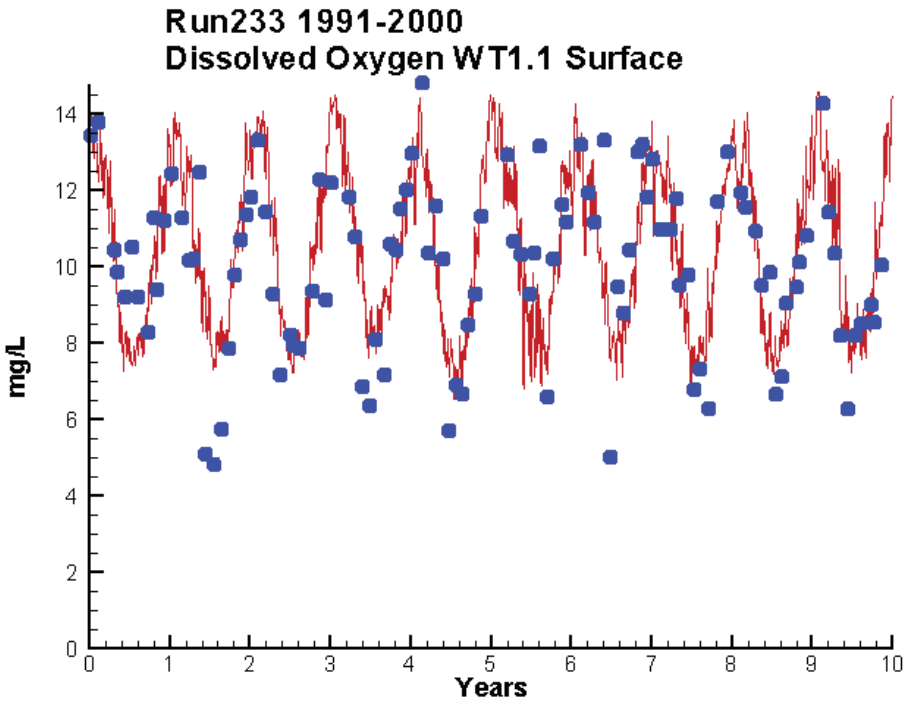

	Mean Difference	Absolute Mean Difference
Top DO	0.2361	1.2389

Station WT1.1

Run233 1991-2000
Light Extinction WT1.1 Surface

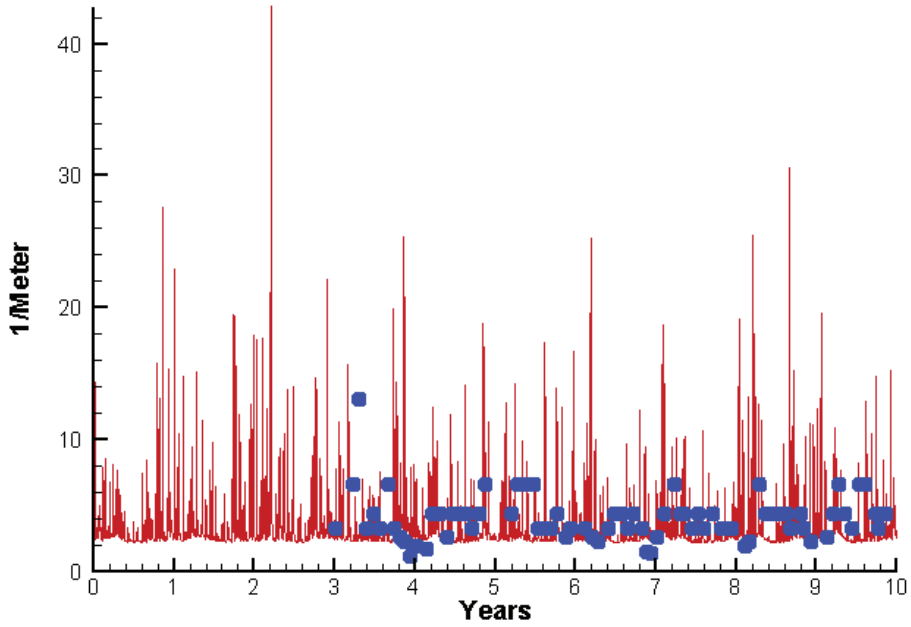

Run233 1991-2000
Total Solids WT1.1 Surface

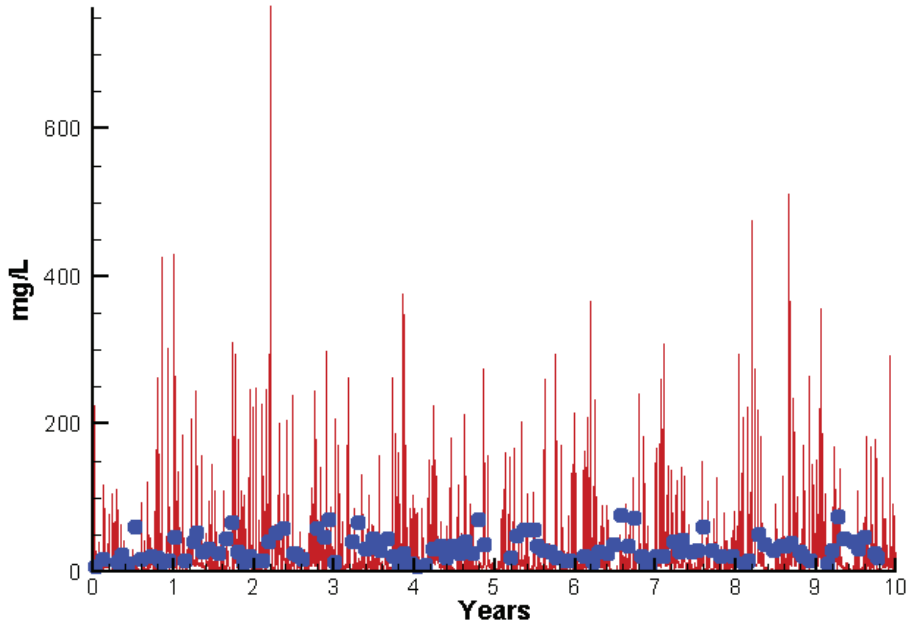

Run233 1991-2000
Solids Surface
Fixed Solids C(33+34+35+36)
Volatile Solids C(33+34+35+36)

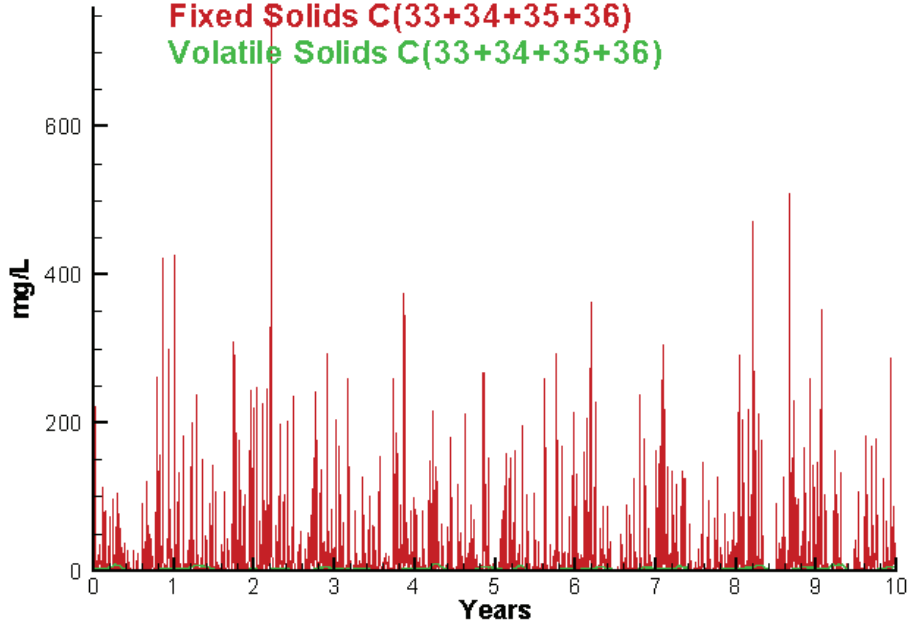

	Mean Difference	Absolute Mean Difference
KE	-0.6288	2.1079
TSS	-2.6122	36.4544

Station WT2.1

Run233 1991-2000
Chlorophyll WT2.1 Surface

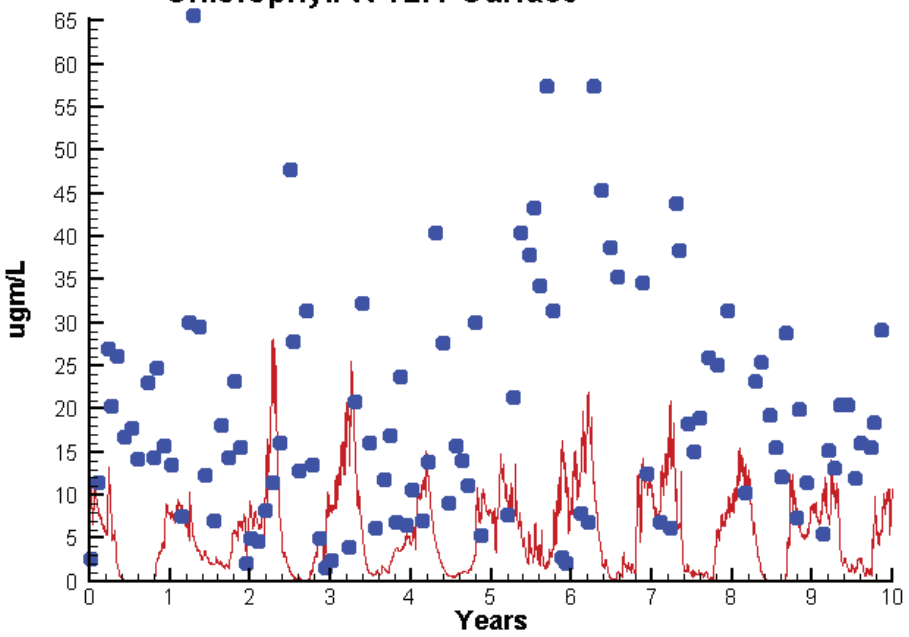

Run233 1991-2000
Light Extinction WT2.1 Surface

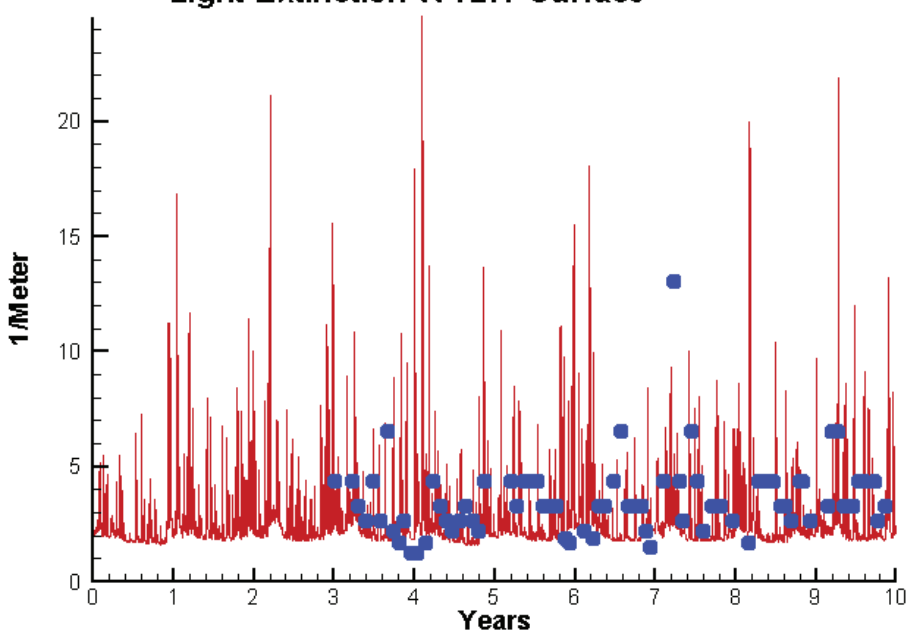

Run233 1991-2000
Dissolved Inorganic Nitrogen WT2.1 Surface

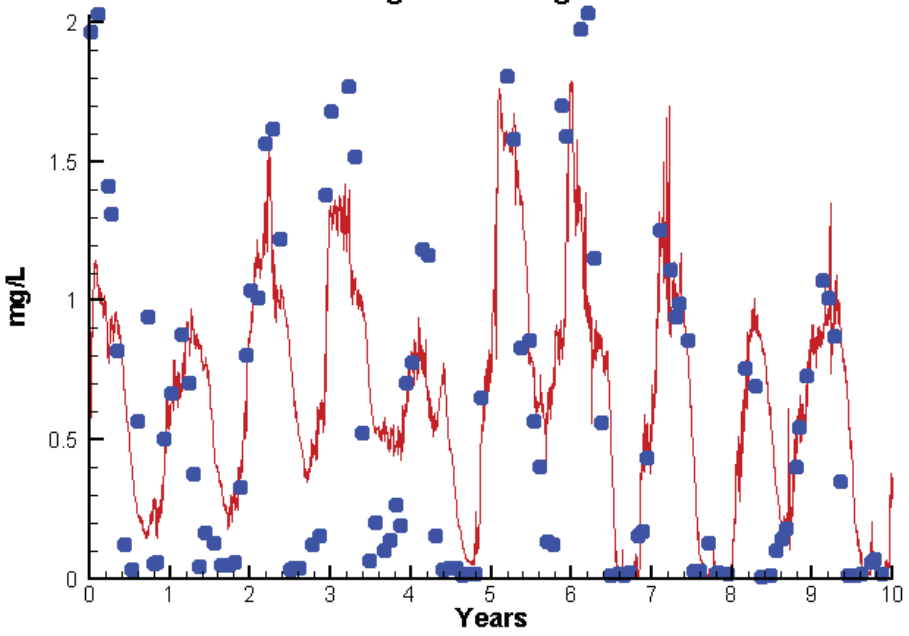

Run233 1991-2000
Dissolved Inorganic Phosphorus WT2.1 Surface

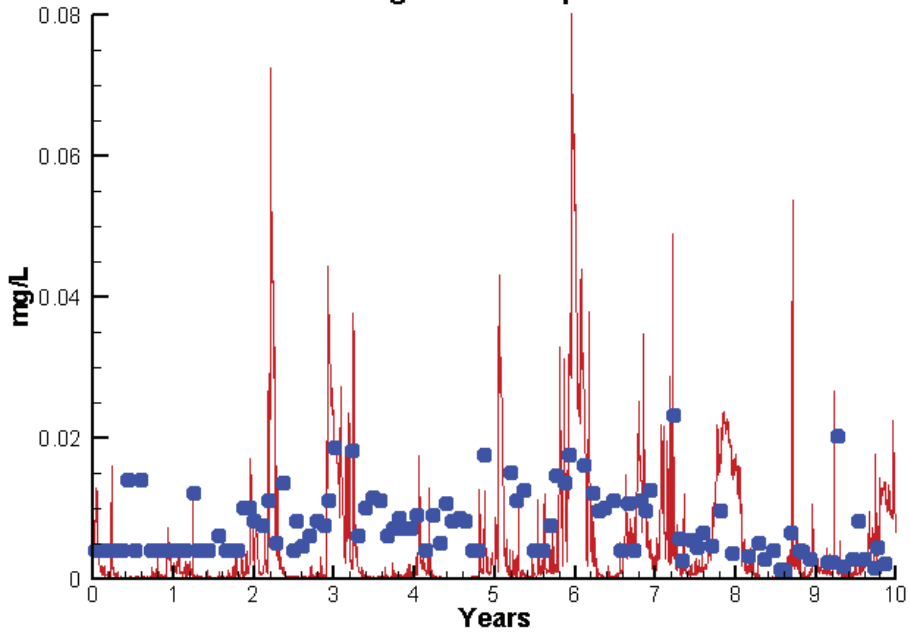

Station WT2.1

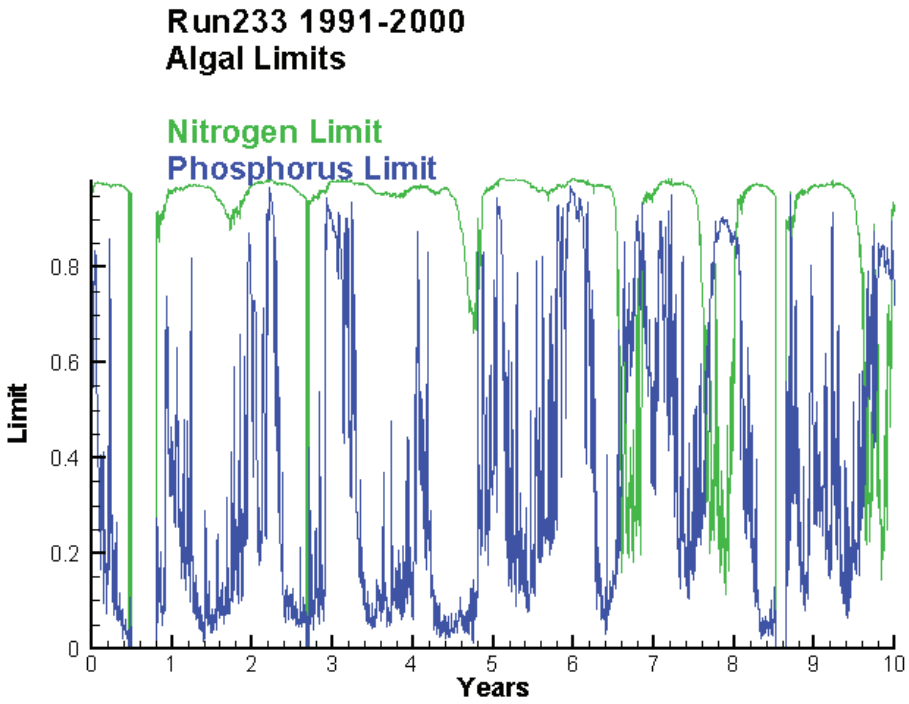

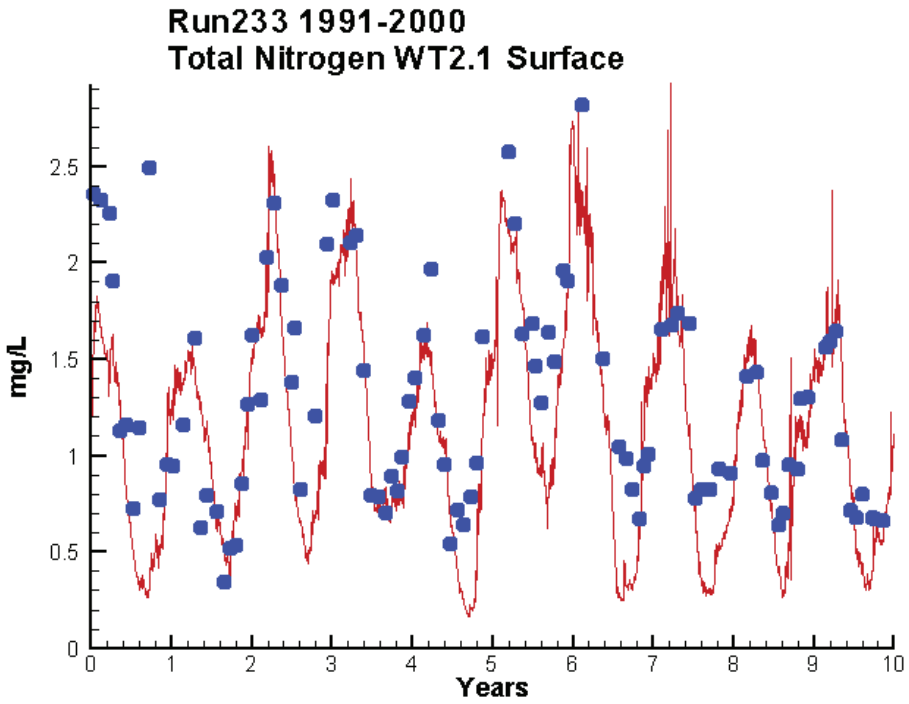

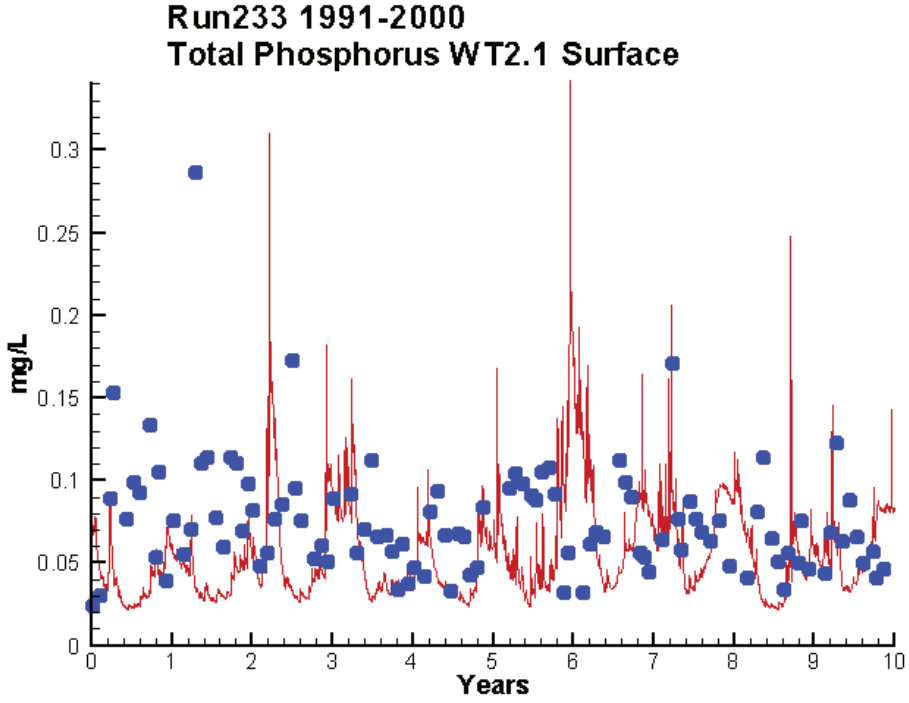

	Mean Difference	Absolute Mean Difference
Chl	-13.9437	16.1802
DIN	0.0564	0.2997
KE	-0.8362	1.8252
DIP	-0.0038	0.0061
TP	-0.0218	0.0393
TN	-0.1926	0.2978

Station WT2.1

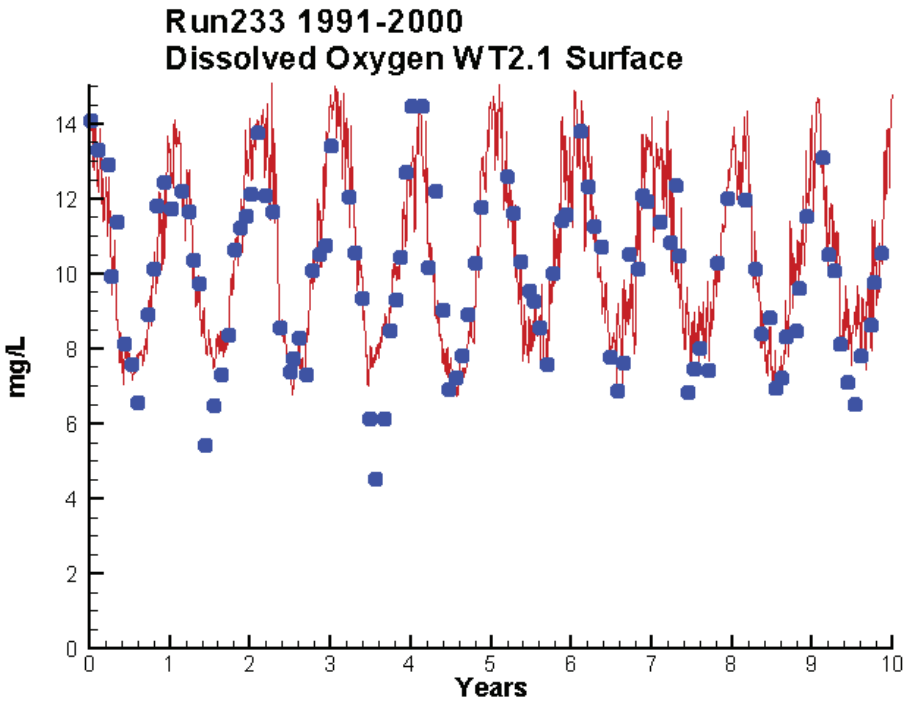

	Mean Difference	Absolute Mean Difference
Top DO	0.2987	0.9009

Station WT2.1

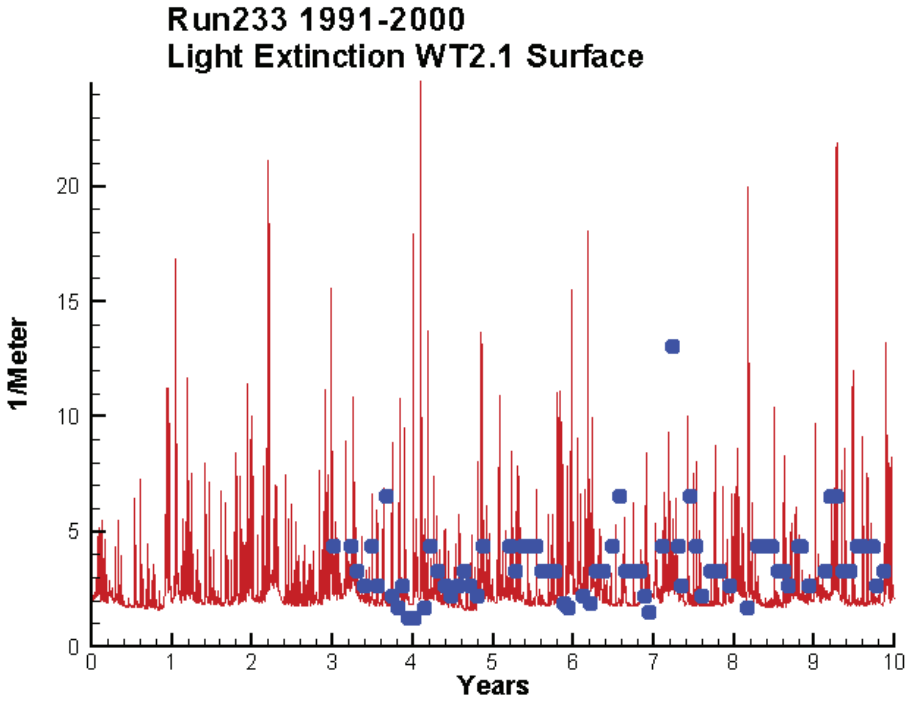

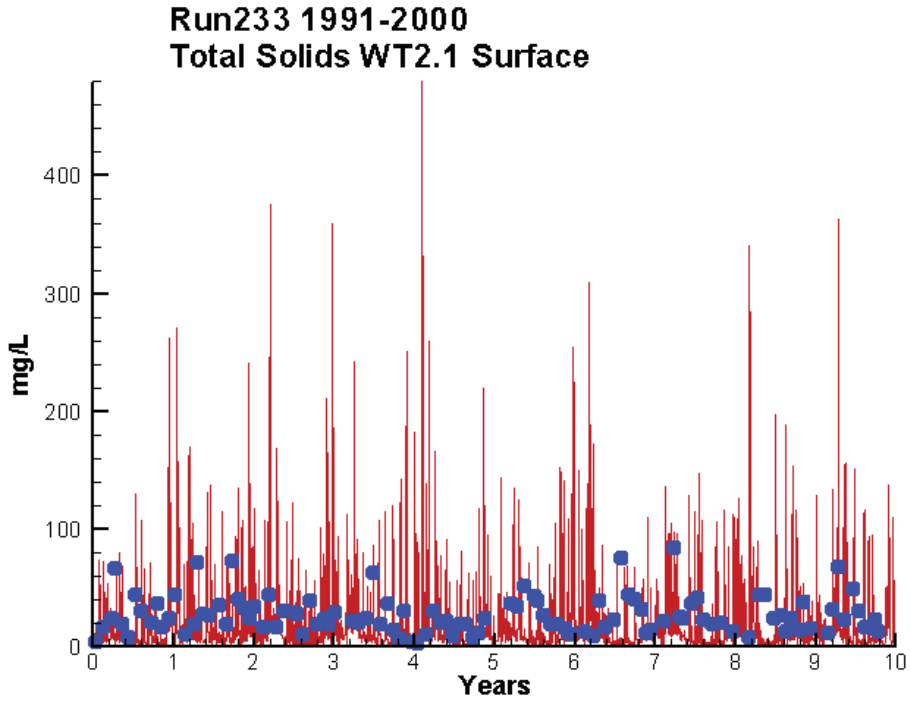

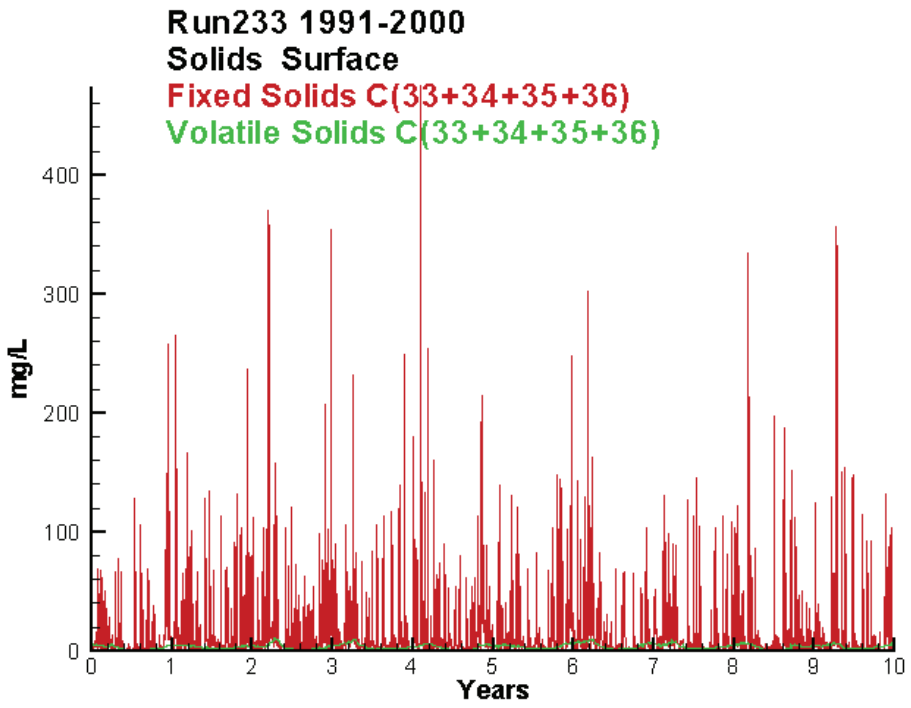

	Mean Difference	Absolute Mean Difference
KE	-0.8362	1.8252
TSS	-5.4664	27.3787

Station WT5.1

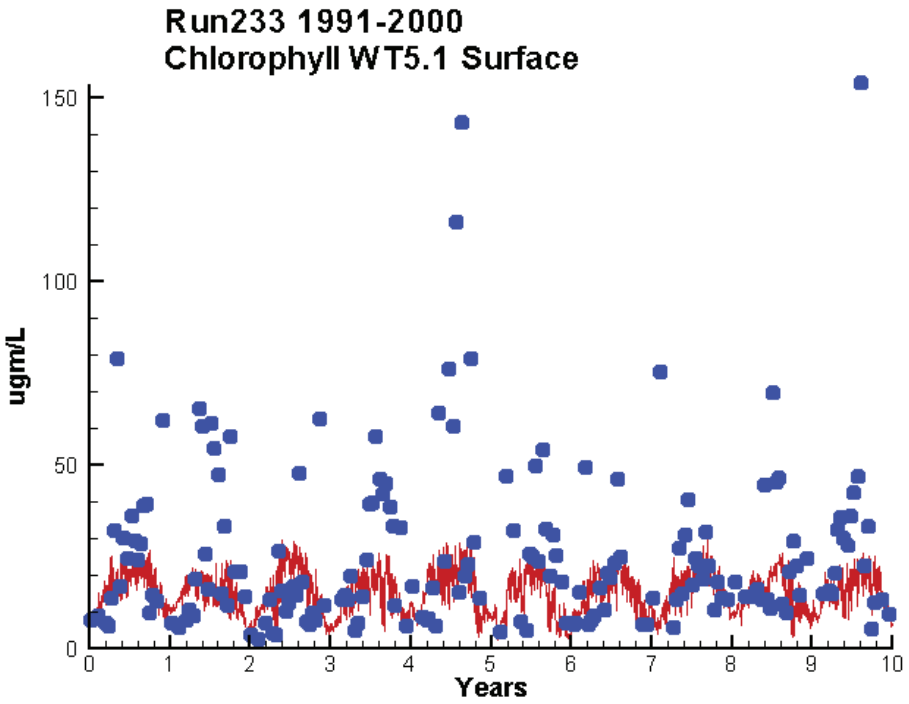

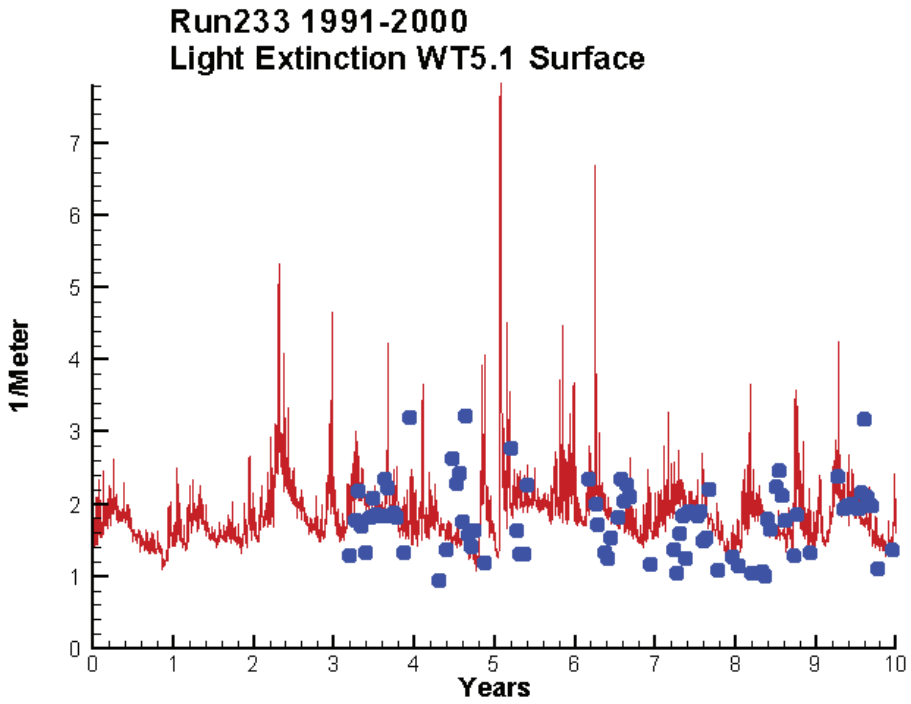

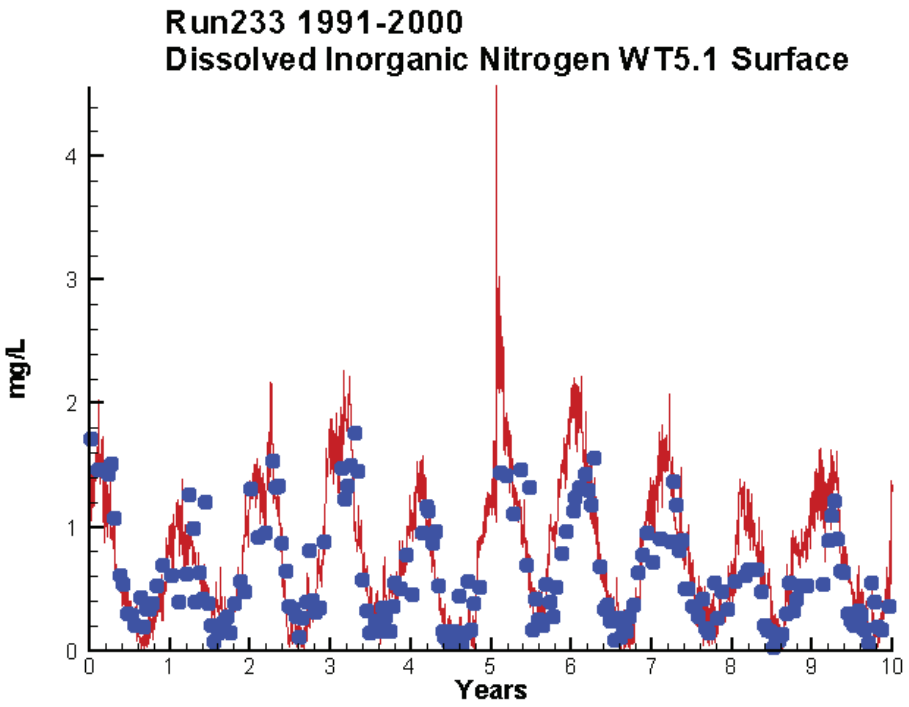

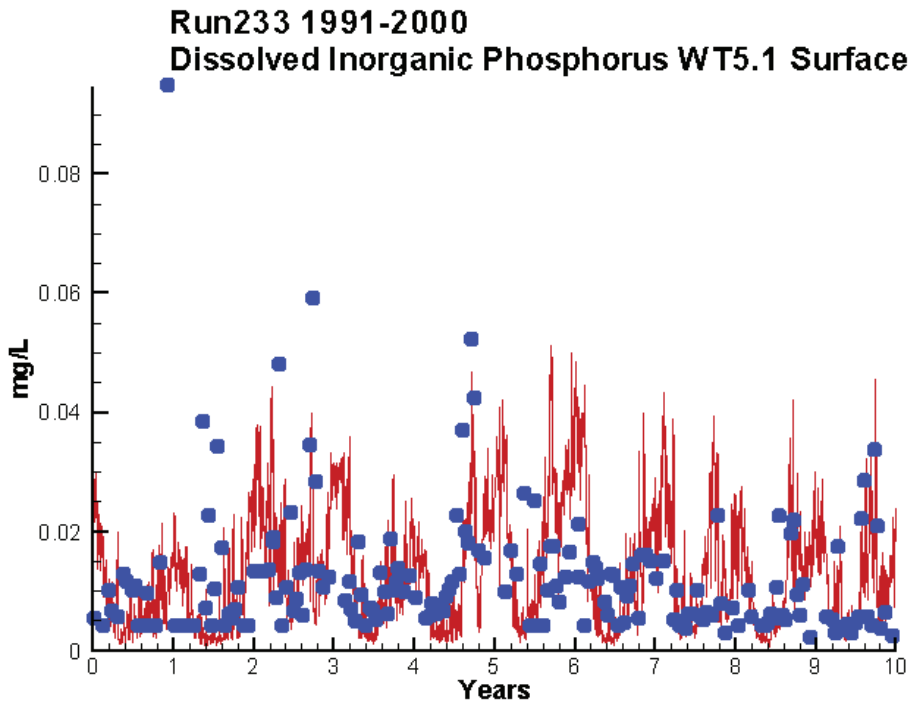

Station WT5.1

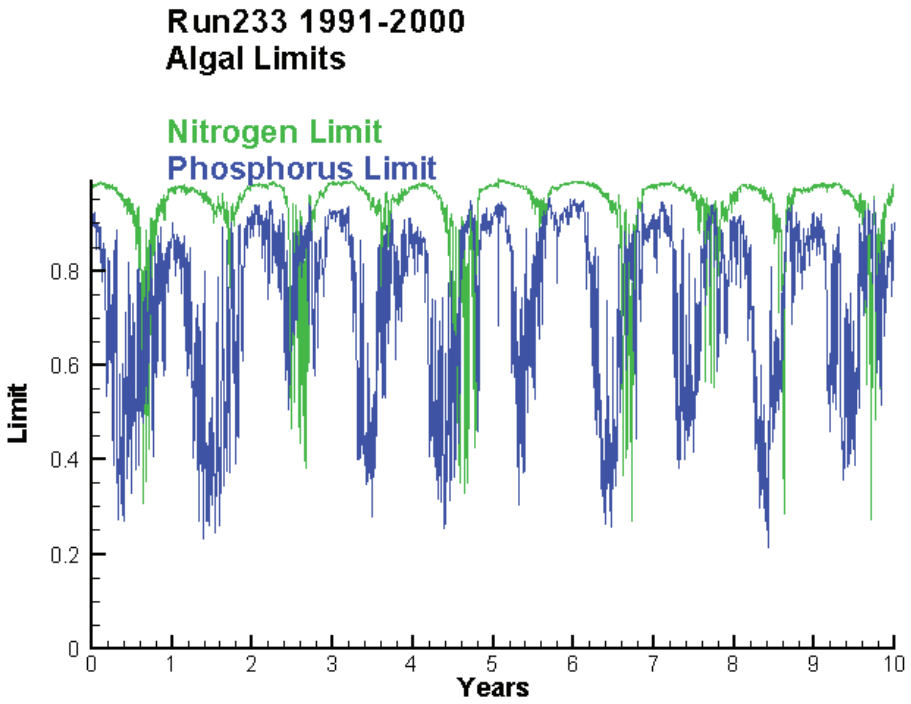

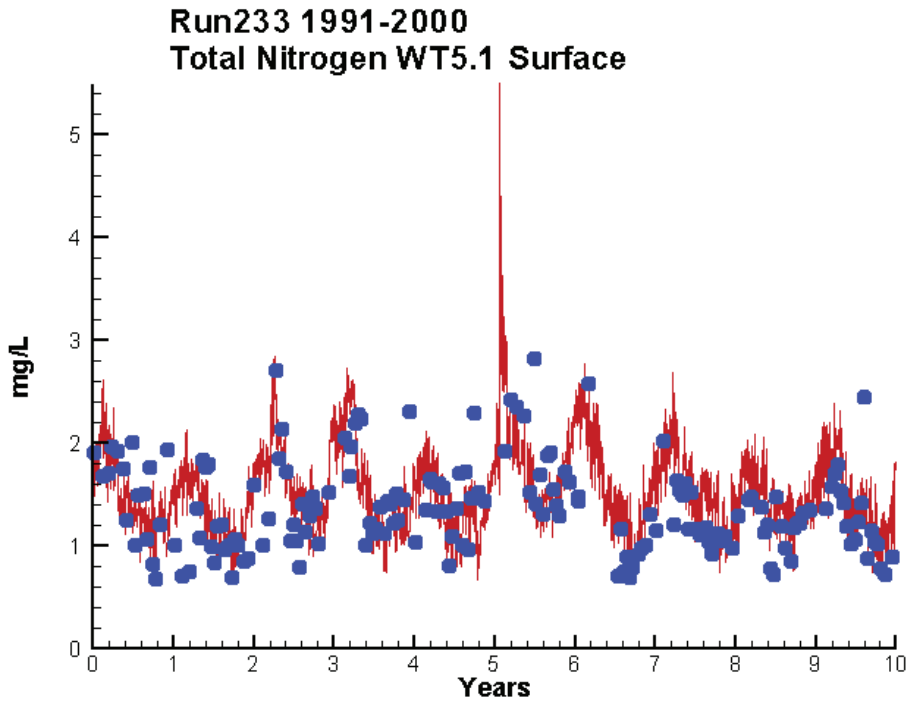

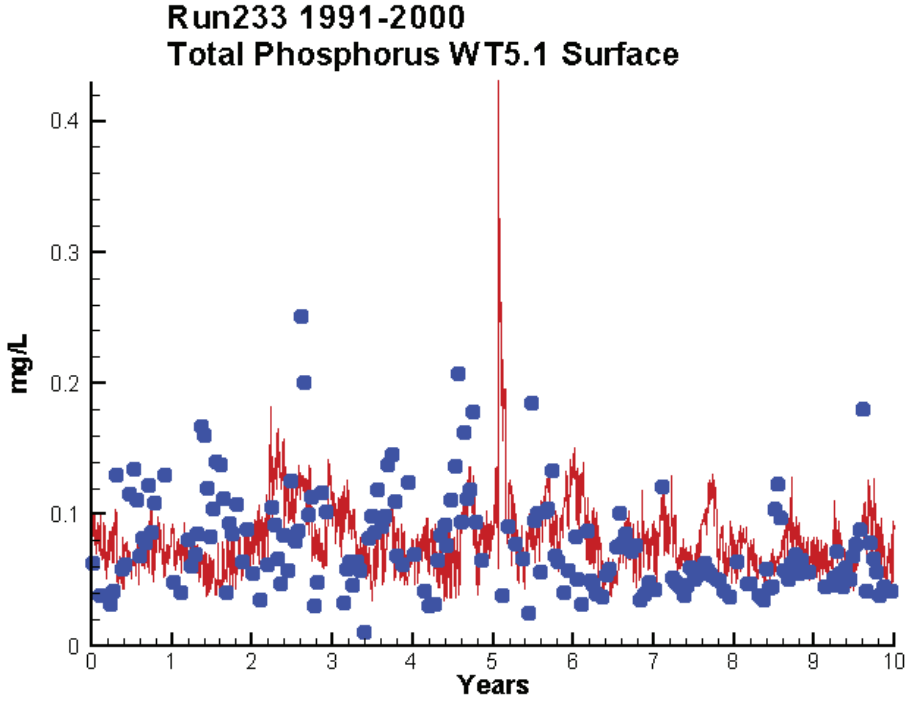

	Mean Difference	Absolute Mean Difference
Chl	-9.5153	14.7139
DIN	0.0870	0.2423
KE	0.1135	0.5187
DIP	0.0000	0.0089
TP	0.0023	0.0343
TN	0.0726	0.3284

Station WT5.1

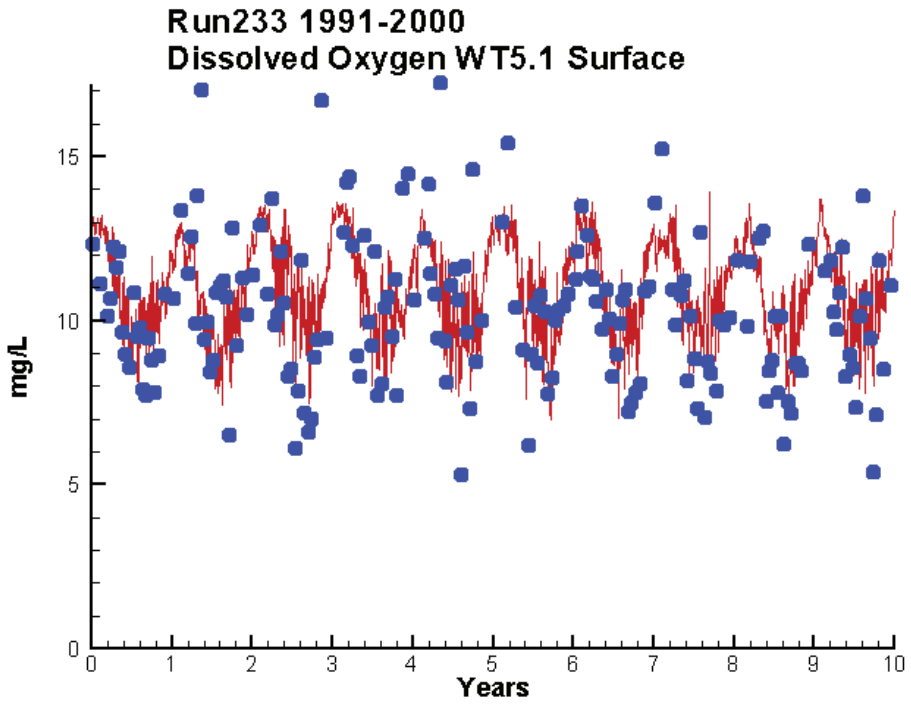

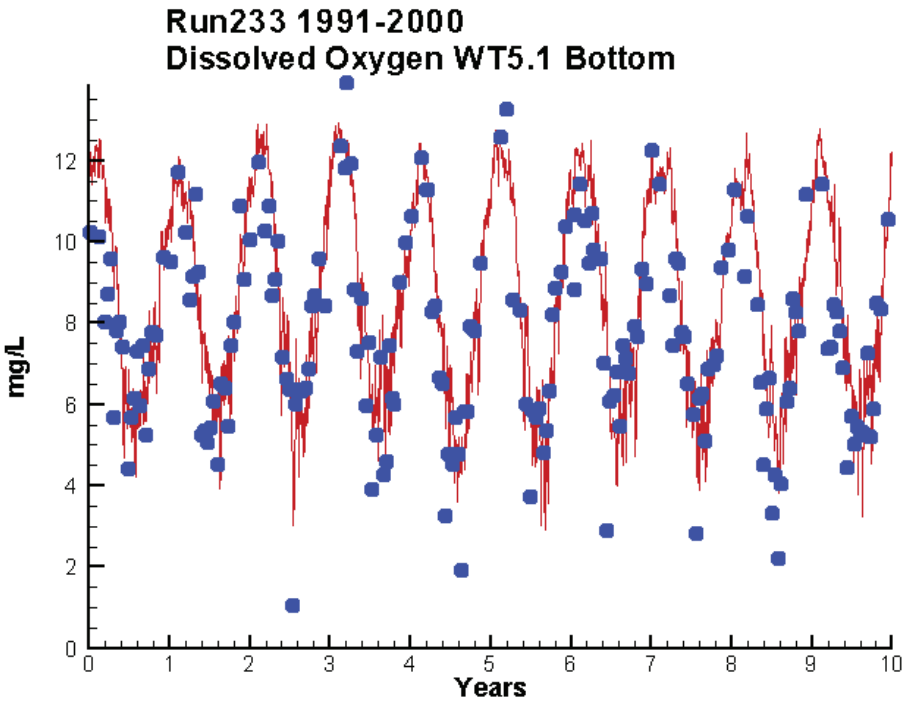

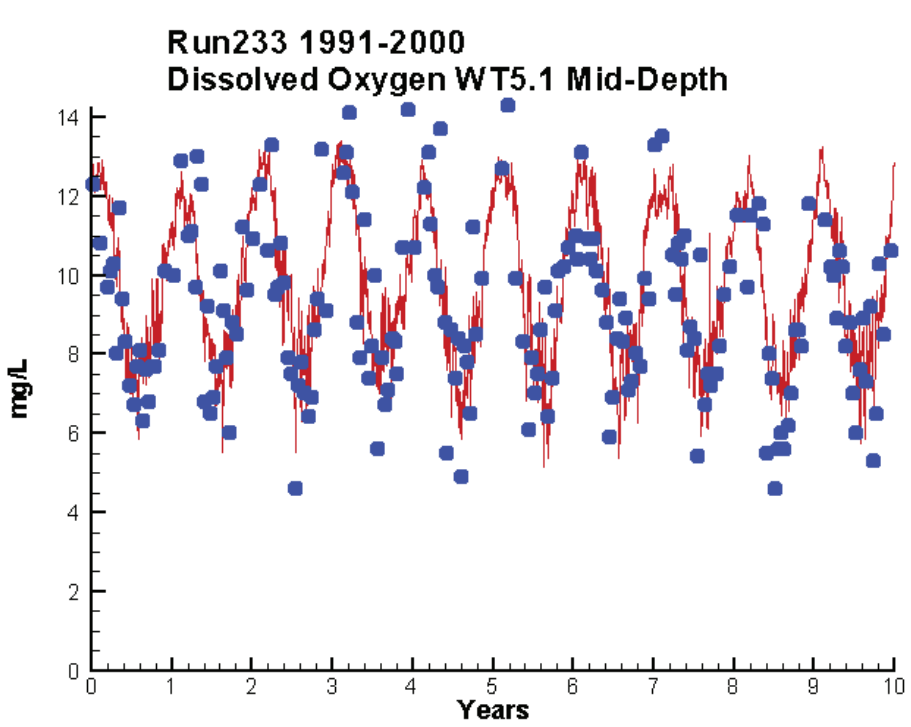

	Mean Difference	Absolute Mean Difference
Top DO	0.4169	1.5415
Mid DO	0.3060	1.1953
Bot DO	0.5509	1.1147

Station WT5.1

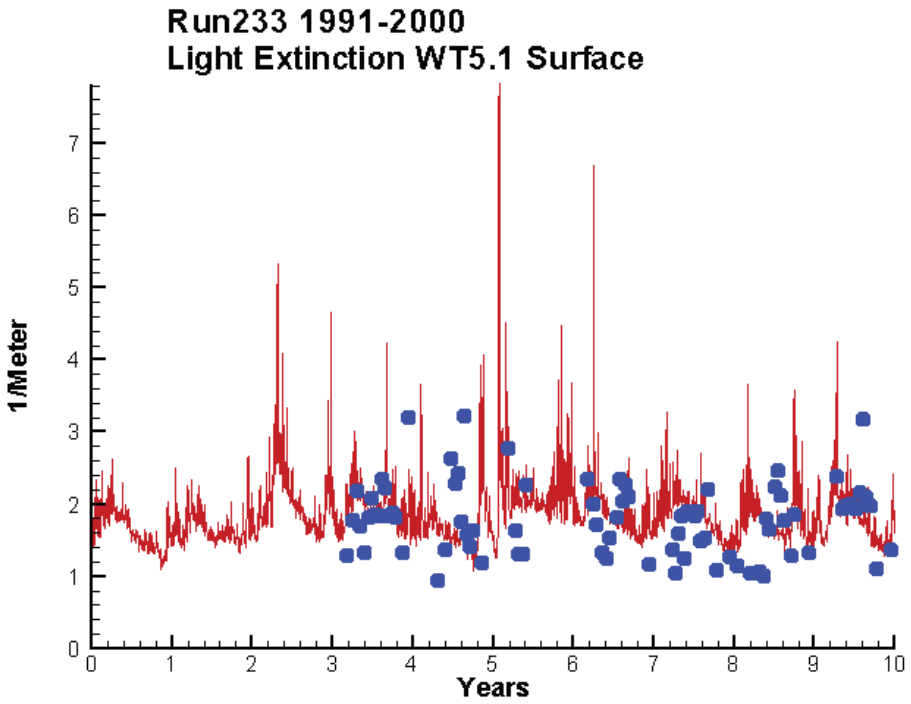

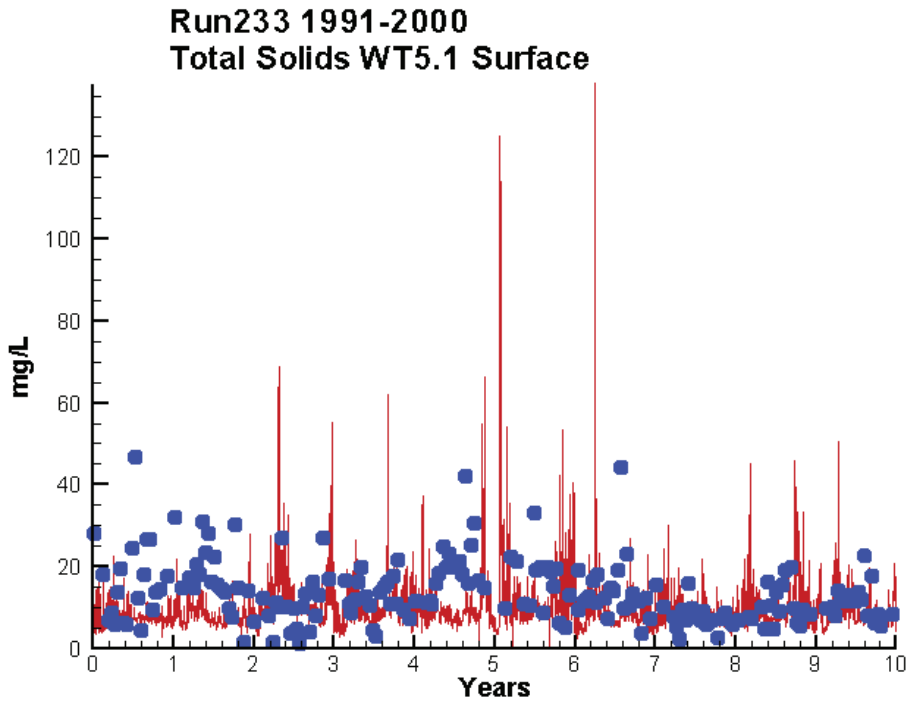

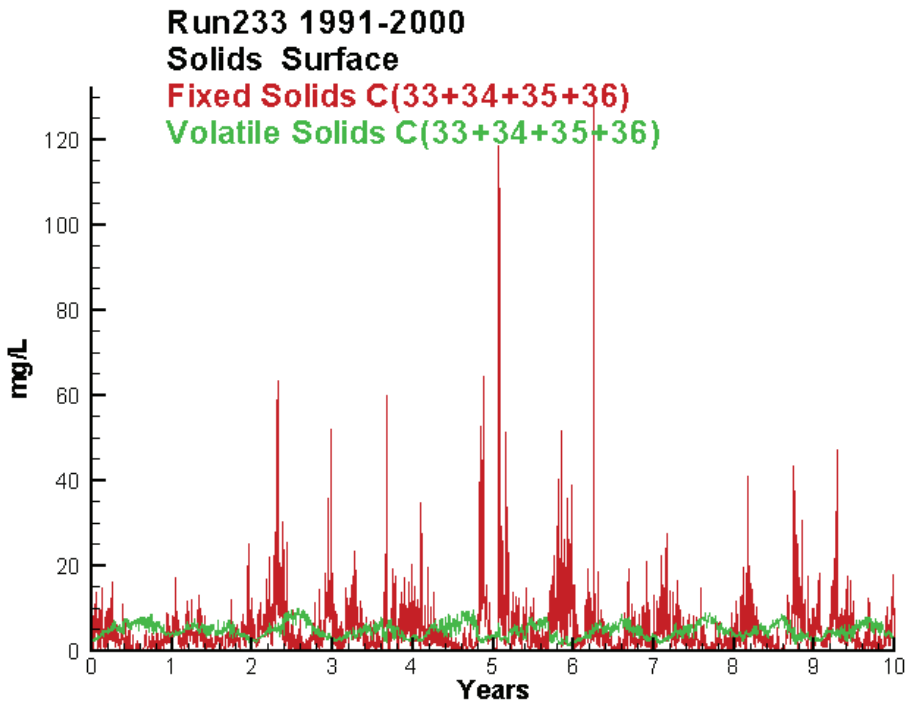

	Mean Difference	Absolute Mean Difference
KE	0.1135	0.5187
TSS	-3.9731	7.6406

Station WT8.1

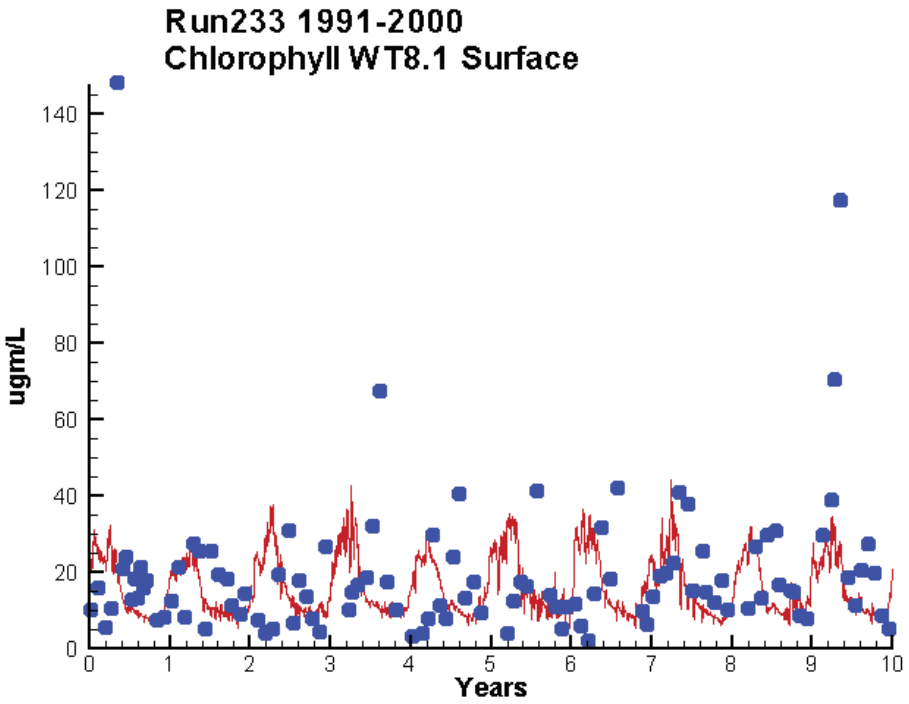

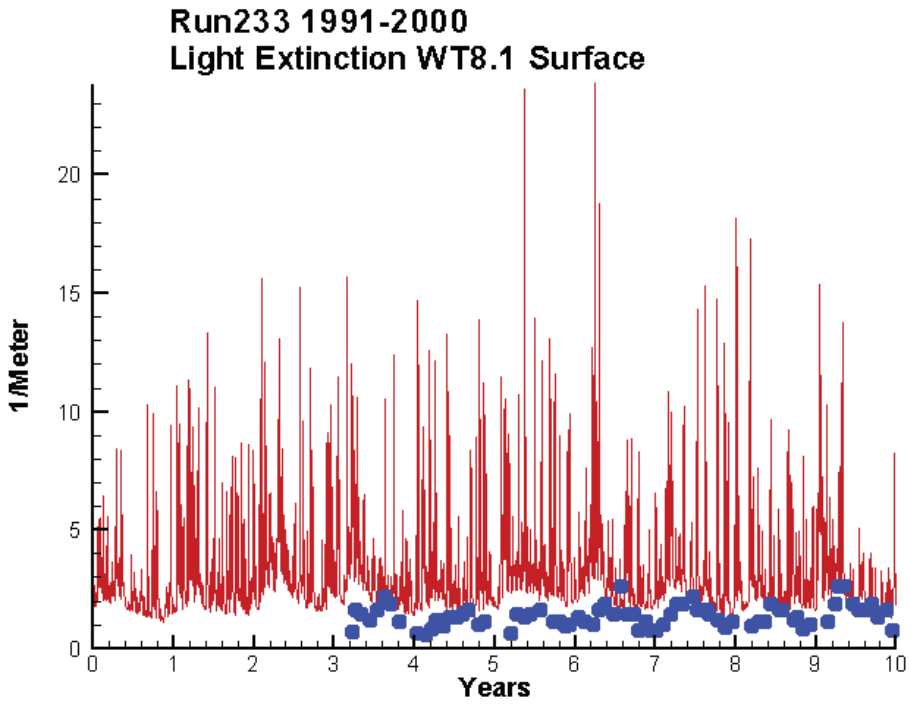

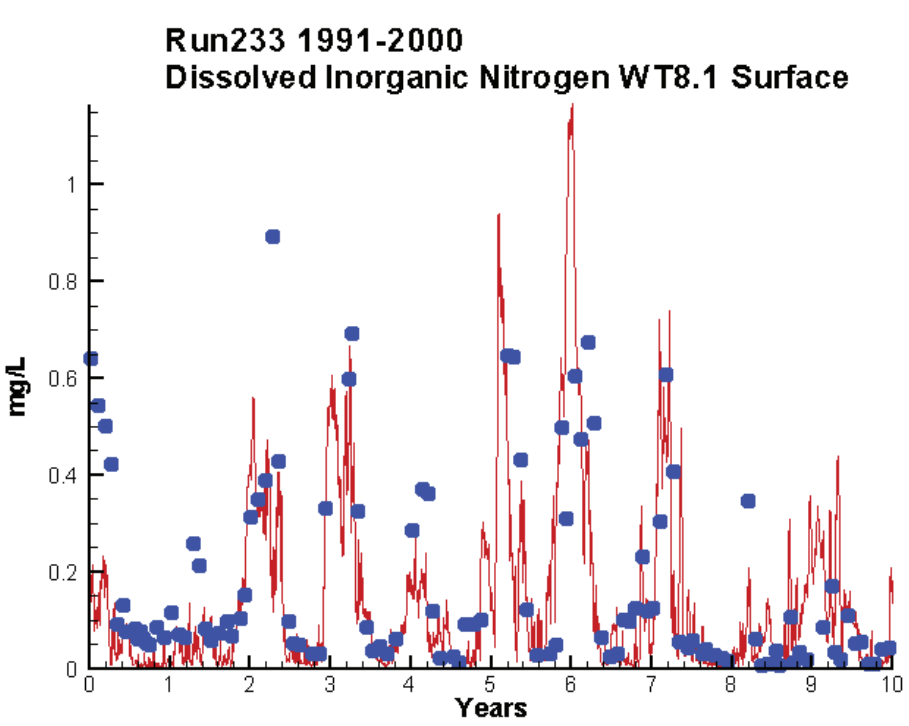

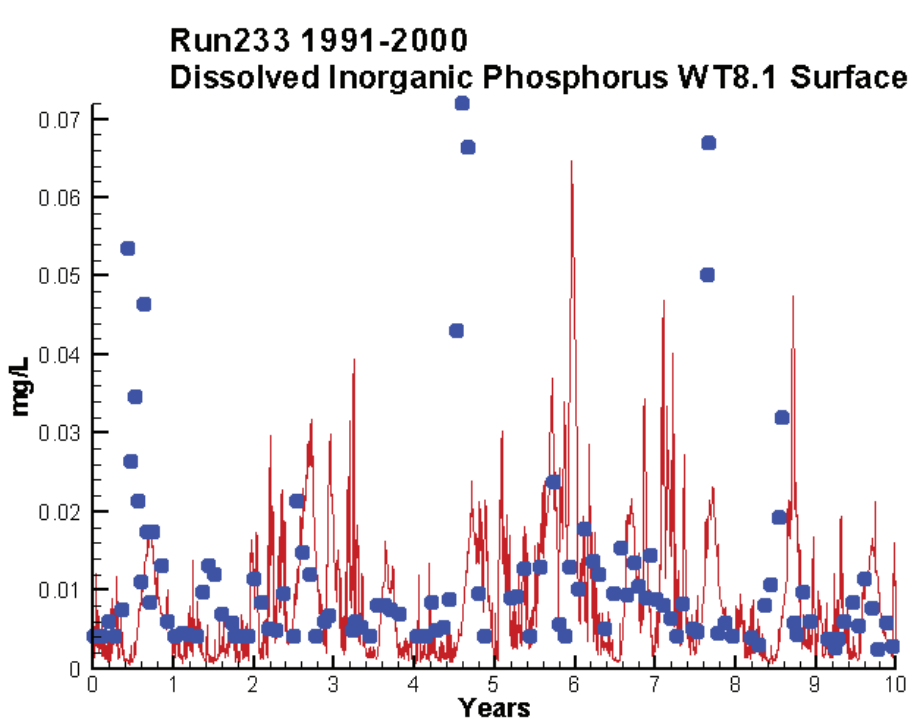

Station WT8.1

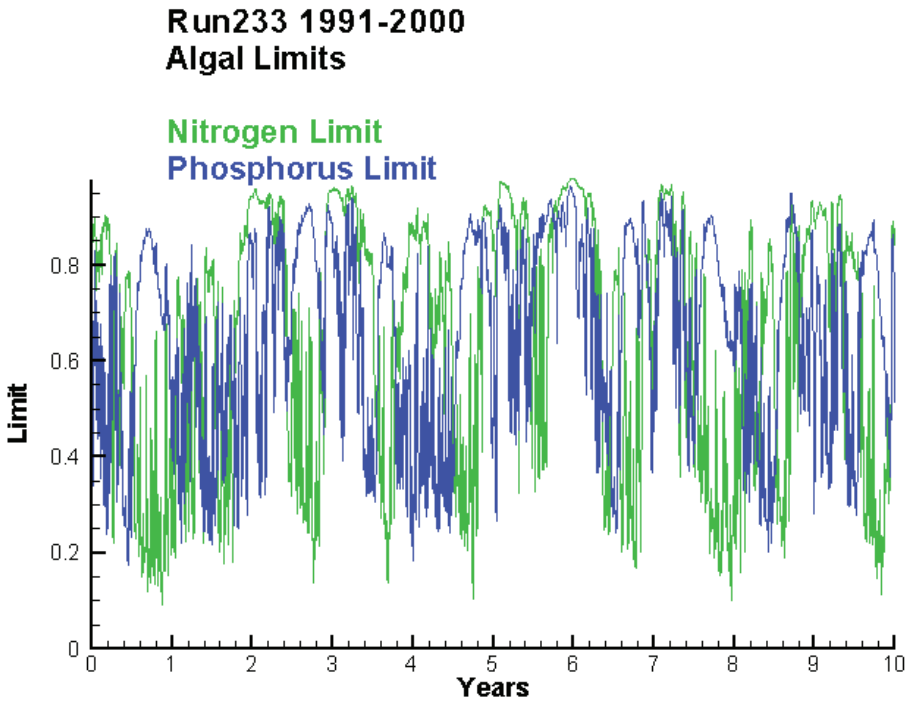

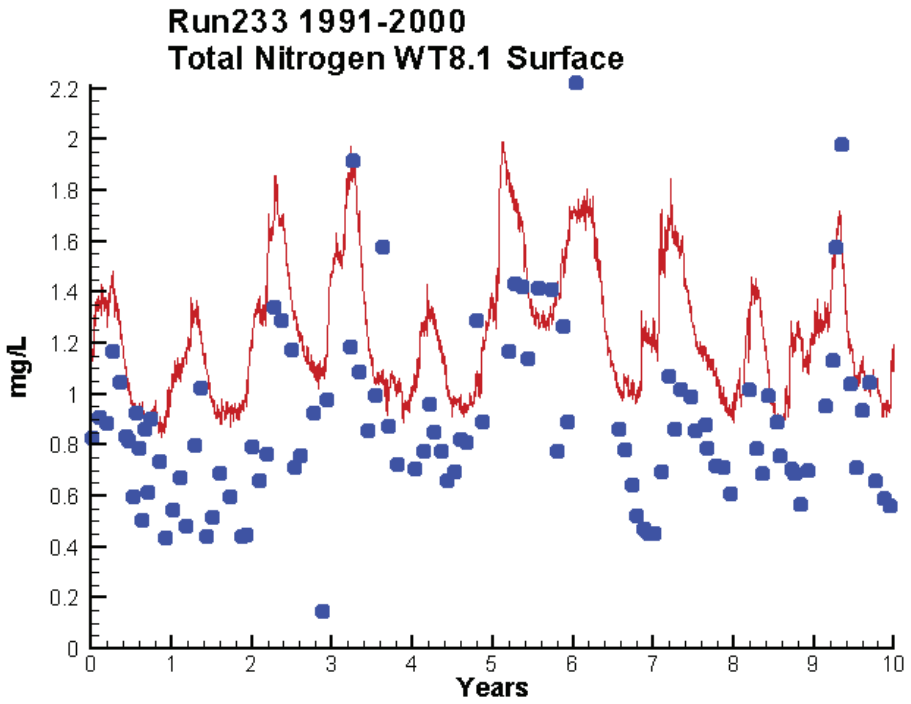

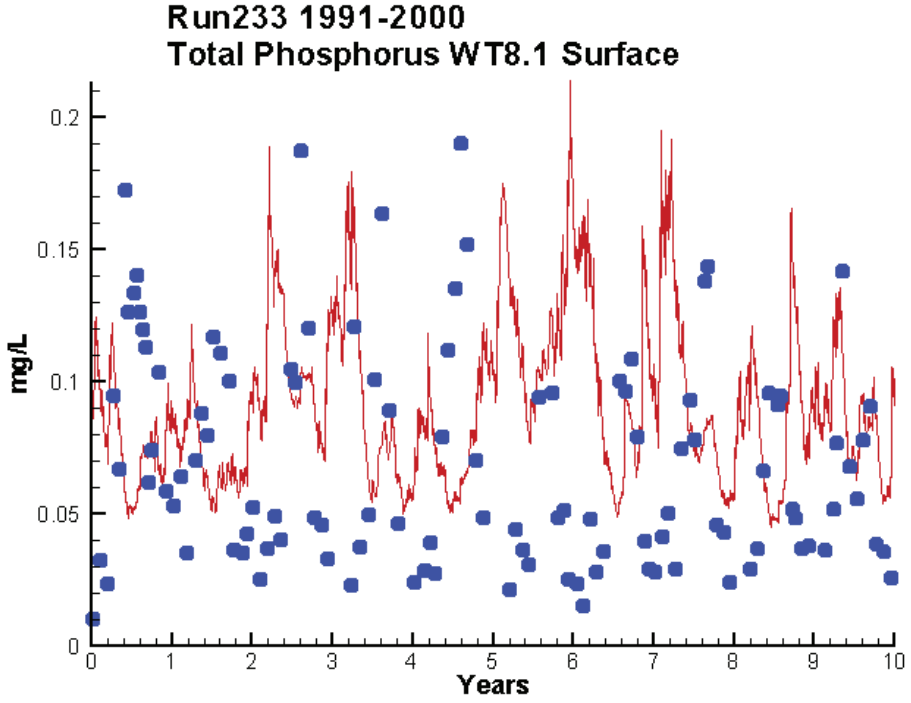

	Mean Difference	Absolute Mean Difference
Chl	-3.3486	12.9475
DIN	-0.0442	0.1023
KE	2.0743	2.0991
DIP	-0.0028	0.0093
TP	0.0208	0.0515
TN	0.3370	0.3746

Station WT8.1

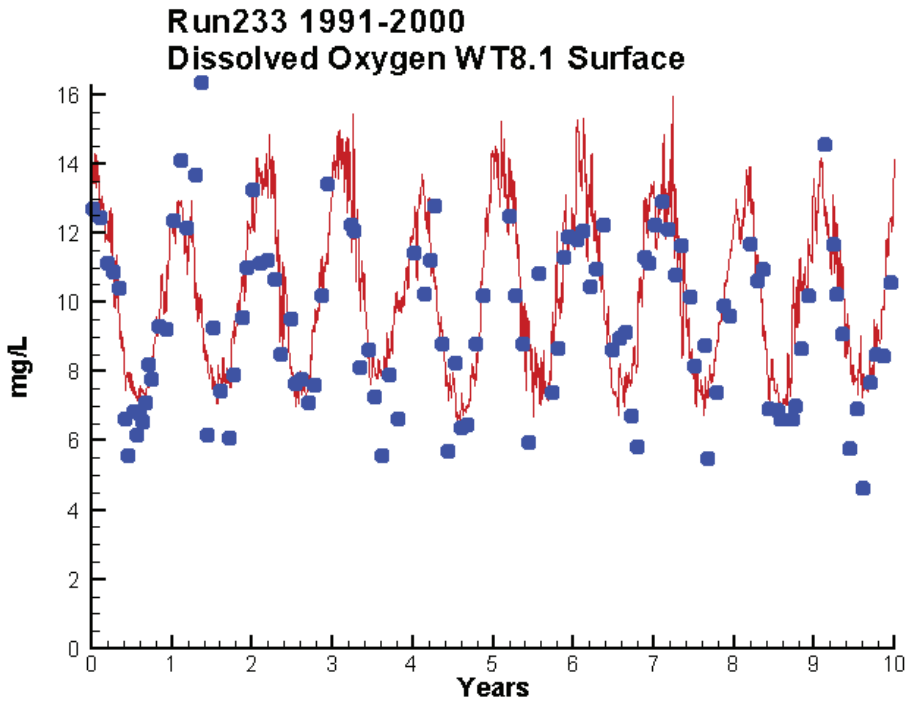

	Mean Difference	Absolute Mean Difference
Top DO	0.6294	1.4363

Station WT8.1

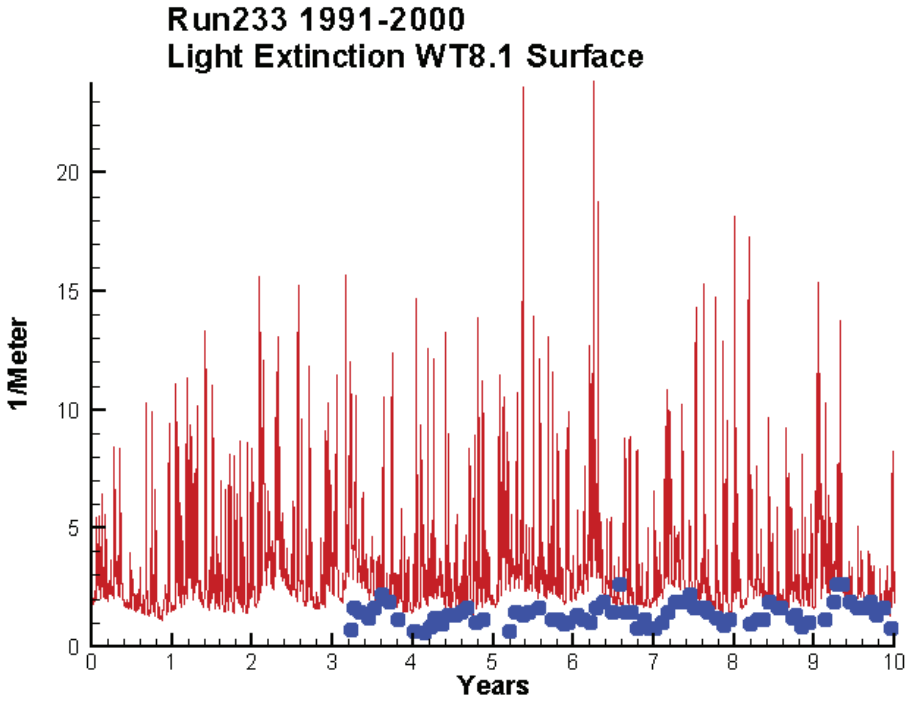

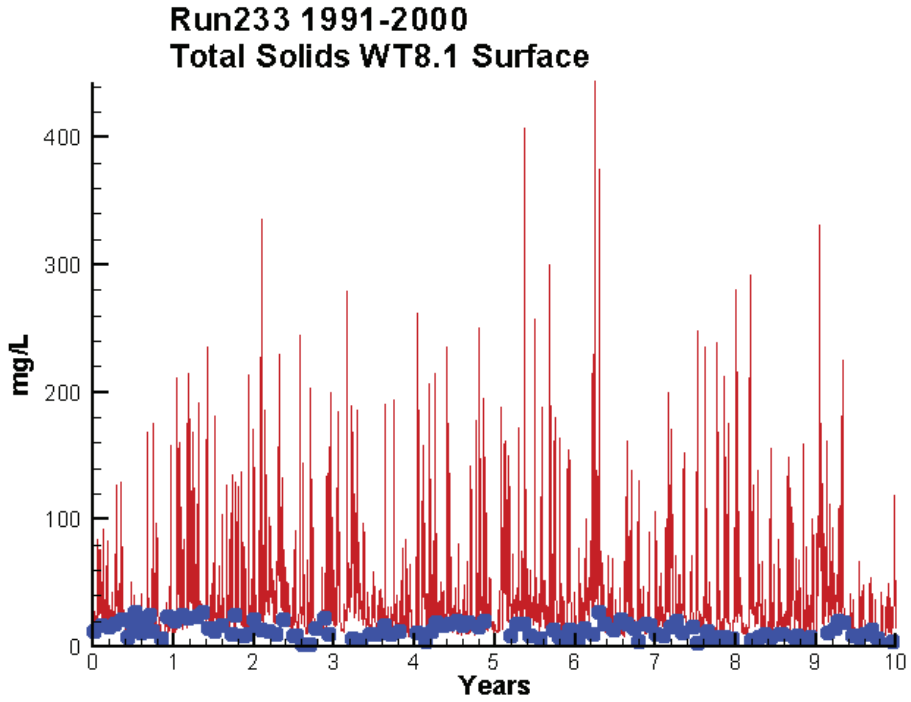

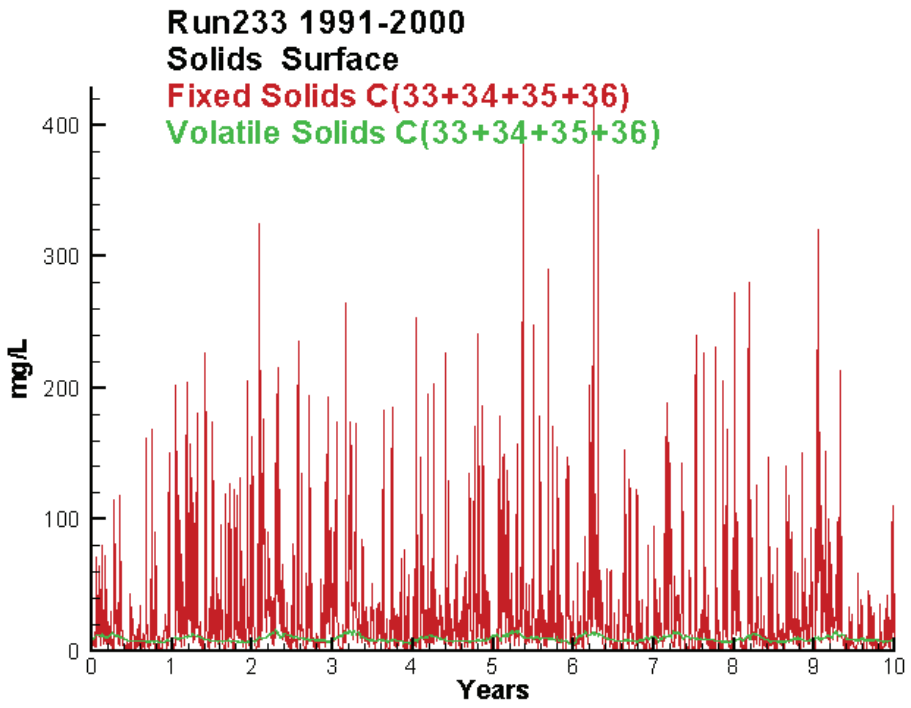

	Mean Difference	Absolute Mean Difference
KE	2.0743	2.0991
TSS	26.7310	28.7080

Appendix B: Time Series Comparisons 2002–2011

The eutrophication model was verified to the period 2002–2011. Verification implies the 2002–2011 observations were not considered in the parameter specification based on 1991–2000 data. Data for model calibration was obtained from the database maintained by the US Environmental Protection Agency's Chesapeake Bay Program at http://www.chesapeakebay.net/data/index.htm. Observations were obtained from 40 stations among the larger number in the monitoring program (Figure B-1). We selected one station in each major Chesapeake Bay Program Segment as well as stations in multiple smaller segments. At each station, time series comparisons were completed for 19 water quality components at one to three depth intervals. Comparisons included physical quantities (salinity, temperature, suspended solids, and light attenuation), chlorophyll, dissolved oxygen (DO), and multiple forms of carbon, nitrogen, and phosphorus. This appendix concentrates on the components that correspond closely to chlorophyll, clarity, and DO. The presentation of each component is described, and four pages of plots for each time series station follow the descriptions.

Chlorophyll Surface. Ten-year time series of computed and observed chlorophyll *a*. The time axis on this and the following plots commences on January 1, 2002, and runs through January 31, 2011. Instantaneous observations from the surface sample (1 meter) are plotted along with daily-average model values in the cell that corresponds to the monitoring station.

Light Attenuation. Ten-year time series of computed and observed diffuse light attenuation. Attenuation was almost exclusively derived from irradiance observed at multiple depths in the water column.

Dissolved Inorganic Nitrogen Surface. Ten-year time series of computed and observed dissolved inorganic nitrogen, which is computed as the sum of ammonium and nitrate nitrogen.

Dissolved Inorganic Phosphorus Surface. Ten-year time series of computed and observed dissolved inorganic phosphorus.

Figure B-1. Monitoring stations. Forty stations were selected from this group for time series analysis.

Algal Limits. Ten-year time series of computed nutrient limitations on phytoplankton production in the model surface cell. Nutrient limits are daily average values. The limitations are biomass weighted according to the algal groups present. A limitation of zero indicates complete limitation to growth. A limitation of unity indicates no limitation.

Total Nitrogen Surface. Ten-year time series of computed and observed total nitrogen.

Total Phosphorus Surface. Ten-year time series of computed and observed total phosphorus.

Statistics. Mean difference and absolute mean difference statistics are provided for the computations and observations at this station. Those statistics are defined in equation 1 and equation 2:

$$MD = \frac{\sum(P-O)}{N} \quad (1)$$

$$AMD = \frac{\sum|P-O|}{N} \quad (2)$$

where:

MD = mean difference
AMD = absolute mean difference
O = observation
P = prediction
N = number of observations

Dissolved Oxygen. Ten-year time series of computed and observed DO. The presentation varies depending on local depth of the monitoring station. Comparisons are always presented for the surface sample. At deeper stations (typically prefixed EE and RET), comparisons are presented at the surface and bottom. At stations deep enough to warrant sampling near the pycnocline (typically prefixed CB and LE), comparisons are presented at the surface, mid-depth, and bottom. Statistics correspond to the number of depths plotted.

Total Suspended Solids Surface. Ten-year time series of computed and observed total suspended solids (TSS). Model TSS is the sum of the four fixed solids variables (fine clay, clay, silt, and sand) plus particulate organic carbon components (algal carbon and labile, refractory, and slow refractory particulate organic carbon). Organic carbon is converted to solids through multiplication by the ratio 2.5 g solids g^{-1} C.

Solids Surface. This graph separates computed fixed (inorganic) and volatile (organic) solids. Volatile solids are obtained from modeled carbon as noted in *Total Suspended Solids Surface*, above. No observations are shown since these fractions are not regularly observed in the monitoring program.

Station CB1.1

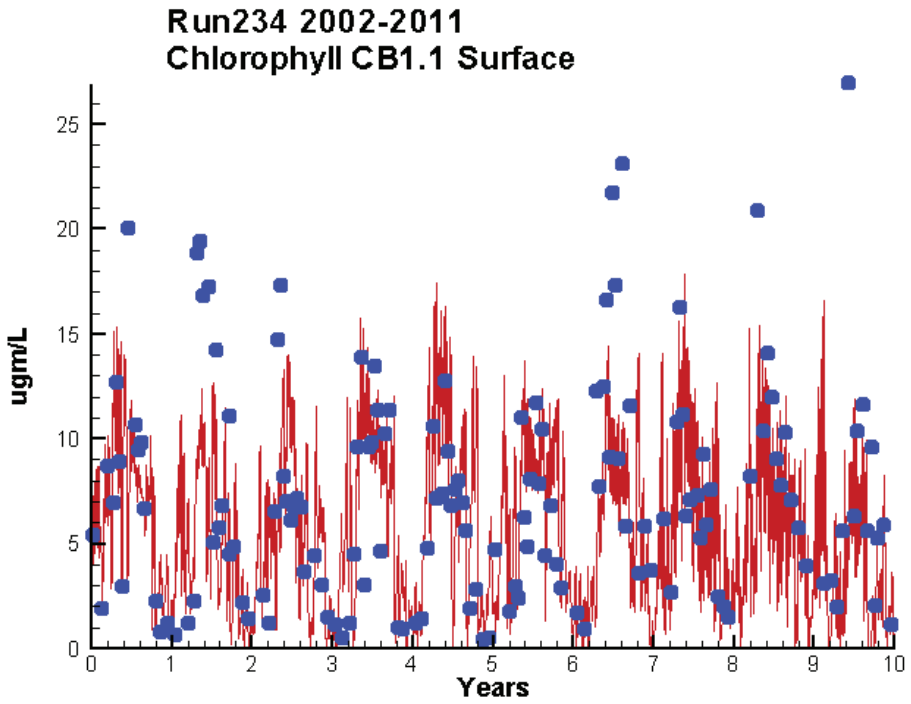

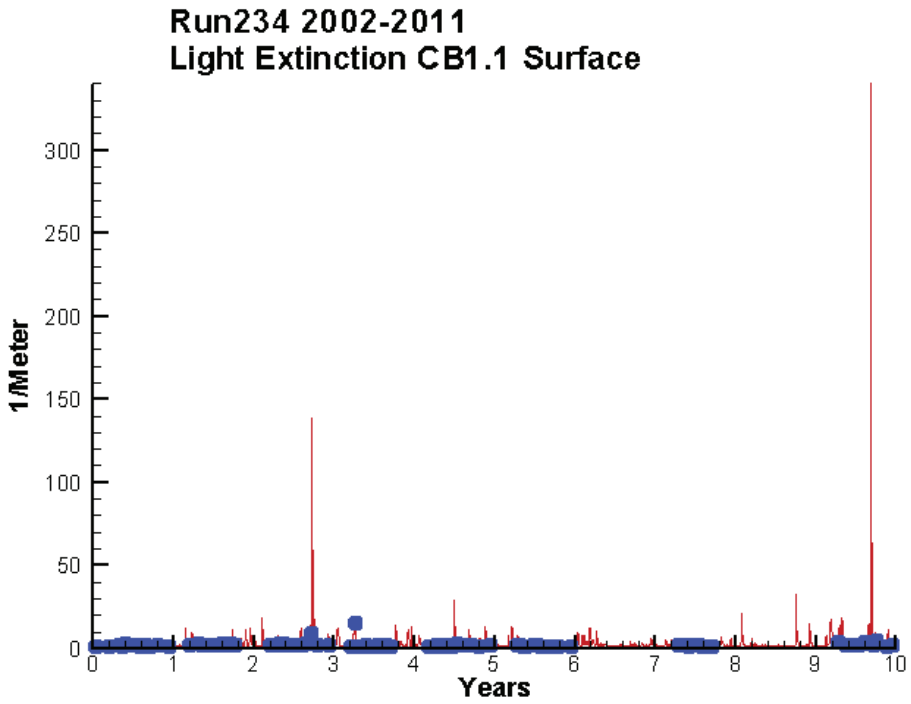

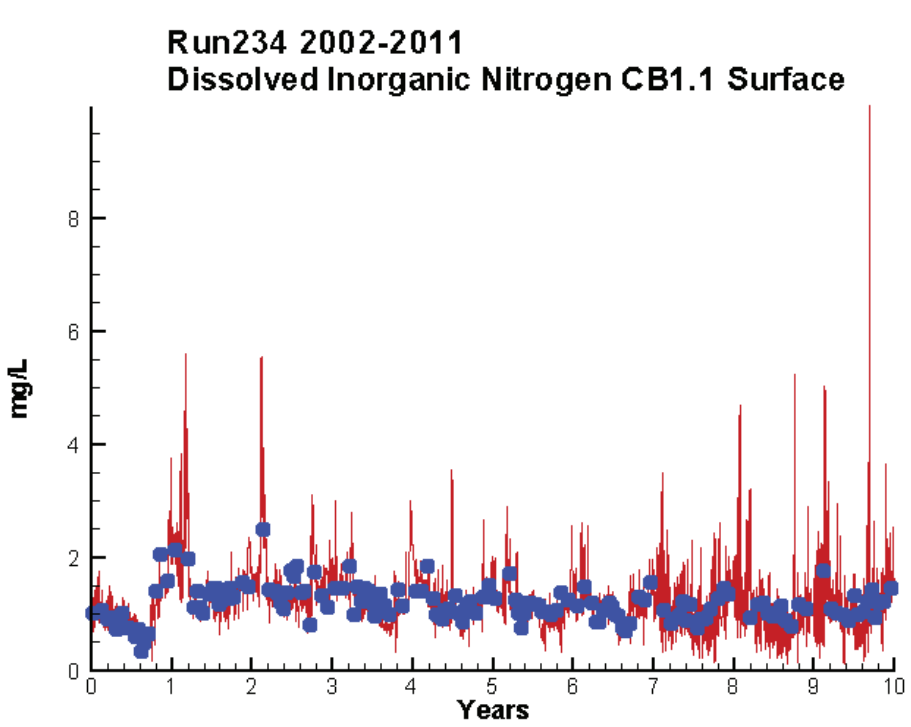

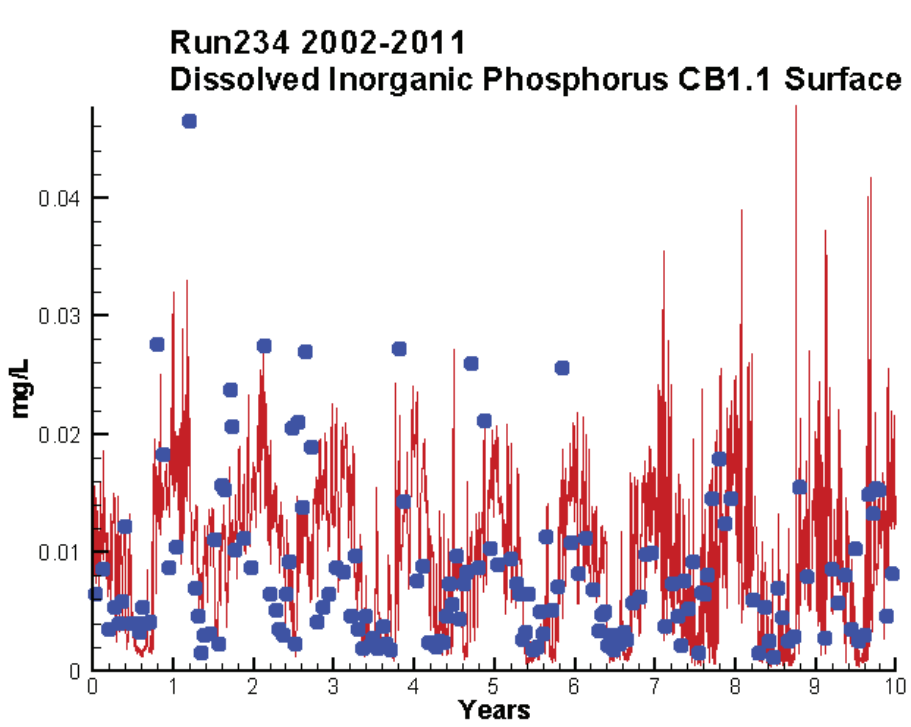

Station CB1.1

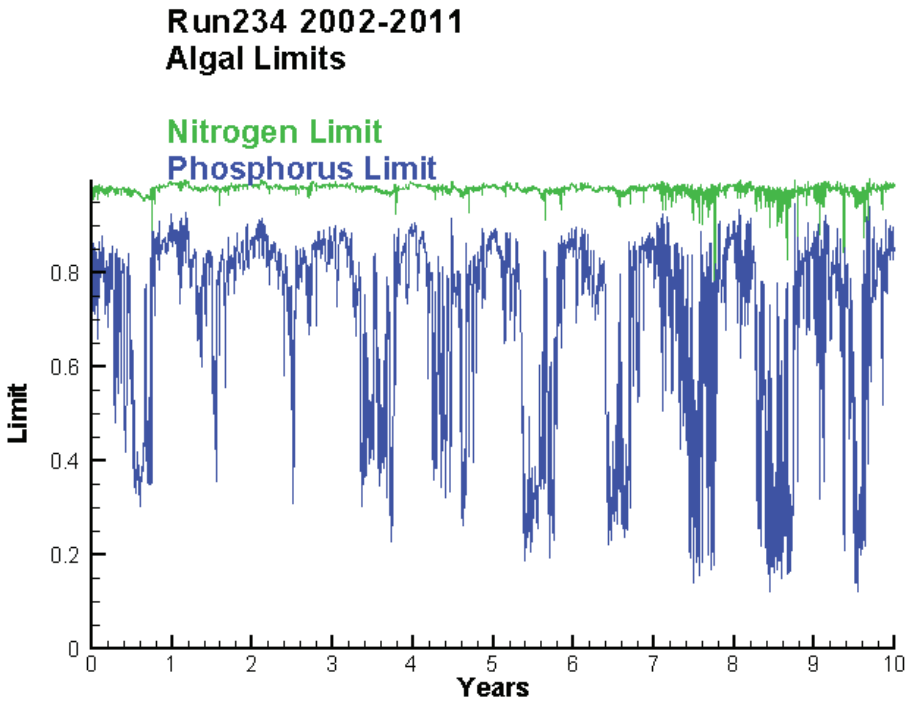

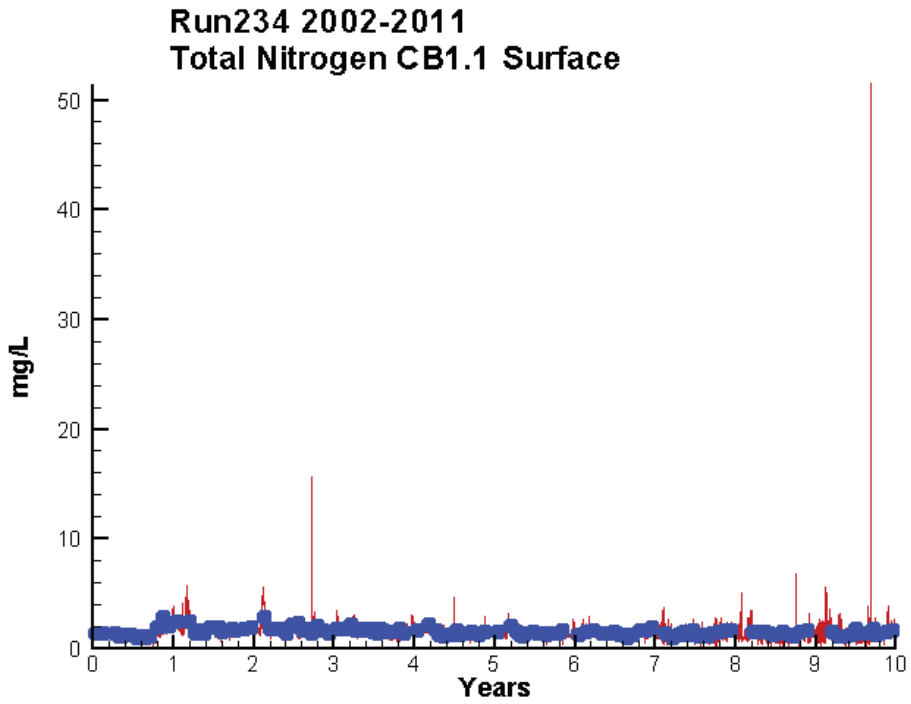

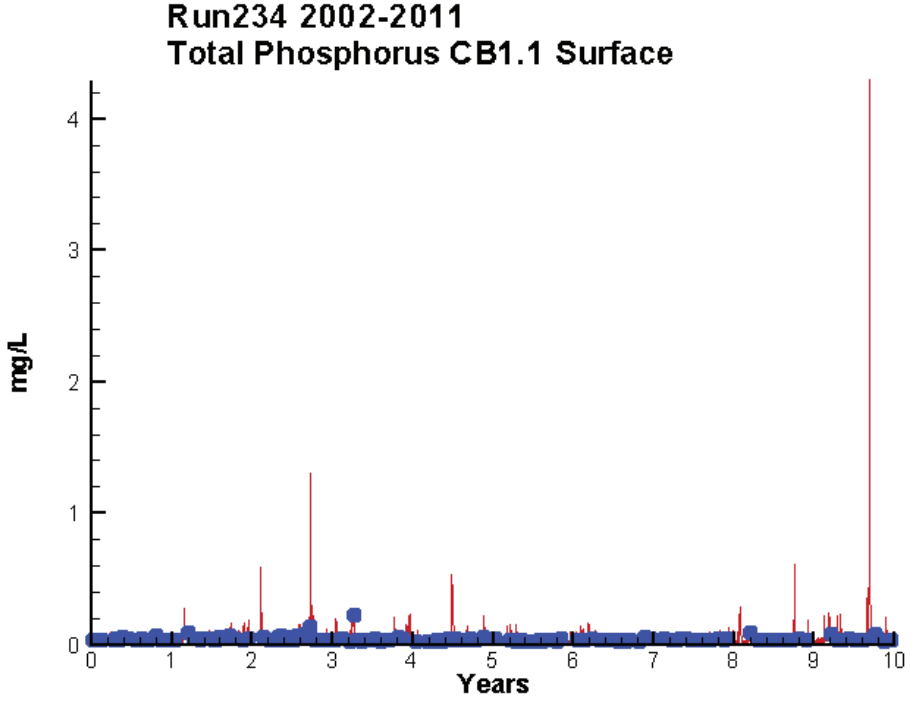

	Mean Difference	Absolute Mean Difference
Chl	-0.7271	3.7647
DIN	-0.0293	0.2664
KE	1.5087	1.6366
DIP	0.0003	0.0047
TP	0.0074	0.0197
TN	-0.1578	0.3550

Station CB1.1

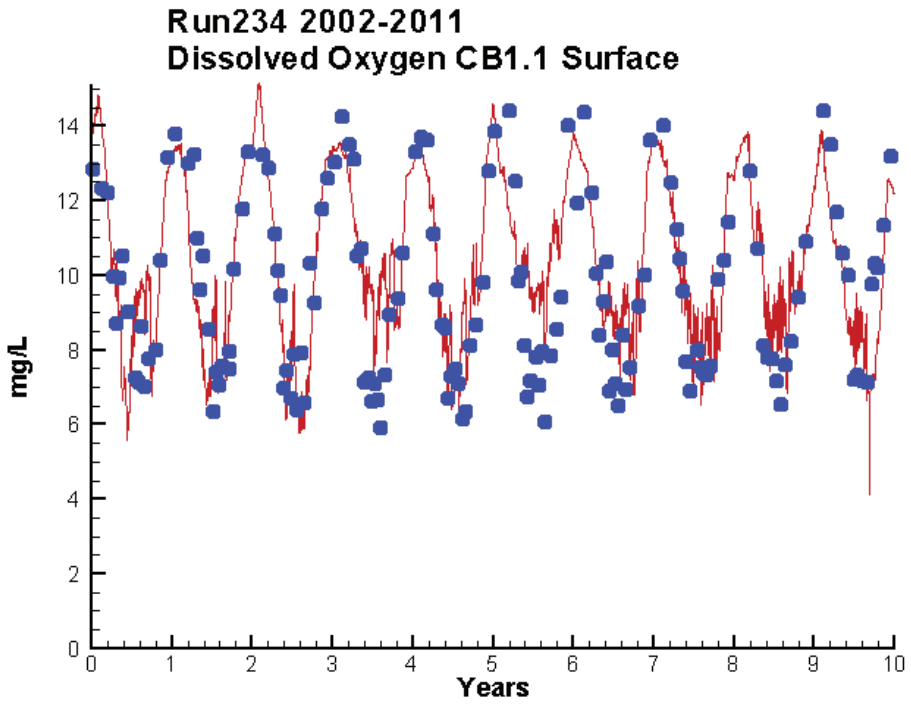

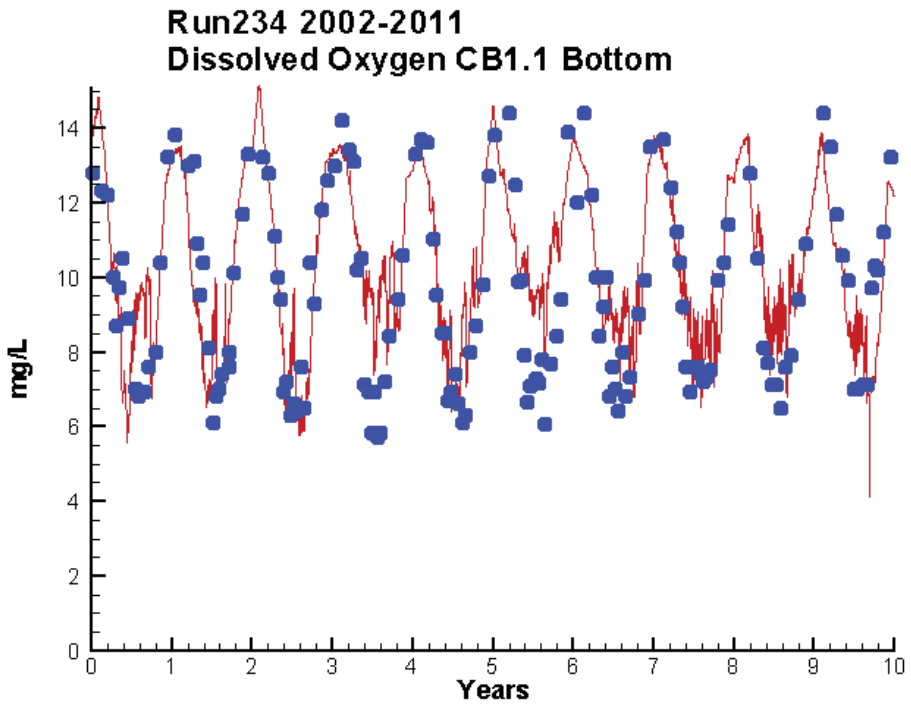

	Mean Difference	Absolute Mean Difference
Top DO	0.2702	1.1129
Bot DO	0.3786	1.1736

Station CB1.1

Run234 2002-2011
Light Extinction CB1.1 Surface

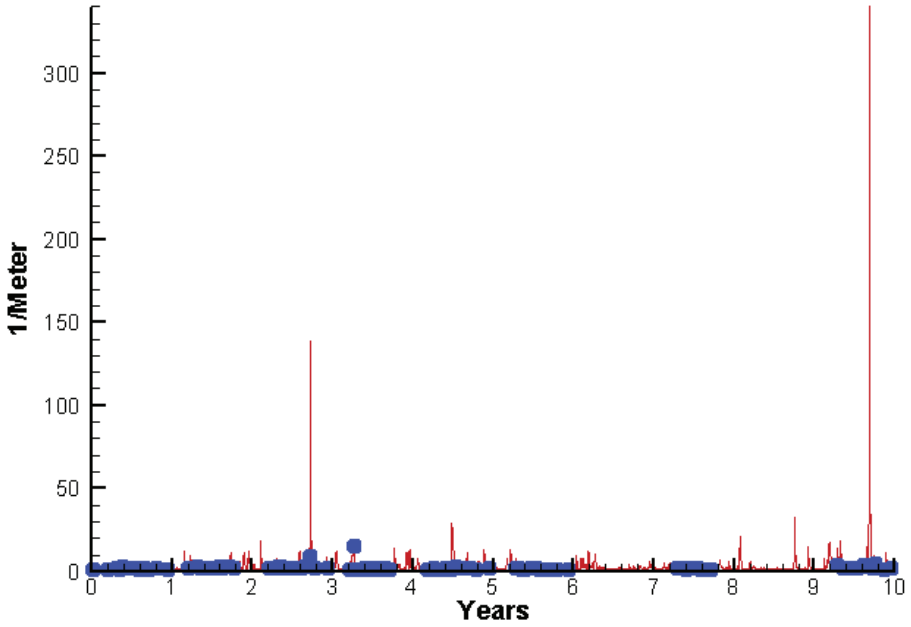

Run234 2002-2011
Total Solids CB1.1 Surface

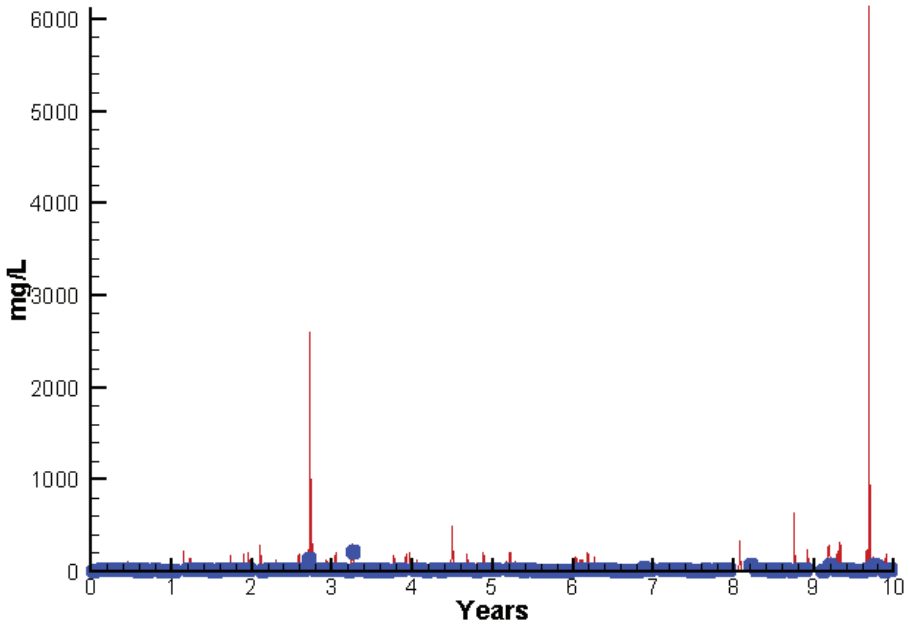

Run234 2002-2011
Solids Surface
Fixed Solids C(33+34+35+36)
Volatile Solids C(33+34+35+36)

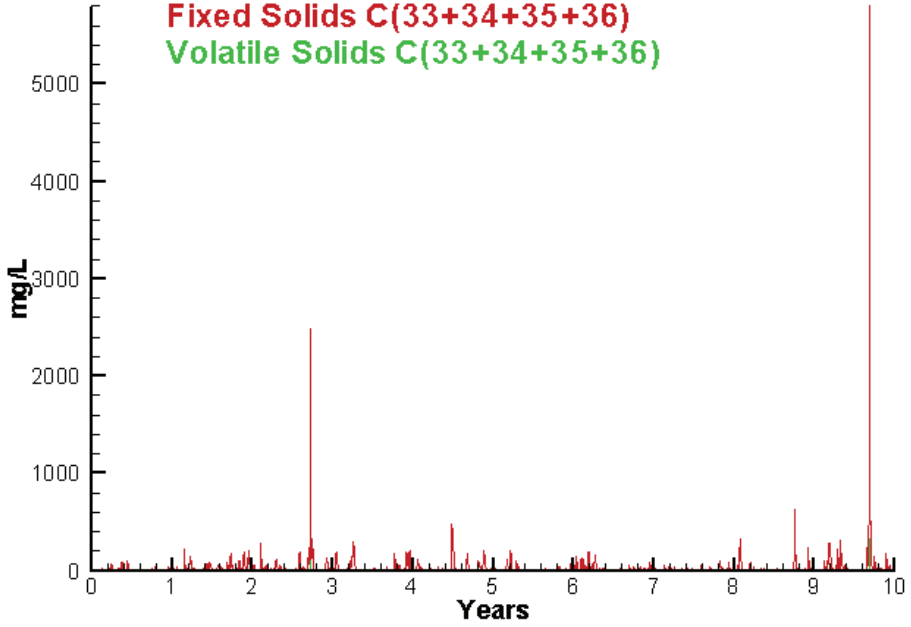

	Mean Difference	Absolute Mean Difference
KE	1.5087	1.6366
TSS	17.6994	20.8495

Station CB2.2

Run234 2002-2011
Chlorophyll CB2.2 Surface

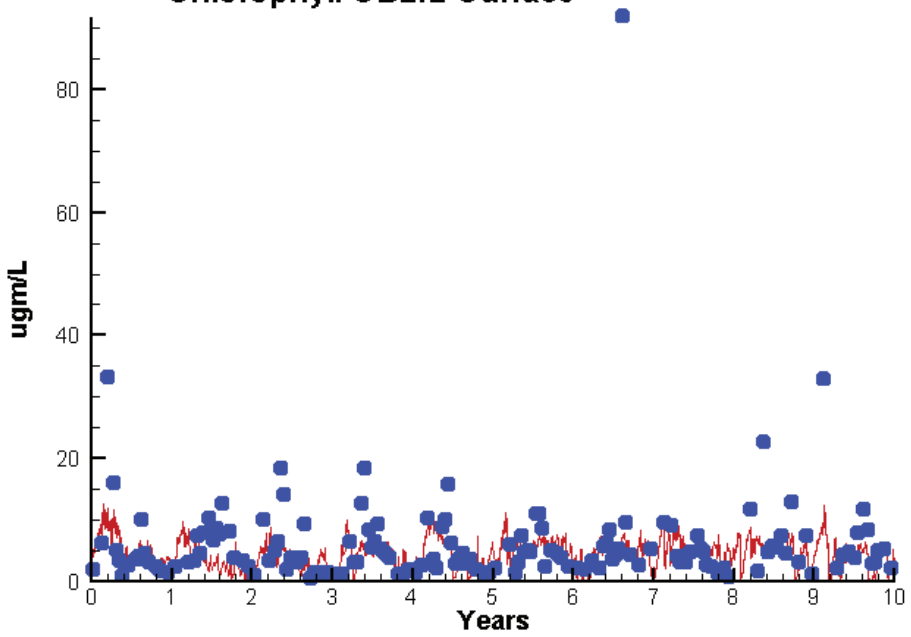

Run234 2002-2011
Light Extinction CB2.2 Surface

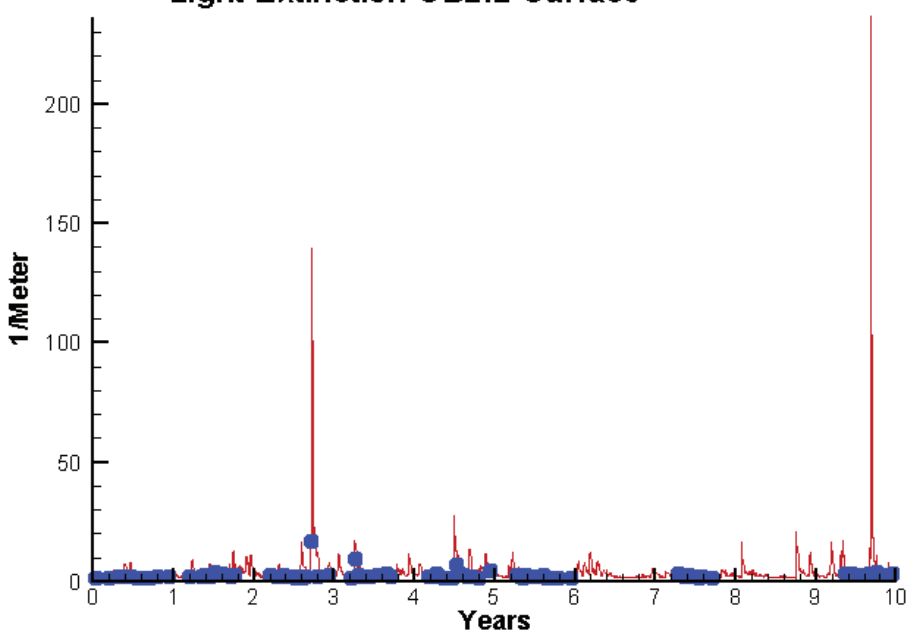

Run234 2002-2011
Dissolved Inorganic Nitrogen CB2.2 Surface

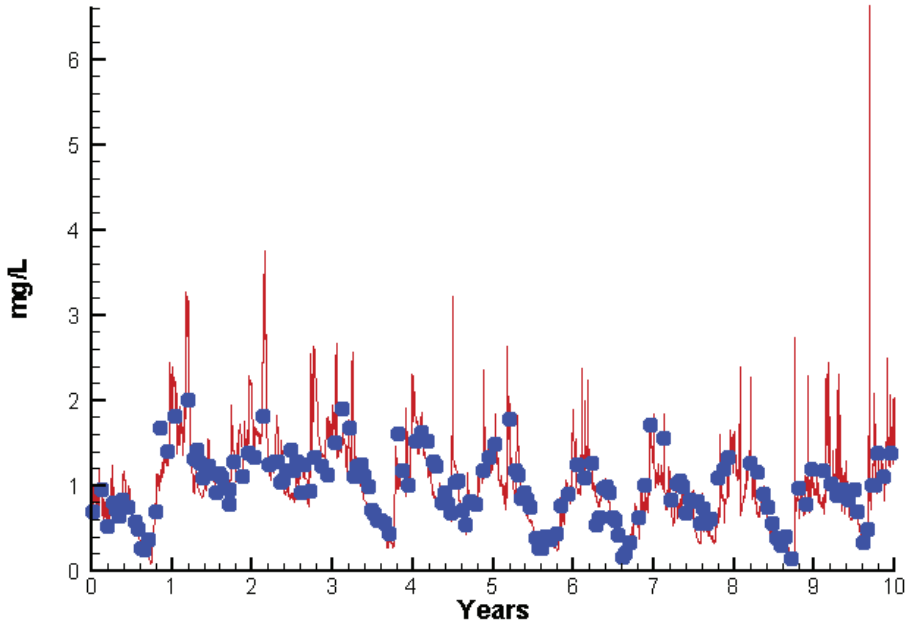

Run234 2002-2011
Dissolved Inorganic Phosphorus CB2.2 Surface

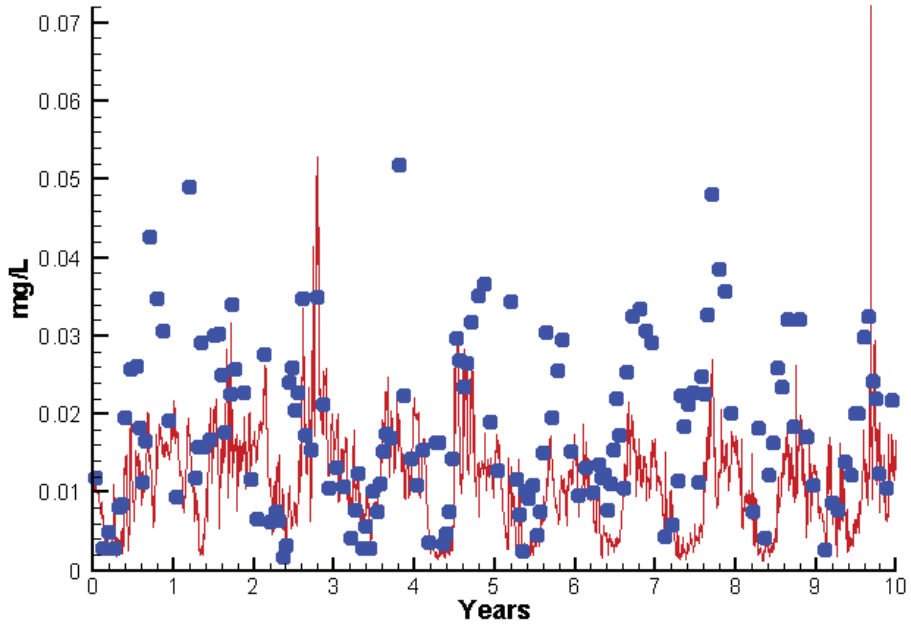

Station CB2.2

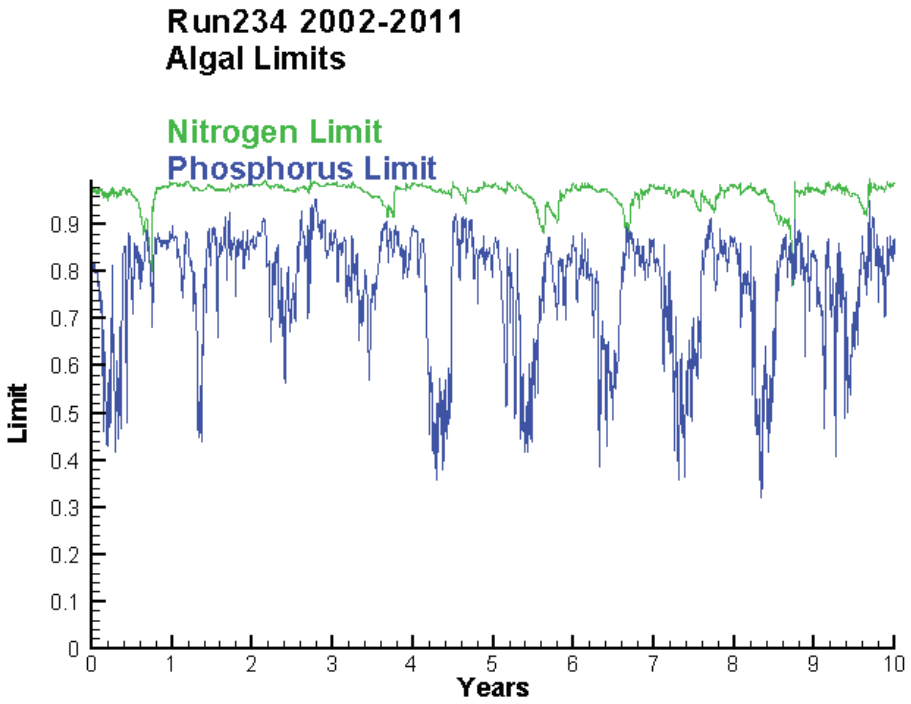

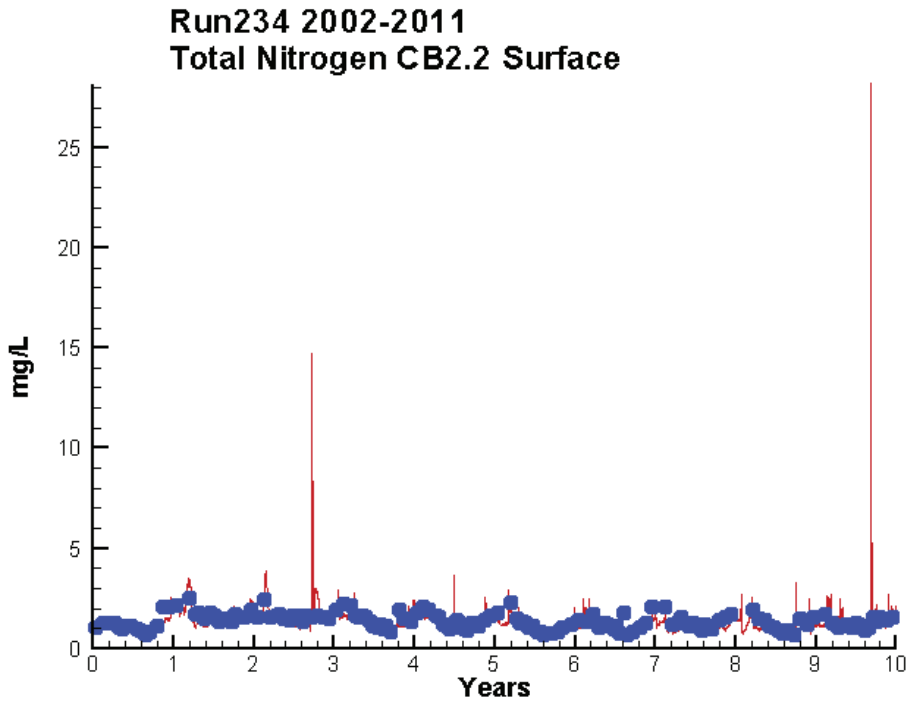

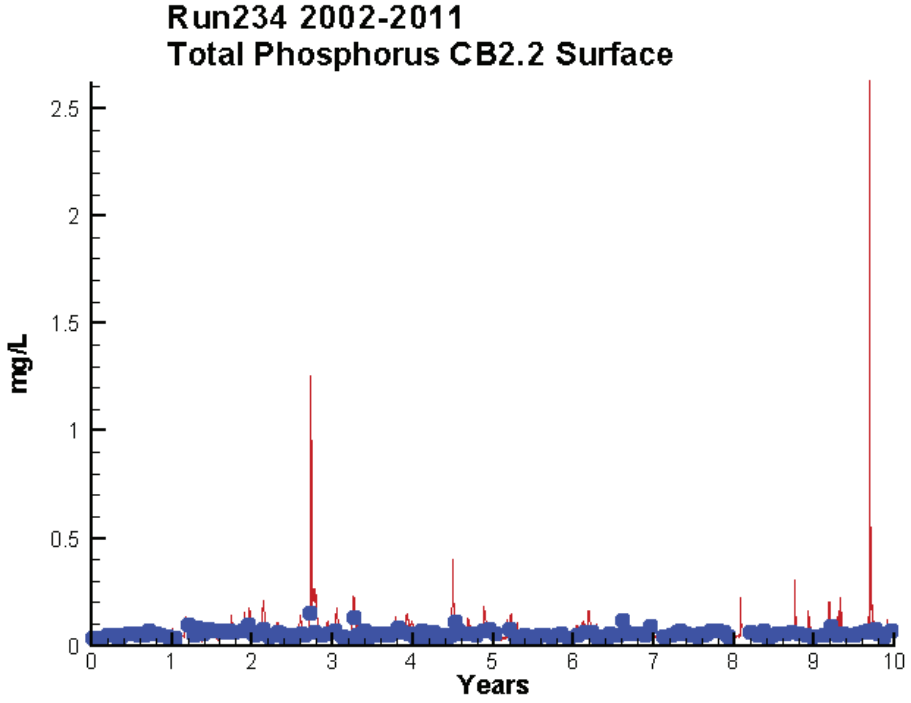

	Mean Difference	Absolute Mean Difference
Chl	-1.6186	3.4881
DIN	-0.0240	0.2011
KE	2.4941	2.5882
DIP	-0.0070	0.0089
TP	0.0060	0.0239
TN	-0.1075	0.2849

Station CB2.2

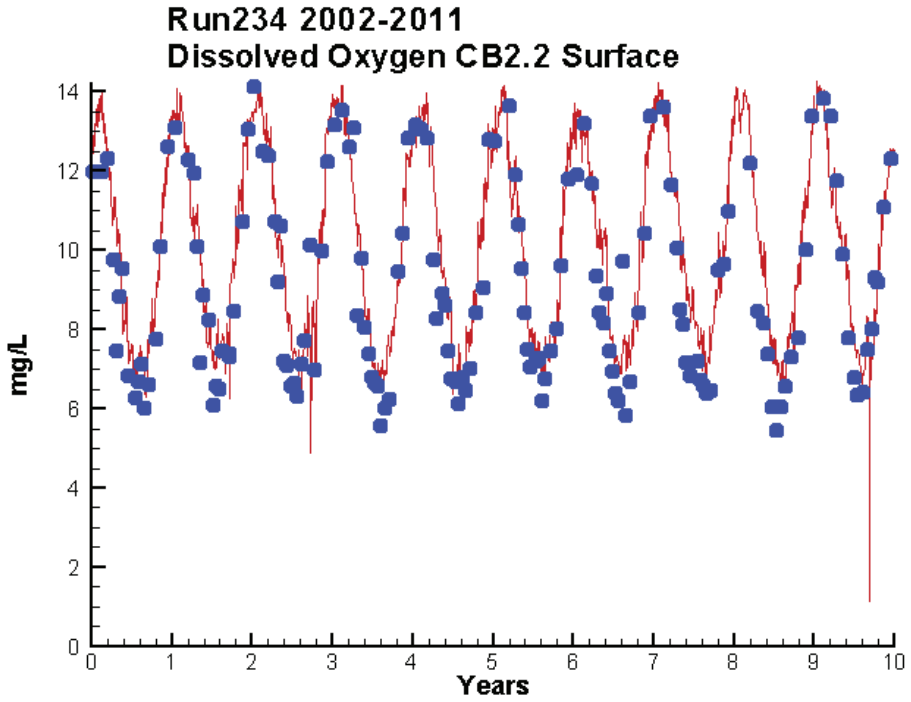

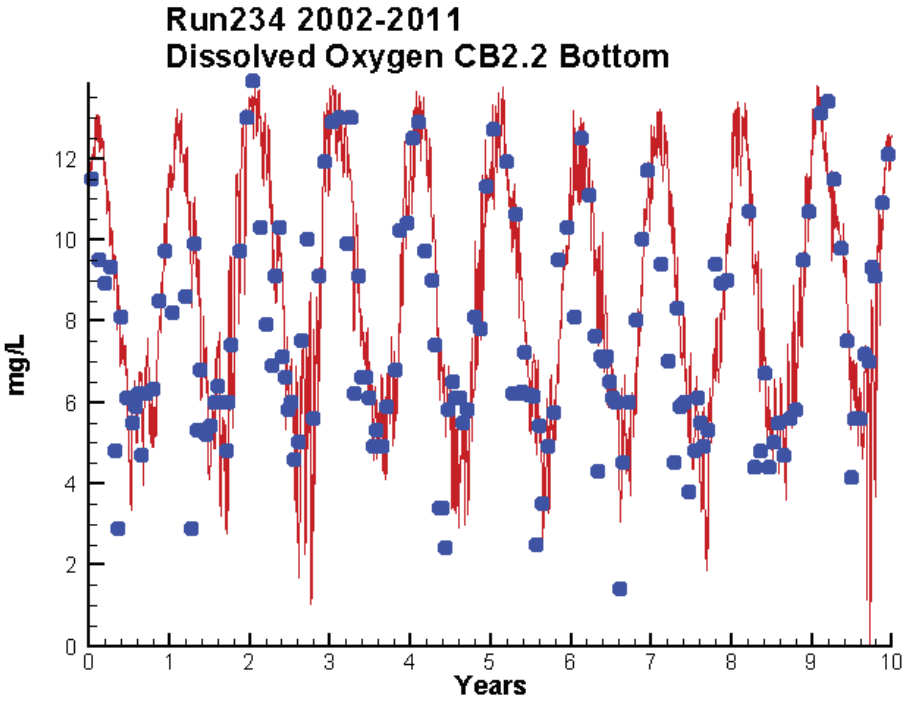

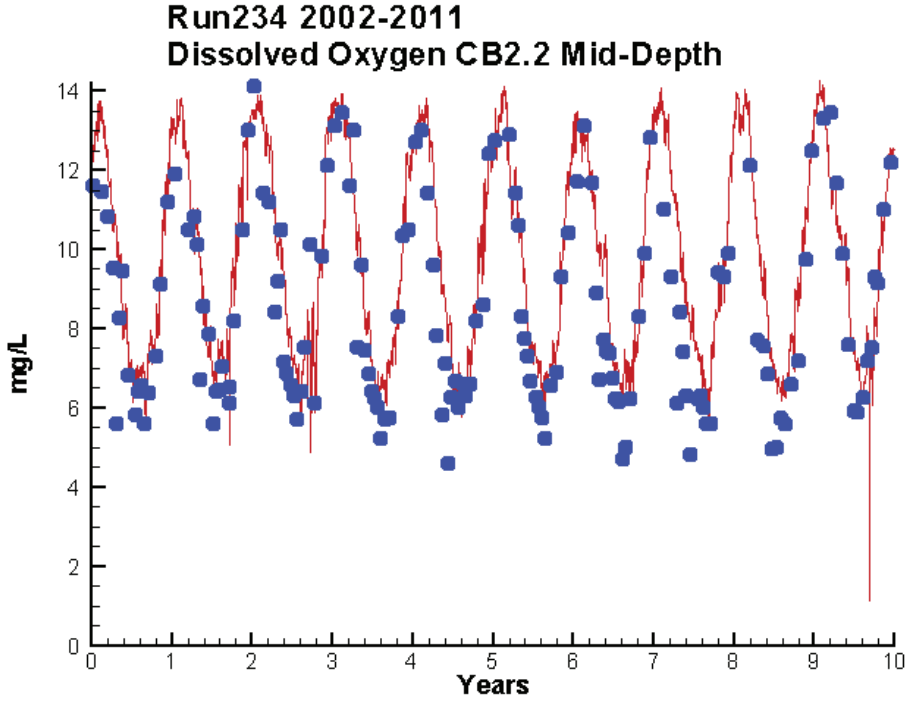

	Mean Difference	Absolute Mean Difference
Top DO	0.5776	0.8949
Mid DO	0.8323	1.0963
Bot DO	0.4348	1.4104

Station CB2.2

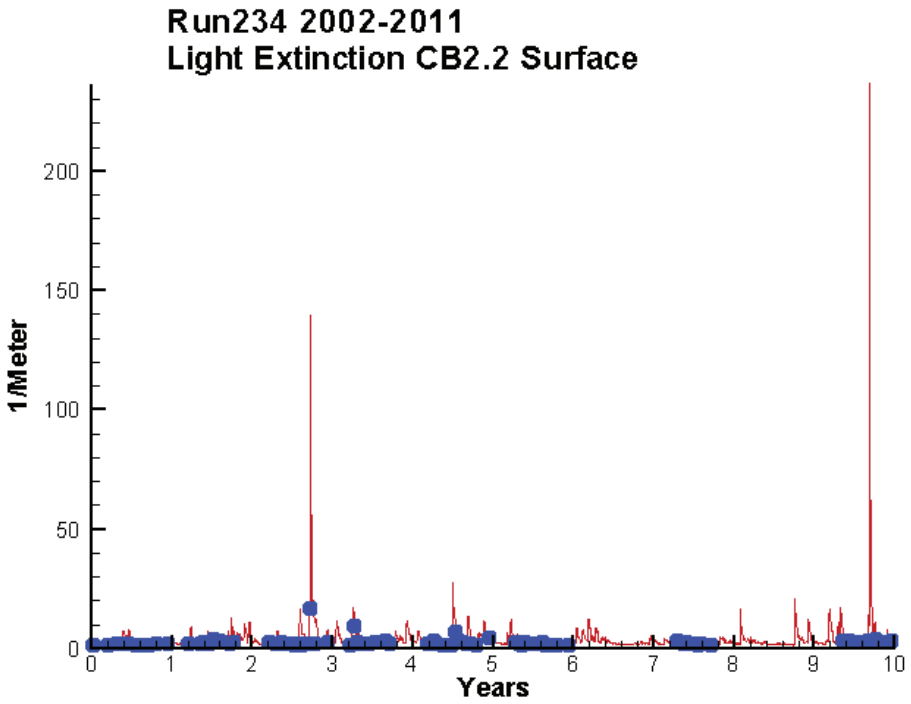

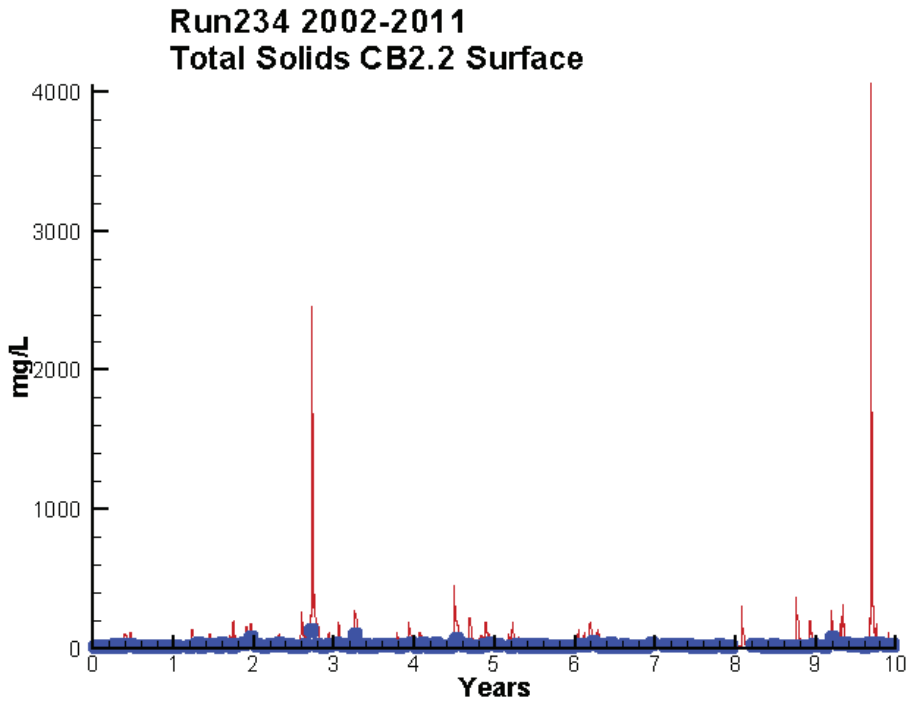

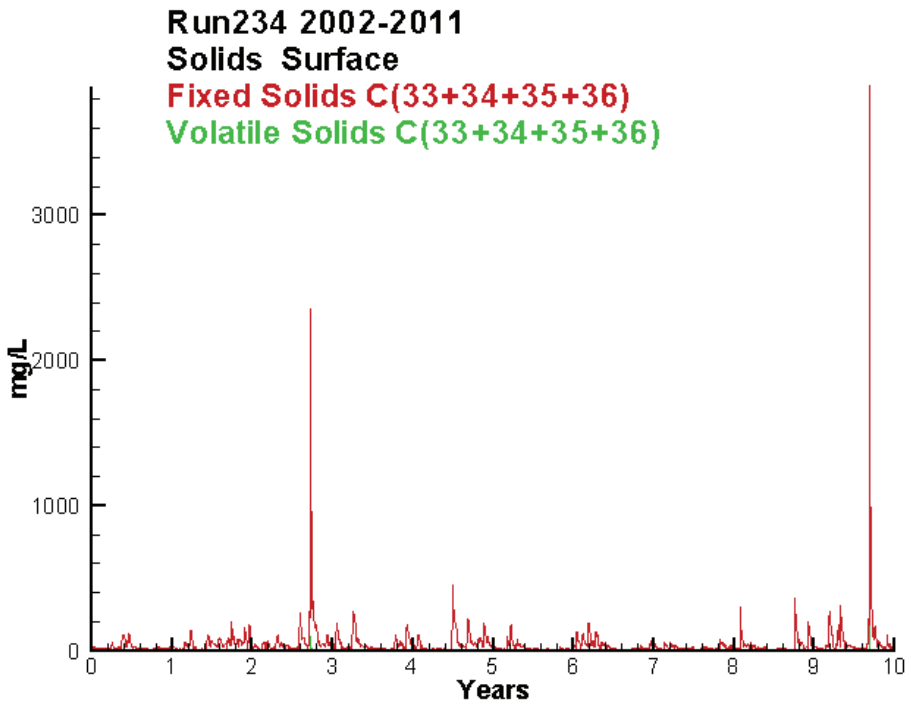

	Mean Difference	Absolute Mean Difference
KE	2.4941	2.5882
TSS	31.5248	32.6656

Station CB3.3C

Run234 2002-2011
Chlorophyll CB3.3C Surface

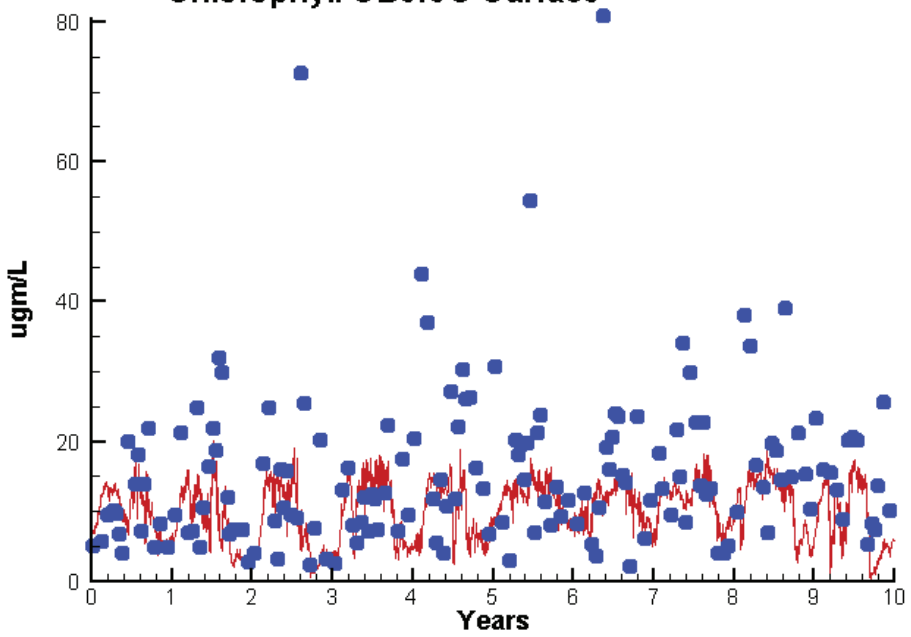

Run234 2002-2011
Light Extinction CB3.3C Surface

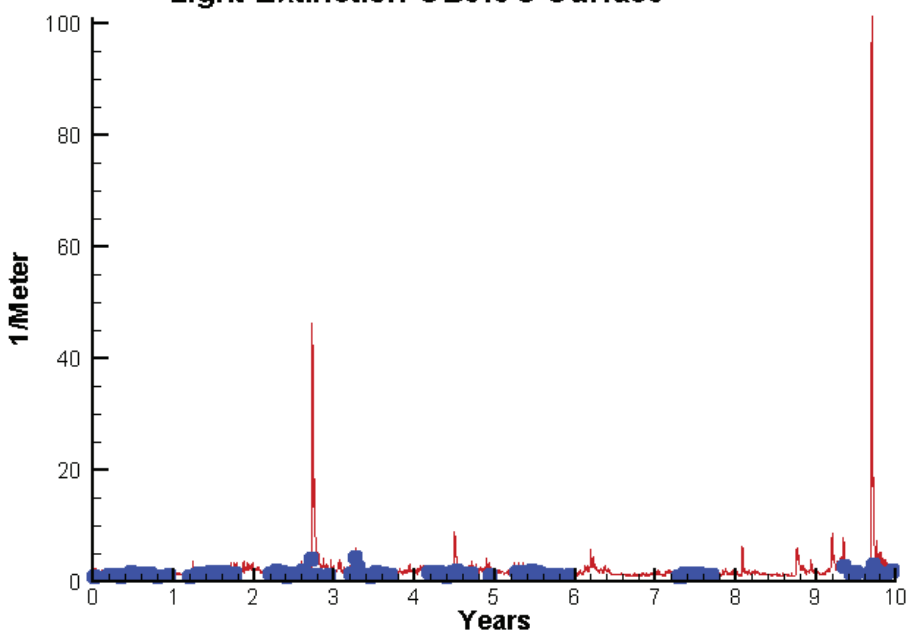

Run234 2002-2011
Dissolved Inorganic Nitrogen CB3.3C Surface

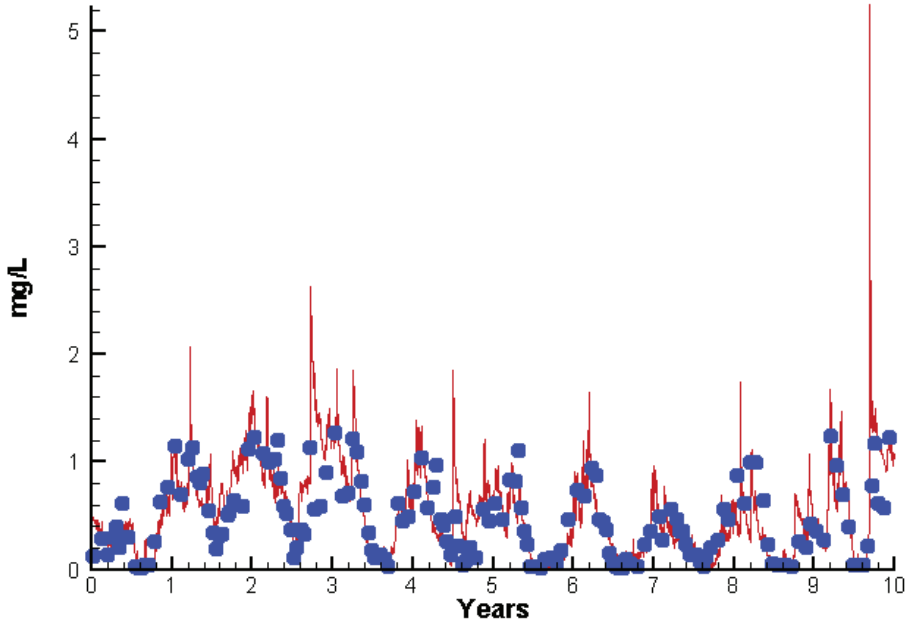

Run234 2002-2011
Dissolved Inorganic Phosphorus CB3.3C Surface

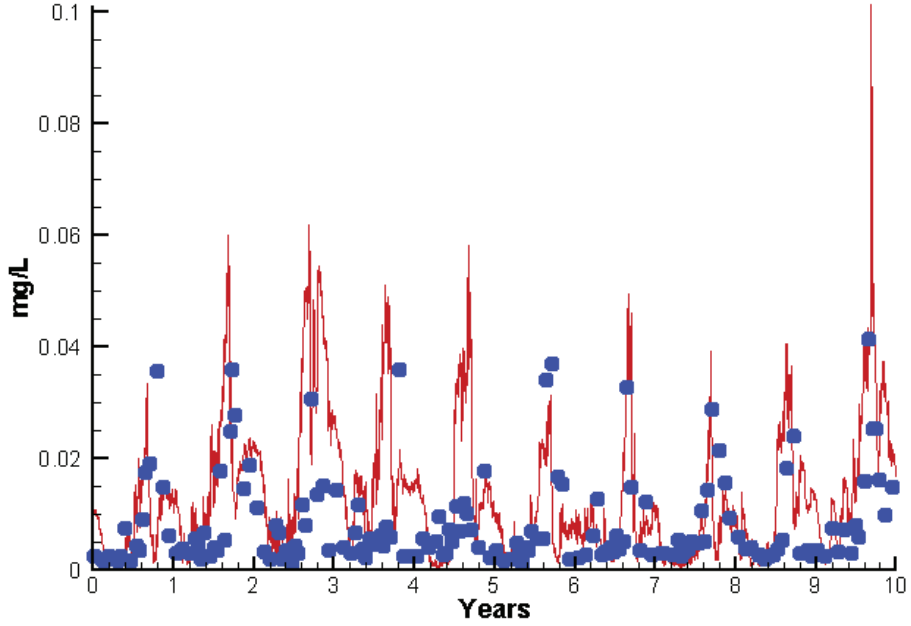

Station CB3.3C

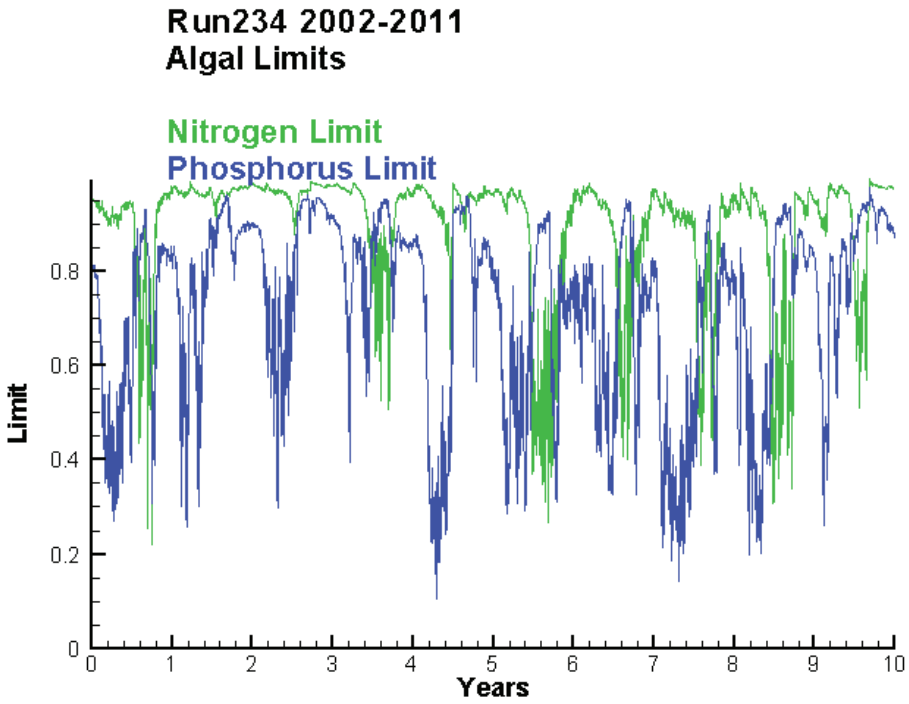

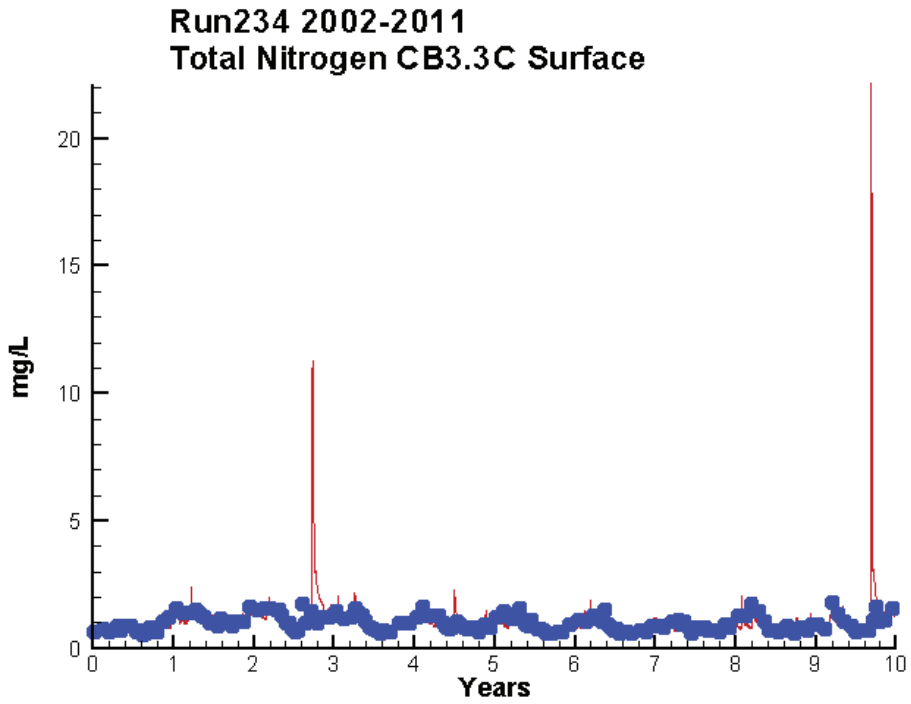

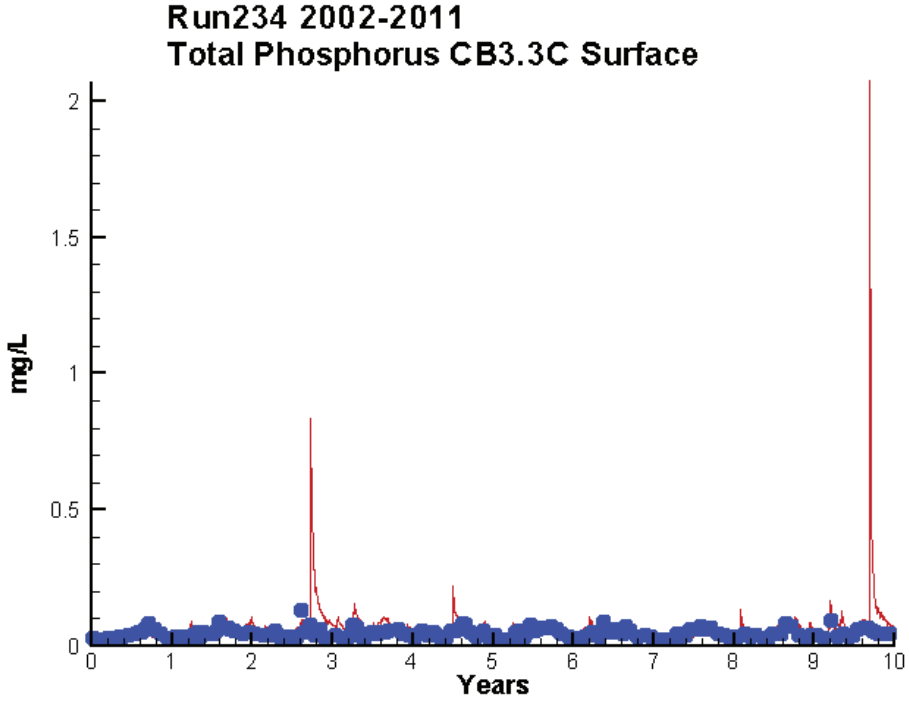

	Mean Difference	Absolute Mean Difference
Chl	-4.6641	7.7102
DIN	0.0363	0.1653
KE	0.8563	0.9219
DIP	0.0048	0.0085
TP	0.0183	0.0244
TN	0.0206	0.1974

Station CB3.3C

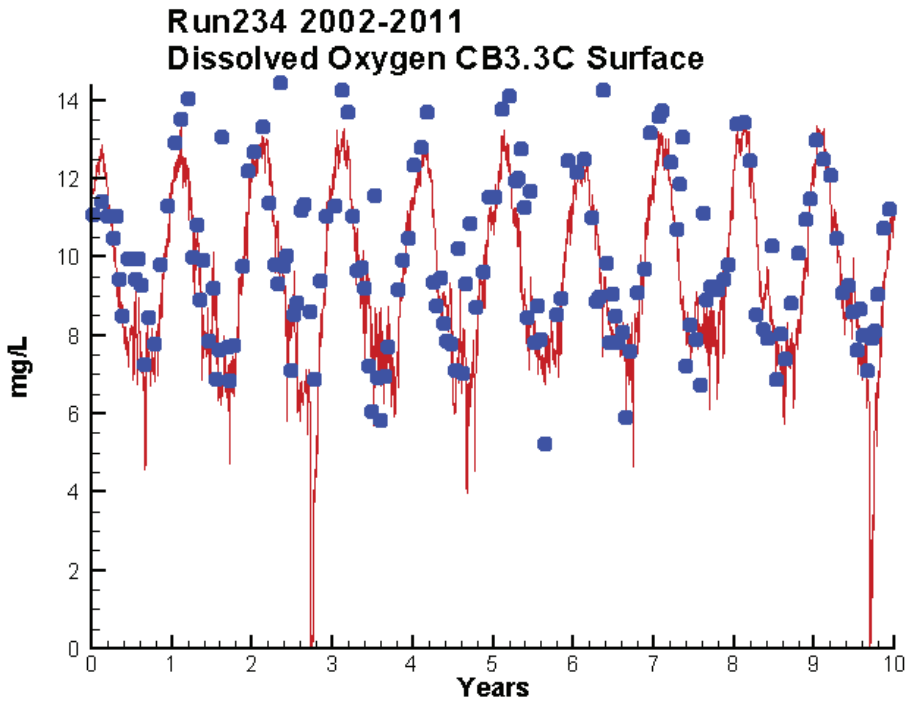

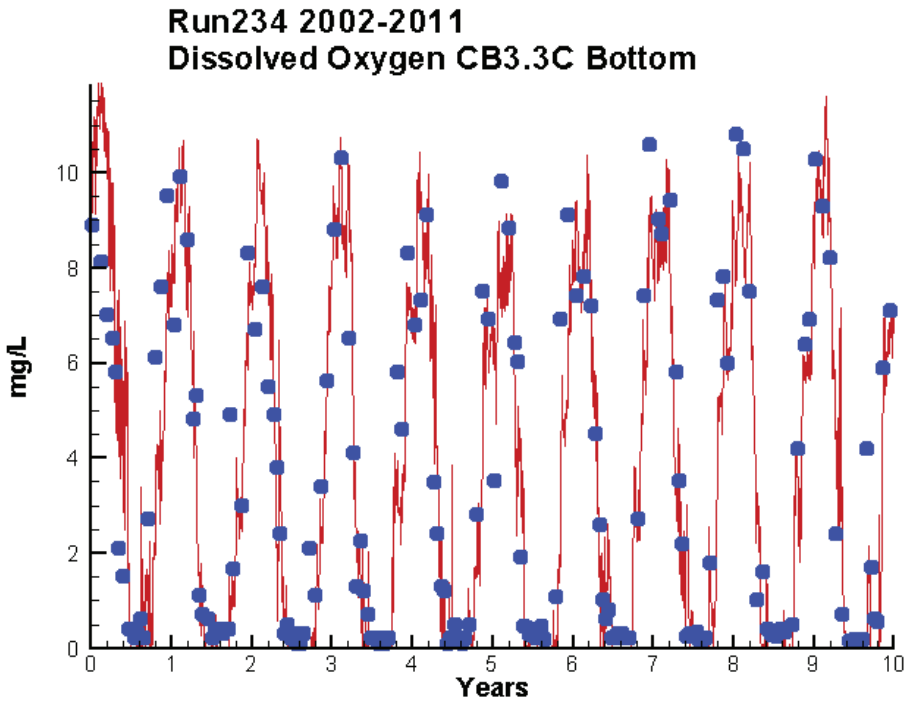

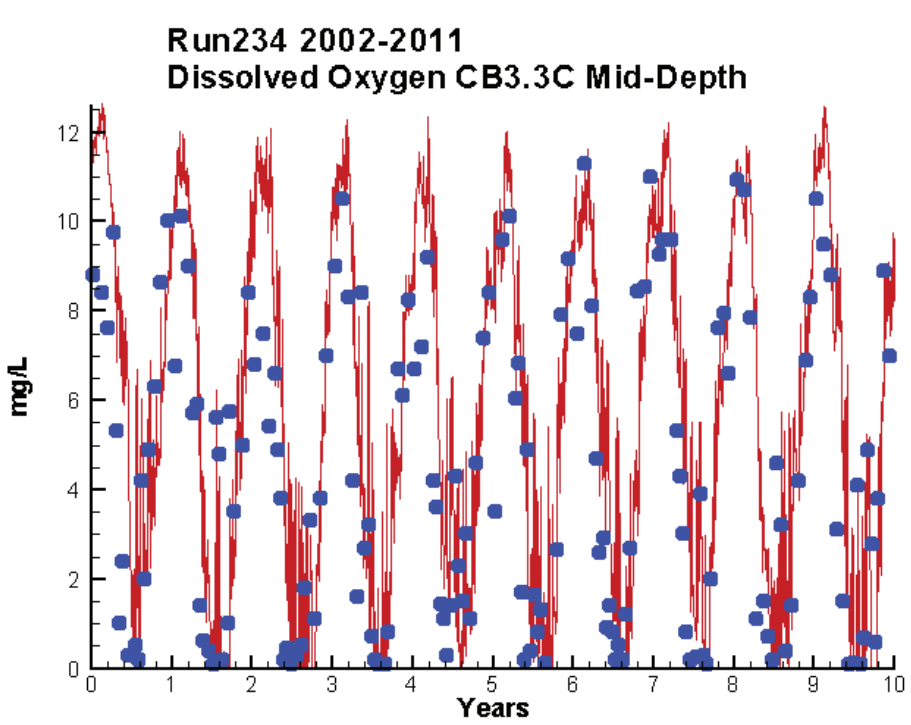

	Mean Difference	Absolute Mean Difference
Top DO	-0.6521	1.1684
Mid DO	1.0601	1.7553
Bot DO	-0.3054	0.9698

Station CB3.3C

Run234 2002-2011
Light Extinction CB3.3C Surface

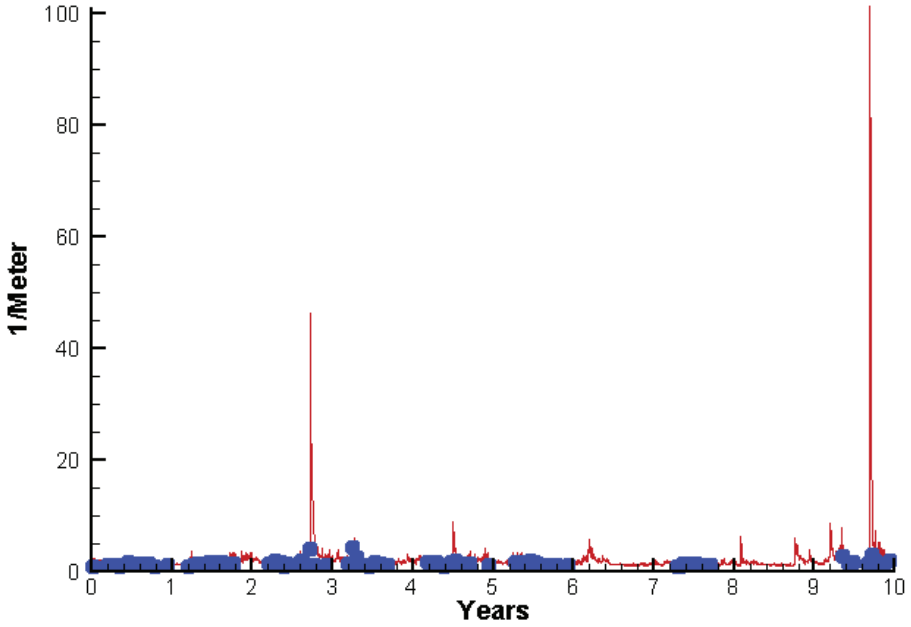

Run234 2002-2011
Total Solids CB3.3C Surface

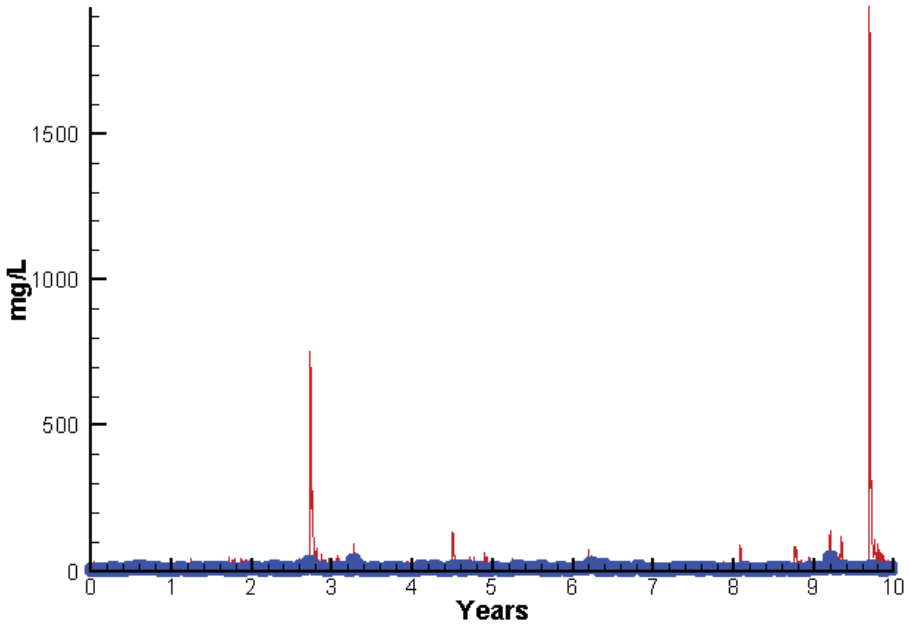

Run234 2002-2011
Solids Surface
Fixed Solids C(33+34+35+36)
Volatile Solids C(33+34+35+36)

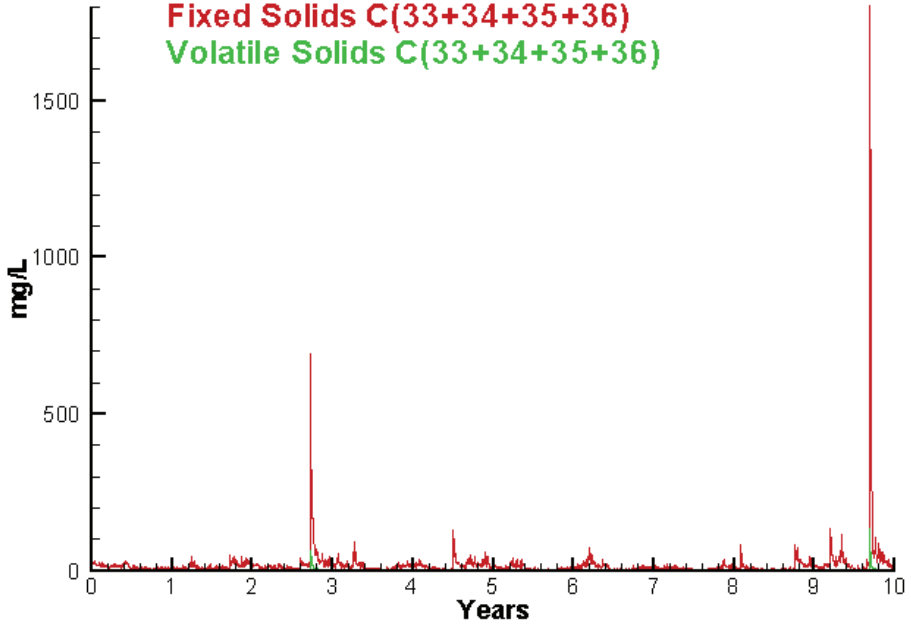

	Mean Difference	Absolute Mean Difference
KE	0.8563	0.9219
TSS	11.7577	12.0672

Station CB4.2C

Run234 2002-2011
Chlorophyll CB4.2C Surface

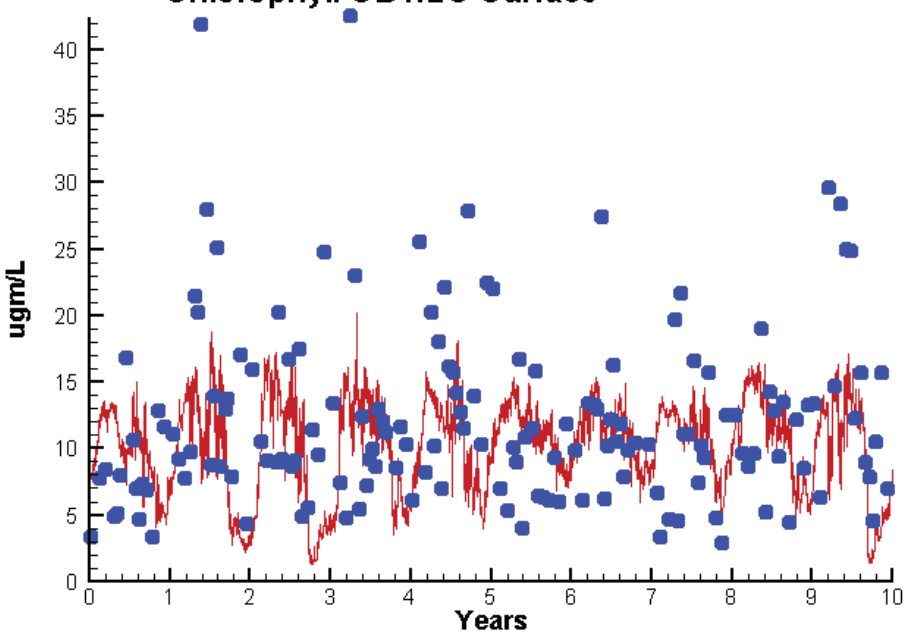

Run234 2002-2011
Light Extinction CB4.2C Surface

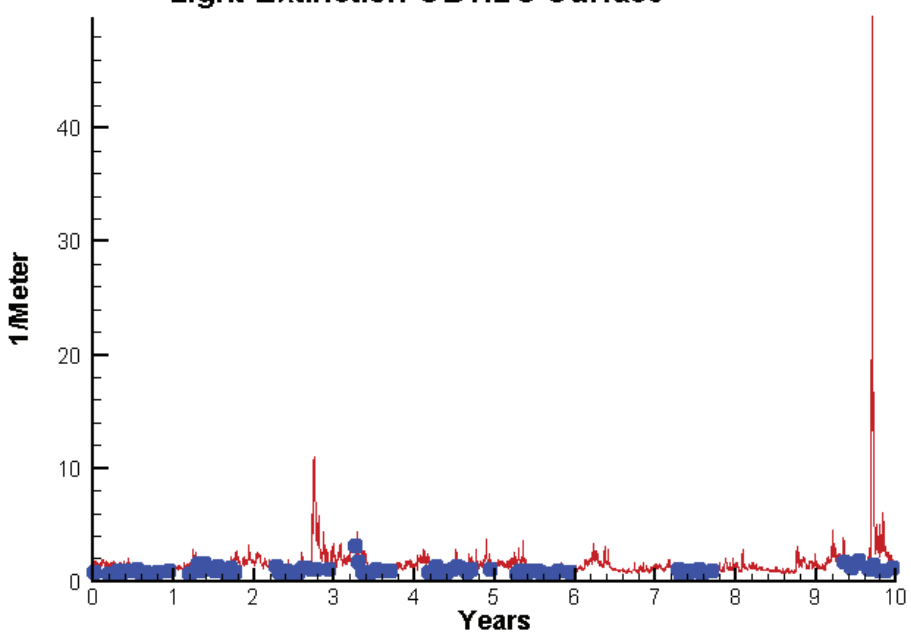

Run234 2002-2011
Dissolved Inorganic Nitrogen CB4.2C Surface

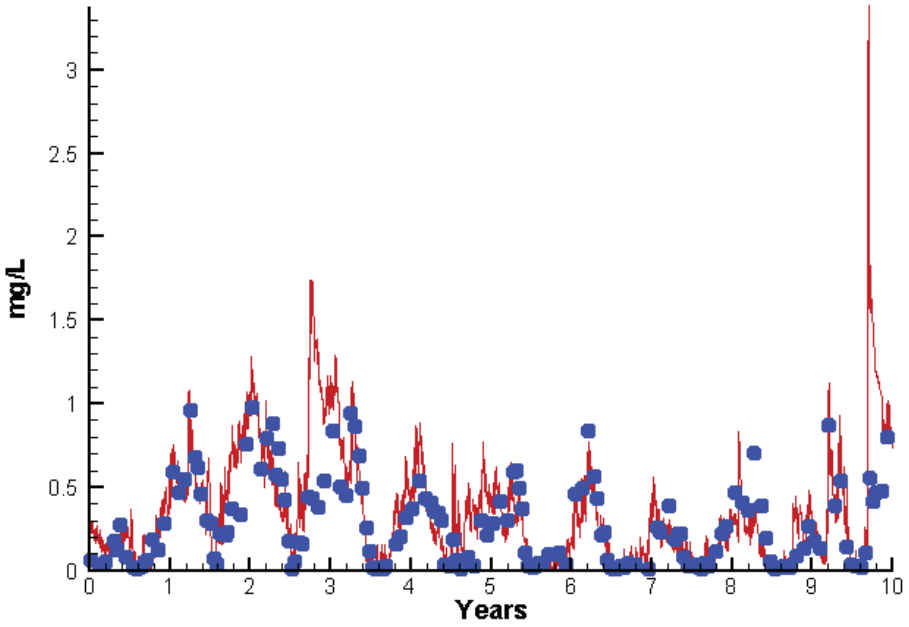

Run234 2002-2011
Dissolved Inorganic Phosphorus CB4.2C Surface

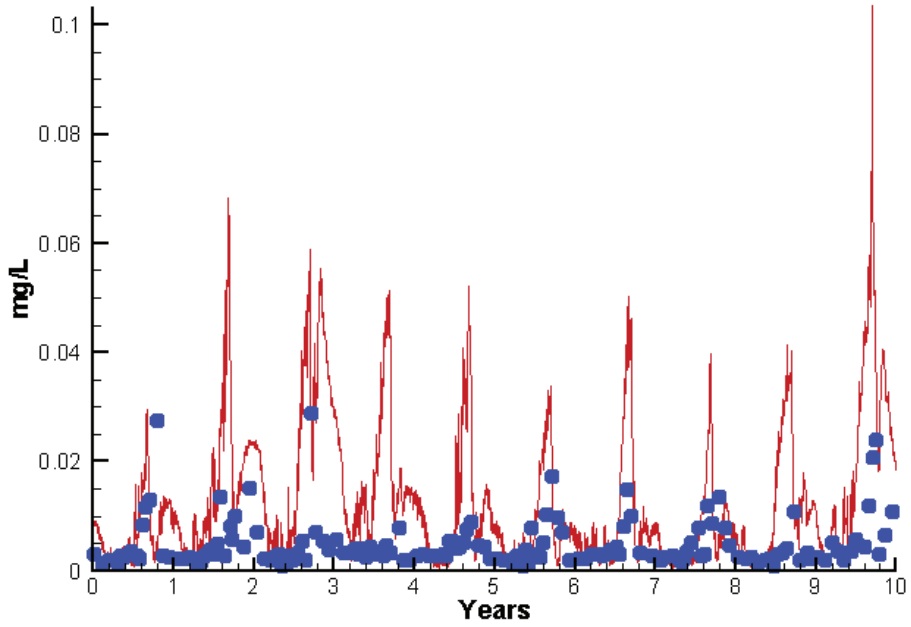

Station CB4.2C

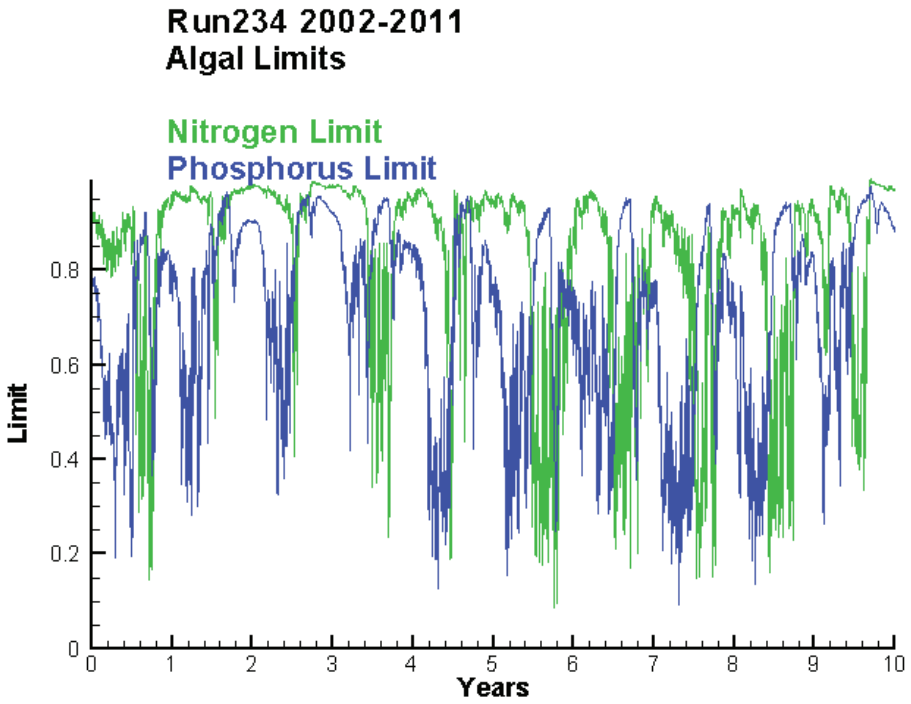

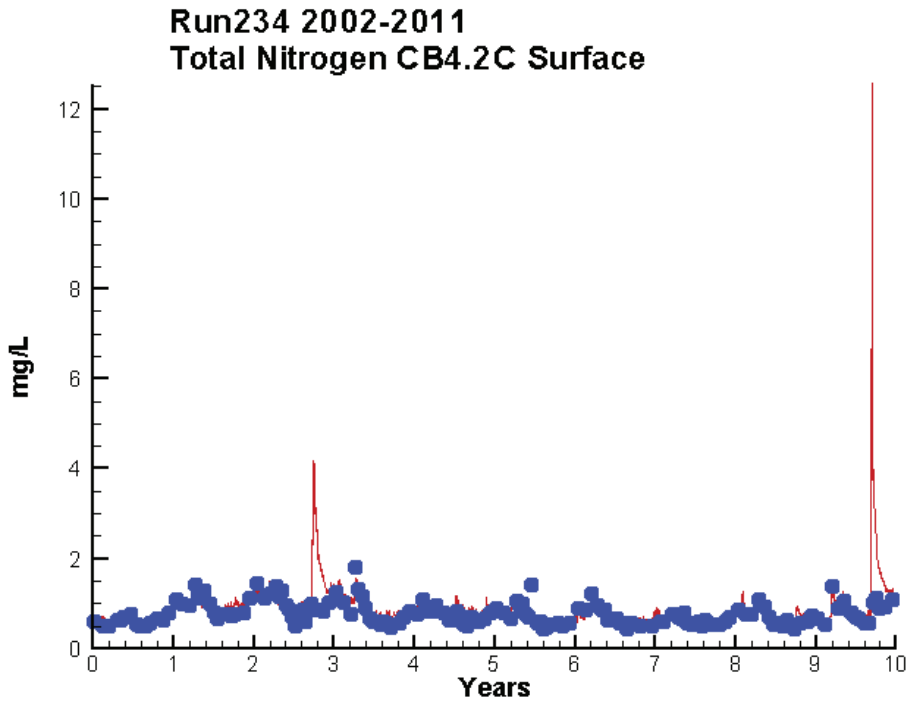

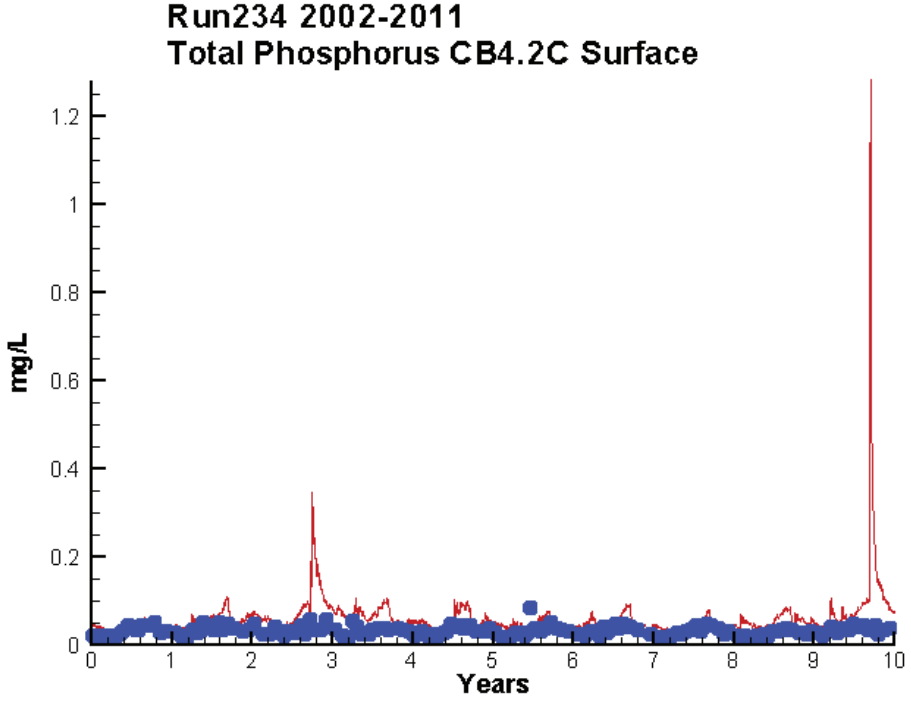

	Mean Difference	Absolute Mean Difference
Chl	-1.4239	5.5655
DIN	0.0552	0.1361
KE	0.5136	0.5736
DIP	0.0081	0.0092
TP	0.0262	0.0277
TN	0.0764	0.1515

Station CB4.2C

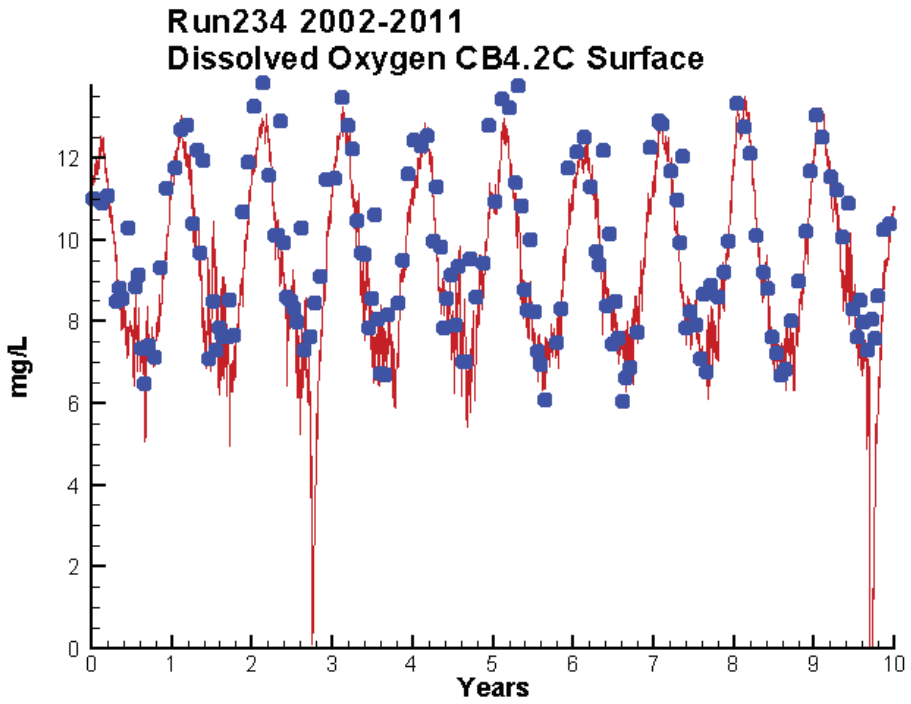

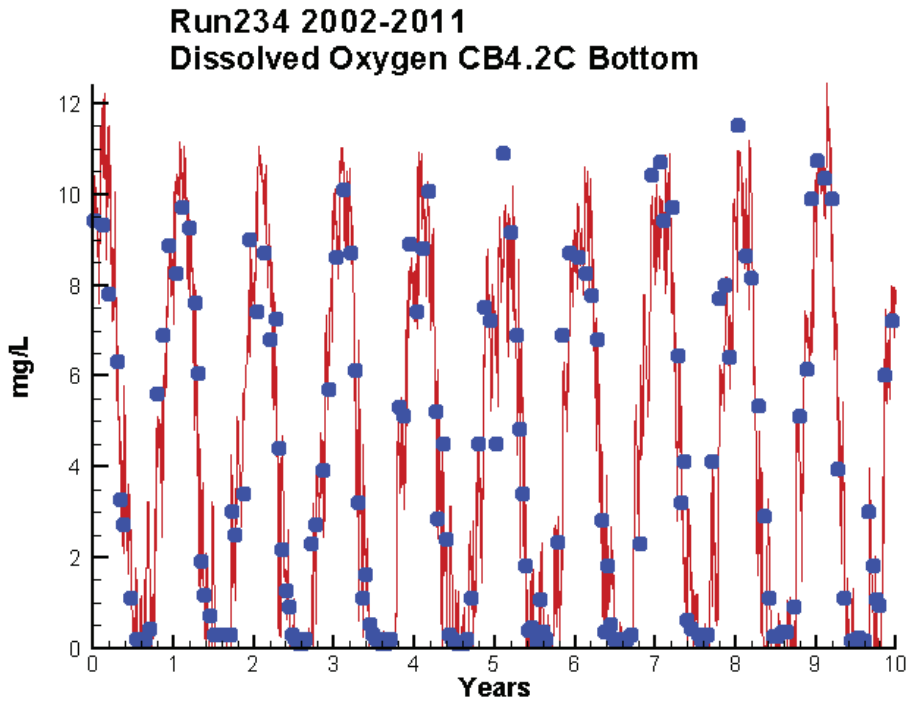

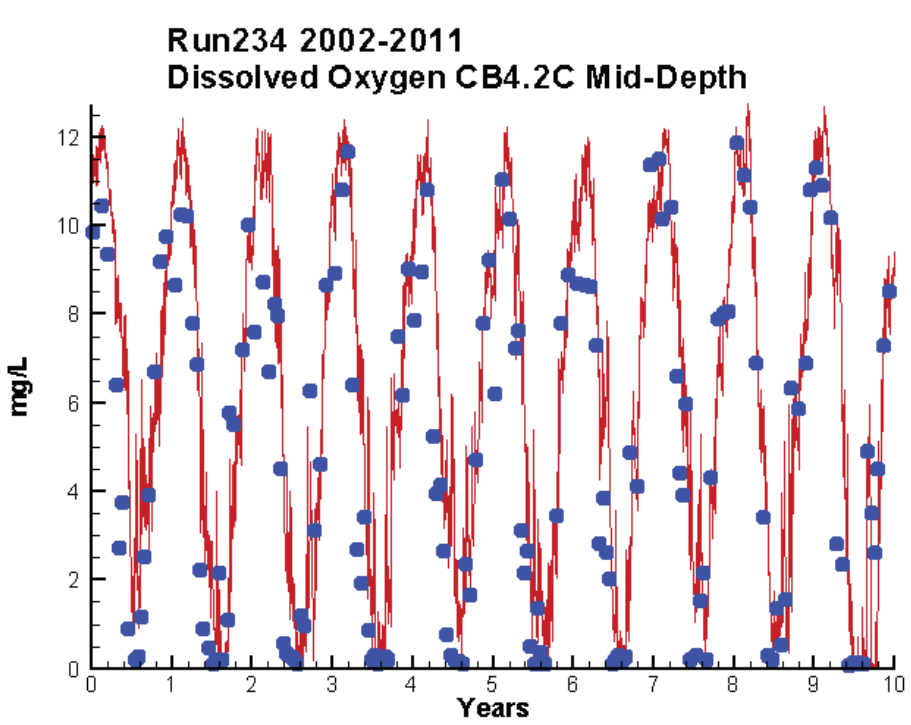

	Mean Difference	Absolute Mean Difference
Top DO	-0.5840	0.8942
Mid DO	1.0407	1.5183
Bot DO	-0.1728	0.8506

Station CB4.2C

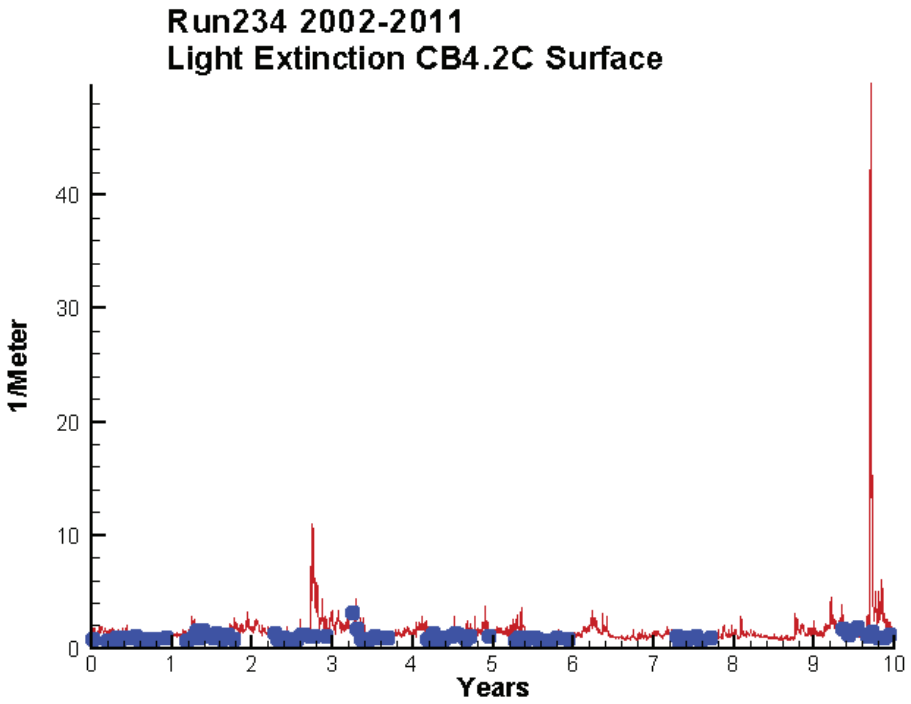

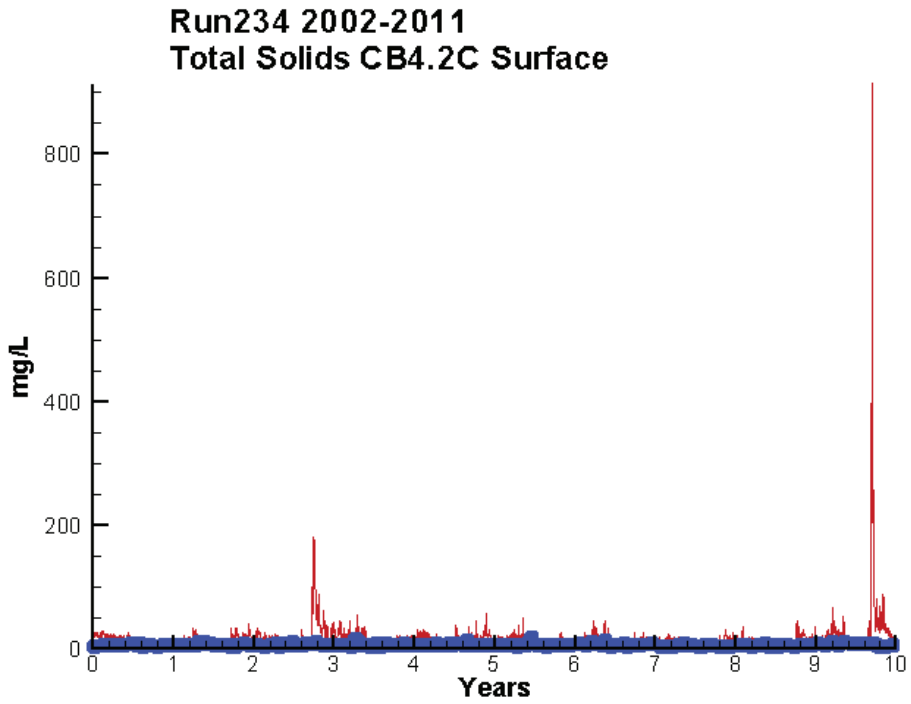

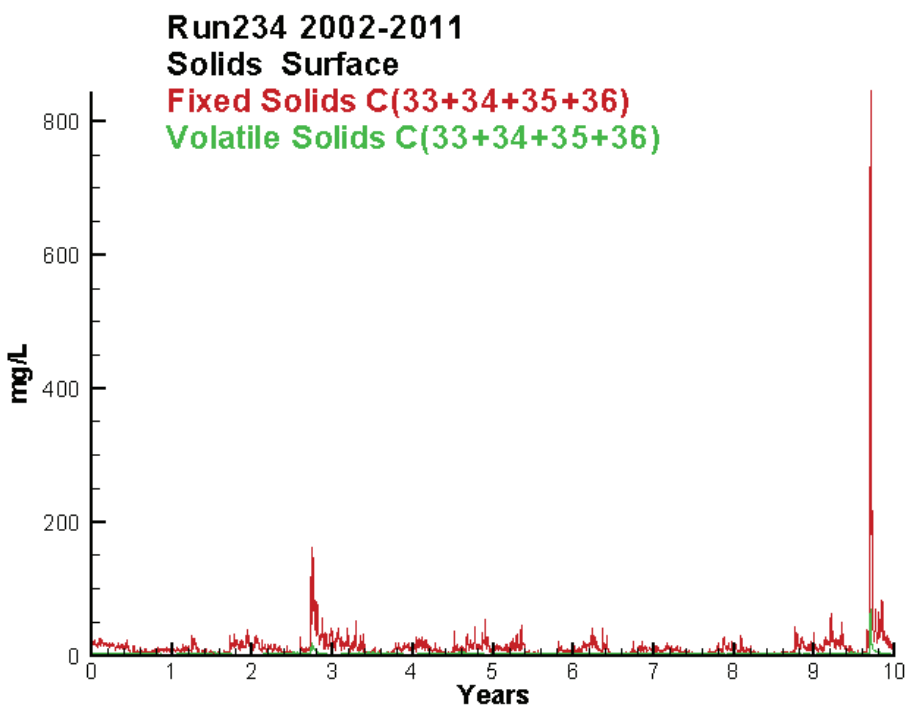

	Mean Difference	Absolute Mean Difference
KE	0.5136	0.5736
TSS	9.4054	9.5406

Station CB5.2

Run234 2002-2011
Chlorophyll CB5.2 Surface

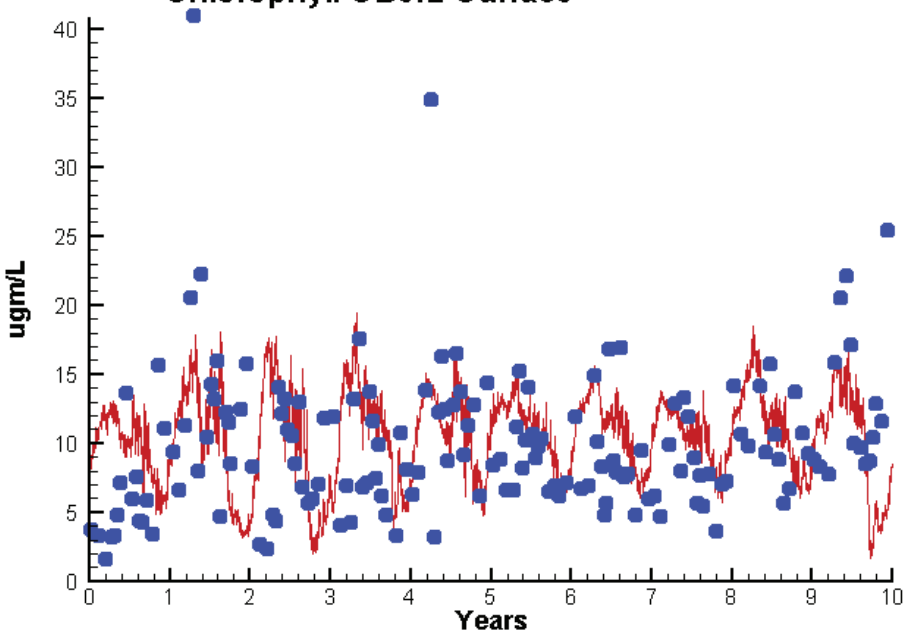

Run234 2002-2011
Light Extinction CB5.2 Surface

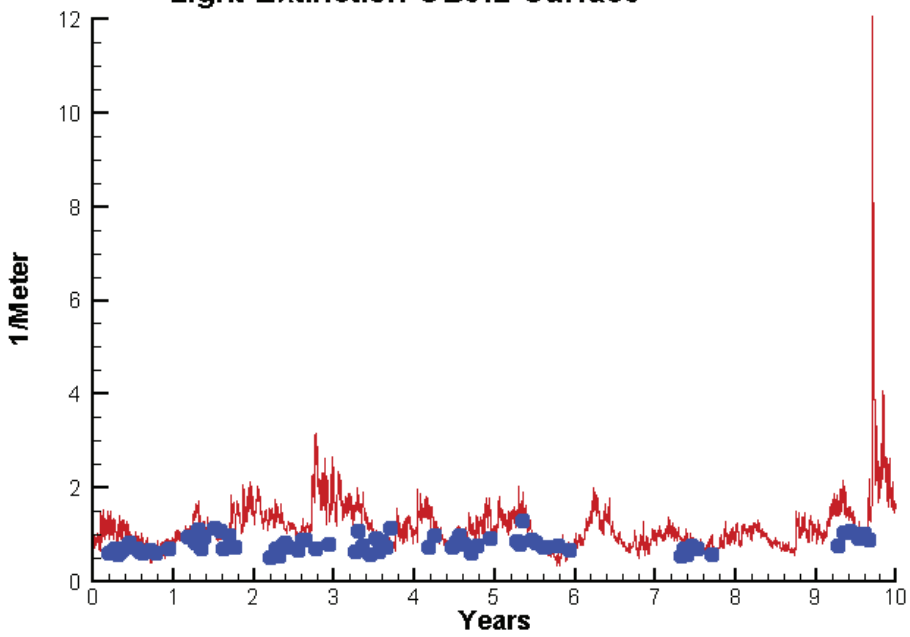

Run234 2002-2011
Dissolved Inorganic Nitrogen CB5.2 Surface

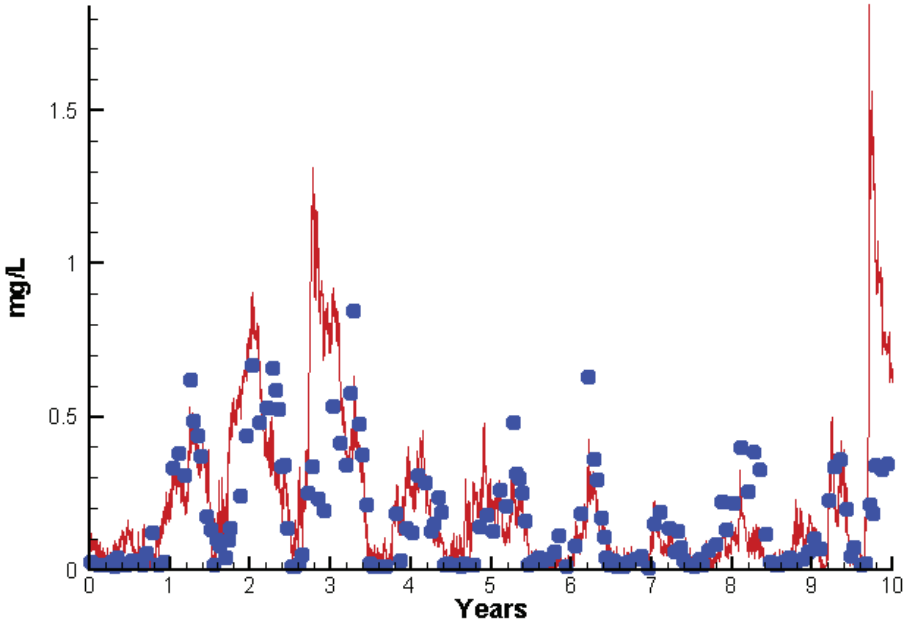

Run234 2002-2011
Dissolved Inorganic Phosphorus CB5.2 Surface

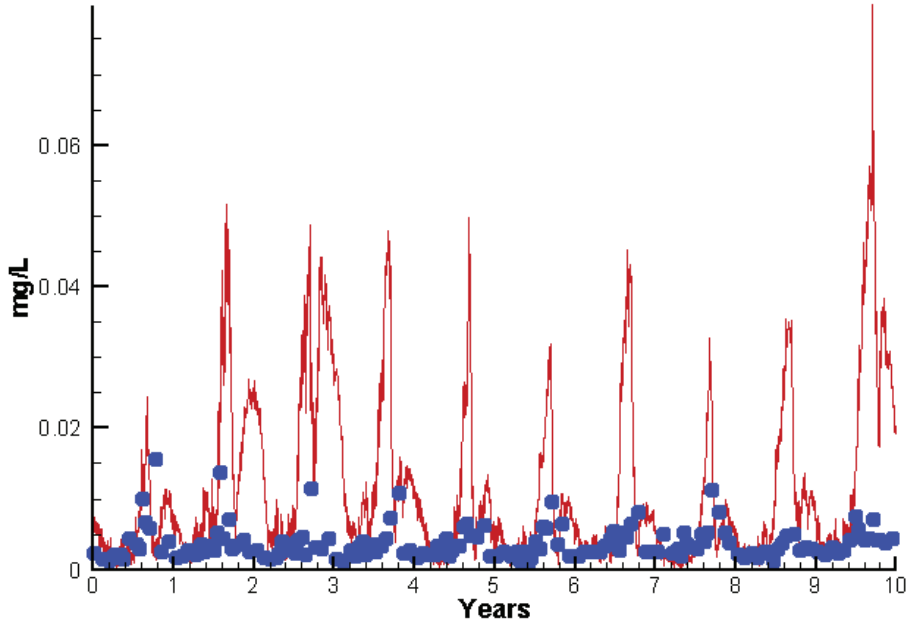

Station CB5.2

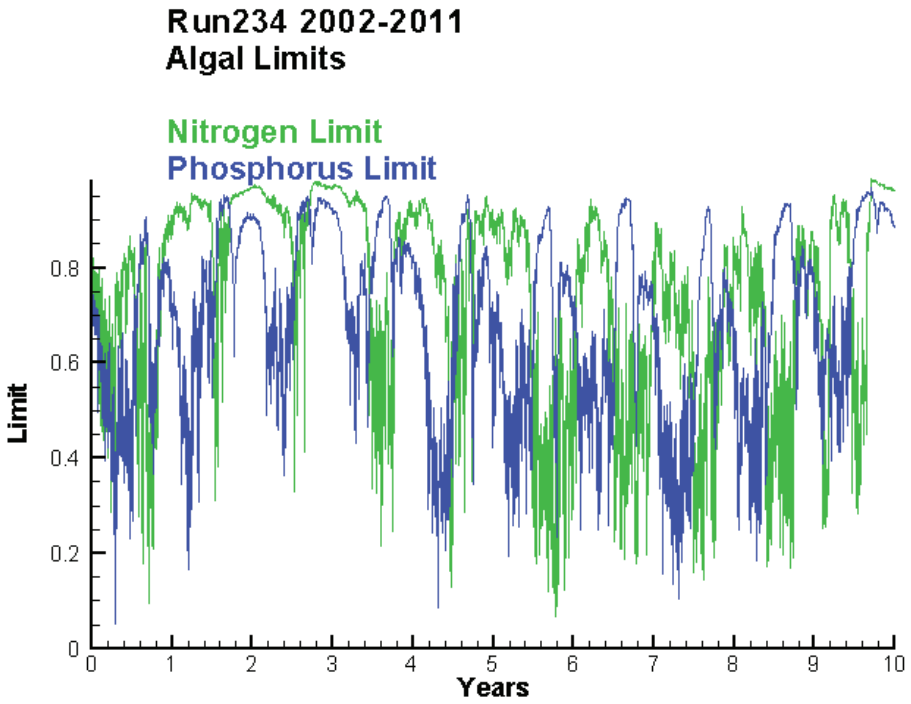

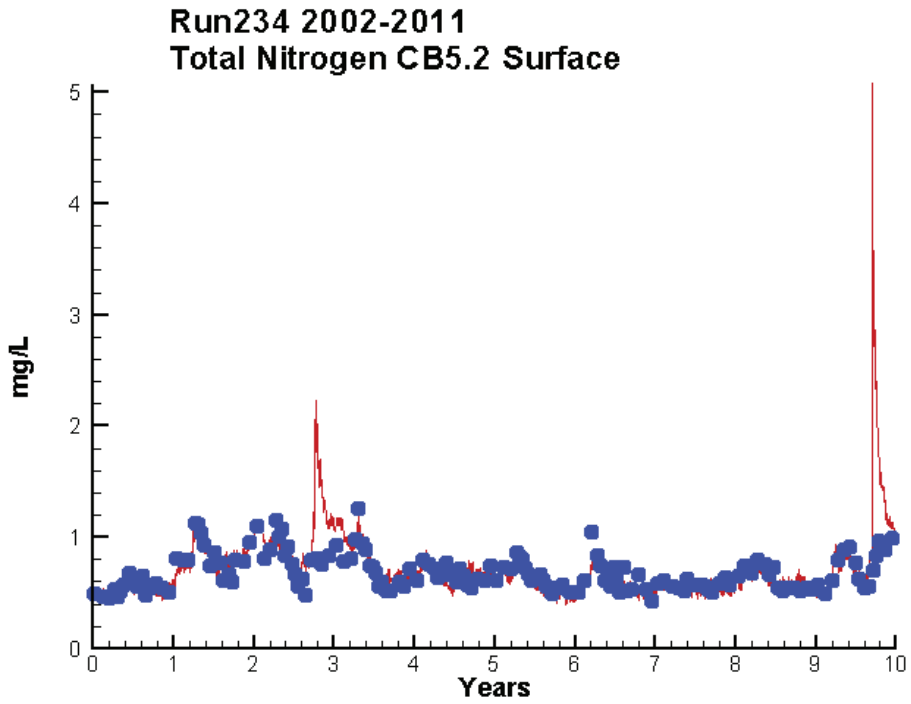

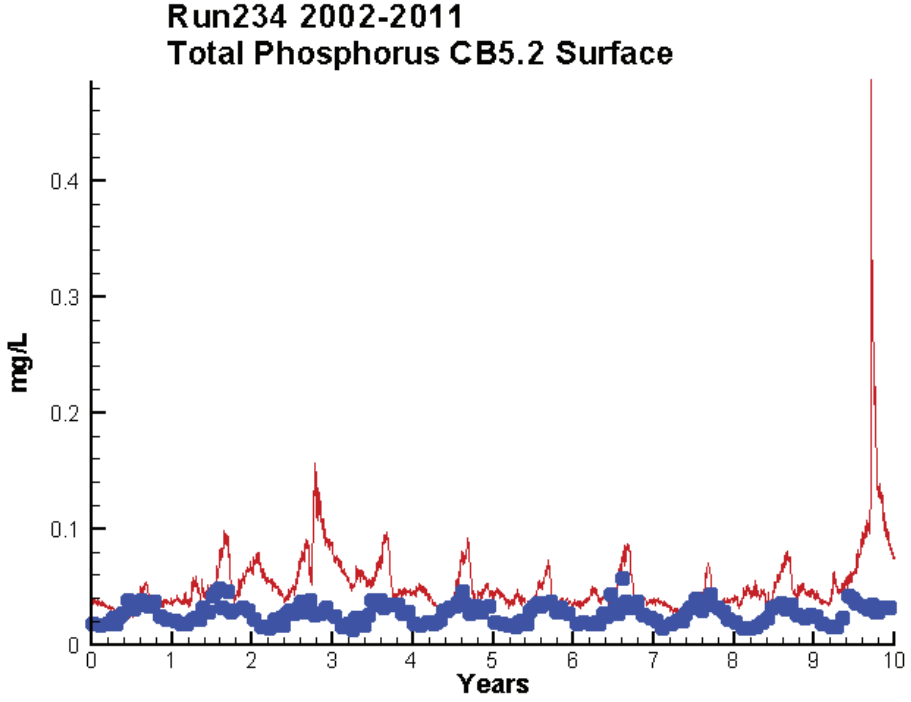

	Mean Difference	Absolute Mean Difference
Chl	0.9079	4.5286
DIN	0.0370	0.1150
KE	0.3417	0.3720
DIP	0.0080	0.0086
TP	0.0257	0.0262
TN	0.0375	0.1039

Station CB5.2

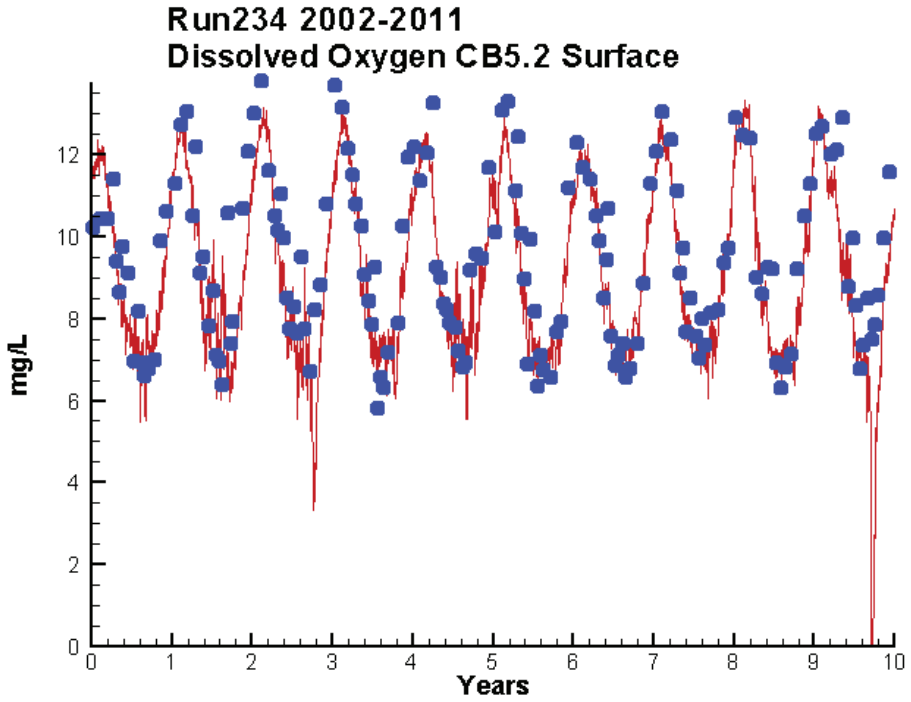

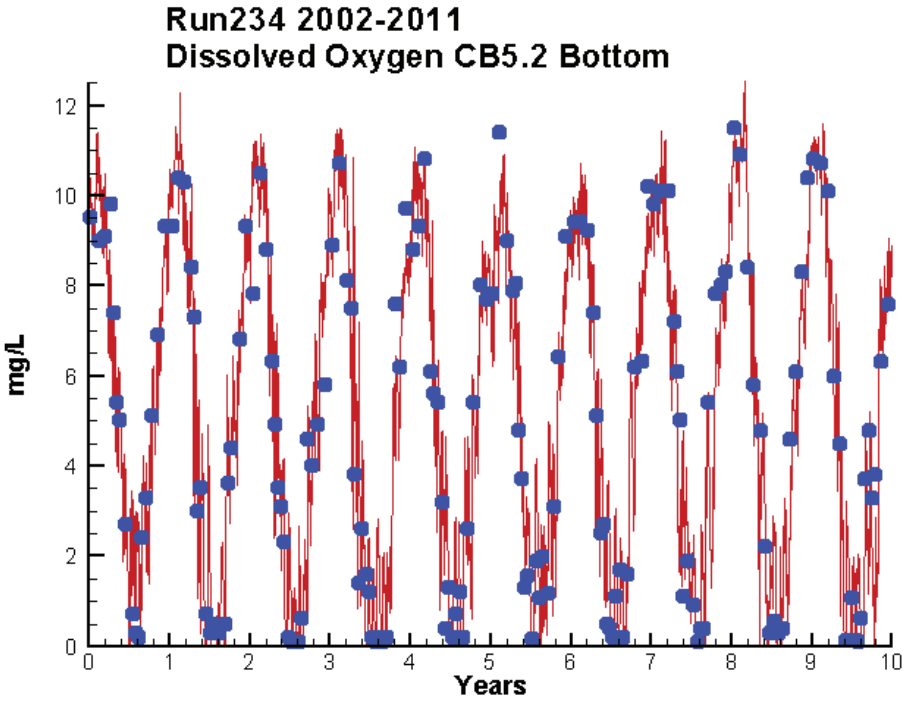

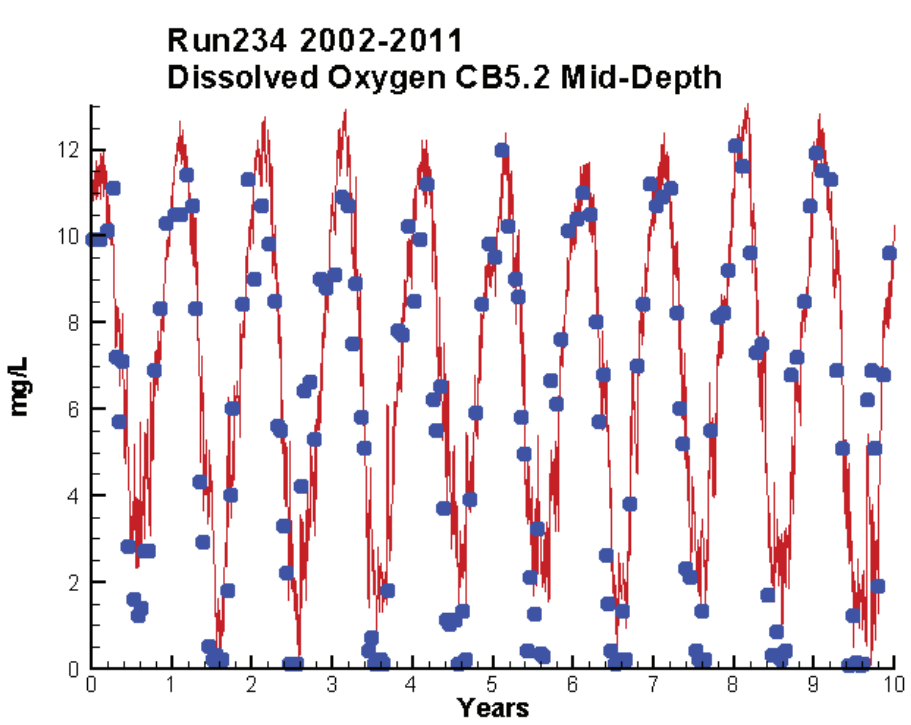

	Mean Difference	Absolute Mean Difference
Top DO	-0.5352	0.8880
Mid DO	0.8904	1.3873
Bot DO	0.0847	1.0483

Station CB5.2

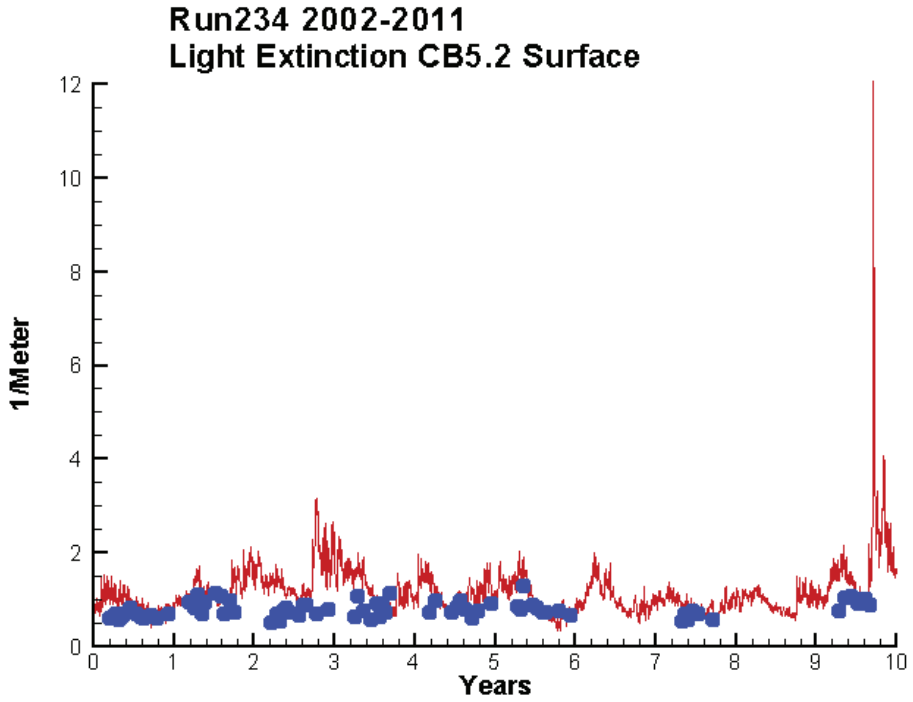

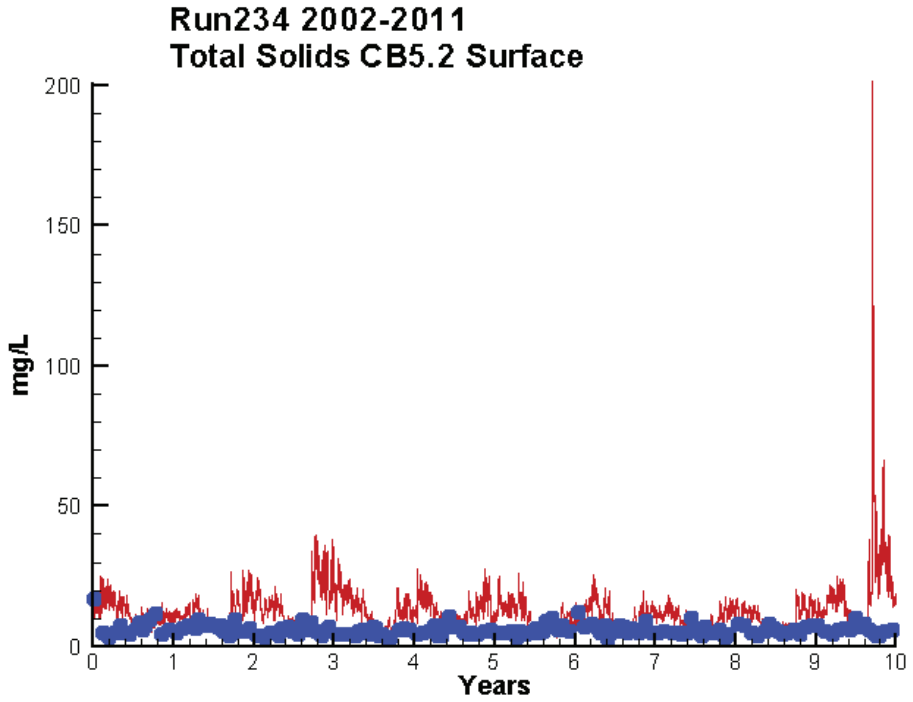

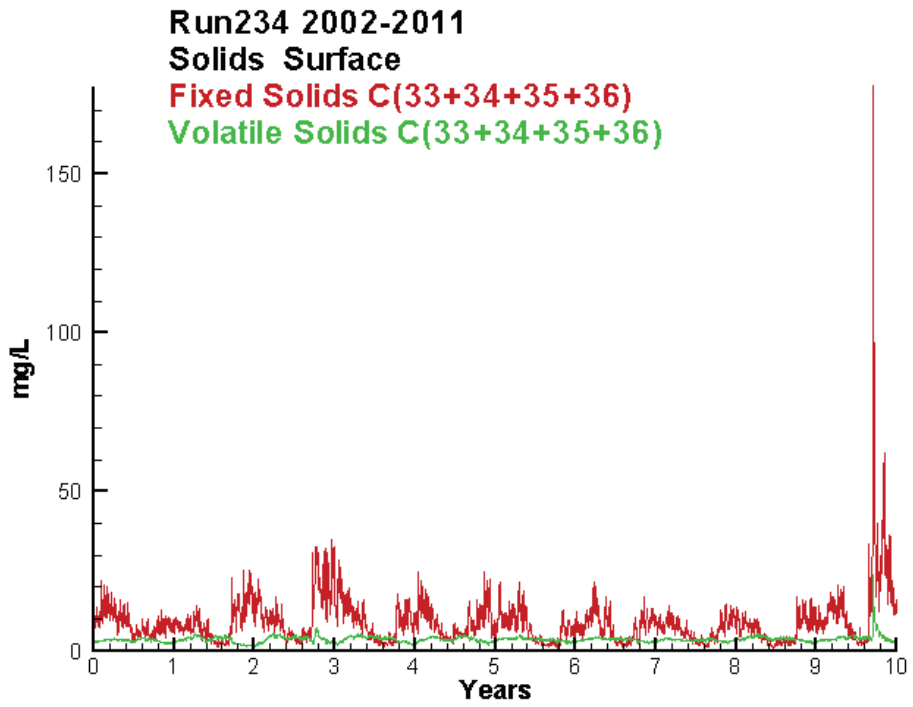

	Mean Difference	Absolute Mean Difference
KE	0.3417	0.3720
TSS	6.2211	6.5652

Station CB6.1

Run234 2002-2011
Chlorophyll CB6.1 Surface

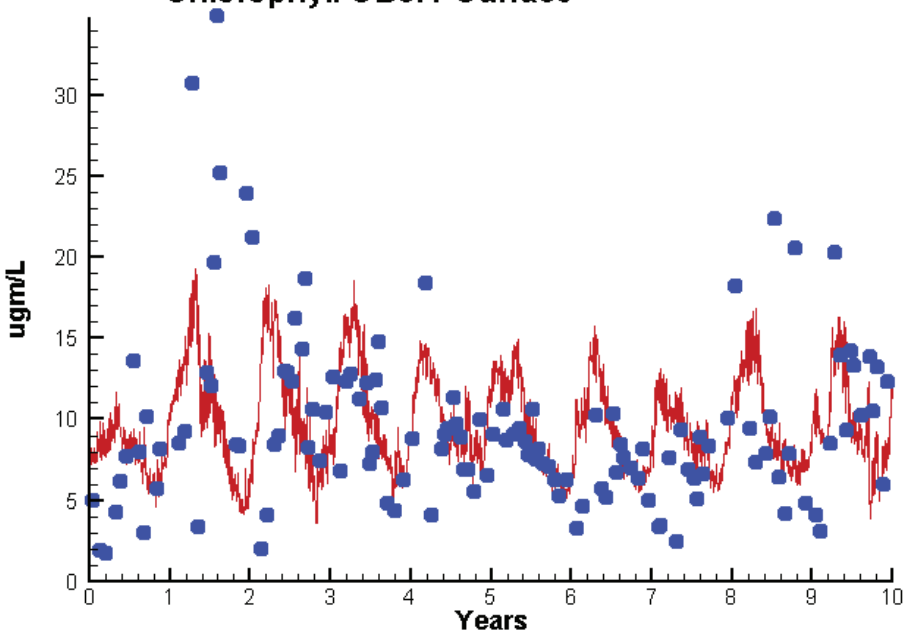

Run234 2002-2011
Light Extinction CB6.1 Surface

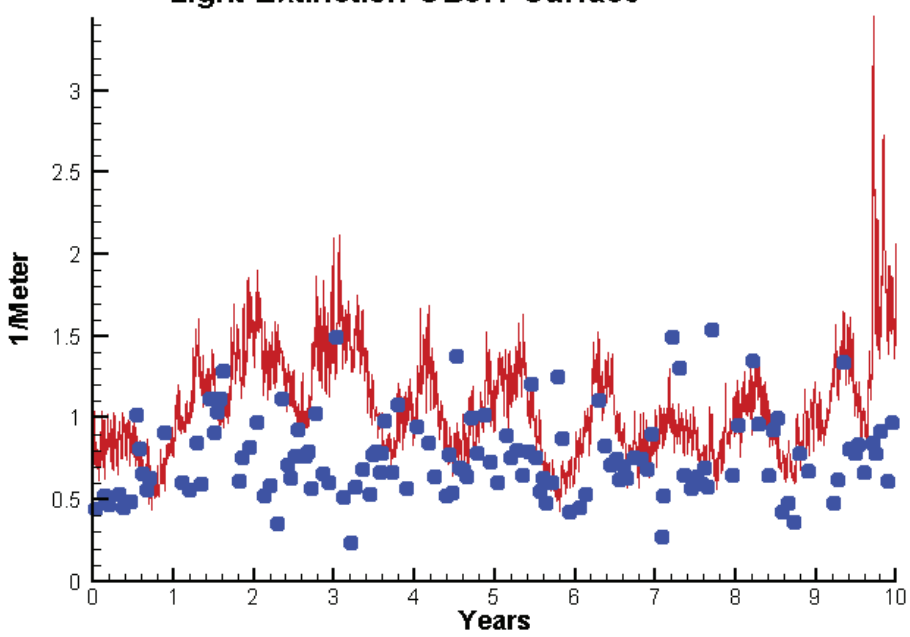

Run234 2002-2011
Dissolved Inorganic Nitrogen CB6.1 Surface

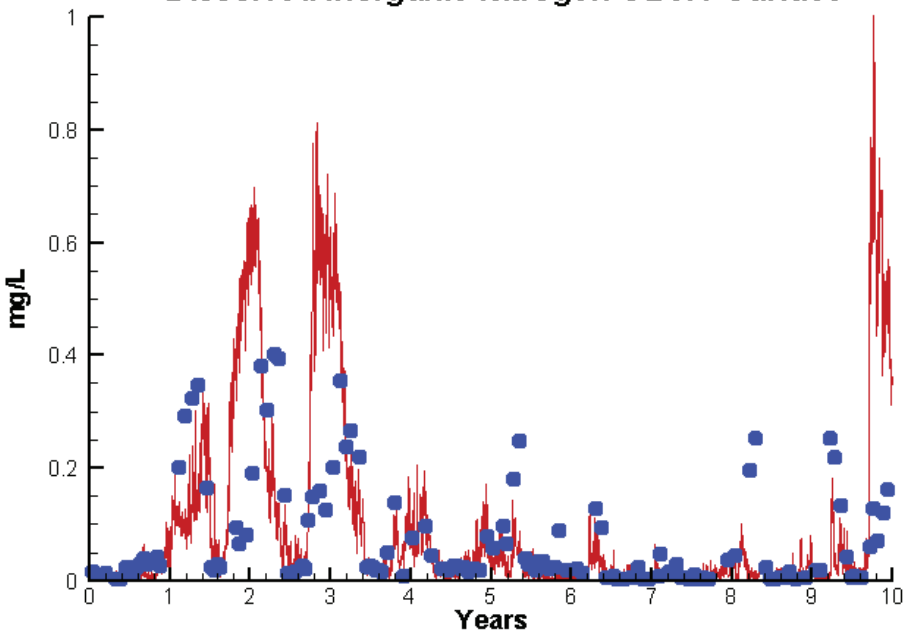

Run234 2002-2011
Dissolved Inorganic Phosphorus CB6.1 Surface

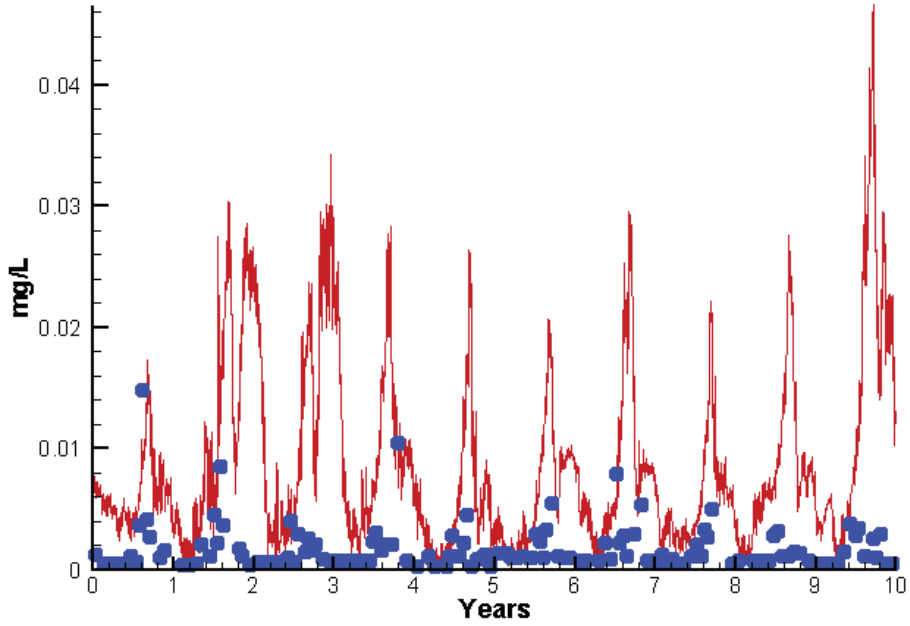

Station CB6.1

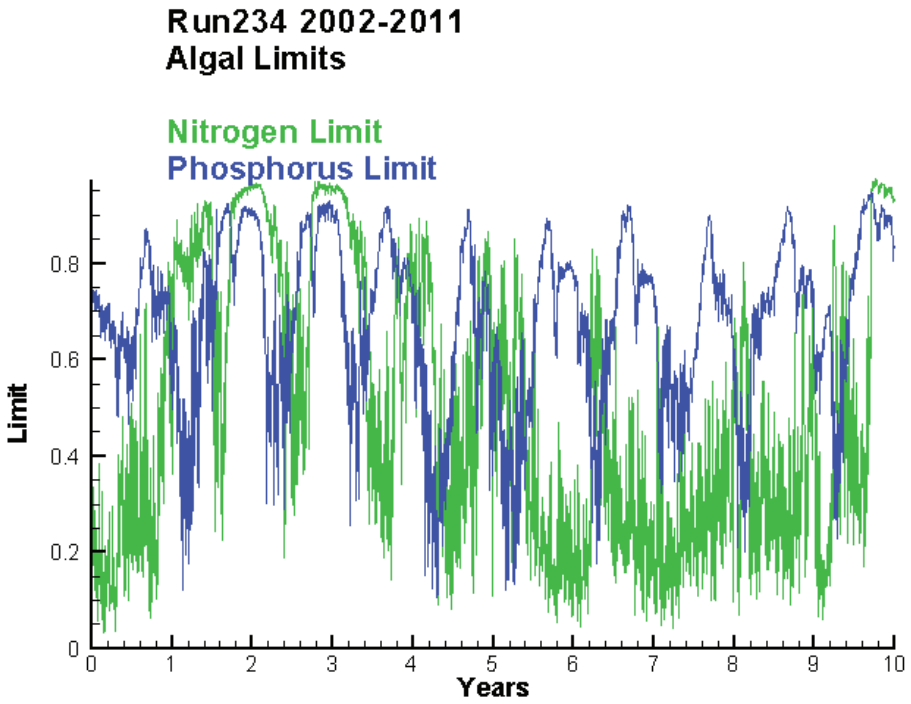

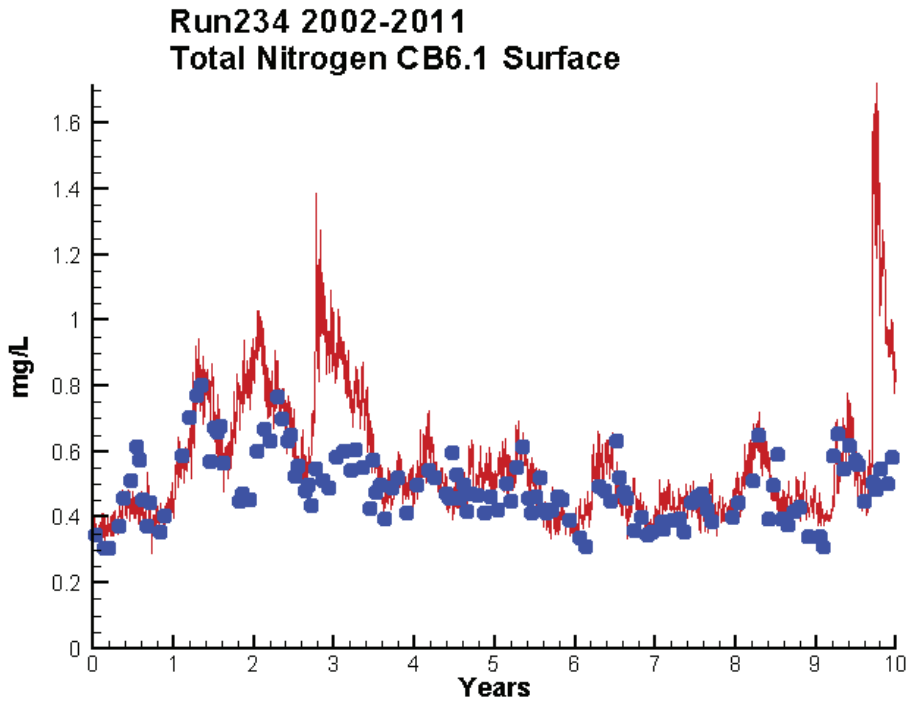

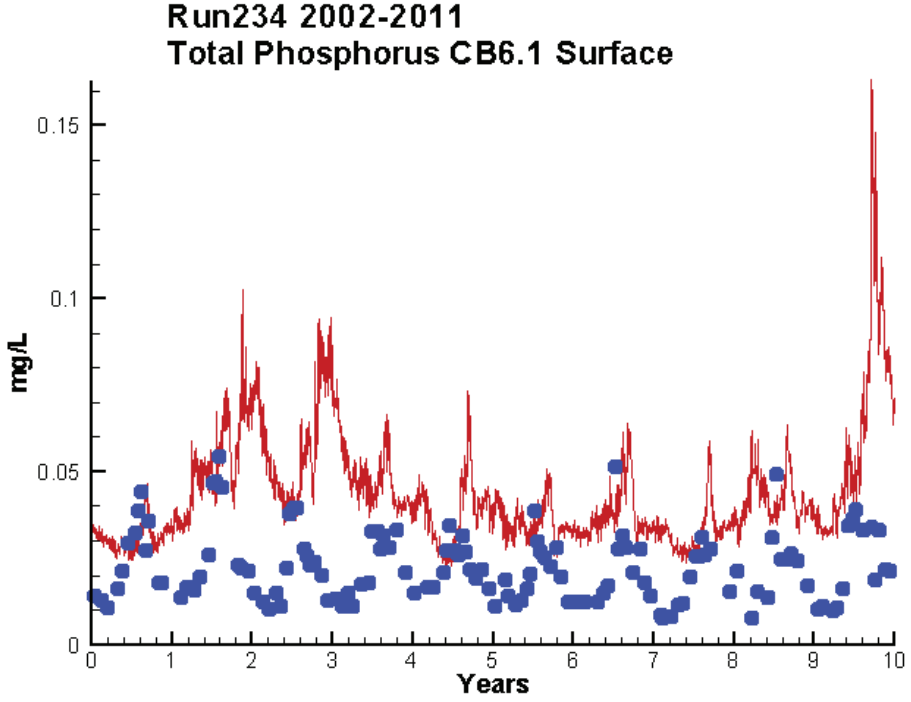

	Mean Difference	Absolute Mean Difference
Chl	0.2233	4.1001
DIN	0.0232	0.0794
KE	0.2981	0.3665
DIP	0.0073	0.0075
TP	0.0219	0.0230
TN	0.0854	0.1177

Station CB6.1

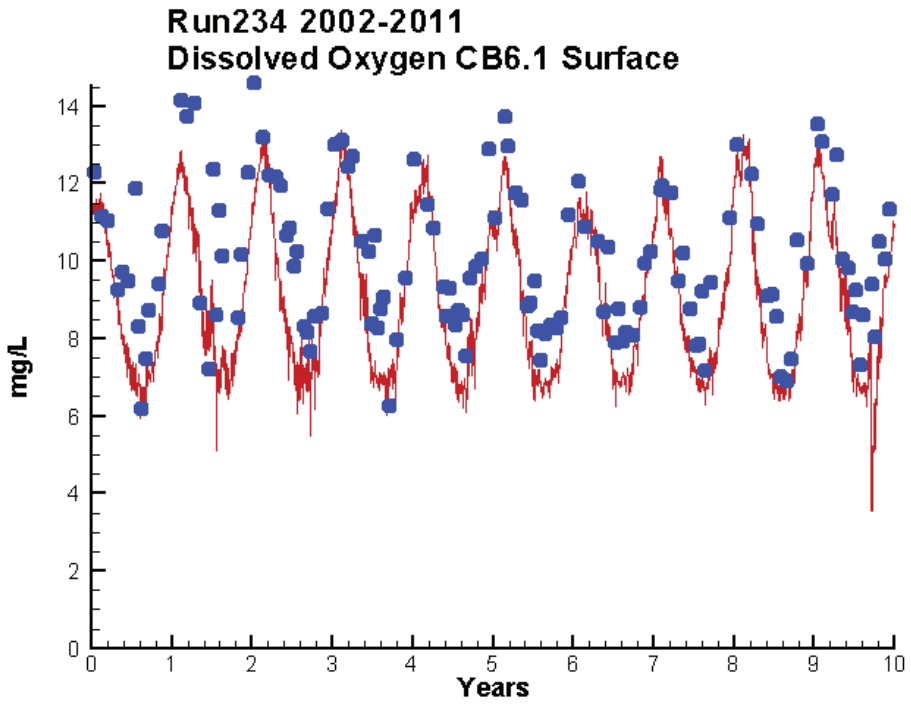

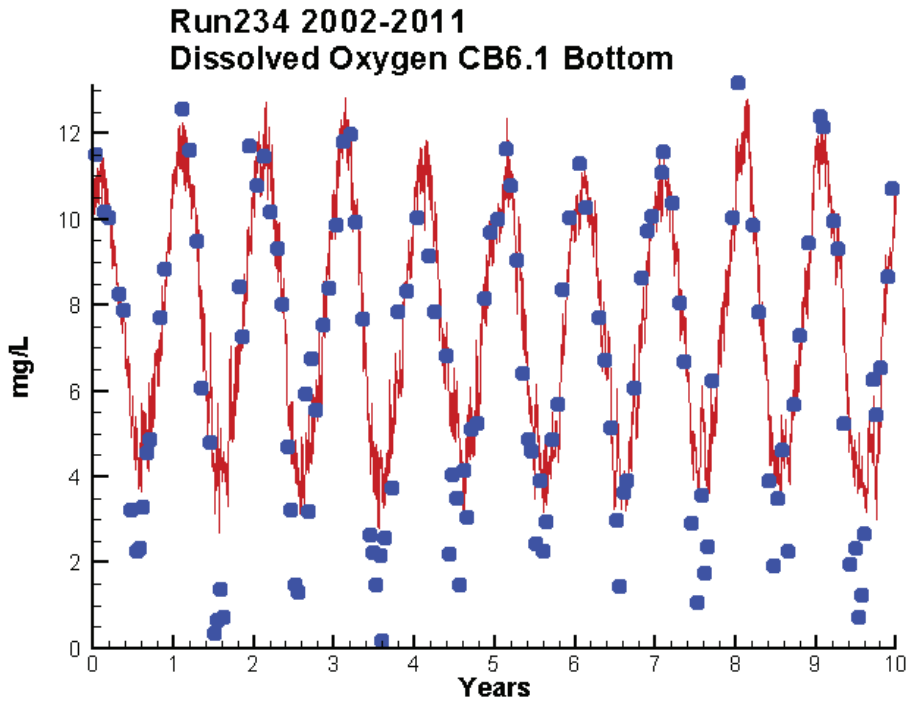

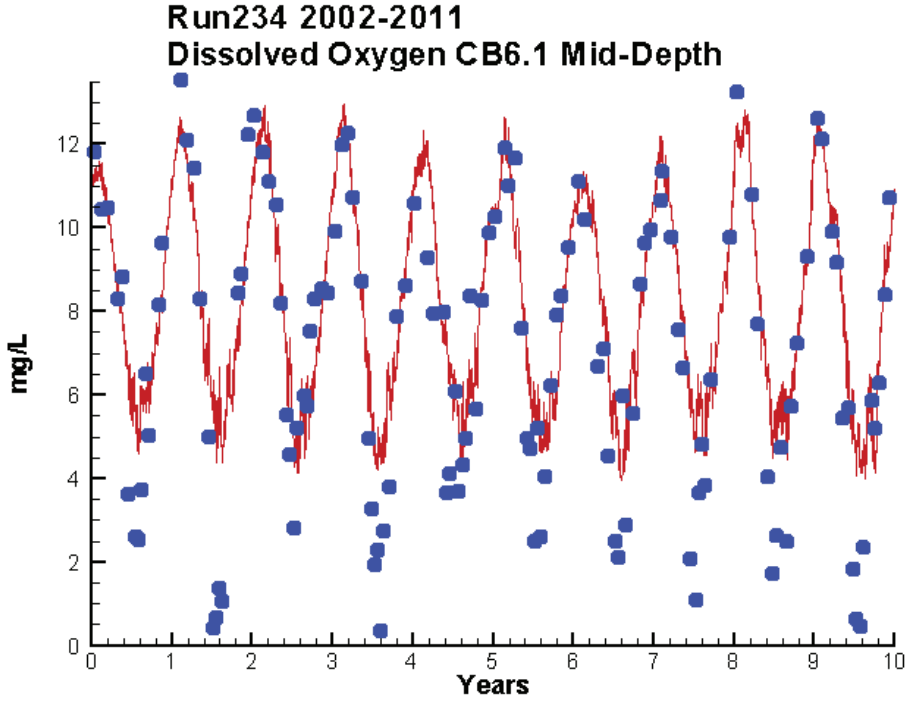

	Mean Difference	Absolute Mean Difference
Top DO	-1.2419	1.3375
Mid DO	0.8982	1.3798
Bot DO	0.6155	1.1977

Station CB6.1

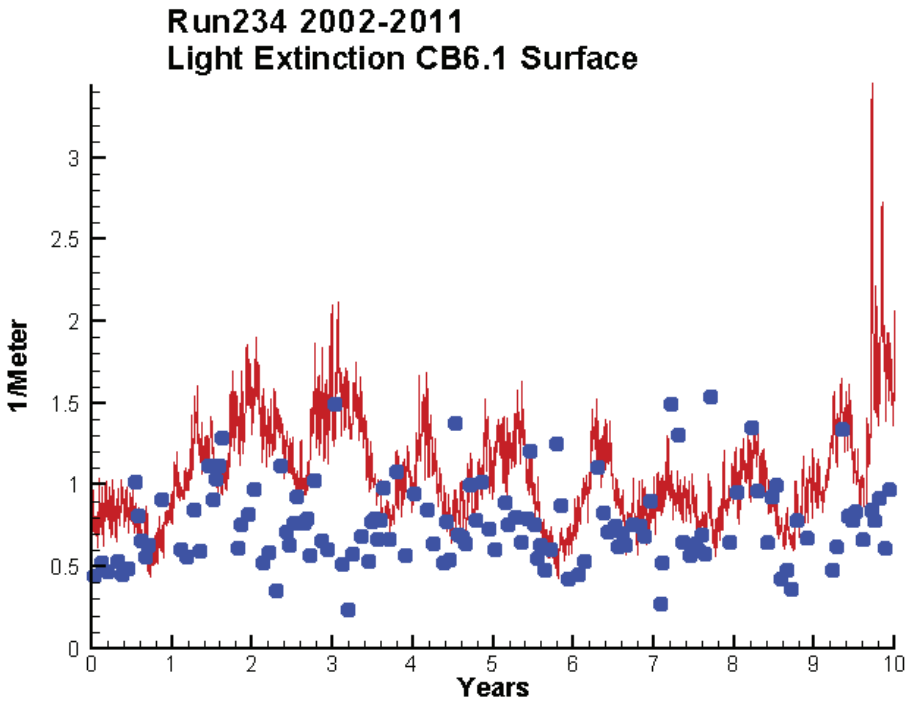

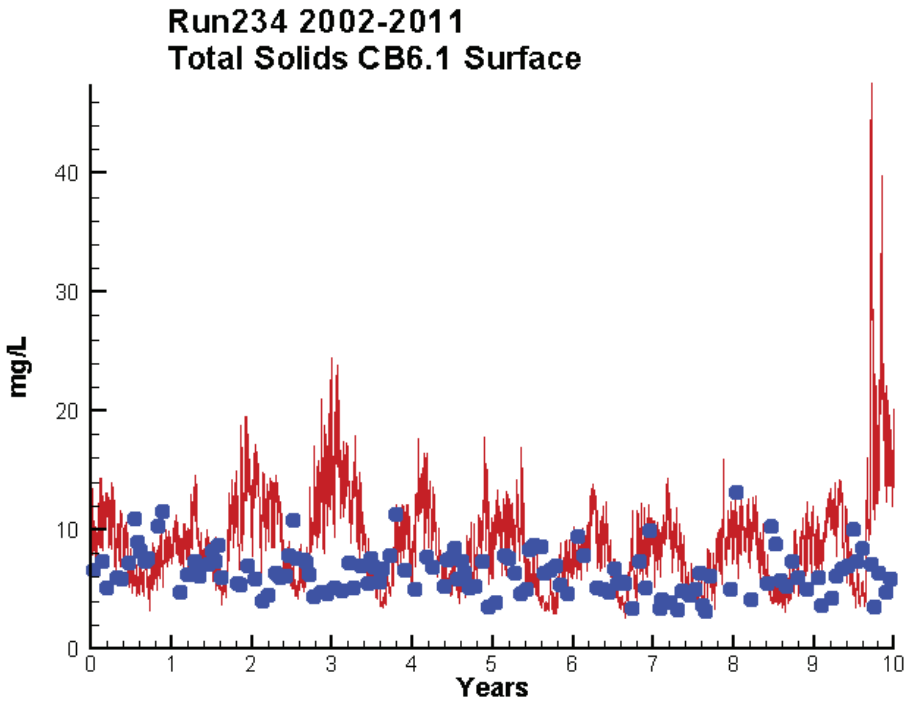

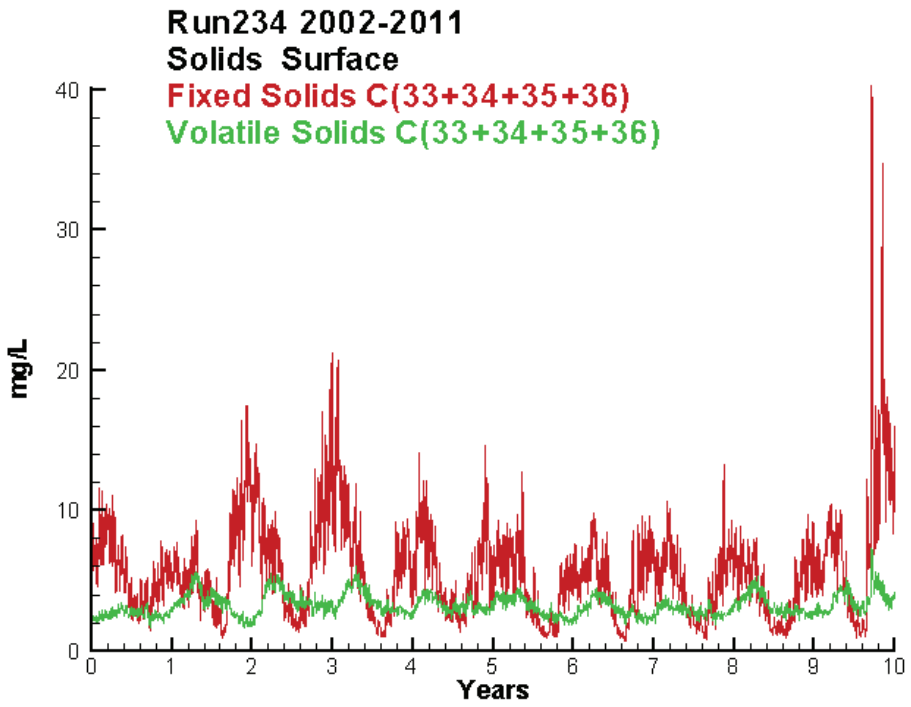

	Mean Difference	Absolute Mean Difference
KE	0.2981	0.3665
TSS	1.6509	3.3753

Station CB7.3

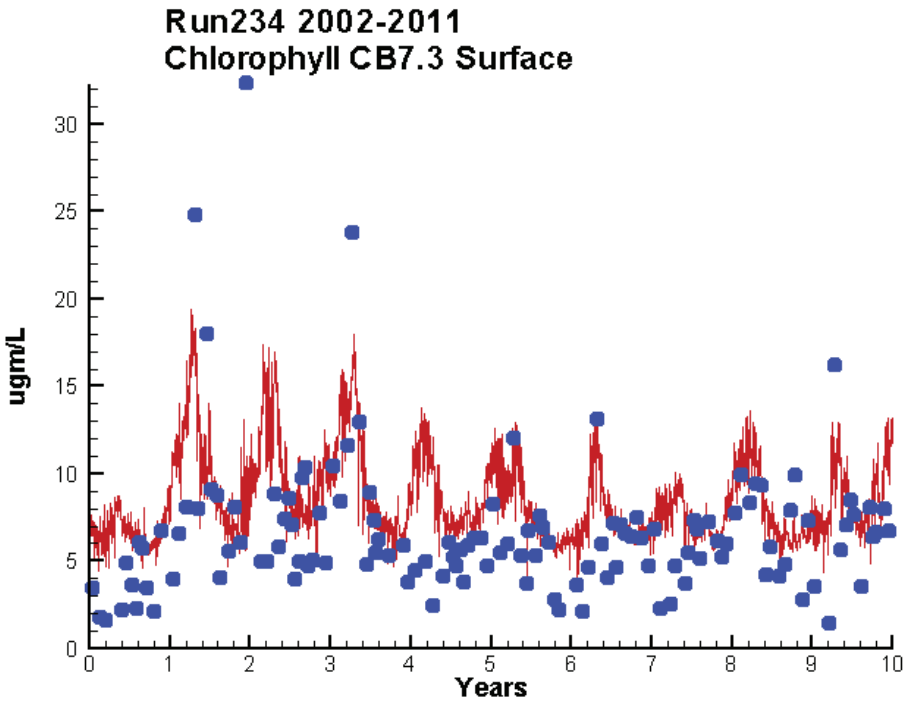

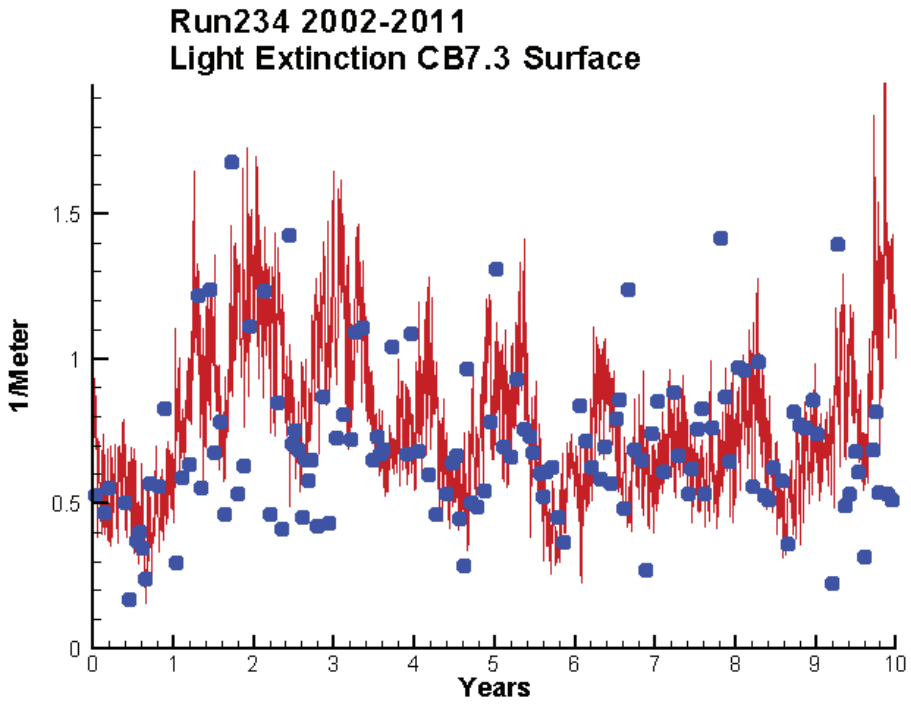

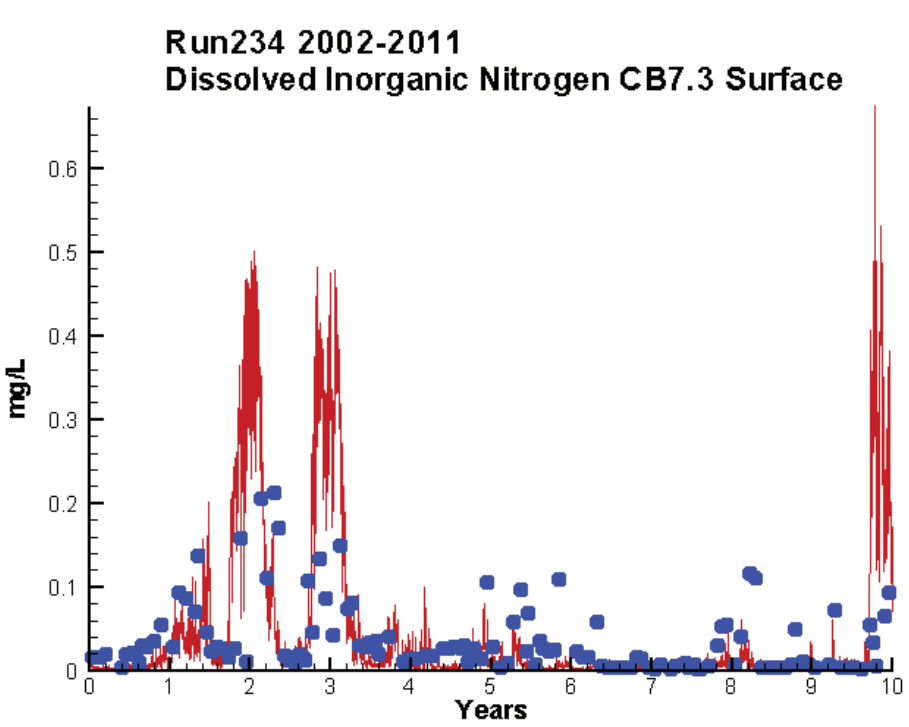

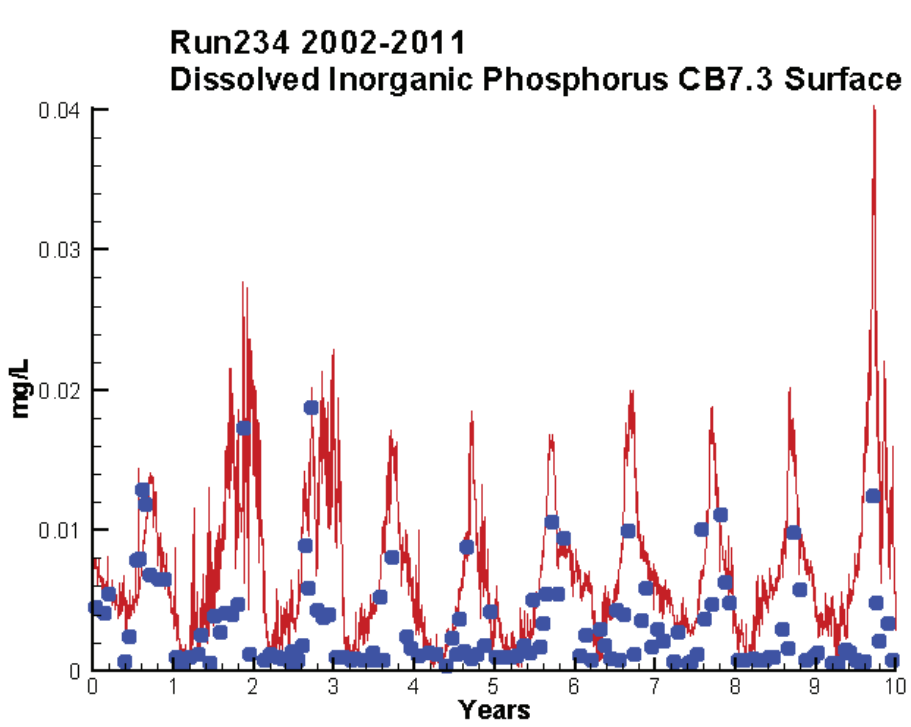

Station CB7.3

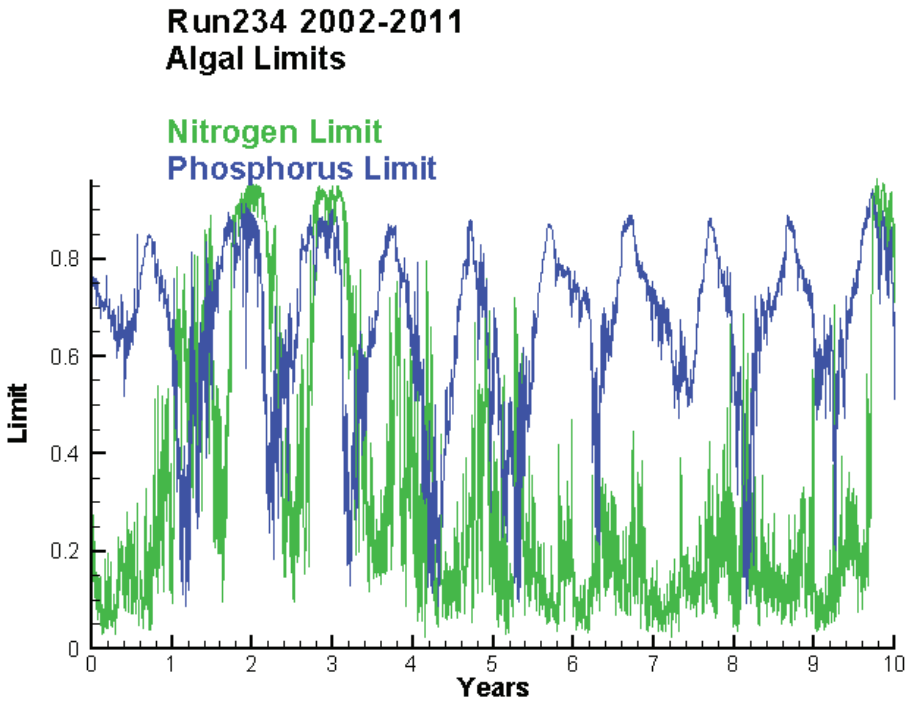

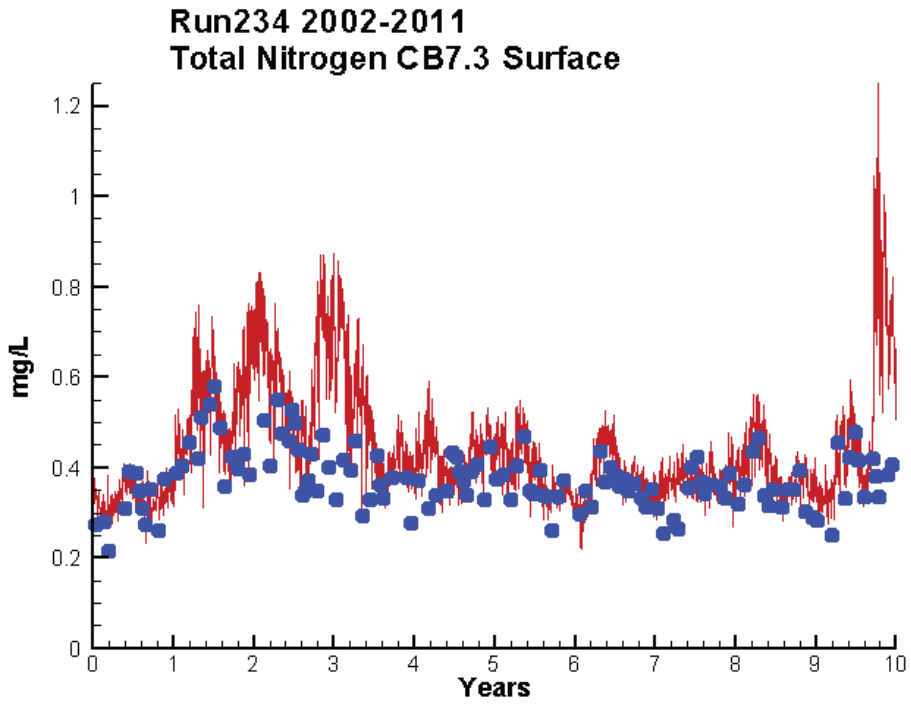

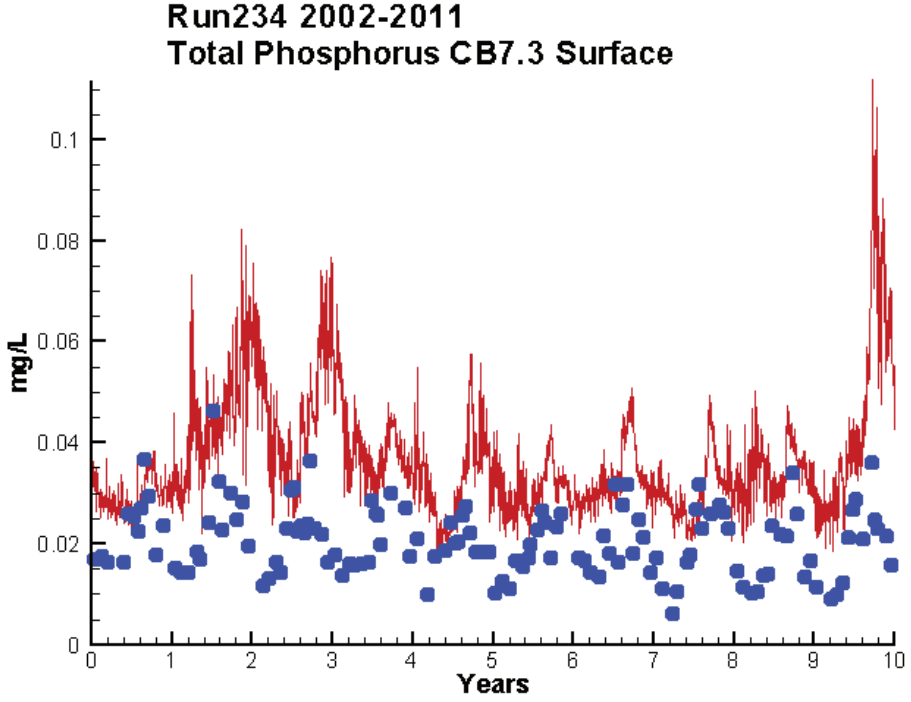

	Mean Difference	Absolute Mean Difference
Chl	1.9769	3.1995
DIN	0.0048	0.0408
KE	0.0962	0.2504
DIP	0.0041	0.0046
TP	0.0162	0.0166
TN	0.0740	0.0878

Station CB7.3

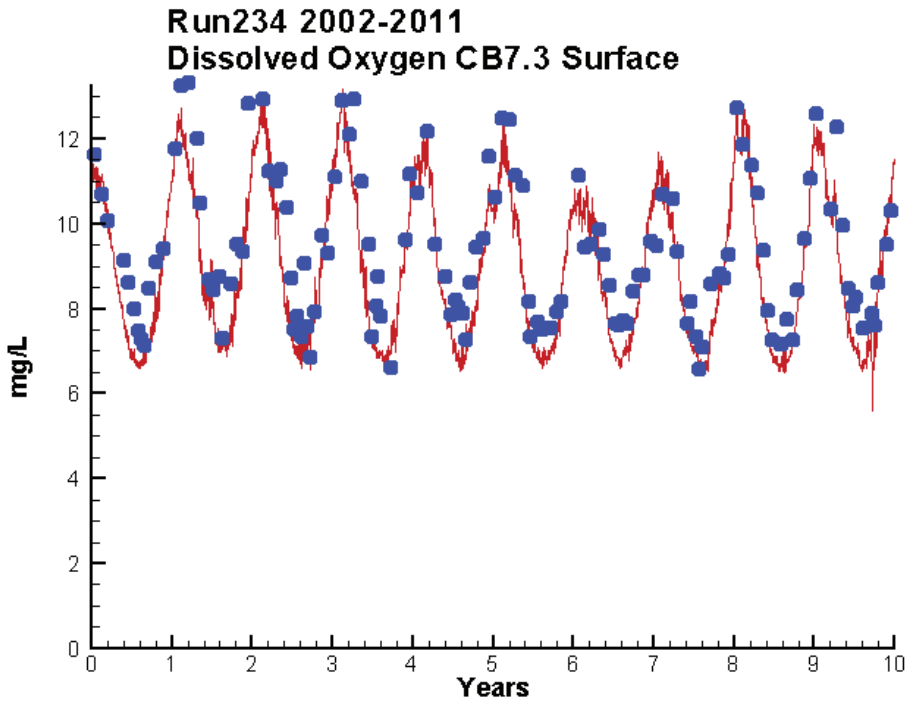

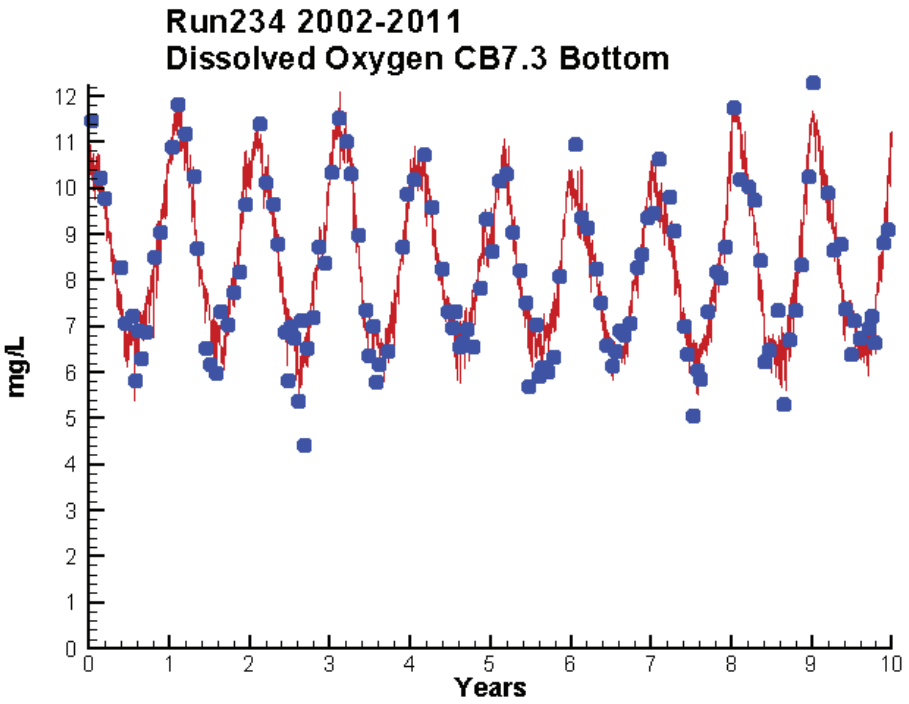

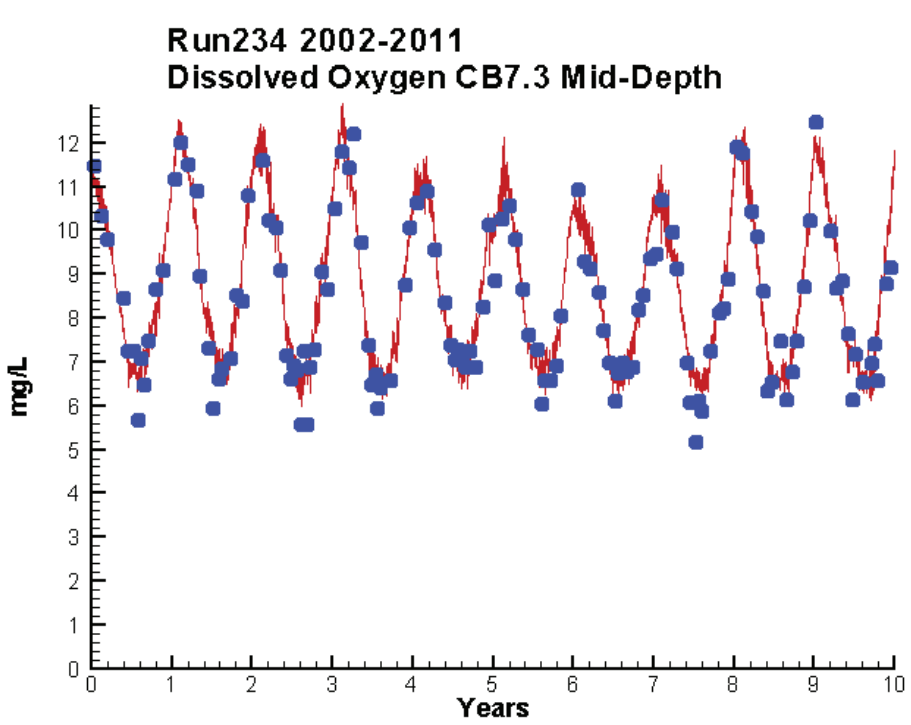

	Mean Difference	Absolute Mean Difference
Top DO	-0.5852	0.7754
Mid DO	0.1932	0.4926
Bot DO	0.0886	0.5646

Station CB7.3

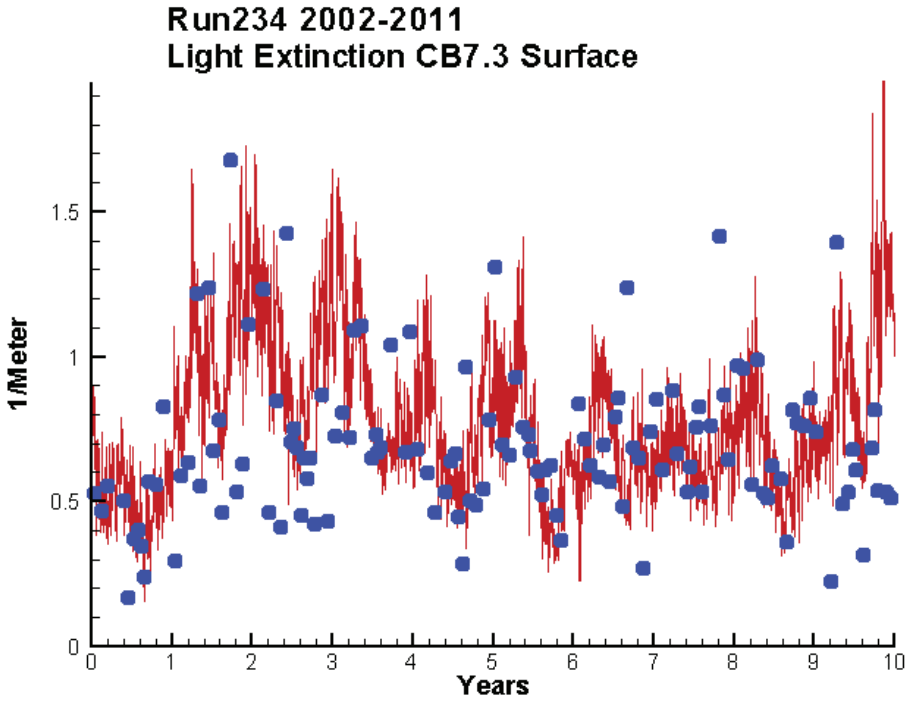

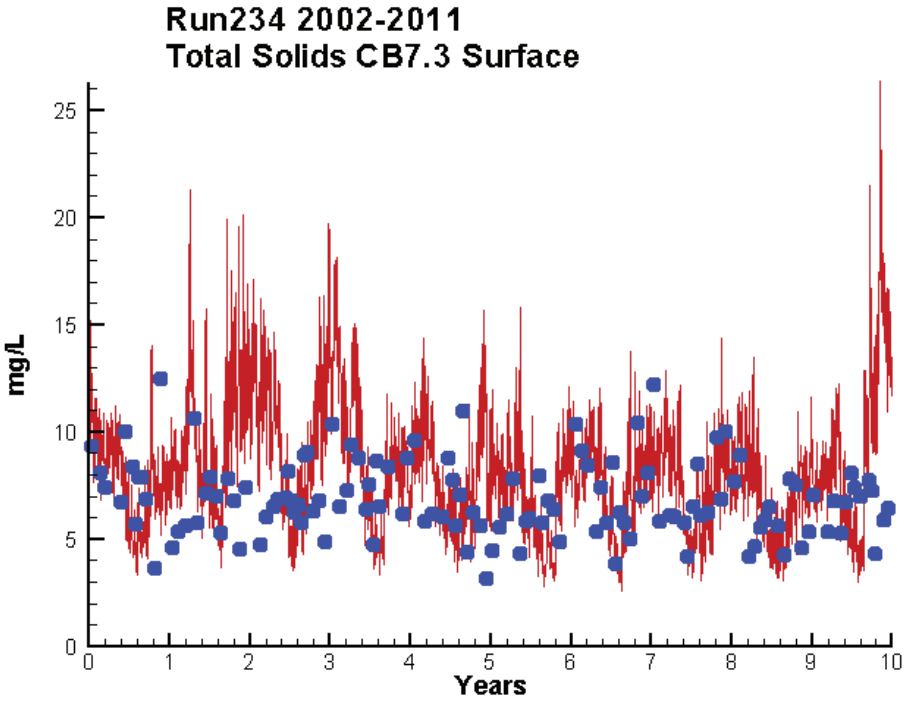

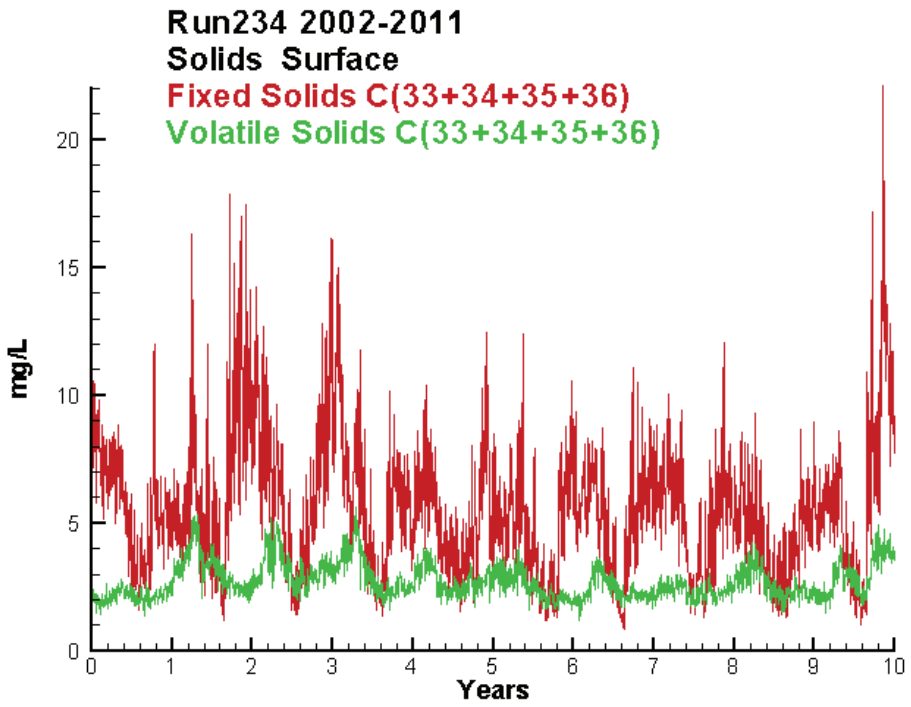

	Mean Difference	Absolute Mean Difference
KE	0.0962	0.2504
TSS	0.7799	2.4362

Station CB7.4

Run234 2002-2011
Chlorophyll CB7.4 Surface

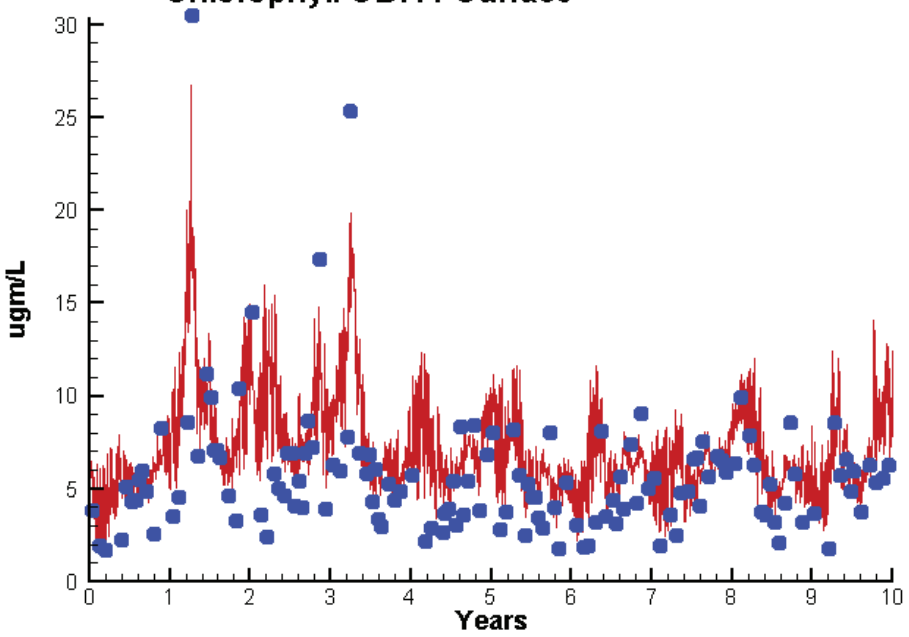

Run234 2002-2011
Light Extinction CB7.4 Surface

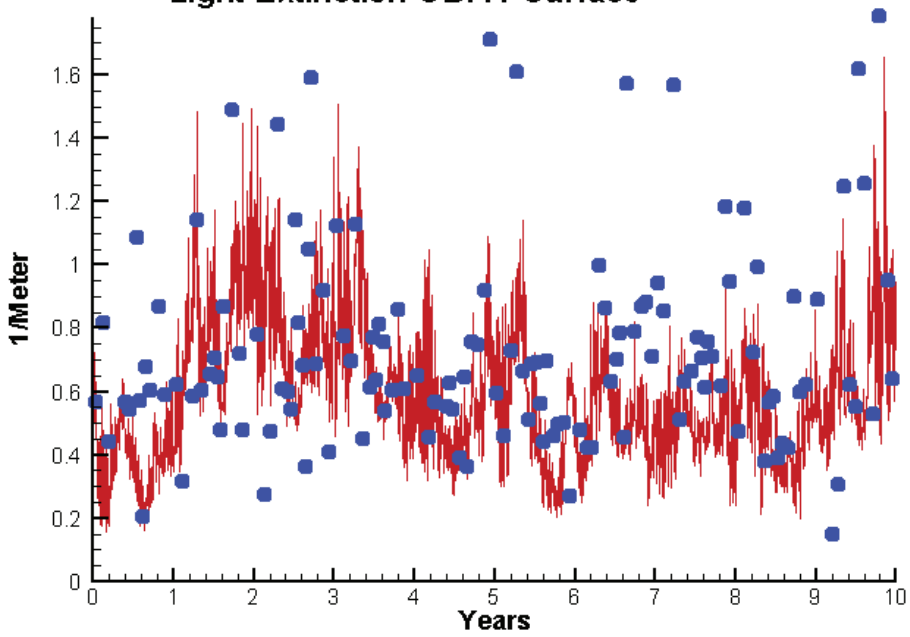

Run234 2002-2011
Dissolved Inorganic Nitrogen CB7.4 Surface

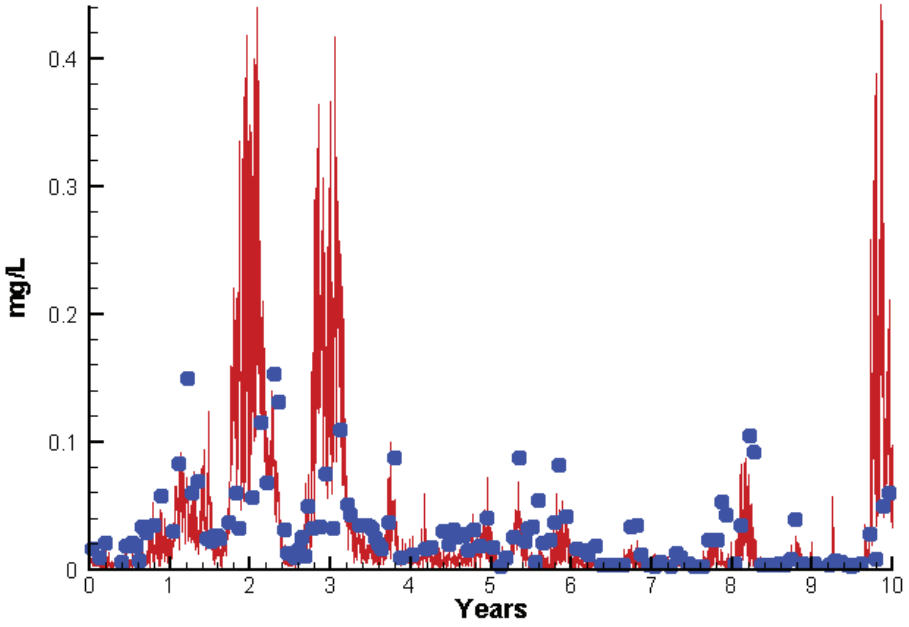

Run234 2002-2011
Dissolved Inorganic Phosphorus CB7.4 Surface

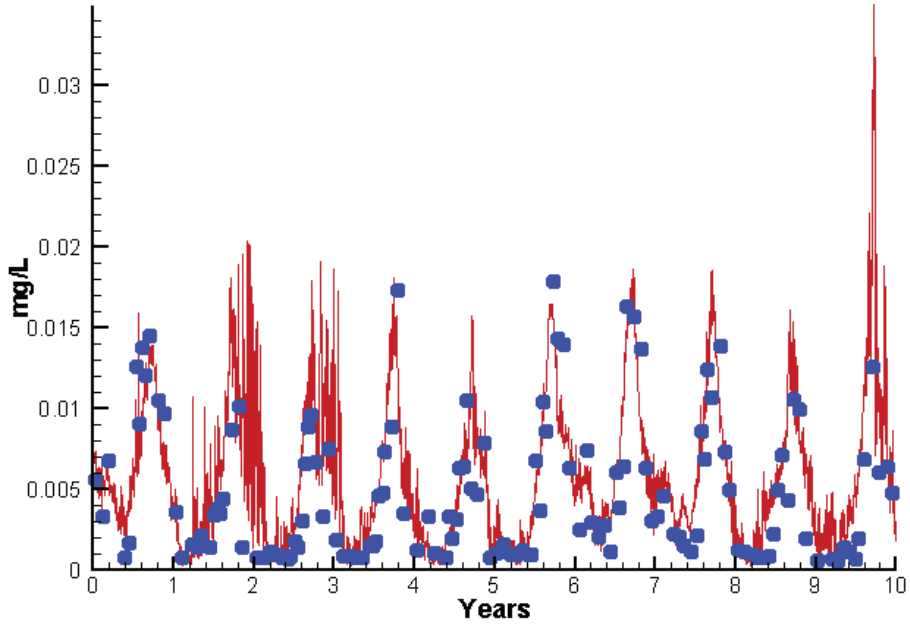

Station CB7.4

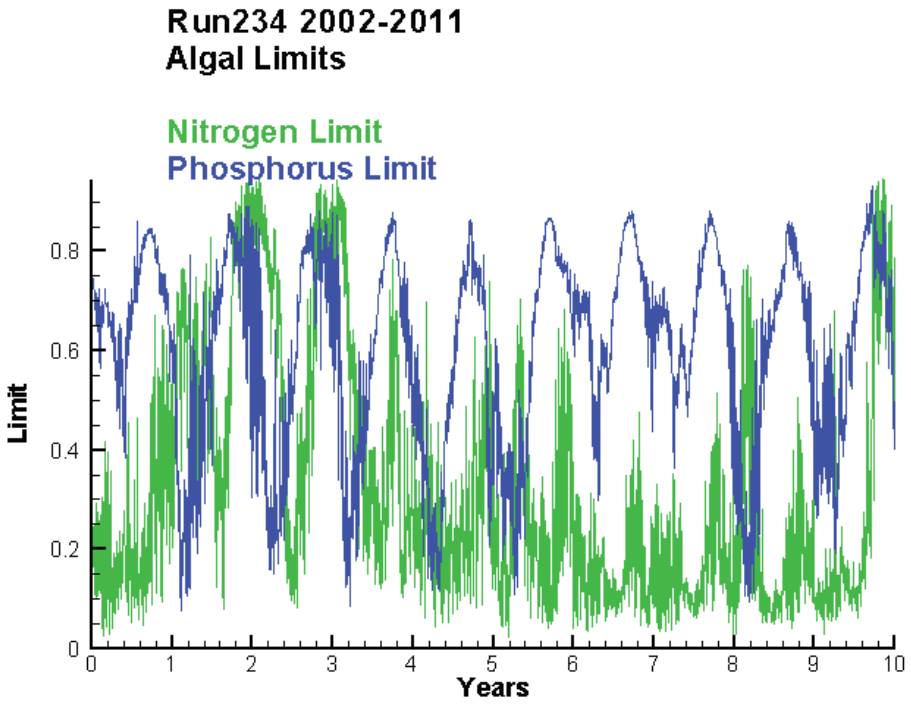

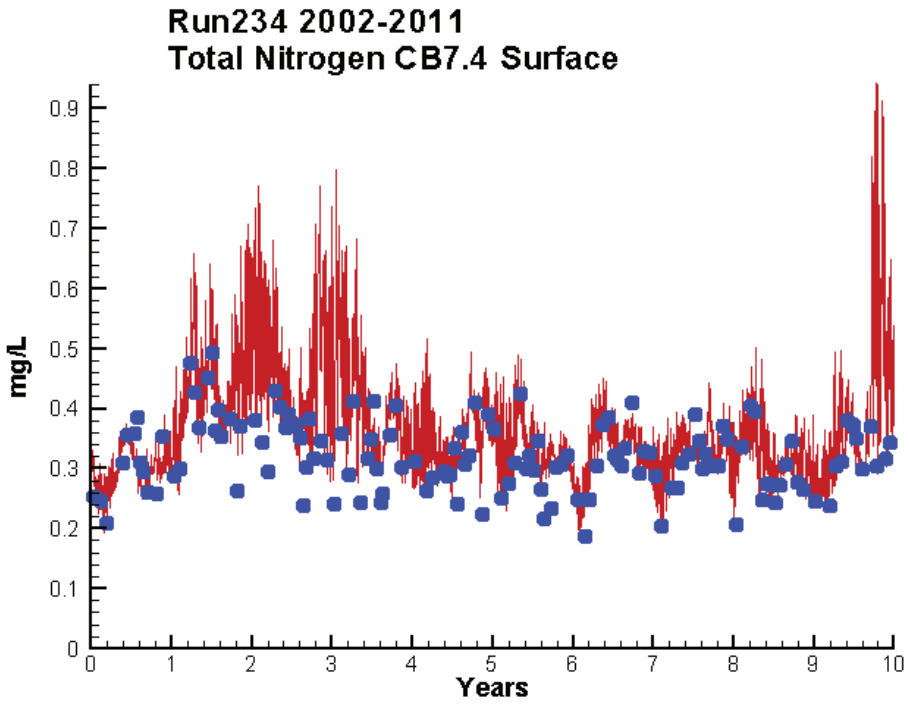

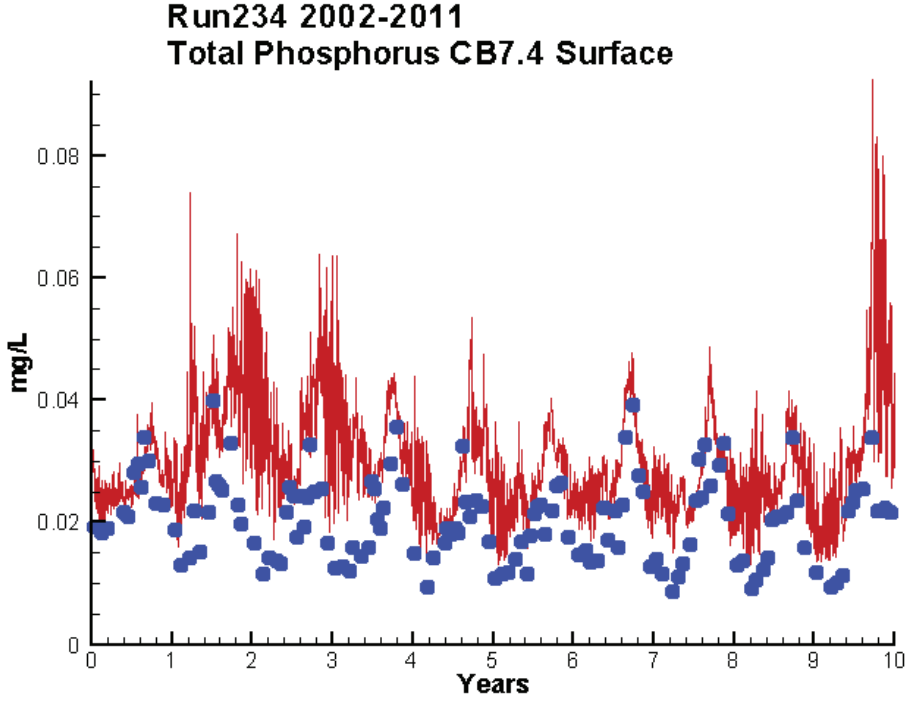

	Mean Difference	Absolute Mean Difference
Chl	1.4230	2.3719
DIN	-0.0041	0.0223
KE	-0.1417	0.2715
DIP	0.0015	0.0026
TP	0.0103	0.0105
TN	0.0481	0.0621

Station CB7.4

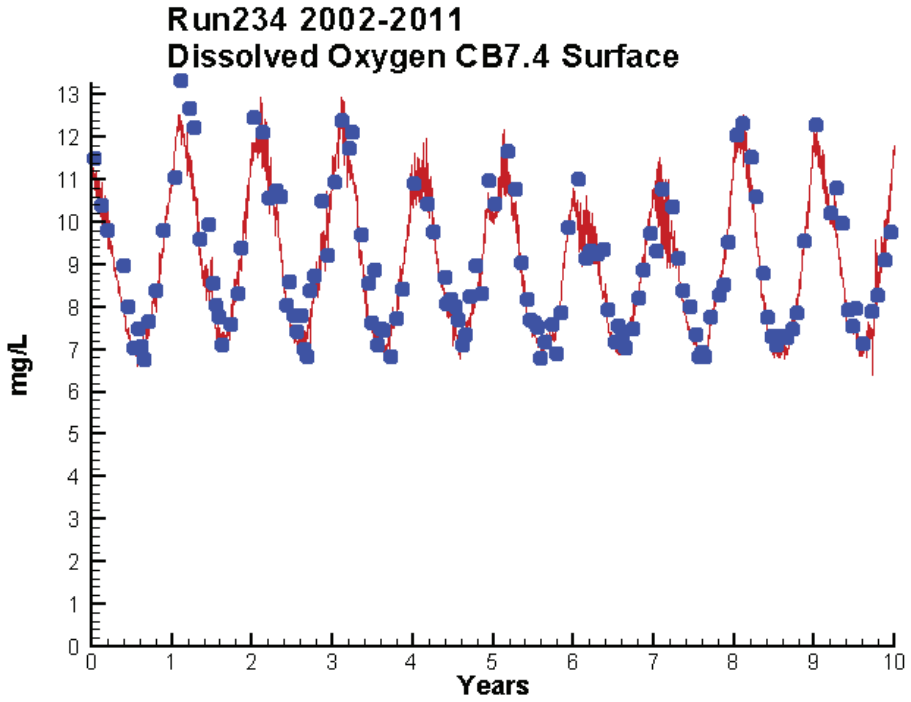

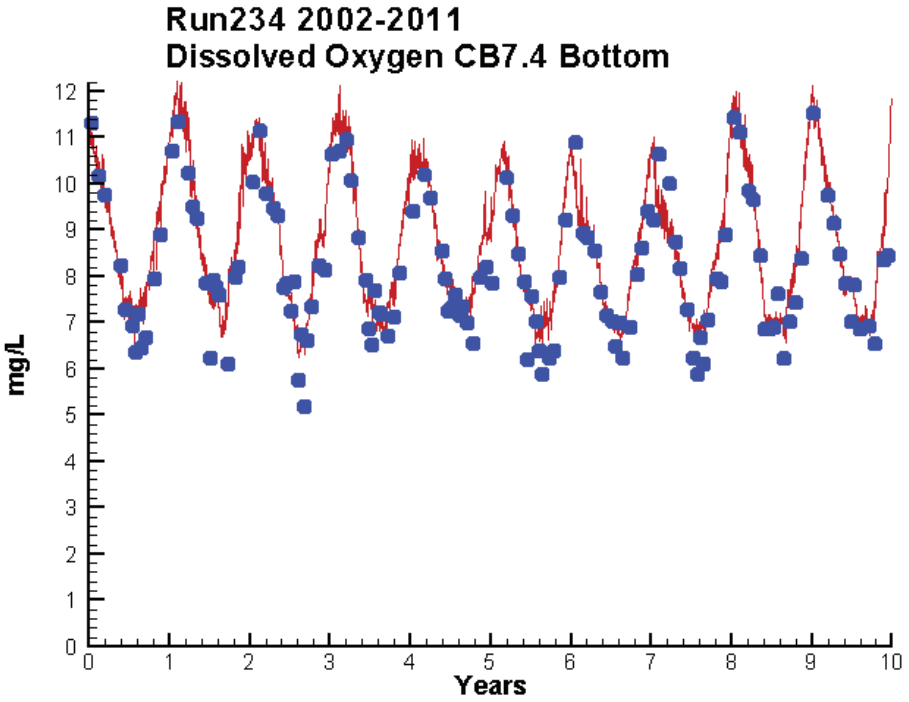

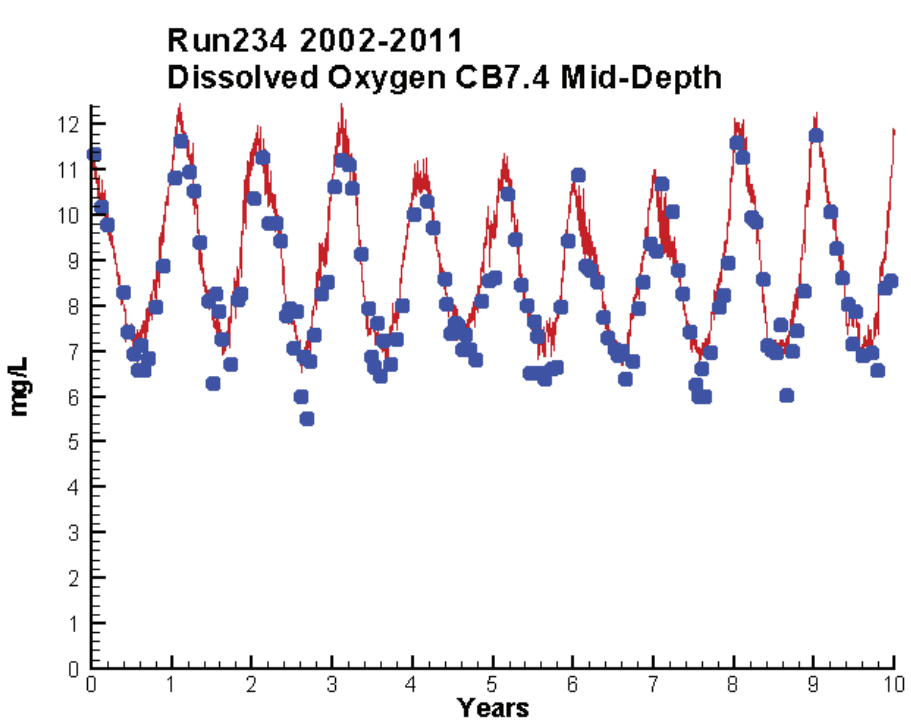

	Mean Difference	Absolute Mean Difference
Top DO	-0.2432	0.5087
Mid DO	0.4067	0.5800
Bot DO	0.3702	0.5619

Station CB7.4

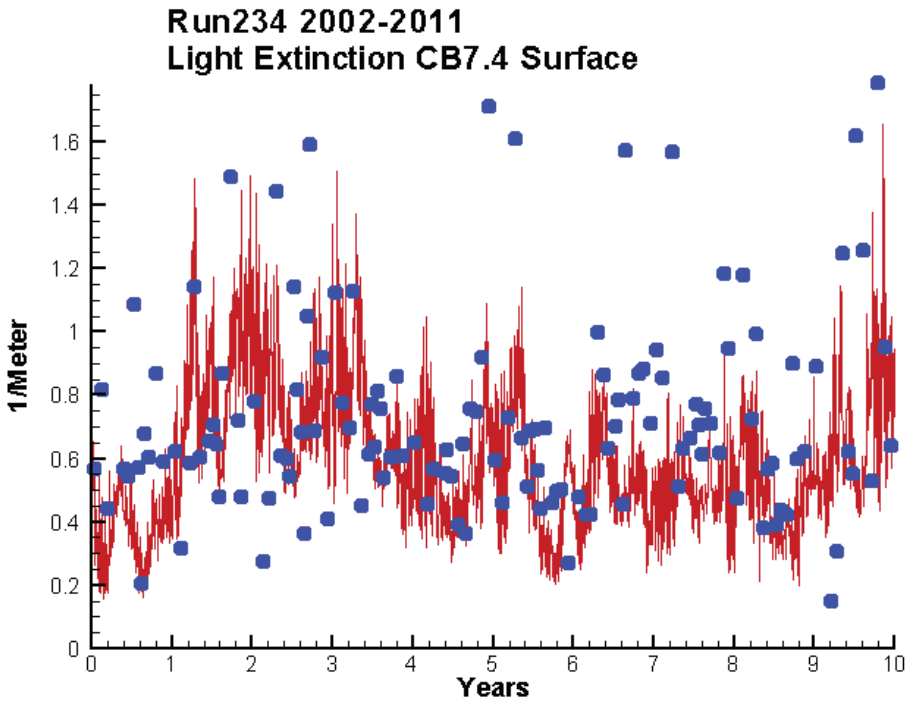

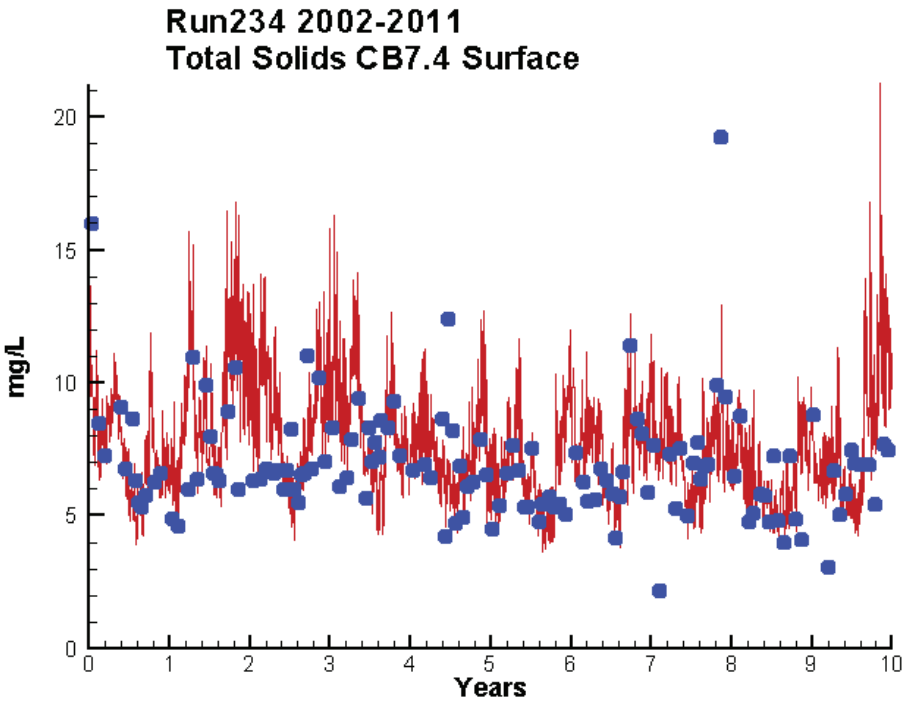

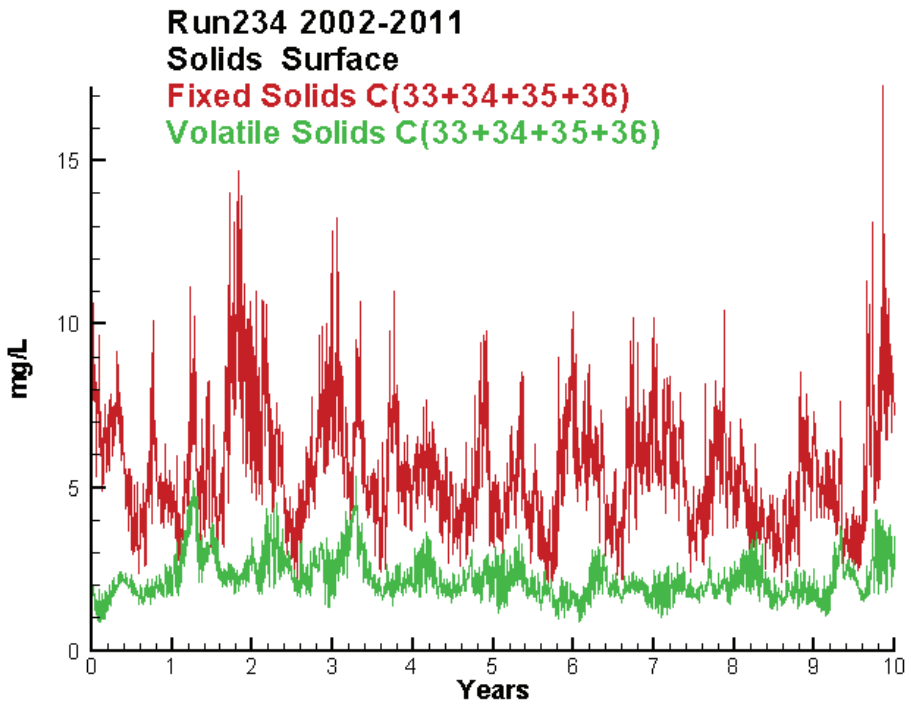

	Mean Difference	Absolute Mean Difference
KE	-0.1417	0.2715
TSS	0.5188	1.6580

Station CB7.4N

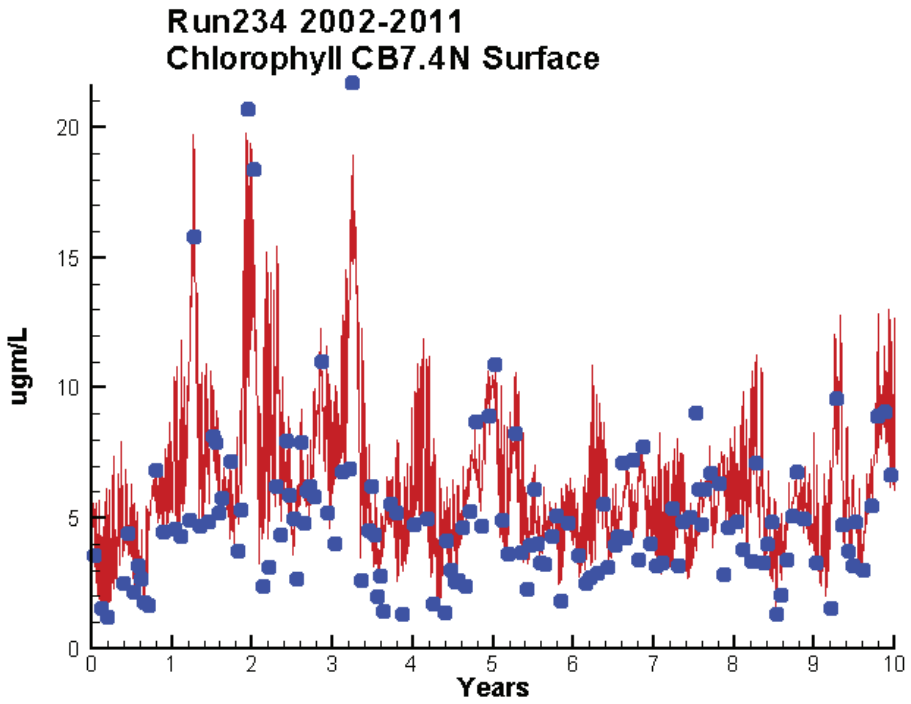

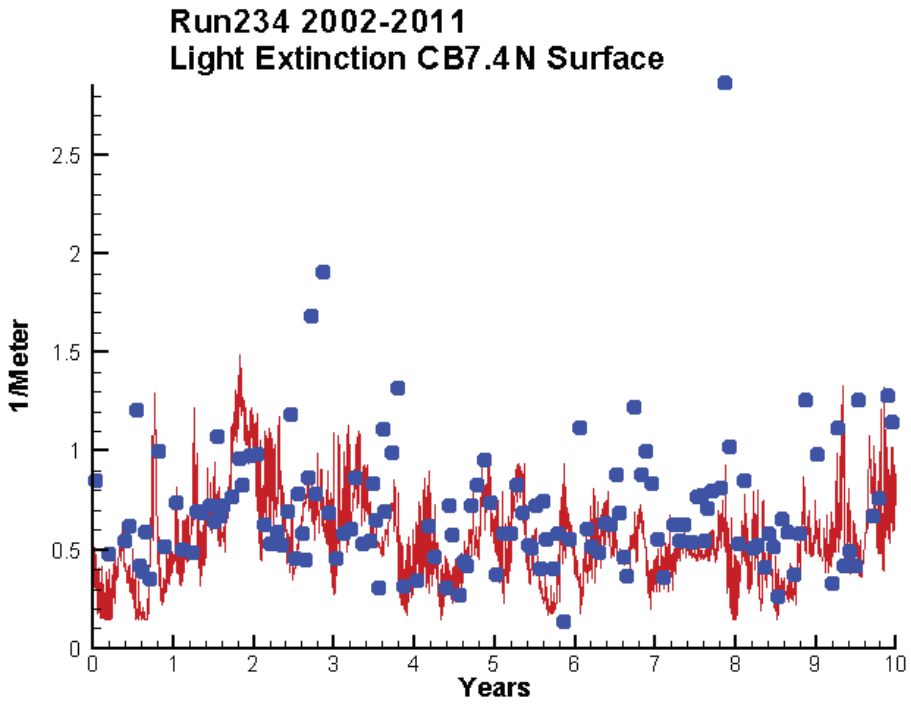

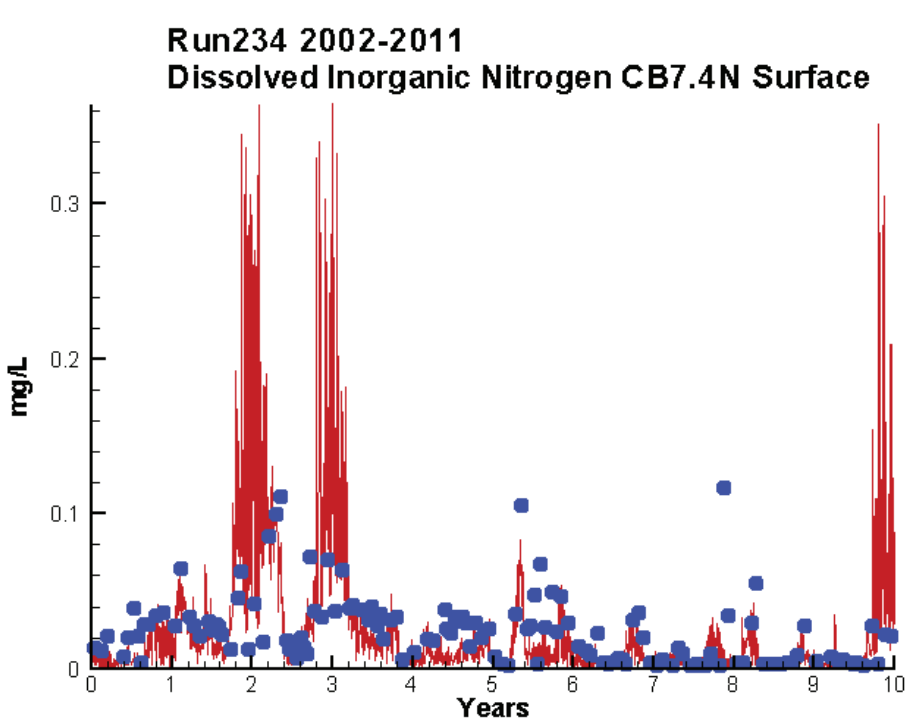

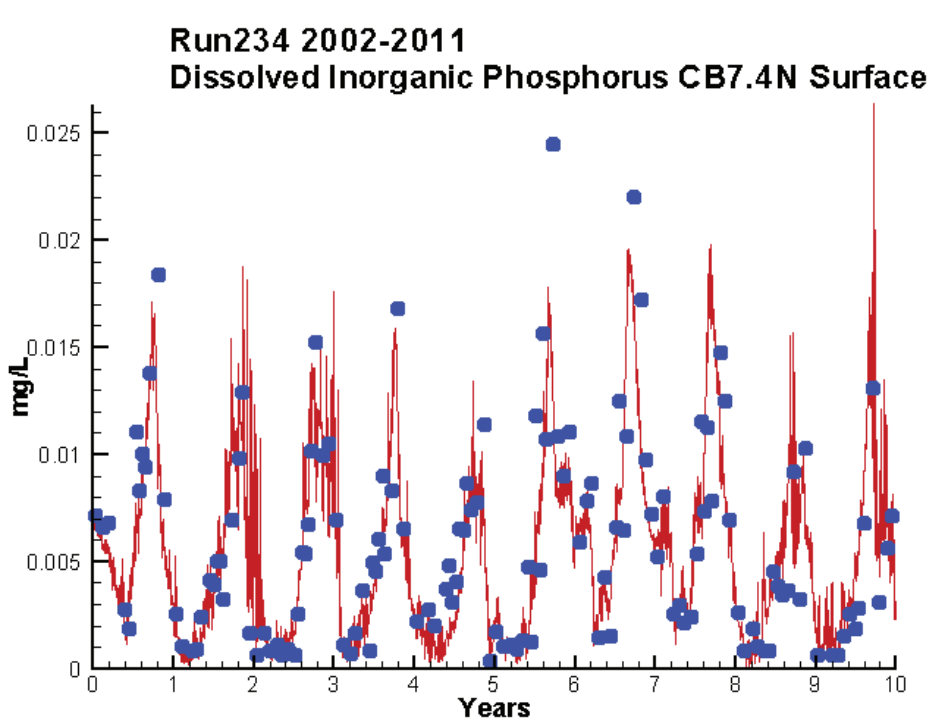

Station CB7.4N

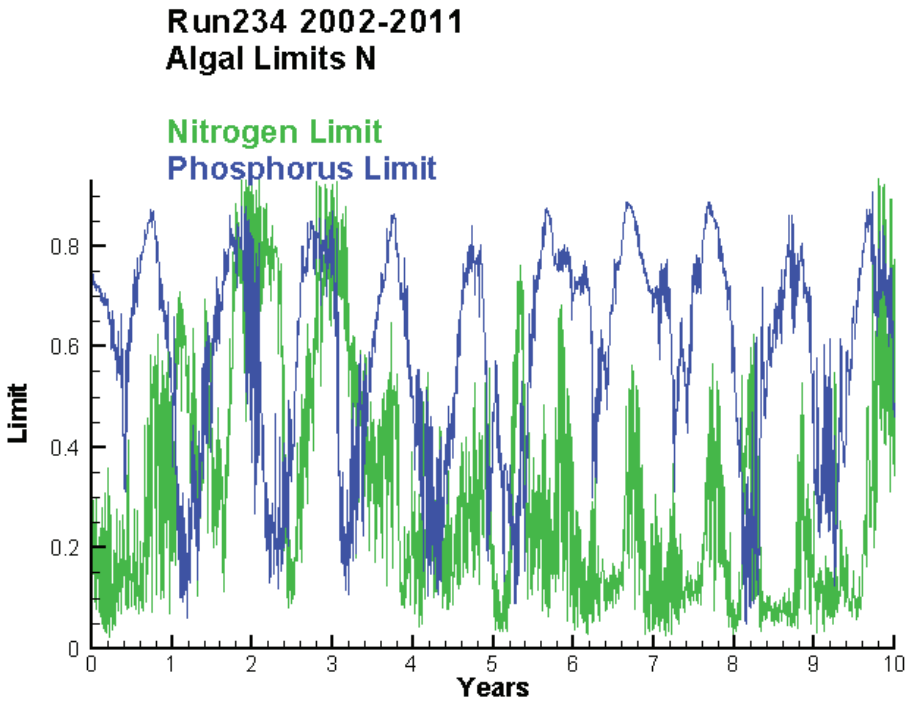

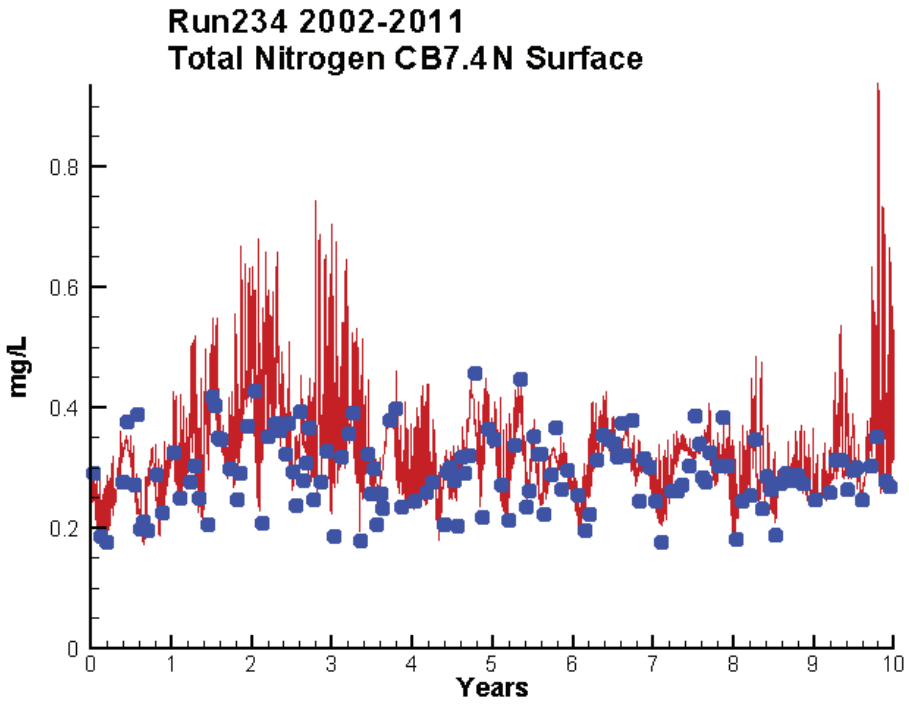

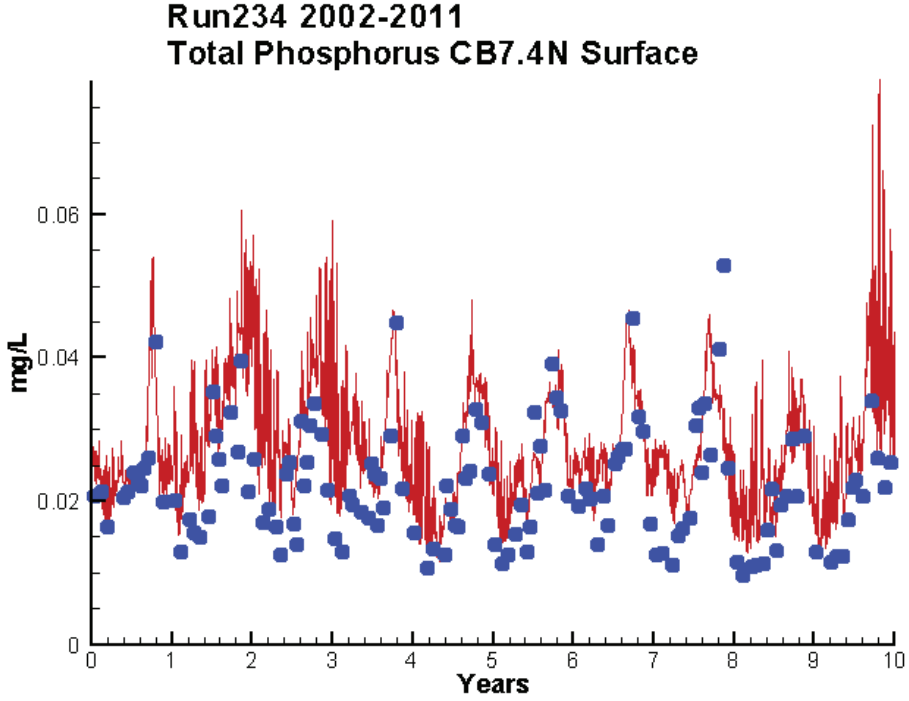

	Mean Difference	Absolute Mean Difference
Chl	1.1009	1.9498
DIN	-0.0030	0.0171
KE	-0.1487	0.2682
DIP	0.0001	0.0024
TP	0.0062	0.0076
TN	0.0365	0.0572

Station CB7.4N

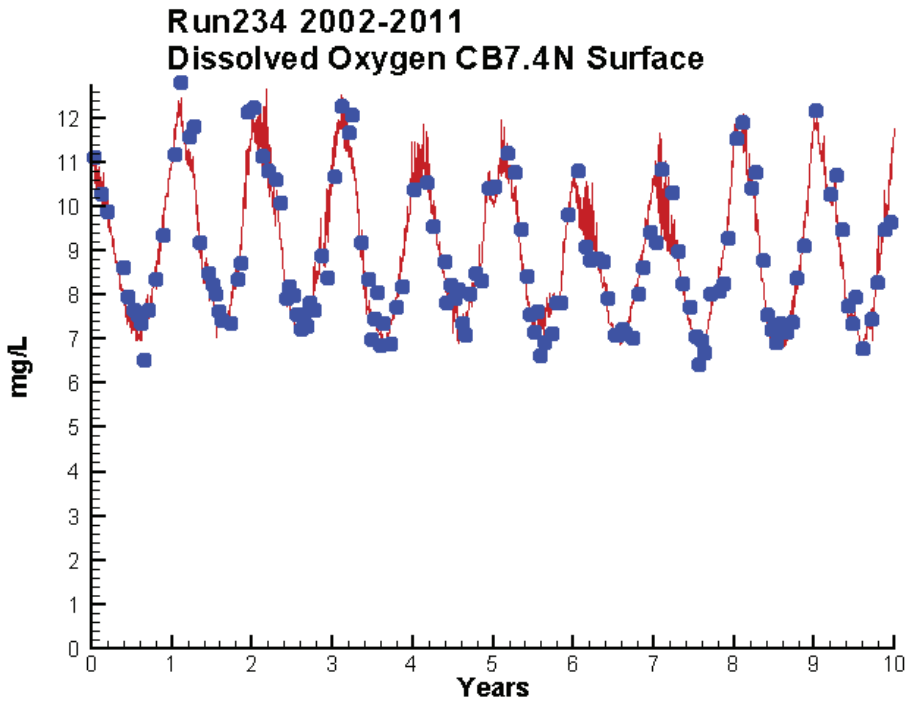

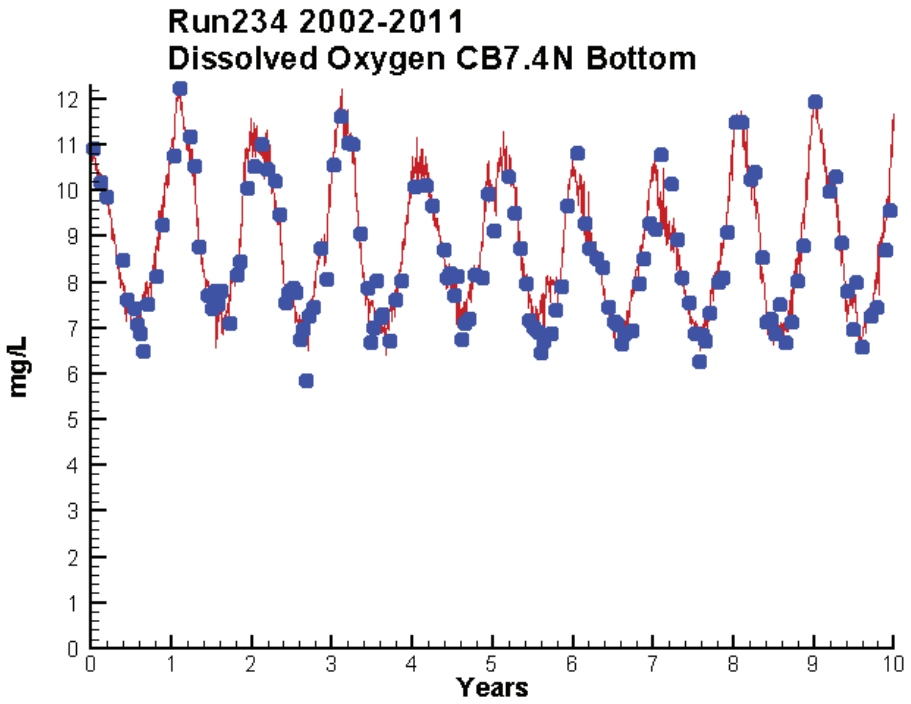

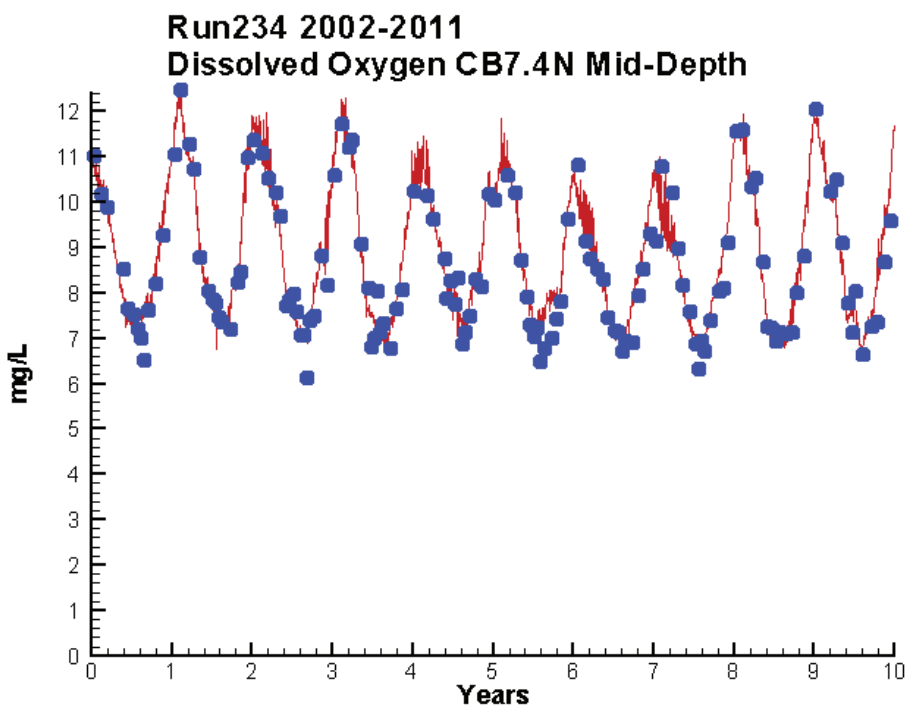

	Mean Difference	Absolute Mean Difference
Top DO	-0.0572	0.4295
Mid DO	0.1386	0.4166
Bot DO	0.1412	0.4265

Station CB7.4N

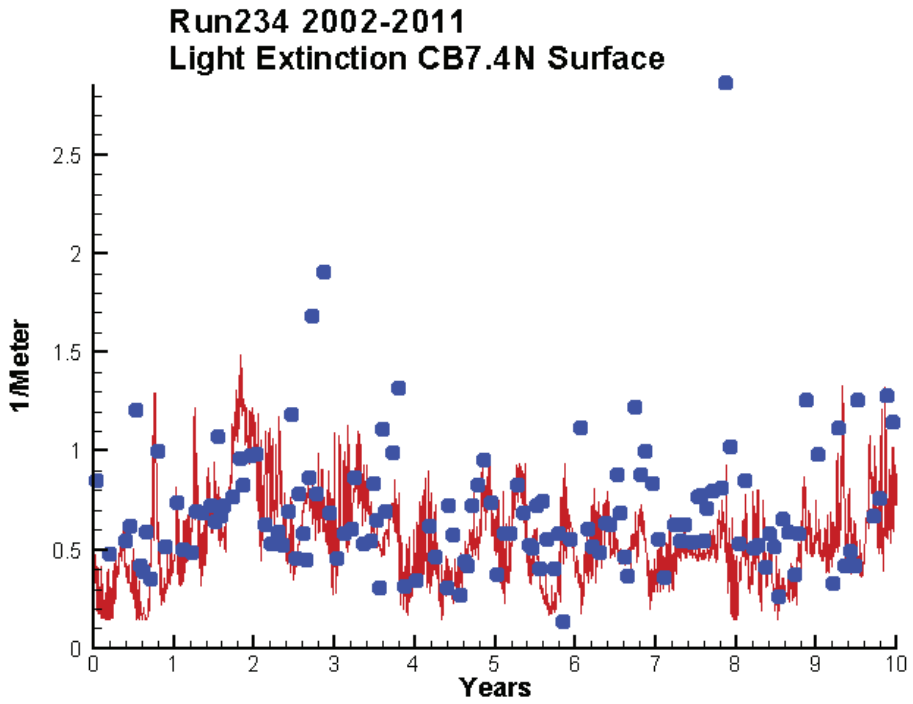

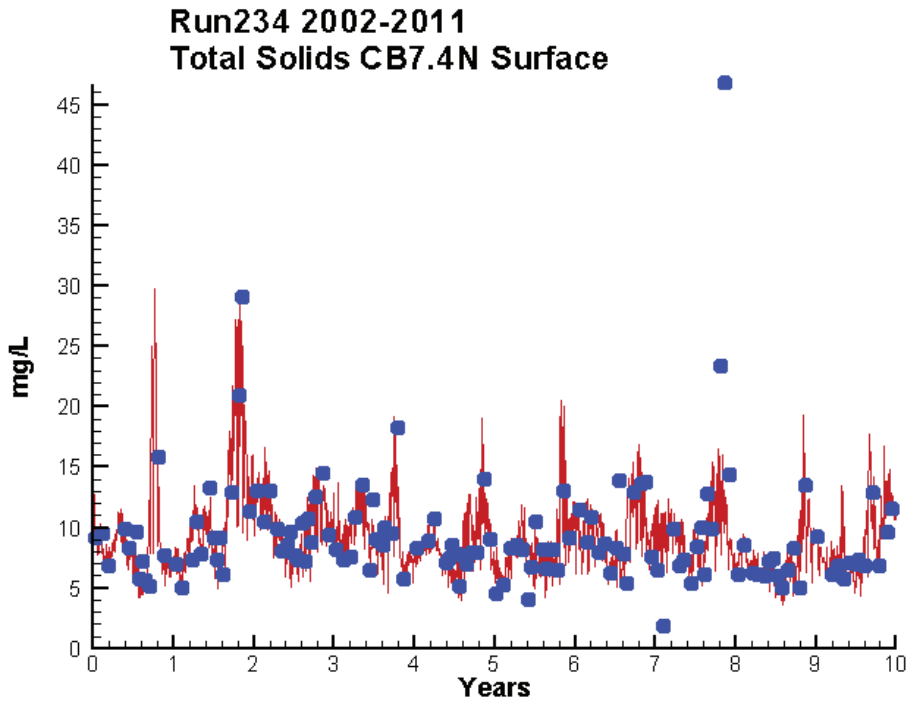

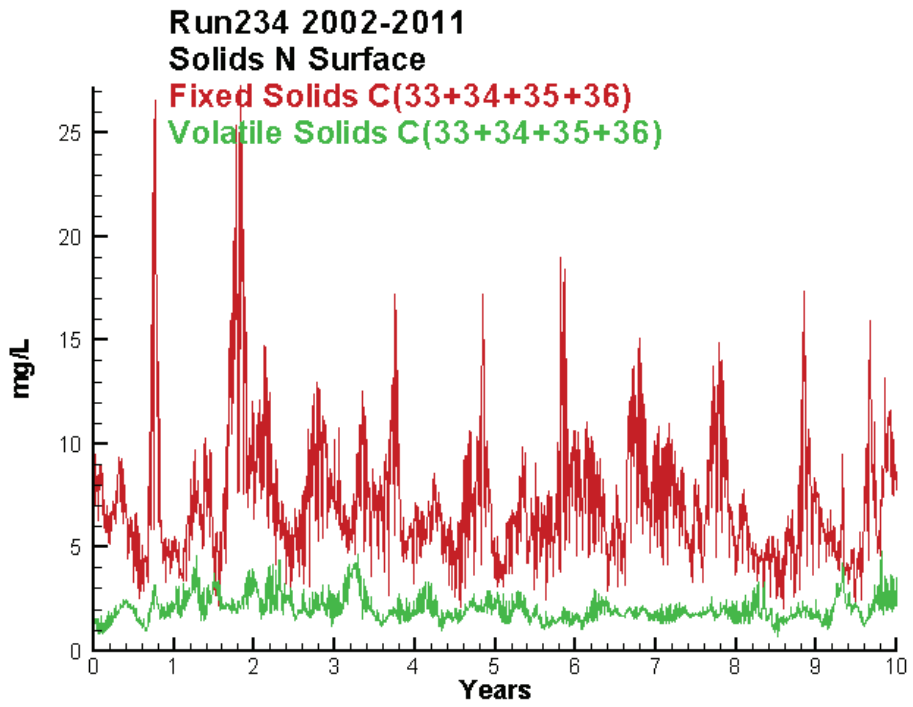

	Mean Difference	Absolute Mean Difference
KE	-0.1487	0.2682
TSS	-0.2023	2.2250

Station CB8.1E

Run234 2002-2011
Chlorophyll CB8.1E Surface

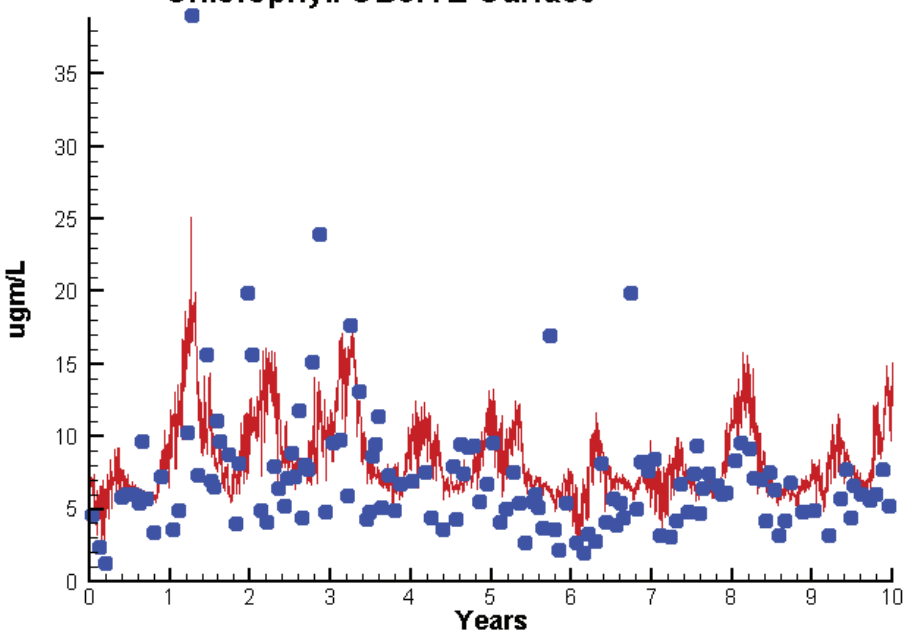

Run234 2002-2011
Light Extinction CB8.1E Surface

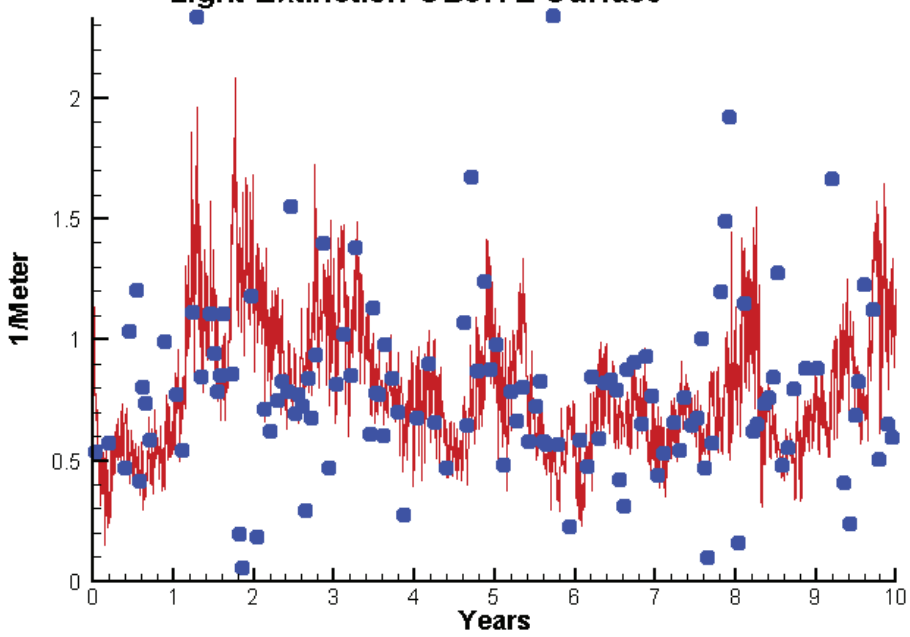

Run234 2002-2011
Dissolved Inorganic Nitrogen CB8.1E Surface

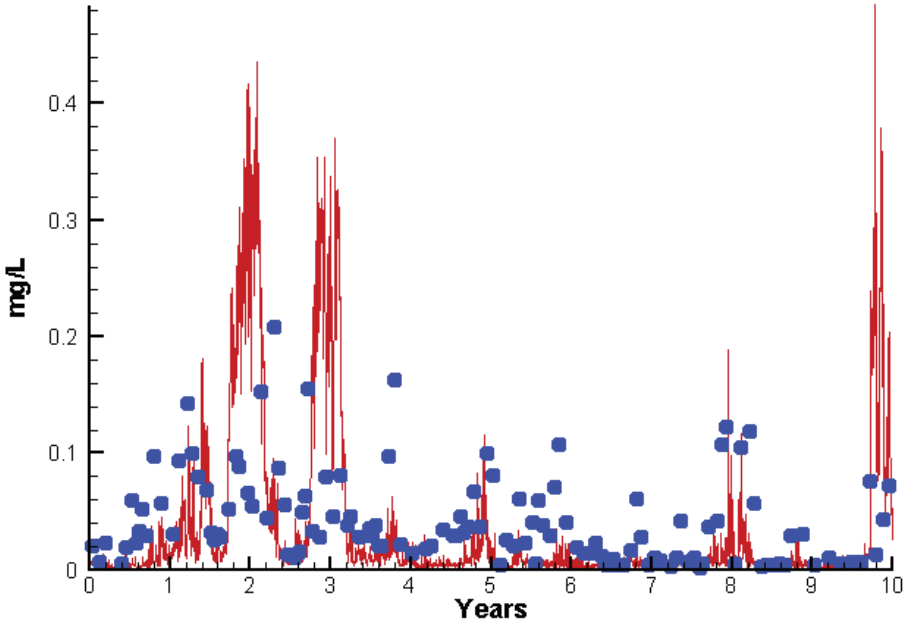

Run234 2002-2011
Dissolved Inorganic Phosphorus CB8.1E Surface

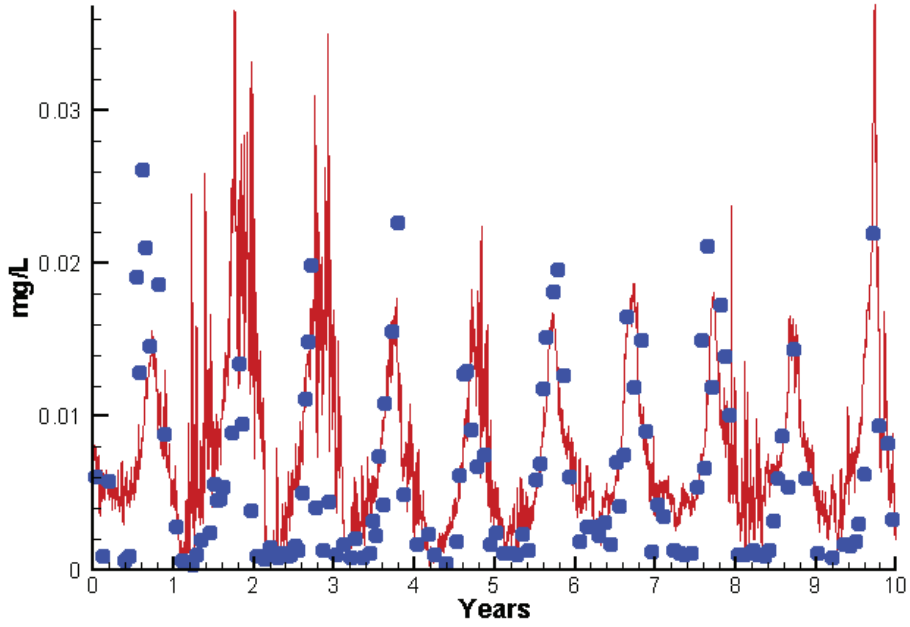

Station CB8.1E

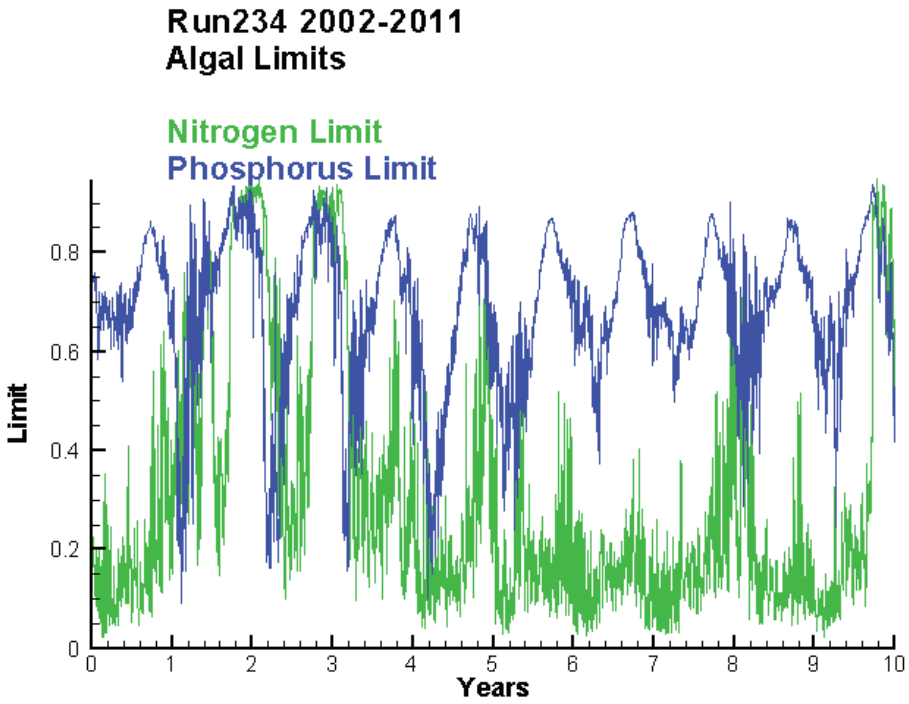

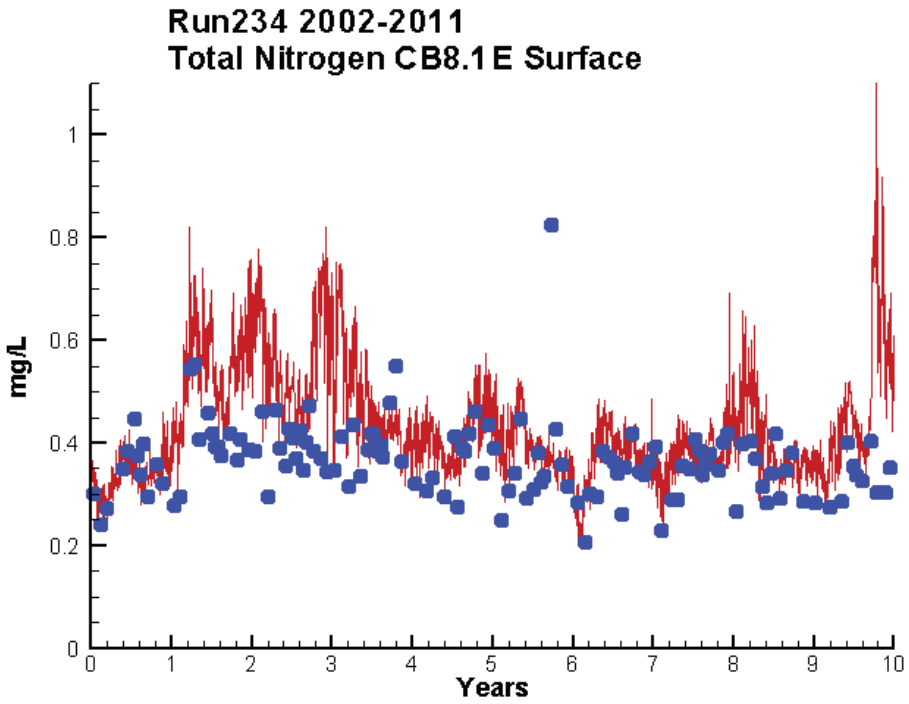

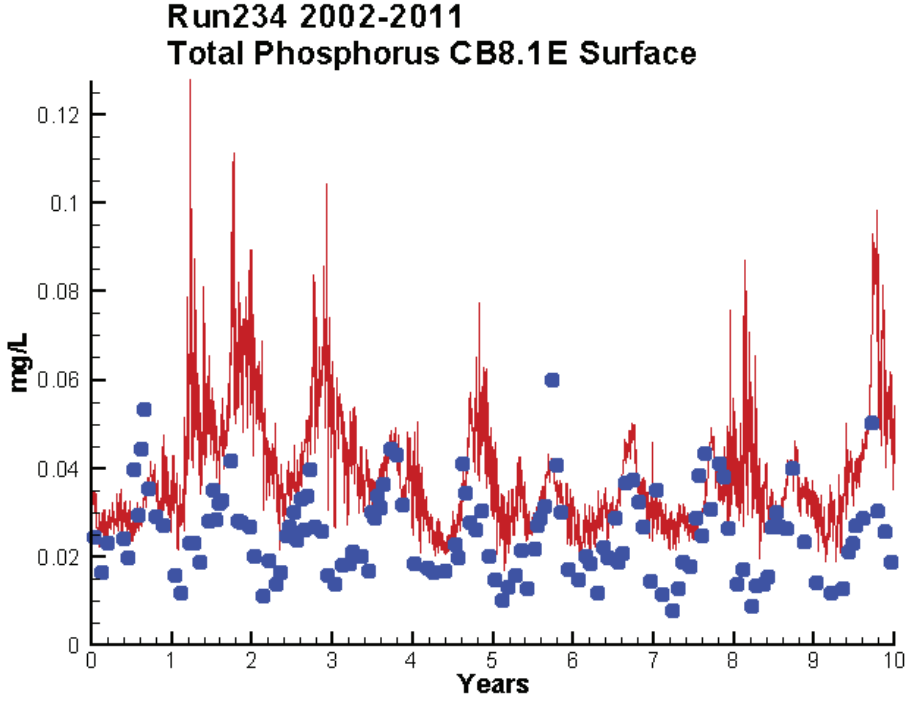

	Mean Difference	Absolute Mean Difference
Chl	1.3635	3.2028
DIN	-0.0091	0.0385
KE	0.0449	0.3120
DIP	0.0020	0.0043
TP	0.0140	0.0158
TN	0.0756	0.0953

Station CB8.1E

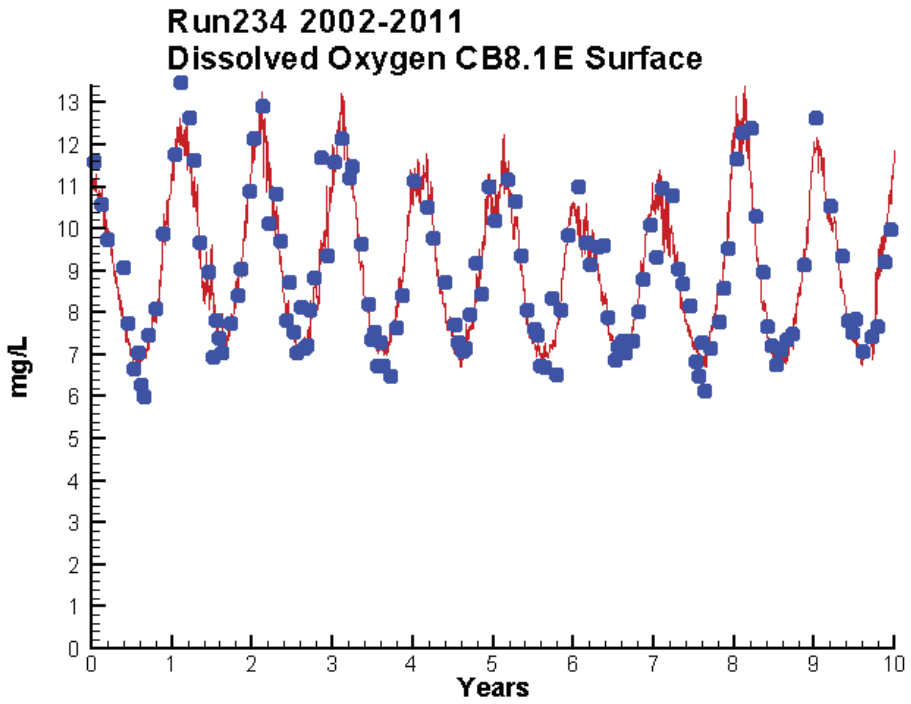

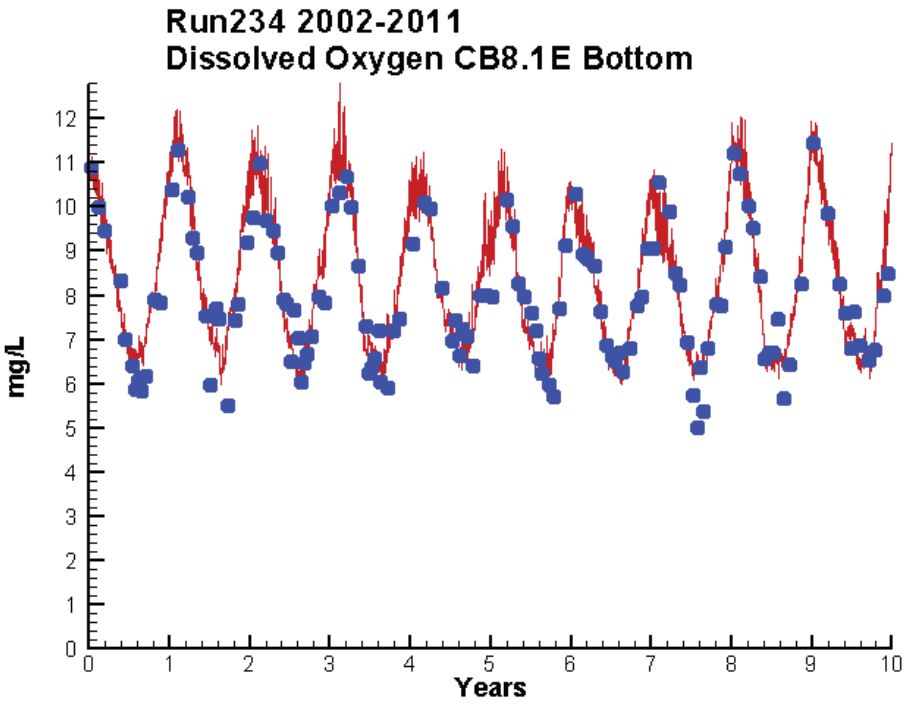

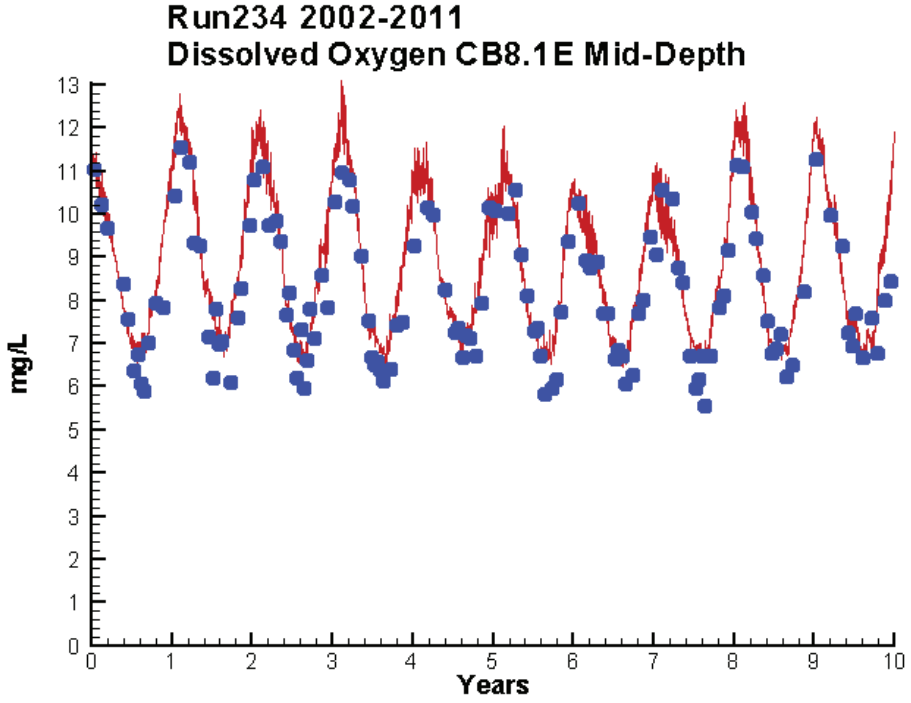

	Mean Difference	Absolute Mean Difference
Top DO	-0.0339	0.5173
Mid DO	0.4885	0.6578
Bot DO	0.2039	0.5901

Station CB8.1E

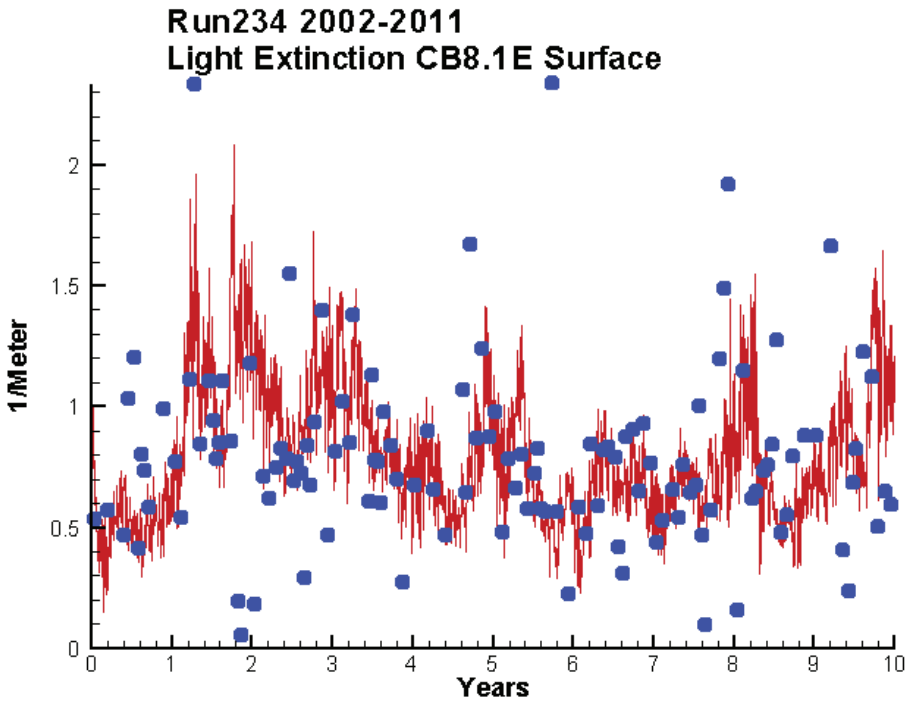

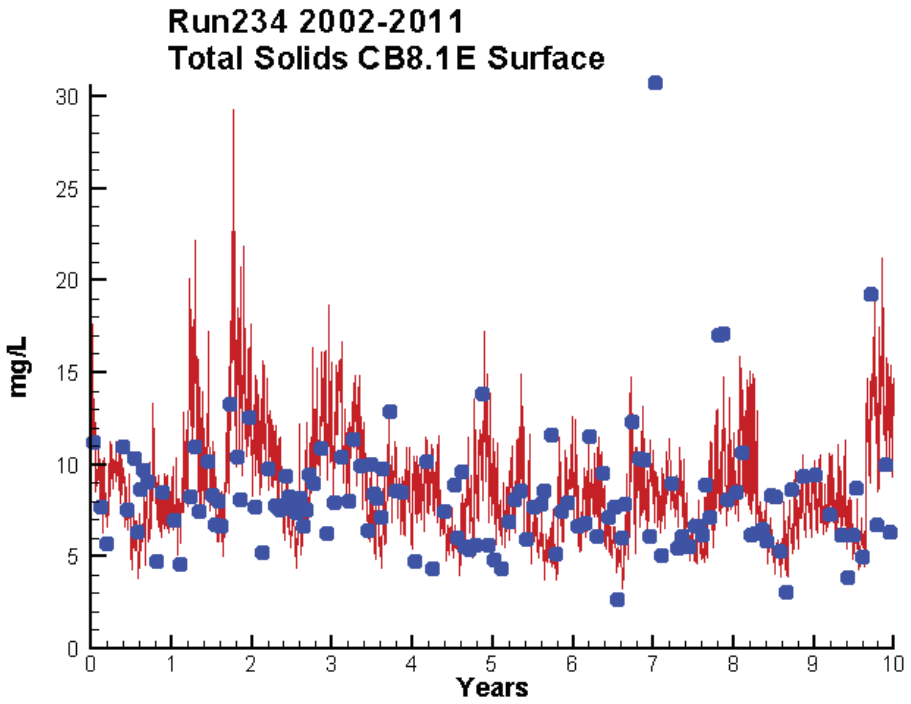

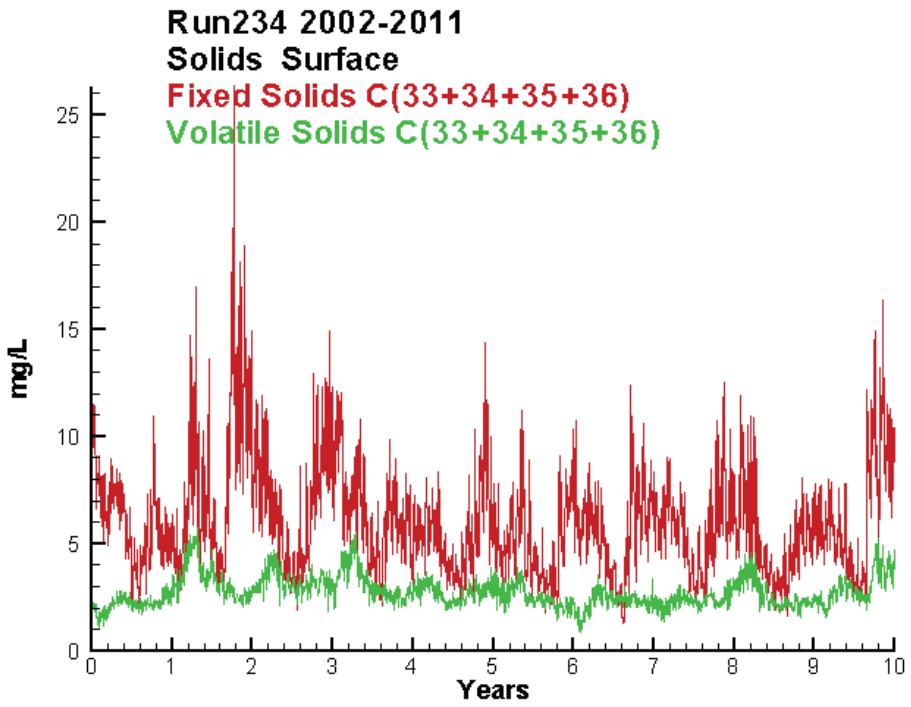

	Mean Difference	Absolute Mean Difference
KE	0.0449	0.3120
TSS	0.2590	2.4117

Station EE3.2

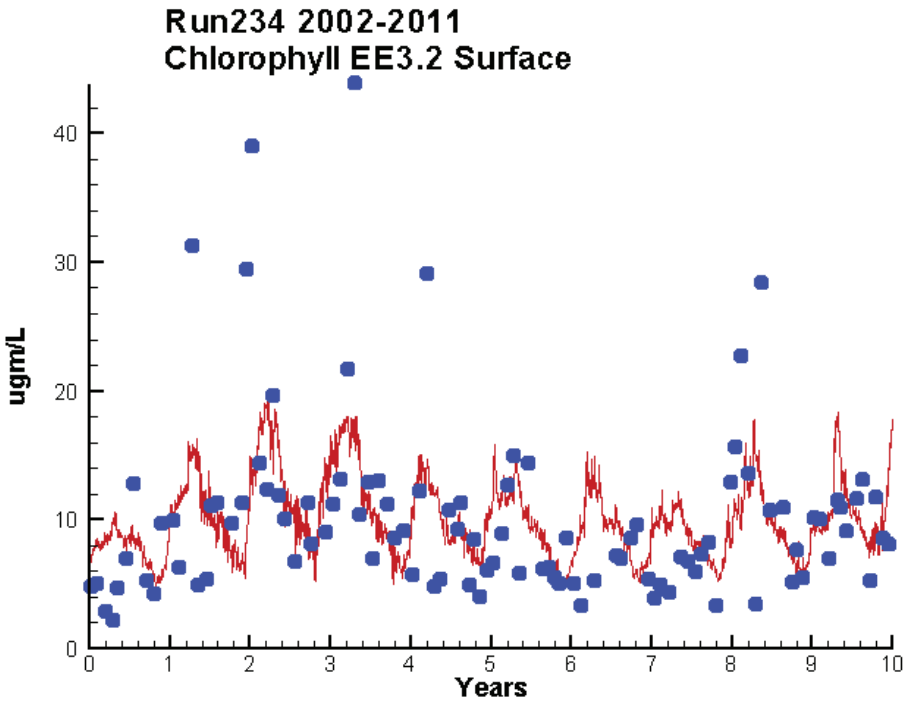

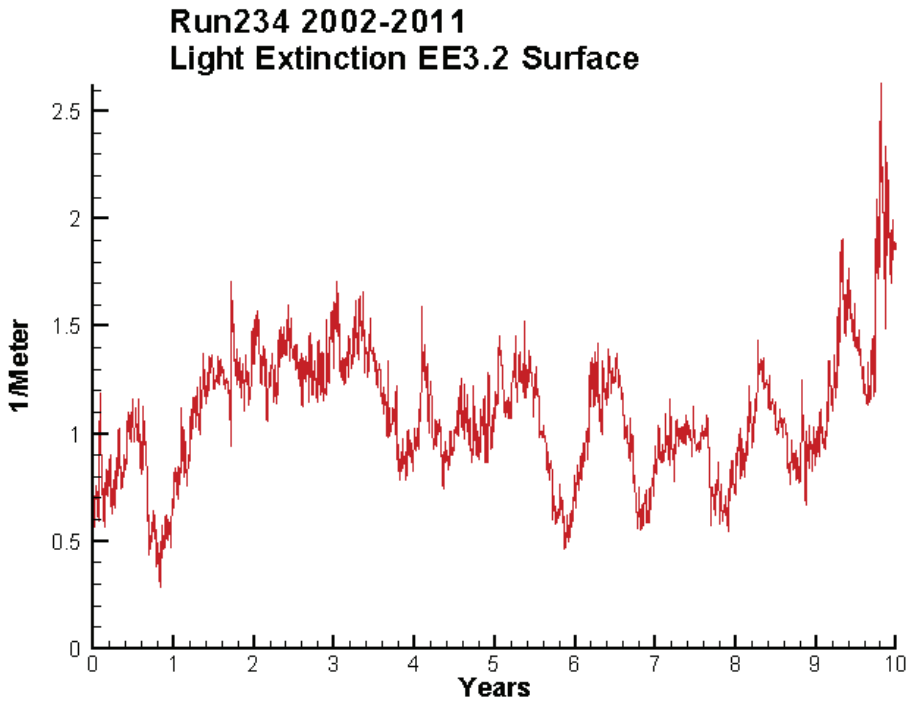

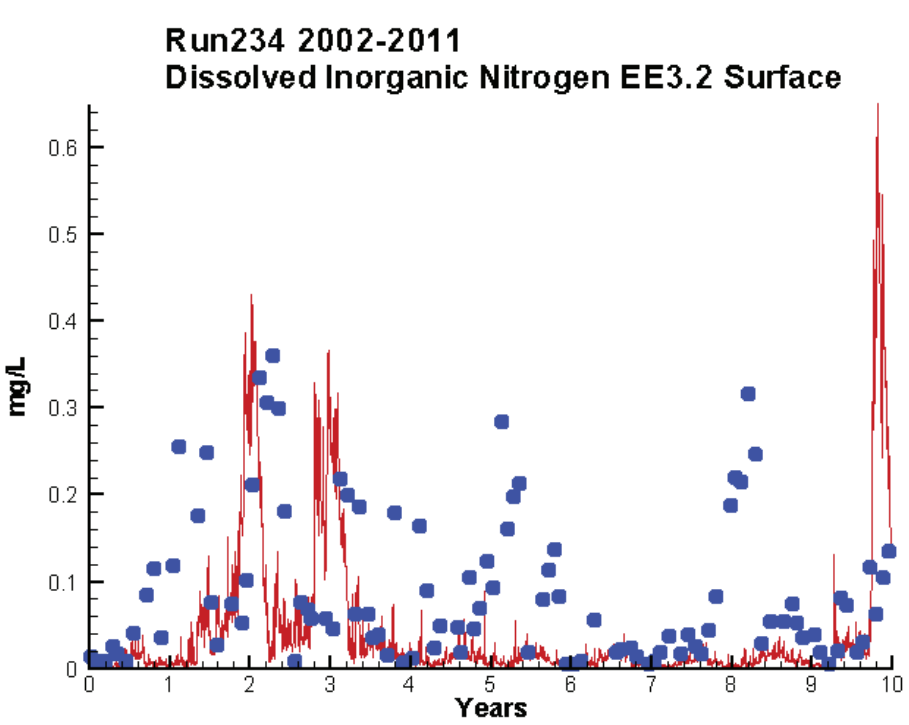

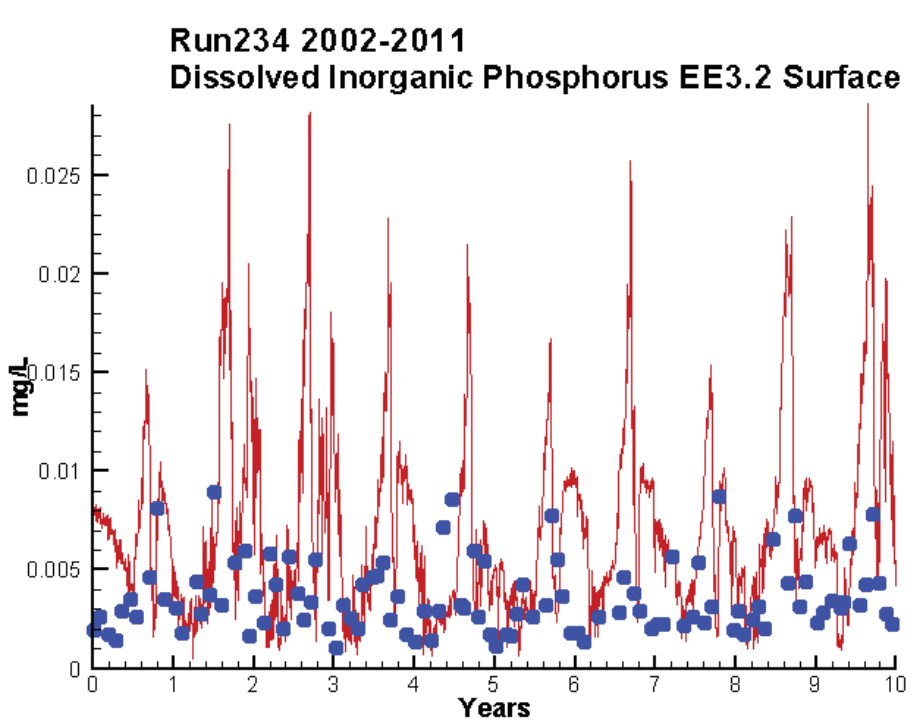

Station EE3.2

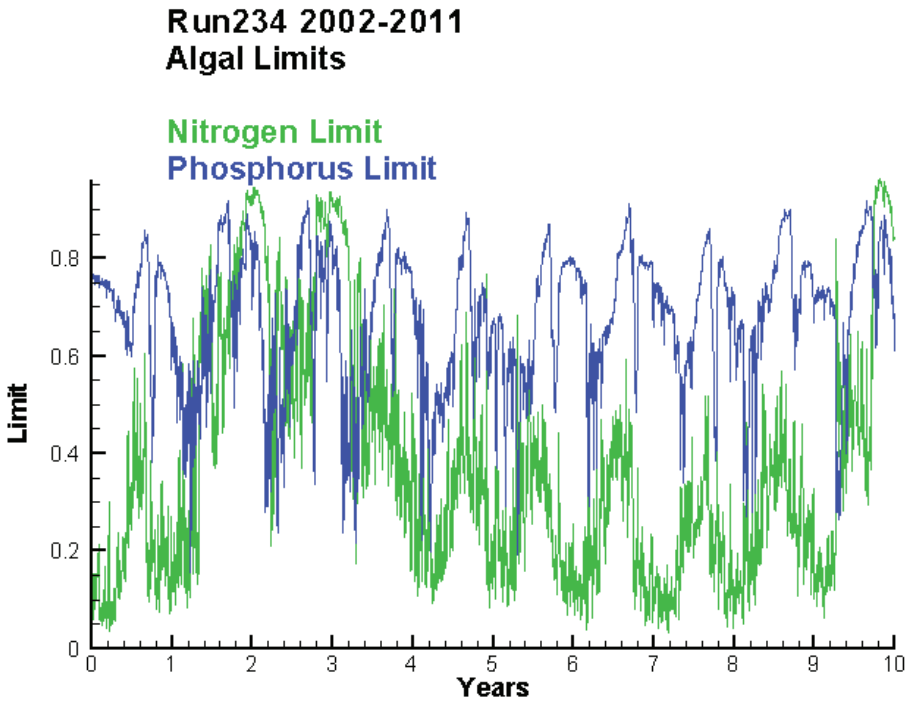

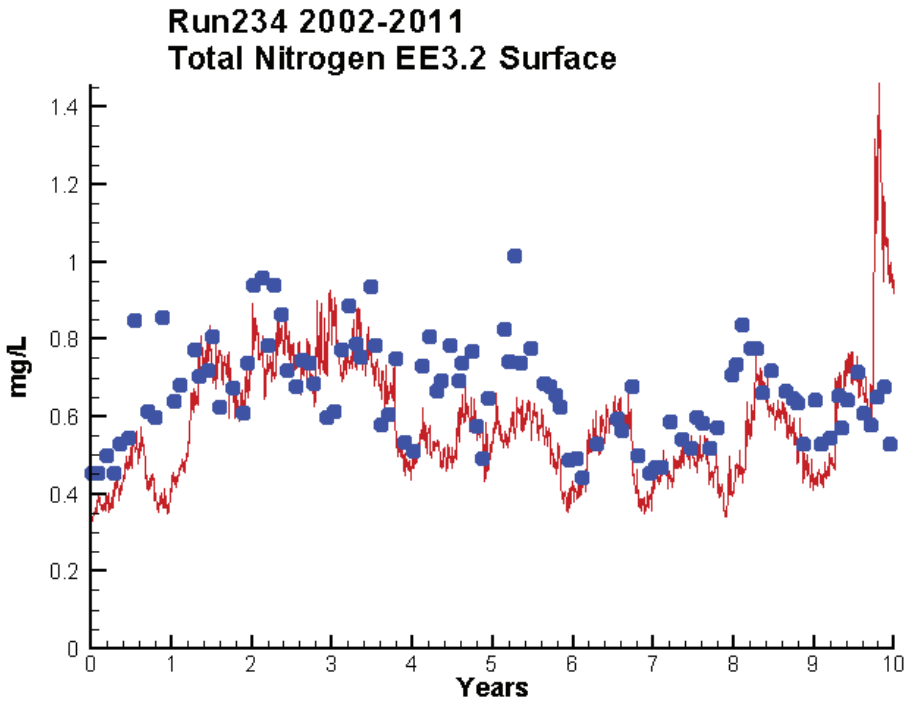

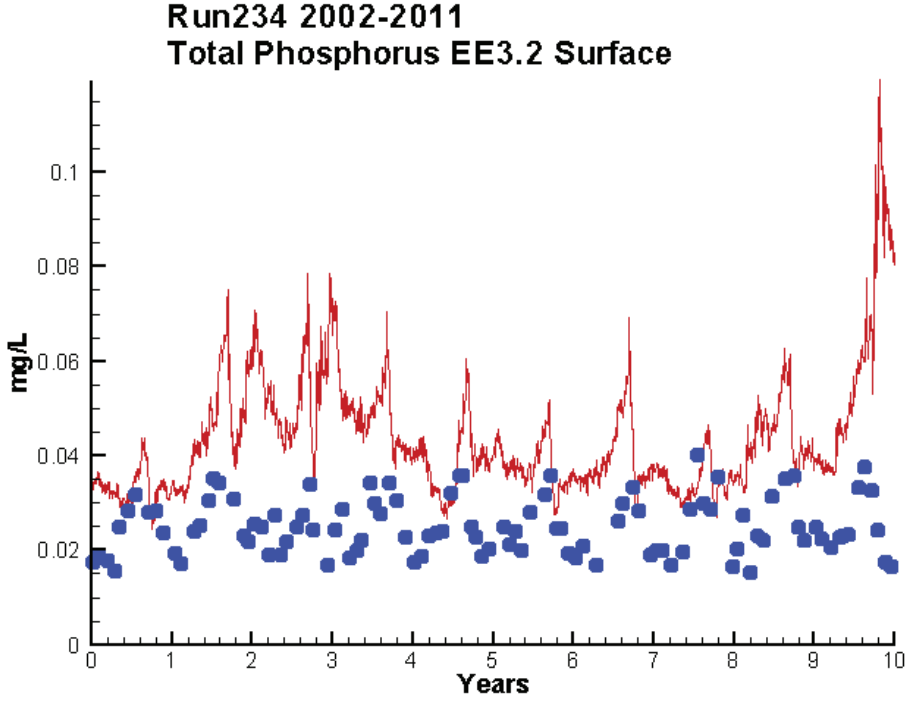

	Mean Difference	Absolute Mean Difference
Chl	-0.0025	4.3295
DIN	-0.0483	0.0800
KE	-0.0483	0.0800
DIP	0.0032	0.0040
TP	0.0185	0.0187
TN	-0.0776	0.1319

Station EE3.2

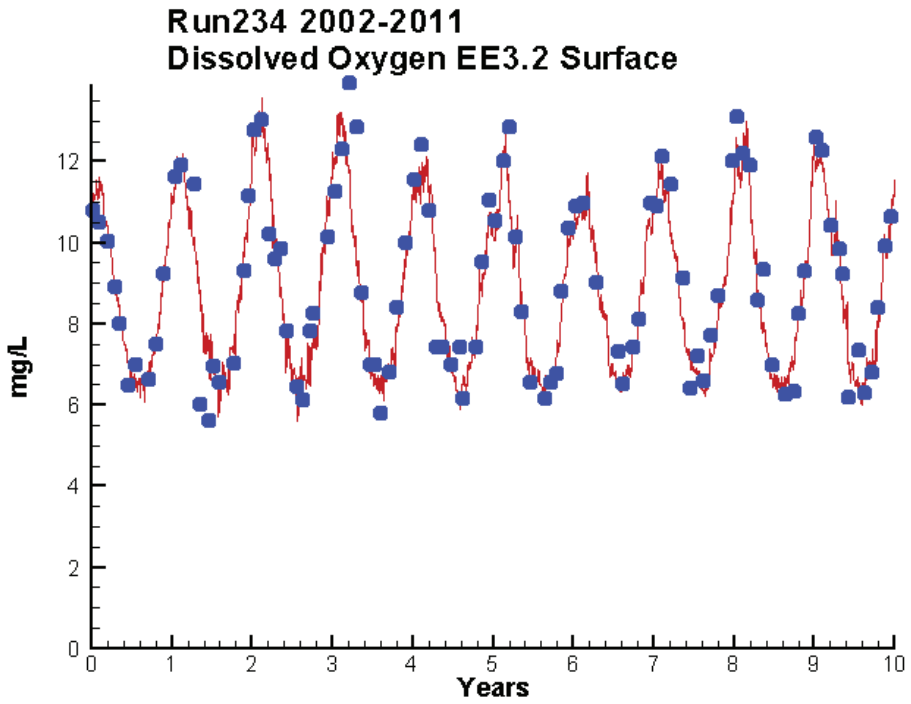

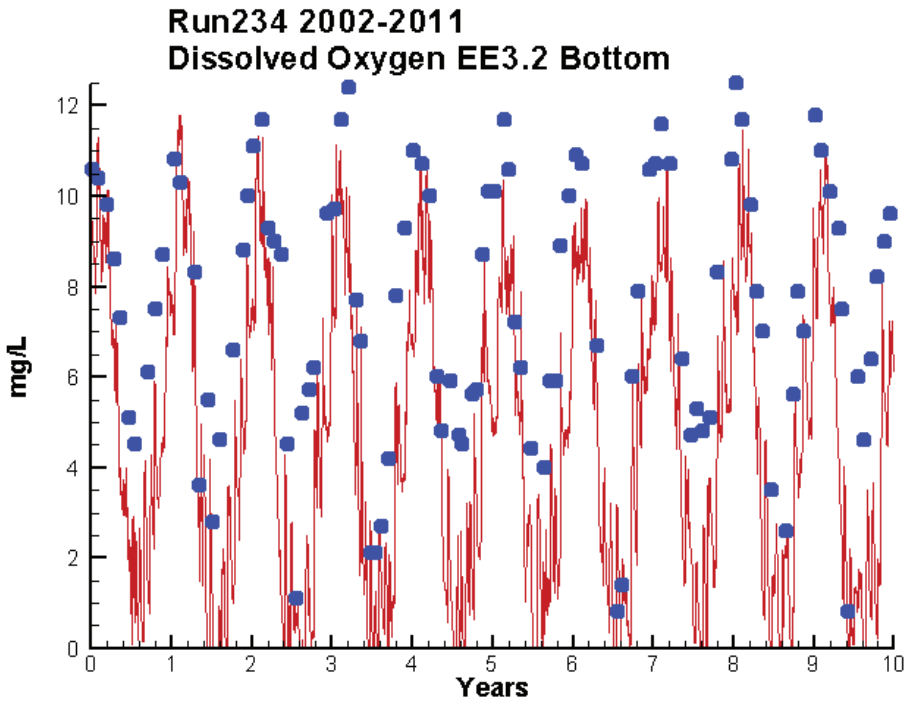

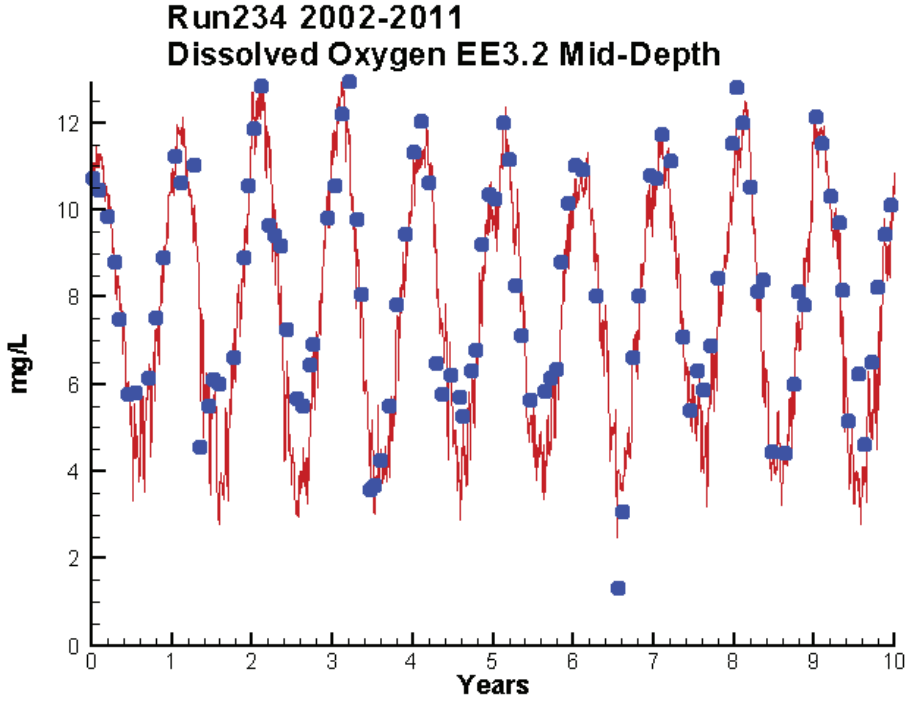

	Mean Difference	Absolute Mean Difference
Top DO	-0.1291	0.5749
Mid DO	-0.3630	0.7782
Bot DO	-2.9790	3.0509

Station EE3.2

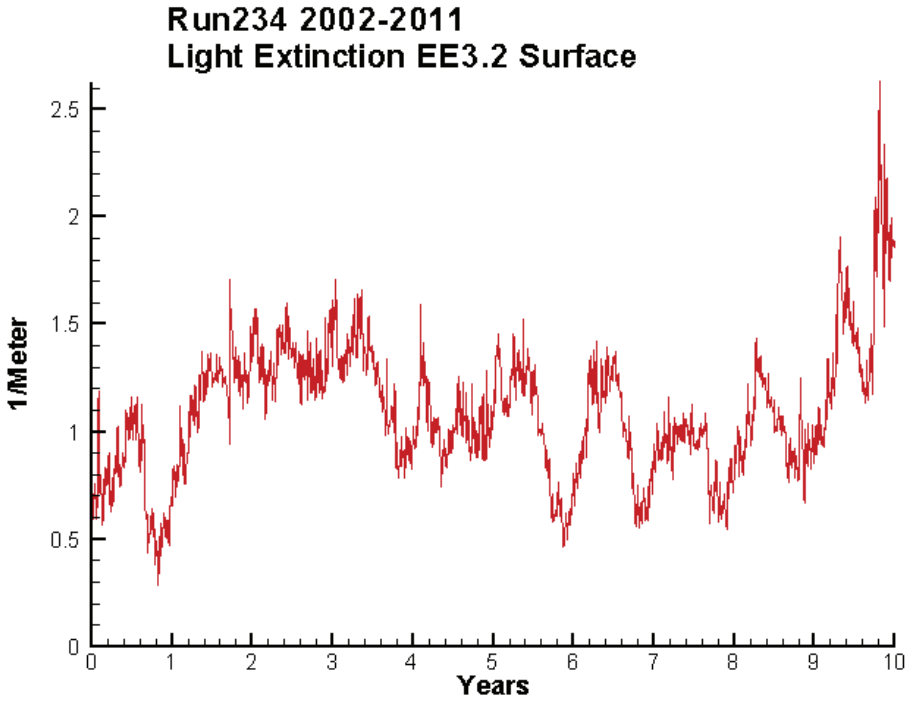

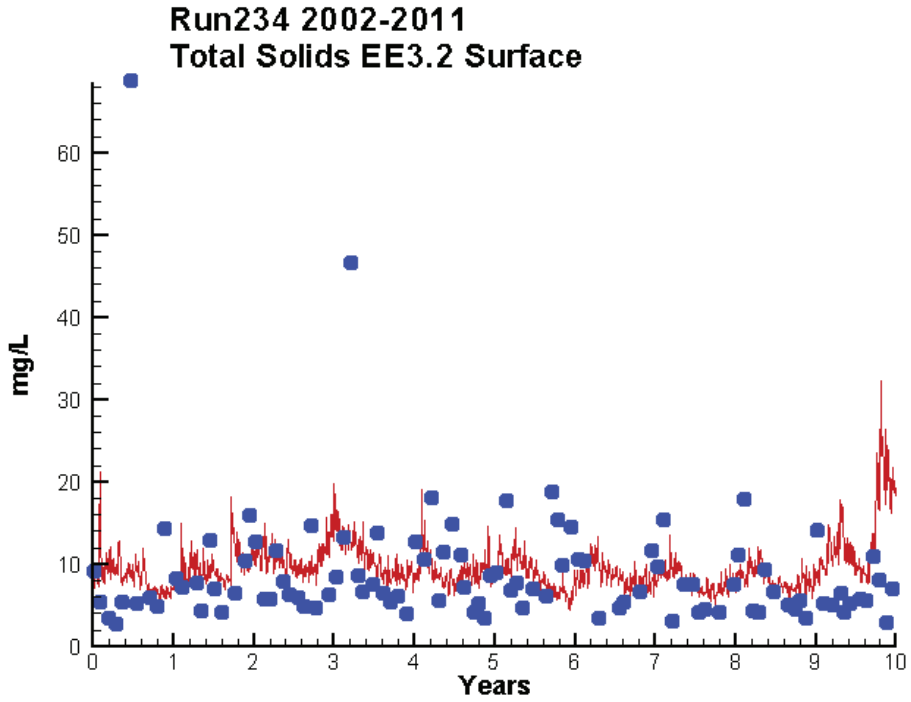

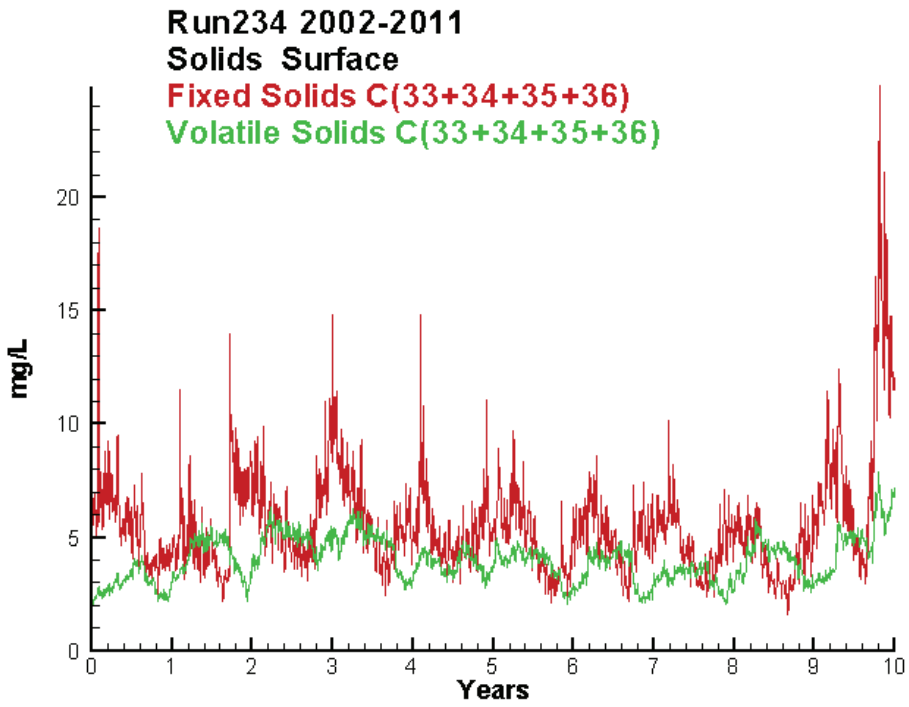

	Mean Difference	Absolute Mean Difference
KE	-0.0776	0.1319
TSS	0.6652	5.0346

Station LE1.3

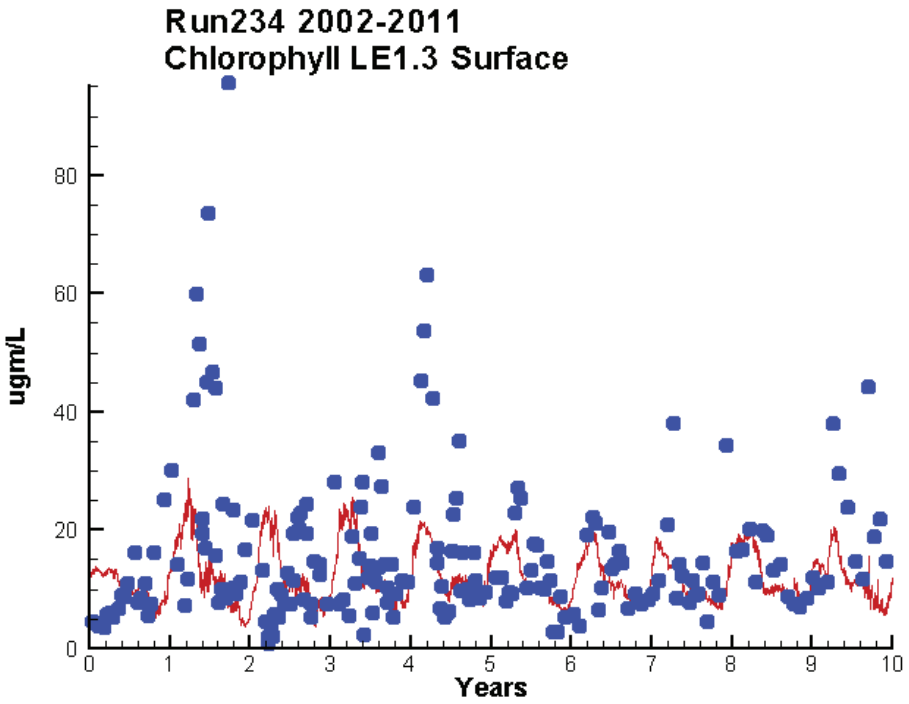

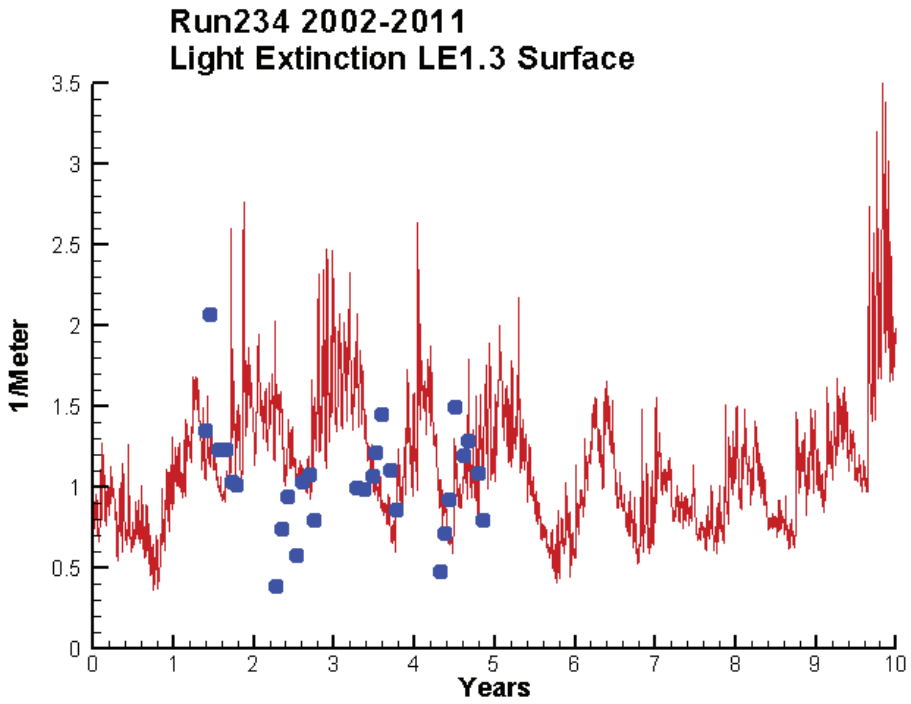

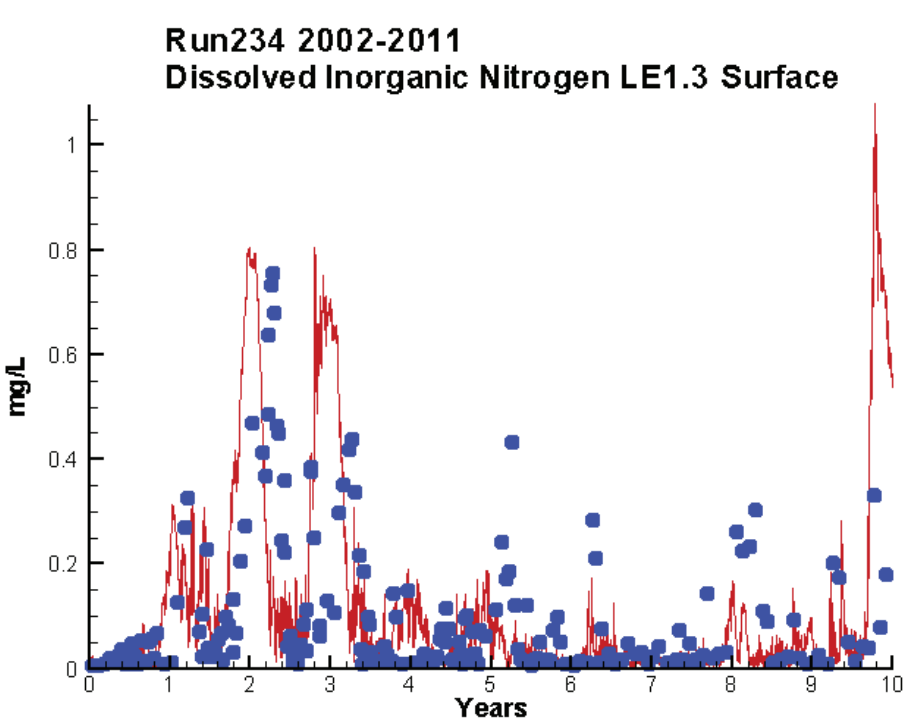

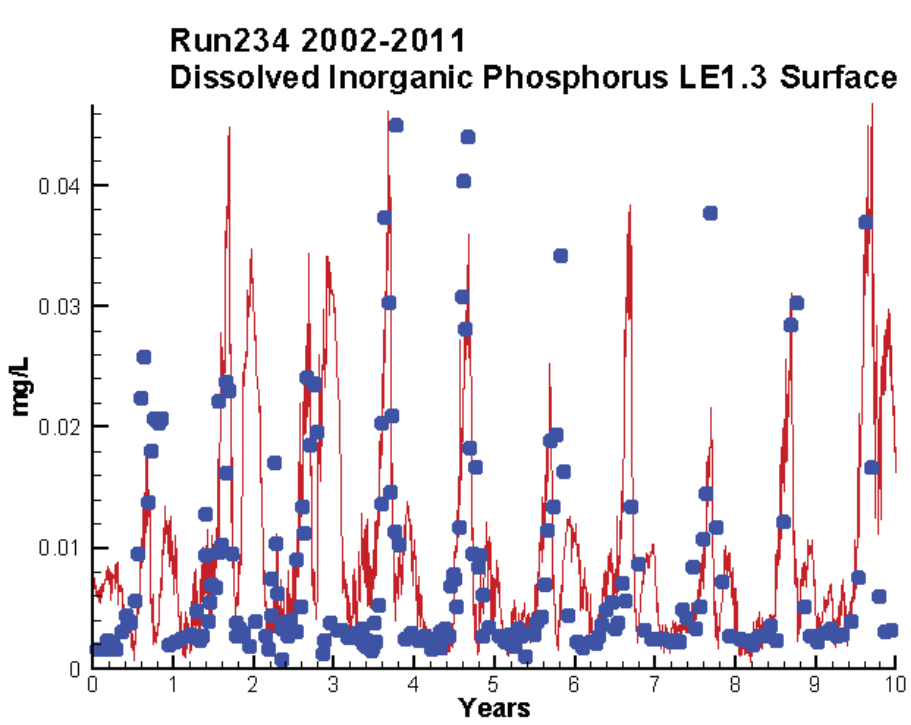

Station LE1.3

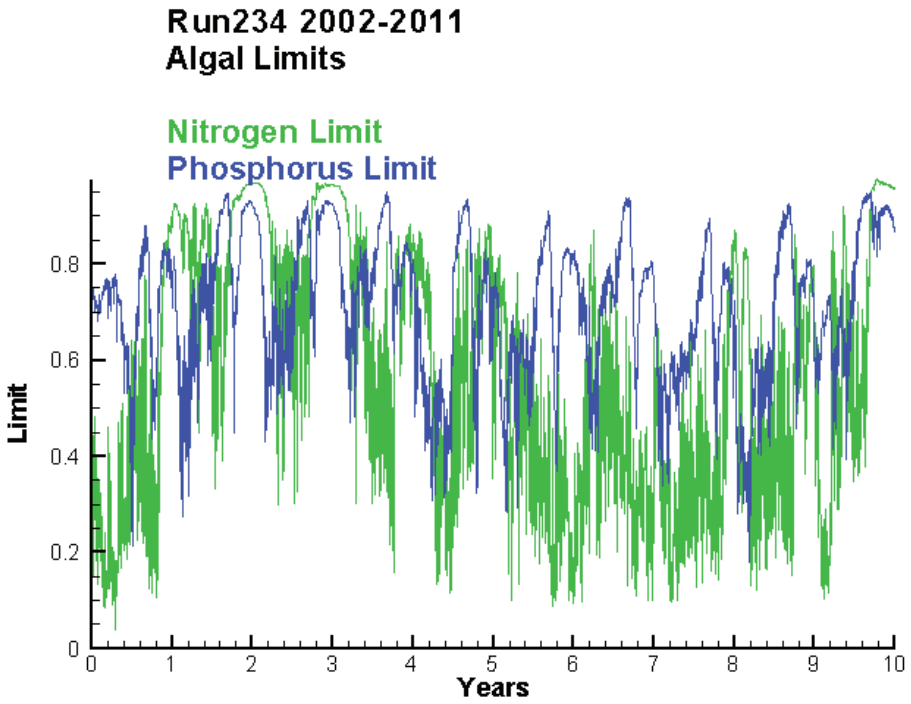

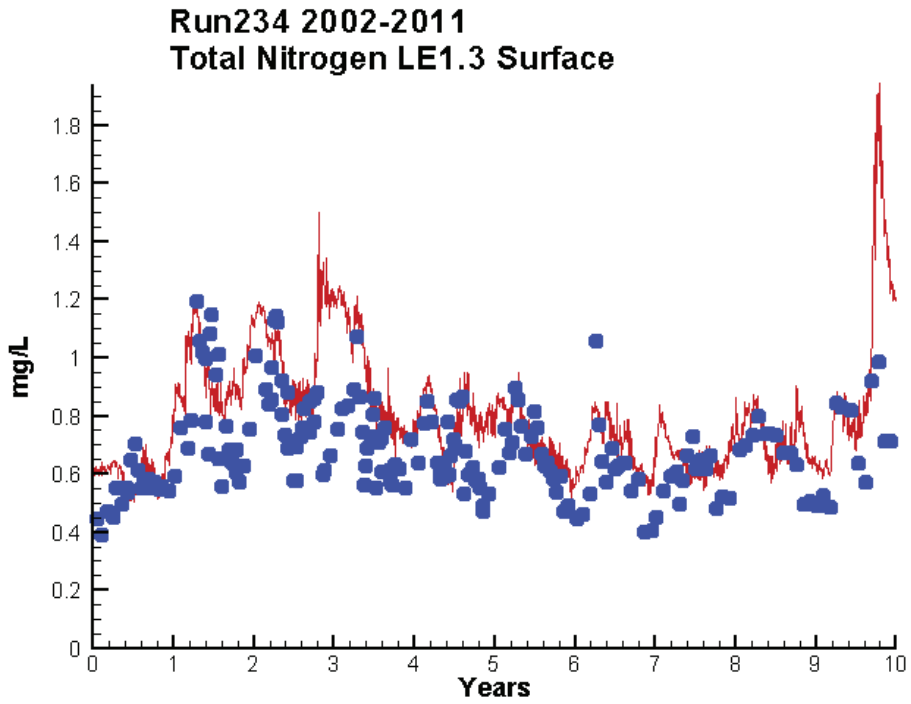

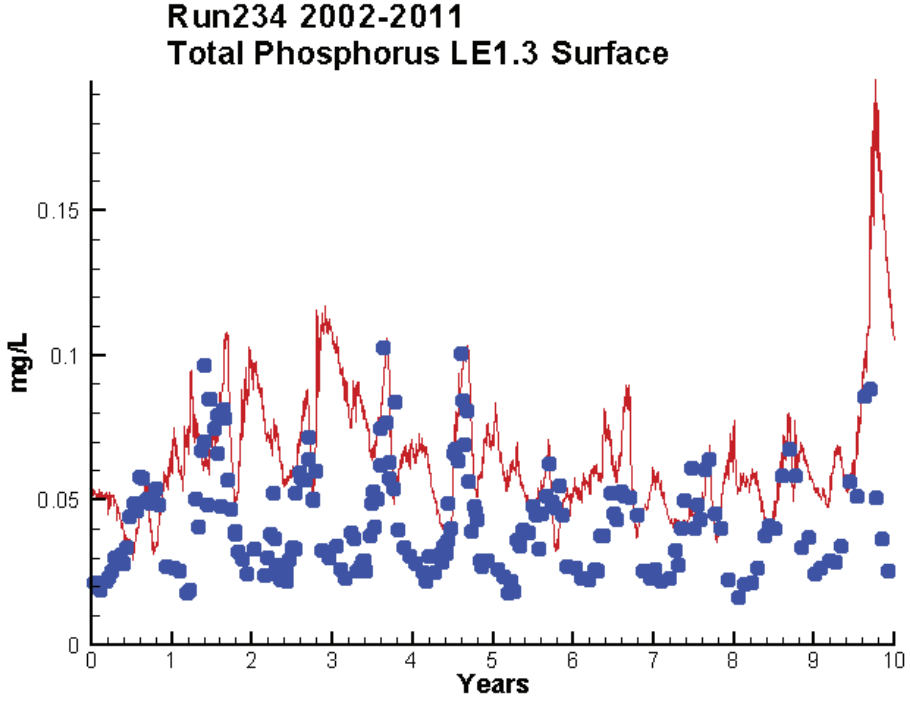

	Mean Difference	Absolute Mean Difference
Chl	-3.4322	8.4271
DIN	-0.0015	0.0973
KE	0.0744	0.3750
DIP	0.0017	0.0063
TP	0.0224	0.0257
TN	0.1213	0.1518

Station LE1.3

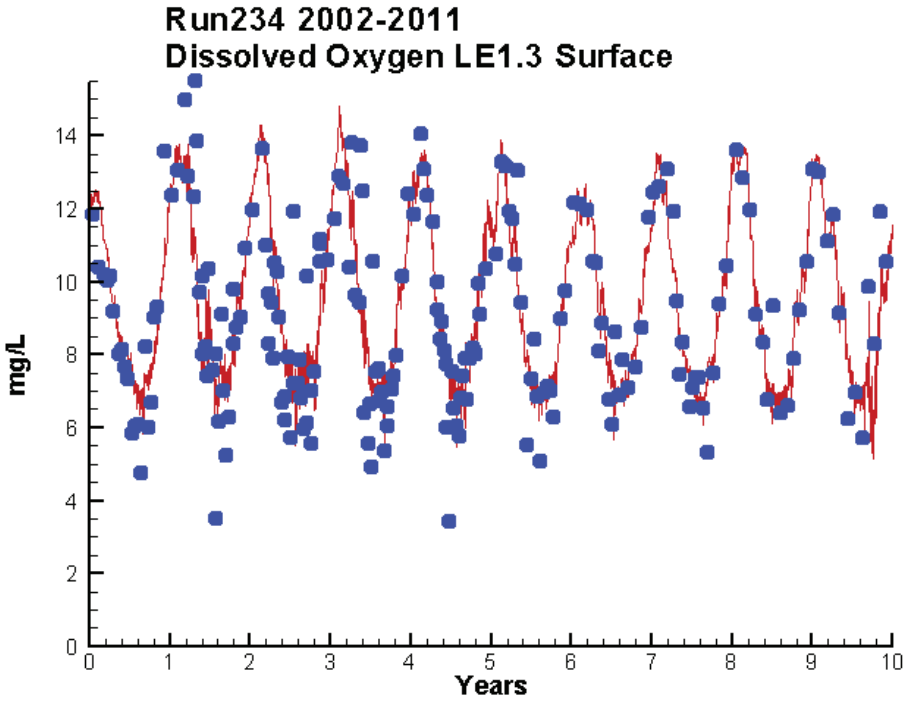

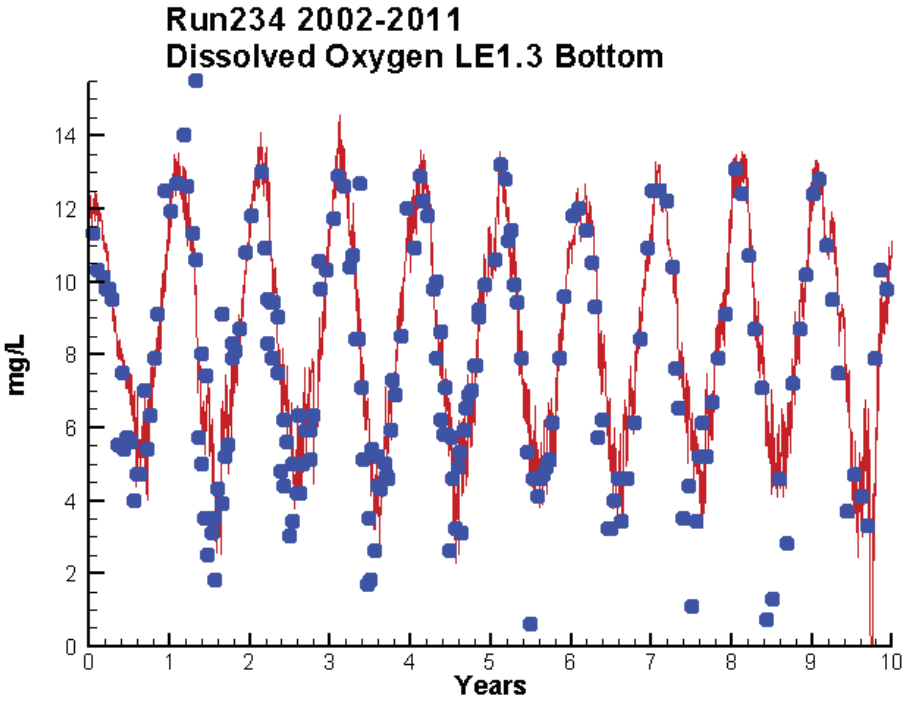

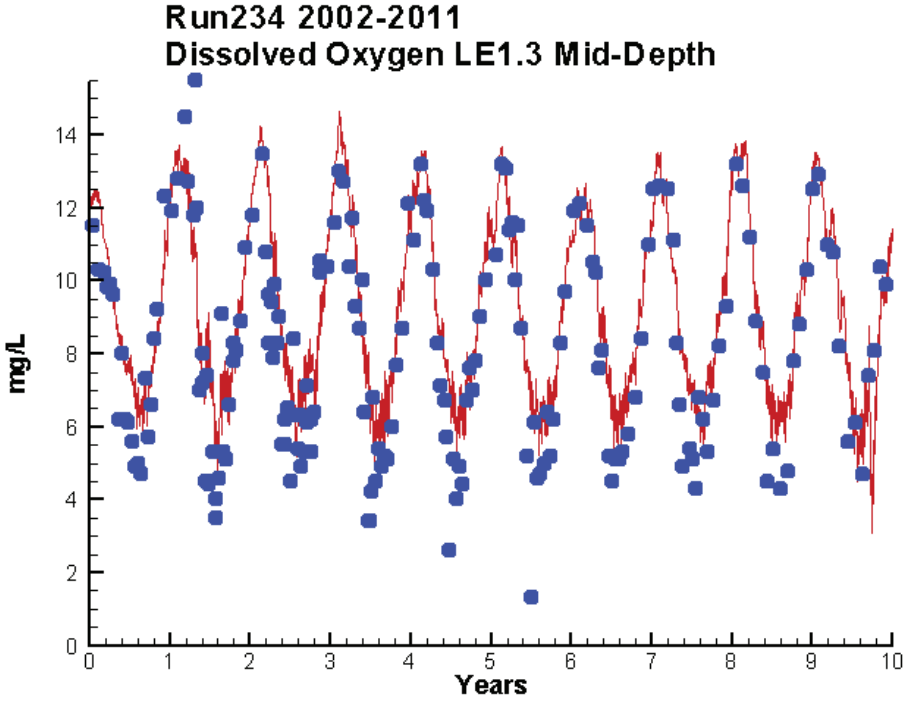

	Mean Difference	Absolute Mean Difference
Top DO	0.1686	1.0010
Mid DO	0.8648	1.2280
Bot DO	0.5411	1.2154

Station LE1.3

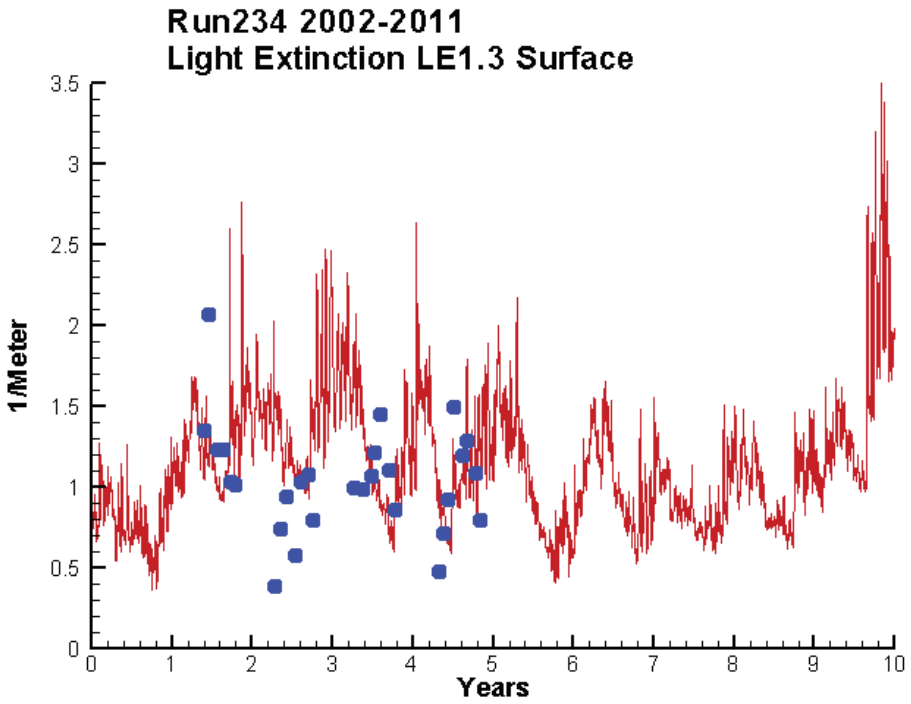

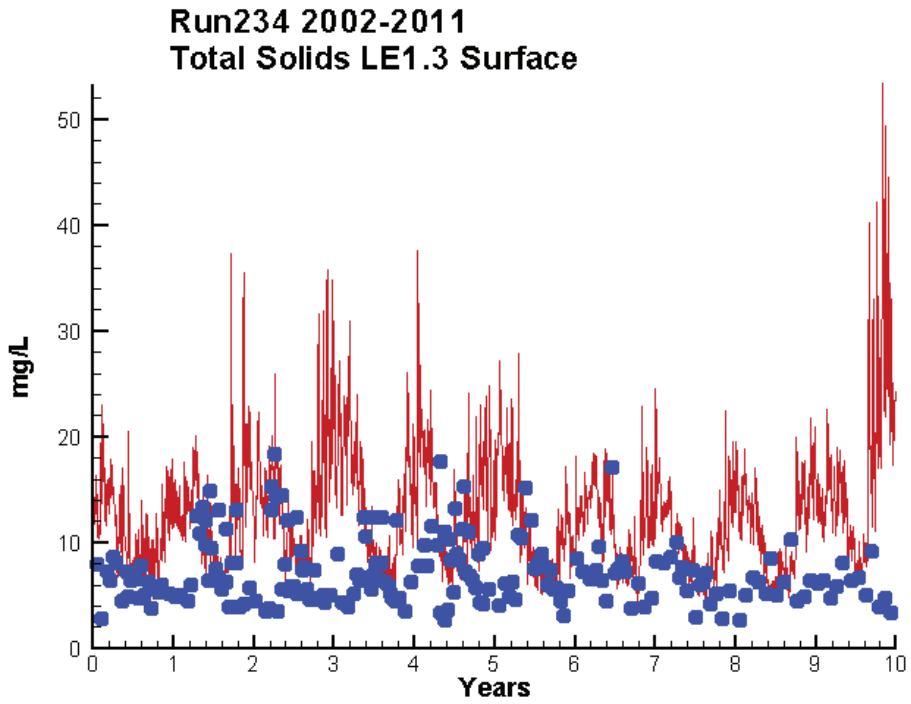

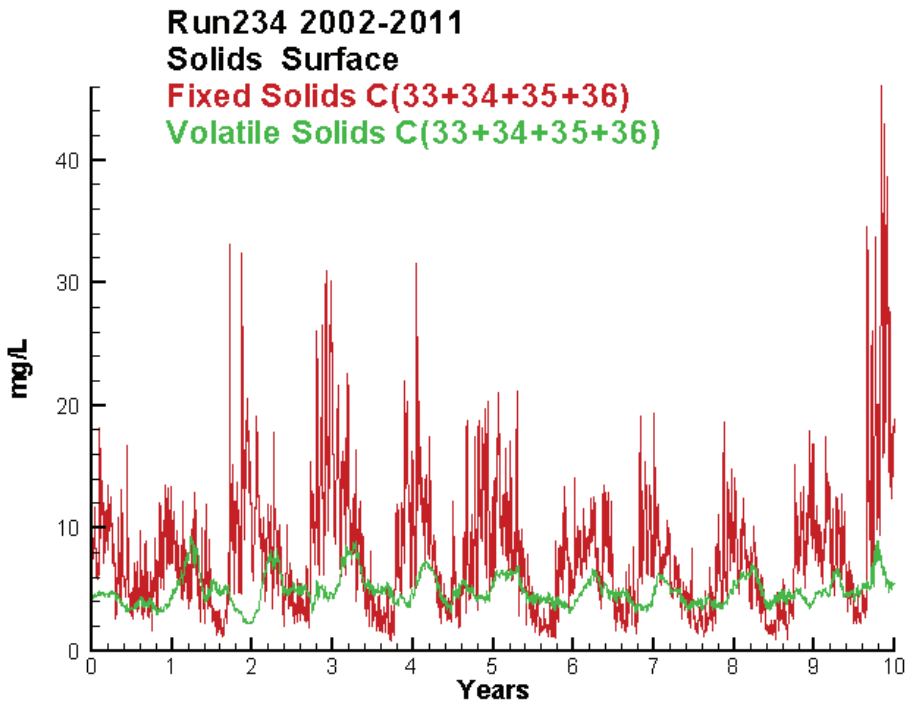

	Mean Difference	Absolute Mean Difference
KE	0.0744	0.3750
TSS	4.9071	5.8473

Station RET1.1

Run234 2002-2011
Chlorophyll RET1.1 Surface

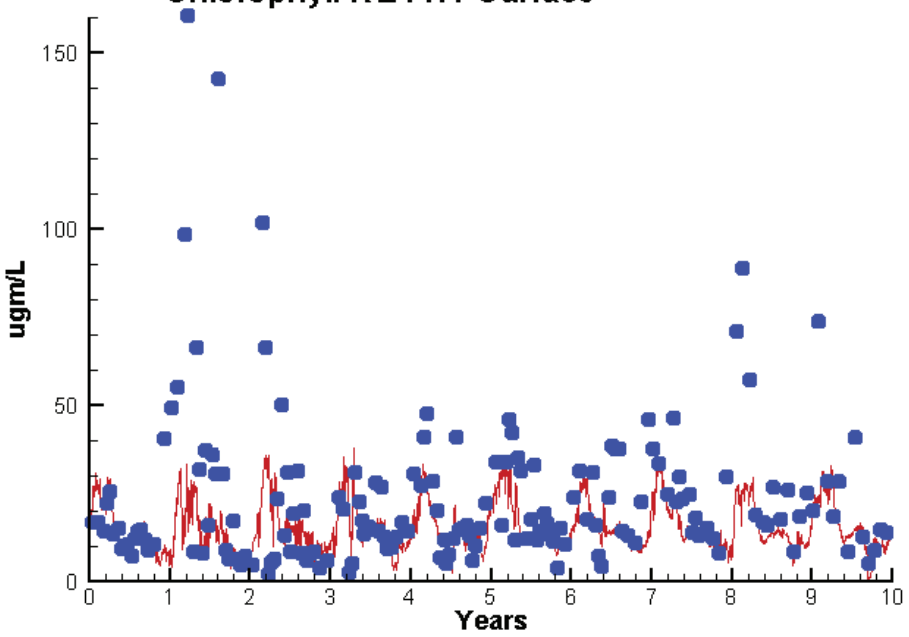

Run234 2002-2011
Light Extinction RET1.1 Surface

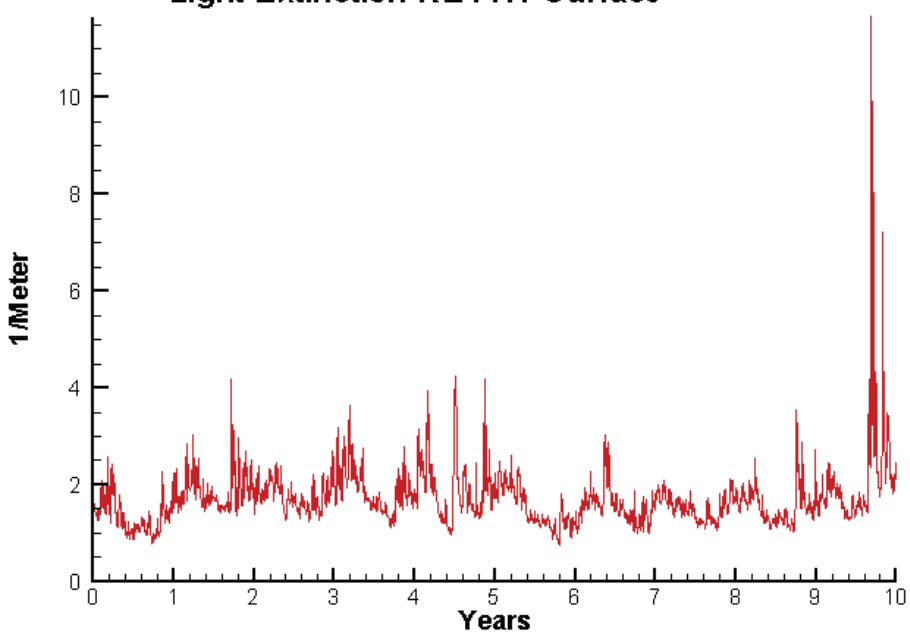

Run234 2002-2011
Dissolved Inorganic Nitrogen RET1.1 Surface

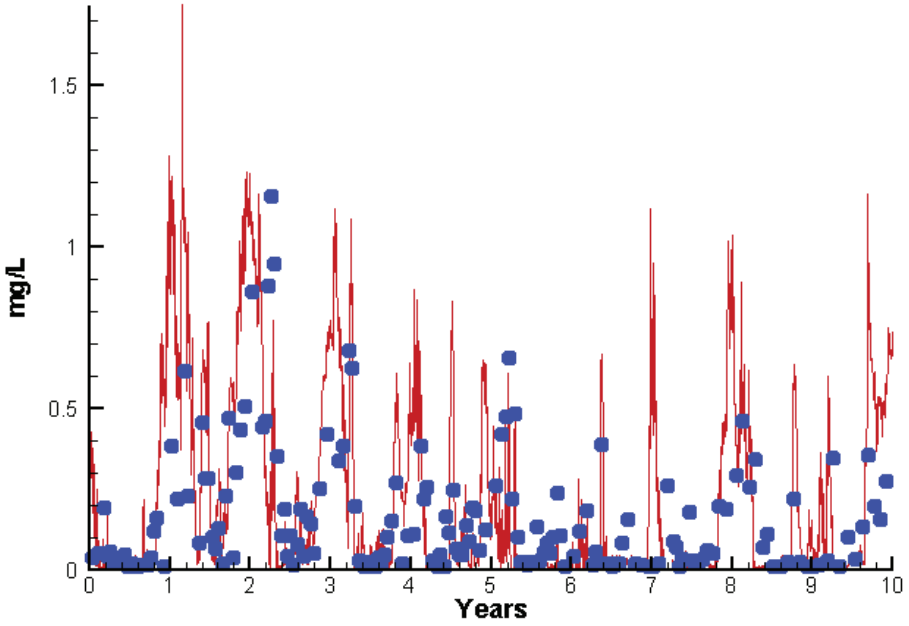

Run234 2002-2011
Dissolved Inorganic Phosphorus RET1.1 Surface

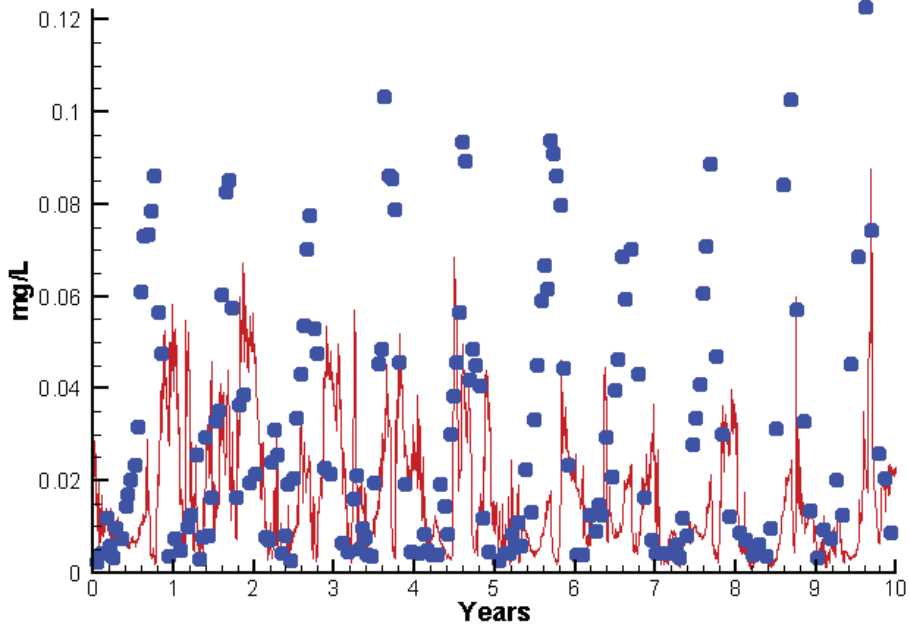

Station RET1.1

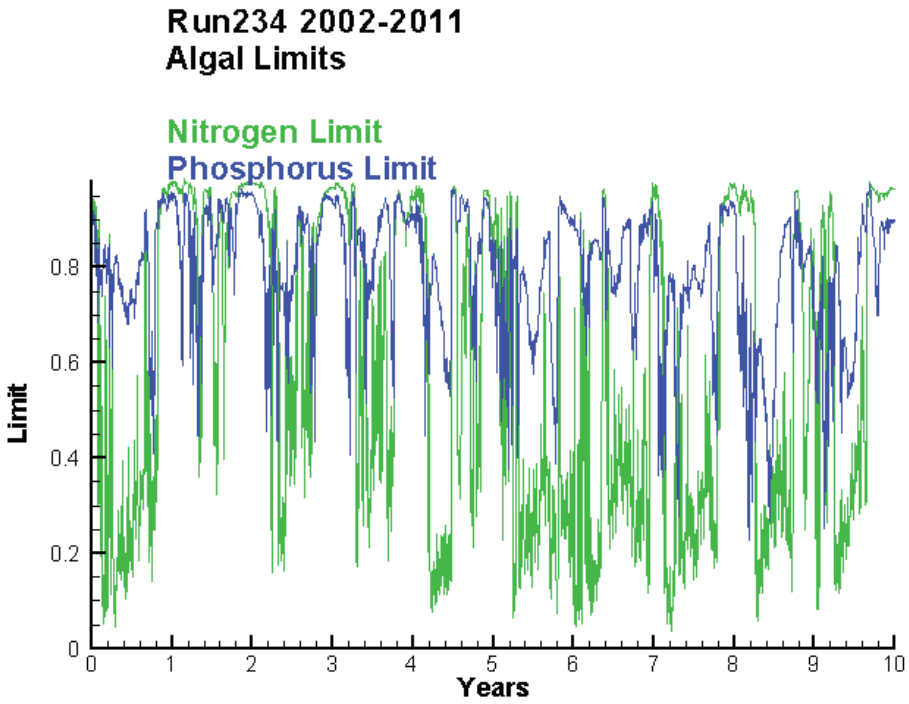

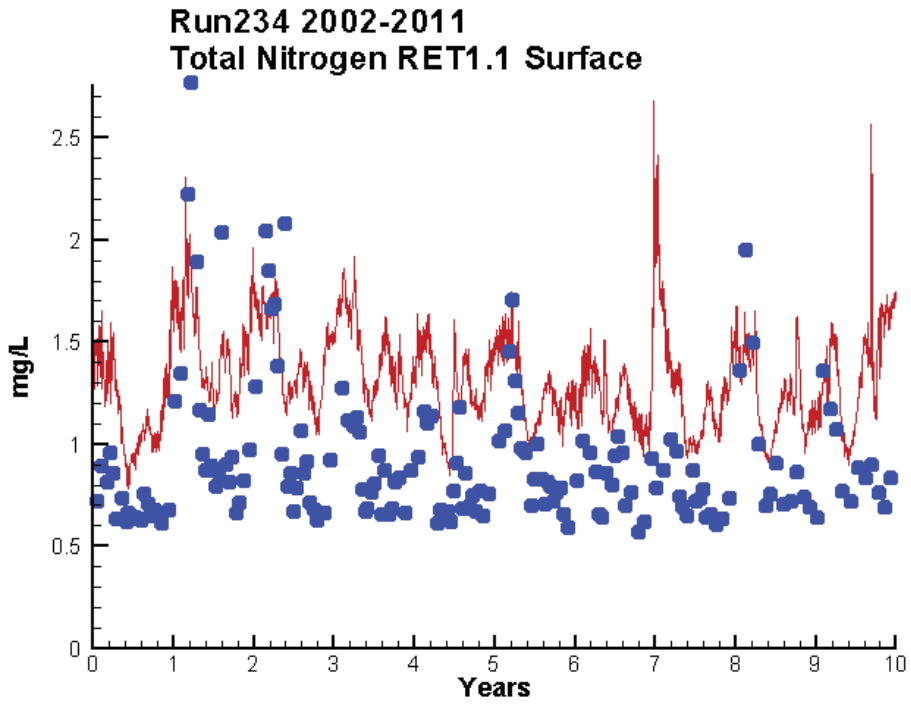

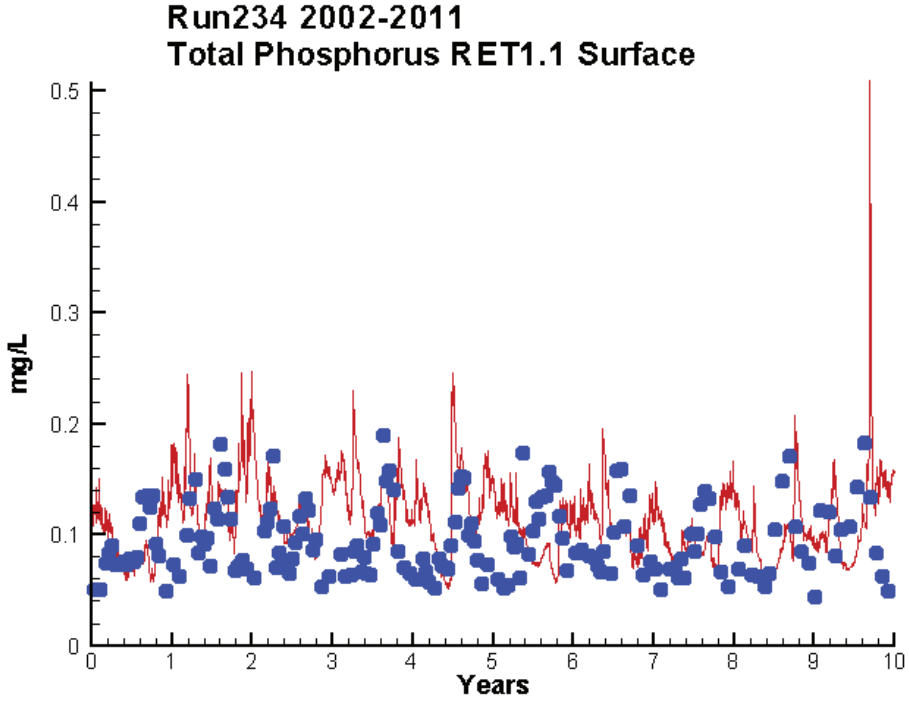

	Mean Difference	Absolute Mean Difference
Chl	-7.8456	11.7403
DIN	0.0330	0.1491
KE	0.0330	0.1491
DIP	-0.0150	0.0227
TP	0.0205	0.0422
TN	0.4050	0.4535

Station RET1.1

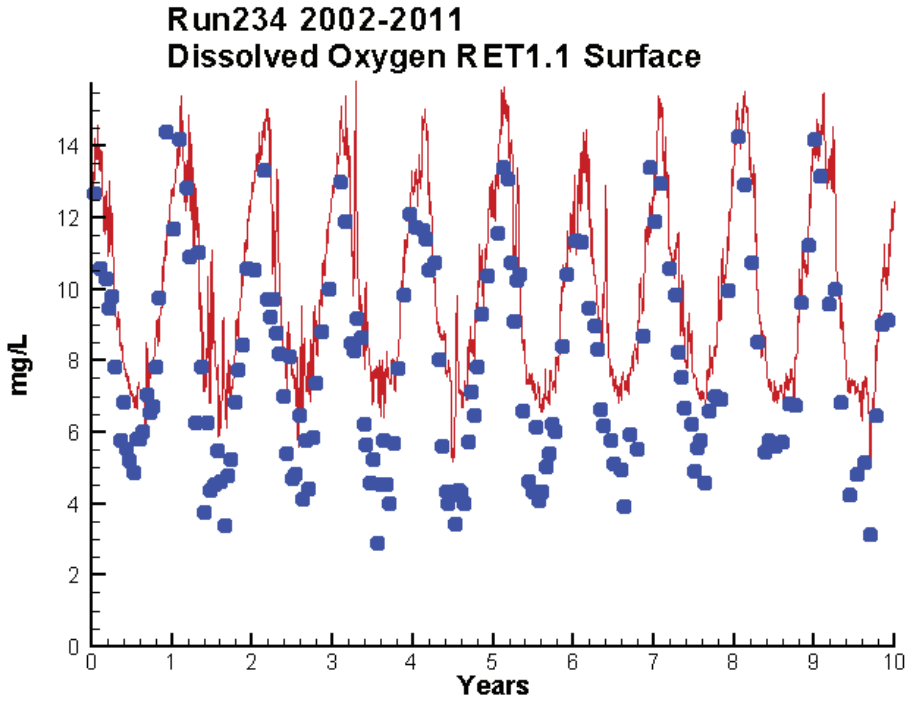

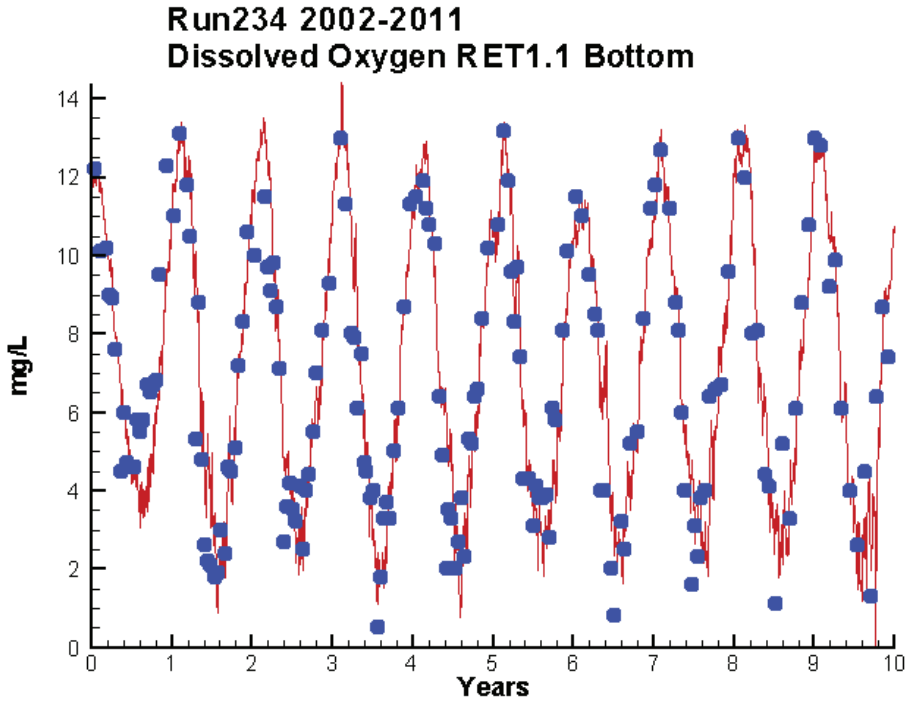

	Mean Difference	Absolute Mean Difference
Top DO	1.9530	2.0456
Bot DO	0.1684	0.9822

Station RET1.1

Run234 2002-2011
Light Extinction RET1.1 Surface

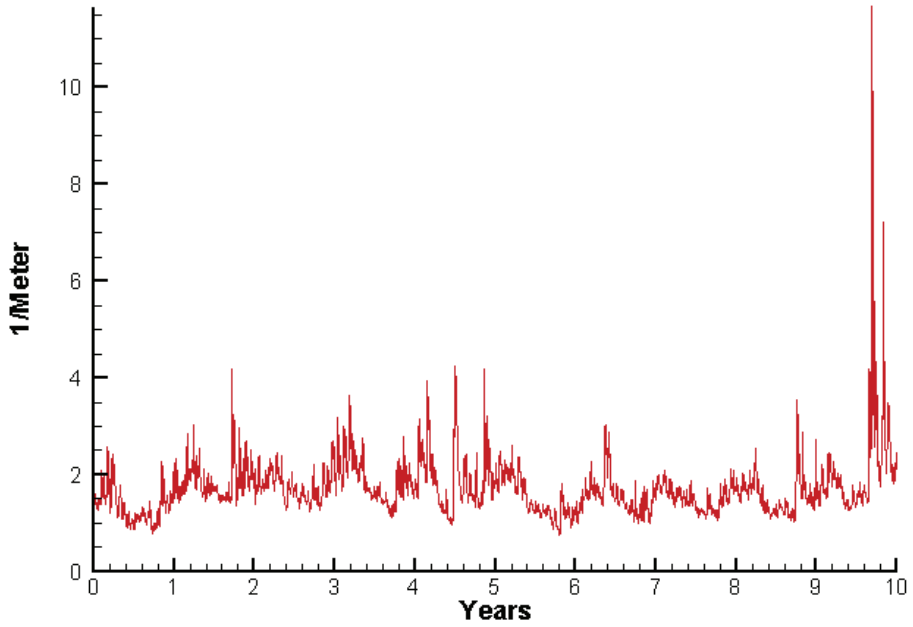

Run234 2002-2011
Total Solids RET1.1 Surface

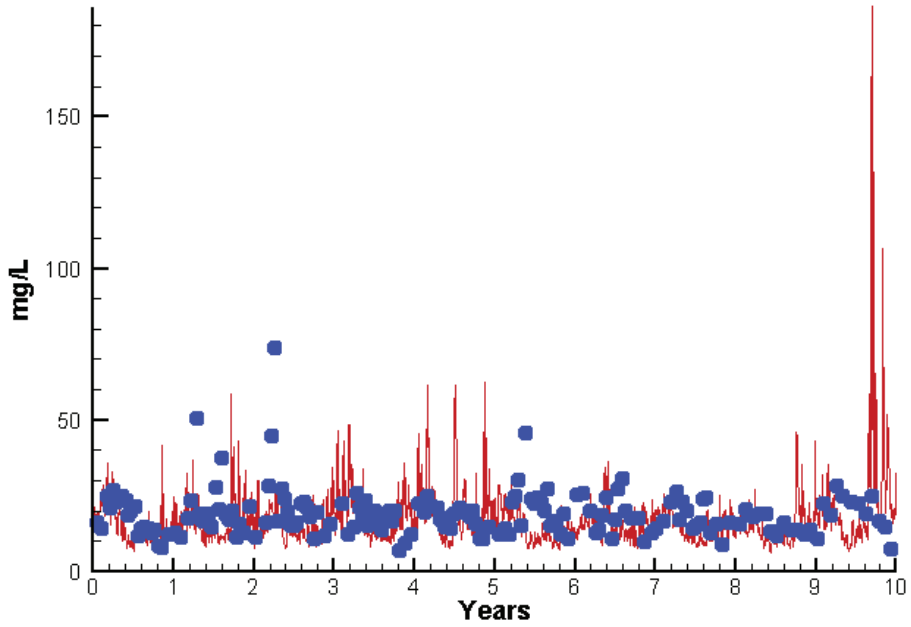

Run234 2002-2011
Solids Surface
Fixed Solids C(33+34+35+36)
Volatile Solids C(33+34+35+36)

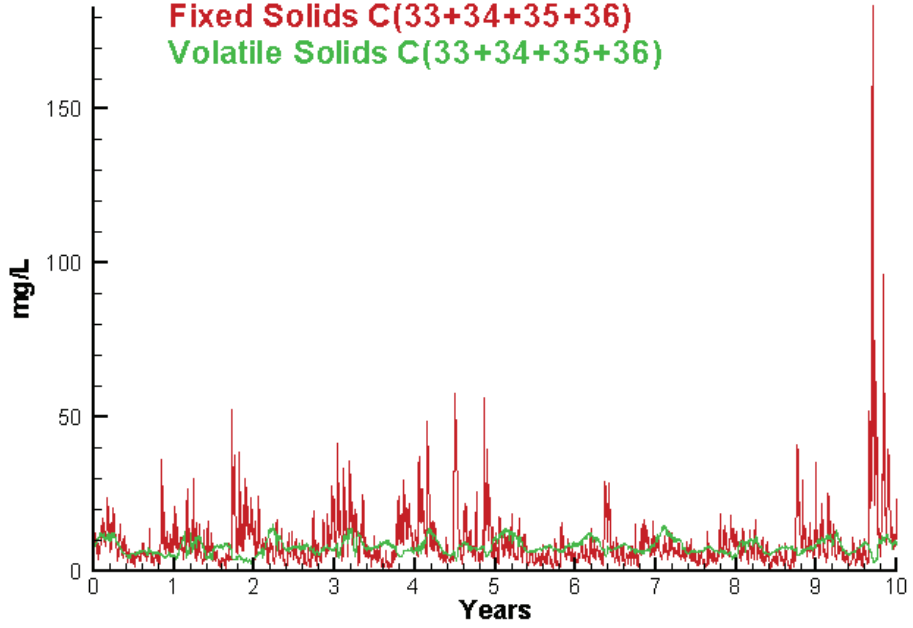

	Mean Difference	Absolute Mean Difference
KE	0.4050	0.4535
TSS	-2.0455	7.2858

Station TF1.7

Run234 2002-2011
Chlorophyll TF1.7 Surface

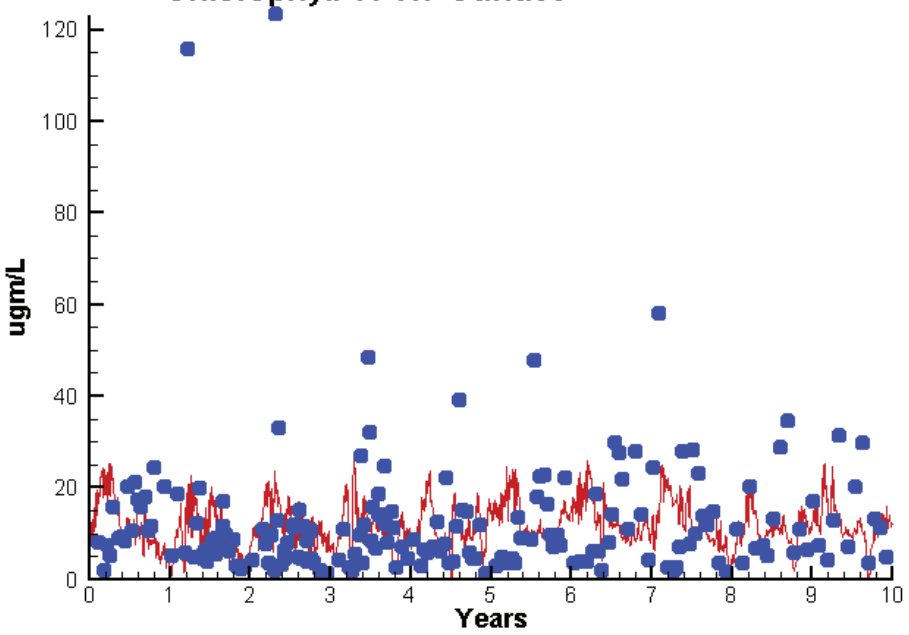

Run234 2002-2011
Light Extinction TF1.7 Surface

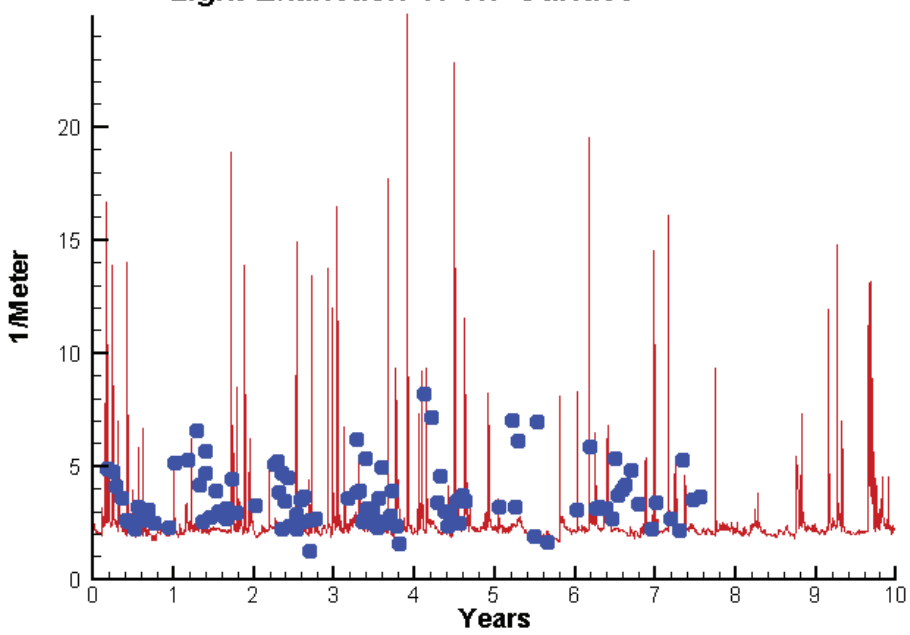

Run234 2002-2011
Dissolved Inorganic Nitrogen TF1.7 Surface

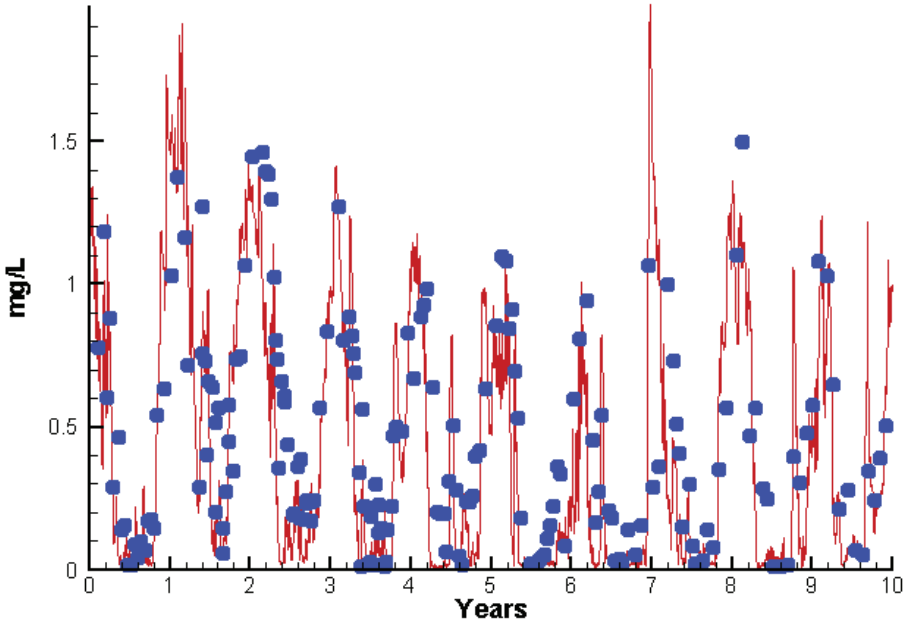

Run234 2002-2011
Dissolved Inorganic Phosphorus TF1.7 Surface

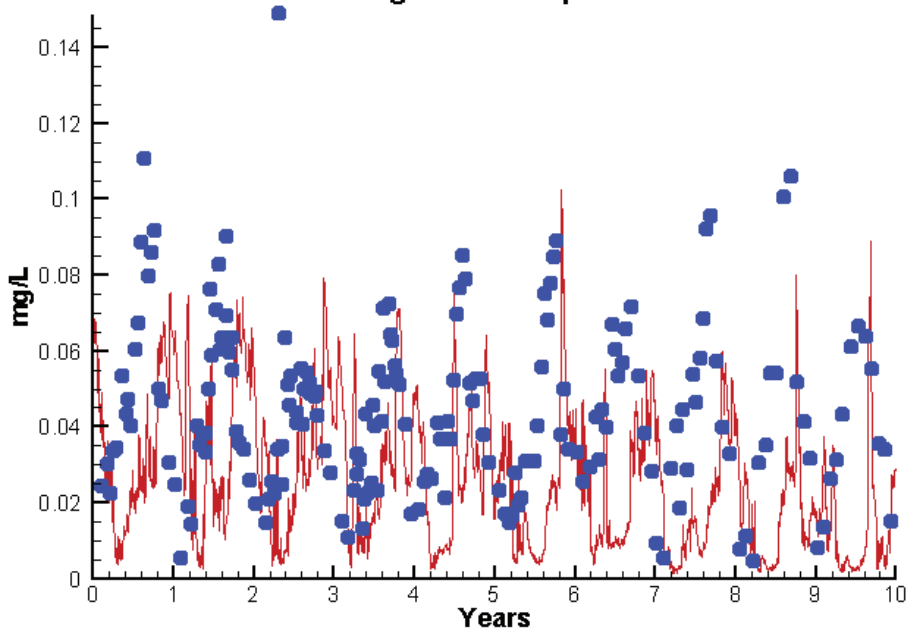

Station TF1.7

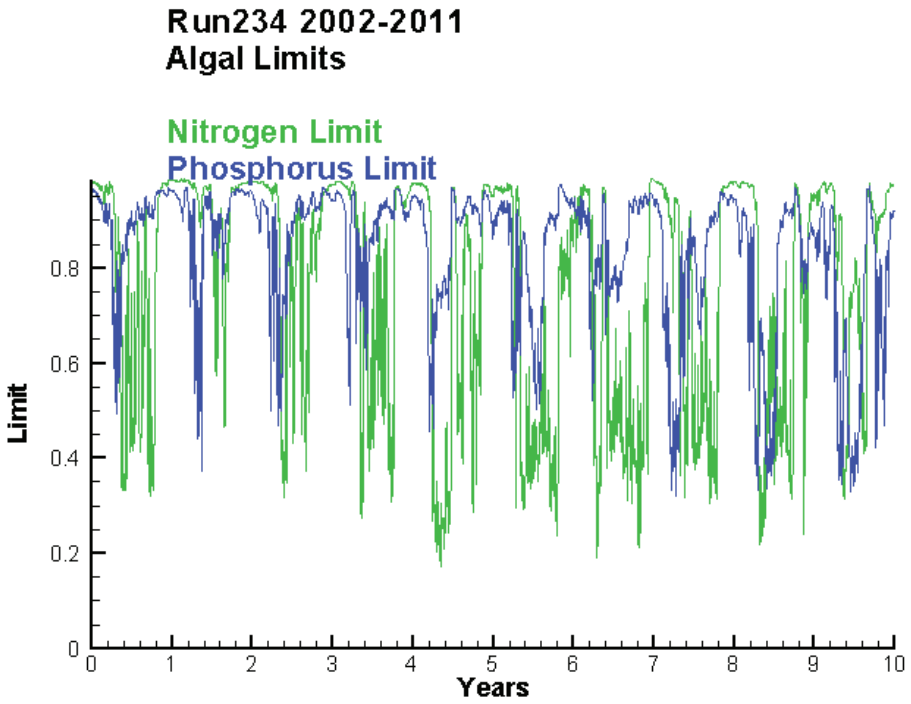

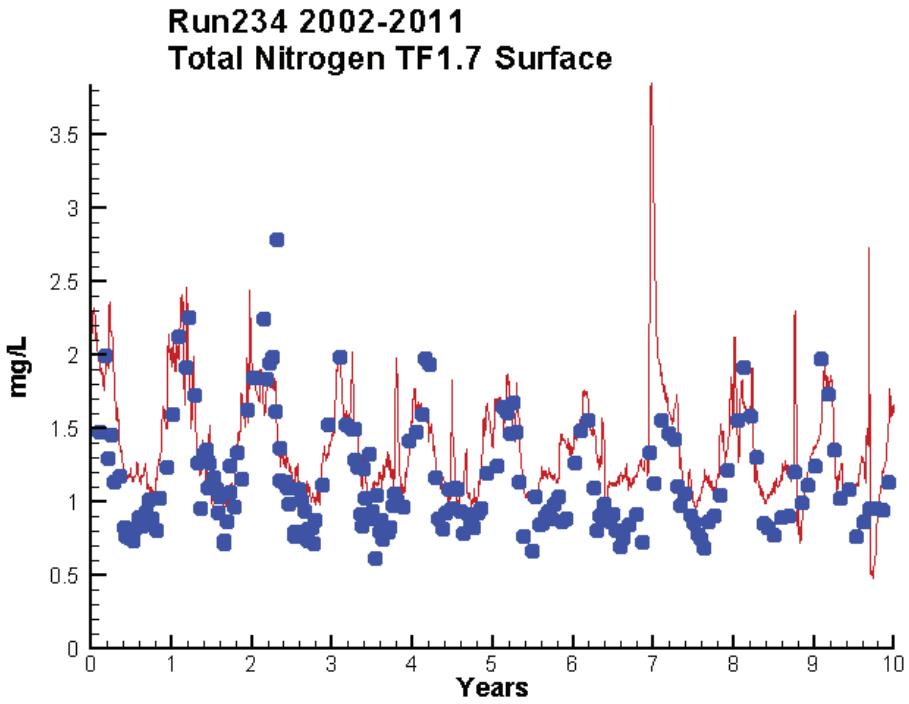

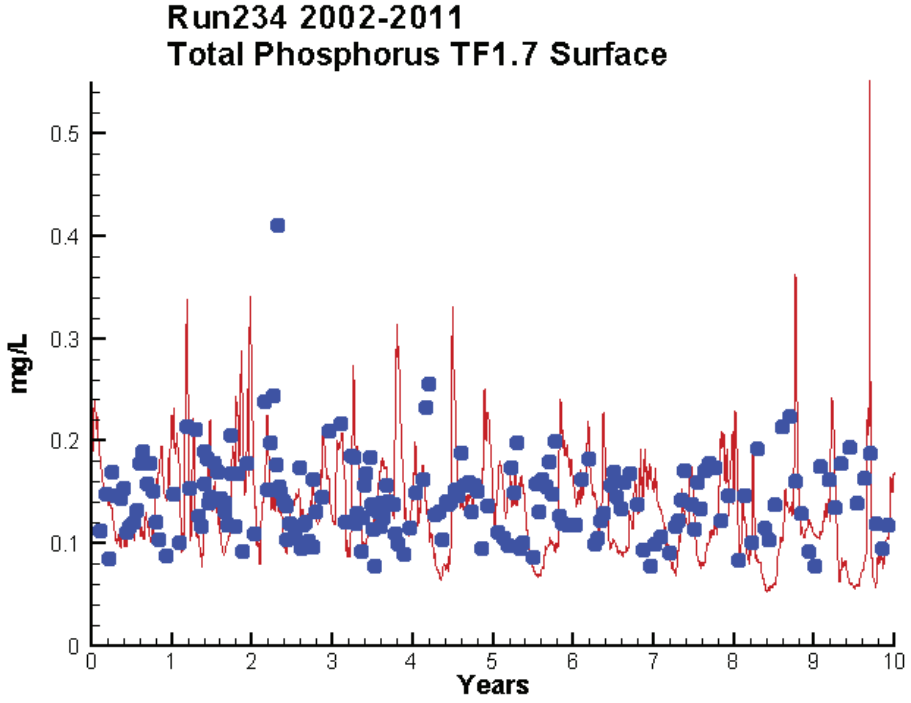

	Mean Difference	Absolute Mean Difference
Chl	-0.4476	9.0097
DIN	-0.0844	0.2090
KE	-1.1840	1.4111
DIP	-0.0192	0.0292
TP	-0.0070	0.0473
TN	0.2066	0.2790

Station TF1.7

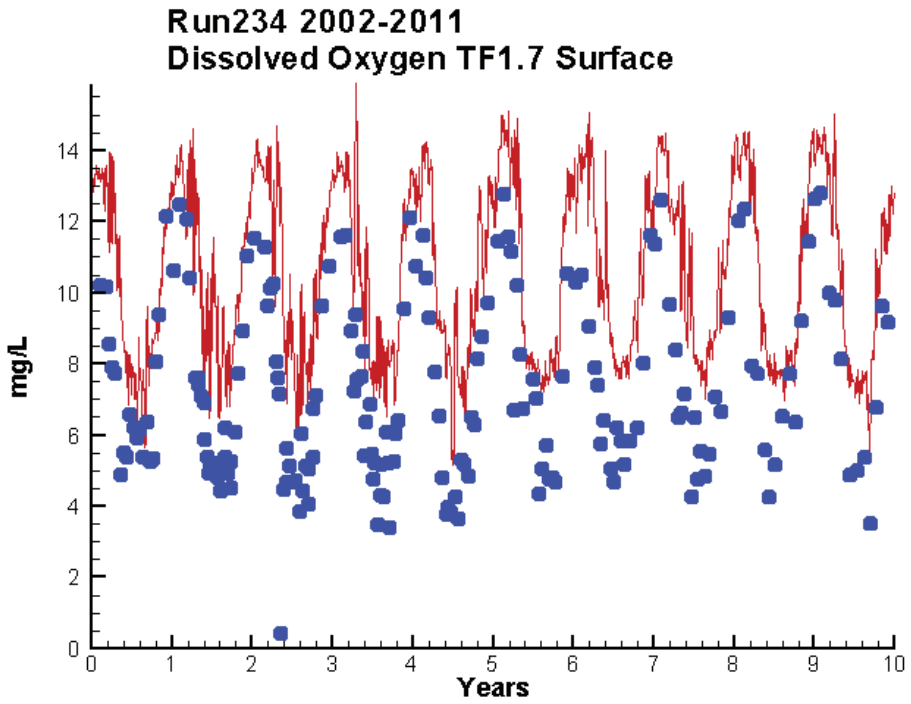

	Mean Difference	Absolute Mean Difference
Top DO	2.9520	2.9576

Station TF1.7

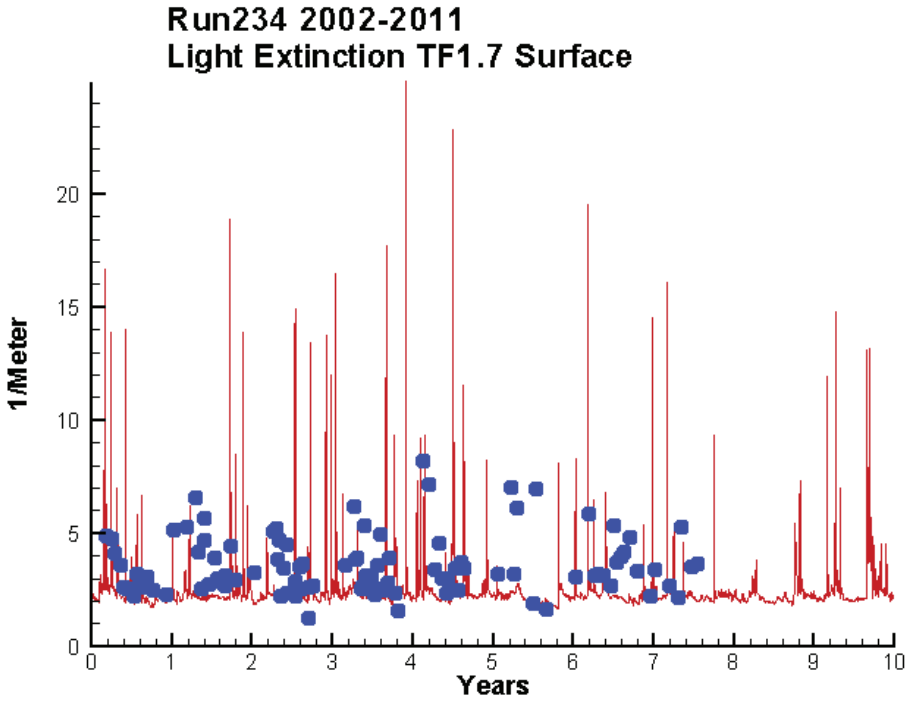

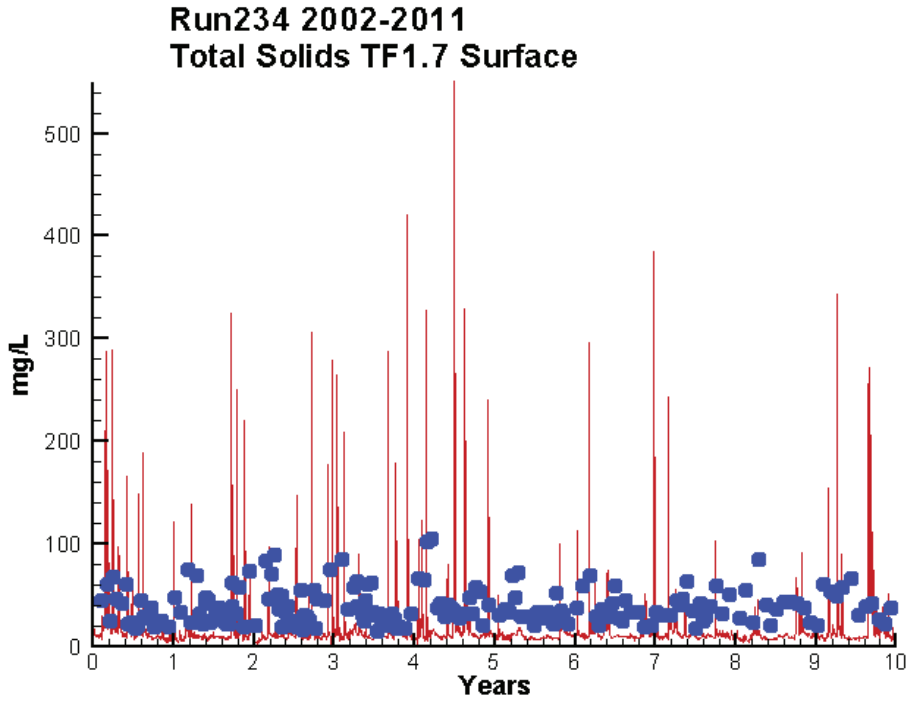

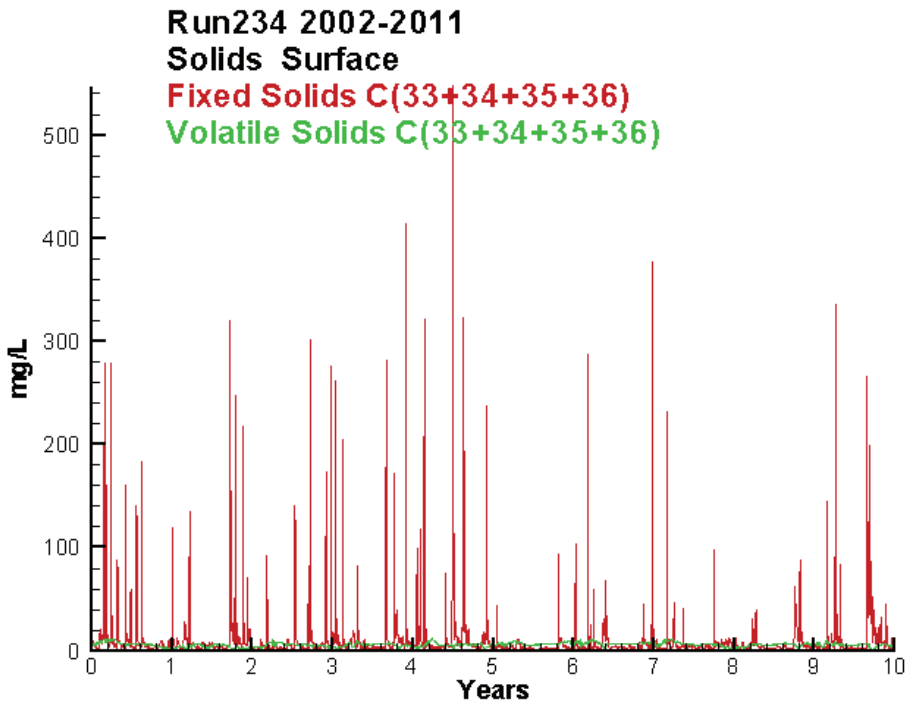

	Mean Difference	Absolute Mean Difference
KE	-1.1840	1.4111
TSS	-22.4619	27.8173

Station LE2.2

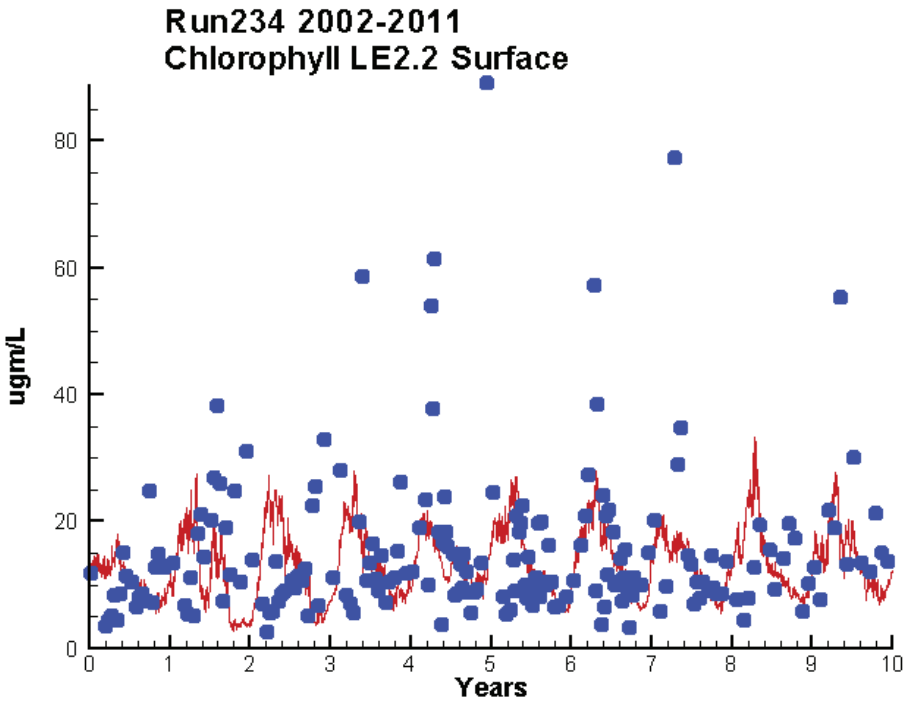

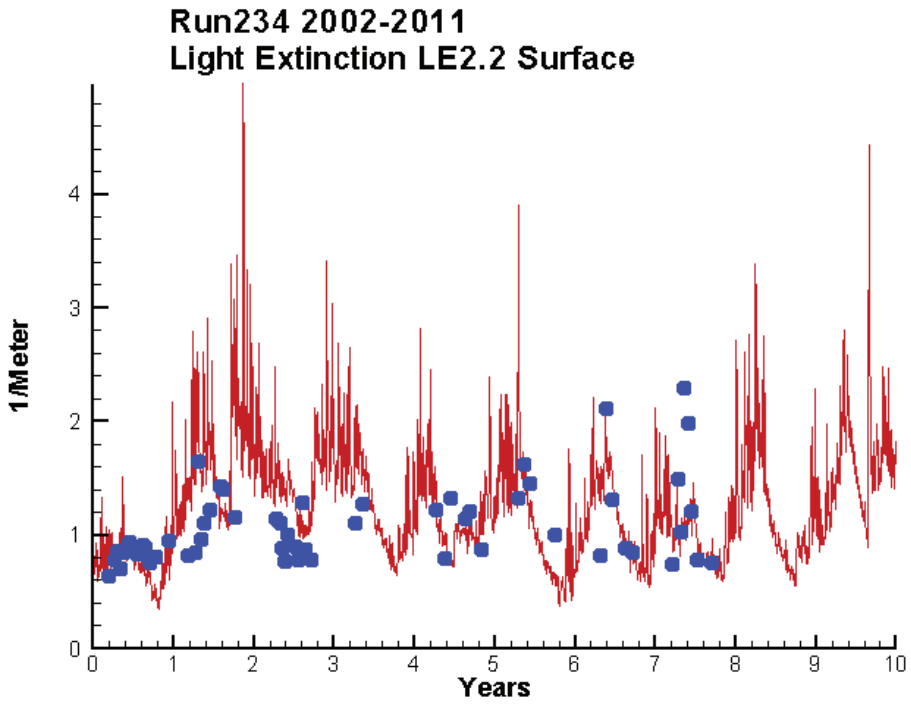

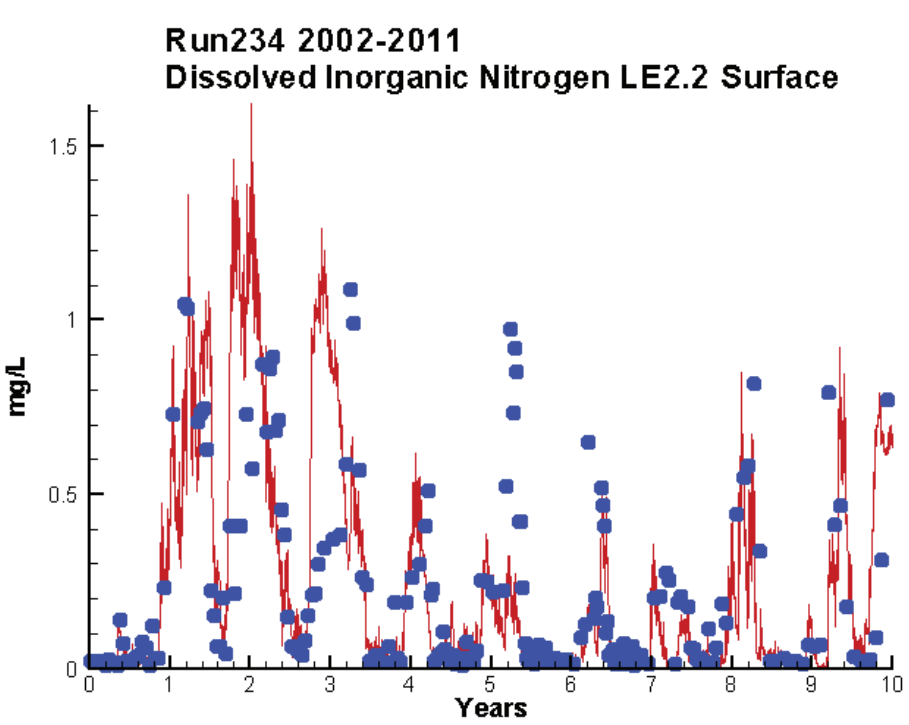

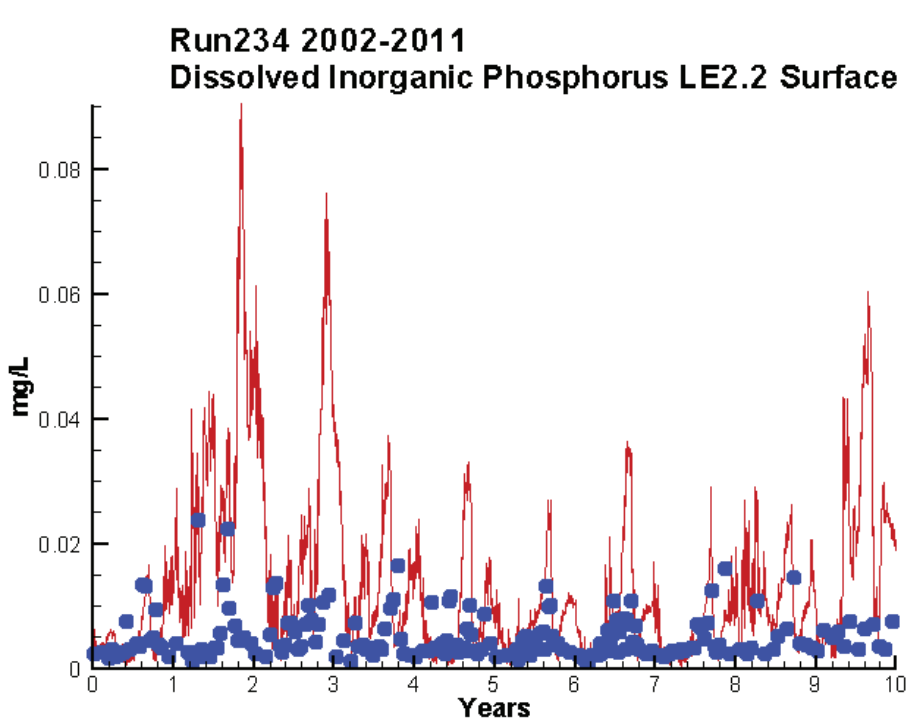

Station LE2.2

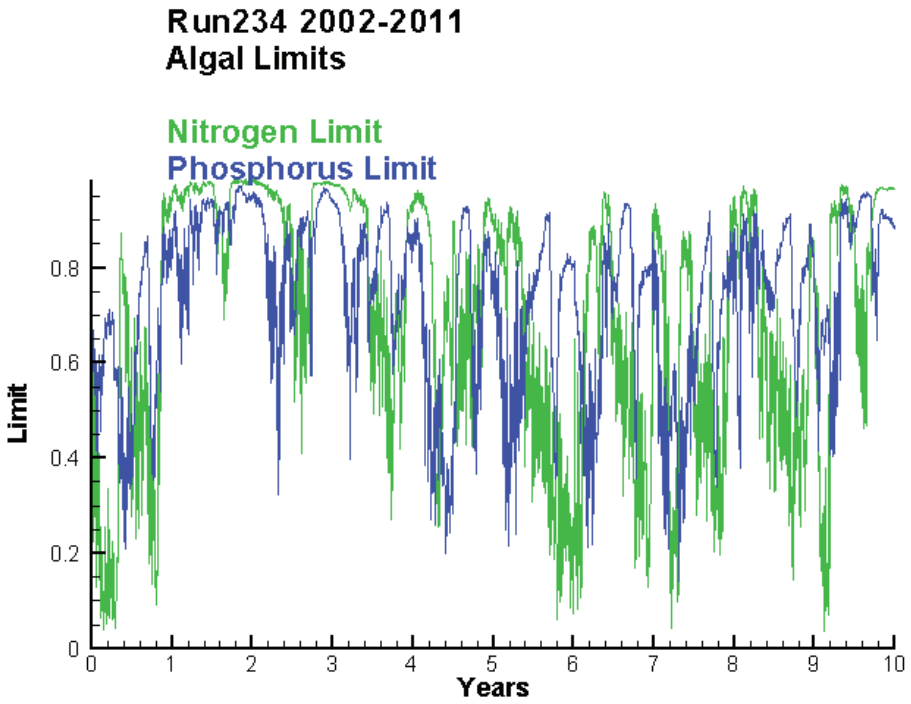

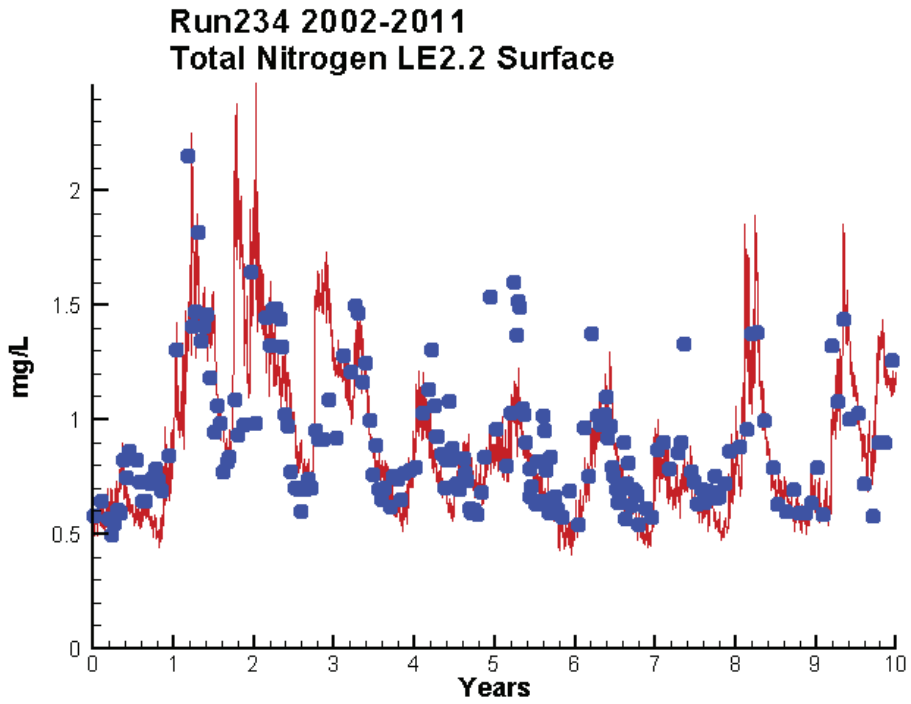

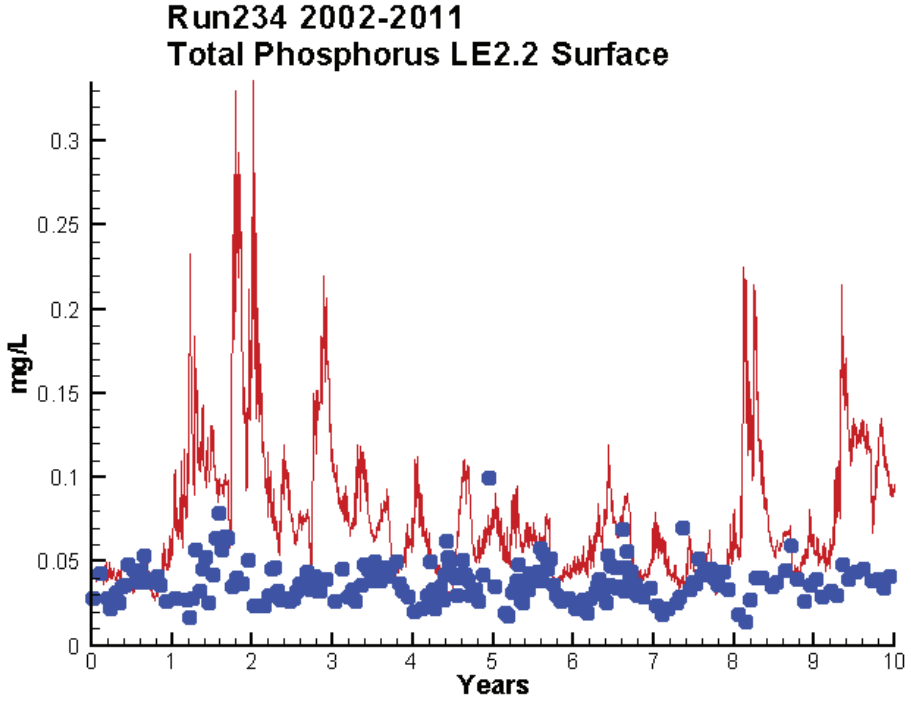

	Mean Difference	Absolute Mean Difference
Chl	-1.4992	7.9650
DIN	-0.0117	0.1407
KE	0.1201	0.3525
DIP	0.0075	0.0089
TP	0.0360	0.0383
TN	-0.0159	0.1703

Station LE2.2

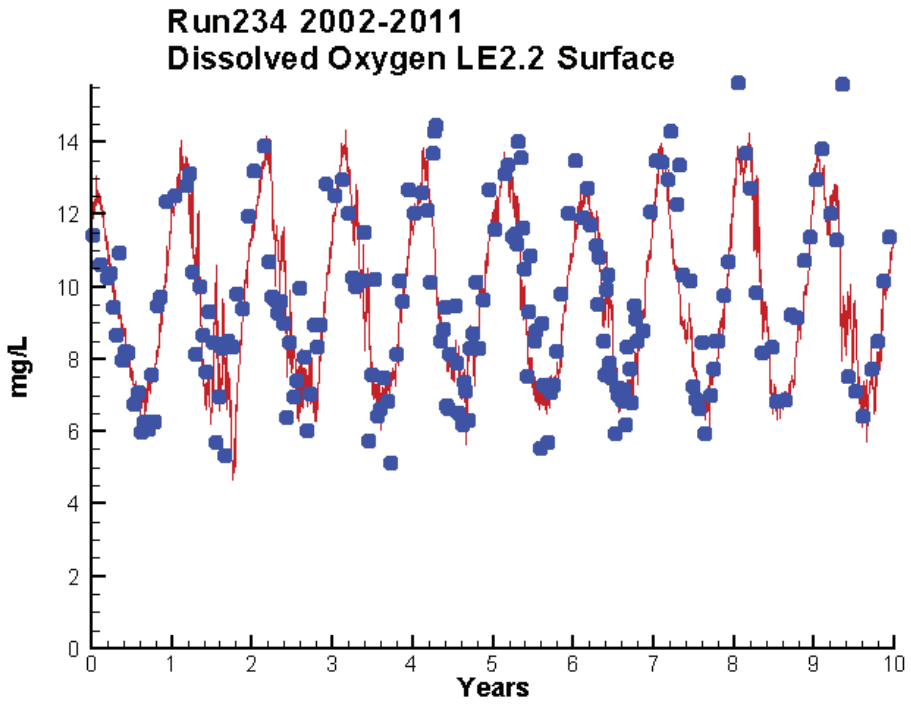

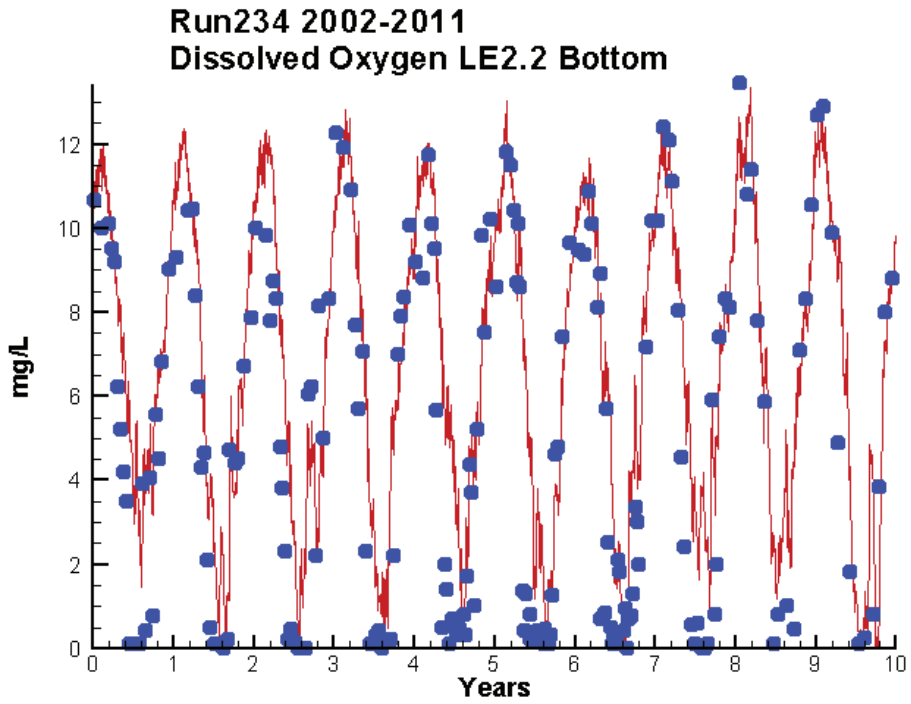

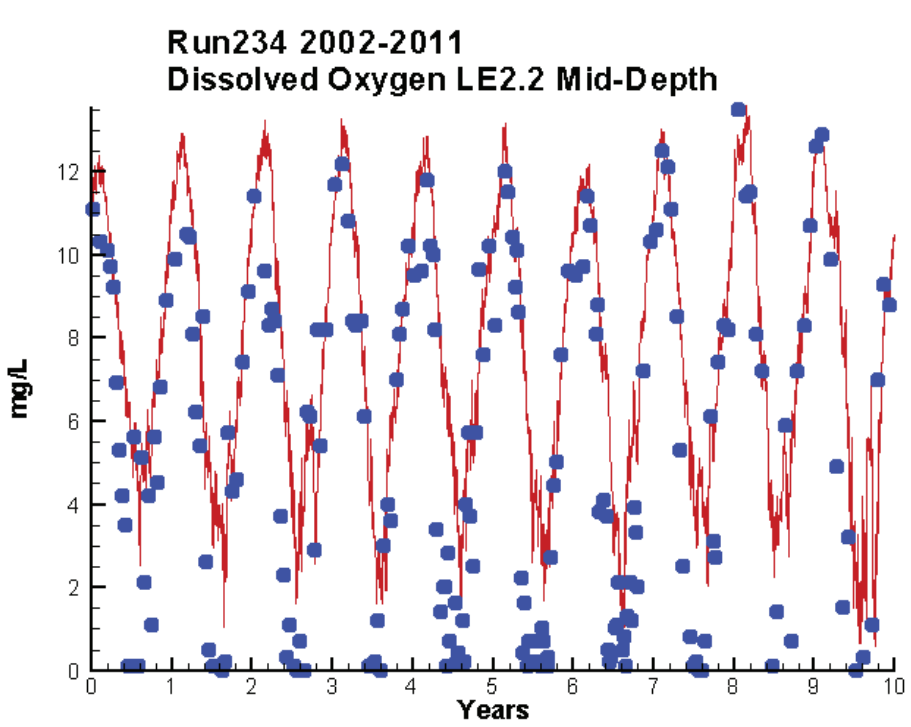

	Mean Difference	Absolute Mean Difference
Top DO	-0.0800	1.0942
Mid DO	2.0622	2.2506
Bot DO	1.4647	1.8082

Station LE2.2

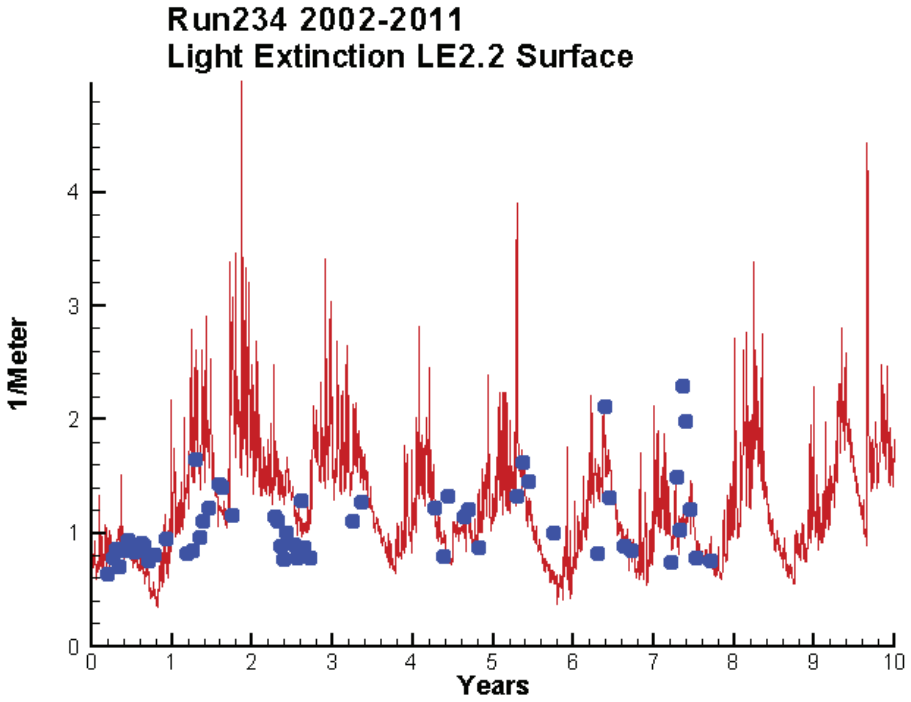

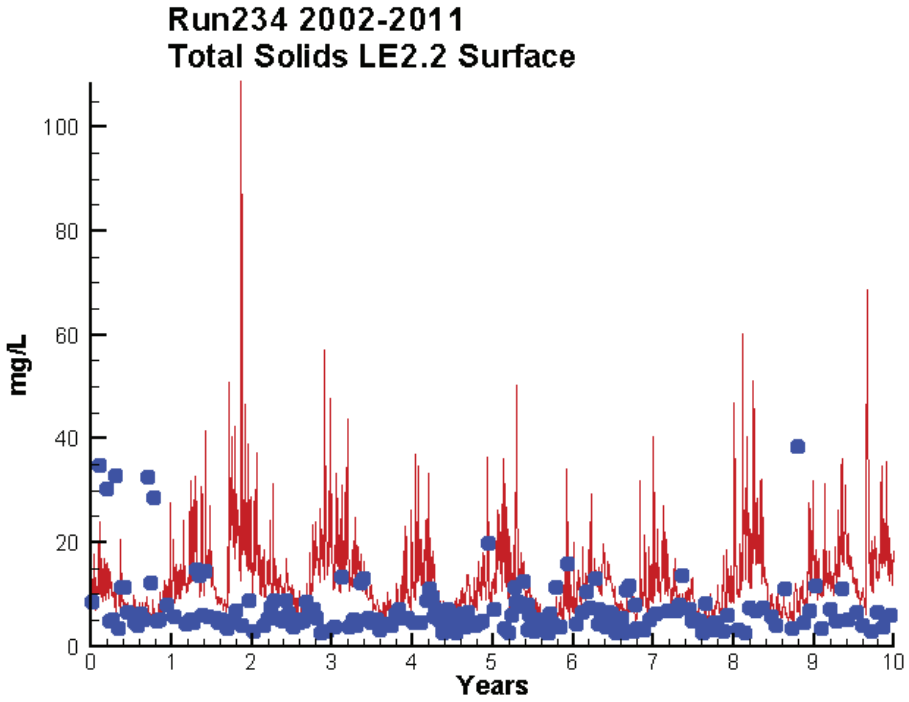

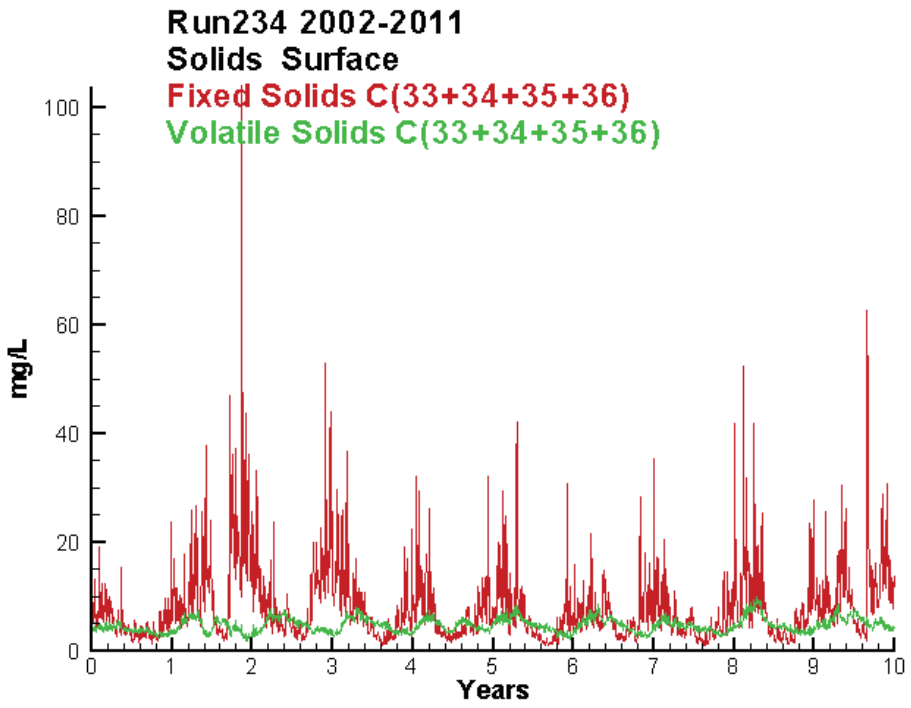

	Mean Difference	Absolute Mean Difference
KE	0.1201	0.3525
TSS	4.2616	6.2609

Station RET2.4

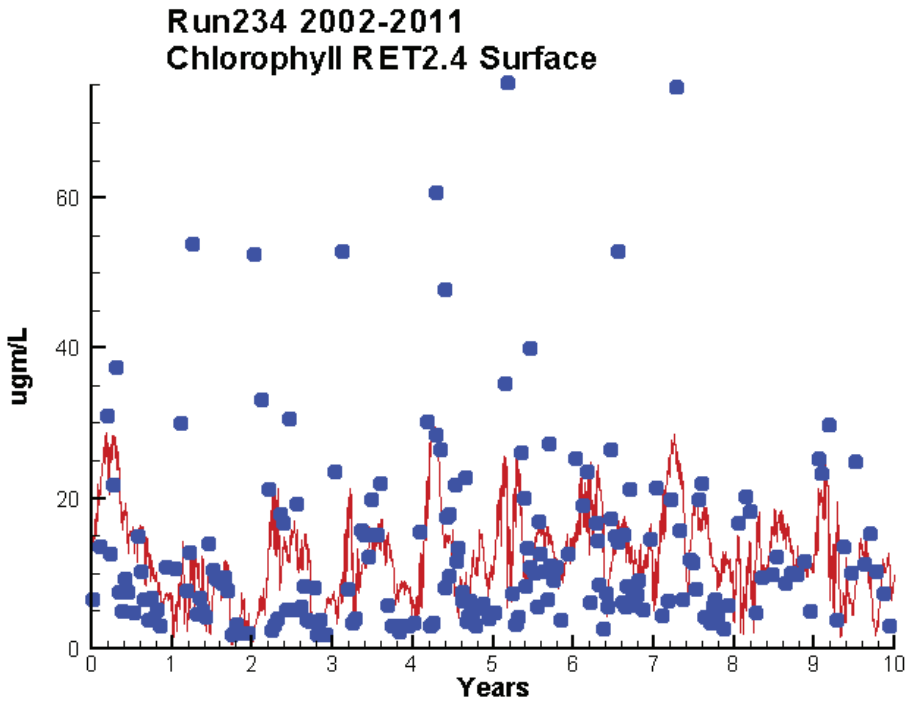

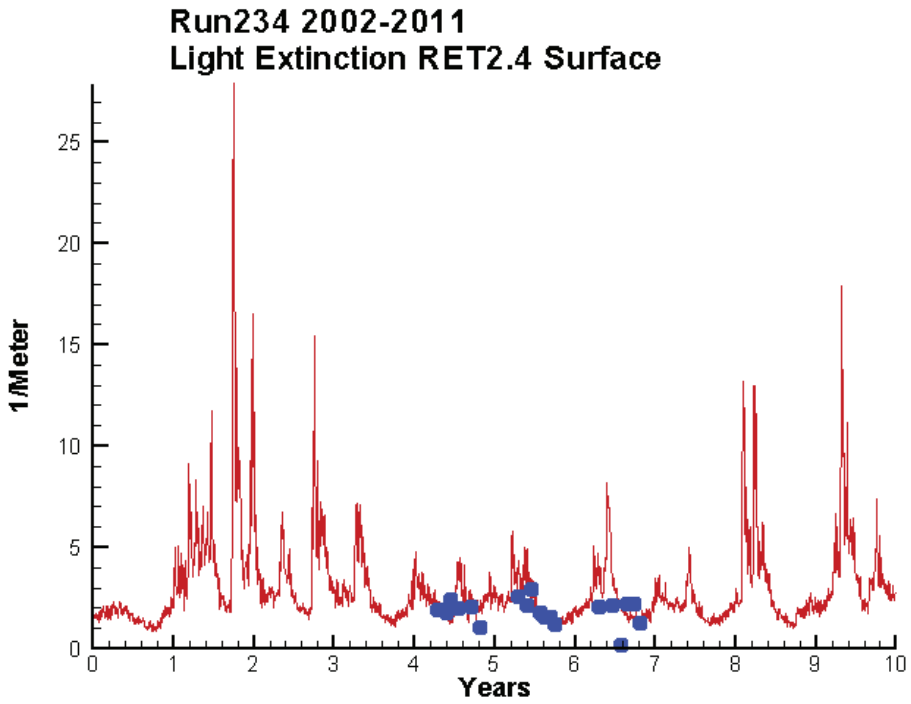

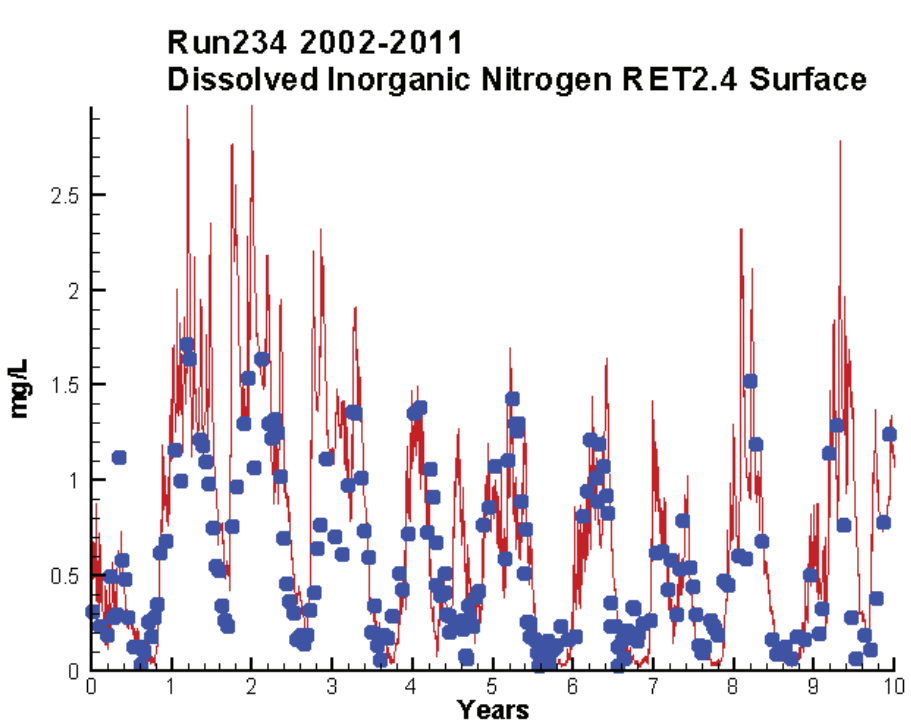

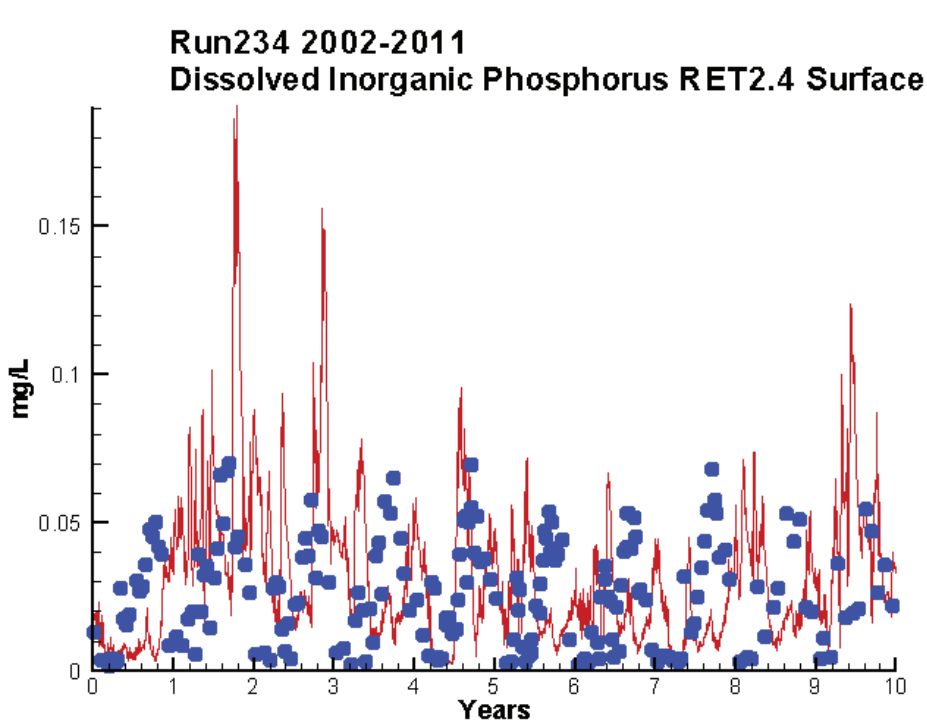

Station RET2.4

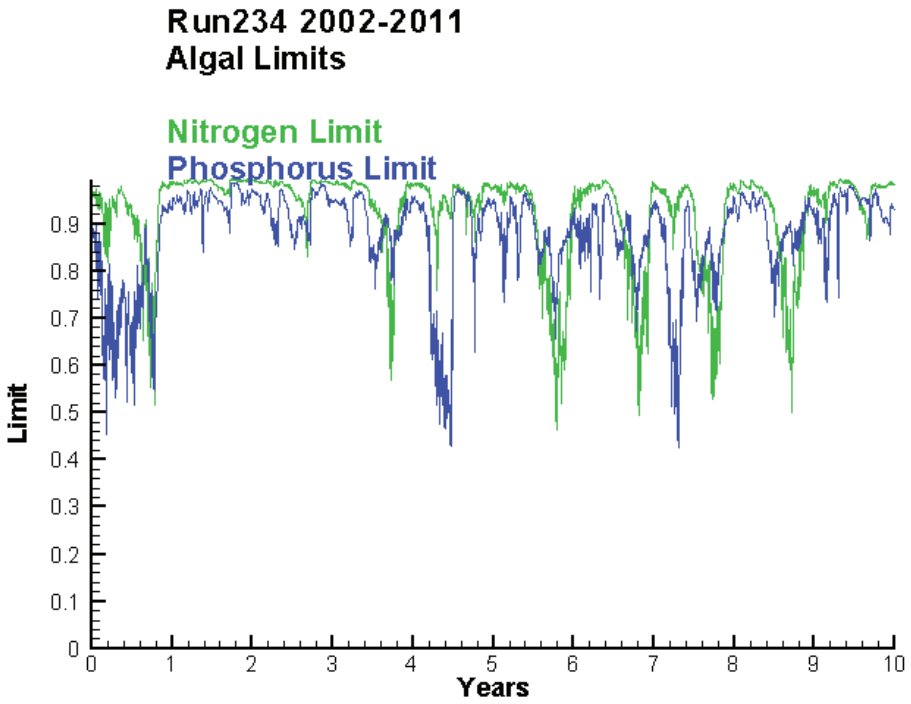

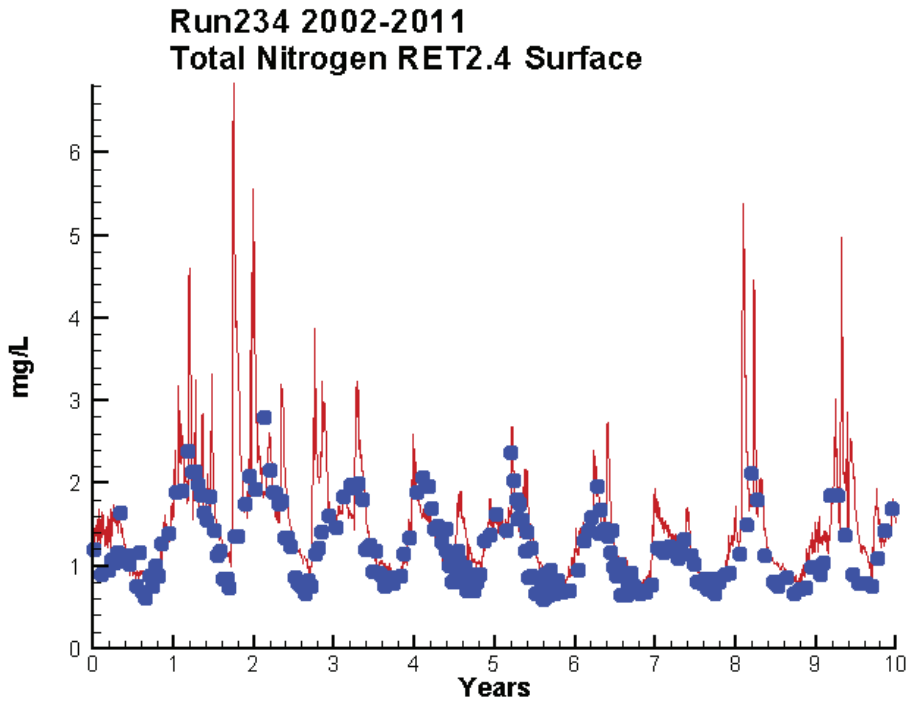

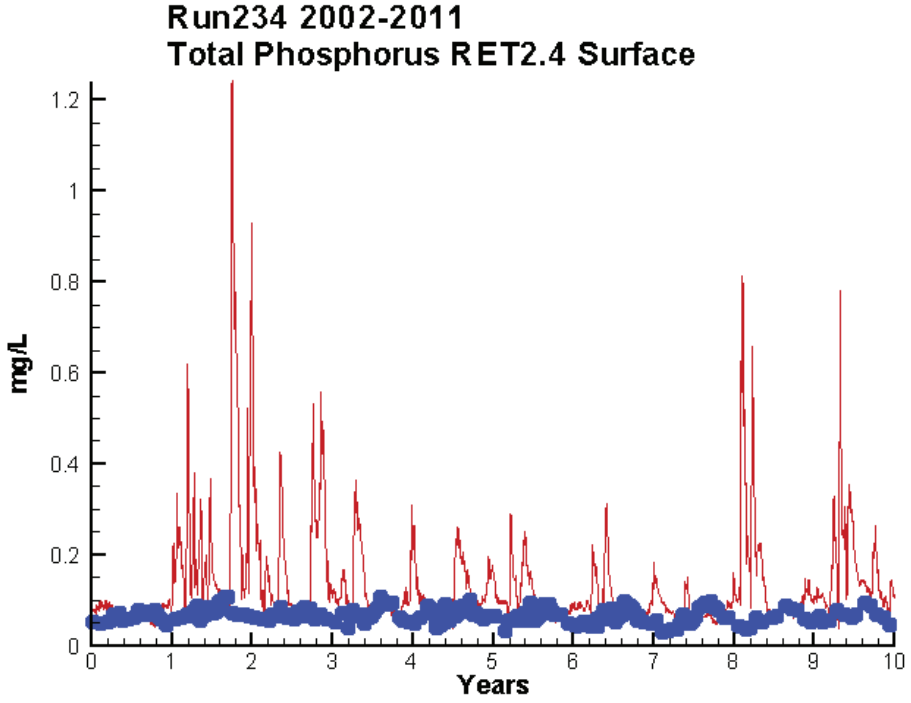

	Mean Difference	Absolute Mean Difference
Chl	-0.0939	8.3410
DIN	0.1040	0.2633
KE	0.4804	0.7807
DIP	0.0029	0.0243
TP	0.0567	0.0649
TN	0.2280	0.3217

Station RET2.4

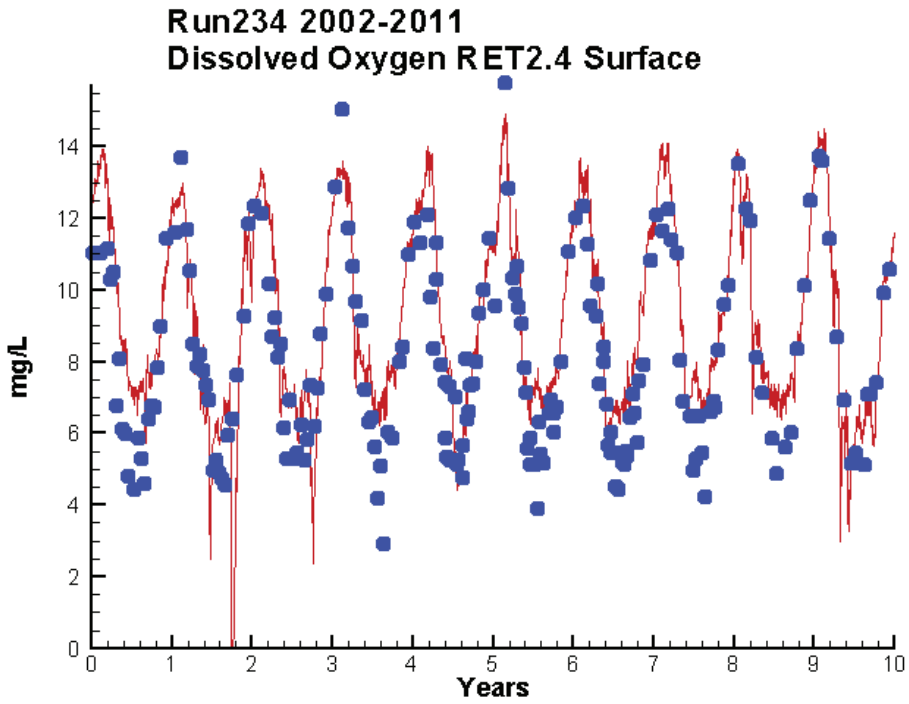

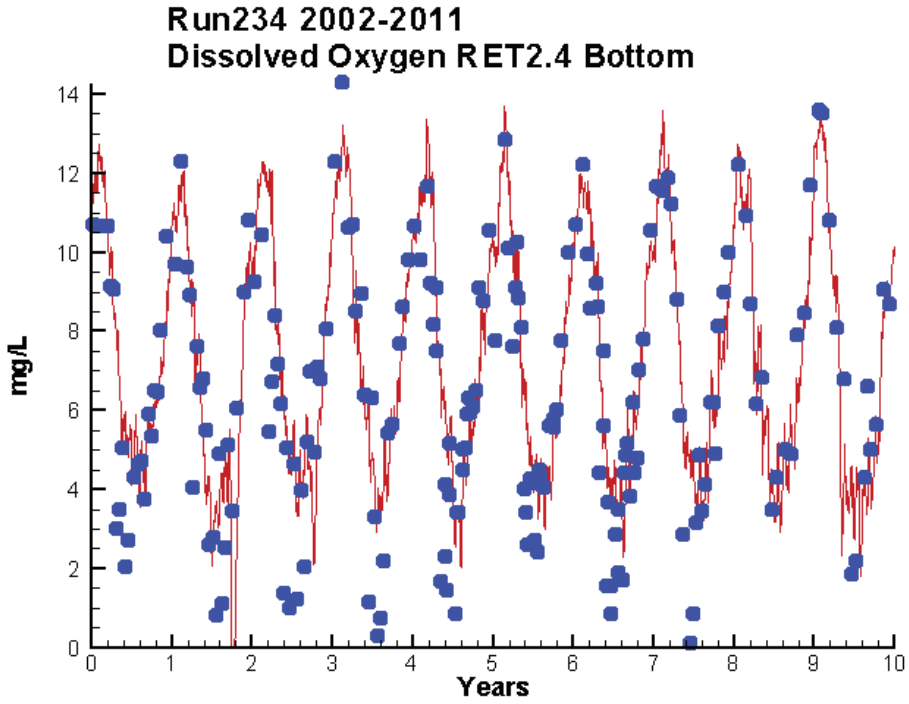

	Mean Difference	Absolute Mean Difference
Top DO	0.8228	1.2107
Bot DO	0.5577	1.3043

Station RET2.4

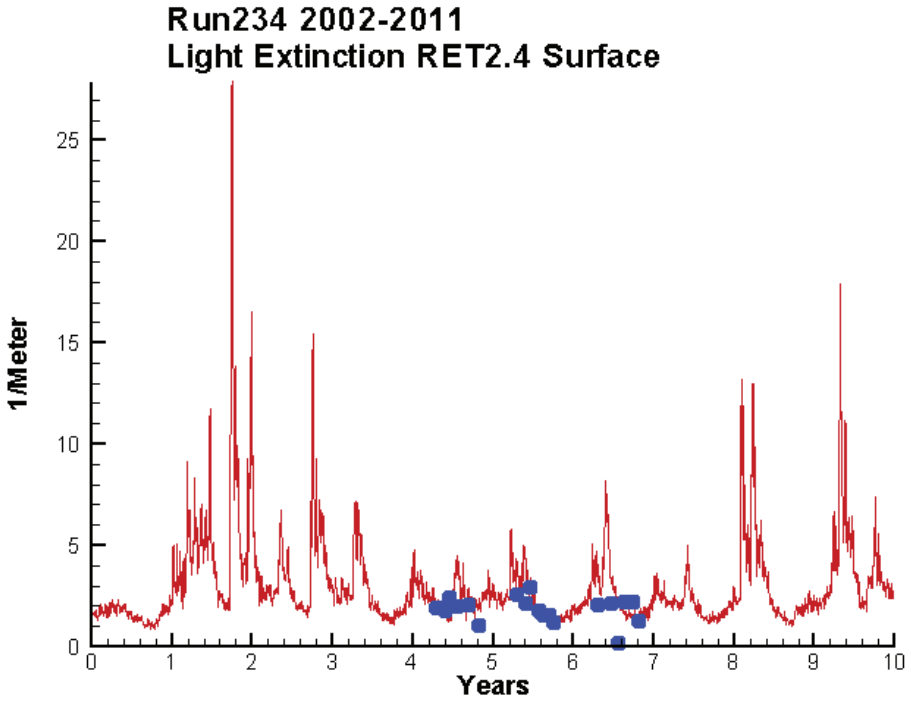

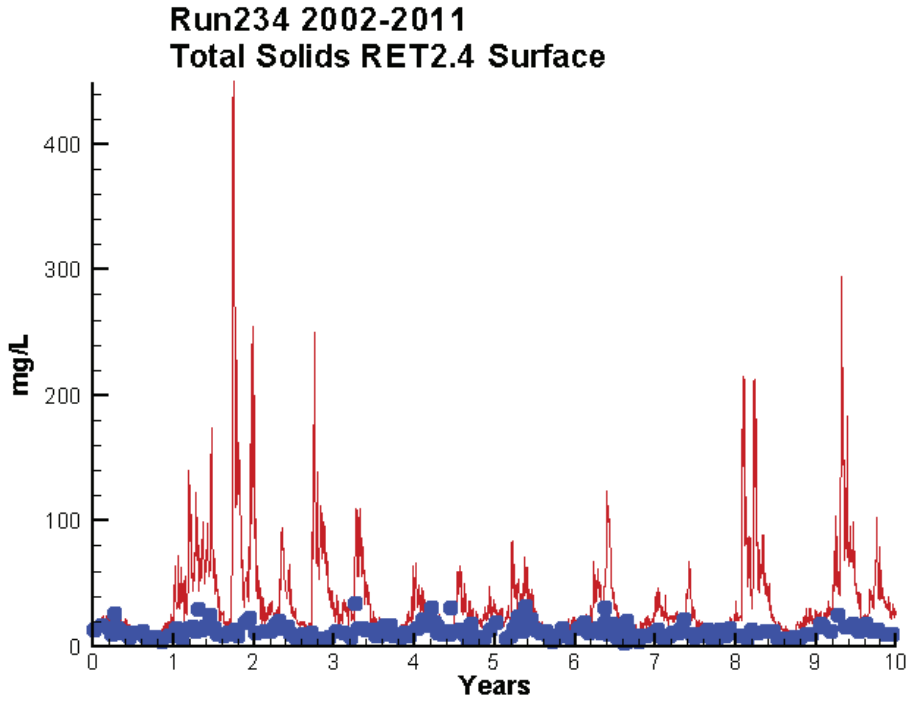

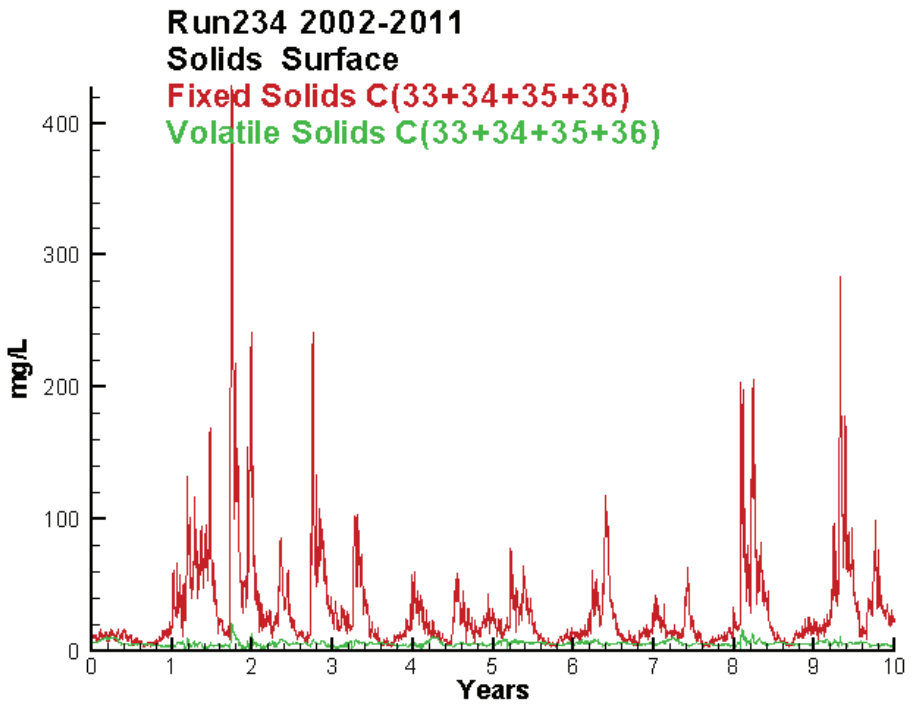

	Mean Difference	Absolute Mean Difference
KE	0.4804	0.7807
TSS	20.2858	20.7739

Station TF2.1

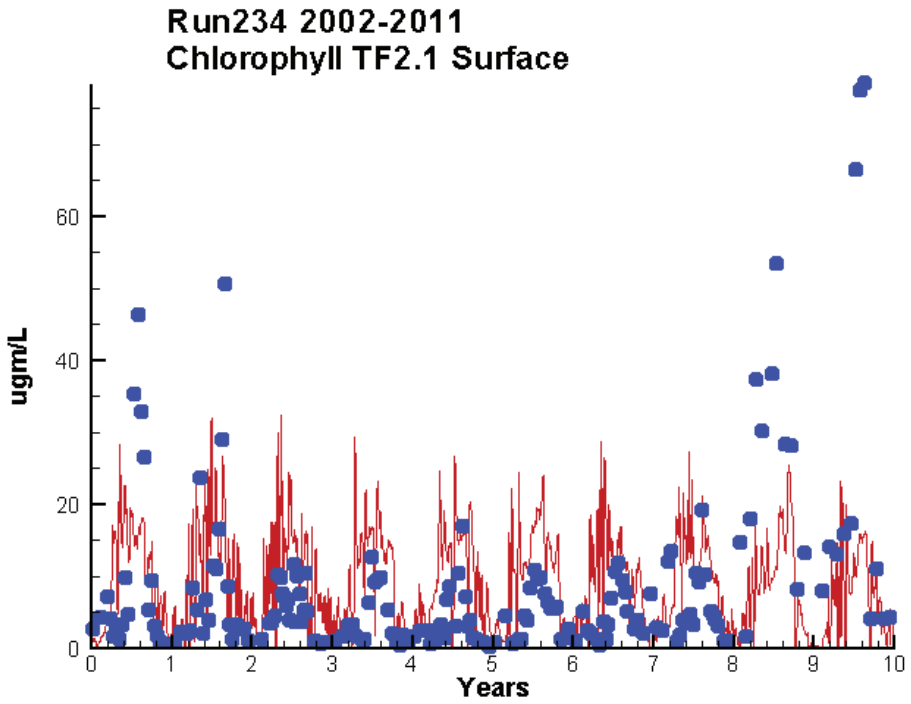

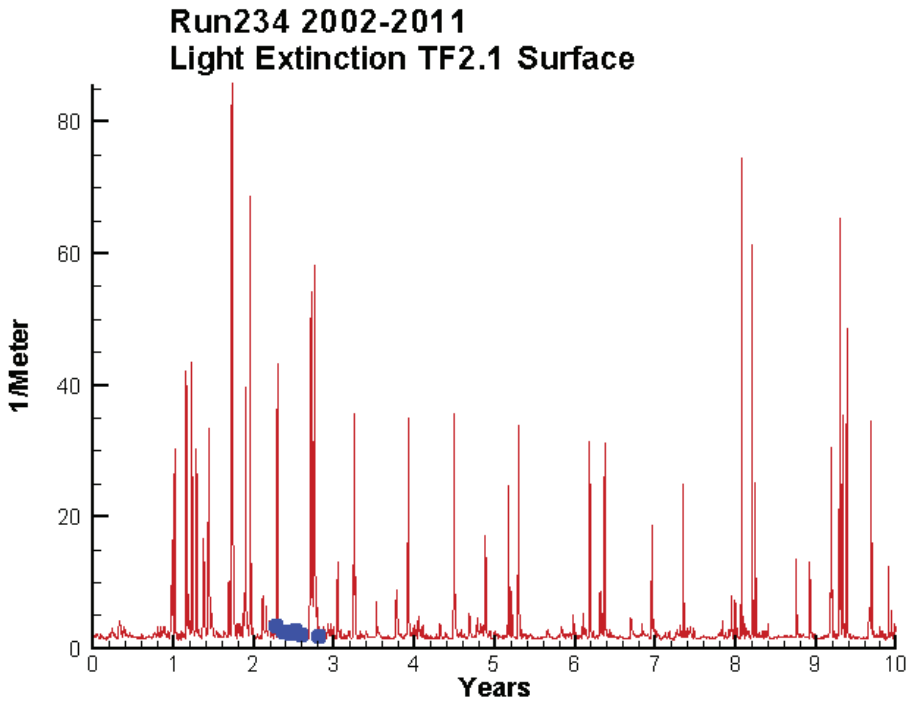

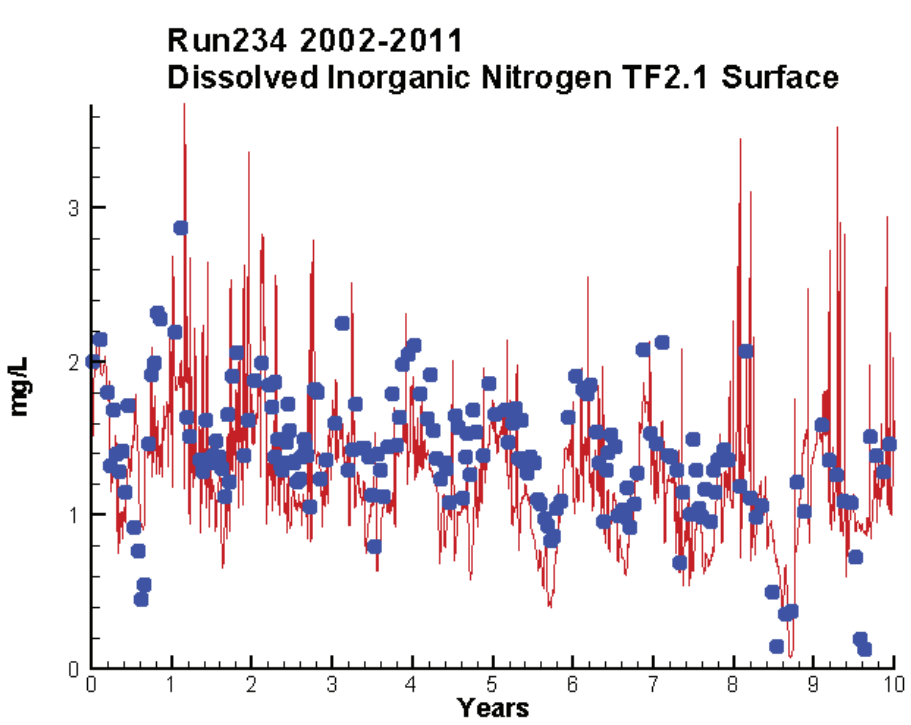

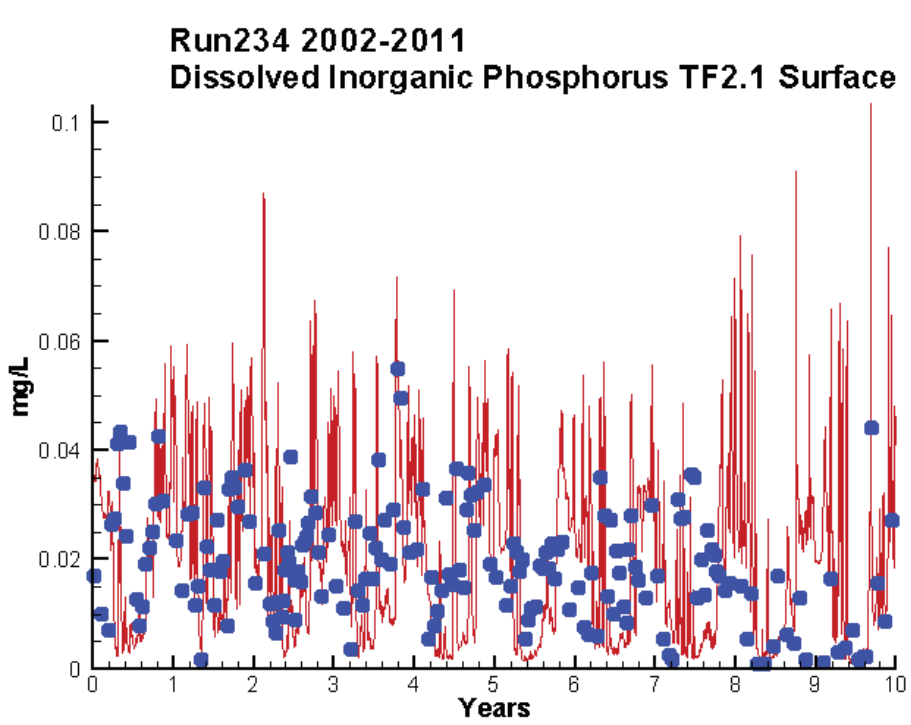

Station TF2.1

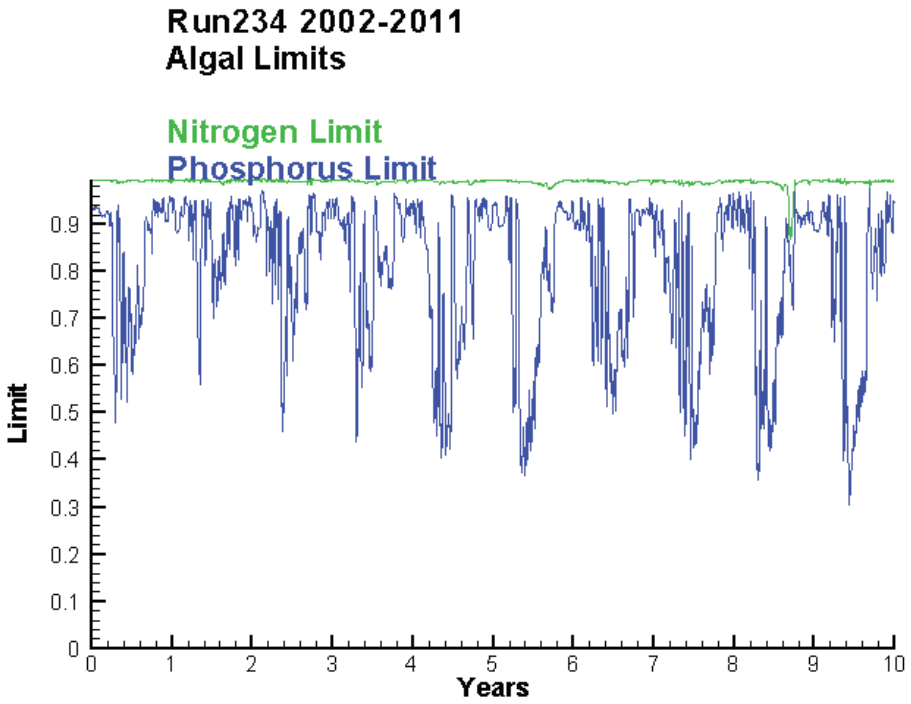

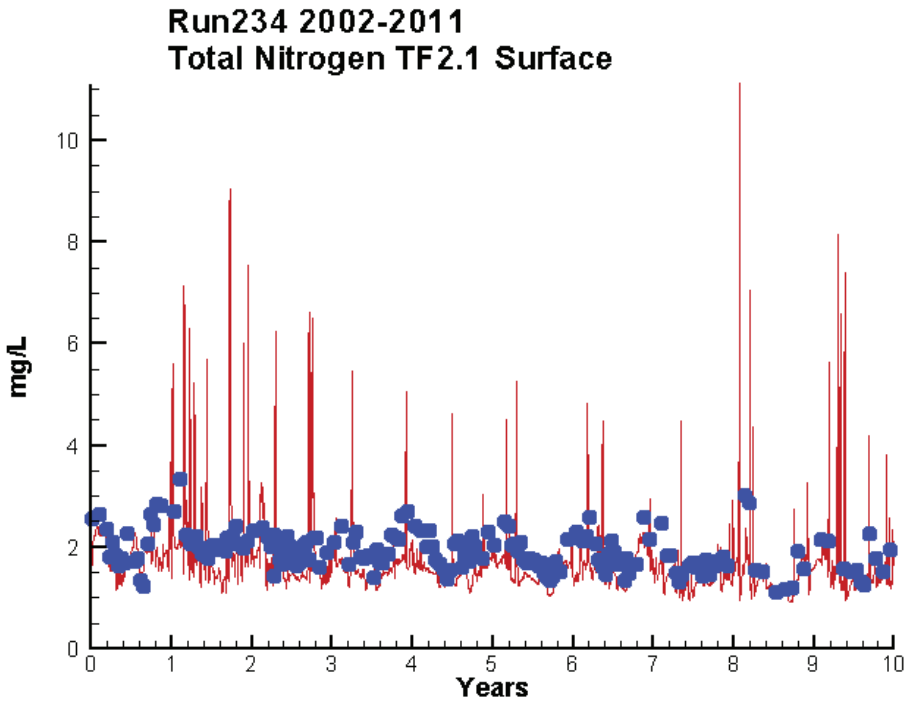

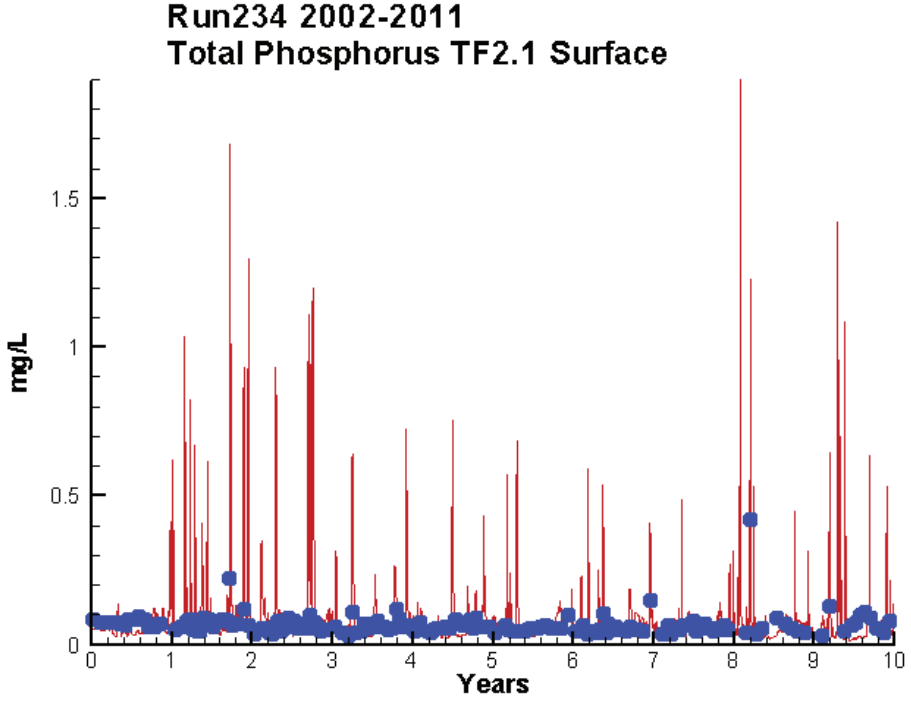

	Mean Difference	Absolute Mean Difference
Chl	2.1354	8.8321
DIN	-0.1867	0.3749
KE	3.6341	4.1056
DIP	-0.0008	0.0134
TP	0.0206	0.0485
TN	-0.2424	0.5049

Station TF2.1

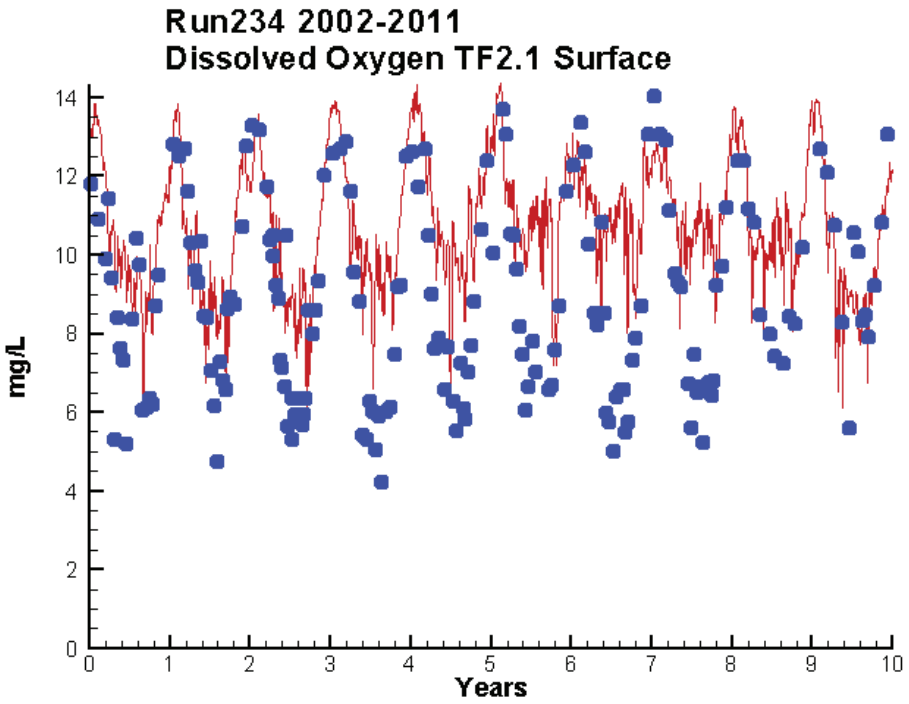

	Mean Difference	Absolute Mean Difference
Top DO	1.6528	2.0936

Station TF2.1

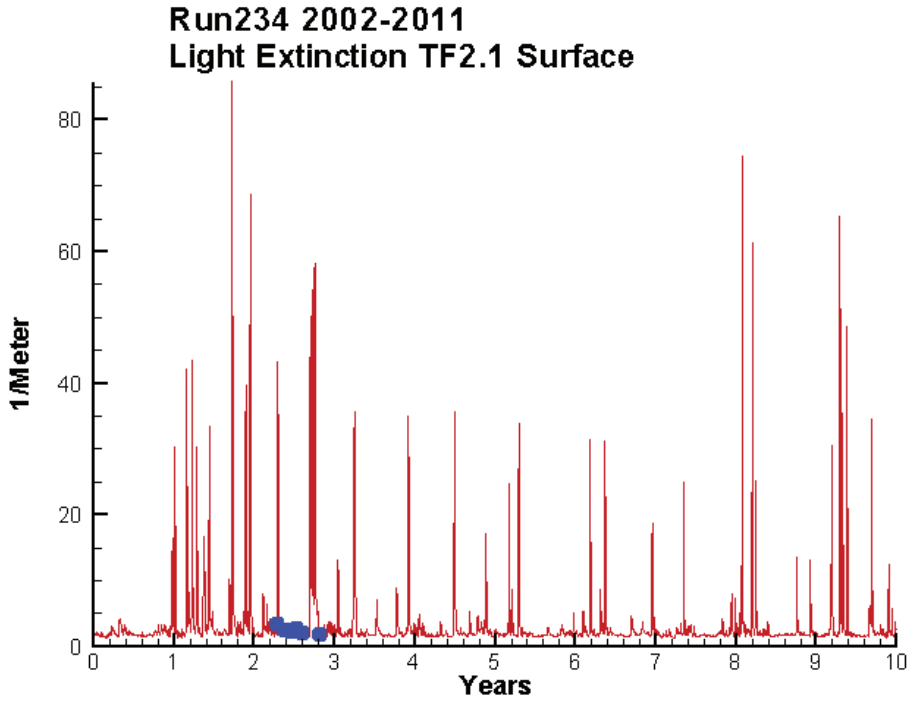

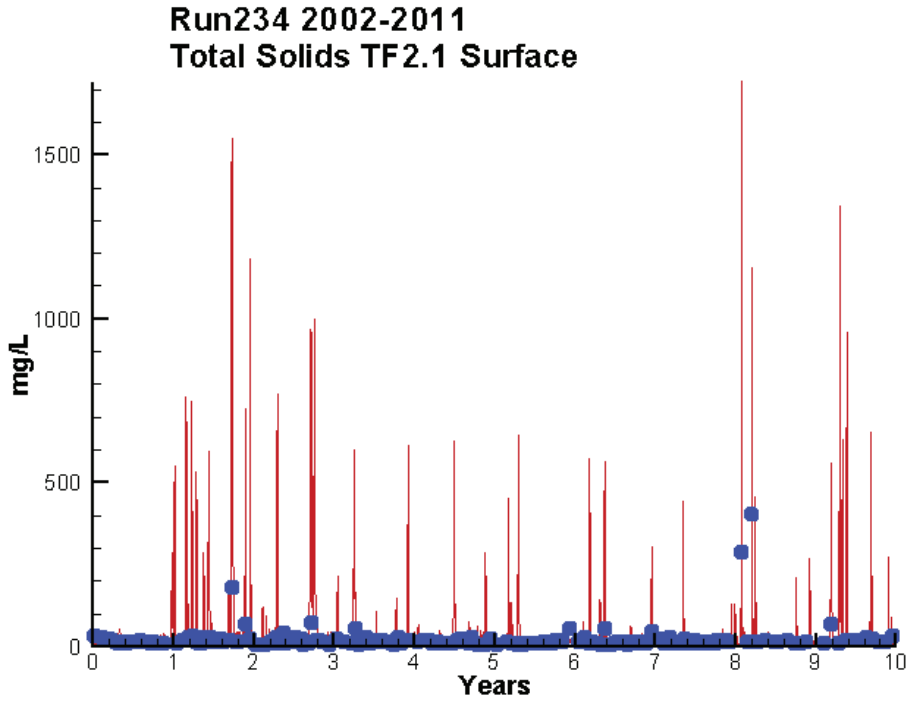

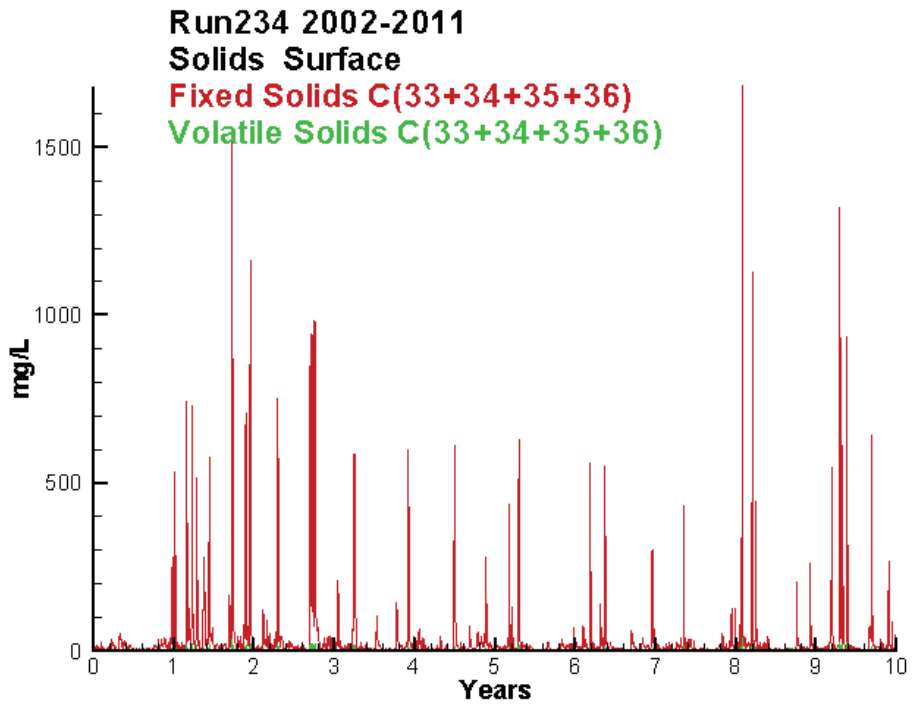

	Mean Difference	Absolute Mean Difference
KE	3.6341	4.1056
TSS	22.2566	31.8525

Station LE3.2

Run234 2002-2011
Chlorophyll LE3.2 Surface

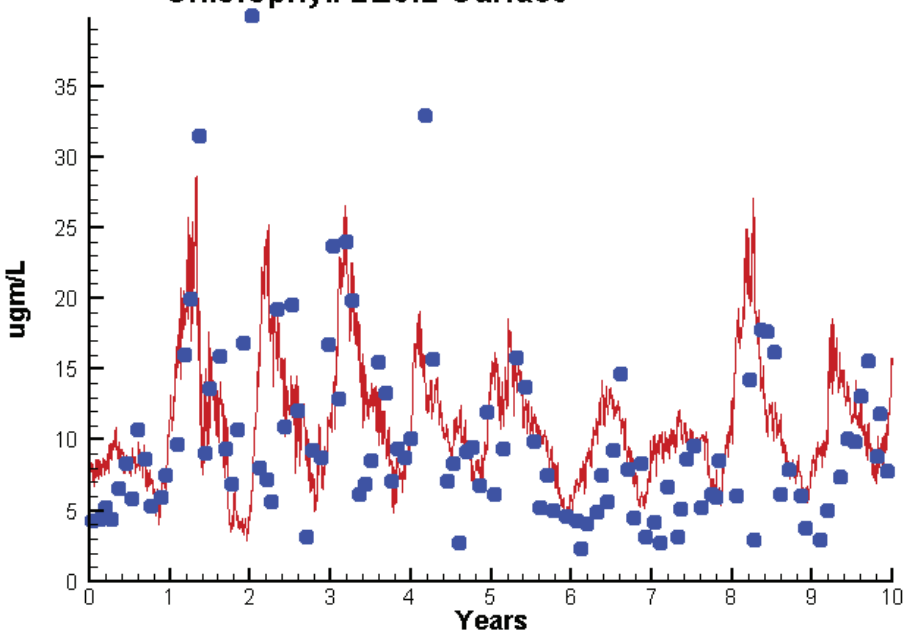

Run234 2002-2011
Light Extinction LE3.2 Surface

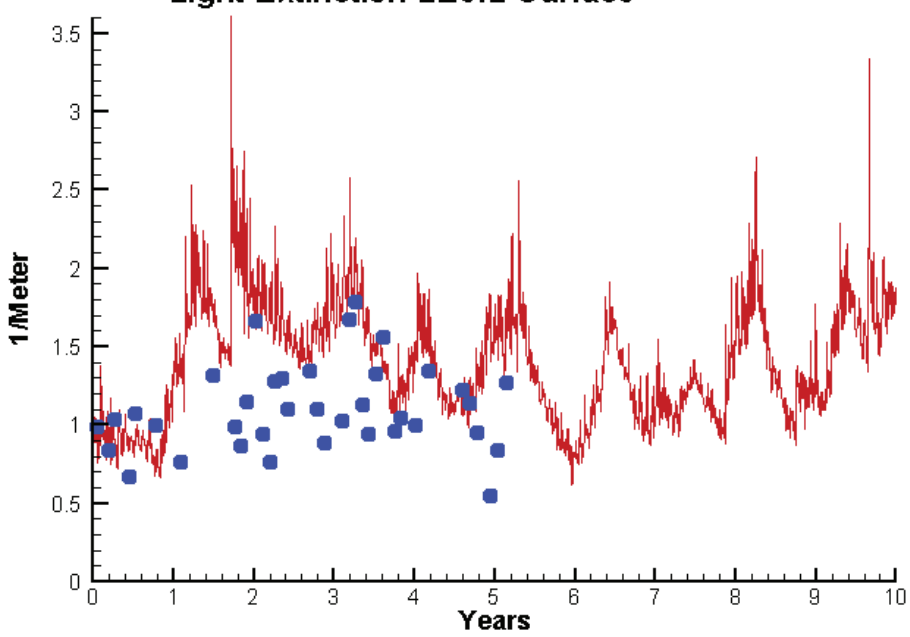

Run234 2002-2011
Dissolved Inorganic Nitrogen LE3.2 Surface

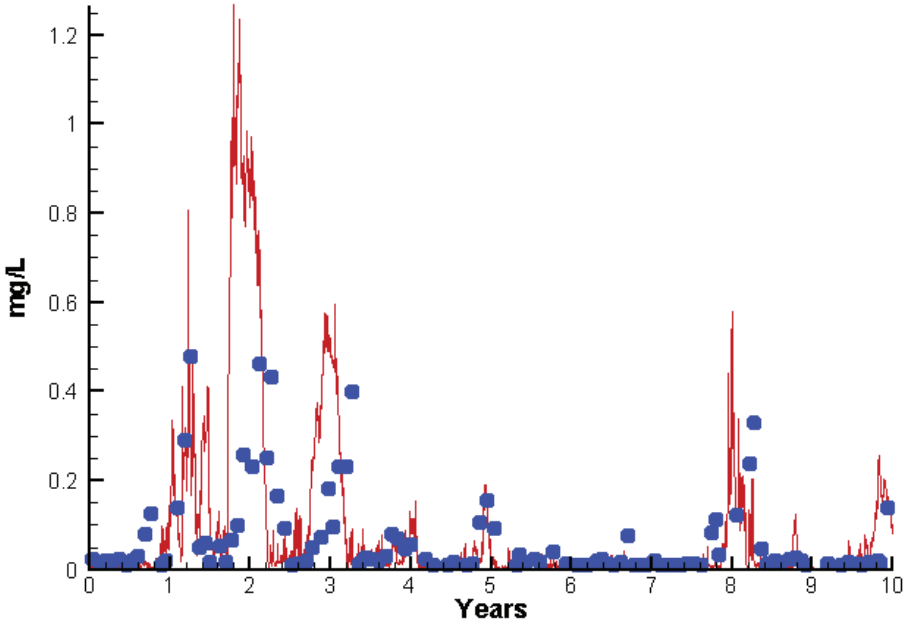

Run234 2002-2011
Dissolved Inorganic Phosphorus LE3.2 Surface

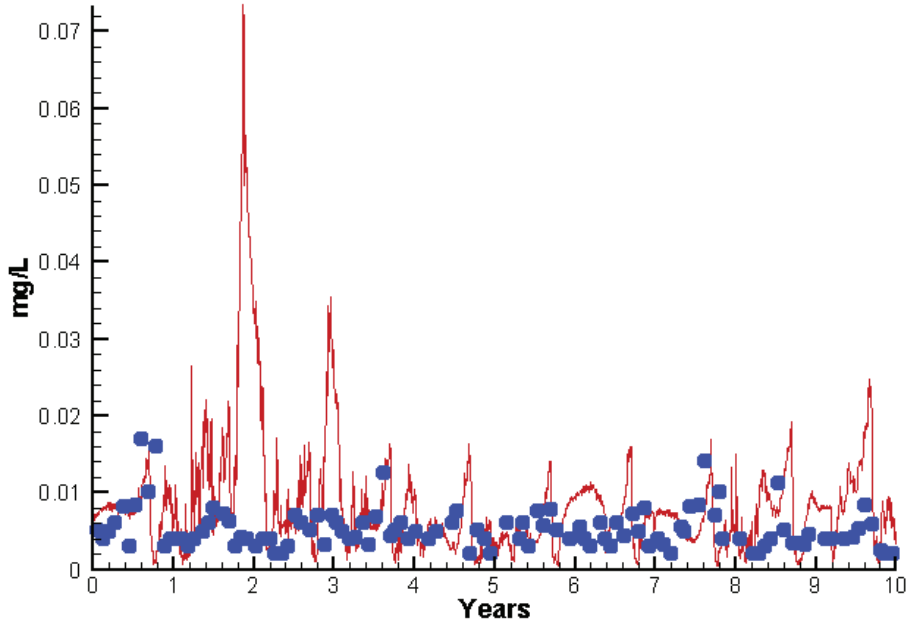

Station LE3.2

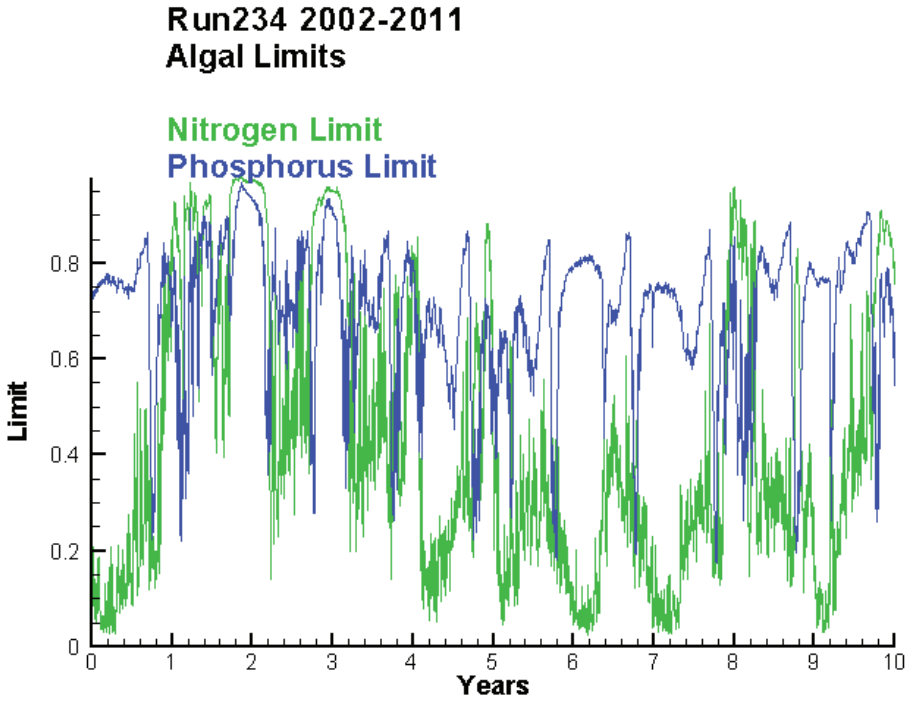

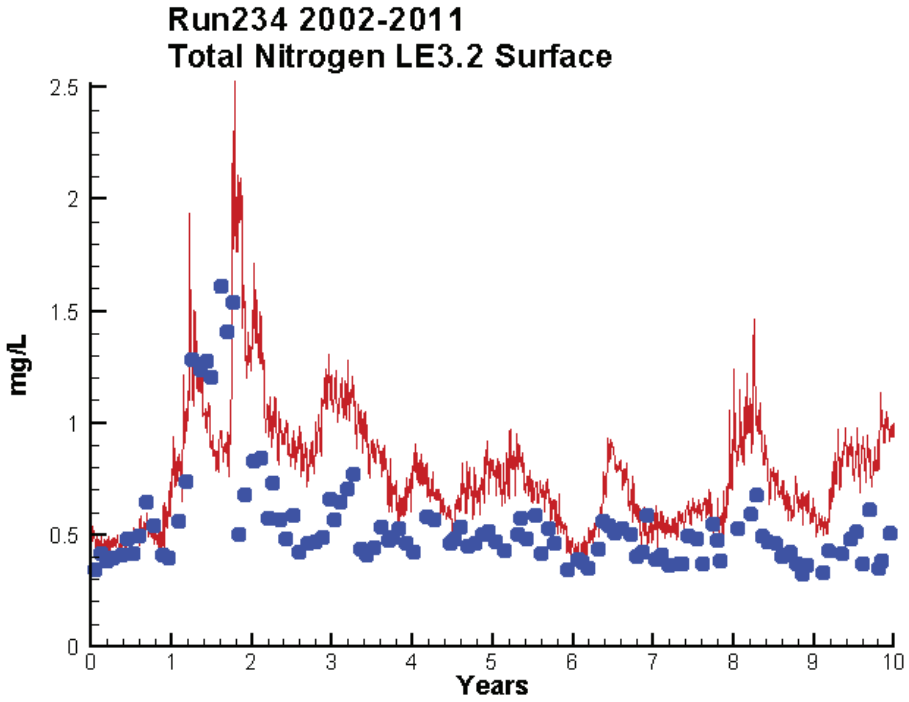

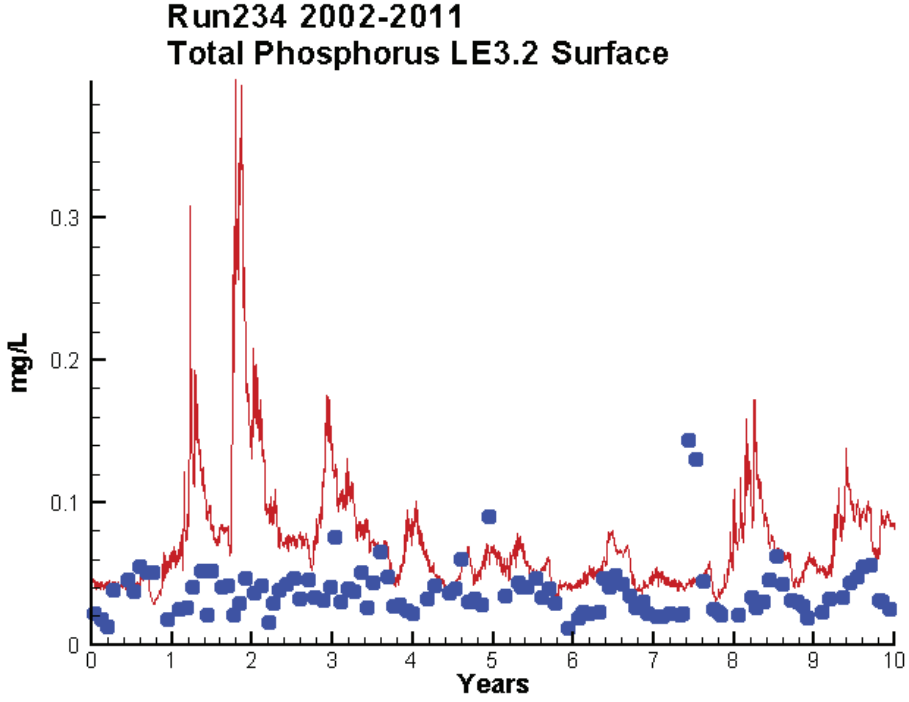

	Mean Difference	Absolute Mean Difference
Chl	1.1537	4.4404
DIN	0.0273	0.0861
KE	0.3920	0.4428
DIP	0.0036	0.0056
TP	0.0360	0.0406
TN	0.2430	0.2812

Station LE3.2

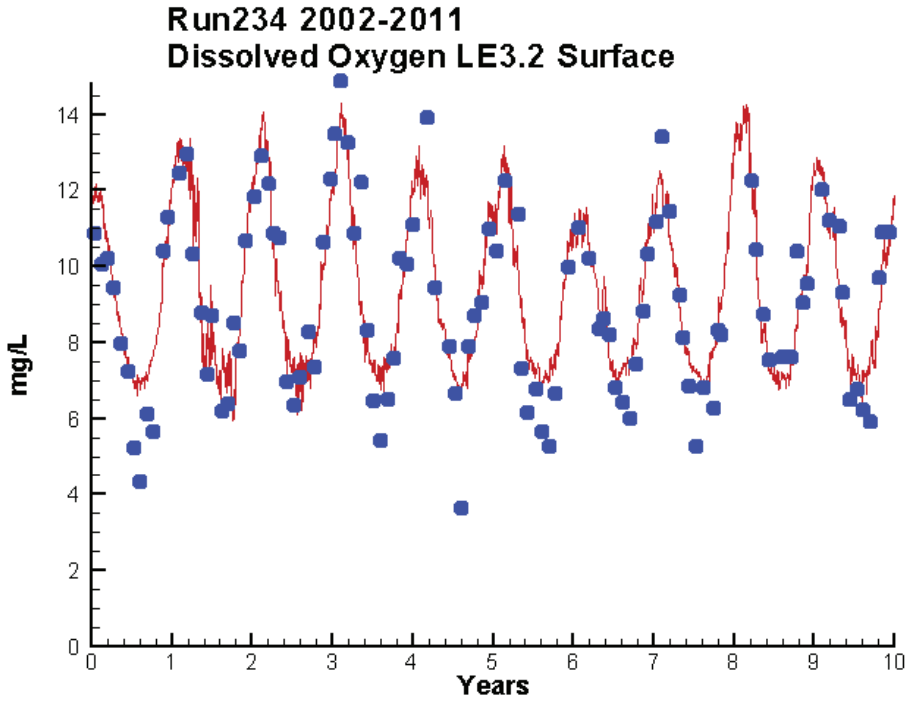

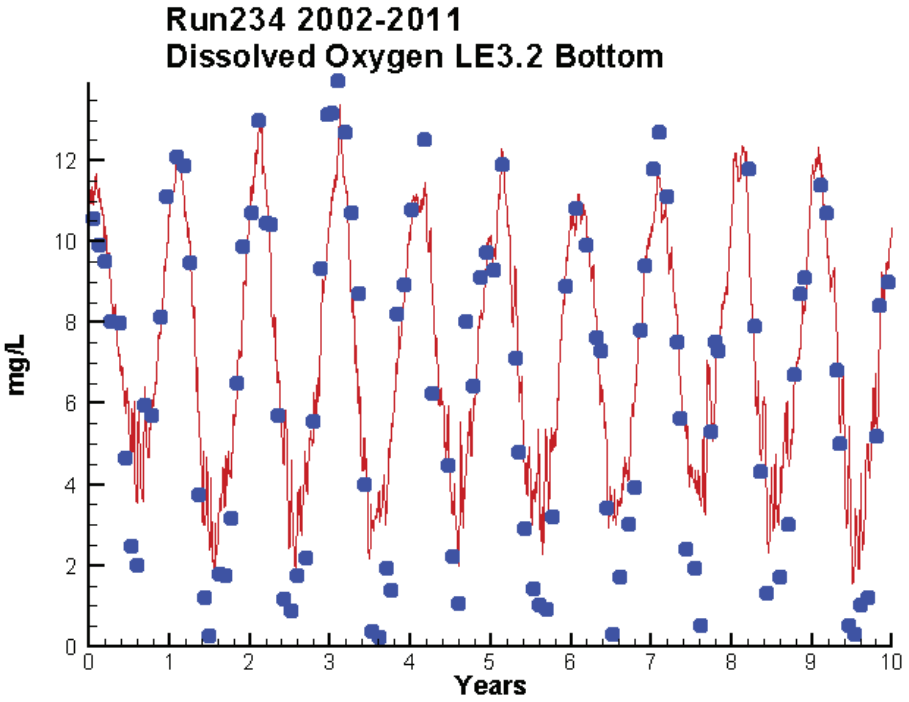

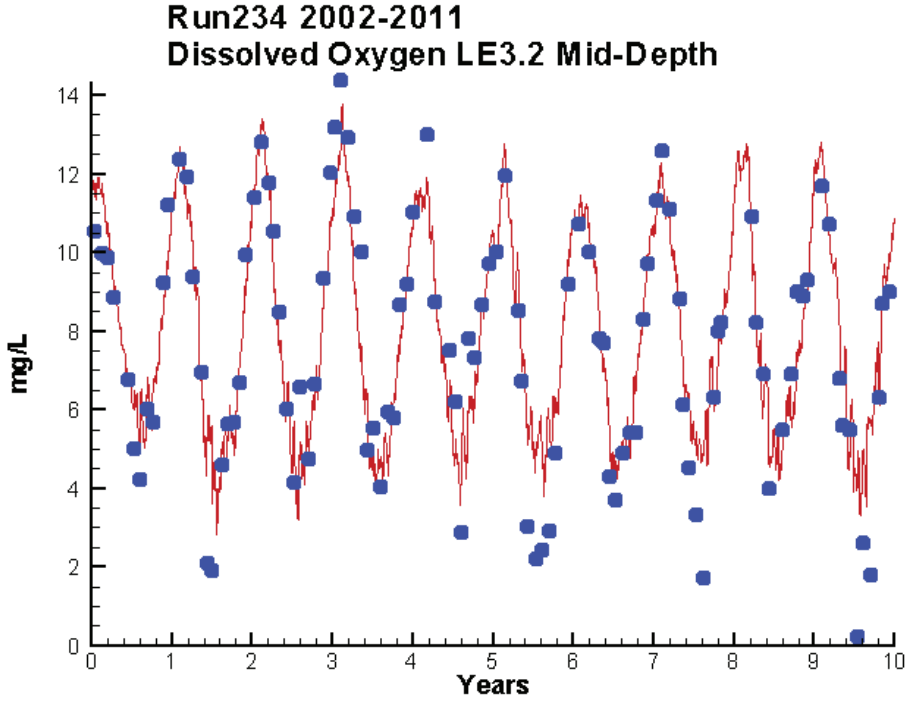

	Mean Difference	Absolute Mean Difference
Top DO	0.2340	0.8697
Mid DO	0.2823	0.9218
Bot DO	0.6430	1.3746

Station LE3.2

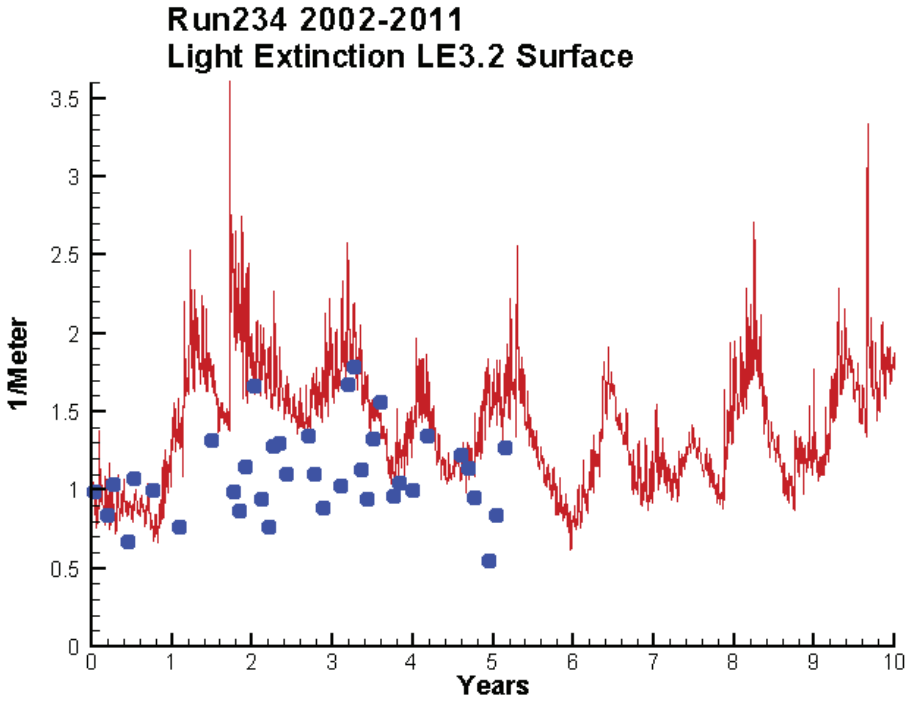

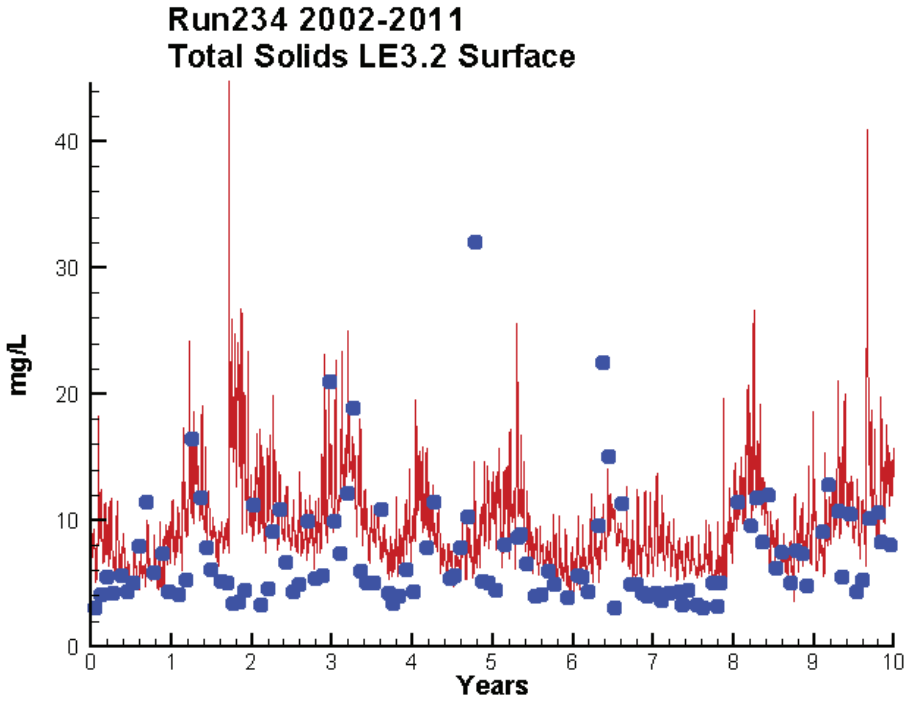

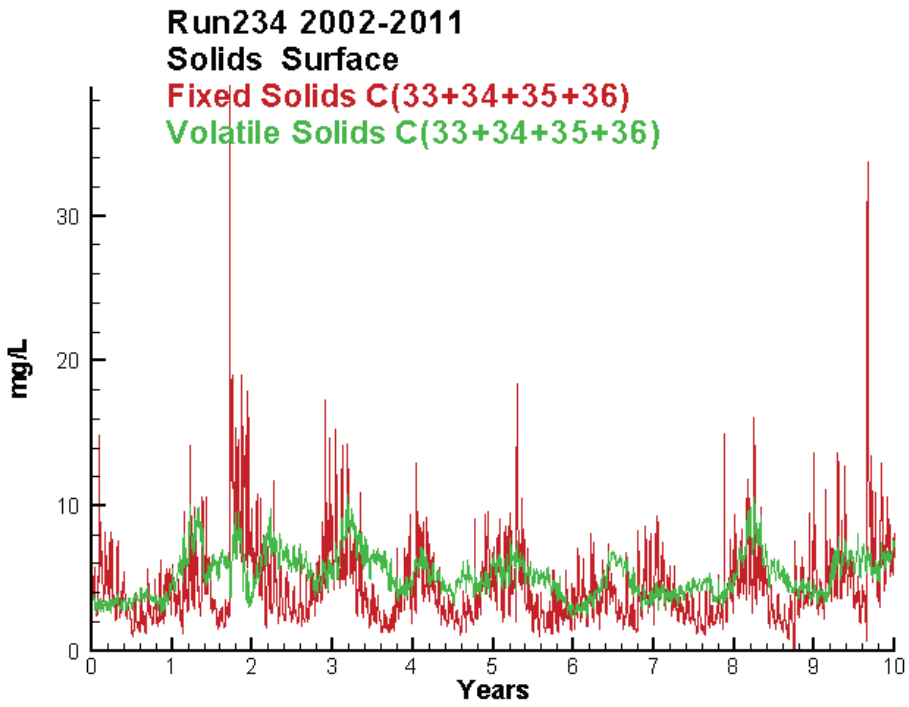

	Mean Difference	Absolute Mean Difference
KE	0.3920	0.4428
TSS	2.2527	3.8175

Station RET3.2

Run234 2002-2011
Chlorophyll RET3.2 Surface

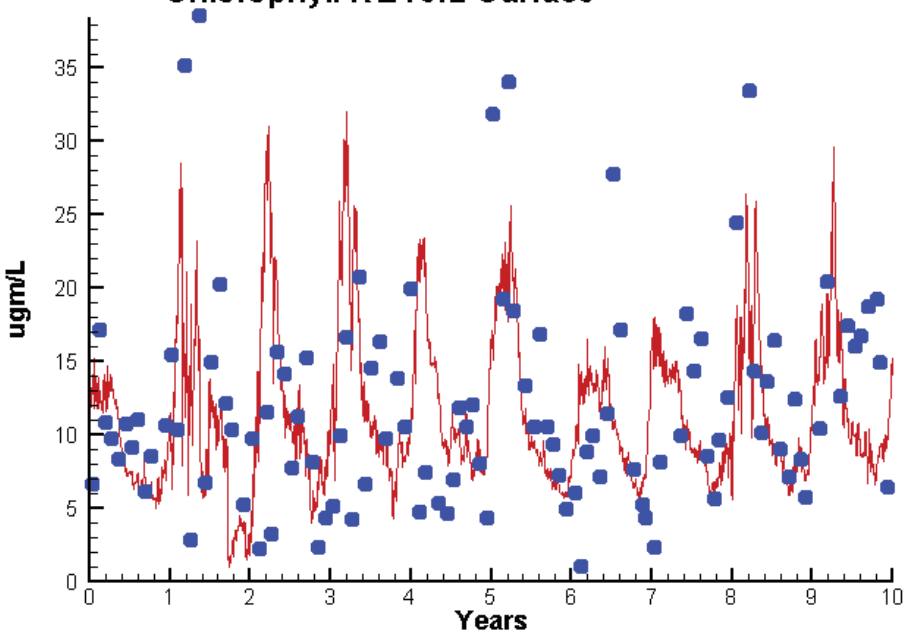

Run234 2002-2011
Light Extinction RET3.2 Surface

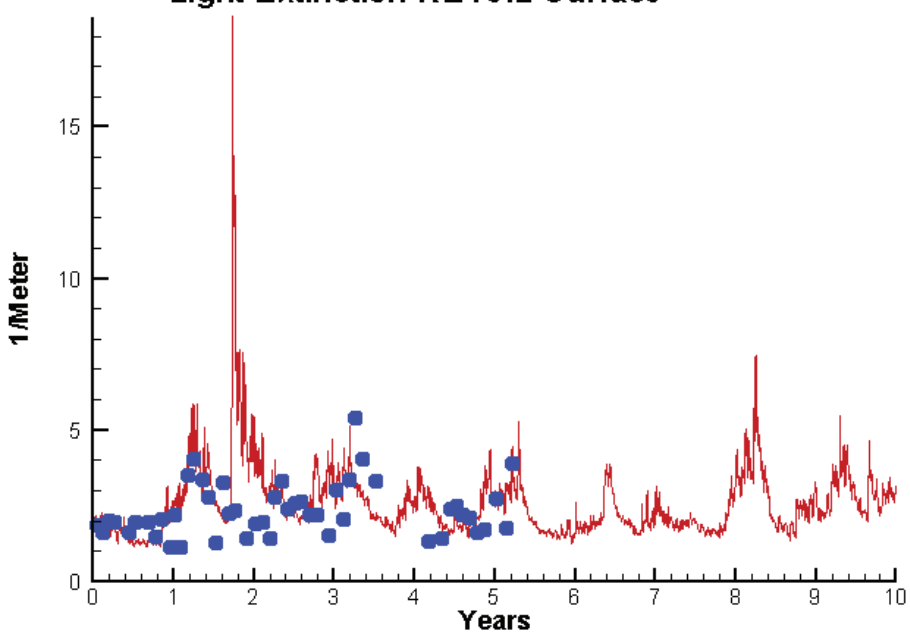

Run234 2002-2011
Dissolved Inorganic Nitrogen RET3.2 Surface

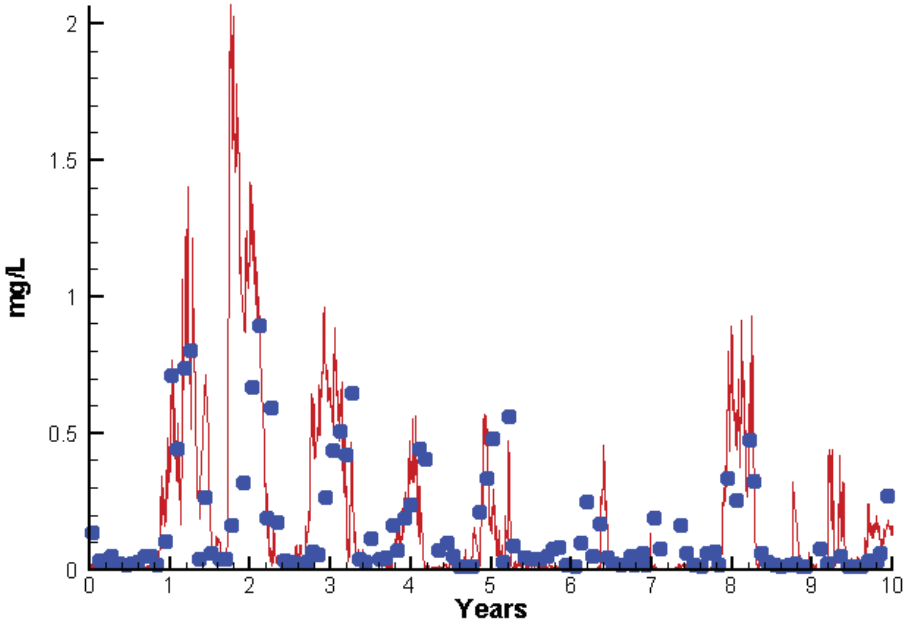

Run234 2002-2011
Dissolved Inorganic Phosphorus RET3.2 Surface

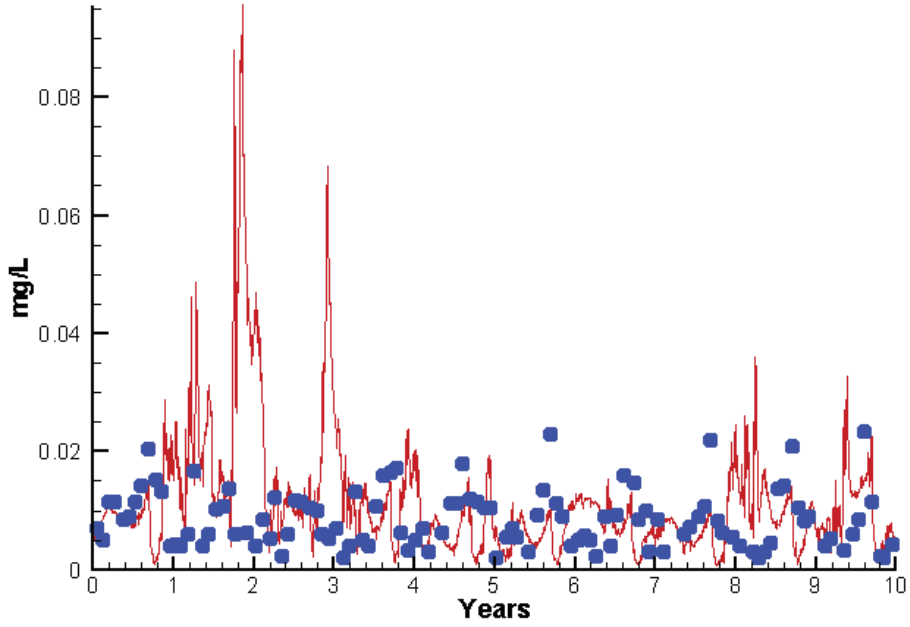

Station RET3.2

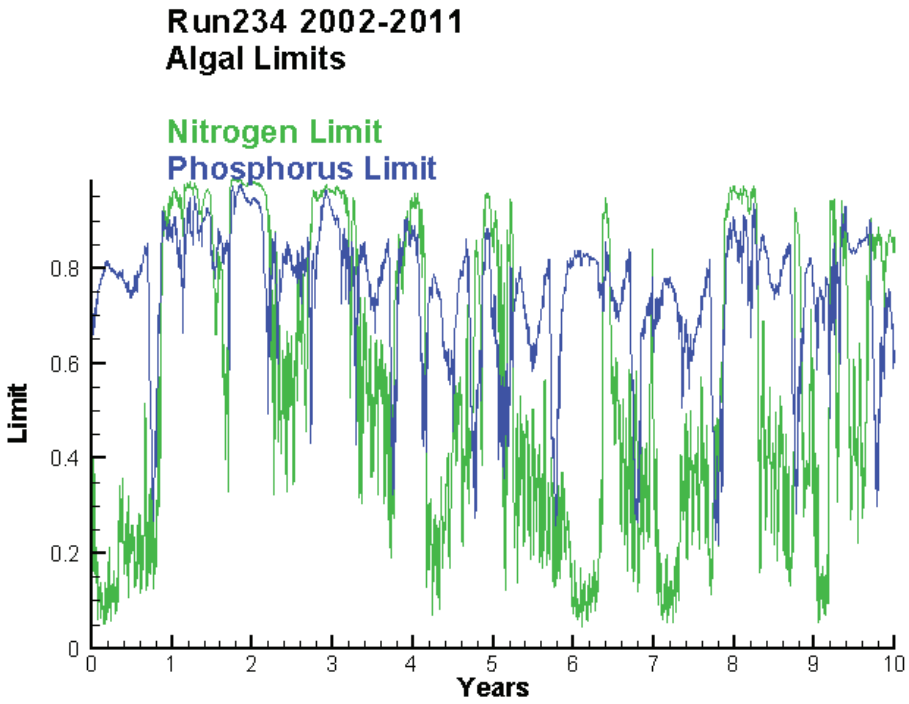

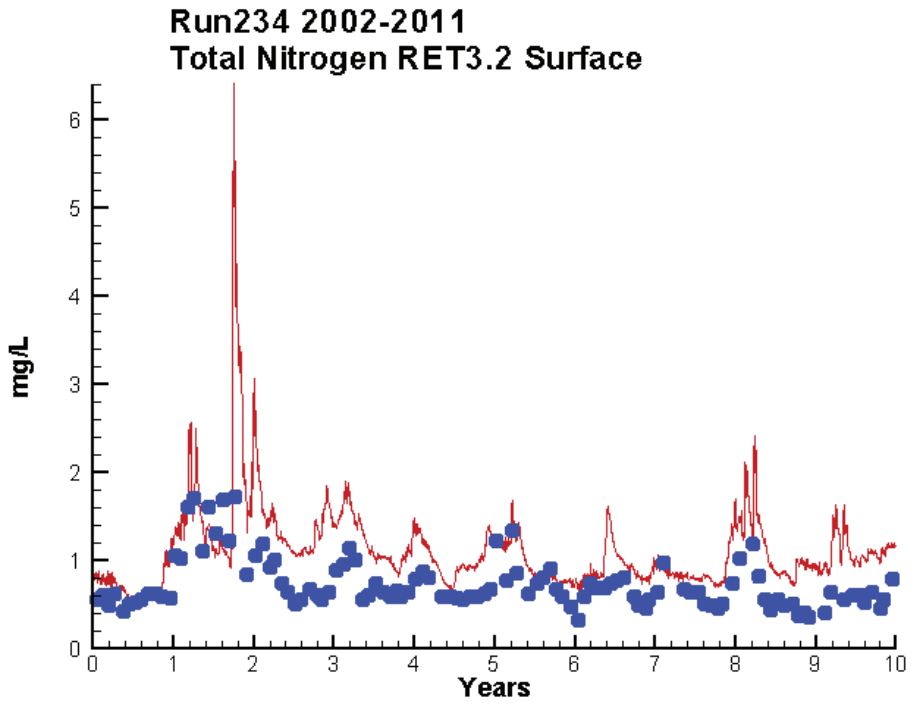

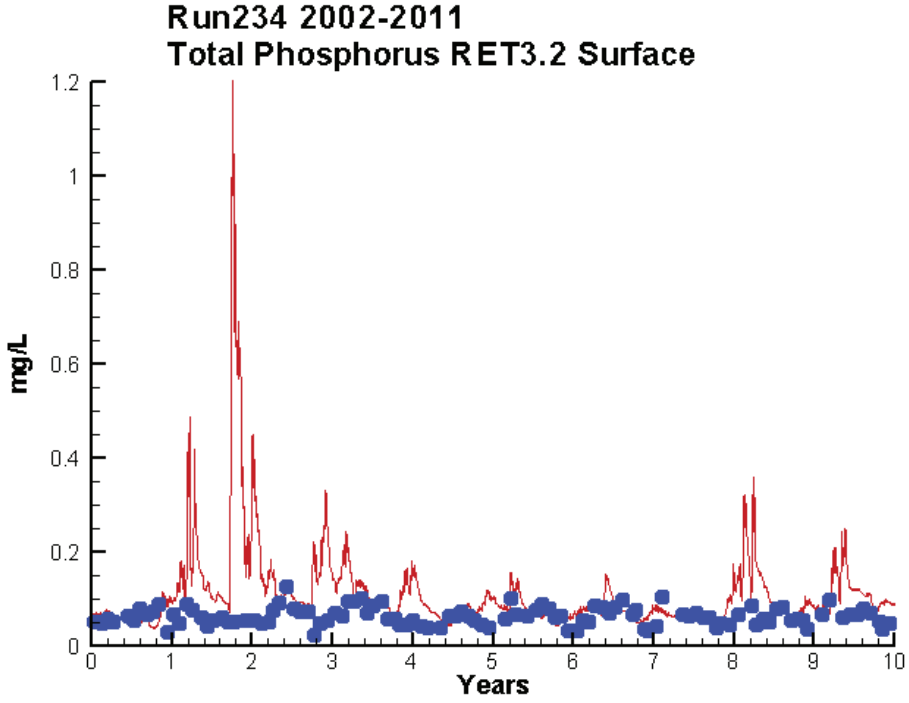

	Mean Difference	Absolute Mean Difference
Chl	-0.5293	5.9024
DIN	0.0224	0.1152
KE	0.5030	0.9503
DIP	0.0025	0.0073
TP	0.0459	0.0526
TN	0.3794	0.4047

Station RET3.2

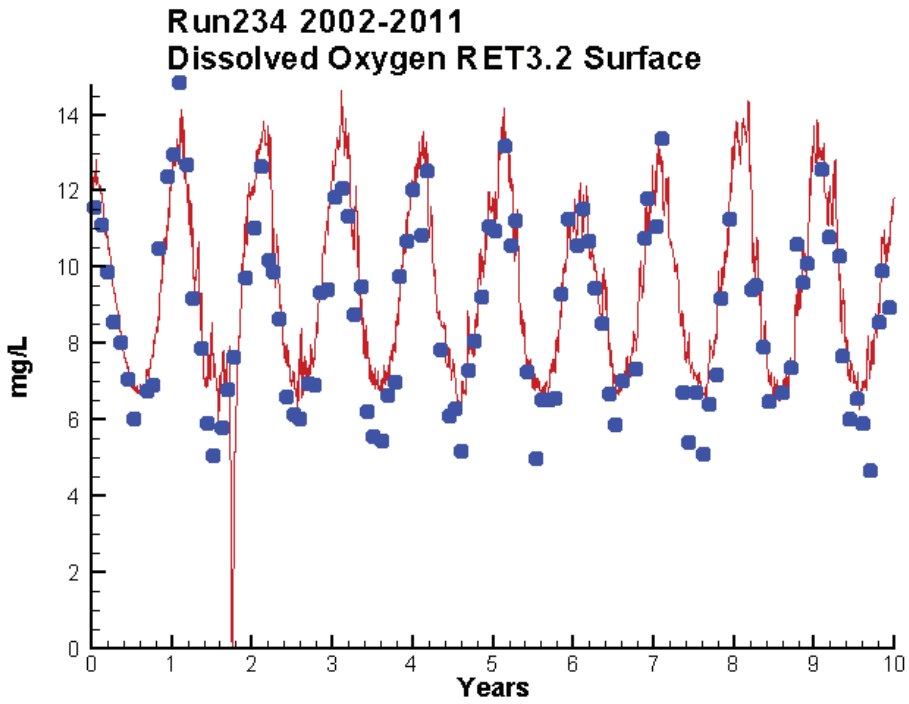

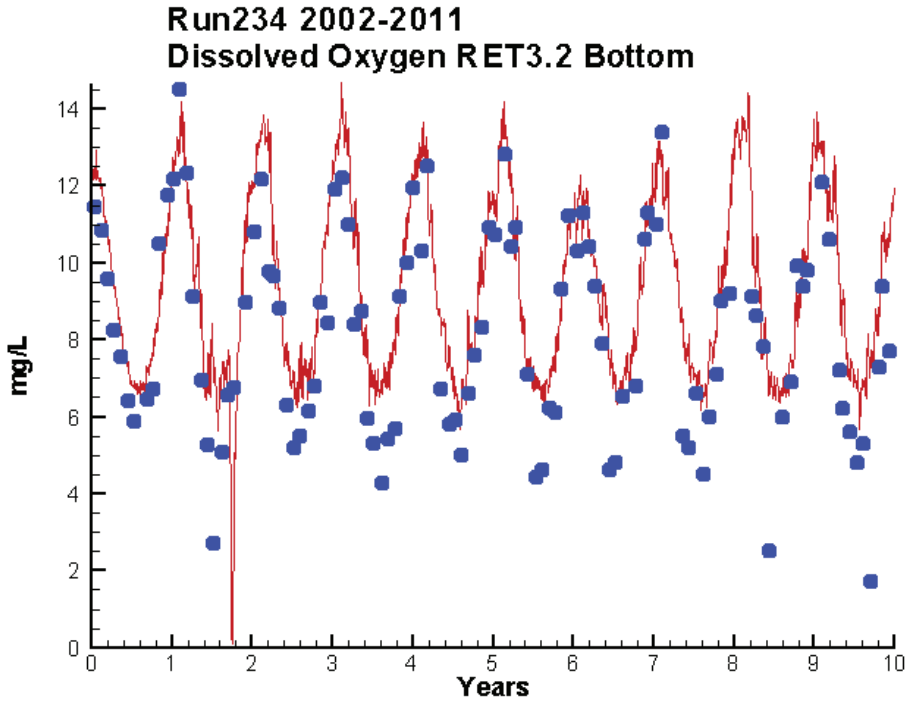

	Mean Difference	Absolute Mean Difference
Top DO	0.6906	1.0031
Bot DO	1.2030	1.4054

Station RET3.2

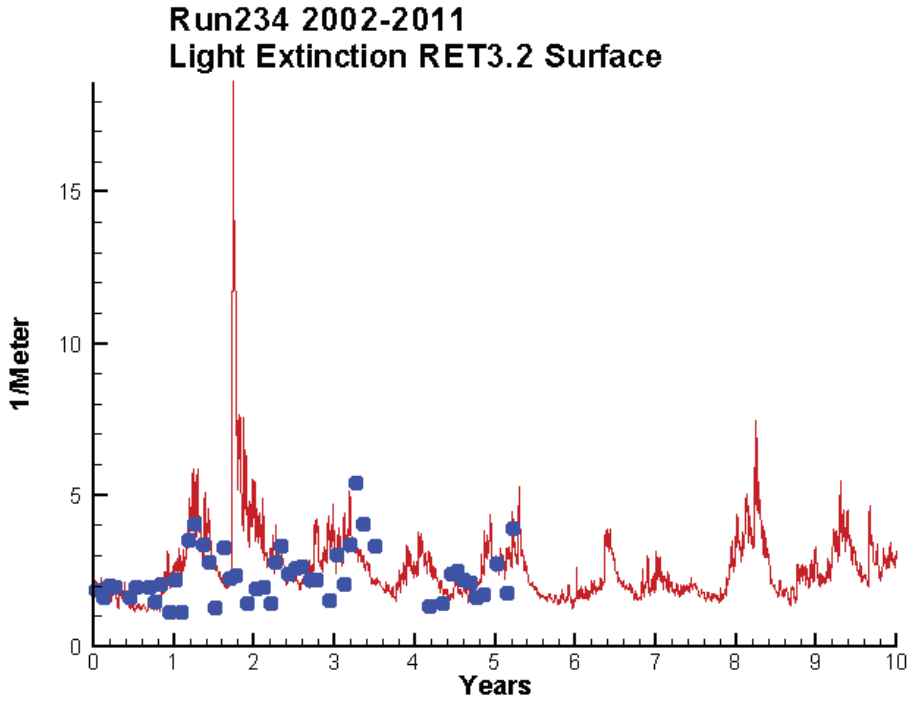

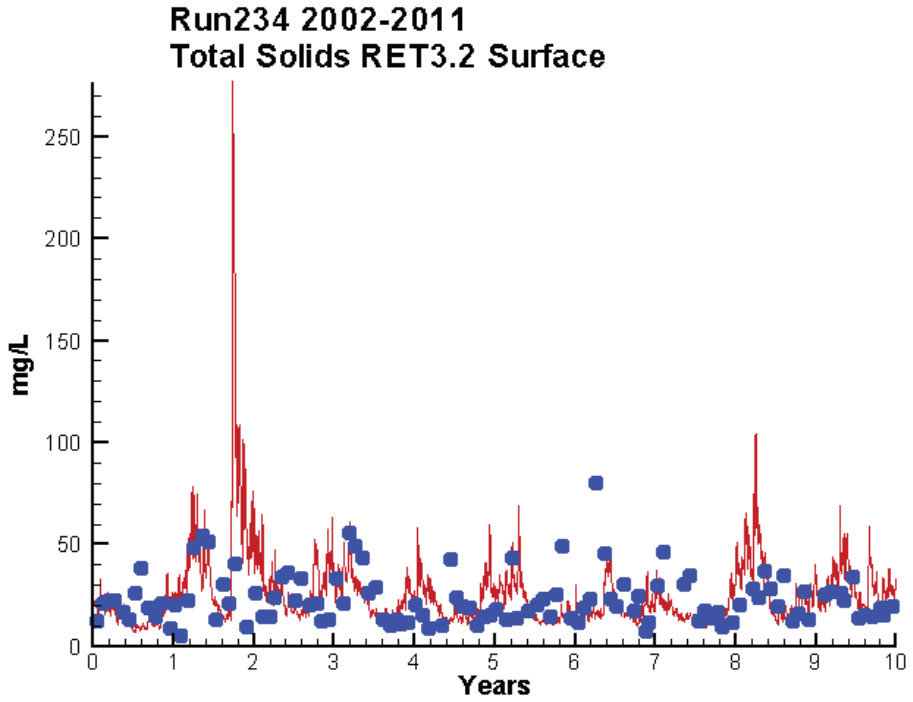

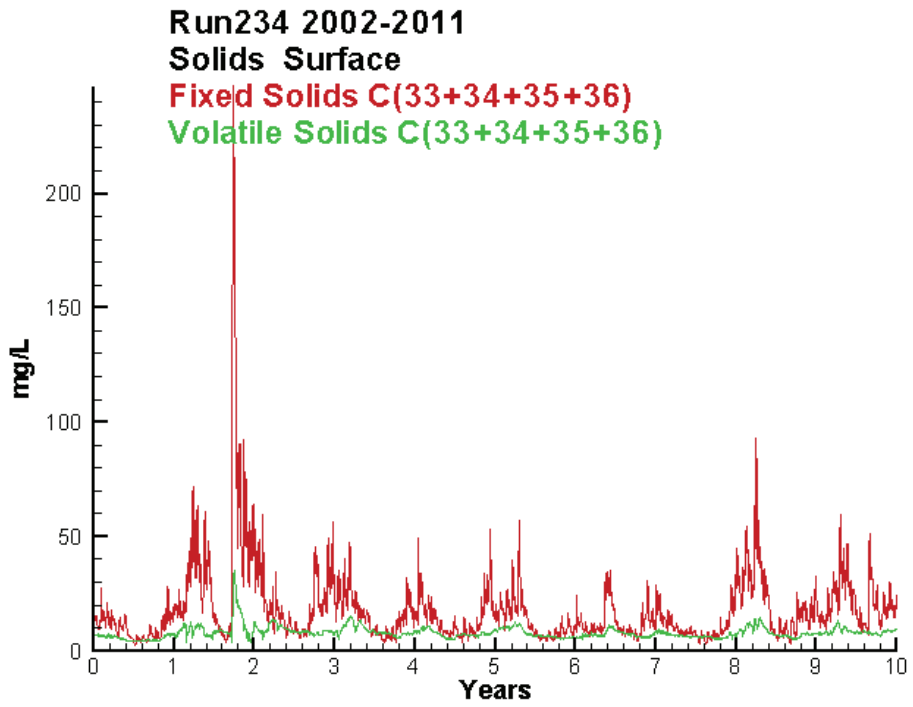

	Mean Difference	Absolute Mean Difference
KE	0.5030	0.9503
TSS	1.9746	11.5527

Station TF3.3

Run234 2002-2011
Chlorophyll TF3.3 Surface

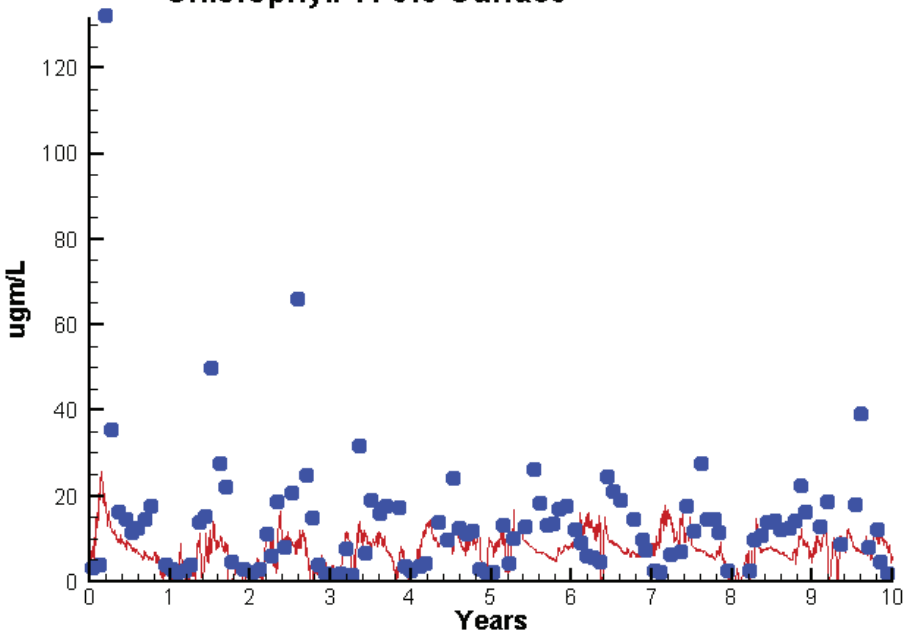

Run234 2002-2011
Light Extinction TF3.3 Surface

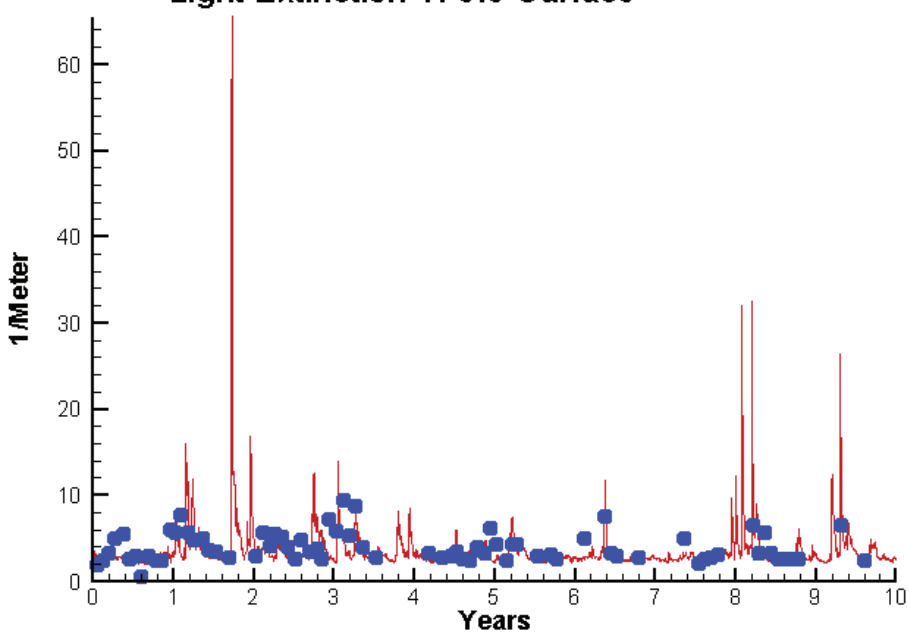

Run234 2002-2011
Dissolved Inorganic Nitrogen TF3.3 Surface

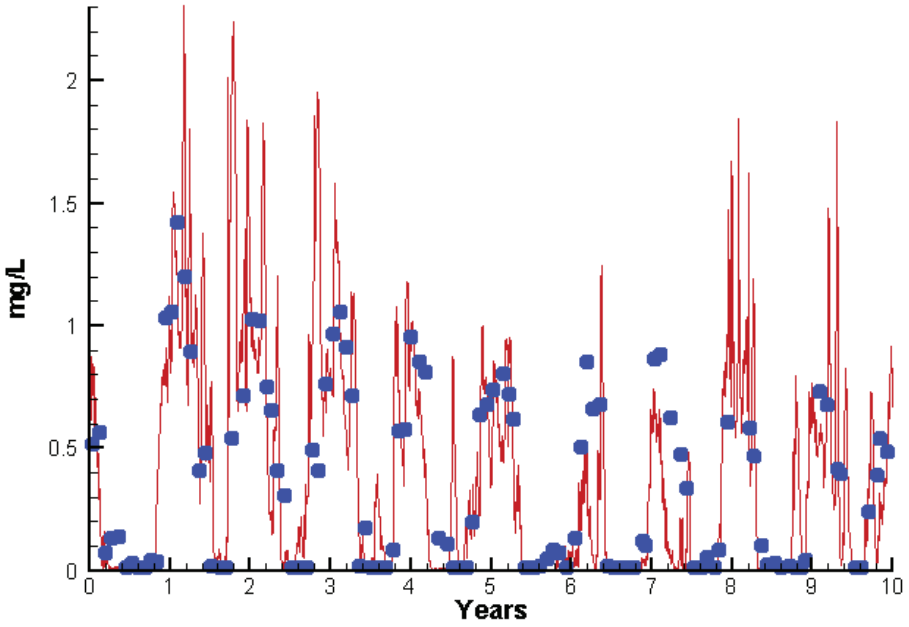

Run234 2002-2011
Dissolved Inorganic Phosphorus TF3.3 Surface

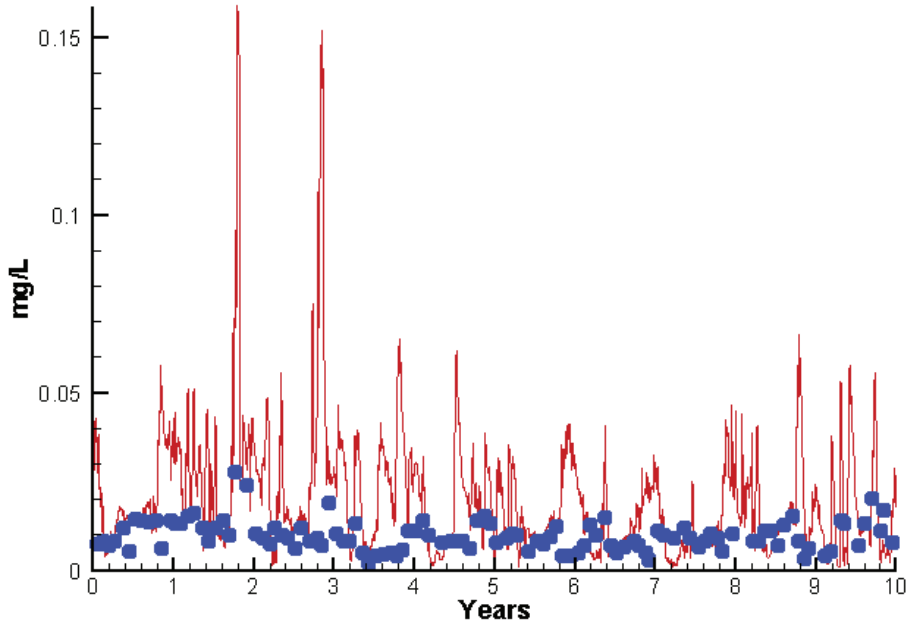

Station TF3.3

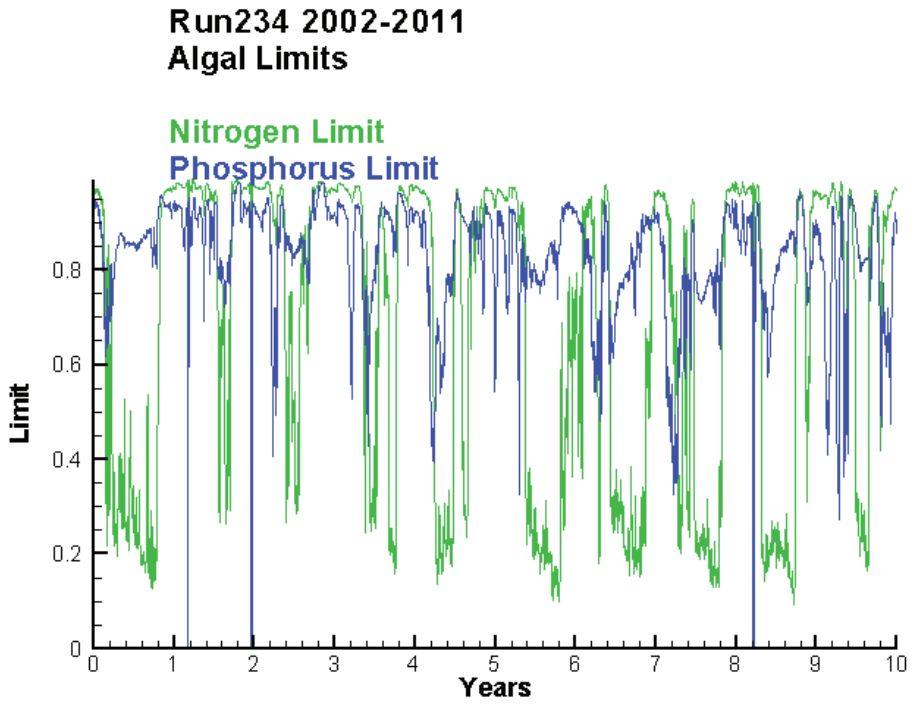

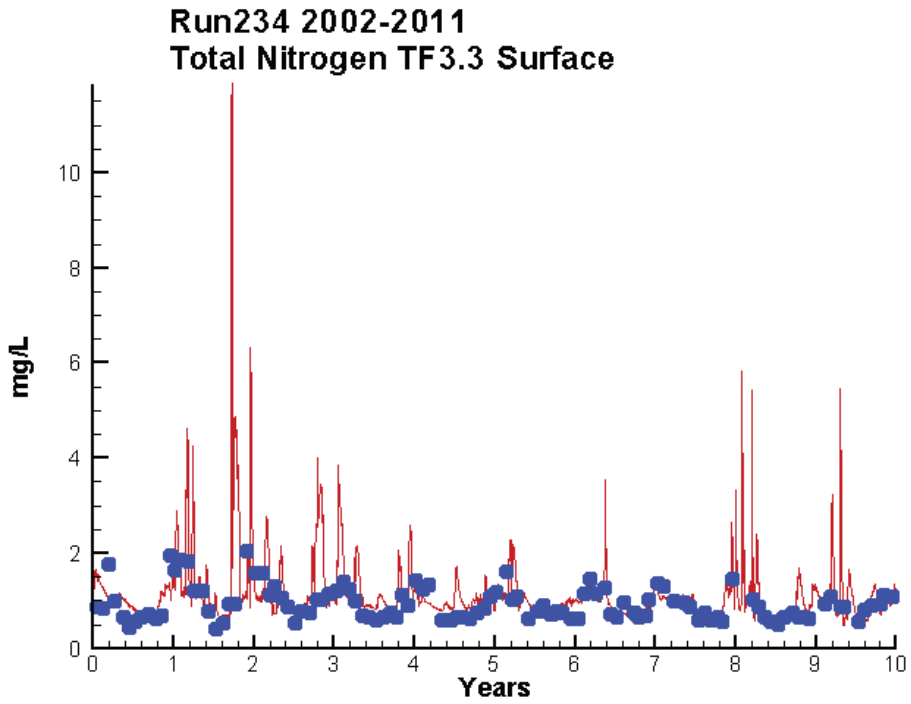

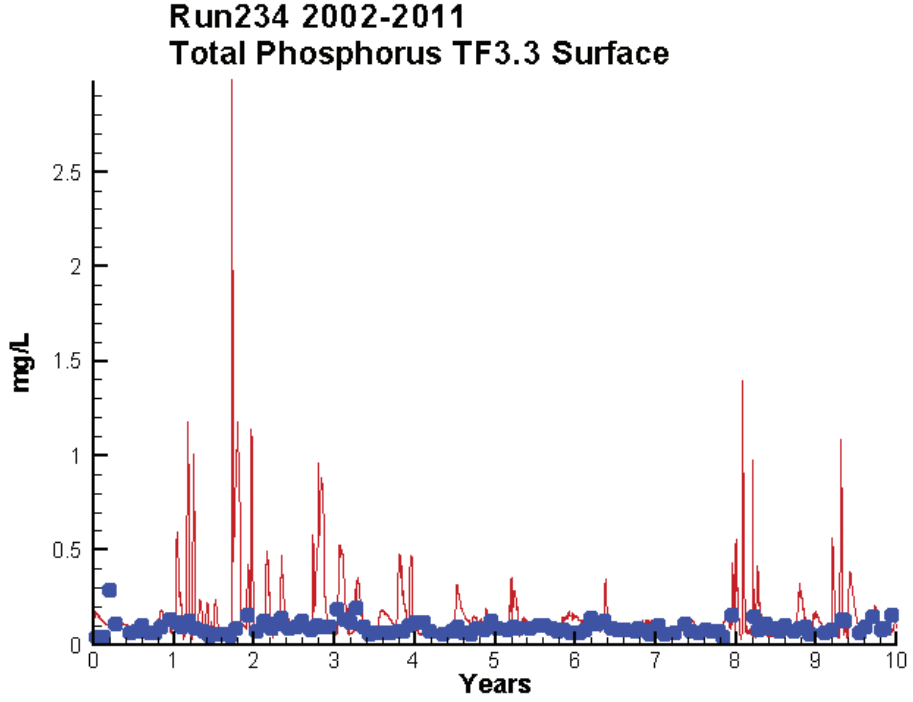

	Mean Difference	Absolute Mean Difference
Chl	-5.8841	8.3570
DIN	0.0230	0.2047
KE	-0.5158	1.2478
DIP	0.0114	0.0132
TP	0.0588	0.0796
TN	0.1973	0.3653

Station TF3.3

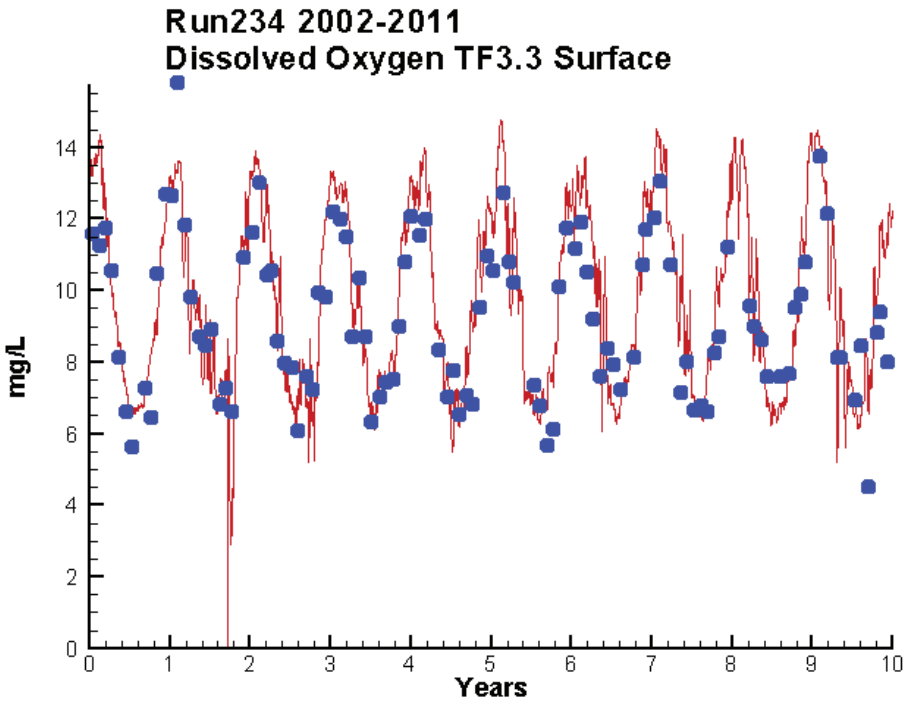

	Mean Difference	Absolute Mean Difference
Top DO	0.5072	0.9864

Station TF3.3

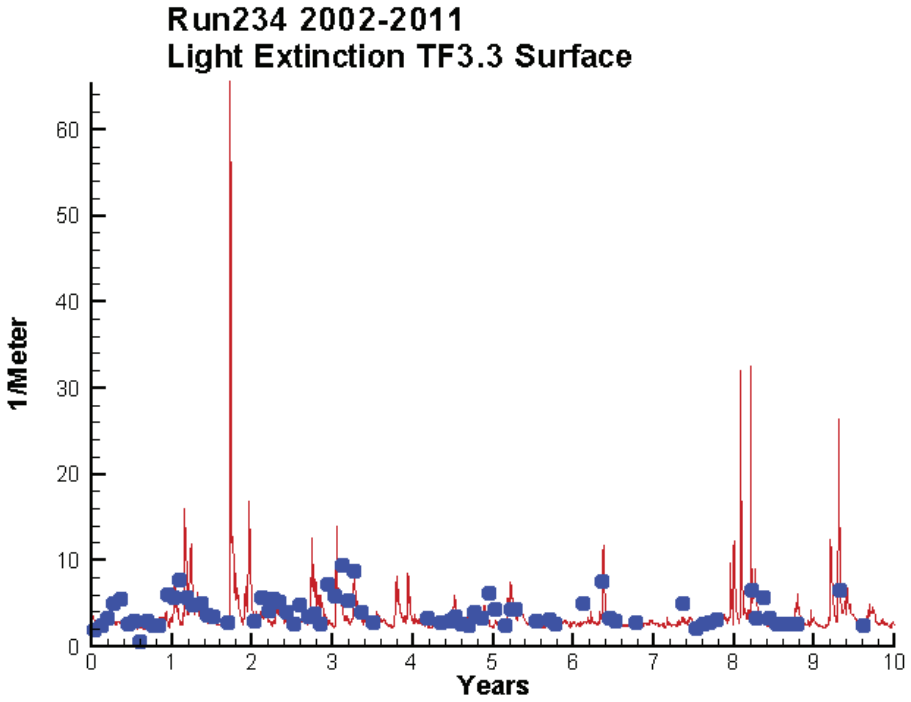

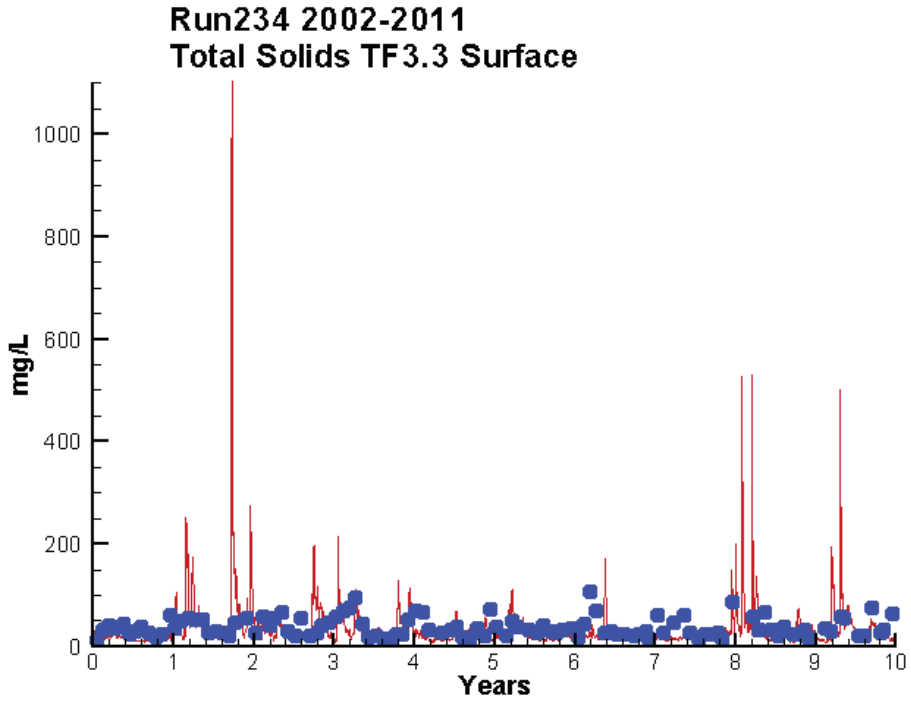

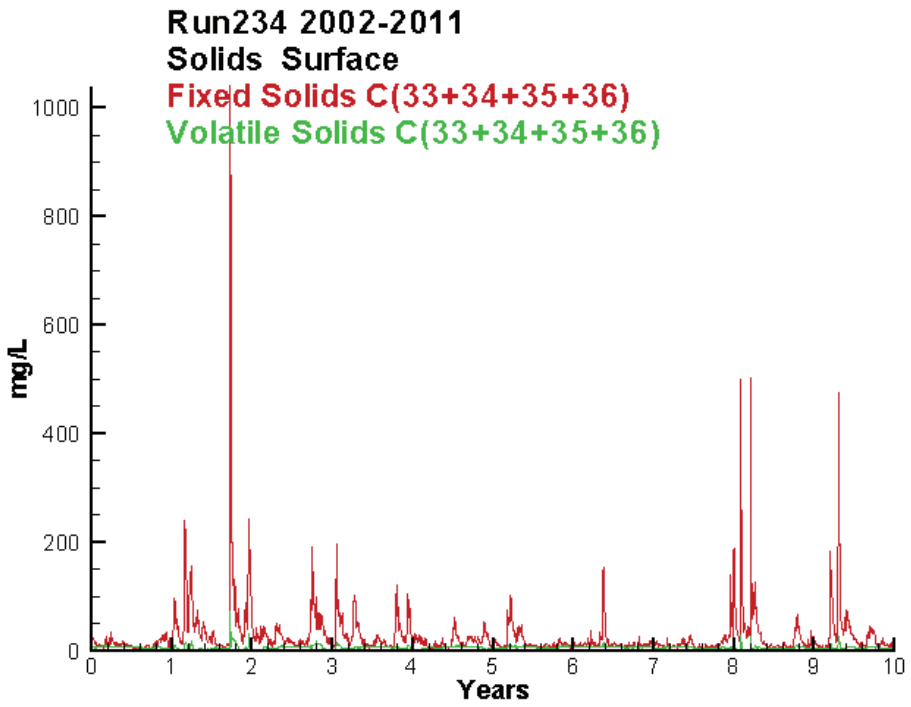

	Mean Difference	Absolute Mean Difference
KE	-0.5158	1.2478
TSS	-4.7839	21.9493

Station LE4.2

Run234 2002-2011
Chlorophyll LE4.2 Surface

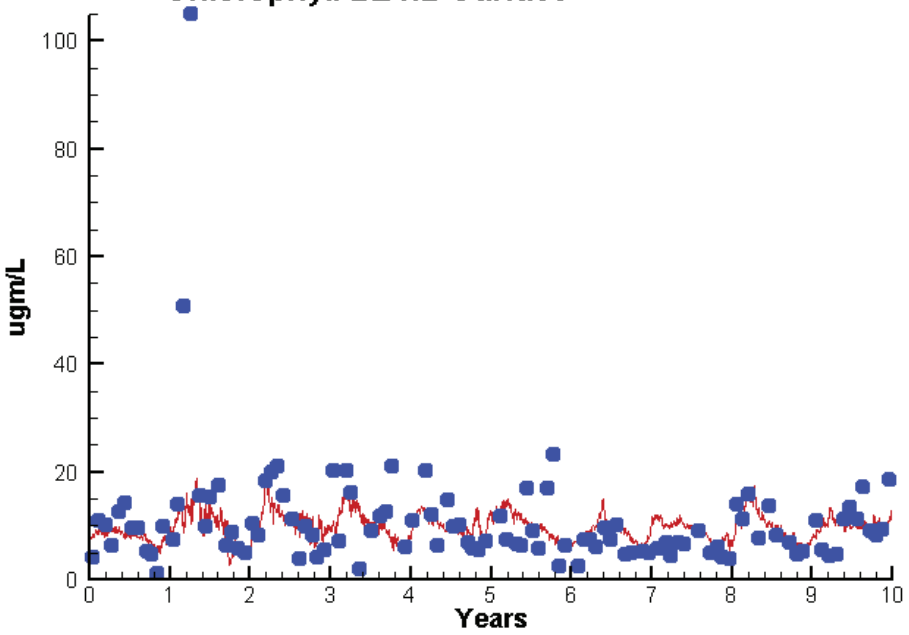

Run234 2002-2011
Light Extinction LE4.2 Surface

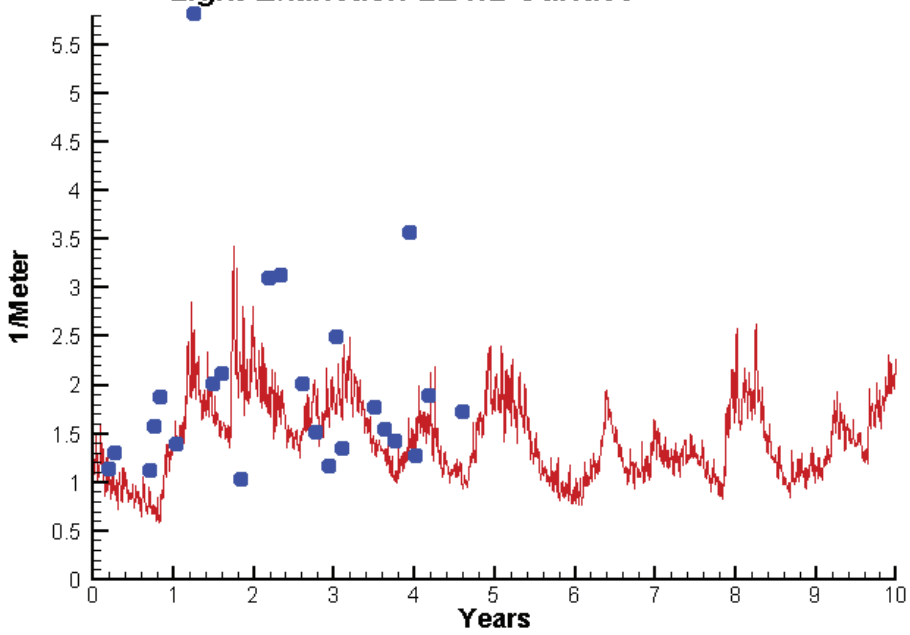

Run234 2002-2011
Dissolved Inorganic Nitrogen LE4.2 Surface

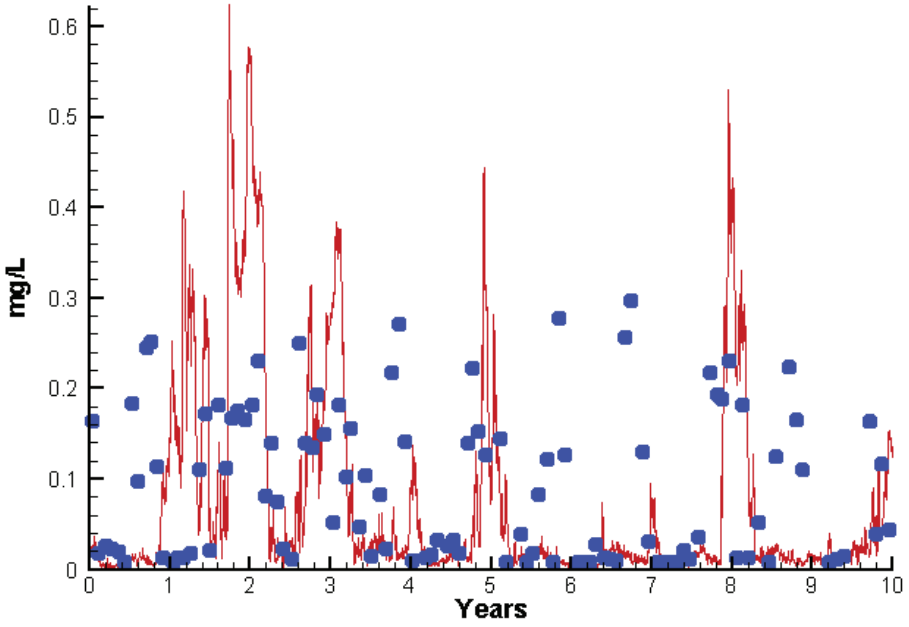

Run234 2002-2011
Dissolved Inorganic Phosphorus LE4.2 Surface

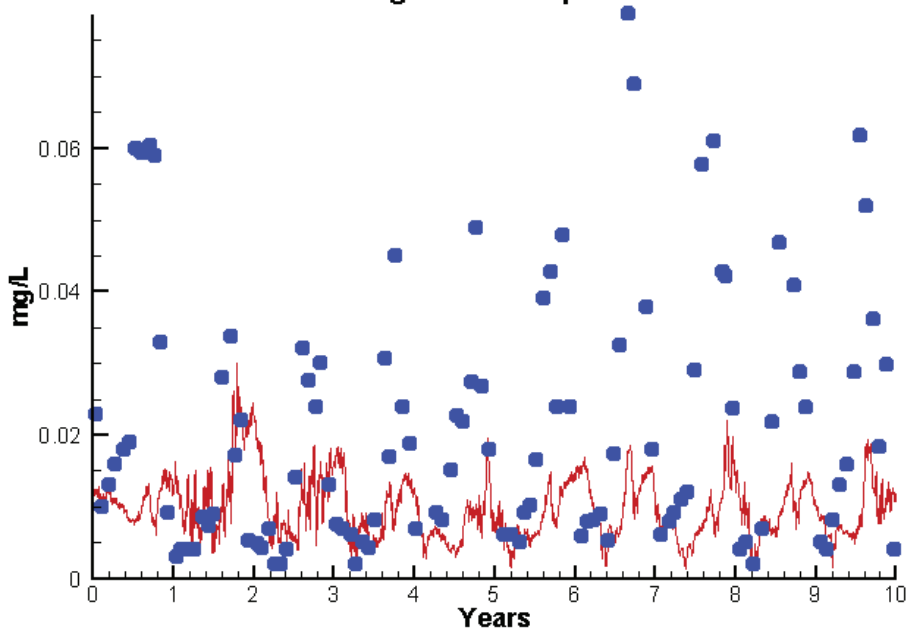

Station LE4.2

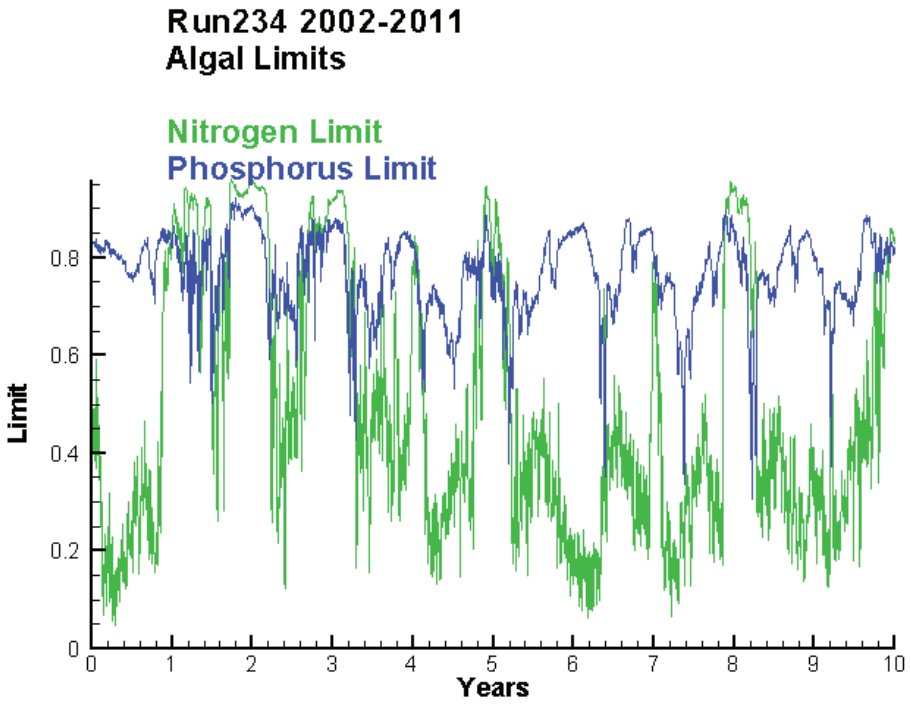

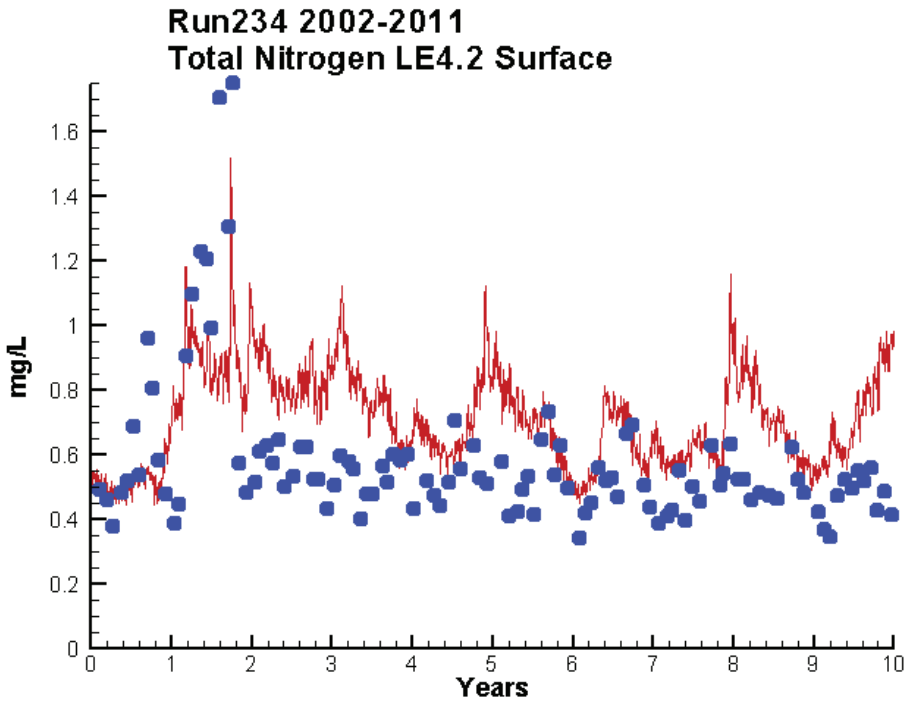

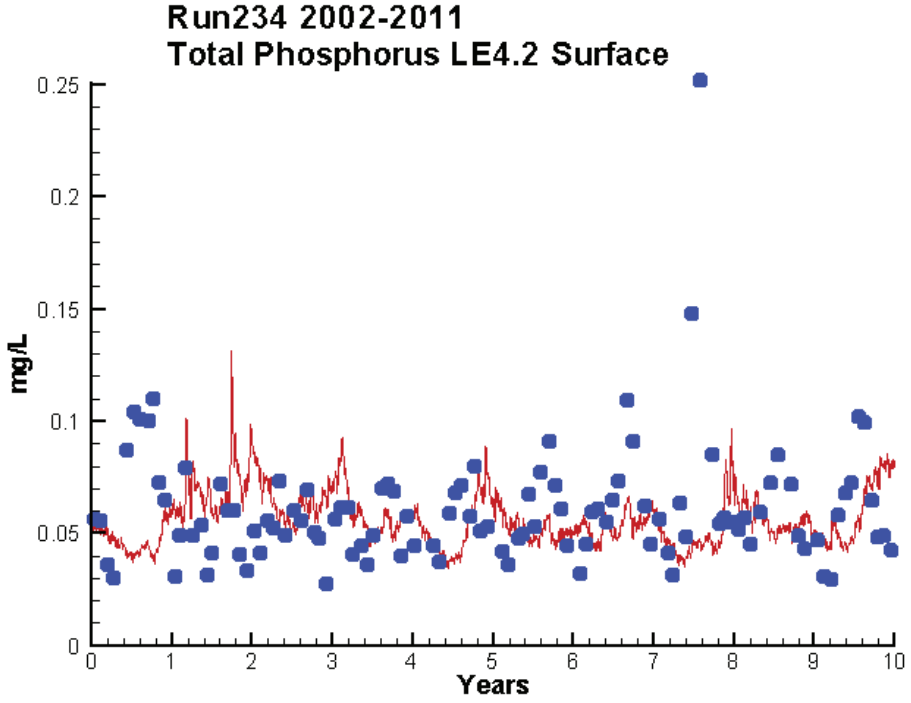

	Mean Difference	Absolute Mean Difference
Chl	-0.9201	4.5752
DIN	-0.0159	0.0899
KE	-0.5407	0.7354
DIP	-0.0111	0.0142
TP	-0.0035	0.0214
TN	0.1394	0.2096

Station LE4.2

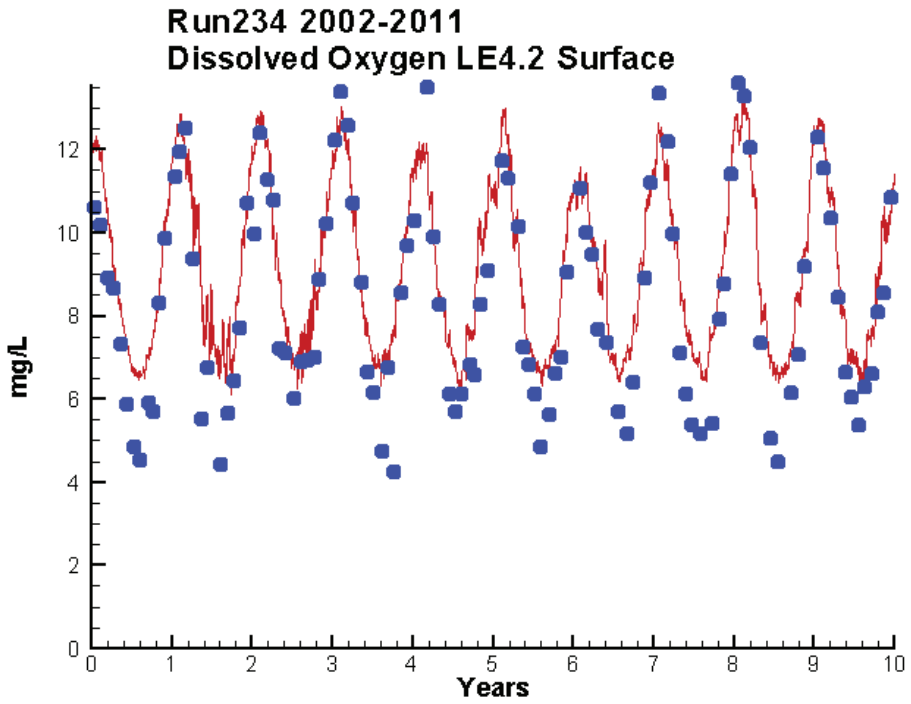

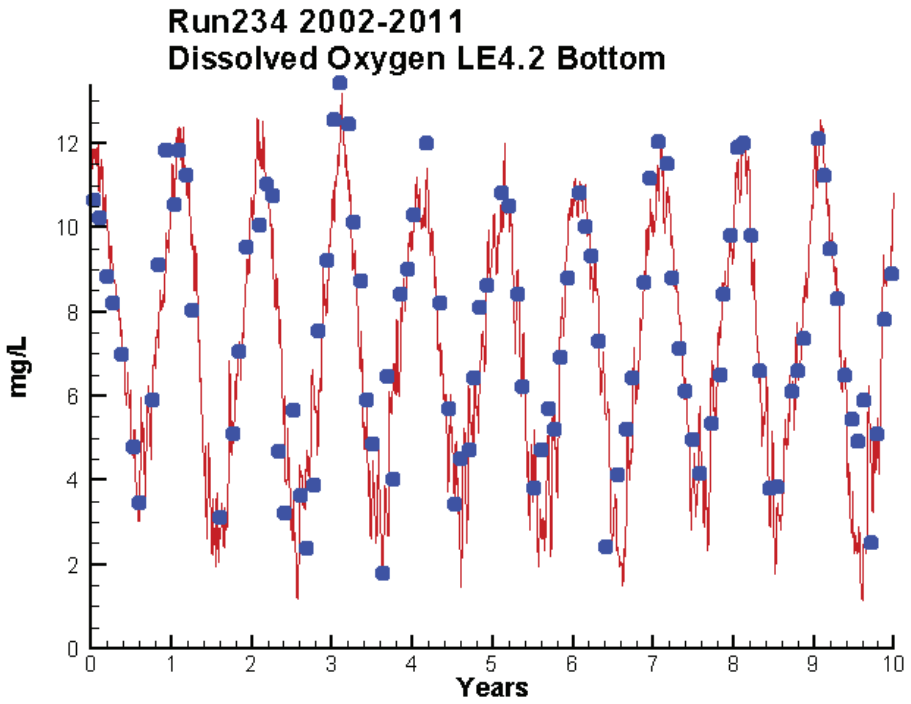

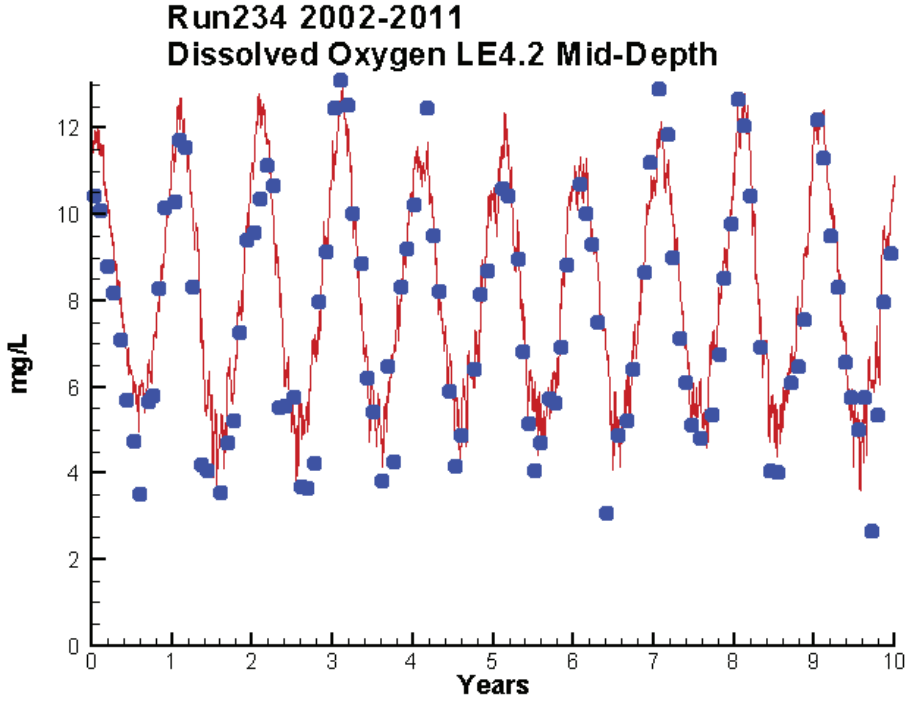

	Mean Difference	Absolute Mean Difference
Top DO	0.8389	1.0432
Mid DO	0.7192	0.9795
Bot DO	-0.1204	0.9208

Station LE4.2

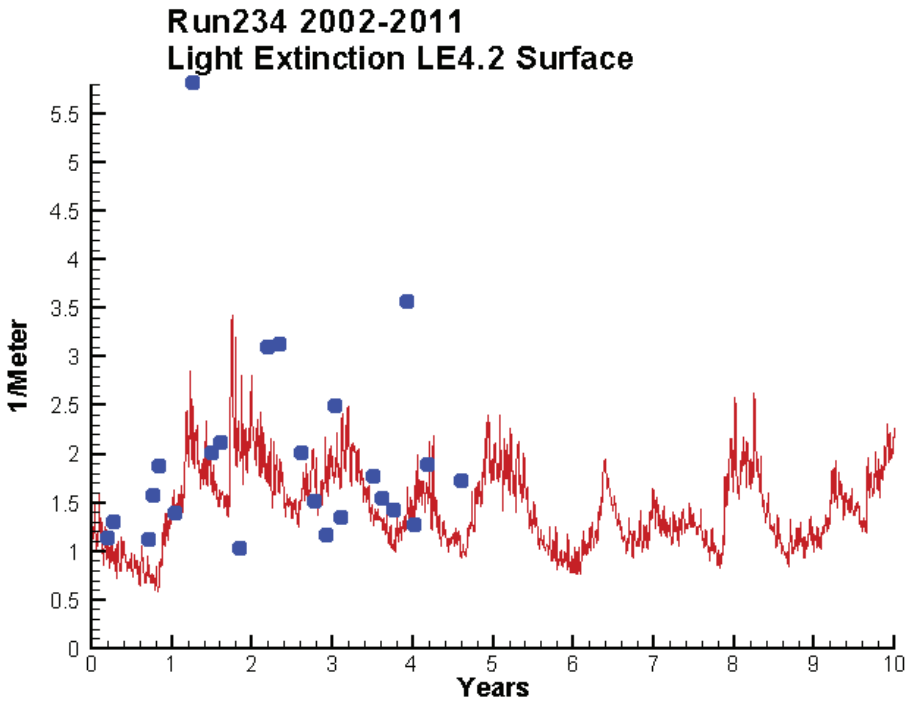

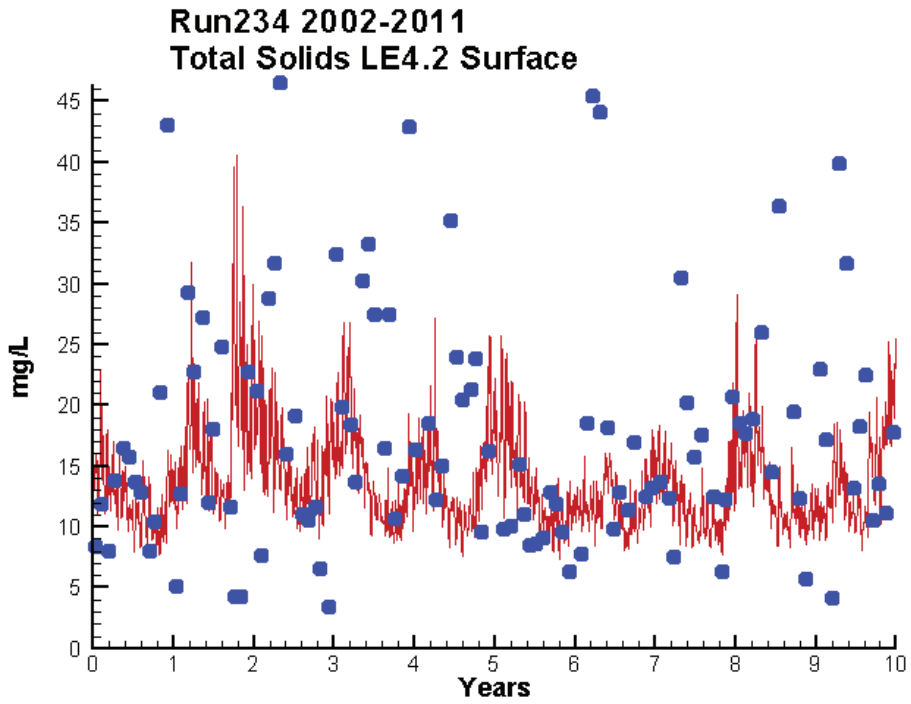

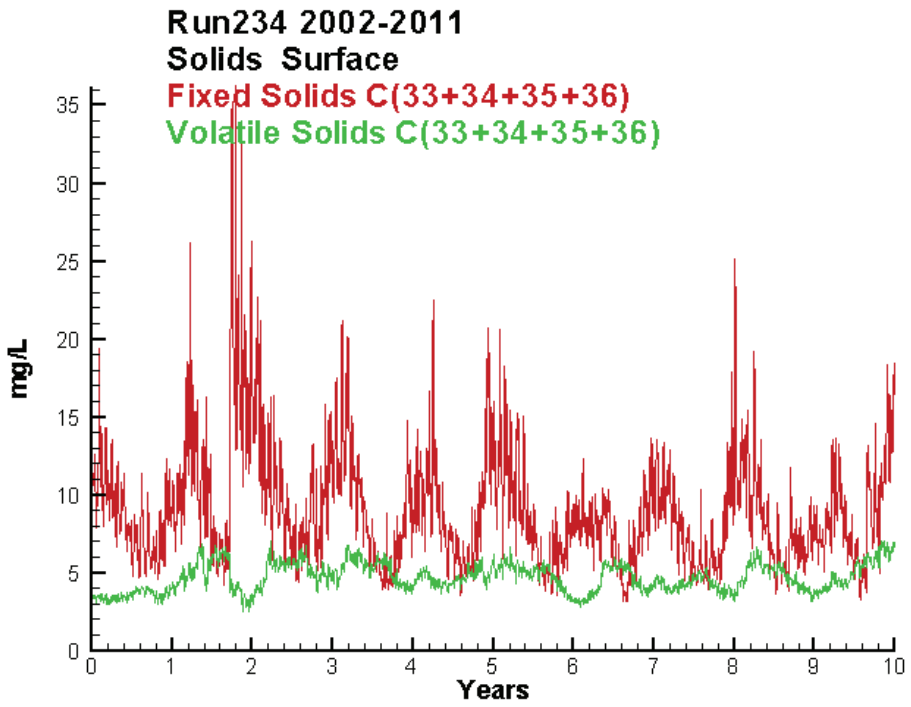

	Mean Difference	Absolute Mean Difference
KE	-0.5407	0.7354
TSS	-3.8362	7.0749

Station RET4.3

Run234 2002-2011
Chlorophyll RET4.3 Surface

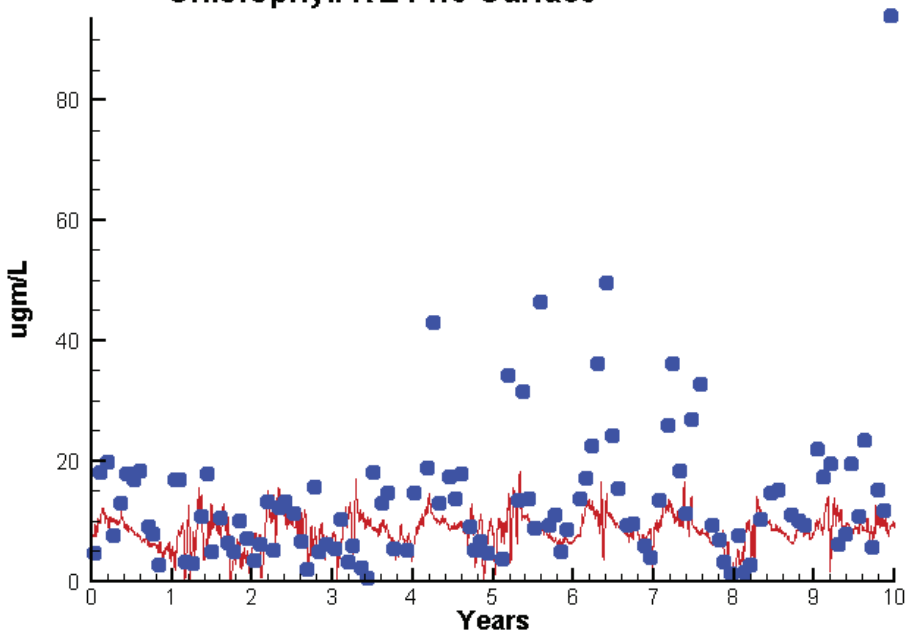

Run234 2002-2011
Light Extinction RET4.3 Surface

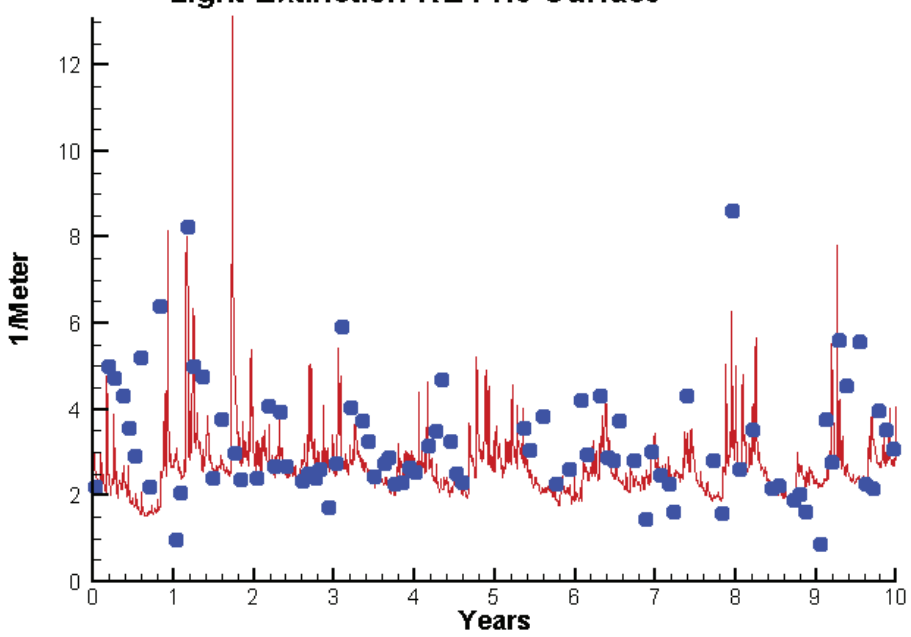

Run234 2002-2011
Dissolved Inorganic Nitrogen RET4.3 Surface

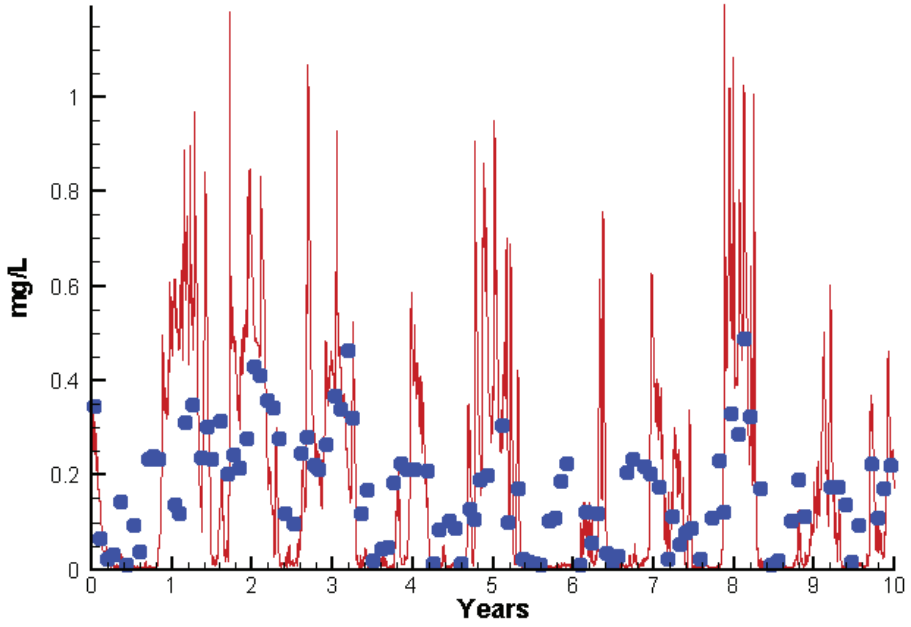

Run234 2002-2011
Dissolved Inorganic Phosphorus RET4.3 Surface

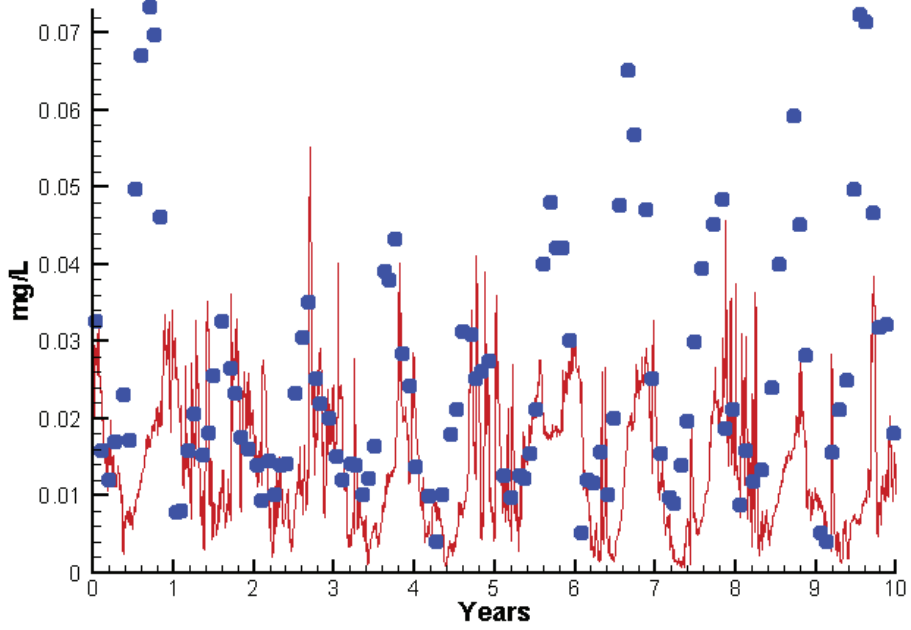

Station RET4.3

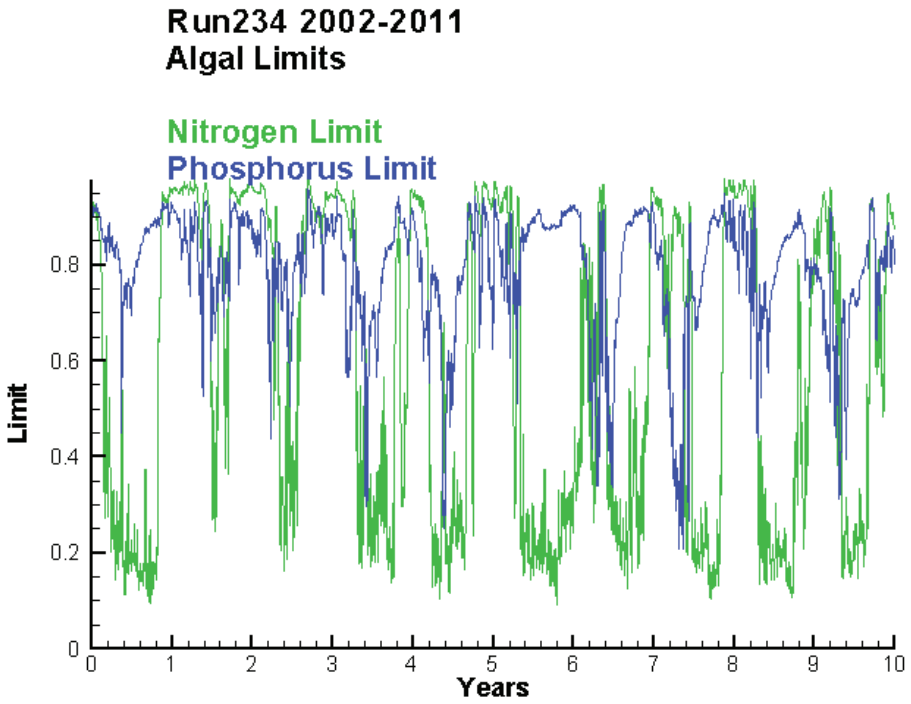

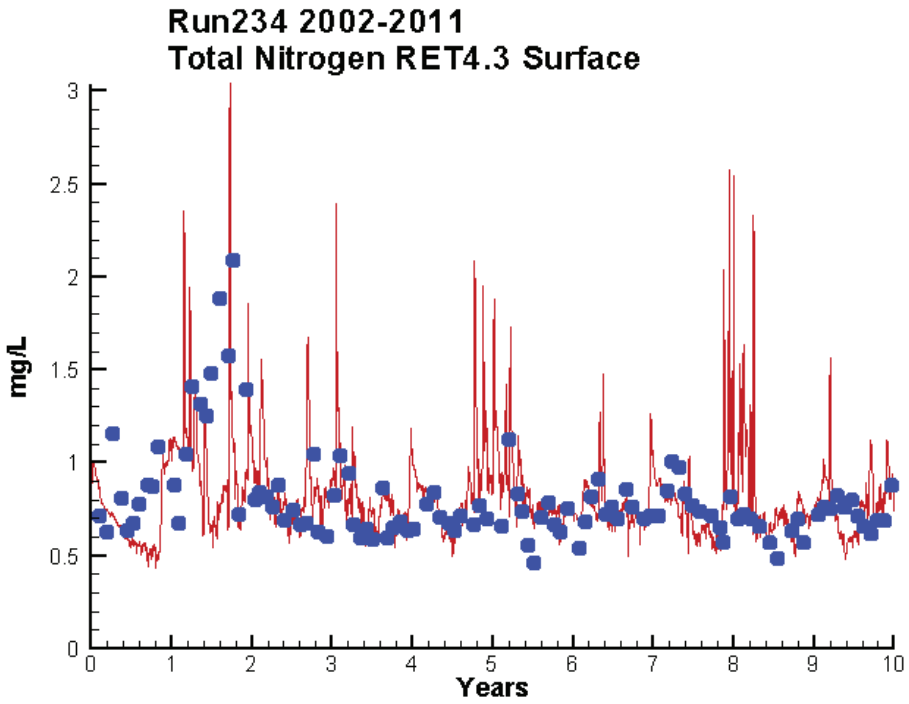

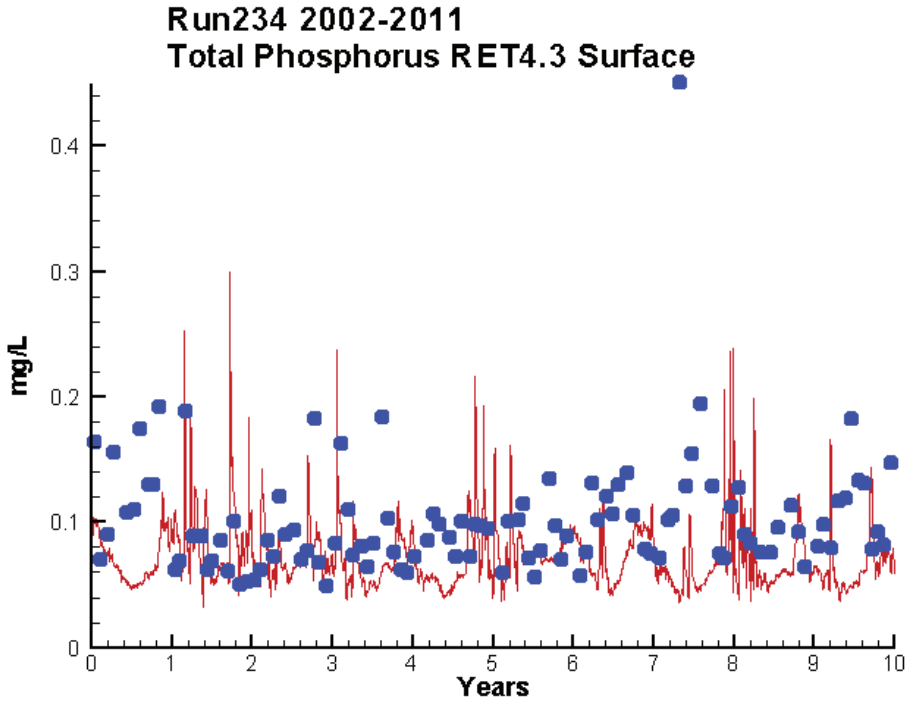

	Mean Difference	Absolute Mean Difference
Chl	-4.9572	7.0271
DIN	0.0062	0.1298
KE	-0.5579	0.9478
DIP	-0.0120	0.0148
TP	-0.0296	0.0430
TN	0.0189	0.2255

Station RET4.3

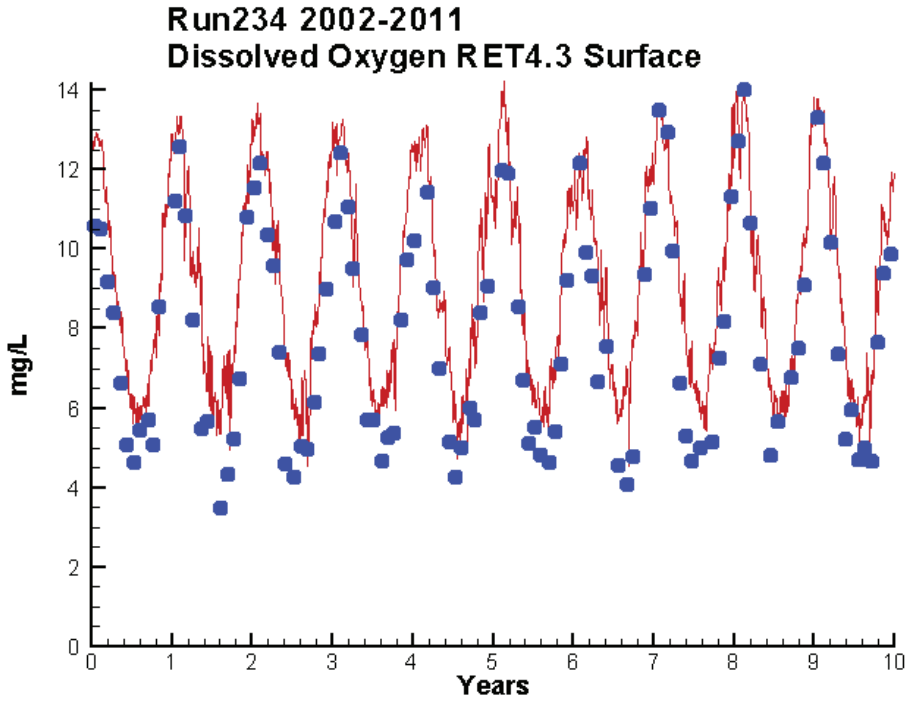

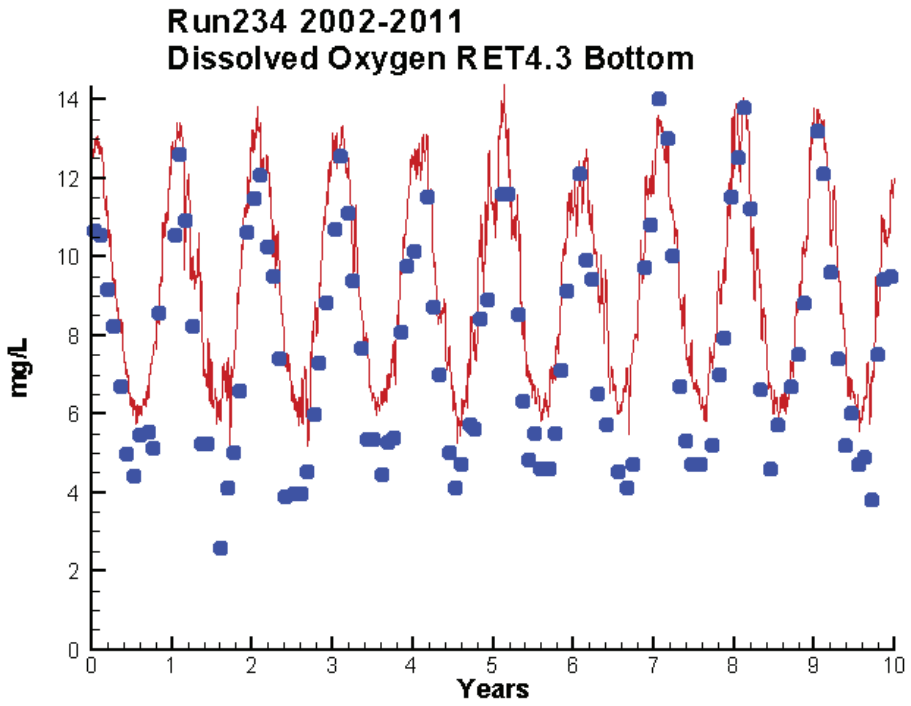

	Mean Difference	Absolute Mean Difference
Top DO	1.4165	1.4473
Bot DO	1.6545	1.6974

Station RET4.3

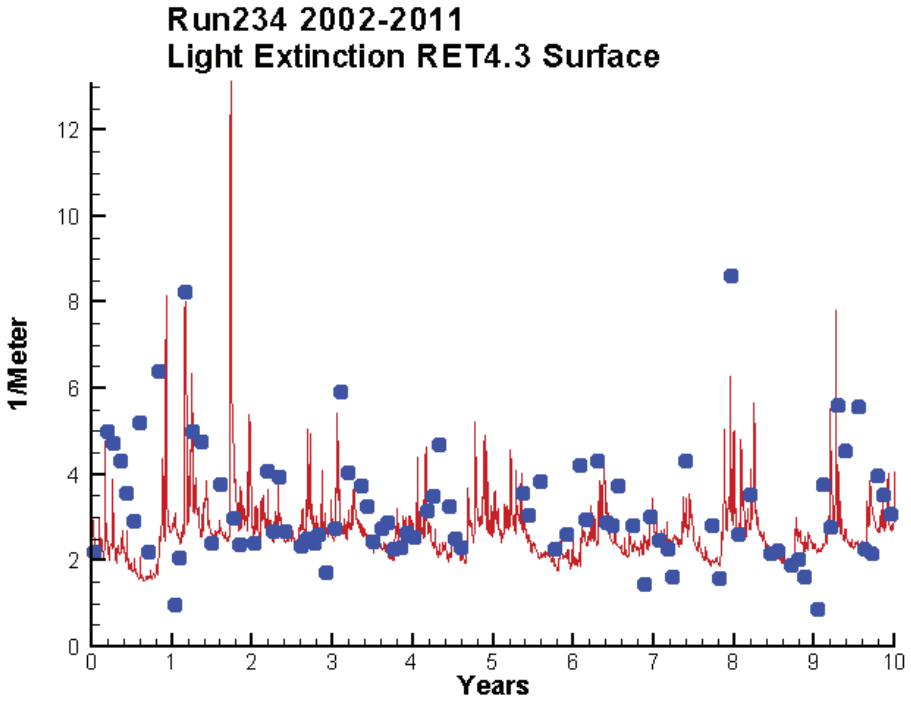

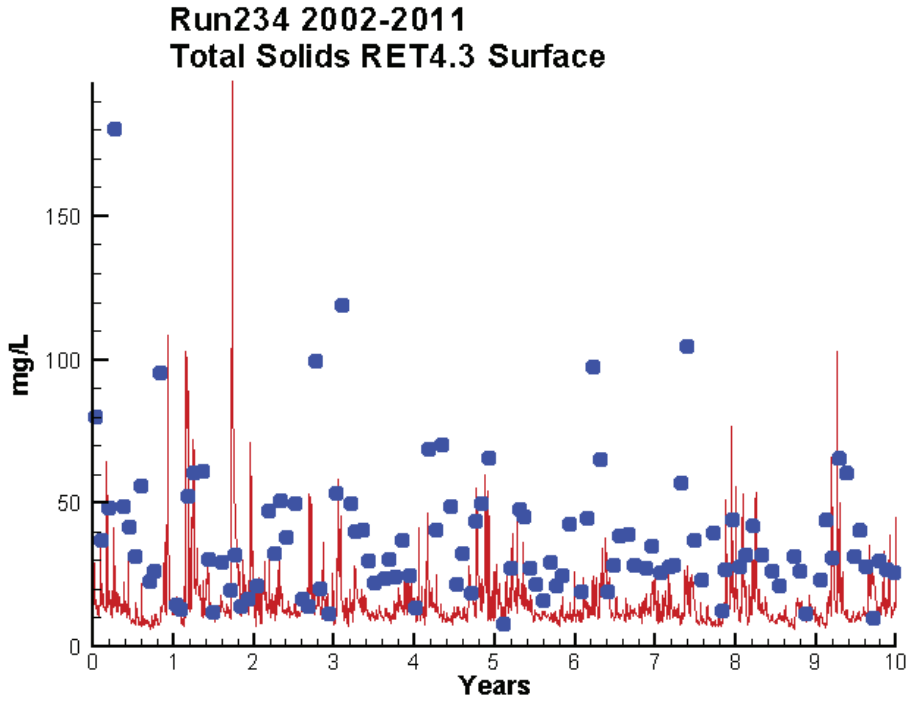

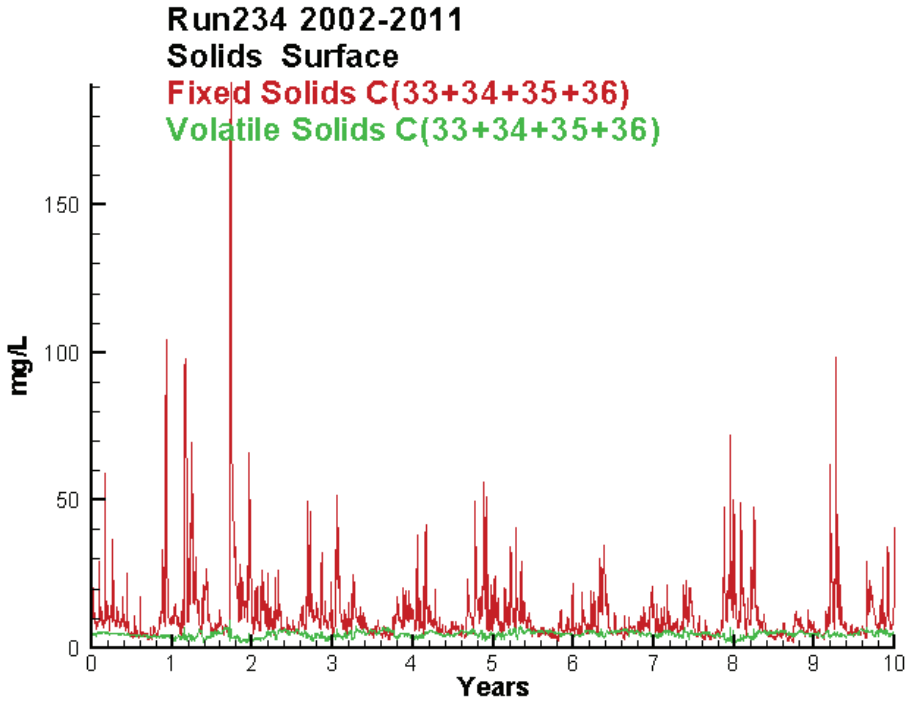

	Mean Difference	Absolute Mean Difference
KE	-0.5579	0.9478
TSS	-22.5304	23.8005

Station TF4.2

Run234 2002-2011
Chlorophyll TF4.2 Surface

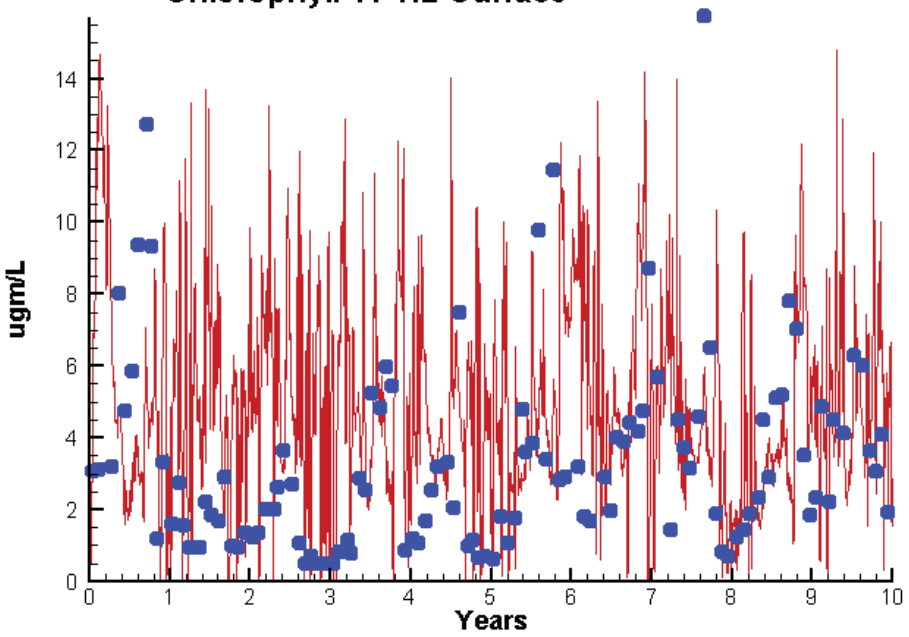

Run234 2002-2011
Light Extinction TF4.2 Surface

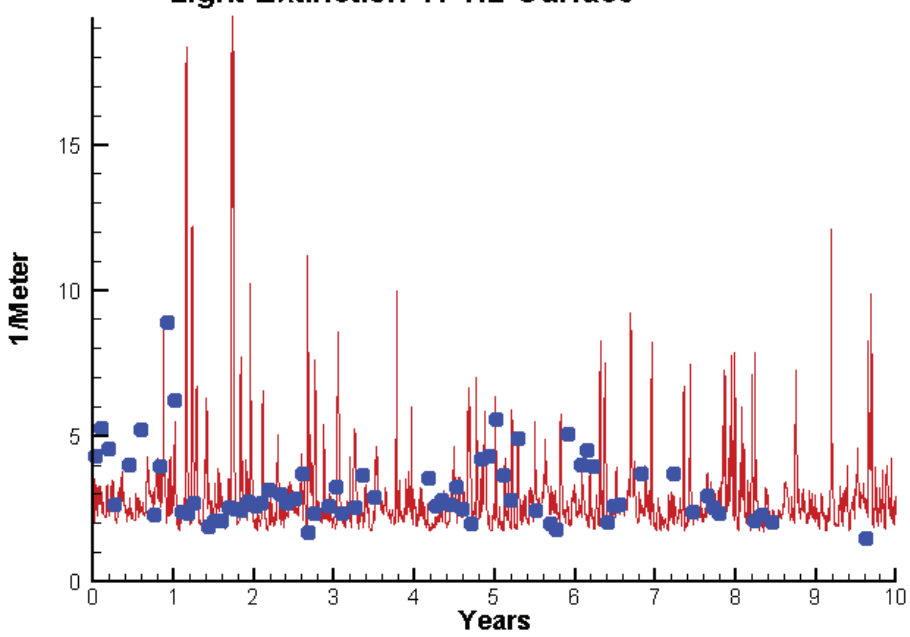

Run234 2002-2011
Dissolved Inorganic Nitrogen TF4.2 Surface

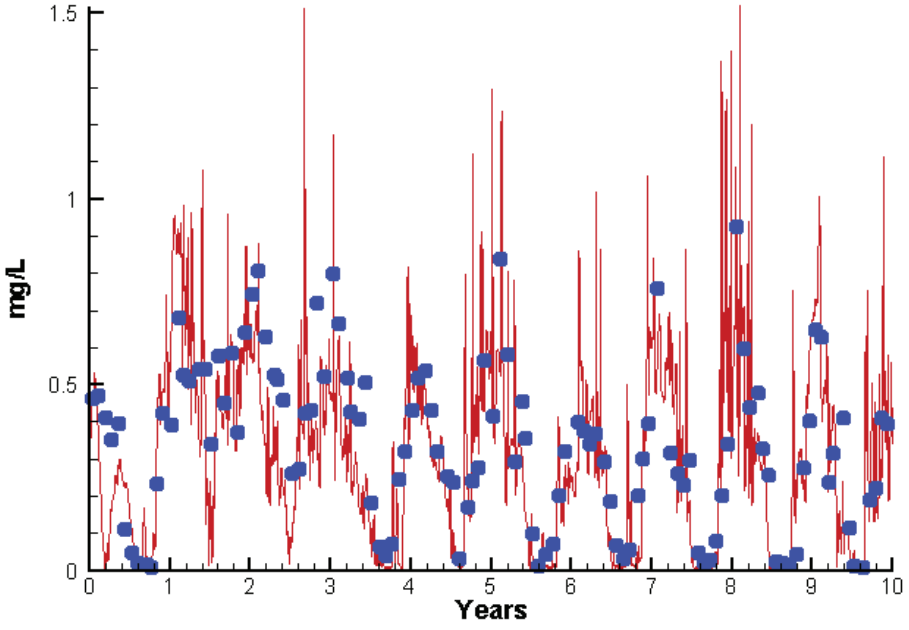

Run234 2002-2011
Dissolved Inorganic Phosphorus TF4.2 Surface

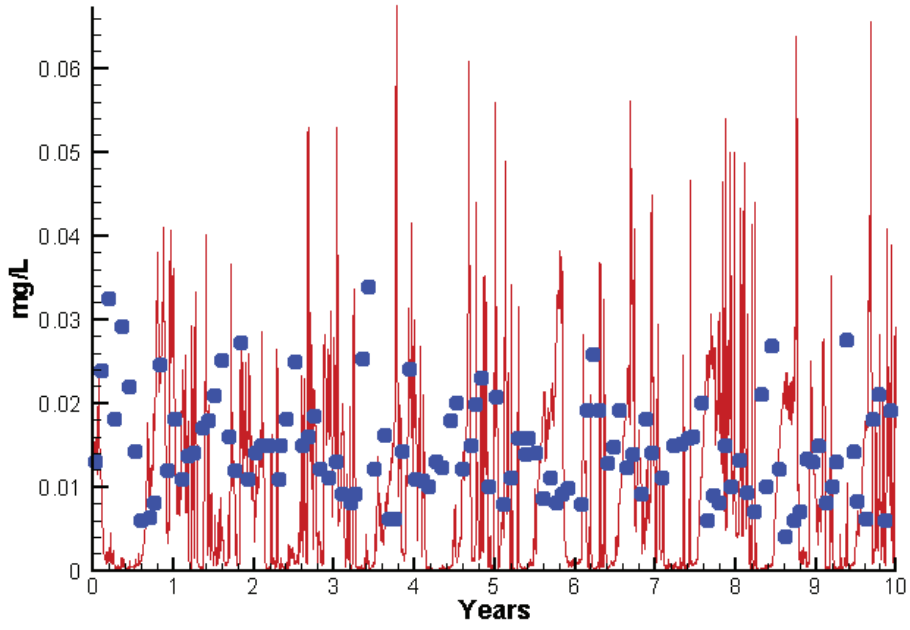

Station TF4.2

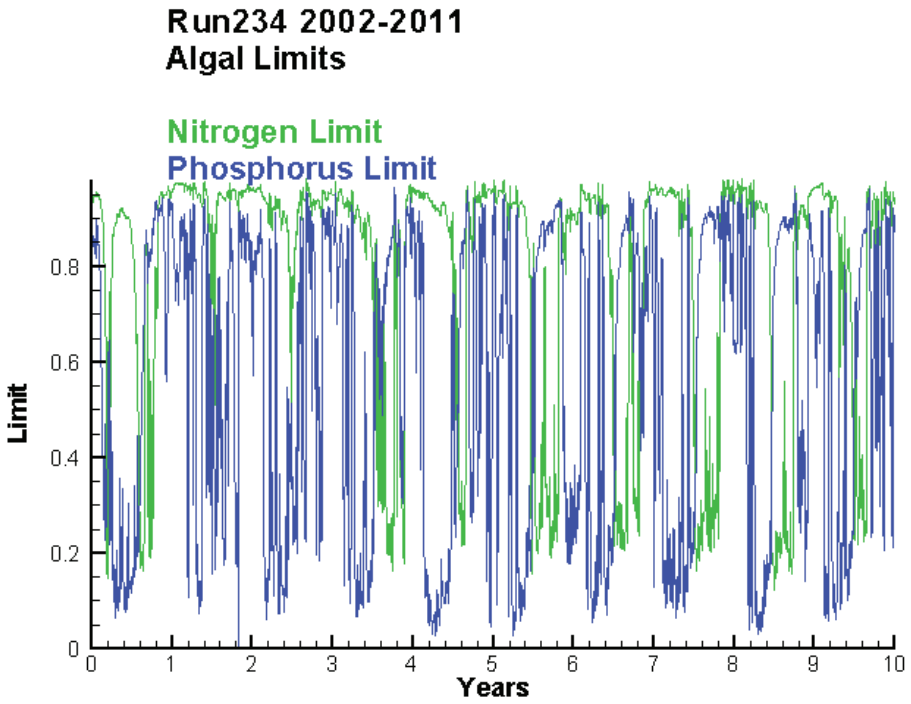

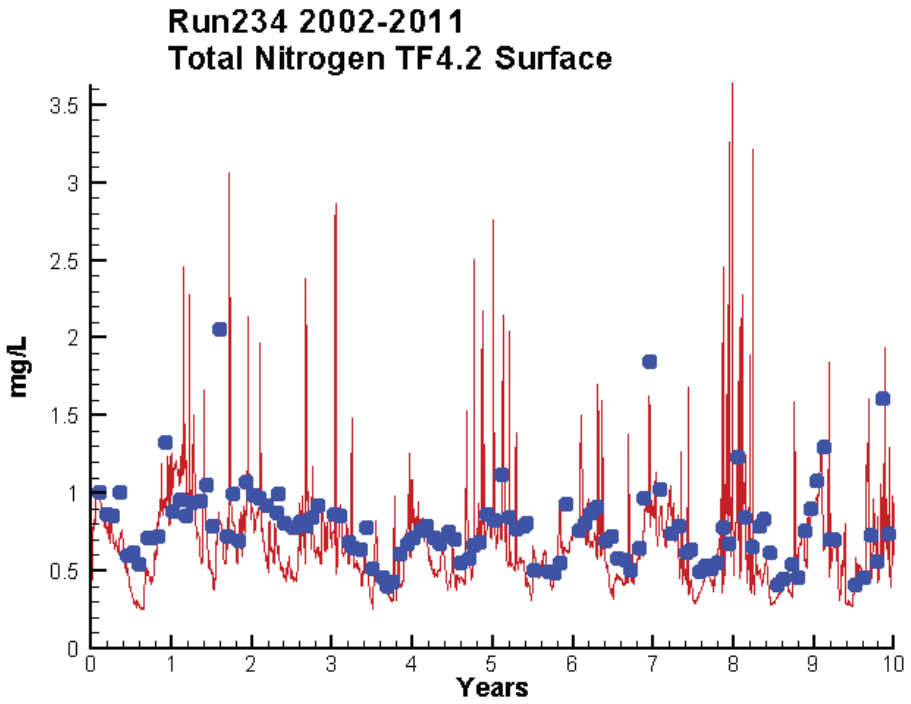

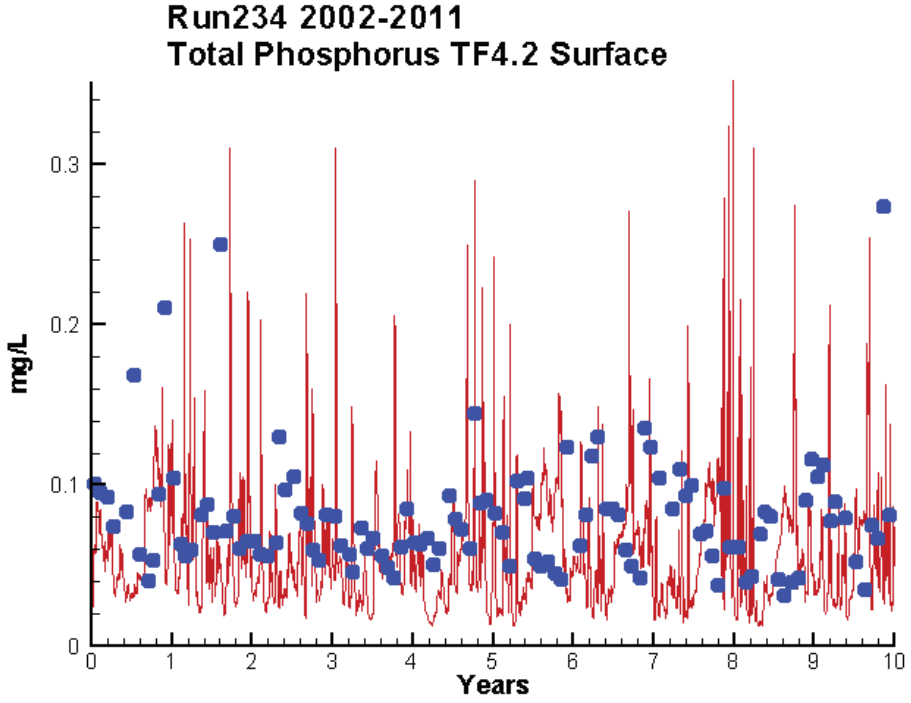

	Mean Difference	Absolute Mean Difference
Chl	1.7180	3.3003
DIN	-0.0331	0.1282
KE	-0.3807	1.1454
DIP	-0.0049	0.0118
TP	-0.0226	0.0436
TN	-0.1066	0.2165

Station TF4.2

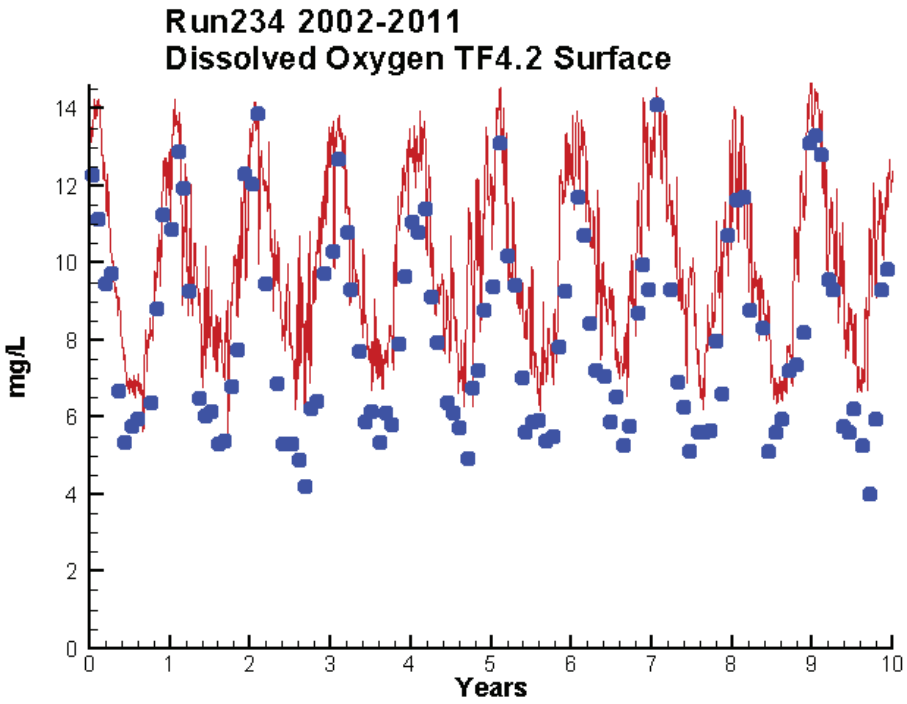

	Mean Difference	Absolute Mean Difference
Top DO	2.0610	2.1071

Station TF4.2

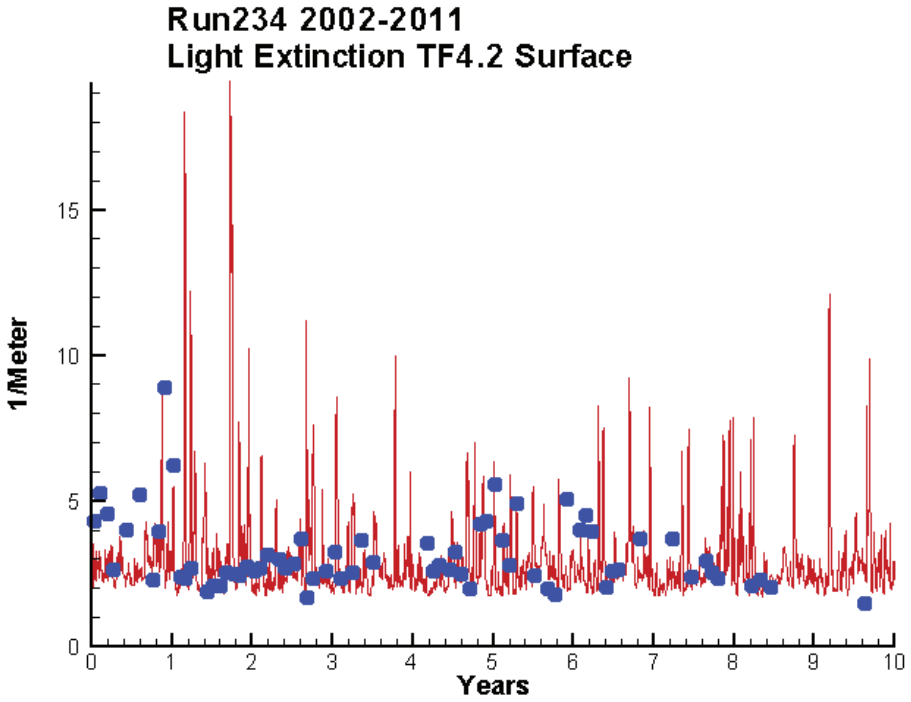

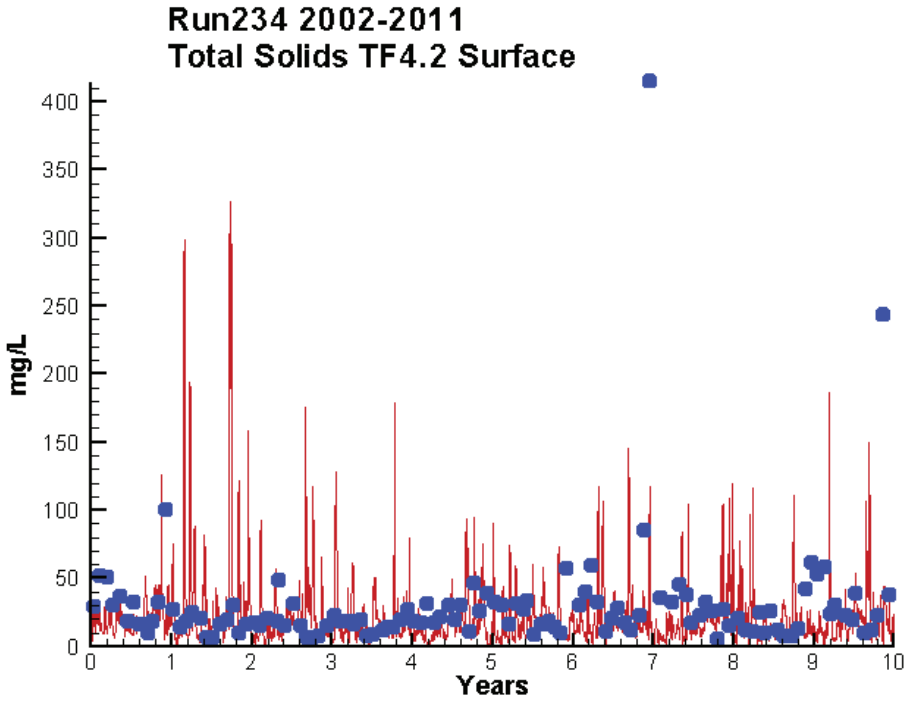

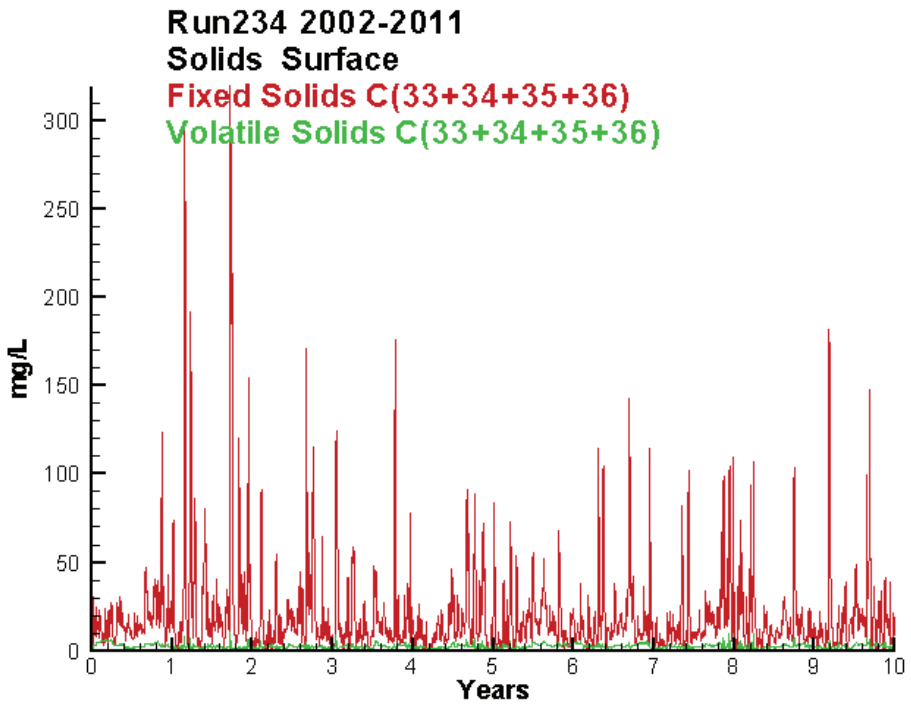

	Mean Difference	Absolute Mean Difference
KE	-0.3807	1.1454
TSS	-8.4507	22.4136

Station LE5.3

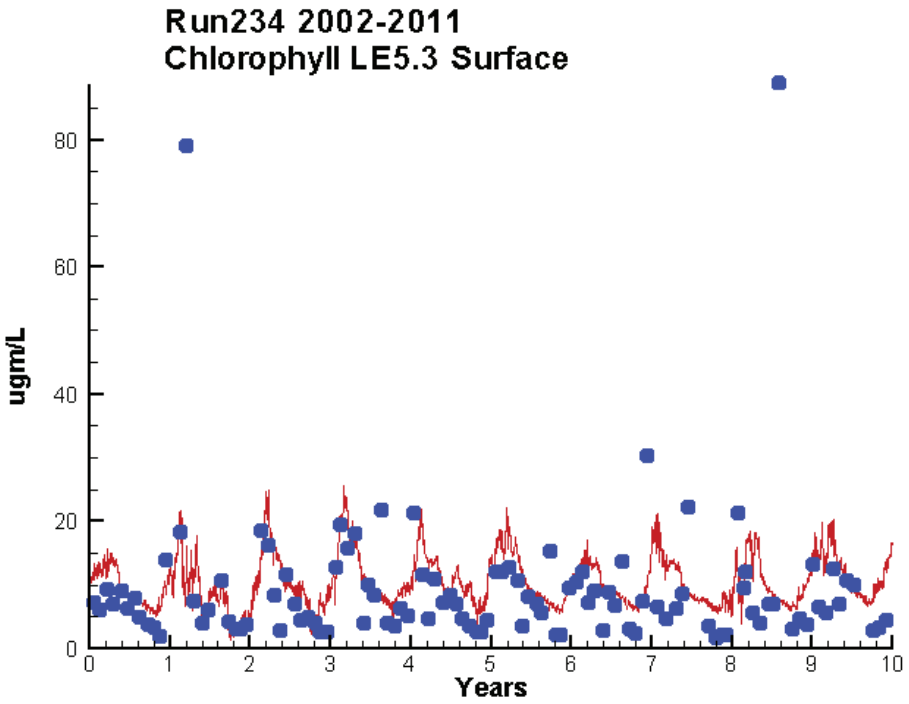

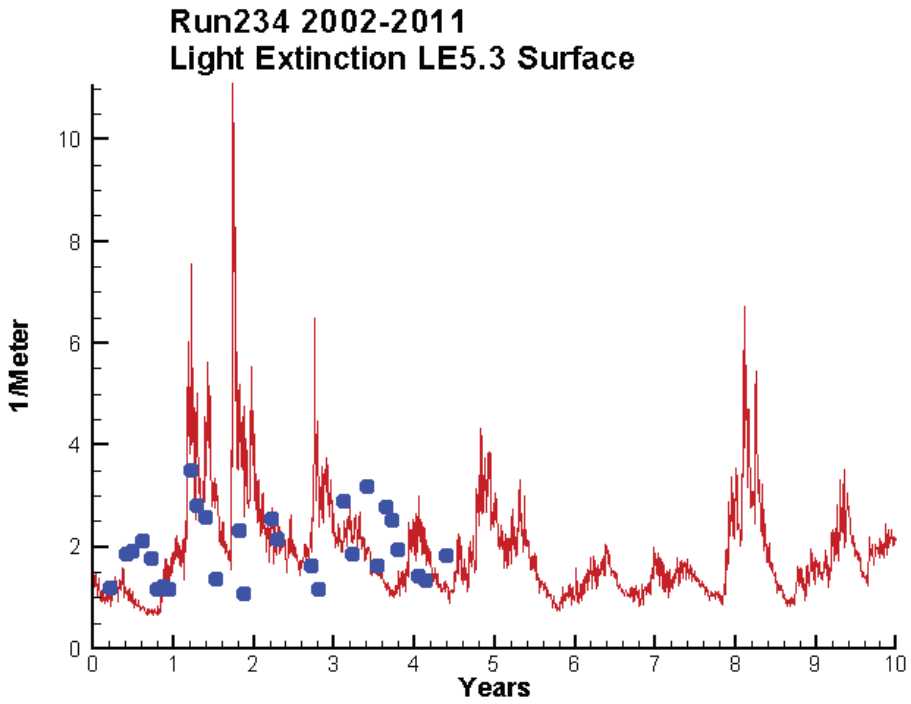

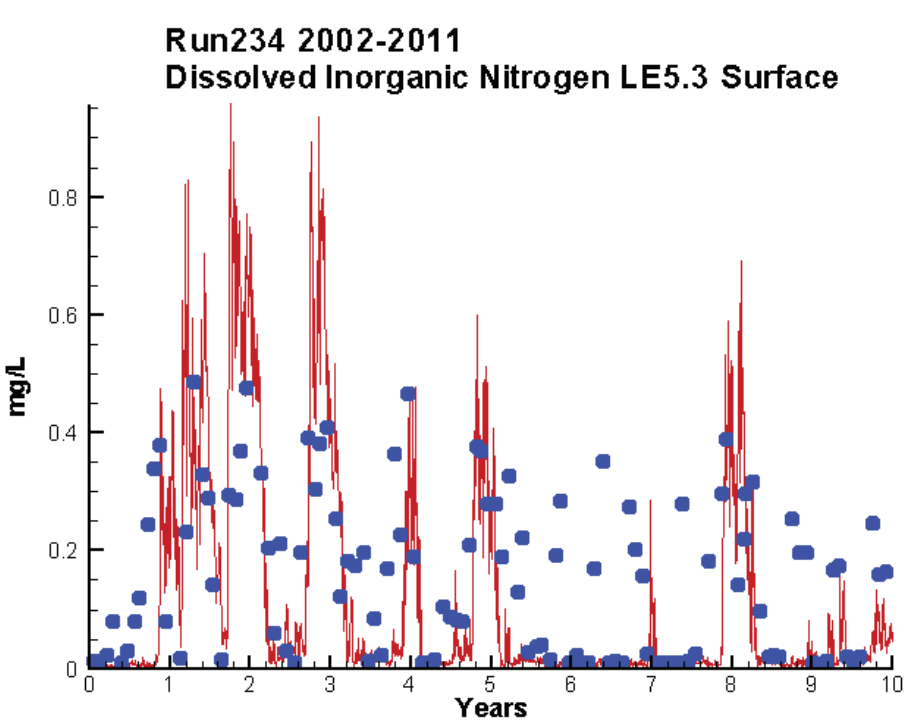

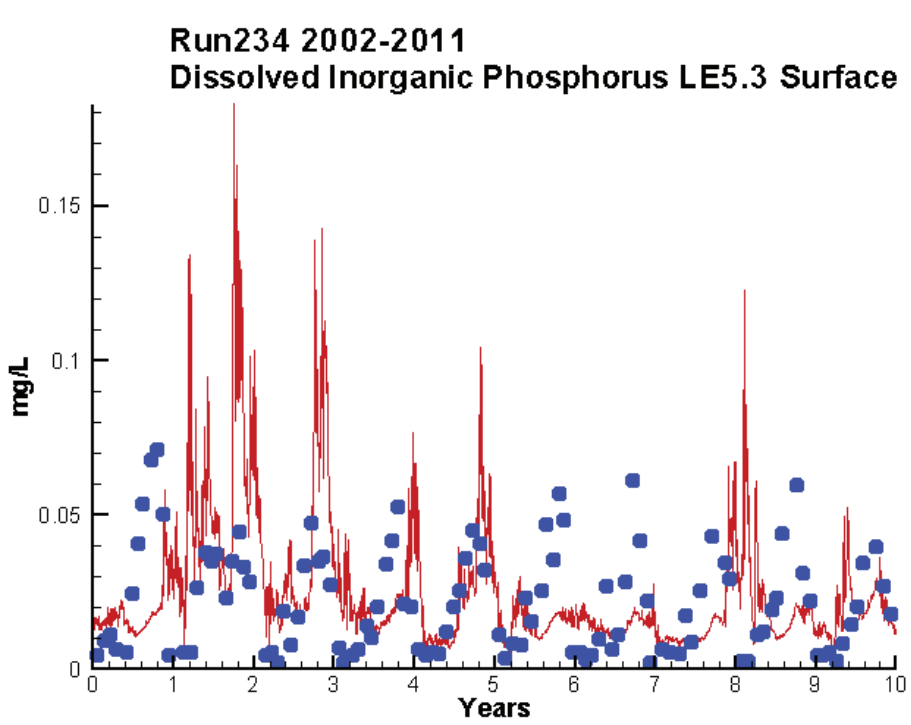

Station LE5.3

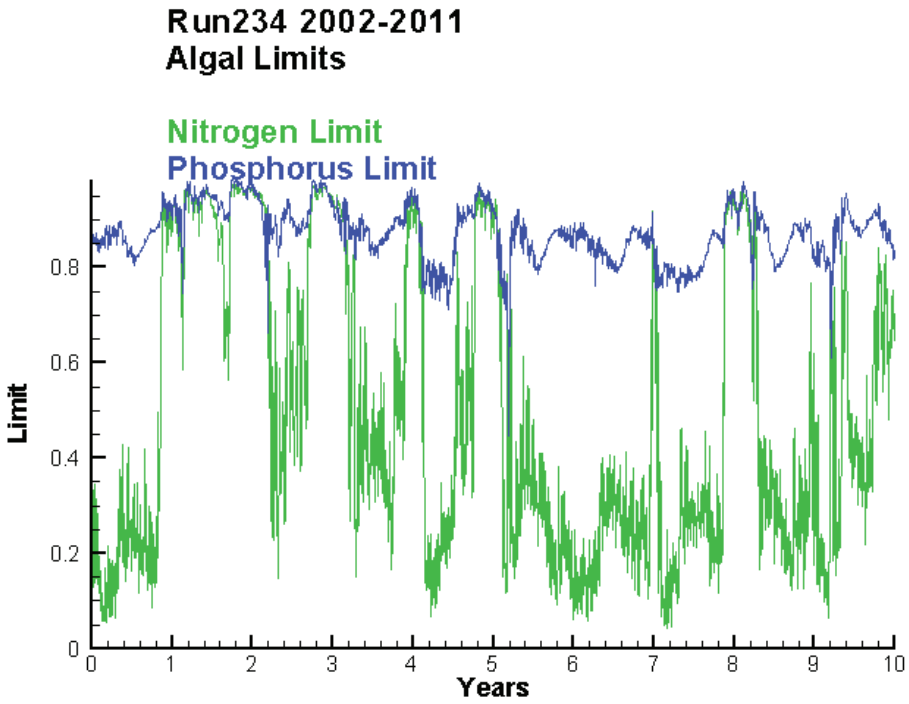

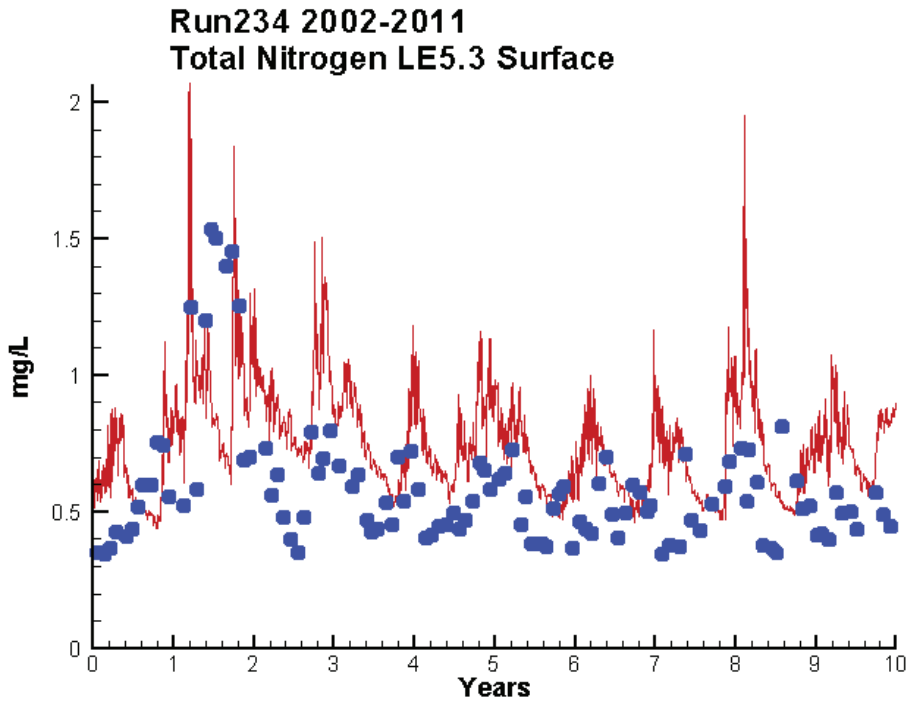

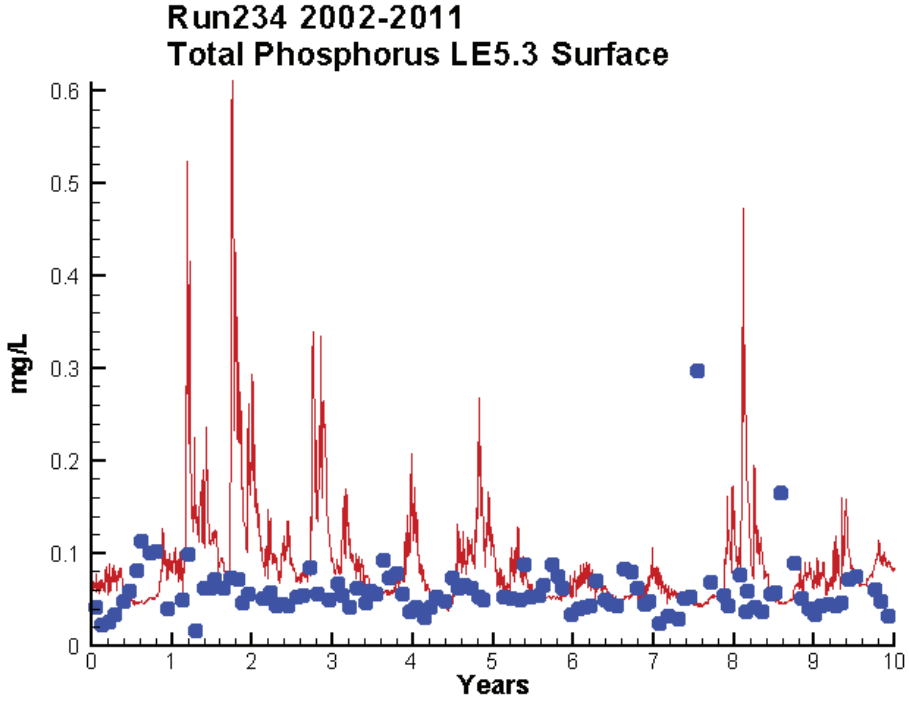

	Mean Difference	Absolute Mean Difference
Chl	1.1927	5.6186
DIN	-0.0388	0.1060
KE	0.1549	0.8937
DIP	0.0038	0.0176
TP	0.0304	0.0463
TN	0.1763	0.2514

Station LE5.3

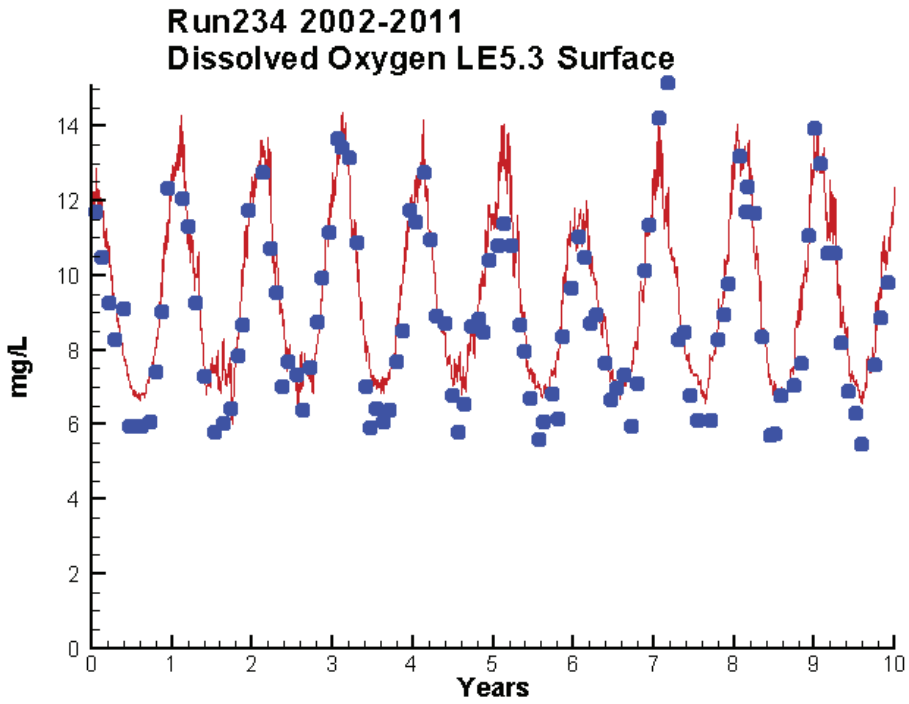

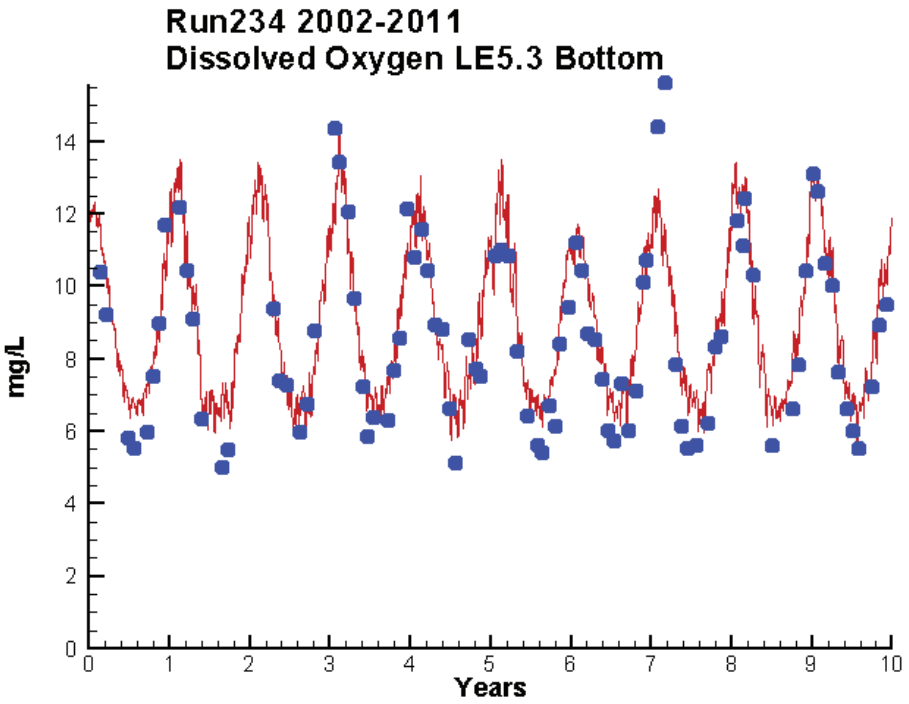

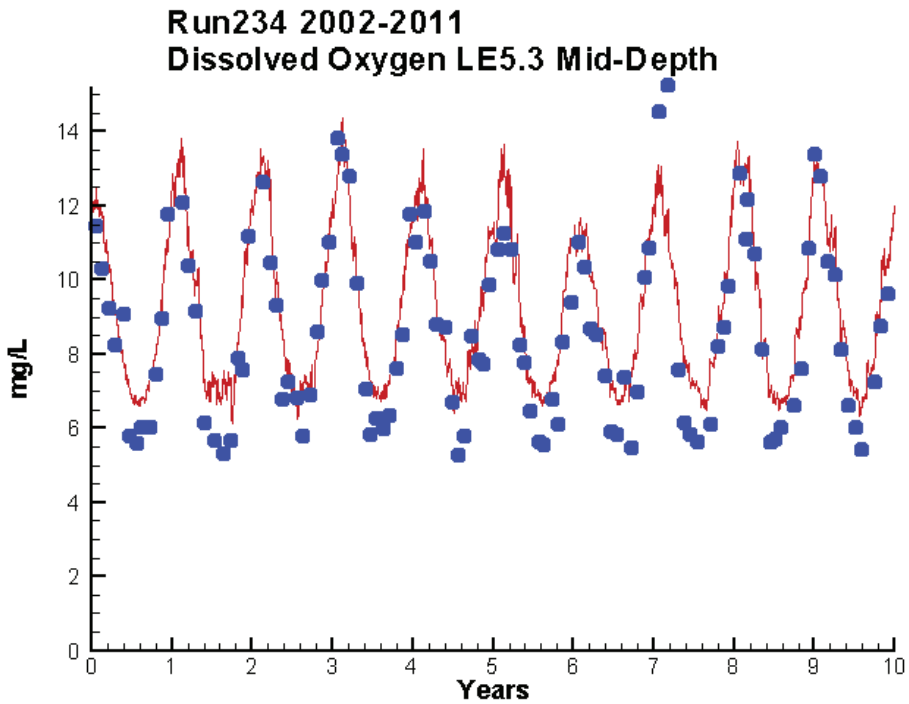

	Mean Difference	Absolute Mean Difference
Top DO	0.6776	0.9358
Mid DO	0.8026	1.0510
Bot DO	0.6061	0.9427

Station LE5.3

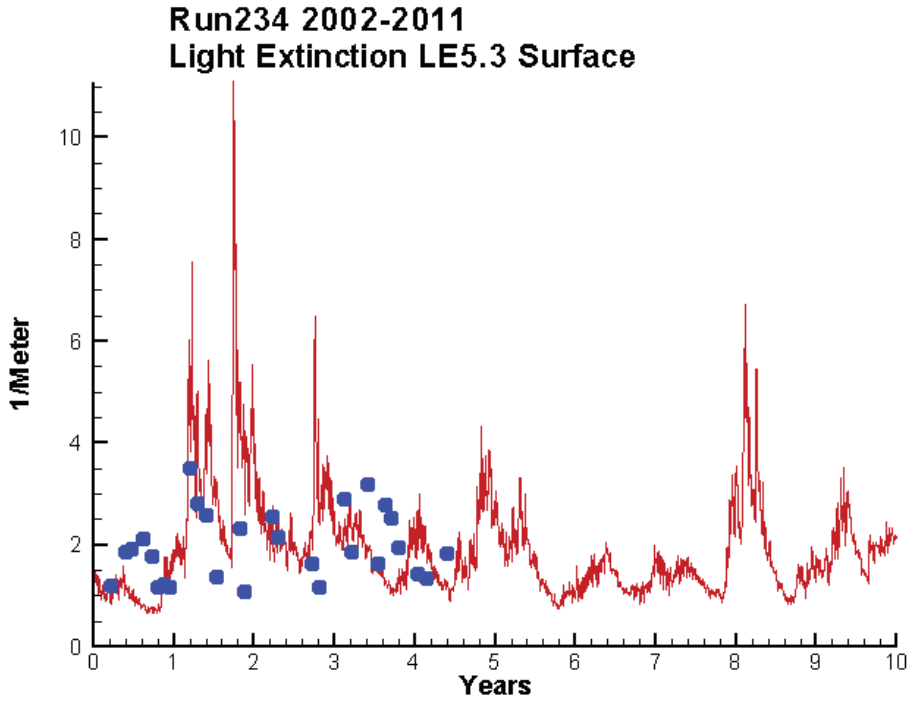

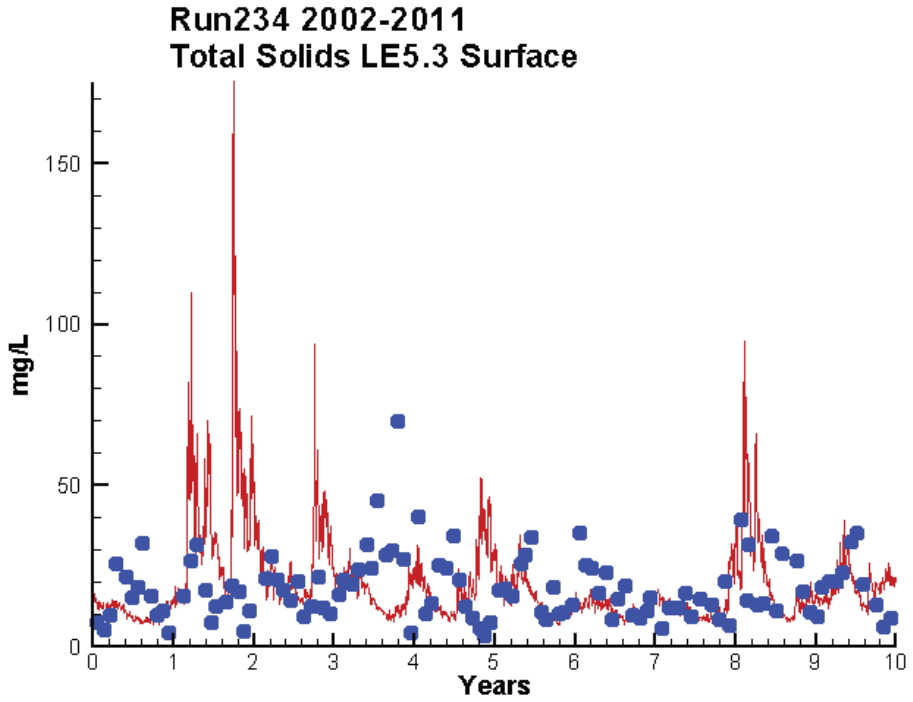

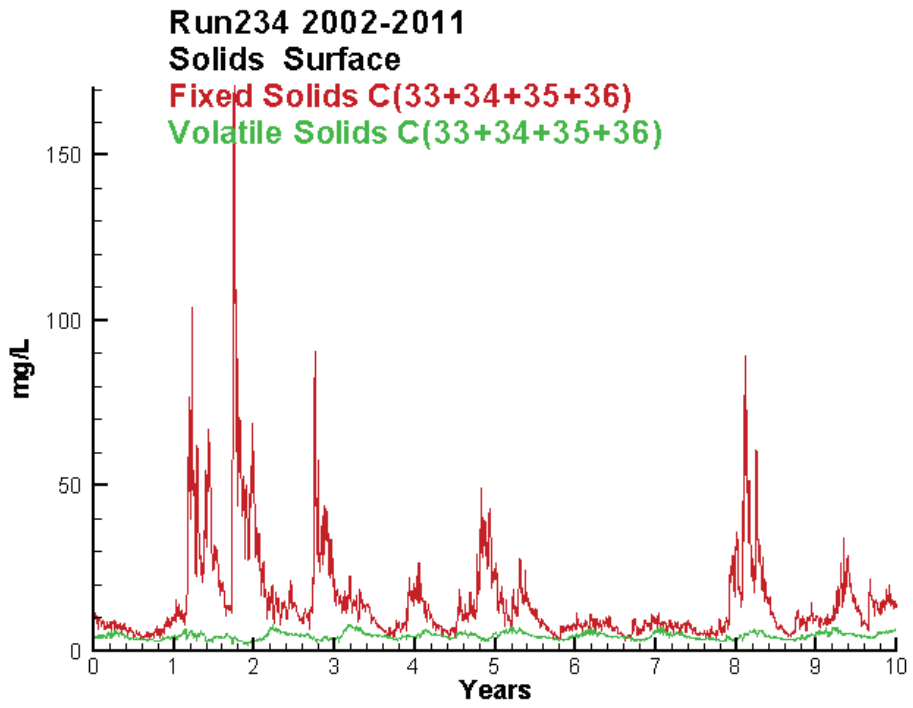

	Mean Difference	Absolute Mean Difference
KE	0.1549	0.8937
TSS	2.0831	11.8614

Station RET5.2

Run234 2002-2011
Chlorophyll RET5.2 Surface

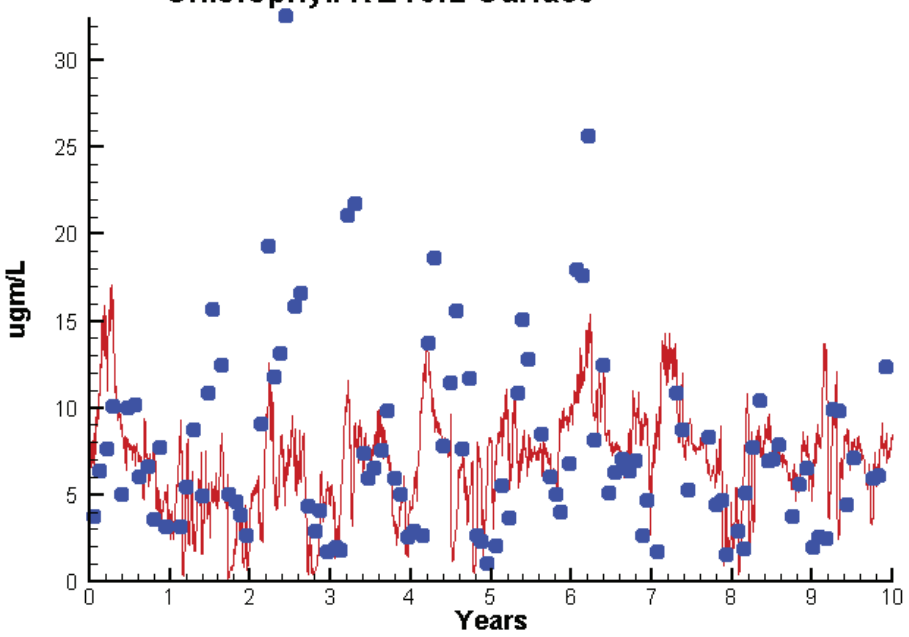

Run234 2002-2011
Light Extinction RET5.2 Surface

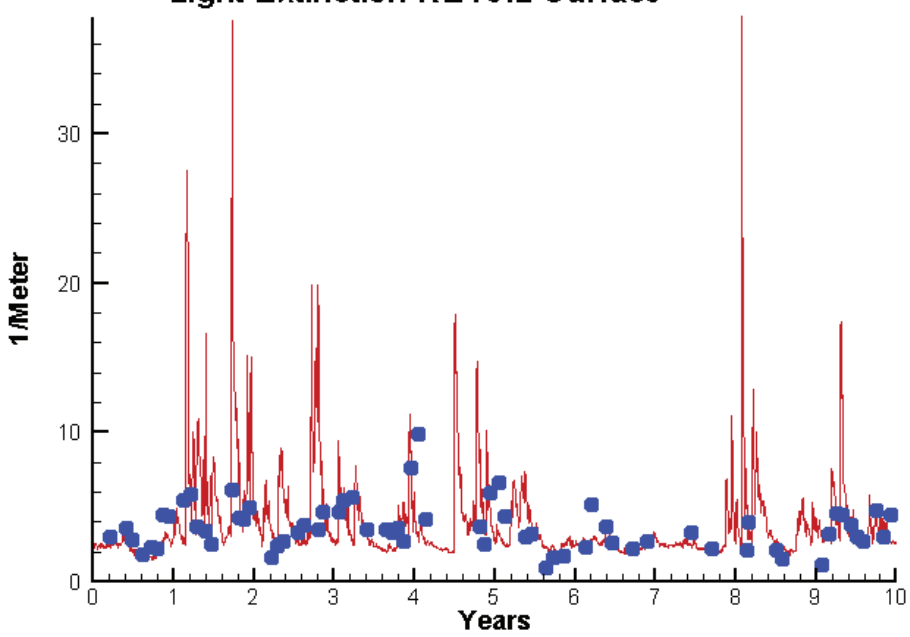

Run234 2002-2011
Dissolved Inorganic Nitrogen RET5.2 Surface

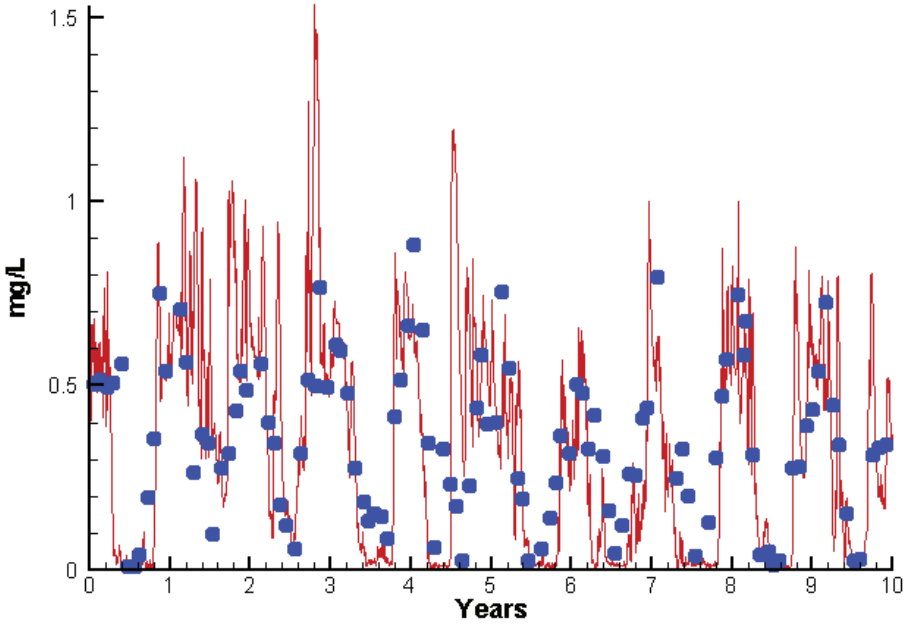

Run234 2002-2011
Dissolved Inorganic Phosphorus RET5.2 Surface

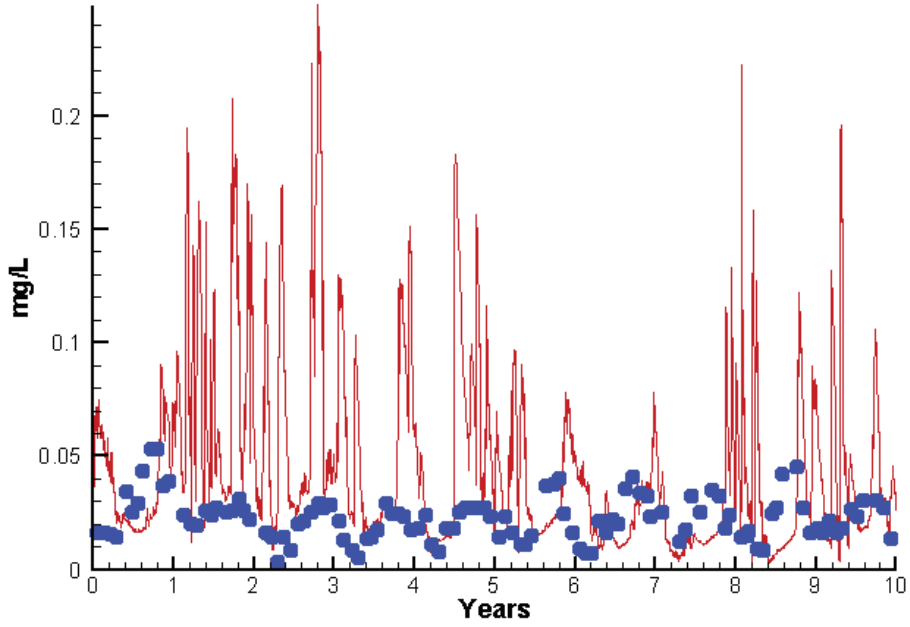

Station RET5.2

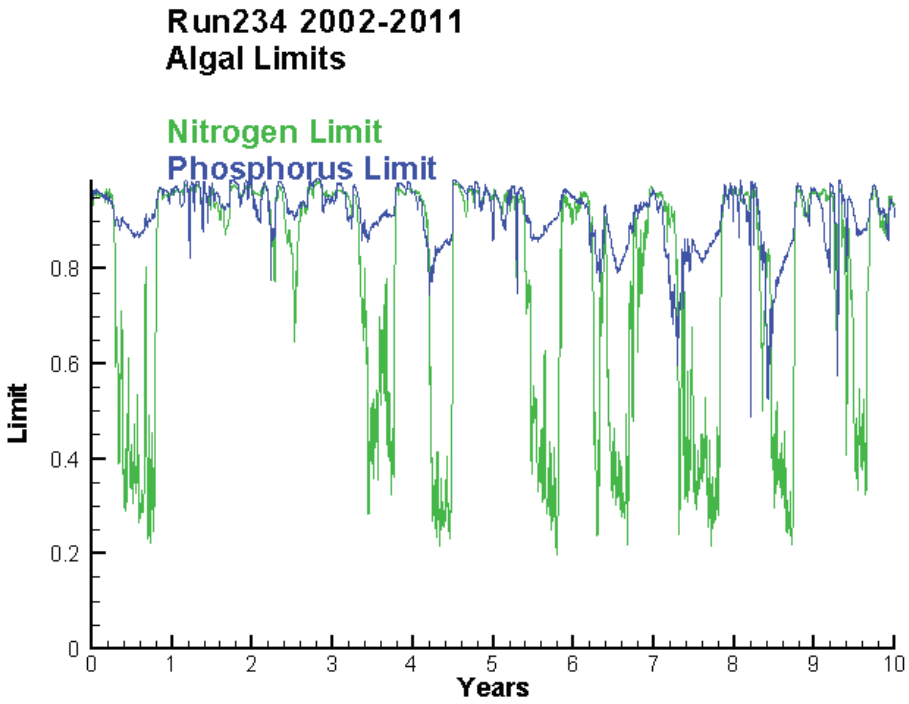

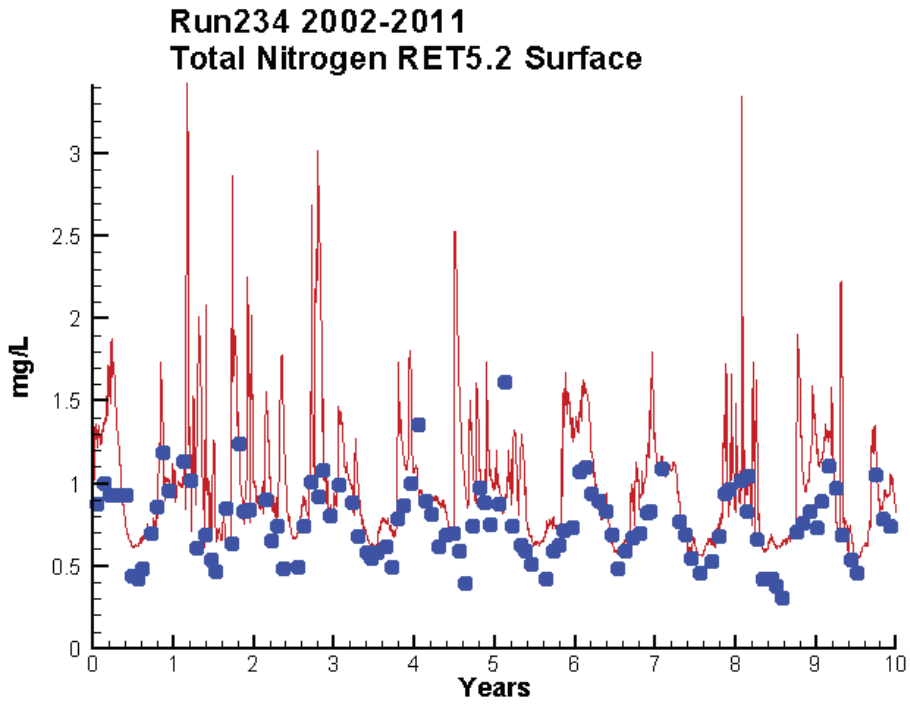

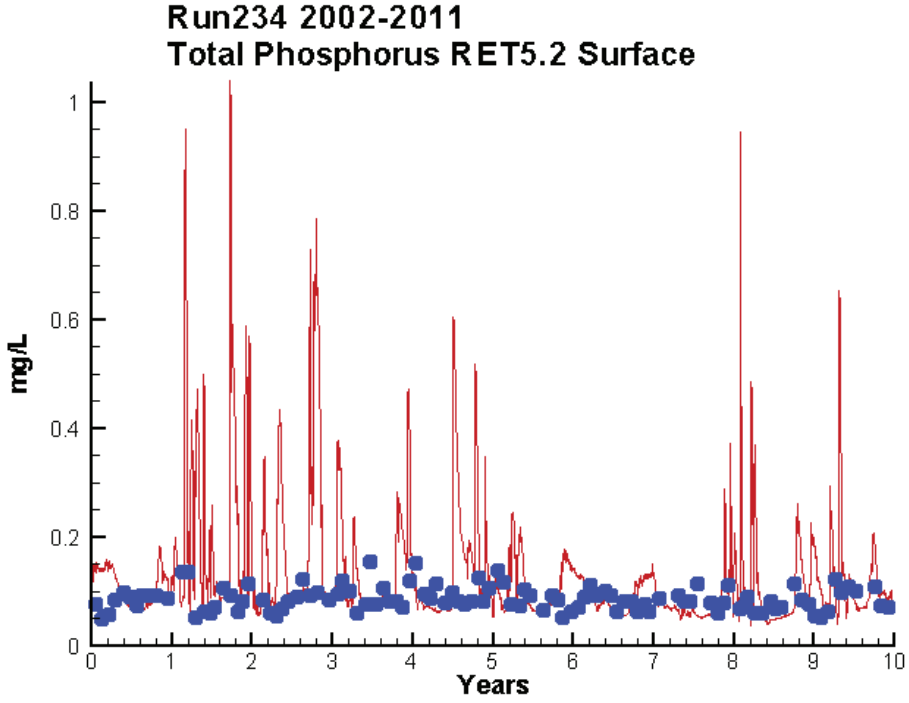

	Mean Difference	Absolute Mean Difference
Chl	-0.7110	3.9782
DIN	0.0142	0.1726
KE	0.7449	1.9932
DIP	0.0269	0.0342
TP	0.0595	0.0784
TN	0.2871	0.3324

Station RET5.2

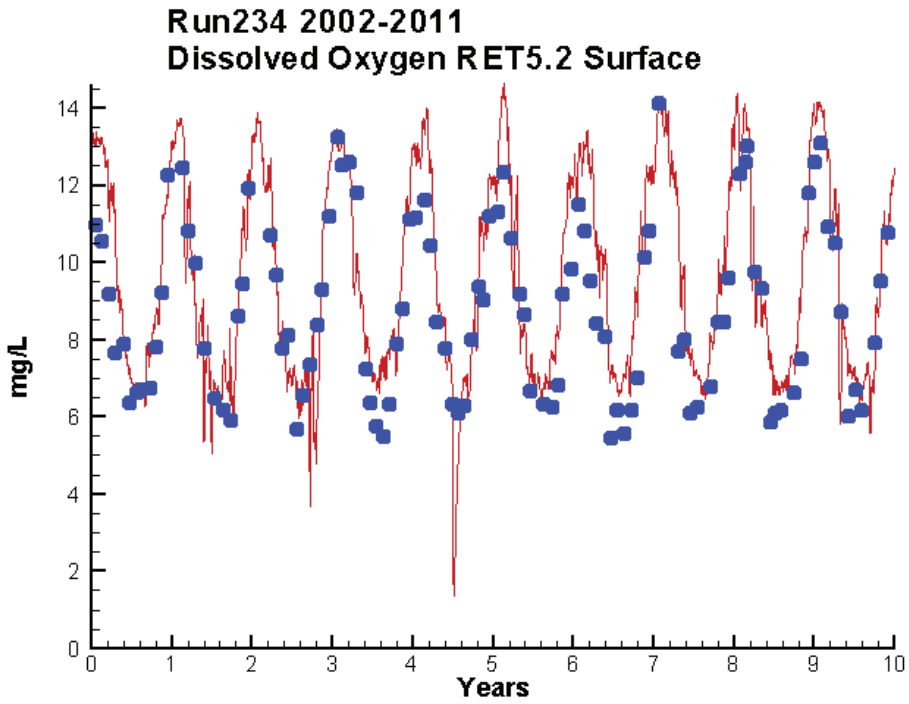

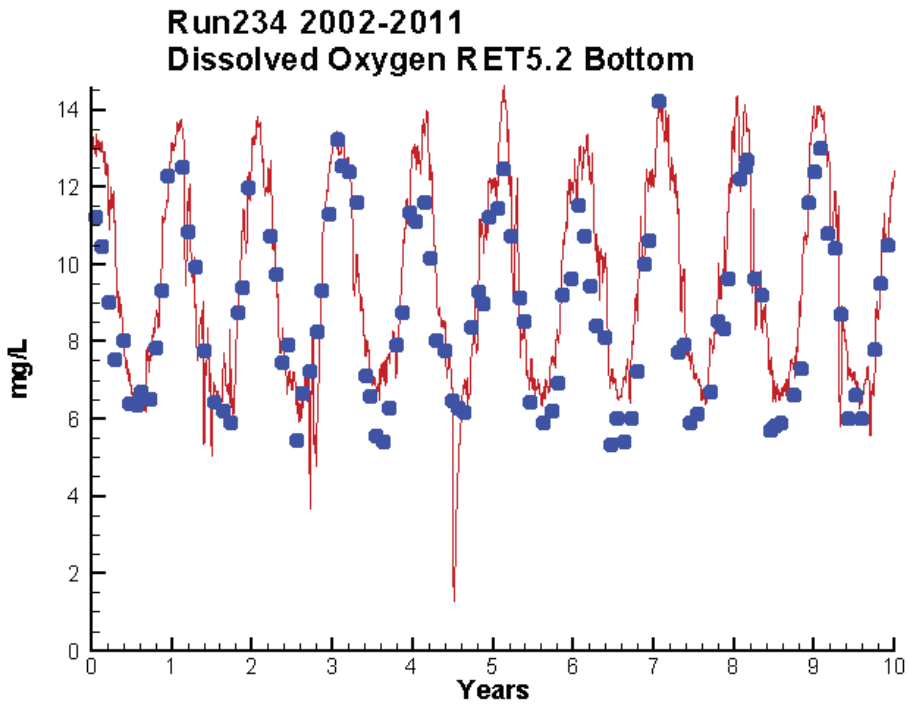

	Mean Difference	Absolute Mean Difference
Top DO	0.8786	1.1822
Bot DO	0.8912	1.2011

Station RET5.2

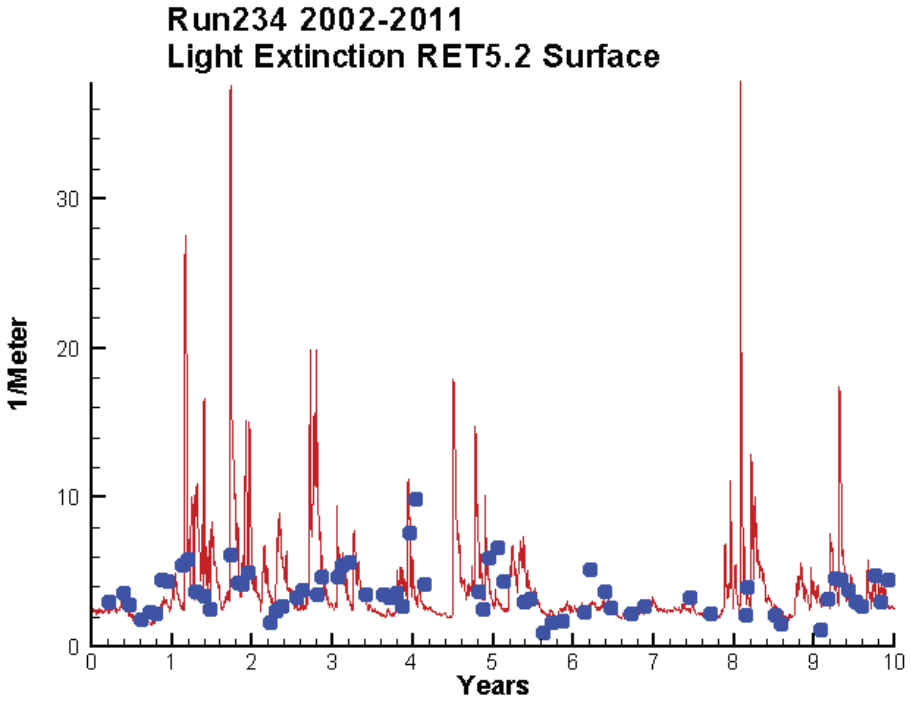

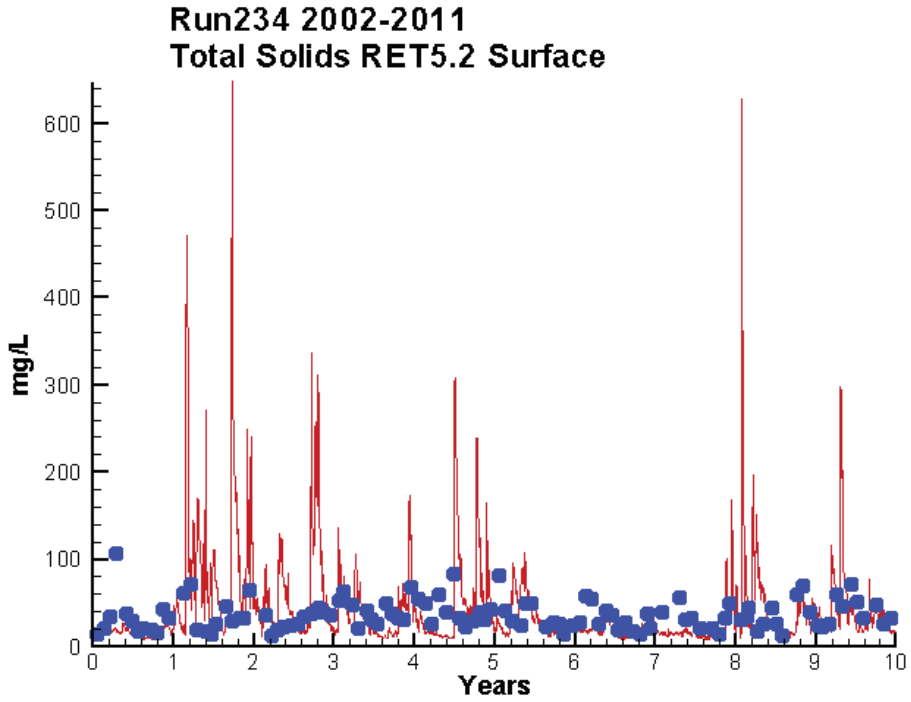

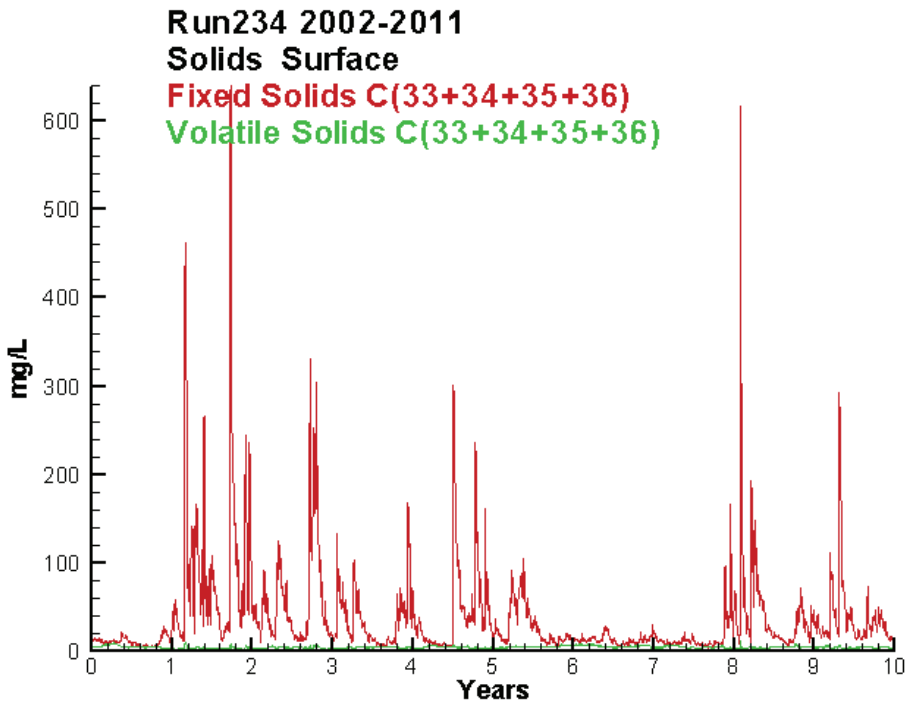

	Mean Difference	Absolute Mean Difference
KE	0.7449	1.9932
TSS	12.9696	35.2804

Station TF5.5

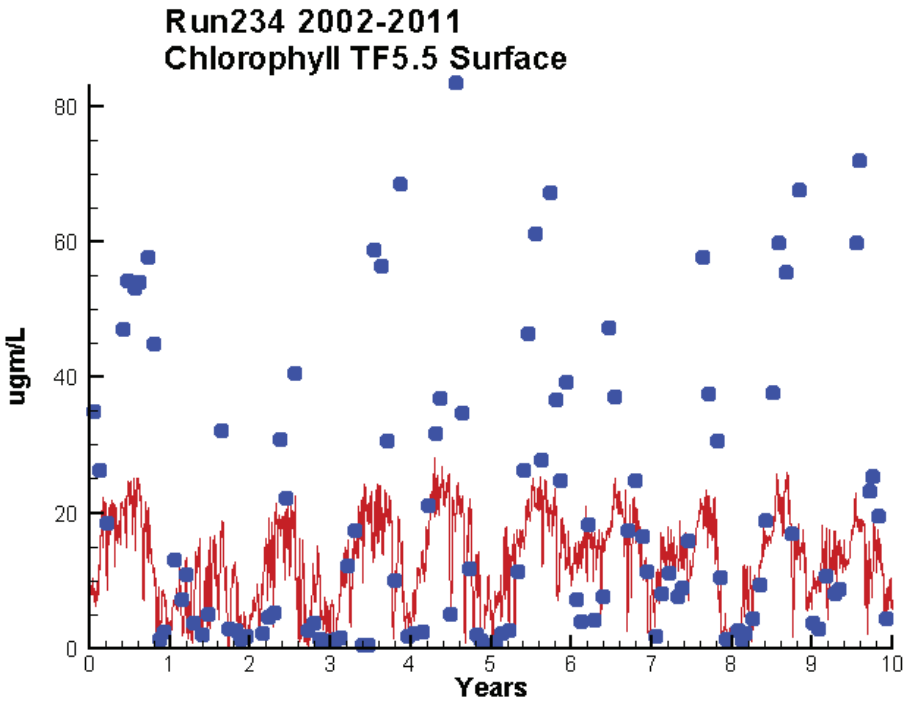

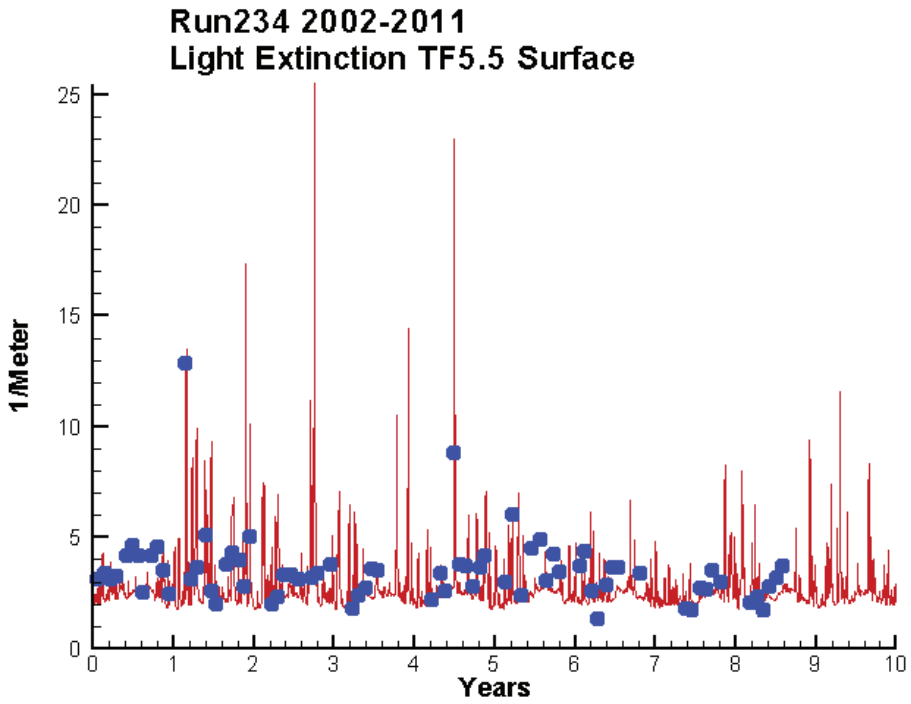

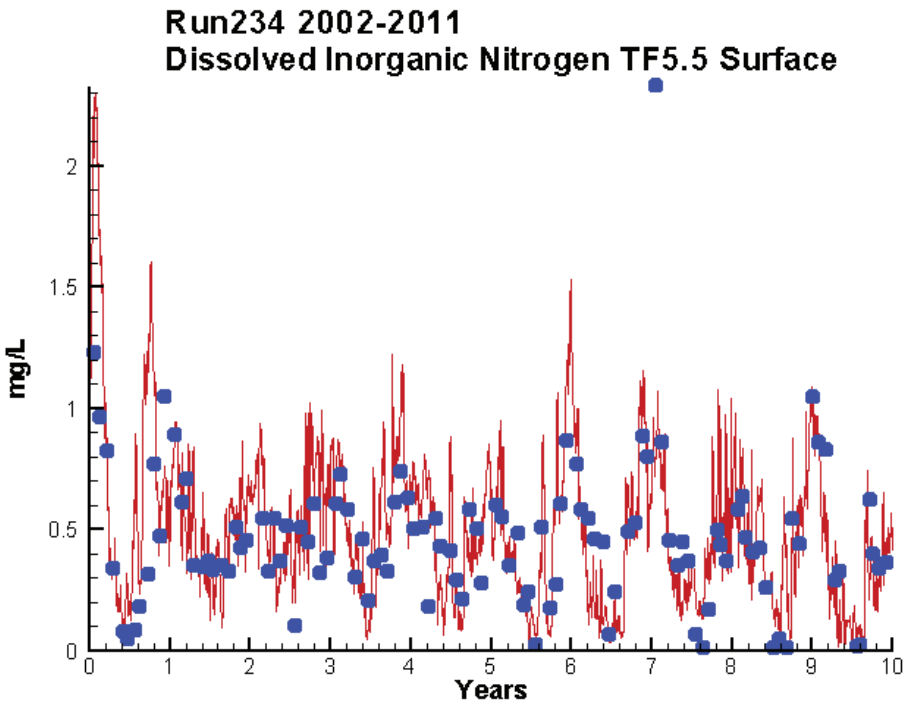

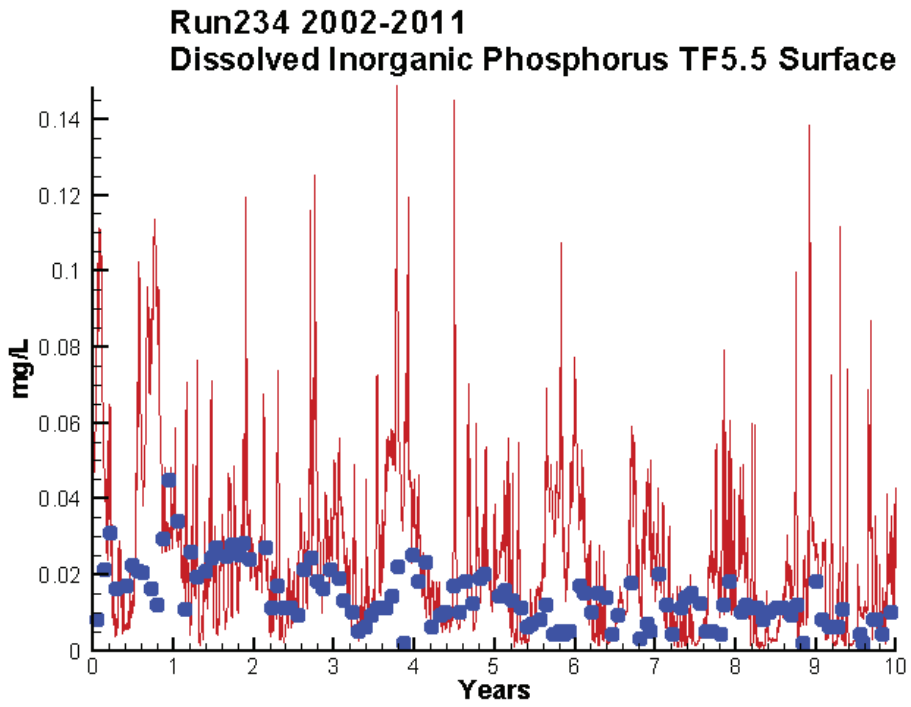

Station TF5.5

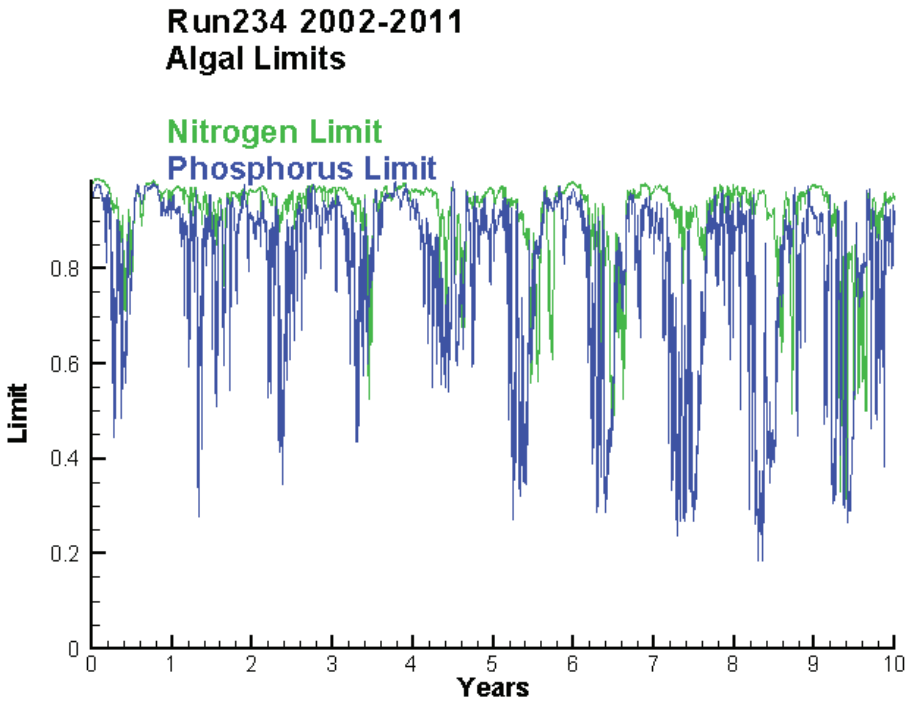

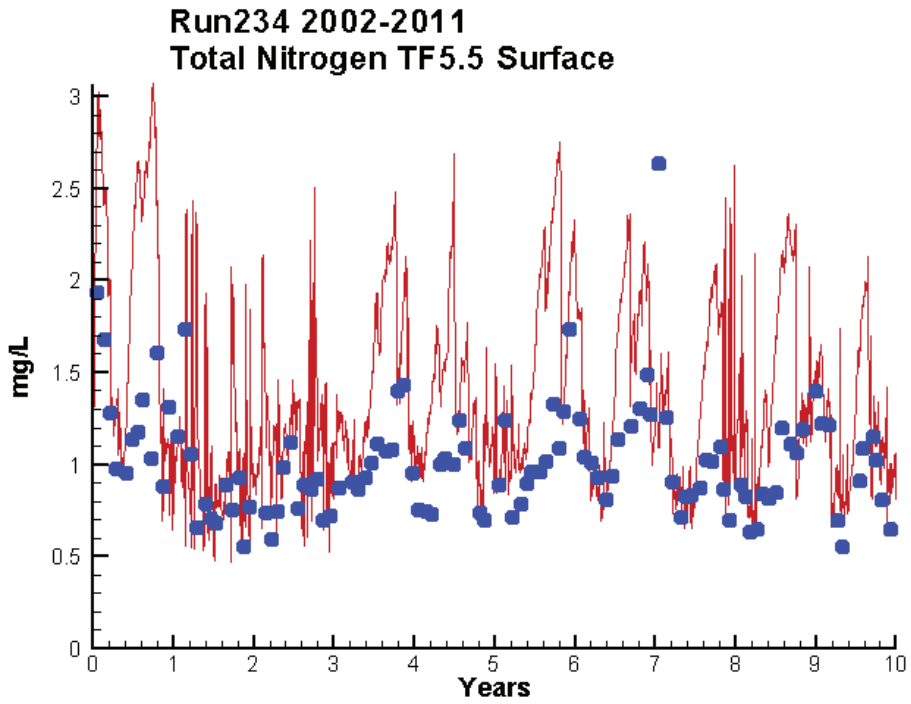

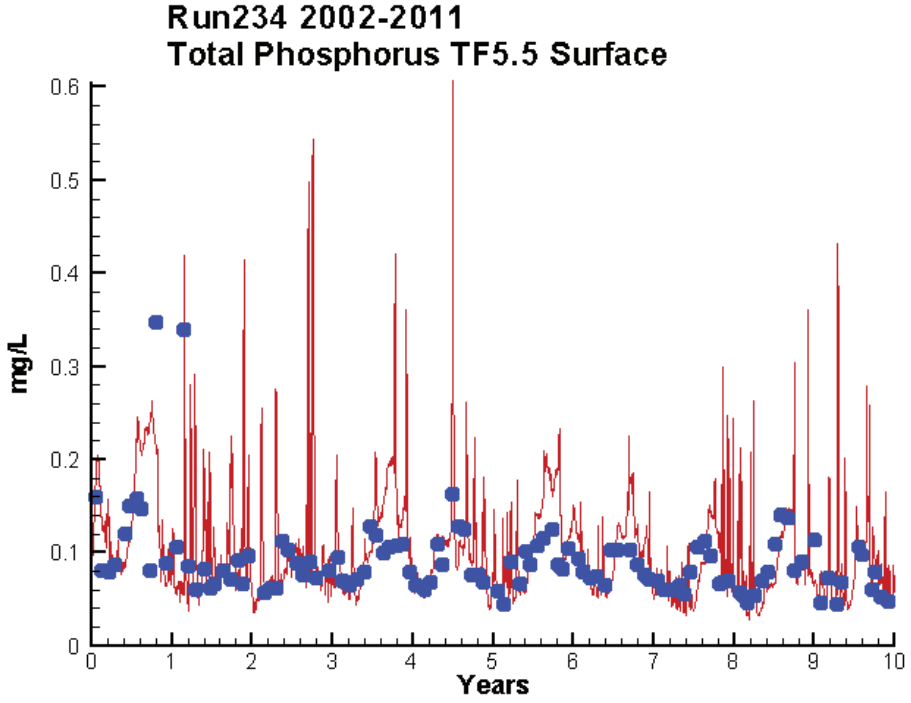

	Mean Difference	Absolute Mean Difference
Chl	-8.0546	12.8969
DIN	0.0520	0.1866
KE	-0.2837	1.2244
DIP	0.0119	0.0172
TP	0.0207	0.0370
TN	0.4295	0.4776

Station TF5.5

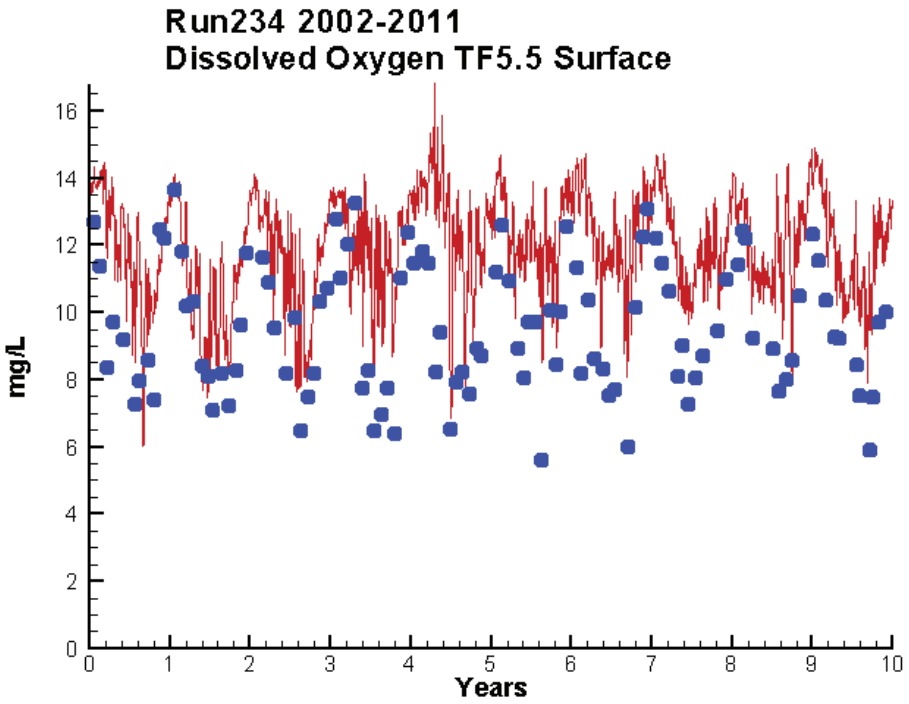

	Mean Difference	Absolute Mean Difference
Top DO	2.4562	2.5249

Station TF5.5

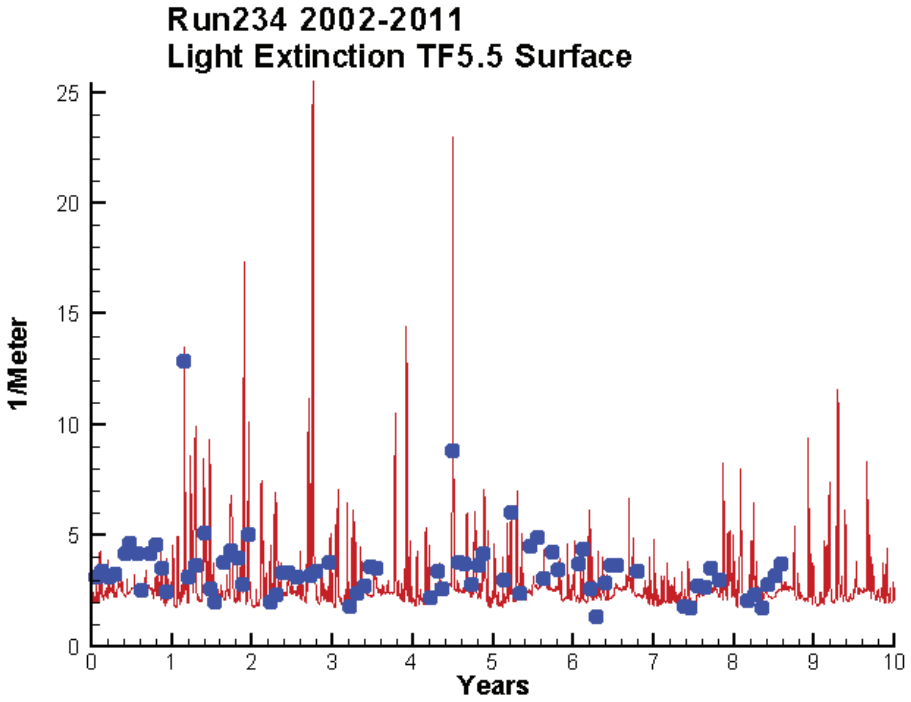

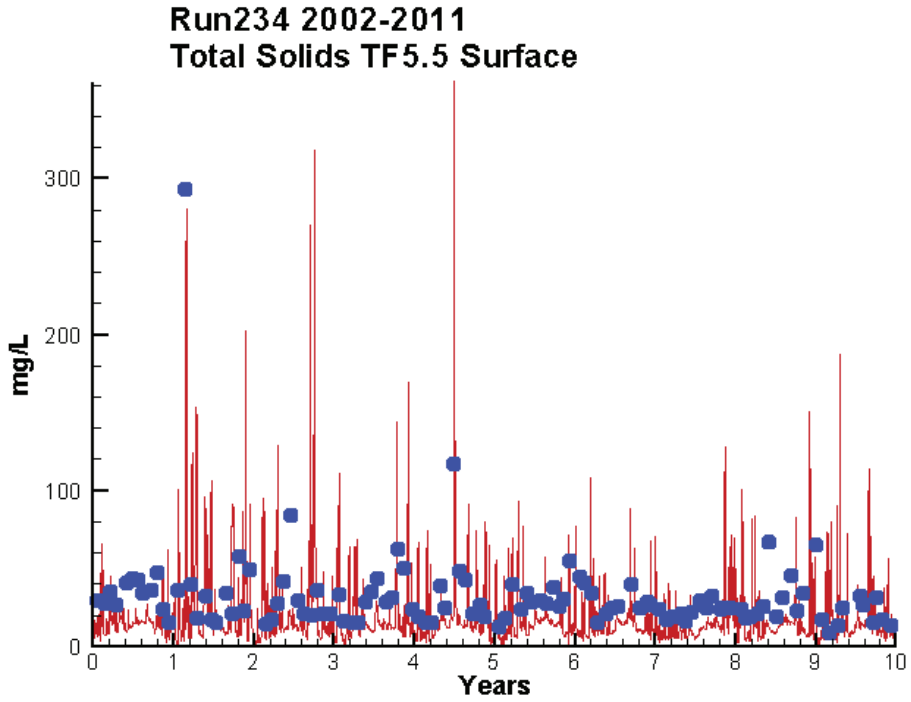

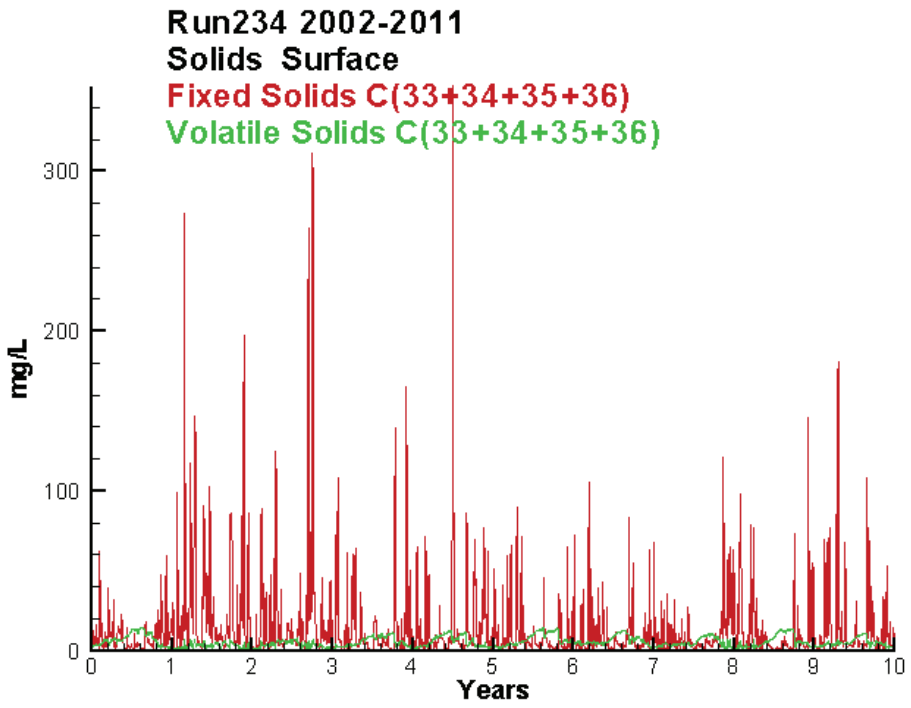

	Mean Difference	Absolute Mean Difference
KE	-0.2837	1.2244
TSS	-9.1523	22.5016

Station EE1.1

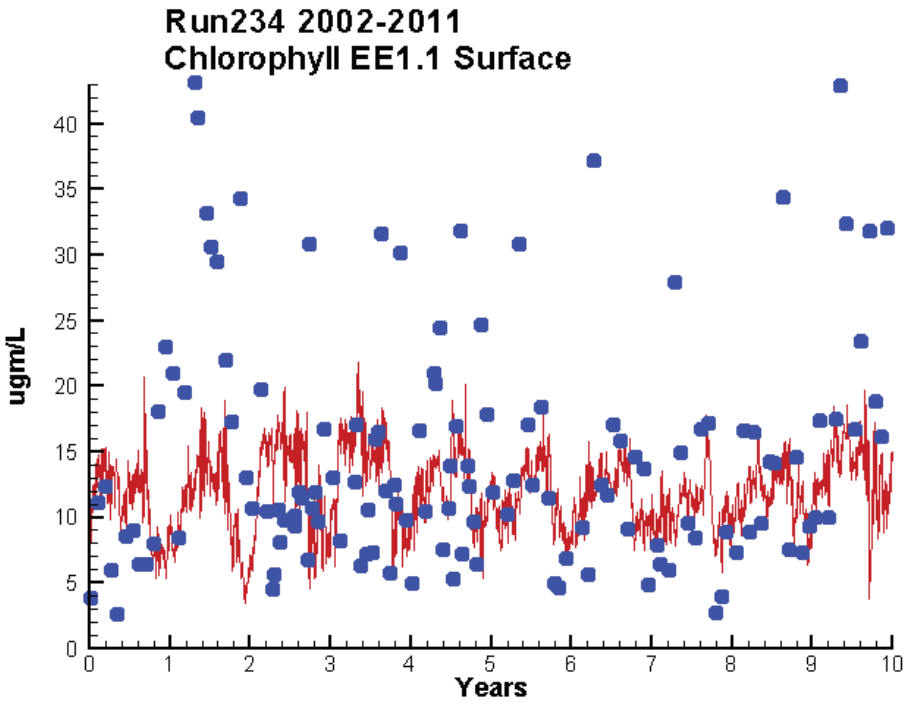

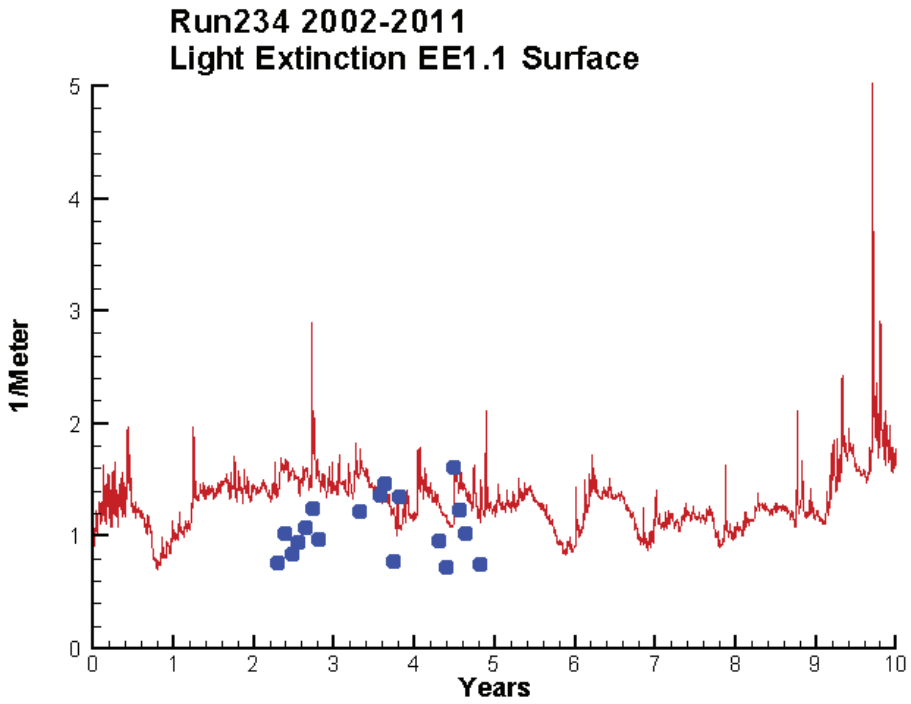

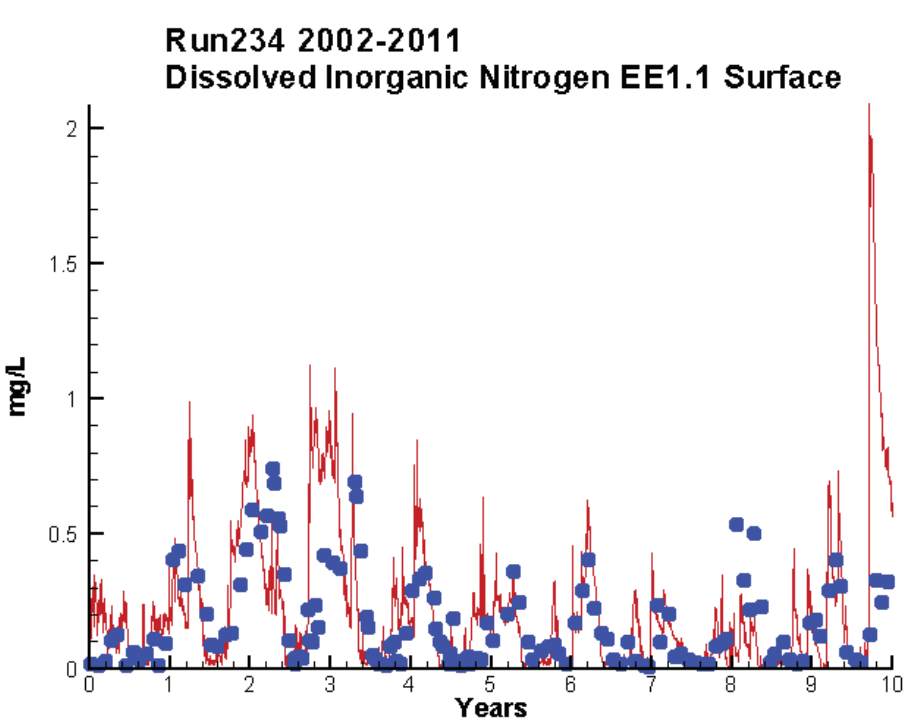

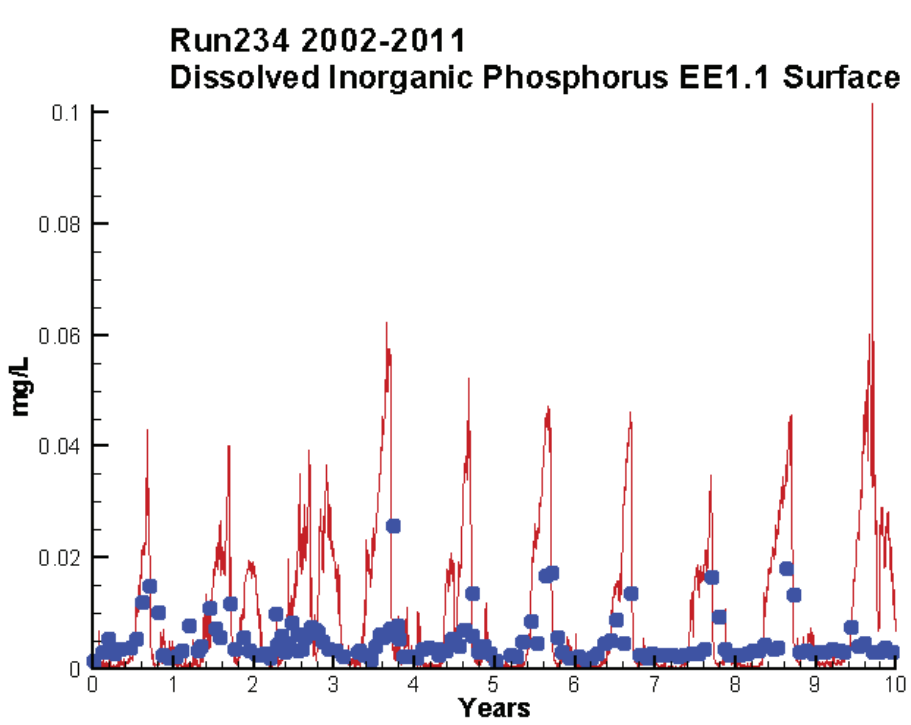

Station EE1.1

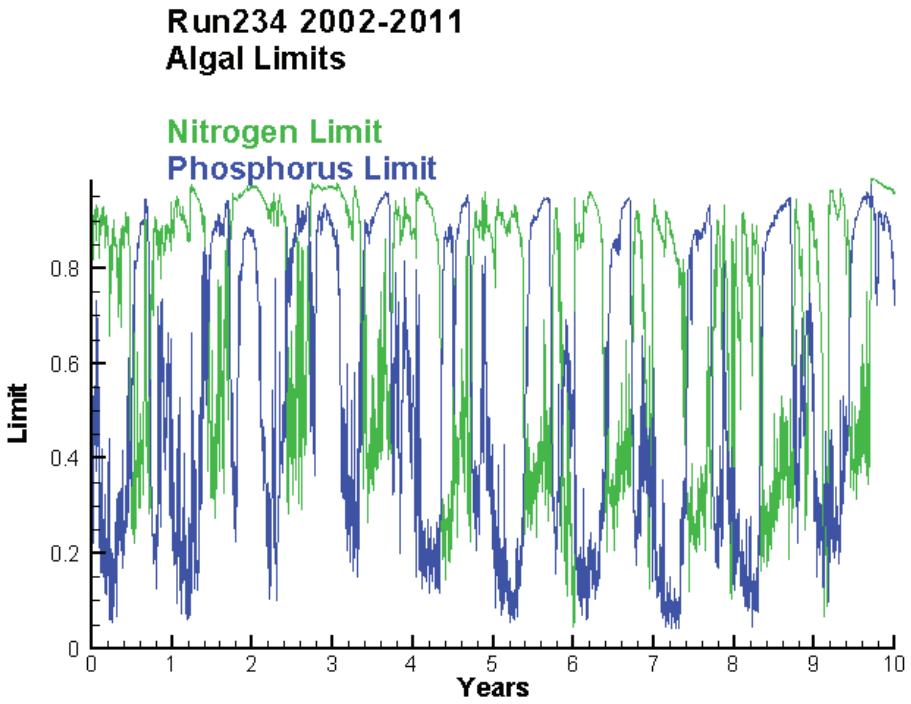

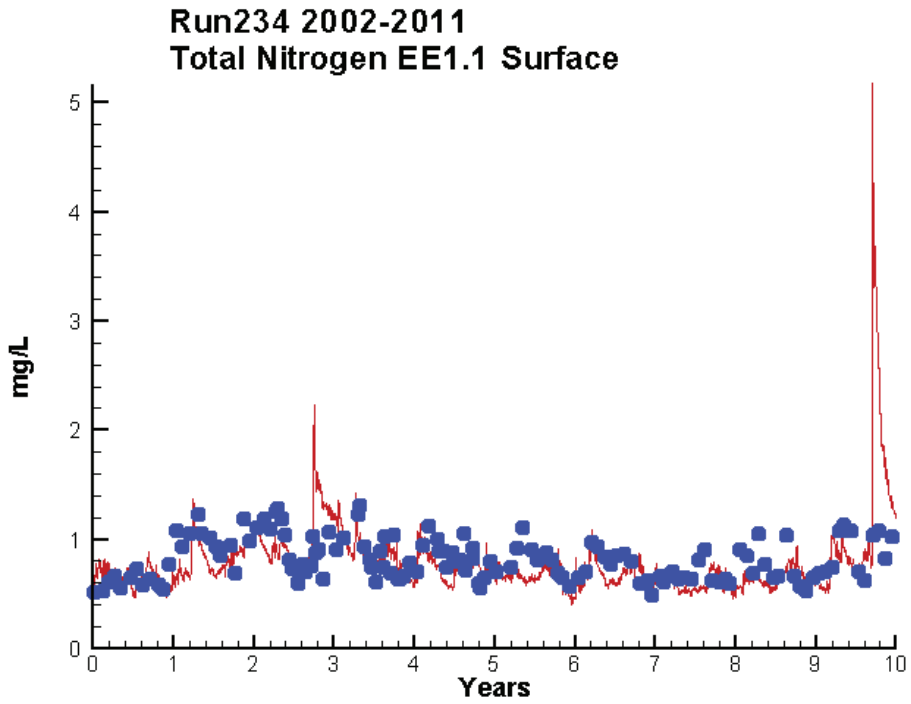

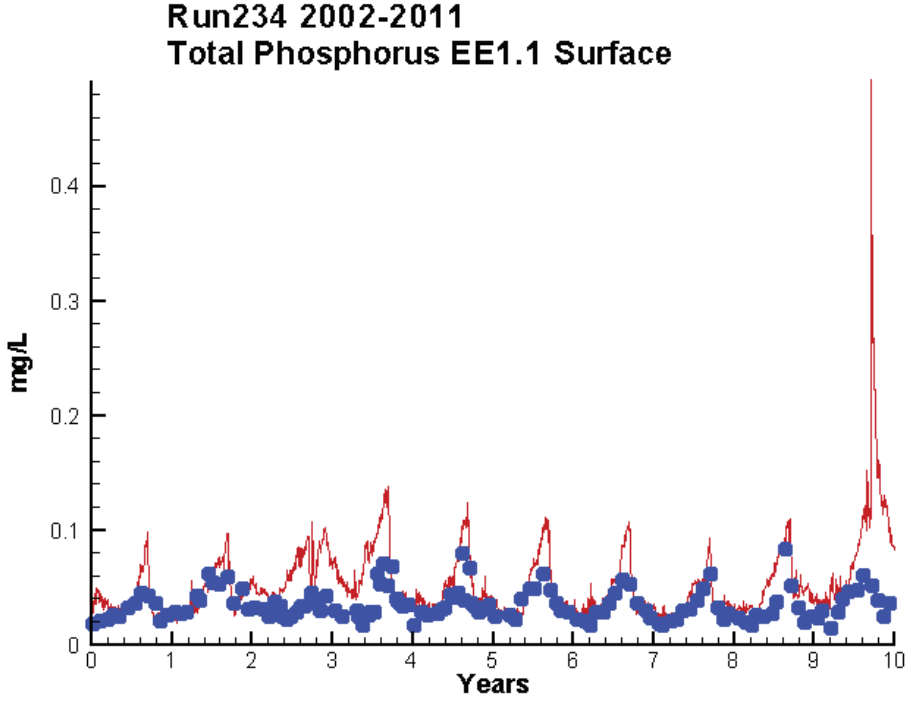

	Mean Difference	Absolute Mean Difference
Chl	-2.4893	6.9307
DIN	0.0422	0.1524
KE	0.5205	0.6038
DIP	0.0052	0.0083
TP	0.0202	0.0218
TN	-0.0151	0.1986

Station EE1.1

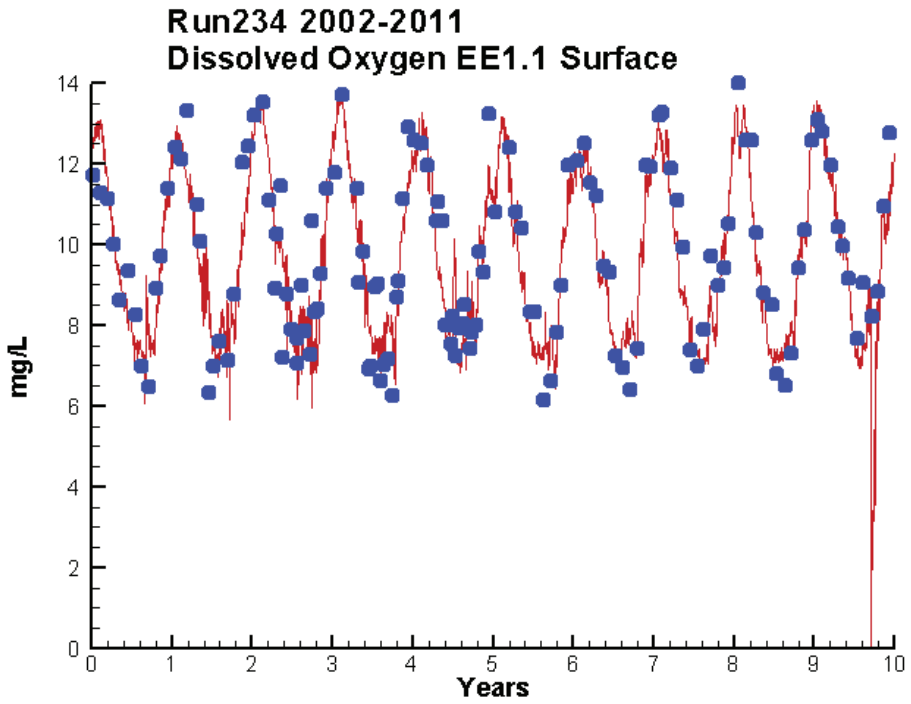

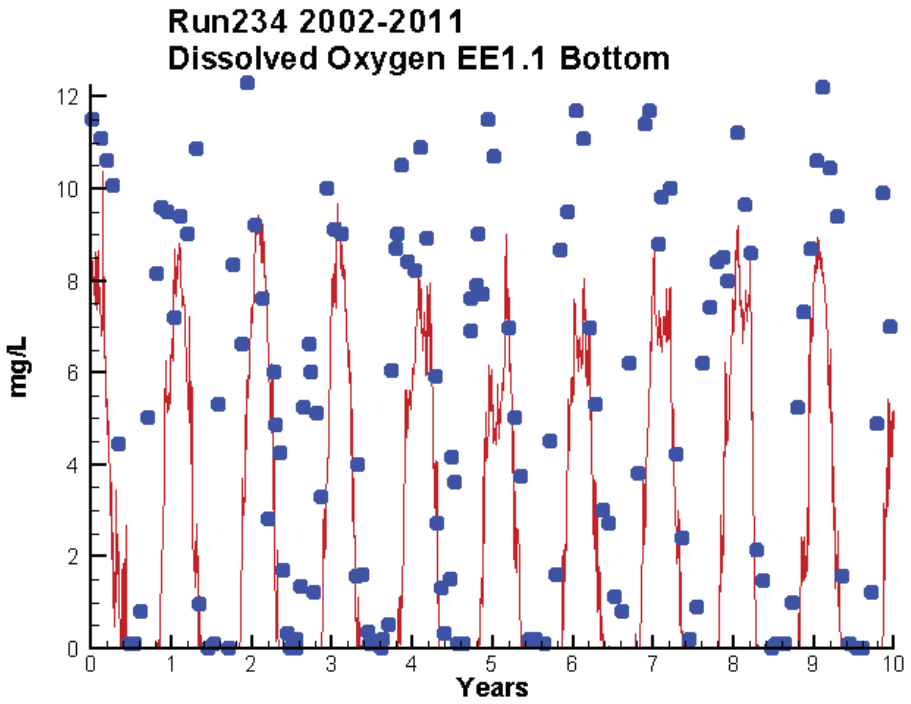

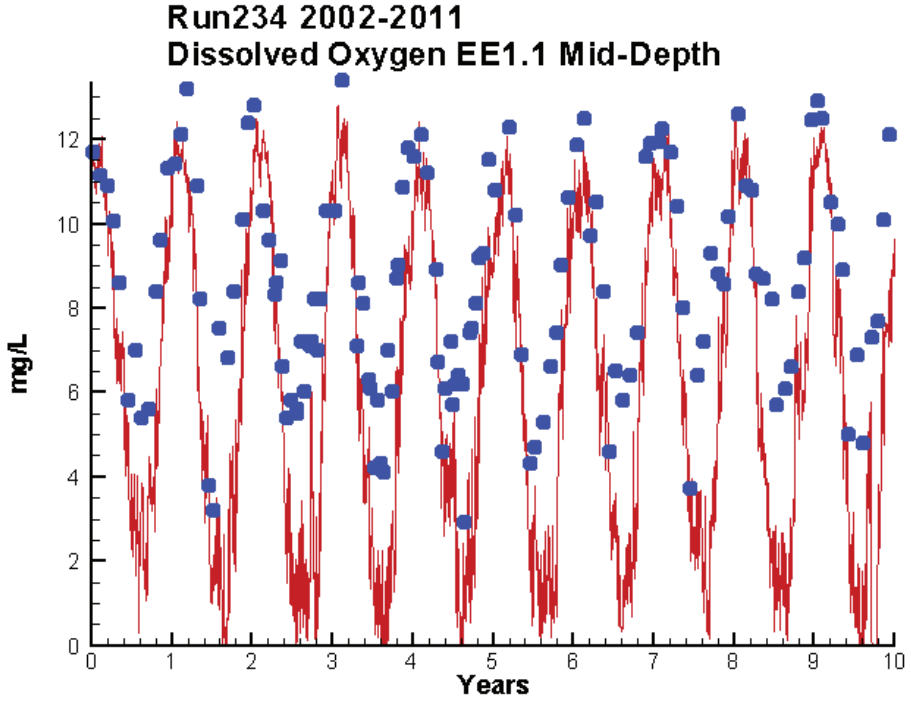

	Mean Difference	Absolute Mean Difference
Top DO	-0.1897	0.8025
Mid DO	-2.6600	2.7171
Bot DO	-3.1025	3.1717

Station EE1.1

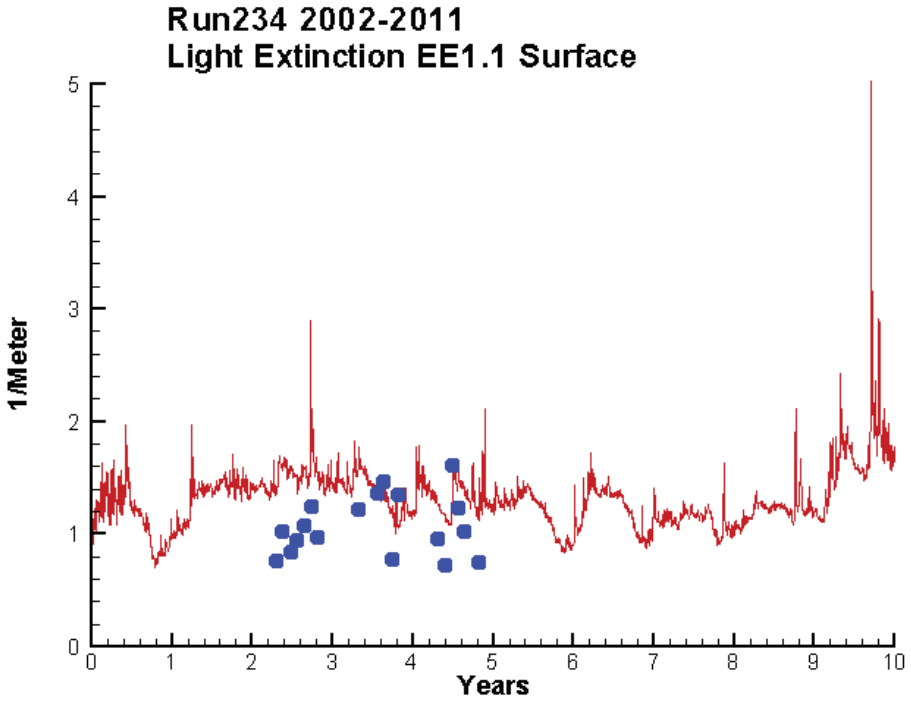

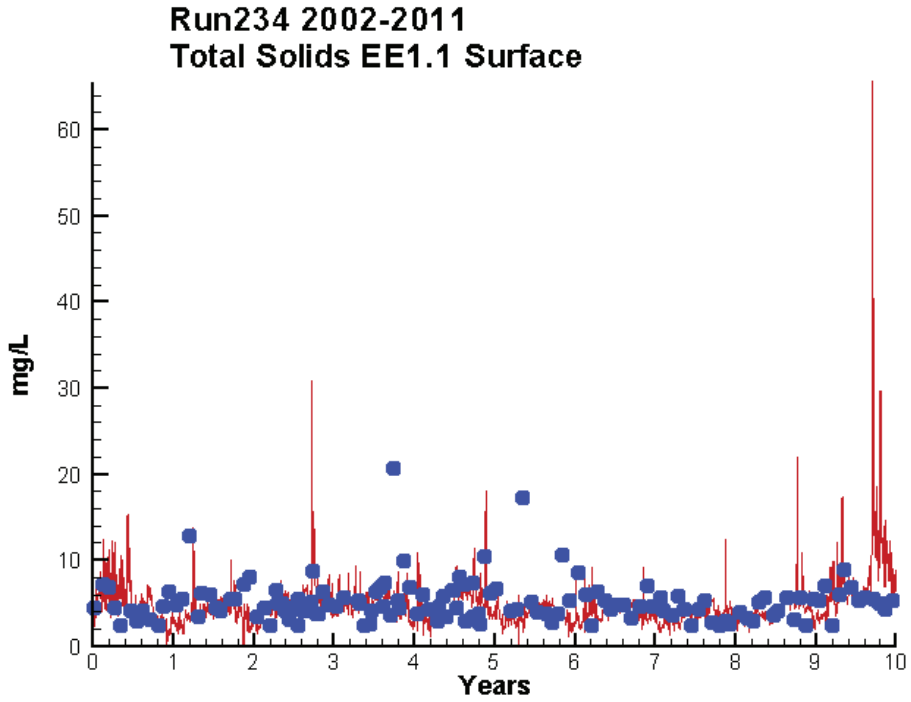

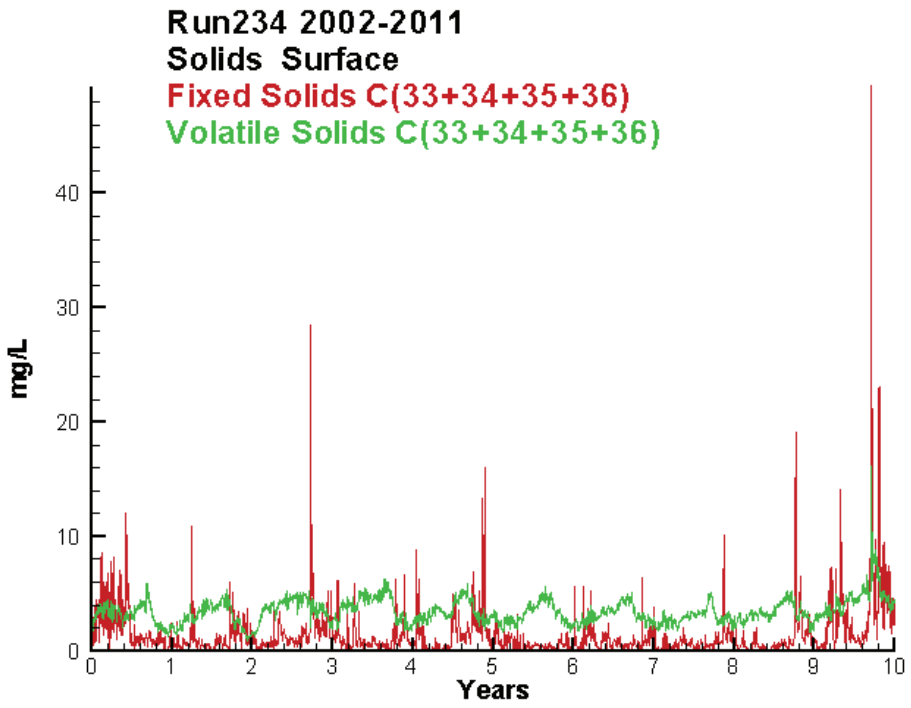

	Mean Difference	Absolute Mean Difference
KE	0.5205	0.6038
TSS	-0.0218	2.4209

Station EE2.1

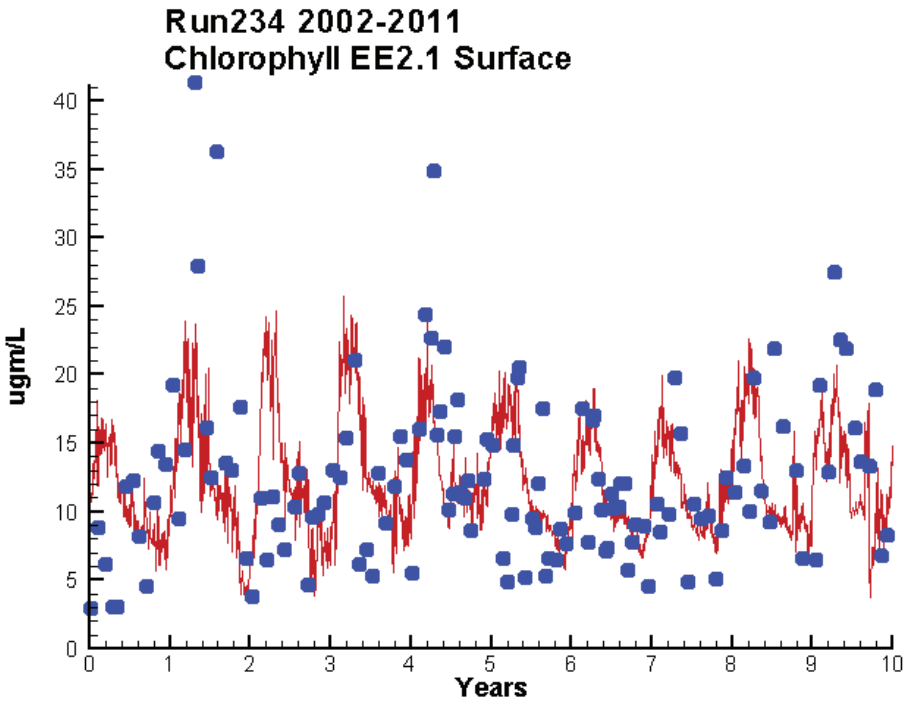

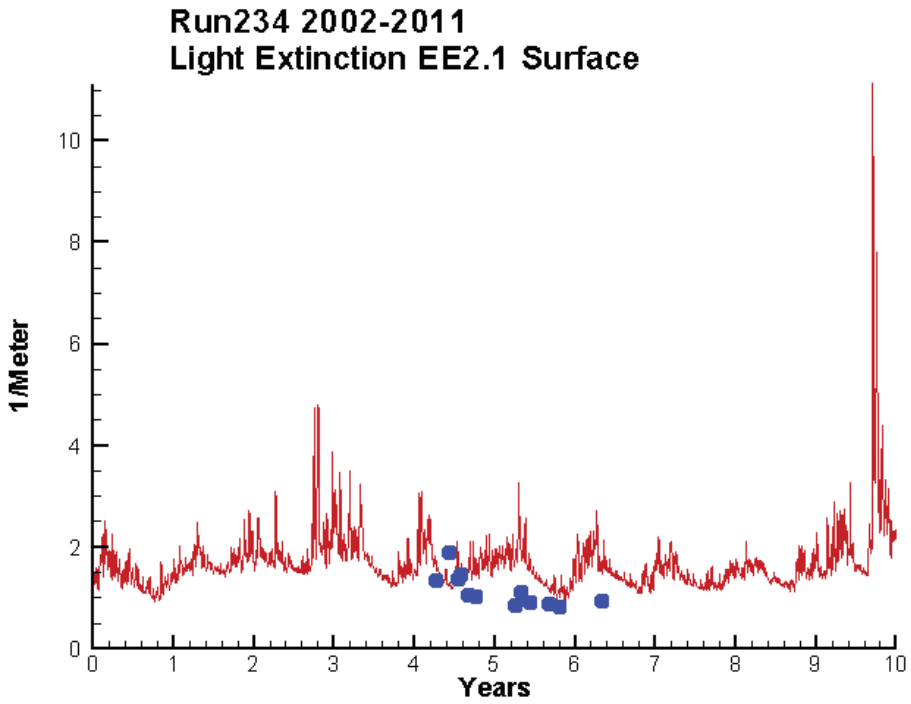

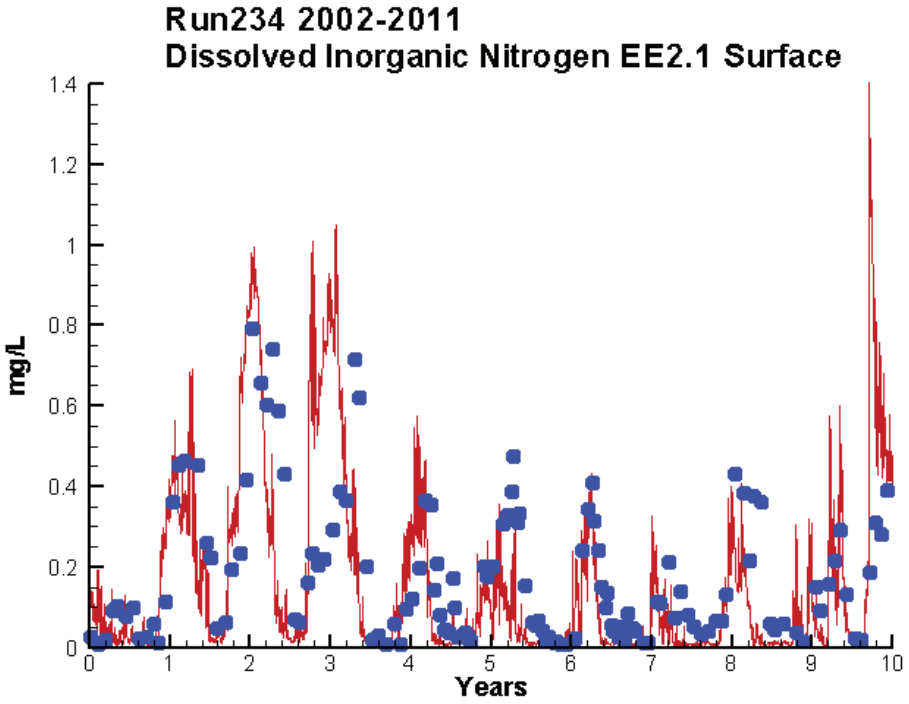

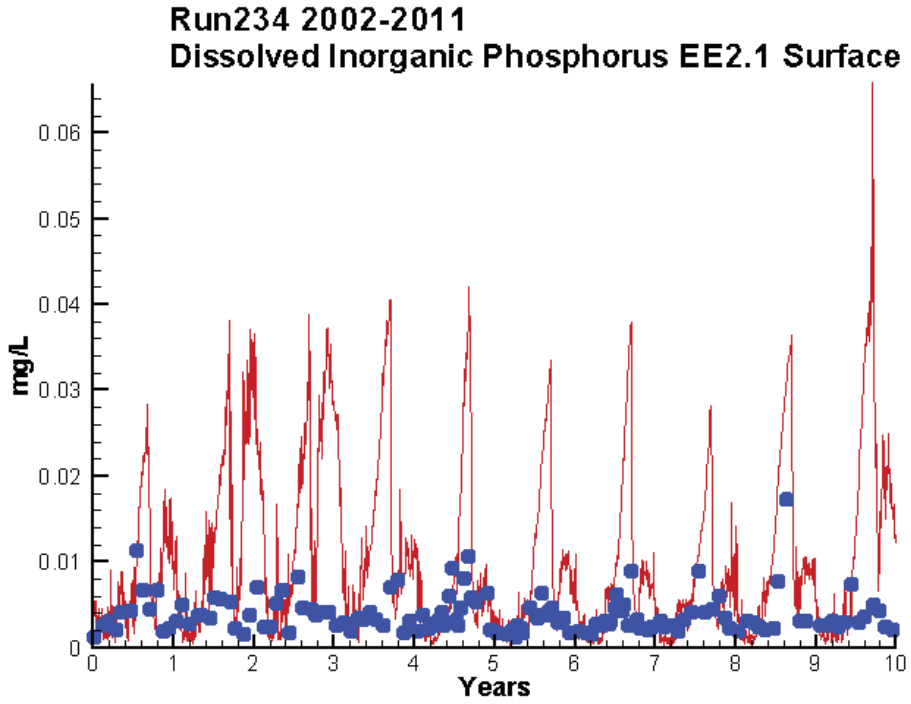

Station EE2.1

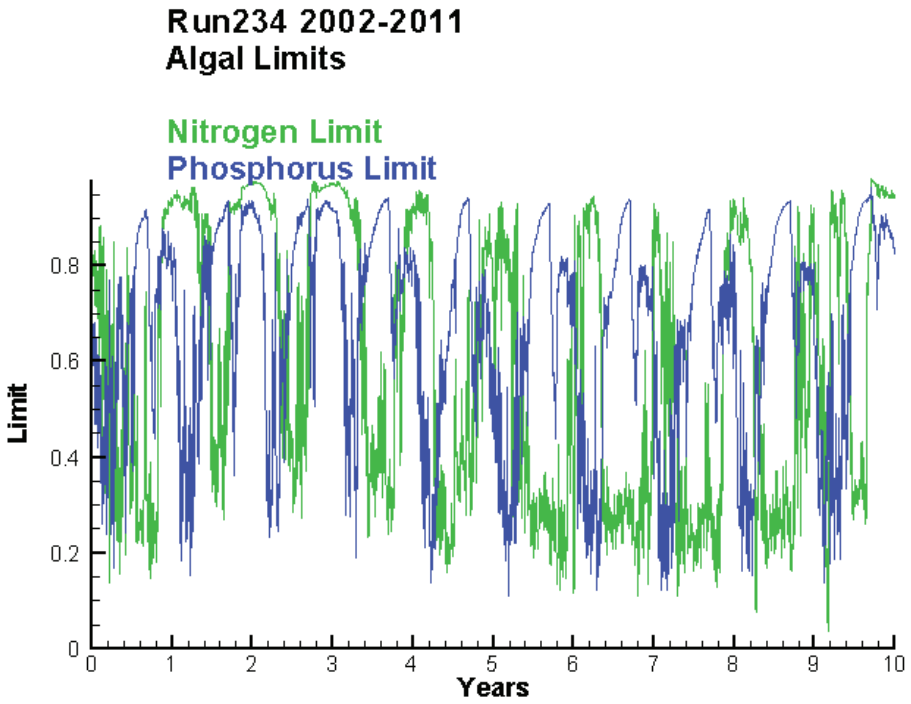

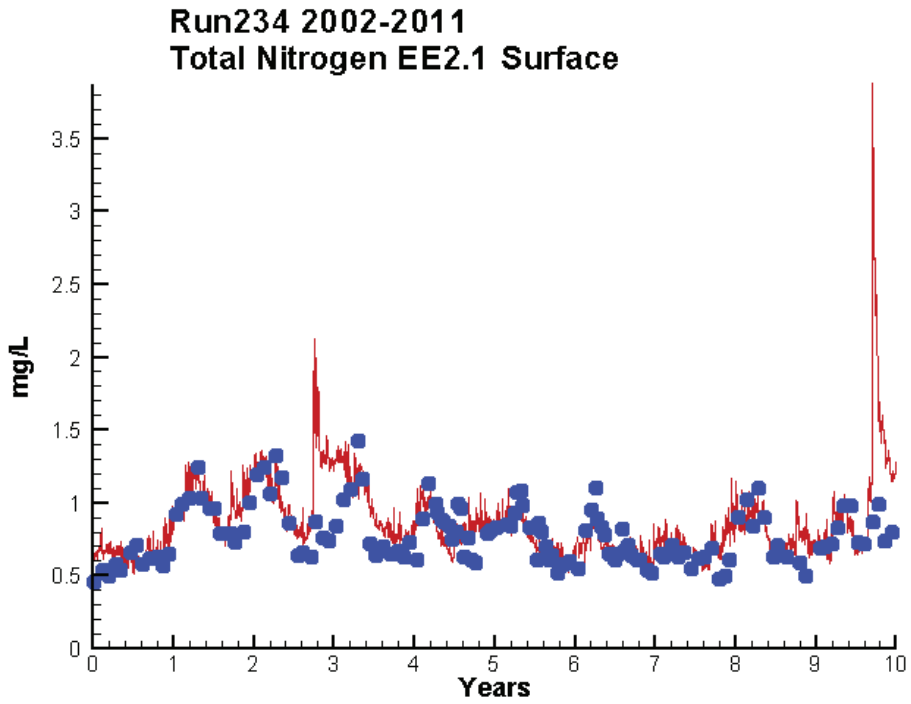

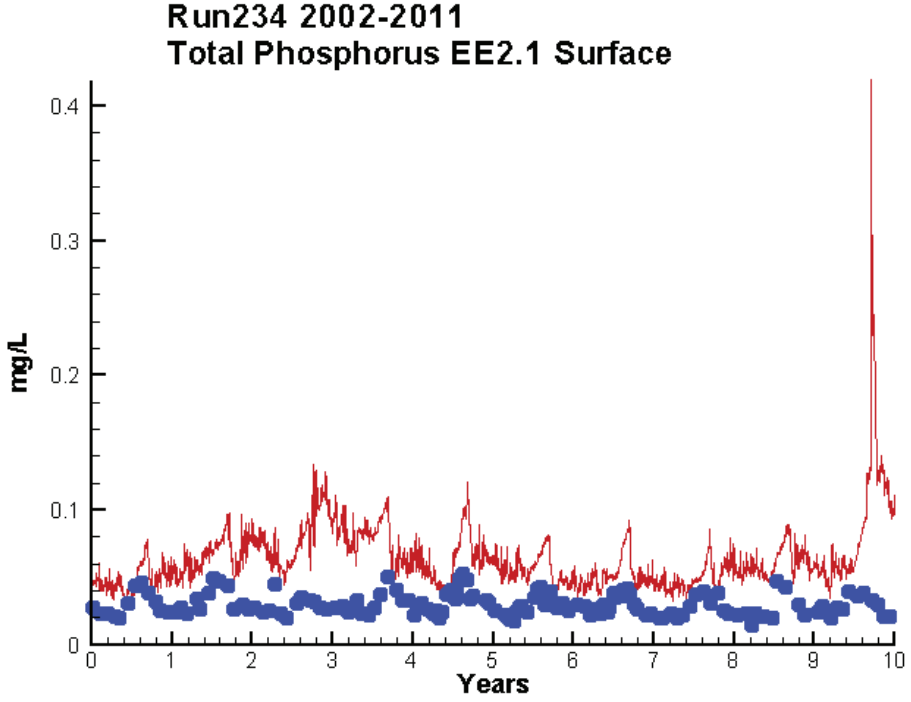

	Mean Difference	Absolute Mean Difference
Chl	-0.0141	4.7750
DIN	-0.0195	0.1314
KE	0.3796	0.4853
DIP	0.0064	0.0072
TP	0.0338	0.0338
TN	0.0742	0.1431

Station EE2.1

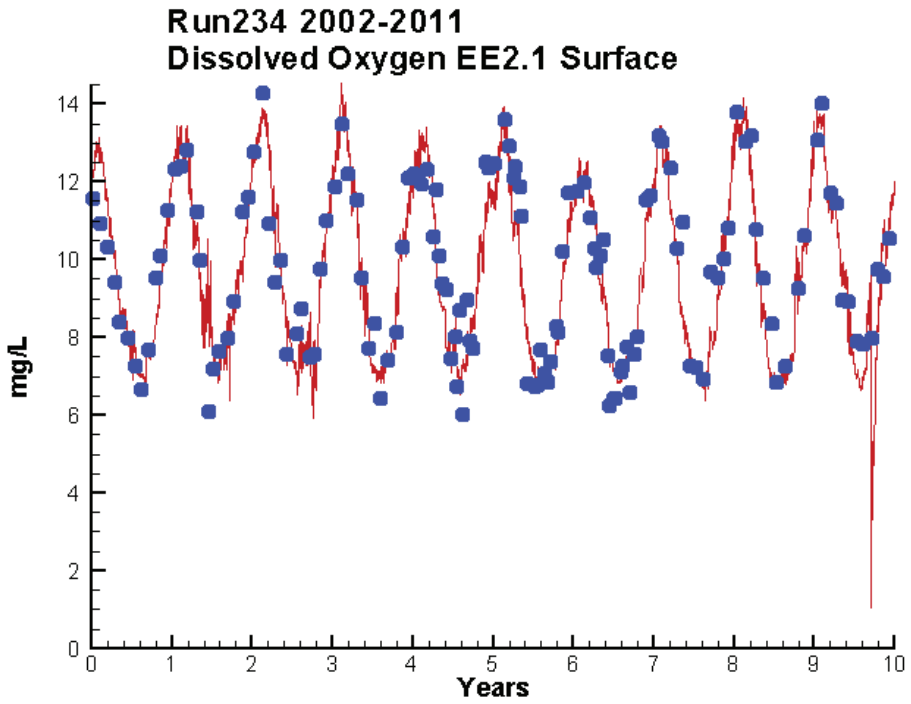

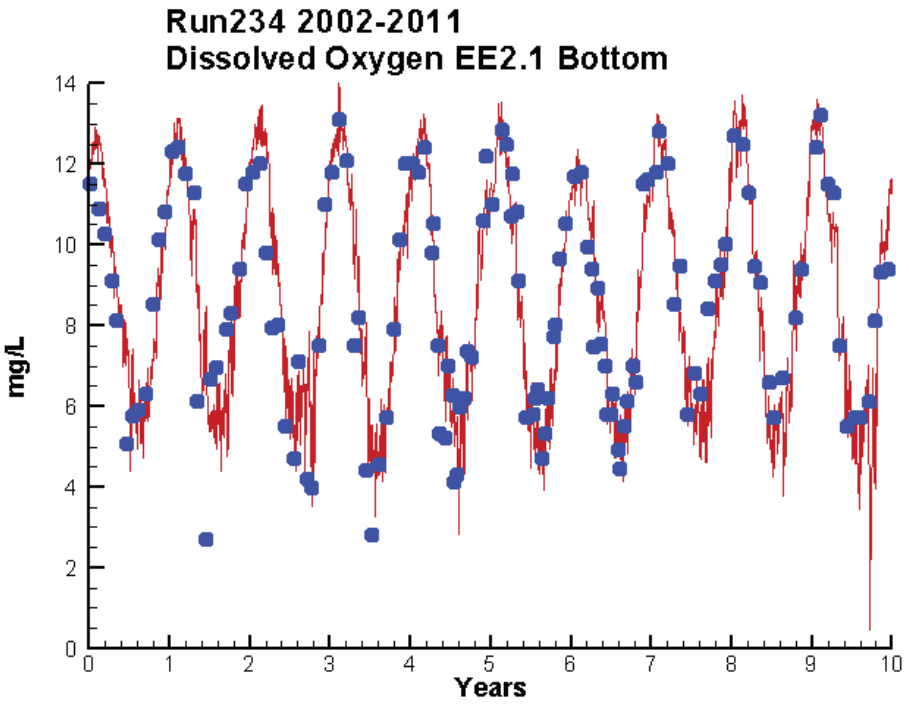

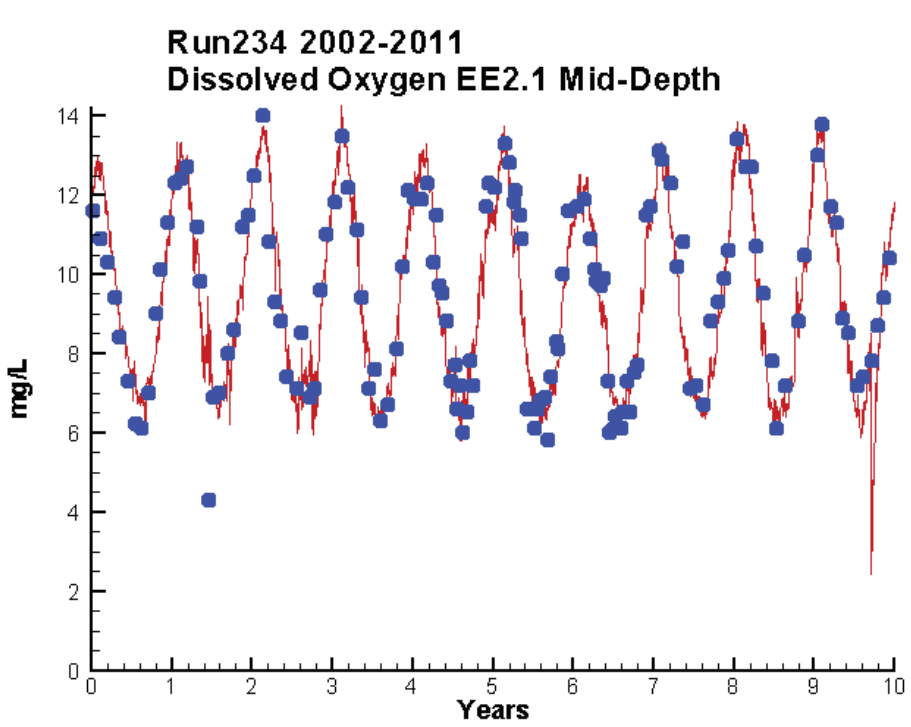

	Mean Difference	Absolute Mean Difference
Top DO	-0.1412	0.6838
Mid DO	-0.0818	0.6671
Bot DO	0.0571	0.8831

Station EE2.1

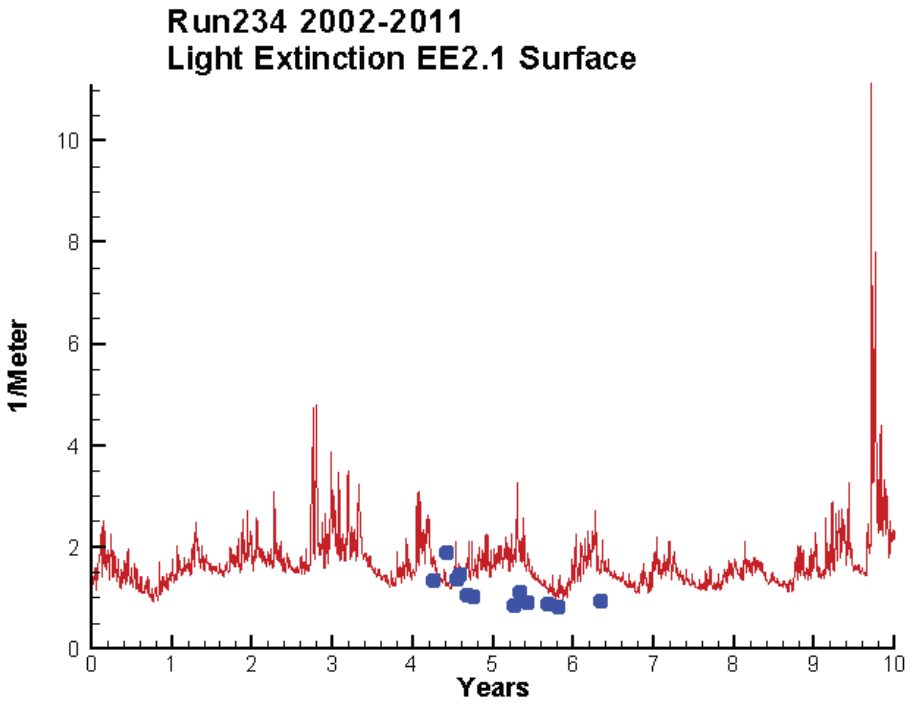

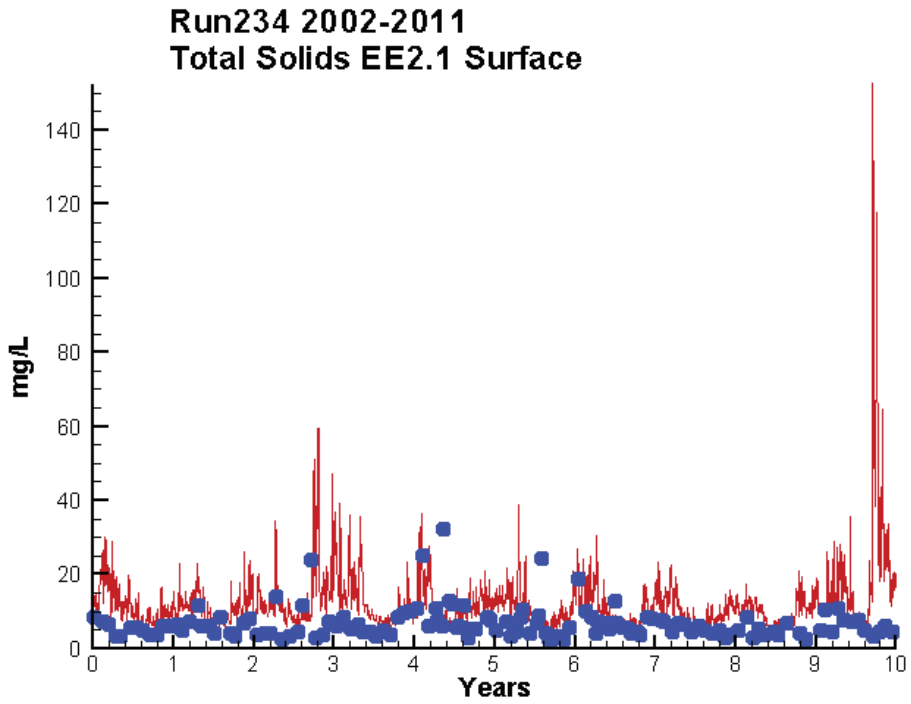

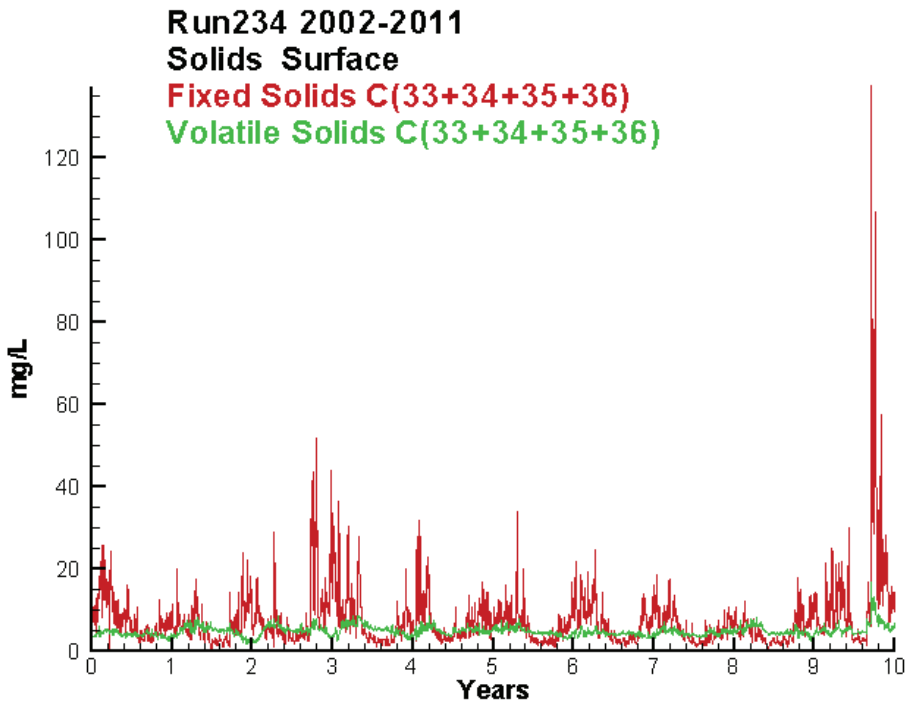

	Mean Difference	Absolute Mean Difference
KE	0.3796	0.4853
TSS	4.9696	6.3311

Station EE3.1

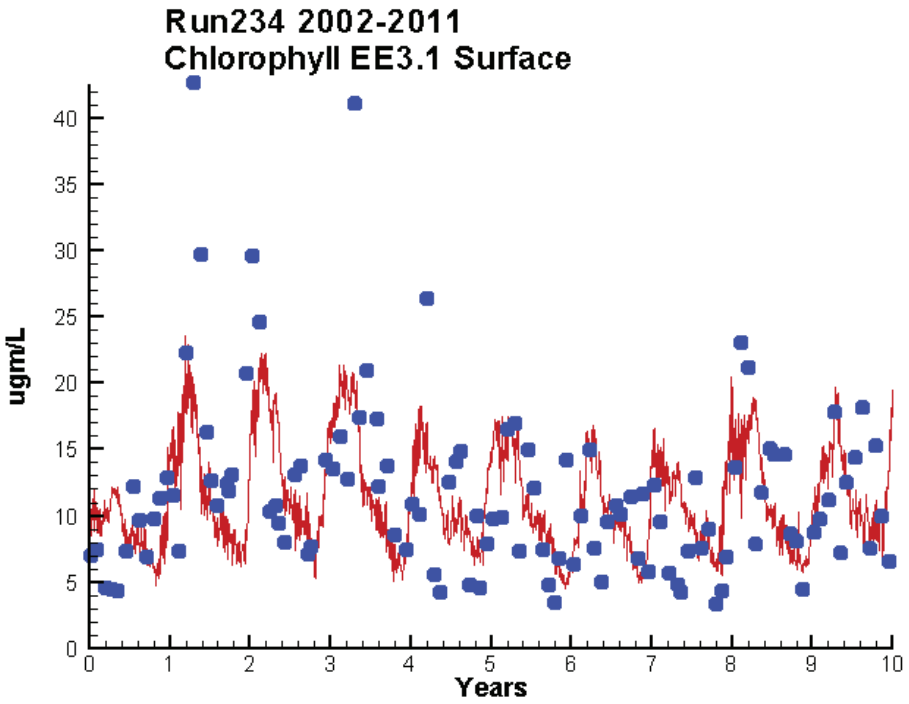

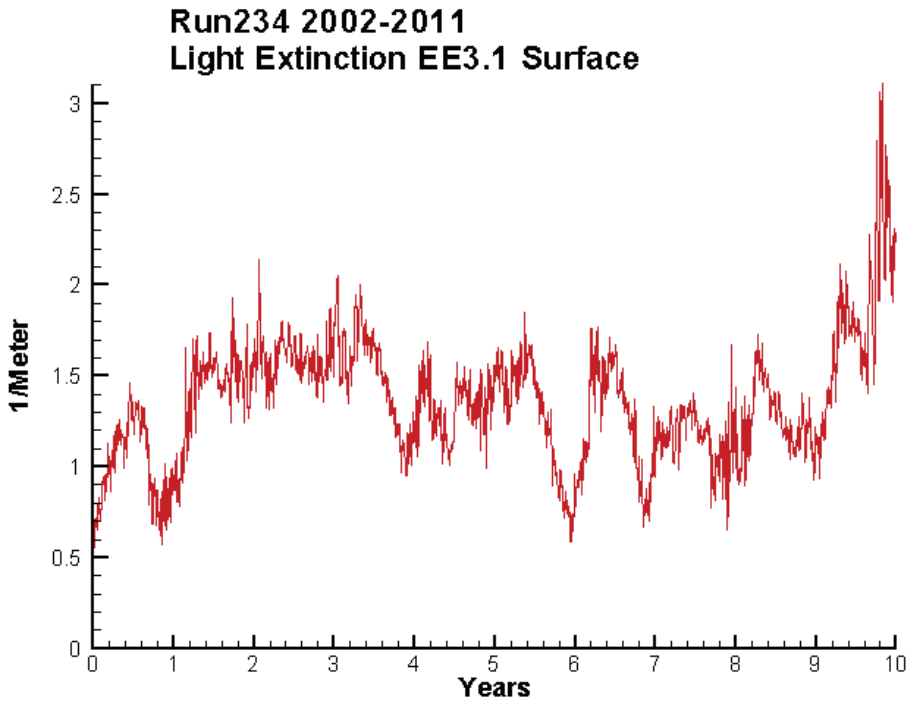

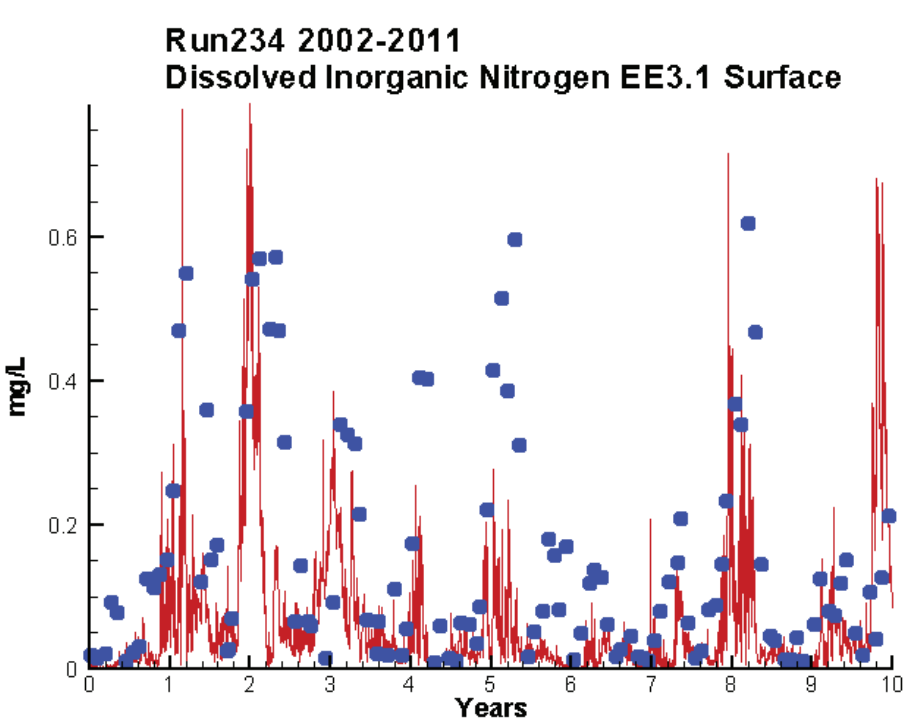

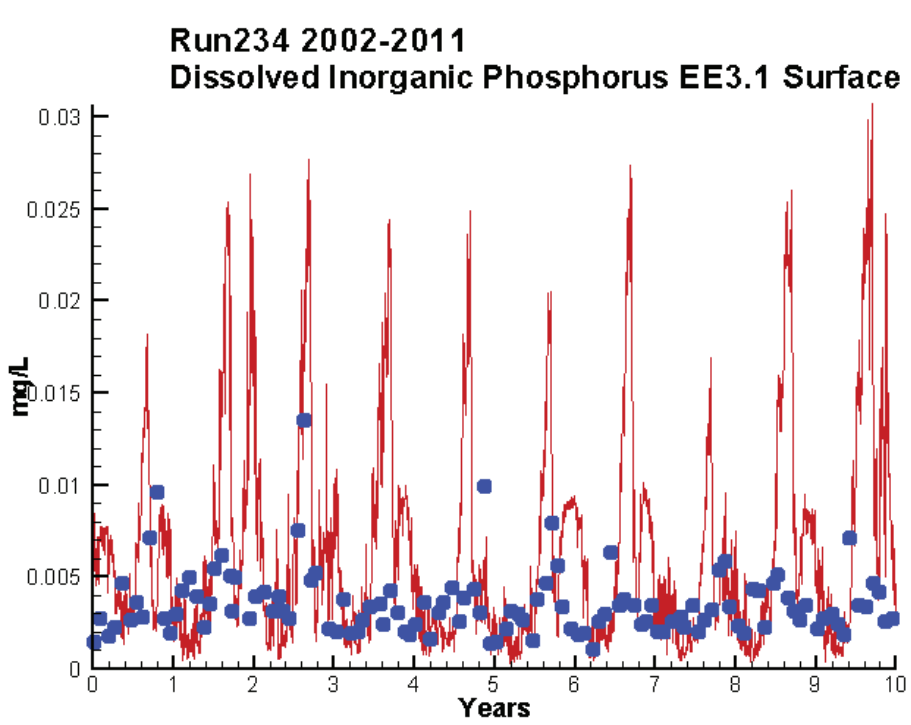

Station EE3.1

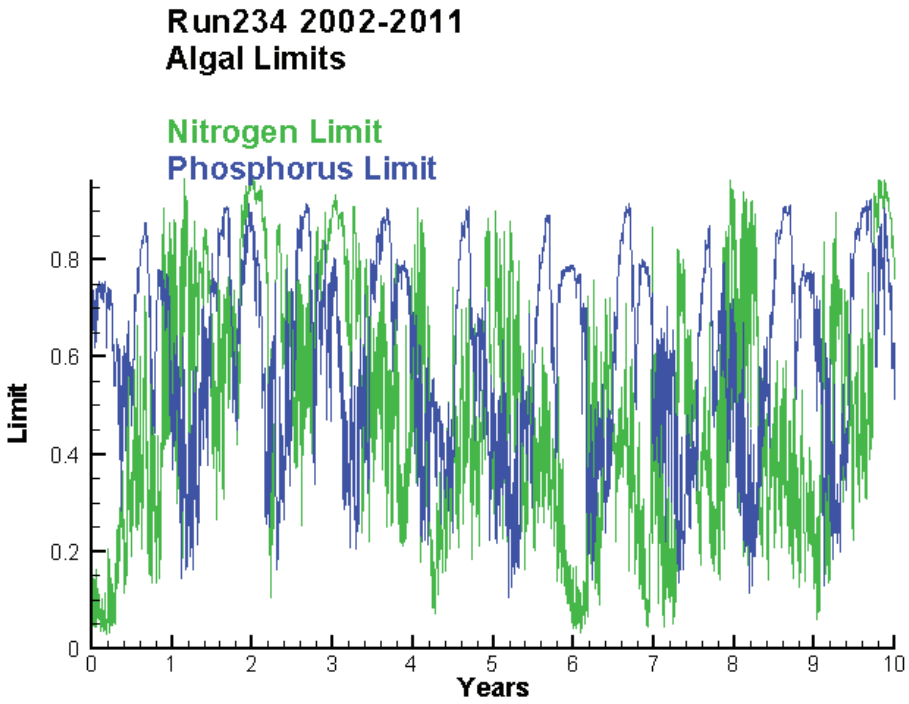

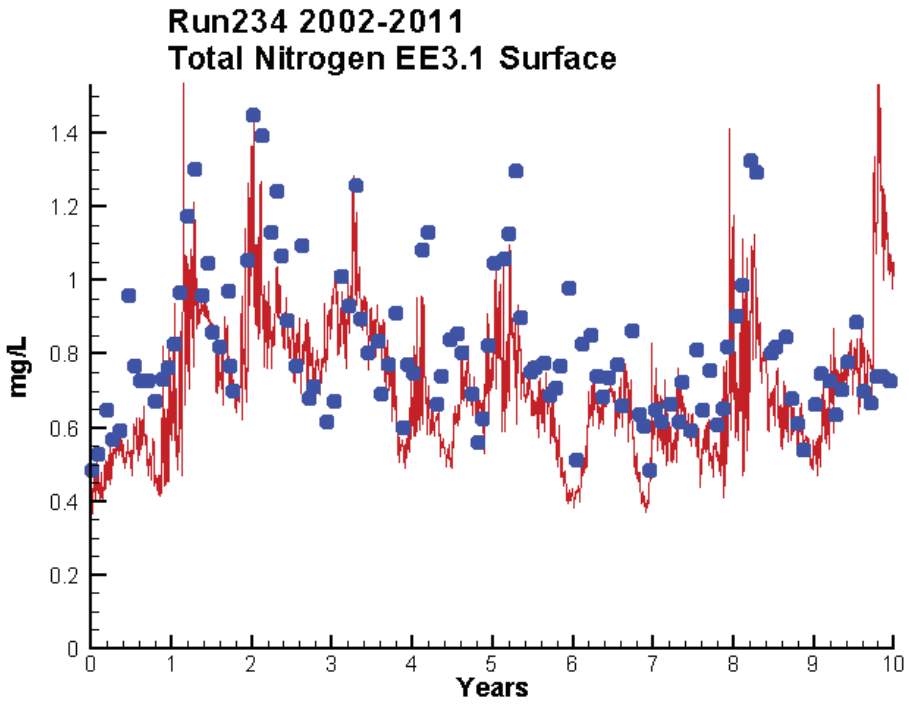

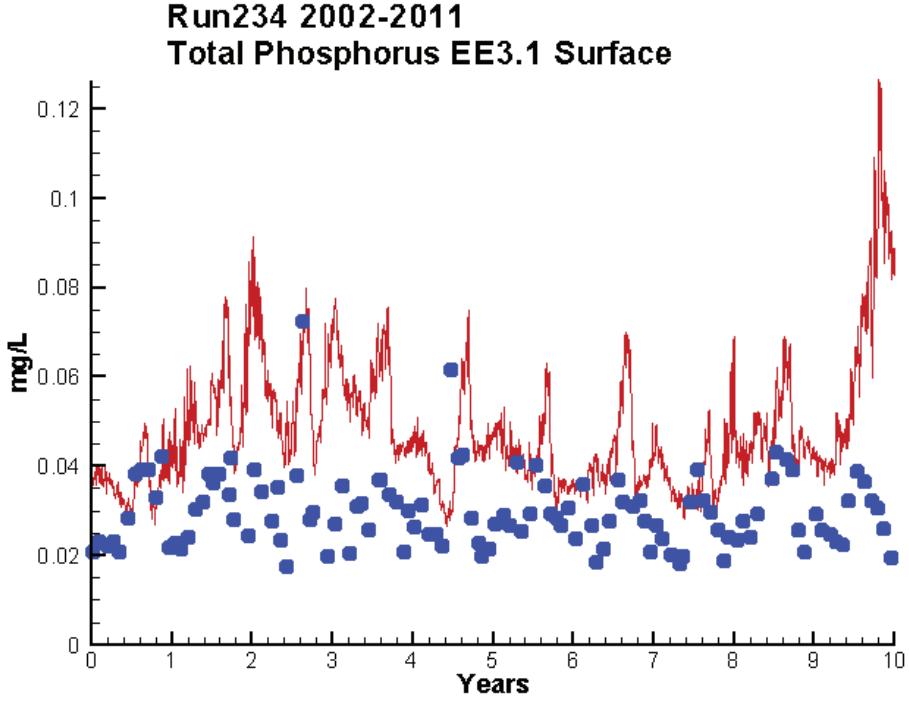

	Mean Difference	Absolute Mean Difference
Chl	-0.2943	4.6986
DIN	-0.0854	0.1193
KE	-0.0854	0.1193
DIP	0.0027	0.0039
TP	0.0181	0.0189
TN	-0.1060	0.1614

Station EE3.1

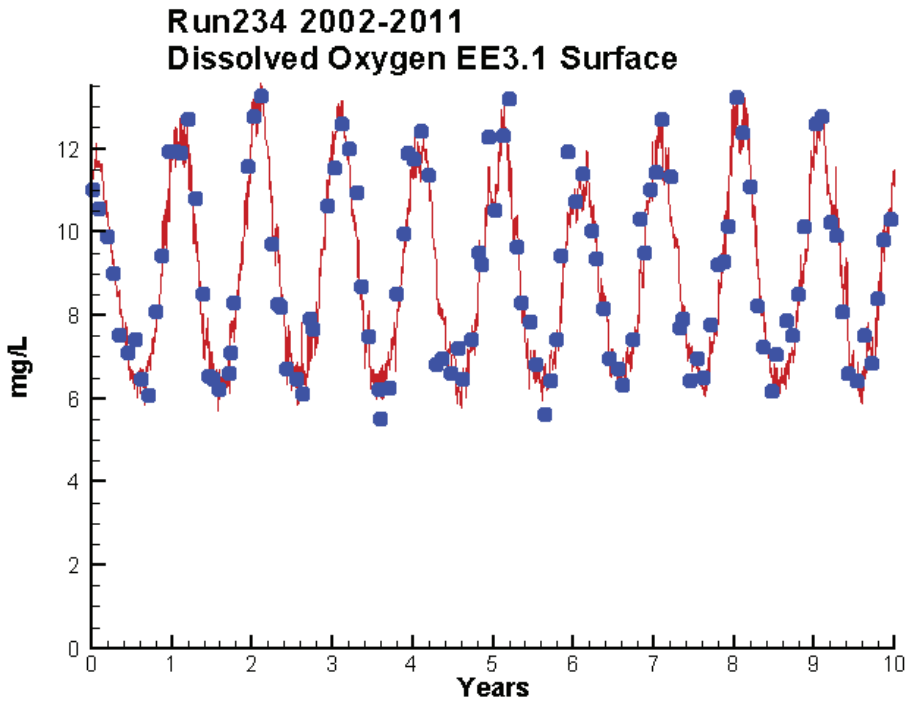

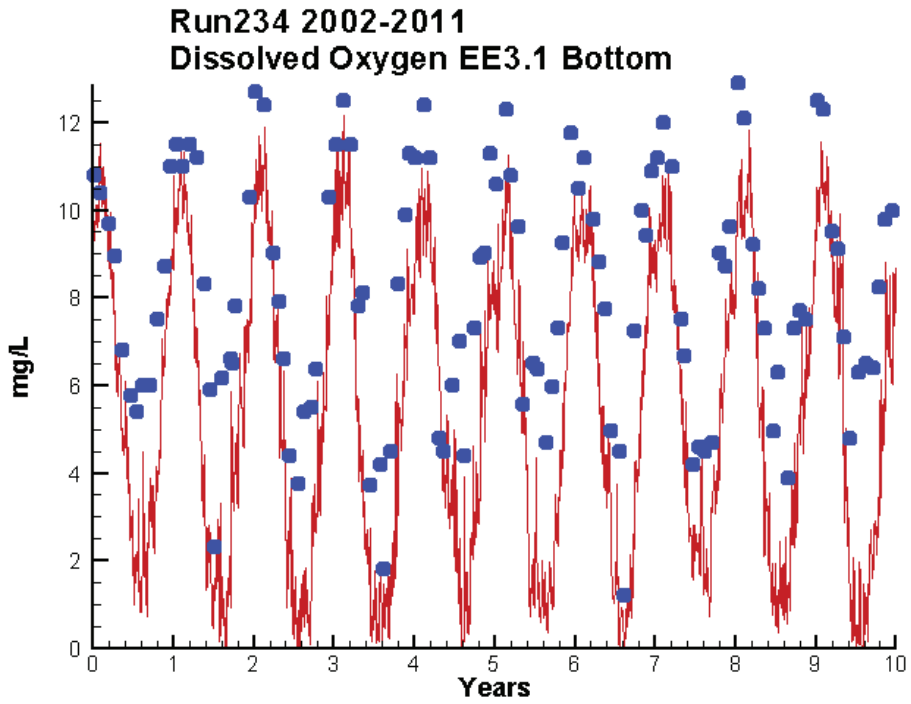

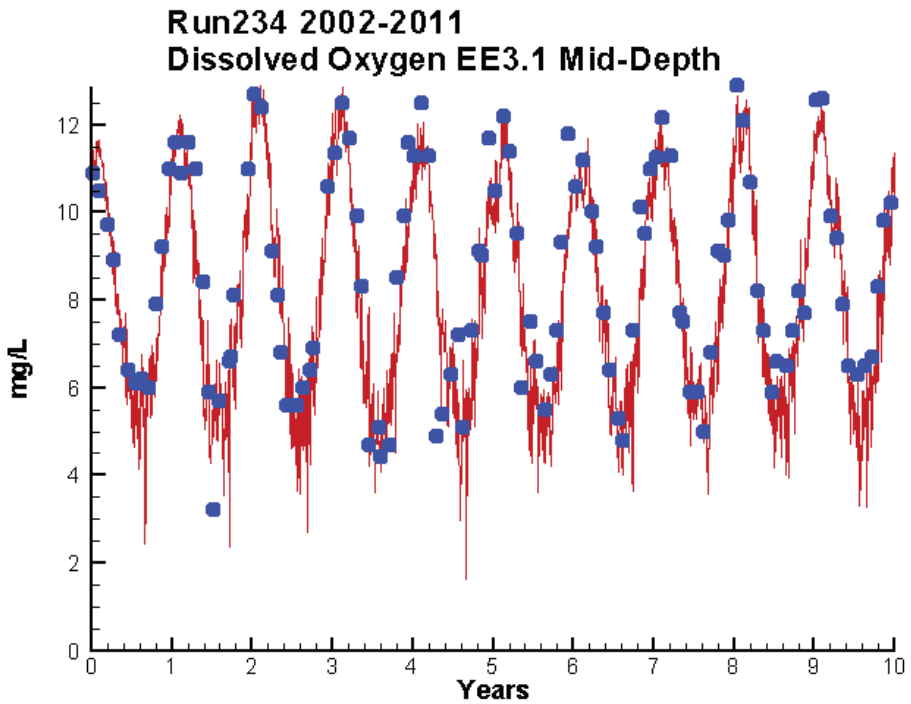

	Mean Difference	Absolute Mean Difference
Top DO	-0.0112	0.5311
Mid DO	-0.4534	0.8188
Bot DO	-2.7341	2.7649

Station EE3.1

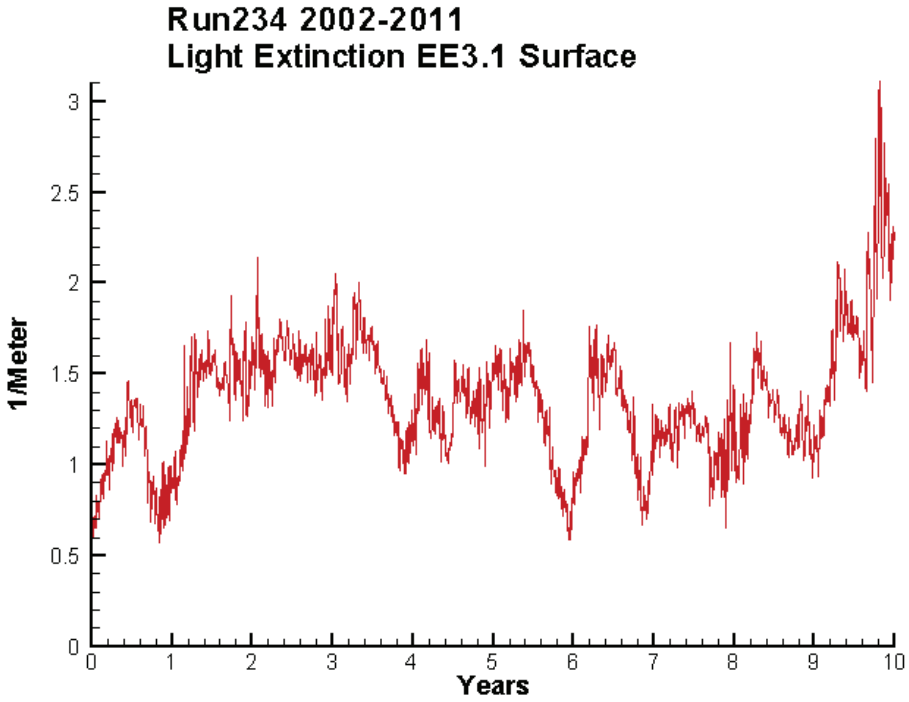

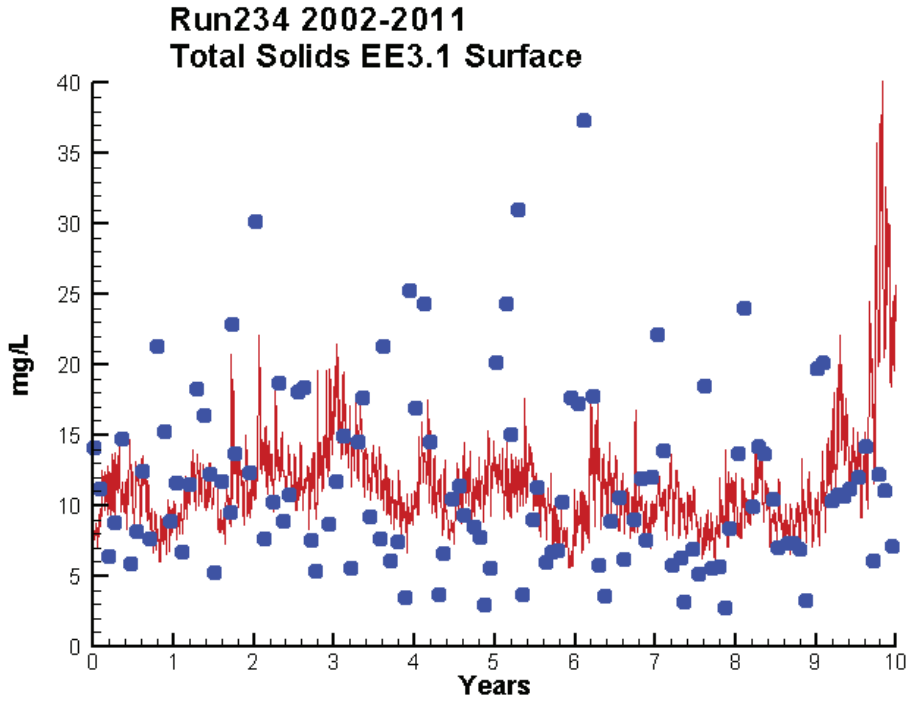

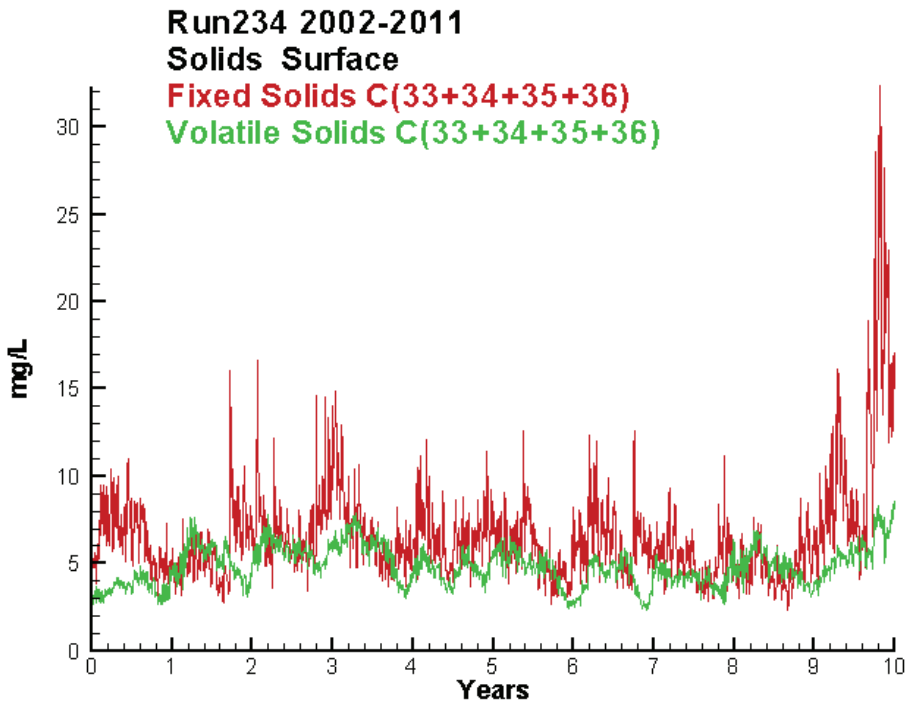

	Mean Difference	Absolute Mean Difference
KE	-0.1060	0.1614
TSS	-0.3194	5.2076

Station ET1.1

Run234 2002-2011
Chlorophyll ET1.1 Surface

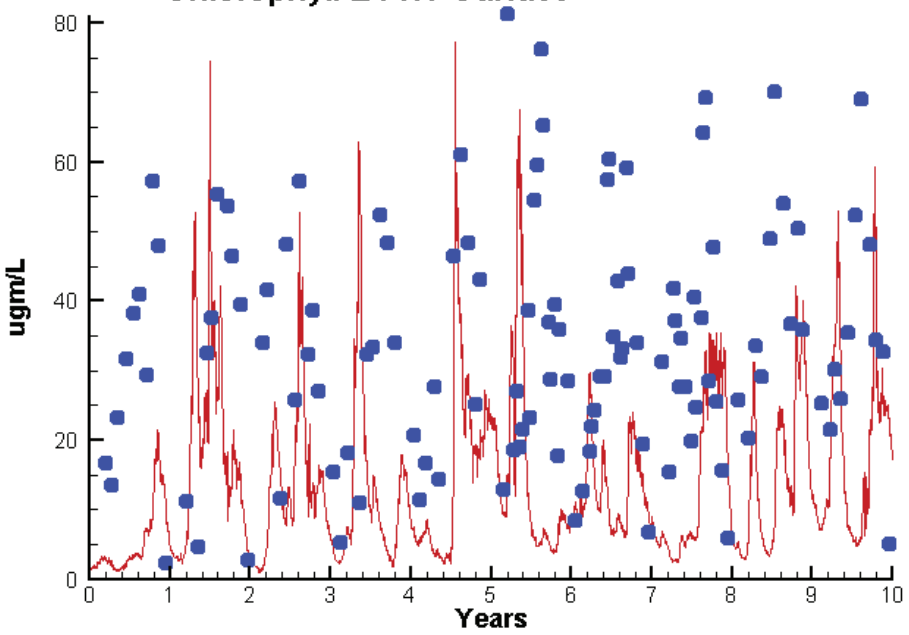

Run234 2002-2011
Light Extinction ET1.1 Surface

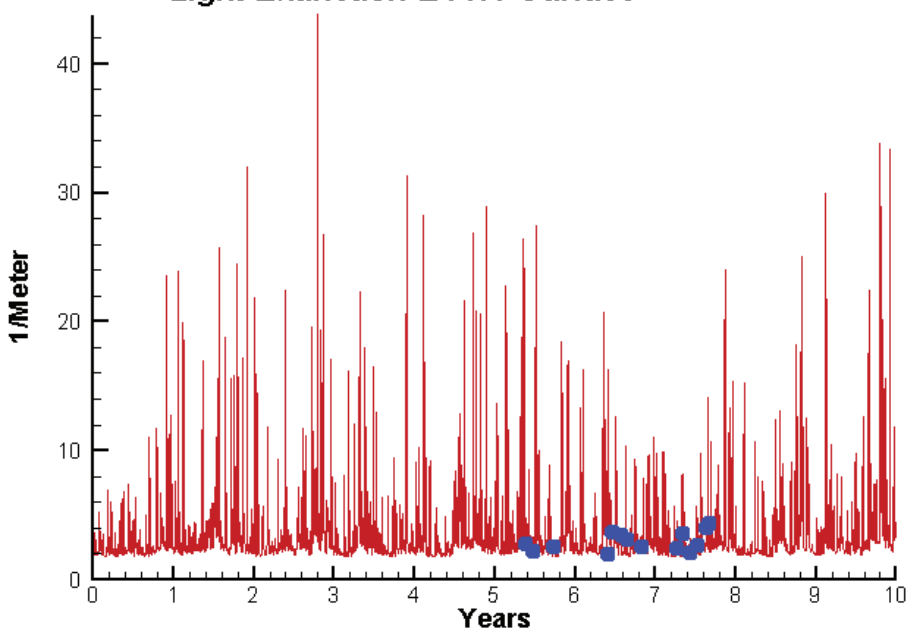

Run234 2002-2011
Dissolved Inorganic Nitrogen ET1.1 Surface

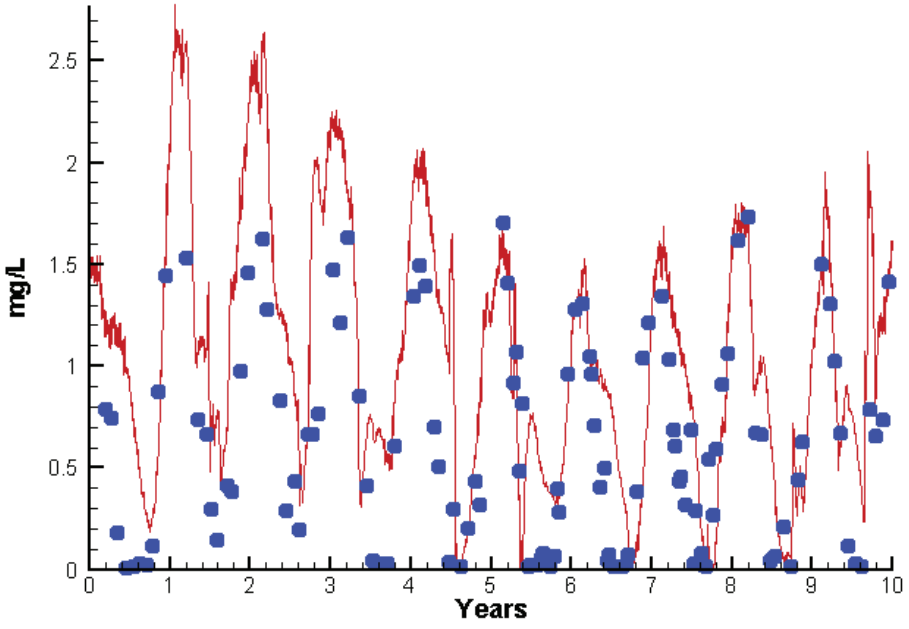

Run234 2002-2011
Dissolved Inorganic Phosphorus ET1.1 Surface

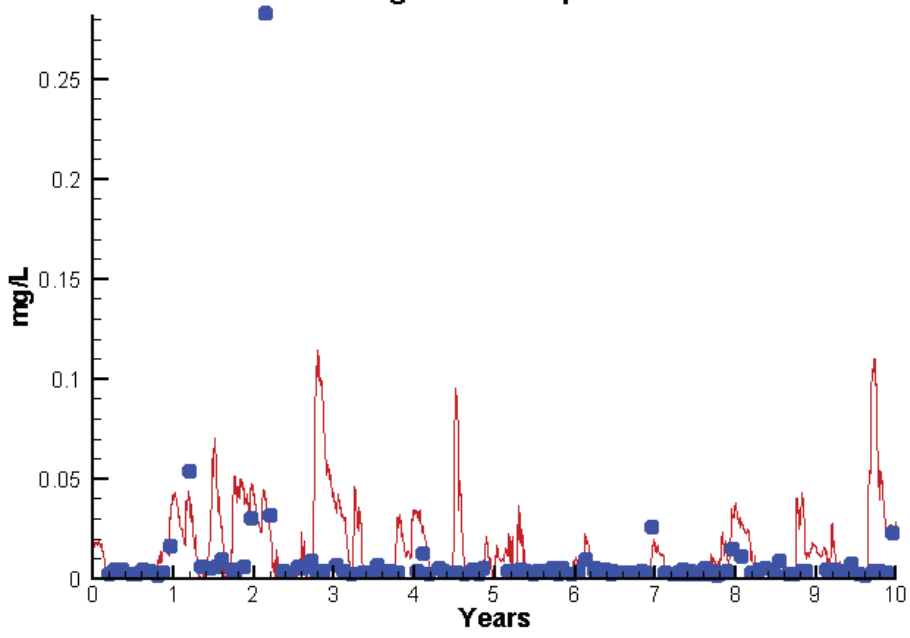

Station ET1.1

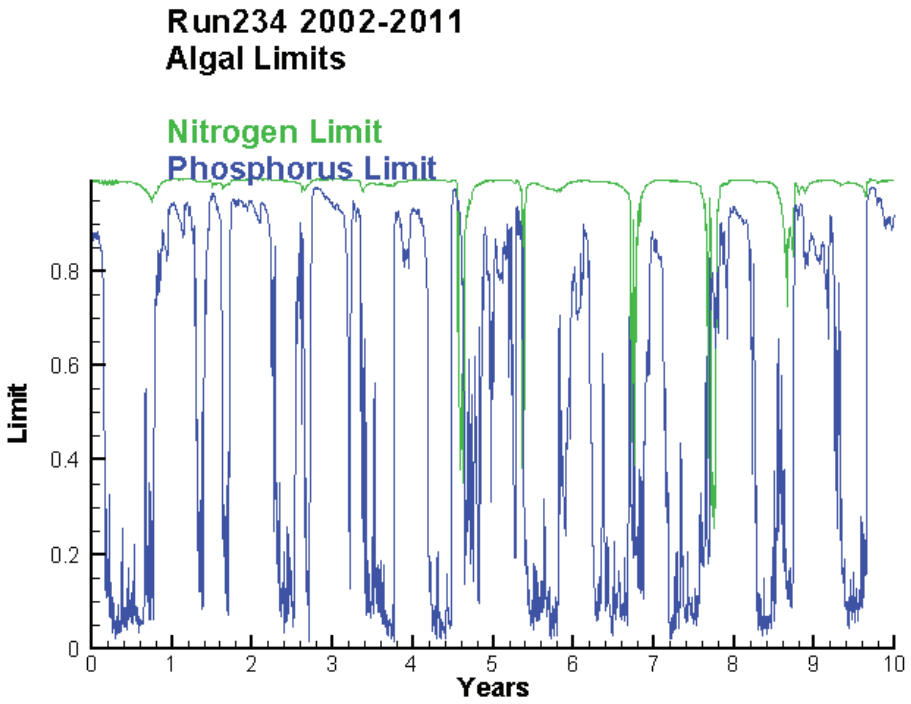

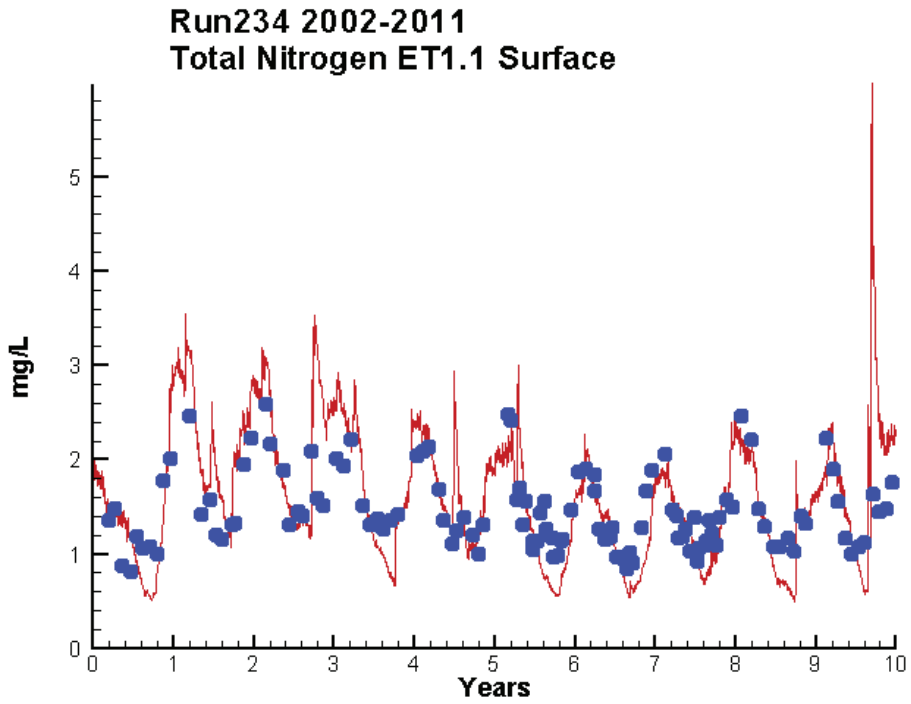

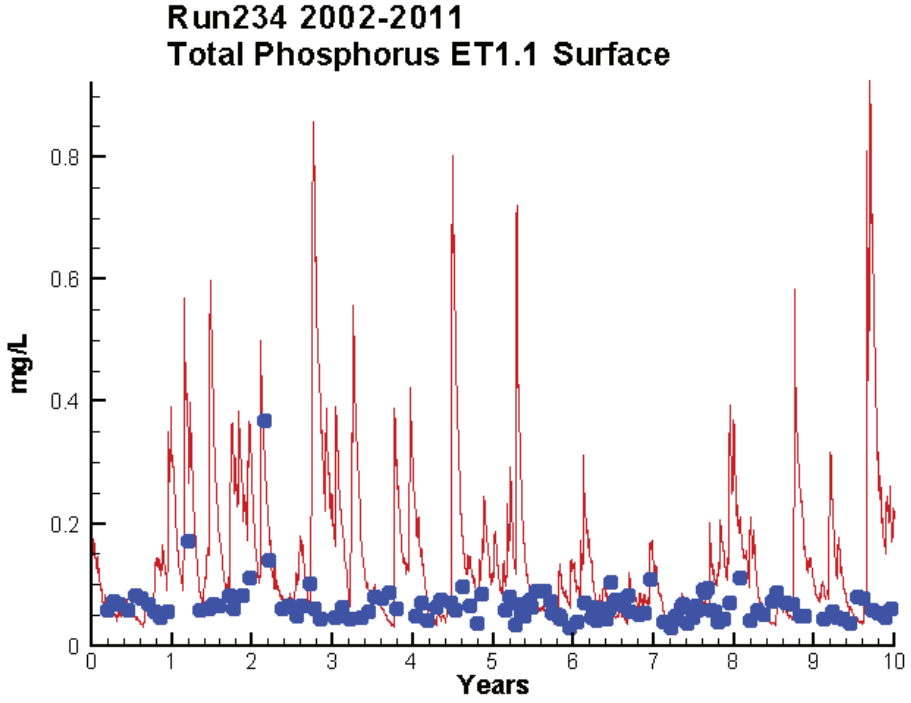

	Mean Difference	Absolute Mean Difference
Chl	-19.0763	23.1118
DIN	0.3425	0.4397
KE	-0.0336	0.8083
DIP	0.0044	0.0121
TP	0.0709	0.0837
TN	0.0450	0.3326

Station ET1.1

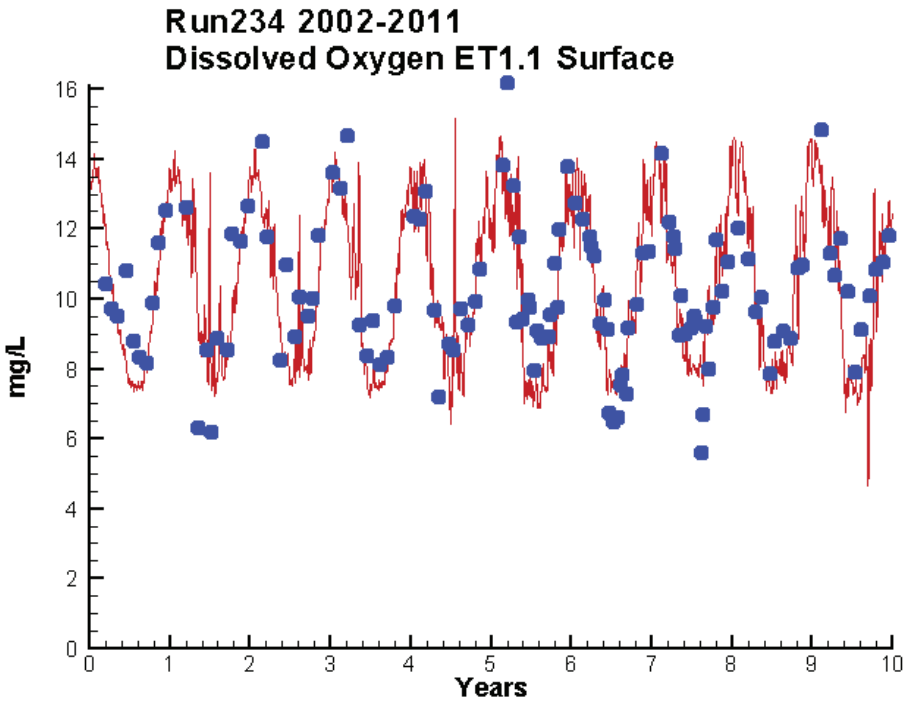

	Mean Difference	Absolute Mean Difference
Top DO	-0.2839	1.0675

Station ET1.1

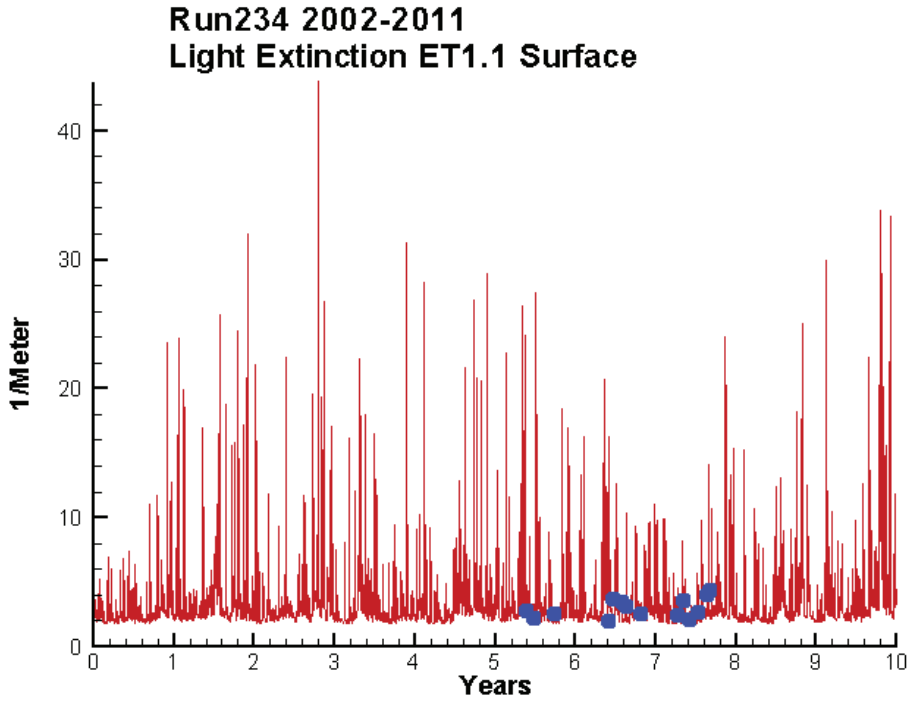

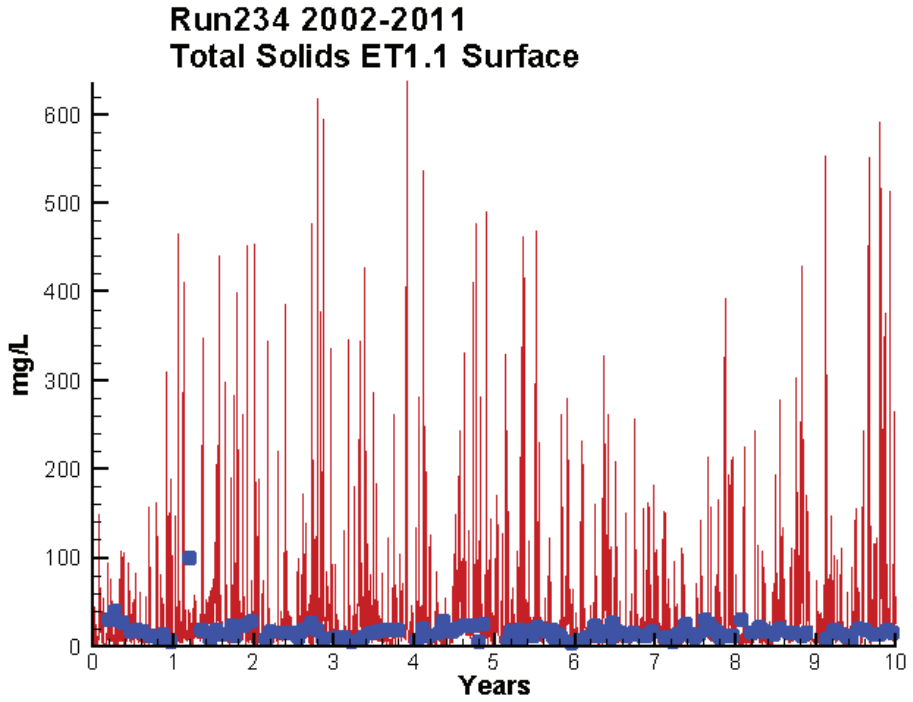

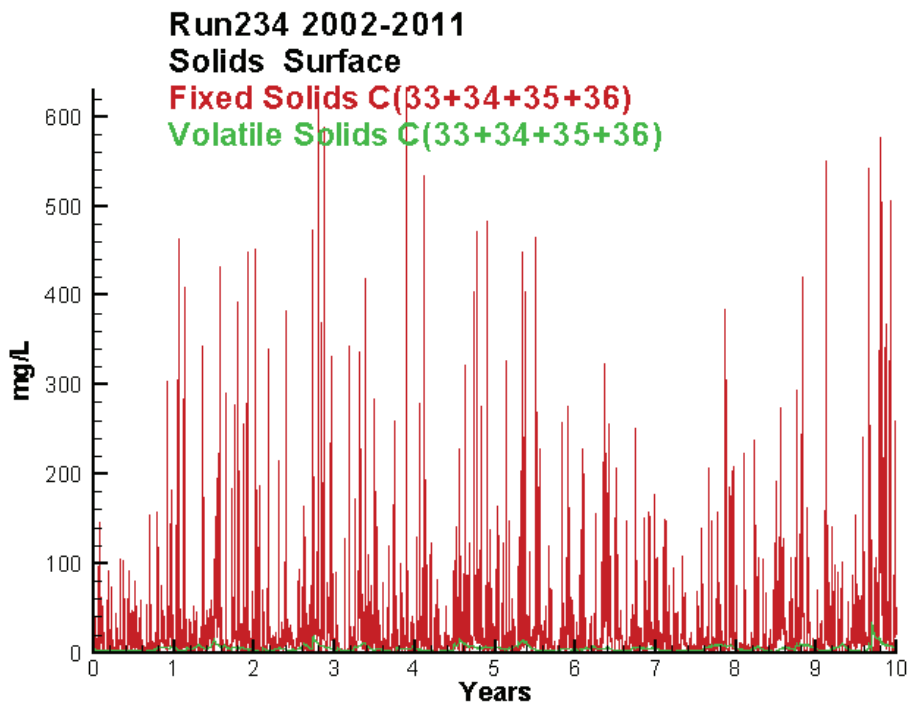

	Mean Difference	Absolute Mean Difference
KE	-0.0336	0.8083
TSS	10.8019	20.2013

Station ET2.3

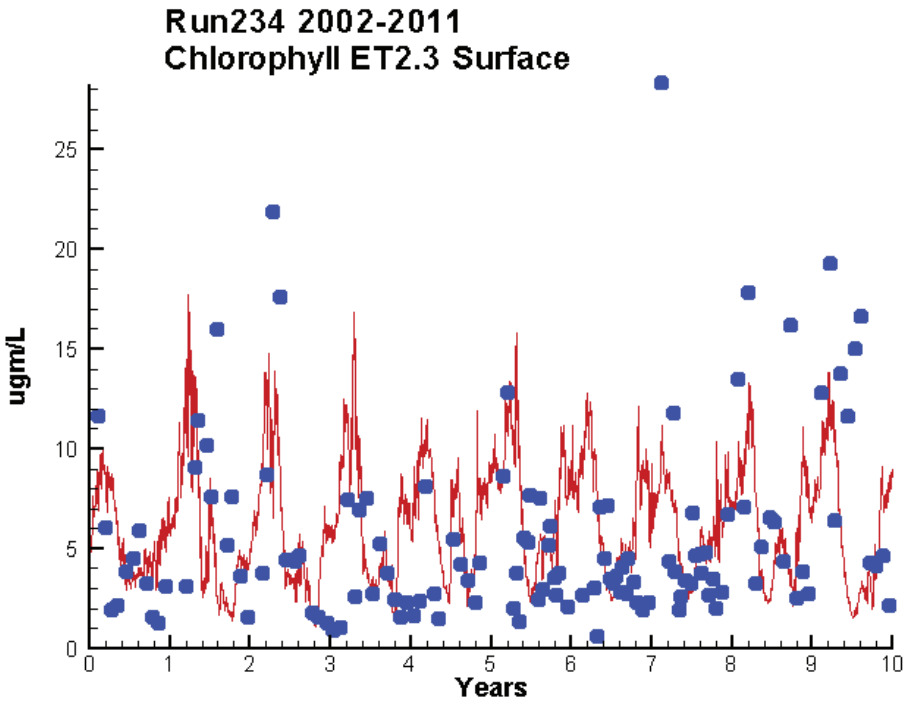

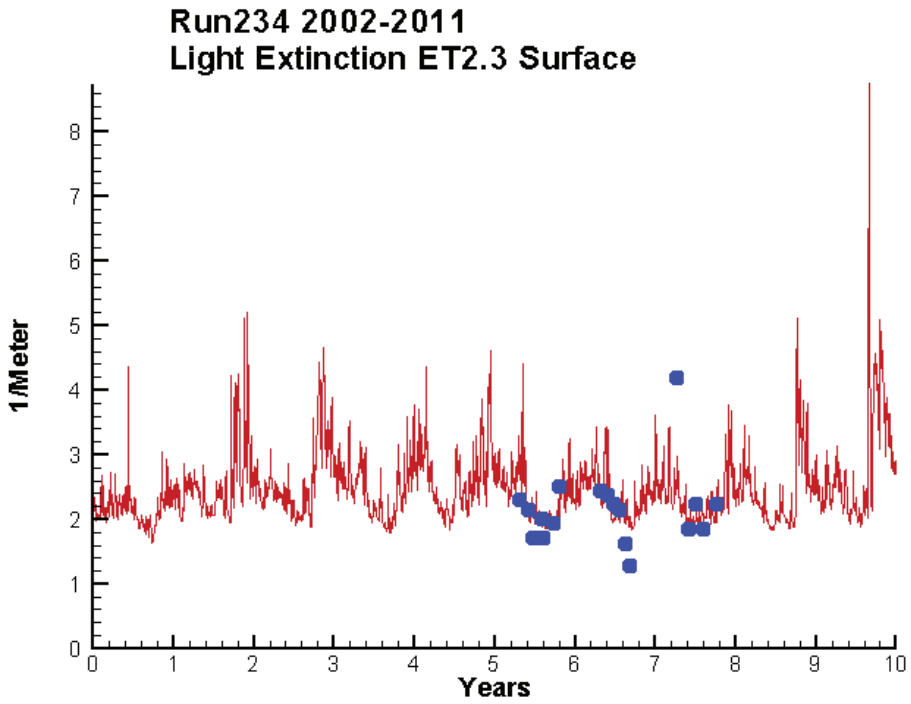

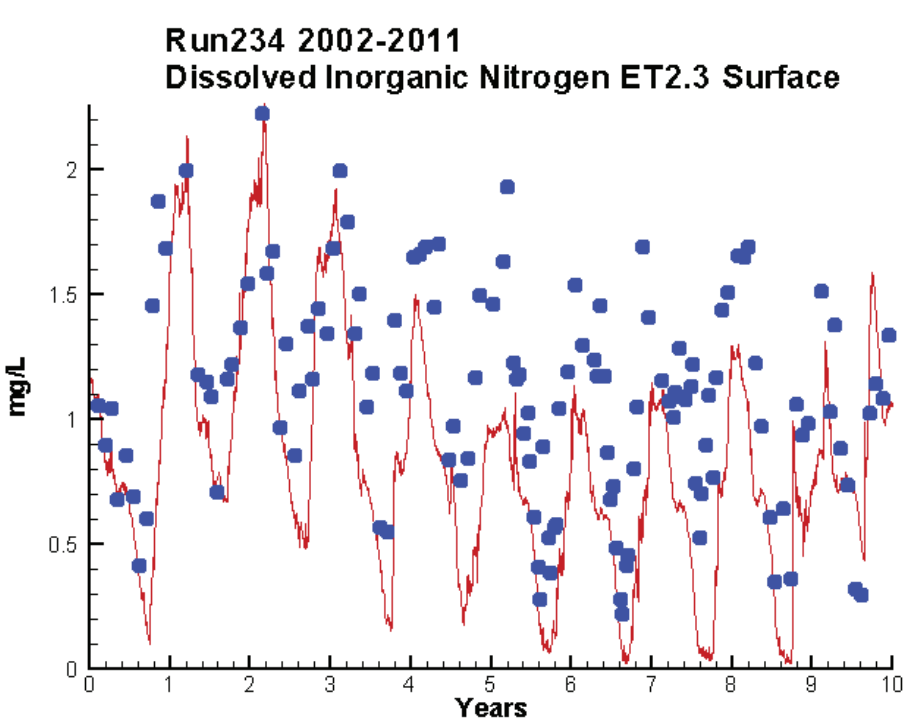

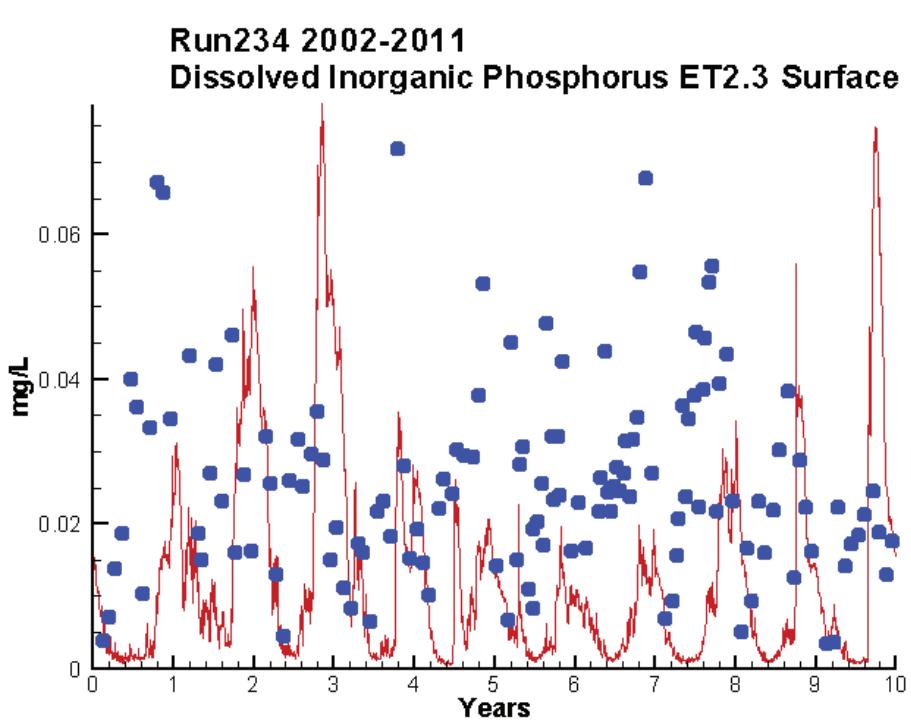

Station ET2.3

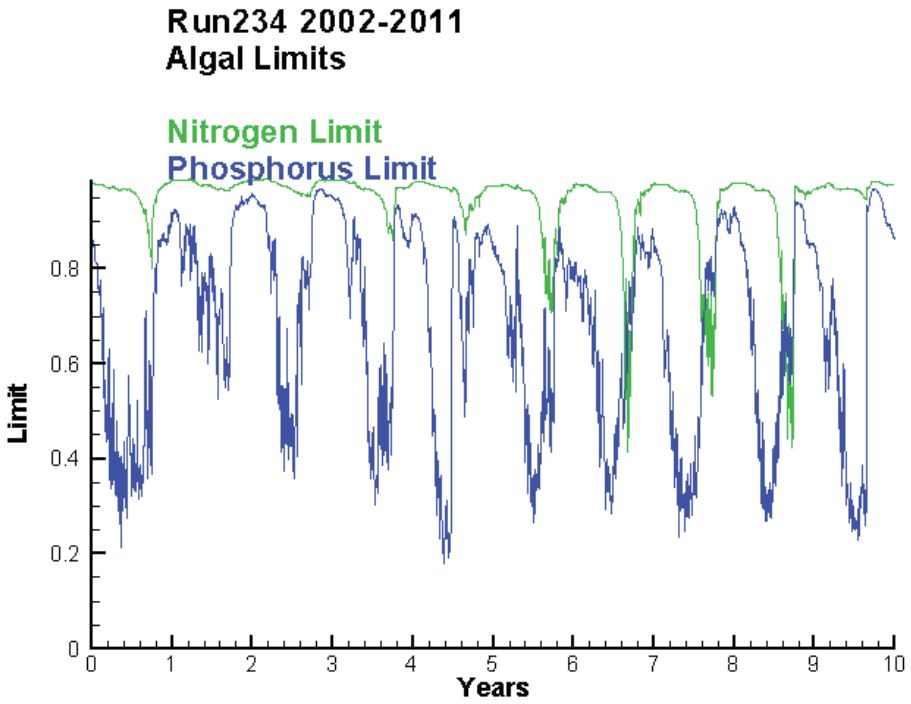

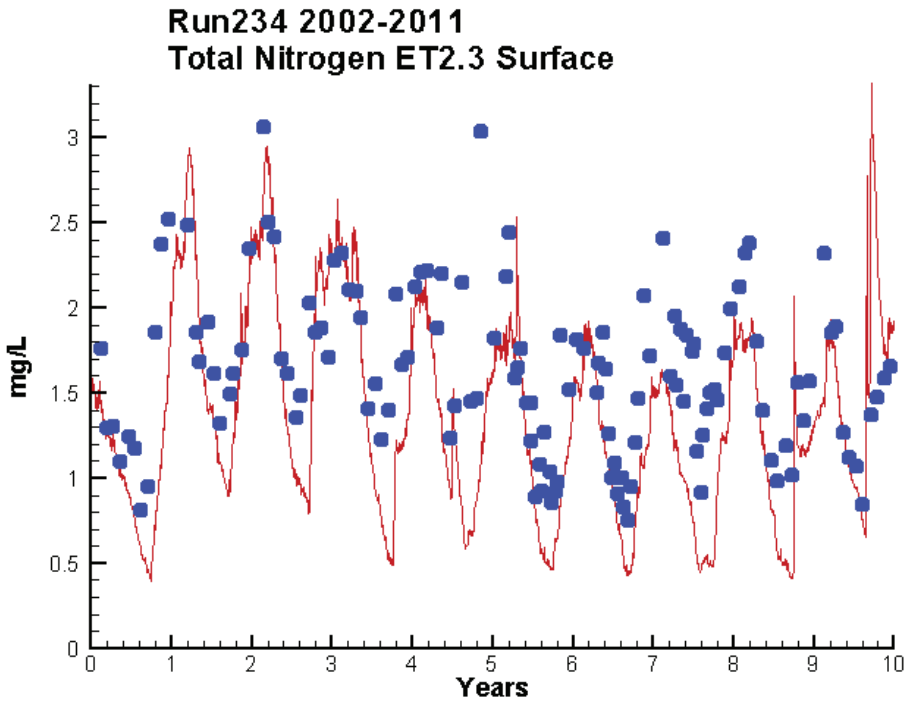

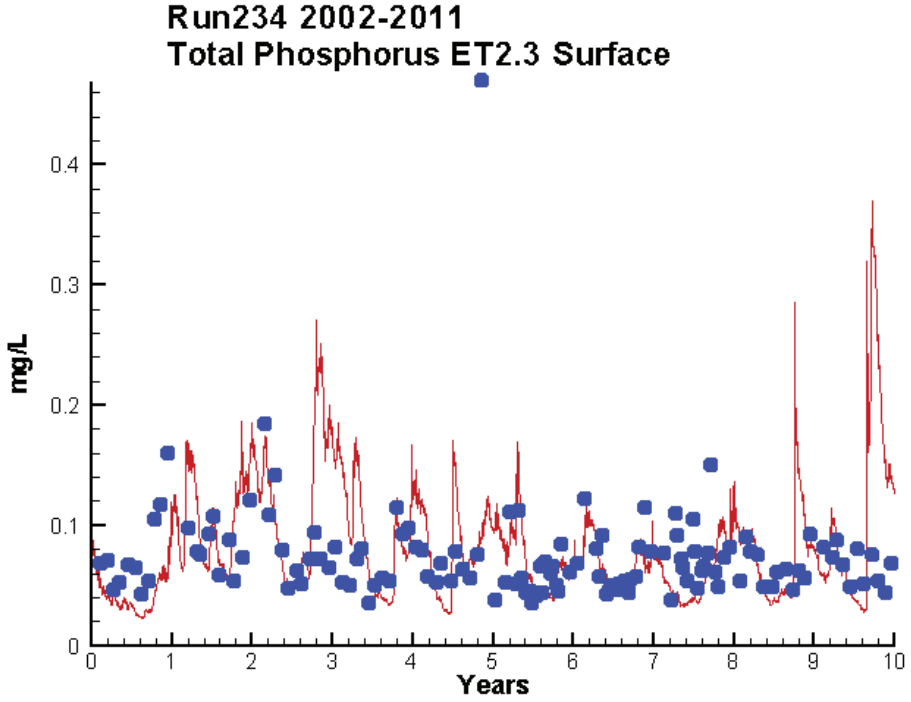

	Mean Difference	Absolute Mean Difference
Chl	0.5705	3.7915
DIN	-0.3638	0.4054
KE	0.0707	0.2885
DIP	-0.0146	0.0196
TP	0.0046	0.0336
TN	-0.3504	0.4340

Station ET2.3

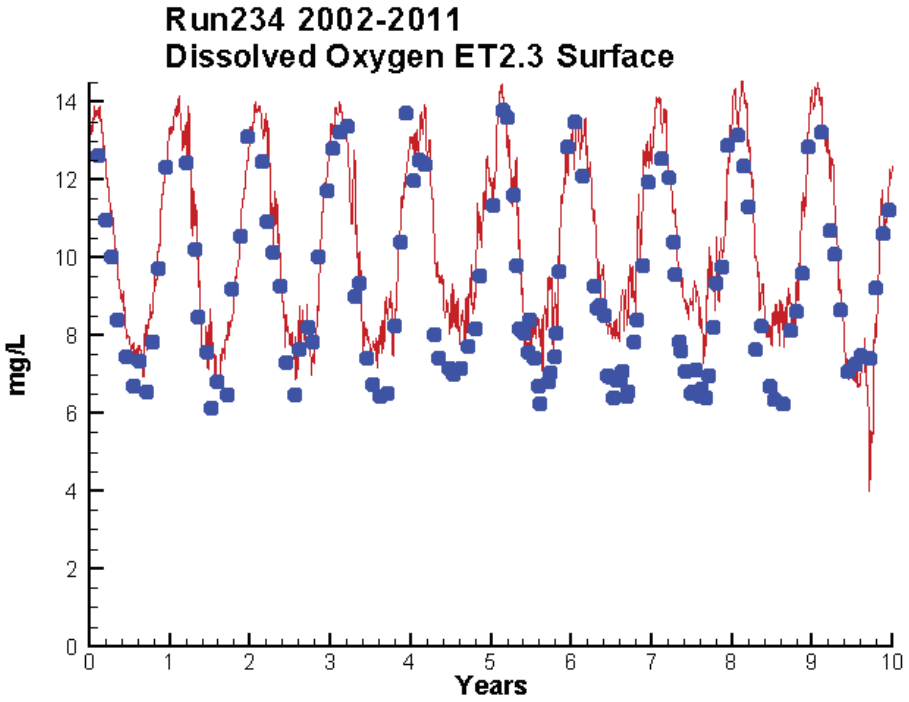

	Mean Difference	Absolute Mean Difference
Top DO	0.9414	1.0993

Station ET2.3

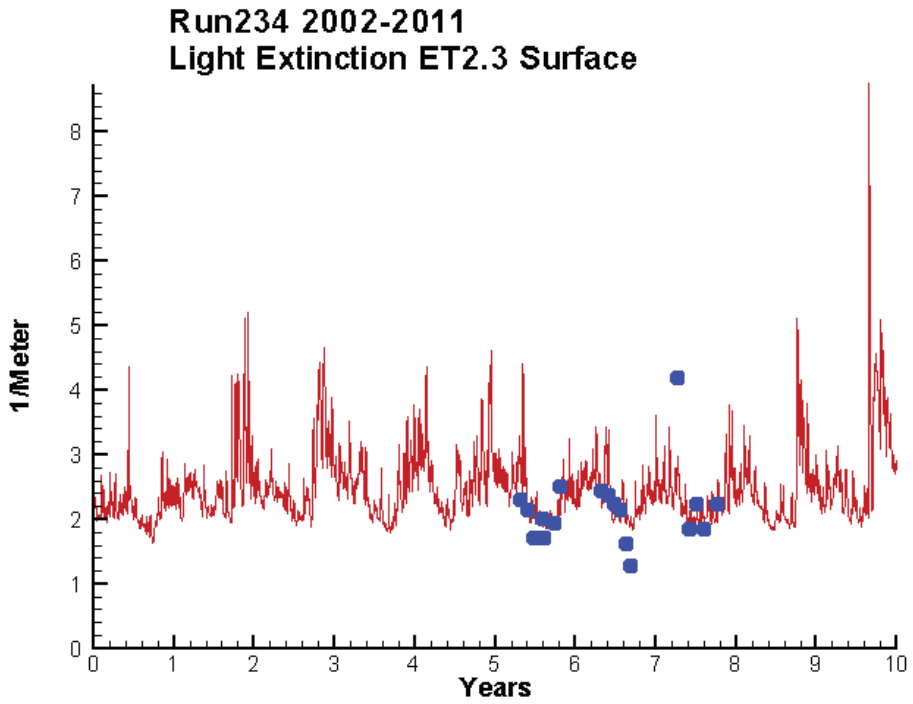

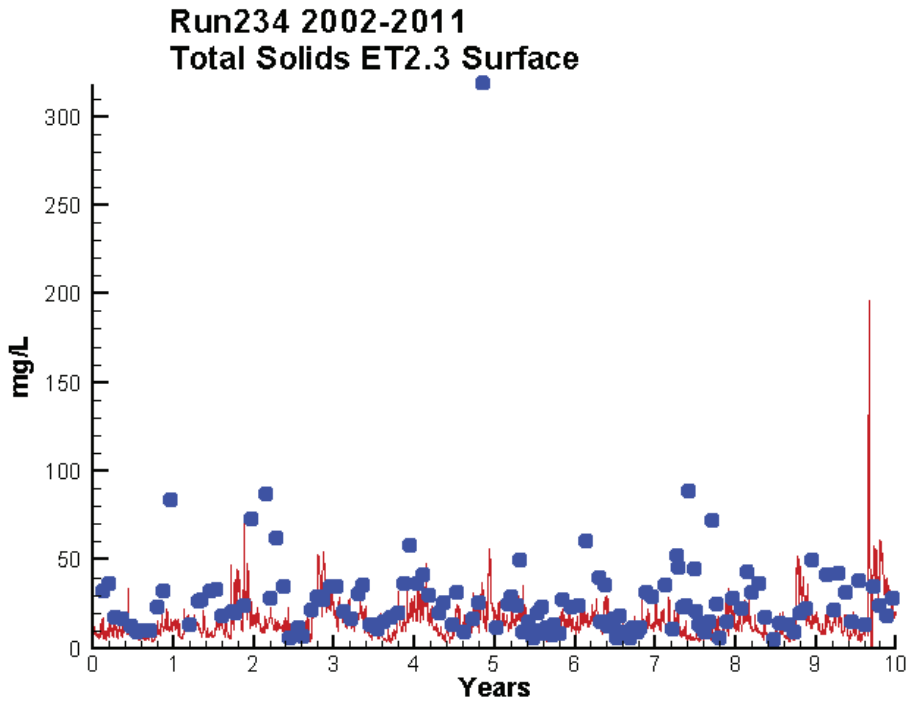

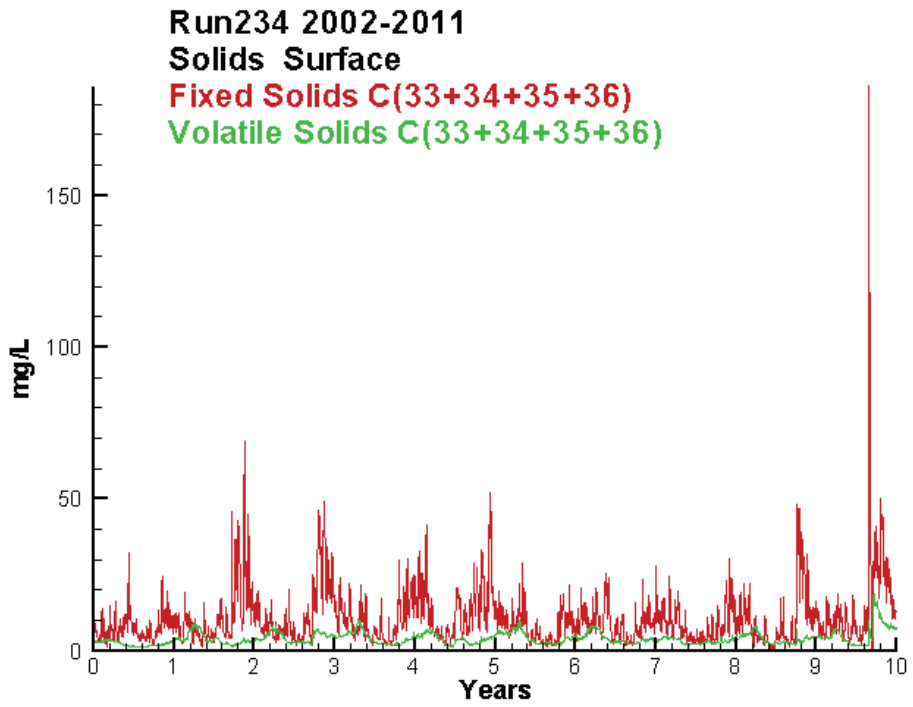

	Mean Difference	Absolute Mean Difference
KE	0.0707	0.2885
TSS	-13.3361	16.4917

Station ET4.2

Run234 2002-2011
Chlorophyll ET4.2 Surface

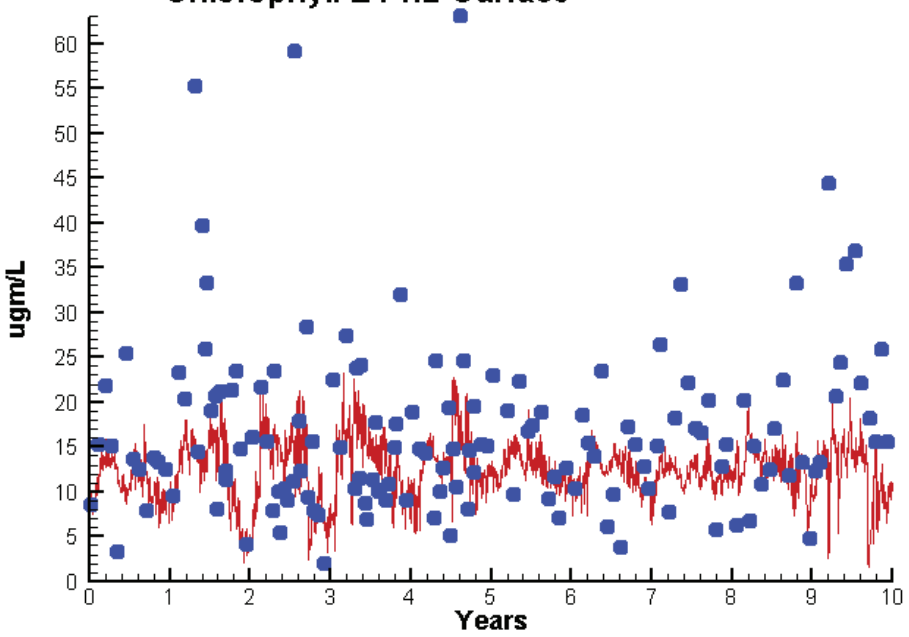

Run234 2002-2011
Light Extinction ET4.2 Surface

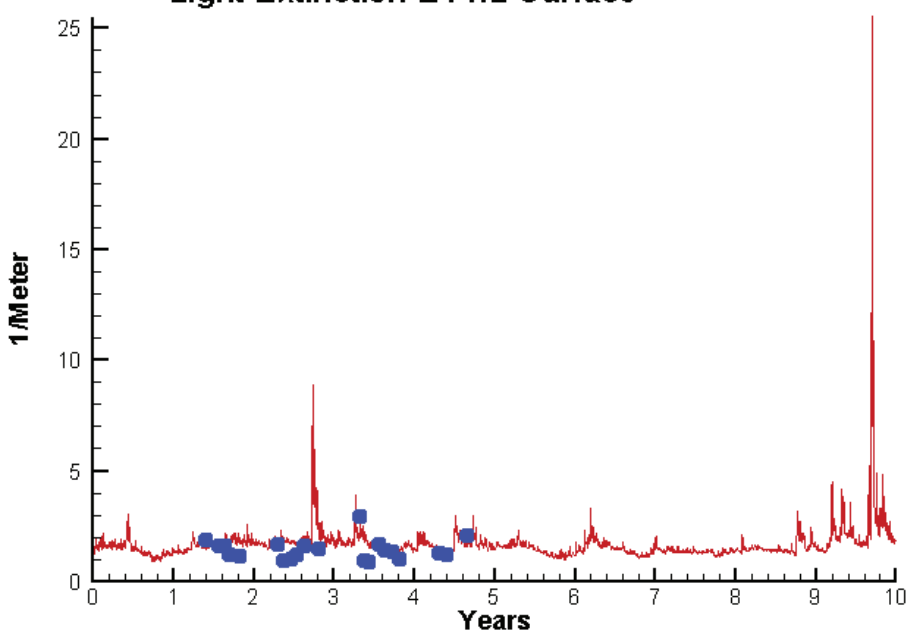

Run234 2002-2011
Dissolved Inorganic Nitrogen ET4.2 Surface

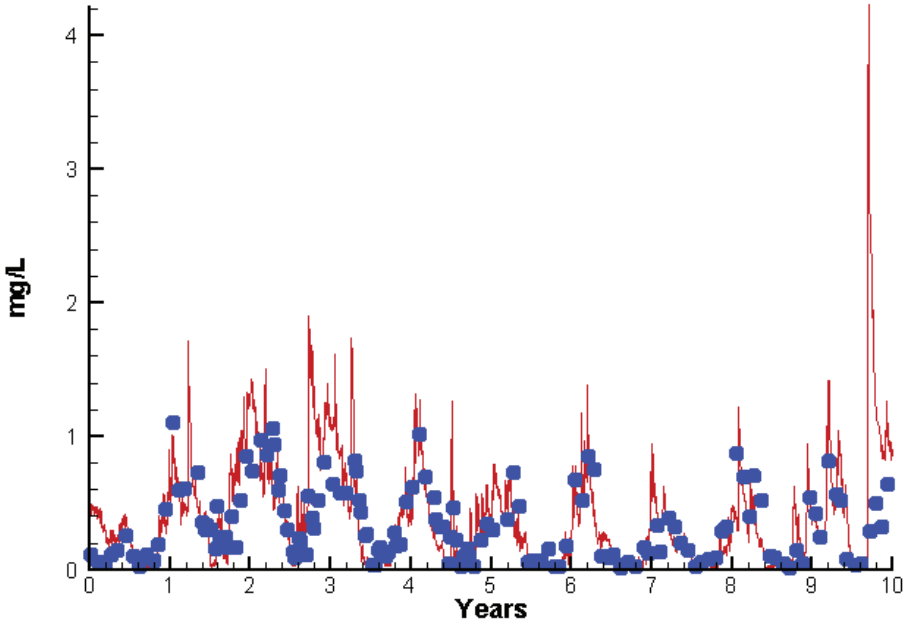

Run234 2002-2011
Dissolved Inorganic Phosphorus ET4.2 Surface

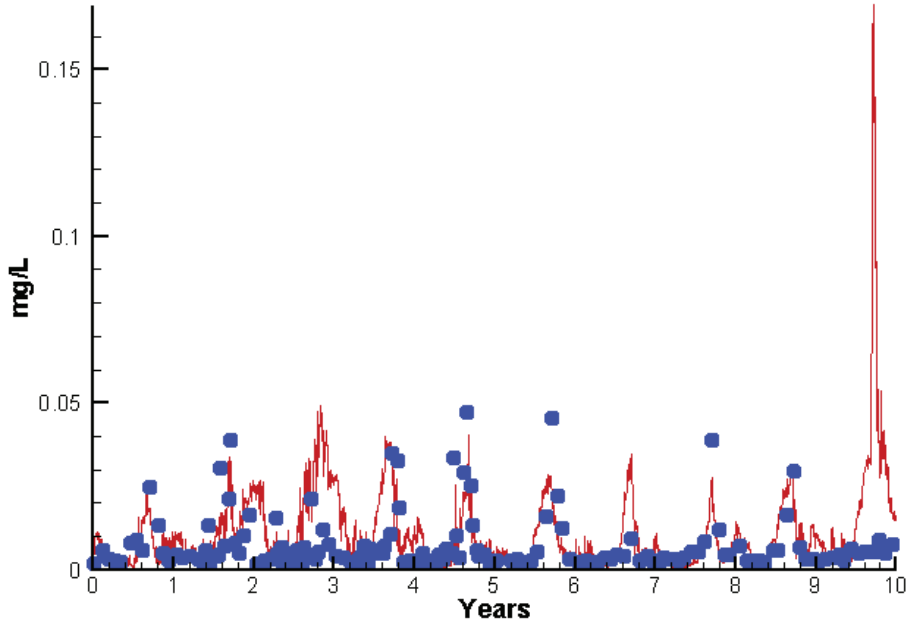

Station ET4.2

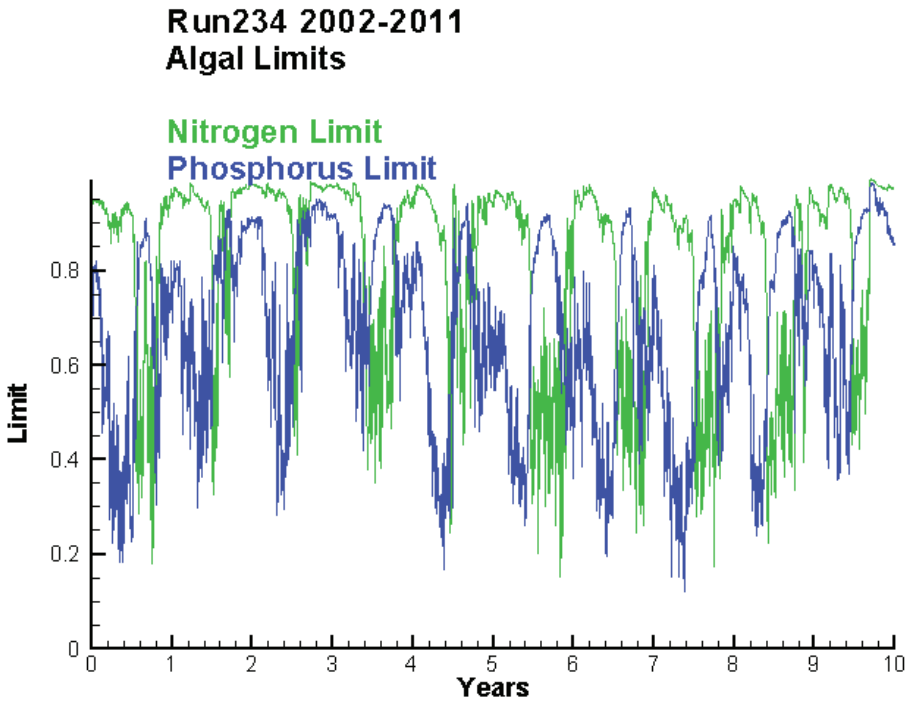

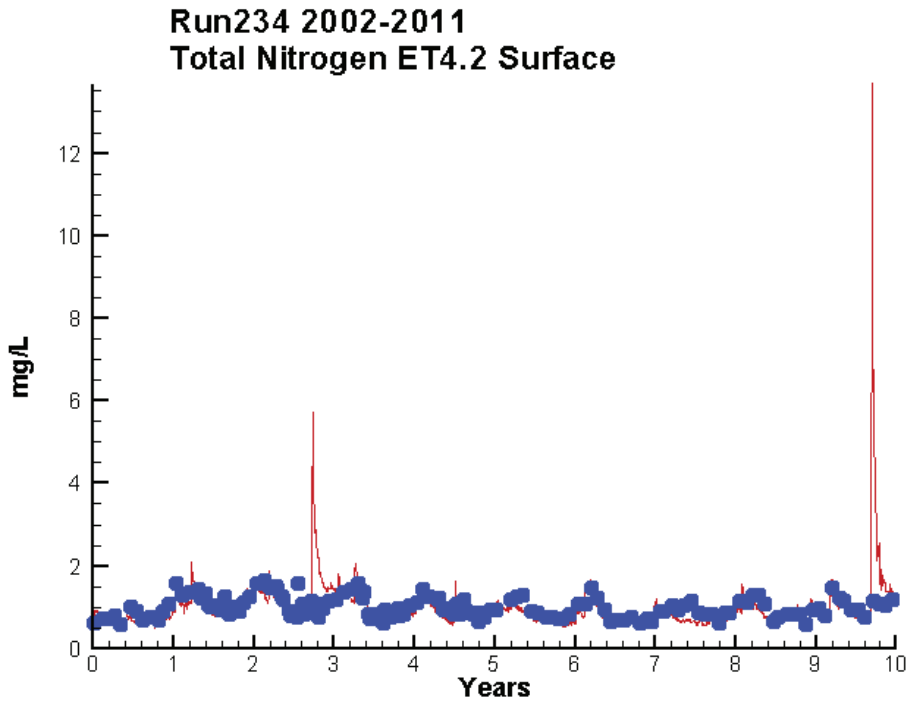

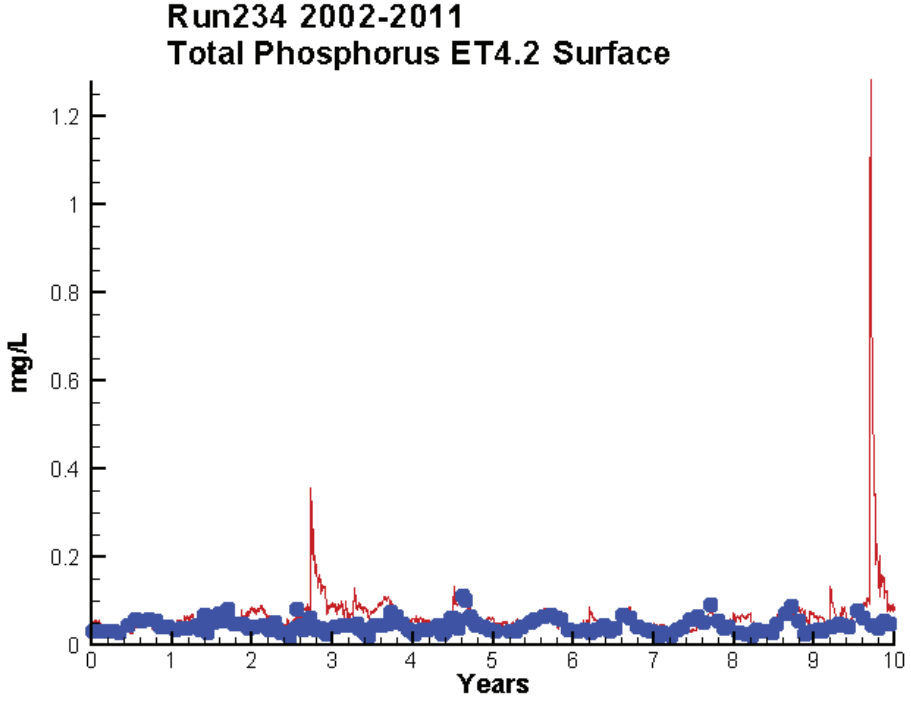

	Mean Difference	Absolute Mean Difference
Chl	-3.9182	7.2145
DIN	0.0399	0.1718
KE	0.3295	0.4326
DIP	0.0036	0.0083
TP	0.0224	0.0264
TN	-0.0180	0.1954

Station ET4.2

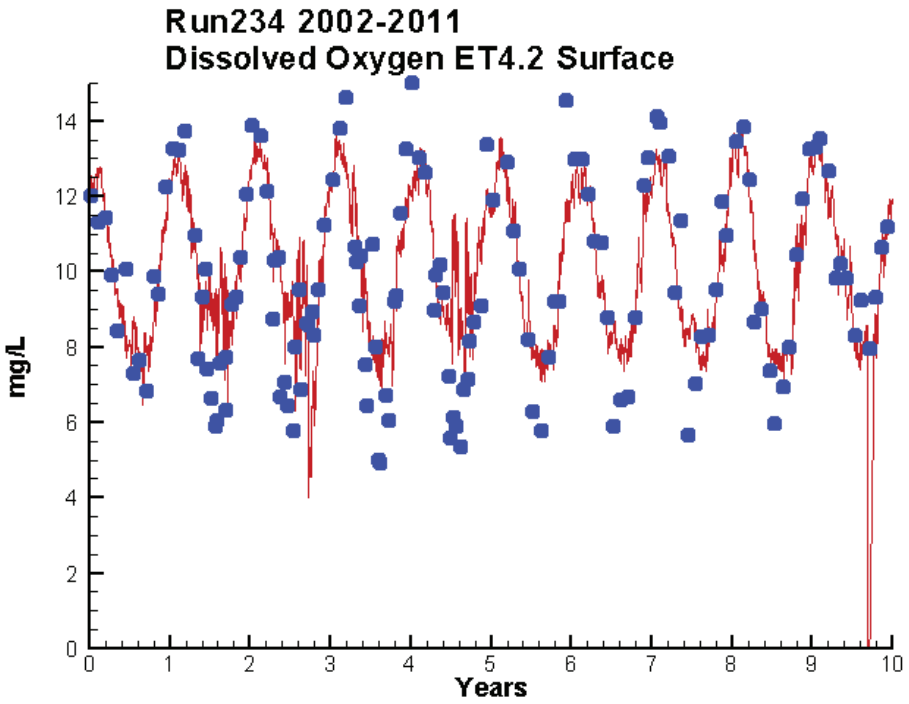

	Mean Difference	Absolute Mean Difference
Top DO	0.3367	1.1786

Station ET4.2

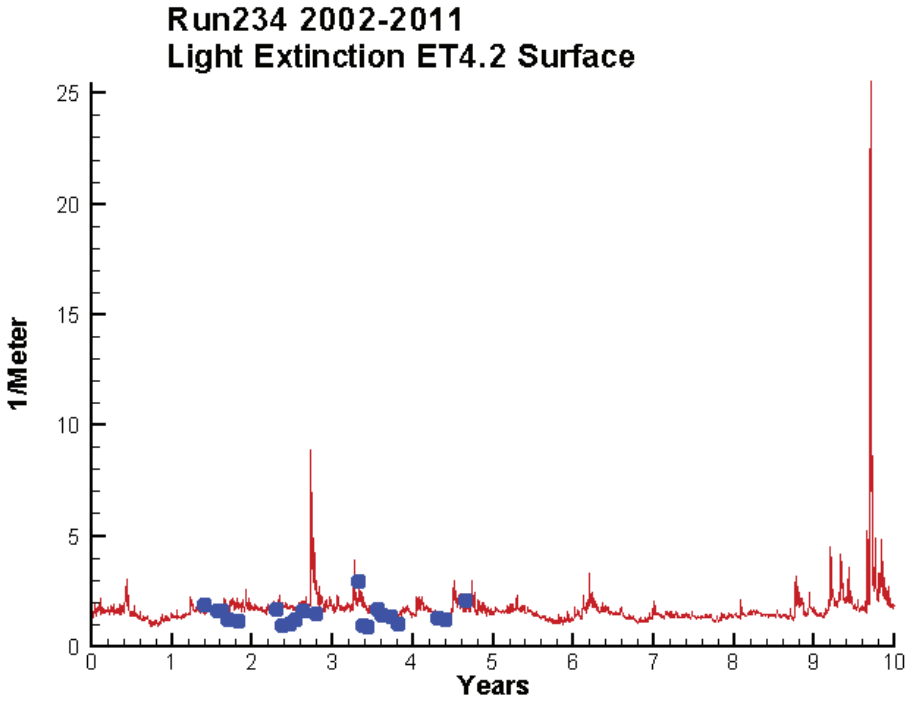

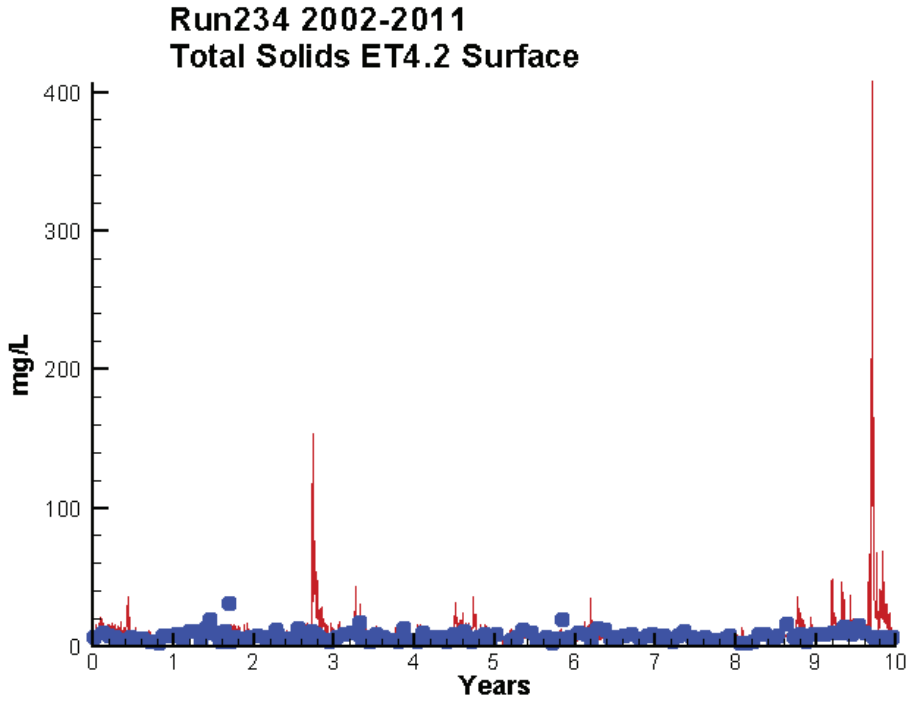

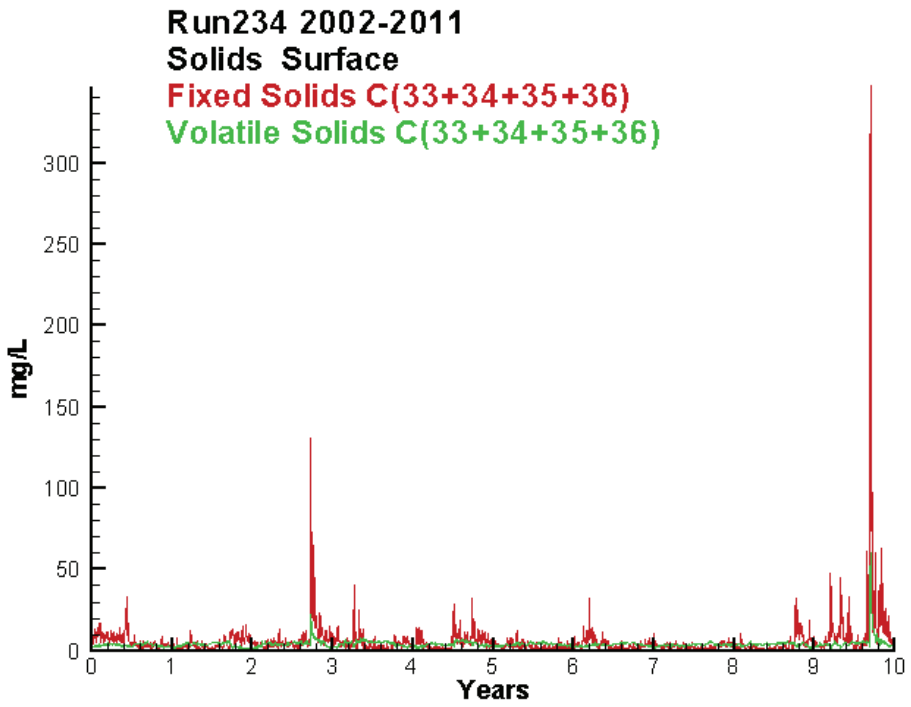

	Mean Difference	Absolute Mean Difference
KE	0.3295	0.4326
TSS	2.2681	4.3650

Station ET5.2

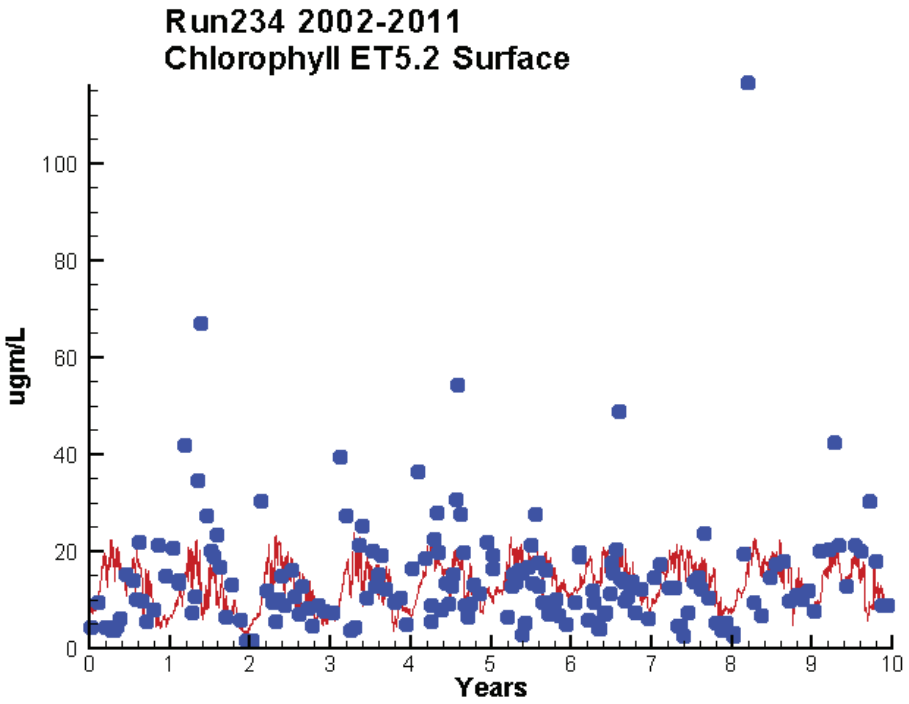

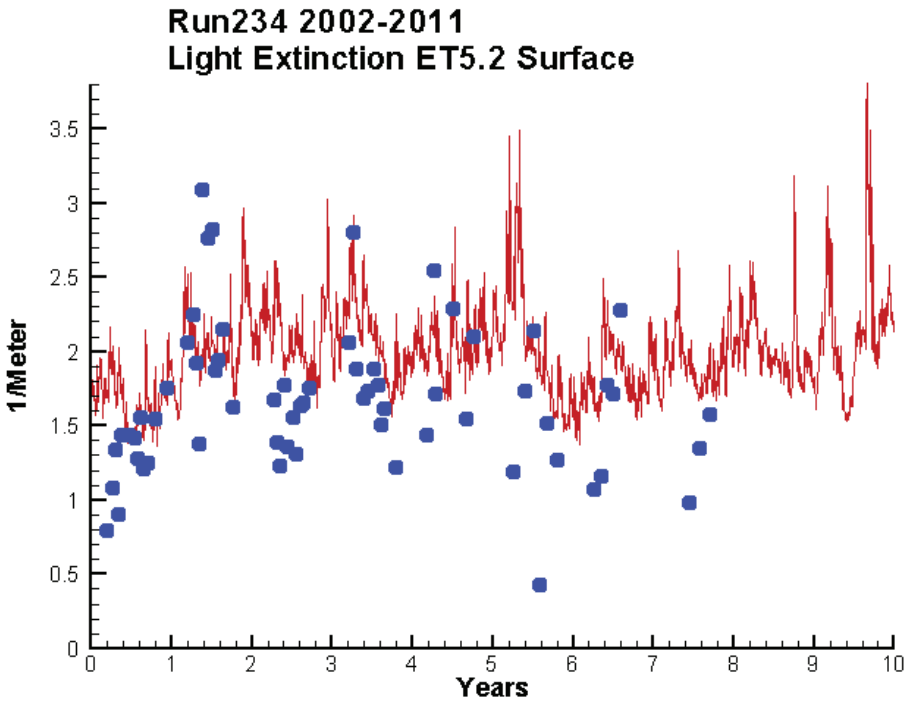

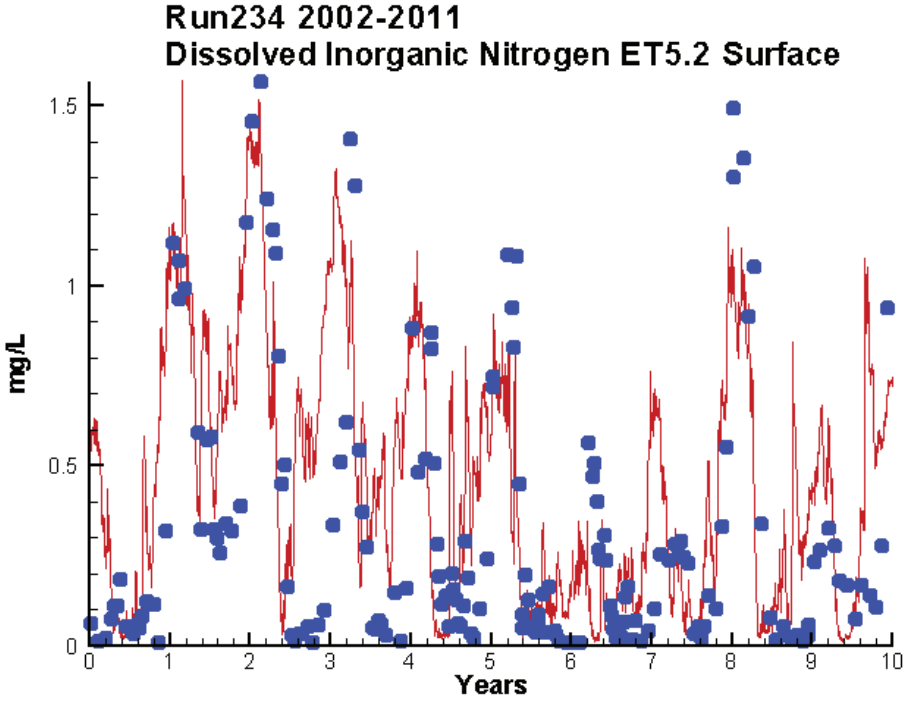

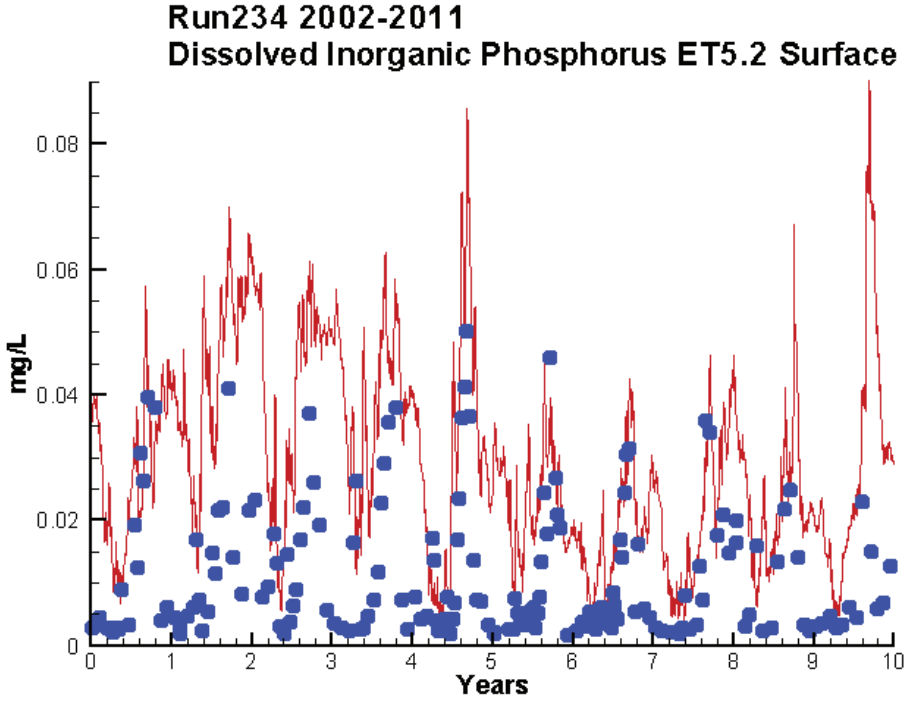

Station ET5.2

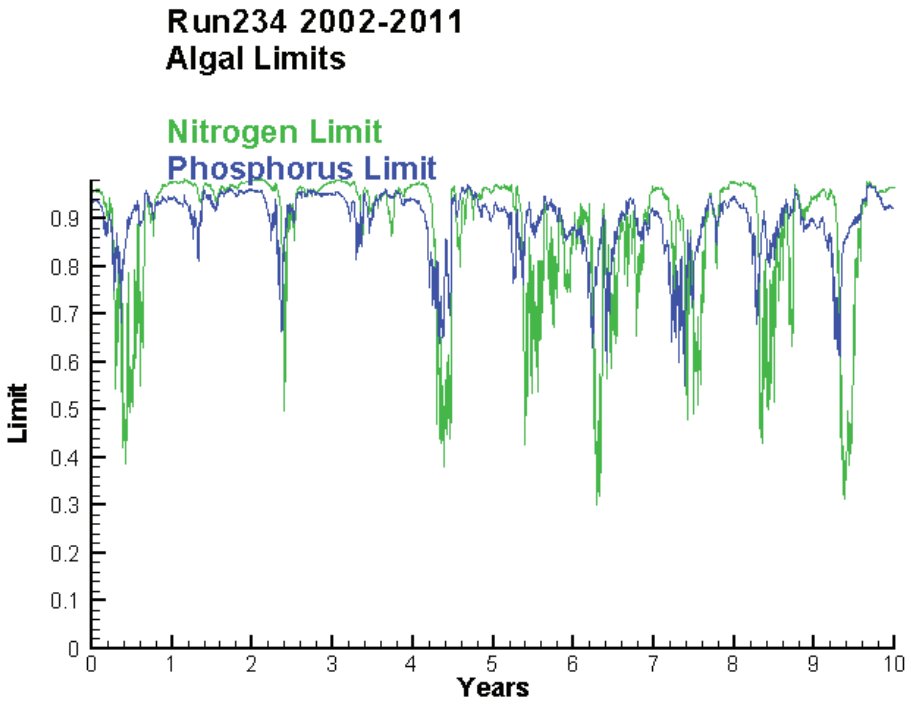

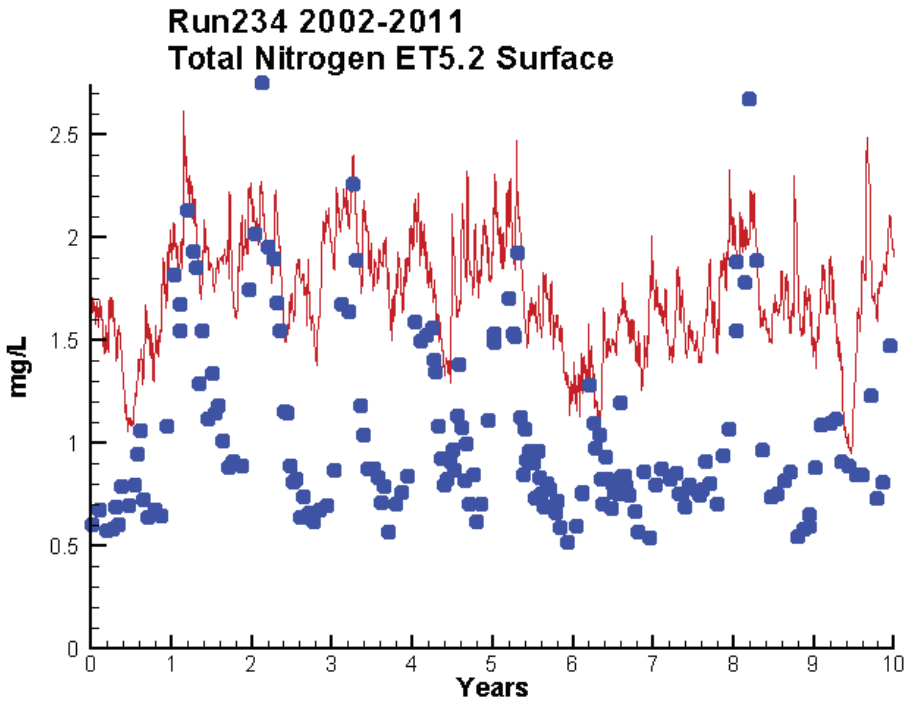

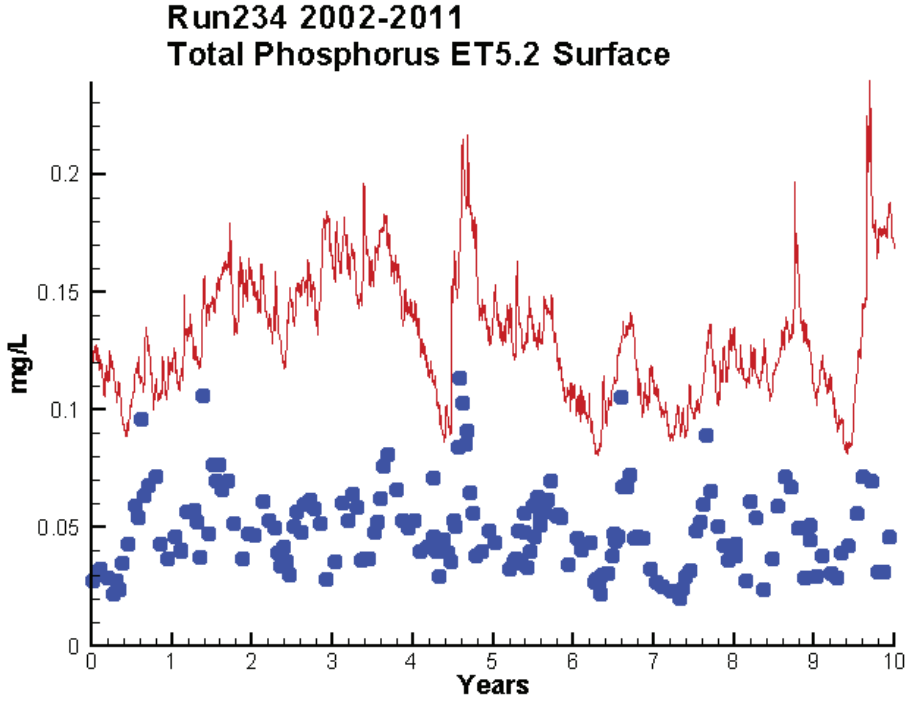

	Mean Difference	Absolute Mean Difference
Chl	-0.3137	7.6720
DIN	0.0825	0.2684
KE	0.3254	0.4485
DIP	0.0168	0.0177
TP	0.0813	0.0813
TN	0.6846	0.6969

Station ET5.2

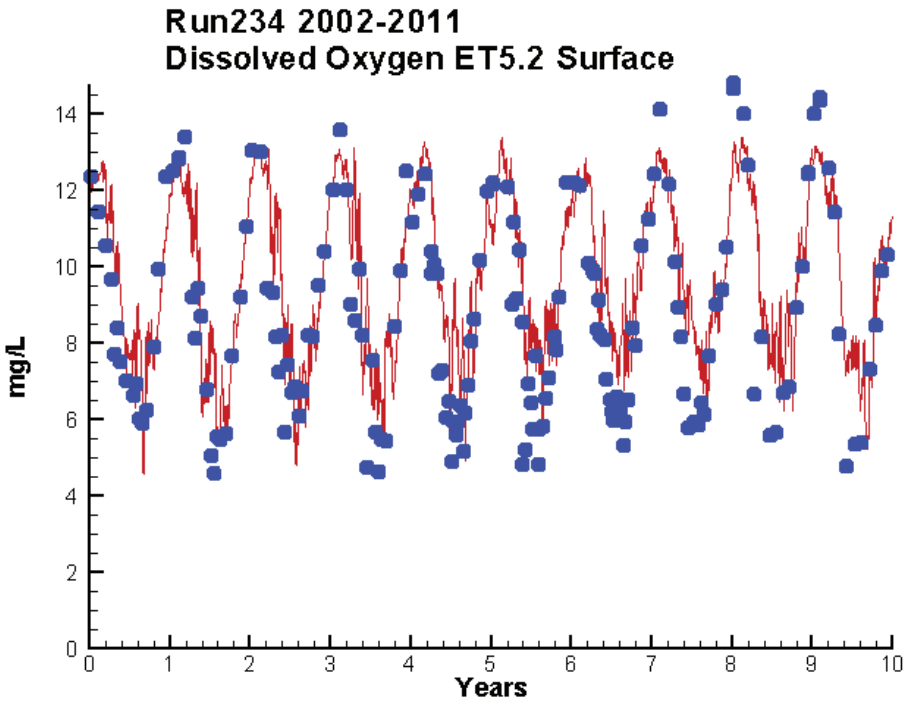

	Mean Difference	Absolute Mean Difference
Top DO	0.8879	1.2705

Station ET5.2

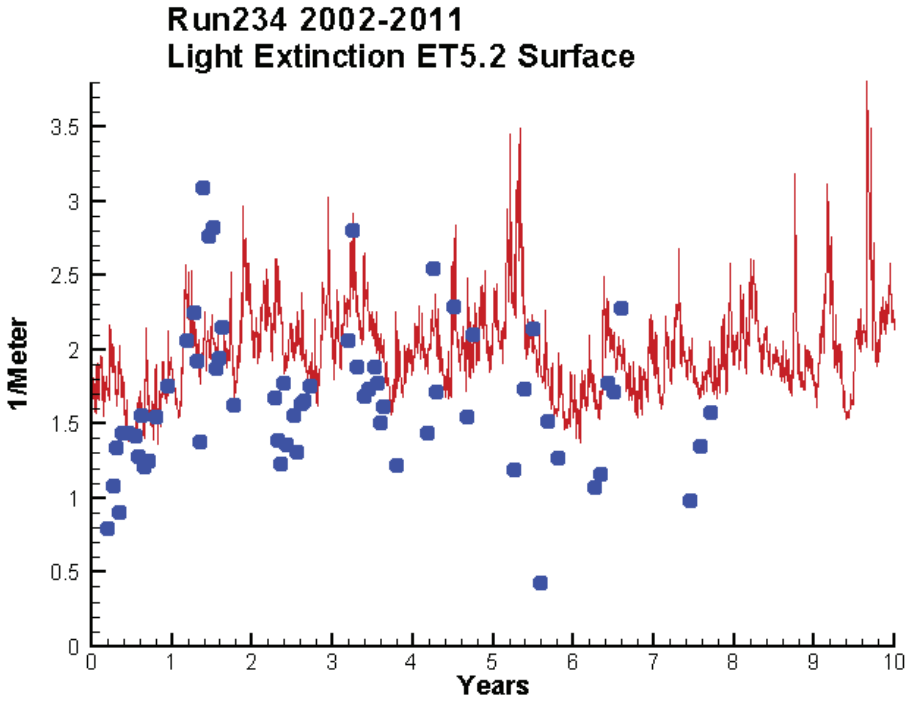

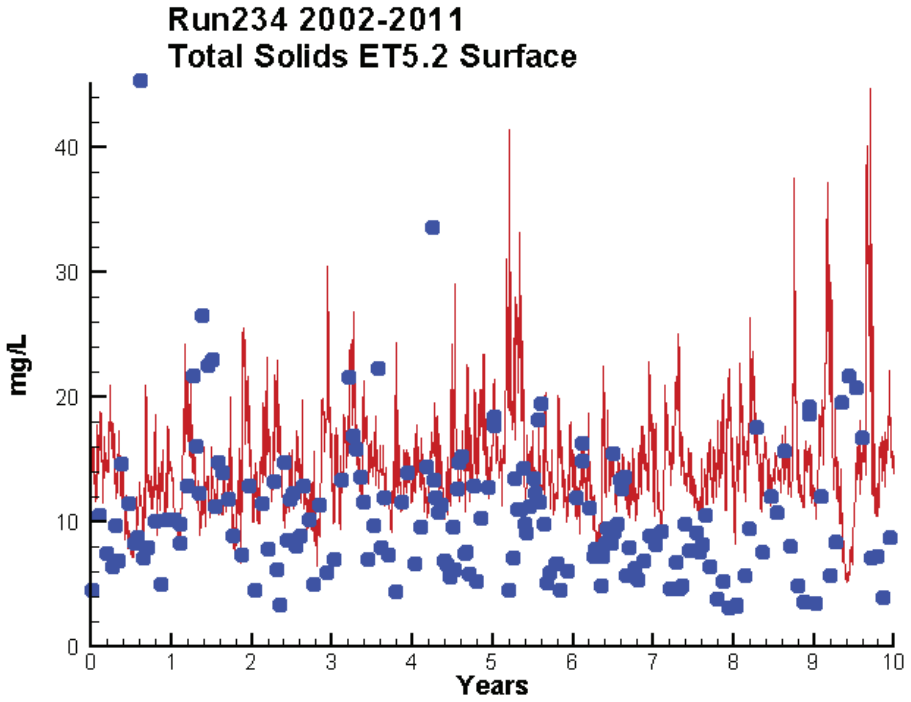

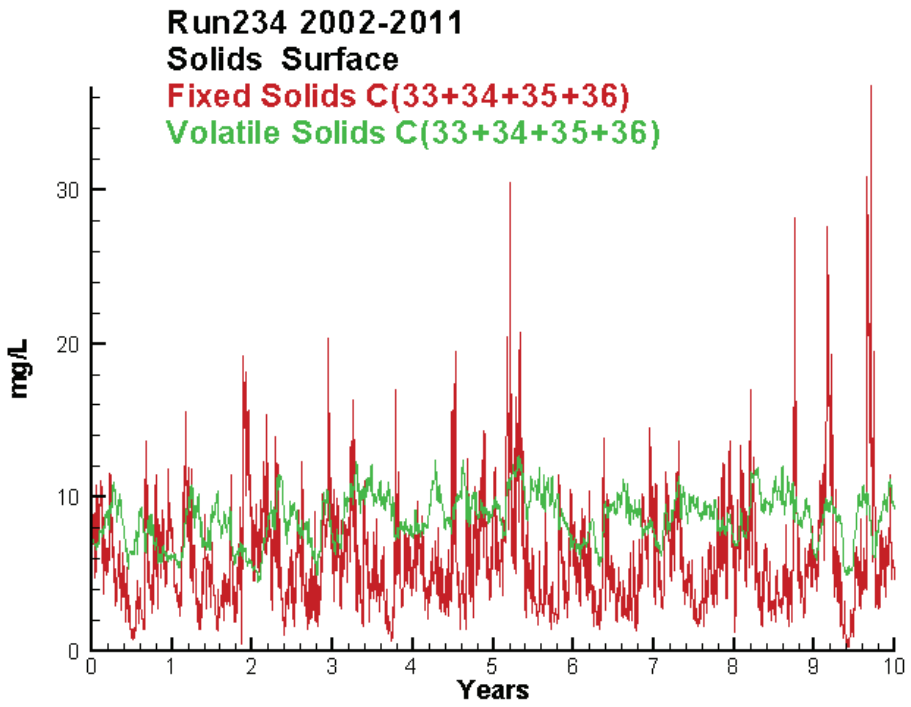

	Mean Difference	Absolute Mean Difference
KE	0.3254	0.4485
TSS	3.6229	5.8855

Station ET6.2

Run234 2002-2011
Chlorophyll ET6.2 Surface

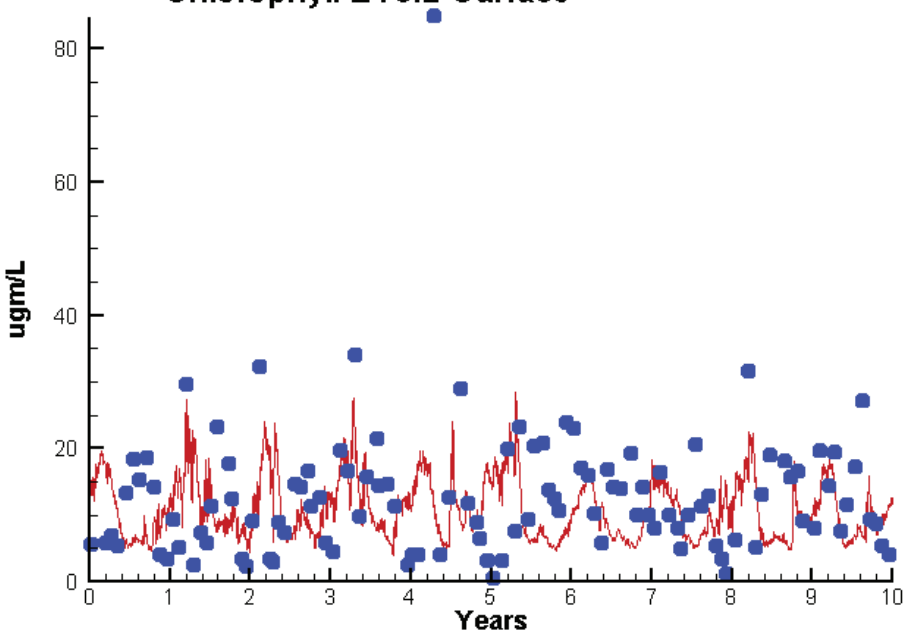

Run234 2002-2011
Light Extinction ET6.2 Surface

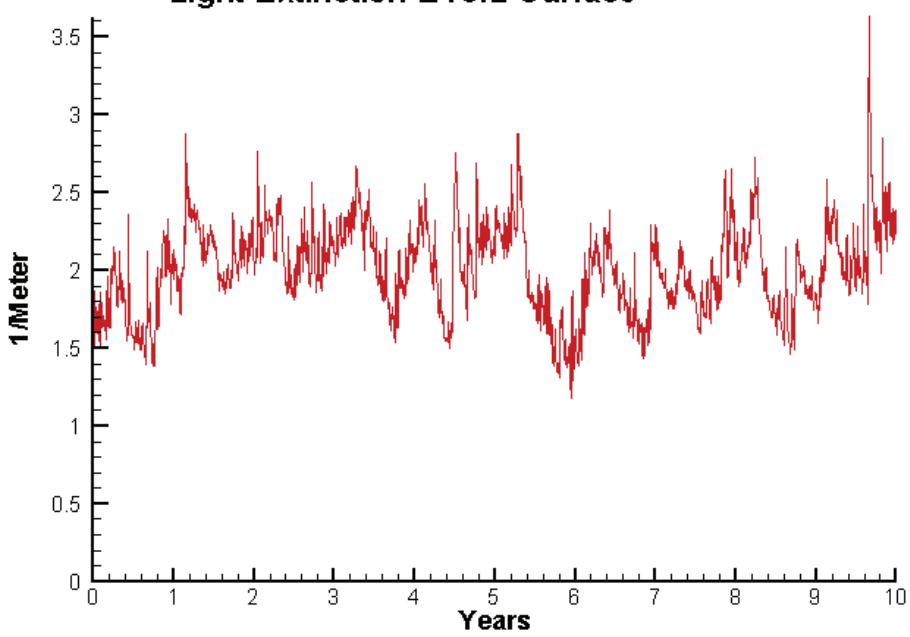

Run234 2002-2011
Dissolved Inorganic Nitrogen ET6.2 Surface

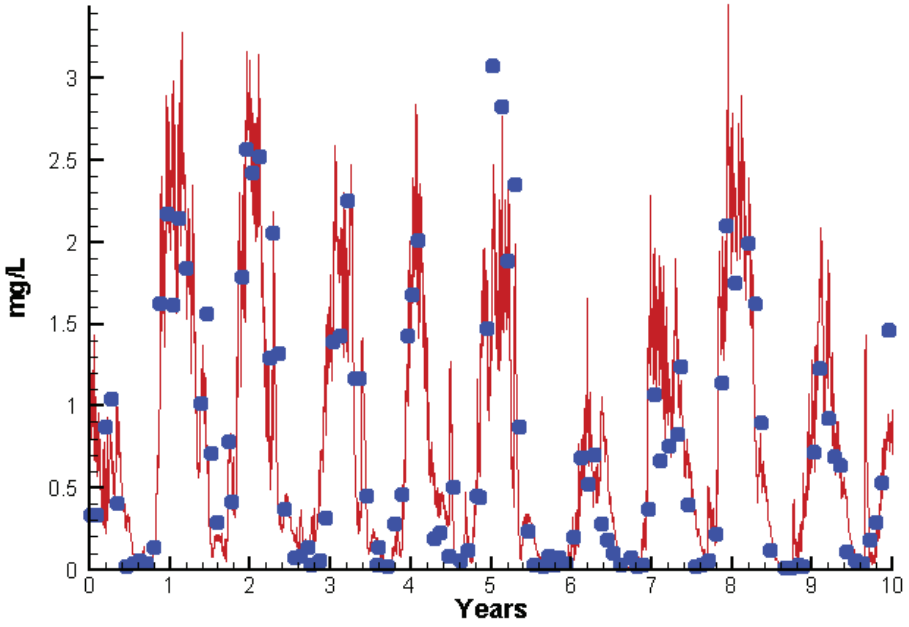

Run234 2002-2011
Dissolved Inorganic Phosphorus ET6.2 Surface

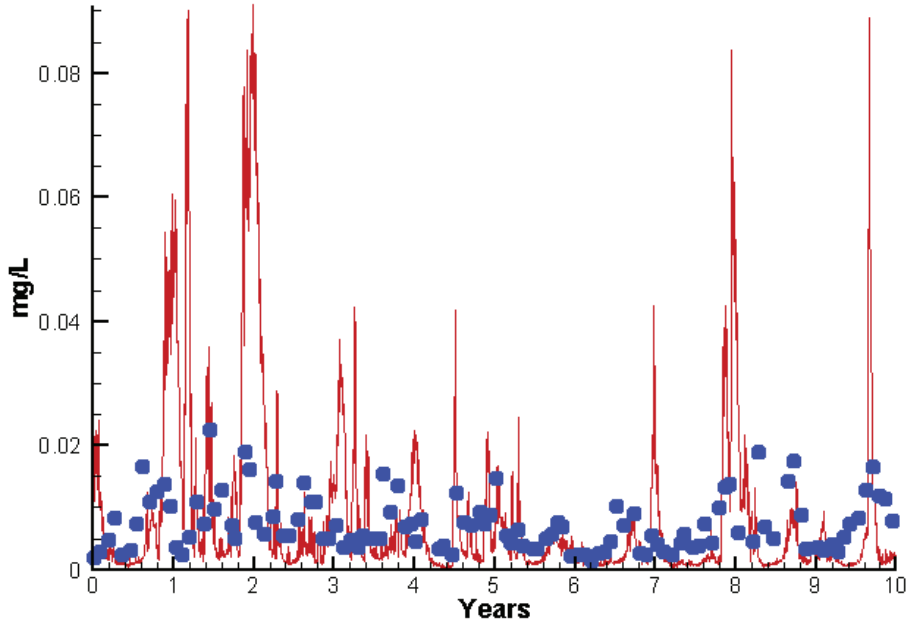

Station ET6.2

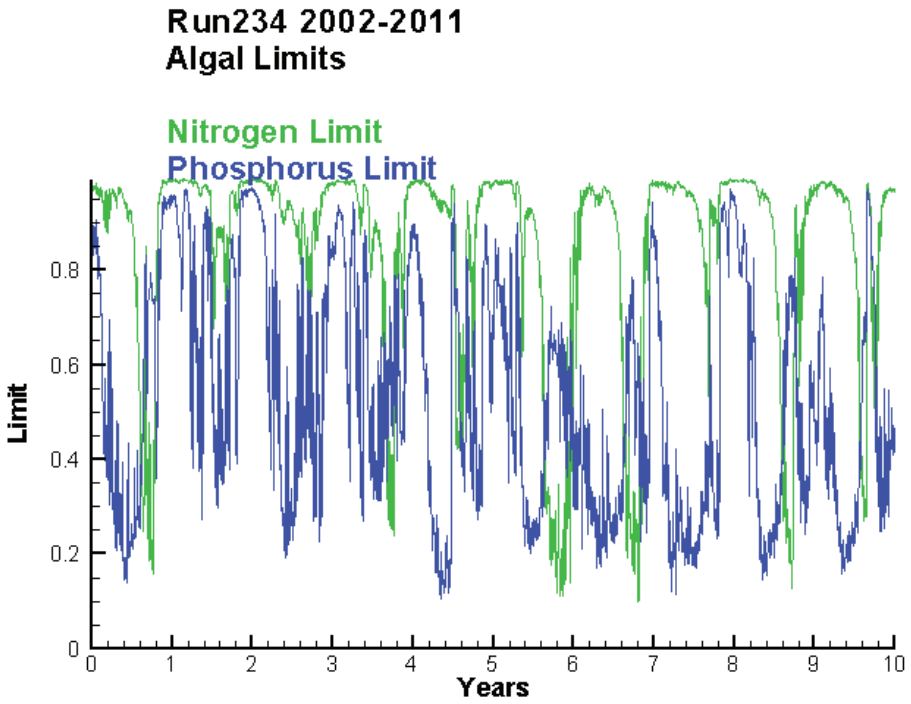

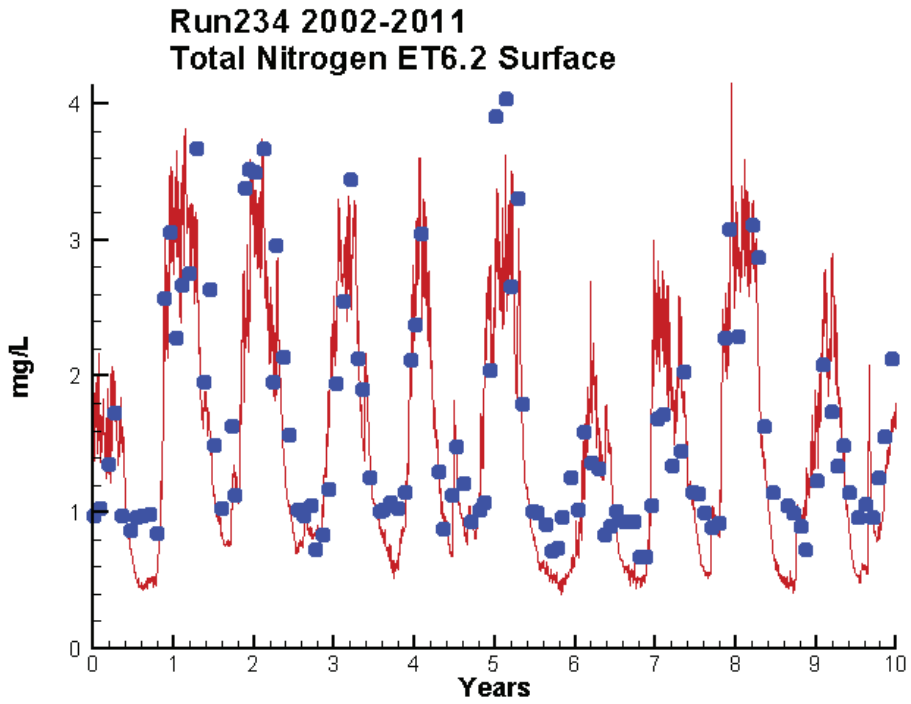

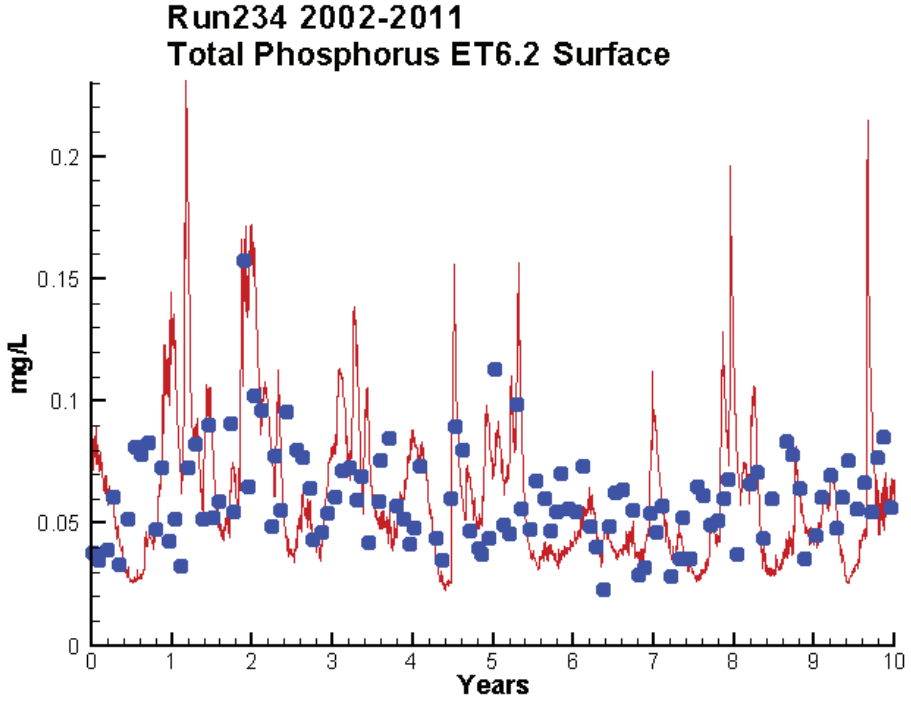

	Mean Difference	Absolute Mean Difference
Chl	-2.0258	7.5925
DIN	0.0609	0.3252
KE	0.0609	0.3252
DIP	0.0016	0.0077
TP	0.0027	0.0229
TN	-0.0630	0.4086

Station ET6.2

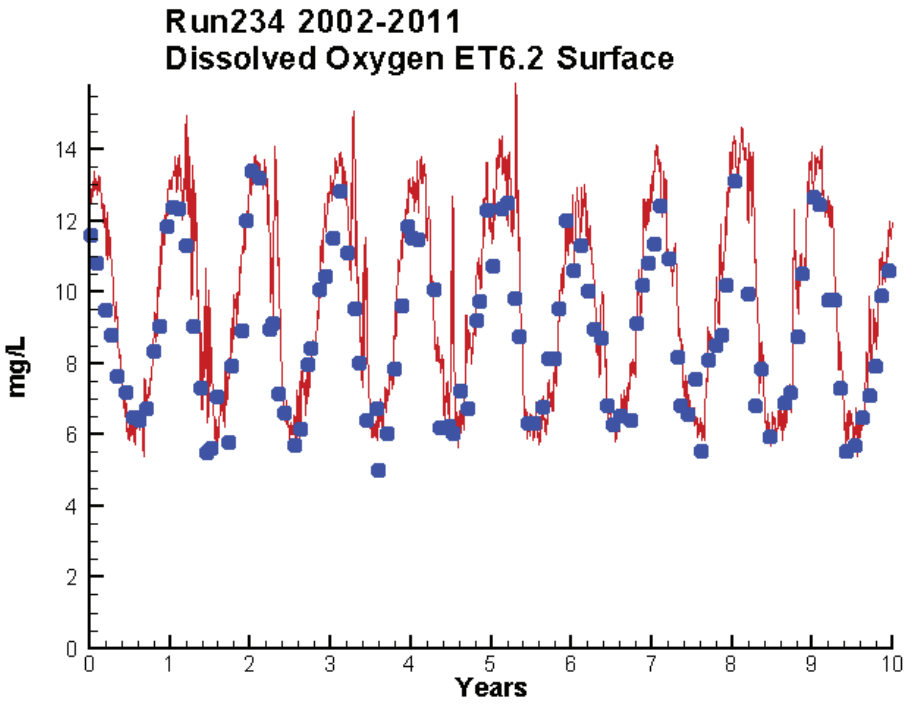

	Mean Difference	Absolute Mean Difference
Top DO	0.9258	1.1330

Station ET6.2

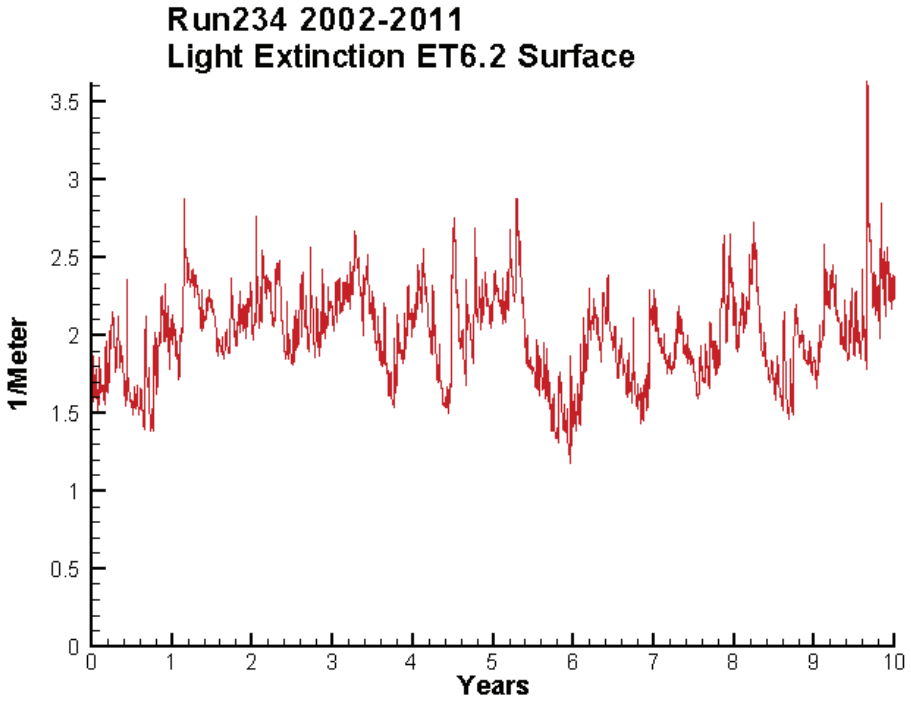

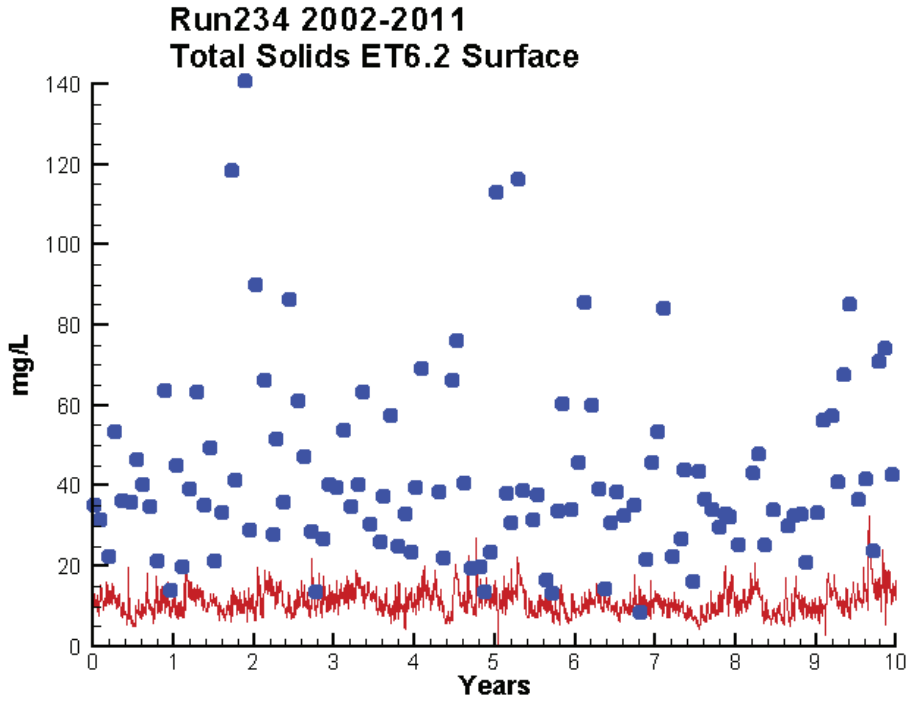

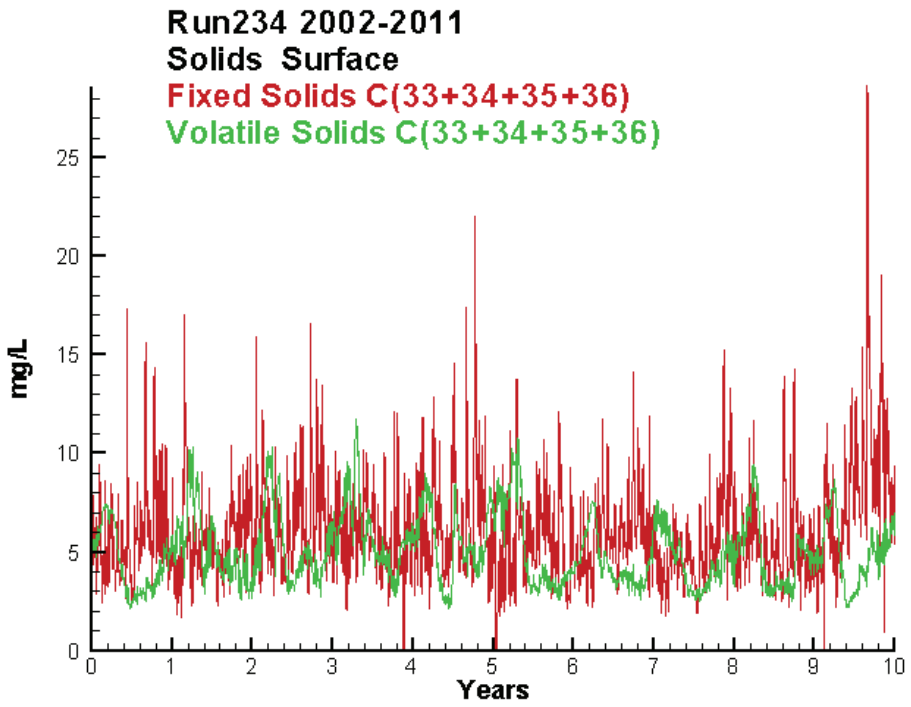

	Mean Difference	Absolute Mean Difference
KE	-0.0630	0.4086
TSS	-31.5701	31.6057

Station ET9.1

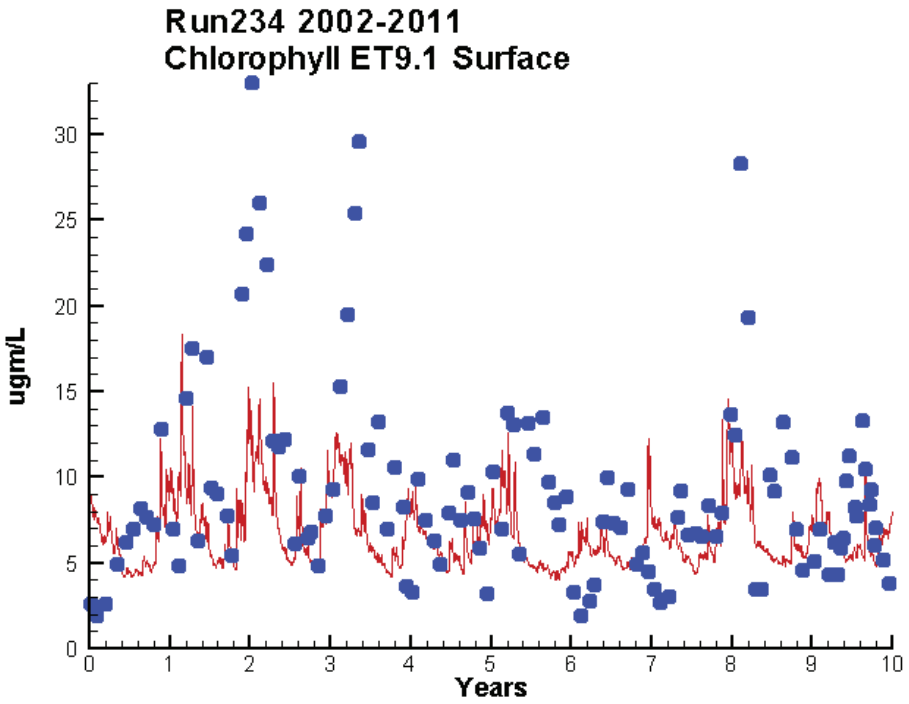

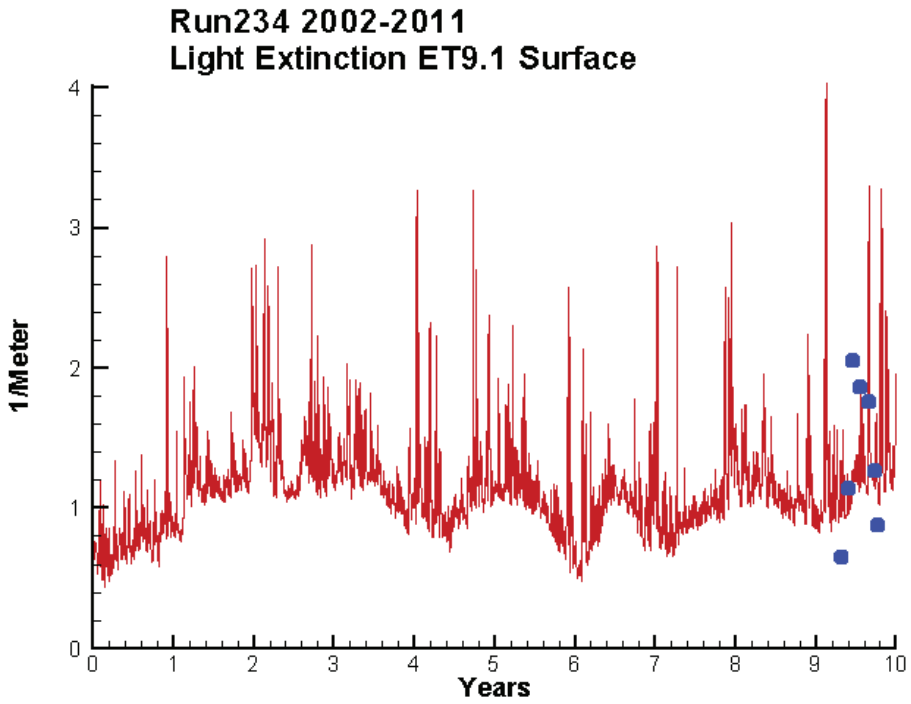

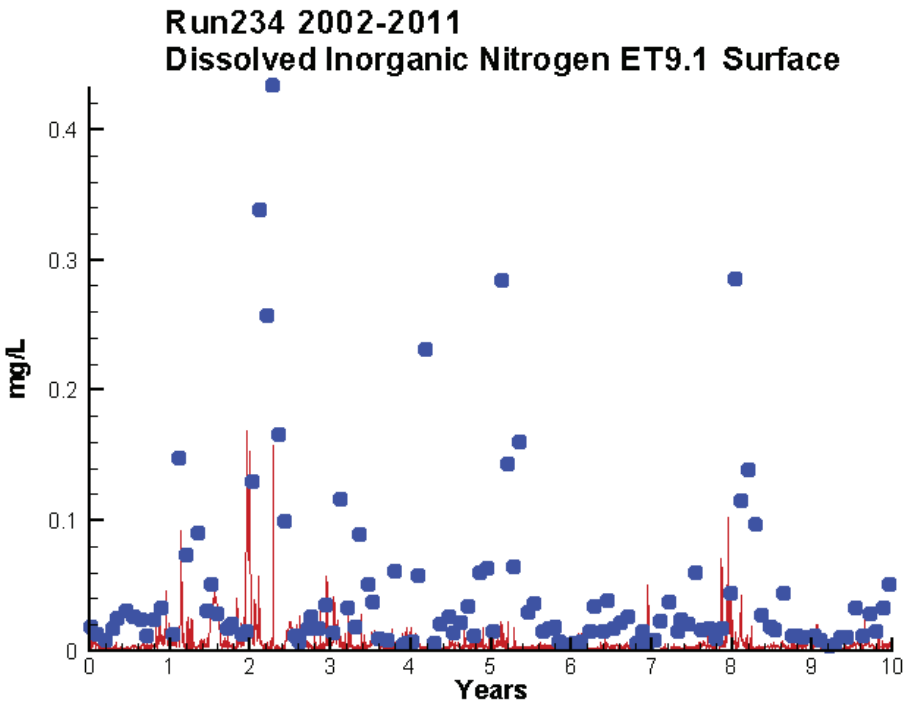

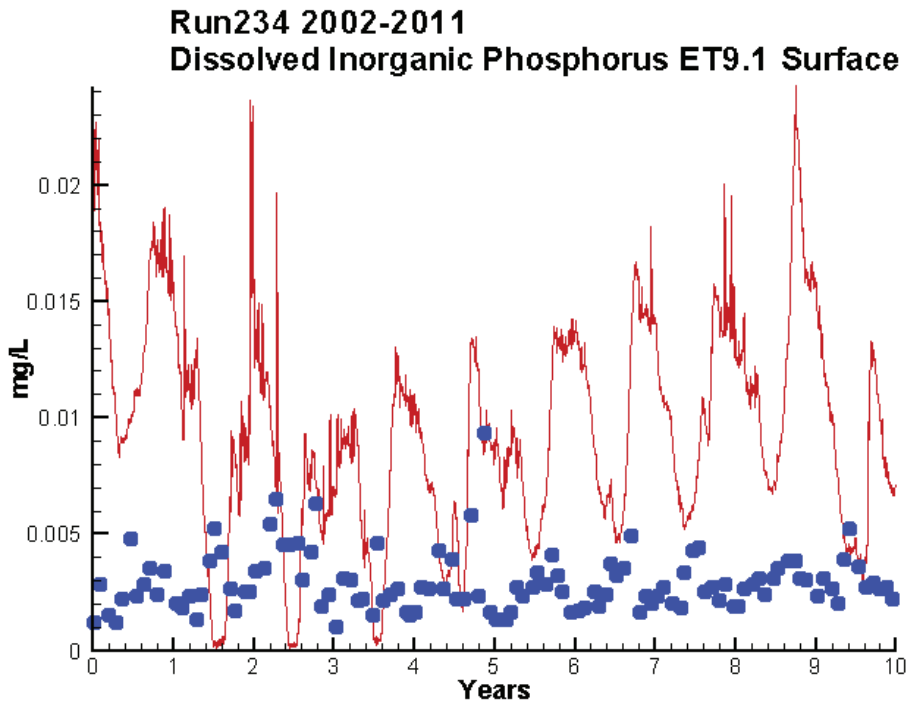

Station ET9.1

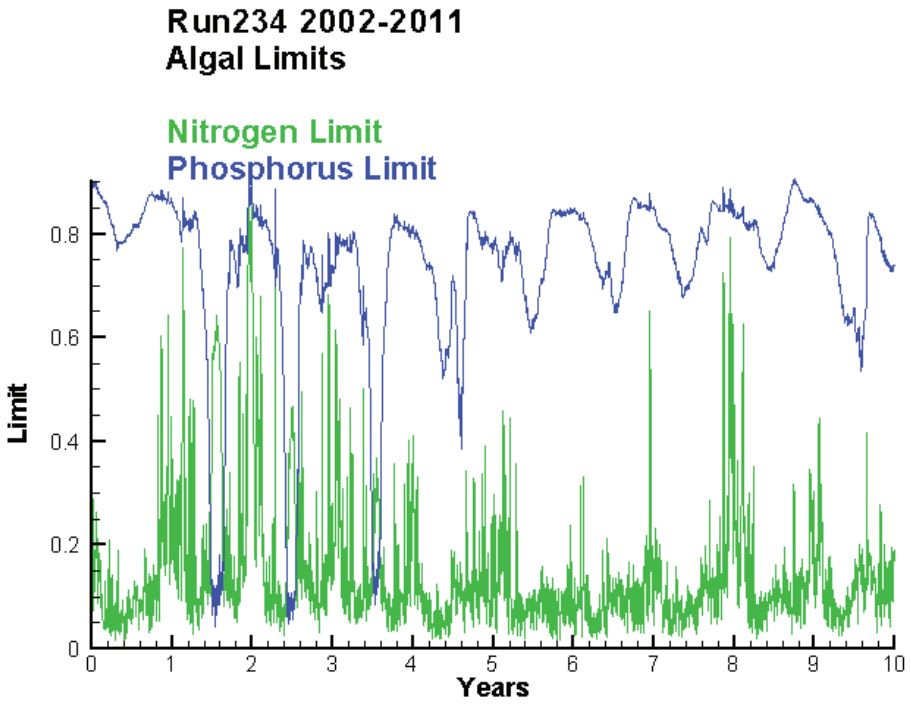

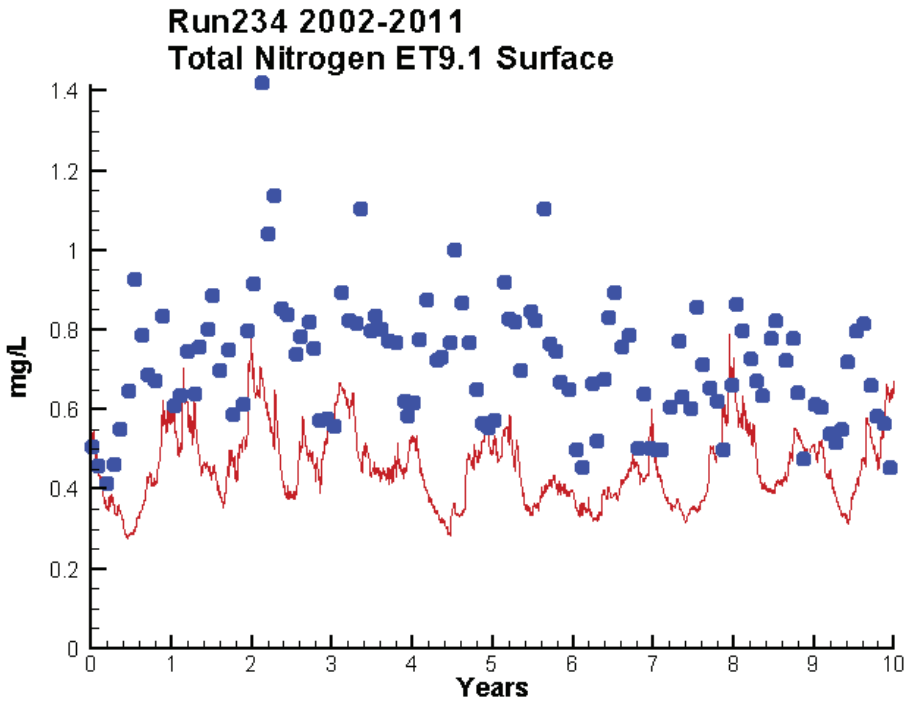

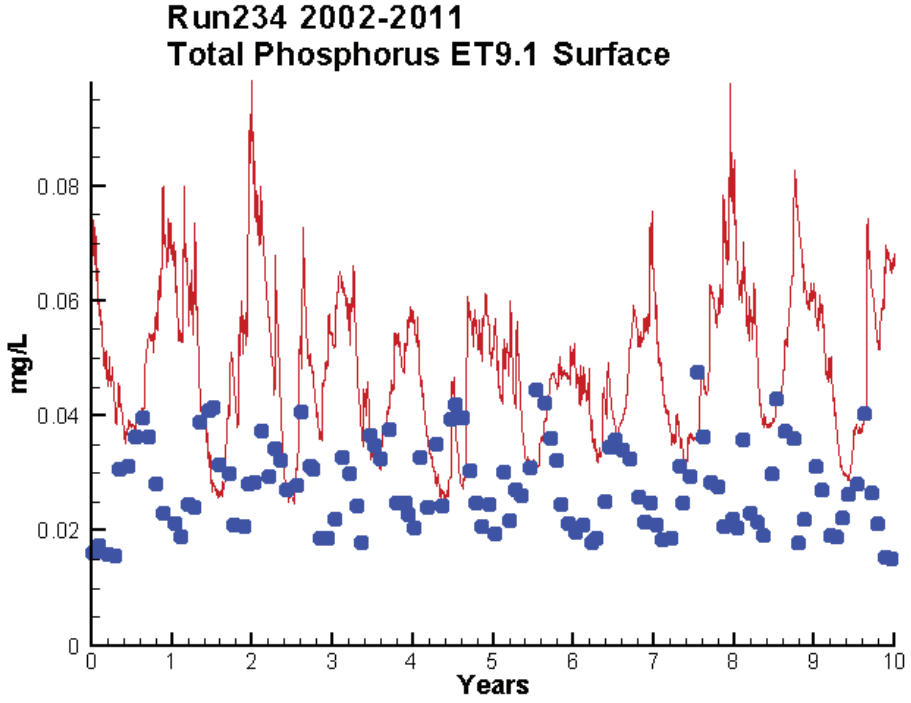

	Mean Difference	Absolute Mean Difference
Chl	-2.5769	4.1119
DIN	-0.0395	0.0424
KE	-0.0967	0.3364
DIP	0.0066	0.0070
TP	0.0210	0.0224
TN	-0.2553	0.2639

Station ET9.1

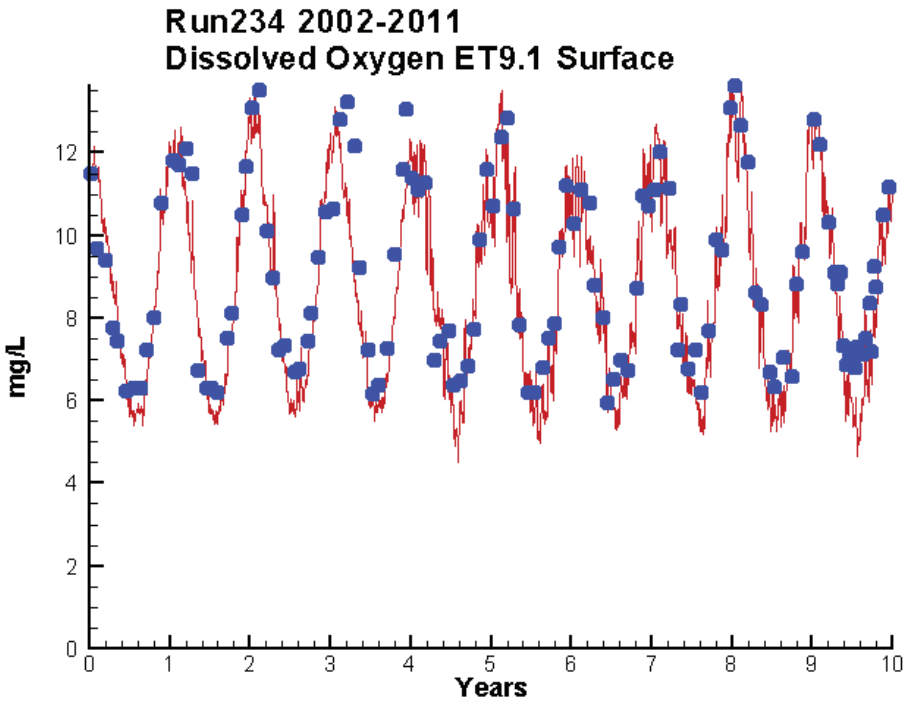

	Mean Difference	Absolute Mean Difference
Top DO	-0.3991	0.7022

Station ET9.1

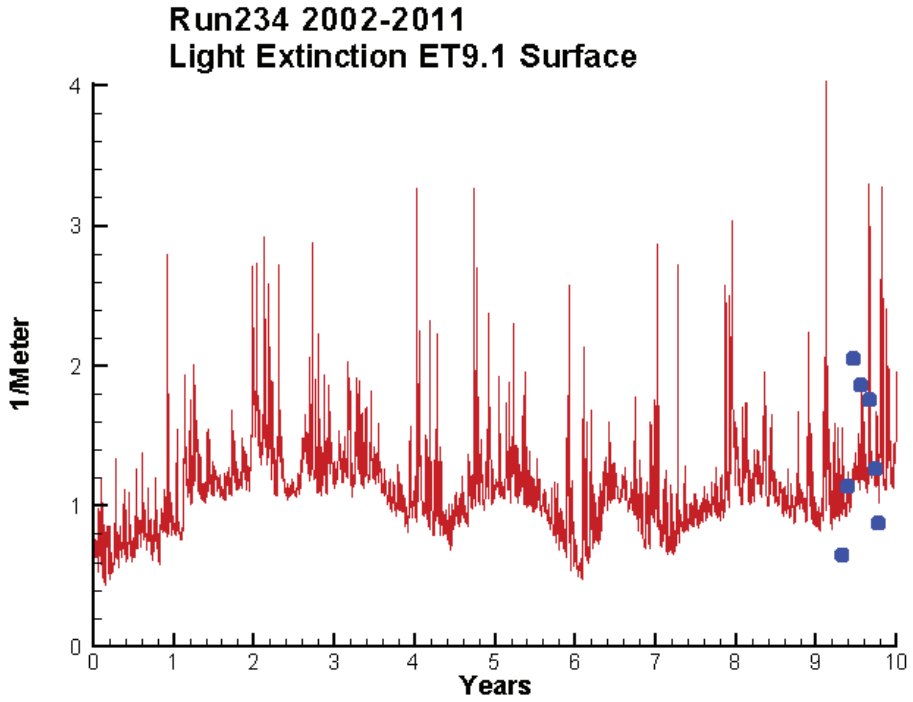

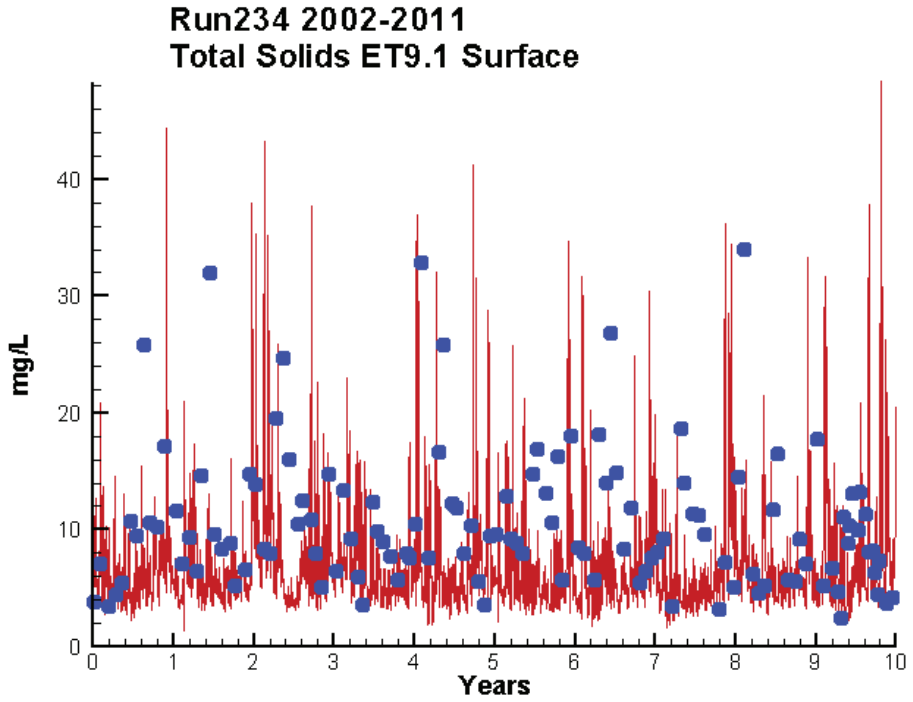

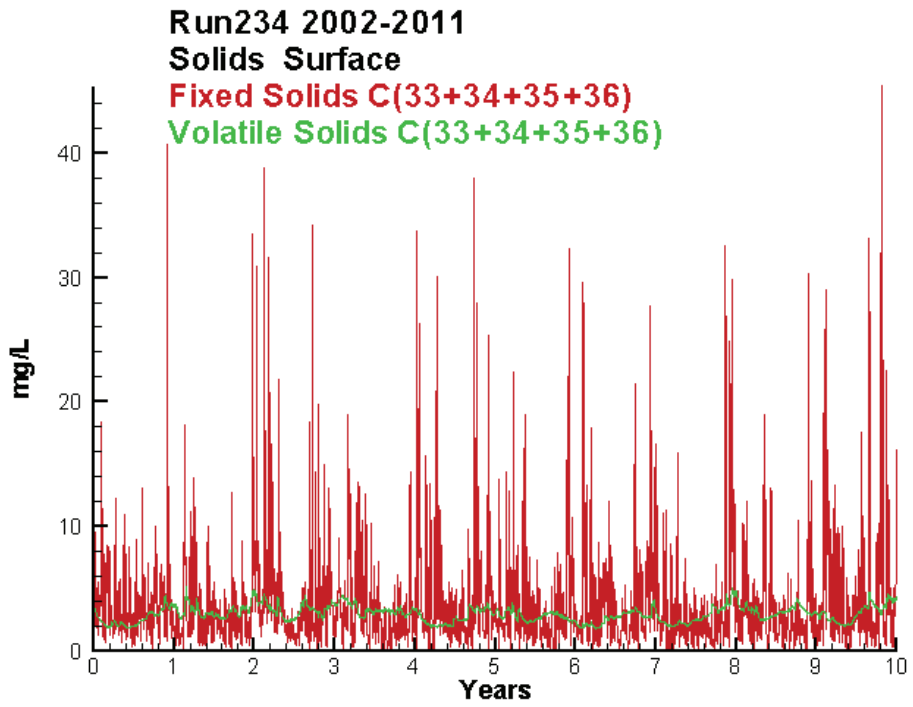

	Mean Difference	Absolute Mean Difference
KE	-0.0967	0.3364
TSS	-3.5602	6.3890

Station WE4.2

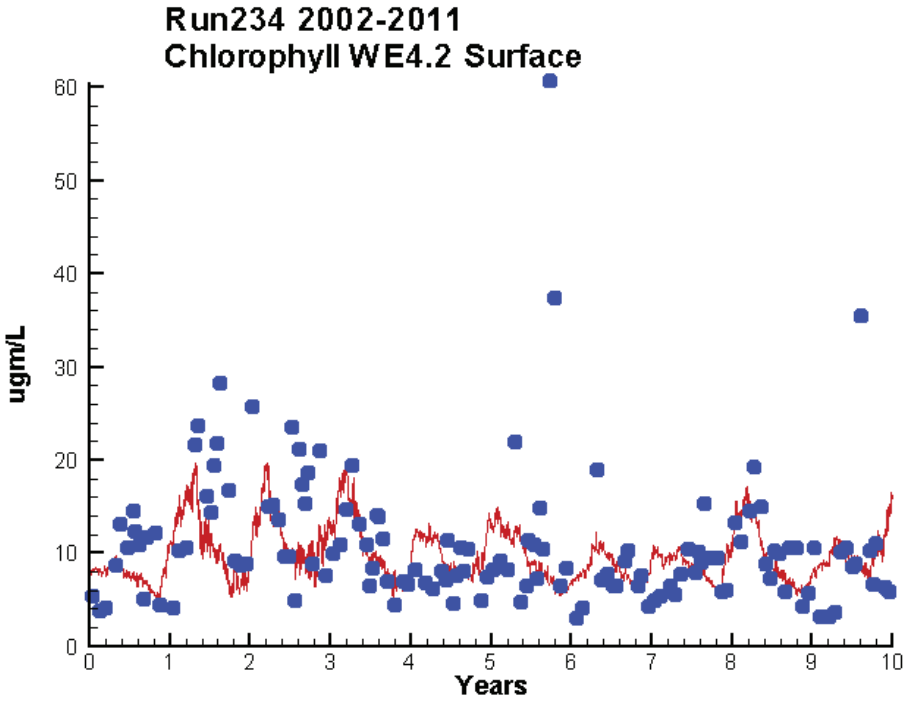

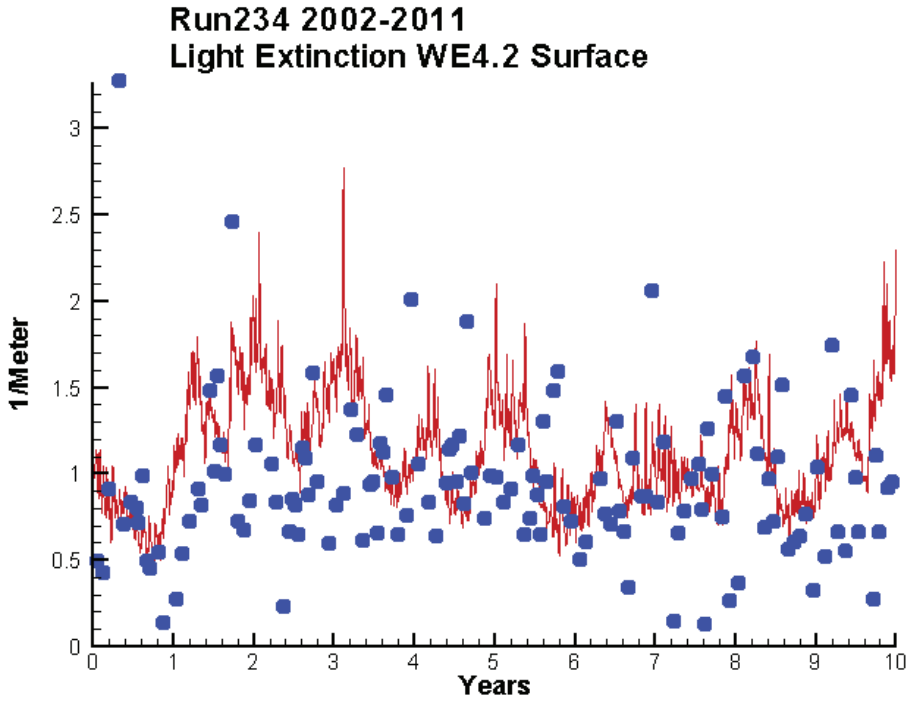

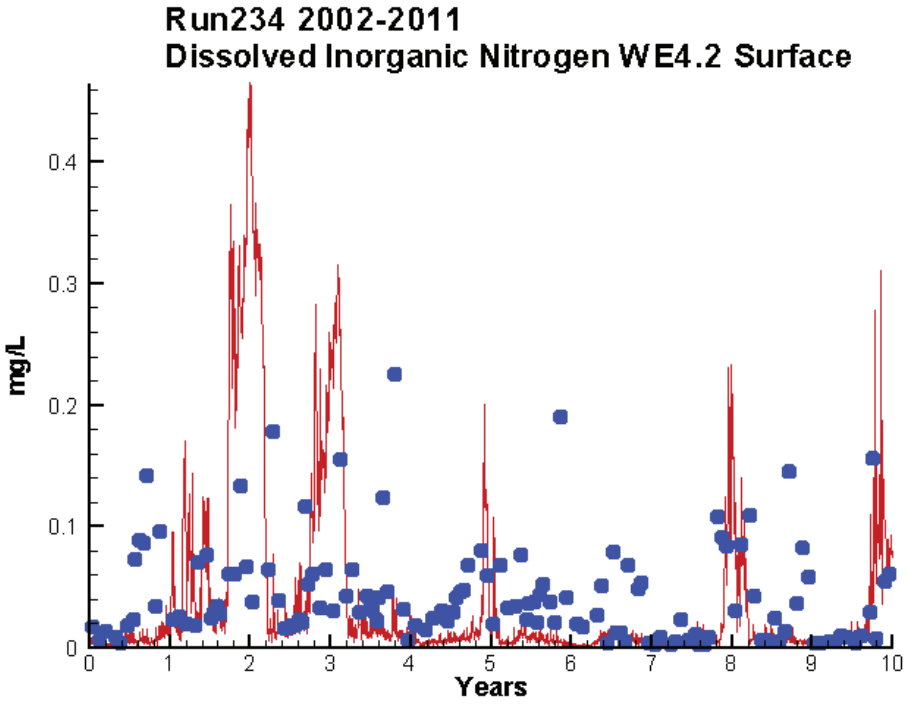

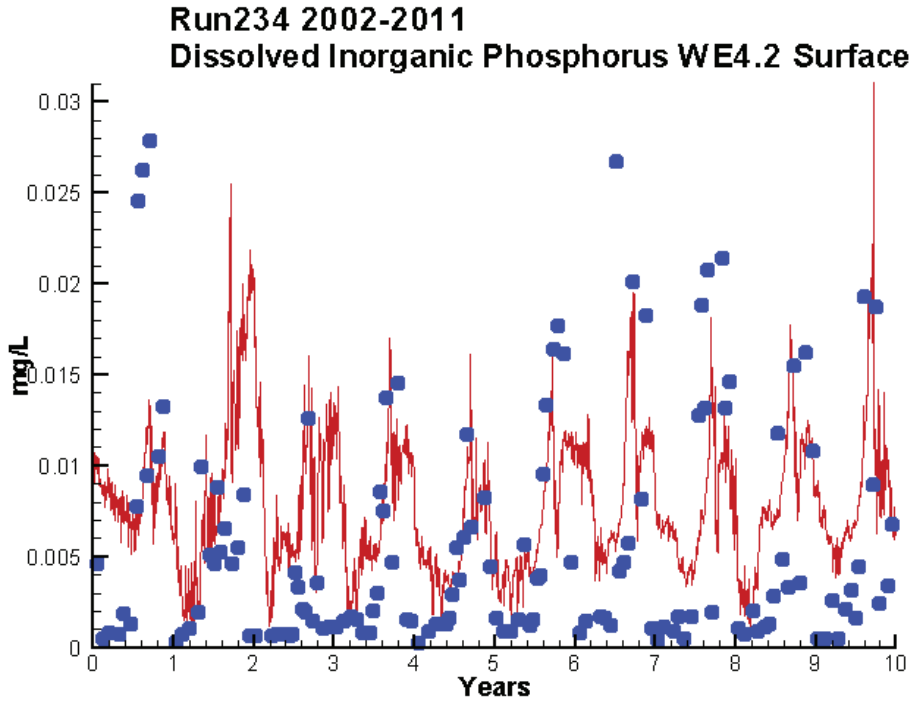

Station WE4.2

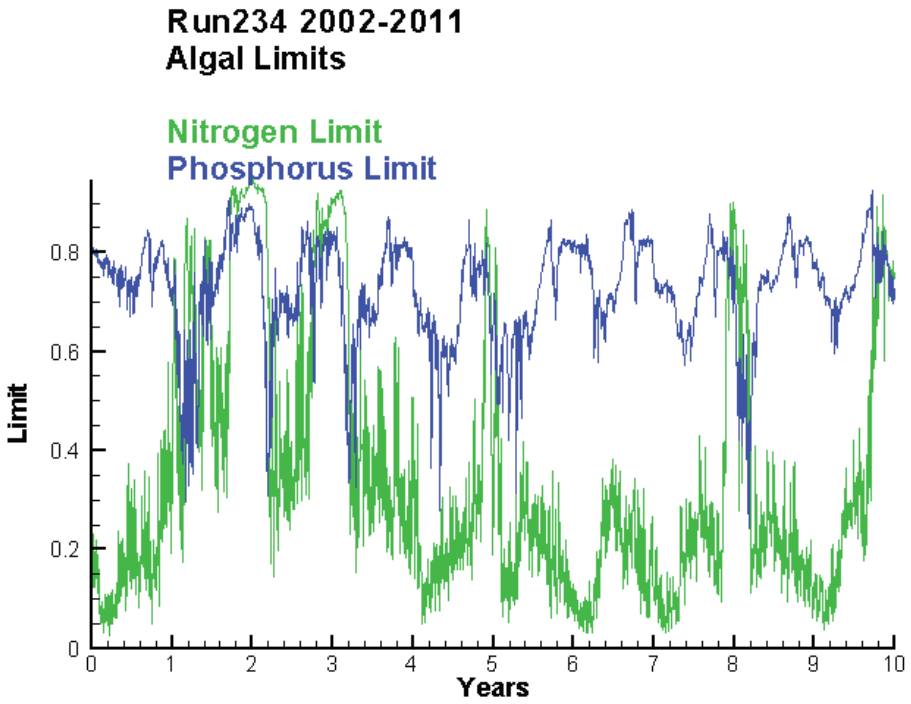

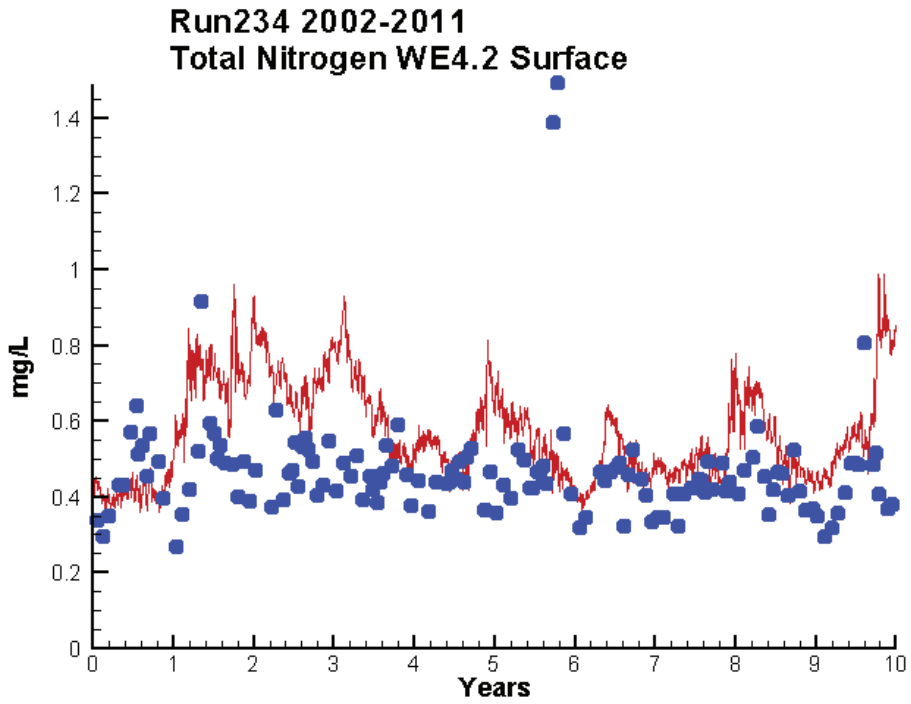

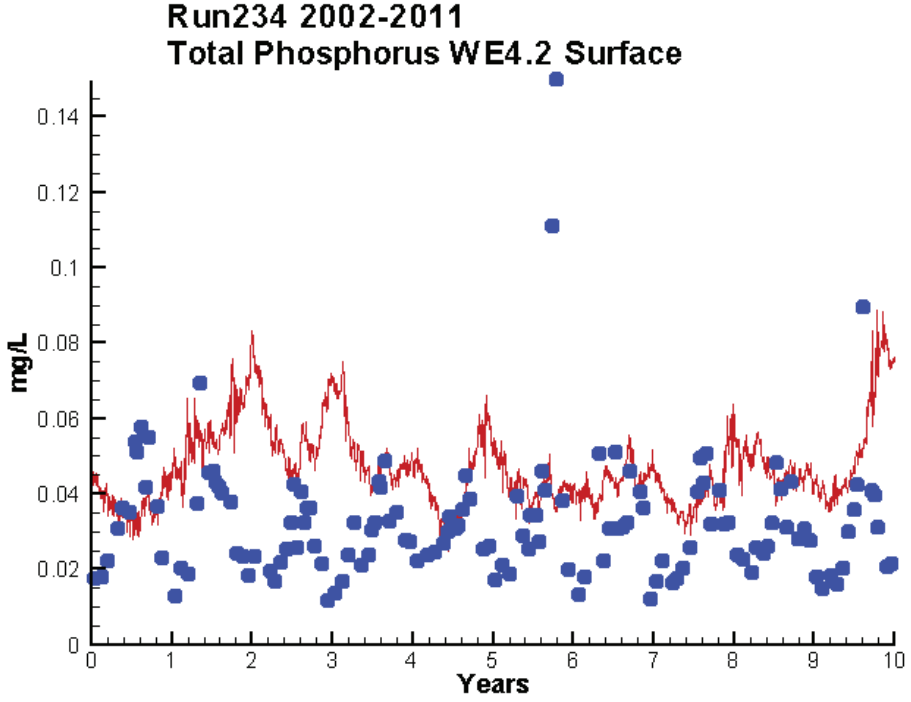

	Mean Difference	Absolute Mean Difference
Chl	-1.2838	4.4508
DIN	-0.0075	0.0422
KE	0.1833	0.4105
DIP	0.0020	0.0052
TP	0.0142	0.0196
TN	0.1080	0.1594

Station WE4.2

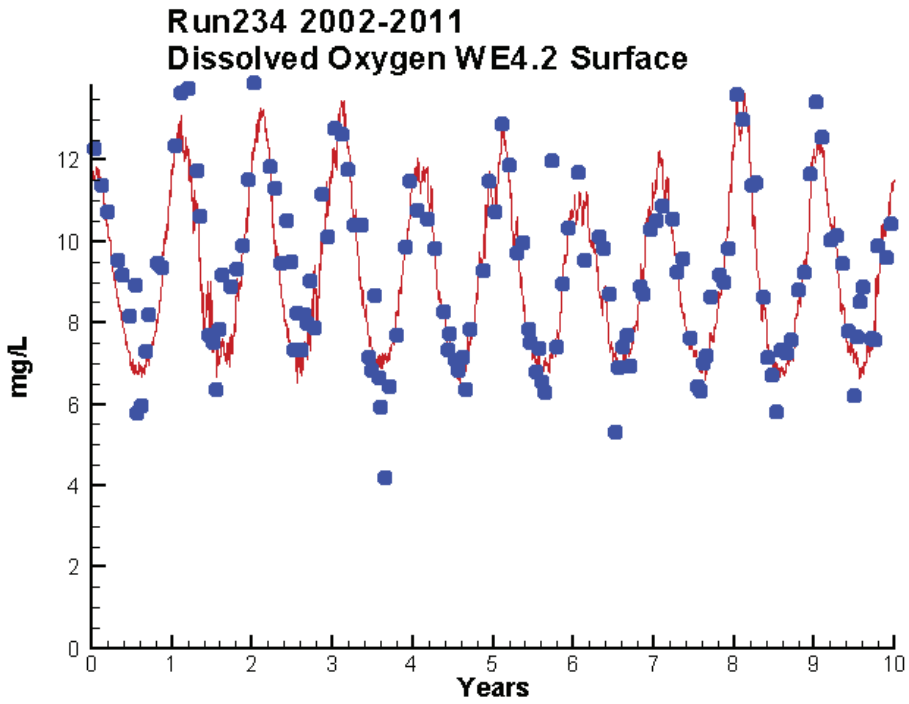

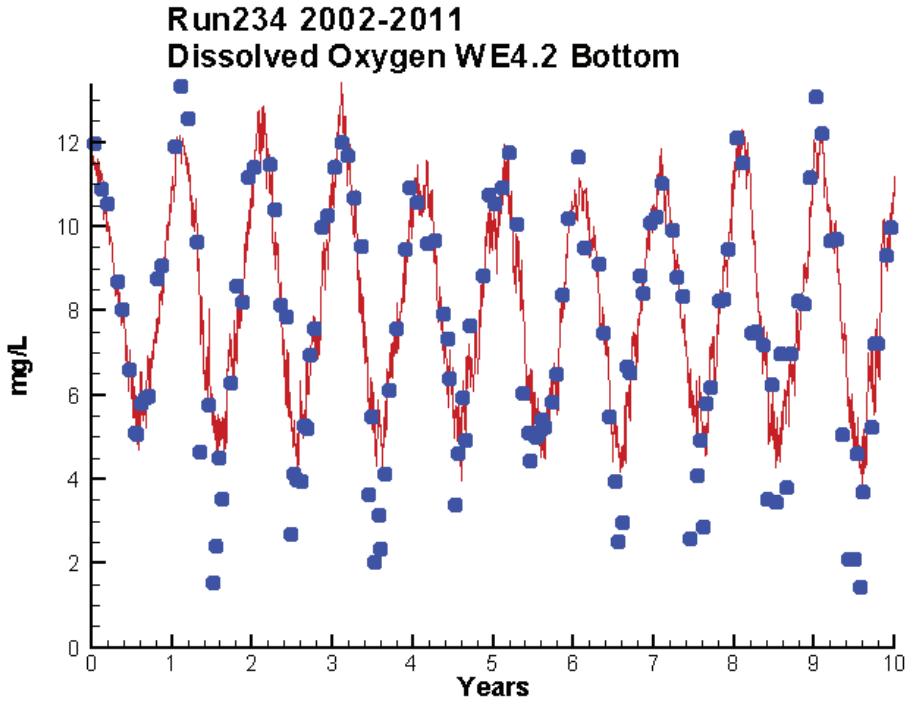

	Mean Difference	Absolute Mean Difference
Top DO	-0.2166	0.7274
Bot DO	0.4051	0.9411

Station WE4.2

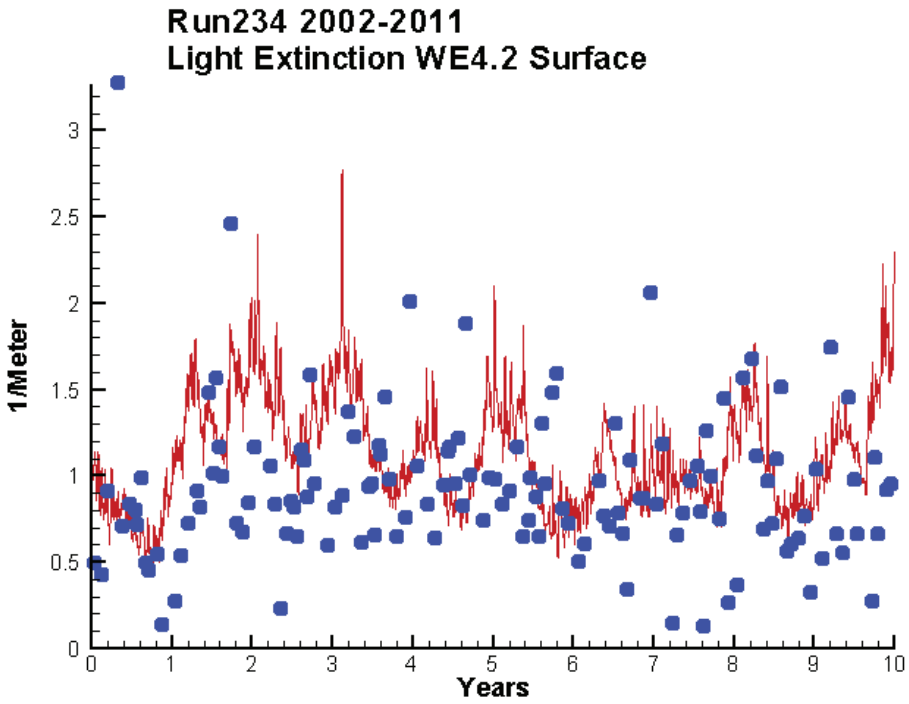

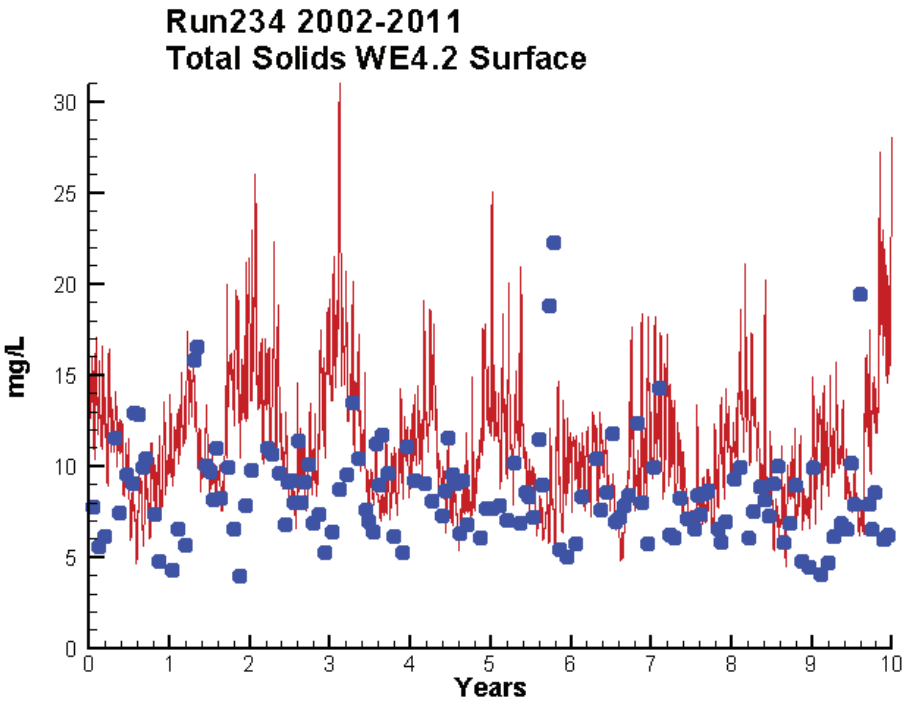

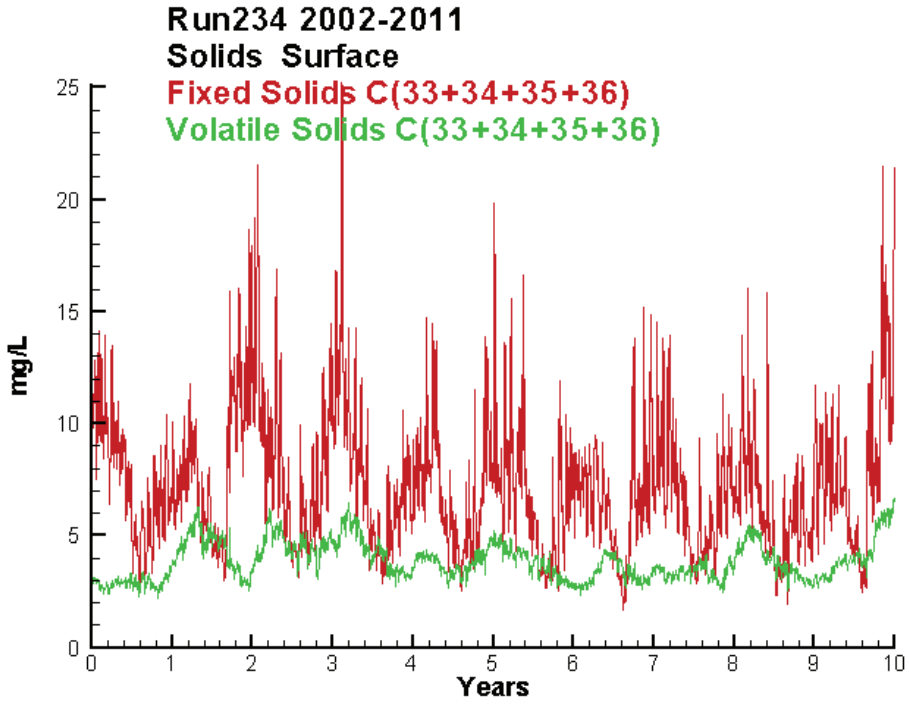

	Mean Difference	Absolute Mean Difference
KE	0.1833	0.4105
TSS	2.1126	3.6486

Station WT1.1

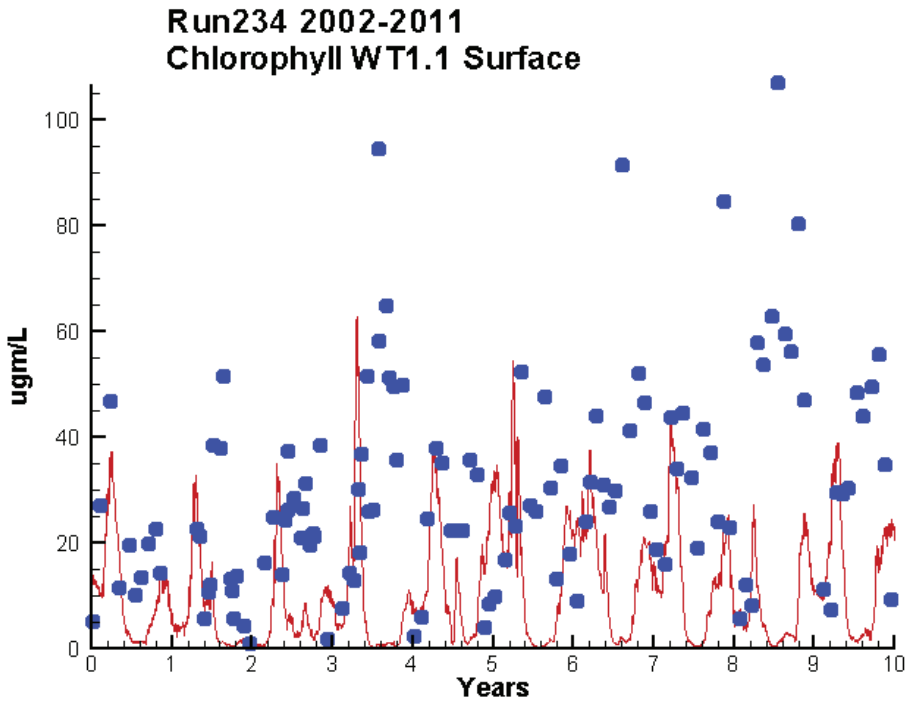

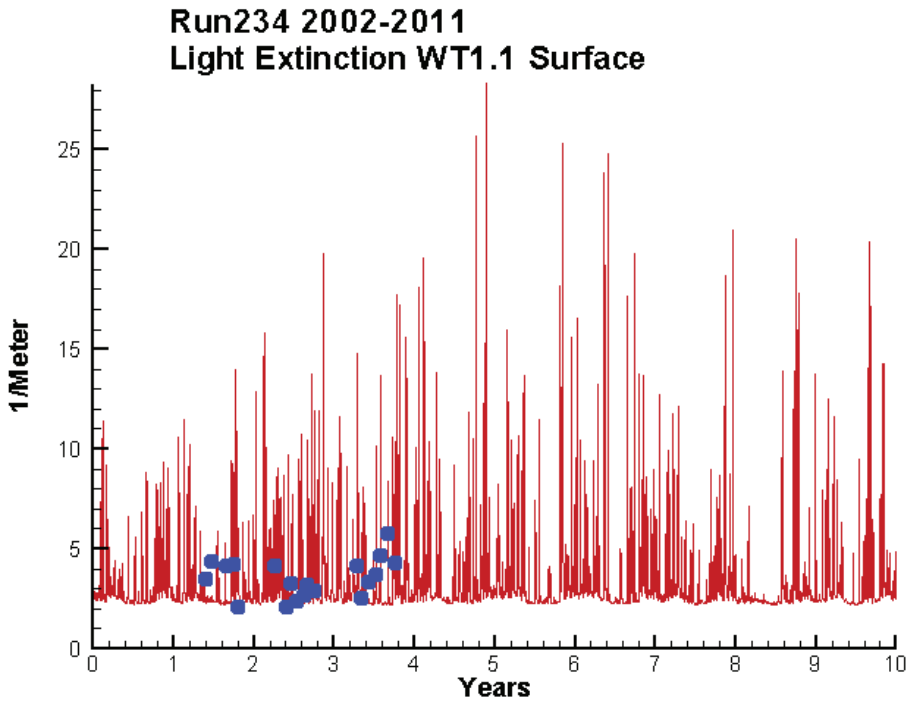

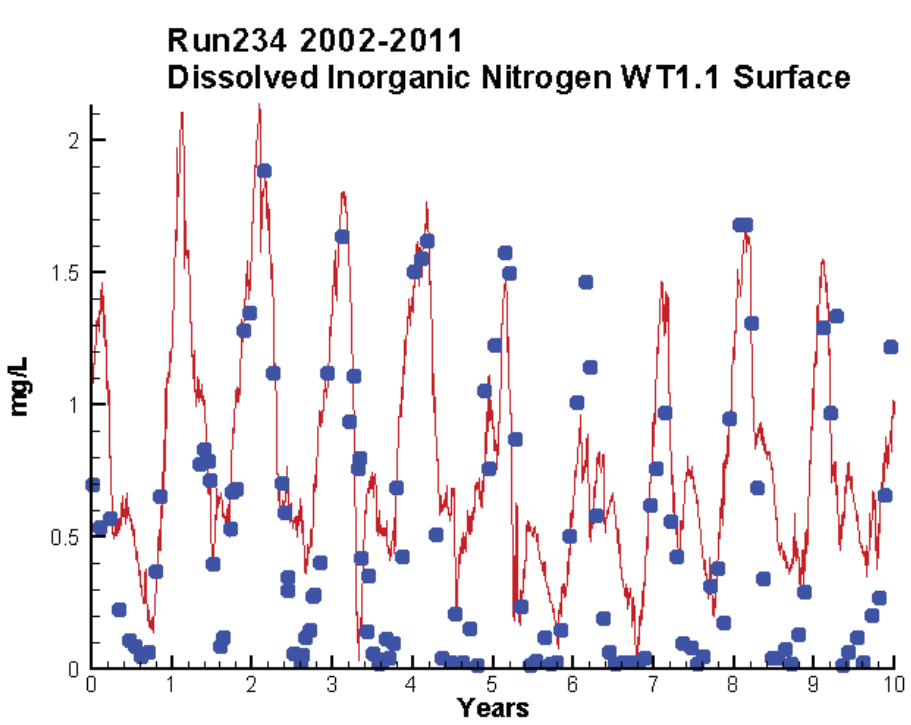

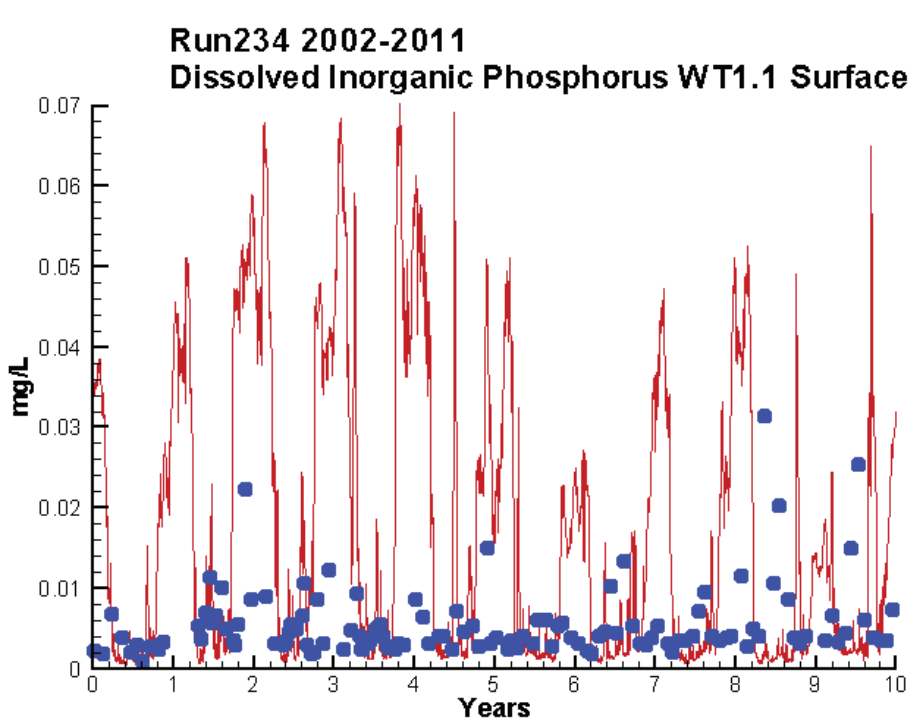

Station WT1.1

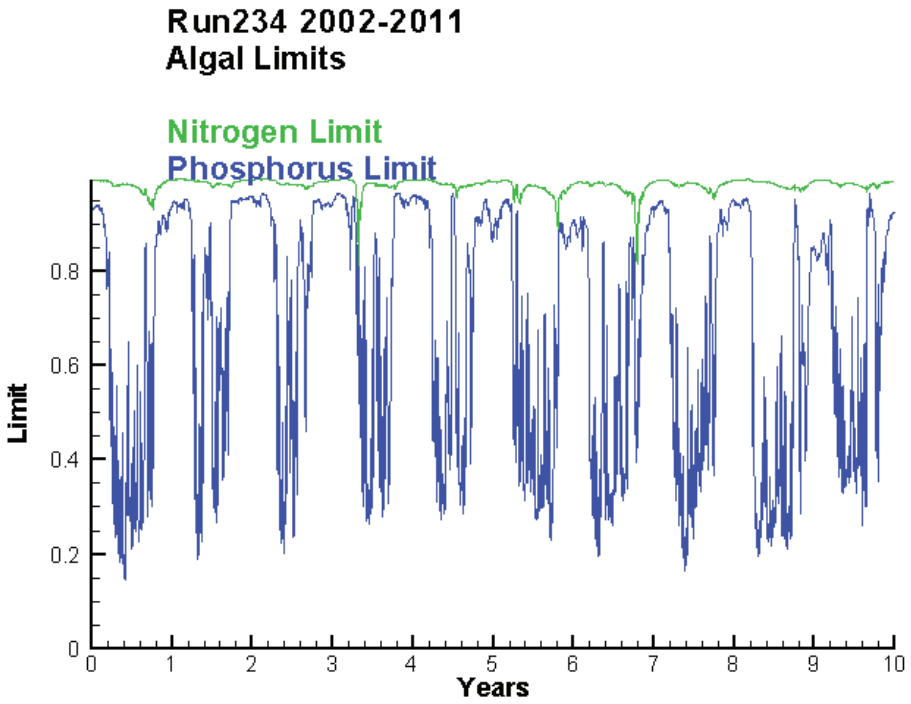

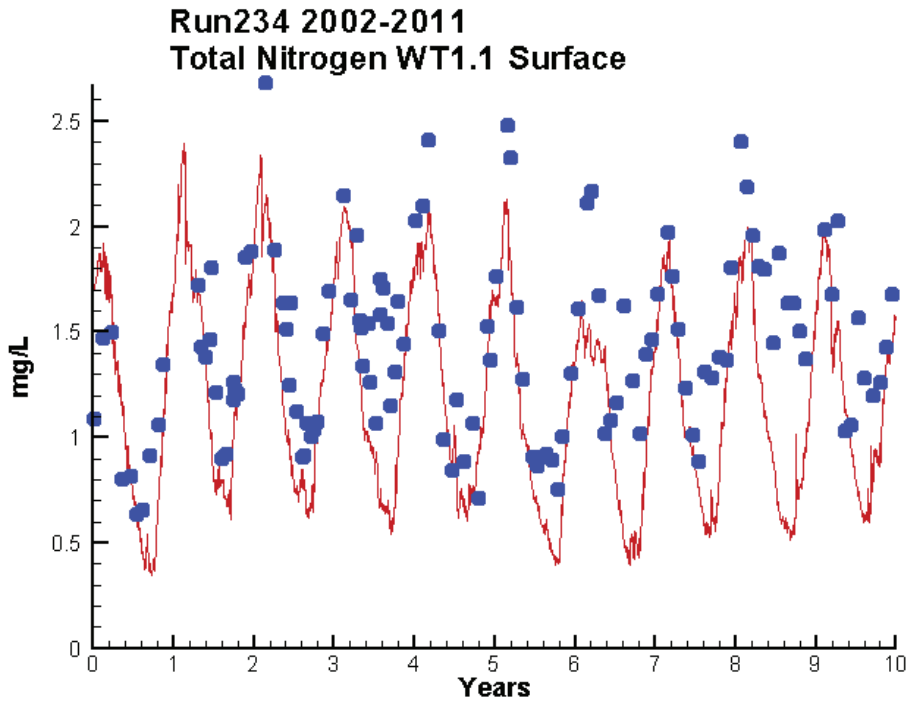

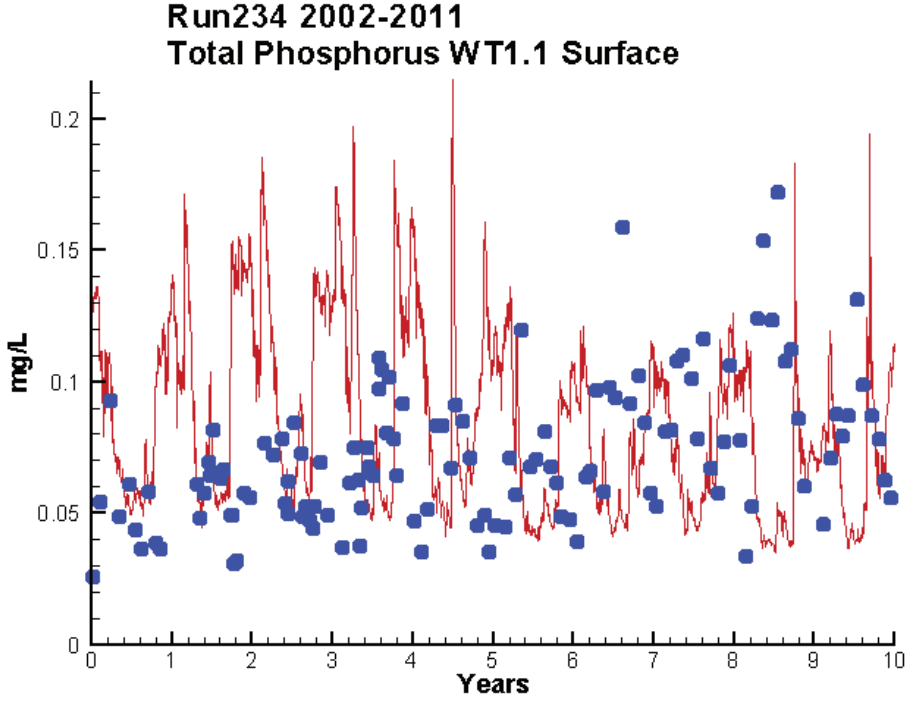

	Mean Difference	Absolute Mean Difference
Chl	-18.9517	22.9533
DIN	0.2153	0.3317
KE	0.1952	1.8020
DIP	0.0108	0.0142
TP	0.0116	0.0426
TN	-0.3090	0.3574

Station WT1.1

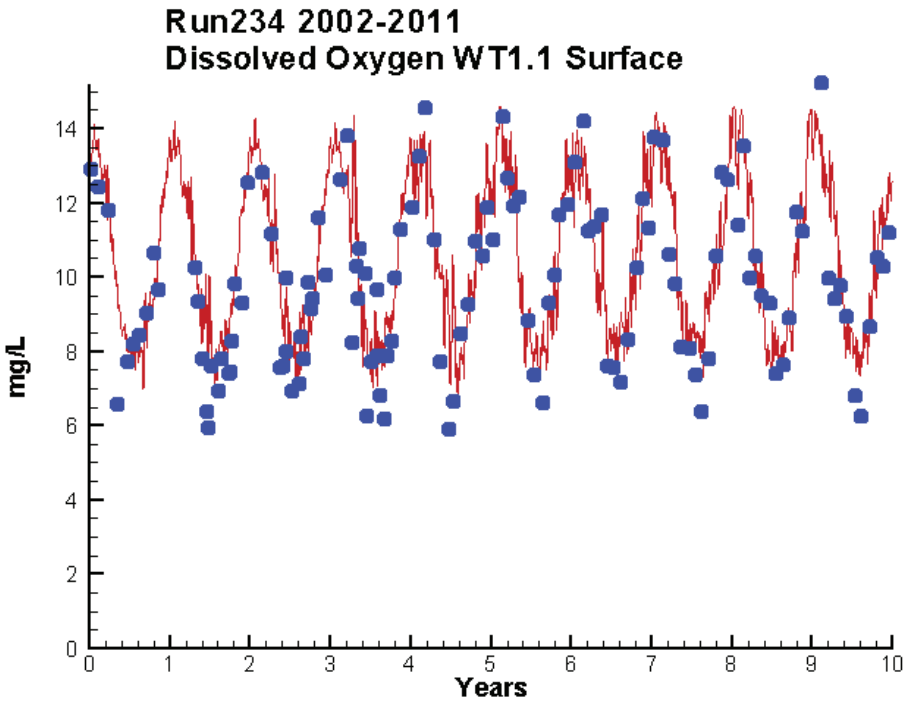

	Mean Difference	Absolute Mean Difference
Top DO	0.4902	1.0302

Station WT1.1

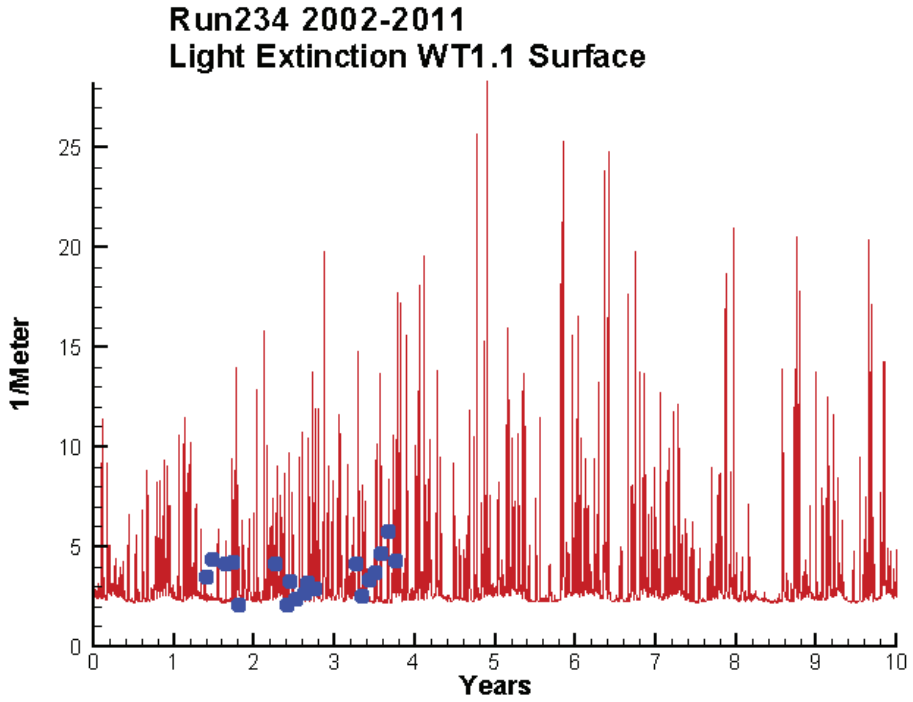

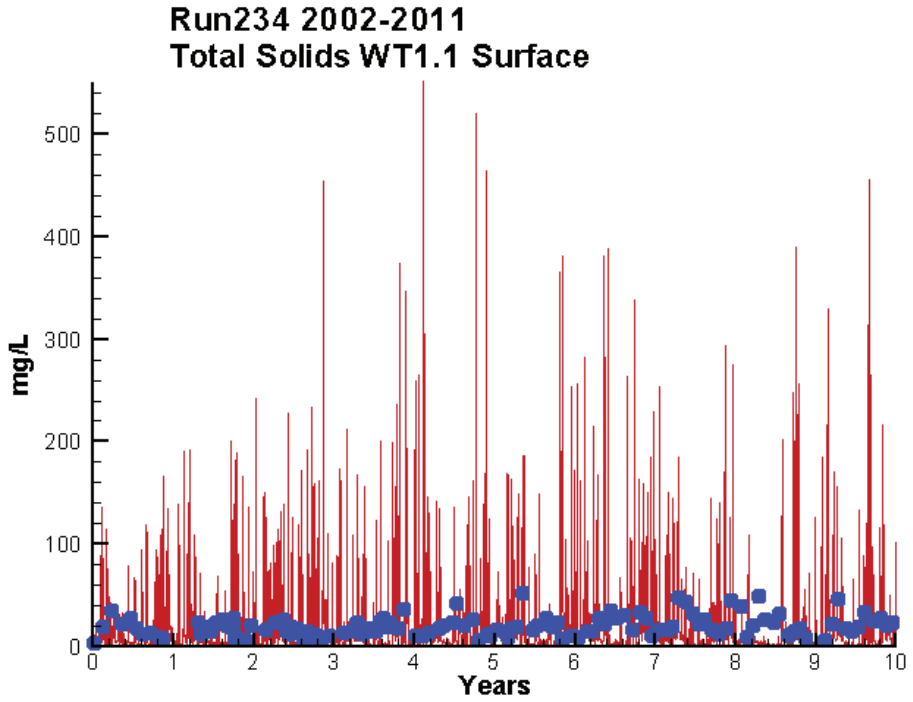

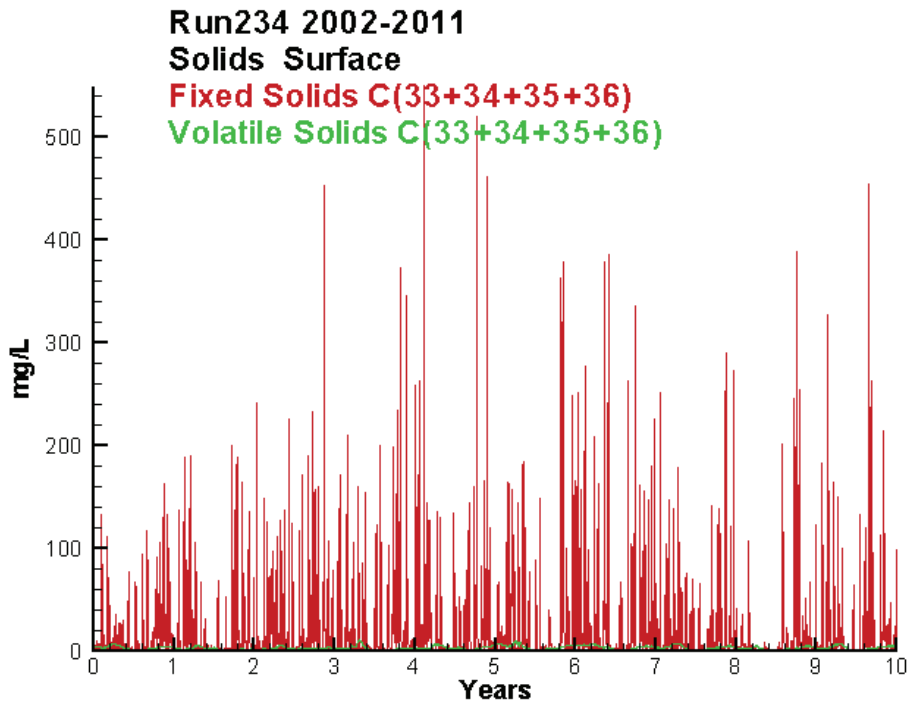

	Mean Difference	Absolute Mean Difference
KE	0.1952	1.8020
TSS	-0.9083	21.2098

Station WT2.1

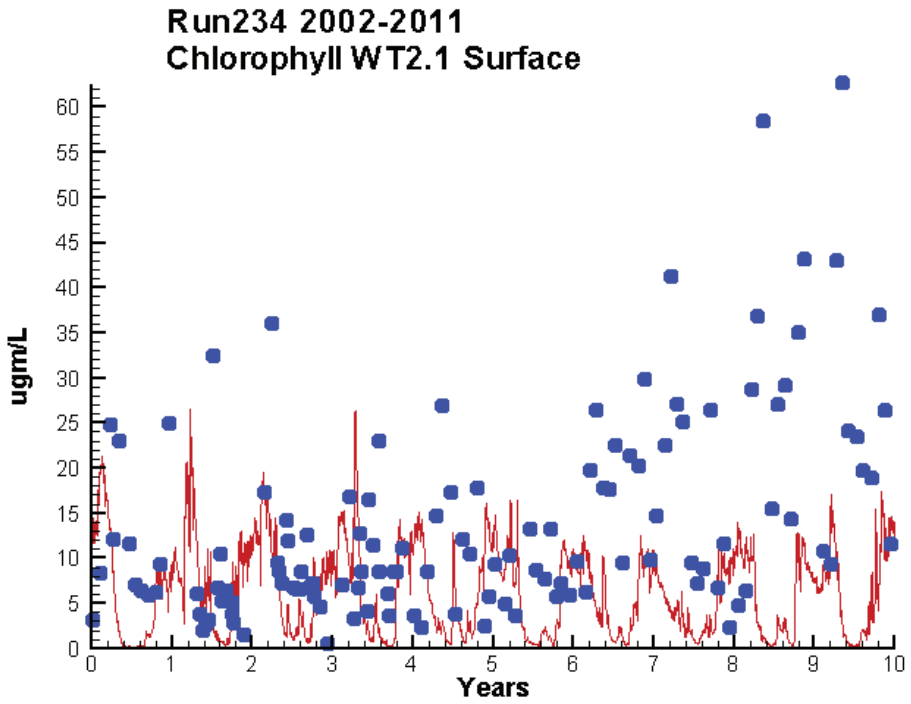

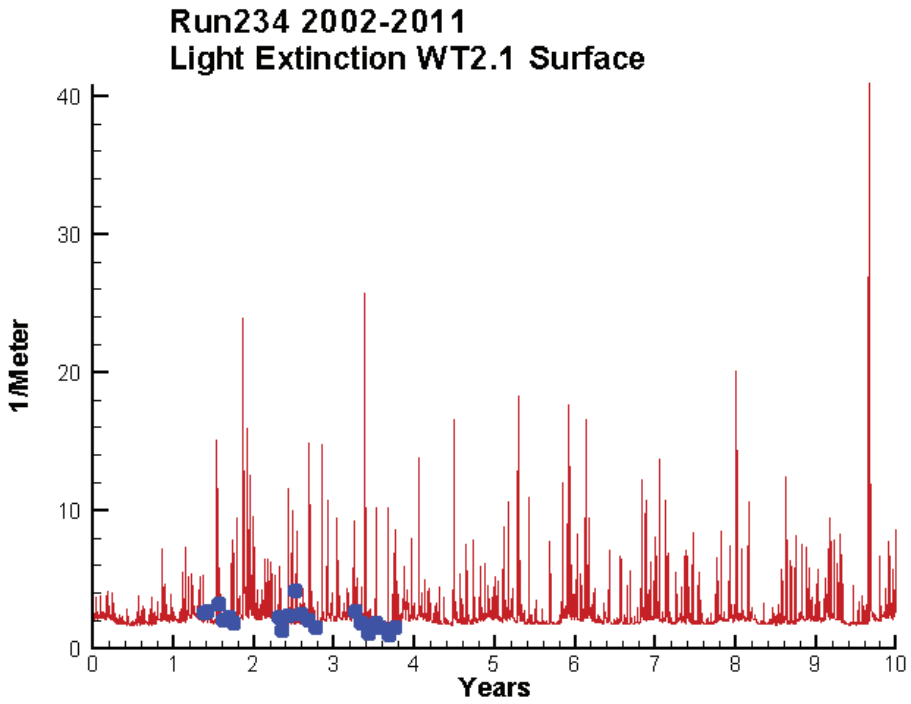

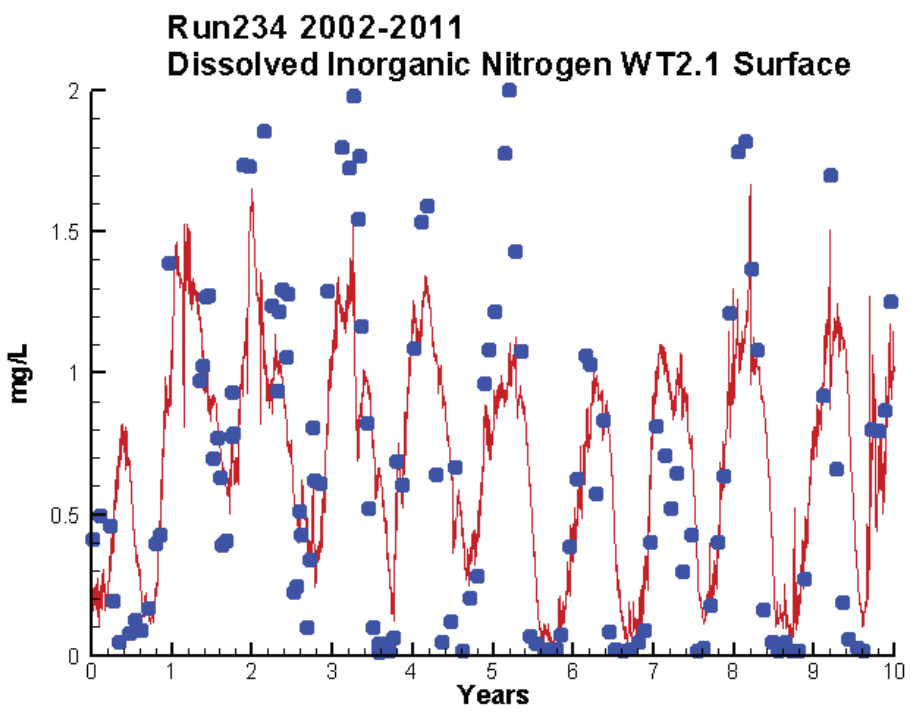

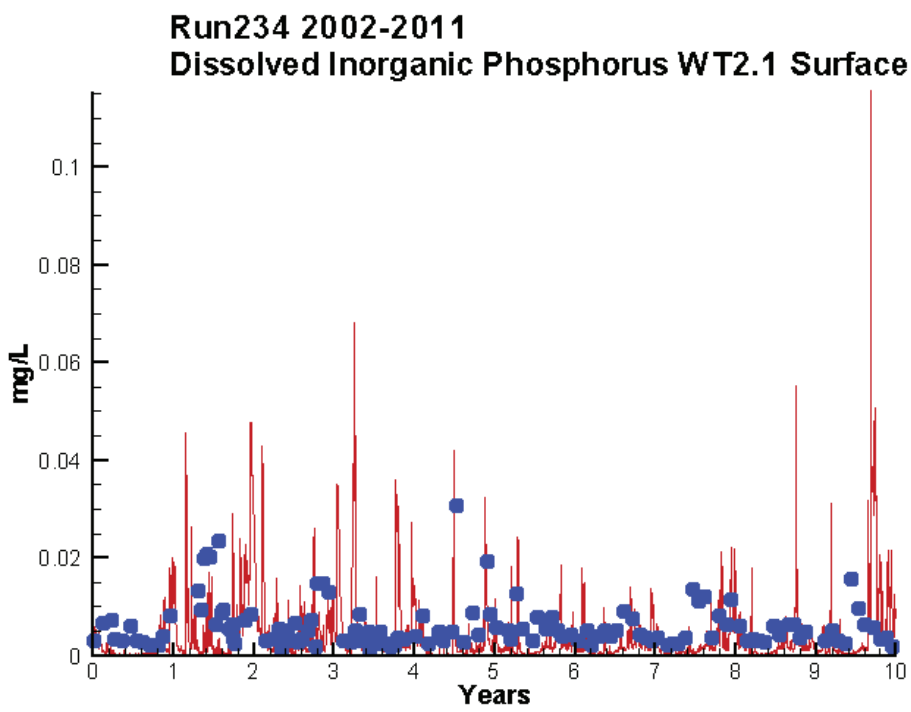

Station WT2.1

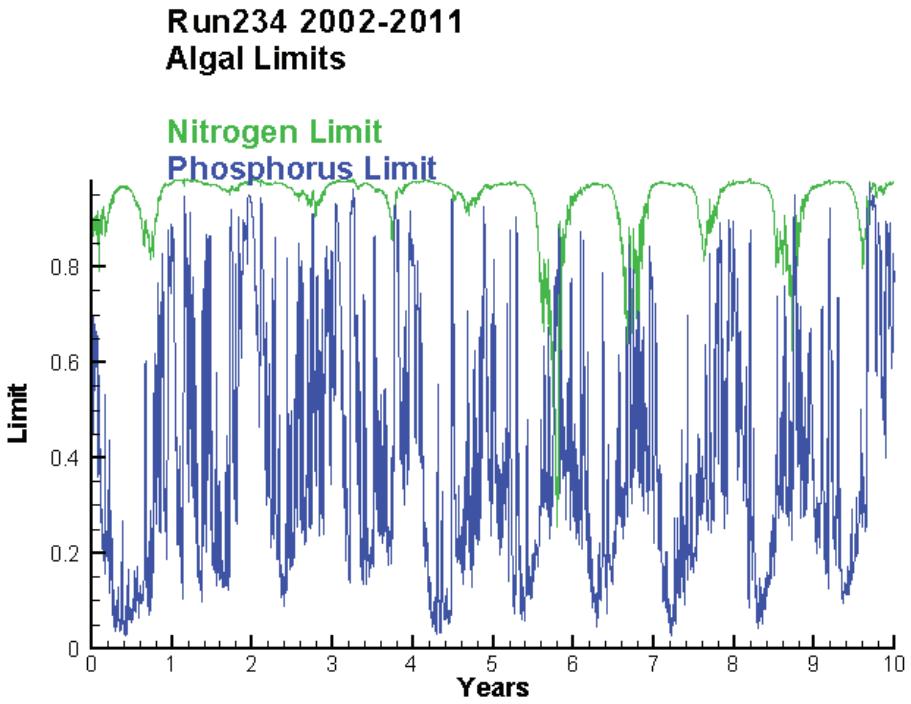

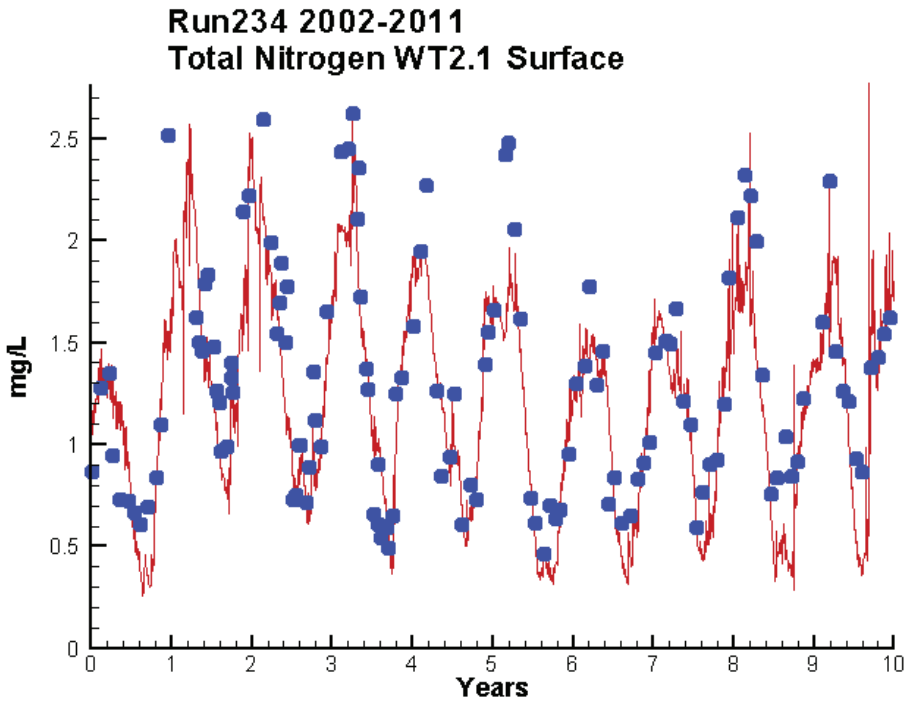

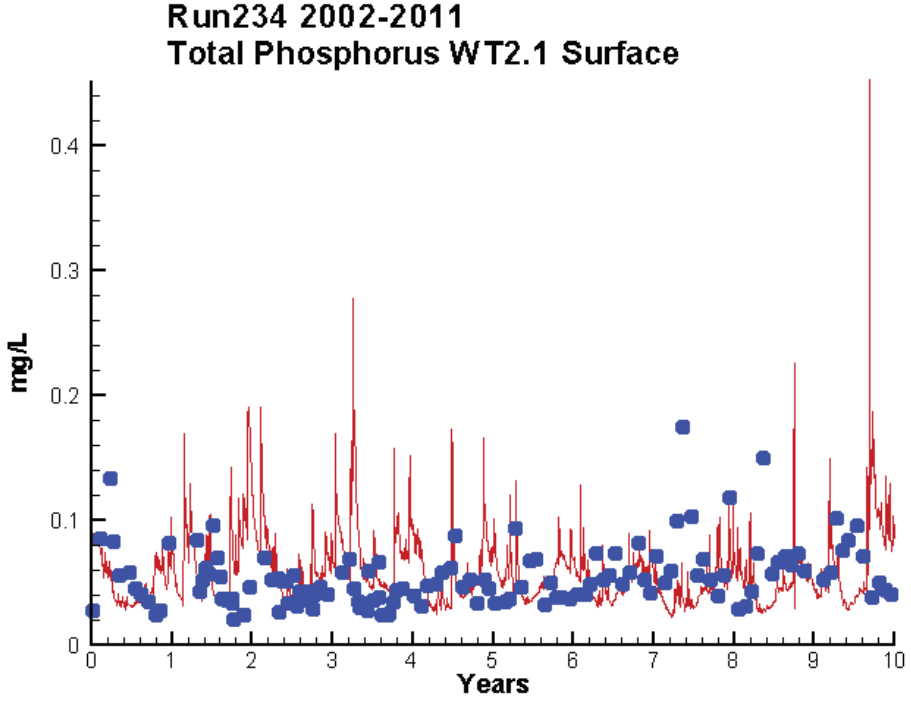

	Mean Difference	Absolute Mean Difference
Chl	-7.9155	10.9743
DIN	0.0119	0.3052
KE	0.5595	1.0273
DIP	-0.0022	0.0054
TP	0.0040	0.0294
TN	-0.1168	0.2396

Station WT2.1

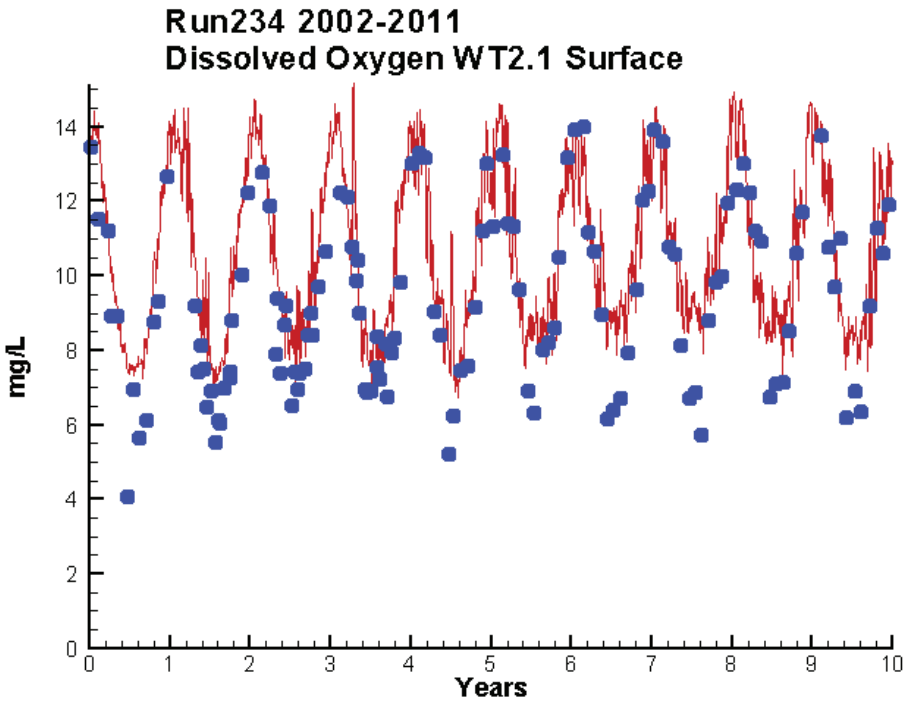

	Mean Difference	Absolute Mean Difference
Top DO	1.0105	1.3018

Station WT2.1

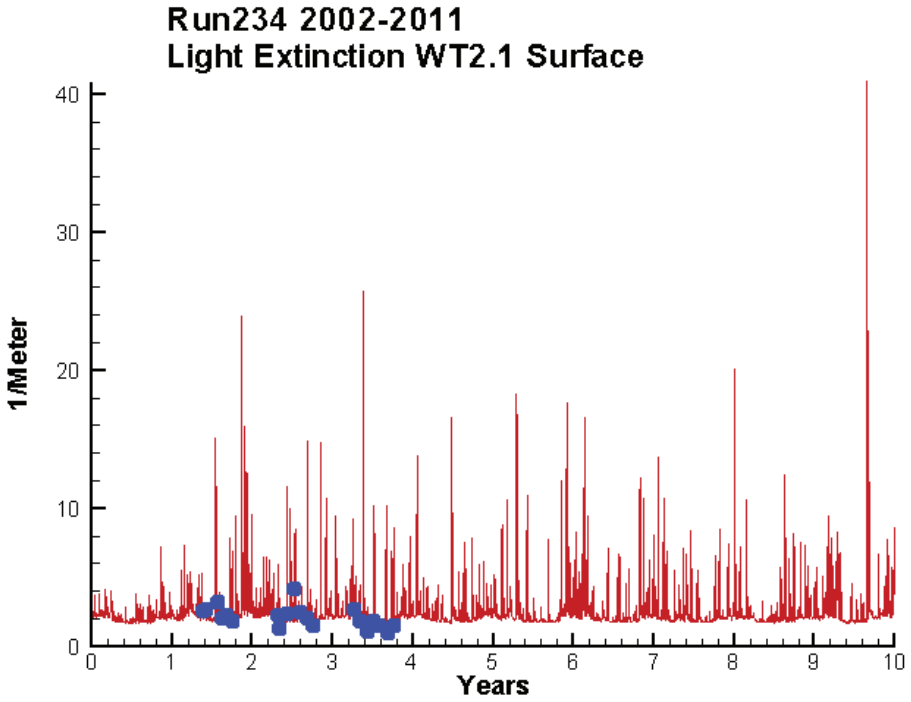

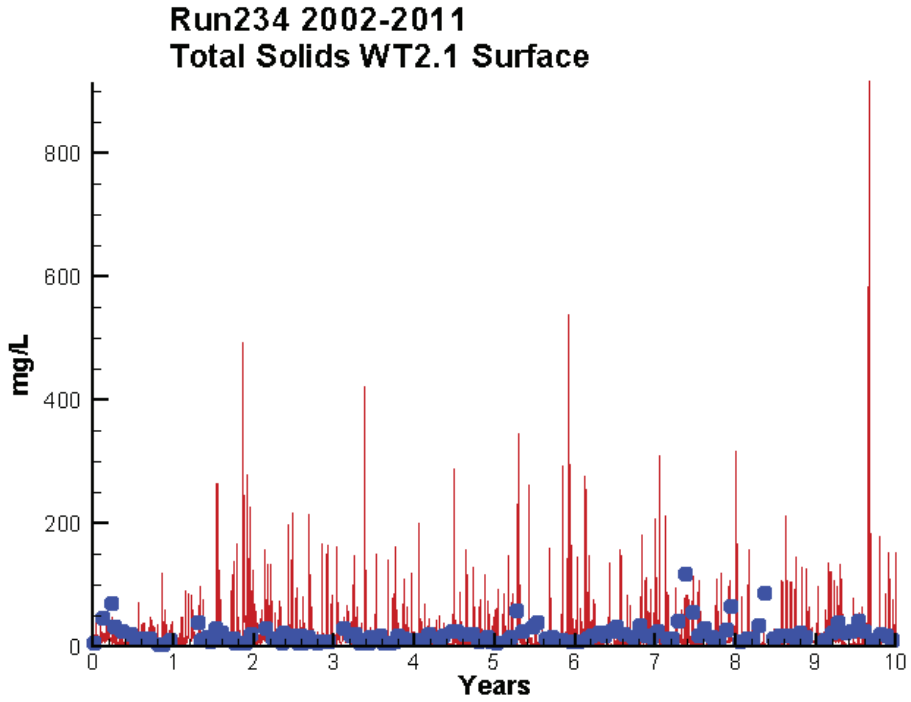

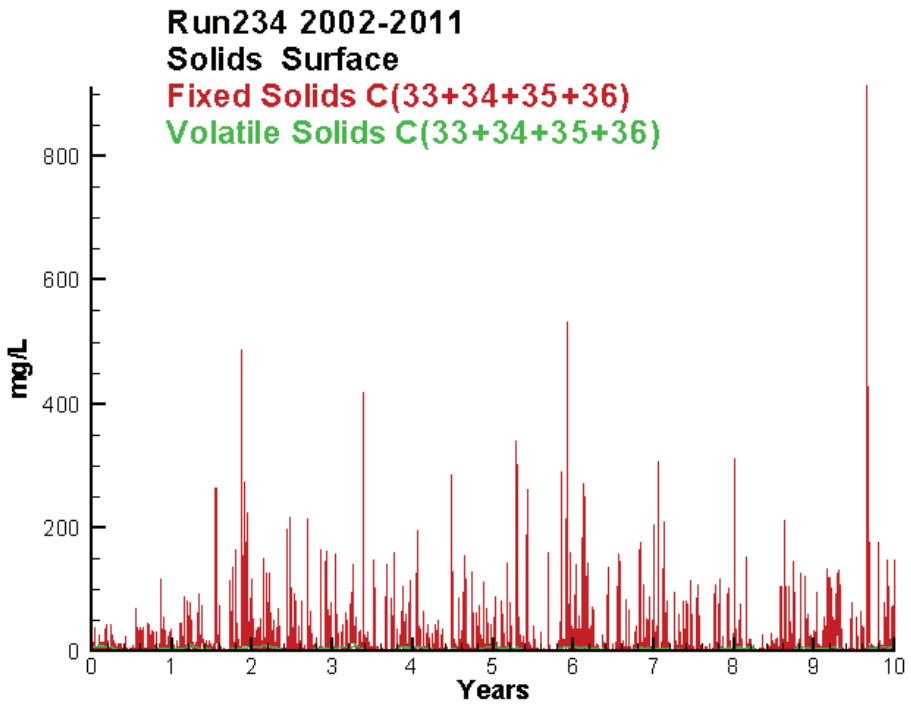

	Mean Difference	Absolute Mean Difference
KE	0.5595	1.0273
TSS	-2.7647	17.9455

Station WT5.1

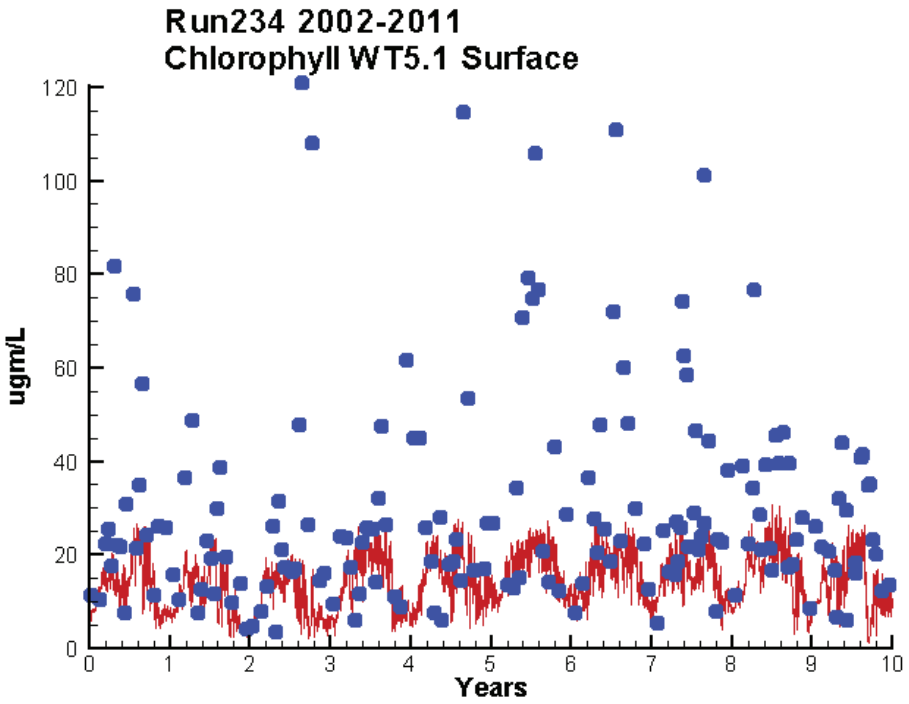

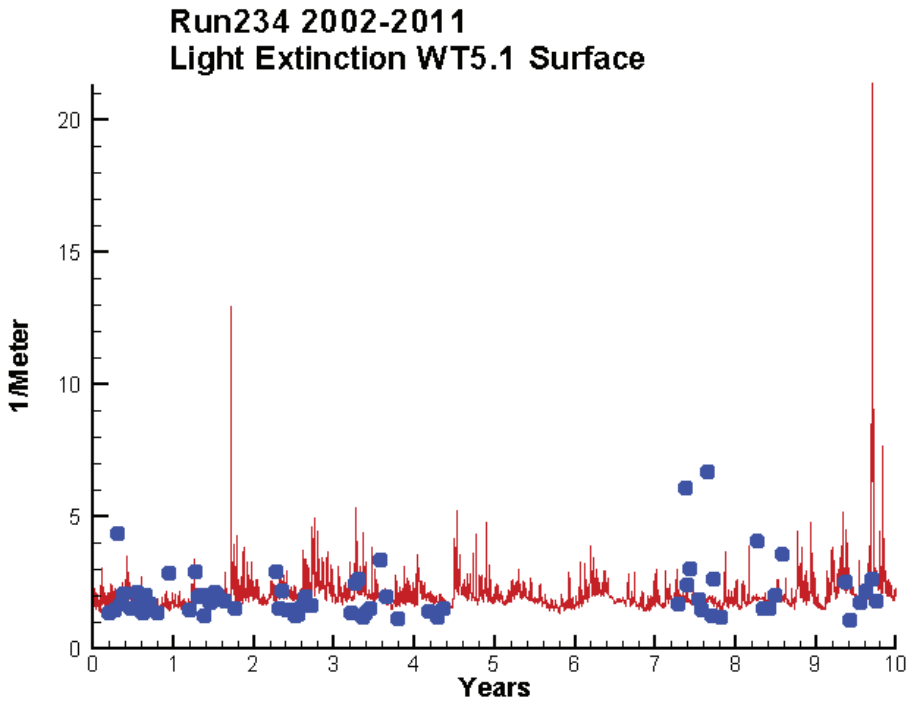

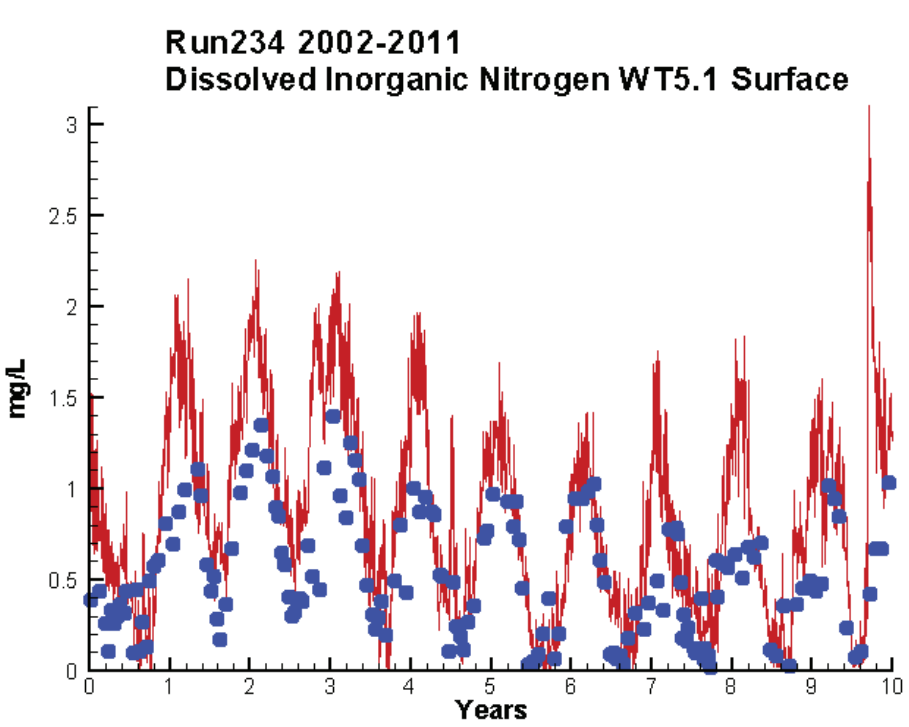

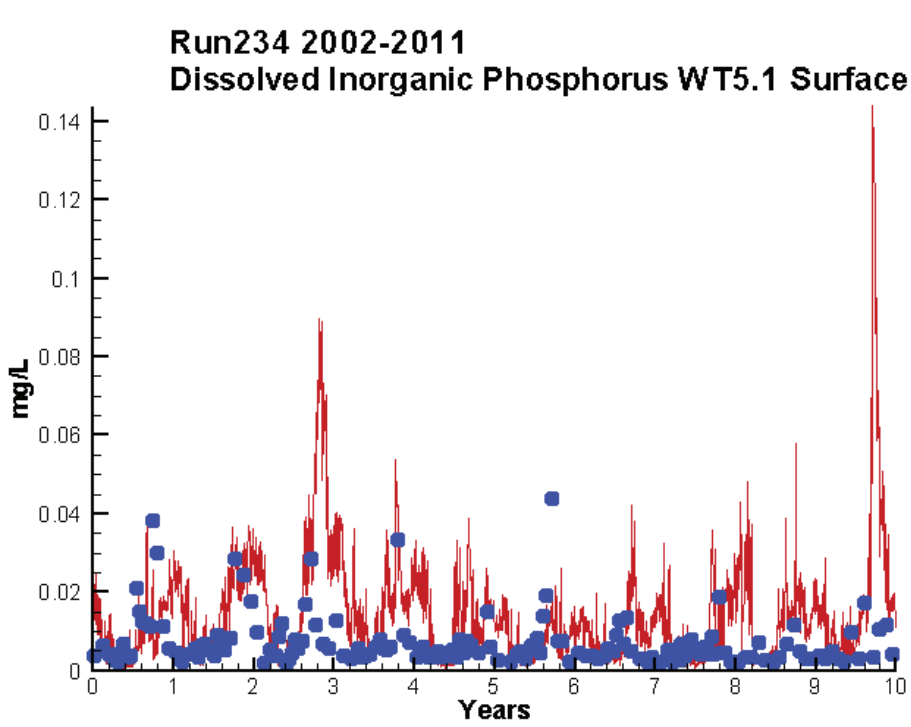

Station WT5.1

Run234 2002-2011
Algal Limits

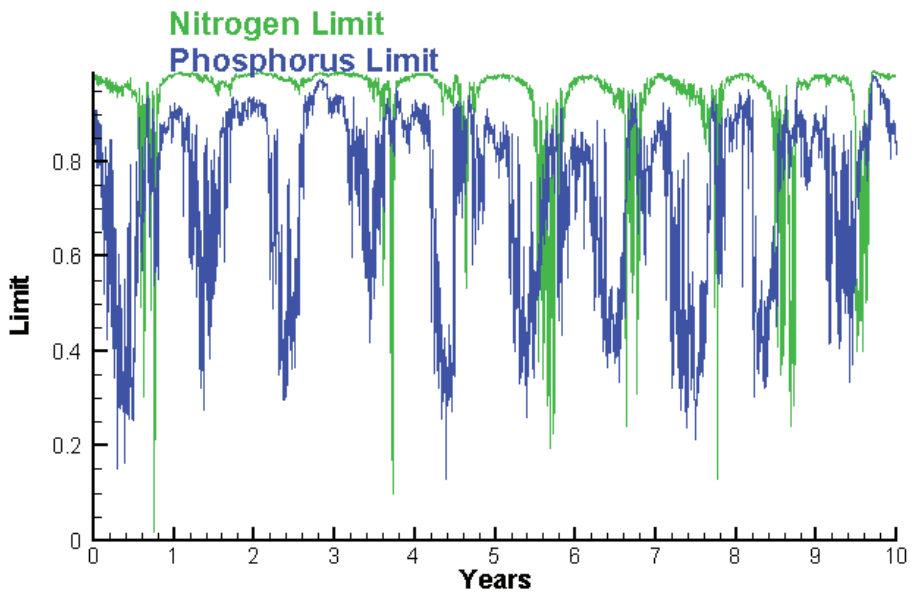

Run234 2002-2011
Total Nitrogen WT5.1 Surface

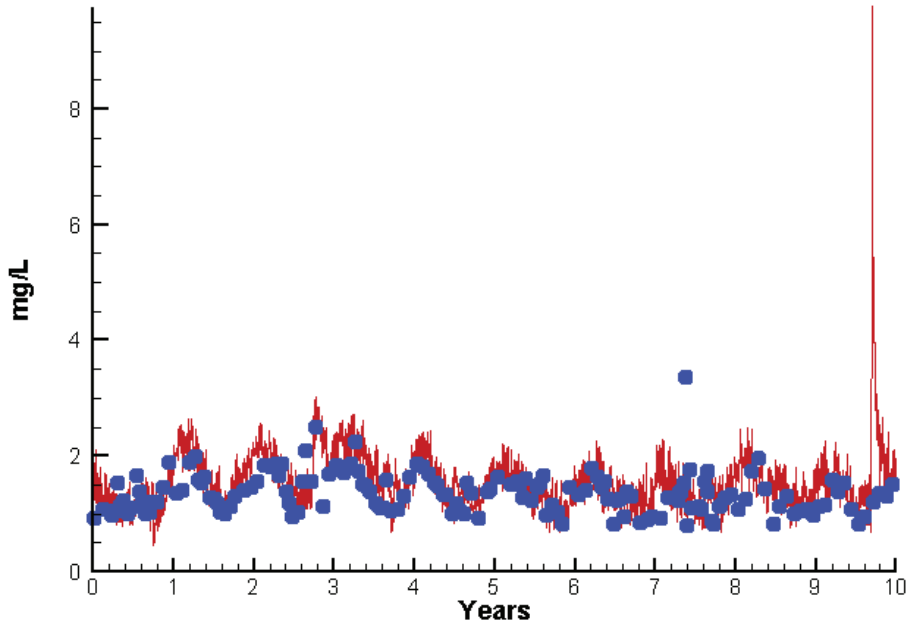

Run234 2002-2011
Total Phosphorus WT5.1 Surface

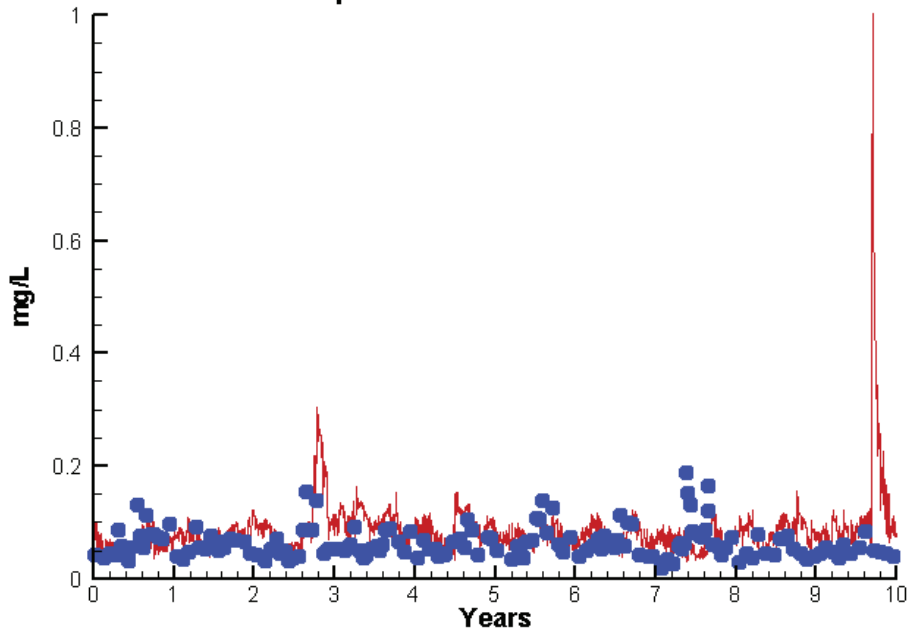

	Mean Difference	Absolute Mean Difference
Chl	-14.6263	17.3151
DIN	0.2481	0.2963
KE	0.1098	0.8723
DIP	0.0057	0.0090
TP	0.0192	0.0347
TN	0.1511	0.3291

Station WT5.1

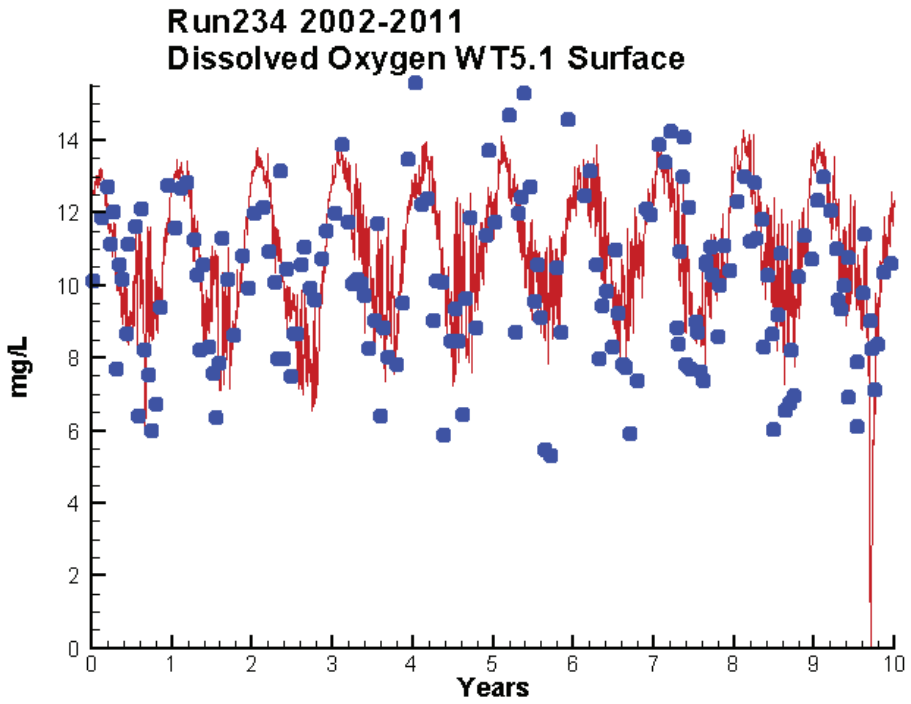

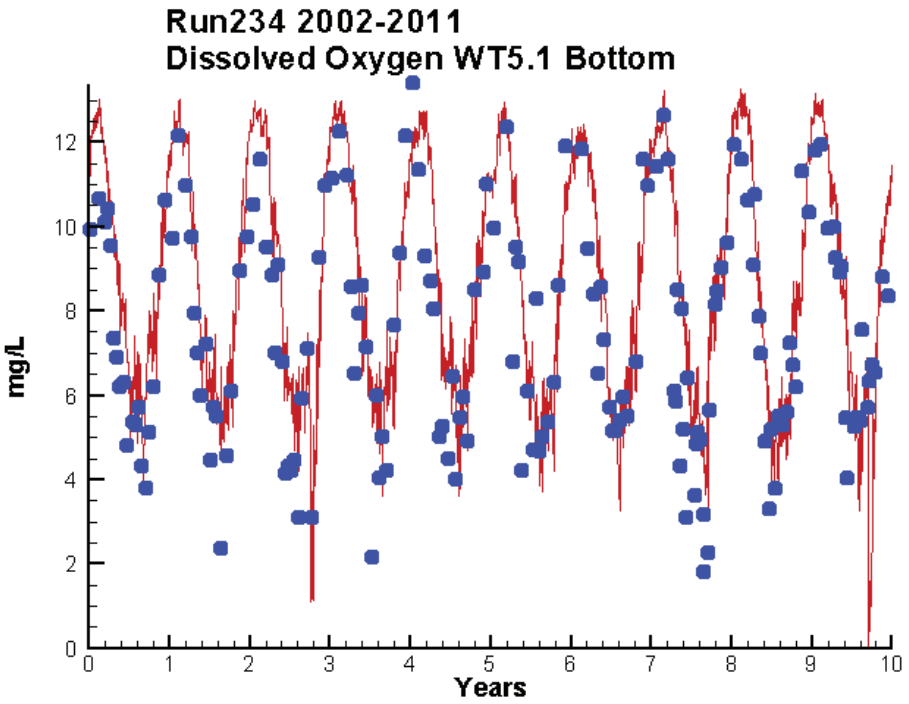

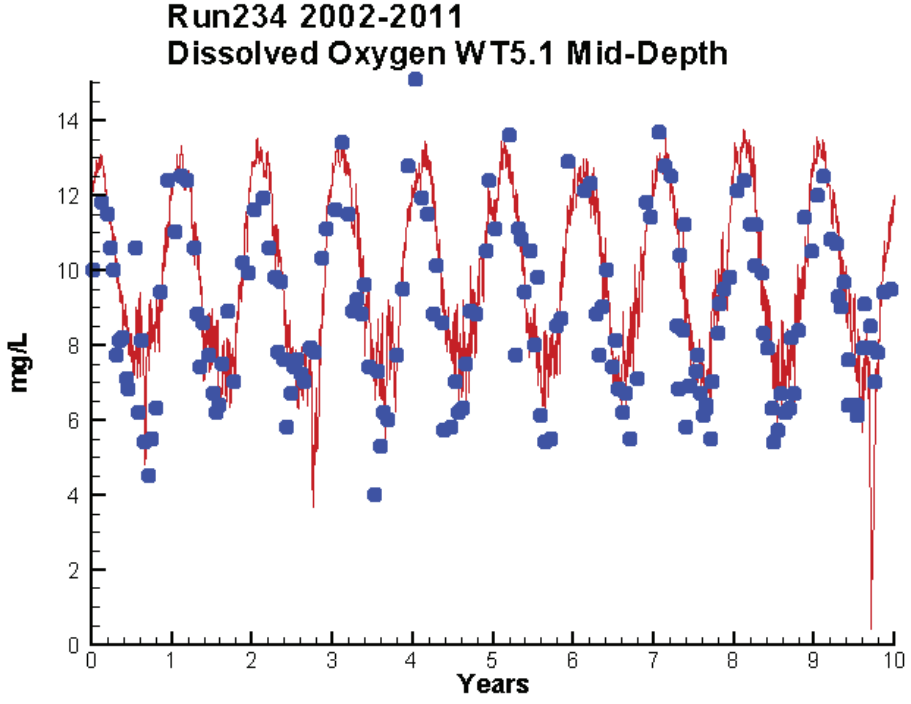

	Mean Difference	Absolute Mean Difference
Top DO	0.6357	1.6984
Mid DO	0.6830	1.3101
Bot DO	0.9034	1.3986

Station WT5.1

Run234 2002-2011
Light Extinction WT5.1 Surface

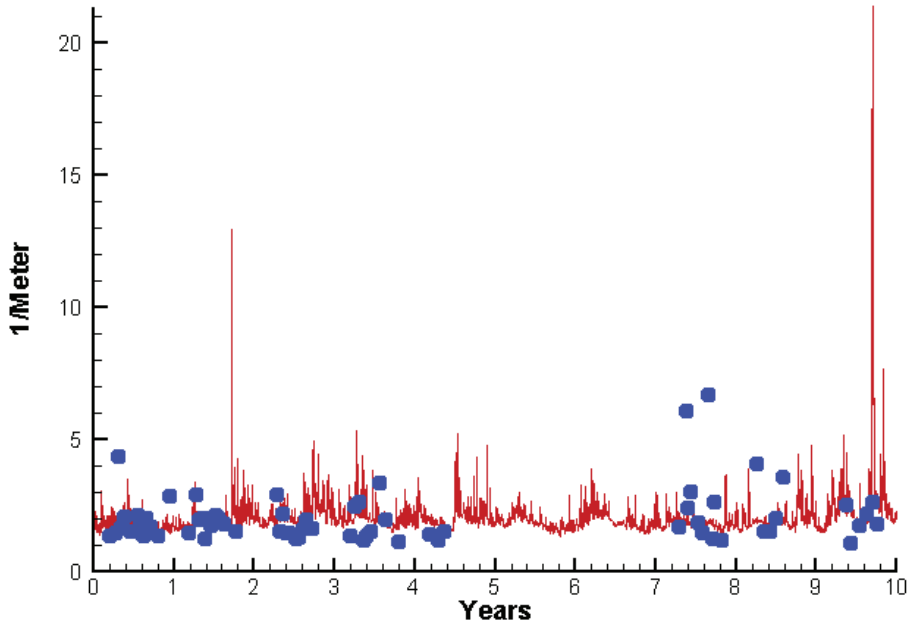

Run234 2002-2011
Total Solids WT5.1 Surface

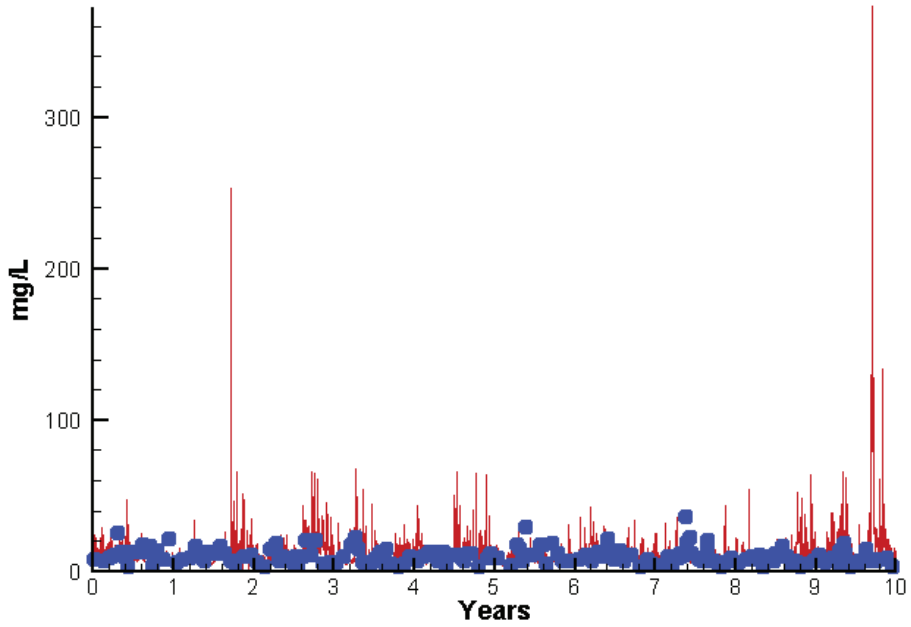

Run234 2002-2011
Solids Surface
Fixed Solids C(33+34+35+36)
Volatile Solids C(33+34+35+36)

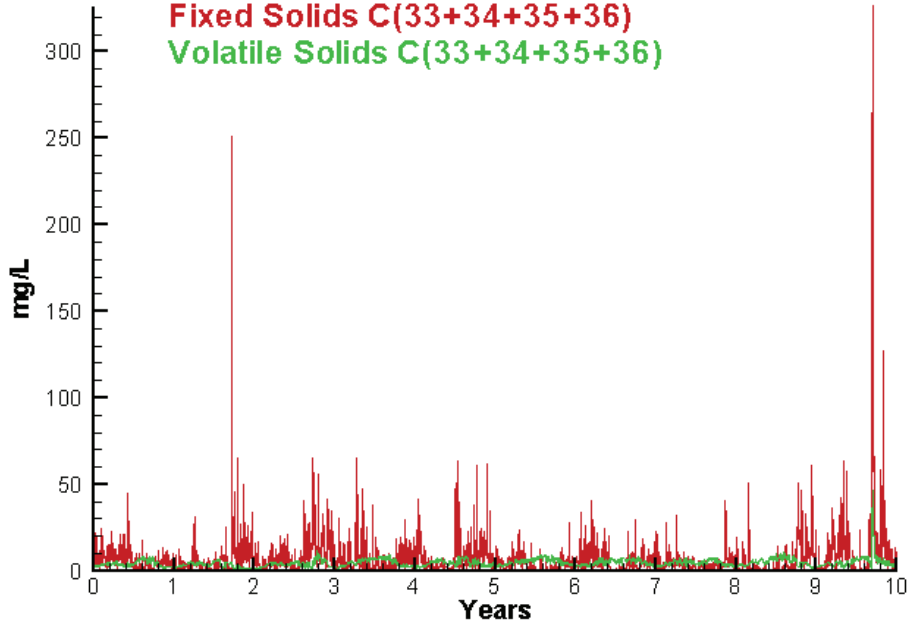

	Mean Difference	Absolute Mean Difference
KE	0.1098	0.8723
TSS	2.0189	6.6601

Station WT8.1

Run234 2002-2011
Chlorophyll WT8.1 Surface

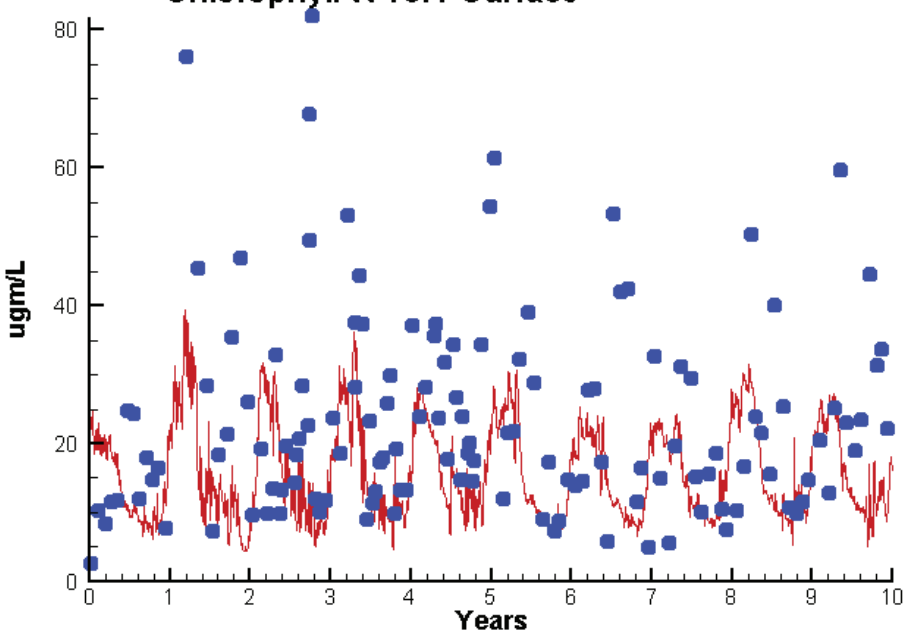

Run234 2002-2011
Light Extinction WT8.1 Surface

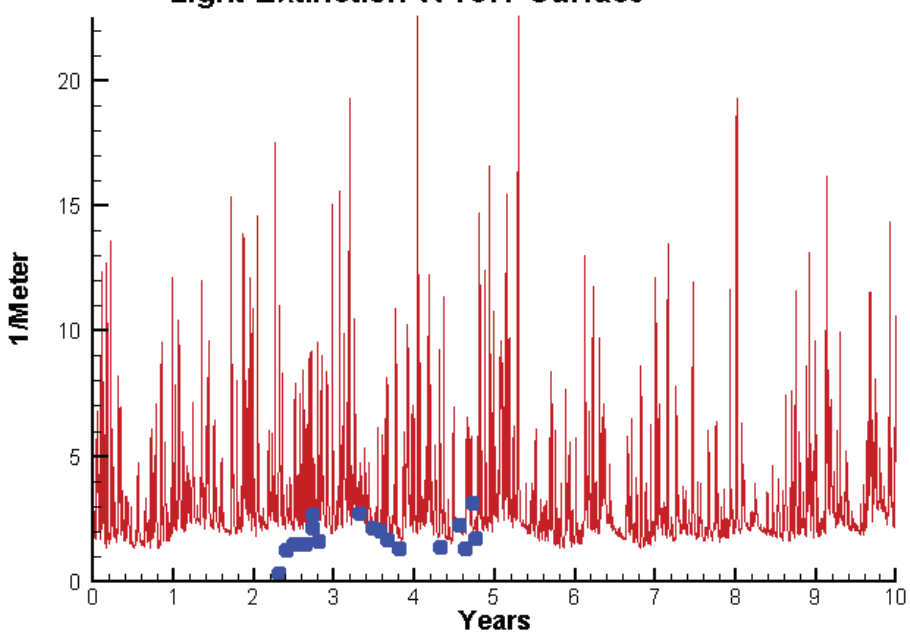

Run234 2002-2011
Dissolved Inorganic Nitrogen WT8.1 Surface

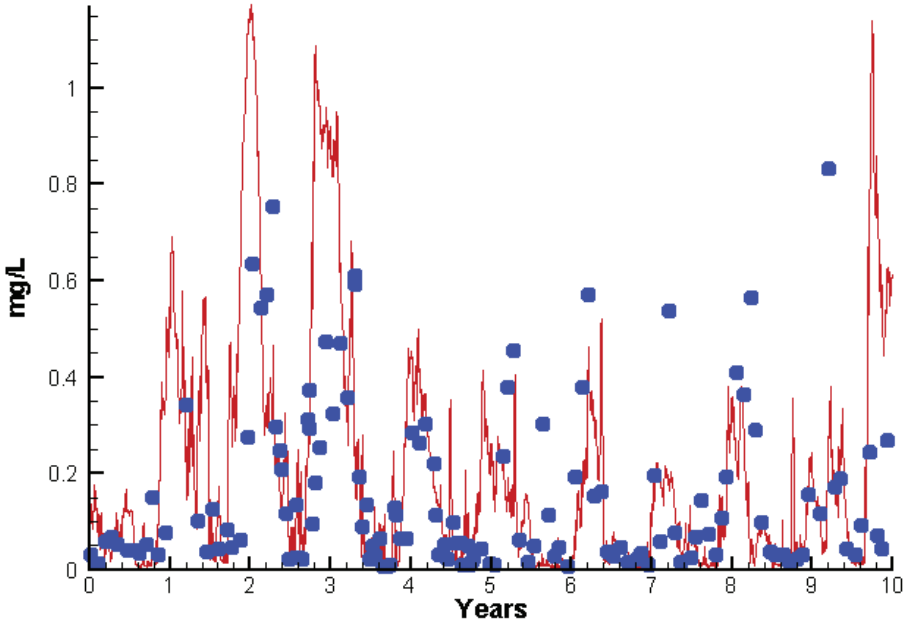

Run234 2002-2011
Dissolved Inorganic Phosphorus WT8.1 Surface

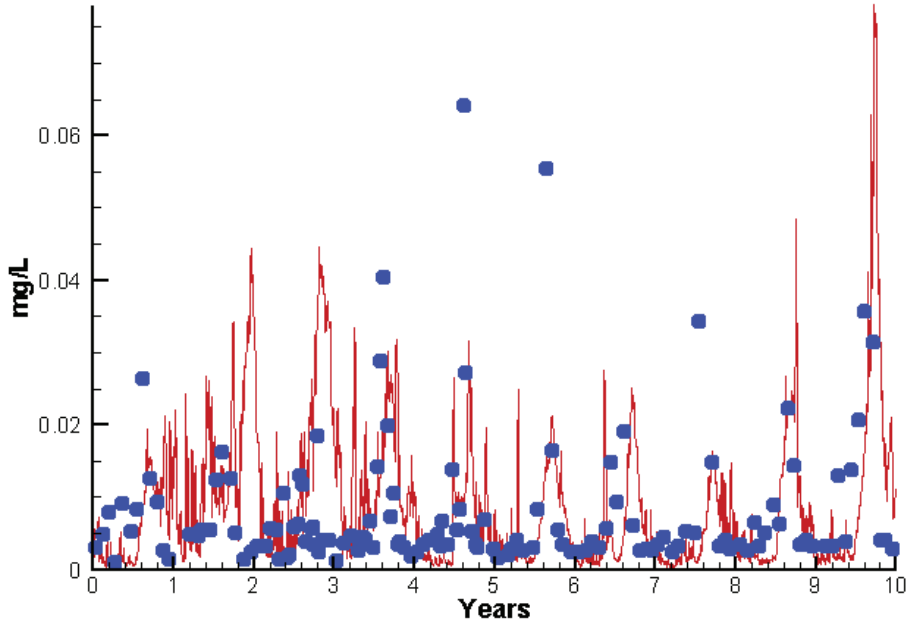

Station WT8.1

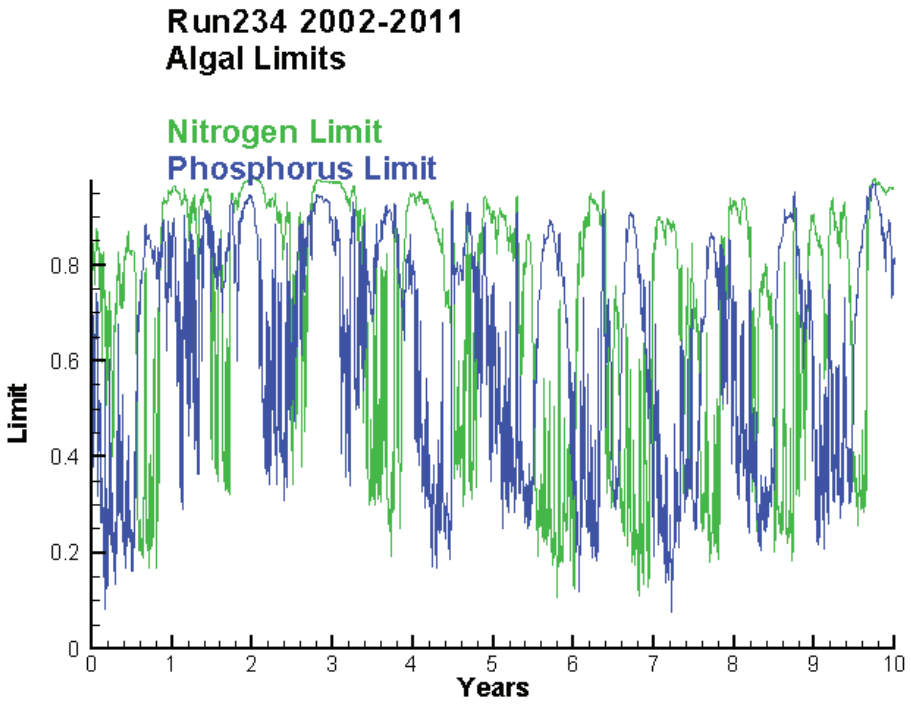

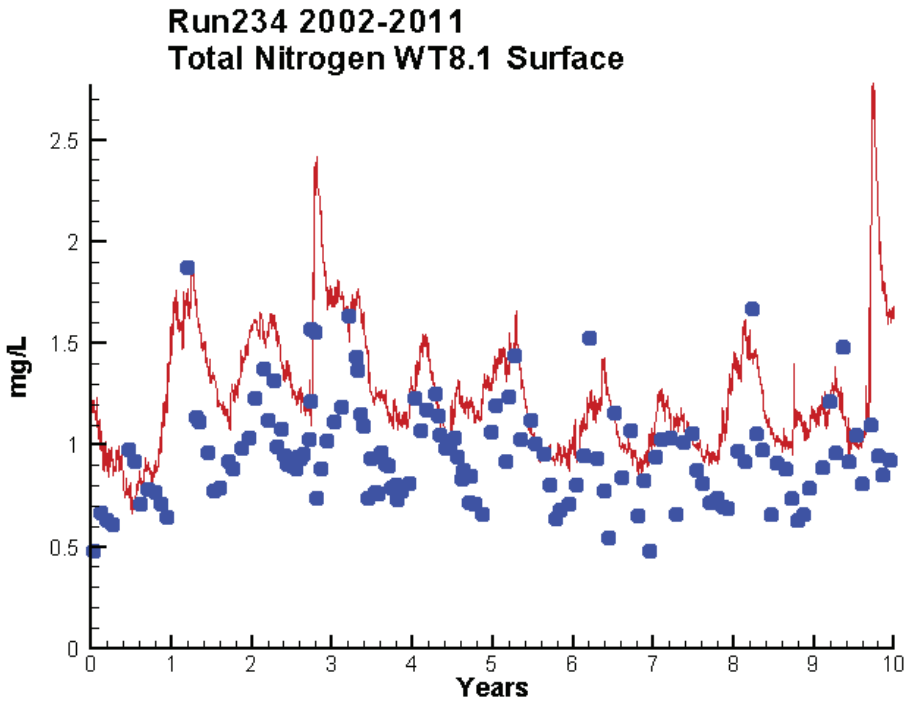

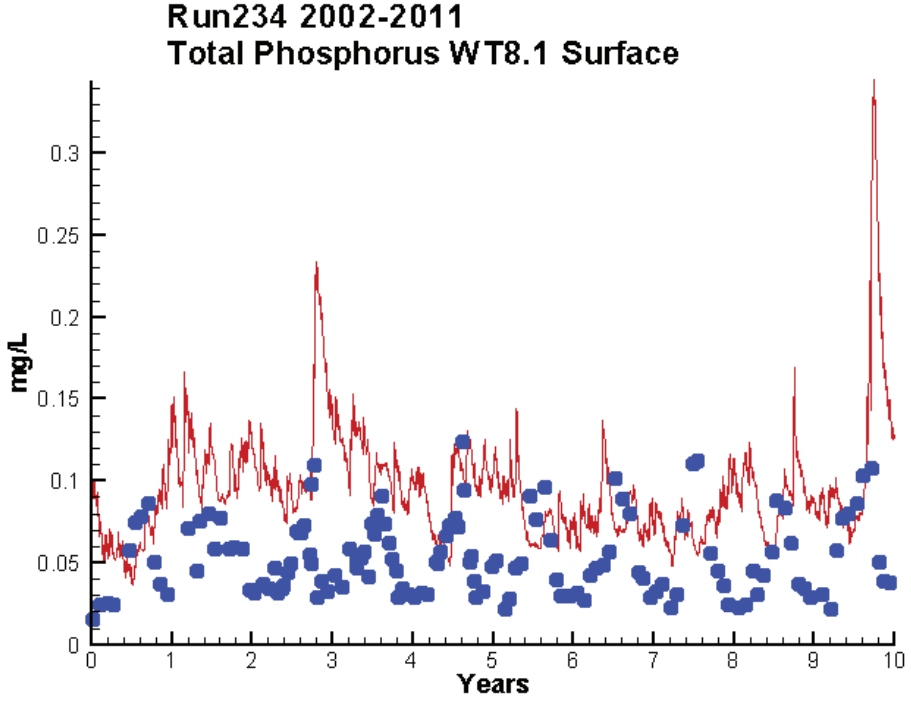

	Mean Difference	Absolute Mean Difference
Chl	-8.0393	12.4024
DIN	0.0399	0.1401
KE	1.4467	1.5791
DIP	0.0017	0.0079
TP	0.0441	0.0497
TN	0.3071	0.3401

Station WT8.1

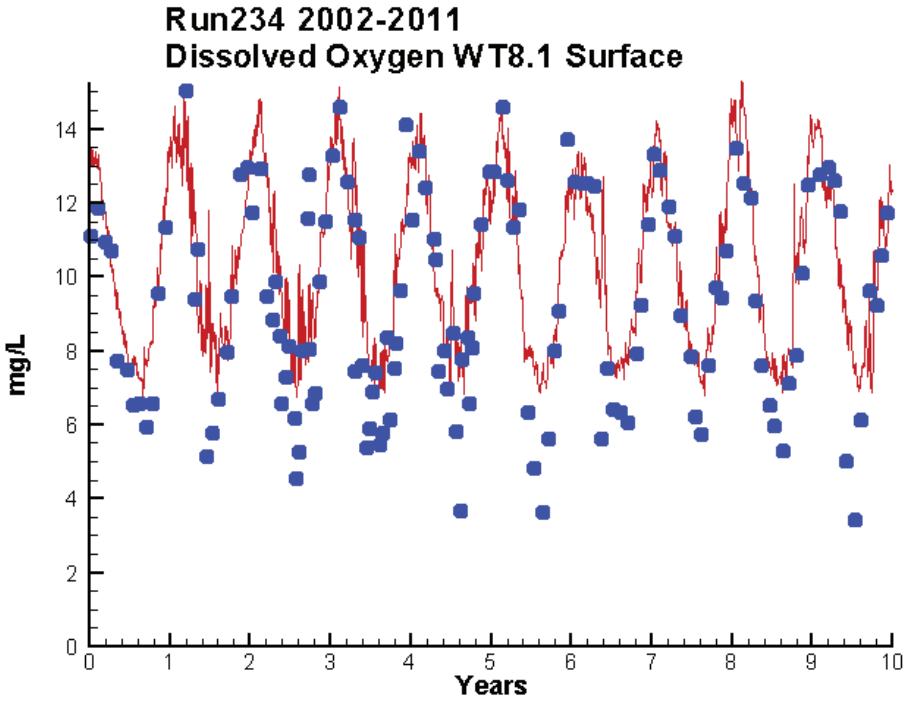

	Mean Difference	Absolute Mean Difference
Top DO	0.9293	1.4243

Station WT8.1

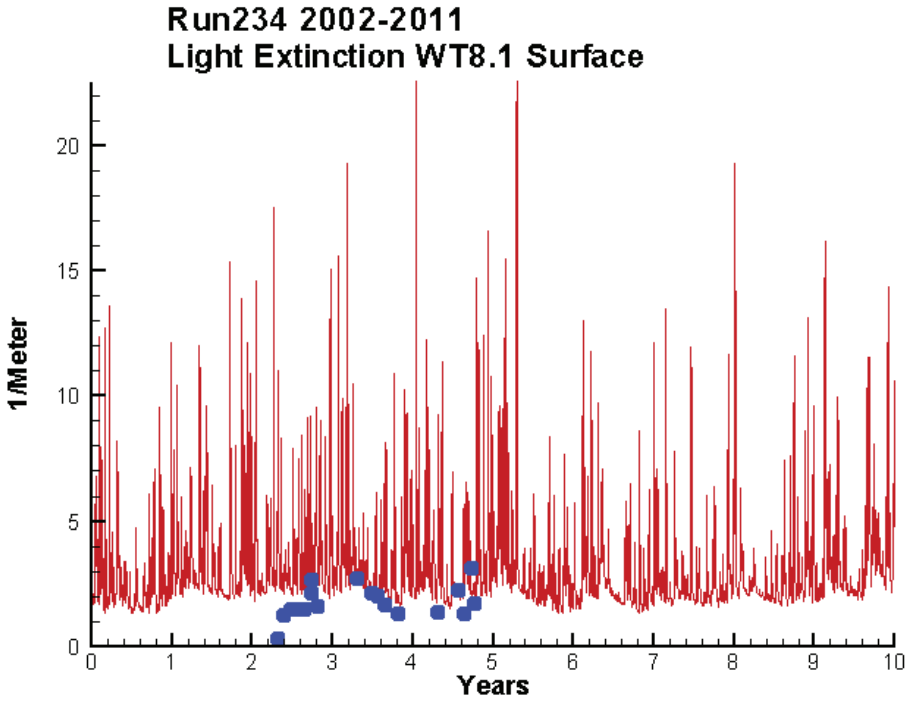

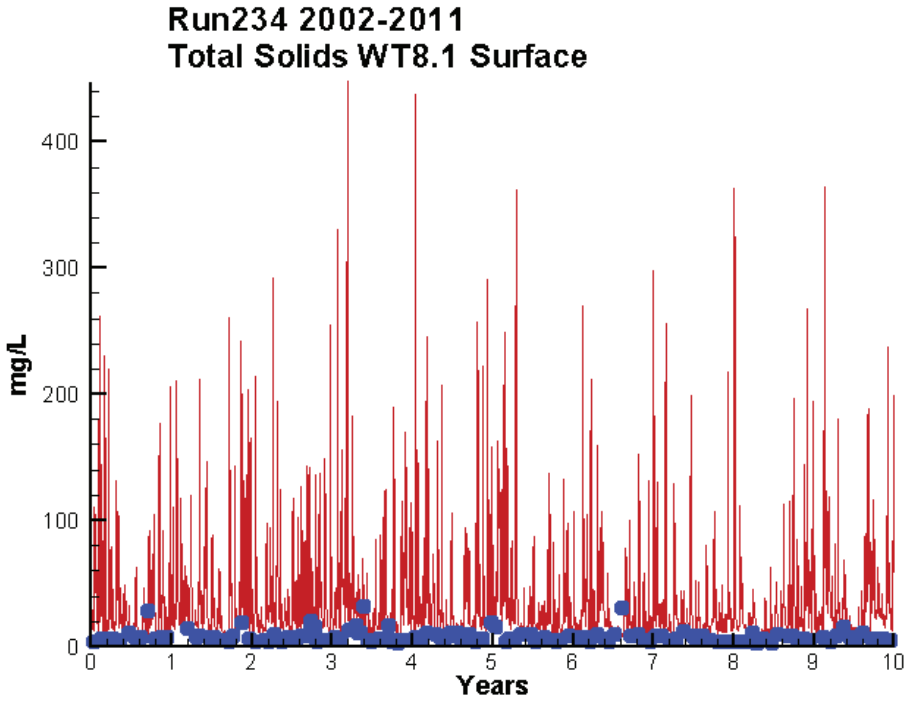

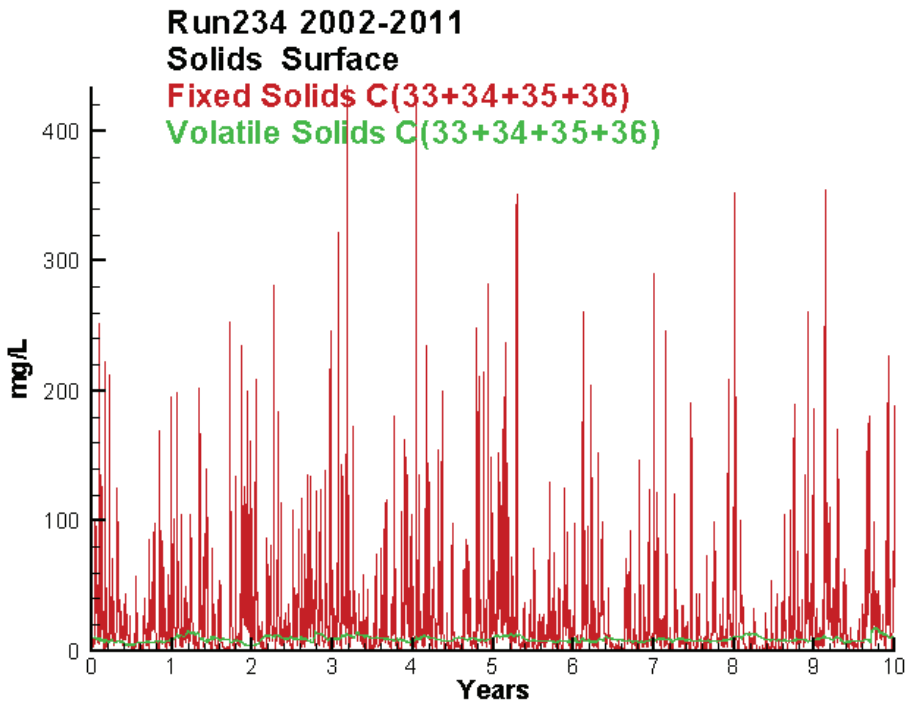

	Mean Difference	Absolute Mean Difference
KE	1.4467	1.5791
TSS	21.5723	22.2018

Appendix C: Longitudinal Comparisons 1991–2000

The spatial distributions of observed and computed properties were compared in a series of plots along the axes of the Bay and major tributaries (Figure C-1). The calibration period encompassed more than 100 cruises. Reducing that number of surveys into a manageable volume of comparisons required selection and aggregation. Three years were selected for comparisons: 1994, 1996, and 1999. The year 1994 was considered a year of average flow in the Susquehanna River, the source of the majority of runoff to the Bay. Flows in 1996 were characterized as above average while 1999 was a year of below-average runoff.

Model results and observations were averaged into four seasons:

- Winter–December through February
- Spring–March through May
- Summer–June through August
- Fall–September through November

Conventional arithmetic means were calculated for the observations. Model results were subjected to a process designated as "cruise averaging." Within each season, model results were considered only during intervals coinciding with sample cruises. Cruise averaging diminished discrepancies between model and observations attributed to consideration of model results for periods when no data were collected. Daily averages of model results were computed within the model code. Cruise averaging was completed in a postprocessor. Arithmetic averages were computed during cruise periods for all modeled substances except light attenuation and total suspended solids. Log averages were calculated for those two components. The variance of the computed values skewed arithmetic means to unrepresentative high values. The postprocessor also extracted the maximum and minimum computed daily averages.

The mean and range of the observations, at surface and bottom, were compared to the cruise average and range of daily-average model results. The longitudinal axes largely followed the maximum depths represented on the model grid. Only stations located on axes were considered for comparison with the model. Comparisons were made for physical quantities (salinity, temperature, suspended solids, and light attenuation), chlorophyll, dissolved oxygen (DO) and multiple forms of carbon, nitrogen, and phosphorus.

Figure C-1. Longitudinal transects in the Bay and major tributaries.

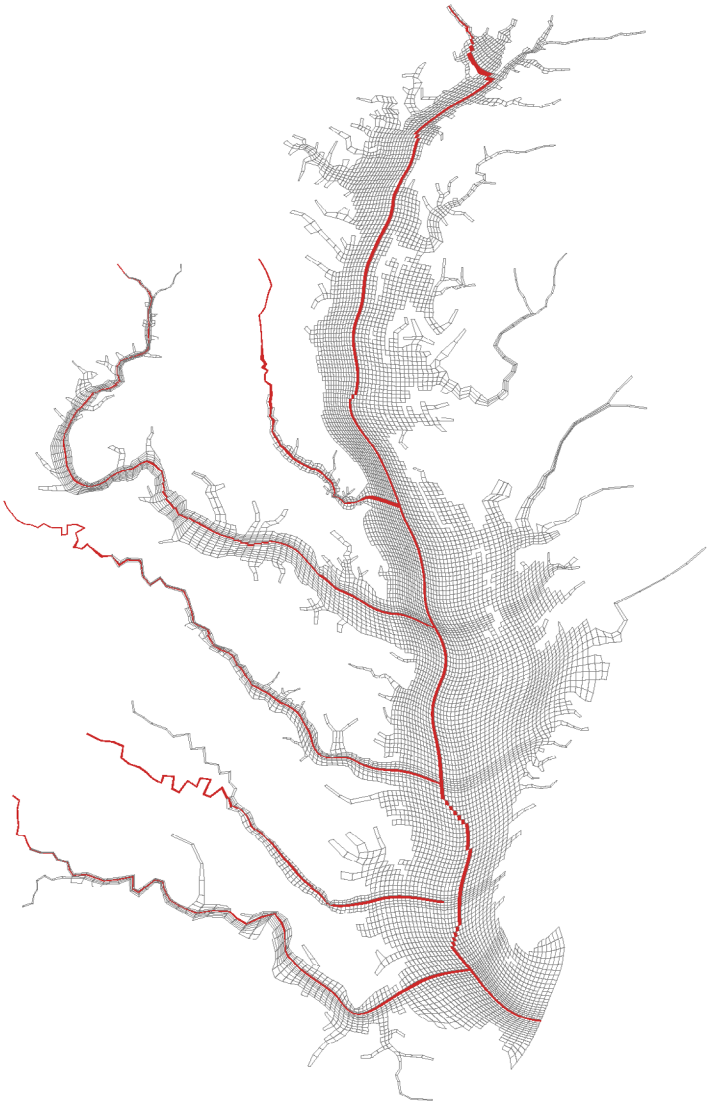

This appendix concentrates on the components that correspond closely to chlorophyll, clarity, and DO in the critical summer period. On the plots provided in this appendix, DO is shown at the surface and bottom. Surface samples are from the 1-meter depth. Bottom samples are typically 1 meter off the bottom and follow local bathymetry. Model values are from surface and bottom cells on the grid. Chlorophyll and light attenuation are presented for the surface only.

For all substances, the blue circles and vertical bars indicate mean and range of the observations, respectively. The continuous red and green traces represent model mean and range, respectively, subject to the selection and averaging process described above.

Mainstem Bay - Summer - 1994

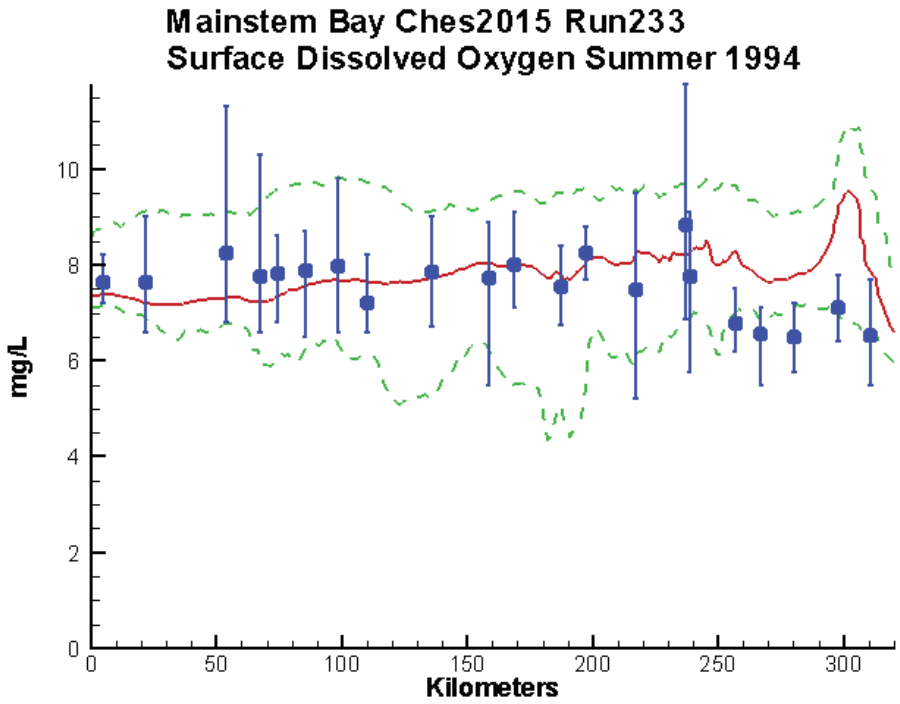

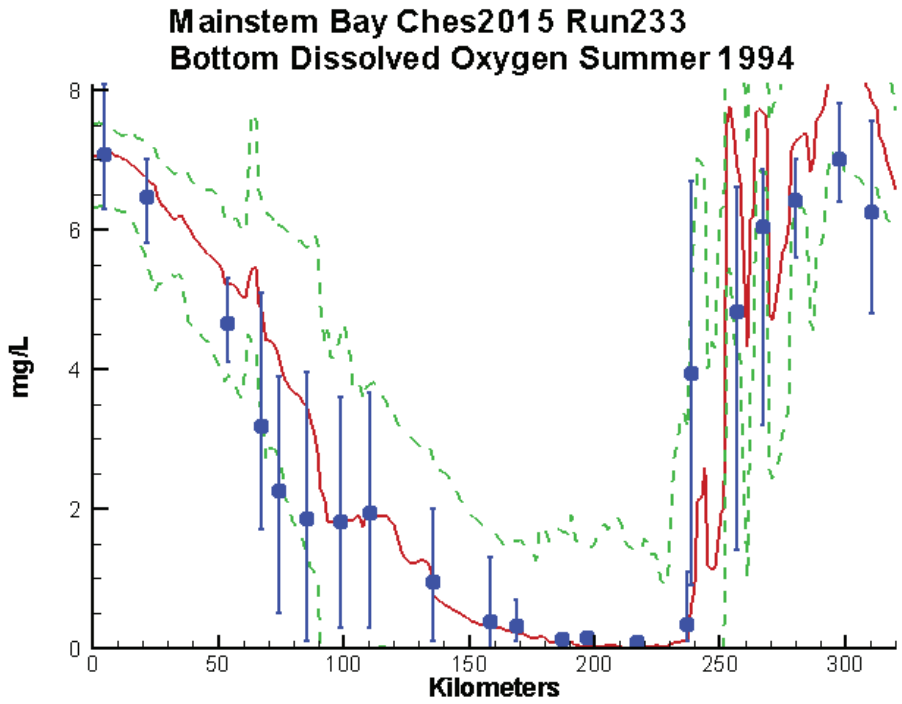

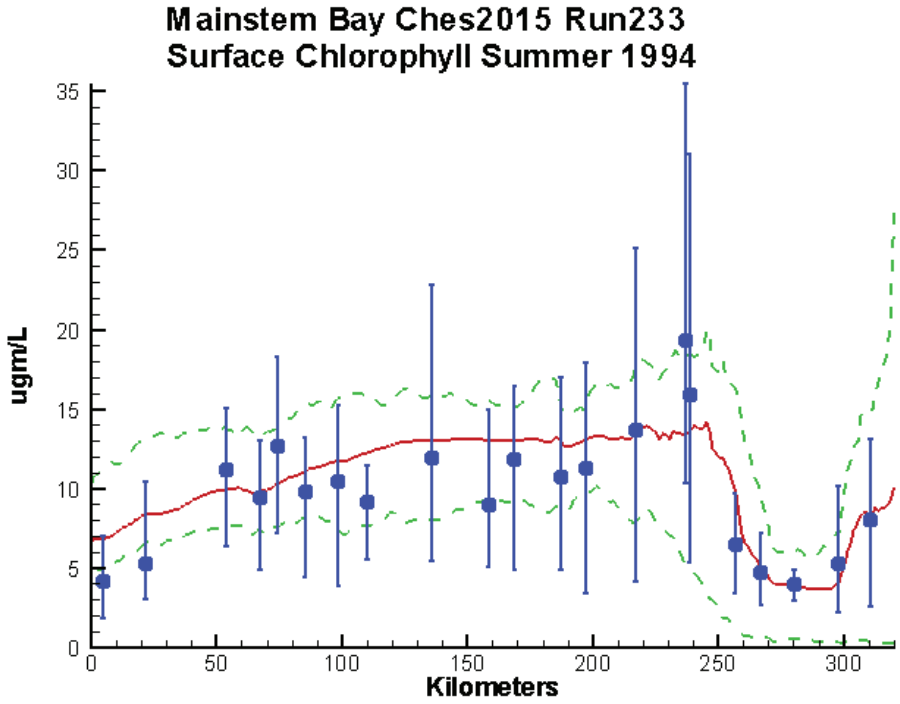

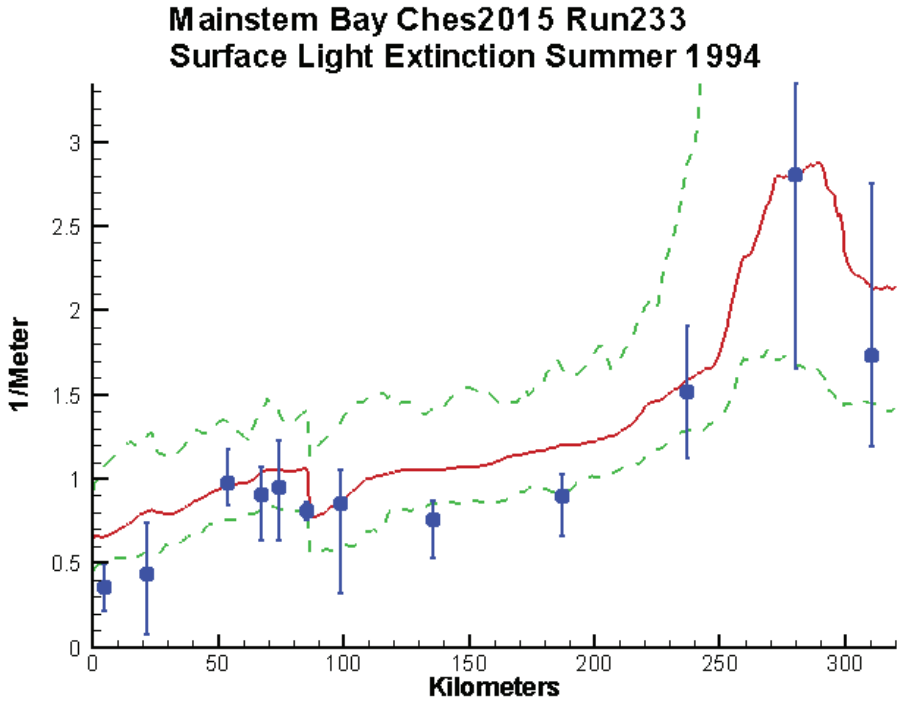

James River - Summer - 1994

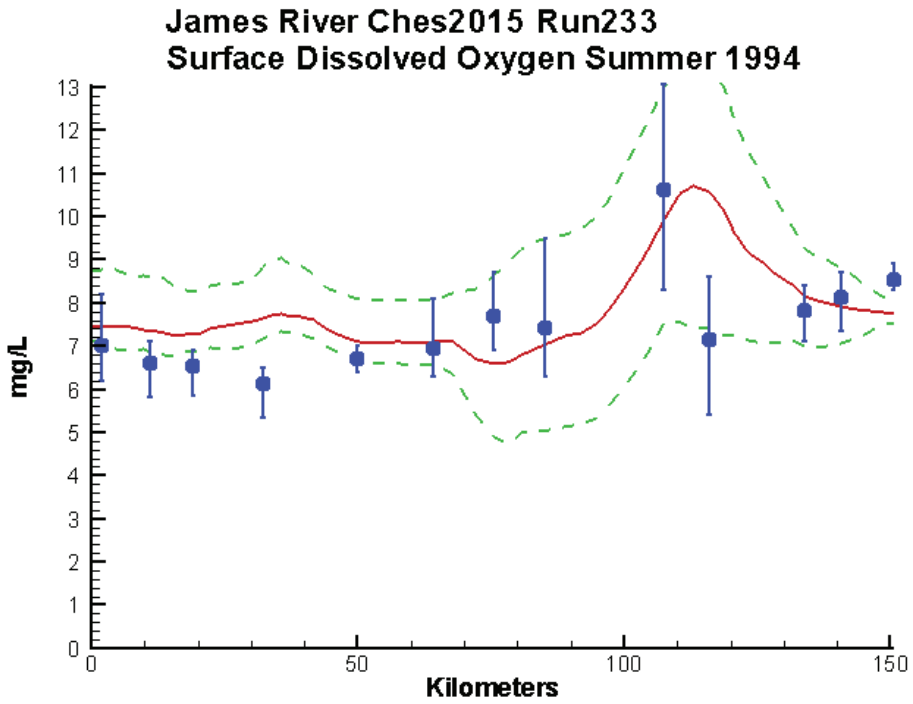

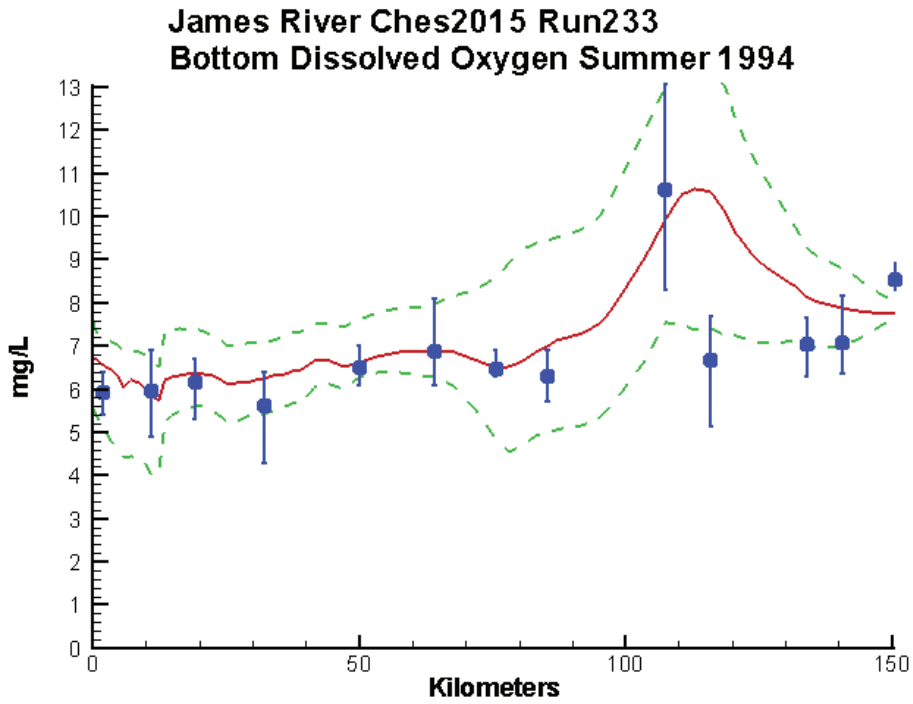

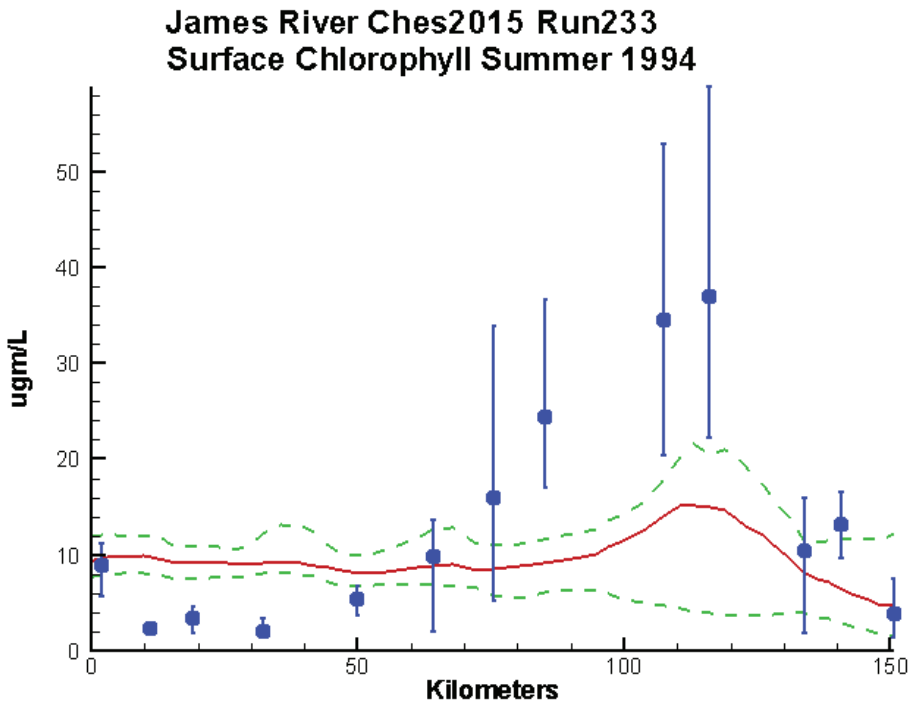

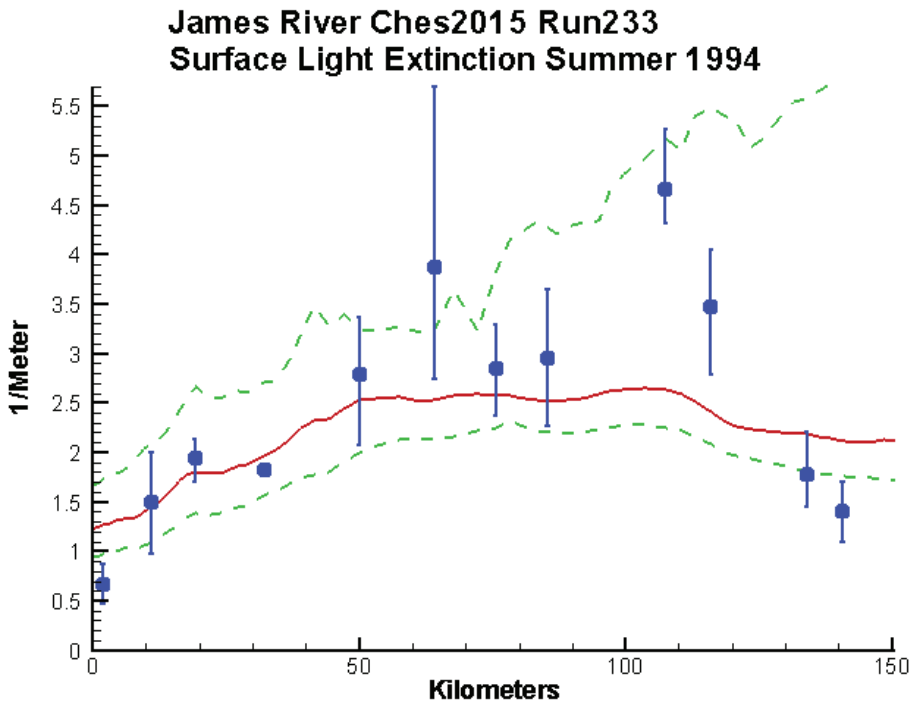

York River - Summer - 1994

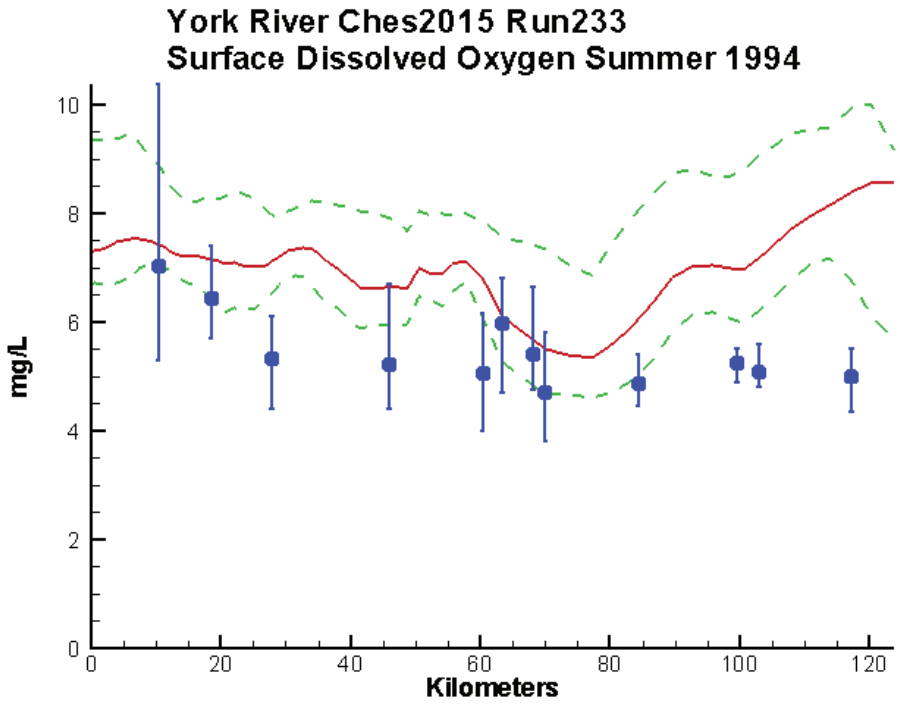

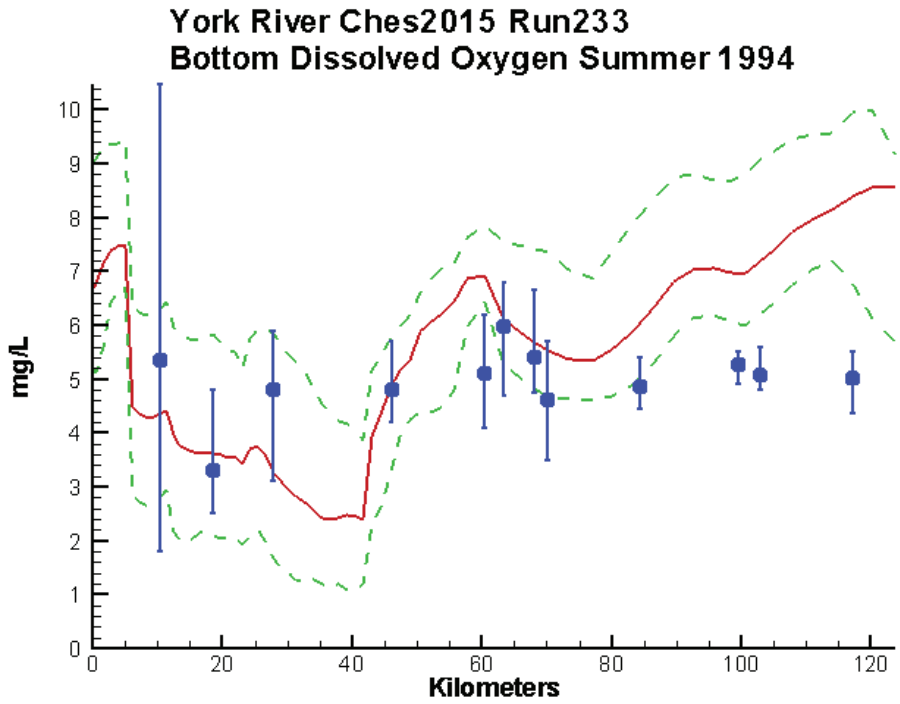

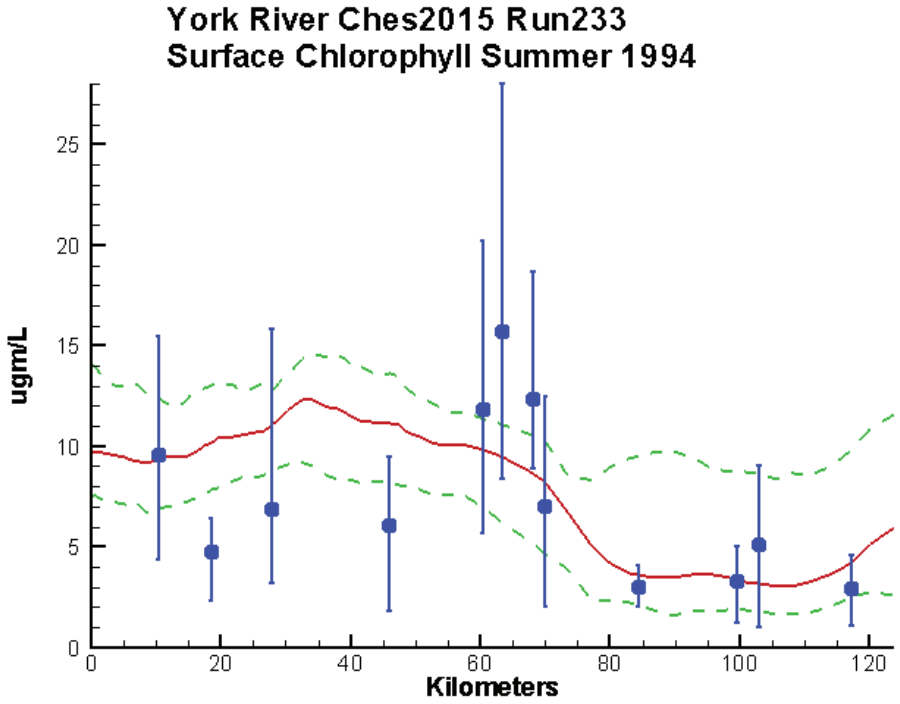

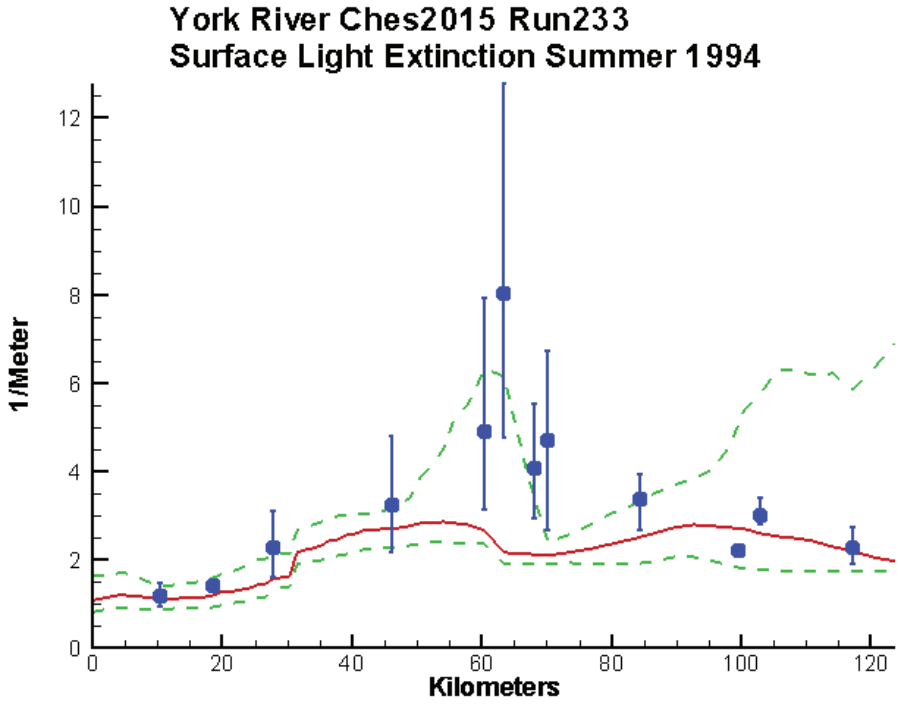

Rappahannock River - Summer - 1994

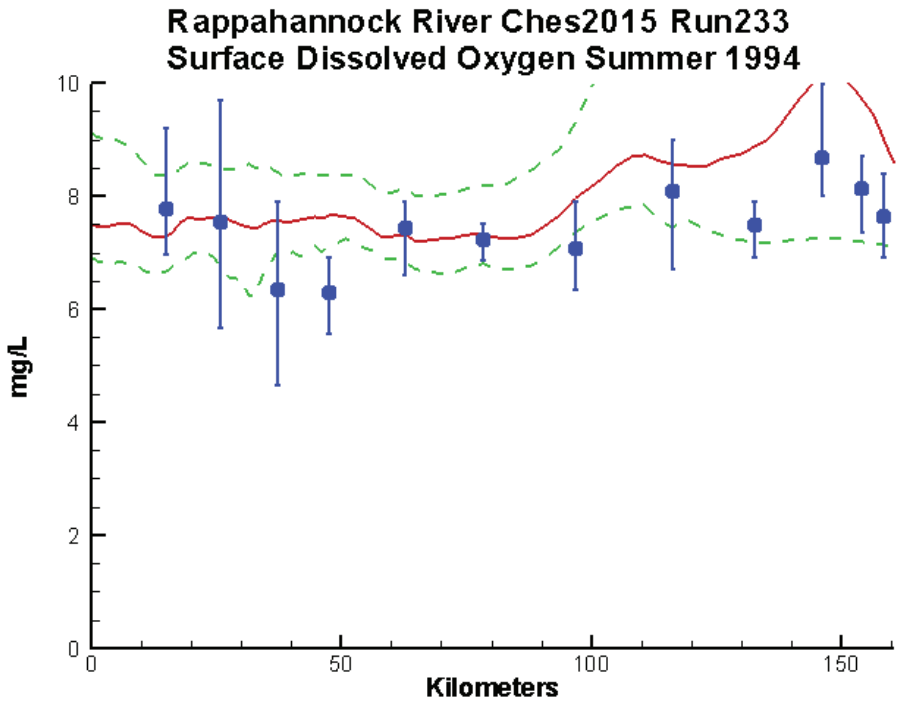

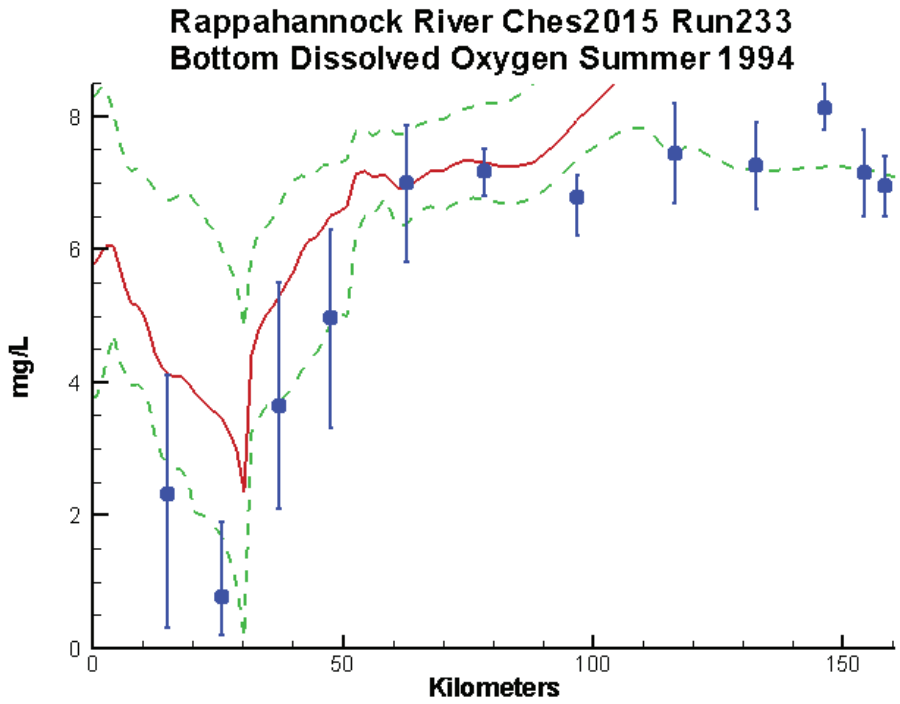

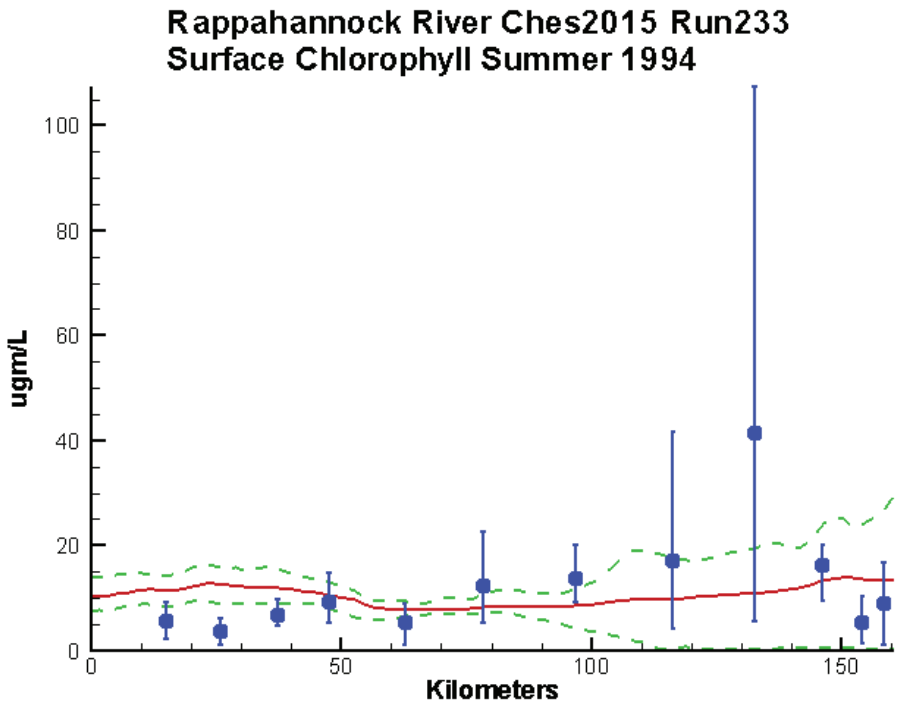

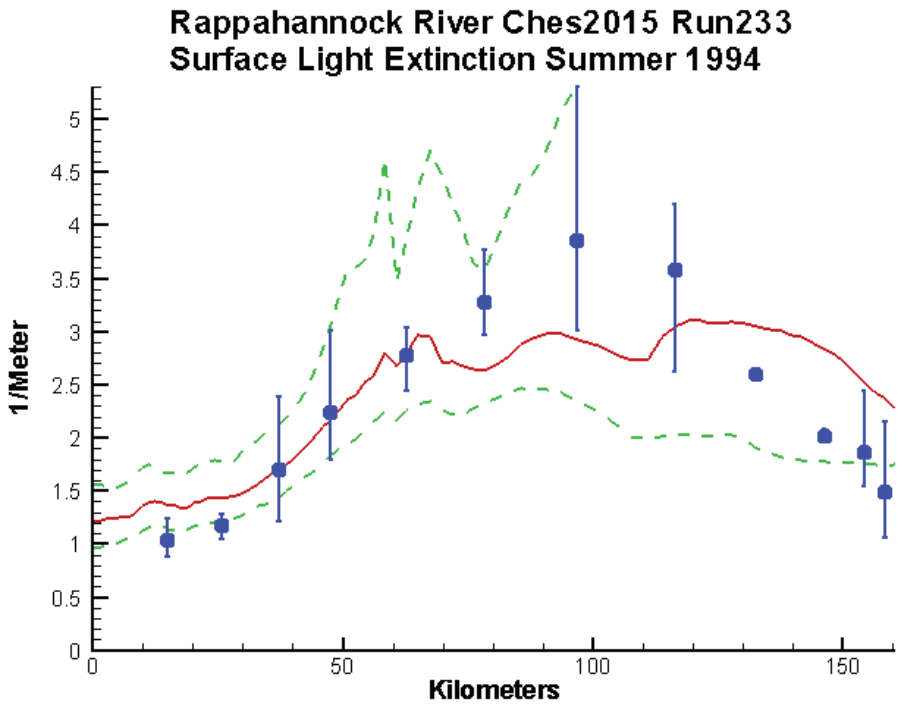

Potomac River - Summer - 1994

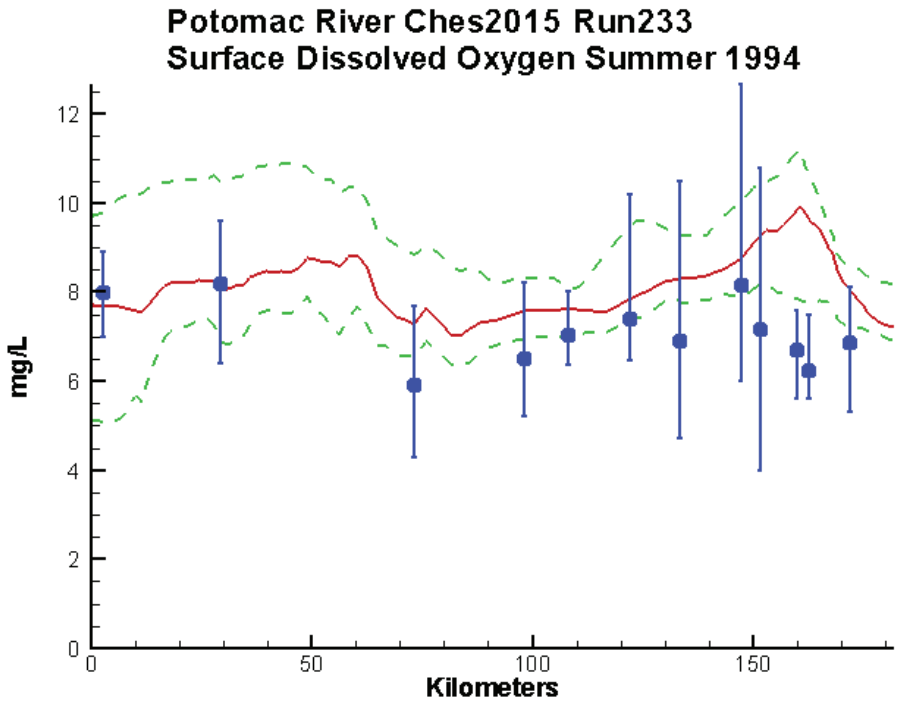

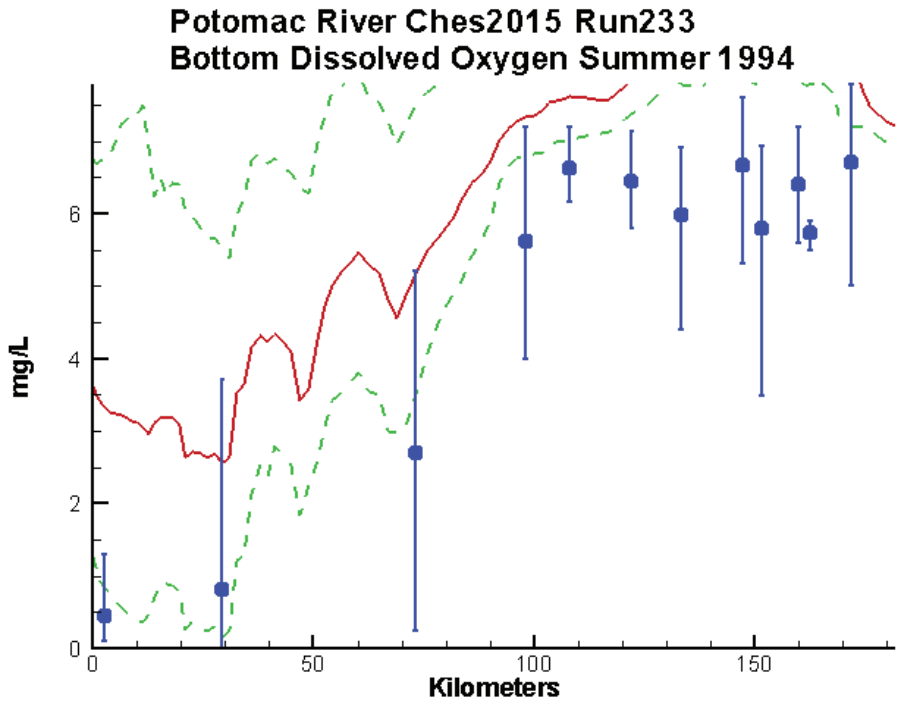

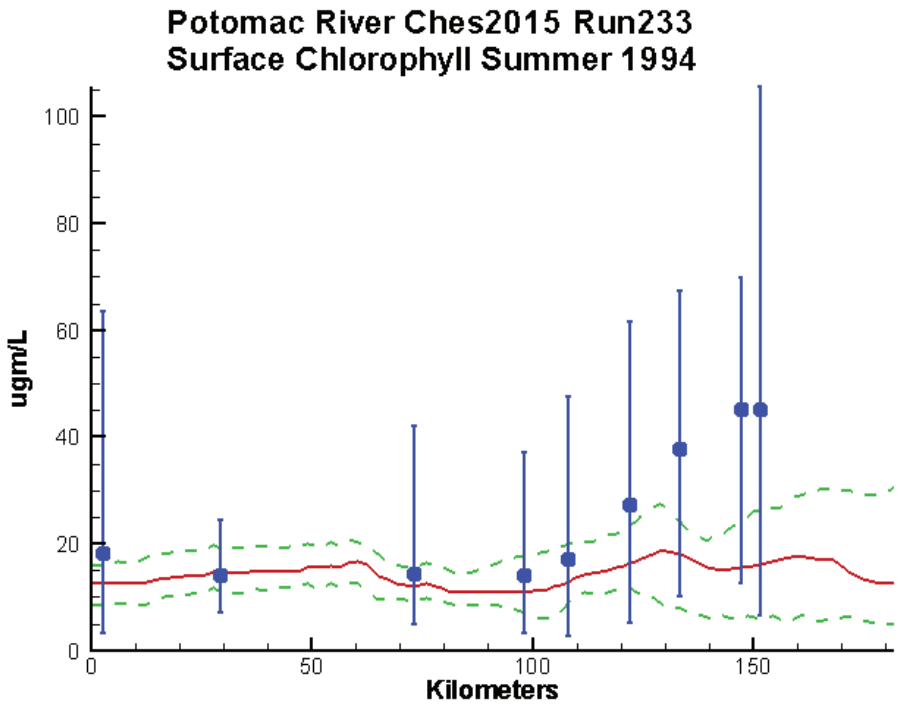

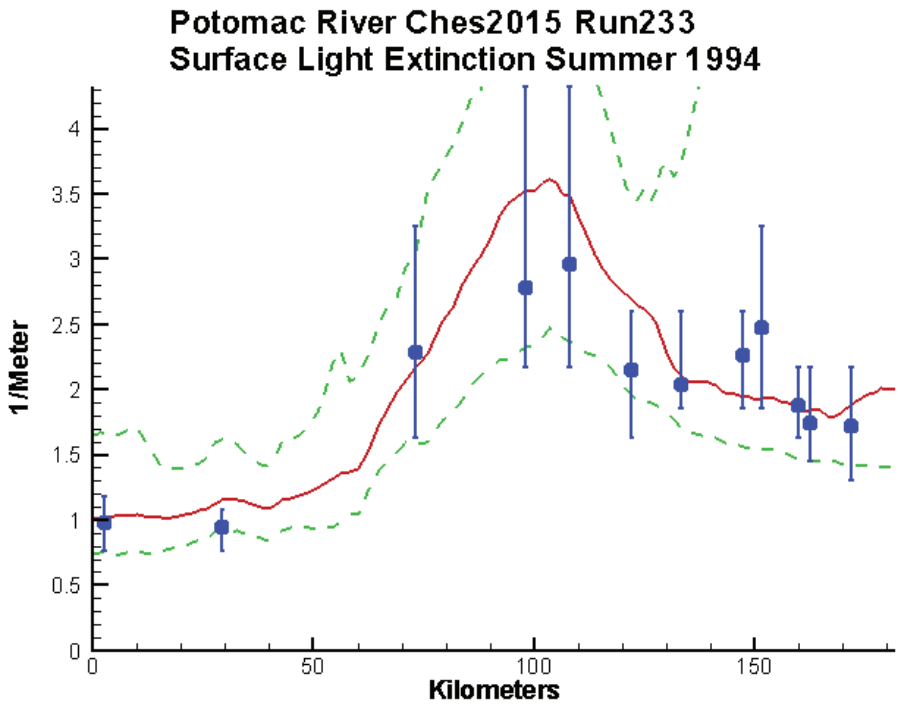

Patuxent River - Summer - 1994

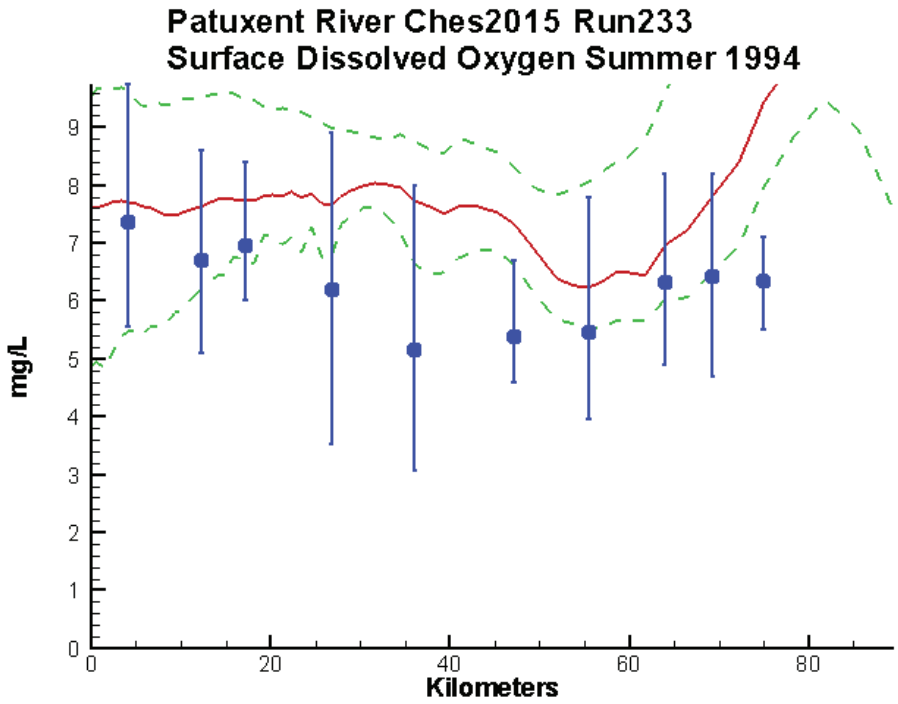

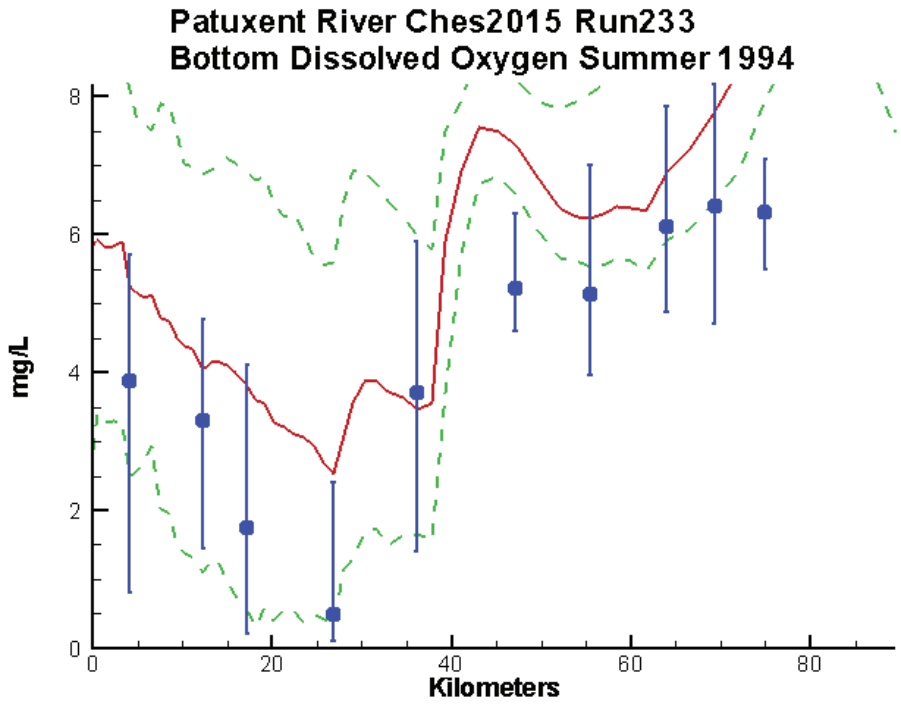

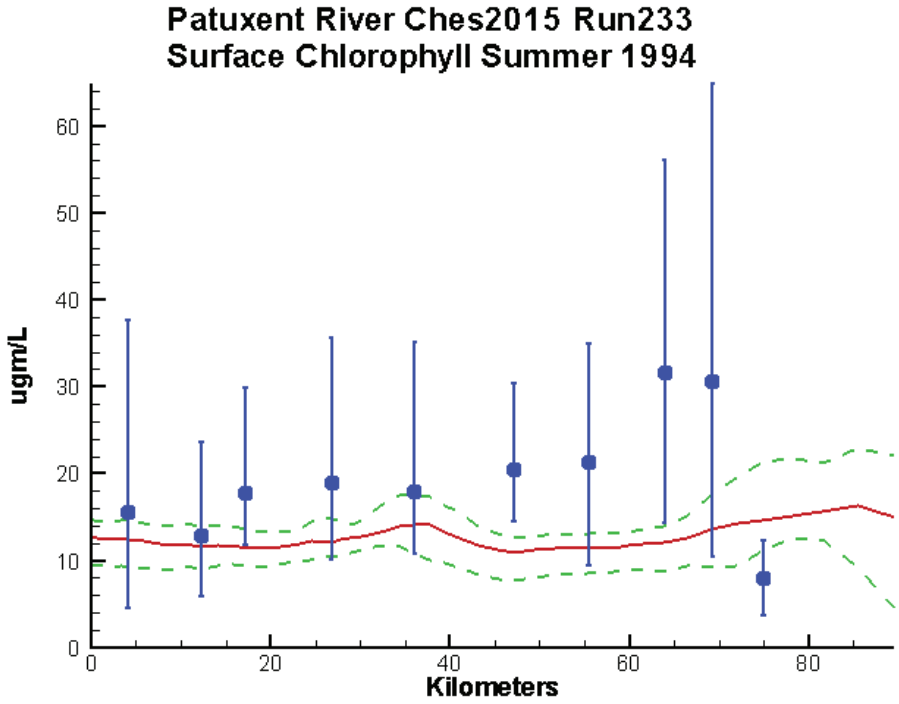

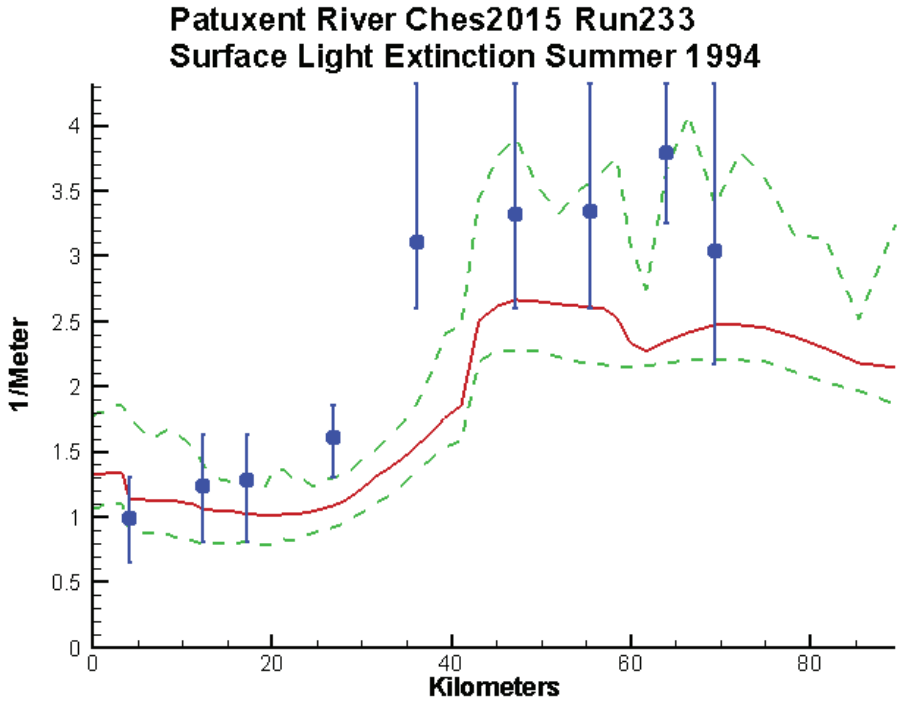

Mainstem Bay - Summer - 1996

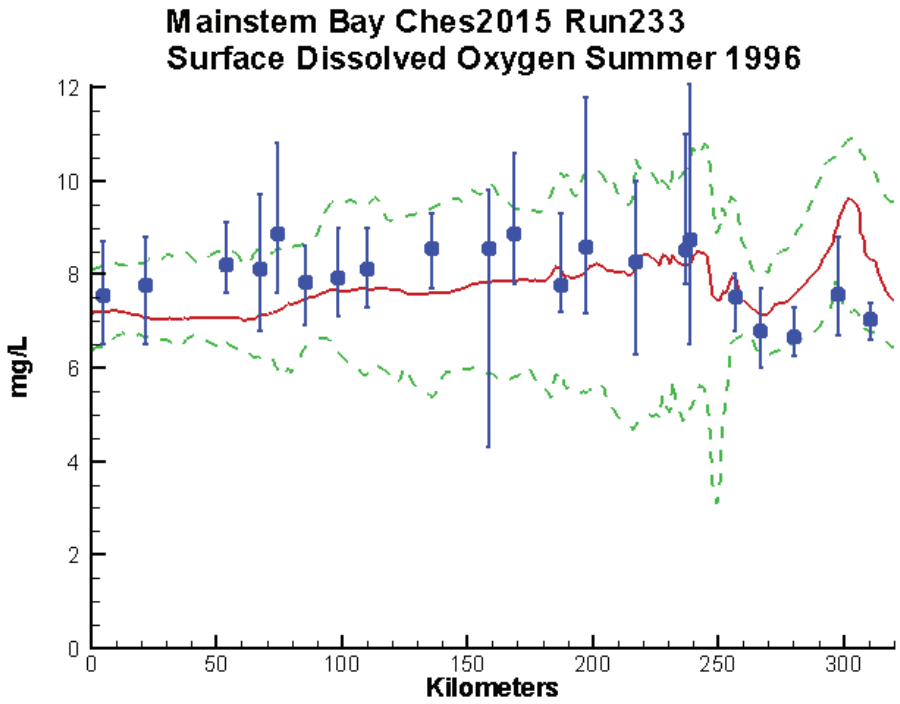

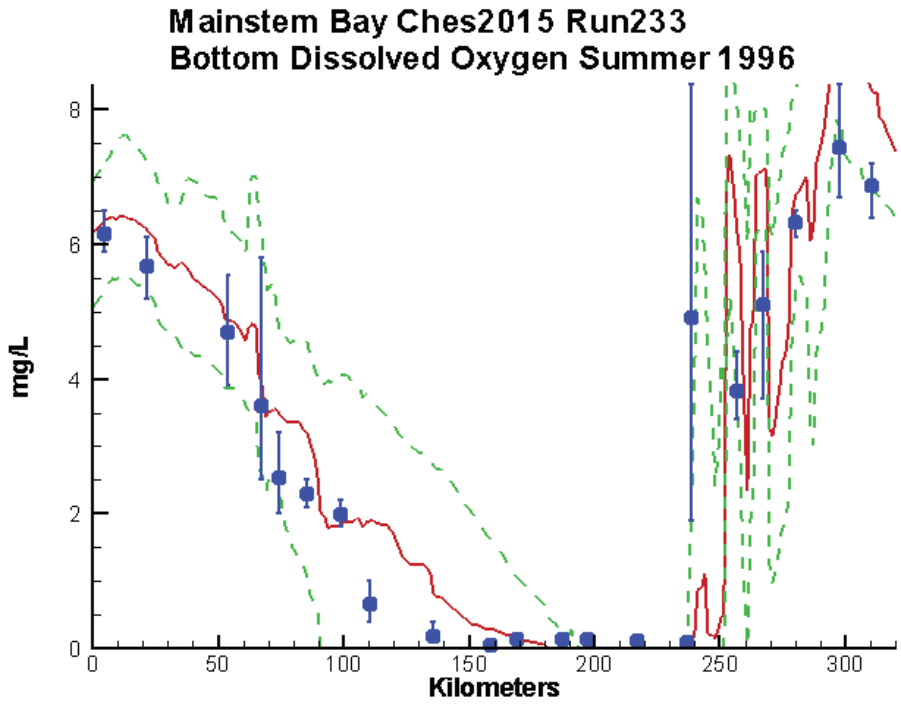

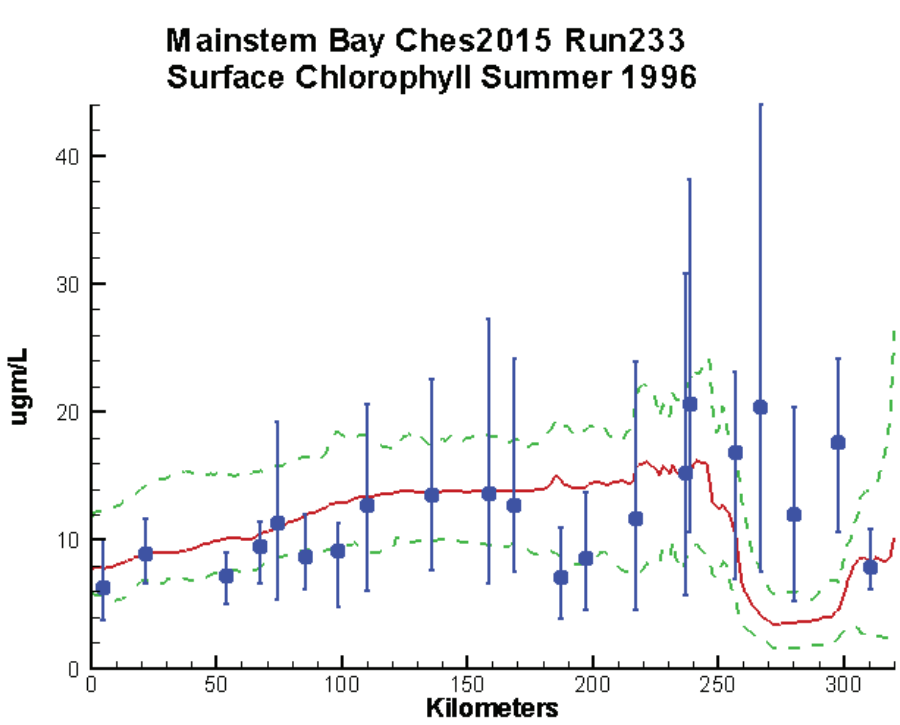

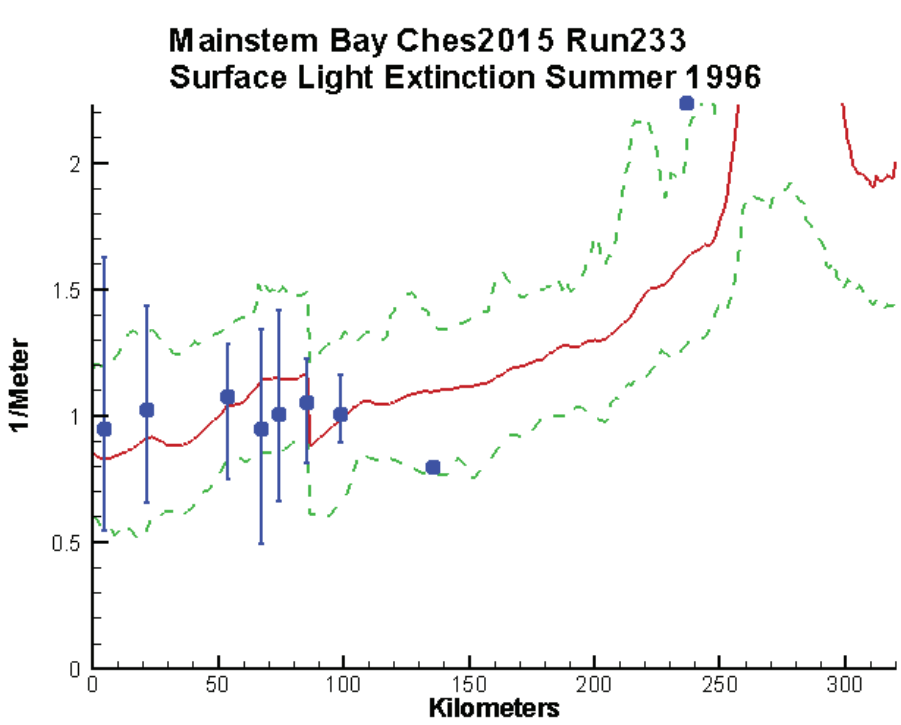

James River - Summer - 1996

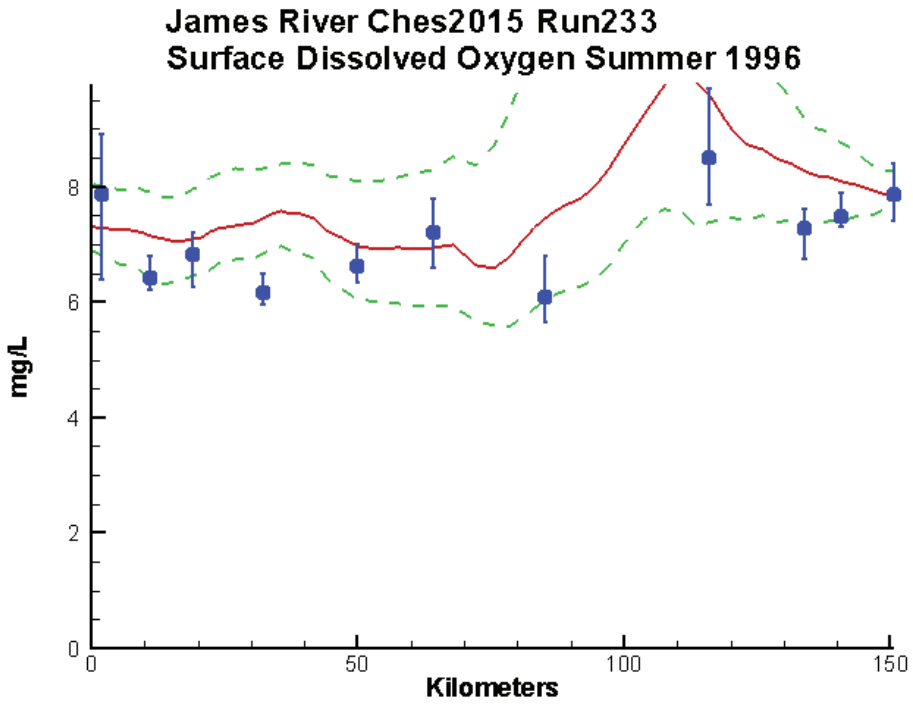

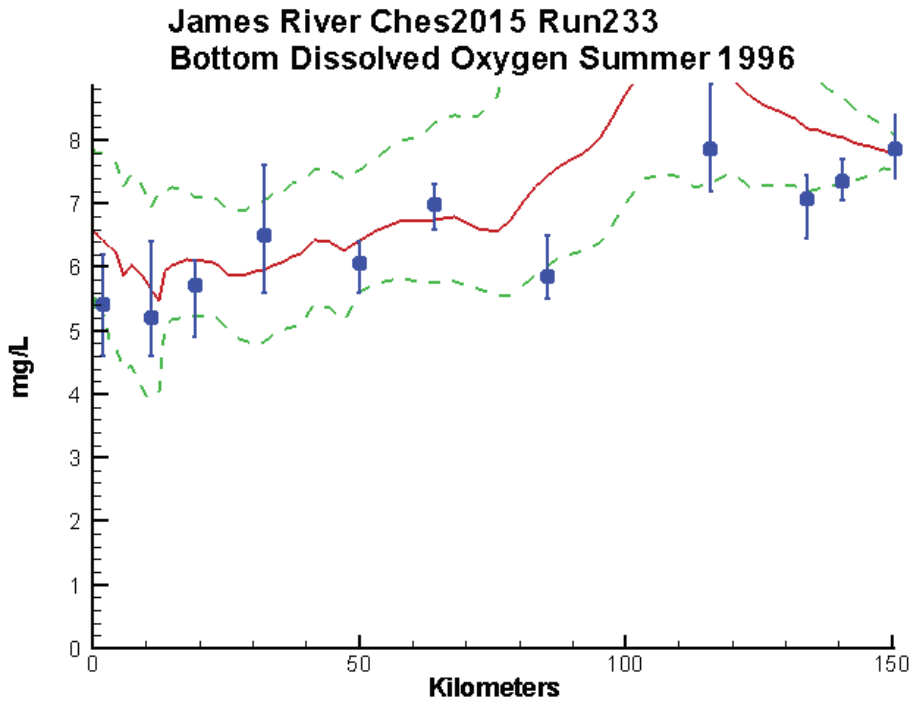

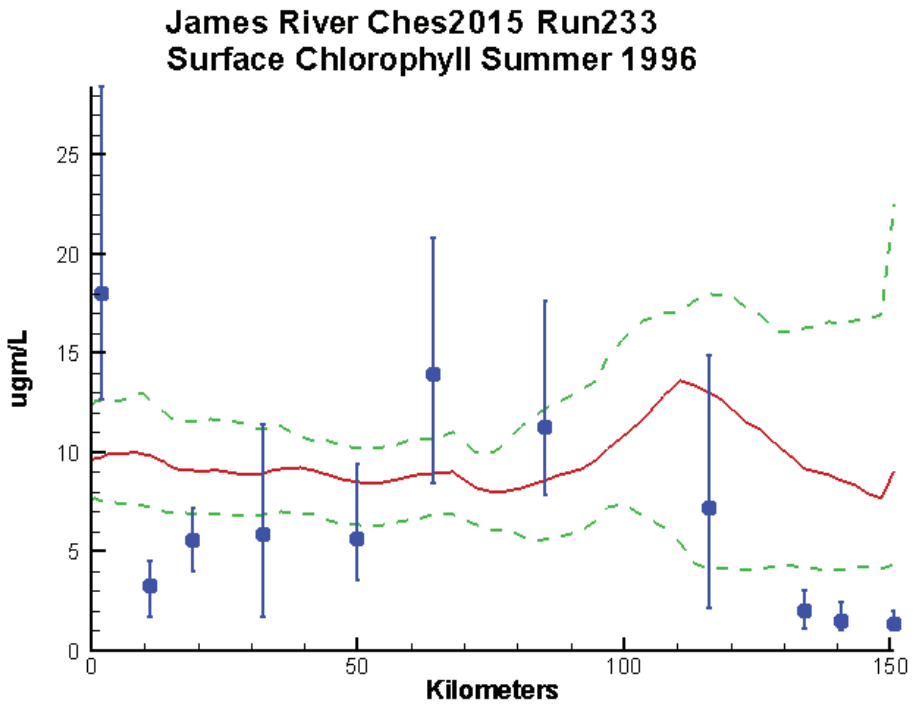

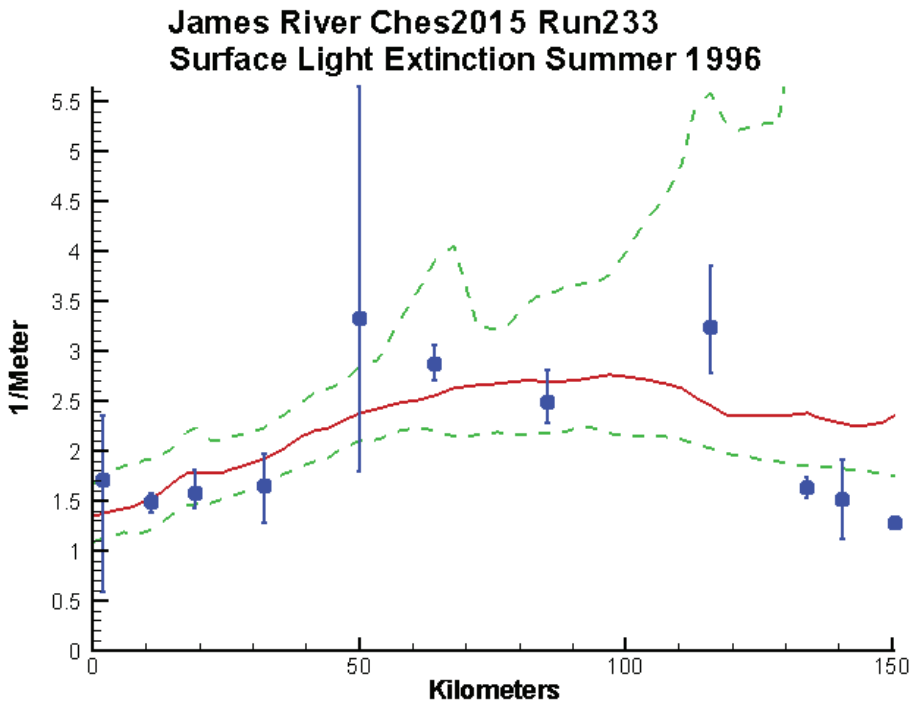

York River - Summer - 1996

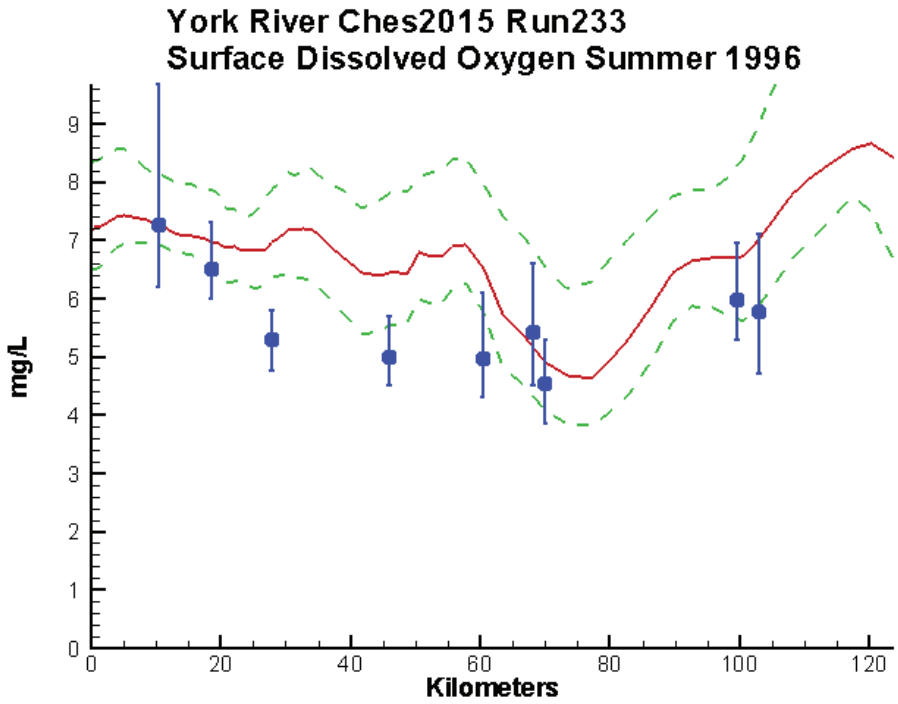

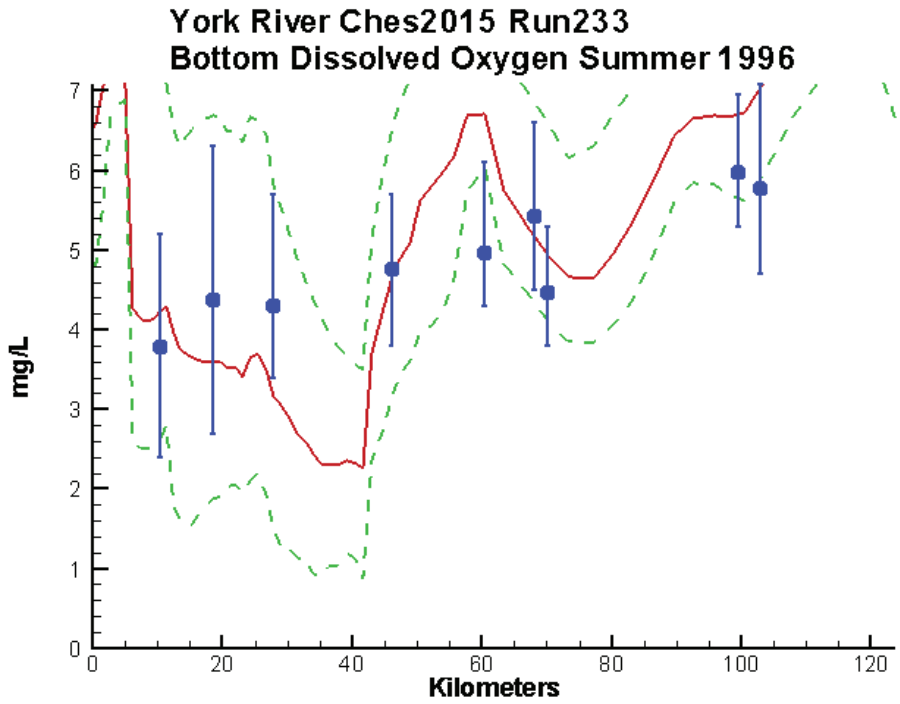

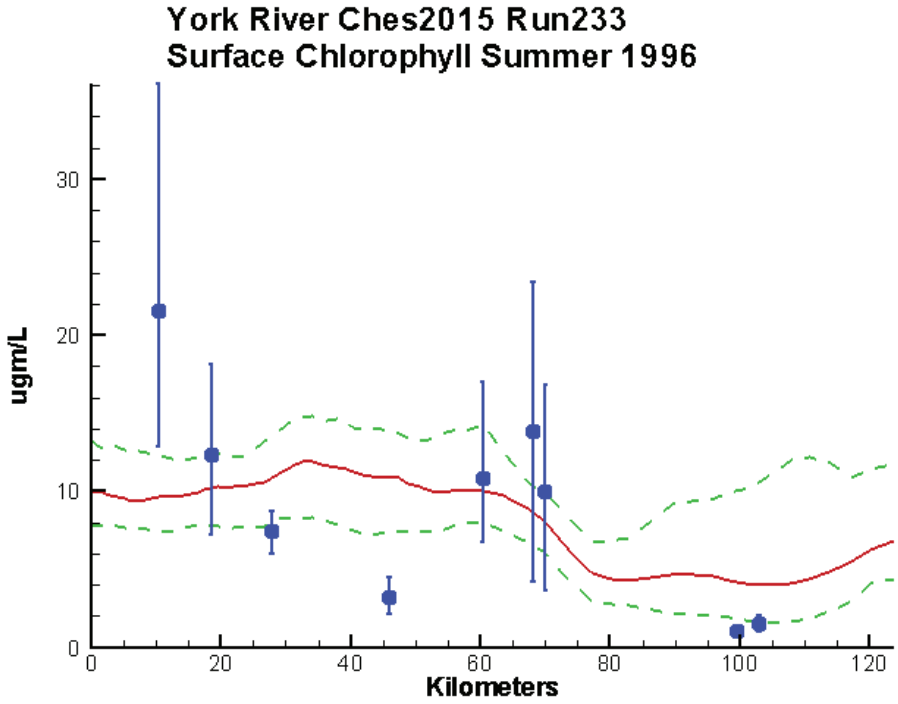

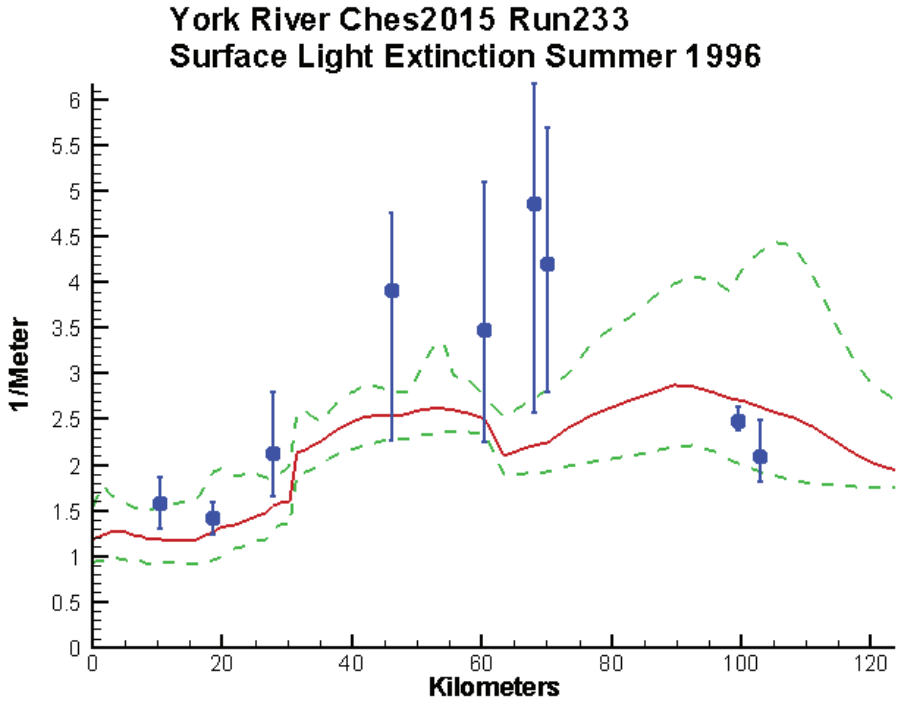

Rappahannock River - Summer - 1996

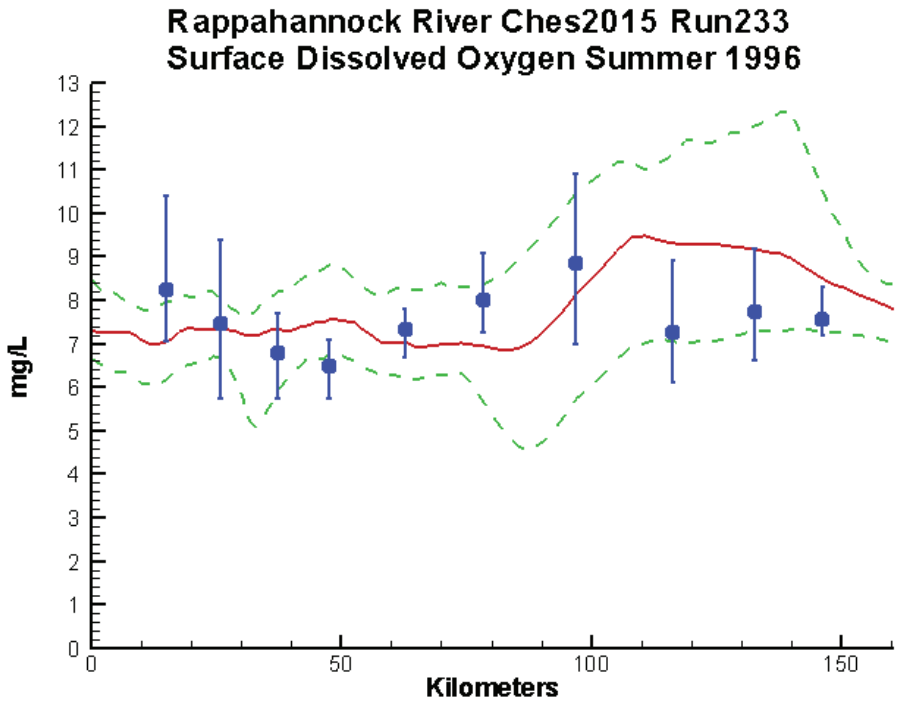

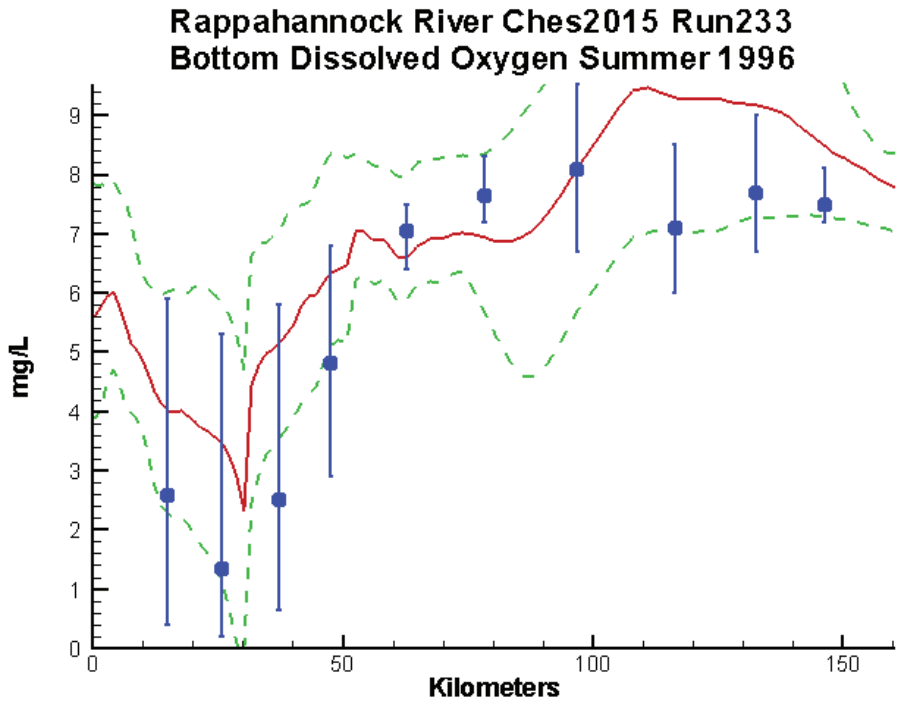

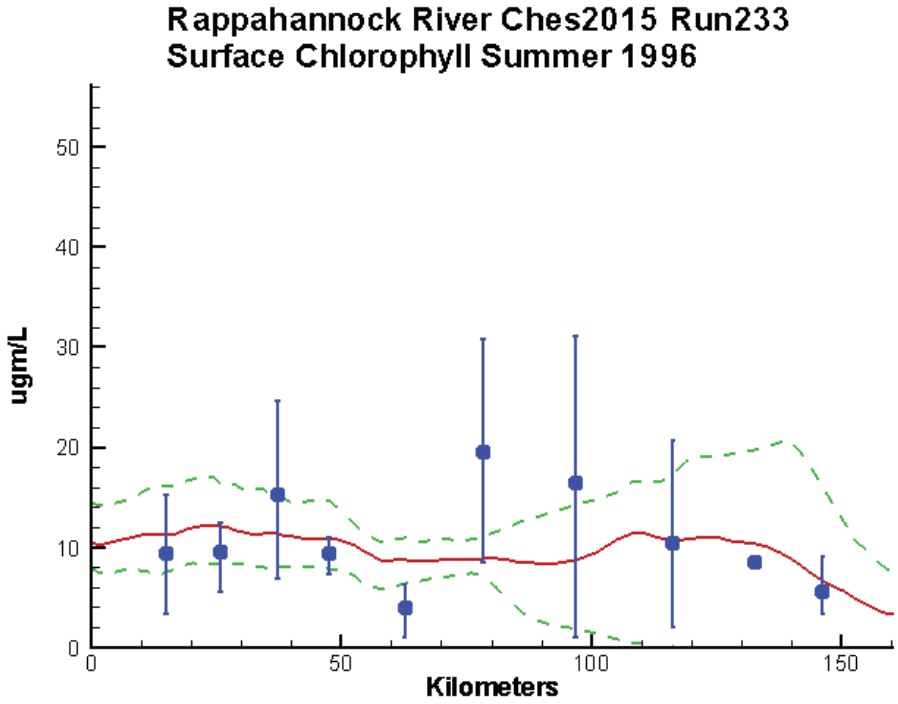

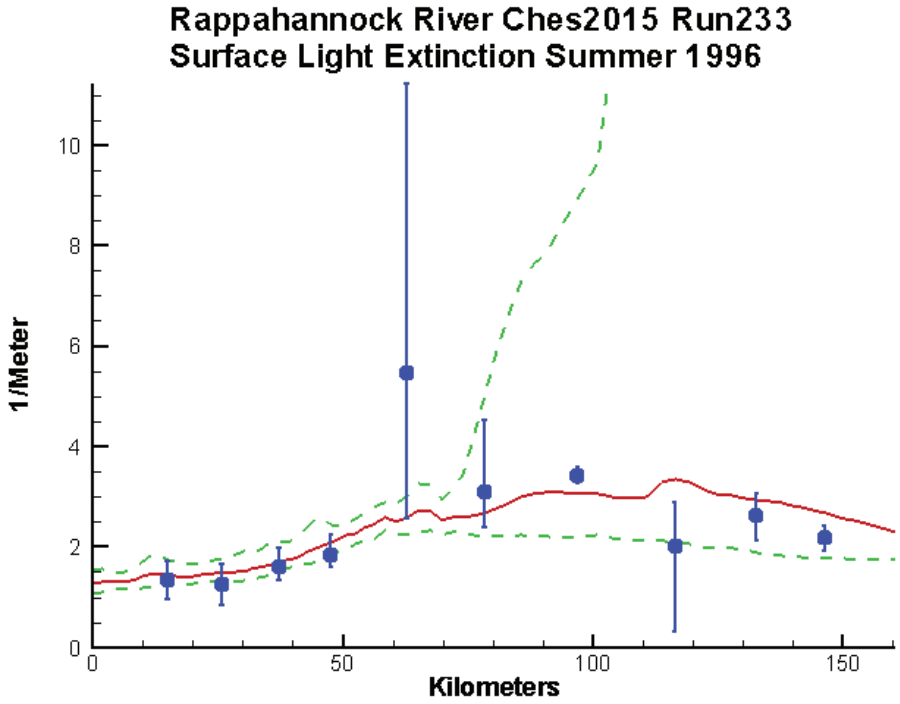

Potomac River - Summer - 1996

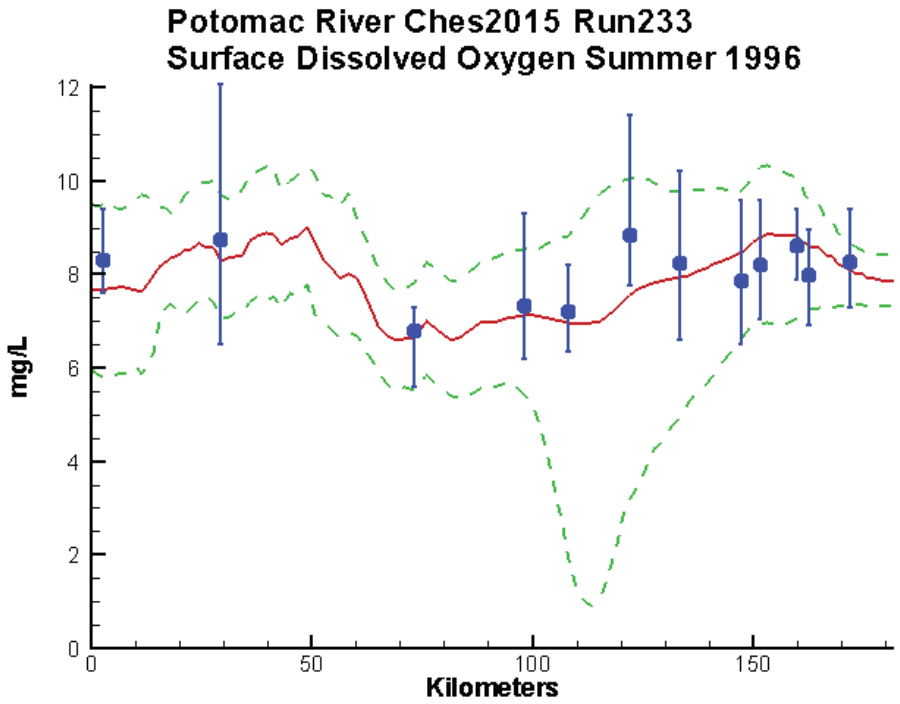

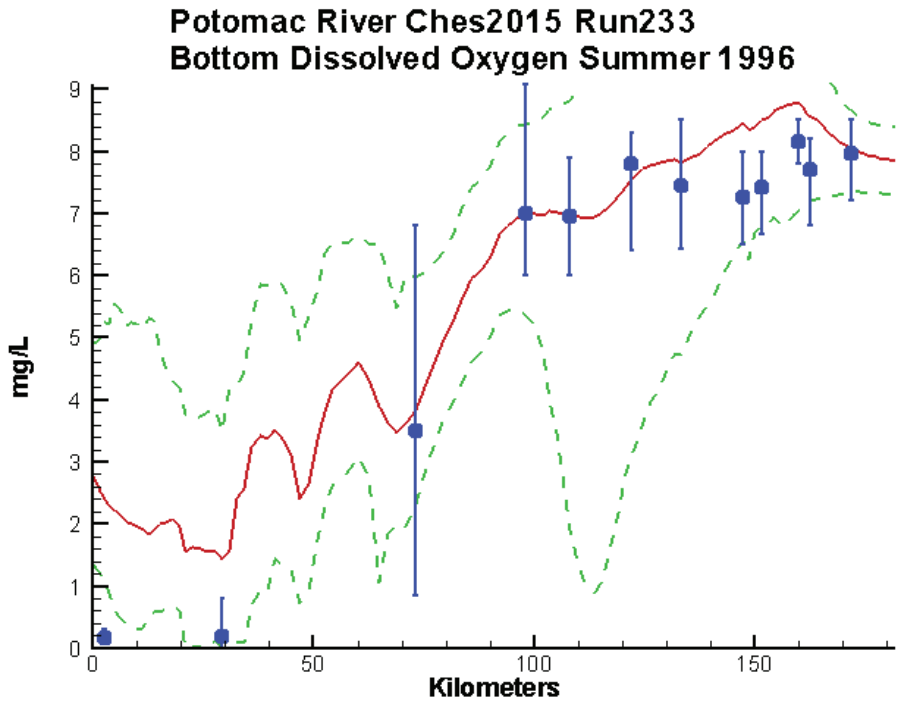

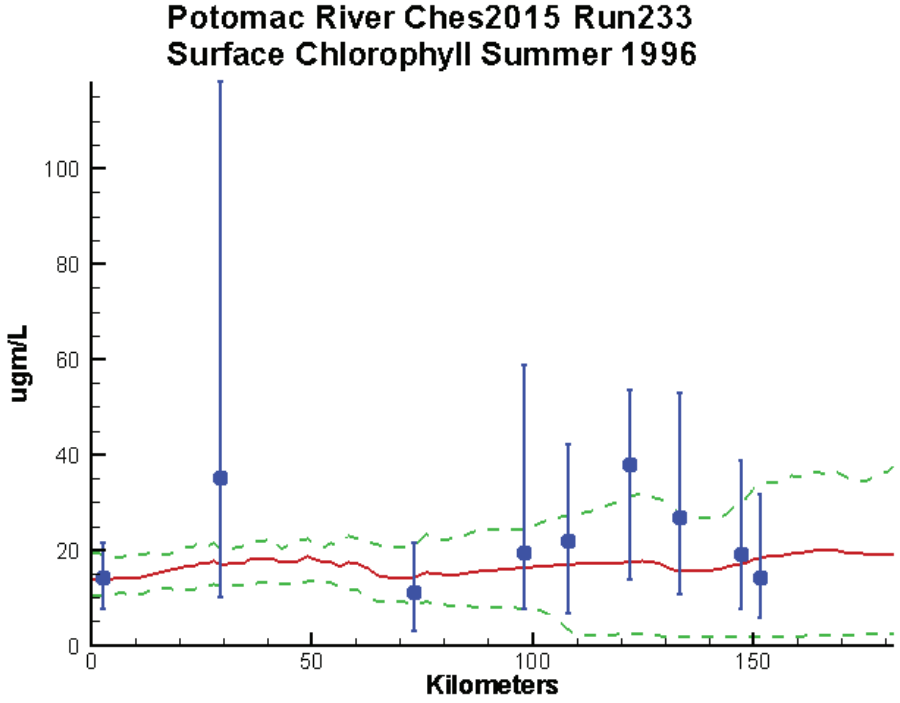

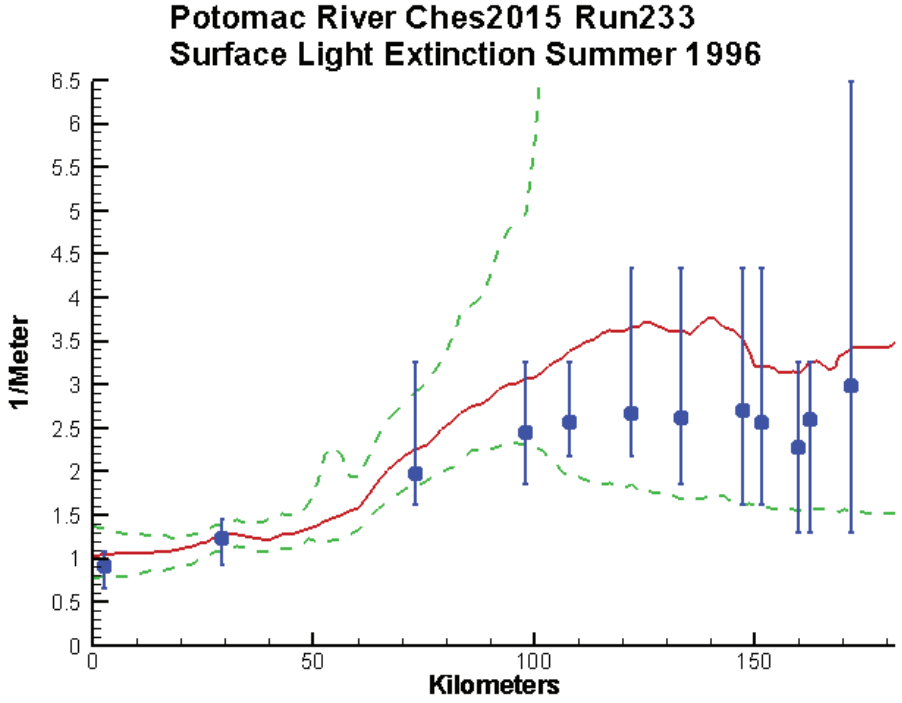

Patuxent River - Summer - 1996

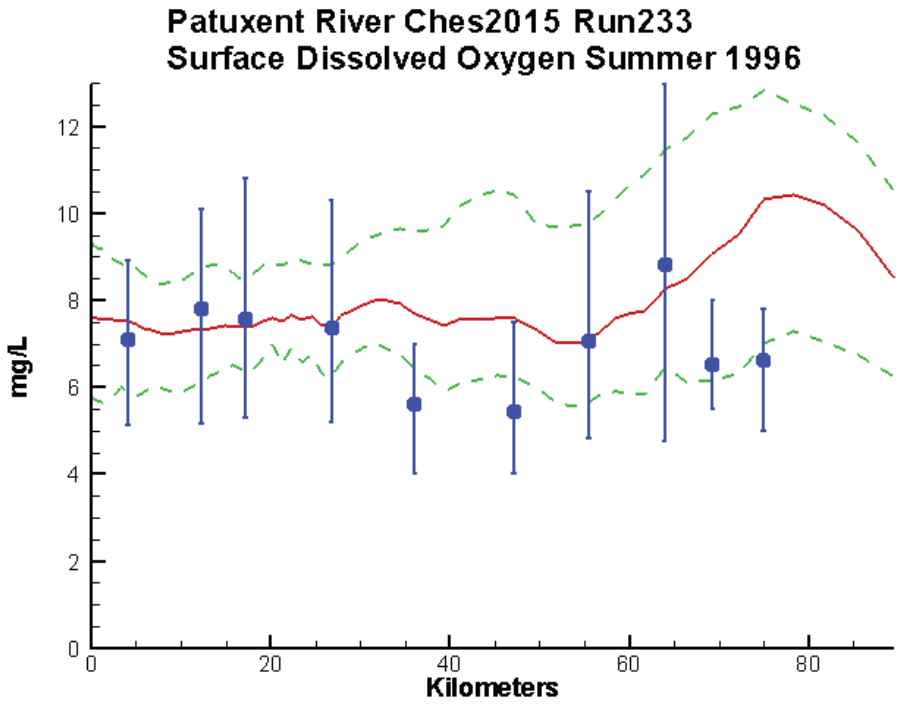

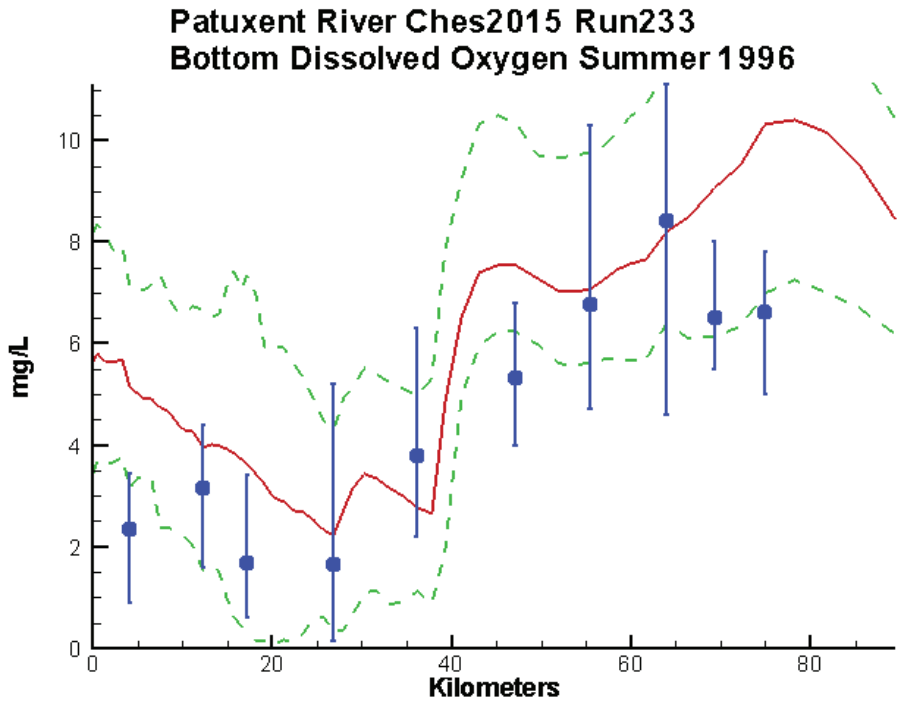

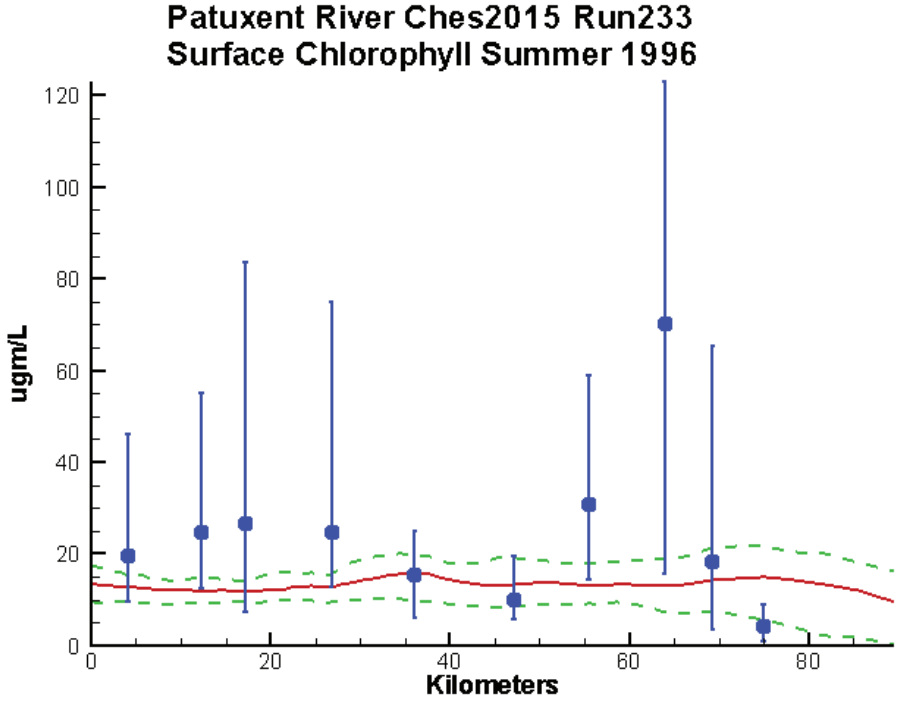

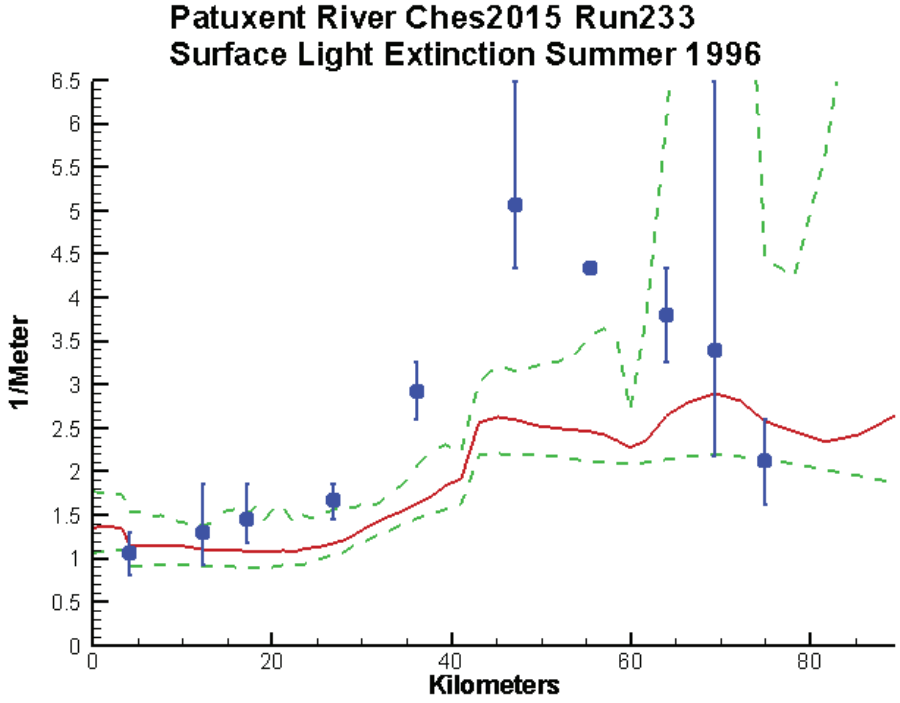

Mainstem Bay - Summer - 1999

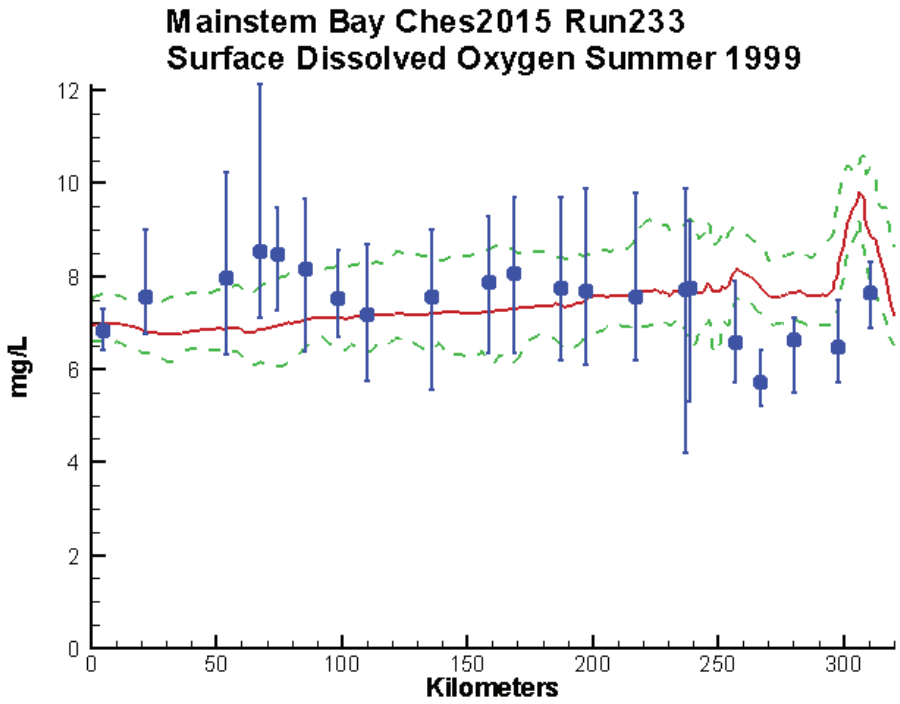

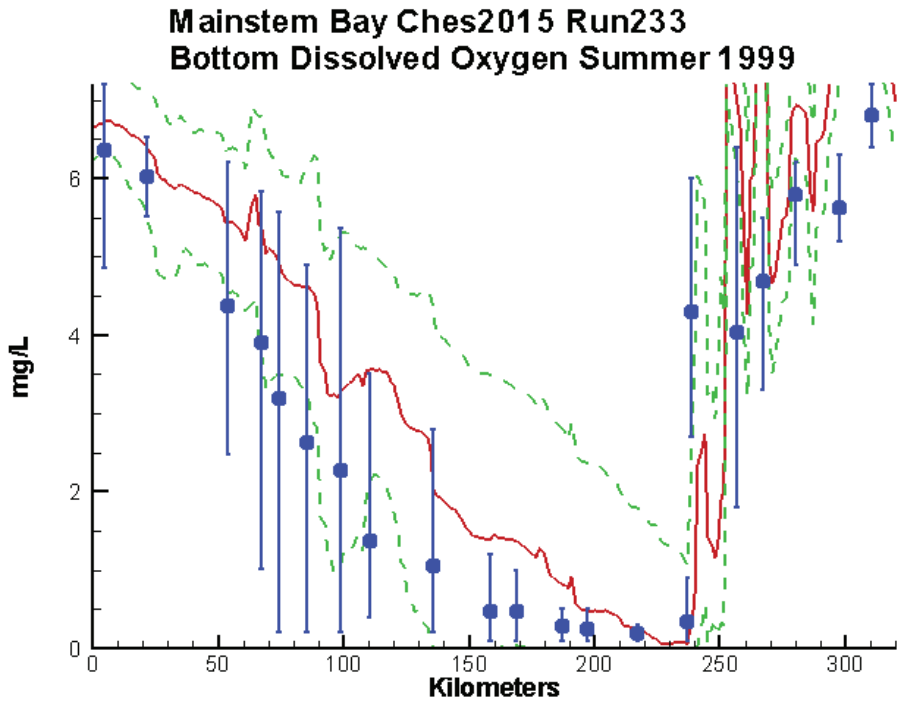

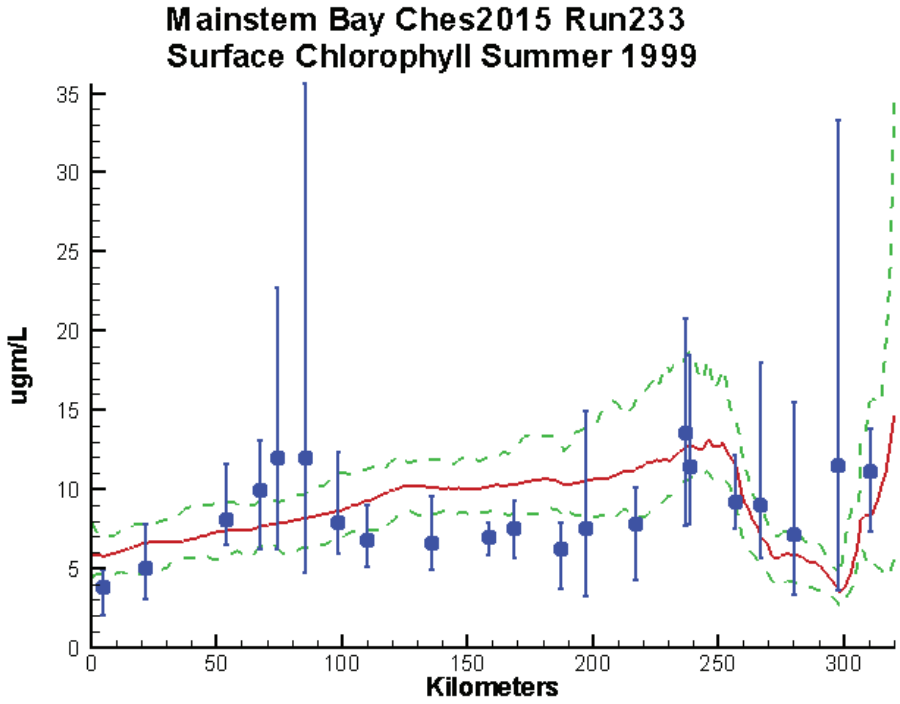

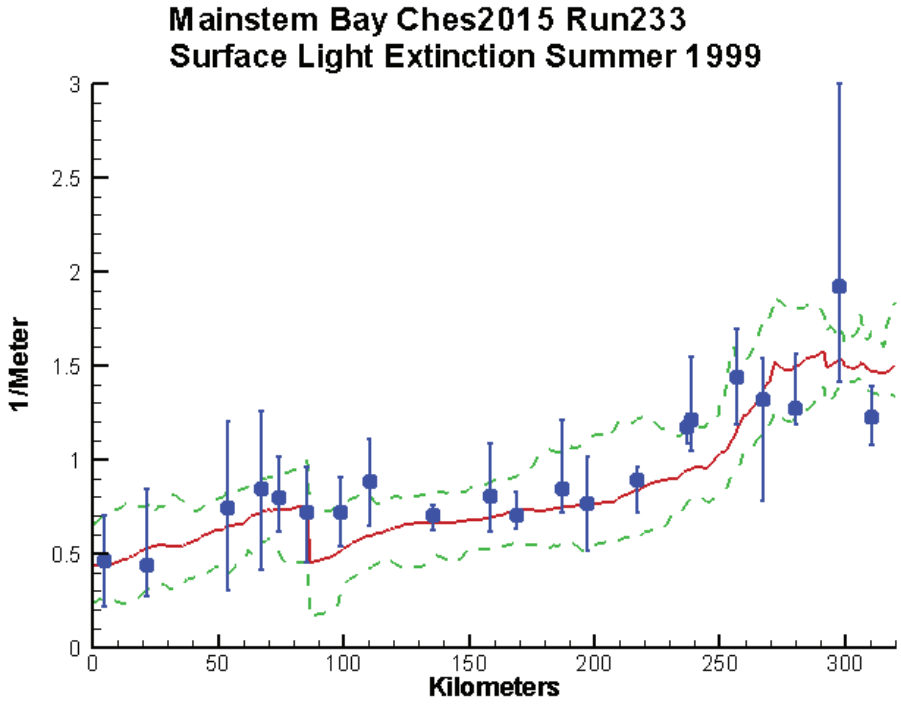

James River - Summer - 1999

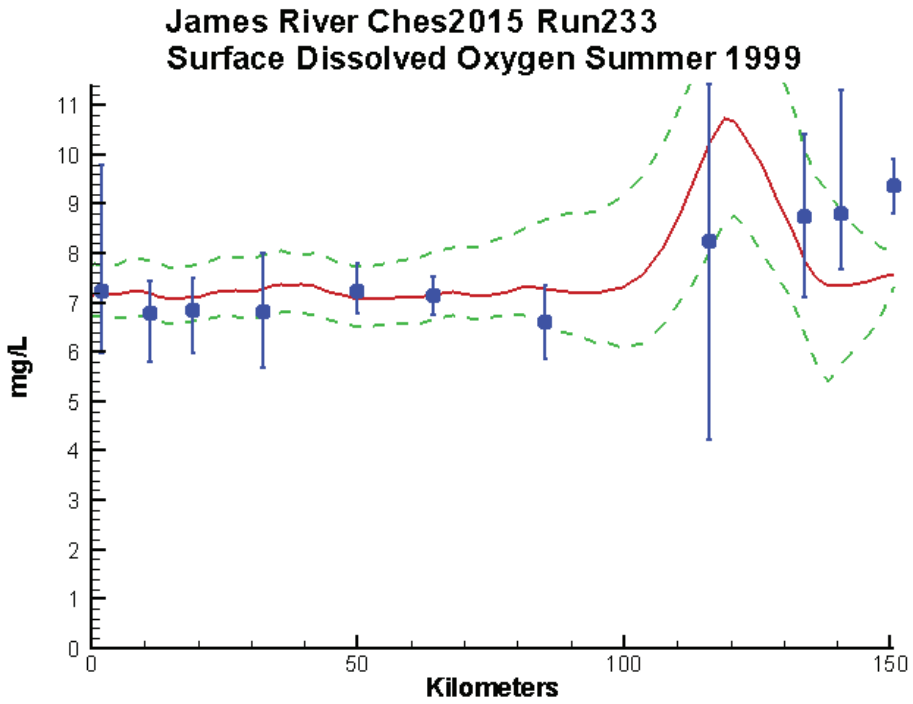

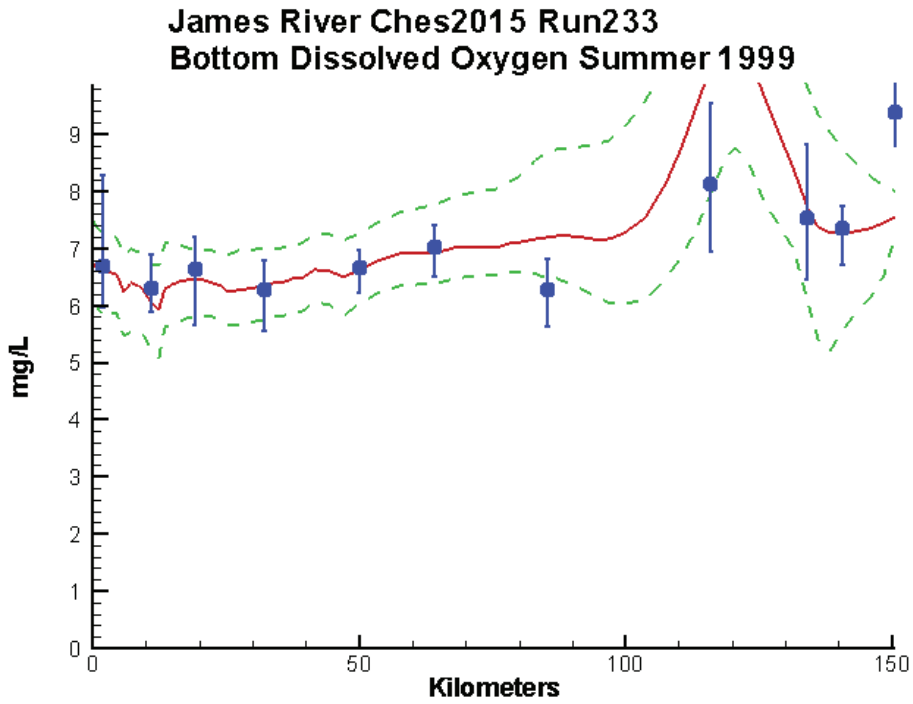

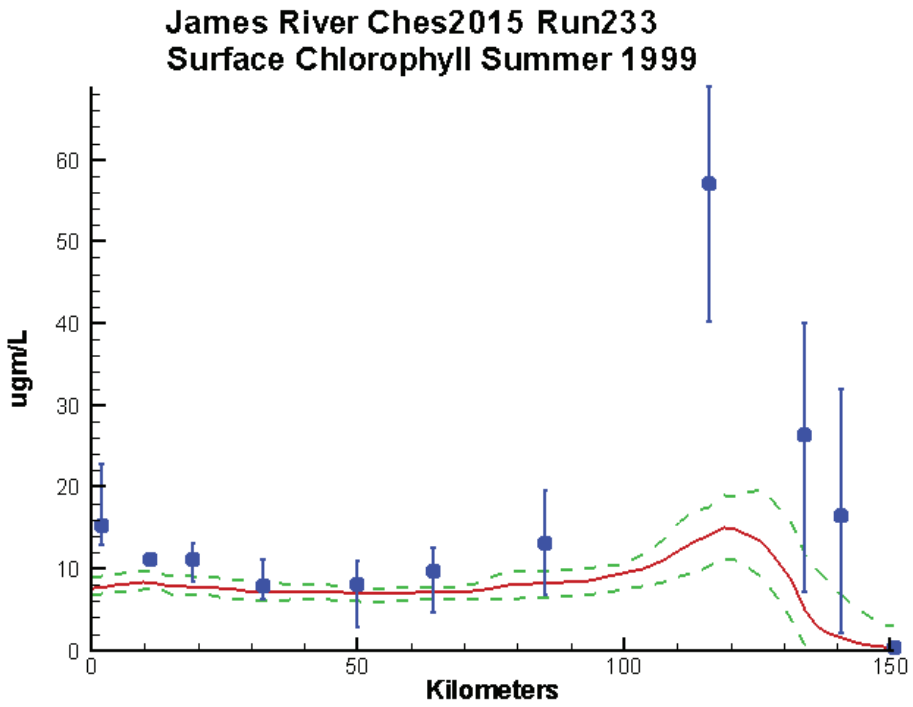

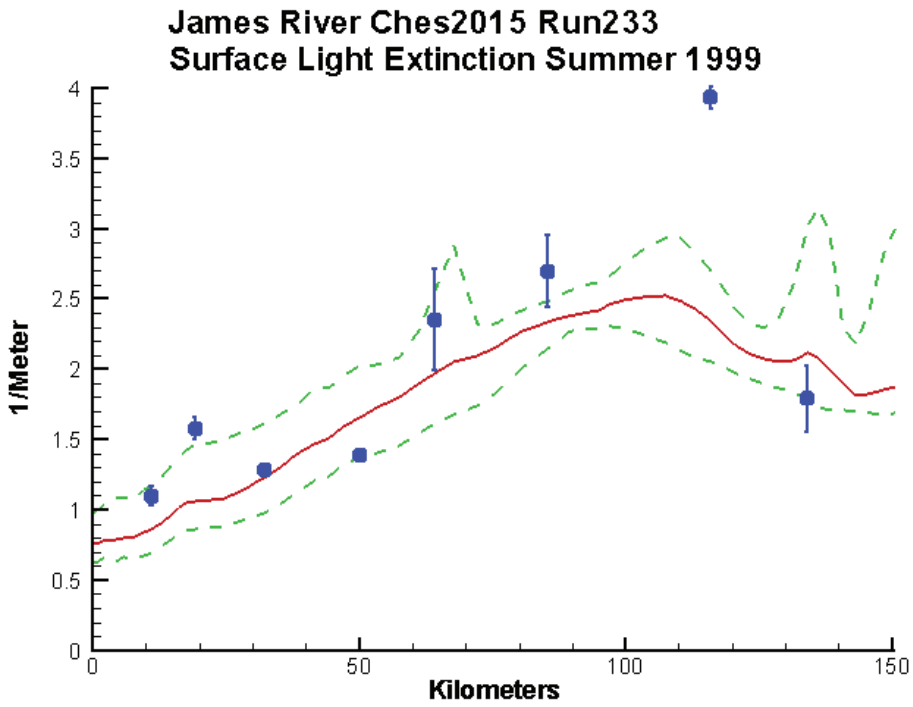

York River - Summer - 1999

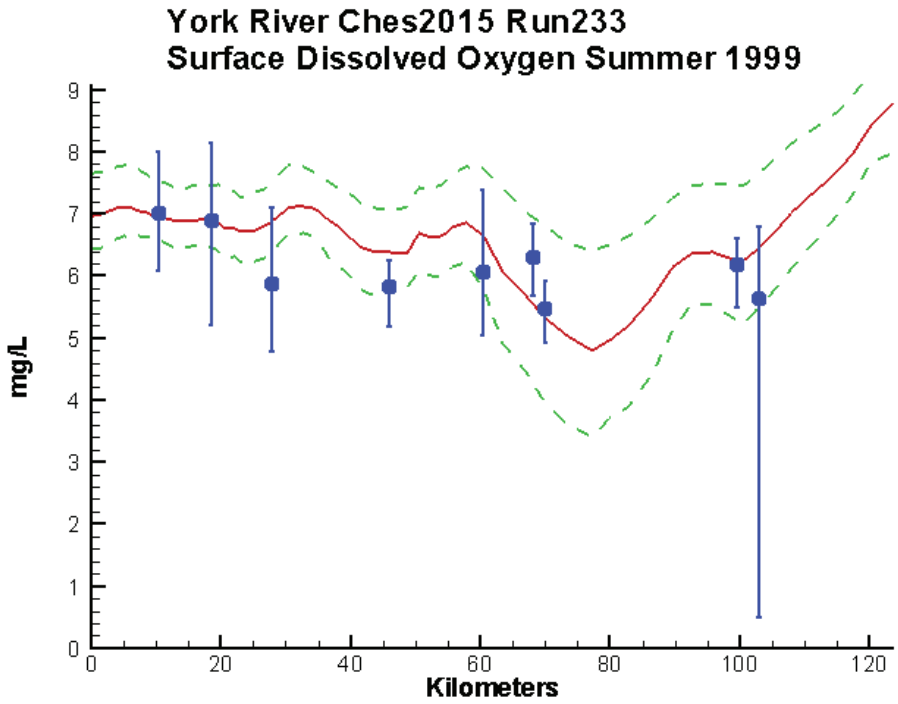

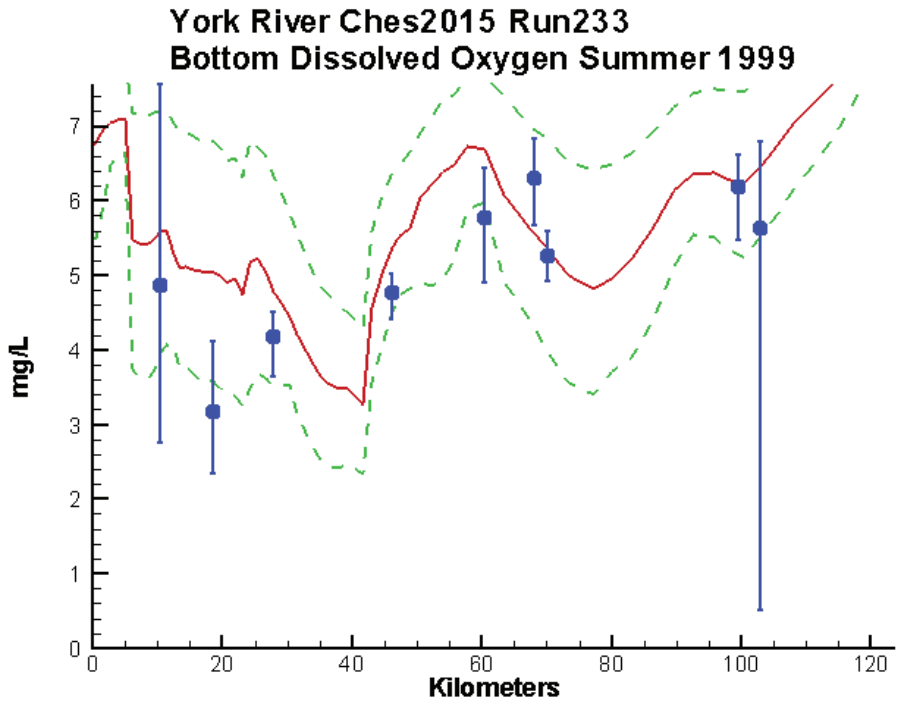

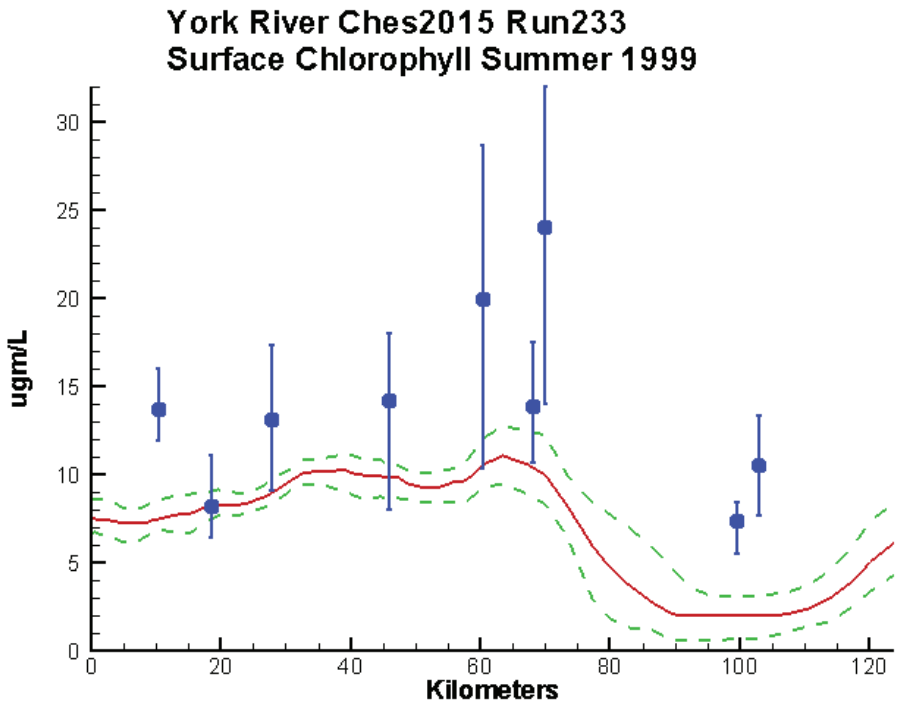

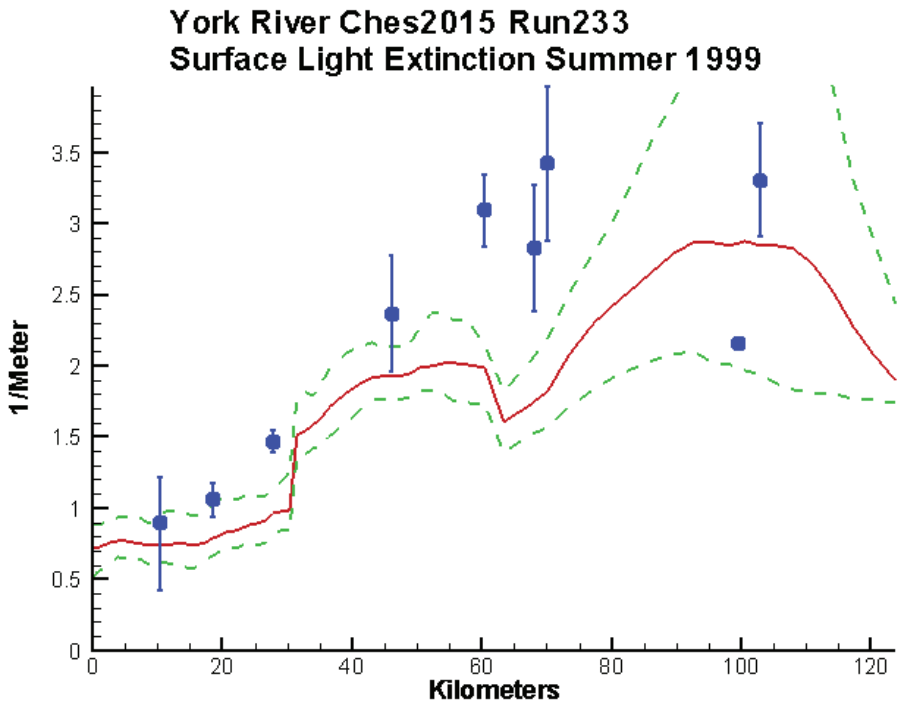

Rappahannock River - Summer - 1999

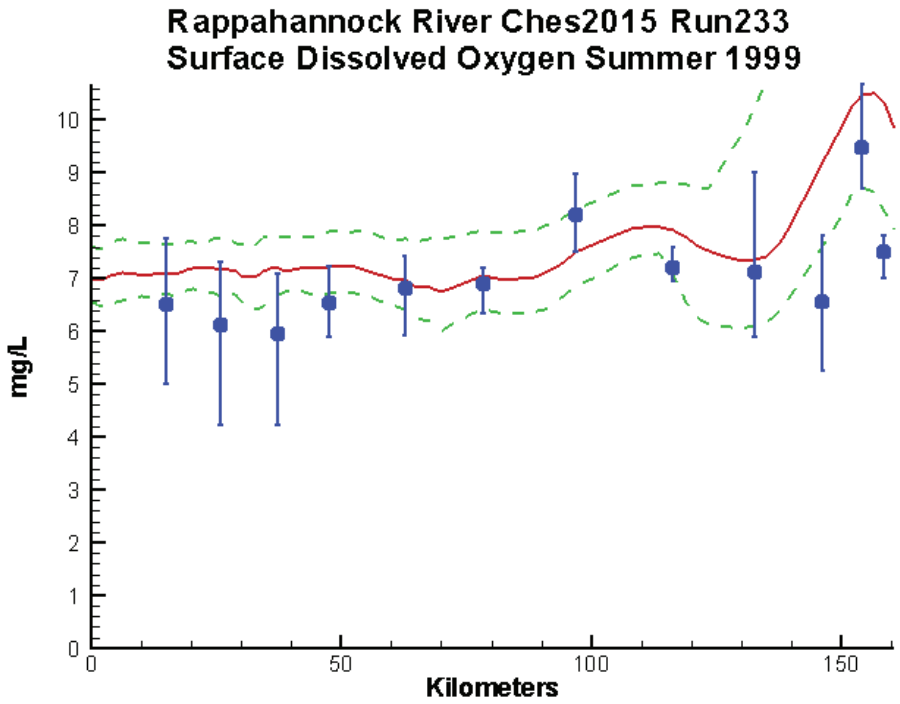

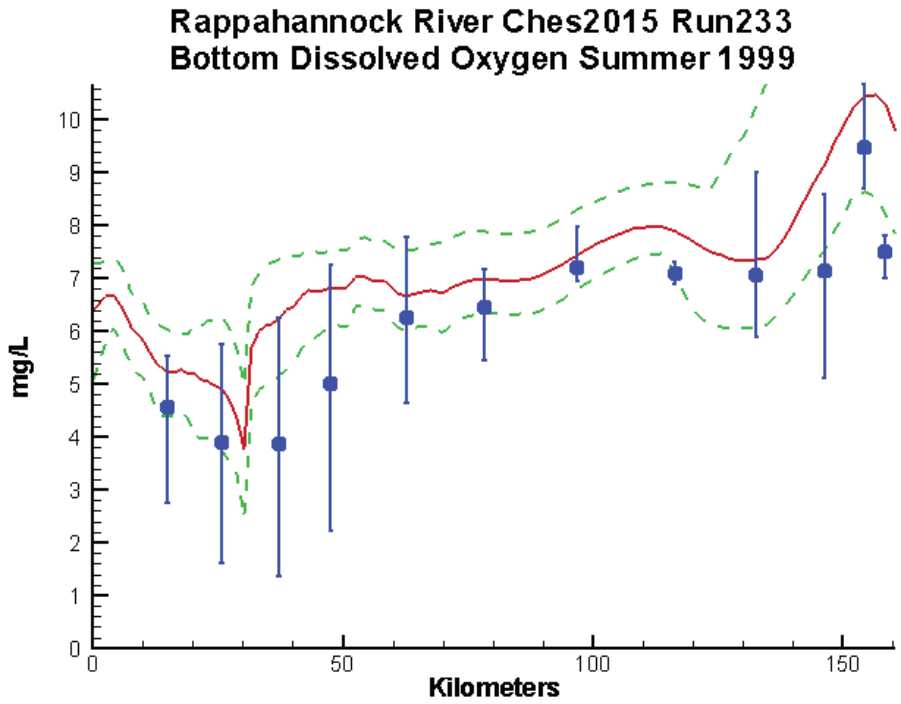

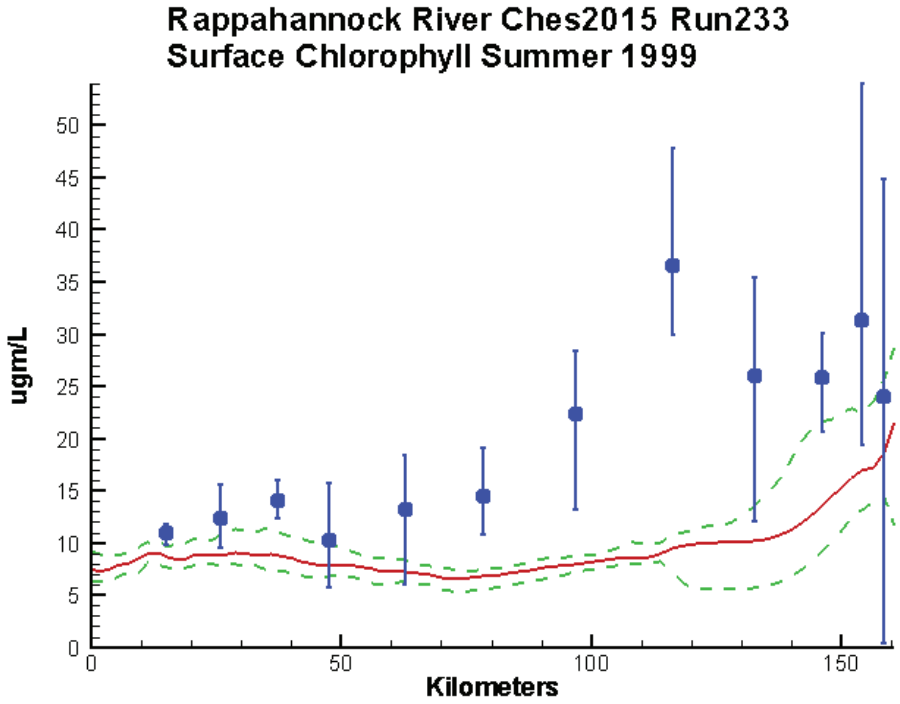

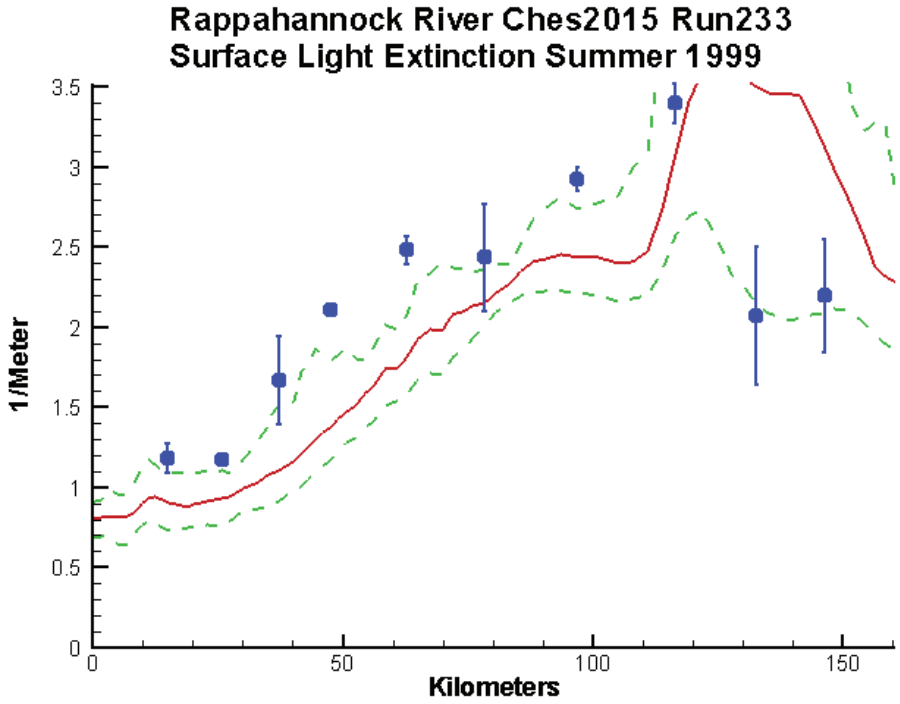

Potomac River - Summer - 1999

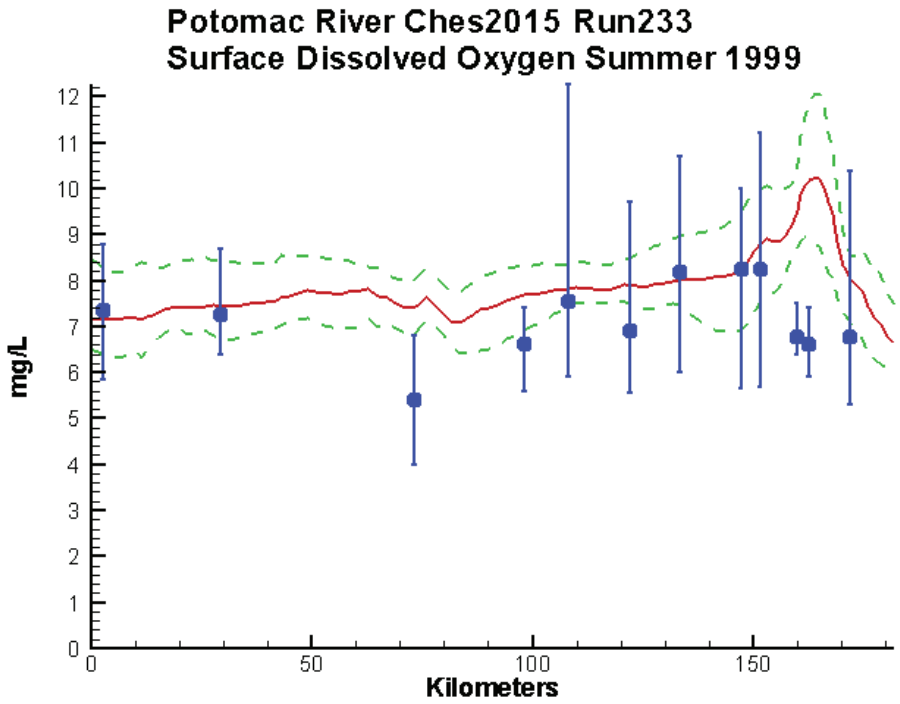

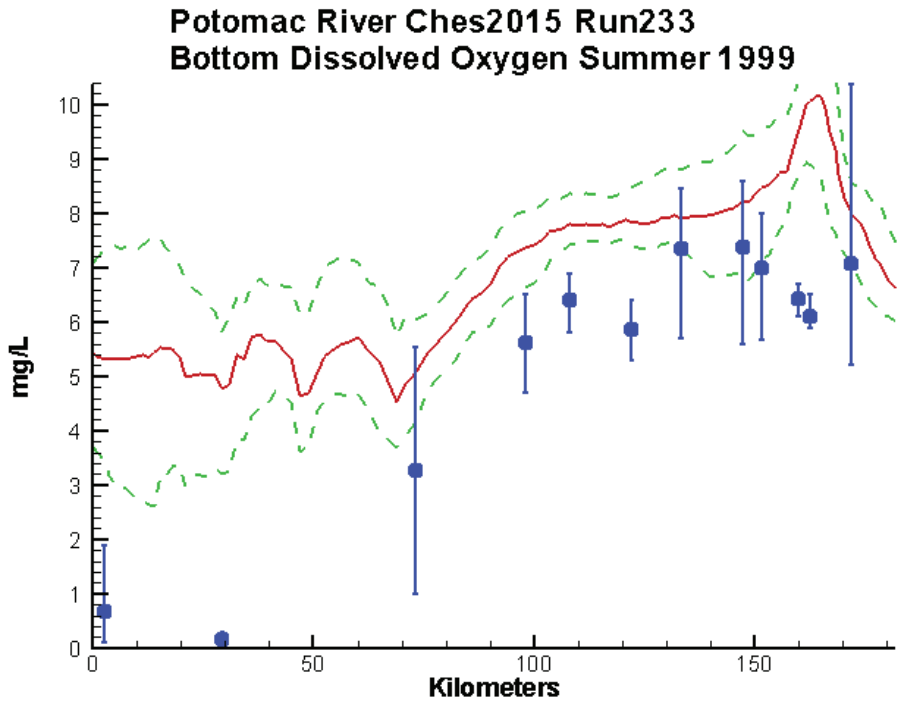

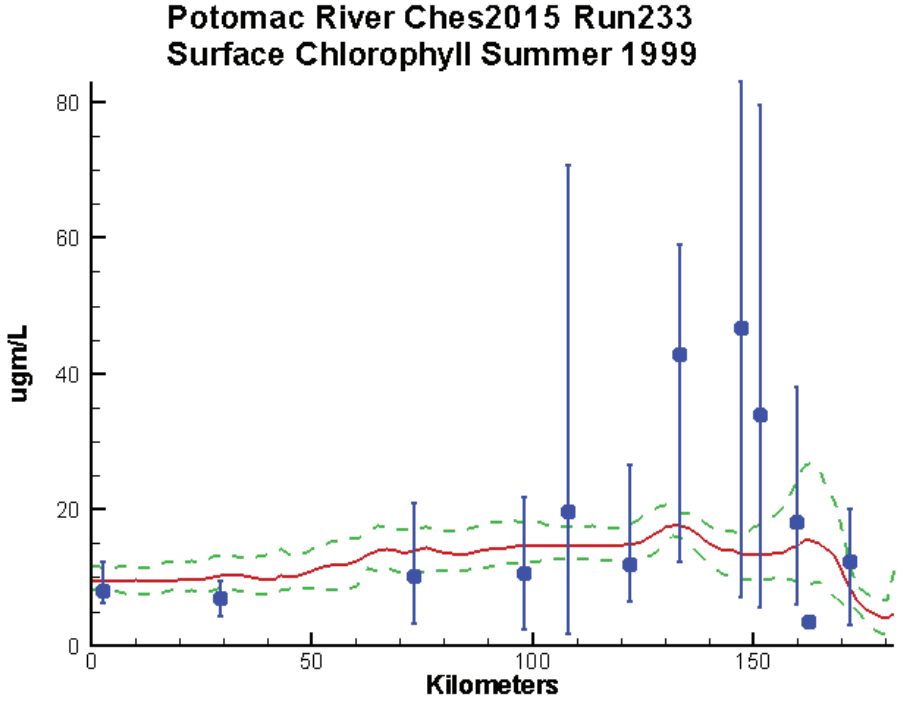

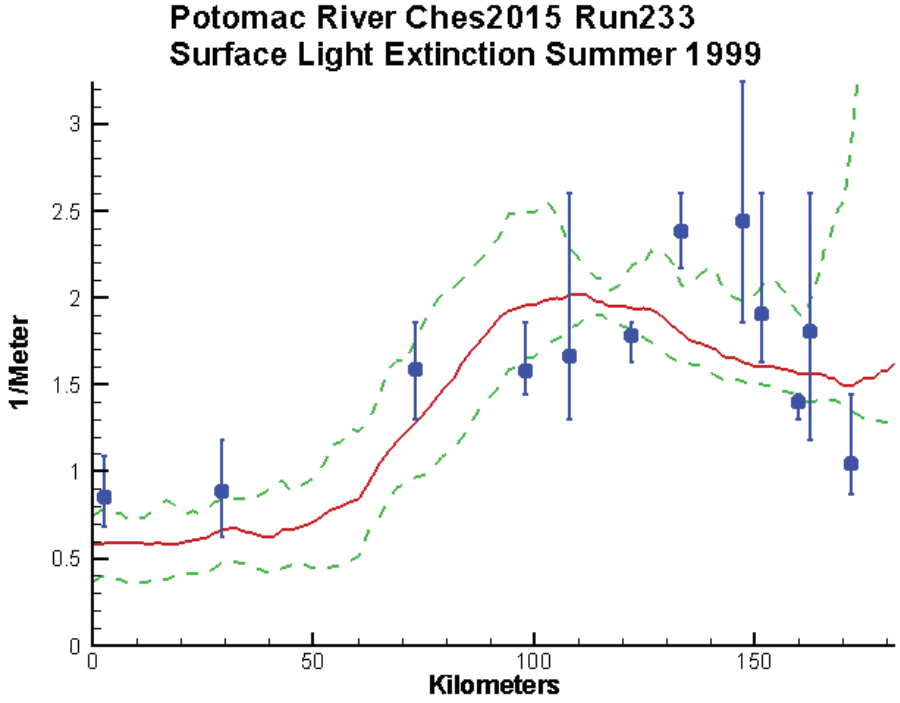

Patuxent River - Summer - 1999

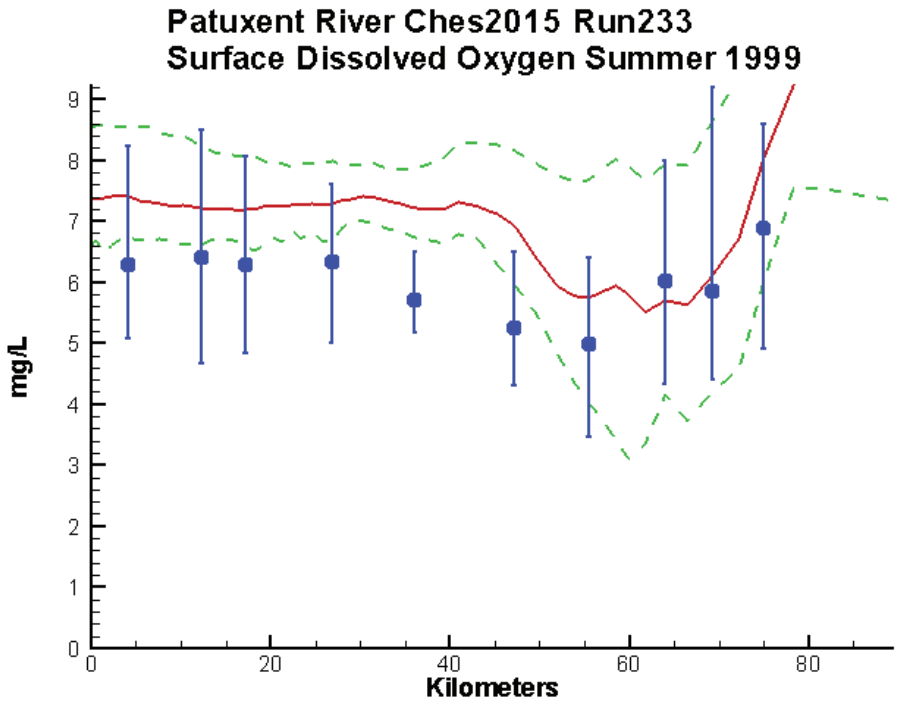

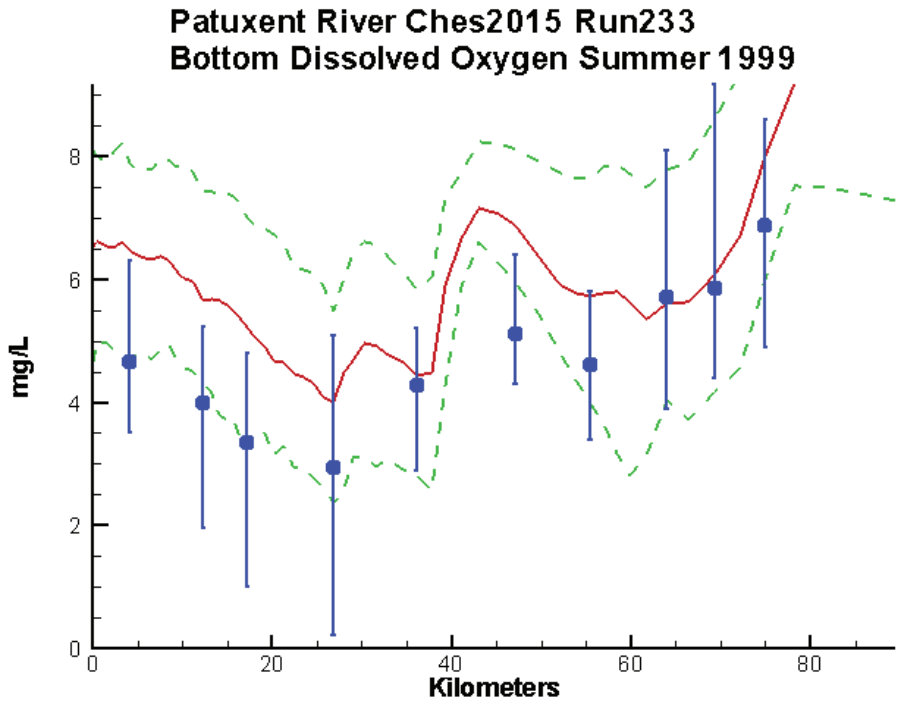

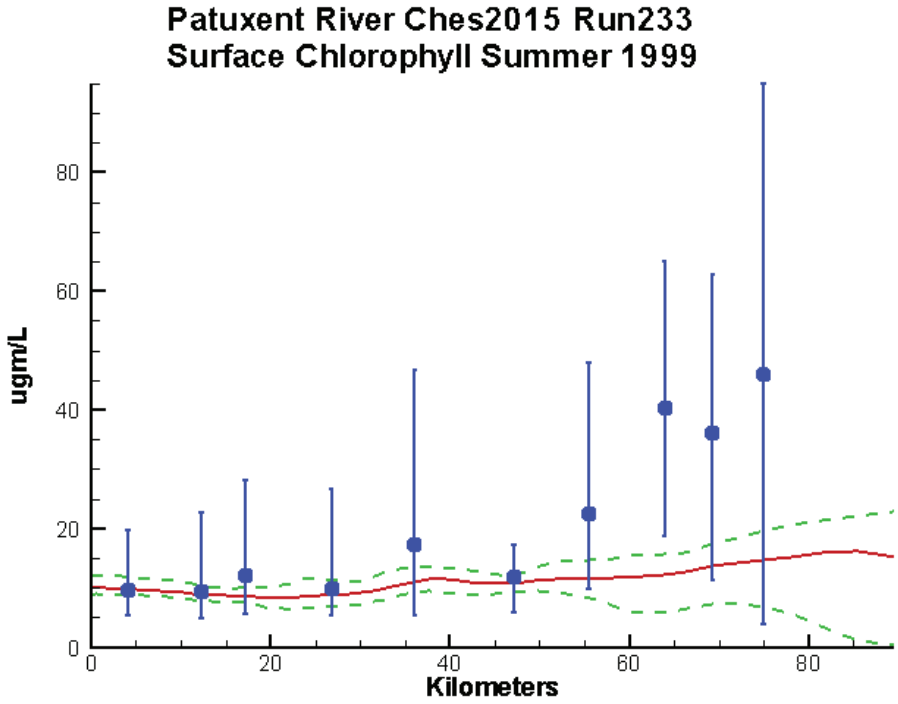

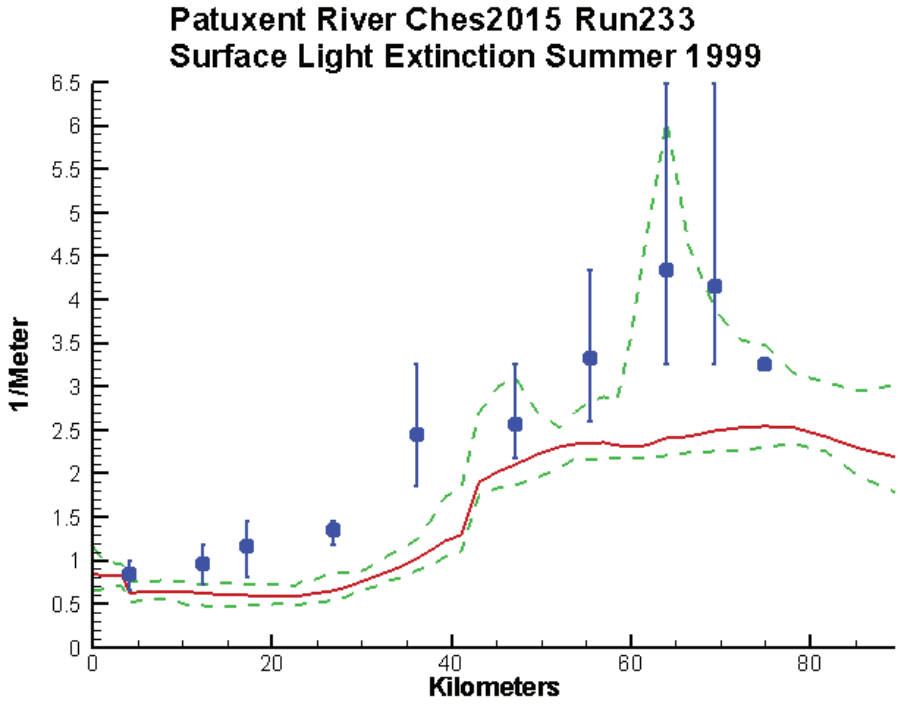

Appendix D: Longitudinal Comparisons 2002–2011

The spatial distributions of observed and computed properties were compared in a series of plots along the axes of the Bay and major tributaries (Figure D-1). The verification period encompassed more than 100 cruises. Reducing that number of surveys into a manageable volume of comparisons required selection and aggregation. Three years were selected for comparisons: 2004, 2007, and 2010. These years are not as readily distinguished by flow as the 1991–2000 sequence addressed in appendix C. The Susquehanna River flows for all three years fall between the 1999 (dry) and 1994 (average) flows of the earlier sequence.

Model results and observations were averaged into four seasons:

- Winter–December through February
- Spring–March through May
- Summer–June through August
- Fall–September through November

Conventional arithmetic means were calculated for the observations. Model results were subjected to a process designated as "cruise averaging." Within each season, model results were considered only during intervals coinciding with sample cruises. Cruise averaging diminished discrepancies between model and observations attributed to consideration of model results for periods when no data were collected. Daily averages of model results were computed within the model code. Cruise averaging was completed in a postprocessor. Arithmetic averages were computed during cruise periods for all modeled substances except for light attenuation and total suspended solids. Log averages were calculated for those two components. The variance of the computed values skewed arithmetic means to unrepresentative high values. The postprocessor also extracted the maximum and minimum computed daily averages.

The mean and range of the observations, at surface and bottom, were compared to the cruise average and range of daily-average model results. The longitudinal axes largely followed the maximum depths represented on the model grid. Only stations located on the axes were considered for comparison with the model. Comparisons were made for physical quantities (salinity, temperature, suspended solids, and light attenuation), chlorophyll, dissolved oxygen (DO) and multiple forms of carbon, nitrogen, and phosphorus.

Figure D-1. Longitudinal transects in the Bay and major tributaries.

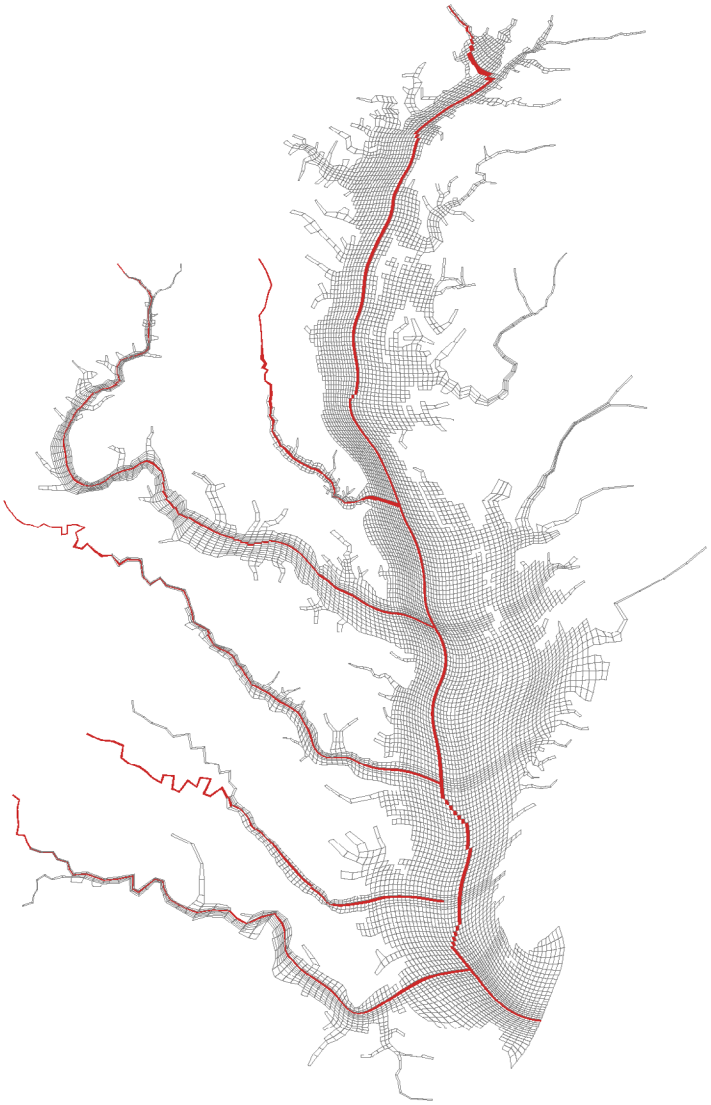

This appendix concentrates on the components that correspond closely to chlorophyll, clarity, and DO in the critical summer period. On the plots provided in this appendix, DO is shown at the surface and bottom. Surface samples are from the 1-meter depth. Bottom samples are typically 1 meter off the bottom and follow local bathymetry. Model values are from surface and bottom cells on the grid. Chlorophyll and light attenuation are presented for the surface only.

For all substances, the blue circles and vertical bars indicate mean and range of the observations, respectively. The continuous red and green traces represent model mean and range, respectively, subject to the selection and averaging process described above.

Mainstem Bay - Summer - 2004

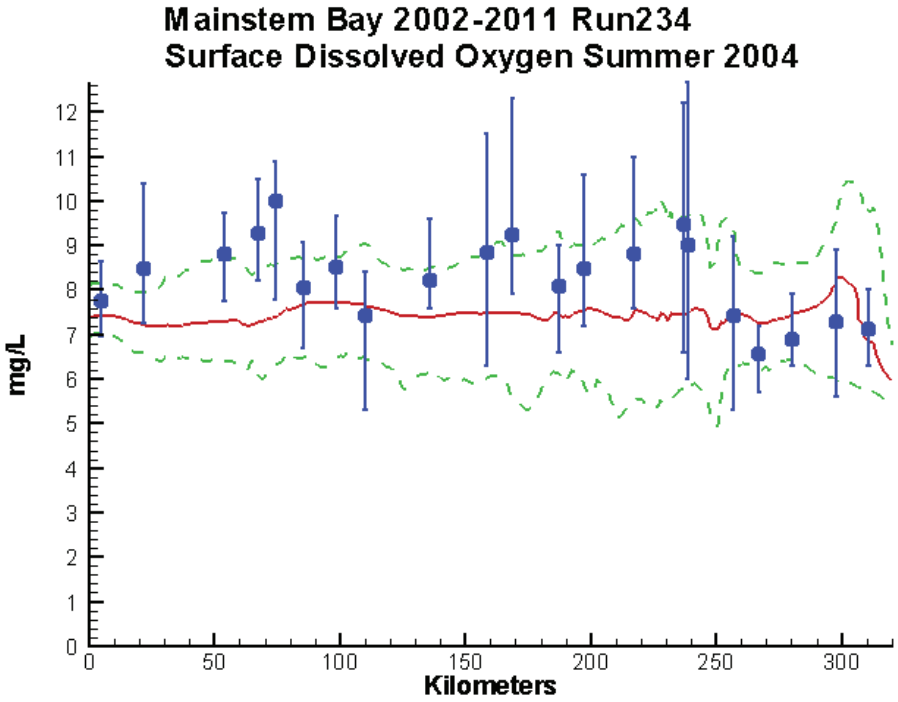

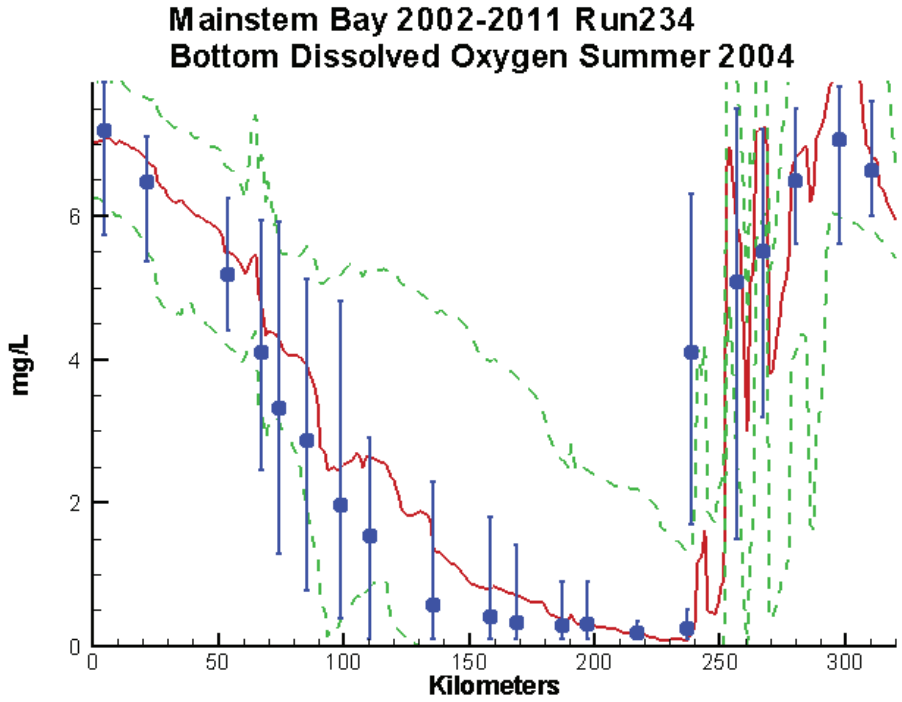

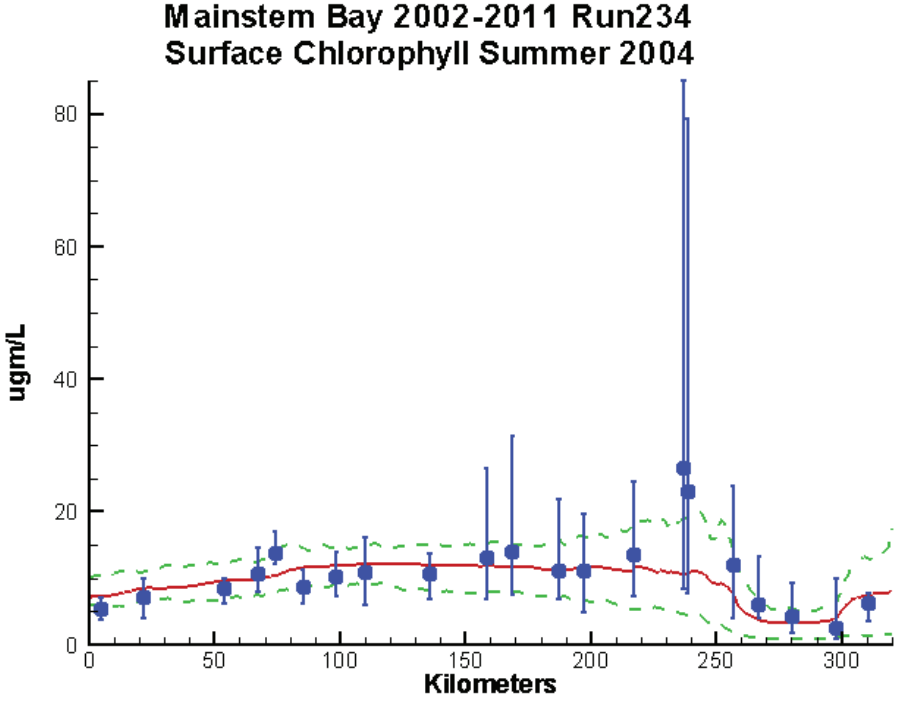

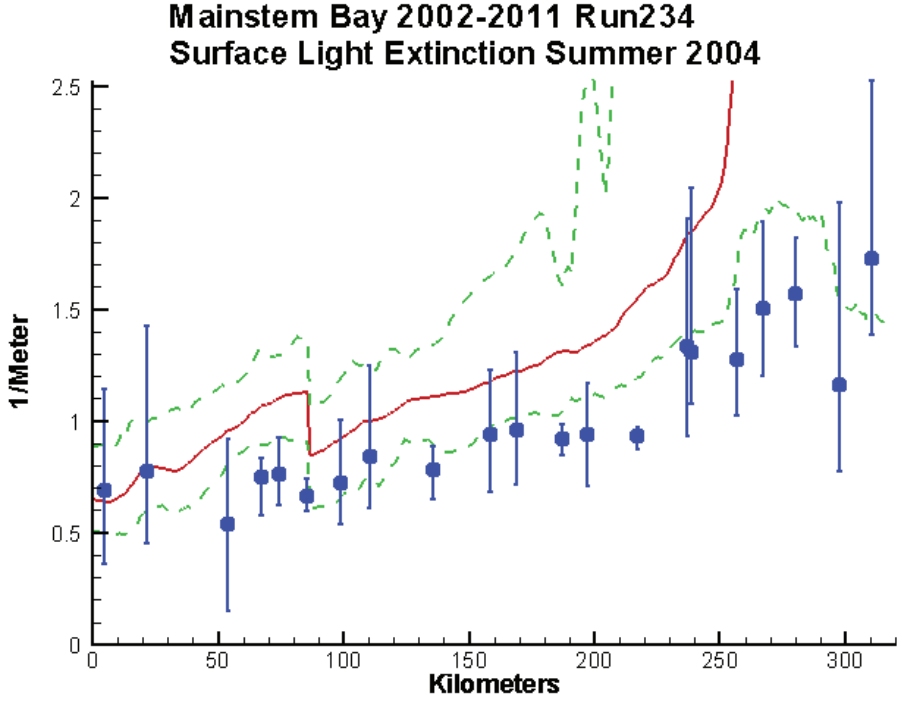

James River - Summer - 2004

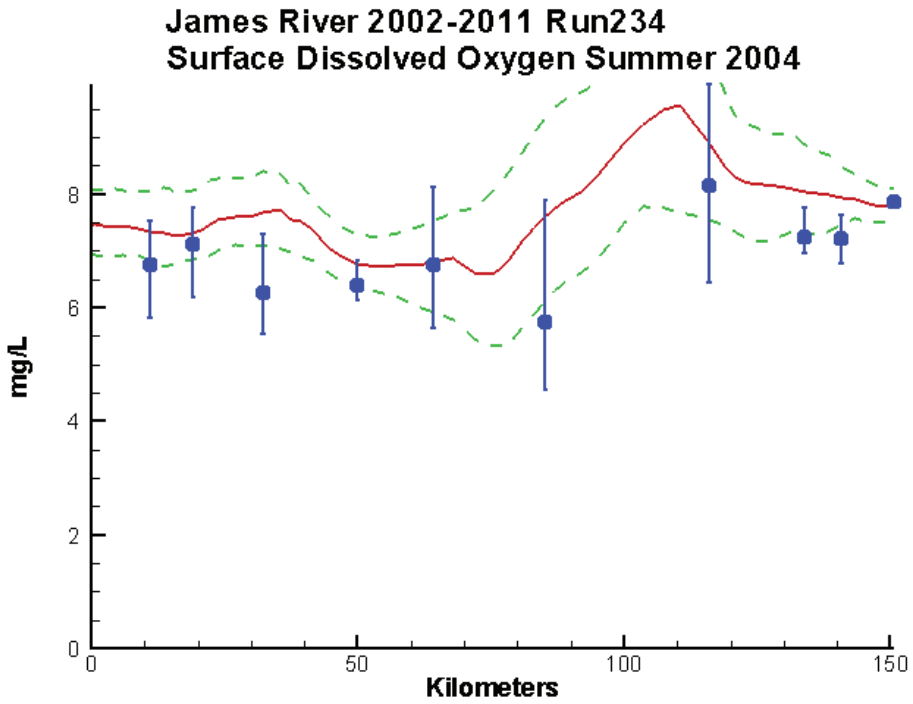

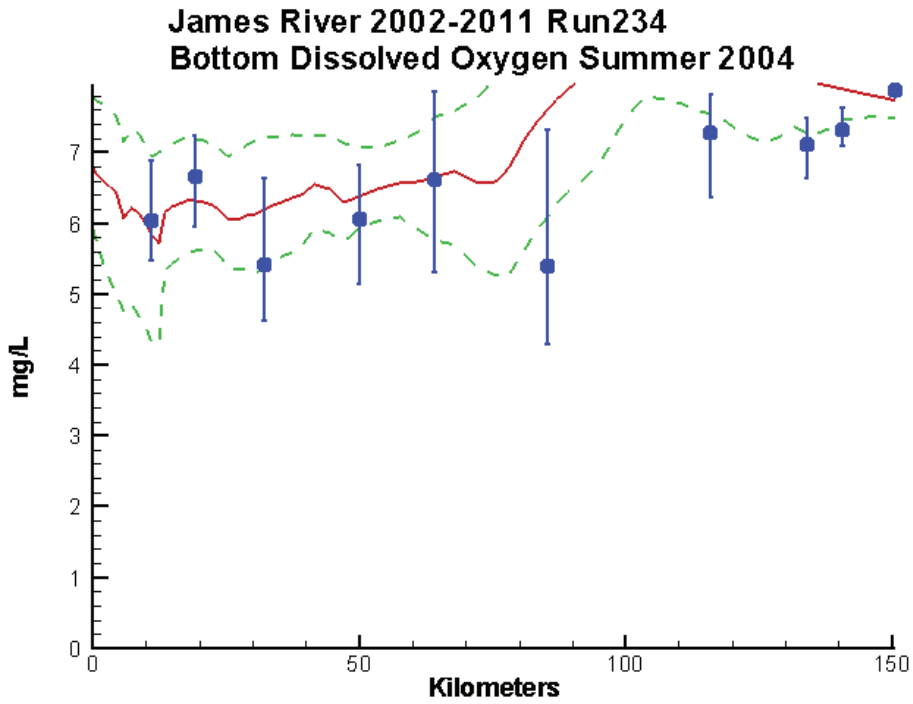

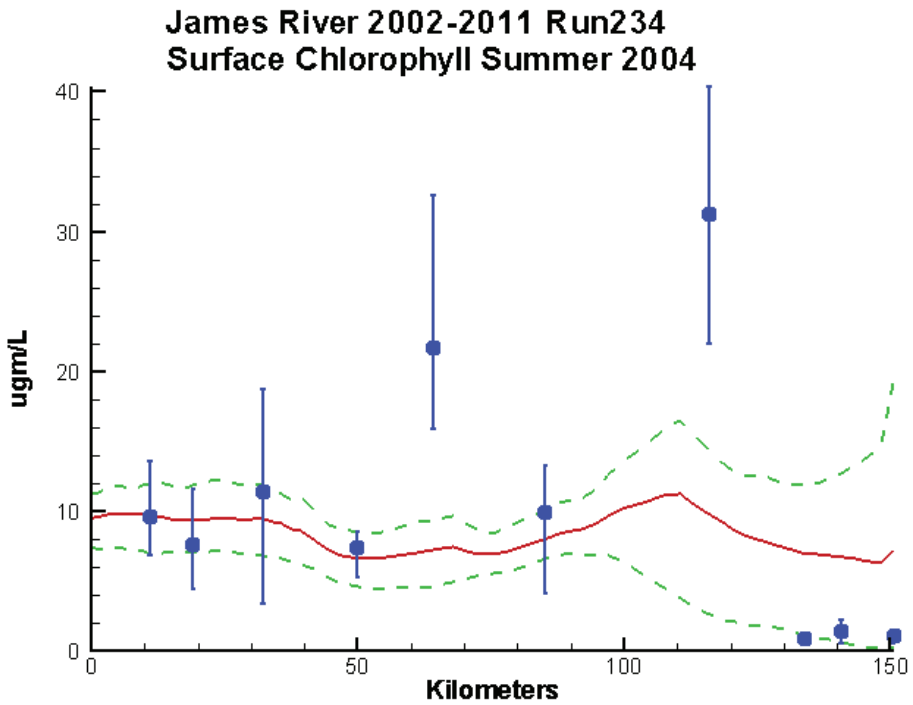

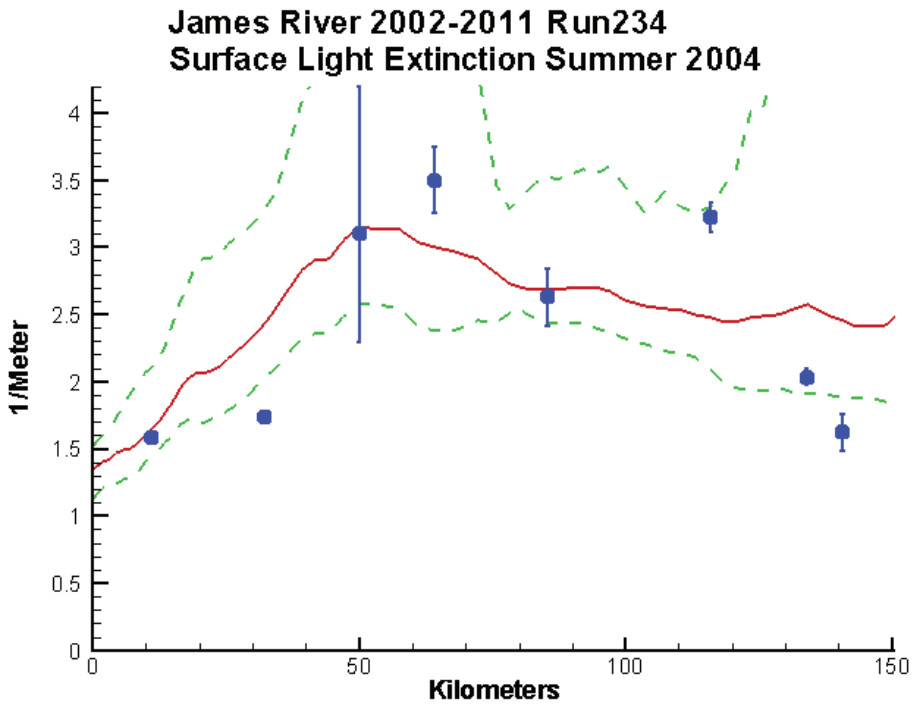

York River - Summer - 2004

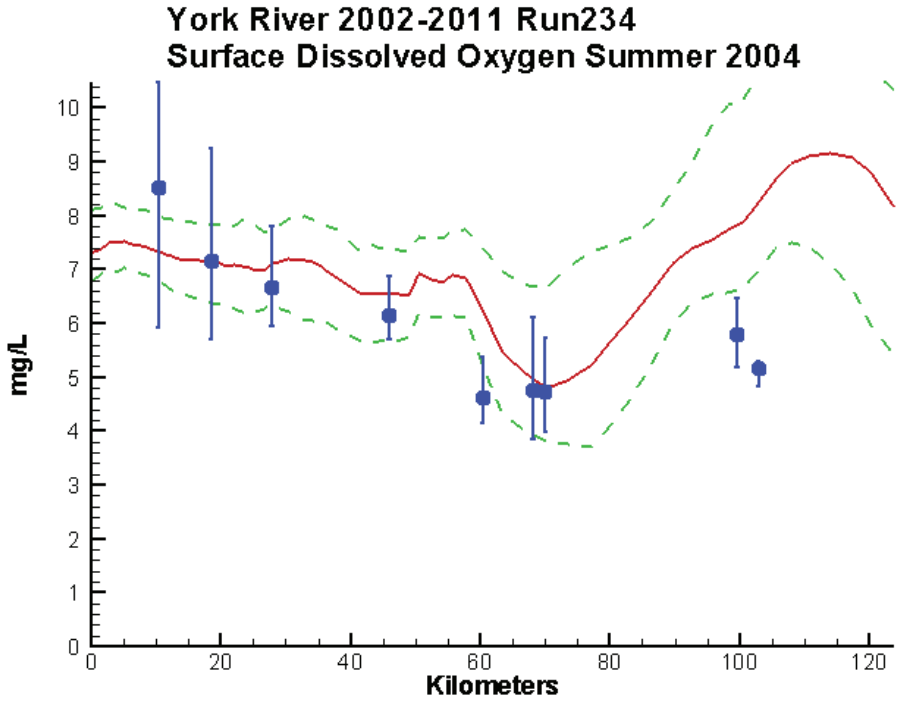

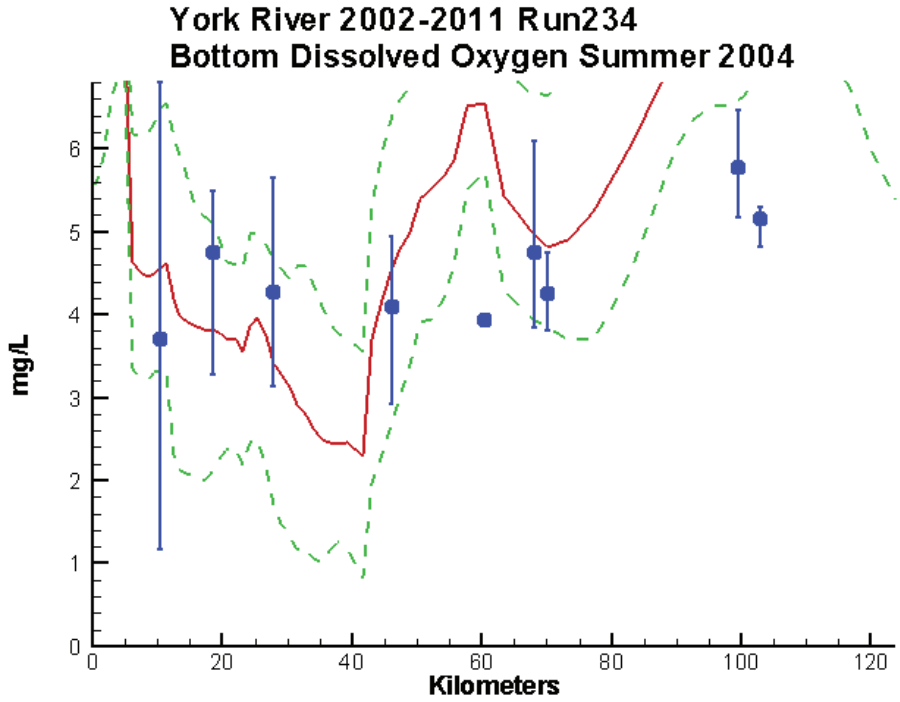

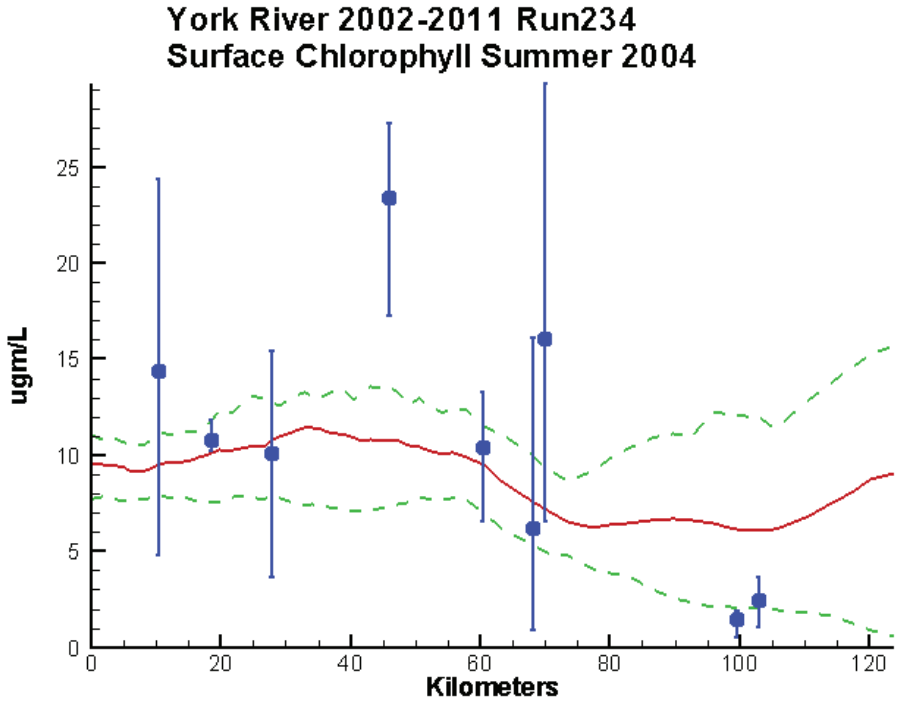

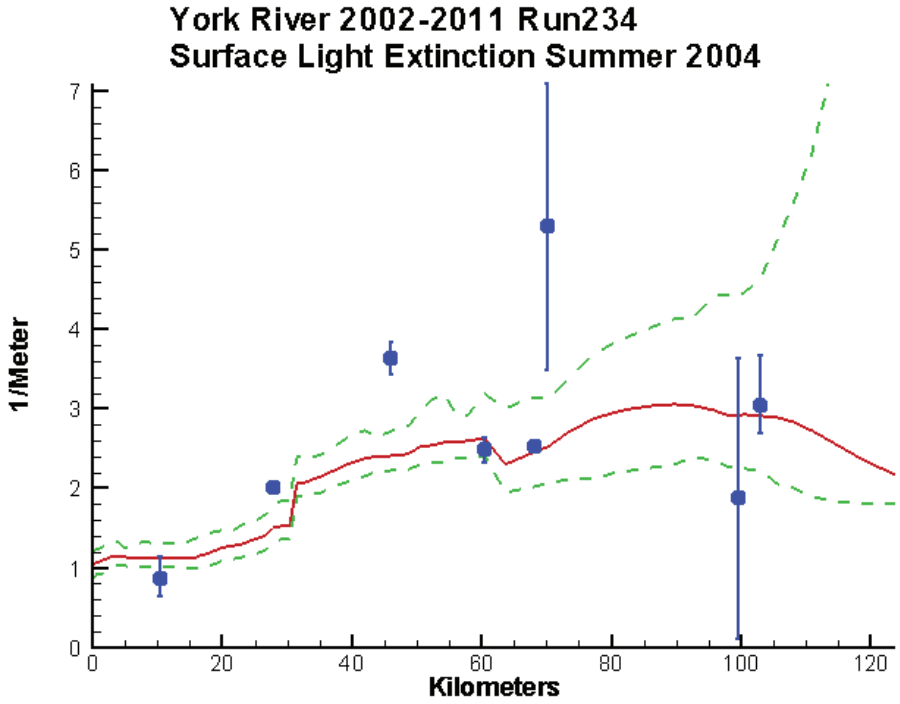

Rappahannock River - Summer - 2004

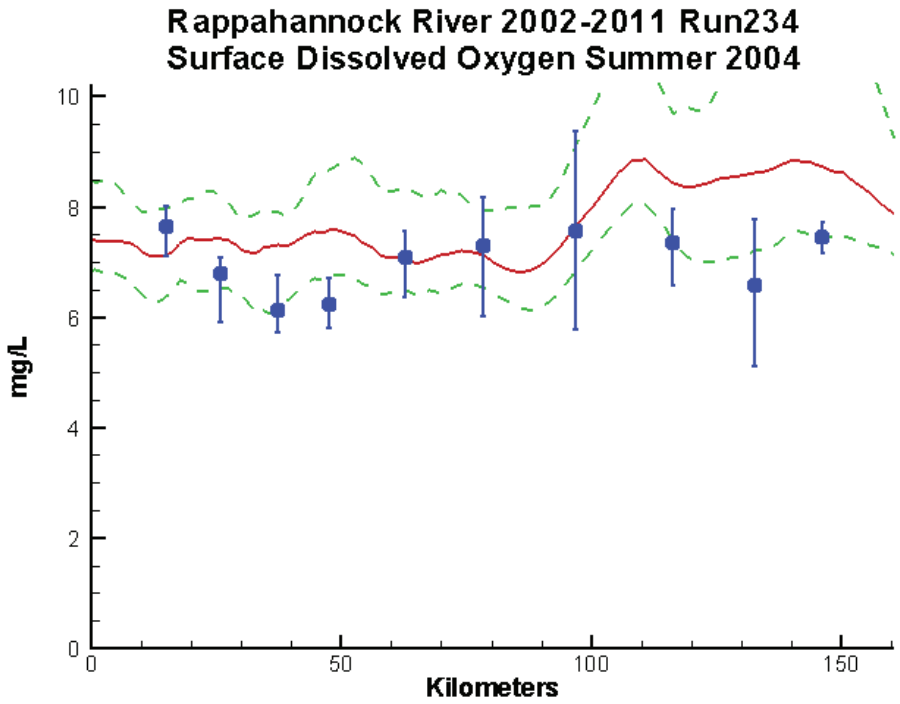

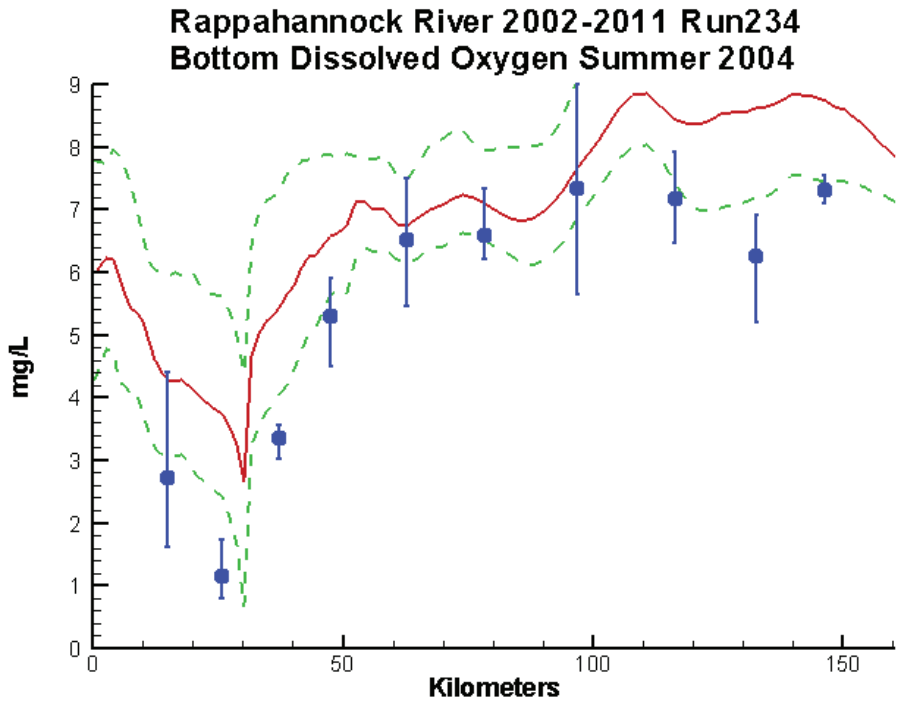

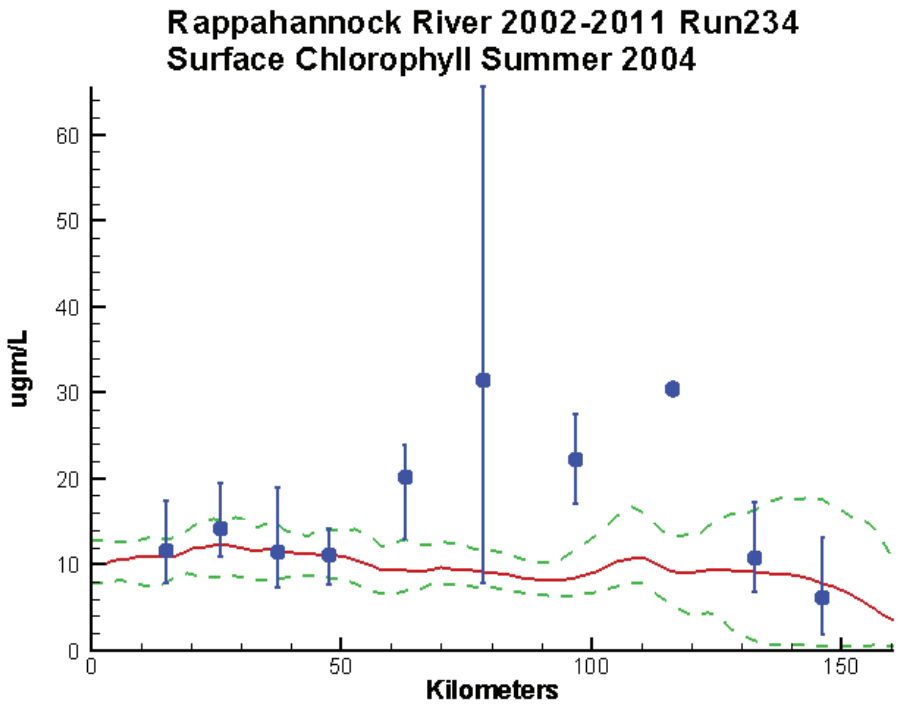

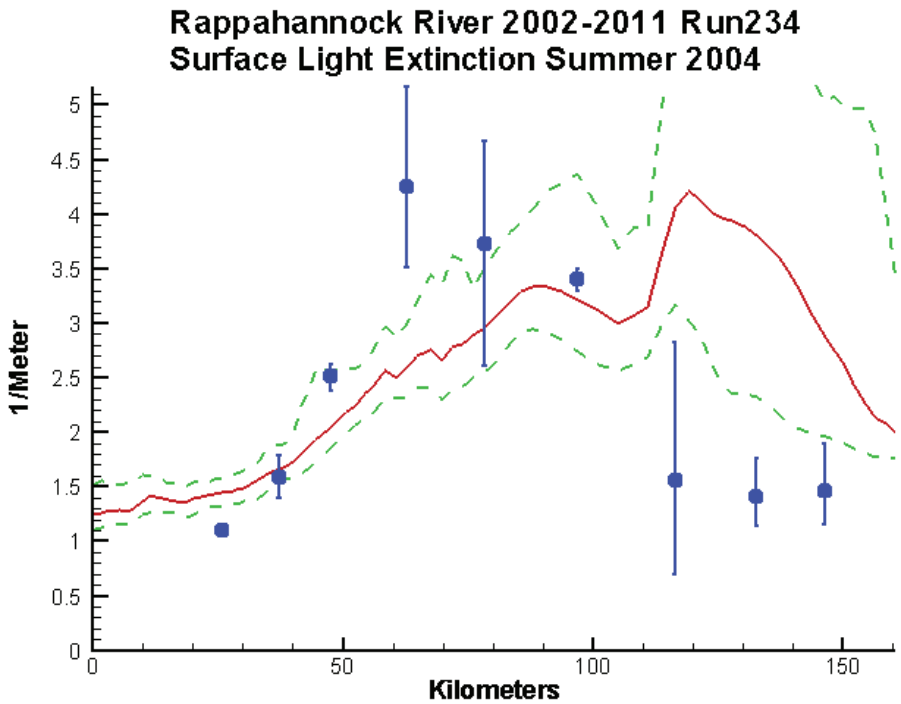

Potomac River - Summer - 2004

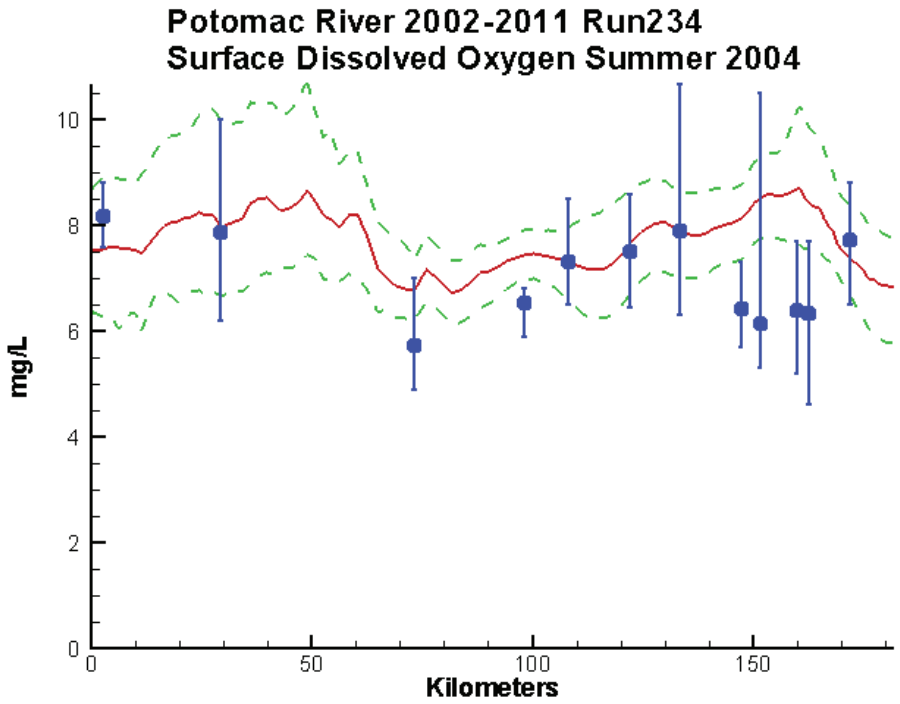

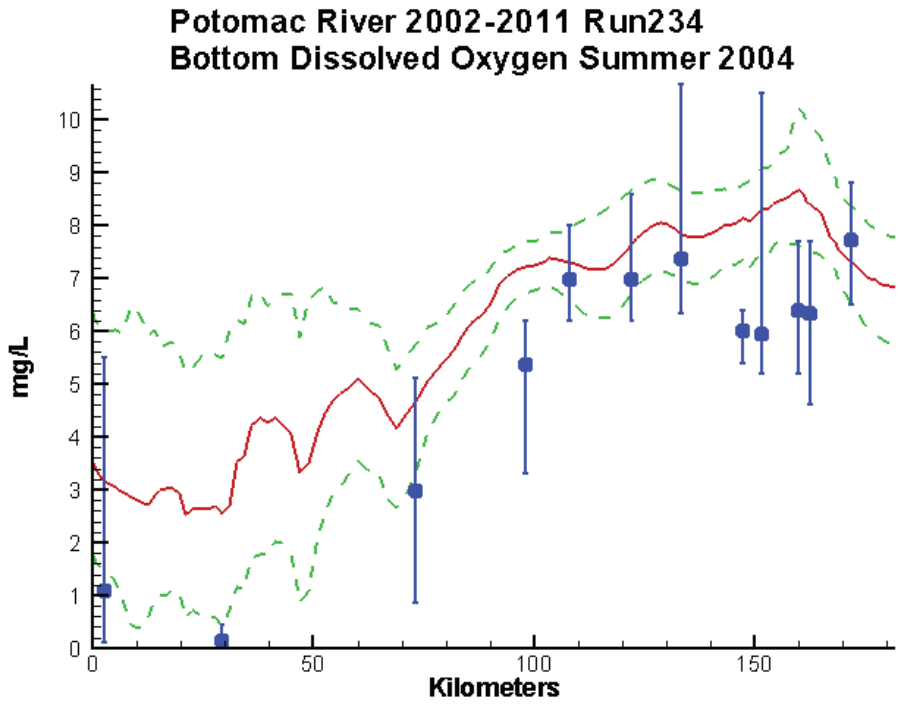

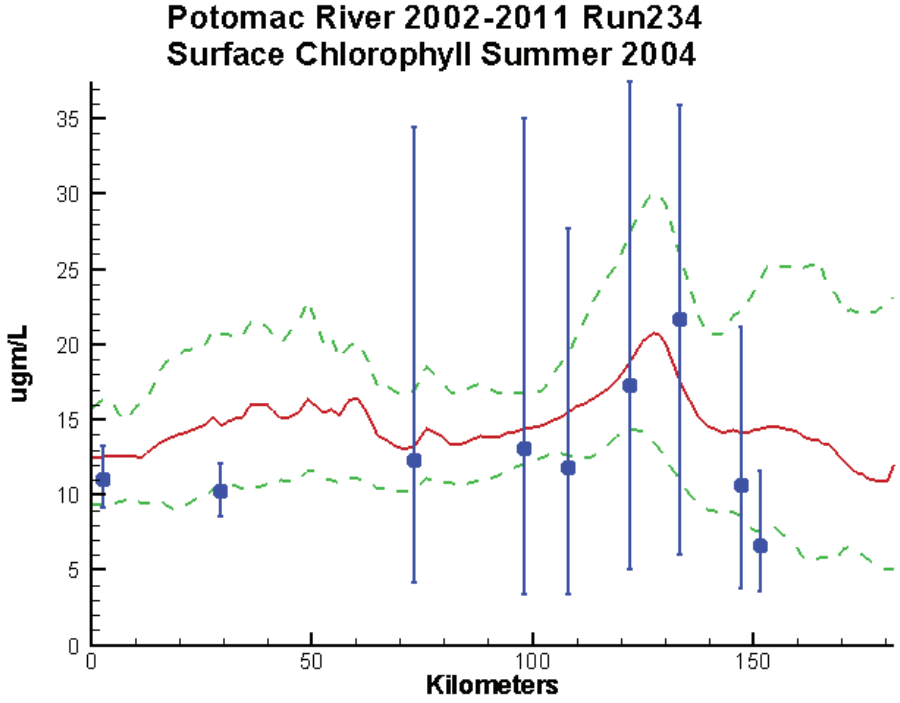

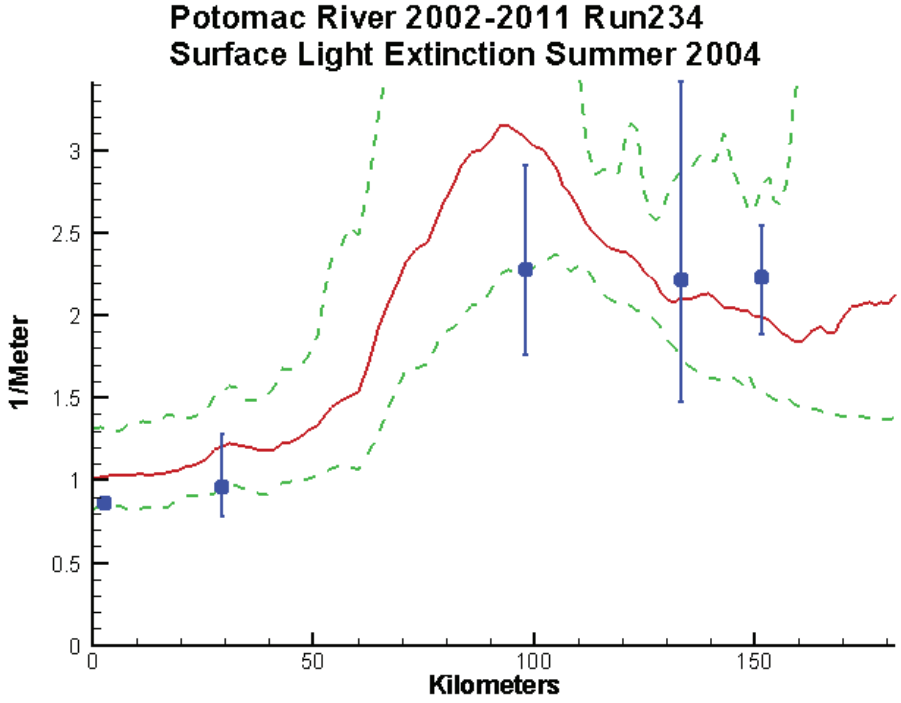

Patuxent River - Summer - 2004

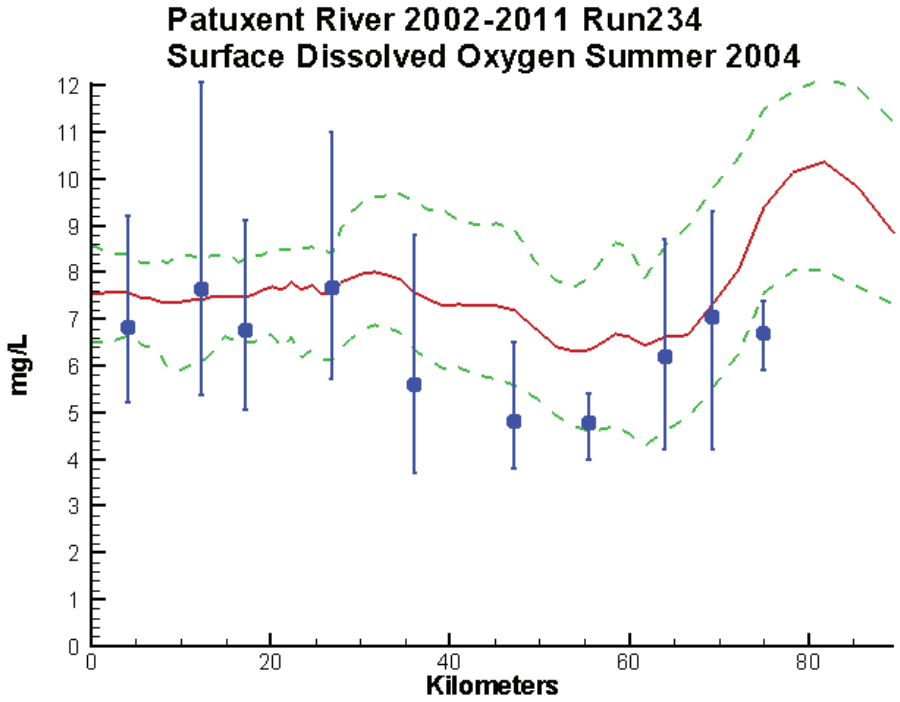

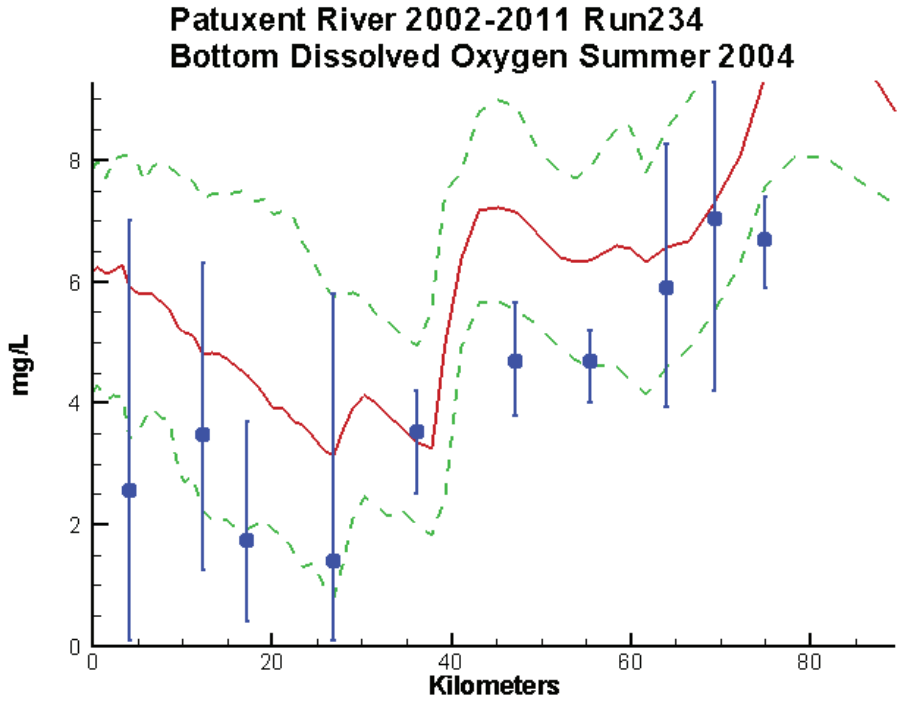

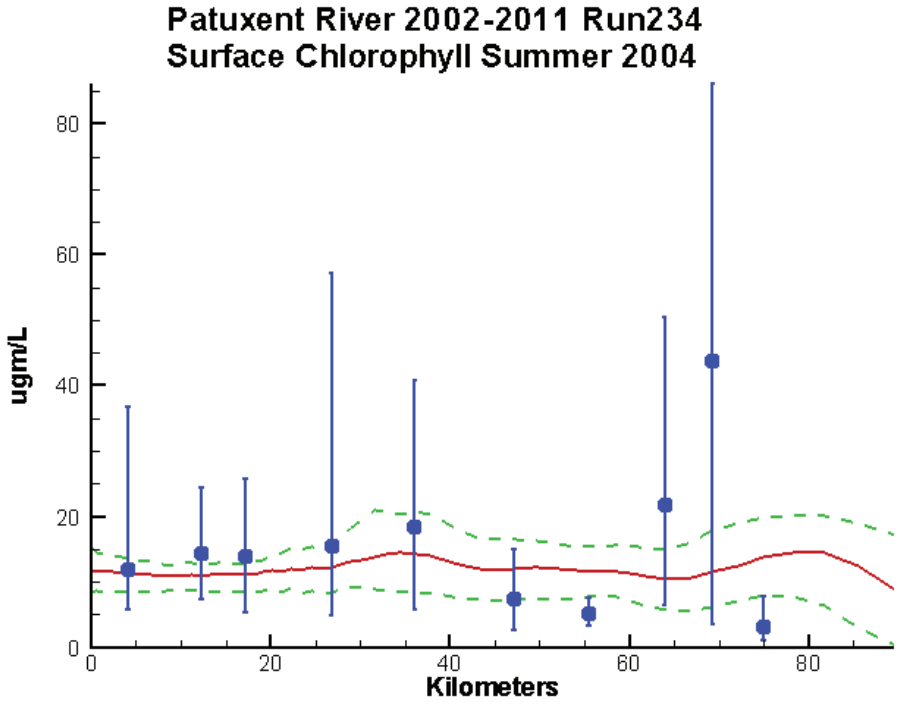

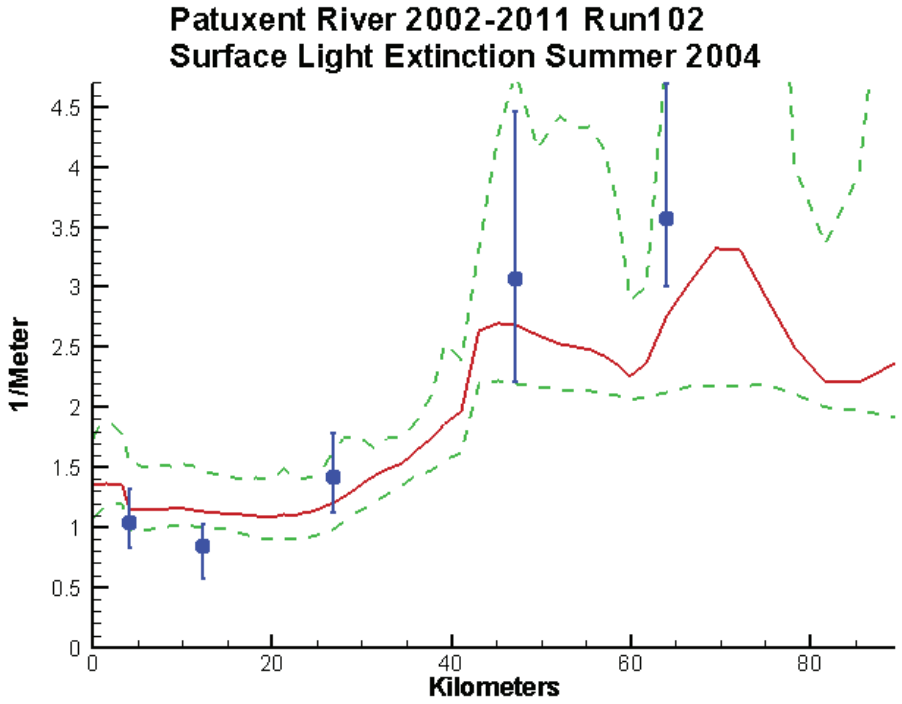

Mainstem Bay - Summer - 2007

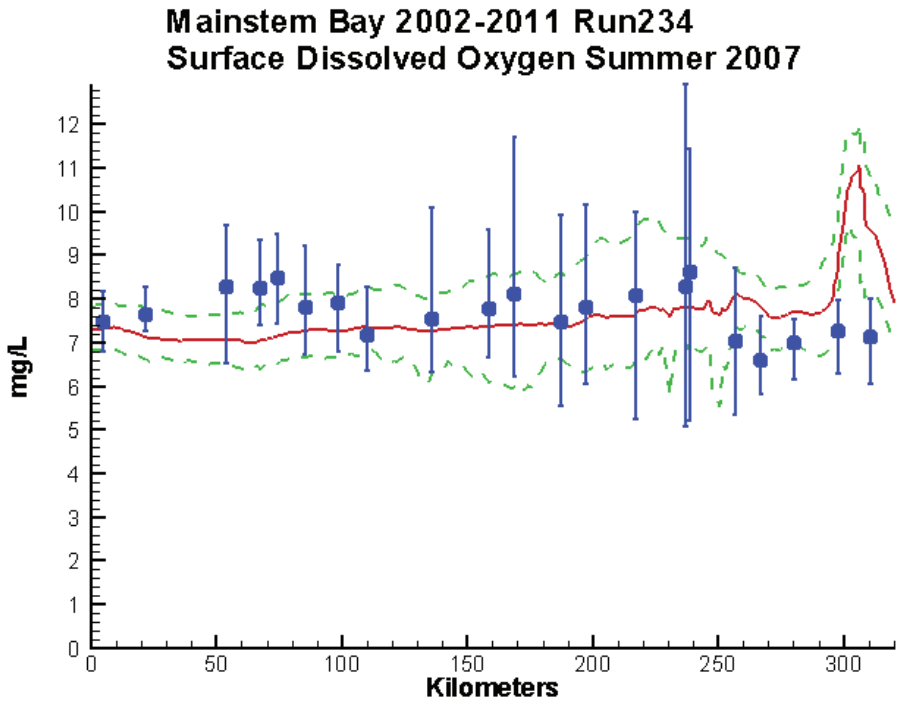

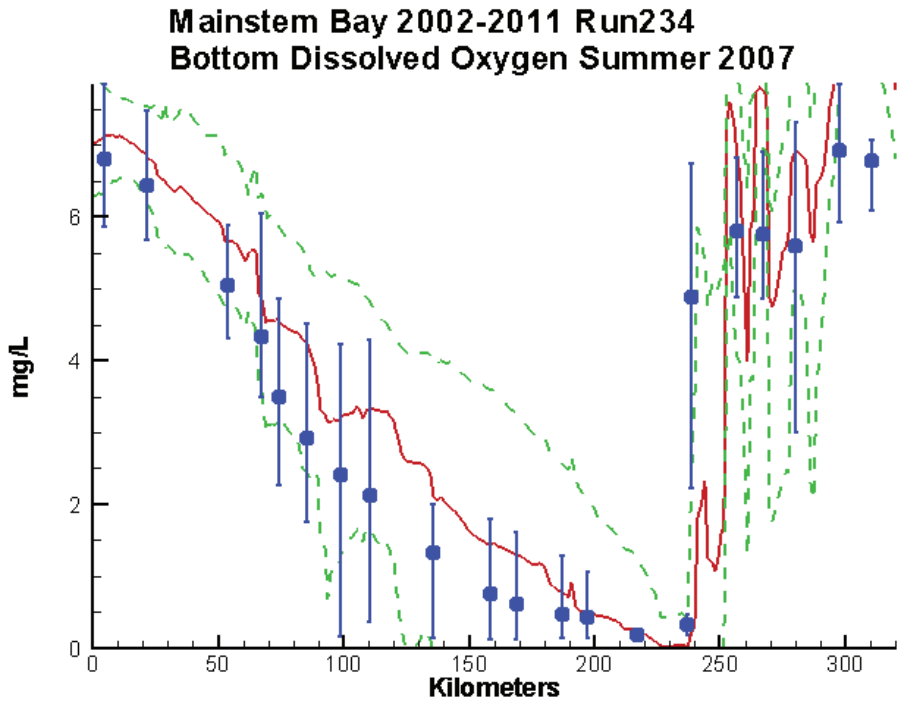

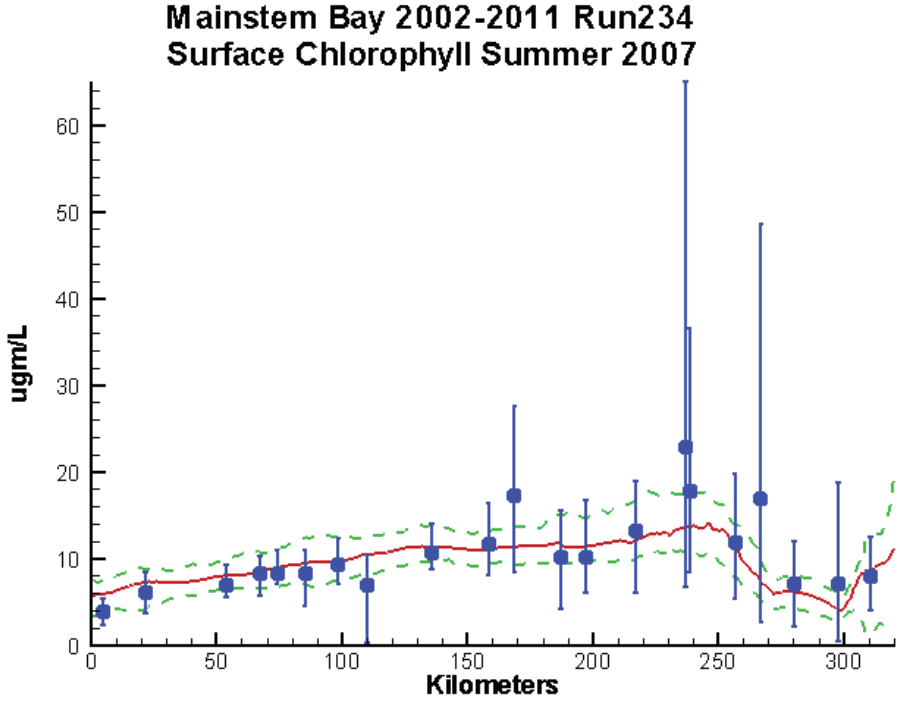

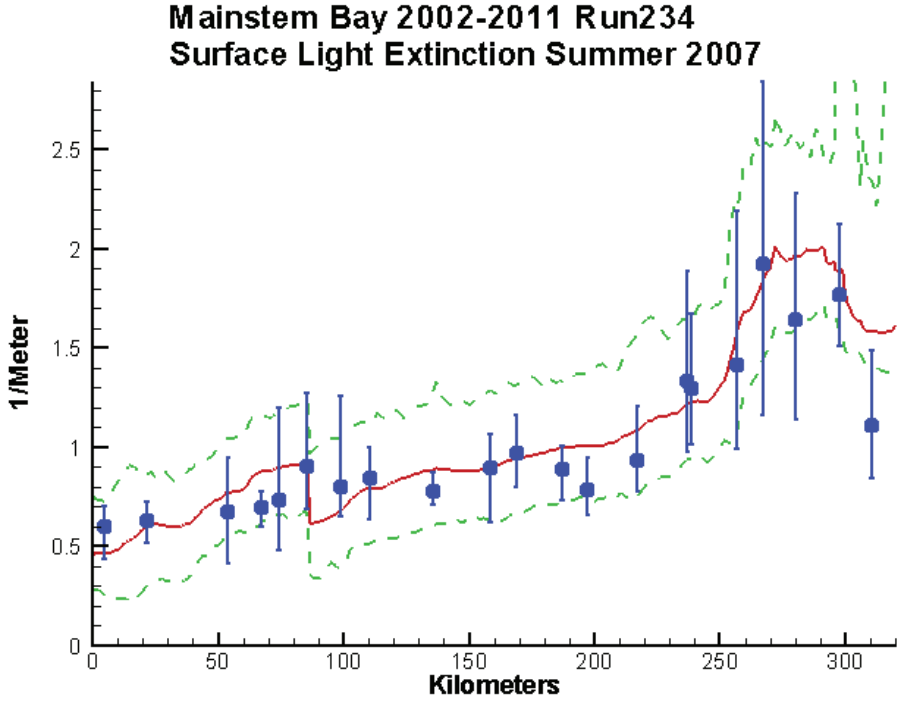

James River - Summer - 2007

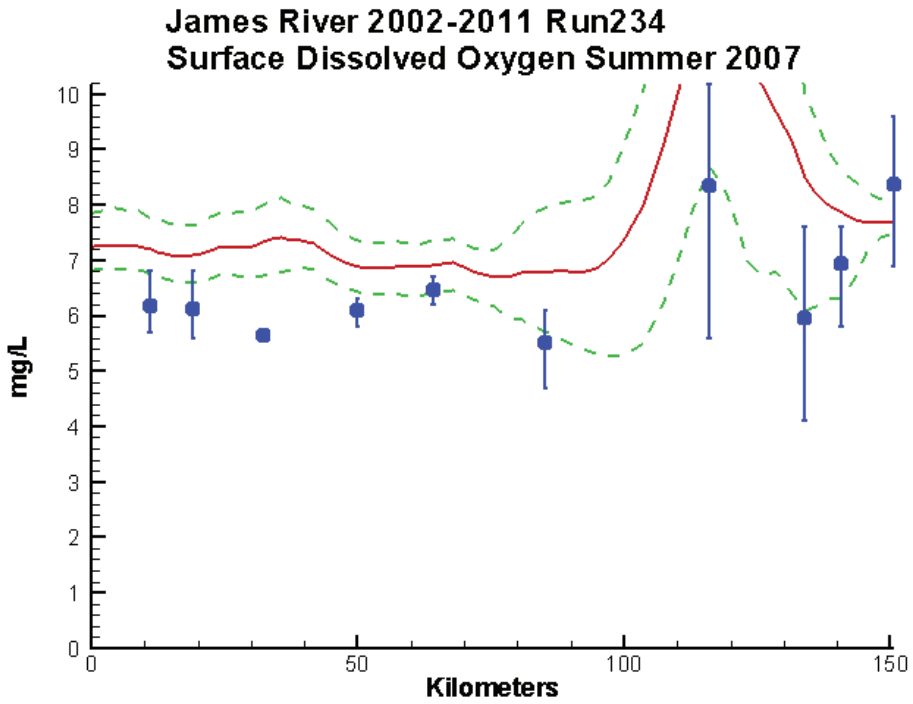

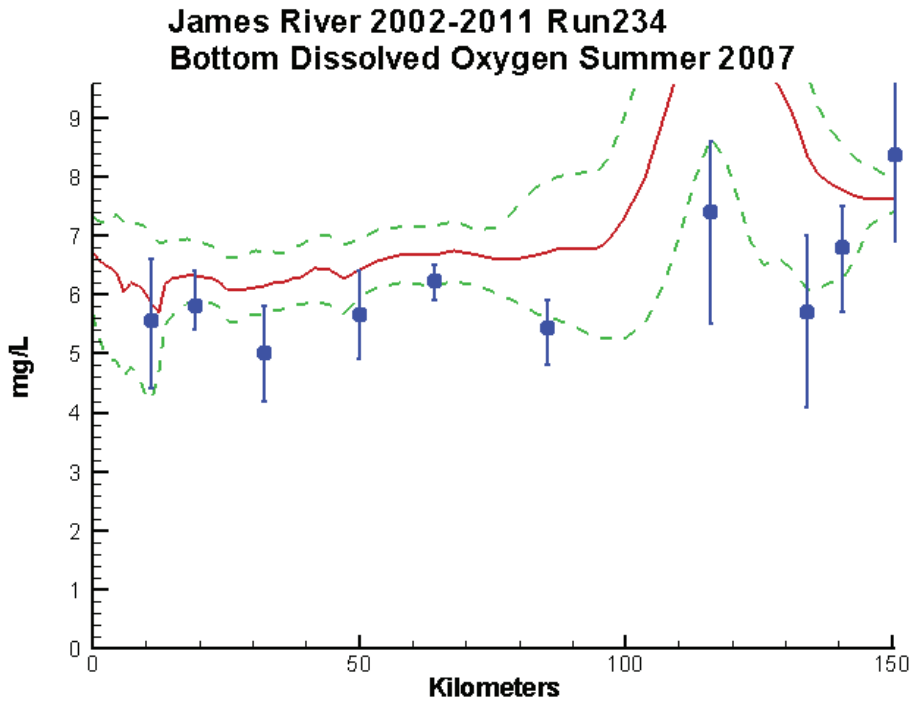

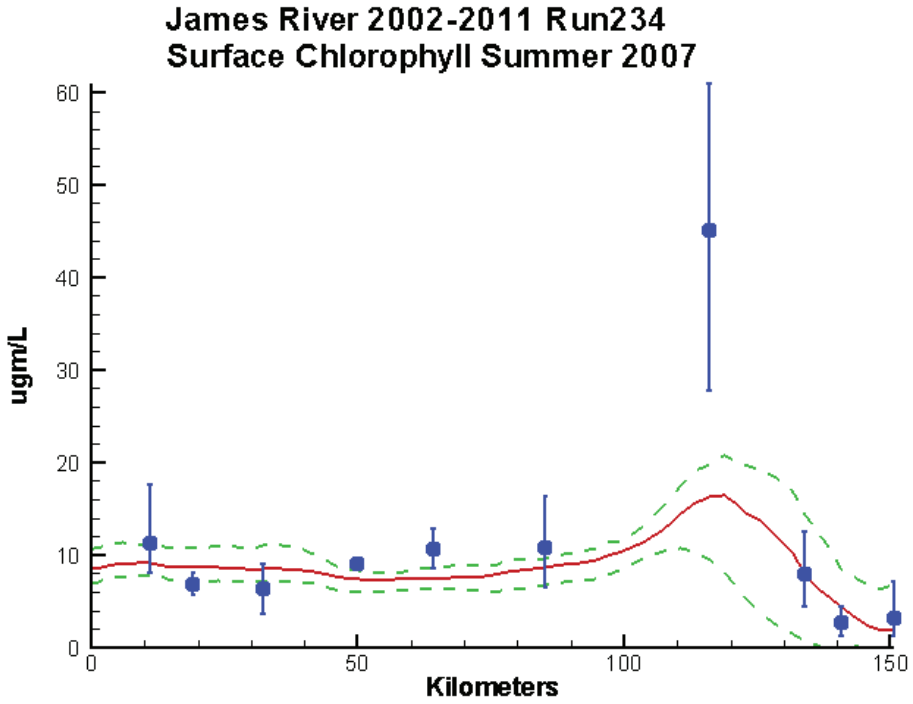

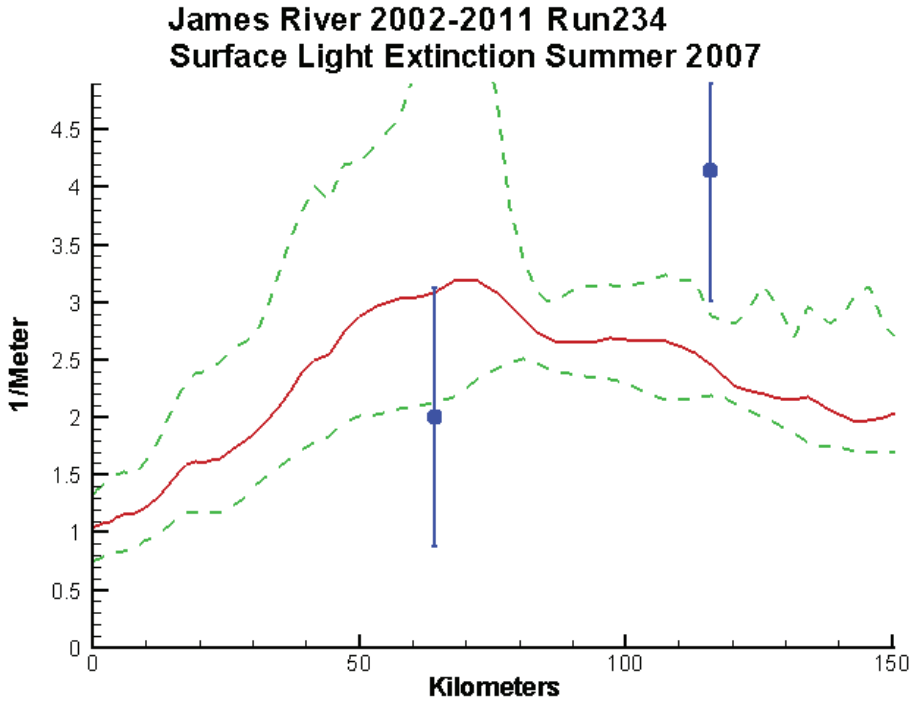

York River - Summer - 2007

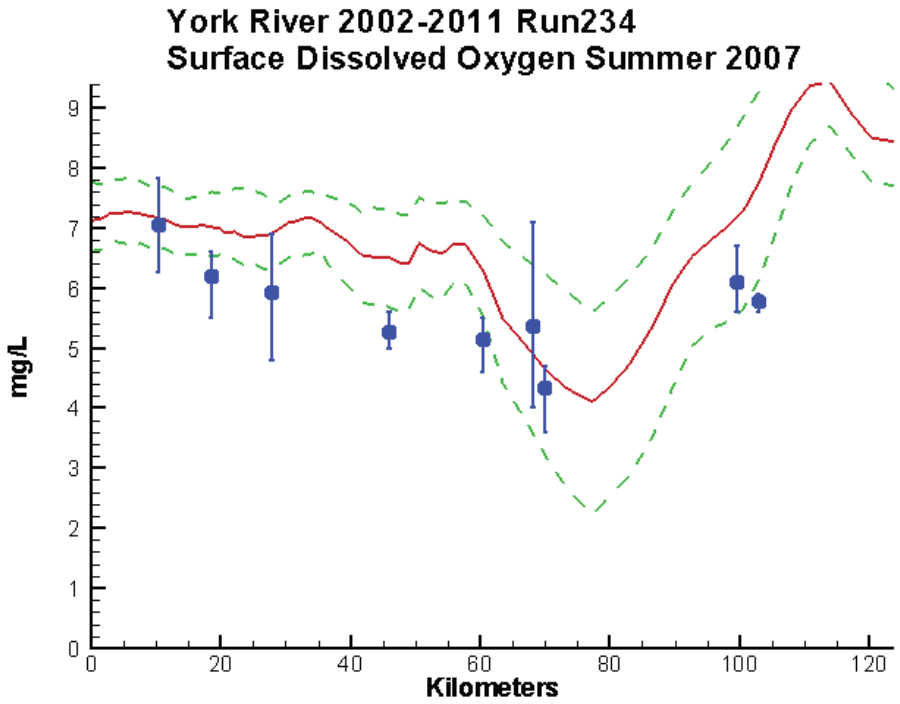

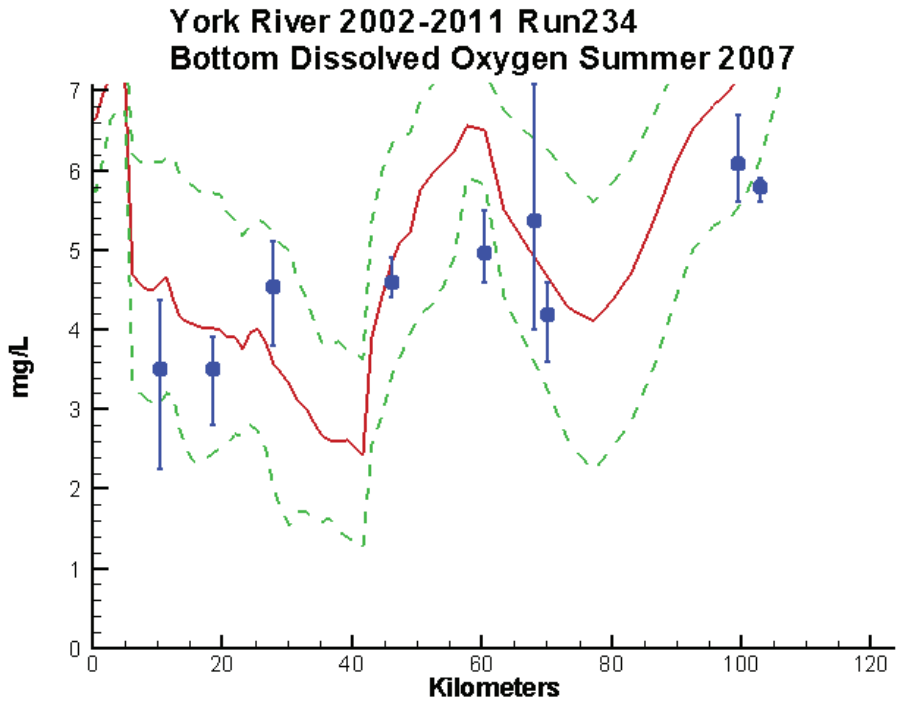

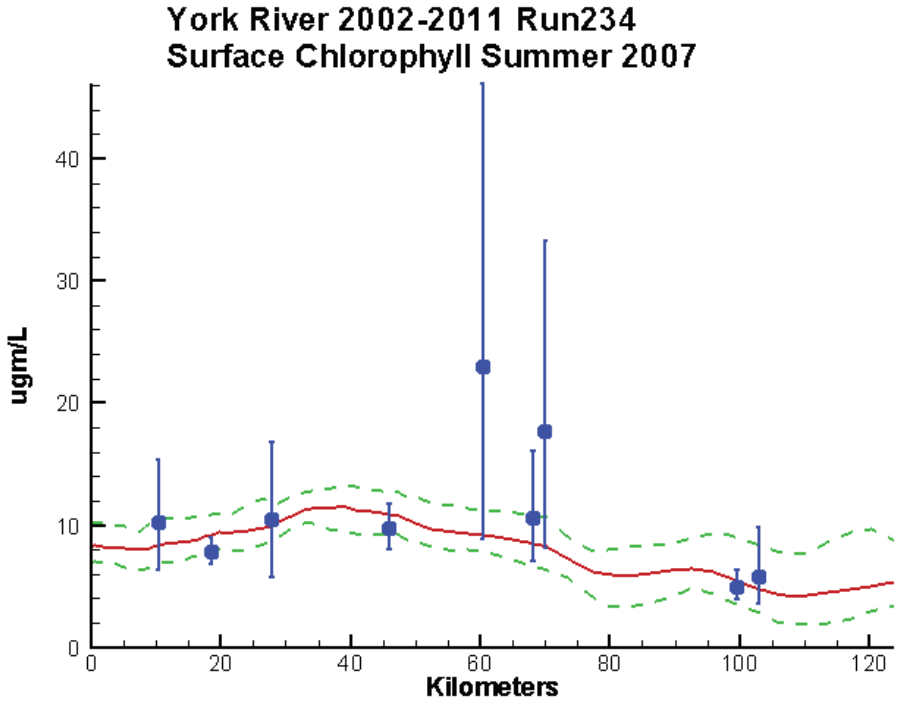

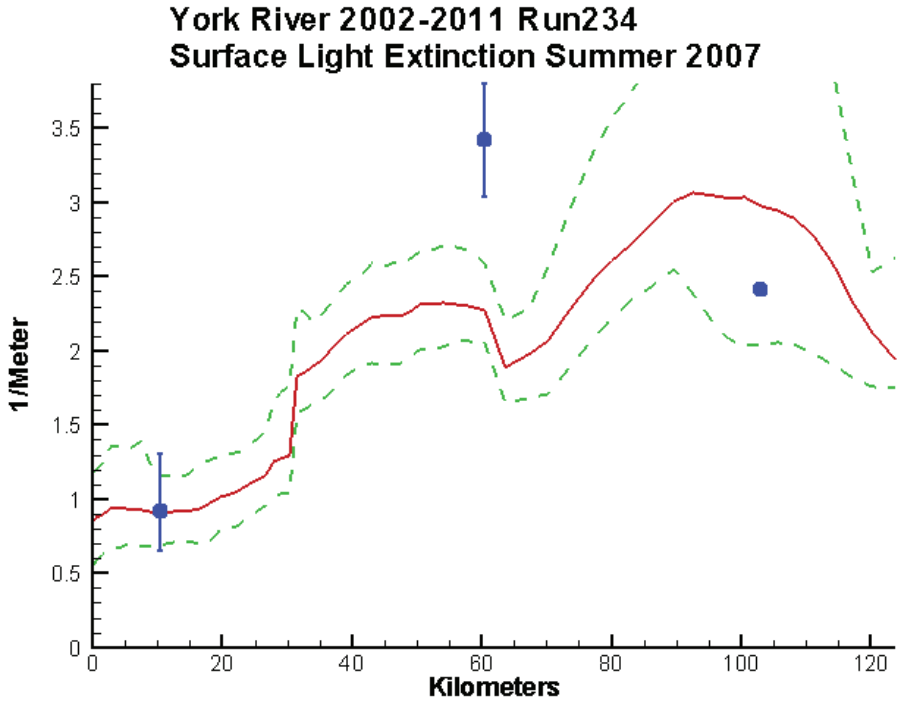

Rappahannock River - Summer - 2007

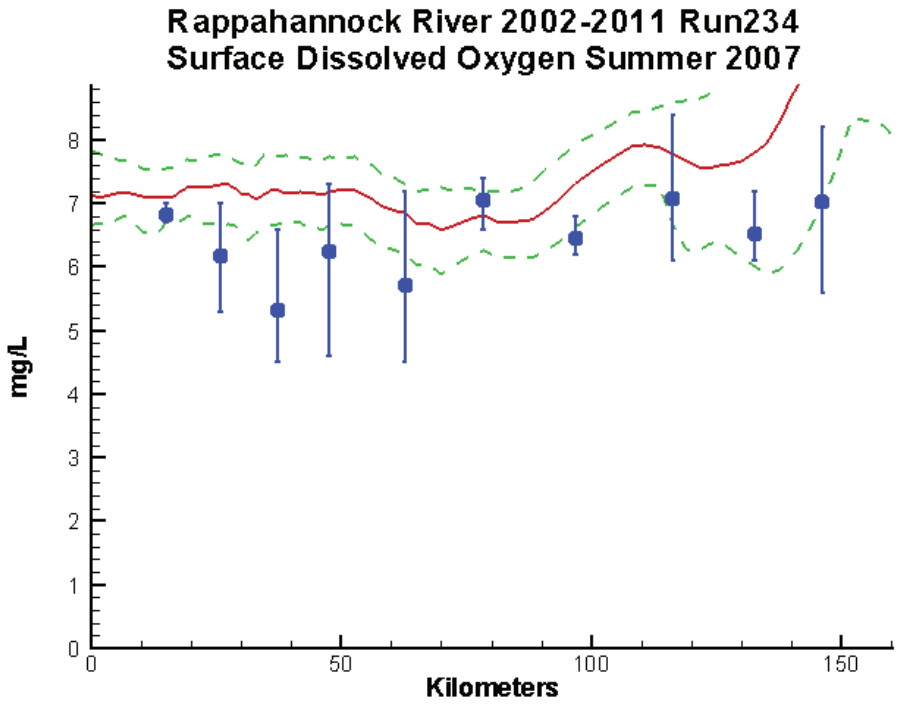

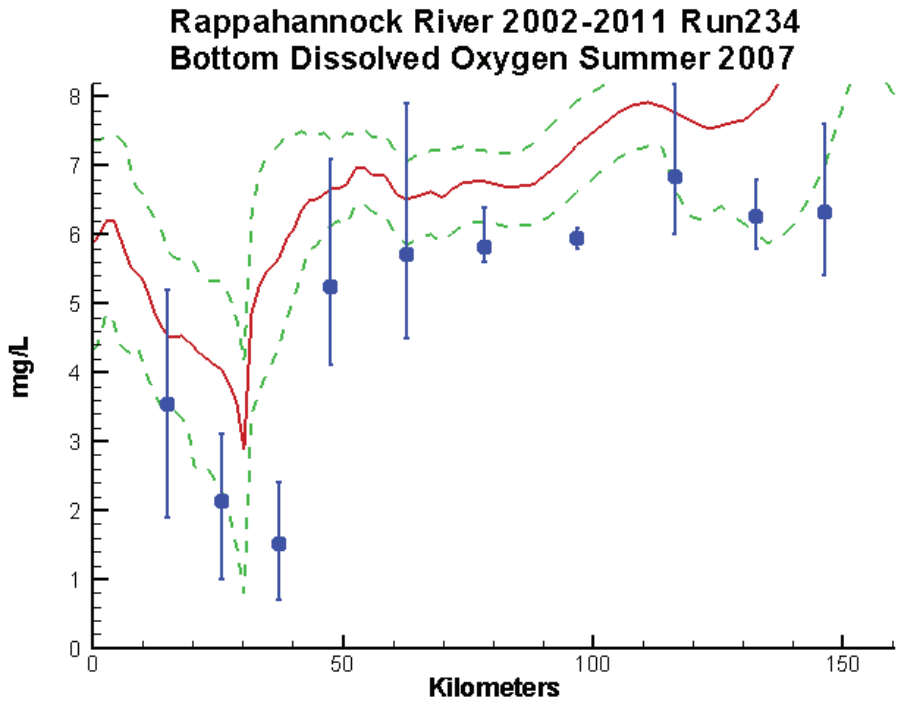

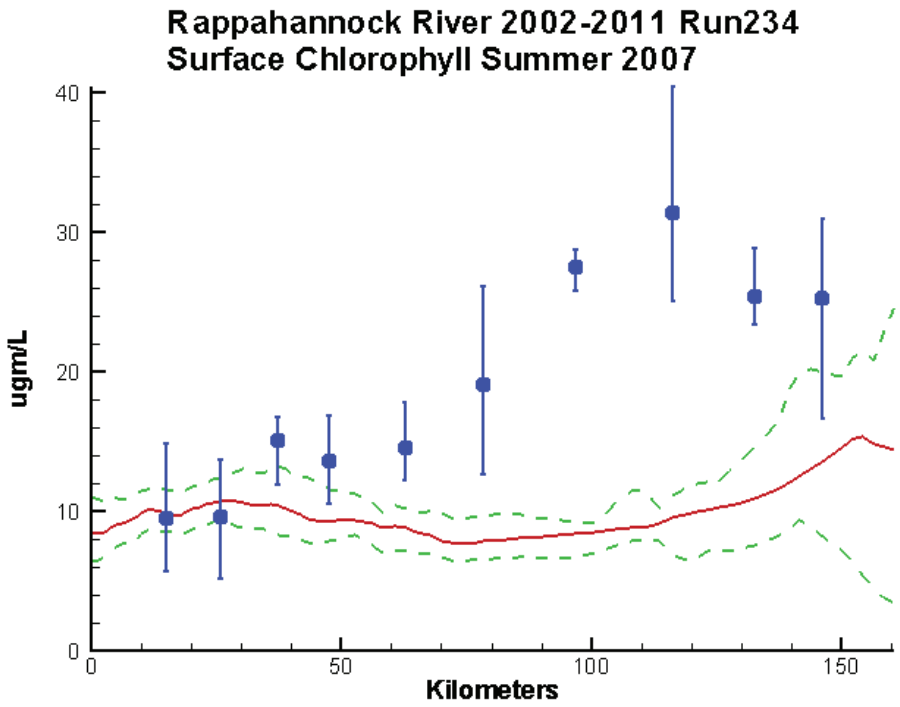

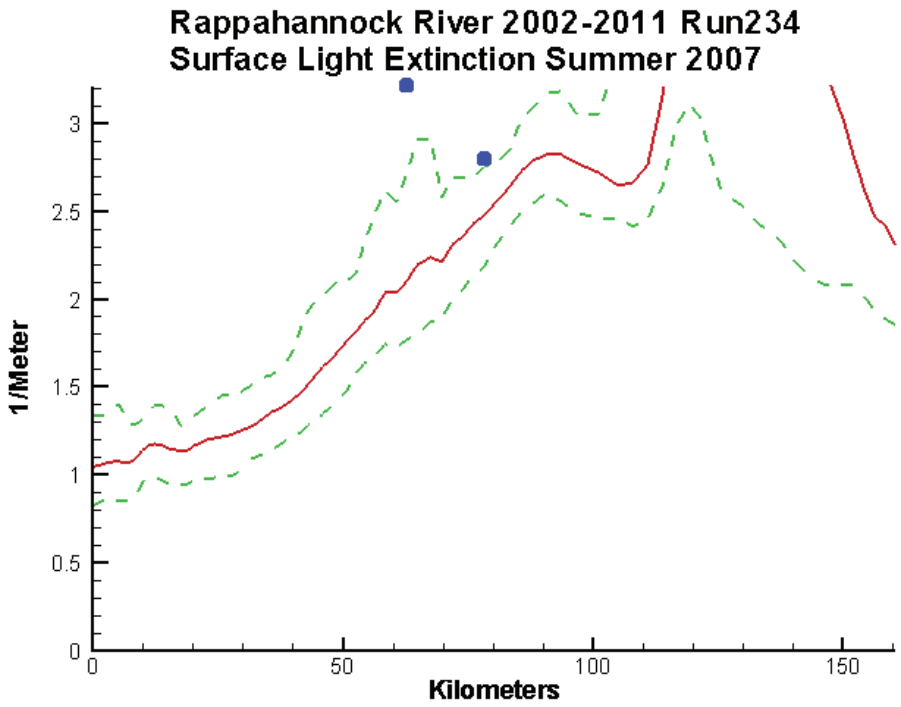

Potomac River - Summer - 2007

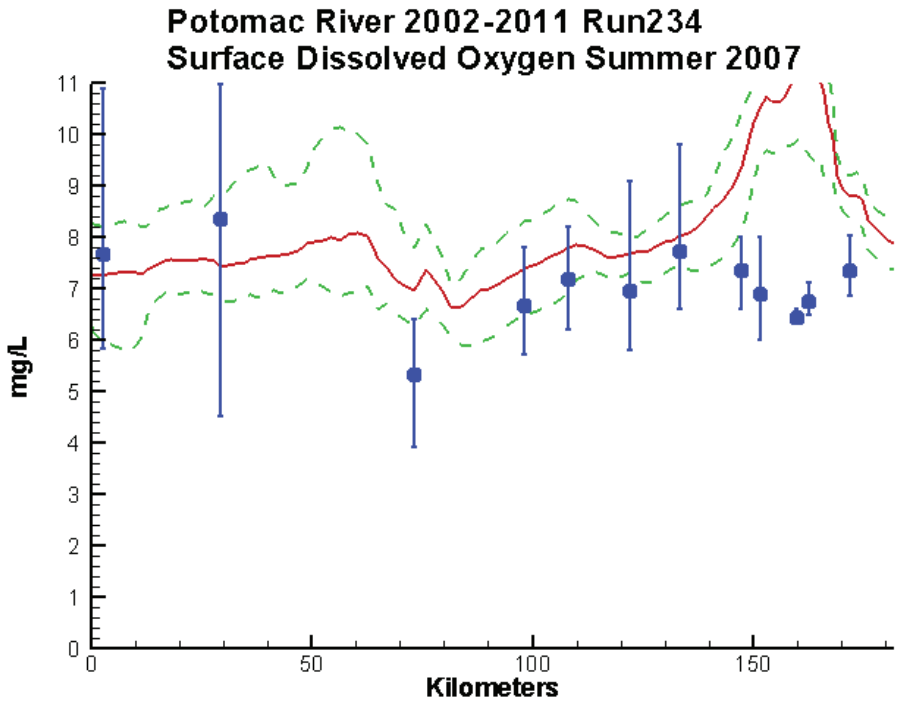

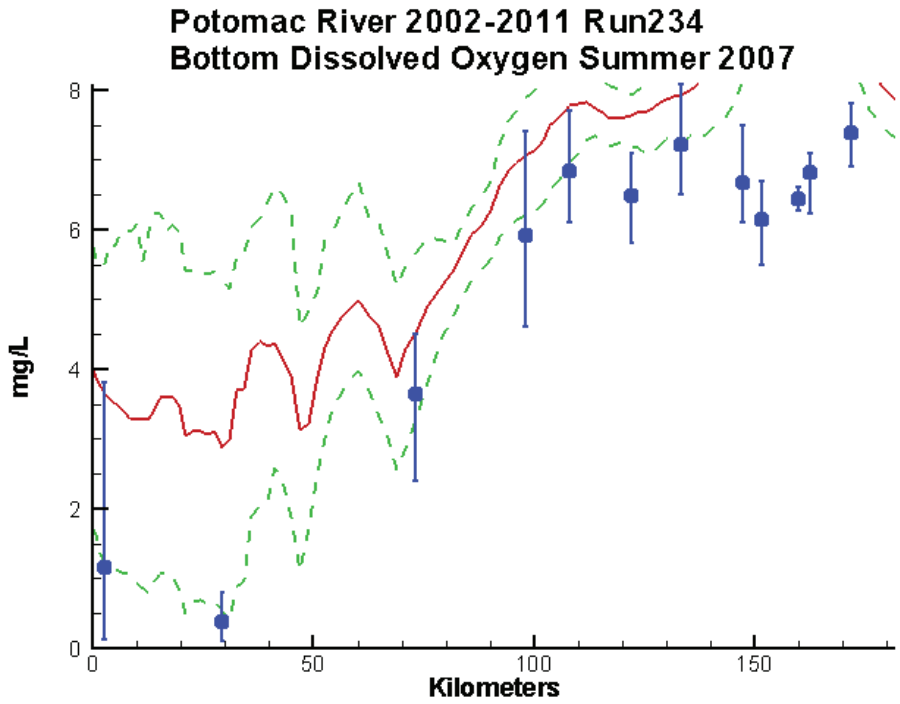

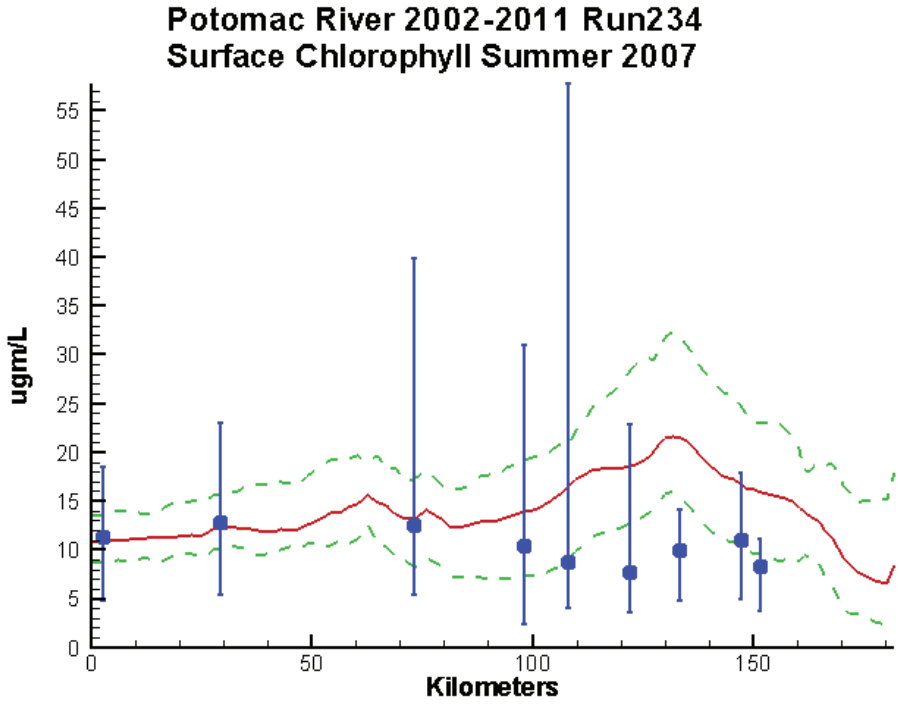

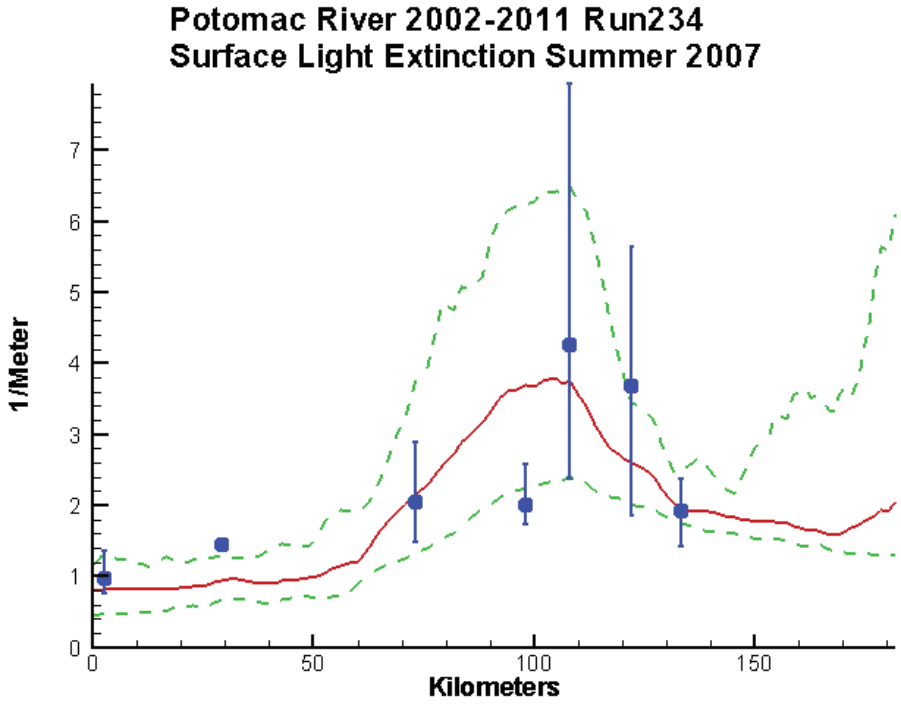

Patuxent River - Summer - 2007

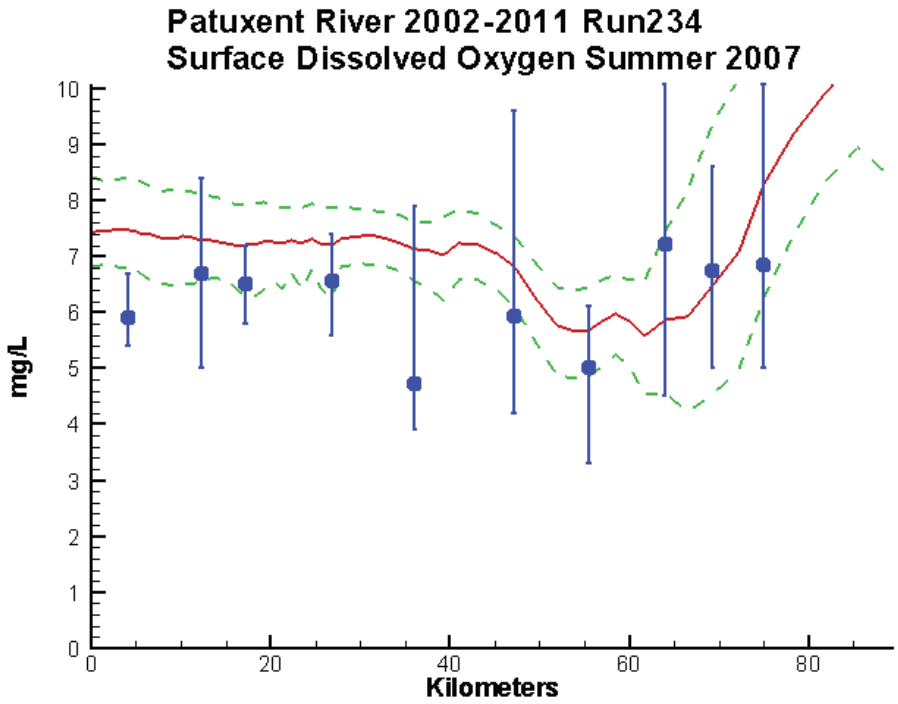

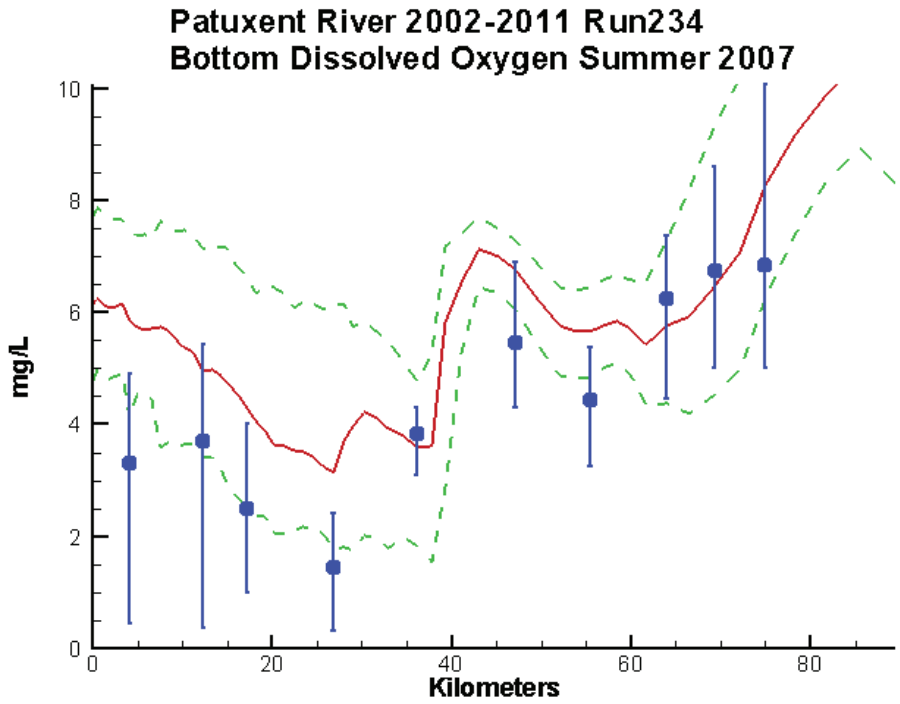

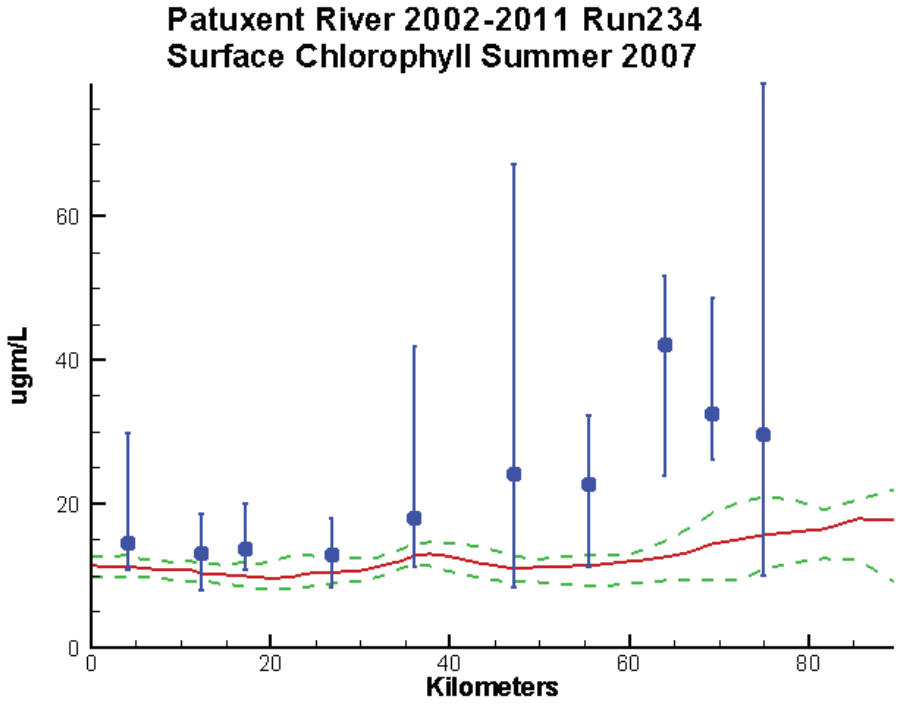

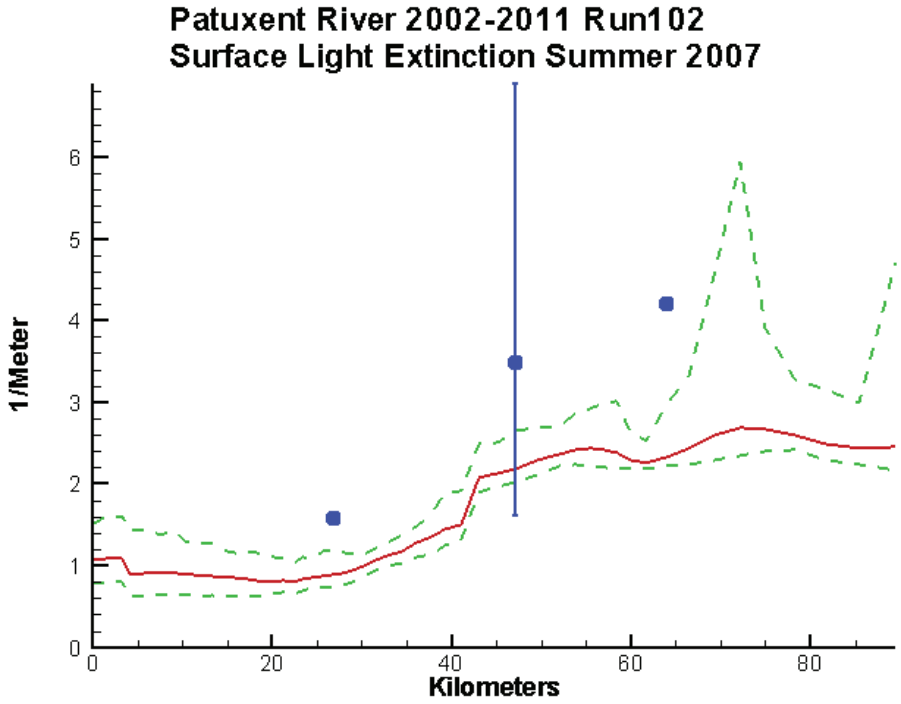

Mainstem Bay - Summer - 2010

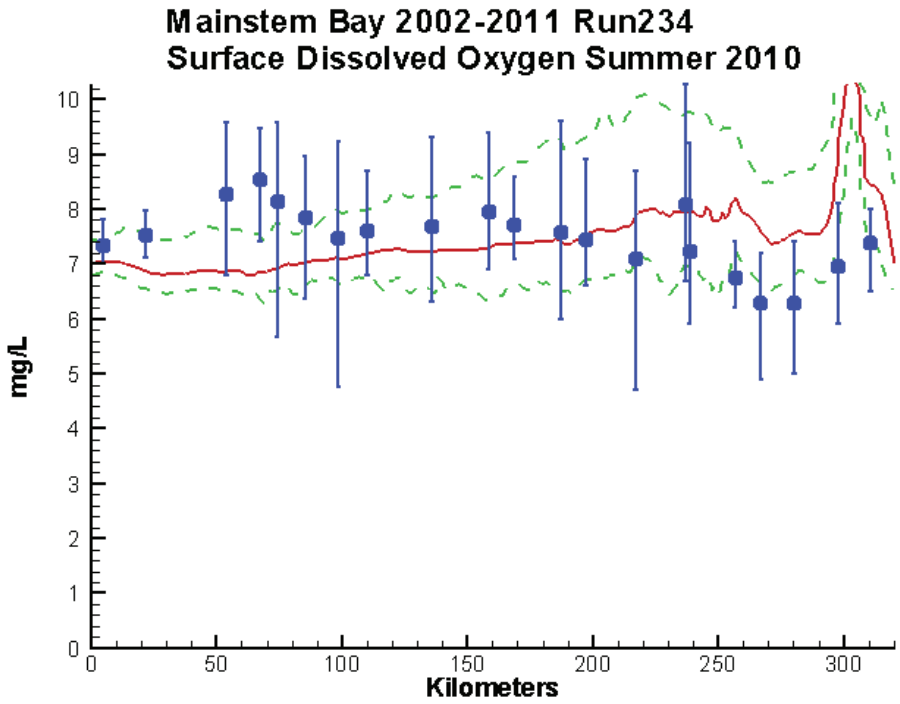

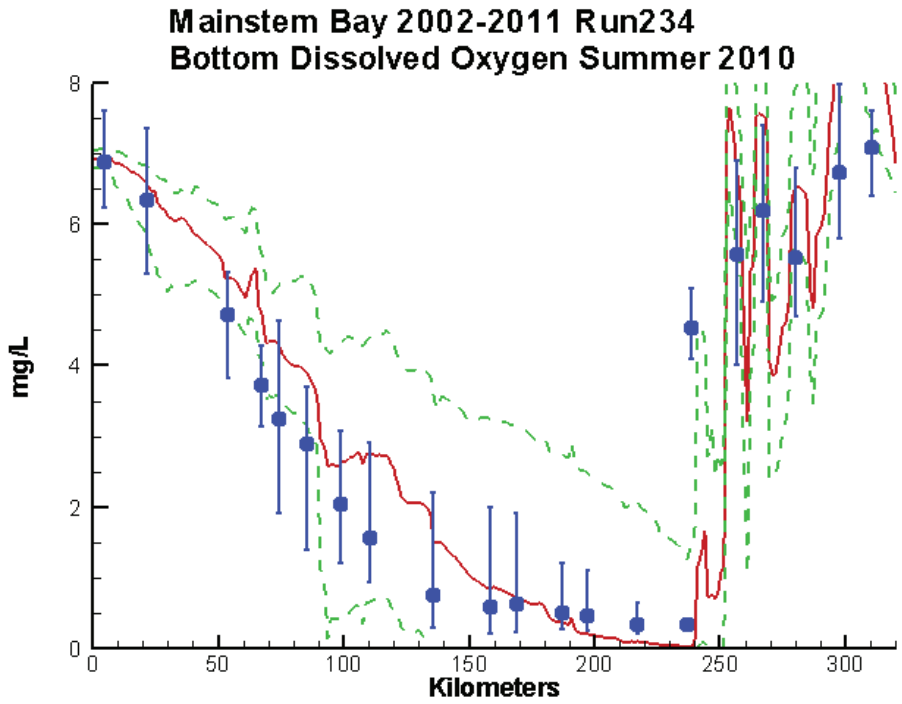

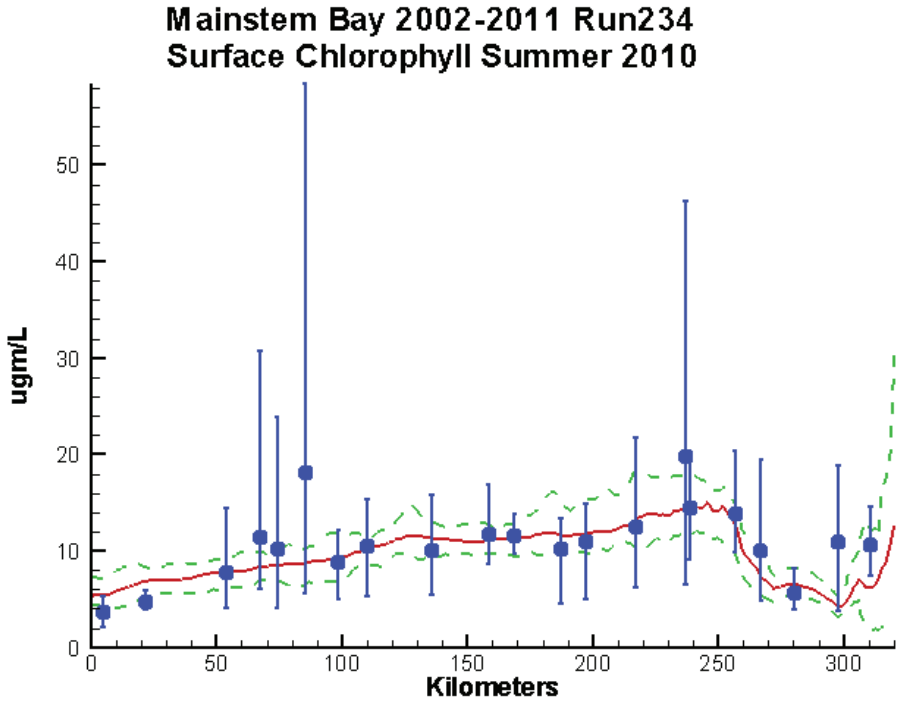

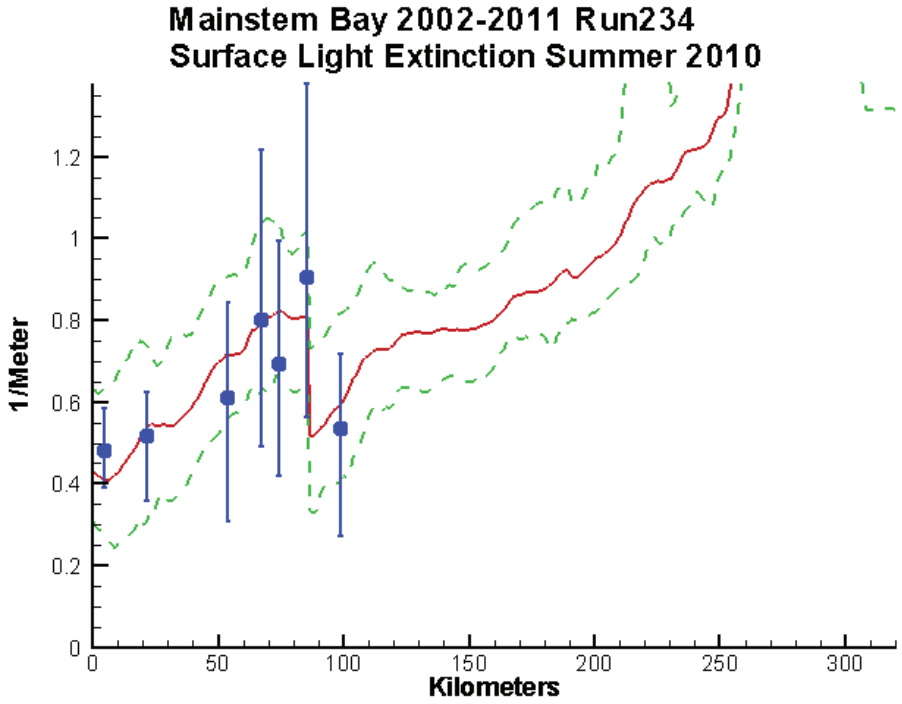

James River - Summer - 2010

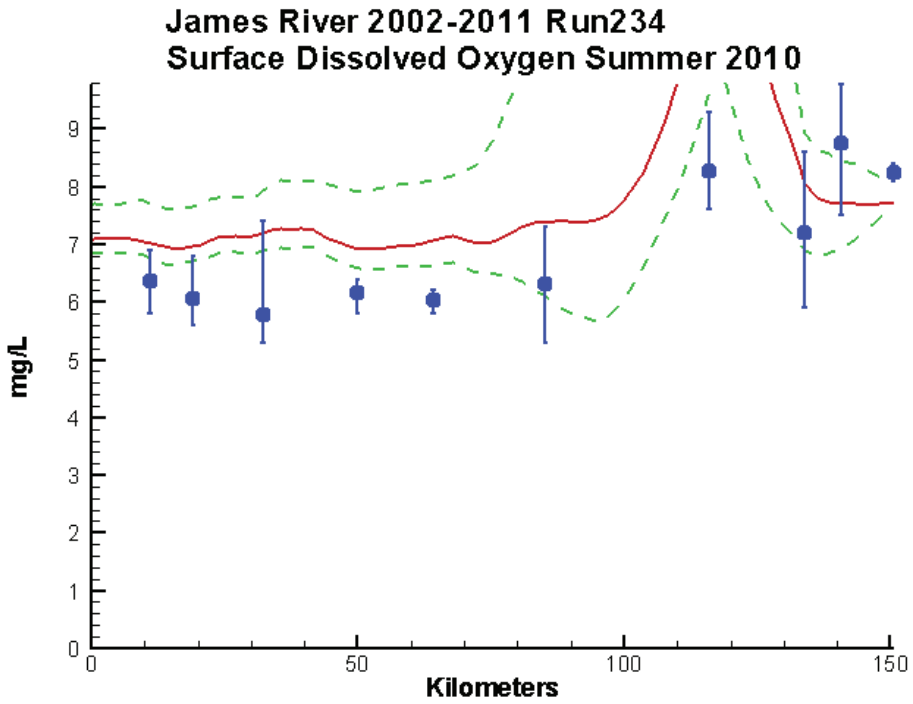

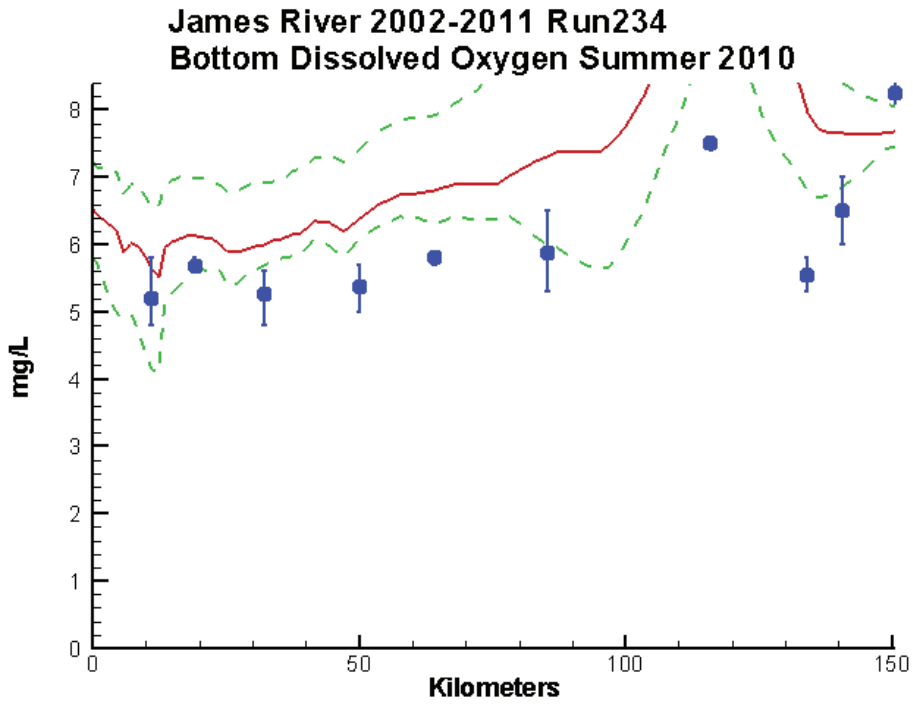

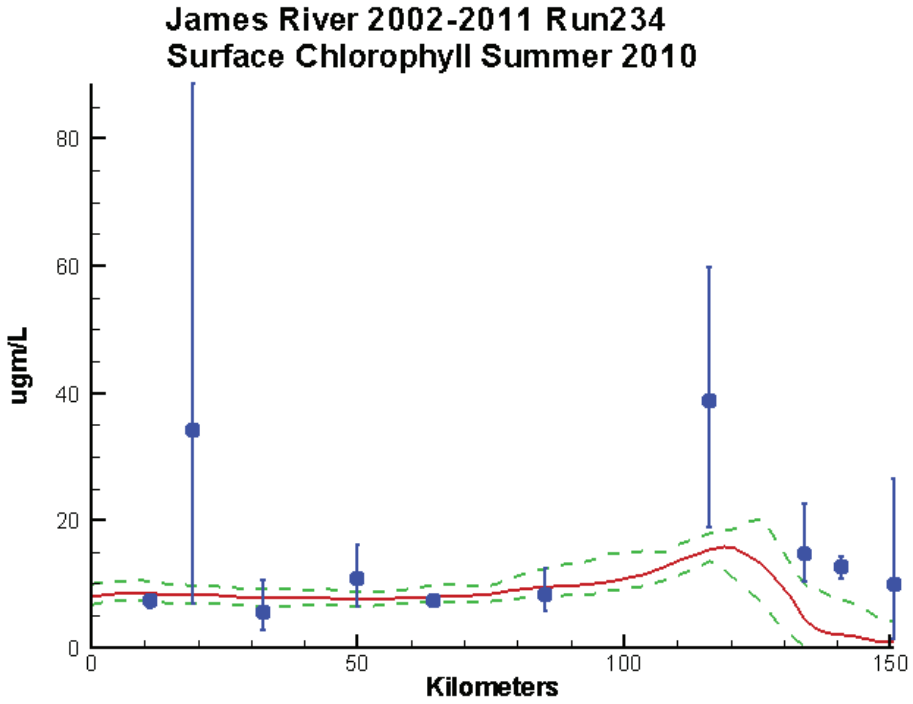

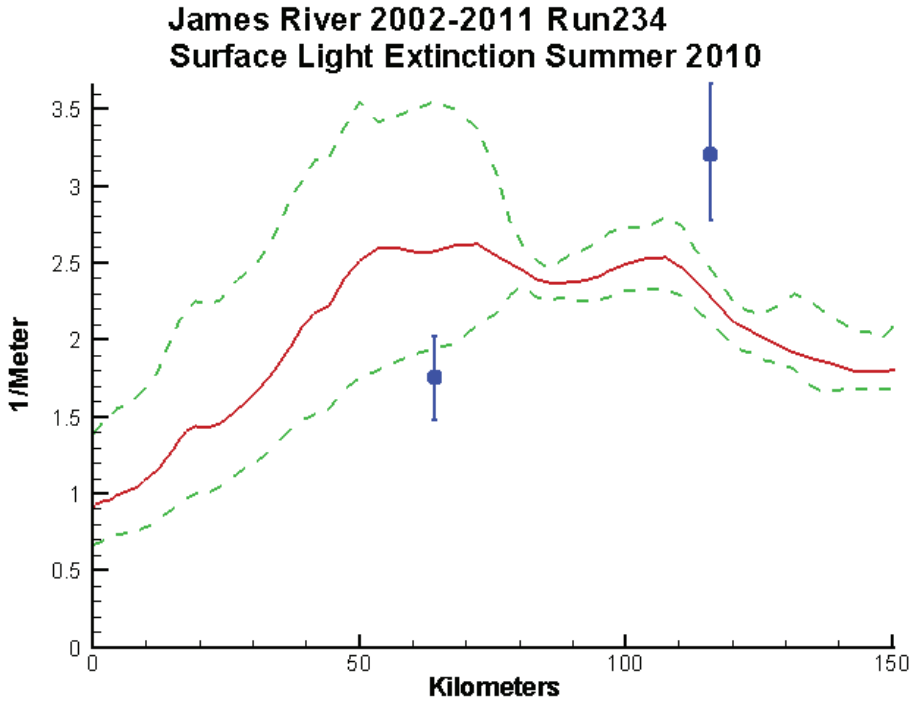

York River - Summer - 2010

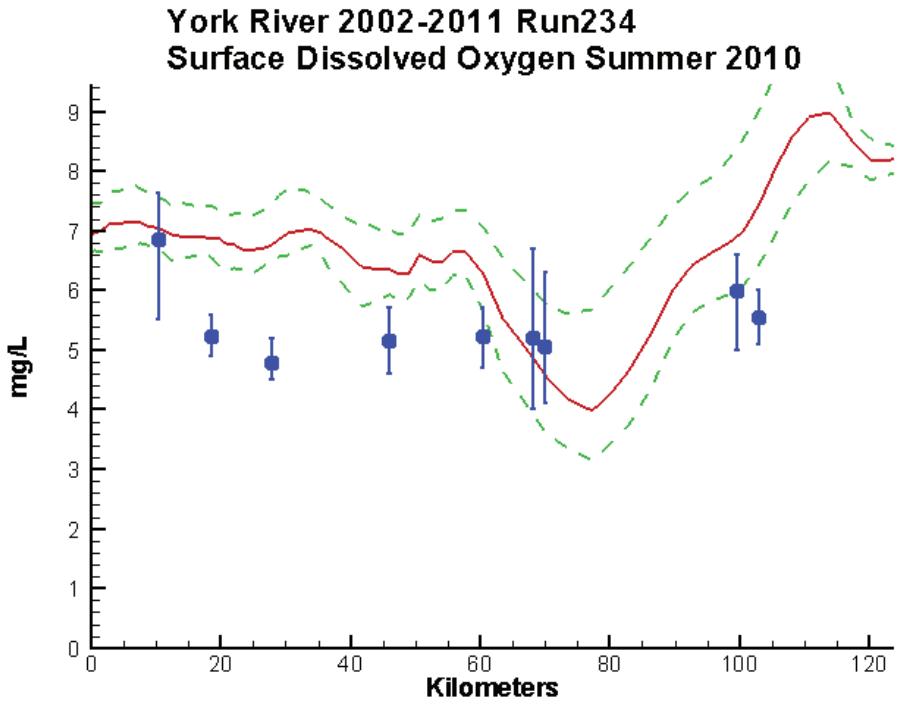

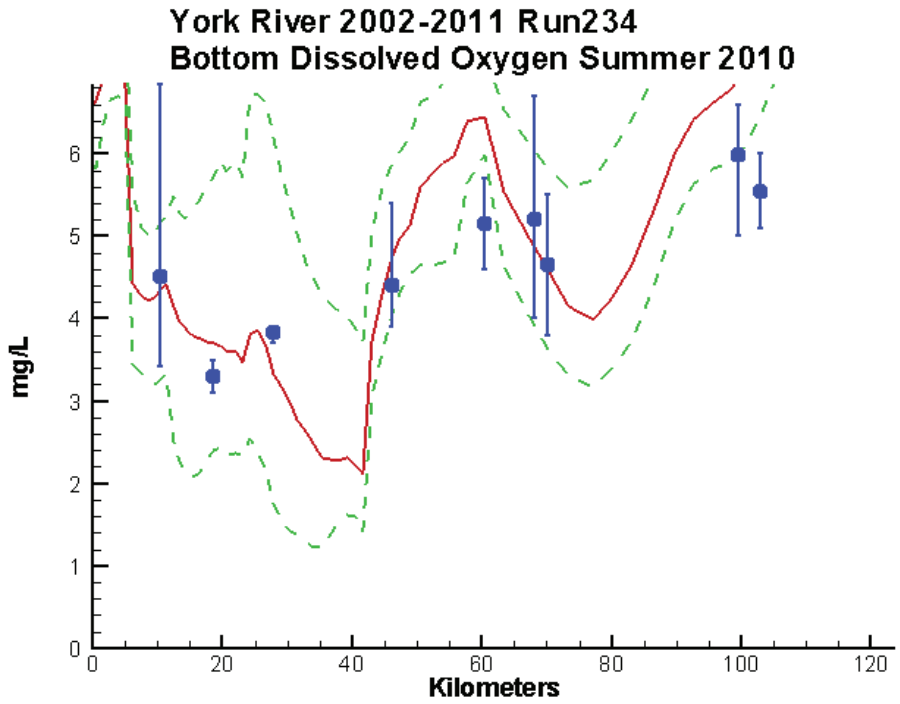

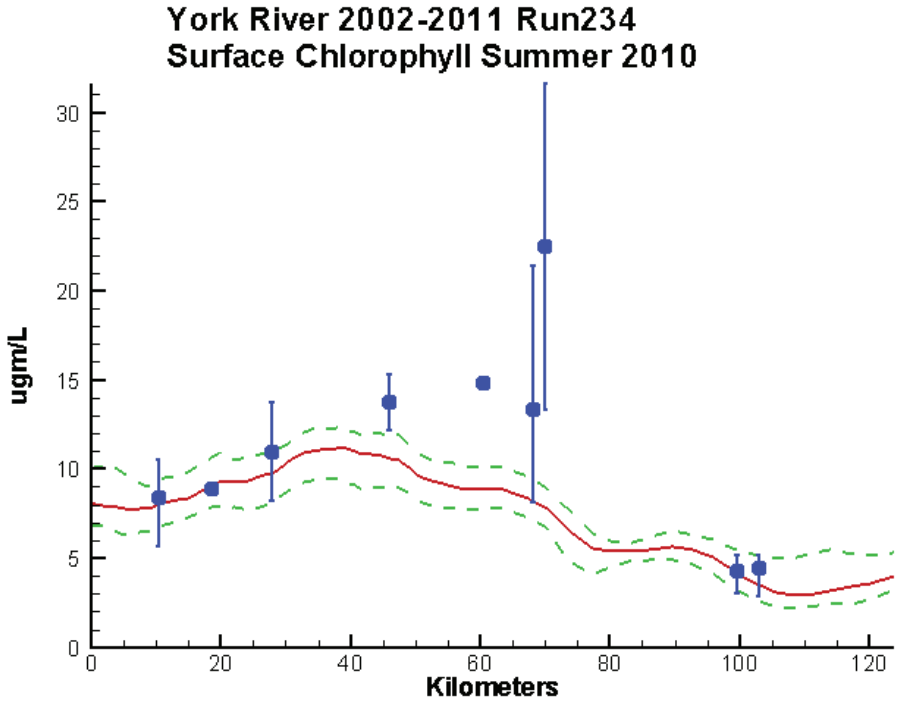

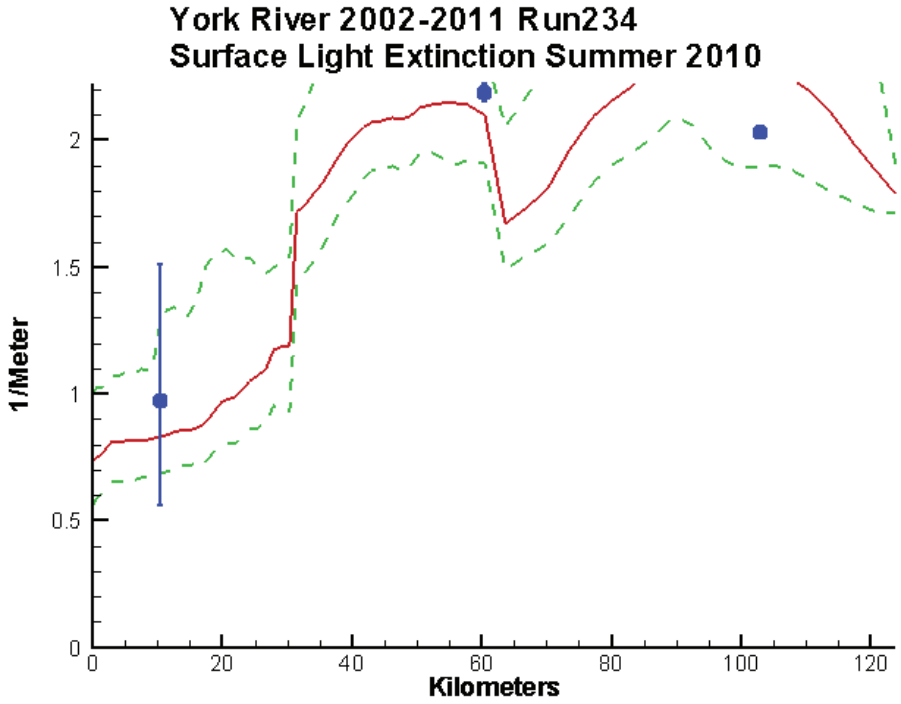

Rappahannock River - Summer - 2010

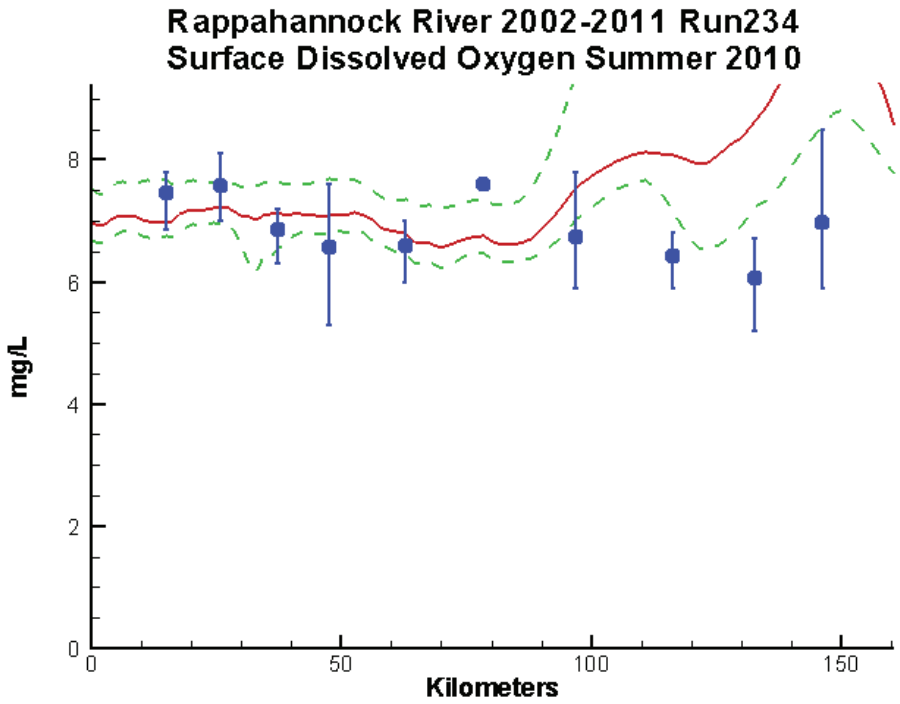

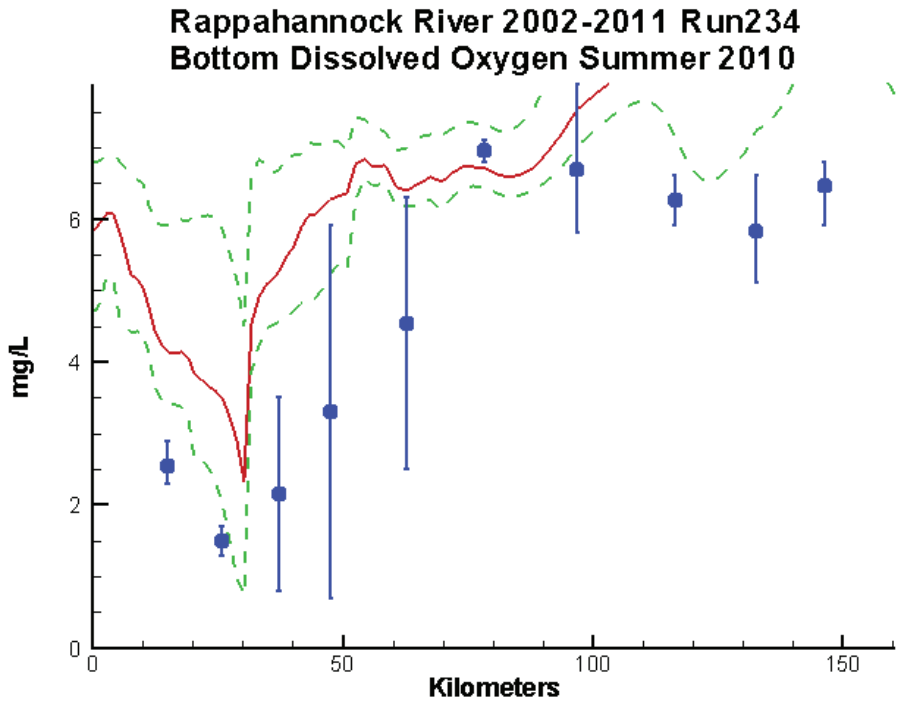

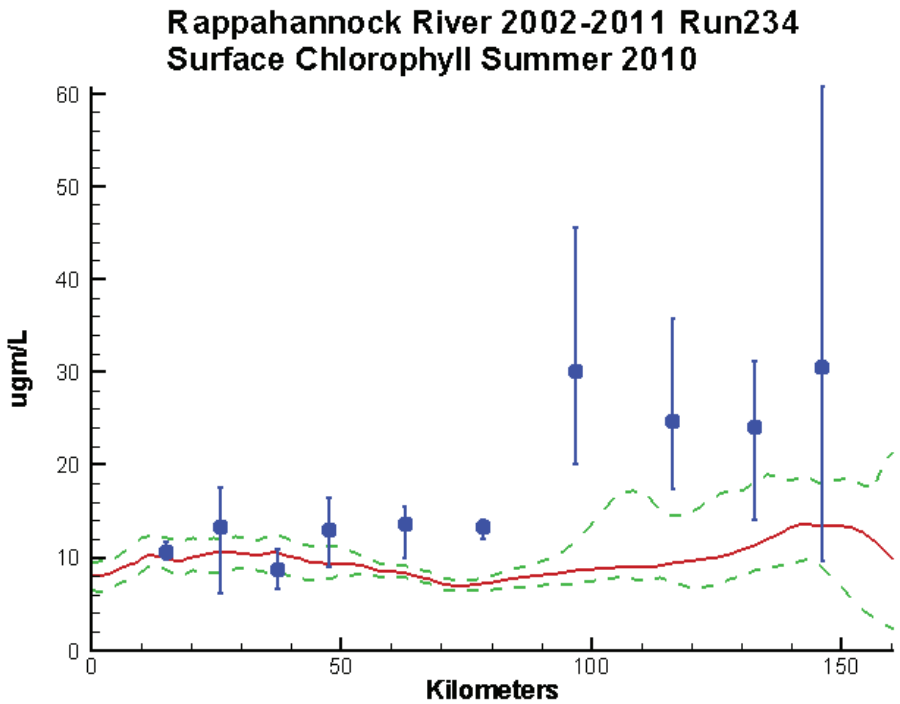

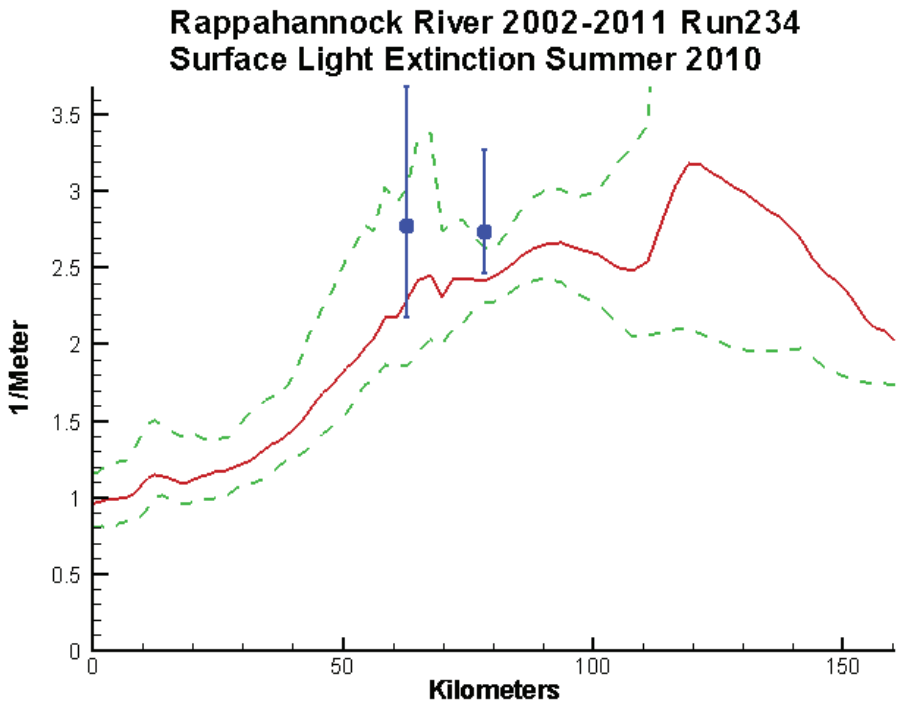

Potomac River - Summer - 2010

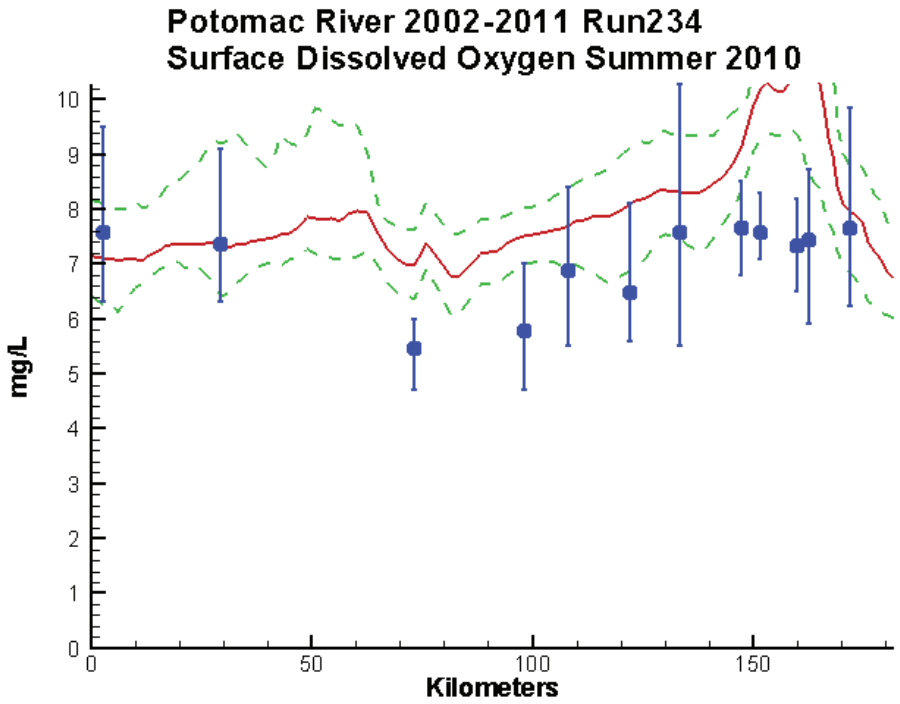

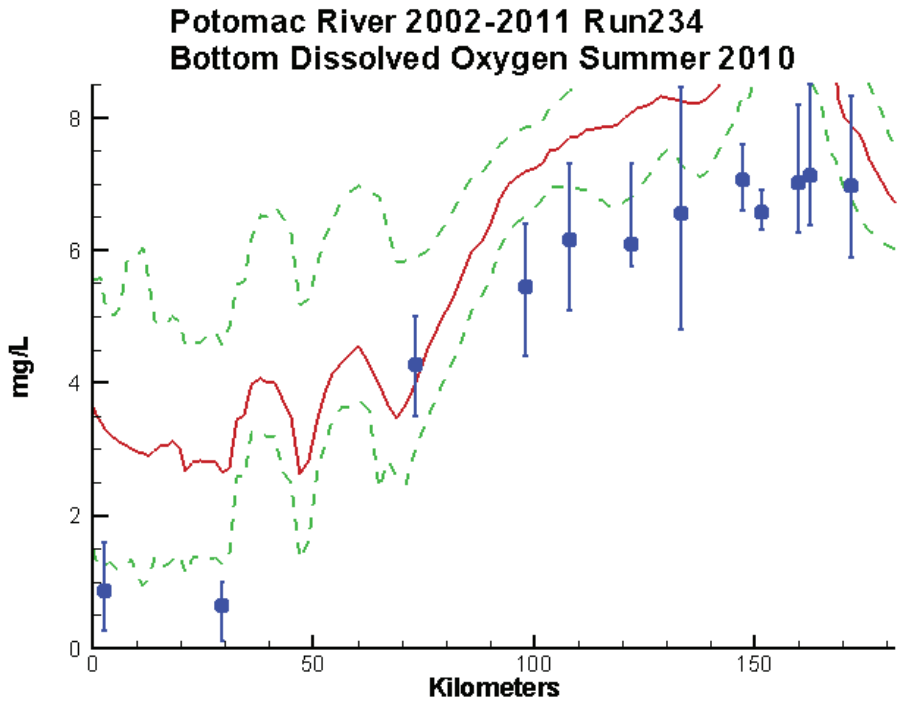

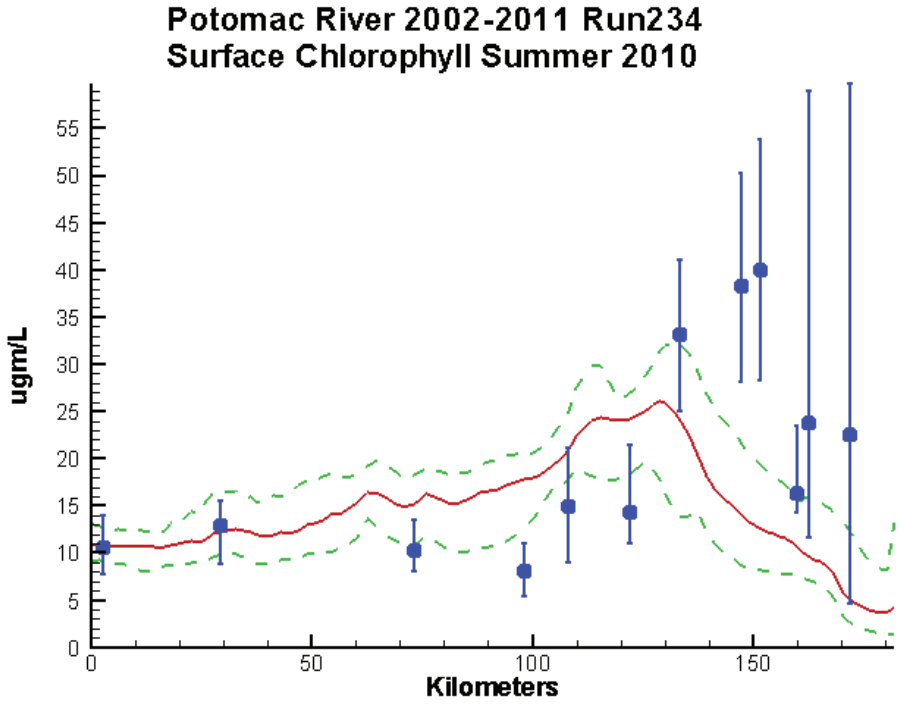

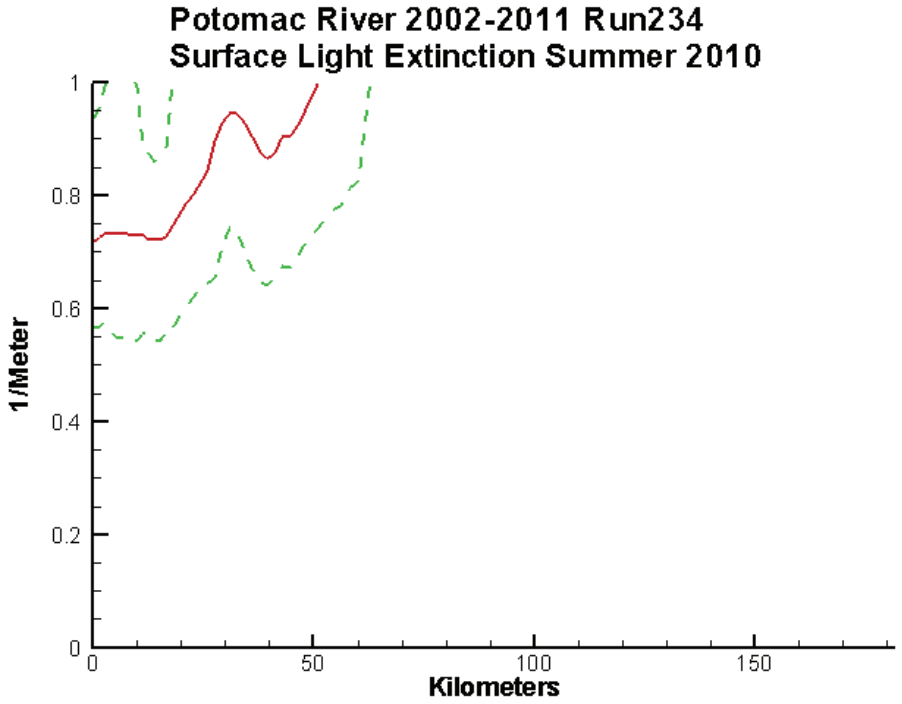

Patuxent River - Summer - 2010

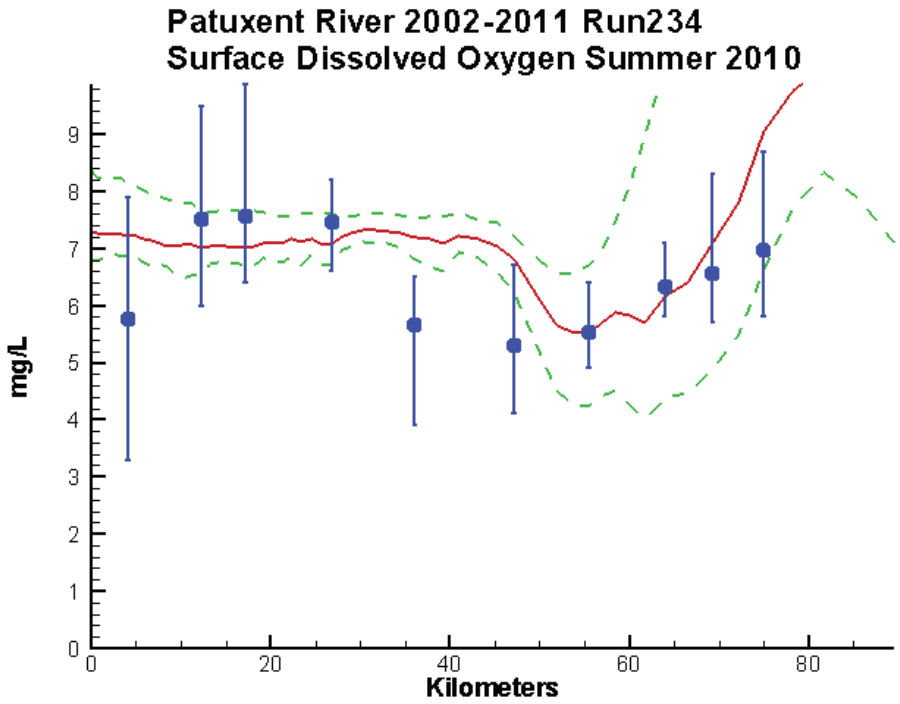

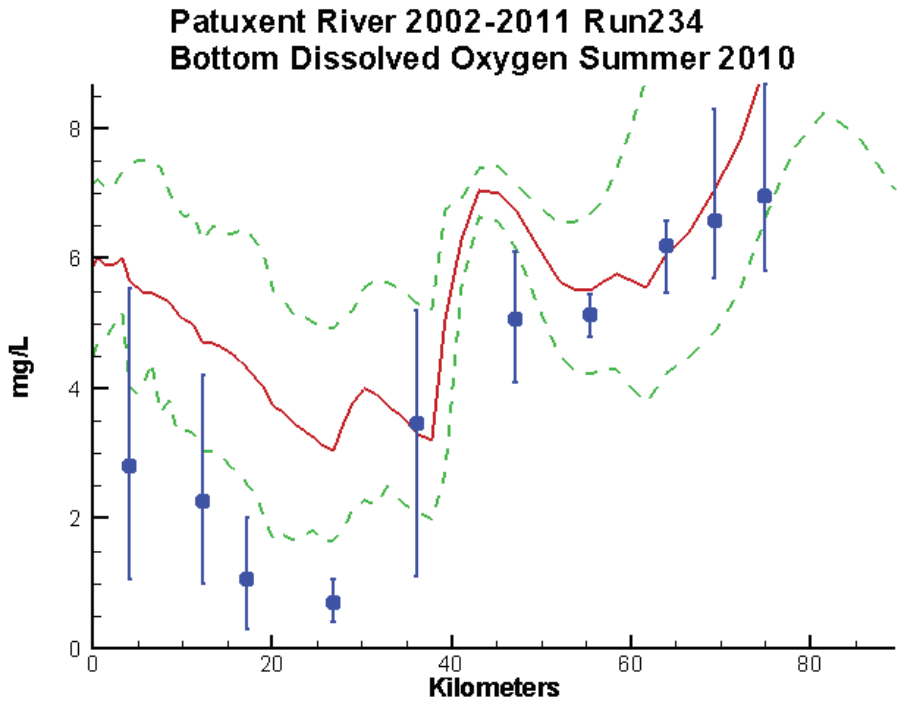

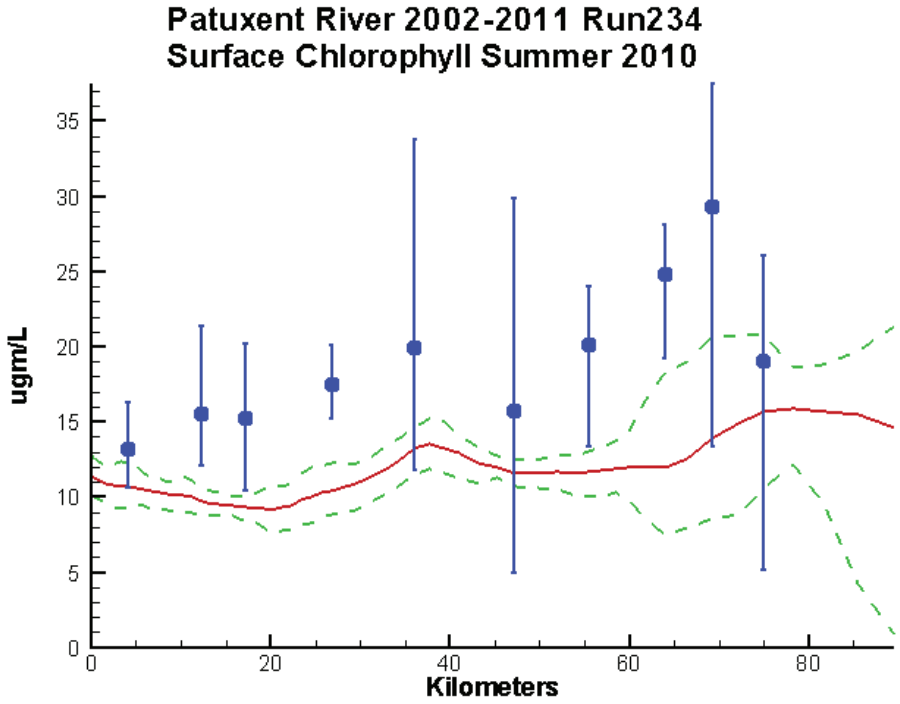

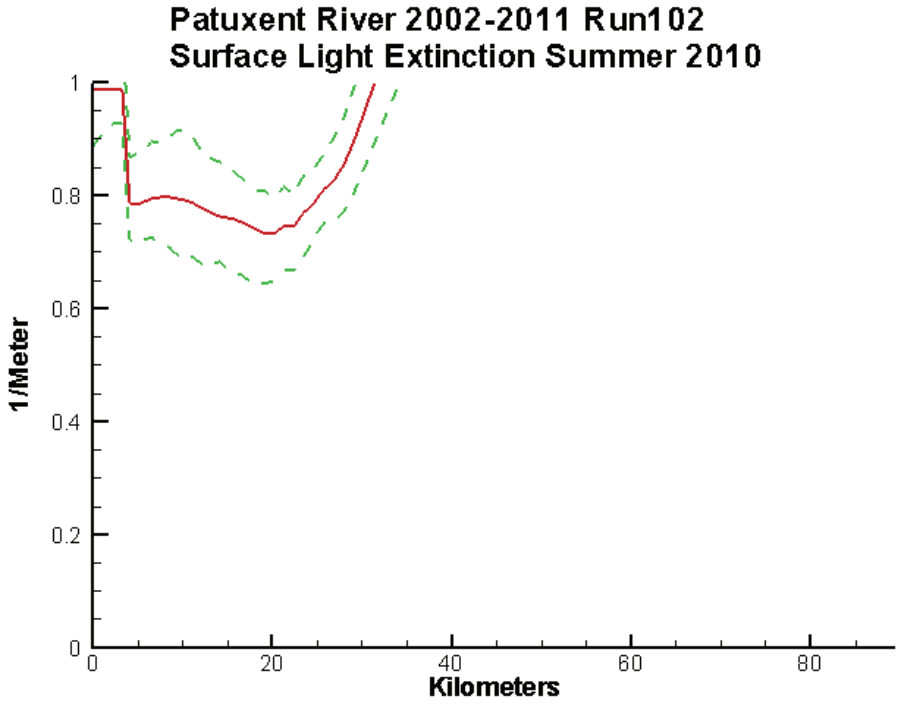

Appendix E: Comparison of Simulated and Observed Nutrient Limitation as a Metric of Model Calibration

Eutrophication and hypoxia are among the most severe anthropogenic stresses to coastal environments, and management efforts to reduce nutrient loading from the watershed are common practice for mitigating and restoring affected ecosystems. Model simulations provide critical information for such nutrient management decision-making by characterizing the effects of changing the quantity and distribution of nutrient loading across the coastal watershed. The assessment of eutrophication and hypoxia in tidal coastal waters is largely dependent on the modeled sensitivity of the dissolved oxygen (DO) response to nutrient loading, and, therefore, it is important to consider nutrient limitation sensitivity when assessing the performance of a model. Eutrophication models in coastal waters, however, are typically calibrated and validated to DO and chlorophyll (Chl) state variables rather than to DO sensitivity to nutrient limitation. Therefore, equifinality poses a challenge to evaluating success of coastal eutrophication model calibration because similar calibration statistics can be achieved through different combinations of parameter values while failing to take into account the observed estimates of nutrient limitation.

To overcome the challenge, the simulated biogeochemistry of four differently calibrated versions of the 2017 Chesapeake Bay Water Quality and Sediment Transport Model (WQSTM) were evaluated with respect to observed DO and Chl as well as the spatiotemporal distribution of biological nutrient limitation, which is a primary determinant of DO sensitivity to nutrient load. The four model versions generated similar goodness-of-fit to observed DO and Chl concentrations in the Chesapeake Bay, but their predictions of the sensitivity of DO to simulated nutrient loading differed considerably. Furthermore, those differences in sensitivity resulted in different estimates of the amount of nitrogen (N) and phosphorus (P) loading reductions needed for DO attainment of water quality standards. Comparing simulated levels of nutrient limitation with observed nutrient limitation estimated by bioassay data showed that three of the model calibrations deviated from observed nutrient limitation. Predicted nutrient limitation was similar to the nutrient limitation bioassay results in space, time, and relative importance of N vs. P in only one version of the model, and that version was selected for management application. Nutrient limitation is a useful metric of model performance and should be included in model calibration assessment for eutrophication management applications.

E.1 Introduction

Nutrients are a principal controlling factor of primary production and phytoplankton blooms in coastal ecosystems. Eutrophication, defined as excessive nutrients, represents one of the most severe anthropogenic stresses to coastal environments and ecosystem functioning. Increasing populations, urbanization, local economy, and excessive fertilizer and manure application to agricultural lands lead to increased nutrient loading to coastal waters. Excessive nutrient loading can result in eutrophication, high phytoplankton production and biomass, and DO depletion caused by increased consumption, a phenomenon that occurs in the main stem of the Chesapeake Bay every summer.

Hypoxia, defined here as DO below 2 mg/l, weakens ecosystem function and reduces tidal water habitat areas. The Chesapeake Bay Program (CBP), a federal and state partnership, was formed in 1983 to restore the Bay to a healthy status. With an aim towards this goal, a major focus of the CBP is to reduce nutrient loading from the watershed. Target nutrient loadings, corresponding to a reduction to approximately half of the loads observed in the mid-1980s high-loading period, were determined for each state-basin based on the state-basin's contribution to hypoxia in the Bay (USEPA 2010). To make these determinations, model simulations provide a measure of the relative nutrient loading effectiveness (i.e., the sensitivity of tidal water hypoxia to watershed nutrient loading reductions from each state-basin). The total nutrient loading is then partitioned across the watershed according to the spatially explicit estimates of load effectiveness at reducing hypoxia.

Nutrient loading effectiveness in the state-basins is primarily determined by nutrient limitation in the tidal Bay, and thus any change in the location, timing, and extent of nutrient limitation might alter effectiveness predictions. Moreover, nutrient management actions in the watershed influence both N and P, each with an independent effectiveness. In the state-basins, nutrient target exchanges between N and P loads are allowed based on their respective effectiveness on DO in the Deep Water and Deep Channel designated uses in the Bay. The relative extent of N vs. P limitation predicted by the model is a critical component in determining the target loadings for total N (TN) and total P (TP) and their exchange coefficients. As such, the robustness of the model predictions in terms of overall target nutrient loadings, their partitioning over the watershed, and their exchange coefficients relies on the accuracy of the simulated nutrient limitation.

This appendix describes the methods and outcomes of an assessment of the accuracy of nutrient limitation predictions that contributed to the selection of the final model version used for the 2017 Midpoint Assessment. Prior investigations and bioassays on nutrient limitation have established spatial and temporal distributions of the relative N limitation vs. P limitation in the Chesapeake Bay (Fisher et al. 1992, 1999; Kemp et al. 2005). Those observations provide a

valuable opportunity to evaluate the accuracy of predicted nutrient limitation in the 2017 WQSTM. Nutrient limitation was computed from the final solutions of the four model versions and compared to bioassay results. The version of the model that yielded the best fit to the bioassay results was ultimately selected for application in the CBP 2017 Midpoint Assessment.

E.2 Data

Bioassays on nutrient limitation and its spatial and seasonal variations were carried out during the late 1980s and early 1990s in the Chesapeake Bay by Fisher et al. (1992, 1999) and Kemp et al. (2005). Bioassays consisted of incubating surface water samples with ammonium additions, phosphate additions, and combinations of nutrients and without nutrient additions to serve as control. The incubations lasted 1-8 days, and Chl concentration and carbon dioxide (CO_2) uptake were measured before, during, and after the incubation. Increases of phytoplankton biomass (measured by Chl concentration) and primary production indicated N limitation or P limitation after ammonium and phosphate additions, respectively. Concurrent N and P limitation (co-limitation) was detected when phytoplankton growth increased only after both N and P were added simultaneously. The first major bioassay series was conducted in 1987 (Fisher et al. 1992) and further cruises were carried out from 1989 to 1994 (Fisher et al. 1999), which revealed spatial and seasonal changes in nutrient limitation in the Bay.

Kemp et al. (2005) summarized the results of the bioassay experiments into a map that displays spatial and seasonal shifts in nutrient limitation in the Bay (Figure E-1). The vertical dimension represents distance from the Bay head and the horizontal axis represents time in months from January through December. The map shows that the upper Bay from the Bay head to 60 km southward, which covers the Chesapeake Bay Program Segments (CBPS) CB1TF, CB2OH, and CB3MH, is mostly P-limited during the phytoplankton growth season (from April through November) and light-limited in winter. The mid-Bay from 60 to 220 km downstream of the head, essentially CB4MH and CB5MH, is primarily P-limited during winter and spring (from January through June), but shifts to N limitation in summer and fall. The lower-Bay CBPSs CB6PH, CB7PH, and CB8PH are mostly N-limited during most of the year, with occasional N-P co-limitation or P limitation in the winter and spring.

Figure E-1. Seasonal and regional variations in N, P, and light limitation of phytoplankton growth synthesized from bioassay experiments conducted in the main stem of the Chesapeake Bay between 1992 and 2002 (reproduced from Kemp et al. 2005). The CBPSs are depicted based on their distance from the Bay head.

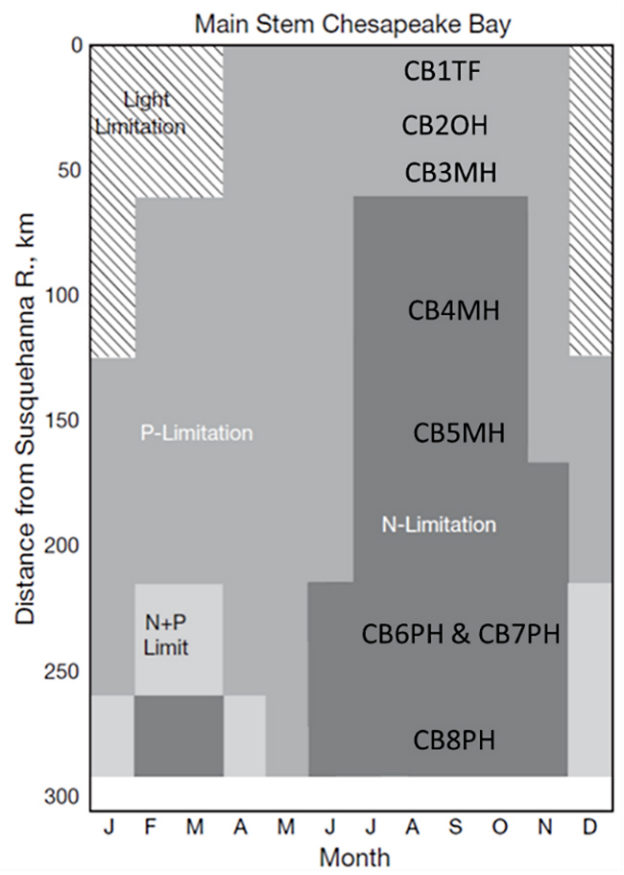

To facilitate model-data comparison in management units, the bioassay data was rearranged on a segment basis for the spring-summer season (March through September) (Figure E-2). The vertical axis indicates the frequency of occurrence of N limitation as a fraction of the total nutrient limitation, which is the sum of N and P. The CBPS CB1TF in the tidal fresh zone (salinity < 0.5 practical salinity unit [psu]) at the Bay head and CBPS CB2OH in the oligohaline region (salinity 0.05–5 psu) in the upper Bay are P-limited from March through September, with all monthly lines overlapping with the horizontal axis and thus corresponding to N/(N+P) equal to zero. In the mesohaline zone (salinity 5–18 psu) of the mid-Bay, represented by CBPS CB3MH, P limitation dominates from March through June, followed by N-P co-limitation in July through September. CBPSs CB4MH and MD5MH in the mid-Bay share the same nutrient limitation pattern: P limitation dominates in spring from March through June and N limitation prevails in summer from July through September. CBPS VA5MH is located in a transitional zone between the mesohaline region in the mid-Bay and the polyhaline region (salinity 18–30 psu), where P limitation dominates in spring from March through May, N-P co-limitation occurs in June, and N limitation

dominates from July through September. Polyhaline region segments, represented by CBPSs CB6PH, CB7PH, and CB8PH, are dominated by N limitation. Only in early spring (i.e., March and April) is the system co-limited by both nutrient species. On the time dimension, P limitation prevails in spring from March through May, with occasional co-limitation in the polyhaline region. June is the transitional time when the upper Bay and the mid-Bay are governed by P limitation whereas the lower Bay is N-limited. N limitation dominates in summer from July through September in most of the Bay, except for the tidal fresh and oligohaline zones, where P limitation remains predominant.

Figure E-2. N and P limitation during the productive season (Mar-Sep) for CBPSs in the main stem of the Bay. The lines for Jul, Aug, and Sep show complete overlap.

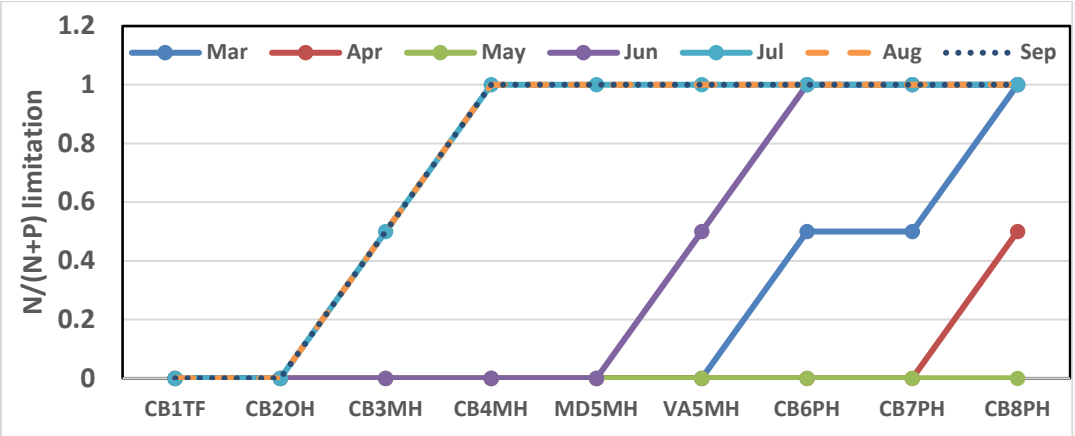

E.3 Model-Data Comparison for Dissolved Oxygen and Chlorophyll Simulations

The Corps of Engineers Integrated Compartment Water Quality Model (CE-QUAL-ICM) is the water quality model component of the overall 2017 WQSTM and is described in detail in chapter 2 of this report. At the last stage of the model calibration, there were four versions of the model that produced similar model-data comparison statistics for the key CBP decision state variables of DO and Chl. Those were most relevant to the decisions and outcomes of the 2017 Midpoint Assessment of the Bay water quality standards.

This section describes the results of model-data comparisons for DO and Chl across the four model versions. Four types of comparisons are presented in accordance with the main report: (1) DO and Chl time series at station CB4.2C, located in CBPS CB4MH in the mid-Bay, where hypoxia is most severe; (2) box and whisker plots at the same station; (3) mean difference (MD) plots; and (4) absolute mean difference (AMD) plots between modeled results and observations. The MD and AMD are computed as shown in equation 1 and equation 2:

$$MD = \frac{\sum_{i=1}^{N}(P_i - O_i)}{N} \quad (1)$$

$$AMD = \frac{\sum_{i=1}^{N}|P_i - O_i|}{N} \quad (2)$$

where:

P_i = i^{th} model prediction
O_i = i^{th} observation
N = total number of data points

Figure E-3 displays the time series of daily bottom DO at station CB4.2C. All model versions reproduced the seasonal variation and magnitude observations well. The DO reached zero in summer, substantially below the hypoxia limit of 2 mg/l, and increased up to 11 mg/l in winter. The earliest version of the model, Run196, predicted slightly higher DO values than other versions, although the difference was negligible, whereas the other three versions estimated similar DO results (Figure E-3 and Figure E-4). The Run199 version predicted slightly lower values than other model versions, but differences were minimal, and Run214 and Run223 were virtually identical.

In terms of surface Chl, Run196's predictions were slightly higher than those of the other model versions, whereas the other predictions mostly overlapped (Figure E-5). No extremely high or extremely low observed values were reproduced by the model, but seasonal dynamics and the magnitude of temporal variations were generally well captured. The box and whisker plot (Figure E-6) shows that the results of the four versions of the model were quite similar in terms of the median and the upper and lower quartiles of surface Chl simulations, even though the maximum simulated by Run196 was slightly higher than that simulated by the other model versions. In some years, model predictions tended to be higher than observations, particularly in 1993, 1994, 1997, and 1999, while model predictions were lower than observations in 2000 (Figure E-6).

Figure E-3. Time series of daily bottom DO at station CB4.2C in the mid-Bay main stem.

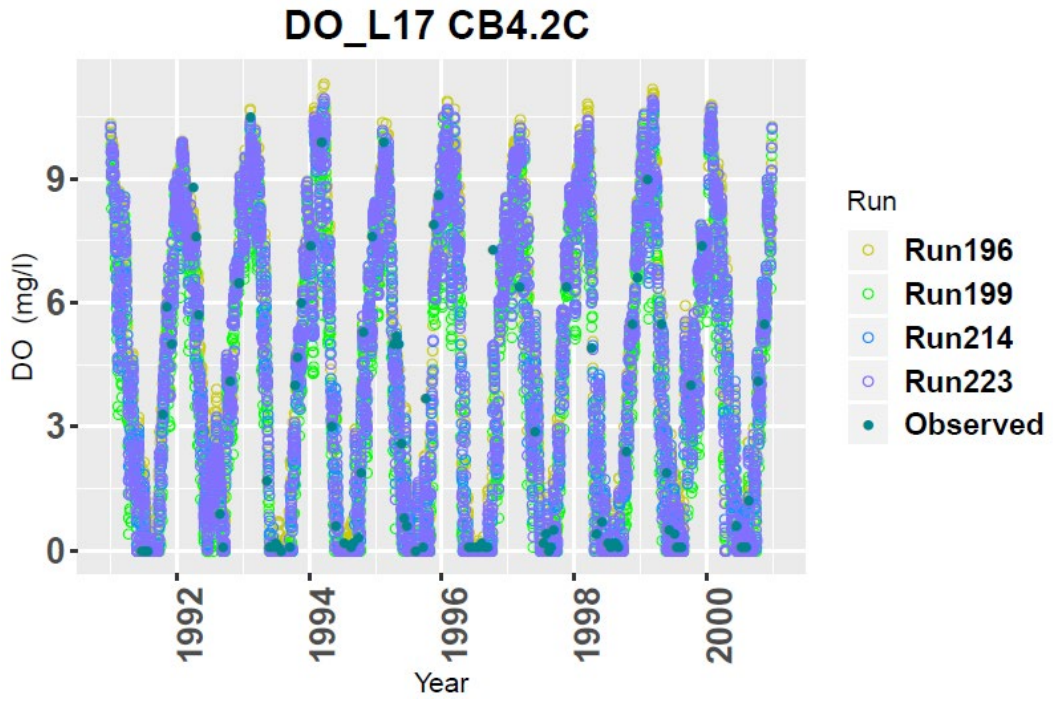

Figure E-4. Box and whisker plot of bottom DO at station CB4.2C in the mid-Bay main stem. The statistics (median, and upper and lower quartiles) are based on all the data for each year.

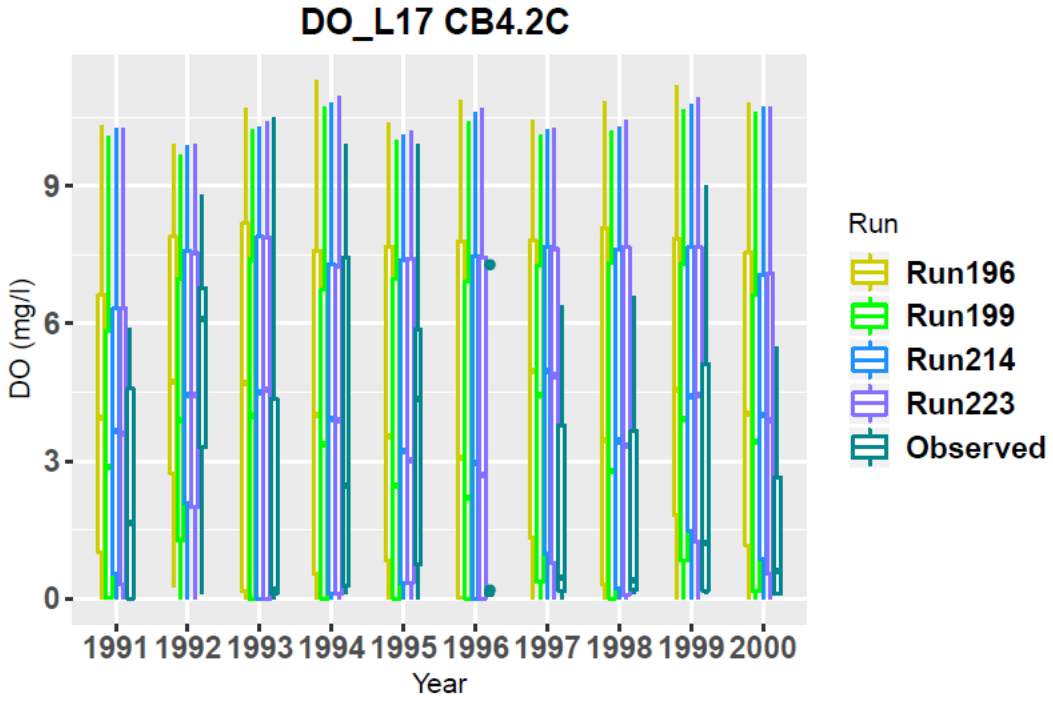

Figure E-5. Time series of daily surface Chl at station CB4.2C in the mid-Bay main stem.

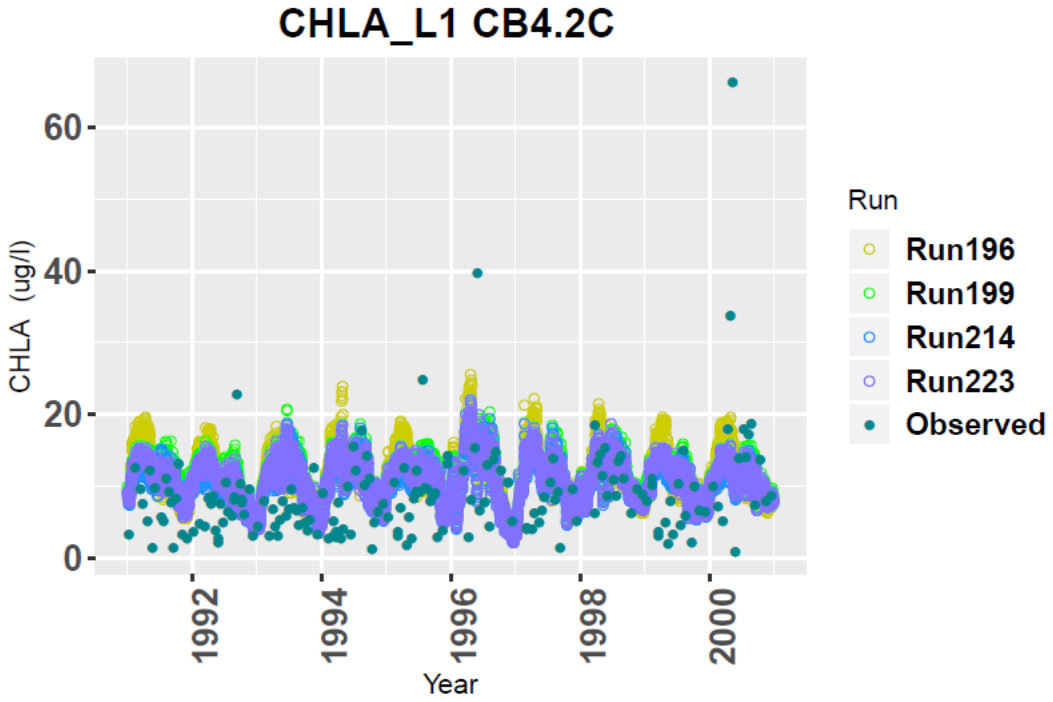

Figure E-6. Box and whisker plot of surface Chl at station CB4.2C in the mid-Bay main stem.

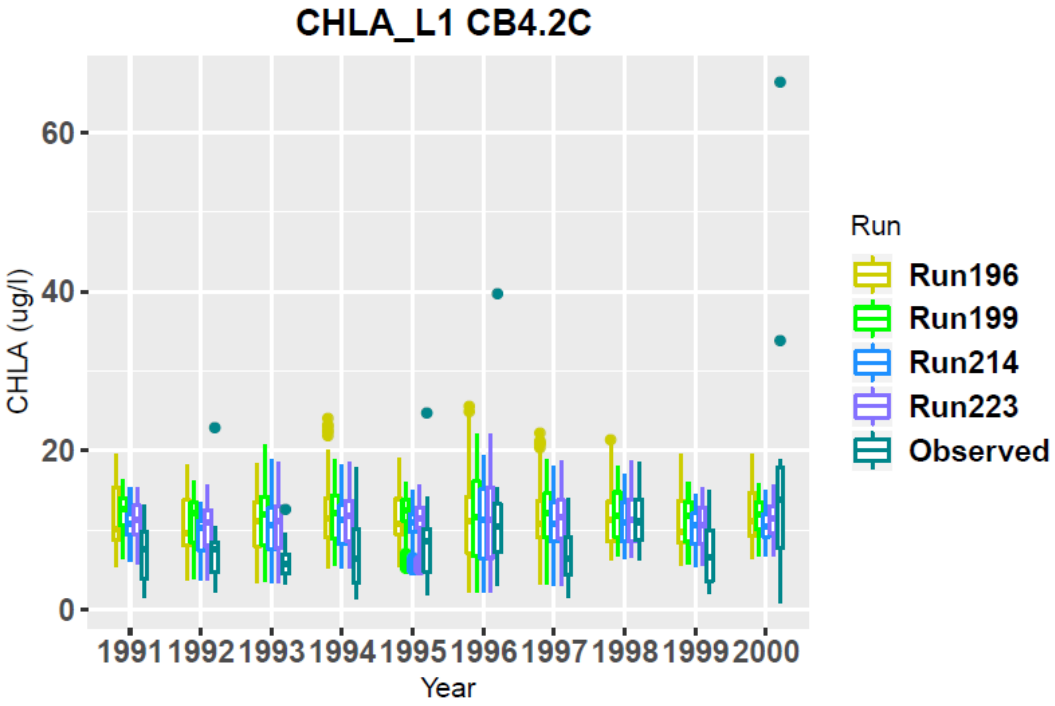

Values of AMD and MD were computed for the main stem Bay and each major tributary, including the Patuxent, Potomac, Rappahannock, York, James, Eastern Shore, and Western Shore for DO. The four versions of the model produced similar AMD values for DO across the whole water column (Figure E-7). Run199 generated slightly higher AMD values than other model versions in some of the tributaries such as the Eastern Shore, Patuxent, and Western Shore, although differences were generally lower than 10 percent. The three other model versions yielded similar results. Values of AMD were lowest in the main stem, where the smallest difference across the four model versions was also observed, and highest in the Eastern Shore. Based on MD values, the model tended to underestimate DO in the Eastern Shore and overestimate it in other major basins (Figure E-8). The simulation performed particularly well in the main stem and the Western Shore, where MD was < 0.25 mg/l. In the other basins, MD was mostly < 1 mg/l.

Simulations of Chl were quite comparable across the four model versions in terms of AMD (Figure E-9). The main stem Bay exhibited the lowest AMD value for Chl, followed by the York, the Rappahannock, and the Eastern Shore, whereas the Western Shore showed the highest Chl AMD. High AMD values in the Western Shore are the result of Chl underestimation by all four model versions, as reflected by negative MD values (Figure E-10).

The model-data comparison in this section is appropriate for comparing the four versions of the equally well calibrated versions of the model for consistency with findings of spatial and seasonal nutrient limitation in the Chesapeake Bay (Fisher et al. 1992, 1999; Kemp et al. 2005). As shown above, the four versions of the model are quite similar in terms of model-data comparison and all produced acceptable values of MD, AMD, and other statistical comparisons with observations. Consequently, all four model versions could theoretically be used for management applications based on DO and Chl goodness-of-fit metrics. But how do these model versions perform when simulating nutrient limitation?

Figure E-7. Absolute mean difference between model-predicted and observed DO (mg/l) across the water column in the main stem and major tributaries.

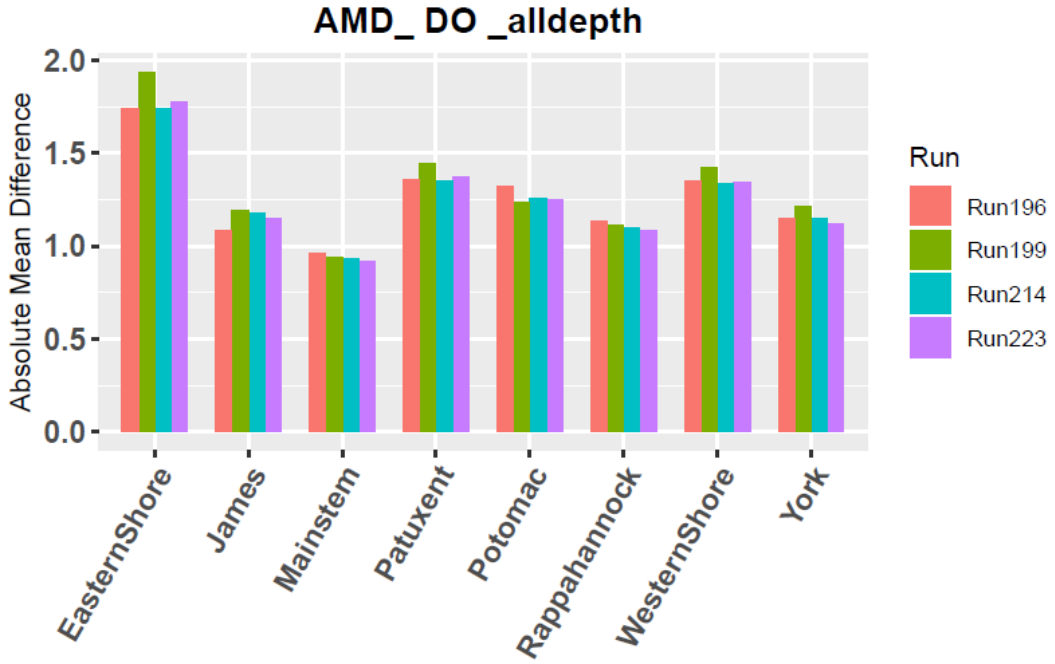

Figure E-8. Mean difference between model-predicted and observed DO (mg/l) across the water column in the main stem and major tributaries.

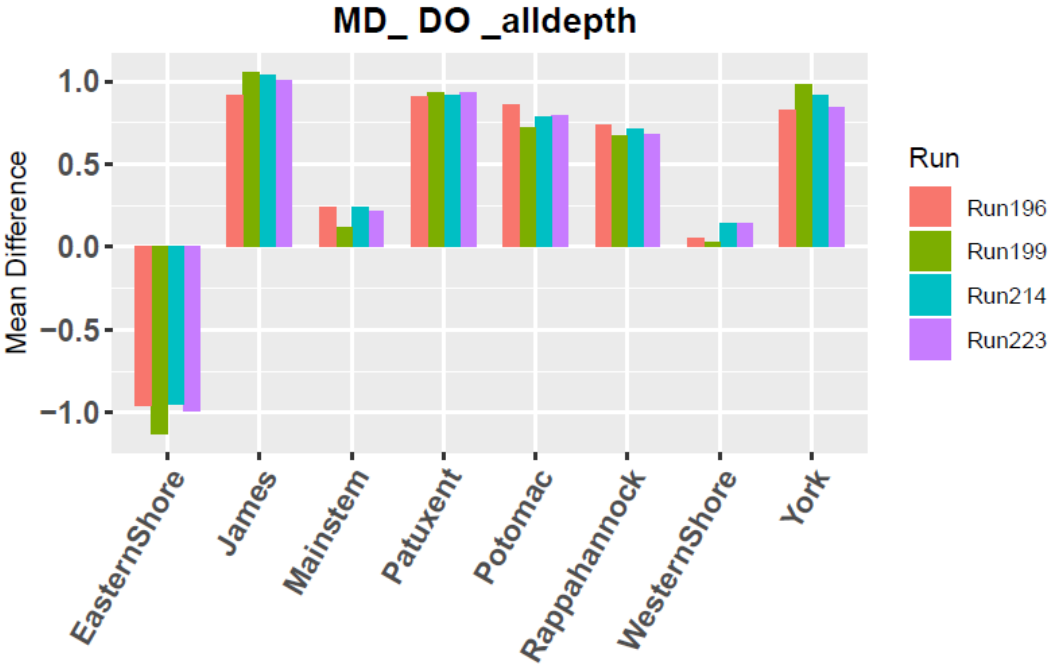

Figure E-9. Absolute mean difference between model-predicted and observed Chl (ug/l) across the water column in the main stem and major tributaries.

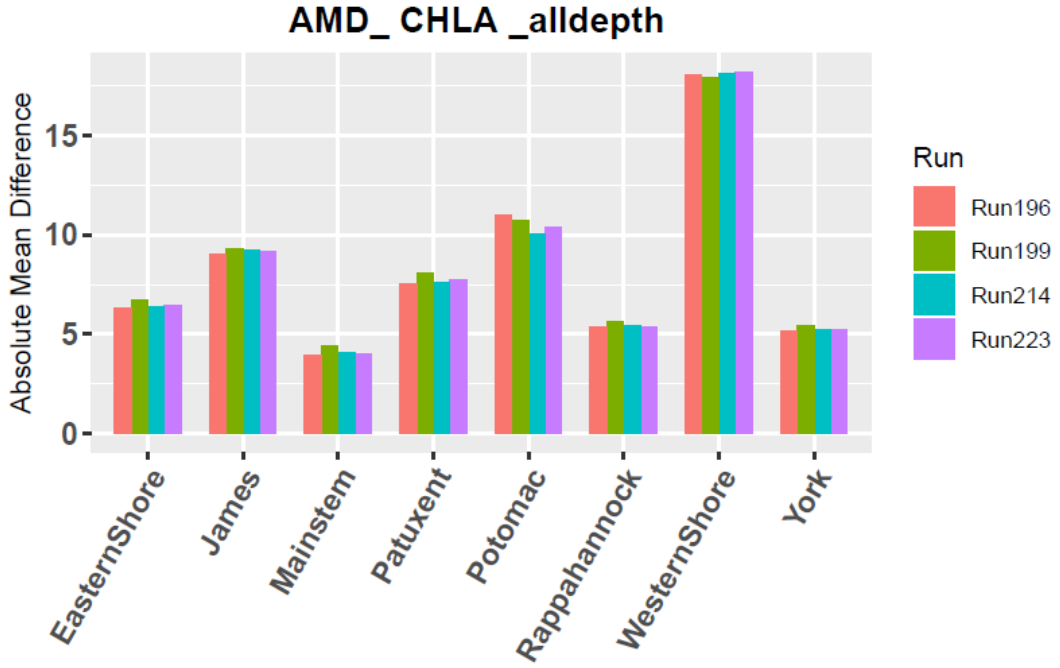

Figure E-10. Mean difference between model-predicted and observed Chl (ug/l) across the water column in the main stem and major tributaries.

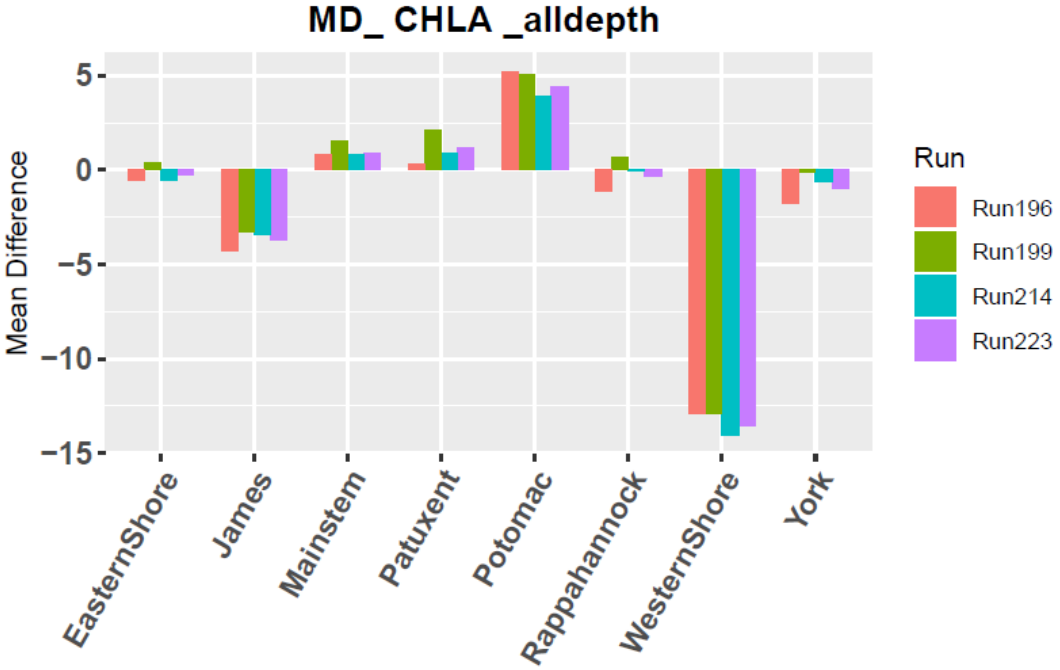

E.4 Modeled Nutrient Limitation

The 2017 WQSTM uses Michaelis-Menten kinetics (Michaelis and Menten 2013) to simulate nutrient limitation of phytoplankton production, as shown in equation 3:

$$f(N) = \frac{N}{N+K_S} \quad (3)$$

where:

N = nutrient (N or P) concentration
K_S = half-saturation constant (i.e., the nutrient concentration at which phytoplankton growth is reduced by half)
$f(N)$ = limiting factor, ranging from 0 to 1

The 2017 WQSTM has three phytoplankton groups. In the case of P, the same half-saturation constant of 0.0025 mg/l is used for all three groups. For N, however, different half-saturation constants are used (Figure E-11). Specifically, a half-saturation constant of 0.01 N mg/l is used for phytoplankton group 1 (cyanobacteria), while group 2 (diatoms) and group 3 (green algae) are each assigned a half-saturation constant of 0.025 N mg/l. During simulations, the limiting factors for each nutrient species and phytoplankton group were recorded at an hourly time step. To compare simulation results with bioassay data, nutrient limitation of the entire phytoplankton community rather than of a single algal group is needed. To this end, a weighted average of the limitation factors of the three phytoplankton groups was computed as in equation 4:

$$f(N) = \frac{f_1(N)P1+f_2(N)P2+f_3(N)P3}{P1+P2+P3} \quad (4)$$

where:

$P1$, $P2$, and $P3$ = biomass of the three phytoplankton groups
$f_1(N)$, $f_2(N)$, and $f_3(N)$ = group-specific nutrient limitation factors of a specific nutrient element (N or P in this case)
$f(N)$ = nutrient limitation factor for the entire phytoplankton community

The computation was carried out in the same way for both N and P.

Figure E-11. N and P half-saturation constants for phytoplankton growth. The right panel displays N limitation on phytoplankton groups P1 and P2.

Half-saturation constants of nitrogen and phosphorus (mg/l) for phytoplankton growth. P1, P2 and P3 are 3 phytoplankton groups.

Phytoplankton	Nitrogen	Phosphorus
P1	0.01	0.0025
P2	0.025	0.0025
P3	0.025	0.0025

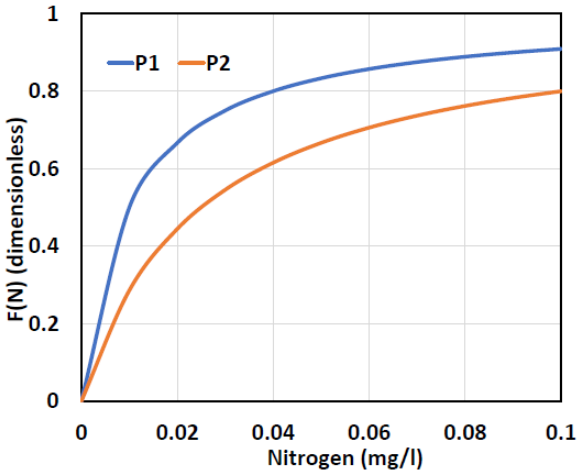

The bioassays used in this study represent the nutrient limitation status at a specific time and location and are averaged on a monthly time scale within a specific geographic segment. The model provides a limitation factor for each nutrient element and each phytoplankton group at each model cell on a daily basis (computed at each hourly time step and averaged daily for output). In the model, phytoplankton growth is determined by the minimum available nutrient based on the Liebig's Law (Liebig 1840) and there is practically no circumstance in which both nutrients are simultaneously the minimum at a specific time step. Relative N limitation vs. P limitation was determined by counting the instances when either N or P was limiting in time and space within a month and CBPS. Specifically, relative limitation was calculated by dividing the number of limitation instances of a specific nutrient (N or P) by the total number of limitation instances of both nutrients. A "limitation instance" is defined as occurring when a nutrient exhibits a concentration lower than its half-saturation constant and lower than that of the other nutrient (N or P). The counting for each month during the period of high production in the Chesapeake Bay (March–September) was performed over the 10-year simulation period from 1991 to 2000 and over all the model cells within a specific CBPS on a daily basis.

Figure E-12 shows nutrient limitation simulated by Run196 during the productive season from March through September in the main stem segments. Compared with nutrient limitation observed through bioassays (Figure E-2), Run196 lacks P limitation in the upper Bay, particularly in CBPSs CB2OH and CB3MH. Based on bioassays, CB2OH is P-limited year-round, while in the Run196 simulation, N limitation dominates in September and August and occurs 40 percent of the time in July. In CB3MH, bioassays show co-limitation in summer from July through September, while Run196 simulated full N limitation during the same period of time. Also, bioassays show a shift from P limitation in spring to N limitation in summer in the lower Bay from CBPS MD5MH through CBPS CB8PH, while Run196 simulated full N limitation year-round. As a general observation, Run196

lacks P limitation in the upper Bay year-round as well as during spring in the lower Bay.

Run199 simulated a shift from P limitation in spring to co-limitation in summer in the upper-Bay CBPSs CB1TF, CB2OH, and CB3MH (Figure E-13). This is an improvement from the full N limitation simulated in summer by Run196 toward the observation of full P limitation in CB1TF and CB2OH (Figure E-2), but P limitation remains lower compared to bioassay results. The Run199 solution in the lower Bay is better than that of Run196, with a transition from P limitation in spring to N limitation in summer, as shown in the bioassay results.

Run214 captured the observation that CBPSs C12TF and CB2OH are P-limited year-round (Figure E-14). The transition from P limitation to N limitation in the lower Bay is also reproduced. However, differences between simulations and observations remain in the mid-Bay CBPSs CB4MH and MD5MH. Bioassay measurements show predominant N limitation in summer (July through September) in the mid-Bay, while Run214 predicted co-limitation of the two nutrient elements during the same period of time and over 70 percent P limitation in July.

Run223 predicted nutrient limitation patterns that most closely matched bioassay observations among the four versions of the model (Figure E-15). The upper-Bay CBPSs C12TF and CB2OH are predominantly P-limited year-round. Only in September did the model predict slight N limitation but, given the manner in which modeled nutrient limitation was calculated (i.e., by counts in space and time), the difference remains minimal when compared to other versions of the model. Also, in the mid-Bay CBPSs CB4MH and MD5MH, the model predicted predominant N limitation in summer and P limitation in spring, in agreement with the bioassay results. In the lower Bay, N limitation generally dominates, with co-limitation in spring and full N limitation in summer. The bioassay results in March and April showed the same pattern of transition from co-limitation in spring to full N limitation in summer. The bioassay results in March, April, and May showed full P limitation for all CBPSs between CB1TF and MD5MH.

Figure E-12. Nutrient limitation simulated by Run196 during the productive season in the main stem segments.

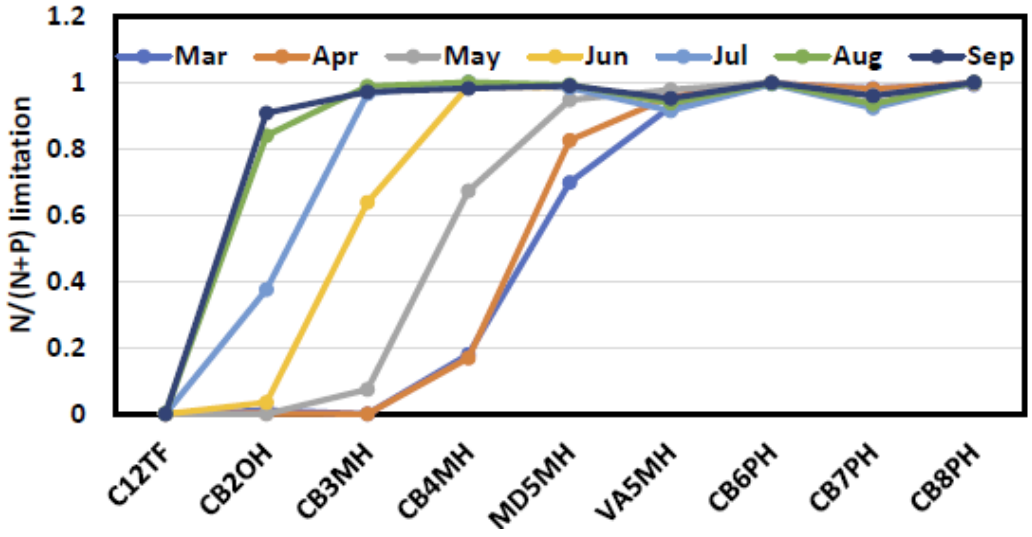

Figure E-13. Nutrient limitation simulated by Run199 during the productive season in the main stem segments.

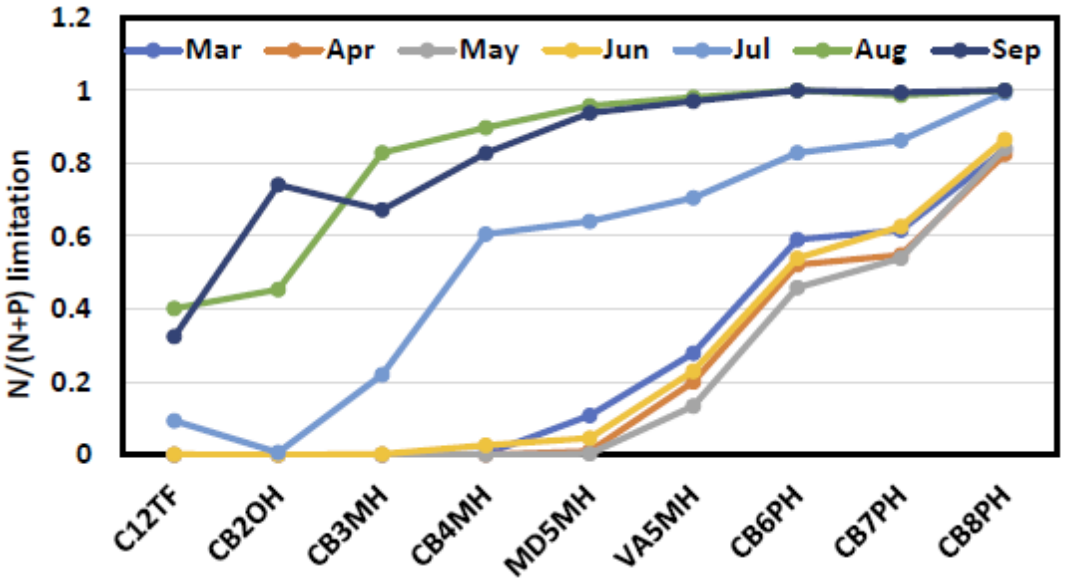

Figure E-14. Nutrient limitation simulated by Run214 during the productive season in the main stem segments.

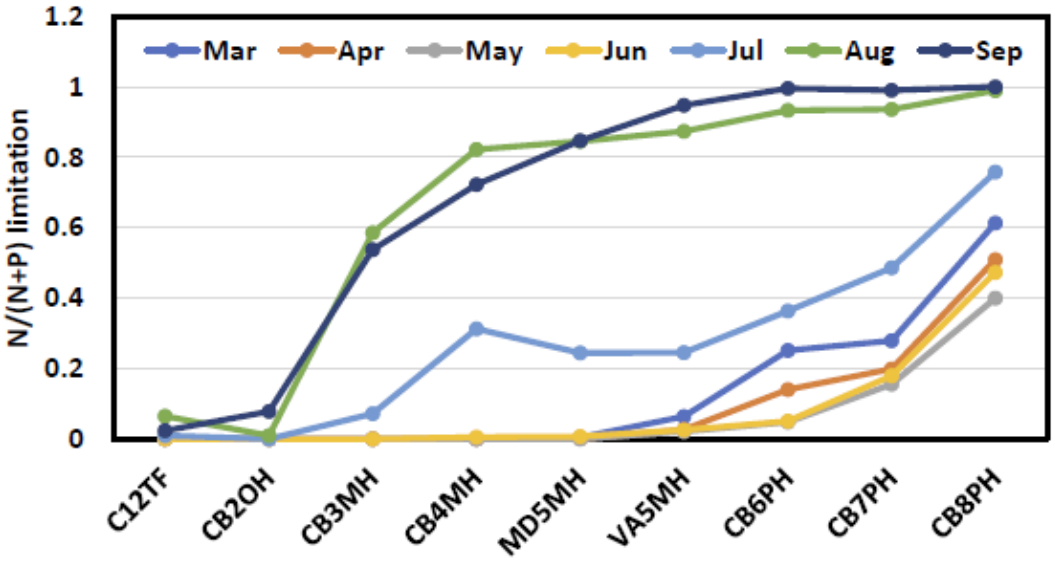

Figure E-15. Nutrient limitation simulated by Run223 during the productive season in the main stem segments.

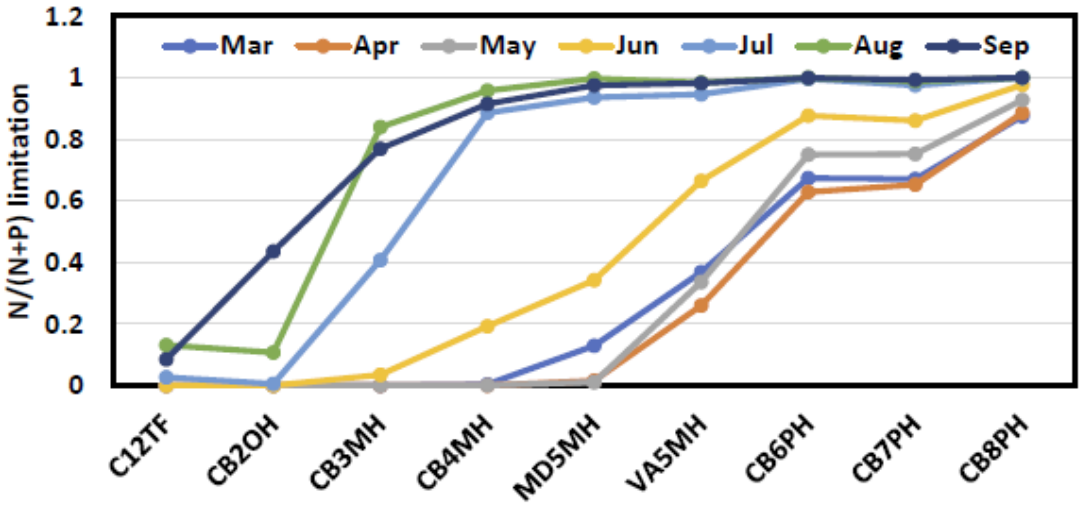

E.5 Sensitivity of Dissolved Oxygen Concentrations to Nutrient Reduction

The objective of this section is to illustrate the importance of nutrient limitation in determining the sensitivity and effectiveness of nutrient loading on water quality in the Bay. Nutrient reduction planning and decisions are based on the effectiveness of nutrient loading on Bay water quality (measured primarily by DO concentration). The effectiveness of each major basin was determined by running the model with changes in nutrient loadings from that basin while keeping the loadings from other basins constant at the level of the Total Maximum Daily Load (TMDL). Those geographically isolated model runs, or "georuns," each isolates a single basin to determine its unique effectiveness on water quality in the Bay. A series of sensitivity analyses was carried out to determine the proper amount of nutrient loading change necessary to have a measurable impact on DO concentration in the Bay, and 1 million lb N and 100 thousand lb P were determined to be the appropriate amounts for the georuns. The Redfield ratio of N and P is 16:1 in moles, yielding a ratio in mass of 7.27 (Redfield 1958). The elemental ratio in phytoplankton can vary across space, time, nutrient limitation conditions, and species. An average N:P ratio of 10 was used in regular model simulations and in the georuns. As nutrient reduction is the purpose and practice for managing nutrient loading from the watershed, it is appropriate to assess the impact of nutrient reductions in this type of sensitivity analysis. However, some small basins have less TN and TP loading than the amount needed to be reduced to have a measurable effect on DO in the Bay (i.e., 1 million pounds N and 100 thousand pounds P). Consequently, in those cases, an addition of the appropriate amount of nutrient loading (1 million pounds N or 100 thousand pounds P) was performed instead of a reduction for the georuns. The watershed was split into seven major drainage basins (in order from north to south and east to west): Susquehanna, Patuxent, Potomac, Rappahannock, York, James, Eastern Shore, and Western Shore. The major river basins (Potomac, Rappahannock, York, and James) are split into above and below fall line and the East Shore of Maryland and Delaware into upper, mid-, and lower East Shore, along with the southernmost Virginia Eastern Shore yielding a total of 16 geographic regions.

Although georuns relate to "effectiveness," the results described in this appendix relate specifically to "sensitivity," which refers to the impact of changes in nutrient loading in a specific drainage basin on the water quality in the Bay. Effectiveness includes not only the change in DO concentration in the Bay after a modification of nutrient loading from a drainage basin, but also the delivery factors that specify nutrient transport from each land-river segment in the watershed to the Bay. In the georuns, changes in nutrient loadings were specified at the fall line or at the coastal cells that directly receive nutrient loadings from land. Delivery factors were added to the results of the georuns, transforming the georun sensitivity to effectiveness, which is not part of this appendix.

The sensitivity metric reported here is defined as the change in the 25th percentile of DO concentrations in a designated use of a segment in the Bay. First, the Bay is divided into 92 segments for management purposes and, depending on the local pycnocline depths, each segment is assigned up to three designated uses: Open Water, Deep Water, and Deep Channel. The term "designated use" is used to refer to regions in a TMDL where a particular criterion is applied. In the case of the Chesapeake TMDL, the Open Water, Deep Water, and Deep Channel designated uses each have an associated DO criterion designed to protect the habitat of a specific group of living resources within the designated use. Open Water above the upper pycnocline is frequented by striped bass, bluefish, mackerel, seatrout, menhaden, silversides, and shortnose sturgeon, an endangered species. Deep Water, between the upper and lower pycnoclines and within those pycnoclines, is occupied by bottom-feeding fish, crabs, oysters, bay anchovy, and other species. The Deep Channel in the main stem of the Bay, below the deeper pycnocline, is occupied by bottom sediment-dwelling worms, small clams, bottom-feeding fish, and crabs. In coastal shallow regions that are well mixed and without a distinguishable pycnocline, the whole water body is classified as Open Water. In the deeper off-coastal region where a pycnocline develops in summer (June-September), the water column is divided into Open Water in the surface layer and Deep Water below the pycnocline. The deep trench along the main stem of the Bay is characterized by two pycnoclines: a shallow pycnocline that separates the Open Water and Deep Water designated uses, and a deeper pycnocline that separates the Deep Water above and Deep Channel below.

The 25th percentile of DO concentrations is determined for each designated use and each segment during the summer season. Each segment-designated use combination is simulated by a few to several thousand model cells over 10 years with daily output. The 25th percentile is calculated among all model cells over 10 years. Sensitivity is computed as the difference between the 25th percentile of DO concentrations (ug/l) in the control run and the georuns. In this appendix, only the average sensitivity of the Deep Water and Deep Channel of CBPSs CB3MH, CB4MH, and CB5MH and Deep Water in the Potomac are presented. Those are the major segments in which hypoxia is most severe. The georuns were initially carried out using model version Run196 for an early test, and Run199 was originally selected as the final product. However, the results of the Run199 georuns showed lack of P-sensitivity in the upper Bay and lack of N-sensitivity in the mid-Bay, which led to the in-depth analysis of nutrient limitation presented above. As nutrient limitation showed that Run214 lacked N limitation in the mid-Bay as well, georuns were not performed with that version of the model. Instead, the final georuns were carried out with model version Run223. In the following paragraphs, we compare relative N and P sensitivities predicted by model versions Run196, Run199, and Run223.

Oxygen sensitivity was calculated only for the Deep Channel and Deep Water designated uses because DO in the surface Open Water is influenced by multiple confounding factors in addition to oxygen consumption through respiration and mineralization, such as surface reaeration and photosynthesis evolution of oxygen. CBPSs CB1TF and CB2OH at the head of the Bay are shallow areas without Deep Water and Deep Channel designated uses. Consequently, CBPSs CB3MH, CB4MH, and CB6PH are used as representative of the upper mid-Bay, mid-Bay, and lower Bay, respectively. For the CB3MH Deep Channel designated use (Figure E-16), sensitivity to N loading was highest in Run196 and lowest in Run199. A greater contrast across model versions is observed for P sensitivity (Figure E-17). The DO sensitivity to P loading in CB3MH Deep Channel is almost an order of magnitude lower in Run196 than in the other two runs, with the sensitivity to loading from the Virginia rivers in the southern part of the watershed being almost negligible. This is a result of the fact that Run196 lacks P limitation in the upper Bay and the mid-Bay. The DO sensitivity to TP loading from the Maryland portion of the watershed is mostly comparable between Run199 and Run223, while Run223 has higher DO sensitivity to P loading from the Virginia portion of the watershed than Run199. The ranking of the major basins in terms of DO sensitivity is similar among the different versions of the model, implying that the ranks are primarily determined by geographic location in the watershed and hydrodynamics in the Bay. The DO concentration in the CB3MH Deep Channel is mostly sensitive to N loading from the Susquehanna and Western Shore, but in terms of P loading, the upper and mid-Eastern Shores have an impact as high as the Susquehanna and Western Shore on DO.

Similar results were obtained in CBPS CB4MH (Figure E-18 and Figure E-19). Run196 has the highest sensitivity of DO to N loading (Figure E-18) but lacks sensitivity to P loading. Run199 has the lowest sensitivity to N loading and the highest sensitivity to P loading, while Run223 predicted sensitivities that lie between the two previous versions of the model. In terms of ranks among the major river basins, the Susquehanna has the highest impact of N loading on DO in the CB4MH Deep Channel, followed by the Western Shore and Patuxent, similar to their ranks in CH3MH. On the contrary, the ranks in P sensitivity changed from those observed in CB3MH. Specifically, the mid-Eastern Shore and Patuxent below fall line have the highest impact on DO in the CB4MH Deep Channel, whereas Susquehanna, upper Eastern Shore, and Western Shore are ranked at the top for P sensitivity in the CB3MH Deep Channel. Thus, it appears that P loading from the Susquehanna influences DO concentration down to CB3MH, whereas CB4MH is more impacted by local P loading than by loading from the upstream Susquehanna.

The lower-Bay CBPSs from CB6PH to CBP8PH are without a Deep Channel designated use and the Deep Water designated use extends from the pycnocline to the bottom. As a result, Deep Water DO sensitivity is presented here as a comparison to Deep Channel DO in the upper and mid-Bay. Run196 yielded the lowest sensitivity of DO concentration to N loadings, whereas it has the highest

sensitivity in the upper and mid-Bay (Figure E-20). This may be partly due to the high sensitivity in the upper and mid-Bay leading to high consumption of N and, as a result, less N available to the lower Bay. Also, Run199 predicted a slightly higher sensitivity to N loading than Run223 did, in the reverse order as compared to that in the upper and mid-Bay. A starker contrast can be observed in the DO sensitivity to P loading in the lower-Bay compared to the upper and mid-Bay (Figure E-21). In the case of Run223, the uppermost basins (Susquehanna, upper Eastern Shore, and Western Shore) have negative DO sensitivity to P loading in the lower Bay, meaning that an increase (or decrease) of P loadings in the upper-Bay basins will lead to a decrease (or increase) in the bottom DO concentration in the lower Bay. The upper Bay is mostly P-limited and phytoplankton production is primarily controlled by P availability. An increase (or decrease) of P loading will lead to an increase (or decrease) in phytoplankton production and to a subsequent increase (or decrease) in N uptake. If larger amounts of N are taken up in the upper Bay, less N will be available in the lower Bay, leading to a decrease in phytoplankton production and DO consumption. Basically, a negative sensitivity results from availability of the alternative nutrient (N in this case) due to the biogeochemical dynamics occurring in the upper Bay.

Average sensitivities were used to determine the effectiveness values upon which the watershed planning targets and exchanges between N and P loadings were based. Specifically, the average sensitivities in the Deep Water and Deep Channel designated uses in the main stem segments (CB3MH, CB4MH, and CB5MH) and the Potomac tributary (POMMH) were used. The average sensitivities to N and P are depicted in Figure E-22 and Figure E-23. The average DO sensitivity to N loadings is mostly comparable across the three versions of the model, with Run196 showing the highest values and Run199 the lowest values (Figure E-22). The Susquehanna has the highest sensitivity among the major river basins, followed by the Western Shore, Potomac, and Patuxent, which mostly have the same level of sensitivity. However, the sensitivity to P loading is quite different across the three runs (Figure E-23). The sensitivity to P loading is virtually negligible in the Run196 solution in the lower-Bay tributaries, including the Potomac, Rappahannock, York, and James rivers. The upper-Bay basins have similar sensitivity, including the Susquehanna, upper and mid-Eastern Shore, and Western Shore. In the case of the Susquehanna, the largest tributary in the Chesapeake Bay, the average sensitivity to P loading is almost an order of magnitude lower in the Run196 solution than in the Run199 solution and six times lower than in the Run223 solution. As mentioned earlier, the relative sensitivity of N vs. P provides key information for nutrient loading exchanges in major state-basins. Assuming a phytoplankton N:P ratio corresponding to the Redfield ratio of 16:1 in moles and 7.226:1 in mass and using the Susquehanna as the most representative nutrient loading source, the relative sensitivity of N vs. P is about 23:1 in the Run196 solution, 2.3:1 in the Run199 solution, and 3.4:1 in the Run223 solution. The extremely high value in the Run196 solution results from its lack of P limitation. The key point is that differences in nutrient limitation across model solutions can lead to greater differences in both DO

sensitivity to nutrient loading and the nutrient exchange coefficients in management practices.

Figures E-16 through E-23 use the following abbreviations for the 16 geographic regions in the Chesapeake Bay watershed:

Susq	=	Susquehanna
EshLow	=	Lower Eastern Shore
EshMid	=	Mid-Eastern Shore
EshUpp	=	Upper Eastern Shore
EshVA	=	Eastern Shore Virginia
Wsh	=	Western Shore
PotA	=	Potomac above fall line
PotB	=	Potomac below fall line
PxtA	=	Patuxent above fall line
PxtB	=	Patuxent below fall line
RapA	=	Rappahannock above fall line
RapB	=	Rappahannock below fall line
YrkA	=	York above fall line
YrkB	=	York below fall line
JmsA	=	James above fall line
JmsB	=	James below fall line

Figure E-16. DO sensitivity in CB3MH Deep Channel to TN loading from the major drainage basins.

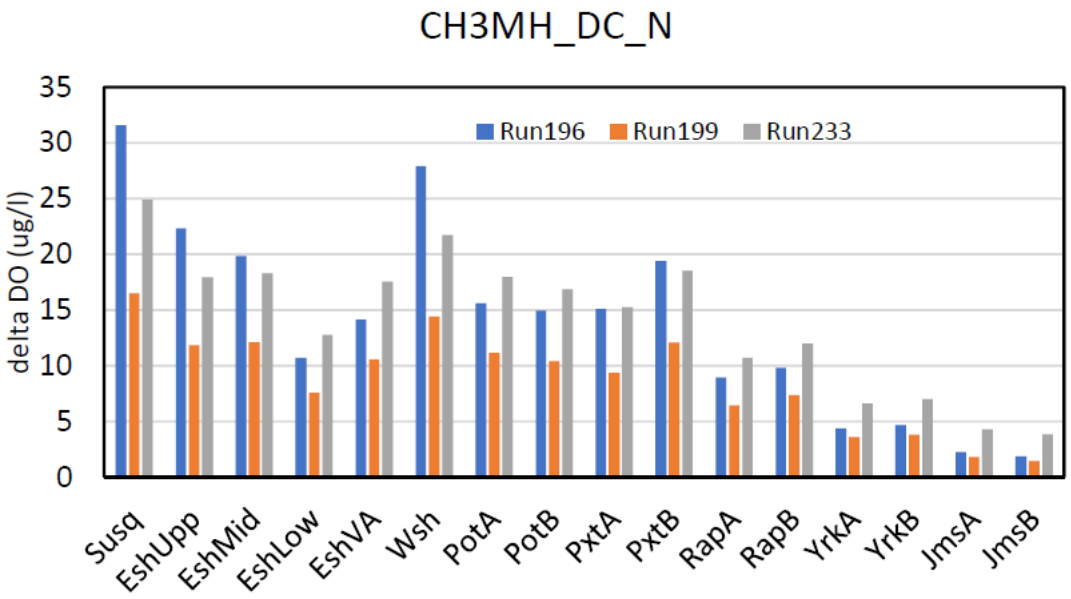

Figure E-17. DO sensitivity in CB3MH Deep Channel to TP loading from the major drainage basins.

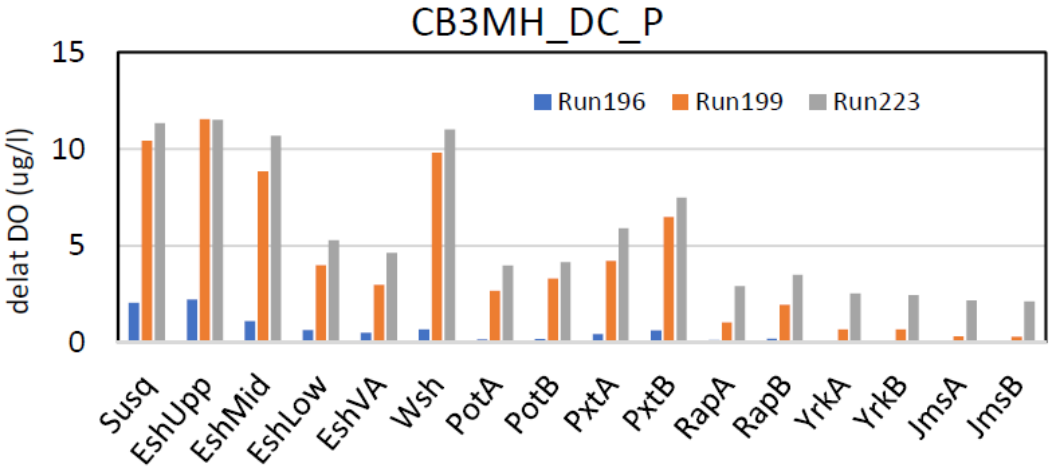

Figure E-18. DO sensitivity in CB4MH Deep Channel to TN loading from the major drainage basins.

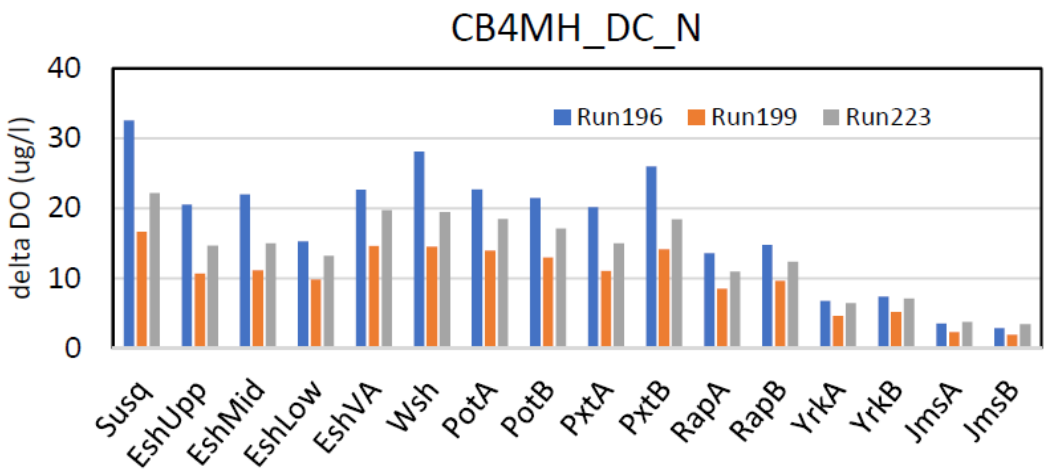

Figure E-19. DO sensitivity in CB4MH Deep Channel to TP loading from the major drainage basins.

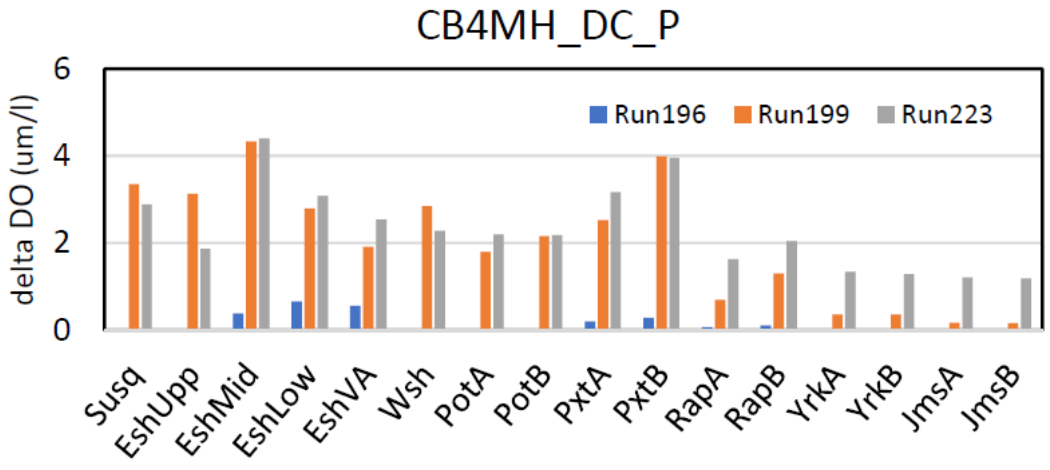

Figure E-20. DO sensitivity in CB6PH Deep Water to total TN loading from the major drainage basins.

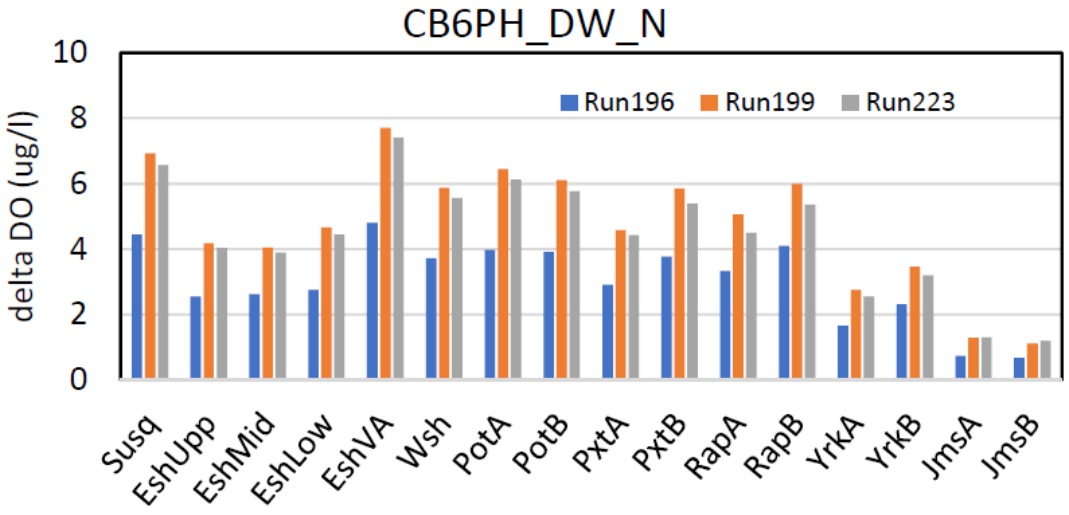

Figure E-21. DO sensitivity in CB6PH Deep Water to TP loading from the major drainage basins.

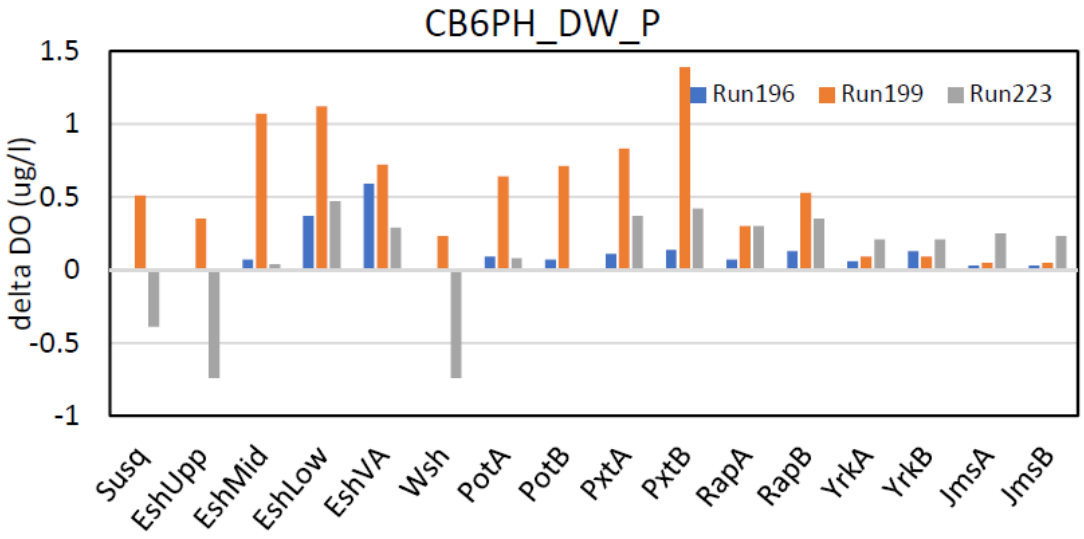

Figure E-22. Average DO sensitivity in CB3MH, CB4MH, CB5MH, and POMMH Deep Water and Deep Channel to TN loading from the major drainage basins.

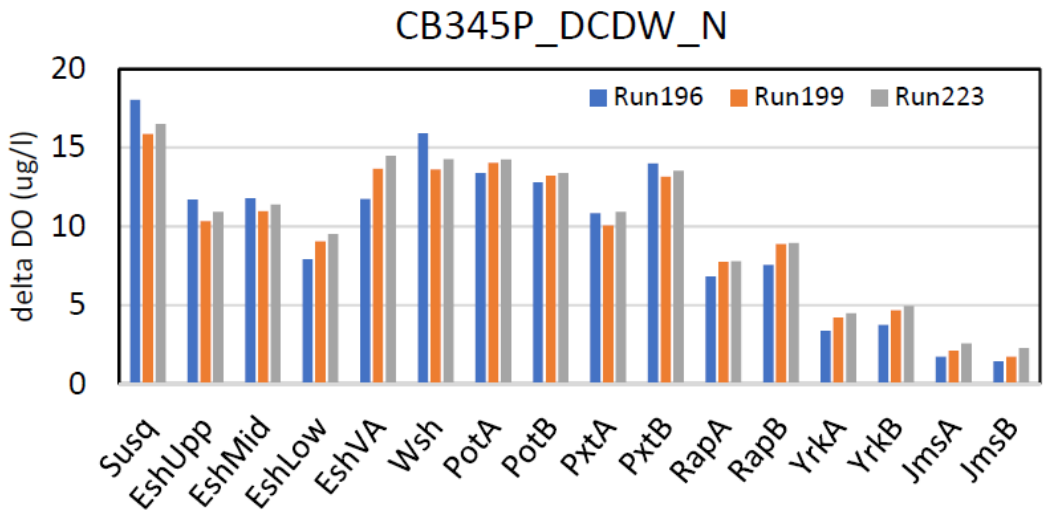

Figure E-23. Average DO sensitivity in CB3MH, CB4MH, CB5MH, and POMMH Deep Water and Deep Channel to TP loading from the major drainage basins.

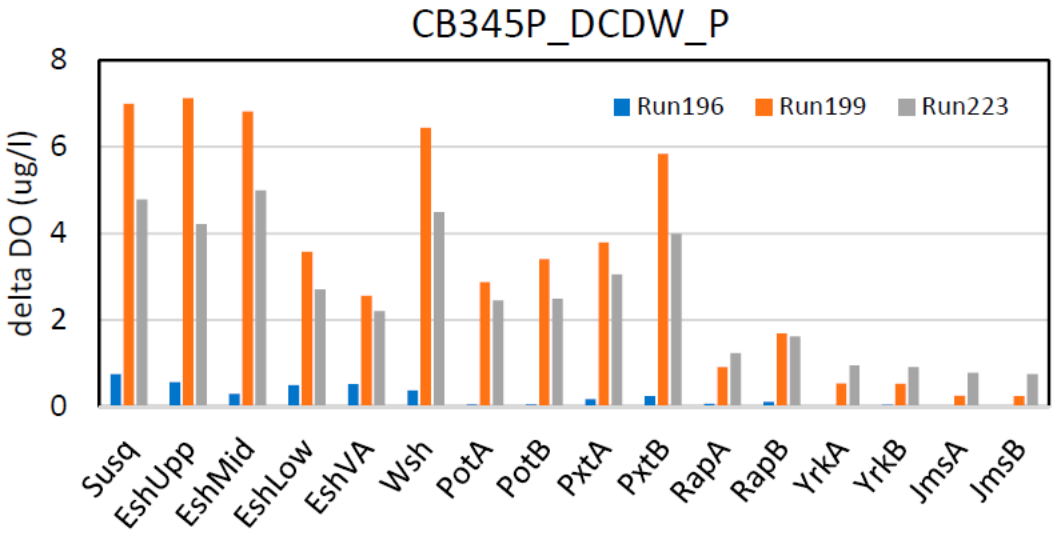

E.6 Conclusions

Eutrophication and associated hypoxic conditions present one of the most severe anthropogenic stresses to coastal ecosystems generally and to the Chesapeake Bay in particular. Nutrient management and loading reductions in the watershed and airshed of coastal ecosystems are primary controls for mitigation and restoration (Linker et al. 2013). Model simulations provide critical information for management decision-making in determining the quantity and spatial partitioning of nutrient reductions on the watershed. This is particularly true when considering the influence of climate change on eutrophic coastal watersheds for which model simulation is the primary method of generating projections and assessing future risks and opportunities. In these contexts, models are usually calibrated and validated using model-data correspondence of state variables, and, in the case of biogeochemical and water quality simulations of eutrophic coastal watersheds, Chl and DO are among the most commonly used calibration variables. Due to equifinality, however, equivalent goodness-of-fit values can be achieved from different model parameter configurations. For nutrient management applications in which various nutrient species are involved, a shift in greater nutrient limitation from N to P, for example, can lead to the same results in terms of DO concentration and hypoxia.

In addition, the spatiotemporal extent over which a specific nutrient is limiting can alter the effectiveness of that nutrient on water quality and, consequently, alter the amount of reduction for that nutrient estimated to be needed to reach water quality criteria. Relative limitation among different nutrient species will also ultimately affect their exchange coefficients in CBP management practice. In this study, we showed that four versions of the same model resulted in similar model calibration and validation statistics. When compared with bioassay results

of nutrient limitation, however, the different versions of the model predicted different nutrient limitation patterns in space, time, and between N and P. Differences in nutrient limitation resulted in large differences in the sensitivity of the Deep Water DO response to nutrient reductions in the watershed. The primary goal of nutrient management is to reduce nutrient loading from the watershed so that DO concentration criteria can be attained. The amount of nutrient reduction and the partitioning of the total allowed nutrient loading over different drainage basins are determined based on DO sensitivity to nutrient loading. Consequently, nutrient limitation in the model solution is critical for management decision-making and planning. The robustness and accuracy of nutrient limitation estimates directly affect the success of nutrient management actions, and the relative limitation factors of different nutrient species play a significant role in determining the exchange coefficients between nutrients for nutrient reduction and trading. This study shows that nutrient limitation is a critical metric of model robustness in management applications.

E.7 References

Fisher, T.R., E.R. Peele, J.W. Ammerman, and L.W. Harding Jr. 1992. Nutrient limitation of phytoplankton in Chesapeake Bay. *Marine Ecology Progress Series* 82:51–63.

Fisher, T.R., A.B. Gustafson, K. Sellner, R. Lacouture, L.W. Haas, R.L. Wetzel, R. Magnien, D. Everitt, B. Michaels, and R. Karrh. 1999. Spatial and temporal variation of resource limitation in Chesapeake Bay. *Marine Biology* 133:763–778.

Kemp, W.M, W.R. Boynton, J.E. Adolf, D.F. Boesch, W.C. Boicourt, G. Brush, J.C. Cornwell, T.R. Fisher, P.M. Glibert, J.D. Hagy, L.W. Harding, E.D. Houde, D.G. Kimmel, W.D. Miller, R.I.E. Newell, M.R. Roman, E.M. Smith, and J.C. Stevenson. 2005. Eutrophication of Chesapeake Bay: Historical trends and ecological interactions. *Marine Ecology Progress Series* 303:1–29.

Liebig, J. 1840. *Organic Chemistry in Its Applications to Agriculture and Physiology*. 4th ed. Taylor and Walton, London.

Linker, L. C., R.A. Batiuk, G.W. Shenk, and C.F. Cerco. 2013. Development of the Chesapeake Bay watershed Total Maximum Daily Load allocation. *Journal of the American Water Resources Association* 49(5):986–1006.

Michaelis, L., and M.L. Menten. Kinetics of invertase action. 1913. *Biochemische Zeitschrift* 49:333–369.

Redfield, A. 1958. The biological control of chemical factors in the environment. *American Science* 46:205–221.

USEPA (US Environmental Protection Agency). 2010. Allocation Methodology to Relate Relative Impact to Needed Controls. Appendix K in *Chesapeake Bay Total Maximum Daily Load for Nitrogen, Phosphorus and Sediment*. US Environmental Protection Agency, Chesapeake Bay Program Office, Annapolis, MD. Accessed June 2019. https://www.epa.gov/sites/production/files/2015-02/documents/appendix_k_-_relating_relative_impact_to_needed_controls_final.pdf.

Appendix F: Hypoxia Volume—An Integrated Scalar for Model Calibration and Validation

Model simulations are increasingly used in environmental management and nutrient reduction programs to address eutrophication and hypoxia. First a model is calibrated and validated in a specific system like the Chesapeake Bay, then model simulations are conducted by altering nutrient inputs or physical conditions to represent nutrient management scenarios or future climate change projections. Model calibration is typically done against observations at sampling stations. As stations and sampling surveys are discrete in space and time, however, they inevitably overlook much of the system variability across space and time. In this appendix, we use hypoxia volume-day as an integrated metric of model performance that includes integration both in space and time.

First, hypoxia volume is computed by integration in space and then hypoxia volume-day is obtained by integrating hypoxia volume through time. That method was applied to four model solutions and compared model assessment statistics with those based on station-specific dissolved oxygen (DO) concentrations. Model calibration assessment statistics based on hypoxia volume-day differed from estimates based on station data. The difference was particularly significant in the tributaries and embayments, where the model is less accurately calibrated than in the mainstem Chesapeake Bay. Given the nature of integration in space or space and time, hypoxia volume and hypoxia volume-day, respectively, have the potential to provide for a more comprehensive and effective metric for model calibration and assessment when added to traditional calibration techniques in model applications of eutrophication and hypoxia in coastal waters.

F.1 Introduction

As described in chapter 2, the 2017 Chesapeake Bay Water Quality and Sediment Transport Model was calibrated to more than 30 state variables, including the key state variables of DO and chlorophyll. Calibration and model-data comparisons were performed at observation stations and across vertical layers (appendices A-D). Those observations represent the status of the Bay at a specific location and time and, because the number of stations is limited, the majority of the Bay regions are inevitably overlooked during calibration. Hypoxia volume (i.e., the total volume of water with DO concentration below 2 mg/l), however, is an integrated metric in space and the hypoxia volume-day metric includes integration in time as well. Because hypoxia—defined here as DO below 2 mg/l—

occurs essentially in the bottom layers of the Bay, it is unrepresentative of water quality in the surface layers. Different DO concentration thresholds, however, can be used to define water quality criteria in addition to the value of 2 mg/l typically used to define hypoxia. Different DO criteria ranging from 1 mg/l to 5 mg/l have been established to more accurately represent the range of DO habitat and ecological conditions in the Chesapeake Bay from surface waters to the bottom. The living resource-based DO criteria values allow a more comprehensive and integrated assessment of DO calibration performance across different depths and estuarine habitats.

Based on living organism occupation and habitats, three DO designated uses were defined in the Chesapeake Bay: (1) the Open Water (OW) use, which is the water volume above the pycnocline typically inhabited by populations of striped bass, bluefish, mackerel, seatrout, menhaden, silverside, and shortnose sturgeon (an endangered species); (2) the Deep Water (DW) use, which extends below the surface pycnocline and above the bottom Chesapeake pycnocline described by Fisher (Dr. Thomas Fisher, University of Maryland Center for Environmental Science, personal communication, October 2019) and inhabited by bottom-feeding fish, crabs, oysters, bay anchovy, and other species; and (3) the Deep Channel (DC) use, which is located at the bottom of the mainstem below the deep pycnocline (USEPA 2010) and occupied by bottom sediment-dwelling worms, small clams, and bottom-feeding fish and crabs. A critical DO concentration was established for each designated use: 1 mg/l for the DC designated use, 3 mg/l for the DW designated use, and 5 mg/l for the OW designated use.

The Bay is divided into 92 Chesapeake Bay Program Segments (CBPSs) for management purposes (USEPA 1983), as shown in Figure 3-1 in chapter 3 of the main report. In the shallow coastal area, where the whole water column is well mixed and without a distinguished pycnocline from the surface to the bottom, only the OW designated use is applied. In deeper areas, where a surface pycnocline develops in summer, both OW and DW designated uses are applied. There is a DC designated use/habitat region in the mainstem of the Bay in which water is separated from the DW of the water column by a second, deeper pycnocline. That bottom water body constitutes the DC designated use. Consequently, a CBPS can have one, two, or three designated uses, depending on its geographic location. In this appendix, we use the integrated water volume where DO is lower than a set of select critical values (1 mg/l, 3 mg/l, and 5 mg/l) based on the DO water quality criteria as a metric to compare water quality model simulations to observations in individual CBPSs and across the whole Bay. In the rest of this document, the terms “hypoxia volume” and “hypoxia volume-day” are, therefore, used with reference to different critical DO values. Results of model performance when using a commonly used critical DO value of 2 mg/l are also included in this report to facilitate comparison with other model applications in the Chesapeake Bay.

F.2 Observed Hypoxia Volume and Interpolator Grid

The DO data have been collected since 1984 within the framework of the Chesapeake Bay Program (CBP). The data provide the basic information for modelling applications and are extensively used for model calibration, validation, and comparison. This section describes how the DO data were used to determine the hypoxia volume in each segment and in the whole Bay based on different DO critical values (1 mg/l, 2 mg/l, 3 mg/l, and 5 mg/l). Raw data were interpolated onto a regular grid with horizontal resolution ranging from 50 m in the coastal embayment and tributaries to 1,000 m in the mainstem of the Bay (Figure F-1) (Bahner 2006). Vertical resolution of the Interpolator grid is 1 m and the number of vertical layers differs for each node point depending on local water depth. Interpolation on the grid is based on inverse-distance weighting (USEPA 2018). The observed hypoxia volume in each CBPS was determined by calculating the total number of Interpolator cells with DO concentration below each critical value multiplied by the cell volume in that segment. The hypoxia volume for the whole Bay was calculated as the sum of the hypoxia volumes of all the CBPSs.

Figure F-1. Interpolation grids.

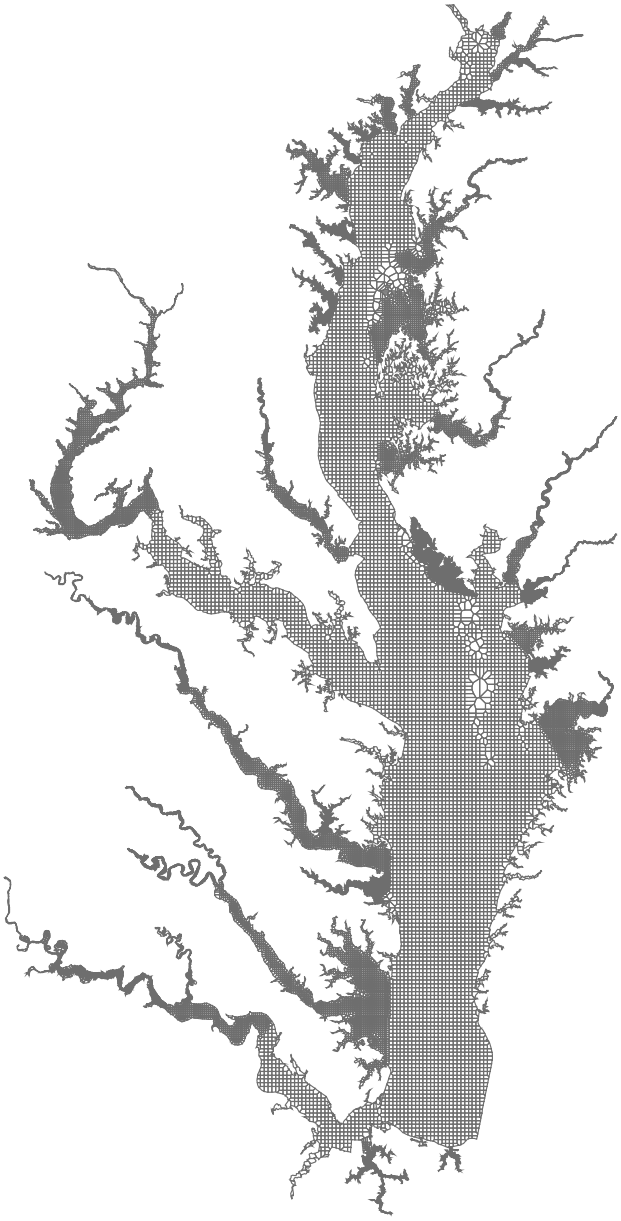

F.3 Modeled Hypoxia Volume and Model Grid

This section explains how modeled hypoxia volumes were computed from model cells. The model grid consists of 1,106 horizontal cells with a z-coordinate in the vertical dimension. The number of vertical layers varies depending on local water depth. The horizontal resolution is approximately 1 km. Surface model cells are 7 feet thick (2.13 m), and all layers below the surface cells are 5 feet thick (1.52 m). The interpolation grid has a total of 76,153 surface cells, while the model has only 11,064 surface cells. As a result, the Interpolator grid has much higher resolution than the model grid in both the horizontal and vertical dimensions. Modeled

hypoxia volume was calculated in a similar manner to observed hypoxia volume (i.e., by calculating the total number of cells with DO concentrations below each critical value multiplied by cell volume). Although the overall water volumes estimated for each CBPS by the model and the Interpolator grids are similar, some differences occur, particularly in shallow segments. To account for those differences, the ratio for each CBPS between the volume of water estimated by the interpolation grid and the volume of water estimated by the model grid was calculated. Modeled hypoxia volumes in each segment were then scaled to the interpolation space by multiplying them by the corresponding volume ratio. In the case of the whole Bay, the model volume is 88 km^3 and the interpolation volume is 75 km^3, yielding a ratio of 0.853. That ratio was applied to the total modeled Baywide hypoxia volume before comparing it to the observed hypoxia volume.

F.4 Model-Observation Comparison

Hypoxia volume was computed for all 92 CBPSs. This section describes results for three mainstem segments (CB3MH, CB4MH, and MD5MH), two Western Shore tributaries (Potomac POMMH and Rappahannock RPPMH), and two Eastern Shore tributaries and embayment (Chester River CHSMH and Eastern Shore EASMH). Those segments are characterized by the most severe hypoxic conditions in the Bay. Results from other segments are included in the Baywide hypoxia volume calculations, which is presented following the figures for the individual segments.

Figures F-2 through F-9 present time series of hypoxia volume from 1993 to 1995, which is the critical period for water quality criteria assessment, and an integrated hypoxia volume-day for each of the seven CBPSs and the whole Bay. In segment CB3MH, time series of model predictions compare reasonably well with observations (Figure F-2, *left panel*). Model-predicted hypoxia volumes based on all water quality DO criteria values (from 1 mg/l to 5 mg/l) show high variability, which is generally supported by observations. Hypoxia starts in May according to both model predictions and observations. The end date of hypoxia occurrence, however, differs between model predictions and observations. Specifically, observations indicate that hypoxia events end in September in this segment, particularly when based on the lowest criteria values of 1 mg/l and 2 mg/l, while some of the model predictions extend hypoxia until late October and early November. A hypoxia event is predicted in early November 1995 by some model versions, which is unsupported by observations.

When considering integrated hypoxia volume-day, model Run196 exhibits predictions that most closely match observations among the four versions of the model in segment CB3MH (Figure F-2, *right panel*). Specifically, model predictions and observations are almost identical when using 1 mg/l (52.5 km^3-days versus 52.3 km^3-days) and 2 mg/l (93.5 km^3-days versus 92.2 km^3-days) and differ by less than 10 percent for hypoxia volume-day based on critical values of 3

mg/l and 5 mg/l. The model Run199 predicted the highest volume-day in this segment, ranging from 82 percent higher than observations below 1 mg/l to 38 percent higher than observations below 5 mg/l. Predictions from the two other model solutions, Run214 and Run223, fall between Run196 and Run199 predictions. Run223, the model version used for the 2017 Midpoint Assessment management decisions based on overall model performance, predicted hypoxia volume-day values 32 percent and 19 percent higher than observations in this segment when using DO critical values of 1 mg/l and 5 mg/l, respectively.

Figure F-2. Hypoxia time series (*left panel*) and integrated hypoxia volume-day (*right panel*) in CBPS CB3MH from 1993 through 1995.

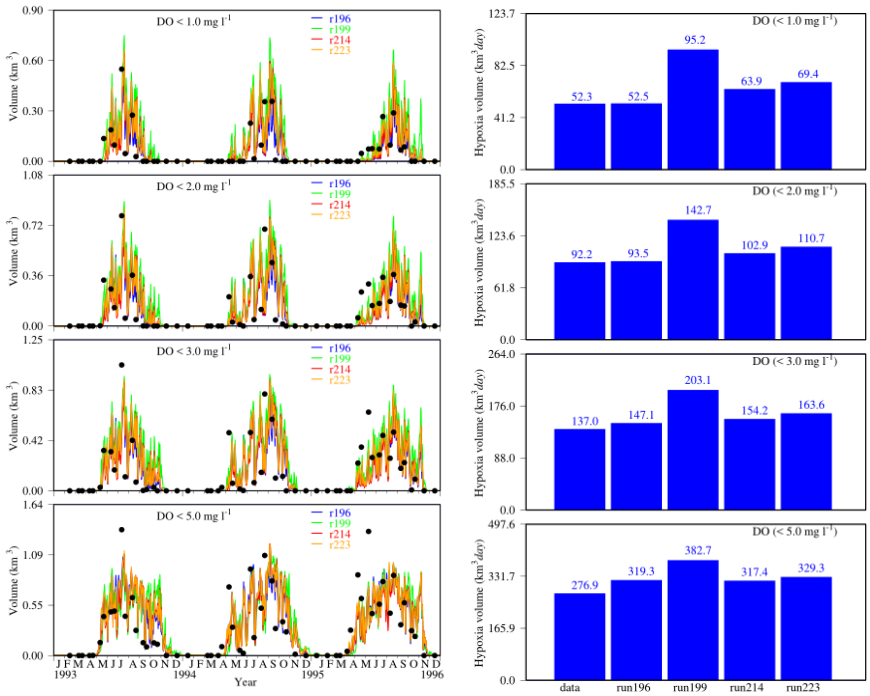

Segment CB4MH is in the central part of the Bay, where hypoxia is most frequent and severe. The magnitude and seasonal cycle of hypoxia from 1993 to 1995 are mostly comparable between model predictions and observations (Figure F-3, *left panel*). Observations revealed, however, an abrupt development of hypoxia in early May 1993. The models also predicted abrupt hypoxia development at the same time, but the magnitudes were lower than observed. Given that hypoxia development was more gradual in other years (1994 and 1995), the mechanisms leading to this abrupt hypoxia development in early May 1993 require further investigation. Also, the variability in hypoxia volume is smaller in CB4MH than in CB3MH because CB3MH is in the region where hypoxia starts to develop, whereas CB4MH constitutes the core part of the DC, where consistent hypoxia persists the longest in the Bay. Run196 predicted significantly lower hypoxia volume-day than observations, whereas this model version performed the best in segment CB3MH. Run196 underestimated hypoxia volume-day by a maximum of 44 percent (DO lower than 1 mg/l) and a minimum of 4 percent (DO lower than

5 mg/l). Run199 predicted 9–10 percent higher hypoxia volume-day than observations when considering DO lower than 1 mg/l and 5 mg/l, respectively. Run223 underestimated hypoxia volume-day by 11 percent with 1 mg/l as the critical value but virtually matched the observed value when using 5 mg/l as the critical value. It is important to note that the mainstem CBPSs CB4MH and MD5MH are part of the DW and DC contiguous regions of the Bay where the DO criteria are most difficult to achieve with nutrient reductions from the watershed and airshed. Therefore, the accuracy of model hypoxia assessments is most important for these mainstem CBPSs because the more easily achieved DO criteria of the Western Shore and Eastern Shore CBPSs (discussed below) will be achieved long before the DO criteria of CB5MH and MD5MH are achieved.

Figure F-3. Hypoxia time series (*left panel*) and integrated hypoxia volume-day (*right panel*) in CBPS CB4MH from 1993 through 1995.

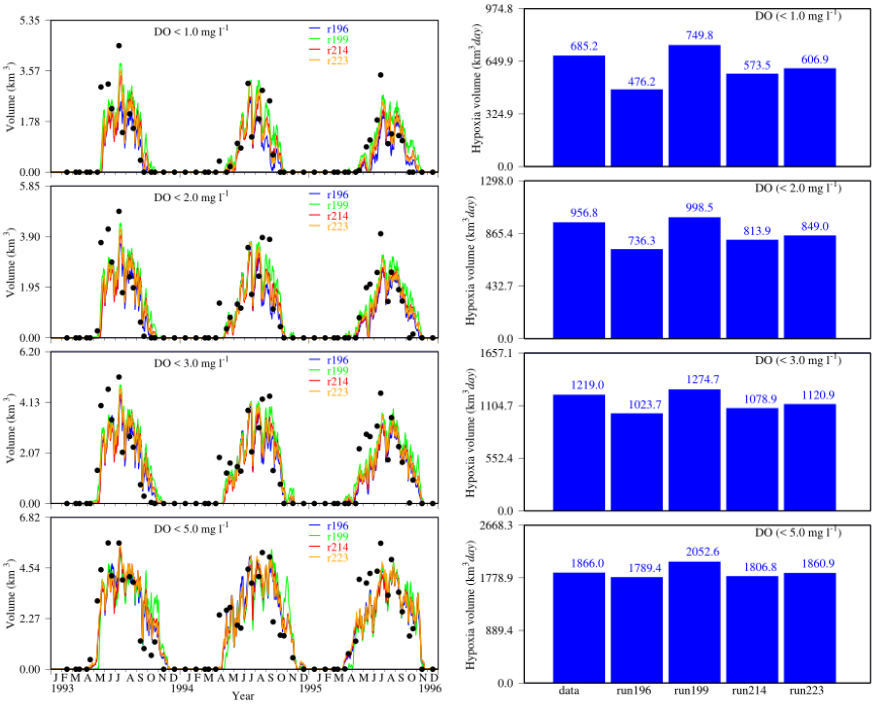

In CBPS MD5MH, as in CBPS CB4MH, deeply established and persistent hypoxia volume shows less variability than in upstream CBPS CB3MH (Figure F-4). High hypoxia volume values observed at the onset of the hypoxia season (late April and early May) are generally slightly underestimated by all model versions, particularly when considering low critical values such as 1 mg/l and 2 mg/l. In 1995, two peaks in hypoxia volume were predicted by all model versions and were also supported by observations. A second phytoplankton bloom with subsequent DO consumption may have occurred in fall 1995, but the mechanisms leading to the second peak in hypoxia require further investigation. Except for Run199, all model versions underestimated hypoxia volume-day when using critical values of 1 mg/l through 3 mg/l. Run196 underestimated hypoxia volume by 56 percent, 33

percent, and 15 percent when adopting a critical value of 1 mg/l, 2 mg/l, and 3 mg/l, respectively, but overestimated the observed volume by 5 percent when using a critical value of 5 mg/l.

Figure F-4. Hypoxia time series (*left panel*) and integrated hypoxia volume-day (*right panel*) in CBPS MD5MH from 1993 through 1995.

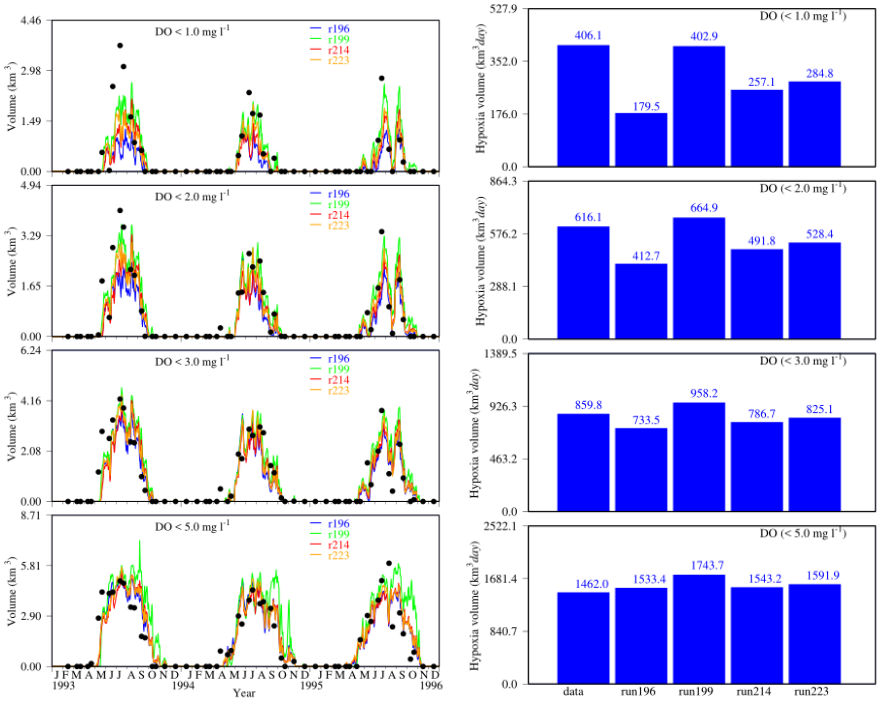

All model predictions of hypoxia were considerably underestimated in the Western Shore tributaries like the Potomac and Rappahannock (Figure F-5 and Figure F-6). Only when using a critical value of 5 mg/l did the model predict results comparable to observations, indicating that model predictions are comparable to observations at high DO concentrations but significantly off at the lower end of DO concentrations. On the other hand, the models overestimated hypoxia volume in the Eastern Shore tributaries and segments, like the Chester River (Figure F-7) and the Eastern Shore (Figure F-8). In the Chester River mesohaline CBPS CHSMH (Figure F-7), observations show that hypoxia starts in April and ends in August. Model-predicted hypoxia also starts in April but ends much later, in November. As a result, the duration of model-predicted hypoxia is about 3 months longer than observed hypoxia and the integrated hypoxia volume-day values predicted by the model are also much higher than observations.

Figure F-5. Hypoxia time series (*left panel*) and integrated hypoxia volume-day (*right panel*) in CBPS POMMH from 1993 through 1995.

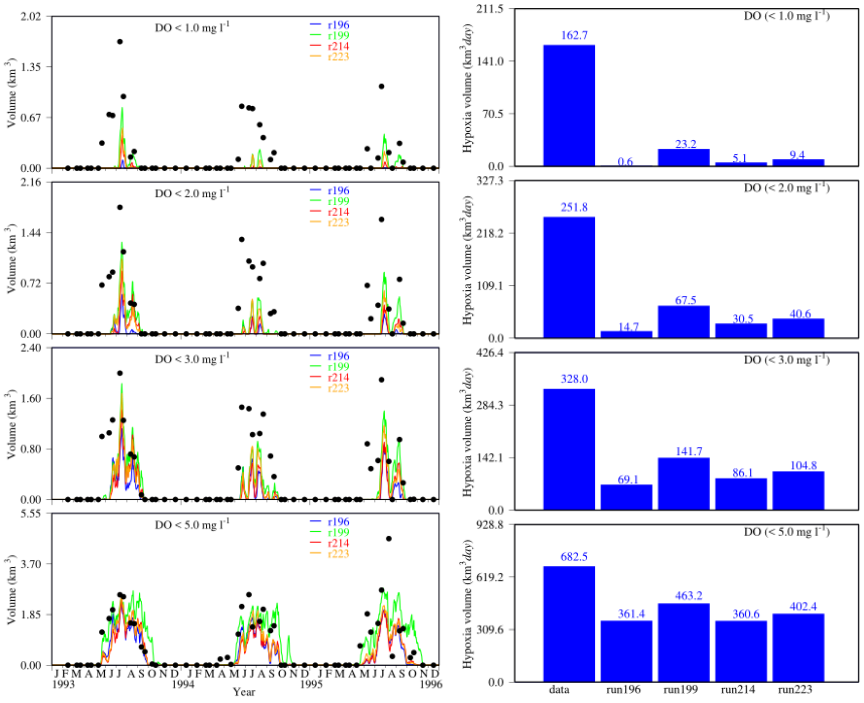

Figure F-6. Hypoxia time series (*left panel*) and integrated hypoxia volume-day (*right panel*) in CBPS RPPMH from 1993 through 1995.

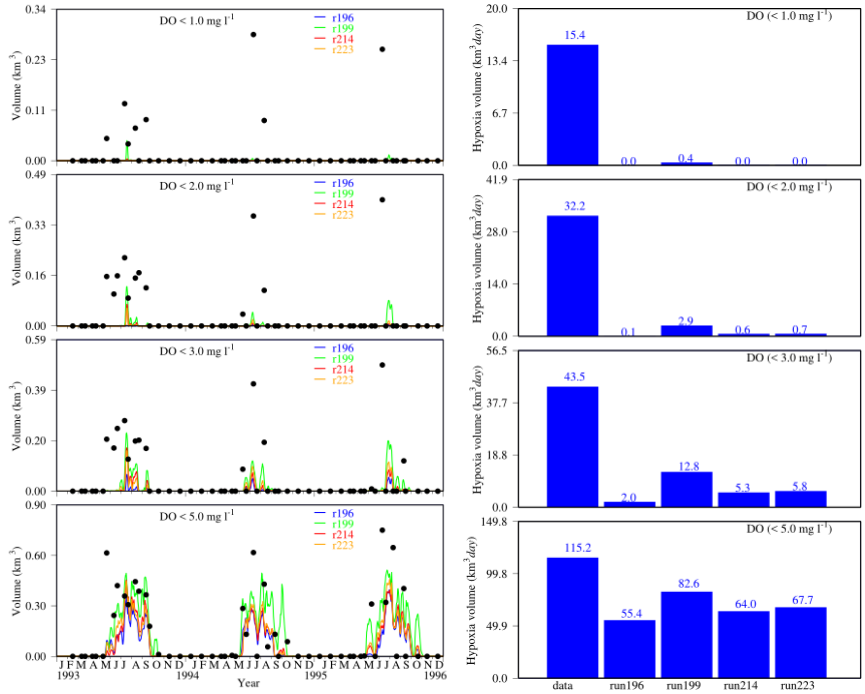

Figure F-7. Hypoxia time series (*left panel*) and integrated hypoxia volume-day (*right panel*) in CBPS CHSMH from 1993 through 1995.

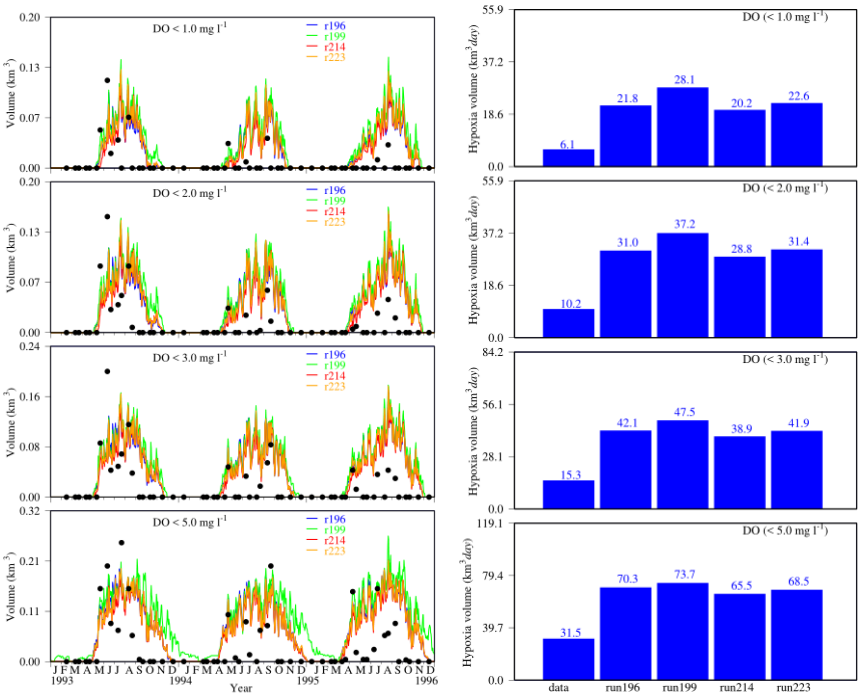

Run223 overpredicted hypoxia volume-day by 2.7-, 2.1-, 1.7-, and 1.2-fold when using critical DO concentrations of 1 mg/l, 2 mg/l, 3 mg/l, and 5 mg/l, respectively. The model-data discrepancy is larger for the Eastern Shore CBPS EASMH than for other segments (Figure F-8). Discrepancies exist in both magnitude and duration of hypoxia occurrence in the Eastern Shore. Observations revealed a relatively short hypoxia event from May through August, but the model predicted a longer hypoxia event lasting from May through November. In terms of hypoxia volume-day, Run223 overestimated observations by 4.5-fold with a 1-mg/l critical value, 3.4-fold with a 2-mg/l critical value, 3.2-fold with a 3-mg/l critical value, and 2.4-fold with a 5-mg/l critical value. Based on the hypoxia volume assessment of EASMH, the CBP decided that model estimates from that CBPS would not be used for the 2017 Midpoint Assessment.

Figure F-8. Hypoxia time series (*left panel*) and integrated hypoxia volume-day (*right panel*) in CBPS EASMH from 1993 through 1995.

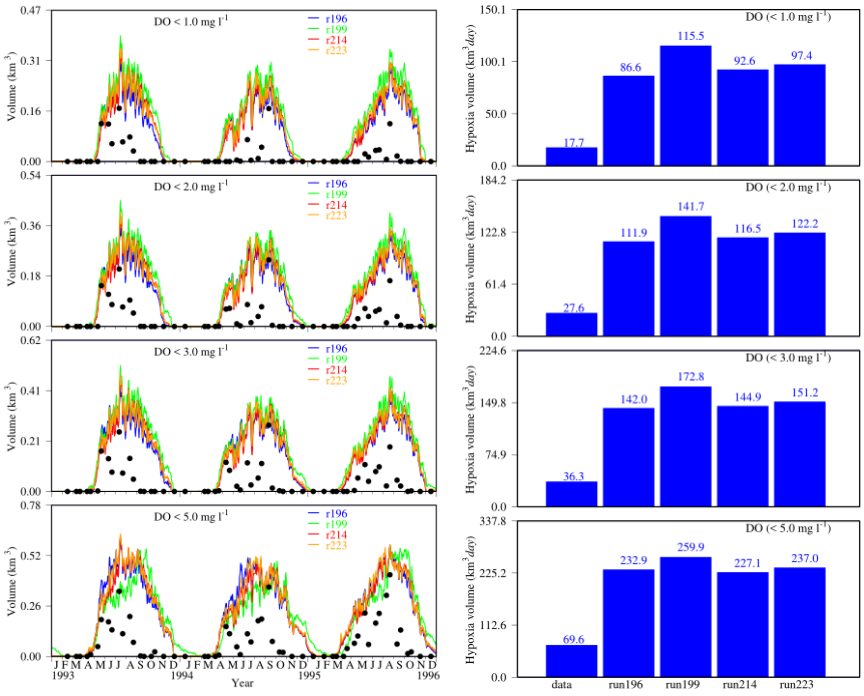

Hypoxia and hypoxia volume-day in the whole Bay integrate hypoxia volume across all segments and provide an overall assessment of model performance in time and space. Because of different sampling frequencies across segments, monthly averages of observed hypoxia volume were computed to compare them with model results (Figure F-9). Model predictions are generally comparable with observations but underestimate the peak hypoxia volume occurring in July primarily because of the underestimated hypoxia in the tributaries. Hypoxia volume tends to be underestimated in June as well. All model solutions underestimate the observed hypoxia volume-day with the exception of Run199 with a critical DO concentration of 1 mg/l. Run223 underestimates Baywide hypoxia volume-day by 20 percent with a critical DO concentration of 1 mg/l, 35 percent with 2 mg/l, 37 percent with 3 mg/l, and 33 percent with 5 mg/l.

Figure F-9. Hypoxia time series (*left panel*) and integrated hypoxia volume-day (*right panel*) in the whole Bay from 1993 through 1995.

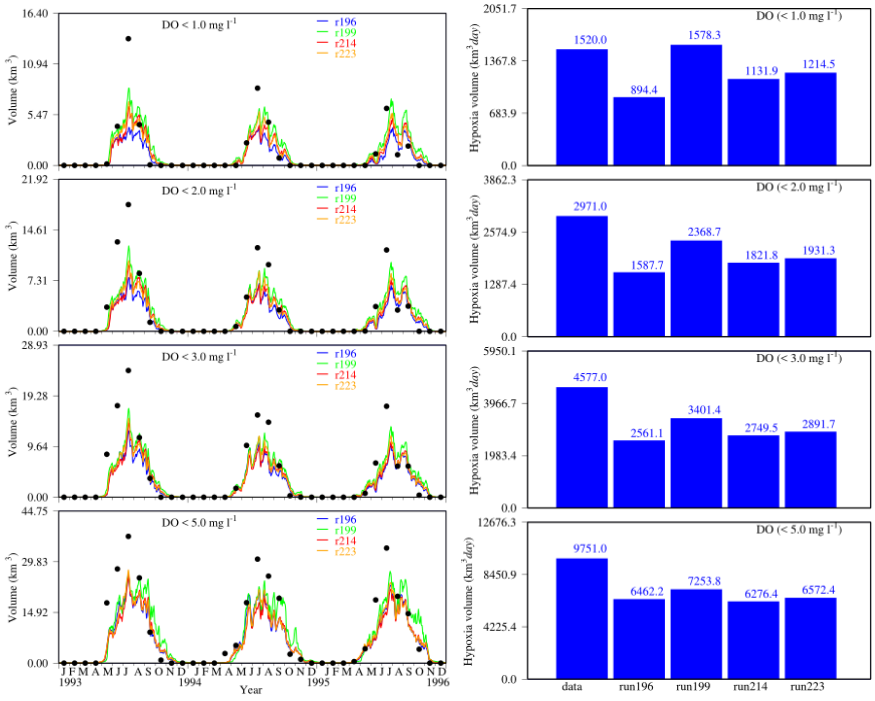

F.5 Model Goodness-of-Fit Statistics Using Hypoxia Volume versus DO Data

The previous section demonstrated that hypoxia volume and hypoxia volume-day can be used as metrics to assess the accuracy of model simulations. The key question is: Does this method result in different outcomes than a more traditional approach to model assessment?

In the main report and in appendix E, the absolute mean difference (AMD) between predicted and observed station-specific DO concentrations is used to assess the goodness-of-fit of model simulations, as shown in equation 1:

$$AMD = \frac{\sum_{i=1}^{N} |P_i - O_i|}{N} \quad (1)$$

where:

P_i = i^{th} model prediction
O_i = i^{th} observation
N = total number of data points for each station

Given that samples were collected over time, this metric does include integration in time to some degree. Because hypoxia volume-day also includes integration in time, a comparison can be made between AMD and the difference between

model-predicted and observed hypoxia volume-day. The units of those two metrics are different, however, making a direct comparison difficult. To overcome that issue, AMD was normalized to observations, thereby obtaining a measure of the Relative Difference (RD_d) between predicted and observed station DO data, as shown in equation 2:

$$RD_d = \frac{\int_{i=1}^{N} |P_i - O_i|}{\int_{i=1}^{N} O_i} \quad (2)$$

Similarly, we can define the Relative Difference (RD_h) between model-predicted and observed hypoxia volume-day, as shown in equation 3:

$$RD_h = \frac{HVD_m - HVD_o}{HVD_o} \quad (3)$$

where:

HVD_m = hypoxia volume-day predicted by model simulations
HVD_o = observed hypoxia volume-day

These two variables already implicitly include integration in time.

The AMD was computed for each major tributary and the mainstem Bay. For brevity, only three examples are illustrated in this appendix:

- The Potomac as an example of a Western Shore tributary
- The Eastern Shore as representative of the Eastern Shore tributaries and embayments
- The mainstem Bay

In the Potomac, all model solutions exhibited RD_h values significantly larger than *RDd* (Figure F-10). RD_h decreased when the critical DO concentration was shifted from using 1 mg/l to using 5 mg/l, showing that the model performed better at high DO concentrations in the OW surface layers than at low DO concentrations in the DC. All model solutions generated comparable RD_h. In the case of model solution Run223, RD_h is approximately five times higher than RD_d with a critical DO concentration of 1 mg/l and 2.5 times higher than RD_d when using a 5-mg/l critical value. As a response to the key question posed in the first paragraph of this section, the two methods of traditional DO calibration metrics and the hypoxia volume and hypoxia volume-day metric can lead to different results in terms of the goodness-of-fit of the model. Given that hypoxia volume-day integrates the model solution in space and time, it has the potential, when combined with traditional calibration methods, to provide a more robust metric for model assessment.

Figure F-10. Relative difference between model predictions and observations in the Potomac (POMMH) based on station DO data and integrated hypoxia volume-day.

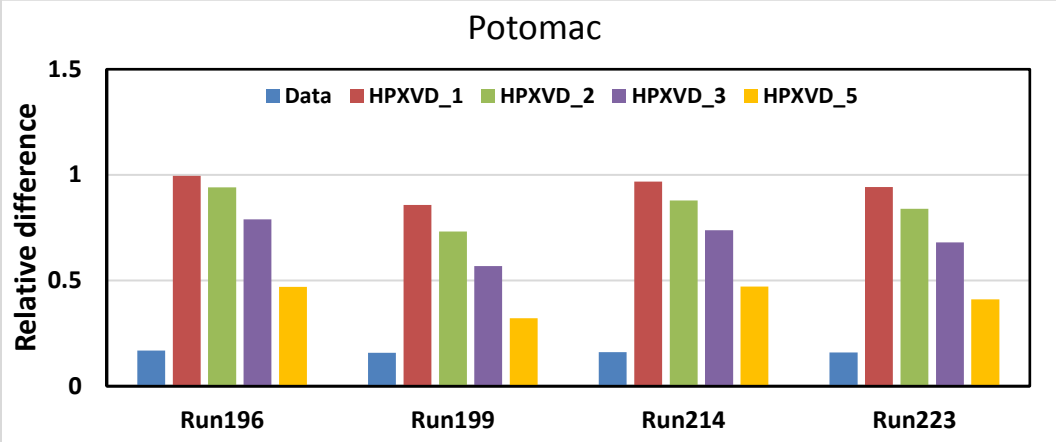

Notes: HPXVD_1 = Hypoxia volume-day based on 1 mg/l critical DO concentration;
HPXVD_2 = Hypoxia volume-day based on 2 mg/l critical DO concentration;
HPXVD_3 = Hypoxia volume-day based on 3 mg/l critical DO concentration;
HPXVD_5 = Hypoxia volume-day based on 5 mg/l critical DO concentration.

The difference between the two methods is more significant in the Eastern Shore (Figure F-11) than in the Potomac (Figure F-10). Run199 showed the largest difference between the two methods, and, in the case of a 1-mg/l critical DO concentration, RD_h is about 24 times higher than RD_d. In the case of the model solution used for the 2017 Midpoint Assessment management decisions (Run223), RD_h is about 21 times higher than RD_d with a 1-mg/l critical DO value and 11 times higher than RD_d with 5 mg/l as the critical DO value. Overall model performance is substantially better in the mainstem Bay than in the previous two cases (Figure F-12). Run196 generated the largest difference between the two methods, with RD_h being three times higher than RD_d when using a 1-mg/l DO critical value. Run199 had the lowest RD_h among all model solutions, but the differences between the two methods remain significant. With a 2-mg/l critical value, RD_d is 18 times higher than RD_h. The results of the two methods are most comparable for model version Run223 in the mainstem Bay. All values of RD_h are relatively close to the corresponding RD_d value. Specifically, RD_h is about 58 percent higher than RD_d when using a 1-mg/l critical DO concentration, 44 percent higher when using 2 mg/l DO, 12 percent higher when using 3 mg/l DO, and 33 percent lower when using 5 mg/l DO. Overall, the model is more accurately calibrated to DO in the mainstem Bay than in the tributaries.

Figure F-11. Relative difference between model predictions and observations in the Eastern Shore (EASMH) based on station DO data and integrated hypoxia volume-day.

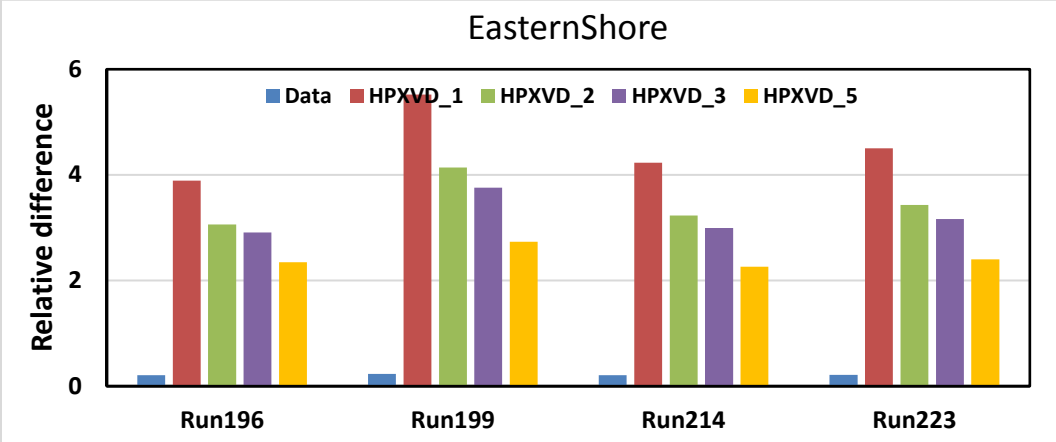

Notes: HPXVD_1 = Hypoxia volume-day based on 1 mg/l critical DO concentration;
HPXVD_2 = Hypoxia volume-day based on 2 mg/l critical DO concentration;
HPXVD_3 = Hypoxia volume-day based on 3 mg/l critical DO concentration;
HPXVD_5 = Hypoxia volume-day based on 5 mg/l critical DO concentration.

Figure F-12. Relative difference between model predictions and observations in the mainstem of the Bay based on station DO data and integrated hypoxia volume-day.

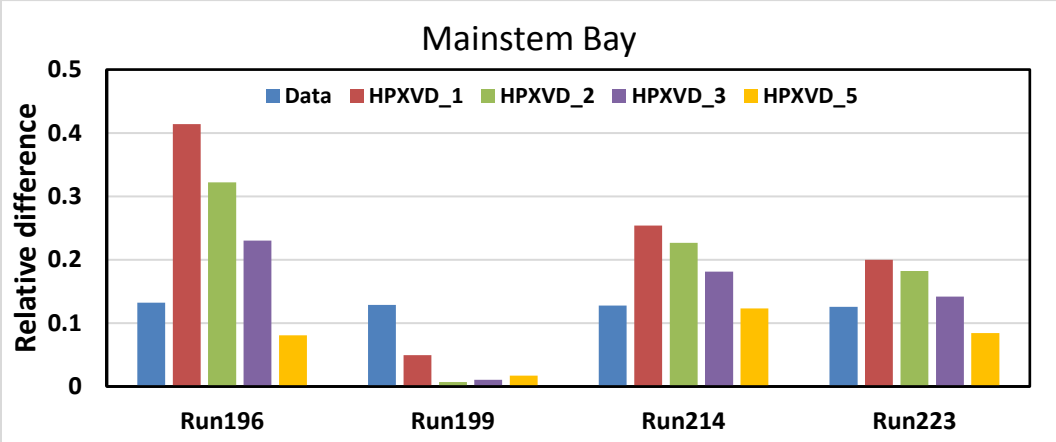

Notes: HPXVD_1 = Hypoxia volume-day based on 1 mg/l critical DO concentration;
HPXVD_2 = Hypoxia volume-day based on 2 mg/l critical DO concentration;
HPXVD_3 = Hypoxia volume-day based on 3 mg/l critical DO concentration;
HPXVD_5 = Hypoxia volume-day based on 5 mg/l critical DO concentration.

F.6 Conclusions

Hypoxia volume and hypoxia volume-day have been used in this study as metrics for model calibration and performance assessment. First, hypoxia volume was computed for both model simulations and observations based on critical DO concentration values of 1 mg/l, 2 mg/l, 3 mg/l, and 5 mg/l. Hypoxia volume-day

was obtained through integration of hypoxia volume in time, both for model simulations and observations. The method was applied to four different model solutions. Comparisons between model predictions and observations were performed using time series plots and measures of hypoxia volume-day. Results show good model performance in the mainstem of the Bay but discrepancies between model predictions and observations in the tributaries and local embayment, indicating a more accurate calibration in the mainstem than in the tributaries and shallow embayments. A comparison between the calibration metrics proposed here for model performance in the assessment of coastal water hypoxia and the more traditional calibration metrics based on station data showed that the two approaches generated different statistics in terms of model assessment and goodness-of-fit. Given their ability to integrate information in space and time, the hypoxia metrics proposed here represent an alternative that allows for a more comprehensive assessment of model performance in modelling applications for nutrient management in hypoxic coastal waters.

F.7 References

Bahner, L. 2006. *User Guide for the Chesapeake Bay and Tidal Tributary Interpolator*. NOAA Chesapeake Bay Office, Annapolis, MD.

USEPA (US Environmental Protection Agency). 1983. The Chesapeake Bay Segmentation Scheme. Chesapeake Bay Program Office, Annapolis, MD. Accessed June 2019. https://nepis.epa.gov/Exe/ZyNET.exe/2000VXXP.txt?ZyActionD=ZyDocument&Client=EPA&Index=1986%20Thru%201990&Docs=&Query=&Time=&EndTime=&SearchMethod=1&TocRestrict=n&Toc=&TocEntry=&QField=&QFieldYear=&QFieldMonth=&QFieldDay=&UseQField=&IntQFieldOp=0&ExtQFieldOp=0&XmlQuery=&File=D%3A%5CZYFILES%5CINDEX%20DATA%5C86THRU90%5CTXT%5C00000014%5C2000VXXP.txt&User=ANONYMOUS&Password=anonymous&SortMethod=h%7C-&MaximumDocuments=1&FuzzyDegree=0&ImageQuality=r105g16/r105g16/x150y150g16/i600&Display=hpfr&DefSeekPage=x&SearchBack=ZyActionL&Back=ZyActionS&BackDesc=Results%20page&MaximumPages=1&ZyEntry=3.

USEPA (US Environmental Protection Agency). 2010. Chesapeake Bay Total Maximum Daily Load for Nitrogen, Phosphorus and Sediment. US Environmental Protection Agency, Chesapeake Bay Program Office, Annapolis, MD.

USEPA (US Environmental Protection Agency). 2018. Chesapeake Bay Program |Indicator Analysis and Methods Document. Chesapeake Bay Program Office, Annapolis, MD. Accessed June 2019. https://www.chesapeakeprogress.com/files/Analysis_and_Methods_2017_Water_Quality_Standards_Attainment_10-12-2018.pdf.

Appendix G: Algal Temperature Parameters for Climate-Change Scenarios

The 2017 Water Quality and Sediment Transport Model represents the effect of temperature on algal production through multiplication of a maximum photosynthetic rate by a temperature function. The temperature function is formulated so that production increases as a function of temperature until an optimum temperature is reached. Algal production declines as temperature increases above the optimum. That relationship is described in equation 1:

$$f(T) = e^{-KTg1 \cdot (T - Topt)^2} \quad when \ T \le Topt$$
$$= e^{-KTg2 \cdot (Topt - T)^2} \quad when \ T > Topt \qquad (1)$$

where:

T = temperature (°C)
$Topt$ = optimal temperature for algal production (°C)
$KTg1$ = effect of temperature below Topt on production ($°C^{-2}$)
$KTg2$ = effect of temperature above Topt on production ($°C^{-2}$)

During the model calibration process, the parameters in equation 1 were derived empirically based on observed temperatures, production rates, and species composition. For climate-change scenarios, we wish to allow for the appearance of algal species with temperature optima above the values derived for existing conditions. We also need to compute production for temperatures beyond those presently observed.

The necessity of revised algal parameters for climate-change scenarios became apparent after model calibration was completed and while the model was being used in load-reduction scenarios. We wanted revised parameters that maintained, to the greatest extent possible, the calibrated production rates for existing conditions while projecting revised production rates for future temperature conditions. Parameter revisions were considered only for algal groups 1 (freshwater) and 3 (other green algae). Group 2 consists of the spring diatom community presently found in saline portions of the Bay system. The parameters for that specific group are not subject to change, although the timing and magnitude of the spring bloom are subject to change in response to future temperature conditions.

Table G-1 presents the revised parameter set. Production computed with the revised parameters largely agrees with calibration values for temperatures less

than or equal to the calibrated optimum (Figures G-1 and G-2). At temperatures above the former optimum, production for climate-change scenarios exceeds values computed using calibration parameters.

Table G-1. Revised Algal Parameters for Climate-Change Scenarios

Parameter	Definition	Group 1 Calibration	Group 1 Climate Change	Group 3 Calibration	Group 3 Climate Change
KTg1	Effect of temperature below optimal temperature on algal production ($°C^{-2}$)	0.005	0.0022	0.0035	0.0013
KTg2	Effect of temperature above optimal temperature on algal production ($°C^{-2}$)	0.004	0	0	0
Pm^B	Maximum photosynthetic rate (g C g^{-1} Chl d^{-1})	200	250	450	600
Topt	Optimal temperature for algal production (°C)	29	37	25	37

Figure G-1. Algal photosynthetic rate versus temperature for Group 1 algae with calibration and climate-change parameter sets.

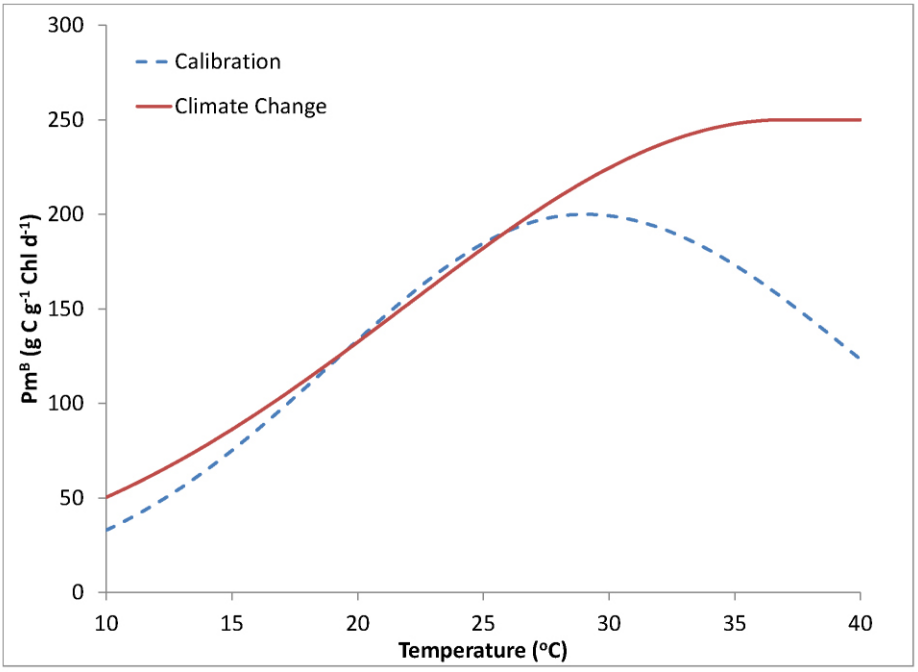

Figure G-2. Algal photosynthetic rate versus temperature for Group 3 algae with calibration and climate-change parameter sets.